

PROCEEDINGS OF THE THIRD INTERNATIONAL CONFERENCE
ON THE PEACEFUL USES OF ATOMIC ENERGY

Volume 8

REACTOR ENGINEERING AND EQUIPMENT

ACTES DE LA TROISIÈME CONFÉRENCE INTERNATIONALE
SUR L'UTILISATION DE L'ÉNERGIE ATOMIQUE À DES FINS PACIFIQUES

Volume 8

TECHNOLOGIE ET ÉQUIPEMENT DES RÉACTEURS

ТРУДЫ ТРЕТЬЕЙ МЕЖДУНАРОДНОЙ КОНФЕРЕНЦИИ
ПО ИСПОЛЬЗОВАНИЮ АТОМНОЙ ЭНЕРГИИ В МИРНЫХ ЦЕЛЯХ

Том 8

ТЕХНОЛОГИЯ И ОБОРУДОВАНИЕ РЕАКТОРОВ

ACTAS DE LA TERCERA CONFERENCIA INTERNACIONAL
SOBRE LA UTILIZACIÓN DE LA ENERGÍA ATÓMICA CON FINES PACÍFICOS

Volumen 8

TECNOLOGÍA Y EQUIPO DE LOS REACTORES

The designations employed and the presentation of the material in this publication do not imply the expression of any opinion whatsoever on the part of the Secretariat of the United Nations concerning the legal status of any country or territory or of its authorities, or concerning the delimitation of its frontiers.

Les désignations utilisées dans cette publication et la présentation des données qui y figurent n'impliquent de la part du Secrétariat de l'Organisation des Nations Unies aucune prise de position quant au statut juridique de tel ou tel pays ou territoire, ou de ses autorités, ni quant au tracé de ses frontières.

Употребляемые здесь обозначения и оформление материала не должны рассматриваться как выражение какого бы то ни было мнения со стороны Секретариата Организации Объединенных Наций относительно правового статуса той или иной страны или территории или ее властей, или относительно делимитации ее границ.

Las denominaciones empleadas en esta publicación y la forma en que aparecen presentados los datos que contiene no implican, de parte de la Secretaría de las Naciones Unidas, juicio alguno sobre la condición jurídica de ninguno de los países o territorios citados o de sus autoridades, ni respecto de la delimitación de sus fronteras.

A/CONF.28/1, Vol. 8

UNITED NATIONS PUBLICATION

Sales No.: 65. IX. 8

Price: \$U.S. 12.50
(or equivalent in other currencies)

PRINTED IN ENGLAND

**Proceedings of
the Third International Conference
on the Peaceful Uses of Atomic Energy**

**Held in Geneva
31 August–9 September 1964**

**Volume 8
Reactor Engineering and Equipment**

MULTILINGUAL EDITION
ÉDITION MULTILINGUE
МНОГОЯЗЫЧНОЕ ИЗДАНИЕ
EDICIÓN PLURILINGÜE



UNITED NATIONS
New York
1965

EXPLANATORY NOTE

The Proceedings of the Third International Conference on the Peaceful Uses of Atomic Energy comprise a single, multilingual publication of sixteen volumes. This form was prescribed by the General Assembly of the United Nations in approving the Conference budget.

Papers accepted for consideration at the Conference are accordingly printed herein only in the original language of submission, each being followed by its abstract in the other three languages of the Conference.*

The budgetary arrangements for the Conference required also that Governments provide abstracts and papers in two of the Conference languages. One of the three abstracts following each paper is, therefore, in a translation provided by the Government concerned. The abstracts were translated into the other two languages either by the Division of Language Services, International Atomic Energy Agency (IAEA) in Vienna, or, with its assistance, through the intermediary of the national atomic energy authorities in London, Paris, Moscow and Madrid.

The Foreword by the Secretary-General of the United Nations, the Preface by the Director General of IAEA, and this Explanatory Note, together with the records of discussion at each of the six scientific general sessions and thirty-six technical sessions of the Conference, are published in all four languages. All other material, which is largely of a formal nature and is confined to Volumes 1 and 16, is published in the language of submission or delivery, followed in the case of French, Russian and Spanish originals by the English translation.

Governments whose national tongue is not one of the four Conference languages were consulted as to their preference for the language in which their papers should appear in these Proceedings.

The Table of Contents in each volume gives the titles of papers in the original language, or language of choice, followed in the case of French, Russian and Spanish titles by the English translation.

Starting from the 992 abstracts submitted by Governments, specialized agencies and IAEA, the Scientific Secretariat, working under the guidance

of the United Nations Scientific Advisory Committee, finally chose 747 papers for inclusion in the Programme of the Conference; of these, 358 were selected for oral presentation at the 42 working sessions.

In arranging the programme, the Scientific Secretariat aimed at achieving a balanced schedule, providing for the oral presentation of as many papers as possible at each session while still leaving adequate time for discussion of the material presented. Two afternoons were left entirely free, to enable informal groups to discuss matters arising out of discussions at the formal sessions of the Conference. No records were taken of such informal meetings.

Wherever possible, the author, or authors, of papers were consulted during the Conference by members of the Scientific Secretariat, who acted as secretaries of session, or by the team of editors made available for the purpose by IAEA,** to ensure maximum accuracy.

The records of discussion at the various sessions, based on notes taken in the meetings by IAEA records officers,** and checked where necessary against the sound recordings made of all sessions, were prepared by the Division of Language Services of IAEA in English, and subsequently translated into French, Russian and Spanish through the intermediary of the atomic energy authorities in the three countries concerned (see third paragraph of the present note).

The editing of the English, French and Spanish papers was carried out at the United Nations Office at Geneva under United Nations supervision by a team of editors, whose services, also, were made available by the atomic energy authorities of their respective countries, with some help from outside consultants. The editing of the Russian papers was done in Moscow in similar circumstances. The following served as editors: Mr. A. de Calmès, Dr. C. E. Granados, Mr. D. H. Hill, Mr. V. F. Kalinin, Cand. Tech. Sc., Dr. R. Lapage, Mr. E. T. Marles, Dr. J. D. C. Mole, Mr. C. Ségot, Mr. J. J. Stobbs, Mr. C. R. Symons and Mr. J. Williamson.

The task of printing this large collection of scientific information has been shared by printers in

* The languages of the Conference were English, French, Russian and Spanish.

** The names of the scientific secretaries, editors and records officers will be found in the list of the Conference Secretariat in Annex 1, Volume 1, of this series.

Belgium, Canada, France, Switzerland, the Union of Soviet Socialist Republics and the United Kingdom.

Full titles of the sixteen volumes of these Proceedings, together with the sessions covered by each volume, are as follows:

<i>Volume No.</i>		<i>Sessions included</i>
1	Progress in Atomic Energy	A, B, 1.6, C, H
2	Reactor Physics	3.1
3	Reactor Studies and Performance	3.2, 3.3
4	Reactor Control	3.4, 3.5
5	Nuclear Reactors — I. Gas-cooled and Water-cooled Reactors	1.1, 1.2, 1.3
6	Nuclear Reactors — II. Fast Reactors and Advanced Concepts	1.4, 1.5, 1.7
7	Research and Testing Reactors	D, 1.9, 1.8
8	Reactor Engineering and Equipment	1.10, 1.11, 3.7
9	Reactor Materials	2.8, 2.9, 2.4
10	Nuclear Fuels — I. Fabrication and Reprocessing	2.3, 2.6, 2.7
11	Nuclear Fuels — II. Types and Economics	2.5, 2.1, 2.2
12	Nuclear Fuels — III. Raw Materials	2.11, 2.12, 2.10
13	Nuclear Safety	3.9, 3.8 3.6
14	Environmental Aspects of Atomic Energy and Waste Management	3.10, 3.11
15	Special Aspects of Nuclear Energy and Isotope Applications	E, 4.1, F, G, 4.2
16	List of Papers and Indexes	

NOTE EXPLICATIVE

Les Actes de la troisième Conférence internationale sur l'utilisation de l'énergie atomique à des fins pacifiques sont publiés ici sous la forme d'une édition unique, multilingue, en seize volumes. Cette présentation a été décidée par l'Assemblée générale lorsqu'elle a approuvé le budget de la Conférence.

En conséquence, les mémoires qui ont été acceptés pour la Conférence sont reproduits ici dans la langue originale dans laquelle ils ont été soumis et sont suivis d'un résumé dans les trois autres langues de la Conférence*.

Aux termes des dispositions budgétaires prises en vue de la Conférence, les gouvernements devaient fournir les résumés et les mémoires dans deux des langues de la Conférence. Ainsi, sur les trois résumés qui suivent chaque mémoire, un est une traduction fournie par le gouvernement intéressé. La traduction des résumés dans les deux autres langues a été faite soit par la Division des services linguistiques de l'Agence internationale de l'énergie atomique (AIEA), à Vienne, soit avec son concours, par les soins des organismes nationaux compétents en matière d'énergie atomique à Londres, Paris, Moscou et Madrid.

L'avant-propos du Secrétaire général de l'Organisation des Nations Unies, la préface du Directeur général de l'AIEA et la présente note explicative, ainsi que les comptes rendus de chacune des six séances scientifiques générales et des trente-six séances techniques de la Conférence, sont publiés dans les quatre langues. Tous les autres textes, qui pour la plupart sont d'un caractère non technique et figurent dans les volumes 1 et 16, sont publiés dans la langue dans laquelle ils ont été présentés par écrit ou oralement et sont suivis, lorsque cette langue est l'espagnol, le français ou le russe, d'une traduction en anglais.

Les gouvernements des pays dont la langue officielle n'est pas l'une des quatre langues utilisées à la Conférence ont été consultés pour savoir dans quelle langue ils préféreraient voir paraître leurs mémoires.

La table des matières de chaque volume donne les titres des mémoires dans la langue originale ou dans la langue choisie; ces indications sont suivies,

pour les titres en espagnol, en français et en russe, de la traduction en anglais.

Sur les 992 résumés présentés par les gouvernements, les institutions spécialisées et l'AIEA, le Secrétariat scientifique, travaillant sous la direction du Comité consultatif scientifique des Nations Unies, en a finalement retenu 747 pour les inscrire au programme de la Conférence; sur ce nombre, 358 ont été présentés oralement aux 42 séances de travail.

En établissant le programme de la Conférence, le Secrétariat scientifique a cherché à réaliser un équilibre: il s'est efforcé de ménager un temps suffisant pour la présentation du plus grand nombre possible de mémoires tout en laissant du temps pour leur discussion. Deux après-midi avaient été laissés entièrement libres afin de permettre aux participants d'organiser des réunions non officielles et de discuter en petits groupes des questions qui se posaient à la suite des séances officielles de la Conférence. Ces réunions n'ont pas fait l'objet de comptes rendus.

Toutes les fois que cela a été possible, l'auteur ou les auteurs des mémoires ont été consultés pendant la Conférence par les membres du Secrétariat scientifique, qui ont assuré le secrétariat des séances, ou par l'équipe d'«éditeurs» que l'AIEA** avait mis à cet effet à la disposition de la Conférence, afin d'assurer l'exactitude la plus grande.

Les comptes rendus des discussions aux réunions, établis d'après les notes prises en séance par les rédacteurs de comptes rendus de l'AIEA** et comparés toutes les fois qu'il le fallait avec les enregistrements sonores, ont été rédigés en anglais par la Division des services linguistiques de l'AIEA, puis traduits en espagnol, en français et en russe par les soins des organismes compétents en matière d'énergie atomique des trois pays intéressés (voir le troisième alinéa de la présente note).

Les mémoires rédigés en anglais, en espagnol et en français ont été mis au point pour l'impression à l'Office européen des Nations Unies à Genève, sous le contrôle de l'ONU, par une équipe de rédac-

** On trouvera les noms des secrétaires scientifiques, des «éditeurs» et des rédacteurs de comptes rendus dans la liste des membres du secrétariat de la Conférence à l'annexe 1 du volume 1.

* Les langues de la Conférence étaient l'anglais, l'espagnol, le français et le russe.

teurs mis à la disposition de la Conférence par les organismes compétents en matière d'énergie atomiques des pays intéressés, avec l'aide de quelques consultants extérieurs. La mise au point définitive des mémoires rédigés en russe a été faite à Moscou dans les mêmes conditions. Voici les noms des rédacteurs qui ont assuré la mise au point des mémoires: M. A. de Calmès, M. C. E. Granados, M. D. H. Hill, M. V. F. Kalinin, M^{lle} R. Lapage, M. E. T. Marles, M^{lle} J. D. C. Mole, M. C. Ségot,

M. J. J. Stobbs, M. C. R. Symons et M. J. Williamson.

Des entreprises de Belgique, du Canada, de France, du Royaume-Uni, de Suisse et de l'Union des Républiques socialistes soviétiques se sont partagé la tâche que représentait l'impression de cette masse importante de documents scientifiques.

Les titres complets des seize volumes des Actes de la Conférence, ainsi que les numéros des séances sur lesquelles porte chaque volume, figurent ci-après:

<i>Numéro du volume</i>		<i>Séances</i>
1	Progrès accomplis dans le domaine atomique	A, B, 1.6, C, H
2	Physique des réacteurs	3.1
3	Etude des réseaux et performance des réacteurs	3.2, 3.3
4	Contrôle des réacteurs.....	3.4, 3.5
5	Réacteurs nucléaires — I. Réacteurs refroidis par un gaz et réacteurs refroidis à l'eau	1.1, 1.2, 1.3
6	Réacteurs nucléaires — II. Réacteurs à neutrons rapides et réacteurs d'avant-garde	1.4, 1.5, 1.7
7	Réacteurs de recherche et réacteurs d'essai de matériaux.....	D, 1.9, 1.8
8	Technologie et équipement des réacteurs	1.10, 1.11, 3.7
9	Matériaux pour réacteurs	2.8, 2.9, 2.4
10	Combustibles nucléaires — I. Fabrication et retraitement	2.3, 2.6, 2.7
11	Combustibles nucléaires — II. Caractéristiques et aspects économiques	2.5, 2.1, 2.2
12	Combustibles nucléaires — III. Matières premières	2.11, 2.12, 2.10
13	Sûreté nucléaire	3.9, 3.8, 3.6
14	Influence sur le milieu de l'emploi de l'énergie nucléaire. Traitement et élimination des déchets	3.10, 3.11
15	Aspects particuliers de l'énergie nucléaire et applications des radioéléments..	E, 4.1, F, G, 4.2
16	Liste des mémoires et index	

ПОЯСНИТЕЛЬНАЯ ЗАПИСКА

Труды третьей Международной конференции по использованию атомной энергии в мирных целях представляют собой единое многоязычное издание из шестнадцати томов. Такая форма была предусмотрена Генеральной Ассамблеей Организации Объединенных Наций при одобрении ею бюджета Конференции.

Принятые к рассмотрению Конференцией доклады соответственно опубликованы здесь лишь на языке оригинала; при этом каждый доклад сопровождается аннотацией на других трех языках Конференции*.

Бюджетные постановления в отношении проведения Конференции также предусматривали, что правительства представят аннотации и доклады на двух языках Конференции. Поэтому одна из трех аннотаций, сопровождающих каждый доклад, является переводом, представленным соответствующим правительством. Аннотации были переведены на другие два языка либо Отделом переводов Международного агентства по атомной энергии (МАГАТЭ) в Вене, либо с его помощью при сотрудничестве национальных органов, ведающих вопросами атомной энергии, в Лондоне, Париже, Москве и Мадриде.

Введение и предисловие Генерального Секретаря Организации Объединенных Наций и Генерального директора МАГАТЭ, соответственно, и настоящая пояснительная записка, наряду с протоколами каждого из шести научных пленарных заседаний и тридцати шести секционных заседаний Конференции, публикуются на всех четырех языках. Все другие материалы, которые по своему характеру в основном относятся к числу официальных и содержатся в томах 1 и 16, публикуются на языке оригинала; и когда речь идет о французских, русских и испанских оригиналах, то к ним приложен английский перевод.

С правительствами стран, язык которых не относится к числу четырех языков Конфе-

ренции, были проведены консультации по поводу того, на каком языке было бы желательно, по их мнению, опубликовать в настоящих трудах представленные ими доклады.

В содержании каждого тома указаны заглавия докладов на языке оригинала либо на другом избранном языке, и в том случае, когда речь идет о французских, русских и испанских заглавиях, их сопровождает английский перевод.

Из 992 аннотаций, представленных правительствами, специализированными учреждениями, а также МАГАТЭ, Ученый секретариат, работая под руководством Научного консультативного комитета Организации Объединенных Наций, в итоге отобрал 747 докладов для включения их в программу Конференции; из них 358 были отобраны для представления в устной форме на 42 рабочих заседаниях.

При составлении программы Ученый секретариат ставил целью добиться сбалансированного расписания, которое дало бы возможность представить в устной форме максимальное количество докладов на каждом заседании при обеспечении достаточного времени для проведения дискуссии по поводу представленного материала. В двух случаях имеющееся во второй половине дня время оставили нераспределенным, с тем чтобы дать возможность неофициальным группам обсудить вопросы, возникшие в ходе дискуссии на официальных заседаниях Конференции. На таких неофициальных заседаниях протоколы не составлялись.

По мере возможности, с автором или авторами докладов консультировались в ходе Конференции члены Ученого секретариата, которые выполняли функции секретарей заседаний, либо такие консультации проводились группой редакторов, которые были выделены МАГАТЭ** для этой цели, с тем чтобы обеспечить максимальную точность.

* Языками Конференции являлись: английский, французский, русский и испанский.

** Фамилии ученых секретарей, редакторов и протоколистов приведены в перечне сотрудников секретариата Конференции в приложении 1-ом к тому 1-му настоящей серии.

Протоколы дискуссии на различных заседаниях, составленные на основе записей, сделанных в ходе заседаний протоколистами МАГАТЭ*, и проверенные, по мере необходимости, путем сравнения со звуковой записью, которая велась на всех заседаниях, были подготовлены Отделом переводов МАГАТЭ на английском языке и впоследствии переведены на французский, русский и испанский языки при сотрудничестве национальных органов, ведающих вопросами атомной энергии, в трех заинтересованных странах (смотри третий абзац пояснительной записки).

Работа по редактированию документов на английском, французском и испанском языках была проведена в Европейском отделении Организации Объединенных Наций, в Женеве, под руководством Организации Объединенных Наций группой редакторов,

* Фамилии ученых секретарей, редакторов и протоколистов приведены в перечне сотрудников секретариата Конференции в приложении 1-ом к тому 1-му настоящей серии.

услуги которых были также предоставлены по линии органов, ведающих вопросами атомной энергии в соответствующих странах, с использованием в некоторой степени помощи приглашенных со стороны консультантов. Русские документы редактировались в Москве в таких же условиях. Нижеследующие лица осуществляли работу в качестве редакторов: д-р К. Э. Гранадос, кандидат технических наук В. Ф. Калинин, г-н А. де Кальмэс, д-р Р. Лепейдж, г-н Э. Т. Марлз, д-р Дж. Д. К. Моул, г-н Ч. Р. Саймонс, г-н Дж. Дж. Стобз, г-н Ш. Сэго, г-н Дж. Уильямсон, г-н Д. Х. Хилл.

В выполнении задачи по печатанию этой обширной научной информации принимали участие типографии в Бельгии, Канаде, Соединенном Королевстве, Союзе Советских Социалистических Республик, Франции и Швейцарии.

Ниже приводятся полные заглавия шестнадцати томов настоящих Трудов, а также указывается, какие сессии охватываются каждым томом:

Номер Тома		Заседания, включенные в том
1	Прогресс в работах по атомной энергии	А, В, 1.6, С, Н
2	Физика реакторов	3.1
3	Изучение реакторов и их характеристики	3.2, 3.3
4	Регулирование реакторов	3.4, 3.5
5	Ядерные реакторы — I. Реакторы с водяным и газовым охлаждением	1.1, 1.2, 1.3
6	Ядерные реакторы — II. Реакторы на быстрых нейтронах и усовершенствованные реакторы	1.4, 1.5, 1.7
7	Исследовательские и испытательные реакторы	D, 1.9, 1.8
8	Технология и оборудование реакторов	1.10, 1.11, 3.7
9	Реакторные материалы	2.8, 2.9, 2.4
10	Ядерное топливо — I. Изготовление и переработка	2.3, 2.6, 2.7
11	Ядерное топливо — II. Типы и экономика	2.5, 2.1, 2.2
12	Ядерное топливо — III. Сырьевые материалы	2.11, 2.12, 2.10
13	Ядерная безопасность	3.9, 3.8, 3.6
14	Исследование окружающей среды и удаление радиоактивных отходов	3.10, 3.11
15	Специальные аспекты применения ядерной энергии и изотопов	E, 4.1, F, G, 4.2
16	Список докладов и указатели	

NOTA EXPLICATIVA

Las Actas de la tercera Conferencia Internacional sobre la Utilización de la Energía Atómica con Fines Pacíficos están constituidas por una publicación única y plurilingüe compuesta de dieciséis volúmenes, en conformidad con lo dispuesto por la Asamblea General de las Naciones Unidas al aprobar el presupuesto de la Conferencia.

Por consiguiente, las memorias aceptadas para ser examinadas en la Conferencia sólo figuran impresas en el idioma original en que se presentaron, y cada una de ellas va seguida de un resumen de la misma en los otros tres idiomas de la Conferencia*.

En los arreglos presupuestarios para la Conferencia se dispuso también que los gobiernos tenían asimismo que presentar resúmenes y memorias en dos de los idiomas de la Conferencia. En consecuencia, uno de los tres resúmenes que siguen a cada memoria es una traducción facilitada por el gobierno interesado. Los resúmenes fueron traducidos a los otros dos idiomas, ya por la División de Idiomas del Organismo Internacional de Energía Atómica (OIEA) de Viena, o, con su asistencia, por conducto de las autoridades nacionales de energía atómica de Londres, París, Moscú y Madrid.

La introducción del Secretario General de las Naciones Unidas, el prefacio del Director General del OIEA y la presente nota explicativa, junto con las actas de los debates celebrados en cada una de las seis sesiones científicas generales y las treinta y seis sesiones técnicas de la Conferencia, se publican en los cuatro idiomas. El resto del material, que reviste en su mayoría un carácter oficial y está contenido exclusivamente en los volúmenes 1 y 16, se publica en el idioma en que fue presentado o entregado, seguido para los originales en español, francés y ruso, de la traducción en inglés.

Se consultó a los gobiernos cuyo idioma nacional no es uno de los cuatro idiomas de la Conferencia para saber en cuál de ellos preferían que se publicaran sus memorias en estas Actas.

El índice de cada volumen contiene los títulos de las memorias en el idioma original, o en el idioma elegido, seguidos, cuando se trata de títulos en español, francés y ruso, de la traducción en inglés.

De los 992 resúmenes presentados por gobiernos, organismos especializados y el OIEA, la Secretaría

Científica, bajo la dirección del Comité Científico Consultivo de las Naciones Unidas, escogió por último 747 memorias que debían ser incluidas en el programa de la Conferencia; de éstas, 358 fueron seleccionadas para ser presentadas oralmente en las 42 sesiones de trabajo.

Al preparar el programa de actividades, la Secretaría Científica trató de conseguir un justo equilibrio, y así se previó la presentación oral del mayor número posible de memorias en cada sesión, pero dejando todavía tiempo suficiente para examinar la información presentada. Se dejaron dos tardes totalmente libres, a fin de que los grupos oficiosos pudieran examinar las cuestiones que surgieran en las sesiones oficiales de la Conferencia. No se levantó acta de tales reuniones.

Siempre que fue posible, el autor, o los autores, de las memorias fueron consultados en el curso de la Conferencia por miembros de la Secretaría Científica, que actuaron de secretarios de sesión, o por un grupo de editores facilitado a dicho efecto por el OIEA**, a fin de asegurar la máxima exactitud.

Las actas de los debates celebrados en las diversas sesiones, basadas en notas tomadas en las reuniones por redactores de actas del OIEA**, y verificadas siempre que fue necesario mediante las grabaciones efectuadas en todas las sesiones, fueron preparadas por la División de Idiomas del Organismo Internacional de Energía Atómica (OIEA) en inglés, y traducidas después al español, el francés y el ruso por conducto de las autoridades de energía atómica de los tres países interesados (véase el tercer párrafo de la presente nota).

La preparación para la publicación del texto de los documentos en español, francés e inglés se efectuó en la Oficina de Ginebra de las Naciones Unidas, bajo la fiscalización de las Naciones Unidas, por un equipo de editores cuyos servicios fueron también proporcionados por las autoridades de energía atómica de sus respectivos países, con alguna ayuda de consultores del exterior. La preparación para la publicación de los documentos en ruso se efectuó en Moscú en circunstancias análogas. Actuaron de editores las personas siguientes: Sr. A. de Calmès, Dr. C. E. Granados, Sr. D. H. Hill,

** Los nombres de los secretarios científicos, editores y redactores de actas figuran en la lista de la Secretaría de la Conferencia, en el anexo 1, volumen 1, de esta serie.

* Los idiomas de la Conferencia fueron el español, el francés, el inglés y el ruso.

Sr. V. F. Kalinin, Dra. R. Lapage, Sr. E. T. Marles, Dra. J. D. C. Mole, Sr. C. Ségot, Sr. J. J. Stobbs, Sr. C. R. Symons y Sr. J. Williamson.

En la impresión de esta gran recopilación de información científica han participado impresores

de Bélgica, el Canadá, Francia, el Reino Unido, Suiza y la Unión de Repúblicas Socialistas Soviéticas.

Los títulos completos de los dieciséis volúmenes de estas Actas, junto con las sesiones comprendidas en cada volumen, son los siguientes:

<i>Número del volumen</i>		<i>Sesiones</i>
1	Progresos realizados en el dominio atómico	A, B, 1.6, C, H
2	Física de los reactores	3.1
3	Estudios sobre reticulados. Funcionamiento de reactores	3.2, 3.3
4	Control de los reactores	3.4, 3.5
5	Reactores nucleares—I. Reactores refrigerados por gas y por agua	1.1, 1.2, 1.3
6	Reactores nucleares—II. Reactores rápidos y conceptos más avanzados	1.4, 1.5, 1.7
7	Reactores de investigación y de ensayo	D, 1.9, 1.8
8	Tecnología y equipo de los reactores	1.10, 1.11, 3.7
9	Materiales de los reactores	2.8, 2.9, 2.4
10	Combustibles nucleares—I. Fabricación y tratamiento	2.3, 2.6, 2.7
11	Combustibles nucleares—II. Características y estudios económicos	2.5, 2.1, 2.2
12	Combustibles nucleares—III. Primeras materias	2.11, 2.12, 2.10
13	Seguridad nuclear	3.9, 3.8, 3.6
14	Influencia del empleo de la energía nuclear sobre el ambiente. Evacuación de residuos	3.10, 3.11
15	Aspectos especiales de la energía nuclear y empleo de los radioelementos....	E, 4.1, F, G, 4.2
16	Lista de documentos e índices	

TABLE OF CONTENTS

Volume 8

Session I.10 Heat transfer

		Page
	<i>Organic media</i>	
P/15	Campbell <i>et al.</i> Development of organic-liquid coolants	3
P/53	Lévêque Etudes technologiques des fluides caloporteurs organiques <i>Technological study of organic cooling fluids</i>	13
P/93	Villeneuve <i>et al.</i> Transferts de chaleur par liquides organiques <i>Heat transfer with organic fluids</i>	22
P/590	van Meel Burn-out in subcooled forced convection boiling of polyphenyls	30
	<i>Gas cooling</i>	
P/135	Cunningham <i>et al.</i> Heat transfer and pressure drop performance of herringbone and helical fin fuel elements for uranium/Magnox reactors	39
P/136	Hadrill <i>et al.</i> Heat transfer performance of the polyzonal can for the CEGB reactors	49
P/226	Troost <i>et al.</i> Thermal design aspects of gas-cooled power reactor cores	59
P/519	Gilli Heat transfer characteristics of helical tube bundles as used in steam generators of gas-cooled reactors	69
P/552	Negrini <i>et al.</i> A method for the calculation of three-dimensional flux and temperature distributions in a Magnox reactor, and comparison with experimental measurements taken at Latina power station	77
P/719	Нестеренко, Шадский Метод моделирования на аналоговых вычислительных машинах нестационарных тепловых процессов газоохлаждаемых энергетических реакторов	85
	<i>Nesterenko, Shadsky A method of simulating transient thermal processes in gas-cooled reactors using analogue computers</i>	
	<i>Water cooling</i>	
P/16	Lane, Collier Thermal and irradiation performance of experimental fuels operating in steam-water mixtures	93
P/96	Le Franc <i>et al.</i> Améliorations apportées au transfert thermique des combustibles nucléaires par l'application du procédé «Vapotron» <i>Improvement introduced into the thermal transfer of nuclear fuels by the "Vapotron" process</i>	104
P/224	Levy <i>et al.</i> Critical heat flux considerations in the thermal and hydraulic design of water-cooled nuclear reactors	114
P/326	Осмачкин Особенности теплообмена в ядерных реакторах, охлаждаемых несжимаемыми жидкостями	128
	<i>Osmachkin Specific heat exchange features in non-compressible liquid-cooled reactors</i>	
P/569	Jannussis The transient heat transfer from hollow cylindrical fuel elements in boiling superheated conditions	141
P/580	Torikai <i>et al.</i> Boiling heat transfer and burn-out mechanism in boiling-water cooled reactors	146
P/600	Rallis, Jawurek The mechanism of nucleate boiling	156
P/699	Novaković, Stefanović Boiling from a liquid interface	166
P/867	Silvestri <i>et al.</i> Basic heat transfer and hydrodynamics studies in two-phase flow	173
	<i>Liquid metal cooling</i>	
P/225	Dwyer, Lyon Liquid-metal heat transfer	182
P/328	Субботин <i>et al.</i> Теплообмен в элементах реакторов с жидкометаллическим охлаждением	192
	<i>Subbotin et al. Heat transfer from fuel elements of liquid metal-cooled reactors</i>	

TABLE OF CONTENTS

(Continued)

	Page
<i>General</i>	
P/527 Schmid	204
Some theoretical problems of heat conduction in reactor fuel elements	
P/776 Schmid, Stach	212
The optimum reactivity control of a multi-zone nuclear reactor in relation to the maximum output of the power station	
Record of session 1.10	219
Compte rendu de la séance 1.10	224
Протокол заседания 1.10	231
Acta de la sesión 1.10	238
 Session 1.11: Hydraulic problems of reactor engineering	
<i>Water cooling</i>	
P/55 Mondin <i>et al.</i>	247
Quelques aspects fondamentaux de l'ébullition dans les réacteurs nucléaires	
<i>Some fundamental aspects of boiling in nuclear reactors</i>	
P/95 Foure <i>et al.</i>	255
La technique des écoulements diphasés tourbillonnaires dans les réacteurs à eau	
<i>Technique for vortex type two-phase flow in water reactors</i>	
P/230 Lottes <i>et al.</i>	263
Fluid dynamics, stability, and vapor-liquid slip in boiling reactor systems	
P/231 Poppendiek, Gambill	274
Helical, forced-flow heat transfer and fluid dynamics in single and two-phase systems	
P/232 Isbin <i>et al.</i>	286
Critical flow phenomena in two-phase mixtures and their relationships to nuclear safety	
P/327 Алексеев <i>et al.</i>	295
Критические тепловые потоки при вынужденном течении воды	
<i>Burn-out heat fluxes under forced water flow</i>	
P/329 Булеев	305
Теоретическая модель турбулентного обмена в трехмерном потоке жидкости	
<i>Theoretical model of turbulent transfer in three-dimensional fluid flow</i>	
P/589 Bogaardt <i>et al.</i>	316
Heat transfer and hydraulic stability in boiling-water reactors	
P/607 Becker <i>et al.</i>	325
Hydrodynamic instability and dynamic burn-out in natural circulation two-phase flow an experimental and theoretical study	
P/801 Kjelland-Fosterud <i>et al.</i>	338
Two-phase flow investigations for a marine boiling water reactor	
<i>Gas cooling</i>	
P/50 Gelin, Milliat	347
Etudes aérodynamiques et thermiques de gaines d'éléments combustibles refroidis par gaz	
<i>Aerodynamic and thermal studies of cans of gas cooled fuel elements</i>	
P/524 Berger, Derian	355
The influence of an electric field on the heat transfer to CO ₂ coolant at high and low pressure in a nuclear reactor	
<i>General</i>	
P/698 Zarić	364
Heat transfer intensification by use of the longitudinally variable pressure gradient	
Record of session 1.11	371
Compte rendu de la séance 1.11	373
Протокол заседания 1.11	376
Acta de la sesión 1.11	379
 Session 3.7: Reactor plant equipment	
<i>Control</i>	
P/126 Hiorns <i>et al.</i>	385
Recent developments in the instrumentation and control of large gas-cooled reactors	

TABLE OF CONTENTS

(Continued)

		Page
P/229	Hanauer Improvements in instrumentation for high-performance power reactors	395
P/330	Емельянов <i>et al.</i> Система управления реакторами <i>Emelyanov et al.</i> <i>Control systems of nuclear reactors</i>	404
P/518	Plumier <i>et al.</i> Résultats pratiques et perspectives de l'utilisation de poison en solution dans les réacteurs à eau sous pression <i>Practical results and prospects for the use of a soluble poison in the pressurised-water reactors</i>	413
<i>Pressure vessels</i>		
P/52	Lamiral <i>et al.</i> Les caissons en béton précontraint des réacteurs français de la filière uranium naturel – graphite – gaz carbonique <i>The prestressed concrete pressure-vessels of the French natural uranium-graphite-carbon dioxide gas sequence reactors</i>	422
P/140	Houghton Brown <i>et al.</i> The design and construction of prestressed concrete pressure vessels with particular reference to Oldbury nuclear power station	433
P/141	Taylor, Williams The design of prestressed concrete pressure vessels, with particular reference to Wylfa	446
P/144	Townley, Procter Investigations to predict the performance of steel reactor pressure circuit components in service	456
P/227	Gaines, Porse Problems in the design and construction of large reactor vessels	464
P/331	Стекольников <i>et al.</i> Корпуса водо-водяных энергетических реакторов высокого давления <i>Stekolnikov et al.</i> <i>Vessels for power reactors cooled and moderated by water at high pressures</i>	473
P/522	Hauer <i>et al.</i> Pressure vessel for the first Czechoslovak nuclear power station	484
P/810	Hellström Design and manufacture of the reactor pressure vessels for the Ågesta and Marviken Power Stations and some future developments	498
<i>Control rods</i>		
P/809	Ericsson, Ahlnäs Design, development and manufacture of control rod drives for heavy-water power reactors	505
<i>Fuelling machinery</i>		
P/54	Saitcevsy, Gaussot Les appareils de chargement et déchargement du combustible dans les réacteurs uranium naturel – graphite – gaz <i>Fuel loading and unloading devices for the natural uranium-graphite-gas sequence reactors</i>	512
P/139	Joss <i>et al.</i> Experience with Bradwell and Latina on-load fuel handling equipment and its influence on future designs	522
P/808	Granelli <i>et al.</i> Fuel handling equipment for the Ågesta D ₂ O moderated pressure vessel reactor	532
<i>Other components</i>		
P/51	Martin, Roche Etude de structures nouvelles adaptées aux réacteurs graphite – gaz et eau lourde – gaz <i>Study of new structures adapted to gas-graphite and gas-heavy-water reactors</i>	541
P/94	Robert <i>et al.</i> Les circuits de gaz carbonique dans les centrales nucléaires <i>CO₂ circuits in nuclear power stations</i>	548
P/137	Warner, Bayer Graphite core structures for large gas-cooled power reactors	560
P/138	Bateman <i>et al.</i> Gas circulators and their drives for large gas-cooled power reactors	569
P/143	Bradley <i>et al.</i> Some engineering problems of the SGHW 100 MW(e) prototype reactor	579
P/228	Monson <i>et al.</i> Components for sodium reactors	588
P/592	Videm Mild steel in primary circuits of water-cooled power reactors	600
P/696	Kägi, Doroszalai Special problems relating to monotube boilers in nuclear power stations	609

TABLE OF CONTENTS

(Continued)

		Page
P/728	de Jong <i>et al.</i> Experience in the design, calculation and manufacture of power reactor components	618
P/770	Klees, Gérard Apport de la réalisation d'une grande centrale nucléaire dans la conception et la construction des équipements pour réacteurs	627
	<i>The effect of the construction of a large nuclear power plant on the design and manufacture of reactor equipment</i>	
P/834	Kuchta Strength problems of the flanged joint	636
P/857	Yoshioka <i>et al.</i> Some engineering studies conducted in introducing a British type reactor for the Tokai atomic power station	642
	Record of session 3.7	653
	Compte rendu de la séance 3.7	657
	Протокол заседания 3.7	662
	Acta de la sesión 3.7	667

Session 1.10

HEAT TRANSFER

LIST OF PAPERS

		Page
Organic media		
P/15	Development of organic-liquid coolants W. M. Campbell <i>et al.</i>	3
P/53	Etudes technologiques des fluides caloporteurs organiques P. Lévêque <i>Technological study of organic cooling fluids</i>	13
P/93	Transferts de chaleur par liquides organiques J. Villeneuve <i>et al.</i> <i>Heat transfer with organic fluids</i>	22
P/590	Burn-out in subcooled forced convection boiling of poly- phenyls D. A. van Meel	30
Gas cooling		
P/135	Heat transfer and pressure drop performance of herringbone and helical fin fuel elements for uranium/Magnox reactors C. Cunningham <i>et al.</i>	39
P/136	Heat transfer performance of the polyzonal can for the CEGB reactors H. F. J. Hadrill <i>et al.</i>	49
P/226	Thermal design aspects of gas-cooled power reactor cores M. Troost <i>et al.</i>	59
P/519	Heat transfer characteristics of helical tube bundles as used in steam generators of gas-cooled reactors P. V. Gilli	69
P/552	A method for the calculation of three-dimensional flux and temperature distributions in a Magnox reactor, and com- parison with experimental measurements taken at Latina power station R. Negrini <i>et al.</i>	77
P/719	Метод моделирования на аналоговых вычислительных машинах нестационарных тепловых процессов в газоох- лаждаемых энергетических реакторов В. Б. Нестеренко, В. М. Шадский <i>A method of simulating transient thermal processes in gas- cooled reactors using analogue computers</i> V. B. Nesterenko, V. M. Shadsky	85
Water cooling		
P/16	Thermal and irradiation performance of experimental fuels operating in steam-water mixtures A. D. Lane, J. G. Collier	93
P/96	Améliorations apportées au transfert thermique des combus- tibles nucléaires par l'application du procédé « Vapotron » J. D. Le Franc <i>et al.</i> <i>Improvement introduced into the thermal transfer of nuclear fuels by the "Vapotron" process</i>	104
P/224	Critical heat flux considerations in the thermal and hydraulic design of water-cooled nuclear reactors S. Levy <i>et al.</i>	114

LIST OF PAPERS

(Continued)

		Page
P/326	Особенности теплообмена в ядерных реакторах, охлаждаемых несжимаемыми жидкостями <i>Specific heat exchange features in non-compressible liquid-cooled reactors</i>	B. С. Осмачкин <i>V. S. Osmachkin</i> 128
P/569	The transient heat transfer from hollow cylindrical fuel elements in boiling superheated conditions	A. Jannussis 141
P/580	Boiling heat transfer and burn-out mechanism in boiling-water cooled reactors	K. Torikai <i>et al.</i> 146
P/600	The mechanism of nucleate boiling	C. J. Rallis, H. H. Jawurek 156
P/699	Boiling from a liquid interface	M. Novaković, M. Stefanović 166
P/867	Basic heat transfer and hydrodynamics studies in two-phase flow	M. Silvestri <i>et al.</i> 173
	Liquid metal cooling	
P/225	Liquid-metal heat transfer	O. E. Dwyer, R. N. Lyon 182
P/328	Теплосъем в элементах реакторов с жидкометаллическим охлаждением <i>Heat transfer from fuel elements of liquid metal-cooled reactors</i>	B. И. Субботин <i>et al.</i> <i>V. I. Subbotin et al.</i> 192
	General	
P/527	Some theoretical problems of heat conduction in reactor fuel elements	J. Schmid 204
P/776	The optimum reactivity control of a multi-zone nuclear reactor in relation to the maximum output of the power station	J. Schmid, V. Stach 212

Development of organic-liquid coolants

By W. M. Campbell,* A. W. Boyd,* D. H. Charlesworth,* R. F. S. Robertson** and A. Sawatzky**

Hydrocarbon mixtures with high boiling ranges have been studied for a number of years as both coolant and moderator for nuclear reactors. Two reactors of this type, the OMRE and PNPf, have operated successfully in the USA. In order to take full advantage of these liquids, however, they should be used only as the coolant, and the operating temperatures should be considerably higher than in those two reactors, necessitating a thorough understanding of the behaviour of the materials under reactor conditions. This paper deals with the coolant studies carried out in Canada which provide confidence that an organic-liquid-cooled heavy-water-moderated reactor can be economically competitive with any of the other reactors currently being studied in the Canadian program. A companion paper deals with the non-coolant aspects of the reactor development [1].

COOLANT DECOMPOSITION

General

The thermal and radiation stabilities of pure terphenyl isomers and of various terphenyl mixtures were studied. The mixtures were Santowax OM (about 70% ortho- and 30% meta-terphenyl) Santowax WR (Santowax R with the para-terphenyl removed) and partially hydrogenated terphenyls.

Pyrolysis

The pyrolytic studies were carried out by heating the samples sealed under vacuum in ampoules at closely controlled temperatures ($\pm 1^\circ\text{C}$) over the range 400–475 $^\circ\text{C}$ [2]. Table 1 shows some typical data.

Samples of pure o- and m-terphenyl decomposed such that the concentration, c , followed first-order kinetics, $dc/dt = -kc$. A mixture of the pure isomers such as Santowax OM also showed first-order decomposition characteristics, but for reactor-grade Santowax OM the kinetics more closely approximated second-order. The kinetics of the formation of decomposition products having very high boiling points (high boilers, HB) varied, and their initial production rate was significantly lower than the decomposition rate of the terphenyls.

Gas-production rates were generally independent of monomer concentration in the liquid. As pyrolysis continued at temperatures above 450 $^\circ\text{C}$, the proportion of H_2 in the gas fell while that of CH_4 and C_2 hydrocarbons increased. Biphenyl was initially produced at significant rates above 450 $^\circ\text{C}$. At lower temperatures the molecular weight of the HB fraction was about 460. After long exposures at temperatures

Table 1. Initial pyrolytic decomposition rates

Hydrocarbon ^a	Initial conversion, %/h			ΔE^* kcal/g mole
	at 400 $^\circ\text{C}$	at 450 $^\circ\text{C}$	at 475 $^\circ\text{C}$	
Santowax OM	0.04	0.8	3.0	66
o-terphenyl	—	1.0	—	—
m-terphenyl	—	0.4	—	—
Santowax HOM	0.2	7.0	30	61

^a See Table 3 for compositions.

$\geq 450^\circ\text{C}$ the molecular weight of the HB fraction climbed to over 700.

Santowax HOM (see Table 2) is less stable than Santowax OM, but it should be noted that the temperature for a given decomposition rate is only 30 $^\circ\text{C}$ lower for HOM than for OM.

The effect of some impurities was also examined—200 ppm chlorine added as chlorinated biphenyl had little effect on decomposition rates while the addition of 10% HB-40 (see Table 2) increased rates by a factor of two.

One experiment was performed to study the effect of prior irradiation on the pyrolysis of o-terphenyl. The total decomposition in a sample which had been irradiated and then heated was found equal to the total expected from pyrolysis and radiolysis alone. There was, however, conversion of lower-molecular-weight radiolysis products to high boilers during the subsequent heating.

Electron irradiations [3]

Samples were irradiated in stainless-steel capsules in the Van de Graaff accelerator at temperatures between 350 and 450 $^\circ\text{C}$. The dose rate was 70 W/g and the temperature was controlled to within $\pm 5^\circ\text{C}$. The energy input was calibrated by measuring the hydrogen yield from benzene.

The decomposition rates for ortho- and meta-terphenyl and Santowax OM at different total doses

* Chalk River Nuclear Laboratories, Atomic Energy of Canada Limited, Chalk River, Ontario.

** Whiteshell Nuclear Research Establishment, Atomic Energy of Canada Limited, Pinawa, Manitoba.

Table 2. Stability of low-melting-point coolants to reactor irradiation [8]

Irradiation: 50% fast neutrons, 50% γ -rays

Coolant	Temperature				
	300 °C	325 °C	350 °C	375 °C	400 °C
Initial rate of coolant decomposition relative to Santowax OM = 1					
DOM	0.87	0.95	0.78	1.01	0.90
HOM	1.27	1.26	1.46	1.44	1.77
HB-40	1.7			2.4	2.4
Initial rate of HB formation relative to OM = 1					
DOM	0.98	1.01	0.90	0.87	0.89
HOM	0.87	1.05	0.71	0.77	0.94
HB-40	1.55	1.40		0.96	1.35
Rate of gas production relative to OM = 1					
DOM	1.17	1.14	1.29	1.32	1.03
HOM	3.8	3.4	2.7	4.0	6.7
HB-40	11	10		14.0	29
Composition of starting materials					
Santowax OM: 3.4% biphenyl, 66.2% ortho, 30.1% meta and 2.1% para terphenyl					
DOM: 29.2% biphenyl, 51.9% ortho, 18.5% meta and 0.4% para terphenyl					
HOM: 0.3% biphenyl, 56.4% ortho, 2.2% meta, 0.1% para terphenyl and 41% hydroterphenyls					
HB-40: 18.1% ortho terphenyl, 82% hydroterphenyls (hydrogenated Santowax R)					

showed a second-order dependence. On the other hand, the gas yields were largely independent of the amount of decomposition. Ortho-terphenyl is less stable than meta-terphenyl but the high-boiler yields are nearly the same for the two compounds. The difference in stability is due to formation of intermediate compounds. Appreciable amounts of benzene, biphenyl and triphenylene have been found.

Reactor irradiations [4]

The irradiations were carried out in capsules inside an annular fuel element in NRX at temperatures

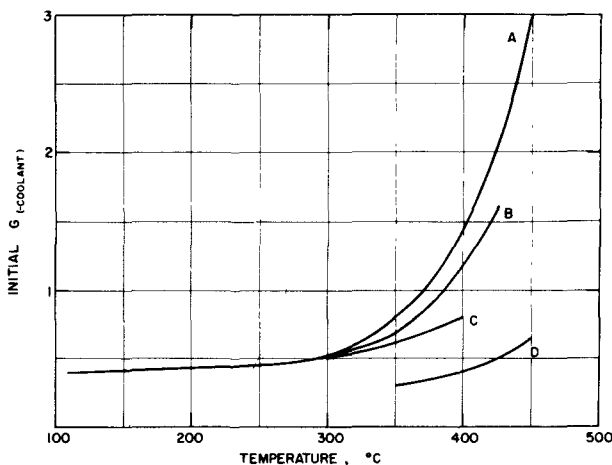


Figure 1. Irradiation of terphenyls

Curve A: o-terphenyl, reactor irradiation 0.1 and 0.3 W/g; Curve B: m-terphenyl, reactor irradiation 0.1 W/g; Curve C: Santowax OM, reactor irradiation 0.1 W/g; Curve D: Santowax OM, electron irradiation 70 W/g

controlled to within $\pm 1^\circ\text{C}$. The dose rates which varied from 0.1 to 0.3 W/g were measured using calorimeters, graphite- CO_2 ion chambers and the hydrogen yield from cyclohexane [5]. In this facility the energy deposition due to gamma rays was very nearly equal to that from fast neutrons.

The results of irradiations at different temperatures and different dose rates are compared with the electron irradiations in Fig. 1. The initial G values on this graph were calculated from integral values assuming second-order dependence on the concentration and have been corrected for pyrolytic decomposition.

The increase in G values with temperature for o- and m-terphenyls was much greater than for Santowax OM. The Santowax OM values are lower for both reactor and electron irradiations. The reason for this is not yet known. At 375 °C, from the known ratios of energy deposition by fast neutrons and γ -rays, a ratio of G_n/G_γ of 3/1 for o-terphenyl can be calculated.

The dependence of the yield of other products upon temperature in the reactor irradiation of ortho-terphenyl is shown in Table 3. The relatively high initial yields of benzene and biphenyl at temperatures

Table 3. Radiolysis of o-terphenyl: initial G values

Radiation: 50% fast neutrons, 50% γ -rays
Dose Rate: 0.1 W/g

Temperature, °C	200	300	350	400	450
HB production ^a	0.40	0.40	0.44	0.69	2.20
Total gas, mole/100 eV	0.06	0.08	0.10	0.14	0.23
Benzene, mole/100 eV	0.03	0.04	0.05	0.17	0.33
Biphenyl, mole/100 eV	0.01	0.04	0.06	0.11	>0.4

^a Molecules of monomer converted to HB per 100 eV.

above 400 °C (accounting for 20% of the total decomposition) are similar to those found in the high-temperature pyrolysis of terphenyl. All these results indicate that in the range 350–400 °C there is a change in the radiolytic reactions with a marked increase in the decomposition rate and in the formation of lower-molecular-weight products.

These effects are most pronounced in o-terphenyl or ortho-rich mixtures. Irradiations of low o-terphenyl mixtures at 400 °C in a loop at the Massachusetts Institute of Technology [6, 7] have not shown any large concentrations of intermediate products.

The stability of low-melting-point coolants relative to that of Santowax OM when subjected to reactor radiation is shown in Table 2. Although the rate of gas evolution is much higher in the hydrogenated compounds their over-all stability at temperatures below 400 °C is comparable to that of terphenyl mixtures and because of their low melting points they may be preferable reactor coolants.

FOULING

The formation of deposits on fuel-element surfaces was one of the major objections cited against organic

coolants in the early days. As shown below two years of satisfactory in-reactor operation have demonstrated that it can be controlled without difficulty. First, it was necessary to set a fouling target. The thermal conductivity of a fouling film was measured and found to be about $0.004 \text{ Wcm}^{-1} \text{ } ^\circ\text{C}^{-1}$. With a heat flux of 100 W/cm^2 a $10 \mu\text{m}$ film will raise the sheath temperature $25 \text{ } ^\circ\text{C}$. Arbitrarily an increase in sheath temperature of $25 \text{ } ^\circ\text{C}$ per year was assumed acceptable which set the maximum fouling rate at $0.2 \mu\text{g/cm}^2 \text{ h}$.

Two types of fouling have been recognized [9] and since their behaviour is quite different they will be discussed separately below. Both types are caused by impurities in the coolant.

Mass-transfer fouling

The film produced here is mainly iron and iron oxide and may contain up to 99% iron. The organic content is very low. Figure 2 shows a cross section of a typical mass-transfer film. To form this film iron from the piping walls at about $350 \text{ } ^\circ\text{C}$ reacts with some trace impurity in the coolant and goes into solution. The iron complex is then carried through the circuit until it contacts the hot fuel element surface at $425\text{--}500 \text{ } ^\circ\text{C}$. At these temperatures the complex breaks down depositing the iron and releasing the complexing agent which is carried around again to pick up another load of iron. The driving force for the transfer is the temperature difference between the hot fuel sheath and the cooler piping.

A number of factors affect the rate of deposition. The rate increases with coolant velocity ($R \propto V^{0.5 \text{ to } 1.0}$) and it doubles when the hot surface temperature is increased by $25\text{--}70 \text{ } ^\circ\text{C}$. Radiation does not appear to be an important factor.

Chlorine is by far the most important of the impurities affecting mass-transfer fouling [10]. Deposition rates as high as $200 \mu\text{g/cm}^2 \text{ h}$ have been found when the total chlorine was 190 ppm. Some chlorine compounds were about 20 times as effective as others.

The active chlorine compound adsorbs on or reacts with the iron pipe wall. Thus the system can be drained and flushed, but surface contamination may still be present and produce a high fouling rate. This means that a low chlorine content in the coolant does not always guarantee a low fouling rate and a better criterion is the total chlorine in the system, i.e., in the coolant plus that on the walls. Operating experience has shown that an acceptably low fouling rate is obtained if the total chlorine is the equivalent of 3 ppm in the coolant.

Mass-transfer fouling can be eliminated by removing all iron-containing materials from the circuit.

Oxygen in the coolant was suspected as a fouling promoter. Tests were carried out with 500–3 000 ppm oxygen in the coolant but fouling was not increased in spite of a 12-fold increase in the total iron content of the liquid. Tests showed, that in the 100 ppm range the effect of water was similar to that of oxygen.

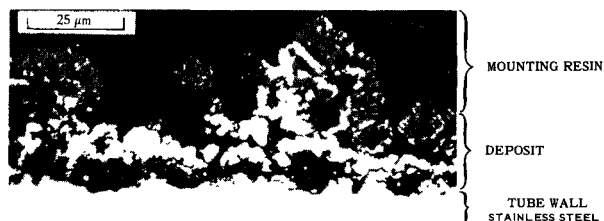


Figure 2. Cross section of typical film deposited by mass-transfer mechanism
Gray portion of deposit is Fe_3O_4 , light portion is mainly αFe .
Composition 85% Fe, 1% C, 0.3% H.
Surface temperature $496 \text{ } ^\circ\text{C}$

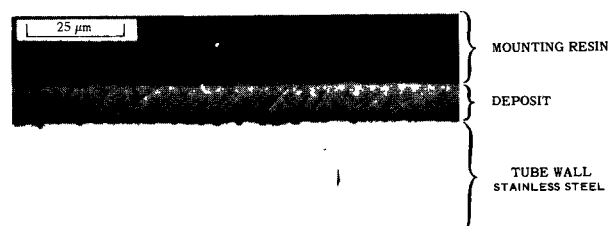


Figure 3. Cross section of typical film deposited by particulate mechanism
Composition 91% organic, 9% Fe_3O_4 .
Surface temperature $485 \text{ } ^\circ\text{C}$



Figure 4. Cross section of film on a fuel sheath typical of recent in-reactor experience
Surface temperature $480 \text{ } ^\circ\text{C}$

The iron complexing agent has not been identified yet. Tracer studies with ^{59}Fe showed that most of the iron in the coolant will pass through a $0.05 \mu\text{m}$ filter. This and other observations indicate the iron is present in solution rather than as a colloid. The active compound is soluble in benzene but not in hexane. Free radicals are known to be present in irradiated coolant but are not thought to be fouling promoters as such, although some trace free radical might be responsible.

Particulate fouling

Films produced by this mechanism are almost entirely organic in nature. Figure 3 shows a cross

section of a typical film. This mechanism, as originally proposed by Gercke [11], depends on micron- or submicron-size particles of organic material, or inorganic particles coated with organic, impinging on the hot surface and sticking to it. Film formation appears to be unaffected by irradiation, it decreases as fluid velocity increases and it doubles with an increase in surface temperature of about 30 °C. Impurities such as chlorine, oxygen, etc., do not have any appreciable effect on particulate fouling.

Practical in-reactor experience

In the Canadian program all the in-reactor experience has been with a 2:1 mixture of ortho- and meta-terphenyls with 30% OMRE high boiler in the X-7 loop in NRX over a period of three years. Early fouling rates were high [9], in the range of 10–40 $\mu\text{g}/\text{cm}^2\text{ h}$, even though the iron content of the coolant was about 2 ppm. Both mass-transfer and particulate mechanisms were present. As coolant quality improved with purification, the rates were reduced and have been very low for the past two years. During a recent irradiation of 82 days in a thermal flux of $5 \times 10^{13} \text{ n}/\text{cm}^2 \text{ s}$ with sheath temperatures of 450–500 °C the deposition rate was less than 0.1 $\mu\text{g}/\text{cm}^2 \text{ h}$. The film is practically nonexistent as evident in Fig. 4. These results show that with adequate purification high sheath temperatures can be used without trouble from fouling.

PURIFICATION

The impurities which must be removed can come from three main sources: from the terphenyl make-up, from the environment when the system is open, and from reactions within the coolant system. Make-up coolant contains from 2–10 ppm Cl, 30–100 ppm H_2O , 1–10 ppm of inorganic material and dissolved oxygen. Air, water and chlorine-containing materials can enter an open system, especially if careful operating procedures are not observed. Decomposition products ranging in molecular weight from hydrogen to high-molecular-weight polymers are formed by radiolysis and pyrolysis. Corrosion products and oxygen-containing compounds are formed by reaction of the system materials and the coolant with air and water.

From experience with several loops it is clear that prevention of coolant and system contamination is by far the most important factor in coolant purity. Once the system has been allowed to become contaminated with air, water, chlorine compounds, etc., it is difficult to restore adequate coolant purity; but it is not difficult to prevent contamination.

Clay adsorption

Contacting coolant with Attapulugus clay followed by filtration is a proved method of reducing the fouling tendency [12]. The clay retains some of the organic component necessary for mass-transfer fouling and much of the insoluble material. It also appears to

modify the remaining insoluble material, perhaps by agglomeration, so that it is more readily removed by filtration.

The clay is dried at 370–400 °C, and used in a down-flow column with a coolant mass velocity of 1.5 $\text{kg}/\text{cm}^2 \text{ h}$ and a temperature greater than 300 °C. The effluent from the columns is filtered through disposable glass-spool cartridges with a nominal rating of one micron. To assess column life the circulating coolant is routinely monitored for its fouling ability (SPFT) [13], iron content and electrical conductivity. During a recent four-month run with one clay column in the X-7 loop, the SPFT rose from 0.1 to 0.3 $\mu\text{g}/\text{cm}^2 \text{ h}$, the iron content from 0.5 to 2.0 ppm, and the electrical conductivity from 5×10^{-4} to $10.5 \times 10^{-4} \text{ M}\Omega^{-1} \text{ cm}^{-1}$. By the end of the period the weight of coolant processed per unit weight of clay was 35 000.

Chlorine removal

Exclusion is the best means of maintaining a low chlorine level. Chlorine can be removed by contacting the coolant at about 325 °C with 0.5% palladium supported on alumina pellets or with magnesium ribbon [14]. The former is preferred since it is effective at lower temperatures and removes a larger variety of chemical forms of chlorine, particularly the form responsible for the fouling complex. When used upstream of the clay column with a mass velocity of 5–10 $\text{kg}/\text{cm}^2 \text{ h}$ through the bed chlorine concentrations near 3 ppm can be maintained. The removal capacity has been 1.2 g Cl/g Pd from high-chlorine coolant and 0.1 g Cl/g Pd from coolant containing 3–10 ppm. The maximum capacity corresponds to a Cl/Pd atomic ratio of 3.6. In systems where steel is exposed to the coolant, iron is usually removed with the chlorine in a Cl/Fe atomic ratio of about two.

There is some evidence that the important chlorine species may be quite volatile and may be removed by a degasser.

Degassing

Degassing during normal operation removes hydrogen formed by radiolysis and corrosion and helps minimize the hydriding of zirconium alloys. Nitrogen and light hydrocarbons are also removed to control the vapour pressure of the coolant. Water may be removed to maintain a concentration in the range 50–100 ppm. If any oxygen gets into the system during maintenance, it should be stripped out below 150 °C.

Initial clean-up of systems

The time required to establish acceptable coolant quality is of special concern during the construction and commissioning of a new loop or reactor system. Recent experience with U-3, a large loop in NRU, has demonstrated that chemical cleaning of the piping and components is not required when mechanical cleaning and careful field inspection is used. The highest iron content observed in the coolant during the initial period was 7.5 ppm. The purification

Table 4. Effect of water on hydriding in autoclaves
400 °C; dissolved H₂ ~ 100 ml/kg

Water content of organic ppm	Hydriding rate, $\mu\text{g}/\text{cm}^2 \text{ h}$					
	Zircaloy-2		Ni-free Zircaloy-2		Zr-2.5% Nb	
	As pickled	Pre-oxidized	As pickled	Pre-oxidized	As pickled	Pre-oxidized
<40	>>0.5	0.032 ±0.007	>>0.5	0.010 ±0.005	>>1.0	0.012 ±0.012
40-60	0.4 ±0.1	0.011 ±0.002	0.280 ±0.020	0.001 ±0.001		0.001 ±0.001
60-1 000	0.045 ±0.02	0.010 ±0.01	0.025 ±0.015	0.002 ±0.002	0.025 ±0.005	0.001 ±0.001

system quickly reduced the level to 1 ppm and achieved good coolant quality in about three weeks.

HYDRIDING OF ZIRCONIUM ALLOYS

When organic liquids were first considered as coolants for reactors the materials which could be used in the core were reviewed. Preliminary studies [15, 16, 17] showed that aluminium materials such as SAP (or APM) were acceptable but zirconium alloys appeared unacceptable due to hydriding. This led to extensive work on SAP but almost nothing on zirconium. Work in Canada over the past two to three years, however, has shown that zirconium alloys can be used provided the coolant impurities are carefully controlled. Work has been done at the Canadian Westinghouse Company Limited in autoclaves at 365-425 °C for periods of 150-300 hours. Long-term tests at 350-400 °C have been performed by CRNL in the X-7 loop in the NRX reactor [18]. Two surface conditions, pickled, and preoxidized (oxidized in air at 400 °C for 48 hours) have generally been used. Alloys investigated have been Zircaloy-2, Zircaloy-4, nickel-free Zircaloy-2 and Zr-2, 5% Nb. (Zr-Nb specimens were heated one hour *in vacuo* at 880 °C, water quenched and tempered *in vacuo* for 24 hours at 500 °C). The hydrogen pick-up varied with the alloy and in general Zircaloy-4 picked up 60% and Zr-2, 5% Nb 20% as much as Zircaloy-2.

The effects of certain variables are reviewed below:

Water

As in steam hydrogen systems [19] water above a certain concentration in the organic liquid reduces

hydriding markedly. The results in Table 4 illustrate that the limiting concentration is about 60 ppm. Water contents as high as 1 000 ppm do not appear to affect the rate. The effect of water is more marked for pickled than for preoxidized surfaces and is more significant with Zr-2, 5% Nb than with the other alloys.

Hydrogen

The effect of hydrogen in autoclave tests with a low water concentration is shown in Table 5. Pickled specimens hydride very readily and the rate increases with increasing H₂ concentration. Preoxidation reduces the rate considerably. With higher water concentrations the effect of hydrogen is negligible.

Chlorine

Chlorine in the coolant was probably the cause of the high pick-up rates found in the early screening experiments [15, 16, 17], and is now thought to be the most important promoter of zirconium hydriding. Table 6 shows the effect. The active chlorine form is unknown.

There are insufficient data yet to show whether chlorine-contaminated Zircaloy surfaces are permanently damaged or whether the hydriding resistance can be restored by contacting the alloy with chlorine-free coolant. One clear fact has emerged, however, and it is that surface contamination of zirconium alloys even from fingerprints must be avoided at all times.

Surface preparation

Tables 4 and 5 show that an oxide film on the alloy reduces hydriding markedly. Table 4 shows that

Table 5. Effect of H₂ concentration on hydriding
425 °C; H₂O < 40 ppm

H ₂ concentration ml/kg	Hydriding rate, $\mu\text{g}/\text{cm}^2 \text{ h}$			
	Zircaloy-2		Ni-free Zircaloy-2	
	As pickled	Preoxidized	As pickled	Preoxidized
~1	0.025	0.005		
8	0.14	0.006	0.050	0.002
~100	7.0	0.030	5.0	0.012
	±4.0	±0.005	±3.0	±0.001

Table 6. Effect of chlorine on hydriding of Zircaloy-2

	No chlorine added	50 ppm C_2HCl_3 Added initially
Temperature, °C	375	370
Chloride in coolant at 370 °C, ppm		
At start	0.8	8.2
At end (after 67 hours)	0.5	1.6
Hydrogen absorbed, $\mu\text{g}/\text{cm}^2 \text{ h}$		
Pickled surface	0.39	9.4
Oxidized surface	0.01	2.1

Table 7. Effect of preoxidation on hydriding of Zr alloys

(X-7 Loop, out-reactor section)

Temperature	300-400°C
Duration	5 000 h
H ₂ content	10-140 ml/kg-usually 40-80 ml/kg
Water content	10-120 ppm

Specimen condition	Hydriding rate, $\mu\text{g}/\text{cm}^2 \text{ h}$		
	Zircaloy-2	Zircaloy-4	Zr-2.5% Nb
Pickled	0.029		
Oxidized in air at 300 °C for 240 h	0.016		
Oxidized in air at 400 °C for 48 h	0.009	0.005 ± 0.001	0.0015 ± 0.001
Oxidized in air at 500 °C for 2 h	0.008		
Autoclaved in water at 300 °C for 216 h	0.011		
Autoclaved in steam at 400 °C for 48 h	0.009		
Autoclaved in steam at 500 °C for 2 h	0.008		

specimens rapidly become oxidized when >60 ppm H₂O is present. Table 7 shows the effect of various preoxidation treatments. A standard preoxidation procedure of 400 °C in air for 48 hours has been arbitrarily selected, but autoclaving in steam at 400 °C for 48 hours or oxidizing at 500 °C for a shorter period appear equally acceptable. Early experiments at 600 °C show that this temperature is too high to produce a satisfactory oxide [18].

Temperature

The data are scattered but with preoxidized specimens there is only a small increase in hydrogen pick-up between 365 and 425 °C.

In-reactor experience; pressure tubes

A Zircaloy-4 pressure tube (10 m long, 3.9 cm inside diameter, 0.11 cm wall thickness) was used in the X-7 loop in NRX from 22 October 1962 to 16 September 1963. The normal fuel-irradiation program was carried out in it during this whole period. For 5 300 hours of this period the outlet coolant temperature varied between 350 and 400 °C while the inlet temperature remained about 320 °C. For the rest of the time the temperatures were considerably lower and hydriding was probably negligible.

A visual examination of the tube at the end of the test showed no appreciable signs of scratches, wear marks, etc. Samples were taken at many points along the tube and analyzed for hydrogen content. The results are shown in Fig. 5. The difference in hydriding at the two ends of the tube may be due to the temperature difference, but the peak in the center

is the first evidence of an irradiation effect. There are two suggested mechanisms for this : (a) neutron damage of the oxide film makes it more "porous" to hydrogen, (b) short-lived hydrogen radicals which are formed by irradiation may be absorbed more readily than normal hydrogen.

A comparison of the data of Fig. 5 with the autoclave data in Table 4 indicates that the hydriding rates in the X-7 loop were lower than the autoclave rates when the water was less than 40 ppm, but are higher than those where the water was above 40 ppm. This may be due to lack of water control in the X-7 loop coolant which varied from 10-120 ppm but was generally about 50 ppm. There may also be a downstream flux effect which accelerated the pick-up in the outlet end of the tube since the difference in hydrogen contents between the inlet and outlet ends is somewhat more than would be expected due to the temperature difference alone.

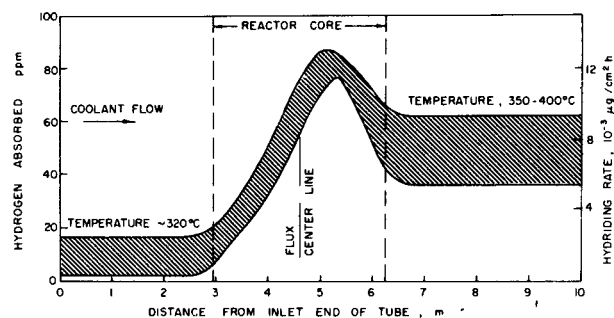


Figure 5. Variation in hydrogen absorbed by a Zircaloy-4 pressure tube irradiated 220 days in X-7 loop.

Table 8. Hydrogen contents of irradiated fuel-element sheaths

Position	H ₂ in Zircaloy-2 sheath ppm	H ₂ in Zr-2.5% Nb sheath ppm
Upstream end	276; 543; average 410	124; 115; average 120
Center	216; 436; average 323	151; 174; average 163
Downstream end	328; 268; average 298	166; 166; average 166
Wire wrap	7 640; 9 136	1 550; 289

In-reactor experience; sheathing

Three UO₂ elements clad in Zircaloy-2 and three in Zr-2, 5% Nb were irradiated in the X-7 loop for 82 full-power days with average sheath temperatures of 480 °C. Each element had a Zircaloy-2 wire wrap spot-welded to it by the method used for CANDU production fuel. All the elements were preoxidized in steam at 55 atm and 400 °C for 30 hours. The main coolant impurities were 20–100 ppm H₂O, 20–70 ml H₂/kg and 0.2–2.7 ppm chlorine.

After the irradiation the elements were examined and while all the sheaths were ductile, the wire wraps, particularly on the Zircaloy-2 elements, were quite brittle. Samples were taken from three positions on the sheath and wire wraps of two elements and analyzed for hydrogen. The results are shown in Table 8. The high hydrogen content in the wire wraps is probably due to thermal migration of the hydrogen from the hot sheaths to the cooler wires. Some of the variation in the sheath samples is undoubtedly due to the same reason.

These hydriding rates are higher than desired. That for the Zr-2.5% Nb sheath was $\sim 18 \times 10^{-3} \mu\text{g}/\text{cm}^2 \text{ h}$. It is possible that these can be reduced considerably by maintaining a higher water content in the coolant.

CONCLUSION

The work to date in Canada has shown very clearly that the control of coolant purity is absolutely essential for an organic-cooled reactor. It has been shown further that coolant purity must never be allowed to get out of control since otherwise the subsequent clean-up will be long and difficult. Several years of operating in-reactor and out-reactor loops has proved that the control of coolant purity is no more difficult than in a water cooled reactor. Provided the proper conditions are observed fouling will not be a problem, at least up to surface temperatures of 500 °C, and zirconium alloys such as Zr-2.5% Nb show real promise for fuel sheathing and pressure tubes.

ACKNOWLEDGMENT

The authors wish to thank all those who have contributed to the work reported here and in particular

to W. D. Mackintosh, M. Tomlinson, J. H. Duerksen and S. R. Hatcher, of Atomic Energy of Canada Limited, and N. A. Graham, of the Canadian Westinghouse Company Limited.

REFERENCES

1. Boxall, D. G., et al., *Development of fuel and coolant tubes for a reactor cooled by organic liquid*, P/23, Vol. 9, these proceedings.
2. Mackintosh, W. D., *Pyrolysis of potential organic coolants for power reactors*, Santowax OM, publication in preparation, Atomic Energy of Canada Limited, Chalk River (1964).
3. Mackintosh, W. D., in publication, U.S. Atomic Energy Commission report TID-7641, Oak Ridge, 202 (1962).
4. Boyd, A. W., and Connor, H. W., *Reactor irradiations of the terphenyls*, publication in preparation, Atomic Energy of Canada Limited, Chalk River (1964).
5. Boyd, A. W. et al., *Trans. Amer. Nucl. Soc.* 6, (1963) 404.
6. Sawyer, C. D., and Mason, E. A., Massachusetts Institute of Technology publication MITNE-39 (IDO-11107), Cambridge (1963).
7. Mason, E. A. et al., Massachusetts Institute of Technology publication SRO-86 (MITNE-45), Cambridge (1964).
8. Tomlinson, M. et al., Atomic Energy of Canada Limited, publication AECL-1915, Chalk River (1964).
9. Charlesworth, D. H., Atomic Energy of Canada Limited, publication AECL-1761, Chalk River (1963).
10. Bancroft, A. R. et al., Atomic Energy of Canada Limited, publication AECL-1913, Chalk River (1964).
11. Gercke, R. H. J., Atomics International, publication NAA-SR-Memo 7328, Rev. 1, Canoga Park (1962).
12. Duerksen, J. H., and Charlesworth, D. H., Atomic Energy of Canada Limited, publication AECL-1683, Chalk River (1963).
13. Bancroft, A. R., Atomic Energy of Canada Limited, publication AECL-1706, Chalk River (1963).
14. Duerksen, J. H., Atomic Energy of Canada Limited, publication AECL-1912, Chalk River (1964).
15. Barker, K. R., and Mausteller, J. W., Mine Safety Appliances Company, Tech. Report No. 54, Callery (1957).
16. Davies, H. E., United Kingdom Atomic Energy Authority, publication AERE M/M153, Harwell (1957).
17. Troutner, V. H., *Corrosion* 16 281t (1960).
18. Sawatzky, A., *The behaviour of zirconium alloys in Santowax OM at high temperatures*, publication in preparation, Atomic Energy of Canada Limited, Pinawa (1964).
19. Shannon, D. W., Hanford Atomic Products Operation, publication HW-67811, Richland (1960).

ABSTRACT—RÉSUMÉ—АННОТАЦИЯ—RESUMEN

A/15 Canada

Mise au point des caloporteurs liquides organiques

par W. M. Campbell *et al.*

Des travaux de recherche et de mise au point effectués, en particulier, dans les boucles d'essai du NRX et du NRU ont permis de constater que les liquides organiques sont prometteurs comme caloporteurs, qu'ils peuvent conserver leur pureté sous l'action des radiations et de la chaleur et qu'ils sont compatibles avec les matériaux dont on peut disposer pour construire les réacteurs.

On a mesuré la vitesse de la décomposition thermique et celle de la décomposition radiolytique des isomères terphényles et des mélanges à des températures allant de 150 à 475 °C. Pour le même apport d'énergie, les neutrons rapides causent environ trois fois plus de dommages que les électrons. On a mesuré également la vitesse de décomposition d'autres liquides ayant des points de fusion convenables pour le démarrage initial du réacteur. L'un d'eux, un mélange terphényle partiellement hydrogéné, avait une vitesse de décomposition semblable à celle des terphényles. La vitesse de formation des gaz était, elle, trois fois plus élevée.

Il est essentiel que le liquide organique soit purifié de façon continue. Le terphényle d'appoint contient de 2 à 10 ppm de chlore, et dans l'ensemble du système la teneur en chlore doit rester inférieure à 5 ppm. Le chlore peut être enlevé sur des lits de copeaux de magnésium ou de palladium placé sur des granules d'alumine chauffés à plus de 325 °C; dans l'utilisation routinière des boucles la teneur en chlore peut être maintenue à moins de 3 ppm. D'autres impuretés sont enlevées par adsorption sur des lits d'argile Attapulgu à 325 °C. Il faut éliminer le plus possible les macro-particules, par exemple par filtration sur laine de verre. Une partie de l'eau et une partie de l'hydrogène sont extraites sous forme de gaz; tandis que l'hydrogène qui reste doit avoir une faible concentration, il importe de maintenir la teneur en eau aux environs de 100 ppm.

On distingue deux types d'encrassement à la surface des éléments de combustible. Le premier type est un dépôt qui contient plus de 70% de fer mais pratiquement pas de matières organiques. Ce dépôt est formé par du fer qui part de la canalisation du circuit, où la température est d'environ 300 °C, et qui atteint la surface des éléments chauffés à 400–500 °C. Le chlore (qu'on trouve surtout sur les parois du système) joue un rôle important dans ce transfert. Si dans le système la teneur totale en chlore correspond à moins de 3 ppm telle que mesurée dans le caloporteur, l'effet d'un tel transfert de masse n'est pas exagéré. Le deuxième type d'encrassement est un dépôt ayant une forte teneur en matières organiques

provenant du caloporteur. Les encrassements organiques sont plus notoires lorsque les surfaces des éléments sont très chaudes; cependant, ces encrassements ne semblent pas beaucoup affectés par les radiations. Une étude effectuée récemment dans la boucle X-7 du NRX a permis d'établir qu'après 82 jours d'irradiation dans un flux de neutrons thermiques d'environ $5 \times 10^{13} \text{ cm}^{-2} \text{ s}^{-1}$, l'épaisseur du film d'encrassement était inférieure à 1 μm sur les gaines chauffées à 450–500 °C.

Les alliages à base de zirconium sont compatibles avec les caloporteurs organiques, à condition que ceux-ci aient les caractéristiques voulues. Le chlore accélère la formation des hydrures mais, lorsque sa teneur est maintenue inférieure à 3 ppm, l'effet est réduit considérablement. La teneur en eau est également très importante: on estime que la teneur optimale est d'environ 100 ppm. Si la teneur en eau était trop faible, on ne pourrait pas avoir en permanence un film d'oxyde imperméable à l'hydrogène. Un tube de force en Zircaloy-4 a été mis à l'essai pendant 10 mois dans la boucle X-7 (essai le plus long de la série). La température de sortie du caloporteur était de 350 à 390 °C et la teneur en eau était faible: 10 à 50 ppm. Au bout de 10 mois d'irradiation, ce tube de Zircaloy-4 avait capté environ 80 ppm d'hydrogène. On a constaté une plus grande capture d'hydrogène dans les régions où le rayonnement avait été plus intense.

A/15 Канада

Разработка органических жидких теплоносителей

В. М. Кэмпбелл *et al.*

Научно-исследовательские и опытно-конструкторские работы главным образом в области испытаний топливных контуров реакторов NRX и NRU показывают, что органические жидкости являются перспективными теплоносителями для реакторов, что их чистота может сохраняться при наличии излучения и тепловых потоков и что имеются конструкционные материалы, которые совместимы с этими жидкостями.

Скорости теплового и радиолитического разложения отдельных видов терфенила и смесей измерялись при температурах от 150 до 475 °C. При равной поглощенной энергии быстрые нейтроны вызывают примерно в три раза большее повреждение, чем электроны. Скорость разложения измерялась также для других жидкостей, которые обладают температурой плавления, подходящей для первоначального запуска реактора. Одна частично гидрированная смесь

терфенилов имеет примерно такую же скорость разложения, как и негидрированный терфенил, однако ее газовыделение примерно в три раза выше.

Непрерывная очистка теплоносителя является важным фактором. Содержание хлора в используемом терфениле колеблется в интервале $2 \div 10 \cdot 10^{-4}\%$, а его количество во всей системе должно превышать $5 \cdot 10^{-4}\%$. Хлор можно удалять путем пропускания через слой магнито-стружки или гранул окиси алюминия, покрытых палладием и нагретых выше 325°C , причем в условиях обычной эксплуатации контуров его уровень можно поддерживать ниже $3 \cdot 10^{-4}\%$. Другие виды загрязнения удаляются адсорбцией на слоях глины аттапульгус при 325°C . Количество взвешенных частиц должно быть сведено к минимуму фильтрацией, например, через фильтры, изготовленные из стекловолокна. Вода и водород могут быть удалены путем продувки инертного газа, и хотя содержание водорода должно поддерживаться на низком уровне, существуют причины для поддержания концентрации воды примерно на уровне 0,01%.

Установлены два типа загрязнения поверхностей тепловыделяющих элементов. Первый тип загрязнения дает осадок, содержащий свыше 70% железа при отсутствии по существу органического вещества. Он образуется в результате переноса железа из трубопроводов контура при температуре около 300°C на горячие поверхности тепловыделяющих элементов, имеющих температуру $400\text{--}500^\circ\text{C}$. Важную роль в этом переносе играет хлор, большая часть которого оседает на стенках системы. Если общее содержание хлора в системе меньше $3 \cdot 10^{-4}\%$ в теплоносителе, то эффект массопередачи приемлемо мал. Второй тип загрязнения вызывается органическими частицами в теплоносителе и приводит к образованию осадка с высоким содержанием органического вещества. Высокие температуры поверхности увеличивают количество загрязнений этого вида, однако облучение, по-видимому, не оказывает существенного влияния. Недавние опыты в контуре X-7 реактора NRX показали, что после облучения в течение 82 дней потоком тепловых нейтронов интенсивностью примерно $5 \cdot 10^{13}$ нейтр/см²·сек пленка загрязнения на оболочках топлива при температуре $450\text{--}500^\circ\text{C}$ была менее 1 мк толщиной.

Циркониевые сплавы при соответствующих условиях оказались совместимыми с органическими теплоносителями. Хлор способствует быстрому гидрированию, но, когда содержание хлора поддерживается ниже $3 \cdot 10^{-4}\%$, этот эффект заметно снижается. Очень важным является также концентрация воды, так как, если она слишком мала, окисная пленка, непроницаемая для водорода, не сохраняется. Оптимальная концентрация воды составляет, вероятно, около 0,01%. Самое длительное испытание

было проведено в контуре X-7 с трубой из циркалоя-4 под давлением. После облучения в течение десяти месяцев при температуре замедлителя на выходе $350\text{--}390^\circ\text{C}$ и небольшой концентрации воды ($1\text{--}5 \cdot 10^{-3}\%$) максимальное поглощение водорода составило примерно $8 \cdot 10^{-3}\%$. Имеются указания на то, что в областях с более высоким потоком нейтронов имеет место более сильное наводороживание.

A/15 Canada

Experimentación con refrigerantes orgánicos líquidos

por W. M. Campbell et al.

Los trabajos de investigación y perfeccionamiento, realizados principalmente en canales de ensayo de combustible de los reactores NRX y NRU, muestran que los líquidos orgánicos ofrecen perspectivas interesantes para la transmisión del calor generado por los reactores, que es posible mantener su pureza en presencia de radiaciones y de flujos térmicos y que existen materiales estructurales compatibles con esos líquidos.

Se han medido, en el intervalo de temperaturas comprendido entre 150 y 475°C , los índices de descomposición térmica y radiolítica de diferentes terfenilos puros y mezclados. Para una misma energía absorbida, los neutrones rápidos causan, aproximadamente, tres veces más daño que los electrones. También se han medido los índices de descomposición de otros líquidos cuyos puntos de fusión son adecuados para la puesta en marcha inicial de un reactor. Uno de ellos, consistente en una mezcla de terfenilos parcialmente hidrogenados, presentó un índice de descomposición aproximadamente igual al de los terfenilos, mientras que el índice de gases fue unas tres veces superior.

La purificación continua del líquido asume capital importancia. La proporción de cloro contenida en el terfenilo utilizado como líquido de reposición varía entre 2 y 10 partes por millón, y la concentración en todo el sistema debe mantenerse por debajo de 5 partes por millón. El cloro puede eliminarse mediante lechos de virutas de magnesio o de paladio sobre gránulos de alúmina calentados a unos 325°C ; en régimen normal, la concentración en los canales de experimentación puede mantenerse inferior a 3 partes por millón. Otras impurezas se separan por absorción en lechos de arcilla Attapulgu, a 325°C . Las impurezas en forma de partículas han de reducirse al mínimo por medio de filtros de lana de vidrio. El agua y el hidrógeno pueden separarse por extracción en atmósfera gaseosa y, si bien debe reducirse al mínimo el contenido de hidrógeno, existen razones que aconsejan mantener la concentración del agua alrededor de 100 partes por millón.

Se han observado dos tipos de incrustaciones en las superficies de los elementos combustibles. El

primero consiste en un depósito que contiene más del 70 por ciento de hierro y prácticamente ninguna sustancia orgánica. Está formado por el hierro arrastrado desde las tuberías del circuito (temperatura del orden de 300 °C) a la superficie de los elementos combustibles (temperatura de 400 a 500 °C). El cloro, la mayor parte del cual se encuentra en las paredes del circuito, desempeña un papel importante en el arrastre. Si la cantidad total de cloro contenido en el sistema es inferior al equivalente de 3 partes por millón en el refrigerante, este efecto de transferencia de masa es tolerable. El segundo tipo de incrustaciones es causado por partículas orgánicas contenidas en el refrigerante y forma un depósito de elevado contenido en sustancia orgánica. La magnitud de este tipo de incrustaciones aumenta en función de la temperatura de la superficie de los elementos combustibles, pero la irradiación no parece afectarla mayormente. Recientes experimentos efectuados en el circuito X-7 del reactor NRX han mostrado que al cabo de 82 d de irradiación en un flujo de neutrones térmicos de $5 \times 10^{13} \text{ cm}^{-2} \text{ s}^{-1}$, aproximadamente, el espesor de la película de incrustación

en los revestimientos del combustible, cuya temperatura se mantuvo comprendida entre 450 y 500 °C, fue inferior a $1 \mu\text{m}$.

Los autores demuestran que las aleaciones de zirconio son compatibles con los refrigerantes orgánicos, siempre que las características de éstos sean apropiadas. El cloro acelera la formación de hidruros, pero cuando el contenido se mantiene por debajo de 3 partes por millón el efecto disminuye considerablemente. La concentración del agua es asimismo muy importante; pues si es demasiado baja, no se conserva la película de óxido impermeable al hidrógeno; la concentración óptima del agua es probablemente de unas 100 partes por millón. El ensayo más prolongado se realizó en un tubo a presión de Zircaloy-4 en el circuito X-7. Al cabo de 10 meses de irradiación, con una temperatura en la salida del refrigerante de 350 a 390 °C y escasa concentración de agua (10 a 50 partes por millón), la fijación máxima de hidrógeno por la aleación fue de 80 partes por millón, aproximadamente. Se observaron síntomas de mayor fijación en regiones de flujo más elevado.

Etudes technologiques des fluides caloporteurs organiques *

par P. Lévêque **

Plusieurs types de réacteurs ont été développés pour utiliser l'uranium naturel comme combustible. Le graphite et l'eau lourde sont, dans ce cas, deux modérateurs possibles. L'emploi de l'eau lourde permet d'envisager divers fluides caloporteurs: l'eau lourde, les gaz sous pression (en particulier le gaz carbonique), les produits organiques. Cette dernière solution a été choisie par la Commission de l'EURATOM, et le projet est connu sous le nom d'ORGEL.

Depuis les premiers travaux effectués aux Etats-Unis sur les fluides organiques on sait que les terphényles sont les produits les plus prometteurs. C'est pourquoi la Commission de l'EURATOM a décidé de concentrer ses efforts de recherches sur le terphényle OM2***.

Cependant la Commission a jugé intéressant d'étudier les possibilités d'utilisation de coupes d'origine pétrolière dans le but d'obtenir des produits à bas point de fusion et moins chers. Les études ont porté principalement sur les alkylphénanthrènes.

C'est une synthèse des résultats obtenus sous différents contrats**** par des équipes comprenant du personnel du Commissariat à l'énergie atomique, de la société Progil, de l'Institut français du pétrole et de la Commission de l'EURATOM qui est présentée dans ce mémoire. Ces différents programmes ont été développés dans les centres de Saclay et de Grenoble du Commissariat à l'énergie atomique.

RECHERCHES SUR LES TERPHÉNYLES

Recherches analytiques

L'étude de la décomposition thermique et radiolytique des terphényles que nous allons traiter a nécessité

* Avec la collaboration de: F. Franzetti, P. Mas, M. Masson et J. R. Puig, Commissariat à l'énergie atomique; A. Houllier, R. Chaudet, J. Normand, D. Rosier et J. L. Trillet, société Progil; P. Giuliani et G. Leleu, Institut français du pétrole; M. Van der Venne et H. Hannaert, EURATOM.

** Commissariat à l'énergie atomique, CEN-Saclay.

*** Terphényle OM2: nom commercial du produit fabriqué par la société Progil dont la composition est: biphényle, 1%; *o*-terphényle, 15-25%; *m*-terphényle, 70-80%; *p*-terphényle, 5%. La température d'apparition des premiers cristaux de ce produit est inférieure à 90 °C; la température de prise en masse est inférieure à 80 °C.

**** EURATOM-CEA: n° 011-60-12-ORGF; 013-60-12-ORGF; 052-62-7-ORGF; 062-62-4-ORGF. EURATOM-PROGIL: n° 015-60-12-ORGF; 016-60-12-ORGF; 017-60-12-ORGF; 059-62-3-ORGF.

Marché d'irradiation EURATOM-CEA-PROGIL n° 117-63-4-ORGF.

des recherches de mise au point de méthodes analytiques appropriées.

Ces recherches ont été effectuées par la société Progil sous contrats EURATOM***** et ont fait l'objet d'une communication [1]. Elles ont permis:

a) De mettre au point des méthodes d'analyses de routine qui sont journalièrement employées, notamment: le dosage de l'eau par la méthode de Karl Fischer; le dosage de traces métalliques par spectrométrie de flamme, absorption atomique ou colorimétrie;

le dosage par chromatographie en phase vapeur du benzène, du diphényle, des trois isomères des terphényles et de certains polyphényles supérieurs, notamment les quaterphényles;

le dosage des produits lourds, de masse moléculaire supérieure aux terphényles, par microdistillation couplée à la chromatographie en phase vapeur.

Cette dernière méthode, qui permet de doser les produits lourds avec une bonne précision (environ $\pm 0,5\%$ en valeur absolue), a été utilisée pour la détermination de tous les résultats qui sont présentés ci-dessous.

b) De développer les techniques d'analyse par chromatographie:

en étudiant des imprégnants stables à haute température;

en employant des détecteurs divers (ionisation de flamme, capture d'électrons, thermistance, conductibilité thermique);

en cherchant à mettre au point la chromatographie préparative.

L'ensemble des connaissances acquises s'est avéré fort utile pour étudier l'évolution des terphényles soumis à la pyrolyse ou à la radiolyse.

Pyrolyse

Les résultats obtenus sur la stabilité thermique des terphényles ont déjà fait l'objet de communications [2, 3, 4]. Nous nous limiterons donc à rappeler les résultats essentiels.

La majeure partie des essais ont été effectués en ampoules à des températures comprises entre 416 et 520 °C. Après pyrolyse on a déterminé les quantités de lourds et de gaz formés.

Nos essais ont porté sur les isomères *para* et *méta* et sur des produits commerciaux, les terphényles OMI

***** Contrats EURATOM-PROGIL n° 006-60-10-ORGF et n° 058-62-3-ORGF.

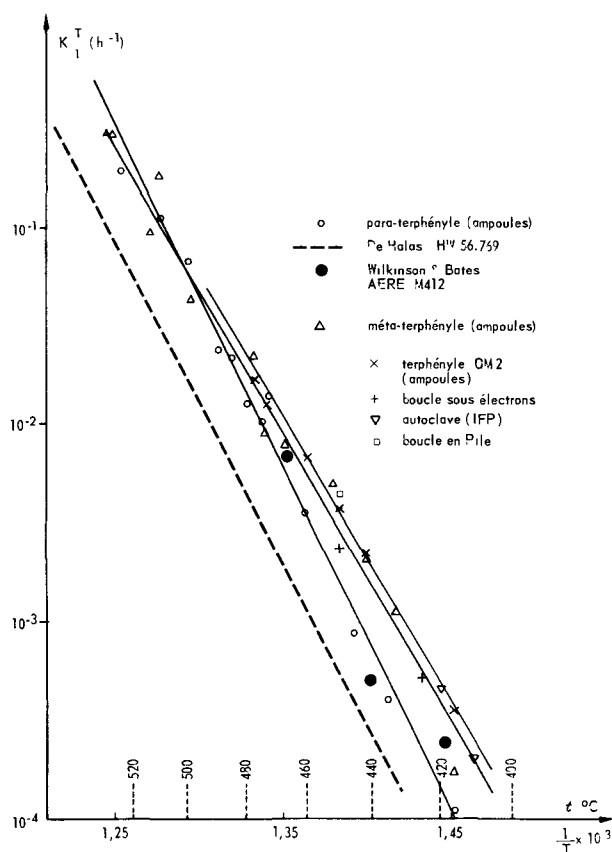


Figure 1. Vitesse de pyrolyse des terphényles; formation de lourds

et OMP, et surtout le fluide de référence d'ORGEL, le terphényle OM2.

La figure 1 montre comment varie la constante de vitesse de pyrolyse en fonction de la température; cette constante de vitesse a été calculée en adoptant une cinétique de réaction d'ordre 1 qui semble parfaitement convenir.

Sur cette figure on voit que:

la stabilité du *para*-terphényle est sensiblement meilleure que celle du *méta*-terphényle ou celle du terphényle OM2;

les stabilités du *méta* et du terphényle OM2 sont très voisines;

nos résultats diffèrent très sensiblement de ceux obtenus par de Halas [5];

les résultats de Wilkinson et Bates [6] pour le *para*-terphényle sont en assez bon accord avec les nôtres.

Les énergies d'activation varient entre 80 kcal/mole pour le *para*-terphényle et 64 kcal/mole pour le terphényle OM2 (formation de lourds).

Enfin on remarquera que les quelques essais en autoclave ou en boucle qui ont été effectués donnent des résultats cohérents avec les essais en ampoules.

Le même travail a été fait en partant de la formation des gaz, mais en admettant une cinétique d'ordre 0. On remarque que le *para*-terphényle présente une stabilité meilleure que celle du *méta*-terphényle et du terphényle OM2.

Les énergies d'activation calculées sont respectivement de 79 kcal/mole pour le *para* et de 67 kcal/mole pour le terphényle OM2.

Radiolyse

Si l'étude de la stabilité thermique représente une connaissance fort importante, il est bien évident que le résultat des études radiolytiques jouera un rôle déterminant dans le choix des conditions d'emploi du fluide caloporteur.

Les essais ont été effectués en ampoules et dans des boucles. Le tableau 1 résume les caractéristiques de celles-ci.

Radiolyse en ampoules

La radiolyse en ampoules a été effectuée alors que nous ne disposions pas de boucles, et, pour défricher le

Tableau 1

Nom	Moyen d'irradiation	Lieu	Volume total	Volume irradié	Intensité moyenne du rayonnement	Intensité neutrons en %	Température d'irradiation	Pressions	Débit	Observations	Références
BLO 1	Mélusine pile		25 à 32 l	8,7 l	0,216 Wg ⁻¹	19	jusqu'à 380 °C	10 kg cm ⁻²			[7]
BLO 2	Piscine de	Grenoble	24 l	8 l	0,168 Wg ⁻¹	17,5	jusqu'à 450 °C	40 kg cm ⁻²	2 m ³ h ⁻¹	Peut travailler à taux constant de polymères	[8] Fig. 2
BLO 3	2 MW		30 l	6 l	0,1 Wg ⁻¹	15	»	25 kg cm ⁻² (40 kg cm ⁻² pour la partie hors pile).	6 m ³ h ⁻¹	Noyau chauffant 50 Wcm ⁻² (effet joule direct)	[9]
SR 2	Accélérateur linéaire d'électrons 4 MeV 150 W	Saclay	270 à 320 ml (250 g)	6 ml environ (4,7 g)	17 Wg ⁻¹	0	»	25 kg cm ⁻²			

problème, les essais ont été effectués dans un four placé dans un convertisseur de la pile EL2 à Saclay.

La dosimétrie effectuée par verres doseurs et détecteurs à seuil et en utilisant le cyclohexane a permis de connaître la dose absorbée avec une précision de l'ordre de 30%. L'énergie d'origine neutronique représentait environ 30% de la dose totale.

Les essais n'ont pu être effectués que dans des fours dont les températures étaient comprises entre 280 et 320 °C et 320–380 °C.

A partir des résultats on a pu déterminer le rendement radiochimique G dans un domaine de températures où la pyrolyse est négligeable et on a trouvé:

$$G(-omp) = 0,23 \pm 0,0$$

$$G_{\text{gaz}} = 0,029 \pm 0,03$$

Compte tenu de l'imprécision sur l'évaluation des doses, ces valeurs peuvent être entachées d'une erreur systématique.

Radiolyse sous électrons

L'idée généralement admise est que, à dose égale, les neutrons ont un pouvoir destructeur beaucoup plus important que le rayonnement γ .

C'est pour essayer de vérifier cette donnée que des essais de radiolyse sous électrons produits par un accélérateur linéaire ont été effectués dans une petite boucle spécialement construite à cet effet par la société Progil. (On admet généralement que les électrons ont un effet comparable à celui du rayonnement γ .)

Les essais ont été effectués à Saclay à des températures comprises entre 200 et 450 °C. Cependant, comme nous le verrons plus loin, la pyrolyse du produit radiolysé étant très importante, nous nous sommes limités pour l'interprétation des résultats à des températures inférieures à 380 °C.

La dosimétrie est faite par calorimétrie sur une cible placée derrière la fenêtre du dispositif. Le rendement radiochimique calculé est de:

$$G(-omp) = 0,12 \mp 0,04$$

Radiolyse en boucle en pile

Cette partie du programme a été réalisée à Grenoble par un groupe de travail groupant le CEA, l'IFP et la société Progil. Les essais ont été effectués dans trois boucles, dont, notamment, les boucles BLO 2 et BLO 3 installées dans la pile MÉLUSINE. Une quatrième boucle (BLO 4), provenant de la transformation de BLO 2, est en construction et fonctionnera dans la pile SILOÉ.

Dosimétrie

Principes de la dosimétrie et choix des méthodes

La situation de la boucle dans le réflecteur nous commande les solutions apportées aux problèmes de dosimétrie:

— le pilotage du réacteur; les expériences voisines ne permettent pas d'avoir un flux constant dans les boucles;

— le volume du vase d'irradiation est suffisamment important pour que les gradients de flux y soient très grands;

— la mesure directe en continu de l'énergie due aux neutrons rapides par des méthodes calorimétriques n'est pas possible actuellement.

Aussi nous avons des détecteurs intégrateurs sur la boucle à l'extérieur dont l'indication est reliée au flux moyen dans le vase d'irradiation par l'intermédiaire de mesures sur une réplique du vase.

Méthodes de mesure des flux

Flux gamma: Calorimètre isotherme à noyau de graphite qui donne à chaque instant la puissance et l'énergie γ reçue par la boucle [10].

Flux rapide: Détecteur à seuil: Ni(1/n)S(1/n)Al.

Méthodes de calcul des dépôts d'énergie

Energie γ : On multiplie l'indication des calorimètres par le rapport des coefficients d'absorption d'énergie dans le liquide et le graphite.

Energie due aux neutrons rapides [11]:

$$\text{On a calculé: } \Pi(x, A) = K(A) \frac{\int_0^{\infty} \Phi(E) \sigma_s(E) E dE}{\int_1^{\infty} \Phi(E) dE}$$

x = distance au cœur de MÉLUSINE

A = masse atomique du corps choqué

$\Phi(E)$ = spectre du flux rapide mesuré au-dessus de 1 MeV, calculé entre 10 keV et 1 MeV en supposant une forme en $1/E\Sigma(E)$

$\sigma_s(E)$ = section efficace de choc élastique

$K(A)$ = coefficient tenant compte des unités, ...

L'énergie rapide est alors $\Pi(x, A) \times \phi(>1)$, $\Phi(>1)$ étant le flux rapide en n/cm² supérieur à 1 MeV.

Mesures sur les boucles

Les valeurs caractéristiques de dosimétrie pour les boucles 1, 2 et 3 (fig. 2) pour 24 heures de fonctionnement effectif de MÉLUSINE à 2 MW sont indiquées dans le tableau 2.

Critique des résultats

Erreurs de mesure:

Flux gamma $\leq 3\%$

Flux rapide $\leq 2\%$

Erreurs systématiques:

Pour l'énergie γ on a fait une série de mesures comparatives avec un calorimètre à compensation

Tableau 2

	BLO 1	BLO 2	BLO 3
D_n , Wh/g	1	0,7	0,36
D_γ , Wh/g	4,2	3,3	2
D_t , Wh/g	5,2	4	2,4
Rapport en			
pile/total	8,7/30	7,7/30	6/28
% D_n/D_t	19%	17,5%	15%

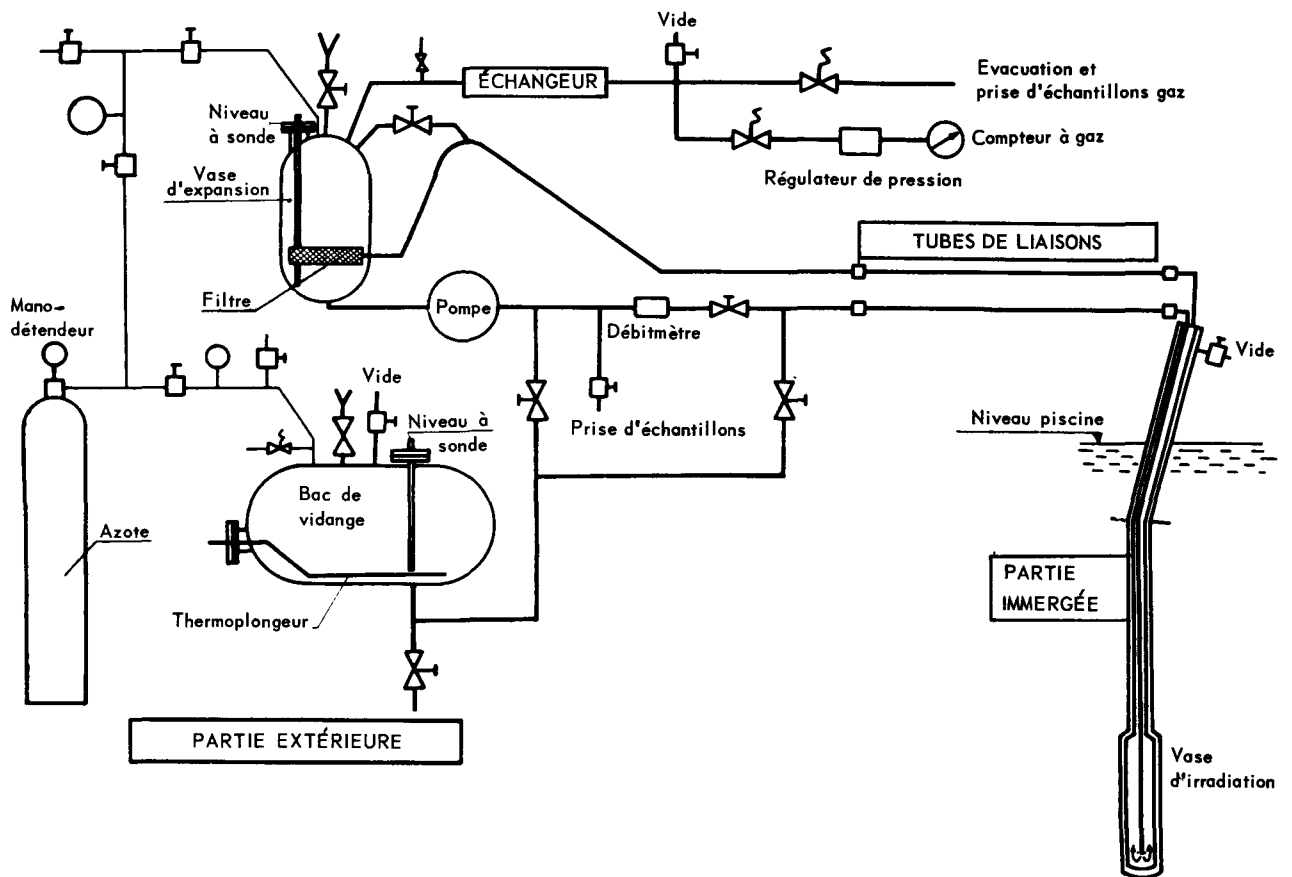


Figure 2. Boucle organique n° 2 — Schéma de principe

électrique [12]. Les mesures coïncident dans une plage de 5%.

Pour l'énergie due aux neutrons rapides: les méthodes calorimétriques utilisées par nous-même (calorimètre à eau) et par Richardson [13] ont démontré la validité de la méthode de calcul.

Erreurs de positionnement:

Elles peuvent donner lieu à des erreurs assez importantes étant donné les forts gradients de flux dans le réflecteur d'une pile piscine. On peut estimer que les doses totales de rayonnement sont connues avec une incertitude égale ou inférieure à $\pm 10\%$.

Mise au point de nouveaux dosimètres

Il faut ajouter qu'un calorimètre de référence a également été réalisé dans le cadre de ces études [14]. Il permet de mesurer avec une bonne précision, grâce à l'étalonnage interne dont il est pourvu, des intensités atteignant 5 Wg^{-1} dans le graphite.

Interprétation des résultats

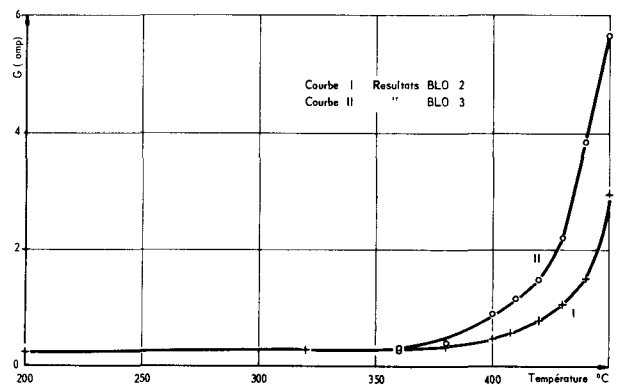
Nous n'insisterons pas sur les problèmes que pose le fonctionnement des boucles et aborderons dès maintenant l'interprétation des résultats.

Une première méthode que nous avons d'abord utilisée consiste à rapporter la décomposition observée à la dose absorbée par le produit irradié. On obtient le rendement radiochimique G bien connu, qui exprime

le nombre de molécules décomposées par 100 eV d'énergie absorbée.

La figure 3 présente les résultats que nous avons obtenus par le mode de calcul avec les boucles BLO 2 et BLO 3.

Cette figure permet de faire deux constatations qui sont à l'origine d'un mode d'interprétation différent, lequel, à notre avis, rend mieux compte des phénomènes observés, et surtout permet de transposer les calculs à d'autres installations pour peu qu'on en connaisse les paramètres essentiels: la première, c'est qu'à partir de 360°C environ, la courbe de variation de G en fonction

Figure 3. Vitesse initiale de radiolyse G (— omp) (BLO 2— BLO 3)

de la température, qui est sensiblement une horizontale, s'infléchit considérablement: le G augmente avec la température; la seconde, c'est qu'à partir de cette température, la courbe initiale se divise en deux, les courbes I et II, chacune d'elles correspondant à une boucle bien déterminée.

Cette anomalie apparente s'explique déjà assez facilement si l'on songe que, par suite d'une position plus favorable, la dose absorbée par le terphényle dans BLO 2 est environ 2,5 fois plus grande que celle absorbée par le terphényle dans BLO 3. Par conséquent, à dose absorbée égale, le temps de fonctionnement de BLO 3 est 2,5 fois plus grand que celui de BLO 2. Dans ces conditions on conçoit très bien que l'effet de la température soit plus sensible dans BLO 3 que dans BLO 2.

Cependant, si l'on essaie de corriger ces courbes en tenant compte des vitesses de pyrolyse du terphényle OM2, on constate toujours un net infléchissement et une séparation des résultats en deux courbes.

Cette observation, recoupée par des mesures de vitesse de pyrolyse du produit radiolysé en autoclave, en boucle et également en ampoules (essais EURATOM) et par l'augmentation de la population de centres actifs mesurés par résonance magnétique nucléaire, à partir d'une température de l'ordre de 380 °C, nous a conduit à penser que la vitesse de pyrolyse du produit radiolysé était beaucoup plus grande que celle du terphényle non radiolysé.

Cette idée étant admise, nous avons cherché à l'exprimer mathématiquement en faisant intervenir des considérations de cinétique et en formulant deux hypothèses qui nous ont paru raisonnables.

La première, c'est que la cinétique de la réaction était d'ordre 1, qu'il s'agisse de pyrolyse pure ou de radiolyse. Le choix de cet ordre n'est pas le produit du hasard: nous avons pu vérifier graphiquement que tous nos résultats obéissaient bien à cet ordre. Nous devons cependant faire remarquer qu'un certain nombre d'entre eux étaient également bien représentés, soit par l'ordre 0, soit par l'ordre 3/2, certains même par l'ordre 2.

Pour lever cette indétermination, BLO 2 a été équipée d'un dispositif permettant de travailler à taux constant de polymère.

Il convient également de signaler qu'EURATOM a calculé, à partir des résultats expérimentaux obtenus, que l'ordre le plus probable était effectivement 1.

C'est également cet ordre que Mason, au MIT, a adopté pour interpréter les résultats qu'il a obtenus en irradiant en pile du Santowax R.

La seconde hypothèse a été d'admettre que les effets radiolytiques et pyrolytiques étaient additifs. Certes, il ne s'agit pas d'une idée bien nouvelle en soi puisque de Halas [5] l'a déjà formulée sans cependant, nous semble-t-il, l'étayer aussi rigoureusement que nous sur des résultats expérimentaux. En tout cas, nos conclusions diffèrent très sensiblement de celles de de Halas puisque les vitesses de pyrolyse du produit radiolysé que nous trouvons sont beaucoup plus importantes.

Donc, partant de l'équation:

$$\frac{dC}{dt} = (Ar + Bp)C$$

et en explicitant les constantes Ar et Bp nous trouvons l'équation:

$$\frac{dC}{dt} = (k_1\bar{d} + k_2)C$$

à partir de laquelle on calcule aisément la valeur apparente Ga^T du rendement radiochimique.

$$(Ga^T)_x = 11,65 \left(k_1 + \frac{k_2}{\bar{d}_x} \right)$$

(l'indice x se rapporte à un boucle donnée; \bar{d}_x est l'intensité moyenne absorbée dans le terphényle, exprimée en Wg^{-1}).

A partir de cette formule nous avons calculé les constantes k_1 et k_2 en résolvant le système de deux équations à deux inconnues qu'on obtient en utilisant les valeurs de $(Ga^T)_x$ et \bar{d}_x des boucles BLO 2 et BLO 3.

Nous pouvons également effectuer une résolution graphique en portant en fonction de $1/T$ la constante globale de vitesse

$$K_x = k_1\bar{d}_x + k_2 = \frac{(Ga^T)_x \bar{d}_x}{11,65}$$

Ce mode de calcul est illustré par la figure 4 (tableau 3).

Il permet de tirer les conclusions suivantes:

a) Au-dessous de 380 °C, la vitesse de radiolyse du terphényle est pratiquement constante et indépendante de la température (courbes I et II). Connaissant $k_1\bar{d}_x$,

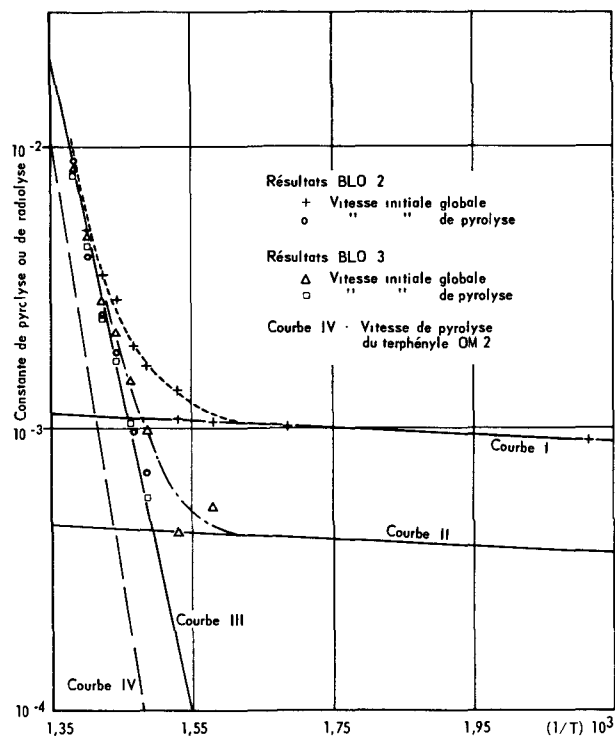


Figure 4. Détermination graphique des vitesses initiales de radiolyse et de pyrolyse à partir des résultats de BLO 2 et BLO 3

Tableau 3

No essai	°C	°K	$1/T \times 10^3$	$G_{\alpha T}$	\bar{d}	$k_1 T + k_2 T$	$k_2 T$
A-14-200	200	473	2,114	0,24	0,044 5	$9,16 \cdot 10^{-4}$	
A-19-320	320	593	1,686	0,26	0,045 4	$1,01 \cdot 10^{-3}$	
B-11-320	320	593	1,686	—	—	—	
A-15-360	360	633	1,579 7	0,31	0,040	$1,06 \cdot 10^{-3}$	
B-1-360	360	633	1,579 7	0,29	0,021	$5,23 \cdot 10^{-4}$	
B-9-360	360	633	1,579 7	0,32	—	—	
A-16-380	380	653	1,531	0,33	0,038 0	$1,075 \cdot 10^{-3}$	
A-23-380	380	653	1,531	0,36	0,044 7	$1,38 \cdot 10^{-3}$	
B-2-380	380	653	1,531	0,36	0,013 8	$4,26 \cdot 10^{-4}$	
A-18-400	400	673	1,485 8	0,48	0,041 1	$1,69 \cdot 10^{-3}$	$6,0 \cdot 10^{-4}$
B-3-400	400	673	1,485 8	0,70	0,016 6	$9,97 \cdot 10^{-4}$	$5,57 \cdot 10^{-4}$
A-12-408	408	681	1,468 4	0,58	0,039 6	$1,97 \cdot 10^{-3}$	$8,7 \cdot 10^{-4}$
B-4-410	410	683	1,464 0	1,16	0,015	$1,49 \cdot 10^{-3}$	$1,04 \cdot 10^{-3}$
A-17-420	420	693	1,443 0	0,78	0,041 6	$2,78 \cdot 10^{-3}$	$1,68 \cdot 10^{-3}$
B-5-420	420	693	1,443 0	1,47	0,017 95	$2,27 \cdot 10^{-3}$	$1,82 \cdot 10^{-3}$
A-20-430	430	703	1,422 4	1,06	0,038 5	$3,5 \cdot 10^{-3}$	$2,4 \cdot 10^{-3}$
B-6-430	430	703	1,422 4	2,20	0,015 24	$2,87 \cdot 10^{-3}$	$2,42 \cdot 10^{-3}$
A-21-440	440	713	1,602 5	1,50	0,039 2	$5,05 \cdot 10^{-3}$	$3,95 \cdot 10^{-3}$
B-8-440	440	713	1,602 5	3,86	0,014 73	$4,85 \cdot 10^{-3}$	$4,4 \cdot 10^{-3}$
A-22-450	450	723	1,383 1	2,96	0,039 1	$9,92 \cdot 10^{-3}$	$8,81 \cdot 10^{-3}$
B-7-450	449	722	1,385	5,67	0,171 8	$8,395 \cdot 10^{-3}$	$7,93 \cdot 10^{-3}$

on calcule aisément k_1 et le rendement radiochimique vrai G_r .

On trouve $G_r = 11,65 K_1$

Ce rendement radiochimique se situe autour de 0,28 et, en attendant les résultats de mesures à des températures comprises entre 200 et 320 °C, la pente calculée des courbes I et II est 0,54 kcal/mole.

b) A partir de 380 °C, la pyrolyse du terphényle radiolysé commence à devenir sensible. La variation de la constante de pyrolyse k_2 est représentée par la courbe III. On constate que les valeurs de k_2 obtenues à partir des résultats des boucles 2 et 3 sont en parfait accord.

L'énergie d'activation calculée est de 54,2 kcal/mole.

La même représentation graphique peut être effectuée pour la formation des gaz.

Discussion des résultats

a) L'ordre des réactions radiolytiques et pyrolytiques a été pris égal à 1. Cela ne fait pas de doute pour la pyrolyse. Par contre, les premiers résultats obtenus sur BLO 2, fonctionnant à taux constant de polymère, semblent indiquer que la radiolyse pure ($\theta < 360$ °C) obéit plutôt à une cinétique d'ordre 2. Il est vraisemblable que, lorsque la pyrolyse se superpose à la radiolyse, l'ordre de la réaction varie de 2 à 1, ce qui complique l'interprétation des résultats. On peut expliquer l'ordre 2 de la radiolyse en admettant que seule l'énergie dissipée dans le terphényle intervient dans la réaction.

b) Il n'en reste pas moins vrai que la vitesse de pyrolyse d'un produit radiolysé est plus élevée que celle d'un produit vierge. Cela peut être dû à l'apparition de dérivés alkylés. Cette hypothèse est étayée par la similitude de l'énergie d'activation de la pyrolyse de tels produits.

c) Mason [15], en reprenant tous les résultats obtenus par des irradiations en piles, arrive à la

conclusion que $G_n = G_y$. Cela semble en contradiction avec nos résultats obtenus sous électrons. Mais si l'on compare l'ensemble des résultats obtenus sous électrons l'on voit que G électron décroît lorsque l'intensité du rayonnement augmente. Or, nos résultats ont été obtenus avec un accélérateur linéaire délivrant une dose instantanée énorme ($29\ 000\ \text{Wg}^{-1}$). Cela explique sans doute notre G électron très faible. D'autre part le G déduit des expériences en ampoules n'est pas assez sûr pour conclure, bien que la contribution des neutrons à l'énergie totale (30% de l'énergie totale) soit plus importante que celle dissipée dans les boucles (17,5 et 15%).

RECHERCHES SUR LES SUBSTITUTS AUX TERPHÉNYLES

Le travail effectué sur les substitués aux terphényles s'est limité à des produits d'origine pétrolière; il comporte deux parties: l'étude extensive des coupes pétrolières et l'étude intensive des coupes «alkylphénanthrène».

Etude extensive des coupes pétrolières

Elle a fait l'objet de communications [16, 7], et nous n'en donnerons que les lignes générales.

D'abord, une évaluation des diverses coupes pétrolières possibles a été faite sur la base de la stabilité thermique mesurée au moyen de différents tests comparatifs dans des autoclaves en acier inoxydable, de la stabilité radiolytique déterminée par des essais à 200 °C sous un accélérateur électrostatique d'électrons à lentille de 600 keV de la société SAMES, de la mesure de la teneur en impuretés et de la radioactivité induite qui en découle, de la détermination de la teneur en aromatiques.

Ensuite, la sélection des meilleures coupes, fruit du travail précédent, a conduit à retenir principalement

Tableau 4. Caractéristiques des charges d'alkylphénanthrènes utilisées dans les essais d'irradiation en boucle en pile (BLO 1)

	AKP. 3	AKP. 4	AKP. 5
Intervalle de distillation A.S.T.M. °C	336-367	312-362	308-328
Densité 25/4	1,082	1,086	1,044
Indice de réfraction n_{25}^d	1,669	1,672	1,6314
Point de cristallisation (apparition des premiers cristaux) °C	10	6	40
Poids moléculaire	200	201	190
Point éclair °C	184	182	170
Point de feu °C	208	203	197
Soufre ppm.	7	8	>8
Stabilité thermique ^a (% monomère transformé):			
360 °C essai statique 8 h	—	1,25	3,3
380 °C essai statique 8 h	3,2	1,60	3,6
400 °C essai statique 8 h	6,3	4,0	3,7
420 °C essai statique 8 h	21	11,4	7,8
Stabilité thermique moles gaz/moles produit:			
360 °C essai statique 8 h	néant	néant	néant
380 °C essai statique 8 h	néant	néant	néant
400 °C essai statique 8 h	0,013	néant	0,03
420 °C essai statique 8 h	0,165	0,075	0,055
Stabilité radiolytique ^a aux électrons:			
accélérés à 177 °C	0,19	0,19	0,19
G monomère transformé 4 Wh/g	0,18	0,18	0,19
8 Wh/g	0,16	0,14	0,18
20 Wh/g	0,11	0,11	0,15
Analyse par activation ^b :			
Na ppm.	0,25	0,04	0,06
Cu ppm.	0,12	0,015	0,02
Mn ppm.	0,01	<5 · 10 ⁻³	0,005
Hg ppm.	<0,02	0,05	0,02
Cl ppm.	—	<0,4	—

^a Les méthodes utilisées pour la mesure de la stabilité thermique et de la stabilité radiolytique sont décrites dans la référence [1].

^b Analyse faite par la Section Application des radioéléments du Centre d'études nucléaires de Grenoble.

les coupes « alkylphénanthrène » dépourvues d'impuretés et entièrement aromatiques provenant du procédé de raffinage appelé *reforming* catalytique, et notamment d'une de ses variantes, le *powerforming*.

Enfin, en vue d'améliorer la stabilité thermique de ces coupes « alkylphénanthrène », il a été nécessaire de vérifier, dans ce but, l'efficacité de différents traitements: hydrodésalkylation, « prépyrolyse », etc.

Etude intensive des coupes « alkylphénanthrène »

Elle a consisté à déterminer la vitesse de décomposition de ces fluides dans des conditions isothermes, en mélange avec leur propre produit de dégradation dans une boucle d'irradiation installée dans la pile MÉLUSINE du CEN, Grenoble.

Appareillage

Les caractéristiques de la boucle dénommée BLO 1 et celles du rayonnement reçu par le vase d'irradiation ont déjà été publiées.

La dosimétrie a été faite suivant les mêmes principes que ceux mentionnés pour le terphényle OM2.

Le bon fonctionnement de l'installation a été vérifié au moyen de deux essais tests avec du diphenyle à 350 °C et du terphényle OM2 à 380 °C.

Résultats

Trois charges d'alkylphénanthrène ont été étudiées. Leurs caractéristiques, leurs propriétés et leur com-

position sont assez voisines ainsi que le montrent les tableaux 4 et 5.

Trois essais ont été réalisés: le premier à 200 °C pour connaître la part de décomposition due à la radiolyse seule; le deuxième et le troisième respectivement à 360 et 380 °C pour chercher la température limite d'utilisation de ces fluides.

a) La stabilité radiolytique a été déterminée en suivant la décomposition du produit mis en œuvre en fonction de la dose et en calculant la constante de vitesse et le G (—) radiochimique initial en supposant que la cinétique de la réaction suivait un ordre 1. Cette hypothèse a été faite parce que les résultats expérimentaux la confirmaient passablement et aussi pour comparer les valeurs obtenues à celles trouvées avec le terphényle OM2; cette comparaison est fournie par le tableau 6.

La contribution de la pyrolyse seule est mesurée au moyen d'un essai en statique dans un autoclave de laboratoire.

Cette contribution est négligeable à 200 °C; elle est de 1/3 et 2/3 respectivement à 360 et 380 °C dans la décomposition de la charge. Elle doit en réalité être plus forte si on admet que, comme pour le terphényle OM2, la pyrolyse d'un produit radiolysé est plus importante. Un essai fait à 400 °C dans BLO 3 avec une charge d'alkylphénanthrène (tableau 6) a du reste montré que la vitesse de décomposition était réellement très grande.

Tableau 5. Composition des charges d'alkylphénanthrènes

	AKP. 3	AKP. 4	AKP. 5	
% en poids ^a noyaux naphthaléniques . . .	—	0,5	% poids C _n H _{2n-12} ^{cd}	1,9
fluoréniques	—	4	% poids C _n H _{2n-14}	17,4
phénanthréniques . . .	48	49	% poids C _n H _{2n-16}	43,5
anthracéniques	3,5	2,1	% poids C _n H _{2n-18}	34,8
pyréniqes	6	6,5		
fluoranthéniques . . .	4	5,2		
% en poids ^b — CH = aromatiques	47	51		
— CH ₂ — et CH ₃ -aliphatiques	13,5	11,5		115

^a Mesuré par spectrométrie U.V.^b Mesuré par spectrométrie I.R.^c Mesuré par spectrométrie de masse^d C_nH_{2n-12}: dérivés du naphthalèneC_nH_{2n-14}: dérivés du diphenylC_nH_{2n-16}: dérivés du fluorèneC_nH_{2n-18}: dérivés du phénanthrène et anthracène

b) La variation des constantes physiques (densité, viscosité, conductibilité thermique, tension de vapeur) en fonction de la température pour un pourcentage de produit de décomposition identique souligne la grande similitude qui existe dans ce domaine avec les terphényles, d'où des coefficients d'échange thermique proches. Une exception cependant existe pour la chaleur spécifique sensiblement plus basse pour les coupes « alkylphénanthrène ».

c) L'activité induite du produit irradié est très faible et équivalente à celle d'un produit de synthèse.

d) L'analyse détaillée par spectrométrie de masse des différentes familles d'hydrocarbures avant et après irradiation [17] a permis de mettre en évidence que c'est la famille du phénanthrène qui a la stabilité la meilleure, qu'une déméthylation importante se produisait, ce qui explique le G gaz important trouvé, qu'une partie du polymère régénèrait des produits initialement présents.

En définitive, cette étude sur les substitués aux terphényles d'origine pétrolière a permis de connaître les possibilités et les limites des coupes « alkylphénanthrène » provenant du résidu de reforming catalytique et retenues comme étant les meilleures.

Elles offrent une combinaison de propriétés qui les rendent comparables aux terphényles jusqu'à la température de 360 °C avec en plus les avantages d'avoir un point de fusion ne dépassant jamais 40 °C et un prix qui pourrait être inférieur.

Des études actuellement en cours permettent d'espérer que leurs mélanges avec du terphényle OM2 (dans certaines proportions) constituent des fluides de bas point de fusion (< 30 °C) et ayant une stabilité

thermique suffisante pour les employer jusqu'à 380 °C. De tels mélanges présentent aussi une solution satisfaisante pour résoudre le problème posé par le démarrage d'un réacteur ORGEL.

BIBLIOGRAPHIE

1. Normand, J. (Progil), et Geiss, F. (CCR-EURATOM), *Progress in analysis of polyphenylic mixtures*, Rome, 15 juin 1962.
2. Houllier, A., et Puig, J. R., *Etude des fluides organiques refroidisseurs/modérateurs de piles atomiques. Stabilité thermique et radiolytique des terphényles*. Communication au XXXIII^e Congrès de chimie industrielle de Bordeaux, octobre 1961.
3. Houllier, A., et Puig, J. R., *Radiolyse et pyrolyse des triphényles à hautes températures*, Colloque sur l'emploi des liquides organiques comme modérateurs et réfrigérants, Rome, 23-24 mars 1961.
4. Puig, J. R., Houllier, A., et Rosier, D., *Radiolyse et pyrolyse des triphényles à hautes températures*, Symposium sur les réacteurs modérés et/ou réfrigérés par les liquides organiques, Rome, 14-15 juin 1962.
5. De Halas, *Kinetics of the decomposition of organic reactor coolants*, HW 56. 769.
6. Wilkinson et Bates, AERE M. 412.
7. Giuliani, P., Leleu, G., de Gorski, E., et de Gaudemans, G., *Caloporteurs organiques d'origine pétrolière pour réacteurs nucléaires*, 6^e Congrès de pétrole, Francfort, 19-26 juin 1963, Section IV - Communication 56.
8. Masson, M., *Boucle n° 2 pour irradiation de coupes pétrolières*, BIST n° 75, 121-125 (août-septembre 1963).
9. Franzetti, F., et Houllier, A., *Boucle de radiolyse pour l'étude des terphényles*, BIST n° 75, 127-131 (août-septembre 1963).
10. Mas, P., Sciens, P., et Droulers, Y., *Etude théorique et expérimentale d'une technique calorimétrique de mesure des dépôts d'énergie dans les matériaux dus au rayonnement complexe de pile*. Rapport CEA n° 2217.
11. Droulers, Y., *Influence du spectre des neutrons sur l'énergie de radiolyse dans les liquides organiques*, Neutron Dosimetry, IAEA, Vienne (1963).
12. Ayela, F., et Derrien, H., *Etude et réalisation d'un calorimètre différentiel à compensation électrique pour la mesure des échauffements en pile*, Rapport CEA n° 2190.
13. Richardson, D. M., Allen, A. O., et Boyle, J. W., *Dosimétrie des rayonnements d'une pile par mesures calorimétriques*. Actes de la première Conférence internationale

Tableau 6. Vitesse de décomposition et G radio chimique initial des coupes « alkylphénanthrène »

Température °C	AKP		OM2	
	k (Wh/g) ⁻¹	G° (-)	k (Wh/g) ⁻¹	G° (-)
200 . . .	0,0129 (BLO 1)	0,17	0,02 (BLO 2)	0,23
360 . . .	0,0136 (BLO 1)	0,18	0,027 (BLO 2)	0,31
380 . . .	0,025 (BLO 1)	0,35	0,030 (BLO 2)	0,36
400 . . .	0,274 (BLO 3)	3,86	0,0605 (BLO 3)	0,70

- sur l'utilisation de l'énergie atomique à des fins pacifiques, P/154, Vol. XIV, p. 234, Nations Unies (1956).
14. Calvet, E., Chatelet, S., Puig, J. R., et Romano, F., *Adaptation du microcalorimètre Calvet à la dosimétrie en pile*. Neutron Dosimetry, AIEA, Vienne (1963).
15. Sawyer, C. D., et Mason, E. A., *The effects of reactor irradiation on Santowax OMP at 610 °F and 750 °F*, IDO 11 107, septembre 1963.
16. *Contribution de l'industrie du pétrole au problème des modérateurs et caloporteurs organiques*. Communication faite par le Département de radiochimie de l'Institut français du pétrole au symposium sur l'emploi des organiques liquides comme modérateurs et réfrigérants, European Atomic Energy Society, Rome, 23-24 mars 1961.
17. Ulrich, I., Copet, A., Bedague, P., et Cornu, A., *Analyse d'un résidu de powerforming, pyrolysé et radiolysé, par spectrométrie de masse en basse tension et par spectrométrie infra-rouge*. 6^e Congrès du pétrole, Francfort, juin 1963.

ABSTRACT—RÉSUMÉ—АННОТАЦИЯ—RESUMEN

A/53 France

A/53 Francia

Technological study of organic cooling fluids

Estudio tecnológico de los fluidos orgánicos para transferencia de calor

By P. Lévêque

por P. Lévêque

Under contract to EURATOM (Van der Venne and Hannaert), the CEA and the Progil society have collaborated on a technological study of the terphenyls. The results obtained from the radiolysis and pyrolysis of the product OM2 (70% *m*-terphenyl, 25% *o*-terphenyl, 5% *p*-terphenyl) are reported. Using two pile loops at temperatures up to 450 °C, a phenomena of accelerated pyrolysis on the radiolysed material has been demonstrated. Some by-products of the petroleum industry have also been studied, with a view to finding substitutes for terphenyl.

El CEA y la Sociedad Progil han emprendido en común, en ejecución de un contrato del EURATOM (Van der Venne y Hannaert), un estudio tecnológico de los terfenilos. Se exponen los resultados de la radiólisis y de la pirólisis obtenidos con el producto OM2 (70 % de *m*-terfenilo, 25 % de *o*-terfenilo y 5 % de *p*-terfenilo). El funcionamiento de dos circuitos de reactor a temperaturas de hasta 450 °C ha puesto de relieve un fenómeno de pirólisis acelerada en el producto radiolizado. Se han estudiado asimismo algunos subproductos de la industria petrolífera con objeto de hallar sustitutos para el terfenilo.

A/53 Франция

Технологические исследования жидких органических теплоносителей

П. Левек

Комиссариат по атомной энергии Франции и фирма «Прожиль» провели совместно по контракту Евратома (ван дер Венне и Ханнаэрт) технологическое исследование терфенилов. Приводятся результаты радиолиза и пиролиза, полученные на продукте OM2 (70% *m*-терфенила, 25% *o*-терфенила, 5% *p*-терфенила). При работе двух контуров реактора при температурах до 450° С наблюдается явление ускоренного пиролиза радиализованного продукта. Были также исследованы некоторые побочные продукты нефтеперерабатывающей промышленности, чтобы найти заменители терфенила.

Transferts de chaleur par liquides organiques

par J. Villeneuve *, R. Ricque *, M. Courtaud * et F. Lanza **

Dans le cadre d'un contrat passé par la Direction du projet ORGEL de l'EURATOM, on a étudié sur deux installations d'essais les caractéristiques d'échange thermique de différents terphényles et l'influence, sur le coefficient d'échange, de l'encrassement des surfaces chauffantes par du terphényle OM2 contenant, dans certains cas, du fer, du chlore ou des produits de décomposition.

LES ÉTUDES DE COEFFICIENT D'ÉCHANGE

Le dispositif expérimental: boucle L0.50.P

L'ensemble de l'installation est représenté par la figure 1.

* Commissariat à l'énergie atomique, CEN-G.

** EURATOM, Ispra.

Le circuit principal de terphényle est construit en grande partie en acier ordinaire et conçu pour fonctionner jusqu'à 450 °C et 20 kg/cm² (pressurisation à l'azote). Il est relié par son point bas à la cuve de stockage, dans laquelle le circuit peut se vidanger à peu près intégralement.

La pompe, classique, à presse-étoupe, est du type centrifuge.

La section d'essais est essentiellement constituée d'un tube d'acier inoxydable de 80 cm de longueur chauffante, 12 mm de diamètre intérieur et 1 mm d'épaisseur.

La mesure du débit est assurée par un orifice déprimogène et un débitmètre à turbine. La pression différentielle de l'orifice déprimogène est transmise à une cellule de pression différentielle par deux lignes de

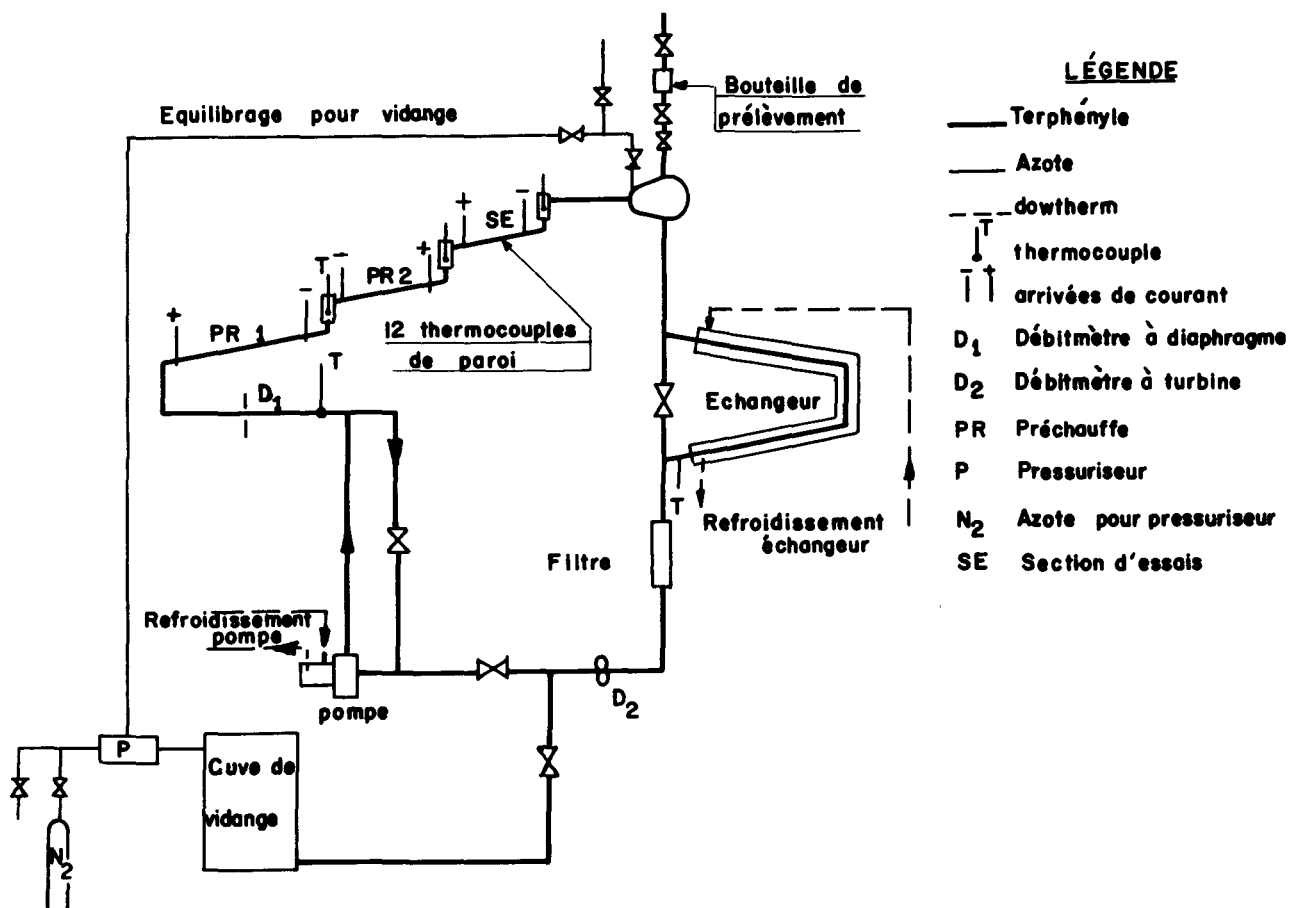


Figure 1. Schéma de la boucle L0.50.P

Tableau I. Composition des terphényles essayés

Produits testés	Composition en pourcentage				
	Légers	Ortho-terphényle	Méta-terphényle	Para-terphényle	Lourds
OMP	Traces	3,4	66,5	30	0,1
OM2 pur	0,5	18,5	76	5	0
(OM2 + HBR) 1	0,4	16,9	66	5,2	11,5
(OM2 + HBR) 2	0,4	15	57	5,1	22,9
(OM2 + HBR) 3	Traces	13	54,8	3,4	28,8

mesure constamment chauffées pour éviter le gel du terphényle. Ces deux appareils sont étalonnés avec une précision de 0,3% au banc d'étalonnage hydraulique à froid; leur concordance en fonctionnement à chaud a toujours été très bonne (mieux que 2% pour 80% des points d'essais).

La densité superficielle de flux thermique est déterminée à partir des mesures de tension et d'intensité du courant continu alimentant la section d'essais.

La mesure de température de fluide est effectuée aux extrémités du canal d'essais par thermocouples et sondes à résistance de platine montés dans une gaine immergée dans un pot assurant le bon mélange de fluide.

Les températures de paroi sont mesurées par des thermocouples thermocoax brasés dans des disques d'argent; ces disques sont serrés contre la paroi et en sont isolés électriquement par une mince feuille de mica. L'isolation thermique y est réalisée au moyen de lames d'air délimitées par trois cylindres en cuivre concentriques au canal d'essais. Entre les deux cylindres extérieurs se trouvent des fils chauffants thermocoax enrobés dans du ciment conducteur Thermon. L'enveloppe chauffante ainsi réalisée fournit un flux bien uniforme. Le troisième cylindre, de diamètre inférieur aux précédents, délimite entre ceux-ci et le canal lui-même deux couches d'air.

On règle, à l'aide de thermocouples brasés sur les tubes de cuivre et montés en différentiel, les gradients radiaux à travers la couche d'air externe. Le gradient radial autour du canal d'essais est ainsi réglé, à 1 ou 2 degrés près, autour d'une valeur voisine de zéro, et le flux de fuite est par suite pratiquement annulé.

Un autre dispositif permet d'annuler également les pertes thermiques par conduction dans les barres d'amenée de courant.

Ces précautions permettent d'obtenir des bilans thermiques toujours compris entre 95 et 105% et donnent une amélioration considérable à la précision des résultats de coefficient d'échange.

Les produits organiques testés

On a effectué les mesures sur des terphényles de la Société Progil, dont la composition chimique est donnée dans le tableau I.

Les produits lourds (HBR) provenaient du réacteur américain OMRE.

Ayant besoin de connaître parfaitement les caractéristiques physiques de ces produits jusqu'à 450 °C et 20 kg/cm², on a construit à Grenoble un calorimètre, un conductimètre thermique, un viscosimètre et un densimètre permettant ces mesures [2]. On a obtenu les valeurs suivantes, valables entre 240 et 450 °C:

$$\text{Densité [(kg/m}^3\text{)} \cdot 10^{-3}] = a + b/T + c/T^2 + d/T^3$$

$$\text{Viscosité [(kg/m s)} \cdot 10^3] = e + f/T + g/T^2 + h/T^3$$

$$\text{Chaleur spécifique (j/kg }^\circ\text{C)} = j + kT$$

$$\text{Conductibilité thermique (W/m }^\circ\text{C)} = 1 + mT$$

T est exprimé en °C

Les valeurs des constantes sont données dans le tableau 2.

Résultats d'essais de coefficient d'échange [3]

Les essais de coefficient d'échange ont été tout d'abord réalisés avec le terphényle OMP dans la gamme de paramètres suivants (44 points d'essais):

Densité de flux	50 et 100 W/cm ²
Vitesse	4 à 9 m/s
Température d'entrée	320 à 410 °C
Nombre de Reynolds	120 000 à 370 000
Nombre de Prandtl	5,5 à 7,8

Ils ont été poursuivis pour 164 points d'essais avec

Tableau 2. Constantes de caractéristiques physiques

Fluide	OMP	OM2	OM2 + 10% lourds	OM2 + 20% lourds	OM2 + 30% lourds
a	-0,532	-0,373	-0,442	-0,361	-0,320
b · 10 ⁻²	10,309	8,887	9,667	8,967	8,600
c · 10 ⁻⁴	-25,929	-21,820	-24,348	-22,172	-20,889
d · 10 ⁻⁶	23,055	19,109	21,796	19,626	18,187
e	0,011	0,180	0,042	-0,127	-0,122
f · 10 ⁻²	0,034	-1,672	-0,063	1,716	1,656
g · 10 ⁻⁴	3,6163	8,7990	3,2628	-2,4538	-1,8834
h · 10 ⁻⁶	-0,1722	-5,5927	1,4641	8,8151	9,3927
j	1,644	1,584	1,587	1,590	1,594
k	2,40	2,43	2,38	2,34	2,29
l	0,1487	0,1442	0,1438	0,1436	0,1432
m · 10 ⁴	-1	-1,05	-0,95	-0,86	-0,76

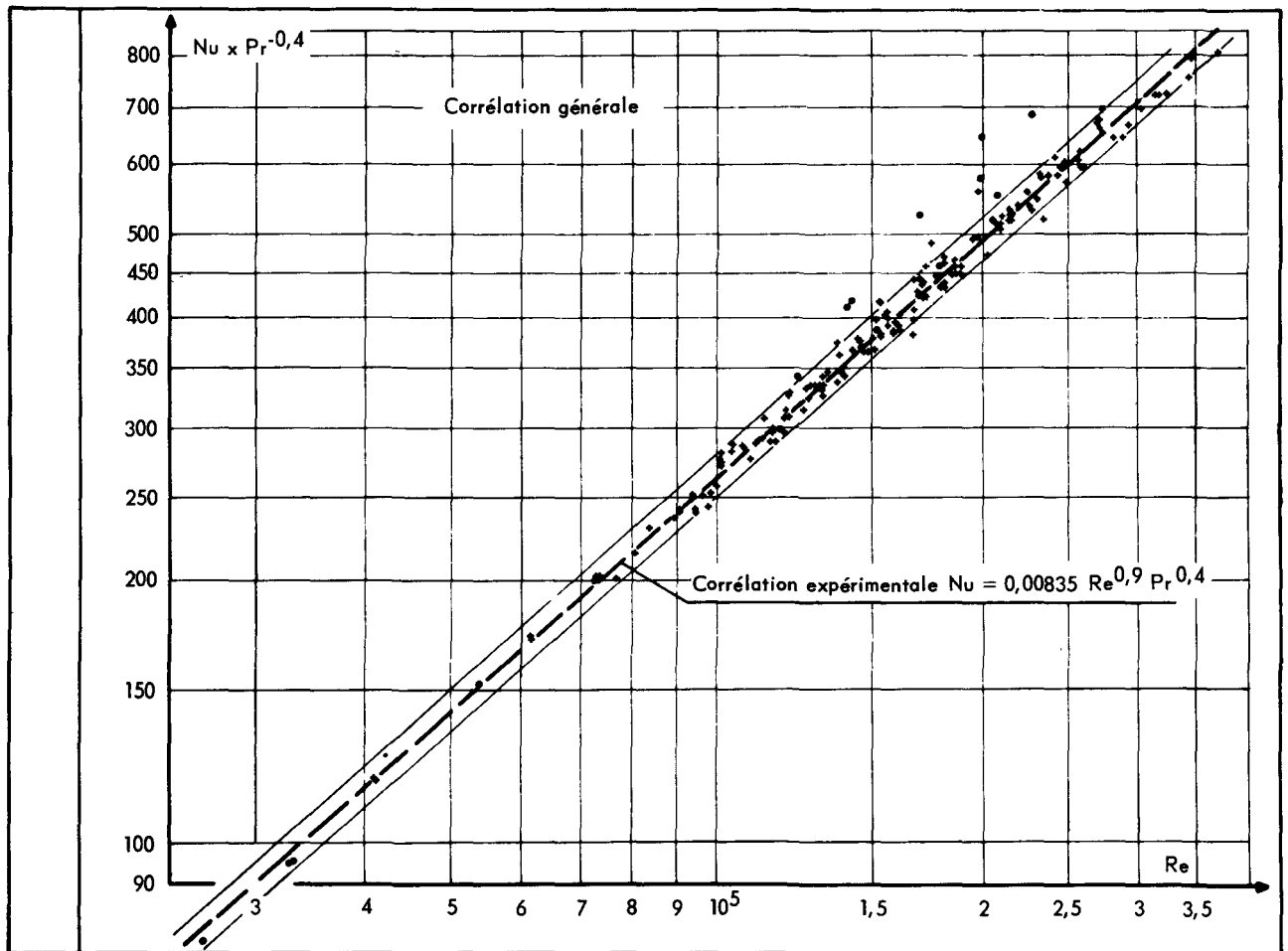


Figure 2. Résultats d'essais

les terphényles OM2 avec et sans produits lourds; la gamme de paramètres explorés est la suivante:

Densité de flux	25 à 50 W/cm ²
Vitesse	1,5 à 8 m/s
Température d'entrée . . .	290 à 380 °C
Nombre de Reynolds	26 000 à 270 000
Nombre de Prandtl	6,5 à 12

La quasi-totalité (95%) des 208 points d'essais répond à la corrélation générale suivante:

$$Nu = 0,00835 Re^{0,9} Pr^{0,4}$$

les nombres sans dimensions étant calculés pour la température moyenne du fluide. 95% des points d'essais sont compris dans une bande de dispersion de $\pm 6\%$ autour de cette corrélation. La figure 2 représente l'ensemble des résultats d'essais. On a constaté que la valeur de la densité de flux thermique n'avait pas d'influence nette sur les résultats.

On a comparé cette corrélation avec les résultats de l'étude théorique de Martinelli [1]; l'analogie de Martinelli conduit à un exposant 0,9 pour le nombre de Reynolds comme la corrélation ci-dessus.

On constate, sur la figure 2, qu'un certain nombre de points présentent une dispersion anormale; ces points correspondent à des terphényles à forte concentration de lourds, circulant à haute température et grande vitesse. On peut penser que, pour ces

conditions, la concentration des lourds ne reste pas uniforme dans l'écoulement et qu'il peut s'établir un gradient de concentration entre la paroi et le noyau turbulent; une étude systématique de ce phénomène reste à faire.

Conclusion

L'étude expérimentale effectuée a donc permis d'établir une corrélation empirique valable pour l'ensemble des produits testés. La faible dispersion des résultats laisse peu d'incertitude sur la détermination de cette corrélation moyenne; par ailleurs, les nombreuses vérifications de mesure effectuées limitent la possibilité d'erreurs systématiques sur la valeur absolue du coefficient d'échange qu'on peut calculer à partir de cette corrélation moyenne.

Les effets séparés des paramètres Reynolds et Prandtl ayant été analysés, l'extrapolation des résultats à l'aide de la corrélation présentée doit pouvoir se faire avec une assez faible incertitude.

ÉTUDE DE L'ENCRASSEMENT DES PAROIS CHAUFFANTES PAR LES POLYPHÉNYLES

Le phénomène d'encrassement des parois chauffantes ou *fouling* étant très complexe et influencé par un

très grand nombre de paramètres, il a paru nécessaire de reprendre cette étude dans le cadre du projet ORGEL à la lumière des résultats déjà enregistrés dans d'autres laboratoires.

Deux séries d'essais ont pu être envisagées :

a) La première, où les différents paramètres sont ajustés aux valeurs qu'ils auront dans le réacteur, en particulier la composition du produit, les conditions thermiques et hydrodynamiques, etc. Cette série permettra de connaître les risques d'encrassement dans le réacteur.

b) La seconde, où on essaiera de déterminer plus particulièrement l'influence de tel ou tel paramètre, dans des conditions pouvant s'éloigner des conditions prévues dans le réacteur, de façon à pouvoir aboutir à une meilleure compréhension du phénomène.

L'étude du phénomène sur un essai s'effectue en deux temps :

1) On suit l'évolution du phénomène par son influence sur le coefficient de transfert de chaleur.

2) Après l'essai, le dépôt obtenu est examiné et analysé.

Le dispositif expérimental: boucle A

La boucle

La boucle d'essais a été conçue pour fonctionner de façon continue pendant toute la durée d'un essai prolongé.

Cela a conduit à automatiser l'installation et à doubler un certain nombre d'éléments du circuit.

La figure 3 représente le schéma de la boucle, dont les caractéristiques principales sont les suivantes :

Pression maximale: 40 kg/cm²

Température maximale sur l'ensemble de la boucle: 450 °C

Débit: 0,6 m³/h à 3 m³/h environ.

Le circuit principal, tuyauteries, vannes, pompes et instruments de mesure, ainsi que les capacités, sont en acier inoxydable. Une portion de circuit en acier doux est montée pour certains essais. Pour éviter des pertes de produits importantes pendant un essai de longue durée, les vannes sont du type à soufflet et les pompes sont du type étanche, à rotor immergé et paliers à roulements à billes. Deux filtres sont montés en parallèle; ils sont constitués chacun par une cartouche filtrante démontable en marche. Les cartouches filtrantes sont en acier inoxydable fritté de porosité 3 μ ou 7 μ .

Une mesure de perte de charge placée aux bornes des filtres permet de connaître leur état de colmatage.

L'ensemble du circuit est «tracé» au moyen de cordons chauffants sous gaine métallique et calorifugés à l'amiante. Il est divisé en une quarantaine de portions ayant chacune un circuit de réchauffage autonome et un thermocouple de contrôle. Un scrutateur mécanique permet de comparer successivement les indications des différents thermocouples à une tension de référence et assure la régulation de chauffage.

Automatismes et sécurités

Prévue pour fonctionner sans surveillance pendant

des périodes assez longues (nuits, fins de semaine), la boucle est dotée d'un certain nombre d'automatismes et sécurités.

La puissance du canal d'essais, le débit et la température du fluide sont réglés automatiquement. Les sécurités sont réparties en deux classes: l'une conduit à l'arrêt du chauffage du canal d'essais; l'autre conduit en outre à la vidange de l'installation. On a conçu l'installation pour éviter le plus possible une telle vidange. En cas de défaut d'un débitmètre ou d'une pompe, l'installation se remet en route automatiquement sur les appareils de secours; de même, en cas de panne de courant de courte durée.

Le canal d'essais

La figure 4 représente ce canal; il est à section annulaire, et l'élément chauffant, à chauffage direct, est un tube lisse en acier inoxydable, de diamètre extérieur 12 mm, d'épaisseur 0,5 mm, et de longueur active 20 cm. Les barres d'amenée de courant, de même diamètre que le tube chauffant, sont frettées sur ce dernier.

L'écoulement du fluide s'effectue entre ce tube et un tube concentrique dit « tube flottant », de diamètre intérieur 16 mm. Le centrage de l'âme chauffante sur ce tube est assuré en trois sections par des aiguilles de quartz calibrées, maintenues dans des plans diamétraux à 120 ° par des méplats usinés sur les cosses d'amenée de courant. L'âme chauffante et le tube flottant sont placés dans un tube de force. Les brides d'extrémité sont isolées électriquement de l'enveloppe. Les barres d'amenée de courant sont percées en leur centre de façon à permettre le passage des fils de thermocouples soudés sur la paroi interne du tube chauffant.

Le canal d'essais ainsi réalisé a un diamètre hydraulique de 4 mm, et les barres d'amenée de courant jouent le rôle de longueurs de tranquillisation sur 50 diamètres à l'amont et 25 diamètres à l'aval. Les vitesses d'écoulement peuvent varier entre 2 et 10 m/s. L'alimentation en courant alternatif permet une puissance réglable entre 0 et 48 kW (24 V, 2 000 A), ce qui permettrait d'atteindre des flux de 350 W/cm².

Conduite des essais

L'essai consiste:

a) A faire circuler le produit aux caractéristiques prévues en mesurant périodiquement le coefficient d'échange et prélevant de temps en temps des échantillons de produits pour analyses.

b) A examiner et analyser la surface du canal chauffant après le démontage de fin d'essais.

Essais effectués et résultats

L'objectif du programme était le suivant:

a) Effectuer deux essais de longue durée avec du téraphényle OM2 propre dans une boucle entièrement en acier inoxydable. Ces essais serviraient ensuite d'essais de référence.

b) Mettre en évidence deux sortes d'encrassement: encrassement particulière prépondérant à faible vitesse

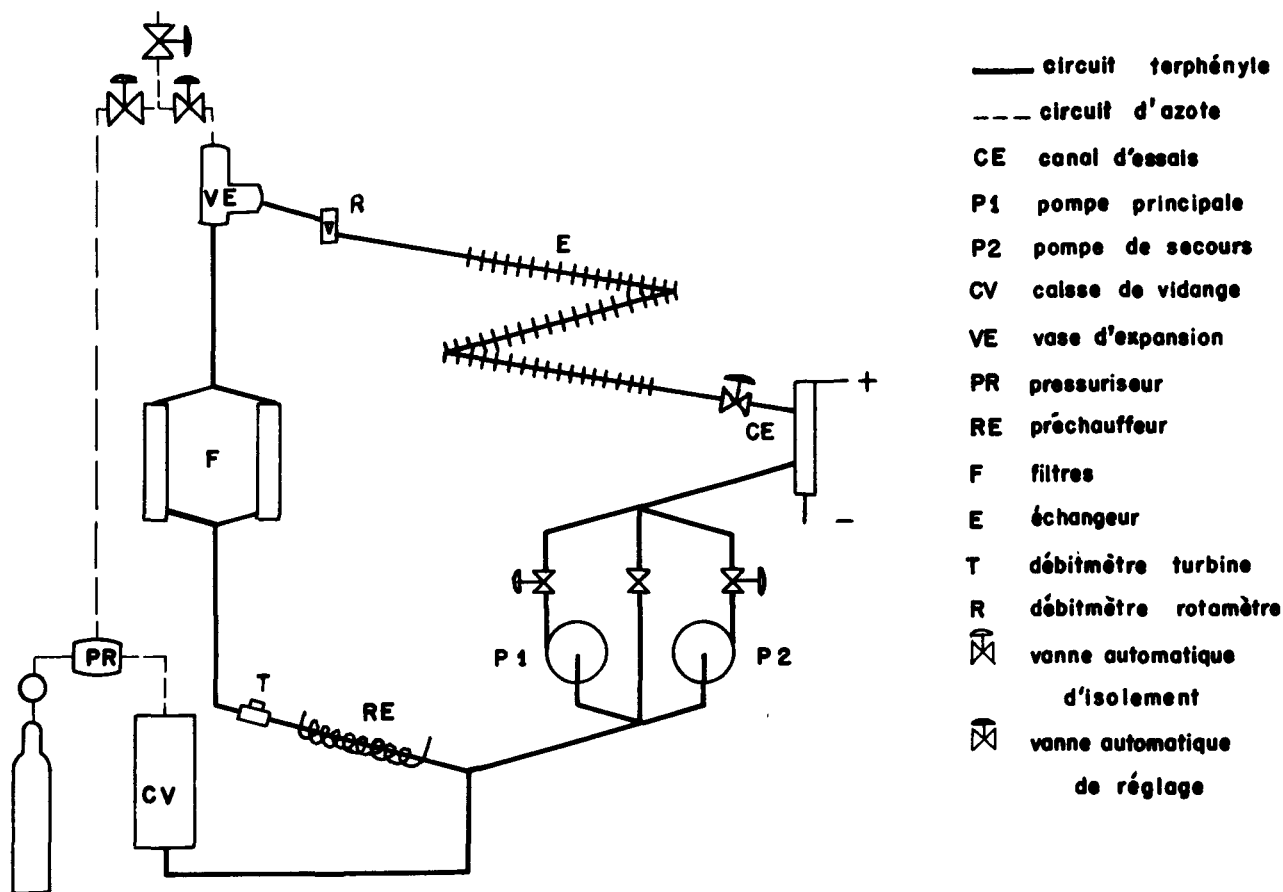


Figure 3. Boucle pour l'étude de l'encrassement, schéma

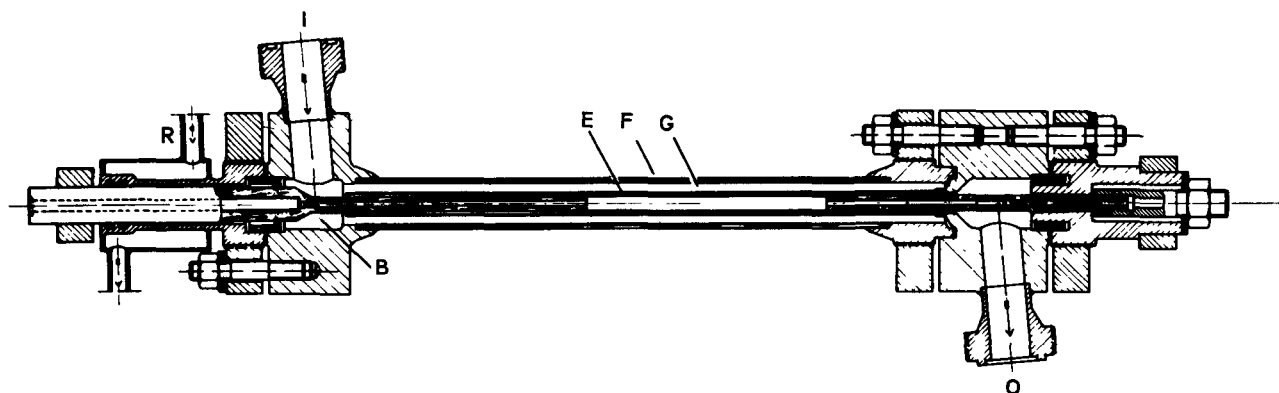


Figure 4. Canal d'essais de la boucle pour l'étude de l'encrassement

I: Entrée du fluide; O: Sortie du fluide; B: Barre d'aménée du courant; R: Refroidissement de la barre B; E: Tube chauffant; G: Tube de guidage; F: Tube de force

et donnant un dépôt lisse contenant 80% environ de matières organiques; encrassement moléculaire prépondérant à grande vitesse et qui donne un dépôt à peu près entièrement inorganique. Il y aurait transport de fer du circuit sur l'élément chauffant.

On a donc mis dans la boucle une section de corrosion en acier doux et on a fait circuler à grande et faible vitesse du terphényle OM2, contenant des produits lourds et du chlore.

Le tableau 3 résume le programme d'essais effectué. La teneur en eau du produit est restée inférieure à 100 ppm, en général.

La variation du coefficient d'échange est donnée par la figure 5.

On peut tirer de ces essais les constatations suivantes [3, 4]:

Lors de l'essai A, le coefficient d'échange n'a absolument pas varié pendant les 918 heures d'essai; la

Tableau 3. Programme des essais d'encrassement

Essai	Durée (heures)	Vitesse (m/s)	Température initiale (°C)		Densité flux (W/cm ²)	Section d'acier doux	Produits lourds (%)	Chlore (ppm)
			Fluide	Paroi				
A	918	3	380	465	52	non	0,5	faible
B	248	3	405	502	62	non	0 à 2,5	faible
C	550	7,5	380	470	140	oui	0,5 à 1	2
D	240	3	380	470	55	oui	15	2
E	280	7,5	382	478	117	oui	28	2
F	120	3	382	478	56	oui	27	3
G	504	7,5	380	476	117	oui	0,5	20
H	414	3	380	478	55	oui	1,5	30
I	515	3	380	482	50	oui	38	40

surface chauffante était très propre après démontage. Rappelons que toute la boucle est alors en acier inoxydable.

L'essai B était destiné à tester un fonctionnement à températures plus élevées; on n'a pas trouvé sur la surface chauffante de dépôt dur et adhérent, mais une boue ressemblant à des produits de pyrolyse qui affectent notablement le coefficient d'échange: il a en effet baissé de 15% en 250 heures. Il semble donc

qu'on ait atteint une limite de fonctionnement en température pour le terphényle OM2.

Les essais C et D devaient montrer l'influence d'une section de tuyautage en acier doux sur l'encrassement tout en utilisant un fluide propre; le coefficient d'échange, lors de l'essai C, a augmenté de 4% en 450 heures. La surface chauffante portait un dépôt rugueux contenant environ 95% de fer.

Lors de l'essai D, le coefficient d'échange est resté

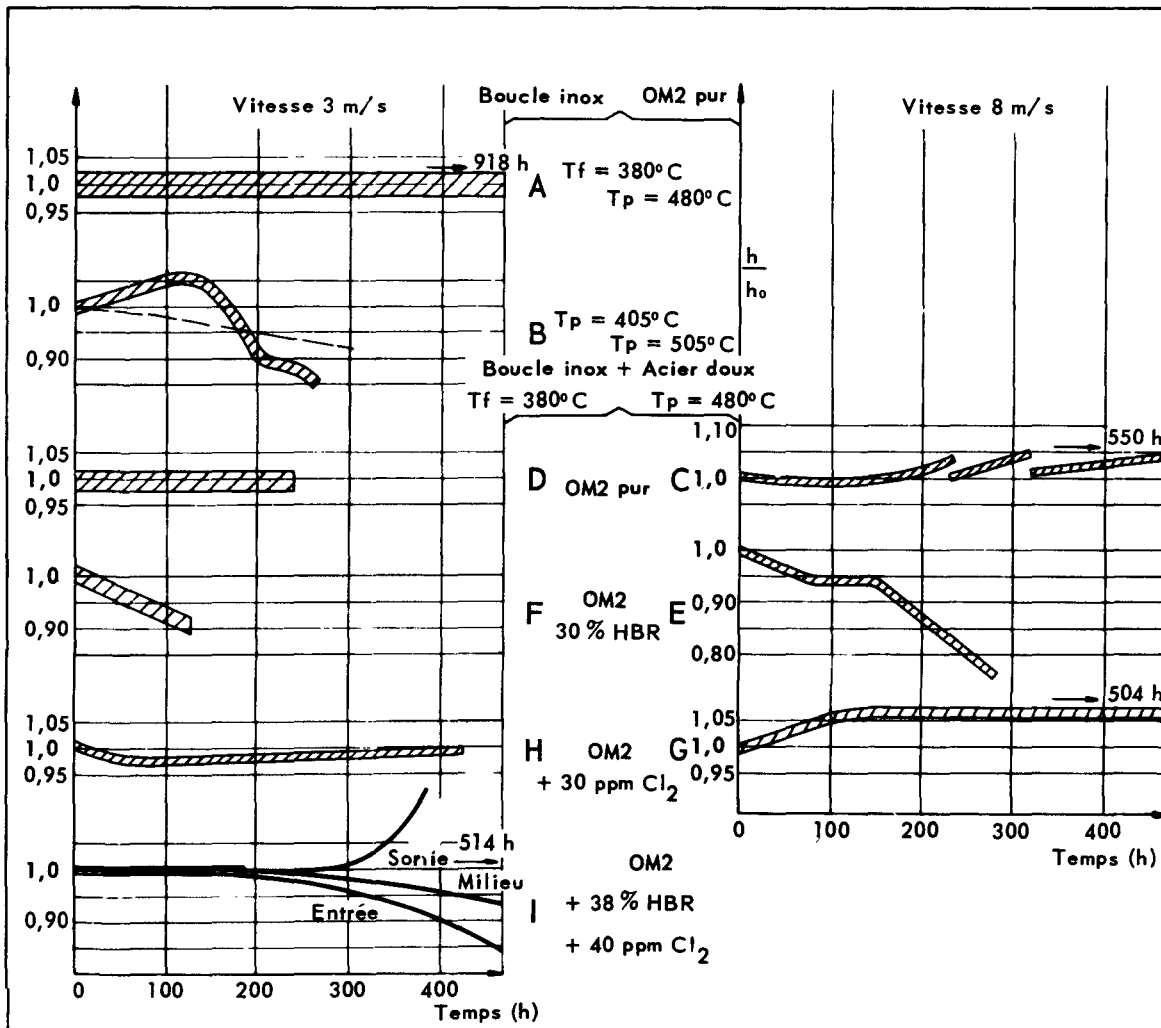


Figure 5. Essais d'encrassement. Variation relative du coefficient d'échange

parfaitement constant, malgré la présence de 15% de produits lourds de pyrolyse; la surface chauffante était parfaitement propre après l'essai.

Les *essais E et F* étaient effectués avec du terphényle OM2 additionné de produits lourds qui — on l'a vu par la suite — contenaient de l'oxygène sous forme combinée. Une section d'acier doux était en place dans le circuit. Le coefficient d'échange a baissé de 20% en 250 heures pour l'essai à grande vitesse (E) et de 8% en 100 heures pour l'essai à basse vitesse (F). La surface chauffante était recouverte, après les essais, d'un dépôt noir lisse et adhérent. Il atteignait une épaisseur de 25 microns pour l'essai E, ce qui correspondrait à une conductibilité thermique de ce dépôt voisine de la conductibilité du terphényle. A l'analyse chimique, ce dépôt contenait 22% de fer et correspondrait à un taux de déposition de $7 \mu\text{g}/\text{h cm}^2$. Le dépôt de l'essai F contenait 8% de fer et correspondrait à un taux de déposition de $6 \mu\text{g}/\text{h cm}^2$ environ.

Les *essais G et H* ont été réalisés avec du terphényle OM2 contenant 30 ppm de chlore, la section d'acier doux étant toujours en place. Les coefficients d'échange ont très peu varié et les surfaces chauffantes ne présentaient pratiquement pas de trace de dépôt à la fin des essais.

L'*essai I* a été réalisé avec du terphényle OM2 additionné de 38% de produits lourds fabriqués par pyrolyse en atmosphère exempte d'oxygène; le terphényle contenait 40 ppm de chlore.

On a observé une diminution du coefficient d'échange de 12% en 500 heures dans la partie amont, sur laquelle on a retrouvé un dépôt lisse; par contre, sur la partie aval, le coefficient d'échange a notablement augmenté et on a retrouvé un dépôt très divisé, sous forme de petites pyramides réparties sur la surface. On n'a pas encore analysé les dépôts, mais cet essai semble montrer que l'effet de l'encrassement n'est pas catastrophique, même avec de fortes teneurs en lourds et en chlore; l'essai confirme que le très fort encrassement observé lors des essais E et F provient probablement de l'oxygène contenu alors dans le produit testé.

En résumé, on a constaté que seule avait une influence nette sur l'encrassement la présence d'oxygène combiné dans le terphényle. Des essais de vérification doivent être poursuivis, mais les essais déjà réalisés permettent de penser que l'encrassement peut être évité dans les réacteurs à liquide organique, même si ces liquides contiennent des produits lourds,

à condition d'utiliser des terphényles très peu chargés en impuretés et ne contenant pas d'oxygène. Si on en croit la référence [5], les essais en pile sous radiation n'apportent pas de changement considérable par rapport aux essais hors pile; les essais décrits ici apportent dès maintenant un élément optimiste aux projets du réacteur ORGEL.

CONCLUSION

Les essais effectués depuis 1961 au Centre d'études nucléaires de Grenoble ont permis de fournir la corrélation de transfert de chaleur $Nu \neq 0,00835 Re_b^{0,9} Pr_b^{0,4}$, valable avec une très faible dispersion pour 5 terphényles différents. D'autre part, ils ont montré que l'encrassement n'était pas sensible si on prenait des précautions pour assurer la propreté du produit et du circuit. On n'a, en effet, noté un encrassement des surfaces chauffantes à 480 °C de température de paroi et 380 °C de température de fluide que lorsque le terphényle contenait de l'oxygène combiné. Par contre, il est apparu qu'une température de paroi supérieure à 500 °C entraînait une diminution du coefficient d'échange par pyrolyse locale du produit sur la paroi.

REMERCIEMENTS

Nous remercions la Communauté européenne de l'énergie atomique, qui a permis ces travaux, exécutés sous contrat pour son compte, et en particulier M. Lesage, qui a été notre correspondant de cet organisme pendant toute la durée du contrat.

Nous exprimons notre gratitude à M. Martin-Lefèvre, qui a participé aux études expérimentales, à MM. Michel et Teytu, qui ont conduit la construction des installations, ainsi qu'au personnel du Service, dont l'activité a permis d'obtenir ces résultats.

BIBLIOGRAPHIE

1. Martinelli, Transaction of ASME, 69-947 (1947).
2. Rapport EURATOM, rapport final du contrat 007-60-12-ORGF, tome 1: *Appareils de mesure de caractéristiques physiques*.
3. Rapport EURATOM, rapport final du contrat 007-60-12-ORGF, tome 2: *Etude du coefficient d'échange et de l'influence de l'encrassement sur l'échange de chaleur*.
4. Rapport EURATOM, rapport final du contrat 085-62-12-ORGF.
5. Charlesworth, D. H., *Fouling in organic-cooled systems*, Rapport CRCE 1096 (Chalk River, Ontario, Canada).

ABSTRACT—RÉSUMÉ—АННОТАЦИЯ—RESUMEN

A/93 France

Heat transfer with organic fluids

By J. Villeneuve et al.

Using a test channel with a circular cross section of 12 mm internal diameter, the following heat transfer

correlation, valid to about $\pm 6\%$, was determined for the terphenyls OMP and OM2 with 0, 10, 20 or 30% of high polymers: $Nu_b = 0.00835 Re_b^{0,9} Pr_b^{0,4}$. This correlation was established with fluxes ranging from 50 to 100 W/cm², temperatures from 290 to 410 °C and Reynolds number from 30 000 to 350 000.

Nine long-term tests were carried out (250 to 1 000

hours continuous running) to determine how deposition on the heating surfaces affects the exchange coefficient. The loop is made of stainless steel except for one part in soft steel. No deposits are observed even if the terphenyl contains 30 ppm of chloride, while, on the other hand, deposition is appreciable when heavy substances containing combined oxygen are added.

A/93 Франция

Свойства теплопередачи органических теплоносителей

Ж. Вильнев *et al.*

В экспериментальном канале с круглым сечением внутренним диаметром 12 мм было определено следующее уравнение теплопередачи, точность которого находится в пределах $\pm 6\%$ для терфенилов ОМР и ОМ2 с 0, 10, 20 или 30%-ным содержанием высокомолекулярных полимеров: $Nu_g = 0,00835 Re_g^{0,9} Pr_g^{0,4}$. Это соотношение было установлено для потока от 50 до 100 $вт/см^2$ при температуре 290—410°С и числах Рейнольдса 30 000—350 000.

Было проведено девять длительных опытов (от 250 до 1000 ч при установившемся режиме) для того, чтобы определить влияние загрязнения нагреваемых поверхностей на коэффициент обмена. Петля была сделана из нержавеющей стали, за исключением одной части, сделанной из мягкой стали. Никакого загрязнения не наблюдается даже в том случае, когда содержание хлора в терфениле достигает 0,003%; напротив, это загрязнение является значительным, когда добавляются тяжелые продукты, содержащие кислород.

A/93 Francia

Tecnología de los fluidos orgánicos para transferencia de calor

por J. Villeneuve *et al.*

En un canal de ensayo de sección circular de 12 mm de diámetro interior, los autores han determinado la correlación de transmisión de calor $Nu_b = 0,00835 Re_b^{0,9} Pr_b^{0,4}$, válida, con un margen de error de $\pm 6\%$ para los terfenilos OMP y OM2, con 0, 10, 20 ó 30% de altos polímeros. Dicha correlación fue establecida en un intervalo de flujos de 50 a 100 W/cm^2 , de temperaturas de 290 a 410 °C y de números de Reynolds comprendidos entre 30 000 y 350 000.

Se efectuaron nueve ensayos prolongados (250 a 1 000 horas en régimen continuo) a fin de determinar el efecto que las incrustaciones que se depositan en la superficie de calefacción ejercen sobre el coeficiente de intercambio. El circuito es de acero inoxidable, salvo una parte que consiste en acero dulce; no se observa ninguna incrustación, aun si el terfenilo contiene 30 ppm de cloro; en cambio, la incrustación es considerable cuando se añaden productos pesados que contienen oxígeno combinado.

Burn-out in subcooled forced convection boiling of polyphenyls

By D. A. van Meel*

The investigations reported in this paper were started in 1961,** since only scarce information was available at that time on the burn-out properties of organic coolants composed of terphenyl isomers which are to be used in the Orgel reactor.

Reliable measurements had to be performed of the burn-out heat flux as a function of the rate of flow, pressure and temperature under conditions to be encountered in the Orgel reactor. Burn-out was studied for upward flow through a vertical round stainless-steel tube heated by the Joule effect using direct current. Since the coolant in the reactor will be pressurized with nitrogen to such an extent that the bulk temperature of the liquid is always lower than its saturation temperature, burn-out will occur only under the condition of subcooled boiling at the heating surface. The experiments were therefore limited to this condition.

The original composition of the coolant will be changed by radiolysis and pyrolysis, and products of higher volatility (gases and low-boilers) as well as of lower volatility (high-boilers) compared with terphenyls may alter the value of the burn-out heat flux if only because the saturation temperature at a given pressure deviates from its initial value. An important part of the experimental programme therefore consists of a study of the burn-out heat flux as a function of the concentration of low- and high-boiling components added to mixtures of terphenyl isomers. This study is not yet terminated at this moment. A calculation of the saturation temperature, which enters directly in the so-called degree of subcooling, is not very reliable for the complex systems under consideration. An apparatus was therefore constructed enabling its accurate measurement even if small amounts of very volatile substances are present.

APPARATUS

The test loop

A schematic diagram of the stainless-steel test loop as used in the experiments on the effects of gases and low-boilers is presented in Fig. 1. The loop is completely filled with about 30 kg of liquid. It contains a vessel allowing thermal expansion of the liquid, in which a diving-bell floats on molten solder. The solder

separates the liquid from the nitrogen which is used to pressurize the liquid. In the experiments in which the liquid was pressurized in direct contact with nitrogen, this expansion vessel was not used. Instead, a vessel was mounted between the pump outlet and the filter. This vessel, as well as the suction vessel, was partly filled with liquid which was pressurized directly with nitrogen.

The loop is trace-heated electrically and insulated with expanded mica. The pump has been specially designed and constructed and consists of a modified single-stage regenerative pump provided with a mechanical seal that is cooled with oil to about 150 °C. Its capacity is 0.75 m³/h at a pressure head of 5 atm.

The test section

A simplified diagram of the test section is given in Fig. 2. The essential part is the test tube which is made of stainless-steel 316. Its dimensions are: length, 500 mm; inner diameter, 5.07 mm; wall thickness, 0.25 mm. Pieces of tube having a relative wall-thickness variation of less than 2% could be selected from commercially available tubing using β -ray wall-thickness measurements.

The test tube is enclosed within a pressure chamber in which the same pressure exists as within the test tube. To avoid deformation of the tube by thermal expansion, the tube is pre-stressed at room temperature, so that it will be practically unstressed when heated.

An unheated length of 500 mm, 5 mm bore tube precedes the test tube.

INSTRUMENTATION

Burn-out detection

A burn-out detector, actuating a switch that cuts off the heating current within 14 ms after a hot spot has been detected, prevents the test tube from being damaged. The detector works on the well-known principle of the Wheatstone bridge, in which the upper half and the lower half of the test tube are incorporated. The bridge signal is differentiated in order to ensure action in the case of fast-changing signals only.

Temperatures

The temperatures at the inlet and outlet of the test tube are measured by means of calibrated bare Ni-NiCr

* Central Technical Institute TNO, The Hague.

** The studies were made under contracts with EURATOM.

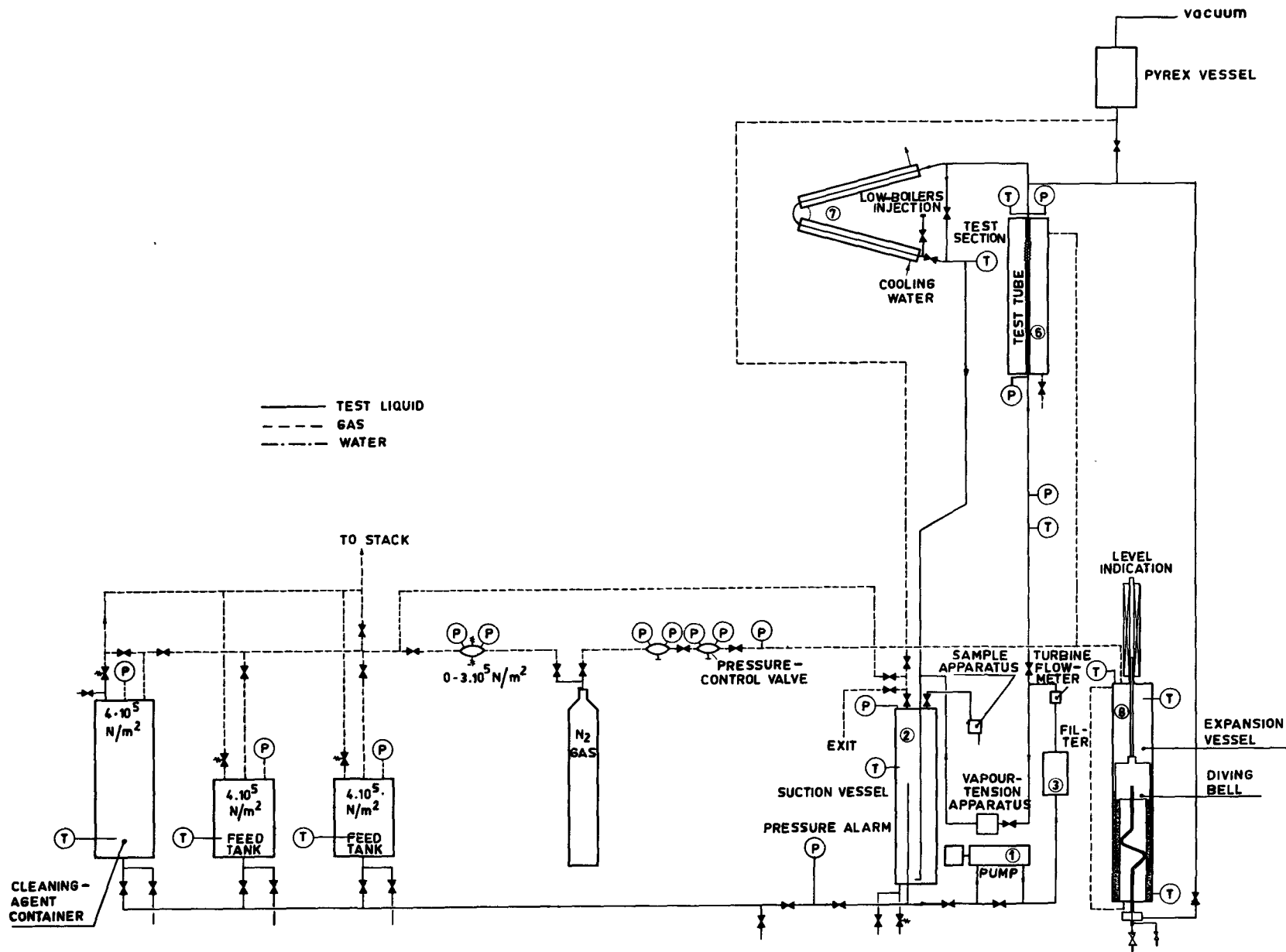


Figure 1. Flow-sheet of loop for burn-out experiments

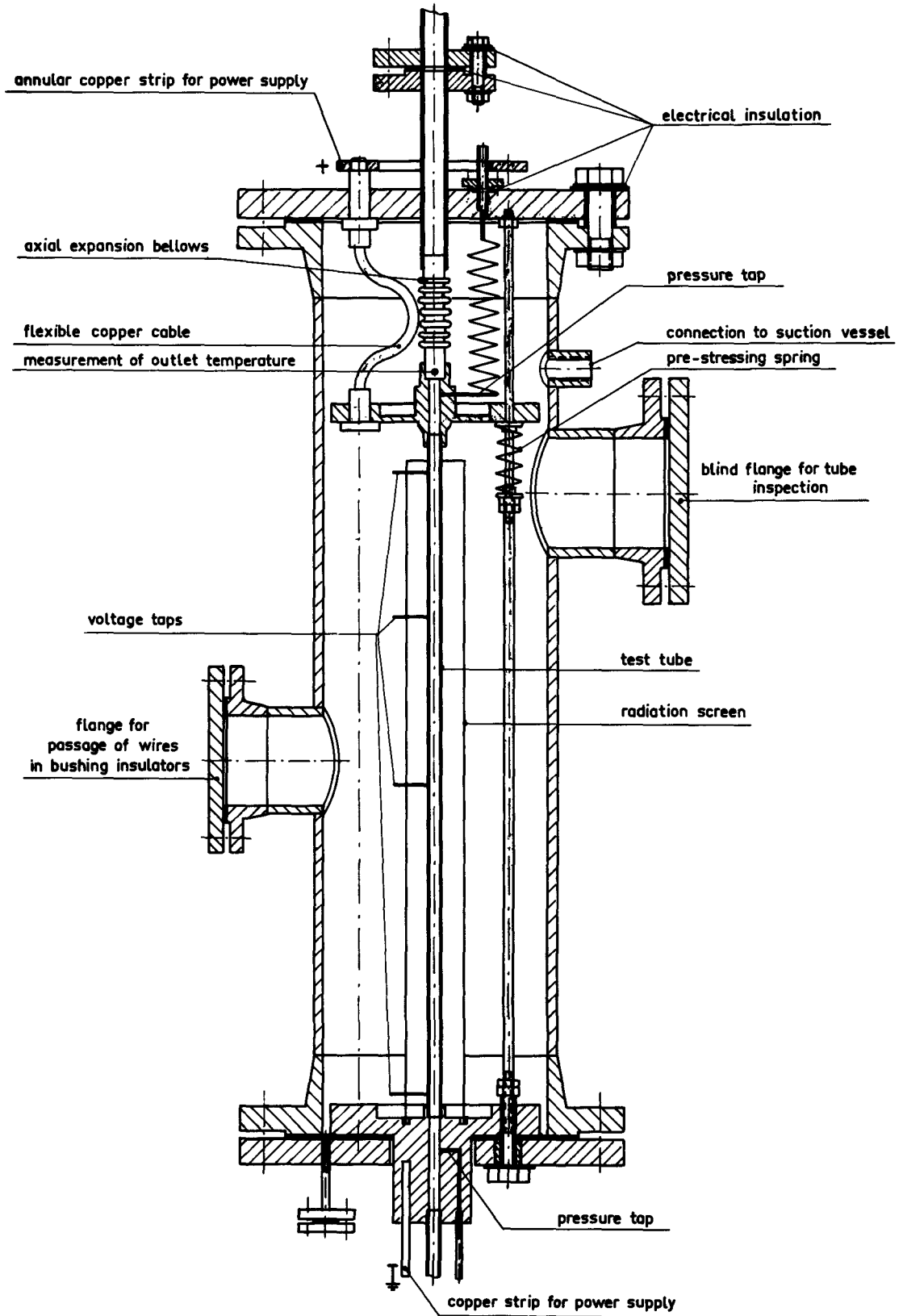


Figure 2. Test section burn-out experiments on terphenyl coolants

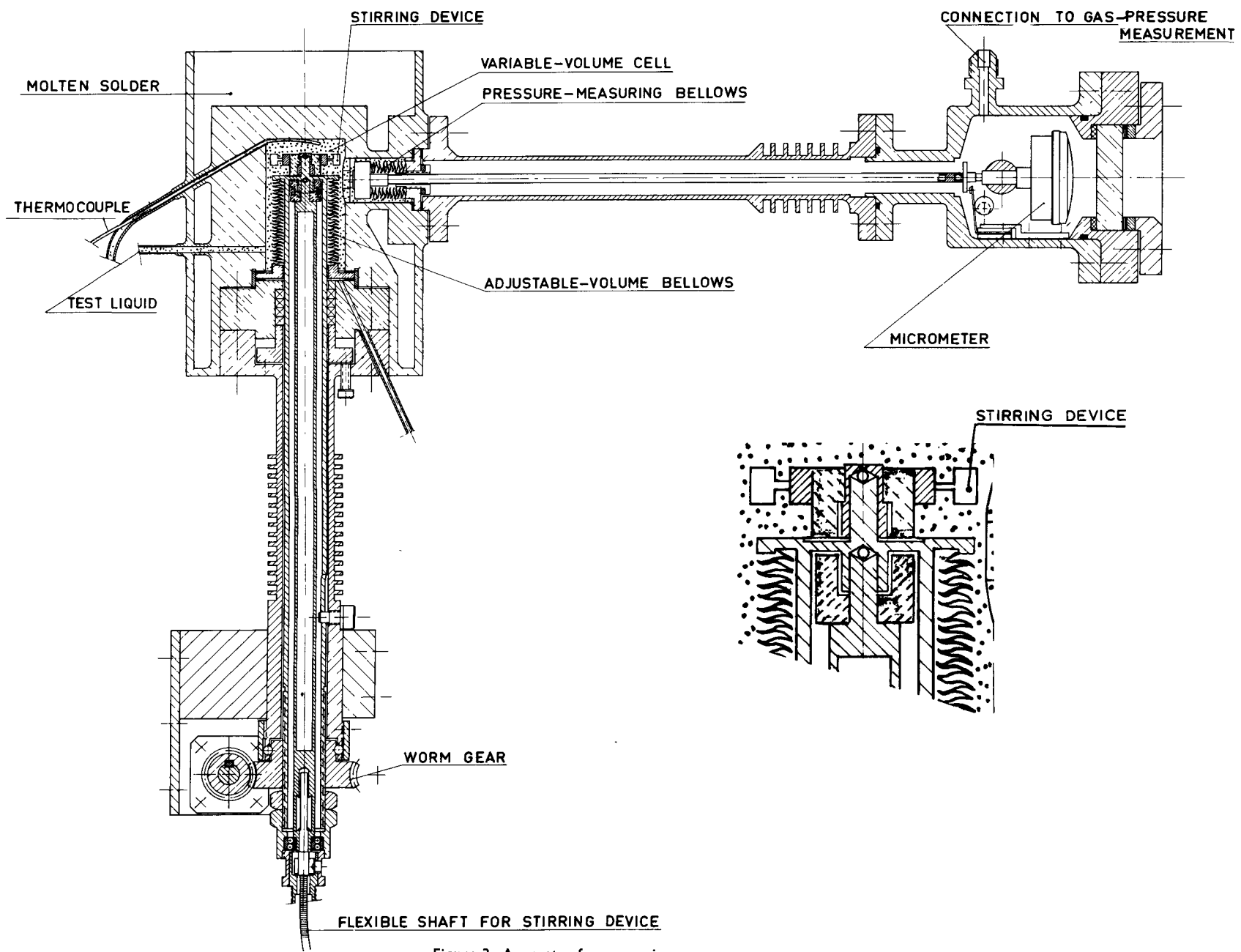


Figure 3. Apparatus for measuring vapour pressure

thermocouples. The temperatures are simultaneously recorded on a double-line recorder. The location at which the outlet temperature, used to derive the degree of subcooling, is measured is indicated in Fig. 2. This location is sufficiently close to the location of the burn-out to neglect heat losses in between. The accuracy of the temperature measurement is 0.5 °C.

Pressure

The static pressure at the outlet of the test tube as well as the pressure drop over the test tube are continuously recorded using Barton differential-pressure cells. The connection tubes to the cells are filled with HB 40* (Monsanto) which has a low melting point. This product was chosen because the cells cannot withstand temperatures above the melting point of the terphenyl mixtures which are investigated. Recently, very thin membranes made of teflon were introduced in this system, in order to separate the contents of the loop from the manometer liquid. The accuracy of pressure measurement is about 1%.

Flow

A recording turbine flow meter is used to measure the volumetric flow rate. Since experiments on the pressure drop over the unheated entrance tube of the section showed very good agreement with the resistance formula of Blasius, the flow meter can be frequently checked. The accuracy of flow measurement is about 2%.

Power

The voltage drop over the upper 10 cm part of the test tube is recorded as well as the direct current through the tube. The accuracy of the value of electrical power, as calculated by multiplication of current and voltage drop, is about 2%.

Saturation temperatures

An apparatus for measuring vapour pressures has been developed, a diagram of which is presented in Fig. 3. The vapour space above the liquid in the measuring chamber (adjustable-volume cell) may be reduced to practically zero during the measurement. As a consequence the composition of the liquid is not changed by evaporation of very volatile components. The adjustability of the volume of the cell is also needed to take up the thermal expansion of the liquid contents. During the measurement, the liquid is stirred continuously. The measuring chamber is surrounded by a bath of molten solder heated with electric-heating cable inserts.

For the measurement of the saturation temperature as a function of pressure, the temperature is kept constant at a predetermined value. Pressure is measured by measuring the gas pressure needed to obtain zero displacement of the small pressure-measuring bellows, the position of which is indicated by a micrometer. Complete liquid-filling of the

variable-volume cell is observed if, owing to the incompressibility of the liquid, this measuring bellows cannot be returned to its zero position. Careful measurements with systems for which well-established data are available showed the accuracy to be 0.5%.

As indicated in Fig. 1, the apparatus is connected permanently with the test loop, which enables measurement of the saturation temperature while burn-out measurements are going on.

HEAT BALANCES

A comparison of the electrical heat input and the increase of the heat content of the liquid shows that the total heat loss of the test tube is about 3%. This agrees with estimates of conduction and radiation losses by calculation. Most of the heat losses are to the lower end flange of the test section. Since only the upper 10 cm part is used for measuring the electrical heat input, no corrections are made as in that part heat losses may be neglected.

PHYSICAL PROPERTIES

Composition of mixtures of terphenyl isomers

The mixtures of terphenyl isomers are manufactured by Progil (France). The liquid to be used in Orgel is indicated as OM₂. Its composition is: diphenyl < 1 wt%, o-terphenyl 14–16 wt%, m-terphenyl 79–81 wt%, p-terphenyl 3–5 wt%. Another liquid tested is OM₁, having the composition: diphenyl < 1 wt%, o-terphenyl 64–66 wt%, m-terphenyl 31–33 wt%, p-terphenyl 2–4 wt%.

Density, viscosity, specific heat

The values of these properties were obtained from EURATOM, Ispra; Centre d'études nucléaires, Grenoble; and Progil. The only property used in the correlations is density.

Saturation temperatures

OM₂. In the burn-out measurements on OM₂ pressurized in direct contact with nitrogen the curve available from CEN Grenoble as given in Fig. 4 was used, since at that time no results of self-performed measurements were available. From recent measurements of vapour pressures with the apparatus described previously the values given in Fig. 4 and indicated by Central Technical Institute TNO were obtained.

OM₁. For this mixture vapour-pressure data of Progil were used (Fig. 4).

OM₂-benzene systems. In Fig. 5 results of measurements with OM₂ containing 0.2, 0.5, 1 and 1.5 wt% benzene are presented. Attention is drawn to the fact that a linear relation is found when a plot of pressure vs. benzene concentration at constant temperature is derived from this graph.

OM₂-diphenyl systems. The results of the measurements with OM₂ containing 3, 5, 6 and 9 wt% diphenyl are presented in Fig. 6. Regarding OM₂ as one and

* Partially hydrogenated terphenyls.

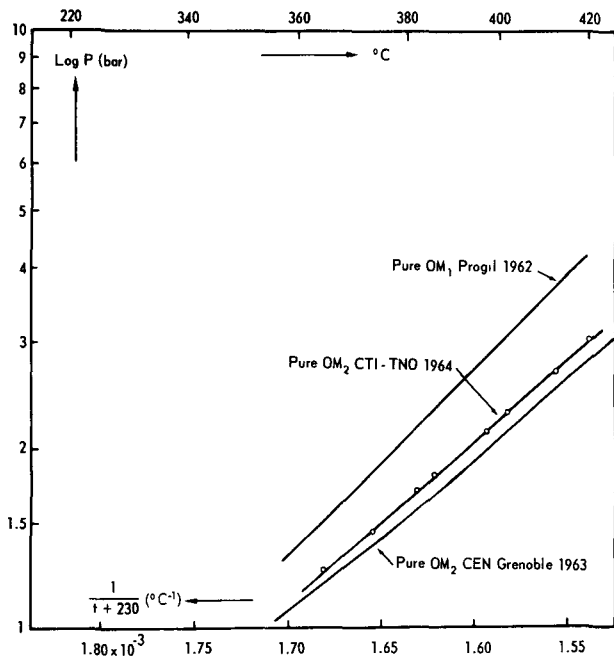


Figure 4. Vapour-pressure data of pure OM₁ and OM₂

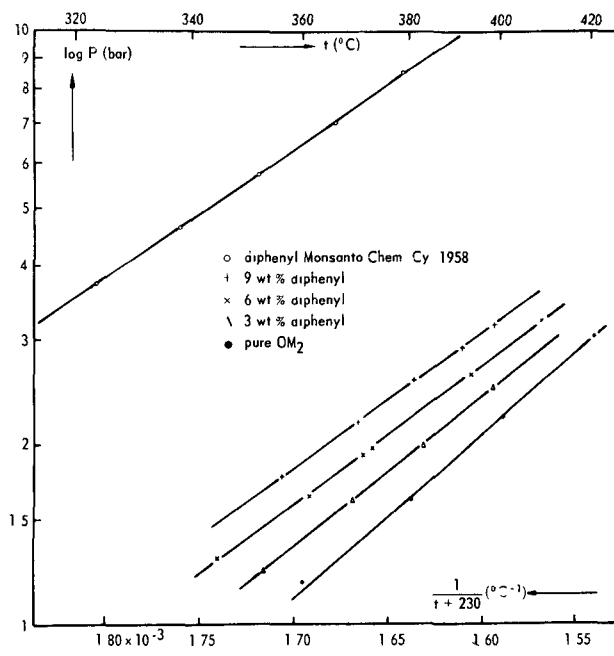


Figure 6. Vapour-pressure data of OM₂-diphenyl mixtures

diphenyl as the other component of a binary system, it may be concluded from these results that Raoult's law can be applied.

RESULTS OF THE MEASUREMENTS OF THE BURN-OUT HEAT FLUX

General

In an early stage of the investigations a series of measurements was made in order to find out whether the heat flux at the moment that the burn-out detector cuts off the heating current differs from the heat flux at

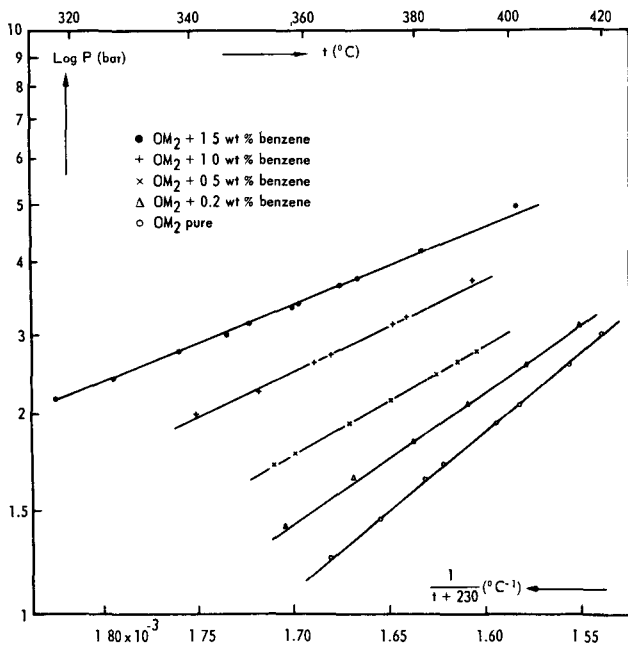


Figure 5. Vapour-pressure data of OM₂-benzene mixtures

which the test tube is really damaged. This was done by stepwise decreasing to zero the sensitivity of the detector. These experiments were made with water as a test liquid. No significant deviations were found, and the heat flux at which the detector cuts off the heating current is therefore considered to be equal to the burn-out heat flux. The degree of subcooling Δt_s is defined as the difference between the saturation temperature at the static pressure at the test tube outlet and the outlet temperature of the liquid.

The measuring procedure is as follows. First, the desired level of pressure is adjusted. Next, a flow rate of the liquid is chosen. The power input into the test tube is then increased until the detector cuts off the current. Because of the heat input into the test tube, the temperature level of the circulating liquid is increased, and consequently the degree of subcooling is decreased. In this way a series of burn-out heat fluxes is obtained at constant mass flow and constant pressure as a function of the degree of subcooling. At the end of a series the liquid is cooled using the water-cooled heat exchanger, another value of mass flow is chosen and the cycle is started again.

At the location of burn-out a very thin black layer is deposited on the inner tube surface. However, even in a case in which about 400 "burn-outs" were produced in one and the same tube, no effects of changing surface conditions on the burn-out heat flux could be detected.

OM₂ pressurized with nitrogen

About 600 runs were made with this system.* For the purpose of correlation 312 runs were used, made

* The complete set of data is given in *Research on the influence of the conditions of flow, subcooling and composition on the burn-out heat flux of polyphenyl reactor cooling agents*, TNO Status Report VIII, Appendix Summary of run data on OM₂.

at an outlet static pressure of 2.9 bar. The other runs, made at pressures in the range of 1.5–4.5 bar, were afterwards compared with the correlation and no significant effect of pressure was found. The equation connecting the burn-out heat flux Φ with the mass velocity G and the degree of subcooling Δt_s is:

$$\Phi = 57 + 9.17 \times 10^{-3} \times G + 3.16 \times 10^{-3} \times G^{3/4} \times \Delta t_s \quad (1)$$

The equation was derived by applying the method of least squares for linear regression on the variables G and $G^{3/4} \times \Delta t_s$. As already mentioned previously, in these experiments the degree of subcooling Δt_s is based on the curve of CEN Grenoble given in Fig. 4. Since this vapour-pressure curve is valid for OM₂ without nitrogen, the real degree of subcooling will be lower. Investigations on this subject are being done at this moment.

Eq. (1) is valid for pressures between 1.5 and 4.5 bar, for mass velocities between 2 100 and 9 650 kg/m² s and for values of Δt_s from 1–93 °C. The correlation coefficient for this equation is 0.96. The mean deviation of the experimental data from the equation is about 8%. Because in individual series of measurements deviations are in the order of only 2%, it is believed that this value of 8% is caused by variations of the isomeric composition of different batches, or possibly by the presence of small amounts of light decomposition products which could not be detected at the time these runs were made.

OM₁ pressurized with nitrogen

With this system 16 runs were made at an outlet pressure of 2.9 bar for three values of the mass velocity. The results were evaluated in the same way as indicated in the previous section.

The resulting equation is:

$$\Phi = 55 + 10.9 \times 10^{-3} \times G + 3.37 \times 10^{-3} \times G^{3/4} \times \Delta t_s \quad (2)$$

The vapour-pressure curve, again for OM₁ without nitrogen, is given in Fig. 4. The equation is valid for mass velocities between 4 000 and 11 000 kg/m² s and degrees of subcooling between 3° and 48 °C. The correlation coefficient is 0.998, the mean deviation about 2%.

OM₂ pure

Experiments on gas-free OM₂ were made in the test loop to which the apparatus for the measurement of vapour pressure was connected. The degree of subcooling is derived from the CTI-TNO curve in Fig. 4. The static pressure at the outlet of the test tube was 2.9 bar. The results could be correlated with the same type of equation as used before:

$$\Phi = 81 + 9.17 \times 10^{-3} \times G + 3.16 \times 10^{-3} \times G^{3/4} \times \Delta t_s \quad (3),$$

the mean deviation being about 4%.

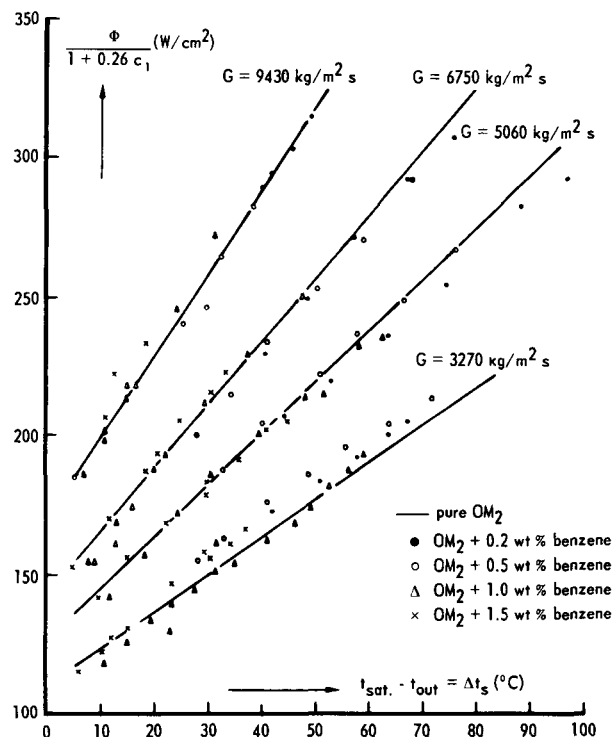


Figure 7. Burn-out heat flux of OM₂-benzene mixtures

In view of what is said about the degree of subcooling used for Eq. (1) the fact that the second and third coefficient are the same in Eqs. (1) and (3) seems to be fortuitous.

Pure OM₂ containing benzene

Again the static pressure at the test tube outlet was 2.9 bar. Basing the degree of subcooling upon the measurements presented in Fig. 5, the results could be correlated within 5% by extending Eq. (3) with a factor that is linear in the benzene concentration. The equation found is:

$$\Phi = (1 + 0.26c_1)(81 + 9.17 \times 10^{-3} \times G + 3.16 \times 10^{-3} \times G^{3/4} \times \Delta t_s) \quad (4)$$

In Fig. 7 the data are presented by plotting $\Phi(1 + 0.26c_1)^{-1}$ against Δt_s for different values of the mass velocity.

Pure OM₂ containing diphenyl

The results obtained with these systems, using vapour-pressure data from Fig. 6, may be correlated in the same way as indicated in the previous paragraph using the equation:

$$\Phi = (1 + 0.01c_2)(81 + 9.17 \times 10^{-3} \times G + 3.16 \times 10^{-3} \times G^{3/4} \times \Delta t_s) \quad (5)$$

DISCUSSION

According to our results there is an effect of mass velocity even if the degree of subcooling tends to zero. This follows also from the formulae given, in contrast to equations of Core and Sato [1] and of Robinson and

Lurie [2] for analogous liquids, which are of the type $\Phi = A + B \times G^n \times \Delta t_s$.

The results obtained with the system OM_2 -benzene prove that the use of the correct degree of subcooling is in itself not sufficient to obtain one single correlation, and that a function of concentration has to be included. It is to be expected, however, that the empirical finding that a correlation is obtained by multiplying the complete equation (1) by a factor depending only on concentration is of only limited validity.

In connection with the influence of benzene on the burn-out heat flux of OM_2 it may be useful to observe that if the burn-out heat flux is not based upon the true degree of subcooling of the solution of benzene in OM_2 , but on the saturation temperature of pure OM_2 ,

benzene is found to decrease the burn-out heat flux considerably.

Symbols

- Φ : burn-out heat flux, W/cm²
 G : mass velocity, kg/m² s
 Δt_s : degree of subcooling, °C
 c_1 : concentration of benzene, weight percentage
 c_2 : concentration of diphenyl, weight percentage

REFERENCES

1. Core, T. C., and Sato, K., USAEC report IDO-28007 (February 1958).
2. Robinson, J. M., and Lurie, H., USAEC Research and Development Report NAA-SR-7954, 1962.

ABSTRACT—RÉSUMÉ—АННОТАЦИЯ—RESUMEN

A/590 Pays-Bas

Caléfaction en convection forcée par ébullition sous-refroidie de polyphényles

par D. A. van Meel

Depuis 1961, le TNO, exécute un vaste programme de recherches sur l'influence de la vitesse du fluide, le degré de sous-refroidissement et la composition de fluide sur le flux thermique critique de polyphényles qui circulent en montant à travers un tube circulaire en acier inoxydable, chauffé par effet Joule.

Une description de la boucle d'essai est donnée.

On présente les résultats obtenus avec un grand nombre d'expériences sur des mélanges d'isomères du terphényle pressurisés par contact direct avec de l'azote. Ces résultats sont bien représentés par une équation du type suivant:

$$\Phi = a + b \cdot G + c \cdot G^{3/4} \cdot \Delta t_s$$

(Φ , flux critique; G , vitesse de masse; Δt_s , degré de sous-refroidissement).

Les valeurs des coefficients seront données pour les compositions suivantes (en poids):

a diphenyle 1%, o -terphényle 14-16%, m -terphényle 79-81%, p -terphényle 3-5%;

b diphenyle 1%, o -terphényle 64-66%, m -terphényle 31-33%, p -terphényle 2-4%.

Des paramètres, comme par exemple le degré de sous-refroidissement, sont basés sur les conditions régnant à l'orifice de sortie du tube d'essai, c'est-à-dire près du lieu de caléfaction.

Le flux, au moment où un brusque accroissement de la résistance du tube d'essai est indiqué par un avertisseur de caléfaction est interprété comme le véritable flux de caléfaction. Quelques expériences, dans lesquelles le tube d'essai était endommagé par un véritable brûlage ont démontré que cela était admissible.

Après ces mesures sur des terphényles sous azote, la boucle a été modifiée de telle sorte que le fluide et le

milieu pressurisant étaient séparés l'un de l'autre dans une cloche à plongeur par de la soudure fondue, permettant d'étudier les effets séparés des corps à bas point d'ébullition et des gaz.

Les résultats portent sur des terphényles ne contenant pas de composants volatils, ainsi que sur les effets de concentrations accrues d'azote, de benzène et de diphenyle. Ces résultats sont interprétés sur la base du degré de sous-refroidissement déduit des courbes de pression de vapeur déterminées expérimentalement. A cet effet, on avait développé un appareil à pression de vapeur permettant de procéder à des mesures exactes de la pression de vapeur en fonction de la température et de la composition de mélanges de terphényles et de substances très volatiles. Cet appareil, branché d'une façon permanente sur le boucle d'essai est caractérisé par la possibilité de faire des mesures dans un très petit volume de vapeur, ce qui permet d'éviter des changements dans la composition du liquide.

A/590 Нидерланды

Кризис кипения полифенилов в условиях принудительной конвекции и разности температуры насыщения и температуры охладителя на входе в реактор

Д. А. Ван-Меел

С 1961 года в Нидерландах ведутся широкие исследования влияния скорости жидкости, степени недогрева и состава жидкости на критический тепловой поток полифенилов, циркулирующий вверх по трубе круглого сечения из нержавеющей стали, нагреваемой джоулевым теплом.

зультаты опытов согласуются с уравнением типа:

$$\Phi = a + b \cdot G + c \cdot G^{3/4} \cdot \Delta t_s,$$

где Φ — критический тепловой поток; G — массовая скорость; Δt_s — степень недогрева.

Приведены значения коэффициентов для смесей следующего состава: 1) дифенил 1% вес., ортотерфенил 14—16% вес., метатерфенил 79—81% вес., паратерфенил 3—5% вес.; 2) дифенил 1% вес., ортотерфенил 64—66% вес., метатерфенил 31—33% вес., паратерфенил 2—4% вес.

Параметры, например степень недогрева, зависят от условий на выходе опытной петли, то есть приближаются к параметрам, соответствующим месту кризиса кипения.

В тот момент, когда детектор кризиса кипения показывает резкое увеличение сопротивления трубы экспериментальной петли, тепловой поток считают реальным тепловым потоком при кризисе кипения. В некоторых опытах труба экспериментальной петли повреждалась вследствие кризиса кипения. Эти опыты доказывают допустимость подобного кипения.

После испытаний с терфенилами, находящимися под давлением азота, петля была видоизменена таким образом, чтобы жидкость и азот были отделены друг от друга в водолазном колоколе плавающимся припоем. Это дает возможность исследовать отдельно влияние низкокипящих веществ и газов.

Приведены результаты исследований терфенилов, не содержащих летучих компонентов, и данные о влиянии увеличения концентрации азота, бензола и дифенила. Эти результаты интерпретируются по величинам степени недогрева, получаемым из экспериментальных кривых давления пара. Для этой цели был разработан аппарат, позволяющий точно определять давление пара в зависимости от температуры и состава примесей терфенилов с различными летучими веществами. Этот аппарат, соединенный непосредственно с экспериментальной петлей, дает возможность проводить измерения в условиях очень маленького пространства, занятого паром, следствием чего является отсутствие изменений состава жидкости.

A/590 Países Bajos

Experiencias de quemado total en ebullición subenfriada por convección forzada de polifenilos

por D. A. van Meel

Desde 1961 el TNO ha venido llevando a cabo un extenso programa de investigación acerca de la

influencia de la velocidad del líquido, grado de subenfriamiento y composición del líquido sobre el flujo térmico crítico de polifenilos fluyendo ascendentemente a través de un tubo de acero inoxidable calentado por efecto Joule.

Se adjunta una descripción del circuito de ensayos.

Se aportan resultados de un gran número de experiencias con mezclas de terfenilos bajo presión por contacto directo con nitrógeno. Estos resultados se correlacionan bien por una ecuación del tipo

$$\Phi = a + b \cdot G + c \cdot G^{3/4} \cdot \Delta t_s$$

(Φ , flujo térmico crítico; G , velocidad másica; Δt_s , grado de subenfriamiento).

Los valores de los coeficientes serán dados para las siguientes composiciones (porcentajes en peso);

a) 1% de bifenilo, 14—16% de *o*-terfenilo, 79—81% de *m*-terfenilo, 3—5% de *p*-terfenilo;

b) 1% de bifenilo, 64—66% de *o*-terfenilo, 31—33% de *m*-terfenilo, 2—4% de *p*-terfenilo.

Los parámetros tales como, por ejemplo, el grado de subenfriamiento, están basados en las condiciones a la salida de la sección de ensayo, es decir, próximo a la localización del fenómeno de quemado total.

El flujo térmico en el momento en que un acusado incremento de la resistencia del tubo es indicado por un detector de quemado se interpreta como el auténtico flujo térmico de quemado. Algunas experiencias en que la sección de ensayo se deterioró al efectuarse un verdadero fenómeno de quemado total mostraron que esto era permisible.

Después de estas medidas con terfenilos bajo nitrógeno, el circuito de ensayos ha sido modificado de manera que el líquido y el medio de presión quedan separados en una campana de bucear por material de soldadura fundido. Ello permite el estudio de los efectos separados de compuestos de bajo punto de ebullición y de gases.

Se presentan resultados sobre terfenilos que no contienen compuestos volátiles y acerca de los efectos de concentraciones crecientes de nitrógeno, benceno y bifenilo. Estos resultados son interpretados con relación al grado de subenfriamiento tal como se deriva de las curvas de presión de vapor determinadas experimentalmente. Con este propósito se desarrolló un aparato de presión de vapor que permite medidas seguras de la presión de vapor como una función de la temperatura y composición de mezclas de terfenilos y sustancias muy volátiles. Este aparato, que está conectado permanentemente al circuito de ensayos, se caracteriza por la posibilidad de medidas bajo condiciones de un espacio de vapor muy pequeño, con lo cual se evitan cambios de la composición del líquido.

Heat transfer and pressure drop performance of herringbone and helical fin fuel elements for uranium/Magnox reactors

By C. Cunningham,* B. E. Boyce,** T. Davis,*** and B. N. Furber****

Fuel elements which employ the principle of polyzonal spiral coolant flow described in [1], [2] and [3] are in use or planned for many gas-cooled reactors, particularly in France and the United Kingdom. The two main types are those with (a) multistart helical finning and (b) herringbone or chevron finning. Typical examples of both types are illustrated in [4] and [5] which also give salient dimensions of elements of current interest in Great Britain. The average heat transfer and pressure drop characteristics of many earlier designs of polyzonal fuel element have been reported in detail in [1], [6] and [7]. This paper has, therefore, been mainly confined to later designs incorporating a larger number of fins for which experimental data has not been published elsewhere. Salient features of experiment design and techniques evolved to measure accurately heat transfer data appropriate to normal operating conditions are discussed. The performance of polyzonal elements under low flow fault conditions is illustrated by typical results together with a note on the measurement of thermal radiation. The paper concludes with a brief presentation of results of tests to assess the influence of deformation and relative element orientation on heat transfer and pressure drop.

RELATIONSHIP BETWEEN REACTOR DESIGN AND OUT-OF-PILE PERFORMANCE TESTS

There are two main phases in reactor design which influence experimental work on fuel element heat transfer and pressure drop. These are (a) the optimisation of the station and (b) the accurate assessment of the performance and operating conditions of the final design.

In the first phase, which is essentially comparative, test data with relatively broad confidence limits on average performance of elements are adequate. For the second, when the major element details have been fixed, its performance must be measured in detail over the complete range of normal and fault conditions

of the reactor. Such information enables the designer to predict accurately core and station performance and fuel element temperatures in detail, to design the gagging pattern, to ensure that levitation of elements does not occur and to assess reactor safety.

Typical experimental data and techniques associated with the two phases of reactor design are discussed in the following sections.

PRELIMINARY SELECTION OF A POLYZONAL FUEL ELEMENT

The fuel element design evolved must be such that its rate of failure during reactor service is acceptable and this implies a stipulated limit on the probability (1 in 1 000, for example) of the maximum allowable fuel element cladding temperature being exceeded when all systematic and random effects have been considered. There are, of course, other design limits, such as maximum fuel temperature, which must also be adhered to, but this paper deals only with the heat transfer and pressure drop performance of the fuel can.

The salient dimensions affecting performance which may be varied are fin outside diameter, fin height and thickness, number of fins, fin lead or angle and channel diameter. In practice, however, limits are set to can volume and to channel and fuel diameters by nuclear and core considerations and to finning dimensions by the manufacturing process.

Mean heat transfer test results are given in Table 1 for helical cans ranging within these limits. The results are compared with predictions using two of the early correlations from [1] and [6]. The relatively poor performance of cans with the thickest fins is not fully understood but it is probably due to the conflict of the requirements of fin efficiency with those for high gas flow between the fins. With this reservation, the correlations enable mean heat transfer for a can to be predicted to better than 10% and this is adequate for preliminary surveys. The correlations tend to give pessimistic values of pressure drop for helical cans when extrapolated beyond the original test range, but correction factors have been derived to overcome this defect. The modified versions can then be used for the preliminary surveys. It may be noted, in passing, that the correlations of [1] and [6] predict accurately the

* The English Electric Company Limited, Whetstone, Leicester.

** United Power Company Limited, Heston, Middlesex.

*** United Kingdom Atomic Energy Authority, Reactor Development Laboratory, Windscale, Cumberland.

**** The Nuclear Power Group, Knutsford, Cheshire.

Table 1. Influence of dimensional changes on the performance of multistart helical cans

Varying dimension	Measured		Predicted [1]		Predicted [6]		Constant element details (dimensions in inches)
	<i>Sr'</i>	<i>F</i>	<i>Sr'</i> ratio	<i>F</i> ratio	<i>Sr'</i> ratio	<i>F</i> ratio	
Number of fins							
36	0.103	39.7	1.05	1.10	1.05	1.08	Fin diam 2.0
40	0.109	47.2	1.07	0.93	1.05	0.91	Lead 12
44	0.116	44.7	1.06	1.00	1.03	0.96	Root diam 1.3
48	0.131	46.6	0.99	0.98	0.96	0.92	Fin thickness 0.025/0.035
54	0.132	35.8	1.05	1.31	1.00	1.19	Channel diam 3.875
60	0.136	35.0	1.08	1.38	1.02	1.22	
Fin height (inches)							
0.425	0.150	48.0	1.05	1.24	1.02	1.18	Lead 13
0.375	0.132	41.0	1.09	1.11	1.01	1.07	Root diam 1.3
0.350	0.131	34.0	1.05	1.19	0.97	1.16	Fin thickness 0.025/0.040
0.325	0.128	30.0	1.01	1.22	0.93	1.15	Channel diam 3.875
0.300	0.118	28.5	1.05	1.15	0.96	1.06	No. of fins 54
Fin tip and root thickness (inches)							
0.016/0.029	0.129	39.0	1.08	1.30	1.14	1.22	Fin diam 2.10
0.016/0.039	0.132	42.0	1.13	1.22	1.11	1.13	Lead 13
0.016/0.050	0.130	37.0	1.32	1.41	1.13	1.28	Root diam 1.3
							Channel diam 3.9
							No. of fins 60
Fin lead (inches)							
12	0.136	35.0	1.06	1.33	1.02	1.22	Fin diam 2.0
13	0.135	34.0	1.02	1.21	0.99	1.16	Root diam 1.3
16	0.121	29.5	1.01	1.15	1.01	1.08	Fin thickness 0.020/0.035
							Channel diam 3.875
							No. of fins 60

and
$$\left. \begin{aligned} Sr' &= St.(S/A) \\ F &= f/(DeA^2) \end{aligned} \right\} \text{ where } \left\{ \begin{aligned} Sr: & \text{ Mean Stanton number} \\ f: & \text{ Friction factor} \\ A: & \text{ Free flow area} \\ De: & \text{ Equivalent diameter} \\ S: & \text{ Surface area for heat transfer per unit} \\ & \text{ length of element.} \end{aligned} \right.$$

All measured values of *Sr'* and *F* are quoted at a Reynolds number = 7.5×10^5 (for the empty channel).
The ratios shown are those for predicted to measured values of *Sr'* and *F*.

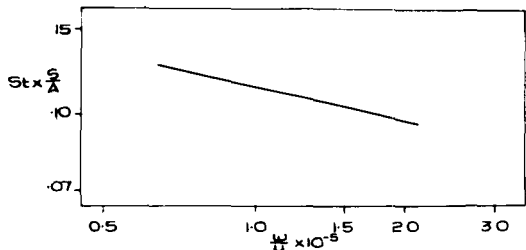
trends of performance associated with changes in can dimensions and may be used with confidence, therefore, when an experimental datum is available within the range of interest.

Two types of herringbone finning have been examined experimentally. One had spiral fins in all its quadrants or sectors and can be compared directly in all its major dimensions with an element having pure multistart helical finning. The finning of the second type was at a constant angle to the element axis over the whole height of the fin, and spiral fin parameters such as number or lead of fins cannot be used to describe it. There is, however, no evidence to suggest any fundamental difference in flow characteristics or performance between the two types of finning. Although experimental data is not so comprehensive it has been found that the trends in mean heat transfer and pressure drop of herringbone cans with changes in dimensions are very similar to those for multistart helical cans.

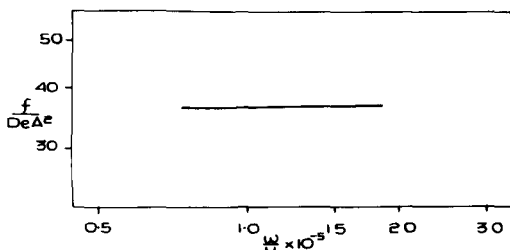
Splitters, braces and spring arm spiders, though not necessarily used on herringbone elements, are an essential feature of the multistart helical design. Splitters are required to establish the flow and are supported by braces which together serve the secondary

function of limiting fuel element bow. The spider helps to locate and stabilise the element. Typical performance data for elements are given in Figs. 1 and 2. The influence on element performance of splitter shape and clearance is discussed in [1] and [6]. Local heat transfer downstream of a brace is reduced, but it is usually possible to choose brace locations and design so that the minimum heat transfer on an element is not unduly affected. It is now possible, from tests on large scale models [3] and similar unpublished work on full scale elements, to explain at least qualitatively the observed pattern of heat transfer variations. Although many devices for increasing the ratio of minimum to mean heat transfer such as variable lead [1] or local flow accelerators [3] have been examined, none has been found which gives a worthwhile increase in over-all performance.

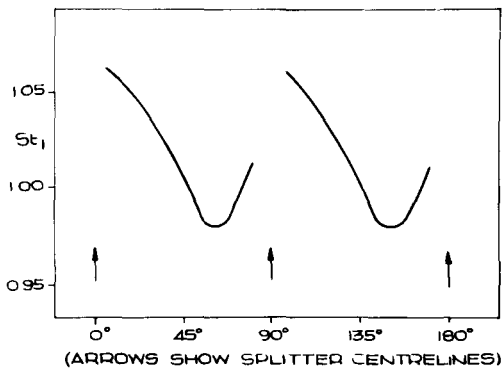
Having first narrowed the field by preliminary optimisation studies based on performance data from correlations and subsidiary experiments to assess effects of the various components like braces, spring-arm spiders, etc., a limited series of tests is carried out on a small number of specimen elements of each of the more promising designs. These tests are similar to those described in [1] and [6] and are adequate for the



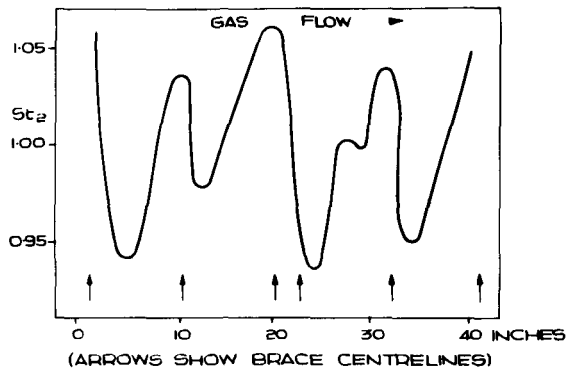
VARIATION OF MEAN HEAT TRANSFER WITH COOLANT FLOW. FIG.1A



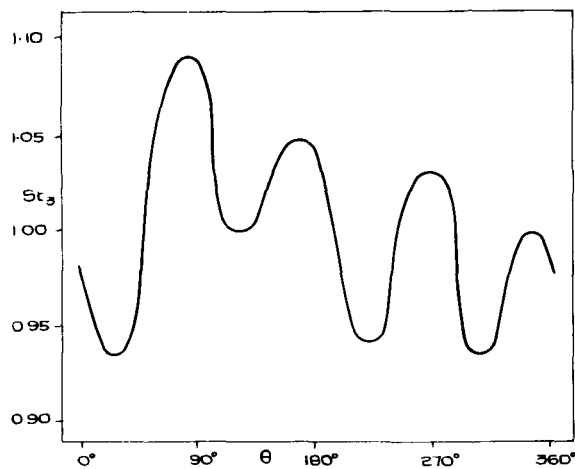
VARIATION OF PRESSURE DROP WITH COOLANT FLOW. FIG.1B



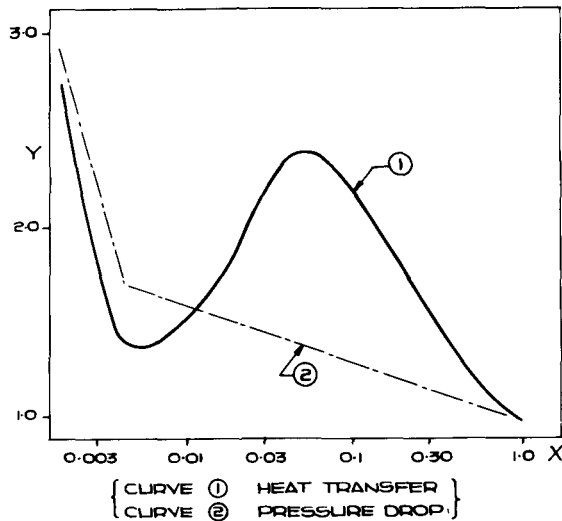
CIRCUMFERENTIAL VARIATION OF HEAT TRANSFER FIG.1C



AXIAL VARIATION OF HEAT TRANSFER. FIG.1D



VARIATION OF HEAT TRANSFER WITH RELATIVE ELEMENT ORIENTATION. FIG.1E



VARIATION OF HEAT TRANSFER AND PRESSURE DROP AT LOW COOLANT FLOW. FIG.1F

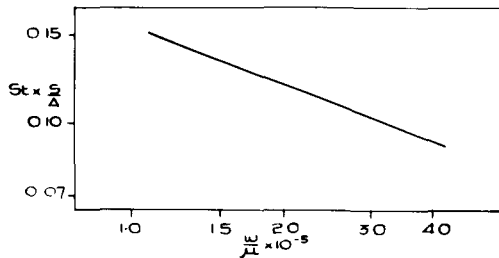
SALIENT ELEMENT DIMENSIONS

NUMBER OF FINS	60
OUTER DIAMETER OF FINS	1.90 INCHES
ROOT DIAMETER OF FINS	1.30 INCHES
FIN THICKNESS	0.0251035 INCHES
CHANNEL DIAMETER	3.875 INCHES

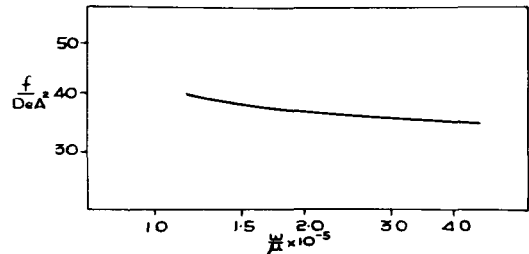
NOTE

COMPLETE NOMENCLATURE FOR ALL GRAPHS IS GIVEN ON FIG 2

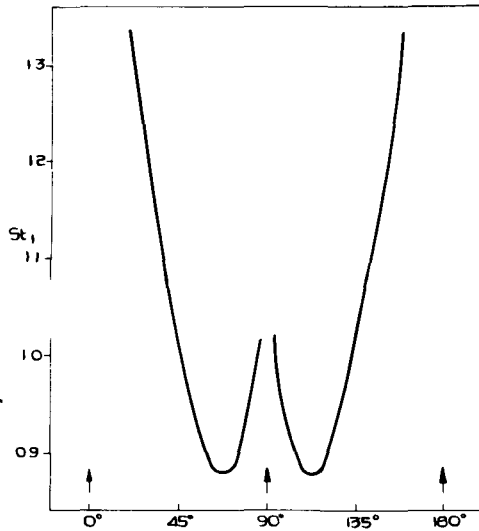
Figure 1. Heat transfer and pressure drop for a helical fuel element



VARIATION OF MEAN HEAT TRANSFER WITH COOLANT FLOW. FIG.2A

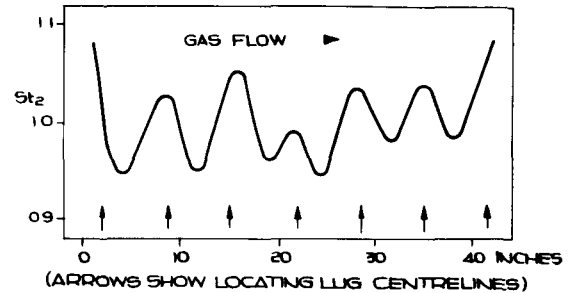


VARIATION OF PRESSURE DROP WITH COOLANT FLOW. FIG.2B



{ ARROWS SHOW SECTOR BOUNDARY CENTRELINES. GAS ENTERS INTERFIN SPACES AT 0° AND 180° POSITIONS AND EXITS AT 90° }

CIRCUMFERENTIAL VARIATION OF HEAT TRANSFER. FIG.2C



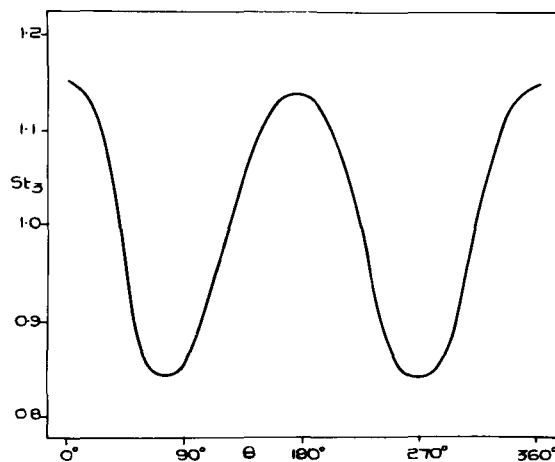
AXIAL VARIATION OF HEAT TRANSFER. FIG.2D

SALIENT ELEMENT DIMENSIONS

FIN ANGLE	: 20°
OUTER DIAMETER OF FINS	: 1.97 INCHES
ROOT DIAMETER OF FINS	: 1.26 INCHES (MIN)
FIN THICKNESS	: 0.035 INCHES
AXIAL FIN PITCH	: 0.261 INCHES
CHANNEL DIAMETER	: 3.95 INCHES

NOMENCLATURE

- A : TOTAL FREE FLOW AREA (ft)²
- D_e : EQUIVALENT DIAMETER (ft)
- S : HEAT TRANSFER SURFACE AREA FOR UNIT LENGTH OF ELEMENT (ft)
- W : COOLANT MASS FLOW. (lb/sec)
- St : AXIAL MEAN STANTON NUMBER AT THE MIDDLE OF A SECTOR ON ALIGNED ELEMENTS.
- St₁ : LOCAL CIRCUMFERENTIAL STANTON NUMBER NORMALISED ABOUT ITS MID-SECTOR VALUE
- St₂ : LOCAL AXIAL STANTON NUMBER NORMALISED ABOUT St.
- St₃ : STANTON NUMBER NORMALISED ABOUT MEAN FOR A COMPLETE 360° ROTATION.
- X : FLOW PARAMETER $\frac{W}{\mu}$ NORMALISED ABOUT ITS CENTRE CHANNEL VALUE AS DATUM
- Y : HEAT TRANSFER OR PRESSURE DROP NORMALISED ABOUT THEIR RESPECTIVE CENTRE CHANNEL VALUES
- μ : ABSOLUTE VISCOSITY OF COOLANT (lb/ft sec)
- θ : ANGLE OF ORIENTATION



VARIATION OF HEAT TRANSFER WITH RELATIVE ELEMENT ORIENTATION. FIG.2E

Figure 2. Heat transfer and pressure drop for a constant angle herringbone element

final selection if reasonable care is taken in their preparation and execution. They usually involve strings of three or four elements with thermocouples spaced uniformly approximately every two or three inches axially in one or two quadrants.

EXPERIMENTAL MEASUREMENT OF PERFORMANCE DATA APPROPRIATE TO NORMAL REACTOR OPERATING CONDITIONS FOR THE SELECTED DESIGN

In the preceding paragraphs heat transfer performance has been considered mainly in terms of mean Stanton number. Having selected a final style of element for a particular reactor, its performance must now be determined for the second design phase. The appropriate experiment must be designed to measure accurately the heat transfer in the light of its complex variations, the special conditions near the ends of elements and the variations within and between elements which are either inherent in the element due to, say, manufacturing tolerances, or those which result from random experimental error. All possible sources of systematic and random error must be eliminated or minimised, so that the design margins may be reduced to the lowest possible level. Some of the most important refinements of technique and apparatus found necessary are described in the following paragraphs. The pressure drop experiments are not discussed here as they are relatively straightforward. The general procedure described in [1] and [6] is usually followed, the pressure drop being determined over an integral number of pitch lengths (i.e., from a point on one element to the corresponding position on another element in the test string) on strings of four or more elements.

In laboratory tests polyzonal elements are heated by passing a current through stainless steel tubes with thin walls fitted inside the bore of the cans. These tubes are coated with a thin layer of ceramic material to insulate them electrically from the element. It is clear from the patterns of circumferential and axial variation, shown in Figs. 1C, 1D, 2C and 2D, that large systematic changes in local heat transfer occur, therefore special precautions must be taken in heater design to minimise spurious effects. A variable thermal resistance between the heater and can barrel or non-uniform heat generation due to changes in heater wall thickness are the most likely sources of error. Of the many different assembly methods investigated, only external pressurising of the element on to the heater tube was found to give a uniform interface thermal resistance. Although tubes with a very close tolerance on wall thickness are used, the variation in heat generation which results from the small changes in thickness which occur in practice around the tube section must be taken into account in deriving accurate experimental heat transfer data. This can be achieved by analysing the experiment described in later paragraphs to derive a correlation for the change in heat transfer coefficient with heater wall thickness

and adjusting the data to compensate. Two further refinements which have been considered are the simulation of the pattern of reactor heat flux in the test channel and of the 7 to 8% heat generation in the moderator. The critical element in a reactor, however, is in a position where the heat flux is not changing significantly so the first refinement was considered to be unnecessary. Tests have shown that the heat transfer coefficient of an element is not influenced by heating of the wall of the containing channel and, therefore, the second refinement is also unnecessary.

The heat transfer performance of the fuel element is sensitive to changes in fin efficiency. For a given geometry the fin efficiency is influenced by gas and metal thermal conductivities which are temperature dependent. It is, therefore, necessary in performance calculations to allow for differences between experimental and reactor gas and metal temperatures. In the past such allowances have been based on the results of specially designed experiments [1] but later work, especially on elements with increased numbers of fins, has shown that the early correlations are not sufficiently accurate. It is preferable for the final performance assessment to minimise the fin efficiency correction by using data obtained from experiments at temperatures as close as possible to those in the reactor.

Unless special precautions are taken in the design of the ends of the element and heater assembly, heat transfer data obtained in these regions may be vitiated by axial conduction along the element or by heat generation in the electrical terminals and connectors. An apparatus designed to avoid these defects is described in [1], but it is cumbersome and not suitable for strings of three or more elements. Better designs have since been evolved which enable true heat transfer coefficients to be measured near the ends of the finning and allow the geometrical configuration between elements of a test string of seven or eight elements to be made similar to that in the reactor.

Again, because of the complex heat transfer patterns associated with polyzonal elements, detailed testing requires the fitting of a large number of thermocouples to each element, often as many as 100. To minimise their disturbance to gas flow the smallest practicable diameter of thermocouple wire should be used, and great care should be exercised in the routing of the couples from the elements to the pressure seal at their exit from the rig channel. Chromel/Alumel thermocouples are usually used because they are compatible with the magnesium alloy of the elements and are readily available. It has been found, in practice, that the calibration of very fine Chromel/Alumel thermocouples shows significant variations between batches and there is also some evidence of calibration instability associated with the temperature history of the wire. Stringent precautions, including re-calibration after use, should be taken to avoid errors due to non uniform or unstable couples.

The heat transfer experiment on the selected fuel element must be designed to meet two main criteria.

It must (a) cover the variables adequately and provide data for the objective assessment of their effect on heat transfer and (b) provide the required performance data for reactor design. Since the heat transfer of a polyzonal element depends on at least nine factors (as listed later) the classical experimental approach in which each variable is investigated in turn is both time consuming and costly. A very powerful, though not necessarily the ideal, method of coping with the situation is the Factorial Experiment. The technique is described in detail in the standard books on experiment design; two recent papers [8] and [9] are specifically related to the present topic. The main advantages of the Factorial Experiment are: (a) it provides, with the minimum of test effort, an accurate estimate of experimental error and hence the datum for the assessment of the statistical significance of each variable included in the experiment, and (b) it enables the interaction, if any, of all variables to be examined; the effect on heat transfer of one variable may be dependent on the level of other variables and this must be investigated.

For the experiment a group of some 20 to 30 cans is chosen randomly from the fuel element production line and each specimen is identified by, say, a letter of the alphabet. A typical Factorial Experiment involves a block of tests on four strings or sets of five elements as illustrated in Table 2, with complete or

Table 2

Set number	Position in set				
	1	2	3	4	5
1	A	B	C	D	E
2	F	G	H	I	J
3	K	L	M	N	O
4	P	Q	R	S	T

partial replication of the block. Each test is carried out following a procedure similar to that described in detail in [1], the elements being assembled and instrumented with due regard to the refinements and precautions discussed above.

The salient factors which influence heat transfer data from such an experiment are: (a) Reynolds number, (b) axial position along the element, (c) between element variations, (d) within element variations (between sectors, say), (e) position of element in string (set), (f) fin efficiency, (g) heater tube thickness variation, (h) relative orientation of successive elements, (i) test errors. As described later, it is the general practice to carry out separate orientation tests, so for the Factorial Experiment elements are fixed with corresponding quadrants aligned, and (h) does not occur as a Factor. Furthermore, a correction for fin efficiency as proposed in [1] or a basically similar one is generally applied, thus eliminating (f) as a Factor. Test errors, as used here, cover all errors associated with the experiment whether they be true

random errors or systematic errors specific to one test of the series or to only one element of a set.

There is some freedom of choice of mass flow levels for the tests but it is more convenient for subsequent analysis if a minimum of three and a maximum of five levels are preselected and all tests performed as close as practicable to these levels. It is relatively simple to adjust the results to the preselected flow levels before the final analysis. The data is also adjusted for heater thickness variation at this stage.

After the initial processing and adjustment of data, an analysis of variance is carried out which enables the significance of the various factors to be assessed together with their influence on the probability distribution for minimum heat transfer on an element. This distribution is required for the calculation of peak random fuel element temperature at the specified probability level.

POLYZONAL ELEMENT PERFORMANCE AT LOW COOLANT FLOWS

During normal reactor operation coolant flows are high and forced convection is the predominant mechanism of heat transfer from the fuel element. At reactor start-up, for part-load running and during a system failure such as gas circulator trip or a major rupture in the coolant circuit, flows are low and in the more severe cases stagnation may occur in one or more channels; heat is then transferred by natural convection or thermal radiation or by a combination of both. Tests have been carried out to obtain data for the performance assessment of fuel elements operating at these conditions.

Convective heat transfer and pressure drop characteristics have been measured using CO₂ at various pressure levels and air at atmospheric pressure from normal operating levels down to 0.3% of full reactor mass flow. Basically the test procedure is the same as for those at higher flows with a number of specific additional features and precautions. It is essential that: (a) a string of at least three or four elements is tested in a vertical channel, (b) heat losses are reduced to a minimum and the rig calibrated to take account of the residual losses, (c) allowance is made for radiative heat transfer, (d) flow metering devices appropriate to the range being covered are used. Results follow the trends illustrated in Fig. 1F. The flow, heat transfer and pressure drop parameters have been normalised using their respective levels at centre channel flow conditions as datum.

In order to measure directly the effective emissivity of an element, the influence of convection must be minimised by testing at low pressures. A small contribution from gas conduction still remains and this can only be eliminated by testing under vacuum conditions. Magnox evaporates under a vacuum at temperatures in excess of 400 °C but by using a different experimental technique the emissivity of small specimens of the material can be determined up to 600 °C in a CO₂ atmosphere. The effective emissivity

of a complete element can then be calculated from this data using a theoretical method similar to that described in [10]. It is important that the small specimens have the same radiation characteristics as the element material and this is best achieved by cutting test specimens from the element itself. The accuracy of this approach has been demonstrated by comparison with experimental results for a complete element at temperatures below 400 °C.

The element surface condition changes during reactor life, consequently its effective emissivity alters and data appropriate to the dwell time of each safety assessment must be used. The effective emissivity of a new element from a production line is about 0.4, while for "aged" elements it can increase to 0.7. In highly rated reactors it may be found that the emissivity of new elements is insufficient to meet the safety criteria, however suitable surface treatments for increasing the emissivity are being developed.

EFFECTS OF ELEMENT ORIENTATION ON PERFORMANCE

When polyzonal fuel elements are loaded in a reactor channel they can assume positions in which the corresponding quadrants of successive elements are randomly orientated with respect to each other unless some device is used to give them a predetermined alignment. Orientation could be included as a Factor in experiments of the type described previously, but this would lead to a very large and costly experimental programme if the required over-all accuracy is to be maintained. Its effect is, therefore, usually investigated in a separate series of tests.

In a typical orientation experiment, three or more elements are placed in the test channel of a pressurised CO₂ loop. A specially designed apparatus enables the relative orientation of the second and third elements to be varied during a test without interrupting the gas flow or power supply. The first element remains at all times in line with the second to establish correct aerodynamic entry conditions, but the orientation of elements following the third can be altered between tests to investigate possible "carryover" of an orientation effect for more than one element length.

Variations in heat transfer with orientation are shown in Figs. 1E and 2E for a position four inches from the upstream end of both styles of element. In general, the heat transfer of a misaligned element varies in a cyclic pattern with angle of misalignment. This pattern is very marked over the upstream half of an element, but it attenuates and generally changes phase over the downstream half. There was little evidence of an appreciable "carryover" of the orientation effect to subsequent elements in a string. The salient difference between the patterns for the two types of finning is that there are four complete cycles in the pattern for multistart helical finning during a 360° rotation, but only two with herringbone fins. The apparent asymmetry of the pattern for the helical element compared to the very uniform variation in all

sectors for the herringbone is mainly due to the presence of a spring-arm spider on the helical element. The amplitude of the variation is dependent on the configuration being tested as well as on axial position along the element, so each design must be investigated experimentally. Subsidiary pressure drop tests indicated that changes of pressure drop with element orientation are relatively small.

It is outside the scope of this paper to describe in detail how the data is incorporated in temperature and performance assessment by the reactor designer, but the following results from typical calculations illustrate the importance of the orientation effect. For a gas-cooled reactor of about 500 MW(e) output with herringbone elements the difference in peak random temperature between the case where all elements are held in-line and that in which elements are randomly aligned is of the order of 25 °C in favour of the former. Therefore, if predetermined alignment can be achieved by a device which is consistent with the diverse requirements of reactor design and economics, gains in reactor performance or margins will accrue.

EFFECT OF DEFORMATION ON ELEMENT PERFORMANCE

As a result of irradiation trials in reactors and out-of-pile tests in laboratories, the manner in which fuel elements are likely to deform during normal reactor life can be predicted. Data has been obtained on deformations of fins, splitters and braces for multistart helical elements and of fins and locating lugs for herringbone elements, as well as on the bowing behaviour for both types. The magnitude of the distortions is governed mainly by operating conditions and details of the geometry of particular designs, and is fully described in [4].

Tests have been carried out on both helical and herringbone elements to determine the effect on heat transfer and pressure drop of deformations calculated to be representative of those occurring during the design reactor life of the elements. The deformation imposed on the herringbone elements was, however, more severe than that on the helical specimens.

Eight elements with multistart helical fins were pressurised on to heater tubes and each was tested in each of five channel positions over a suitable range of Reynolds number. For the first part of the test series the elements were undeformed while for the second part the representative deformation was applied. Closely spaced thermocouples were placed in groups along the axes of two diametrically opposite quadrants at regions where the probability of occurrence of a low heat transfer was known to be high. Other thermocouples were spaced uniformly in an axial row in one of the quadrants to measure mean heat transfer before and after deformation. Statistical analysis of the test results showed that mean heat transfer did not change significantly with deformation and that a small but significant reduction in minimum heat transfer occurred. At reactor conditions this decrease was

2.6% with 95% confidence limit of $\pm 0.3\%$. The pressure drop of deformed cans was lower than that for undeformed elements by about 6%.

A less precise series of tests was carried out on two constant angle herringbone elements of comparable design with the helical elements mentioned above. Similar trends in heat transfer were observed, the reduction in minimum heat transfer was 5% with associated 95% confidence limits of $\pm 5\%$. A small increase in pressure drop was noted after deformation. Further work is in hand to assess the effect of element bow on performance. The magnitude of this effect is expected to be small.

PERFORMANCE COMPARISON OF HERRINGBONE AND HELICAL ELEMENTS

The data shown in Figs. 1 and 2, although specific to the elements tested, illustrate the salient features of heat transfer and pressure drop of four-sector constant angle herringbone and multistart helical fuel elements. (The evidence available on elements with more than four sectors is insufficient to justify their inclusion here.)

The axial variations of heat transfer for both designs (Figs. 1D and 2D) are strikingly similar, showing local depressions downstream of braces and locating lugs. On the other hand, the circumferential variations (Figs. 1C and 2C) are markedly different. The differences in effect of orientation have been discussed earlier; in general, random orientation has a greater influence on the heat transfer of herringbone elements than on that of helical types. The mean axial heat transfer at midquadrant on the herringbone element (Fig. 2A) is substantially higher than this parameter for the helical design (Fig. 1A) but it can be shown that, when all the systematic and random departures from the mean have been considered, the difference in

minimum heat transfer between the two elements is only slightly in favour of the herringbone finning. The pressure drops over a pitch length of element (Figs. 1B and 2B) are comparable for both designs.

In general there is no marked performance advantage in favour of either design, and the ultimate choice of element is governed by factors from all the relevant fields, e.g., aerodynamic stability, endurance, safety, production costs, etc.

ACKNOWLEDGEMENTS

The authors wish to thank their Directors for permission to publish data obtained in their laboratories, and the many colleagues who assisted in the experimental work associated with this paper.

REFERENCES

1. Cunningham, C., and Slack, M. R., Proceedings of the Symposium on the use of secondary surfaces for heat transfer with clean gases. I. Mech. E., 57 (1961).
2. Ritz, H. L., Proceedings of the Second International Conference on the Peaceful Uses of Atomic Energy, p. 48, Vol. 7, p. 725, United Nations (1958).
3. Neal, J., and Hitchcock, J. A., J. British Nuclear Energy Soc., 1, 4, 307 (1962).
4. Hughes, J. W., *et al.* The development and evaluation of uranium/Magnox fuel elements, p/147, Vol. 10, these proceedings.
5. Stewart, J. C. C., I. Mech. E., Nuclear Energy Group Paper 9/64.
6. Wise, A. F. E., Proceedings of the Symposium on the use of secondary surfaces for heat transfer with clean gases, I. Mech. E., 85 (1961).
7. Milliat, J. P., *Ibid.*, 110.
8. Wilkie, D., UKAEA, TRG Report 217 (W) (1962).
9. Wilkie, D., Applied Statistics, X, 2, 83 (1961).
10. Rapier, A. C., and White, L., UKAEA, TRG Report 54 (W) (1961).

ABSTRACT—RÉSUMÉ—АБХОТАЦІЯ—RESUMEN

A/135 Royaume-Uni

Caractéristiques de transfert de chaleur et de chute de pression des éléments de combustible à ailettes hélicoïdales et en chevrons pour les réacteurs uranium/Magnox

par C. Cunningham *et al.*

Les éléments de combustible polyzonaux conçus au Royaume-Uni pour les réacteurs uranium/Magnox à réfrigérant gazeux ont soit des ailettes hélicoïdales décalées, soit des ailettes en chevrons, en tant que surfaces supplémentaires d'échange. Cet exposé traite principalement de la détermination expérimentale des caractéristiques de transfert de chaleur et de chute de pression de ces éléments.

Dans la première partie, on discute des données sur le comportement qui sont nécessaires pour la sélection

d'une forme appropriée d'élément de combustible. On présente des résultats d'essais pour illustrer les effets qu'exercent sur le transfert de chaleur et sur la chute de pression des changements dans les caractéristiques des parties saillantes de l'élément, par exemple le nombre ou le pas des ailettes. On compare ces résultats avec les prédictions faites en utilisant des corrélations publiées précédemment.

Lorsqu'une forme d'élément de combustible a été choisie pour un réacteur, il est nécessaire de connaître son comportement en détail et avec une haute précision pour permettre au constructeur du réacteur de calculer la puissance de la centrale et les températures de l'élément de combustible dans des conditions normales de fonctionnement. Ce mémoire décrit les perfectionnements apportés aux appareils d'essai et le programme d'une expérience type pour la mesure du transfert de chaleur dans ces conditions.

L'élément de combustible choisi doit être également conçu pour un fonctionnement sûr lorsque le réacteur est exploité en charge partielle avec un faible débit de réfrigérant ou lorsque des défaillances dans le système provoquent une perte partielle ou presque complète de réfrigérant. Des expériences sur le comportement, permettant de se rendre compte de la valeur de l'élément dans de telles conditions, sont décrites ainsi que des résultats caractéristiques.

Le mémoire traite enfin de deux aspects importants du comportement des éléments de combustible polyzonaux sur lesquels peu ou pas de données ont été publiées. Ce sont: *a*) l'influence de l'orientation au hasard des éléments successifs dans un canal de réacteur sur le transfert de chaleur et la chute de pression, et *b*) les changements de comportement associés à la déformation des ailettes par les forces de gaz. On présente les résultats d'expériences qui illustrent l'ampleur des effets de ces deux facteurs sur le transfert de la chaleur et la chute de pression.

A/135 Соединенное Королевство

Данные теплопередачи и перепада давления у тепловыделяющих элементов с шевронными и винтовыми ребрами для уран-магноксовых реакторов

К. Каннингем *et al.*

Многозонные тепловыделяющие элементы, сконструированные в Соединенном Королевстве для уран-магноксовых реакторов с газовым охлаждением, имеют в качестве поверхностей, способных расширяться, многозаходные винтовые или «шевронные» ребра. Данная работа была направлена главным образом на экспериментальное определение данных теплопередачи и перепада давления при использовании таких тепловыделяющих элементов.

В докладе обсуждаются данные, необходимые для выбора подходящей конструкции тепловыделяющего элемента. Чтобы показать действие изменений наиболее важных параметров тепловыделяющих элементов, например числа или шага спирали ребер, на теплопередачу и перепад давления, в докладе представлены результаты испытаний. Эти результаты сопоставимы с данными, предсказанными на основе ранее опубликованных зависимостей.

Когда была выбрана конструкция тепловыделяющего элемента для реактора, потребовалась подробная и очень точная разработка его конструкции, чтобы дать возможность конструктору реактора рассчитать мощность станции и температуры тепловыделяющего элемента при нормальных рабочих условиях. Во второй части доклада описываются наладка аппаратуры для испытания и типовая эксперименталь-

ная конструкция тепловыделяющего элемента для измерения теплопередачи при этих условиях.

Выбранный тепловыделяющий элемент должен быть также спроектирован с учетом требований безопасности эксплуатации, когда реактор работает с неполной нагрузкой и небольшим расходом теплоносителя или когда повреждения в системе приводят к частичной или почти полной потере теплоносителя. Эксперименты для получения данных, касающихся оценки тепловыделяющего элемента при таких условиях, описываются наряду с типичными результатами.

Наконец рассматриваются два важных аспекта рабочих характеристик многозонного тепловыделяющего элемента, по которым было опубликовано мало сведений или они не были опубликованы совсем. Один аспект включает изучение влияния хаотического расположения следующих один за другим тепловыделяющих элементов в качестве реактора на теплопередачу и перепад давления. Второй аспект состоит в изучении изменений характеристик, связанных с деформацией ребер под напором газа. Представлены экспериментальные результаты, которые указывают на степень влияния этих двух факторов на теплопередачу и перепад давления.

A/135 Reino Unido

Características de caída de presión y transmisión de calor de los elementos combustibles de aletas helicoidales y en espina de pez en los reactores de uranio-Magnox

por C. Cunningham *et al.*

Los elementos combustibles polizonales proyectados en el Reino Unido para los reactores de uranio-Magnox, refrigerados por gas, tienen, como superficies ampliadas, aletas, bien helicoidales de varias entradas, o bien en «espina de pez» o espigón. Esta memoria trata principalmente de la determinación experimental de las características de transmisión de calor y caída de presión de tales elementos.

Primero se discuten las características de funcionamiento que es necesario conocer para la elección de un diseño adecuado del elemento combustible. Se presentan los resultados de las pruebas para demostrar los efectos de cambios en los parámetros más importantes del elemento, *v.g.* número o ángulo de inclinación de las aletas, sobre la transmisión de calor y caída de presión. Estos resultados se comparan con las predicciones que se obtienen utilizando correcciones publicadas anteriormente.

Cuando se ha elegido un proyecto de elemento combustible para un reactor, es necesario conocer sus características con gran detalle y elevada exactitud para que el proyectista del reactor pueda calcular la potencia de la central y las temperaturas del

elemento combustible en condiciones normales de funcionamiento. La memoria describe los refinamientos en los aparatos de pruebas y el proyecto de un experimento típico de desarrollo para medir la transmisión de calor en estas condiciones.

El elemento combustible elegido debe ser también proyectado para trabajar con seguridad cuando el reactor esté funcionando a carga parcial con caudales bajos de refrigerante, o cuando fallos del sistema den lugar a pérdida parcial o prácticamente completa del refrigerante. Se describen experimentos y resultados típicos de los mismos, para obtener características de funcionamiento que permitan la evaluación del

comportamiento del elemento en las condiciones citadas.

Al final se tratan dos aspectos importantes del comportamiento del elemento combustible polizional sobre el cual se han publicado pocos o ningún dato. Estos son: *a)* la influencia de la orientación al azar de elementos consecutivos en un canal sobre la transmisión de calor y caída de presión, *b)* los cambios en las características provocados por la deformación de las aletas, debido a efectos dinámicos del gas. Se presentan resultados que muestran la magnitud de los efectos de estas dos facetas sobre la transmisión de calor y caída de presión.

Heat transfer performance of the polyzonal can for the CEGB reactors

By H. F. J. Hadrill, E. W. V. Acton,* J. A. Hitchcock and S. B. H. C. Neal**

The first phase of the civil nuclear power programme in the United Kingdom comprises eight twin reactor power stations under the control of the Central Electricity Generating Board and one station under the control of the South of Scotland Electricity Board. All these reactors, which have a total design output of 4 500 MW, have fuel elements consisting of solid rods of natural uranium contained in magnesium alloy cans. The extended surface which provides for effective heat transfer is a polyzonal spiral for the first thirteen reactors.

The responsibility for these reactors achieving their design output rests with the Consortia of manufacturers engaged in the nuclear field. Consequently they have laboratories which provide detailed information on the heat transfer and pressure drop performance of particular fuel elements. However the information necessary to justify a design and provide the basis for an output guarantee does not always cover the requirements of the reactor operator. The anticipated dwell time of the fuel elements in the reactor is between four and five years and creep deformations of the extended surface will alter the heat transfer performance. The extent of the deformations will be governed by local areas of high temperature on the can surface. Both the polyzonal can and the herringbone can exhibit axial and circumferential variations in their heat transfer performance, that of the latter being more marked. In examining the data presented by different laboratories on their cans it became evident that results were influenced both by the techniques employed and by the particular heat transfer loops used in the experiments. Consequently the Board decided in its capacity of reactor operator to conduct its own heat transfer experiments. These provide a comparison of fuel can performance and when allied with complementary measurements at the power stations enable the Board to assess directly the magnitude of some of the major variables affecting the heat transfer performance inside the reactor.

Such work started at the Central Electricity Research Laboratories (CERL) in 1958 and has been continued at the Berkeley Nuclear Laboratories (BNL) since March 1962. During the last two years CERL have

undertaken a fundamental investigation into the gas flow processes around a polyzonal can using a large scale model. The work of both Laboratories is described in the paper.

Large scale model studies of the polyzonal can

A schematic diagram of the rig is shown in Fig. 1. The test section represents one quadrant of a basic polyzonal can, four times normal size, which was heated electrically. The upstream entry length would accommodate an unheated length of can when this was required. Air was drawn over the test section by a fan which normally exhausted to atmosphere, but a closed loop could be formed when flow tracer techniques were employed. The model quadrant, which had 40 thermocouples along its length measuring can surface temperature, was based upon an actual fuel element can. The good agreement between the heat transfer patterns of the can and the model justified the use of the latter for flow investigations. The test section was contained inside perspex covers which represented the channel wall. These allowed flow visualization techniques to be used and temperature and velocity probes to be inserted into observed positions.

Basic fluid flow and heat transfer patterns

A picture of the fluid flow pattern was obtained using tracers and wool tufts together with velocity and temperature surveys, both around the quadrant and between the fins. Relationships were thus established between the flow pattern along the channel and the axial variation in heat transfer [1].

The observations show that the primary effects responsible for the heat transfer variation are the levels of fin channel gas flow and fin entry temperature which in turn are controlled by the flow pattern along the fuel channel. Furthermore the flow over the can may be divided into two régimes, a developing flow

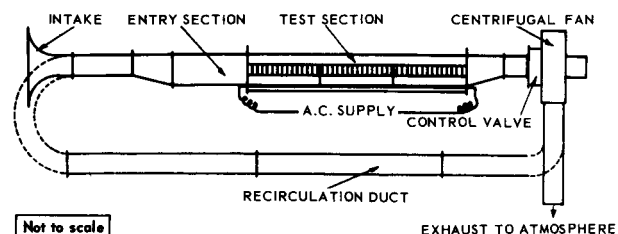


Figure 1. Schematic diagram of test rig

* CEGB, Berkeley Nuclear Laboratories, Berkeley, Gloucestershire.

** CEGB, Central Electricity Research Laboratories, Leatherhead, Surrey.

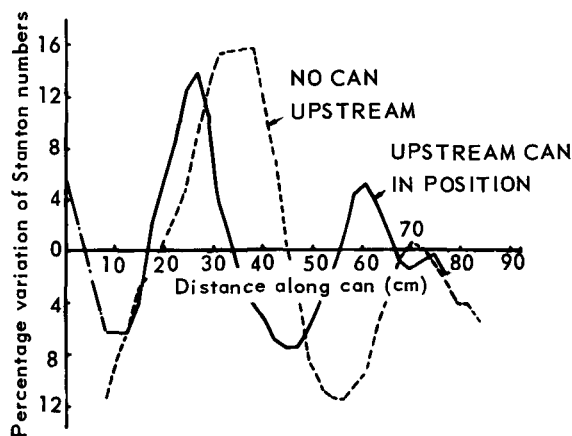


Figure 2. Axial heat transfer variation

and a fully established flow. The flow system is also dependent, especially at the start, as to whether or not an upstream can precedes the can being considered.

With no upstream can present, axial flow approaches along the fuel channel; poor entry conditions result in low fin channel velocities and hence poor heat transfer (Fig. 2). The gas emerging from the first fin channels at the downstream splitter is both warmer and slower than the mainstream, with which it mixes to some extent. However, the emergent gas soon develops into a stream of warmer, slower gas which follows a spiral path around the periphery of the main channel. It displaces the cool, axially flowing gas from the main channel, forcing it down into the fin channels at a progressively faster rate thus causing fin channel velocities, and hence heat transfer, to rise rapidly. A peak value of heat transfer is reached immediately before the warmer, slower gas begins to re-enter the fin channels, usually about a third of the way along the can. The entry of this gas into the fin channels causes a sharp fall in heat transfer.

Beyond this stage, the flow pattern can be regarded as fully established and consists of a shell of slow, warm, spiralling gas surrounding a core of fast, cool, near axially-flowing gas. The shell is composed of gas which becomes progressively warmer and slower towards the downstream end of the can, whilst the core slowly accelerates and warms only gradually, since it mixes little with the spiralling shell. The core pursues a spiral path along the fuel channel and this results in a cyclic variation in the fin channel gas velocities, their local value depending upon the proximity of the core to the fin tips at that point. The heat transfer variation is primarily dependent upon the fin channel gas velocity variation, the temperature of gas entering the fin channels being of second order in the régime of fully developed flow.

The detailed investigations already described were repeated with an unheated quadrant model can placed upstream of the test section, this being equivalent to

an *in line* splitter arrangement. The modified heat transfer pattern is included in Fig. 2.

Gas approaches the first fin channels on the test can in a direction close to that of the fin lead, the flow spiral from the upstream can maintaining much of its form past the cup-and-cone end fitting and on to the test can. The entry condition is considerably improved over that with no upstream can present. This results in improved heat transfer at the start of the can. The improved entry conditions also reflect in a slightly shorter flow pattern development length, resulting in an upstream displacement of the heat transfer pattern. The flow pattern is otherwise similar to that over the upstream can.

Effects of splitter orientation and ancillary fittings

In practice the flow conditions at the start of a can are determined by the type of end fitting and by the generally random orientation of the splitters on successive cans. These effects have been investigated on the model. When the splitters are a few degrees out of alignment, the spiralling flow rising away from the fins may be caught by the start of the splitter on the downstream can. The alignment between the three armed spider and the four quadrants is such that one quadrant will be shielded by a spider arm. This situation makes the entry conditions as poor as those with no upstream can.

From such studies it seems likely that whatever the inlet conditions a point of minimum heat transfer will occur near the upstream end of a can. The value will depend upon splitter orientation and will not necessarily be the point of minimum heat transfer on the can.

The effect on the flow pattern of braces is shown in Fig. 3. The gas velocity immediately downstream of each brace is markedly reduced, but heat transfer is less affected due to axial conduction. It was found that the general level of heat transfer over the upstream third of the can was further reduced due to the braces delaying the development of the flow pattern and encouraging the persistence of low fin channel

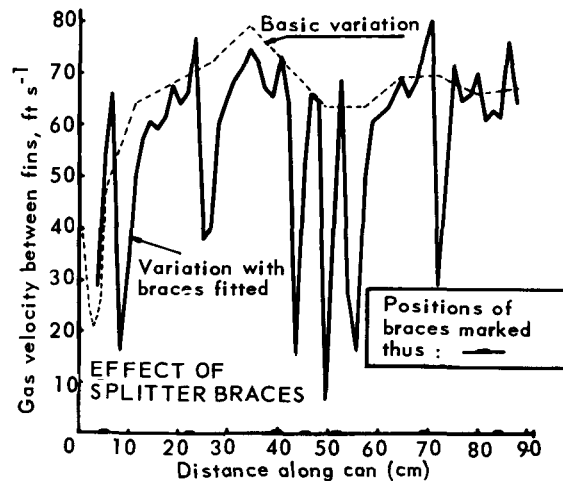


Figure 3. Fin channel gas velocity variation

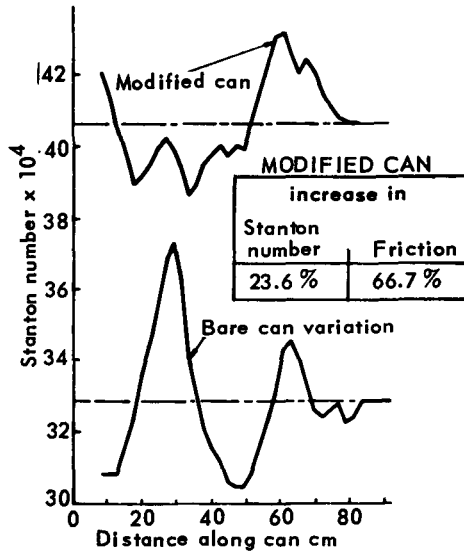


Figure 4. Axial heat transfer variation. Effect of modifications and splitter braces

velocities near the start of the can. However better gas mixing is promoted by the braces and the general level of heat transfer is increased over the last two-thirds of the can, leading to an over-all increase in the mean level of heat transfer by 2–3%.

Laboratory experimental techniques and some factors affecting performance

Considerable changes in experimental techniques have taken place in most laboratories over the last few years to improve the accuracy of heat transfer data. Air rigs at substantially atmospheric pressure are rarely used to evaluate heat transfer coefficients or friction factors; steam heating has ceased and direct current electrical heating is most commonly used to simulate heat generation. Flame sprayed aluminium oxide ceramic is the most widely used high temperature insulation between the stainless steel heater tube and the can. Since experiments in 1962 on the effect of heaters [2], most heat transfer tests have required the cans to be pressurized on to the heater tubes to reduce variations in local can temperatures caused by poor fit of the can on the heater.

Heater tubes

It is important to ensure uniform local heat generation and this is proportional directly to tube wall thickness. Figure 6 shows how the temperature varies in a cylindrical primary surface heated by a heater tube with a variable circumferential wall thickness [3]. The heater tubes used to test polyzonal cans are of 1 in (2.54 cm) od and 0.028 in (0.07 cm) wall thickness, and are manufactured by drawing; a variation in thickness of $\pm 10\%$ is the best normally obtainable and this generally remains constant along the tube. It can be shown that the difference in $St.(S/A)$ ($St.$ = Stanton number, S = heat transfer surface area, A = flow area) between diametrically opposite quadrants is approximately proportional to the change in heater tube wall thickness from the mean value (assuming uniform heat generation) [4]. However, the effect is reduced by circumferential conduction in the wall of the can. An electrical analogue study [5] has shown that the temperature difference between the can root and the gas changes by a maximum of $\pm 6.5\%$ and a minimum of $\pm 4.7\%$ for a variation of $\pm 10\%$ in heater tube wall thickness. A further correction has to be applied for the variation of electrical resistance with temperature. Thus any variation in thickness will lead to a variation in temperature which in turn causes a variation in the local heat generation rate. The above effects are shown in Fig. 7. The change in thermal resistance due to doubling the ceramic insulation thickness from 0.0075 in (0.019 cm) to 0.015 in (0.038 cm) was found to have negligible effect.

Figure 8 shows a typical variation in normalized $St.(S/A)$ along a Hinkley Point can when testing with a heater to normal tolerances. The positions of maximum and minimum heat transfer are determined by the gas flow pattern and the positions of the braces. On average the two curves are separated by about 7% in $St.(S/A)$ which suggests that although other effects were present in the tests, this scatter was largely due to the variations in heater tube thickness.

In reactor performance assessments the minimum value of $St.(S/A)$ wherever it occurs and the mean of the minima found in all four quadrants are often evaluated. Figure 9 shows two such curves plotted against w/μ (w = gas mass flow, μ = viscosity). The

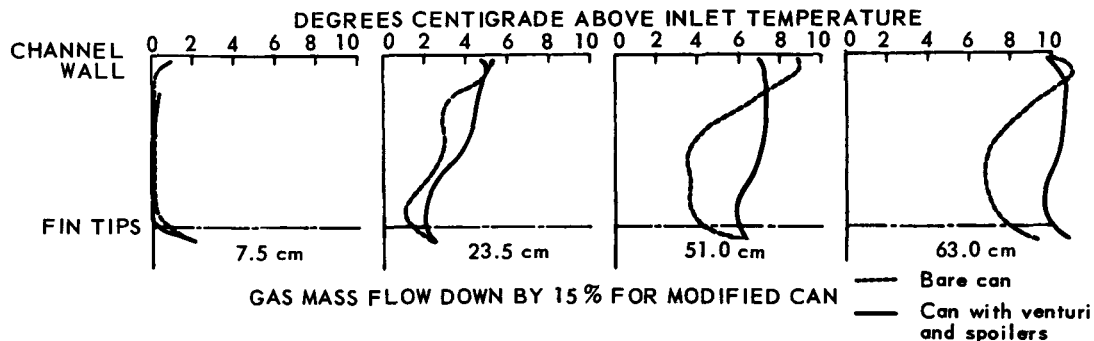


Figure 5. Effect of modifications on gas temperature distribution within fuel channel

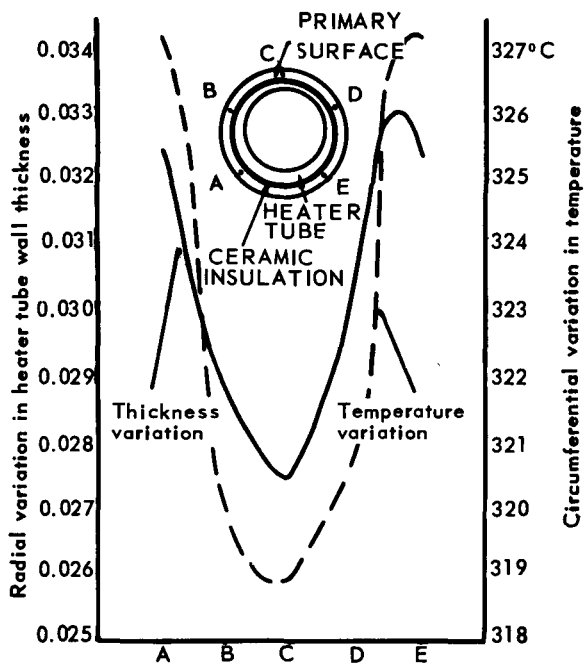


Figure 6. Variation of temperature with heater tube thickness for primary surface

former curve probably defines the quadrant of maximum heater thickness, the difference between the two curves being approximately 5% in $St.(S/A)$. The analogue results have a mean of $\frac{1}{2}(6.5\% + 4.7\%) = 5.6\%$ and hence agree quite closely as other effects are neglected.

Cumulative effects of manufacturing tolerances

Allowance has to be made for variations in the physical dimensions of fuel element cans due to manufacturing tolerances. Changes in the diameter over the fins, the root diameter and the lead of the spiral have been assessed [6] and show a variation of $\pm 2.4\%$ in $St.(S/A)$ over the normal range of w/μ . Thus if all the tolerances are cumulative the variation

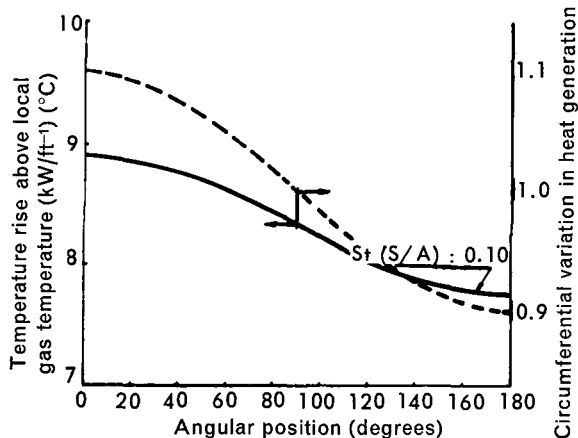


Figure 7. Can temperature distribution for a heater tube with a 10% variation in heat generation

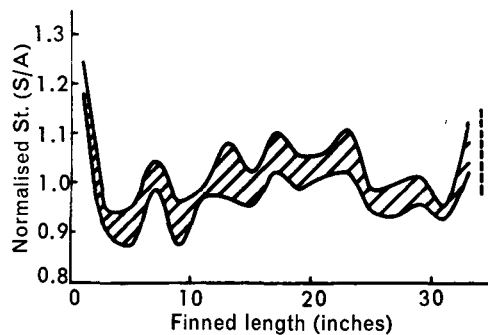


Figure 8. Typical envelope of the over-all scatter band between quadrants for a Hinkley Point fuel can

in $St.(S/A)$ will be approximately 4.8%. In many heat transfer investigations the same can, or cans, are tested several times and are thus subjected to repeated thermal cycles. This leads to small dimensional changes which have been found to introduce variations of $\pm 3.2\%$ in $St.(S/A)$ [6]. Where the repeated use of cans is necessary the test assemblies should be measured before and after an investigation.

Effects due to thermocouples

This is probably the most vexed subject in laboratory heat transfer techniques and can be divided into two main parts, namely: (a) the effect on the temperature being measured due to the presence of thermocouples; (b) changes in thermocouple signal due to variations in temperature level and gradient.

The number of thermocouples used in a normal heat transfer test on a fuel element can has tended to increase. The normal procedure is to measure the can root temperature at 2 in (5.08 cm) intervals along the centre line of each quadrant making a total of some 80 thermocouples on each can. Nickel-chromium, nickel-aluminium alloy 32G (0.201 mm) (B. & S.) wire is used, each reel being calibrated. Figure 10 shows a typical test assembly with the thermocouples grouped together and led downstream along the splitters. One group may be seen on the first can, two groups at the centre of the second can and five at the centre of the third can. This leads to increasing interference with the gas flow over the length of the assembly. The effect of the thermocouples on $f/A^2 de$ (f = fanning

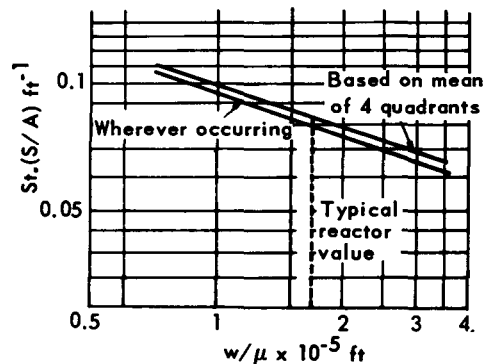


Figure 9. Minimum heat transfer performance

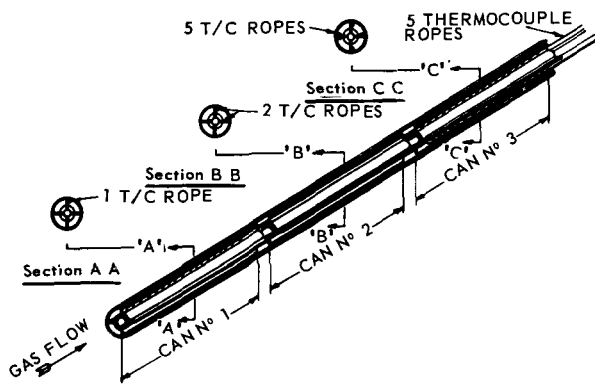


Figure 10. Section through test channel showing disposition of thermocouple cables in "ropes"

friction factor, de = hydraulic diameter) can be seen in Fig. 11, an 11.7% increase being obtained on the third can at a value of $w/\mu = 2 \times 10^5$ ft. It is not possible to measure the change in $St.(S/A)$ directly under the same conditions but its value must be affected. This difficulty has been overcome by leading the thermocouples along slots cut into the bottom, and within the thickness, of the splitters, which arrangement has no effect upon $f/A^2 de$ and by implication upon $St.(S/A)$. This procedure is now standard practice at the Laboratories.

At temperatures above about 300 °C at the hot junction, the thermoelectric properties of nickel-chromium/nickel-aluminium wire change with time. Many heat transfer tests are undertaken at temperatures below 300 °C, but in assessing fuel element performance at reactor temperature it is necessary to maintain values of up to 450 °C for several hours. The change in measured temperature during this time is relatively small, but a more serious effect can follow changes in the structure of the thermocouple wire [7]. If the temperature gradient between hot junction and detector is changed, then much larger errors in temperature readings will occur [8]. To eliminate these errors completely requires calibration *in situ*, and

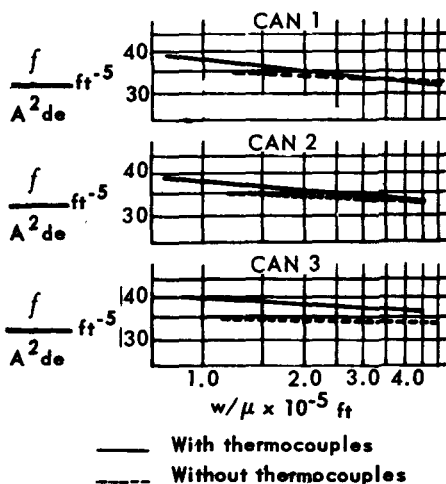


Figure 11. Effect of thermocouple arrangement in Fig. 10 on $f/A^2 de$

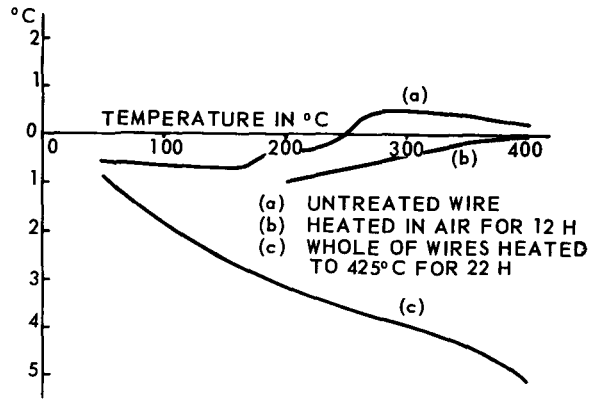


Figure 12. Typical error curves for 32G (BS) nickel-chrome/nickel-aluminium thermocouples

since this is not practicable, the effects are minimized by repeating low temperature readings taken early in heat transfer tests. Figure 12 shows typical results obtained from several specimens of nickel-chromium/nickel-aluminium thermocouples. Curve (a) is the error obtained from calibrating normally, (b) is obtained on heating the hot junction from 200 °C to 400 °C in air in 100 °C steps over a 13 hour period. Curve (c) is an extreme case: it was obtained by heating several specimens 10 yards long in air for 22 hours at 425 °C. For accurate results at elevated temperatures the use of noble metal thermocouples is recommended.

Fuel element end effects

In laboratory tests the end plug making the electrical connexions to the heater tube interferes with the simulation of an actual fuel element. Consequently the values obtained for $St.(S/A)$ over the last few inches of the test element are often ignored. In the reactor a thermal insulation disc is incorporated between the end of the uranium bar and the magnesium alloy end cap. This is shown diagrammatically on Figure 13, together with the can axial temperature distribution, predicted on an electrical analogue. Improved end fittings have been developed in the Laboratories to provide a better simulation of the reactor case and it can be seen that the expected accuracy at 1.6 in (4.26 cm) from the end of the can is 0.25 °C at 1 kW per foot (30.5 cm) heat generation rate. Results previously obtained on production cans are also shown in the figure. Heat is conducted into the end fittings of fuel elements inside the reactor; to obtain representative results in the laboratory it is necessary to ensure that: (a) the heated length of can is equal to the length of the uranium bar; (b) the length of can projecting beyond the ends of the heater bar should equal the length of can projecting beyond the uranium; (c) the end plugs should have low electrical resistance. (The necessarily high value of thermal conduction is fortunately unimportant.)

Evaluation of Berkeley reactor parameters

A detailed temperature survey of No. 1 reactor operating at near full power was made as part of the

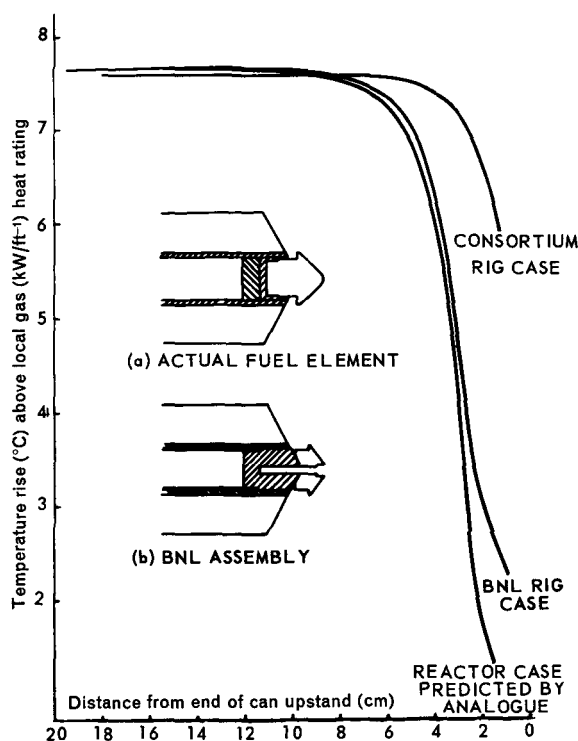


Figure 13. Comparison of can temperature distributions for a reactor fuel element, a BNL can assembly and a consortium can assembly

commissioning programme. The results were analysed by The Nuclear Power Group (TNPG) and are reported in their paper [9]. A second survey in December 1962 [10] enabled the Generating Board to further assess the fuel element performance [11].

The reactor operated under steady conditions during the survey and measurements were made of power, gas mass flow and neutron flux as well as can and gas temperatures. The axial flux plots, taken in positions remote from control rods, were interpolated to give the flux at particular channels. The channel mass flow was estimated from the total mass flow and the individual flow patterns established during previous commissioning tests. This enabled the heat transfer parameter $St.(S/A)$ to be calculated at the position of the tenth fuel element which carried a thermocouple. The flow parameter w/μ was calculated in a similar manner. The heat output falls off in the outer channels of the core and the reactor is gaged to maintain sensibly constant maximum can temperatures. The value of w/μ varied from approximately 1.6×10^5 ft at the centre of the core to 0.5×10^5 ft at the outer channels. $St.(S/A)$ is plotted against w/μ in Fig. 14. The graph is based on results calculated for 78 of the 118 thermocouple fuel elements present in the reactor (the other positions were rejected owing to their proximity to control rods).

The standard deviation of the observed values of $St.(S/A)$ recorded in Fig. 14 is estimated to be 10.0%. Following a statistical analysis in which allowance has been made for the azimuthal variation in channel

heat generation rate, a correction has been made to this standard deviation. Consequently the actual variation in $St.(S/A)$ is believed to reduce to 9.1%. The reactor power during the survey was determined by five different methods which agreed to within $\pm 5\%$. A value of 544.3 MW has been used in this analysis.

From the same basic data, TNPG have also determined the variation in $St.(S/A)$ with w/μ . Their estimate agrees almost exactly with the reactor line in Fig. 14. The design line of $St.(S/A)$ Vs w/μ adopted by TNPG following laboratory heat transfer and pressure drop tests is also given in Fig. 14, together with the line obtained experimentally at BNL. The TNPG design line is approximately 10% below that measured in the flattened zone of the reactor. The reasons for the discrepancy most probably lie in the assumptions made in the theoretical analysis and in the accuracy of measurement both within the reactor and in the laboratory experiment. The following assumptions in the reactor analysis could affect the comparison:

- (a) 5.3% of the heat is generated in the graphite;
- (b) 4% of the gas leaks out of the channel before the thermocouple fuel element is reached;
- (c) 7% of the channel flow passes behind the struts;
- (d) The variation of axial heat generation rate is exactly proportional to the neutron flux as measured in a nearby flux plotting hole.

Thus an increase of 1% (i.e., from 5.3% to 6.3%) in the graphite heat generation would lead to a 1.1% reduction in $St.(S/A)$. If the out-of-channel gas leakage is reduced by 1%, $St.(S/A)$ is reduced by 2%. A further 2% reduction in $St.(S/A)$ results if only 5% of the channel flow passes behind the struts. A 3% error in estimating the neutron flux at the thermocouple fuel element position would reduce $St.(S/A)$ by

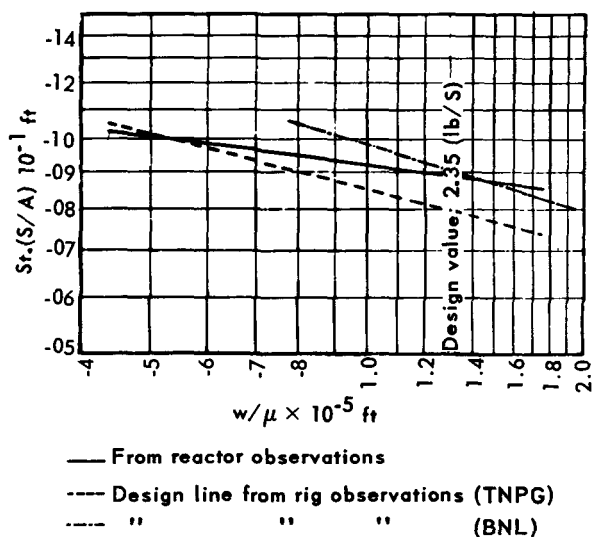


Figure 14. Comparison of Berkeley Reactor and laboratory experimental data.

Note: $St.(S/A)$ and w/μ are both based on total channel flow rate at the point of measurement

3%. Perhaps even more significantly an error of 3 °C on the channel inlet gas temperature (equivalent to one standard deviation) would reduce $St.(S/A)$ by 4%.

It is unlikely that the errors that do exist will all act cumulatively, but in comparing the results from laboratory experiments which have an estimated variation of $\pm 3.5\%$ with the reactor results, agreement such as that shown in Fig. 14 seems not unreasonable. Furthermore having once established a basis for the performance of fuel elements within the reactor at an early stage in their life, any changes which take place at a later stage are far more readily assessed.

Deformation of surfaces exposed to coolant gas flow

To facilitate the prediction of creep deformation of fins, splitters and braces caused by the coolant gas forces in the reactor channel, accelerated long-term hot loop tests have been carried out by the UKAEA Consortia and CEGB. In principle the tests consist of measuring the elements carefully relative to fixed datum points, subjecting them to gas forces usually in excess of reactor values for prolonged periods at high temperatures, followed by repeating the measurements to find the distortion suffered.

Fin deformation

On most of the current polyzonal cans, fin deformation can be considered to be made up of the superposition of several systematic patterns:

(a) The main pattern of displacement varies circumferentially but is axially constant, and can be attributed to the circumferential variation in differential pressure over the fins. Maximum deformation is in the direction of the gas flow and occurs about 10° from the leading edge of the fin (on the lee side of the splitter) reduces to a minimum at the centre of the quadrant, and changes sign at the trailing edge of the fin;

(b) Waving of the fins at the anti-ratchetting grooves is initiated by pressurizing the can on to the fuel and increases with thermal cycling and gas loading;

(c) Deformation caused by abrupt changes in gas flow pattern, e.g., at braces and at the extreme ends of the can where the fins become deformed in pairs or groups;

(d) At the fin leading edge, interaction of the fin deformation in (a) causes some of the fins to bend away from the splitter and increases the gap between the lee side of the splitter and the fin leading edge.

Figure 15 shows the deformation suffered by fins in an endurance test.



Figure 15. Example of fin deformation found in endurance test



Figure 16. Berkeley fuel element showing both splitter and brace deformation after endurance tests

Splitter deformation

The mode of splitter deformation varies from design to design, but in general is characterized by tilting and waving of the splitter. The splitter tends to lean away from the helical path of the gas: the braces oppose this movement but eventually they too lean over slightly so that the splitter tilts over its whole length. Due to the localized support of the braces and the axial variations in gas force, the splitter tilt varies along its length and a wave is produced.

On some of the fuel element designs there is a tendency for one or two braces per quadrant to lift radially away from the fin tips. Initially this is caused by the system of forces acting on the splitter/brace assembly producing a radial deflection of the brace arch. A backwards tilting of the brace arch occurs due to the drag forces and this produces a positive angle of attack to the gas stream and results in a lift force approximately normal to the brace arch. Excessive amounts of brace lift have been reported: in the case of the Berkeley element up to 0.4 in. in an endurance test of 3 000 hours duration [12]. Figure 16 shows the deformation suffered by the splitter cage in an endurance test.

Impact damage and fast bursts

The effect of local impact damage on fuel element heat transfer has been investigated by Lyall [13]. Unless the damage is both severe and widespread, the changes in performance are small; for example a change of 10% in Stanton number occurs locally when four adjacent fins are bent together to touch each other right across a single quadrant. If, however, an end weld suffers a small indentation, this may lead to ingress of CO₂ and subsequent oxidation of the uranium bar. This produces a local swelling some distance from the end of the element [14], leading rapidly to a rupture of the container, which is termed a fast burst.

An investigation into the behaviour of such an element has been made both using an electrical analogue [15] and by experimental simulation [16]. In the experiment a normal heater tube representing the uranium heat source was placed inside a Magnox cylinder to assist axial heat conduction. A ceramic mound was built up on the outside of the cylinder to simulate uranium oxide and finally a Magnox fuel element can was pressurized down onto the assembly as shown in Fig. 17. Tests in a pressurized carbon dioxide loop [17] at a heat rating of 2.76 kW/ft



Figure 17

(a) Simulated fast burst test assembly 35% circumferential strain; (b) Radiograph of fast burst; (c) An actual fast burst

(0.09 kW/cm) yielded the temperature differences between the can and the gas shown in Fig. 18. It can be seen that the can temperature at the point opposite the centre of the oxide mound was depressed by 7.5°C below the average can temperature. At a point 2 in (5.08 cm) downstream however, it had risen 16°C above the average value. At a reactor maximum heat rating of 18 kW/ft (0.59 kW/cm) the temperature values would be 49°C and 104°C respectively, at the same Reynolds number.

Referring back to Fig. 17 it can be seen that the oxide mound on the radiograph of an actual failed fuel element is asymmetric, the gradient on the downstream side of the mound being much less than on the upstream side. Comparison with Fig. 18

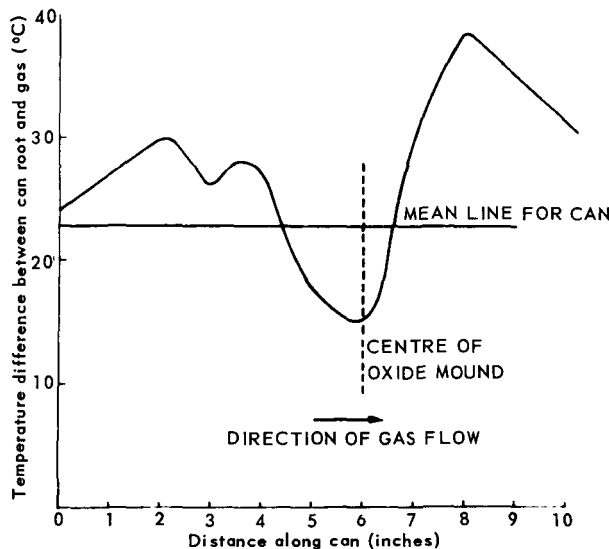


Figure 18. Temperature difference between can and coolant in the area of an oxide mound

suggests that once the uranium has started to oxidize, the increase in temperature downstream of the mound leads to further oxidation of the bar and the mound grows progressively in the direction of the coolant flow.

CONCLUSIONS AND FUTURE WORK

The variation of heat transfer along the length of a polyzonal can has been explained in terms of the flow pattern. This shows that better gas mixing and better entry conditions would lead to a significant improvement in the mean level of heat transfer at the expense of over-all pressure drop.

The present laboratory techniques for testing fuel element cans yield results which agree quite closely with data obtained directly from reactors. The work on deformations allied with post irradiation examination should enable an accurate assessment to be made of the performance of fuel elements in the reactor as progressively higher irradiations are achieved.

Apart from establishing as accurately as possible the heat transfer performance of different fuel elements as successive reactors are commissioned, future work in the Laboratories will include investigations into the transient performance of the polyzonal surface and the applicability of alternative extended surfaces to replacement fuel charges.

REFERENCES

1. Neal, S. B. H. C., and Hitchcock, J. A., *Large scale model investigation of heat transfer from polyzonal spiral surfaces*, J. British Nuclear Energy Soc., 1 (4), 307 (October 1962).
2. Ruddick, C. A., and McMullin, *The circumferential variation in temperature and Stanton number of a finned can with various heater assemblies*, NRC 62/51.
3. Kimpton, A. D., *Various methods of thermocouple attachment*, CEBG note RD/B/N (1963).
4. Watson, M. A. P., *Heat transfer and pressure loss performance of Hinkley Point cans*, CEBG note RD/B/N. 214 (December 1963).
5. Bennet, E. J., and Crisp, R. J., *Effects upon circumferential temperature distribution of heater tube wall thickness*, CEBG note RD/B/N (23 October 1963).
6. Owen, I., *Experimental heat transfer and pressure loss tests on Standard polyzonal fuel element cans*, CEBG note RD/B/N.215 (December 1963).
7. Berry, J. H., and Martin, D. L., *Thermocouple immersion errors*, A.S.T.M. Spec. Tech. Public; No. 178 (1955).
8. Fenton, A., *Thermocouples*, UKAEA TRG Memo 1884 (R).
9. French, P. R. J., Millard, D. J., Cartmell, M. J., and Cesterton, B. K., *Experience in relating the observed thermal performance of civil Magnox-uranium power reactors to design predictions and operating criteria*, P/171, Vol. 3, these Proceedings.
10. Berkeley Power Station CEBG report C. 9.2 (30th January 1963).
11. Mantle, P. L., *Heat transfer performance of fuel elements in Berkeley Reactor No. 1*, CEBG note RD/B/N.216 (January 1964).
12. Smith, S. L., and Hayes, D. J., *Endurance Tests on Berkeley Fuel Elements*, CEBG note RD/B/N.133 (June 1963).
13. Lyall, H. G., *Localized Damage: Effect on Can Heat Transfer*, CEBG note RD/B/N.55 (June 1962).

14. Greenwood, G. W., and Sharpe, B. F., *Post irradiation examination of CEGB fuel elements*, P/148, Vol. 10, these Proceedings.
15. Bennet, E. J., and Crisp, R. J., CEGB note RD/B/N (7 March 1963).

16. Knights, C. J., *On Simulation of fast burst geometry*, CEGB note RD/B/N (14 February 1962).
17. Marrow, A. R., *Heat transfer from simulated Bradwell fast burst*, CEGB note RD/B/N.217.

ABSTRACT—RÉSUMÉ—АННОТАЦИЯ—RESUMEN

A/136 Royaume-Uni

Flux de transfert de chaleur de la gaine polyzonale dans les réacteurs du Central Electricity Generating Board

par H. F. J. Hadrill *et al.*

Ce mémoire décrit les recherches sur le transfert de chaleur entreprises par le Central Electricity Generating Board, en ce qui concerne l'élément de combustible polyzonal. On expose les problèmes qui sont intéressants pour l'exploitant du réacteur et qui rendent nécessaire l'obtention d'une corrélation aussi exacte que possible entre les données de laboratoire et le comportement de l'élément de combustible dans le réacteur.

La nature complexe de l'écoulement du fluide et des processus de transfert de chaleur qui y sont associés autour de la surface spirale polyzonale, qui avait jusqu'alors échappé au traitement théorique pur, a été étudiée en utilisant un modèle à une échelle quatre fois plus grande que la normale. La compréhension de base ainsi acquise de ces mécanismes est décrite dans cet exposé, et on fait des suggestions pour améliorer le flux de transfert de chaleur de la surface.

Des études sur le transfert de chaleur avec surface polyzonale avaient montré que les résultats dépendent très fortement de la variation circonférentielle de l'épaisseur de la paroi du tube de chauffage, des effets accumulés des tolérances de fabrication, ainsi que de la présence des thermocouples et des erreurs en résultant. Les autres facteurs qui ont été étudiés expérimentalement comprennent les effets des pics de flux aux extrémités des éléments de combustible et les différences entre l'extrémité d'un élément de combustible dans un réacteur et l'assemblage de laboratoire chauffé électriquement.

Les mesures des paramètres de transfert de chaleur de l'élément de combustible dans un réacteur de Berkeley sont comparées avec les résultats de laboratoire. On discute la détérioration de l'efficacité qui provient de la déformation par fluage des ailettes, déflecteurs et entretoises, et on donne une indication de l'amplitude des effets. Le cas d'un élément de combustible défectueux contenant une excroissance d'oxyde sur la surface de la barre d'uranium a été considéré et on a évalué l'échange thermique à l'aide d'une expérience dans laquelle on simule la géométrie, et on compare ces résultats avec ceux d'une étude analogique.

A/136 Соединенное Королевство

Характеристики теплопередачи в полизональных оболочках для реакторов Центрального энергетического управления

Х. Ф. Дж. Хэдрилл *et al.*

В докладе представлены исследования теплопередачи в полизональном тепловыделяющем элементе, проведенные Центральным энергетическим управлением. Кратко рассматриваются проблемы, представляющие интерес для оператора на реакторе и требующие установления как можно более точной корреляции между лабораторными данными и данными испытаний тепловыделяющего элемента внутри реактора.

Сложная картина потоков жидкости вокруг полизональной спиральной поверхности и связанные с ними процессы теплопередачи, рассматриваемые ранее с чисто теоретической точки зрения, были исследованы экспериментально на модели, выполненной в четырехкратном масштабе. В докладе представлены основные результаты, которые были получены в этих исследованиях, и высказаны предложения, направленные на улучшение характеристик теплопередачи с поверхности.

Проведенные исследования характеристик полизональной теплопередачи показали критическую зависимость результатов от изменения толщины стенок нагревательных трубок, от эффектов накопления производственных допусков и ошибок в термонарах. Среди других факторов, подвергнутых экспериментальному изучению, исследовались эффекты всплеска потока на концах тепловыделяющих элементов и различия между тепловыделяющим элементом в реакторе и электрически нагреваемой лабораторной сборкой.

Результаты измерений параметров теплопередачи для тепловыделяющего элемента на реакторе в Беркли сравниваются с результатами лабораторных измерений. Обсуждается ухудшение рабочих характеристик, связанное с деформациями за счет ползучести в ребрах, скобах, распорках, и указываются величины этих эффектов. Рассматривается случай выхода из строя тепловыделяющего элемента, имеющего наложение окиси на поверхности уранового

стержня. Оценка тепловых характеристик делается на основании эксперимента, в котором имитируется данная геометрия, и затем сравнивается с результатами аналогичных исследований.

A/136 Reino Unido

Características de transmisión de calor de las vainas polizonales de los reactores CEGB

por H. F. J. Hadrill *et al.*

La memoria describe la investigación sobre transmisión de calor efectuada por la Central Electricity Generating Board sobre un elemento combustible polizonal. Señala los problemas que son de interés para el operador del reactor y que hacen necesario el obtener una correlación tan exacta como sea posible entre los datos de laboratorio y el comportamiento del elemento combustible en el reactor.

Se han investigado, usando un modelo de cuatro veces, la escala natural, la naturaleza compleja tanto del flujo del fluido como de los procesos asociados de transmisión de calor alrededor de la superficie polizonal helicoidal; estos fenómenos habían eludido previamente un tratamiento teórico. Se describen en esta memoria los conocimientos básicos que se han llegado a obtener sobre estos mecanismos y se hacen

sugerencias para mejorar las características de transmisión de calor de la superficie.

Las investigaciones efectuadas en los laboratorios sobre las características de transmisión de calor de las polizonas, han mostrado que los resultados dependen en gran manera de las variaciones circunferenciales del espesor de la pared del tubo calentado, de los efectos acumulativos de las tolerancias de fabricación y de la presencia de errores en los termopares. Se han investigado experimentalmente otros factores, como los efectos de los picos de flujo en los extremos de los elementos combustibles y las diferencias entre el extremo de un elemento combustible en un reactor y un conjunto calentado eléctricamente en el laboratorio.

Se comparan con los resultados de laboratorio las medidas de los parámetros de transmisión de calor de los elementos combustibles de un reactor de Berkeley. Se discute la disminución de rendimiento que resulta debido a la deformación por fluencia de aletas, separadores y soportes y se da una indicación de la magnitud de estos efectos. Se ha considerado el caso de un elemento combustible averiado, con una formación de óxido sobre la superficie de la barra de uranio y se ha evaluado el comportamiento térmico a base de un experimento en el cual se simula la geometría; se hace una comparación con los resultados basados en un estudio analógico.

Thermal design aspects of gas-cooled power reactor cores

By M. Troost,* P. Fortescue,* R. N. Lyon,** G. Melese* and G. Samuels**

Before considering in detail thermal designs of selected reactor cores, it is desirable to look at the picture somewhat more broadly, in order to understand the principles responsible for the wide design diversities exhibited by the many variants of the gas-cooled reactor. Considerable insight into the general characteristics of gas cooling as applied to reactors is forthcoming at once from the most elementary arguments. For simplification, only perfect, constant-property gases and smooth uniform passages are used. Acceleration of the gas is neglected and a uniform flow distribution is assumed. Temperature drops inside fuel elements are not included. Some useful relations between reactor parameters are now derived.

The following basic relations are used:

Frictional pressure drop:	$\Delta p = 2fLV^2\rho/(Dg_c)$	(1)
Mass balance:	$w = \rho\epsilon SV$	(2)
Heat balance:	$Q = wc_p \Delta T$	(3)
Heat transfer:	$\Delta t = Q/(\rho V c_p FAN_{St})$	(4)
Pumping power in the core:	$W = (w \Delta p/\rho)[T_0/(T_0 + \Delta T/2)]$	(5)
Reynolds analogy:	$N_{St} = \alpha f$ (for smooth surfaces and $N_{Pr} = 1, \alpha = 1/2$).	(6)
Hydraulic diameter:	$D = 4\epsilon SL/A$	(7)
Specific heat:	$c_p = C_p/M$	(8)
Average density:	$\rho = pM/[R(T_0 + \Delta T/2)]$	(9)

Here, Δp = core pressure drop
 L = core length
 ρ = average coolant density
 V = average gas velocity
 D = hydraulic diameter of channel
 w = total mass flow
 g_c = conversion factor (32.2 ft × pounds mass) (sec² × pounds force)
 ϵ = void fraction
 ΔT = coolant temperature rise in the core
 Δt = average surface to coolant temperature drop
 N_{St} = Stanton number ($h/V\rho c_p$)
 W = pumping power in the core
 N_{Pr} = Prandtl number ($c_p\mu/k$)
 C_p = coolant molar heat capacity

The required heated surface per unit frontal area of the core is

$$FA/S = \epsilon \Delta T / (N_{St} \Delta t), \quad (11)$$

and the required hydraulic diameter of a channel is

$$D = 4LN_{St}F \Delta t / \Delta T. \quad (12)$$

Using the friction factor correlation for turbulent flow in smooth tubes

$$f = 0.046N_{Re}^{-0.2}, \quad (13)$$

we find an expression for the hydraulic diameter,

$$D = 0.136(2\alpha LF \Delta t / \Delta T)^{0.835} [S\epsilon C_p \mu \Delta T / (QM)]^{0.166} \quad (14)$$

p = average ambient pressure
 N_{Re} = Reynolds number ($DV\rho/\mu$)
 f = friction factor
 S = frontal area of core
 c_p = coolant specific heat capacity
 Q = total thermal output
 F = heated fraction of the channel surface
 A = total frictional area in the core
 h = heat transfer coefficient
 T_0 = absolute inlet temperature
 μ = absolute viscosity
 k = thermal conductivity
 M = molecular weight
 R = universal gas constant

Appropriate manipulation yields a general relation between thermal output per unit frontal area of the core Q/S as a function of the allowable core pumping fraction W/Q , the void fraction ϵ and $\Delta t/\Delta T$, without any knowledge of the detailed core structure,

$$Q/S = \frac{\epsilon p \Delta T}{RT_0} \left(\frac{C_p^3 W}{M Q} \frac{F \Delta t 2\alpha g_c}{1 + \Delta T/2T_0} \right)^{\frac{1}{2}}. \quad (10)$$

The term $(C_p^3/M)^{\frac{1}{2}}$ emerges as a criterion of usefulness of coolants, Eq. (10), but the required heated surface varies for different coolants, Eq. (14). The choice of coolant, however, is mainly determined by such factors as inertness, irradiation damage, and availability. Since gross output varies as rapidly as the square root of the pumping fraction, it often pays to devote a substantial fraction of the reactor output to pumping. The gross output is found to be proportional to the gas pressure and independent of the core length.

* General Atomic, San Diego, California.

** Oak Ridge National Laboratory, Oak Ridge, Tennessee.

The ratio of the heated surface to flow area, $FA/\epsilon S$, depends only on the Stanton number for a given temperature limitation, Eq. (11). For a fixed flow area, it is shown in Eq. (10) that the thermal output does not change if the friction factor and the Stanton number are increased by the same factor, i.e., α is constant but there is a corresponding reduction in the heated surface FA , Eq. (11). As shown later, we can use surface roughening that almost doubles the Stanton number for a penalty of locally tripling the friction factor. Since only the hotter 1/2 to 2/3 downstream section of the fuel element needs roughening, the over-all channel pressure drop is only doubled. When the surface temperature is limiting, the fuel element diameter may thus be doubled and the number of fuel elements decreased by a factor of four, for a fixed total fuel element volume, reactor size, total power and coolant temperature; increased internal temperatures may then become a limiting factor.

MAIN FEATURES OF US GAS-COOLED REACTORS

One type of gas-cooled reactor, e.g., EGCR (Experimental Gas-Cooled Reactor) and EBOR (Experimental Beryllium Oxide Reactor), uses oxide fuel with metallic cladding. These reactors are designed to take advantage of the high burn-up potential of oxide fuel and the design freedom allowed by enrichment. The poor conductivity of the oxide, coupled with the desire for high power density, forces the use of groups of thin rods in channels. High surface temperatures necessitate the use of stainless steel or Hastelloy-X cladding, whose low thermal conductivities render fins inefficient. By using roughened surfaces, the allowable surface heat flux may be increased. The corresponding higher fuel temperatures may be limited by using hollow fuel elements. Hot-spot temperatures are usually obtained by comparing the results of calculations with several assumptions on their causes, rather than by using multiplying factors.

In another type of gas-cooled reactor, e.g., HTGRs (High Temperature Gas-Cooled Reactors) and pebble bed reactors, all-ceramic fuel elements are used. The elimination of metallic cladding allows very high surface temperatures. As the fuel is heavily diluted by moderator, structural fuel irradiation damage is virtually eliminated as a burn-up limiting factor. The incentive to seek high coolant temperatures, and accompanying high plant efficiency, goes far beyond the direct effect on fuel costs, for, in general, it implies increased useful output from a given reactor thermal power and hence reduced unit capital costs of that substantial part of the plant. As shown by Table 1, the HTGR class of reactors is capable of very satisfactory core power density. By virtue of the high temperature differentials and good steam conditions available, the associated boilers and turbines can also be very compact. HTGR type designs optimized for large scale power production have, in fact, exploited these features to the point where powers of the order

of 500 MW(e) are contemplated from total plant containment volumes little larger than the 40 MW(e) Peach Bottom, for similar core power densities.

Some thermal design parameters of US gas-cooled reactors under construction or in operation are presented in Table 1. The corresponding fuel elements are shown in Fig. 1. Rocket and airplane reactors are not discussed, nor are fast gas-cooled reactors. EGCR and HTGR will be described in more detail in later sections. A common problem to all gas-cooled reactors is the possibility of a loss-of-coolant-flow accident. This is more serious for gas-cooled reactors than for liquid-cooled reactors because the afterheat cannot be absorbed by the coolant. US gas-cooled reactors have therefore been equipped with internal heat sinks which absorb the heat of the initial transient resulting from temperature equalization within the fuel element which causes a rapid rise in surface temperature. Some kind of emergency cooling is supplied to remove the afterheat after the initial transient is over. Thus, the design power density of the reactor may be limited by afterheat removal considerations.

EBOR, now under construction, is designed to test the high-temperature behavior of BeO as a reactor moderator [1]. The selection of the present EBOR fuel element was based, in part, on the inherent simplicity, the readily predictable thermal performance, and satisfactory behavior in the event of a loss-of-coolant accident. To achieve proper performance, the fuel rods must be closely spaced in the annular passage. The ratio of the minimum clearance between rods to the rod diameter is 0.14. The ratio of the pitch of the helical rod spacers to the rod diameter is 20. The coolant flow to each fuel element is orificed so that the maximum cladding temperature in each element is about the same. The local heat transfer coefficient around a fuel pin may vary 20 to 30% from its average value [2].

The 630-A reactor [3], which is derived from the Aircraft Nuclear Propulsion program, is proposed as an integral nuclear steam generator for ship propulsion. In this reactor the thickness of the coaxial fuel rings within a fuel assembly is varied to give approximately equal heat fluxes from all rings. A re-entrant water-filled moderator tube is centered in each of the fuel tubes to reduce the flux depression through the assembly. The diameter of the moderator tube is varied in four radial zones in the reactor to obtain nearly the same surface heat flux for all radial positions. Heat losses to the water moderator have to be tolerated to ensure enough cooling by radiation if coolant flow is lost.

The ML-1 reactor [4] is a small portable unit using a closed-cycle gas turbine for power generation. The spacing of the stainless steel pressure tubes, which contain the fuel element bundles, is varied to flatten the radial power distribution. The fuel loading of the pins within the bundle is varied to equalize the cladding temperatures. A 40 mil Hastelloy-X wire separates the pins from each other and from the inner

Table I. Thermal characteristics of some US gas-cooled reactors

	EGCR	HTGR	EBOR	630-A	ML-1	UHTREX
Power						
Thermal, MW(th)	85	115.5	10	67.4	3.3	3
Electrical, MW(e)	25	40	None	20	0.33	None
Active core						
Diameter, m	3.6	2.8	0.59 side	1.22	0.56	0.585 id 1.78 od
Length, m	4.4	2.3	1.93	0.70	0.56	1.0
Power density, kW/liter of core	1.87	8.3	13.7	82.5	15.3	1.3
Power conversion	482 °C steam 87 atm	537 °C steam 95 atm	None	510 °C steam 60 atm	Closed-cycle gas turbine	None
Heat flux						
W/cm ²	55 (max)	35 (max)	84 (max)	19 (avg)	44.5 (max)	35 (max)
W/cm	330 (max)	980 (max)	251 (max)	1 000 (avg)	85 (max)	140 (max)
Maximum temperature, °C						
Surface	816	1 050	815	—	955	1 593
Fuel	1 650	1 330	1 040	813	1 180(UO ₂ -BeO) 1450 (UO ₂)	1 610
Coolant gas	Helium	Helium	Helium	Air	N ₂ or Air	Helium
Total mass flow, kg/s	53.5	55.5	6.3	160	11.3	1.29
Inlet temperature, °C	266	345	400	300	422	870
Outlet temperature, °C	566	728	700	650	650	1 320
Pressure, atm	22	23.0	72.5	27	20.5	34
Coolant void fraction, %	6.2	12.8	11	—	—	—
Reactor pumping fraction, %	2	0.55	1.4	3 ^a	3.3 ^a	0.07
Moderator	C	C (in element)	BeO	Water	Water	C
Number of channels	234	804 elements	36	85 ^b	61 ^b	312 ^c
Fuel	UO ₂	UC ₂ , ThC ₂ in C	UO ₂ -BeO	UO ₂ ^d	UO ₂ , UO ₂ -BeO	UO ₂ in C
Enrichment, %	2.46	93.5	62.5	93.5	93.5	93.5
Cladding material	304 SS	C	Hastelloy-X	80Ni-20Cr	Hastelloy-X	None
Cladding thickness, cm	0.05	0.95	0.05	0.10	0.075	—
Fuel region id and od, cm	0.82 × 1.8 ^e	4.45 × 7.0	0.0 × 0.85 ^f	0.45 ^g	0.0 × 0.46 ^h	1.27 × 2.54
Fuel element length, cm	6 × 73.6	366	210	9 × 7.65	79	4 × 14

^a Primary loop. ^b Pressure tubes. ^c 13 levels of 24 radial channels. ^d 38.2 wt-% UO₂ in 80 Ni-20 Cr alloy. ^e An element contains 7 pins. ^f An element consists of an annular ring of 18 rods around a BeO spine. ^g 10-13 concentric rings 0.45 cm thick, cooled on both sides. ^h An element contains 19 pins (18 fueled).

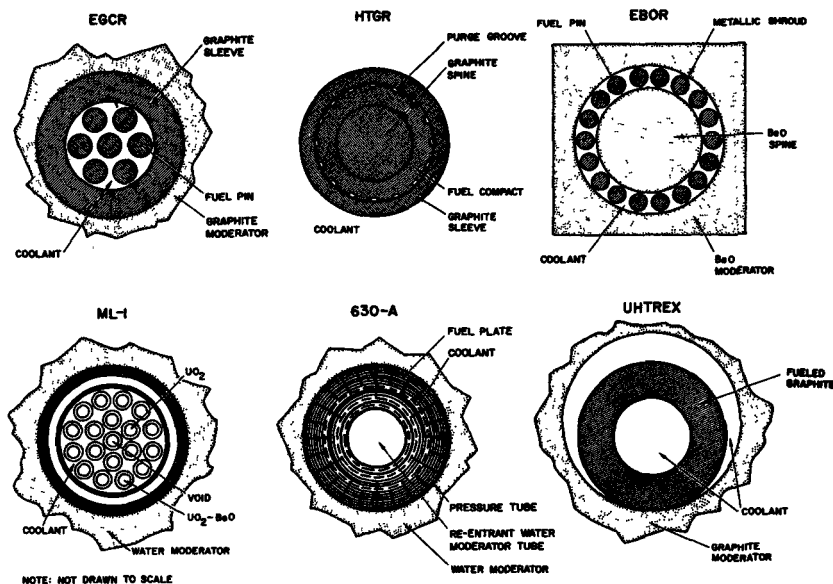


Figure 1. Schematic fuel element cross sections for the reactor of Table 1

liner that is itself insulated from the pressure tube by a 0.112 in. layer of Thermoflex ($\text{Al}_2\text{O}_3\text{-SiO}_2$).

The Ultra High Temperature Reactor Experiment (UHTREX) [5] is designed to supply process heat at very high temperatures. Since no cladding is used, the primary circuit contains large amounts of fission products.

EGCR THERMAL DESIGN

The fuel assembly for the EGCR consists of a seven-rod cluster of stainless steel tubes filled with cored UO_2 pellets, each cluster supported within a 1 in. thick graphite sleeve of 3 in. id and 5 in. od (see Fig. 1). There are six stacked fuel assemblies in each coolant channel [6].

As unsymmetrical temperature variations around the rods result in differential expansion and bowing, initial emphasis was placed on minimizing the circumferential temperature variations in the six outer rods of the seven-rod cluster by proper radial location in the coolant channel. Since the rods are supported at the ends, such bowing restricts gas passage along the hotter portion of the rod, and results in further bowing. It is important to design the fuel assembly so that the total bowing and flow restriction does not result in a local rod-surface temperature that will damage the stainless steel fuel-rod tubes. To determine the temperature structure within a cluster, a rather extensive series of heat-transfer and fluid-flow experiments was conducted [7, 8]. The most convenient qualitative experimental method was found to be measurement of the local removal of a naphthalene coating on one of the outer cluster tubes in an isothermal test using air [9]. Naphthalene removal is most uniform when the outer rods are equidistant between the center rod and the channel wall. However, heat-transfer tests indicate that the axial temperature rise of the gas is not uniform, and mixing between the passages of the cluster is very small; therefore, more space is required between fuel rods than between a rod and the channel wall [10]. Minor variations in the roughness of the outer channel wall do not seriously influence the flow distribution at the expected Reynolds number of about 50 000.

The stability of the fuel rods in the assembly is enhanced further by mid-length spacers. Both the end fixtures and the mid-length spacers disturb the flow so that the entire length of the rods is in a hydrodynamic entrance region. The most recent correlation of air data [11] fits the data within +6% and -8%

$$N_{Nu_b} = 0.041 N_{Re_b}^{0.77} (L/D)^{-0.15}$$

where the temperature difference associated with the Nusselt number ($N_{Nu} = hD/k$) is based on the mixed mean gas temperature and the average surface temperature of the outer rods at a distance L from the nearest upstream spacer; the subscript b refers to mixed mean temperatures.

The rotational position of the assemblies in the coolant channel will be random. Thus, outer rods of a preceding assembly may partially block entrance to

the spaces between the outer rods in the next assembly. The blockage will be most complete with a relative rotation of 30 degrees, while 60 degrees rotation is equivalent to no rotation. Apparently because of the mixing action of the spacers, a 30 degree rotation has little effect except just downstream from the spacers, but a 15 degree displacement of the preceding assembly produces a large eccentric variation in circumferential temperature along the entire first half of the rod and is easily detectable even beyond the mid-rod spacer. This effect results from a rotational flow component introduced by the unsymmetrical displacement of the preceding rods.

Pressure-drop measurements with atmospheric air [12] are well correlated over a range of Reynolds numbers by separating spacer and end effects from the remaining pressure drop. For the EGCR configuration $f = 0.17 N_{Re_b}^{-0.18}$.

For spacers, the loss coefficients, defined as $c = 2 \Delta p g_c / (\rho V^2)$, were largely independent of the main-stream Reynolds number, and were approximately 0.43 for the end supports for the rods and about 0.34 for the mid-rod spacers.

In calculating the local temperatures within the cluster, the following effects are considered: radial and axial heat-generation gradient, thermal radiation within the cluster, variable heat-transfer coefficient around the element and along the channel, gas temperature differences between the various flow passages, circumferential heat conduction around the graphite sleeve, and mixing between the flow passages. The flow of heat in the UO_2 pellets is assumed to be radial only. Analysis shows that at the end of the second assembly, where the heat generation is highest, the circumferential temperature difference between opposite sides of a fuel rod is 80 °F to 90 °F.

THE PEACH BOTTOM HTGR THERMAL DESIGN

The Peach Bottom HTGR [13, 2] is a helium-cooled reactor with semihomogeneous graphite fuel elements. The inlet temperature of 652 °F lies above the level at which the Wigner effect in the graphite reflector is important, but still allows the pressure vessel to be made of low-alloy steel. The outlet temperature of 1 342 °F is limited by the external circuits and not by the core.

The fuel element consists of a graphite spine of 1.75 in. diam, surrounded by a fuel ring of 2.75 in. diam that is contained in a graphite sleeve. The fuel ring consists of coated uranium and thorium carbide particles embedded in a graphite matrix. The elements form a closely packed hexagonal pattern with the 3.50 in. elements on a 3.55 in. pitch. Each element is surrounded by six tricuspid cooling passages. The elements are separated by four ring-shaped spacers.

A fuel ring was chosen rather than a solid central fuel cylinder of the same diameter to limit the peak temperature in the fuel; the present thickness of the ring is convenient for fabrication reasons. The sleeve is provided to keep fission products out of the primary

coolant stream and to provide structural rigidity to the fuel element. Volatile fission products are purged from the element into fission-product traps.

The fuel element has no sharp temperature limitation (e.g., melting point, phase change) but fission-product release from the fuel particles increases appreciably between 2 700 °F and 3 000 °F. The maximum design fuel temperature was taken to be 2 700 °F. A small local hot spot is not very serious, as a somewhat larger than normal fission-product release can be accepted in small areas of the core. It becomes more important, therefore, to know what percentage of the fuel is above certain temperatures rather than to try to prevent any fuel from reaching a limiting temperature.

The average heat-transfer coefficient and the circumferential variation of the heat-transfer coefficient around a fuel element were obtained experimentally [14]. Other uncertainties, such as the flow distribution in the reactor core and the effects of bending of fuel elements, were investigated analytically.

Experimental work [14] has shown that the smooth tube correlation using the hydraulic diameter of the tricuspid-shaped channel yields answers which are about 5% too high. The heat-transfer coefficient around the circumference varies between 55 and 130% of its average value. The friction factor for the channel lies slightly below the correlation for a smooth tube; however, the four spacers contribute approximately as much pressure drop as the channel friction [15].

The following heat-transfer and friction-factor correlations are used in the design for Reynolds numbers between 15 000 and 100 000:

$$N_{Nu_f} = 0.021 N_{Re_f}^{0.8} N_{Pr_f}^{0.4} \quad \text{and} \quad f = 0.079 N_{Re_f}^{-0.25},$$

where the subscript *f* refers to properties evaluated at film temperature.

Temperature and pressure-drop calculations in the HTGR are complicated because the HTGR employs an open core, i.e., all cooling channels are interconnected and orificing is not possible. The local and total power input into the coolant varies from channel to channel; therefore, the resistance to flow also varies as a result of the differences in coolant viscosity and acceleration. The resulting pressure differences between channels are equalized by flow from one channel to another, i.e., cross flow. At first sight, it is not obvious whether cross flow is beneficial or disadvantageous: the hottest channel loses gas continuously because of higher accelerational and frictional local pressure drops, but more gas enters at the inlet of the hottest channel than would be possible for a closed hot channel. For the HTGR, it has been shown that these two effects approximately cancel each other, as far as maximum temperatures are concerned.

The change in coolant outlet temperature [2] in the HTGR resulting from sudden changes in power, coolant inlet temperature, or coolant flow rate is quite slow in comparison with other reactor systems because of the large heat capacity of the fuel element.

HTGR transients are usually limited not by fuel element temperatures but by the outlet temperatures that the ducts and steam generator can withstand. When coolant flow is interrupted, followed by a reactor scram, the fuel cools initially due to temperature equalization. The structural parts of ceramic elements (graphite) can withstand quite high temperatures without damage to the structural integrity of the element. In the Peach Bottom HTGR, emergency cooling is supplied by cooling the pressure vessel and transporting the afterheat from the fuel elements by conduction, natural convection, and radiation.

PEBBLE BED REACTOR CORE DESIGN

In selecting the core for a pebble bed reactor, assuming that the gas temperatures and total heat output are fixed, the relationship between the variables and the thermal-stress limitation places narrow limits on the range of values that one may select. In general, one wants the core power density large to minimize core dimensions, and the fuel elements large to minimize fuel fabrication cost and to simplify fuel handling. Typical core power densities are 5 to 10 kW/liter and ball diameters 1.5 to 2.5 in.

The importance of the core pressure drop depends on the direction of flow through the core. For a downward or radial-flow core, the restriction on pressure drop is the pumping power or structural-restraint limitations, whereas for an upward flow through the core, the limitation on pressure drop will be the levitation flow or flow rate at which the upper layer of fuel elements begins to move. Experiments with gas flowing upward through beds of spheres have indicated that when the pressure gradient equals 80% of the bulk bed density, spinning of the balls in the upper layer begins [16]; at still higher flow rates, actual levitation of some spheres will occur. Recent studies have been summarized by Bundy [17].

The relations used below are taken from Refs. [18 to 21]. Later data [22] indicate that the equation for pressure drop is not valid for $N_{Re} > 15\,000$. Above this value, the friction factor becomes a constant. The pressure drop through a bed of spheres may be expressed as

$$\Delta p = \frac{15 G_s^{1.73} \mu^{0.27} L}{g_c \epsilon^3 \rho [d/(1 - \epsilon)]^{1.27}}$$

where G_s is the approach mass velocity, and d is the sphere diameter. The limit that thermal stress places on the mean power density in the ball bed is

$$q = 60(1 - \nu)k\sigma_u(1 - \epsilon)/(\alpha E d^2 \gamma),$$

where q is the maximum allowable mean power density, ν is Poisson's ratio, σ_u is the ultimate tensile strength, E is the modulus of elasticity, α is the coefficient of linear expansion, and γ is the maximum/mean power ratio.

The heat-transfer correlation for a bed of spheres is

$$N_{St} = 0.5 N_{Pr}^{-0.66} [N_{Re}/(1 - \epsilon)]^{-0.3},$$

with N_{St} and N_{Re} based on the superficial gas velocity and the ball diameter.

The mean surface-to-gas temperature drop is $\Delta t = qd/6h(1 - \epsilon)$.

SURFACE ROUGHENING AND SWIRL FLOW

In gas-cooled reactors the film temperature drop is usually a larger fraction of the total temperature drop than in other types of reactors. It is therefore worth while to decrease the film temperature drop Eq. (11). This may be accomplished in several ways: the heat-transfer surface FA may be increased, the flow area ϵS may be decreased, and the Stanton number N_{St} may be increased. These three effects are compared in Ref. [23]. Many investigators, both in the United States and in other countries [24–30], have studied experimentally and theoretically the ways of improving heat transfer with roughened surfaces. To obtain good performance, they found that the height of the turbulence promoters should be about the thickness of the laminar sublayer and the buffer layer. The friction factor becomes nearly independent of the Reynolds number, while the Stanton number decreases very slowly with increasing Reynolds number for turbulent flow of gases. For a given roughness height, there is an optimum ratio of pitch to height that produces the largest values of friction factor and Stanton number: ~ 7 to 8. The best results given in Refs. [26, 28] may be correlated by plotting the increase in Stanton number versus the increase in friction factor. Data from Refs. [24, 25 and 29], among others, check with this correlation. The two following approximations seem to represent several sets of published data within $\pm 10\%$ for turbulent flow of gases such as air, nitrogen, CO_2 , or helium ($N_{Pr} \approx 0.7$), for $3 \times 10^4 < N_{Re} < 6 \times 10^5$, and for $1 \leq f^+/f \leq 3$

$$N_{St}^+/N_{St} = (f^+/f)[1 + (f^+/f - 1)/4]^{-1}$$

$$f^+/f = (N_{St}^+/N_{St})^3[1 + 5(N_{St}^+/N_{St} - 1)/3]^{-1},$$

where $+$ refers to roughened surfaces. These equations show that doubling the Stanton number triples the friction factor. Surface roughening is currently used in the Windscale Advanced Gas-Cooled Reactor and is now incorporated in the design of most advanced metal-clad gas-cooled reactors.

Swirl-flow heat transfer with gases in tubes has been studied with swirl induced by an internal twisted tape [31, 32] and by tangential tube-wall slots [33]. The results show ratios of swirl/axial-flow heat-transfer coefficients at a given Reynolds number of 1.1 to 3.0 with increased friction factors. A good summary of data is given in Ref. [34].

NUMERICAL METHODS AND APPLICATIONS

Most of the thermal design analysis is performed by analysing a model by numerical methods. A number of digital computer codes have been developed in which thermal problems are solved by replacing the

relevant differential equations by finite-difference equations. For coolant flow, one usually makes the approximation that the transit time of the gas through the coolant channel is small compared with the calculational time step. The finite-difference equations are often made implicit to avoid time-step limitations in transient problems. The solution of the simultaneous finite-difference equations is usually obtained by iterative methods as the number of unknown points is generally too large for effective matrix inversion and nonlinearities make it impractical in any case. Good, commonly used, methods are the Peaceman-Rachford method for regular two-dimensional geometries or an extrapolated Liebman method for irregular or three-dimensional geometries. Nonlinearities (temperature-dependent properties, thermal radiation) are treated by re-evaluating the properties between iterations as a function of the current temperatures.

Codes for one-, two- and three-dimensional geometries have been developed in which all thermal properties may be temperature dependent, heat generation rates may be space and time dependent, radiation across internal gaps is permitted, and thermal expansion is taken into account. The boundary conditions may be completely general, e.g., radiation, conduction, and convection.

Such codes and also analytical methods have been applied to obtain temperature distributions in reactor cores and in complicated geometries such as those encountered in homogeneous fuel elements, e.g., fuel elements pierced by coolant channels, or fuel elements in which the fuel is concentrated in some regions of the element. With uniform convective cooling at the surface of circular equidistant cooling holes inside a circular cylinder, and with uniform heat generation, the optimum location of the holes is nearly independent of their dimension, for a given number of holes [35]. This optimum radial location is about $0.6r$ for six holes or more, independent of the Biot number ($N_{Bi} = hr/k$). A similar problem is solved in Ref. [36] for a triangular or square cooling hole arrangement in a large solid with given coolant-hole surface temperature.

The fuel concentration in the annulus of an HTGR type fuel element which gives the lowest internal hot spot and average temperature is found to be 50 to 65 volume % for ratios of fuel/matrix thermal conductivities of 5 to 20%, respectively. This result is nearly independent of the total fraction of fuel in the element below about 25 volume %; the thermal conductivity of fuel dispersed in the matrix may obey either a linear law or Maxwell's law [37]. For ratios of thermal conductivities above 45 to 50%, the annulus should contain fuel only, subject to metallurgical limitations.

The optimum shape of radial fuel holes in a spined cylindrical fuel element, cooled at the outside, has been studied as a function of various parameters, such as number of fuel holes of given total area, and ratio of conductivities of fuel to matrix [38]. The maximum internal fuel temperature is minimized with respect to

the length/diameter ratio of the fuel holes. Circular holes are usually not as good as elongated pie-shaped holes for low fuel/matrix conductivity ratios.

Good neutron economy and high coolant temperatures can be obtained in all-ceramic (i.e., BeO) cores, but the heat flux for a given size of fuel element is usually limited by tensile thermal stresses. Other coolants besides helium, e.g., CO₂, may be used at high temperatures in an all-BeO reactor. Steady-state temperatures and elastic thermal-stress distributions for several geometries with uniform internal heat generation have been tabulated [39]. It may be noted that the maximum tensile stress that occurs at the cooler boundary is proportional to the difference between average and surface fuel element temperatures. Nonuniform internal heat generation has been studied extensively [40]. Elastic plastic deformation of a cylinder insulated on the outside and cooled inside, with uniform heat generation, has been studied [41]. The thermal-stress limitation for a given heat flux may be eased by cooling the ceramic fuel element both internally and externally. One can also use a graphite sleeve to provide structural strength to a BeO fuel element [42].

Bounds for the efficiency of longitudinal fins of arbitrary shape with variable surface heat-transfer coefficient are given in Ref. [43]. The optimum shape of a fin with a given profile area and the corresponding maximum heat flux are quite different from the values obtained by using a constant heat-transfer coefficient.

In conclusion it may be stated that the design trend of gas-cooled power reactors in the USA has been towards high coolant outlet temperatures combined with simple (all-ceramic) fuel elements.

REFERENCES

1. *Experimental Beryllium Oxide Reactor Program Quarterly Progress Report*, USAEC report GA-4386, General Atomic (31 July 1963).
2. Katz, R., and Troost, M., *Thermal Design Aspects of Gas-Cooled Reactors*, USAEC report GA-2944, General Atomic (1962).
3. *The 630-A Marine Reactor*, Nucl. Eng., 9, 50 (February 1964).
4. *Army Reactor Systems Program*, Power Reactor Technology, 6, 3, 57 (June 1963).
5. *Ultra High Temperature Reactor Experiment (UHTREX), Hazard Report*, USAEC report LA-2689, Los Alamos Scientific Laboratory (20 April 1962).
6. Samuels, G., *Design and Analysis of the Experimental Gas-Cooled Reactor Fuel Assemblies*, USAEC report ORNL-3478, Oak Ridge National Laboratory (27 September 1963).
7. Crandall, W. H., and Higgins, R. M., *Pressure Drop Experiments of the Title II Fuel Assembly for the Experimental Gas-Cooled Reactor, Section III of the Fuel Assembly Heat Transfer and Channel Pressure Drop Experiments for the EGCR Research and Development Program*, USAEC report RD-0009, Allis-Chalmers Mfg. Company (3 October 1960).
8. *Heat Transfer Experiments of the Title II Fuel Assembly for the Experimental Gas-Cooled Reactor*, USAEC report RD-0010, Allis-Chalmers Mfg. Company.
9. Wantland, J. L., and Miller, R. L., *Heat Transfer in Septafoil Geometries by Mass-Transfer Measurements*, USAEC report CF-59-6-9, Oak Ridge National Laboratory (30 June 1959).
10. *Gas-Cooled Reactor Project Quarterly Progress Reports*, USAEC reports ORNL-2964, ORNL-3015, ORNL-3049, Oak Ridge National Laboratory (1960).
11. Kidd, G. J., *Experimental Determination of the Temperature Structure and Heat-Transfer Characteristics of the EGCR Title II Fuel-Element Assembly*, USAEC report ORNL-TM-807, Oak Ridge National Laboratory, to be published.
12. Kidd, G. J., and Wantland, J. L., *Pressure Drop Characteristics of Circular Ducts Containing Septafoil Rod Clusters*, USAEC report ORNL-TM-703, Oak Ridge National Laboratory (15 October 1963).
13. Fortescue, P., Nicoll, D., Rickard, C., and Rose, D., *HTGR-Underlying Principles and Design*, Nucleonics, 18, 1, 86 (1960).
14. Palmer, L. D., and Swanson, L. L., *Measurements of Heat-Transfer Coefficients, Friction Factors, and Velocity Profiles for Air Flowing Parallel to Closely Spaced Rods*, Proc. International Heat Transfer Conference, August 1961, Part III, 535, ASME, New York (1961).
15. Ross, S., Day, E. A., and Skeeahan, R. A., *Tests on Half-Scale Model of 40 MW(e) Prototype HTGR*, USAEC report GA-2963, General Atomic (20 June 1962).
16. Bundy, R. D., *Full-Scale Packed-Bed Reactor Core Experiments, Gas-Cooled Reactor Program Semiannual Progress Report, Period ending March 31, 1962*, USAEC report ORNL-3445, Oak Ridge National Laboratory, 308 (1962).
17. Bundy, R. D., *Summary of Recent Literature with Application to Pebble Bed Reactors*, USAEC report ORNL-TM-806, Oak Ridge National Laboratory, to be published.
18. *Design and Feasibility of a Pebble Bed Reactor Steam Plant*, USAEC report NYO-8573, Sanderson and Porter (1958).
19. Fraas, A. P., Carlsmith, R. S., Coran, J. M., et al., *Preliminary Design of a 10 MW(th) Pebble Bed Reactor Experiment*, USAEC report ORNL-CF-60-10-63 (rev.), Oak Ridge National Laboratory (8 May 1961).
20. Fraas, A. P., Carlsmith, R. S., Coran, J. M., et al., *Design Study of a Pebble Bed Reactor Power Plant*, USAEC report ORNL-CF-60-12-5 (rev.), Oak Ridge National Laboratory (11 May 1961).
21. *Conceptual Design of The Pebble Bed Reactor Experiment*, USAEC report ORNL-TM-201, Oak Ridge National Laboratory (17 May 1962).
22. Touchton, W. F., Jr., *Pressure Drops Through Cylindrical Beds of Packed Spheres*, Franklin Institute report F-B 1994 (February 1963).
23. Melese, G. B., *Comparison of Partial Roughening of the Surface of Fuel Elements with Other Ways of Improving Thermal Performance of a Nuclear Reactor*, Trans. Amer. Nucl. Soc., 6, 337 (November 1963).
24. Kemeny, G. A., and Cyphers, J. A., *Heat Transfer and Pressure Drop in an Annular Gap with Surface Spoilers*, J. Heat Transfer, 83, 189 (1961).
25. Dipprey, D. F., and Sabersky, R. H., *Heat and Momentum Transfer in Smooth and Rough Tubes at Various Prandtl Numbers*, Intr. J. Heat Mass Transfer, 6, 329 (1963).
26. Kattchee, N., and Mackewicz, W. V., *Heat Transfer and Fluid Friction Characteristics of Tube Clusters with Boundary Layer Turbulence Promoters*, ASME paper 63-HT-1 (1963).
27. Kattchee, N., and Mackewicz, W. V., *Effects of Boundary Layer Turbulence Promoters on the Local Film Coefficients of ML-1 Fuel Elements*, Nuclear Sci. Eng., 16, 1, 31 (1963).
28. Walker, V., and Rapier, A. C., *Fuel Element Heat Transfer*, J. Brit. Nucl. Energy Soc., 2, 268 (April 1963).
29. Nunner, W., *Heat Transfer and Pressure Drop in Rough Tubes*, VDI Forschungheft 455, Series B, 22, 5 (1956). AERE Lib/Trans., 786 (1958).
30. Malherbe, J. M., *Influence des rugosités de paroi sur les*

- coefficients d'échange thermique et de perte de charge, CEA-2283 (1963).
31. Kreith, F., and Margolis, D., *Heat Transfer and Friction in Turbulent Vortex Flow*, Appl. Sci. Res., Sec. A, 8, 457 (1959).
 32. Smithberg, E., and Landis, F., *Friction and Forced Convection Heat-Transfer Characteristics in Tubes with Twisted Tape Swirl Generators*, ASME Paper 62-WA-176 (1962).
 33. Green, N. D., and Gambill, W. R., *A Preliminary Investigation of Air Film Heat-Transfer Coefficients for Free- and Forced-Vortex Flows Within Tubes*, USAEC report CF-58-5-67, Oak Ridge National Laboratory (23 May 1958).
 34. Gambill, W. R., and Bundy, R. D., *An Evaluation of the Present Status of Swirl-Flow Heat Transfer*, ASME paper 62-HT-42 (1962): also USAEC report CF-61-4-61, Oak Ridge National Laboratory (24 April 1961).
 35. Rowley, J. C., and Payne, J. B., *Steady State Temperature Solution for a Heat-Generating Circular Cylinder Cooled by a Ring of Holes*, J. Heat Transfer, Trans. ASME (1964).
 36. Sparrow, E. M., *Temperature Distribution in an Internally Cooled, Heat-Generating Solid*, ASME paper 60-SA-15 (1960).
 37. *Advanced Beryllium Oxide Concepts, Progress Report for the Period ending March 31, 1964*, USAEC report GA-5036, General Atomic, to be published.
 38. *Advanced Beryllium Oxide Concepts, Progress Report for the Period ending December 31, 1963*, USAEC report GA-4966, General Atomic.
 39. Hankel, R., *Stress and Temperature Distribution*, Nucleonics, 18, 168 (November 1960).
 40. Melese, G. B., and Wilkins, J. E., Jr., *Heat Conduction in a One Dimensional Geometry with Nonuniform Internal Heat Generation*, Trans. Amer. Nucl. Soc., 5, 1, 142 (June 1962).
 41. Beyer, W. A., *An Elastic-Plastic Cylinder with Free Ends and Internal Heat Generation*, Nuclear Sci. Eng., 17, 179 (October 1963).
 42. McWhirter, A. D., and Goodjohn, A. J., *Beryllium Oxide as a Moderator in High-Temperature, Gas-Cooled Reactors*, Trans. Amer. Nucl. Soc., 6, 2, 330 (1963).
 43. Melese, G. B., and Wilkins, E. J., Jr., *On the Efficiency of Longitudinal Fins of Arbitrary Shape with Variable Surface Heat Transfer Coefficient*, report GA-4559, General Atomic (1963).

ABSTRACT—RÉSUMÉ—АННОТАЦИЯ—RESUMEN

A/226 Etats-Unis d'Amérique

Étude thermodynamique des cœurs de réacteurs de puissance refroidis par un gaz
par M. Troost et al.

Aux Etats-Unis, on utilise couramment l'air, l'azote et l'hélium comme fluide de refroidissement dans les réacteurs refroidis par un gaz. Les puissances spécifiques dans le cœur vont de 2 kW/l pour l'EGCR (réacteur expérimental refroidi par un gaz) ou 8-10 kW/l pour les HTGR (réacteurs à haute température refroidis par un gaz) à environ 250 kW/l dans l'étude préliminaire d'un réacteur à neutrons rapides refroidi par un gaz. Le rapport entre la puissance de soufflage et la puissance thermique se situe généralement entre 2 et 5%. Les températures à la sortie du cœur vont de 565 °C pour l'EGCR à 760 °C pour l'HTGR. Les températures superficielle et interne des éléments de combustible sont telles que l'on doit tenir compte du transfert de chaleur par rayonnement. On a utilisé des éléments de combustible à gainage métallique: oxyde d'uranium en dispersion dans de minces manchons concentriques ou oxyde d'uranium dans des faisceaux de barreaux. Dans l'HTGR et les réacteurs à éléments sphériques, on utilise du carbure d'uranium sous gaine en graphite.

On a procédé à de nombreuses expériences de transfert de chaleur pour déterminer les coefficients locaux et moyens pour ces divers types d'éléments de combustible. On a fait également des expériences de transfert de masse avec du naphthalène pour connaître les distributions du transfert de chaleur dans les situations complexes. Il semble qu'en général les corrélations du transfert de chaleur en régime parallèle sont très proches des corrélations normales, bien que les déviations locales puissent être grandes, ce qui

oblige à les étudier avec soin pour les éléments à gainage métallique. Par exemple, le coefficient de transfert de chaleur local dans le réacteur expérimental à l'oxyde de béryllium (EBOR) varie de 20 à 30% autour de sa valeur moyenne.

On a étudié la possibilité de rendre les surfaces rugueuses afin d'augmenter les coefficients de transfert de chaleur superficielle et d'améliorer ainsi les performances du cœur. L'expérience a montré que l'on peut réduire jusqu'à un quart le nombre des éléments de combustible d'un réacteur en rendant rugueuse seulement la fraction de la surface pour laquelle cette opération a le rendement le plus élevé. On a montré pour les tubes circulaires qu'en provoquant des tourbillons dans le gaz de refroidissement, on peut obtenir des coefficients de transfert de chaleur de 1,1 à 3 fois plus élevés que ceux que l'on obtient en régime turbulent. Le tourbillon peut être provoqué par injection tangentielle ou par des vannes d'une forme appropriée.

On a recours à la détermination statistique des facteurs de points chauds pour les éléments de combustible à gainage métallique refroidis par un gaz. Pour les éléments de combustible céramique, les points chauds locaux sont moins importants que la fraction de combustible qui se trouve au-dessus d'une température donnée lorsque le dégagement de produits de fission augmente rapidement. Le problème des contre-courants entre les canaux de refroidissement des réacteurs HTGR n'affecte pas d'une façon appréciable l'analyse thermique.

On a obtenu expérimentalement des corrélations spéciales entre le transfert de chaleur et la chute de pression pour les réacteurs à éléments sphériques. On a étudié des contraintes thermiques dans les sphères, la lévitation et la dispersion non uniforme du courant.

Comme la plupart des analyses thermiques sont effectuées en employant des méthodes numériques, on a mis au point de nombreux programmes de calculatrices numériques pour analyser les problèmes à deux et à trois dimensions. Les équations aux différences finies résultant des équations différentielles pertinentes sont généralement rendues implicites pour éviter les limitations dues aux échelons de temps dans les phénomènes transitoires. Les séries d'équations non linéaires ainsi obtenues sont résolues par itération; les coefficients non linéaires (comme les propriétés dépendant de la température et le rayonnement thermique) sont traités en réévaluant les coefficients en fonction de la température normale, après chaque itération.

Dans plusieurs réacteurs refroidis par un gaz, le problème de la perte de fluide de refroidissement vient limiter la puissance spécifique et détermine souvent la géométrie des éléments de combustible. Les contraintes thermiques provoquées par les phénomènes transitoires d'énergie ou de fluide de refroidissement peuvent limiter la liberté de conception des éléments de combustible céramique.

A/226 США

Теплофизический расчет активных зон энергетических реакторов с газовым охлаждением

М. Труст *et al.*

В американских реакторах с газовым охлаждением в качестве теплоносителей обычно используются воздух, азот и гелий. В активной зоне мощность, отнесенная к единице объема, может составлять от 2 *квт/л*, как это имеет место в экспериментальном реакторе с газовым охлаждением (EGCR), и 8—10 *квт/л*, как в высокотемпературных реакторах с газовым охлаждением (HTGR), до приблизительно 250 *квт/л* — значения, предусмотренного в предварительных расчетах для реактора на быстрых нейтронах с газовым охлаждением. Отношение мощности, расходуемой на перекачку, к тепловой энергии обычно составляет от 2 до 5%. Температурные пределы на выходе из активной зоны составляют от 565°С до 760°С соответственно для реакторов EGCR и HTGR. Поверхность тепловыделяющих элементов и внутренние температуры находятся в такой области, в которой теплопередача излучением должна приниматься во внимание. Используются тепловыделяющие элементы в металлических оболочках, содержащих окись урана, диспергированную в тонких пластинках цилиндрической формы, или окись урана в виде сборки стержней. Тепловыделяющие элементы с топливом из карбида урана с графитовым покрытием используются в реакторах HTGR и в реакторах с гранулированным топливом.

Опыты по теплопередаче широко применяются при определении местных и средних коэффициентов теплопередачи всех указанных типов тепловыделяющих элементов. Опыты по массопереносу, в которых используются нафталин и бензойная кислота, применяются для того, чтобы определить интенсивность теплопереноса в сложных условиях. Соотношения теплопереноса для параллельного потока в общем, по-видимому, близки к нормальным, хотя местные отклонения могут быть большими и должны быть тщательно исследованы в случае тепловыделяющих элементов в металлической оболочке. Например, величина местного коэффициента теплоотдачи в экспериментальном реакторе с окисью бериллия (EBOR) отклоняется на 20—30% от его среднего значения.

Изучается возможность повысить значения коэффициентов теплоотдачи поверхностью и улучшить рабочие характеристики активной зоны путем увеличения поверхностной шероховатости. Результаты показывают, что количество тепловыделяющих элементов реактора может быть уменьшено в четыре раза за счет увеличенной шероховатости только одного лишь оптимального участка поверхности. Для труб круглого сечения показано, что завихрение газообразного теплоносителя может повысить коэффициенты теплопередачи от 1,1 до 3 раз, чем при турбулентном течении. Завихрение может быть создано путем тангенциального ввода или изогнутых лент.

В отношении тепловыделяющих элементов, заключенных в металлическую оболочку и охлаждаемых газом, факторы концентрации радиоактивных изотопов определяются статистическим методом. В керамических тепловыделяющих элементах местные концентрации радиоактивных изотопов менее важны, чем процент горючего, достигшего температуры, при которой выход продуктов деления быстро возрастает. Показано, что противоток между каналами теплоносителя в реакторах типа HTGR не оказывает существенного влияния на термический анализ.

Получены специфические величины соотношения для теплопереноса и перепада давления в реакторах с гранулированным топливом. Исследованы термические напряжения в шарообразных формах, взвешенное состояние и неравномерное распределение потока.

Создано большое число кодов для цифровых вычислительных машин применительно к анализу дву- и трехмерных задач, так как большая часть теплового расчета конструкции производится численными методами. Конечные дифференциальные уравнения получаются обычно неполными, чтобы избежать ограничений по времени и этапам при решении переходных задач. Полученные нелинейные уравнения решаются итеративными методами; нелинейные коэффициенты (такие, как тепловое

излучение и показатели, зависящие от температуры) подвергают обработке путем переоценки коэффициентов как функцию температуры между итерациями.

В нескольких реакторах с газовым охлаждением потери теплоносителя ограничивают удельную мощность и часто определяют геометрию тепловыделяющих элементов. Техническое проектирование керамических тепловыделяющих элементов ограничивается термическими напряжениями, обусловливаемыми переходными условиями охлаждения или выделения энергии.

A/226 Estados Unidos de América

Aspectos del diseño térmico de los reactores de potencia refrigerados por gas

por M. Troost *et al.*

El aire, nitrógeno y helio son los gases que se utilizan normalmente como refrigerantes en los reactores norteamericanos refrigerados por gas. Las densidades de potencia en el núcleo fluctúan de 2 kW/litro para el Reactor Experimental Refrigerado por Gas (EGCR) y 8 a 10 kW/litro para los Reactores de Alta Temperatura Refrigerados por Gas (HTGR) hasta, aproximadamente, 250 kW/litro previstos en el proyecto preliminar de un reactor rápido refrigerado por gas. La relación entre la potencia de bombeo y la potencia térmica oscila corrientemente entre 2% y 5%. Las temperaturas a la salida del núcleo varían desde 1 050 °F en el EGCR a 1 400 °F en los HTGR. Las temperaturas interna y de la superficie del elemento combustible se encuentran en la zona en que ya debe tenerse en cuenta la transmisión de calor por radiación. Se han usado elementos combustibles con vaina metálica con óxido de uranio disperso en láminas delgadas cilíndricas coaxiales o bien con óxido de uranio en haces de barras. En los HTGR y en los reactores de lecho de bolas se utilizan elementos combustibles con vaina de grafito y carburo de uranio como combustible.

Se han realizado numerosos experimentos sobre transmisión de calor con objeto de determinar los coeficientes de transmisión locales y medios para todos estos tipos de elementos combustibles. Se han llevado a cabo experimentos de transferencia de materia con naftaleno con objeto de determinar las distribuciones de transmisión de calor en los casos complicados. Parece, en general, que las correlaciones de transmisión de calor en lo que se refiere al flujo paralelo resultan muy próximas a las correlaciones corrientes, si bien las desviaciones locales pueden ser grandes y deben ser estudiadas cuidadosamente en los elementos de vaina metálica. Por ejemplo, el coeficiente

local de transmisión de calor en el Reactor Experimental de Oxido de Berilio (EBOR) varía de 20% a 30% alrededor del valor medio.

Se ha estudiado la adopción de una superficie rugosa como medio de aumentar los coeficientes de transmisión de calor a través de la superficie y de mejorar las características del núcleo. Los resultados demuestran que el número de elementos combustibles en un reactor puede reducirse hasta por un factor de cuatro con sólo que una proporción óptima de la superficie total sea rugosa. Esto se ha puesto de manifiesto en el caso de tubos cilíndricos en los que un movimiento rotacional del gas refrigerante puede dar coeficientes de transmisión de calor que son de 1,1 a 3 veces mayores que los obtenidos con flujos turbulentos. El movimiento de rotación puede conseguirse por inyección tangencial o por medio de cintas retorcidas.

Para los elementos combustibles con vaina metálica y refrigerados por gas se ha usado una determinación estadística de los factores de puntos calientes. En los elementos combustibles cerámicos la aparición de puntos calientes locales es menos importante que la fracción de combustible que se encuentra por encima de una cierta temperatura a partir de la cual la liberación de productos de fisión aumenta rápidamente. Se ha demostrado que el problema del flujo transversal entre los canales de refrigeración de los reactores del tipo HTGR no afecta de forma apreciable al análisis térmico.

Se han obtenido experimentalmente correlaciones especiales entre transmisión de calor y pérdida de carga para los reactores de lecho de bolas. Se han estudiado las tensiones térmicas en las esferas, la levitación y la distribución no uniforme del flujo del gas.

Como la mayor parte del análisis térmico se lleva a cabo con métodos numéricos, se han desarrollado numerosos programas para las calculadoras digitales que permiten analizar problemas de dos y de tres dimensiones. Las ecuaciones en diferencias finitas que resultan de las correspondientes ecuaciones diferenciales se hacen normalmente implícitas para evitar limitaciones de intervalo de tiempo en los problemas transitorios. El sistema resultante de ecuaciones no lineales se resuelve por métodos de iteración; los coeficientes no lineales (tales como las propiedades que dependen de la temperatura y la radiación térmica) se tratan, entre iteraciones, volviendo a calcular los coeficientes, considerados como una función de la última temperatura obtenida.

En varios reactores refrigerados por gas el problema de la pérdida de refrigerante limita la densidad de potencia y determina a menudo la geometría del elemento combustible. Las tensiones térmicas producidas por los transitorios de potencia o del refrigerante pueden limitar la libertad de diseño de los elementos combustibles cerámicos.

Heat transfer characteristics of helical tube bundles as used in steam generators of gas-cooled reactors

By P. V. Gilli*

Basically, four alternatives of tube configurations are being used for steam generators of gas-cooled reactors:

(a) straight tubes in cross-flow with hairpin type bends to form multiple coils (as employed in the British Magnox stations and in the Windscale AGR);

(b) straight tubes in axial flow (as in the evaporator sections of the French natural uranium, CO₂-cooled reactor EDF-1 [1, 2]);

(c) involutes in cross-flow (as in the German AVR High temperature reactor); and finally

(d) concentric helical coils in cross-flow (as in EDF stations [1, 2] and in the DRAGON Reactor Experiment [3]).

Tubes are either plain or employ—in the economizer and evaporator sections—gills, fins or studs pointing in the direction of gas flow.

For steam generators of future large gas-cooled reactors, all four of the above alternatives appear feasible and have their merits. This paper deals with the heat transfer properties of alternative (d), i.e., helical coils. In this context, the six steam generator units (primary heat exchangers) of the OECD High temperature reactor project DRAGON that have been designed and manufactured by the Waagner-Biro AG in co-operation with the DRAGON project are of particular interest since they are compact units of an extremely high power density that compare very favourably with all other existing conventional or nuclear steam generators with gas as the heat transfer medium. Amongst other reasons, the high density of heat transfer and steam production (Table 1) is due to the particular arrangement of the helical coils that was chosen.

EXPERIMENTAL WORK

Design principles and data

The final design of the tube bundles of the DRAGON steam generators (Fig. 1) exhibits the following features: Between the central by-pass duct and the annular cage of downcomers, seven concentric cylinders of plain evaporator tubes with uniform longitudinal pitches have been provided (Fig. 2), fitting into each other and consisting each of right-handed multi-start helicoils with numbers of starts increasing with helix diameter. Thus the angles of inclination as well as the heated lengths of the tubes

are virtually equal despite the different diameters of the seven helices. This feature of approximately equal heated and total tube lengths, in conjunction with the equal heat input per tube, leads to essentially equal steam/water flow resistibility and hence to equal mass flow per tube and to equal tube exit enthalpy. It should, however, be noted that the tube arrangement depends on angular position: it changes continuously between in-line and fully staggered arrangements. Geometric and thermal data of the final design are compiled in Table 1.

Gas-side heat transfer

Little published data are available on the heat transfer characteristics of bundles of plain helically-wound tubes in general [4; 5; 6] and no data for the particular geometry described above. Under participation of the OECD high temperature reactor project DRAGON, full scale heat transfer experiments were therefore carried out on a prototype tube bundle of the DRAGON steam generators. Air of atmospheric pressure and ambient temperature was heated up when flowing across the tube bundle and hot water of 41 atm (583 psig) and 245 °C was pumped through the tubes. Air flow rate was adjusted so as to cover the range of mean Reynolds numbers from 740 to 12 000 corresponding to the range from less than 10% to almost 150% load under DRAGON working conditions.

In order to be valid for air as well as for helium and other gases, the measured gas-side heat transfer coefficient for the bundle is written in dimensionless form as:

$$Nu_t = a Re_t^m Pr_t^{0.333},$$

or

$$j = St_t Pr_t^{0.667} = \frac{Nu_t}{Re_t Pr_t} Pr_t^{0.667} = a Re_t^{m-1}$$

where the subscript f refers to gas properties evaluated at the mean film temperature (defined as the arithmetic mean between gas and wall temperatures at the logarithmic mean of the heat transfer area) and where Nu stands for the Nusselt number, Pr for the Prandtl number of the gas and St for the Stanton number. j is called the heat transfer factor. The Reynolds number Re is defined by $Re = GD/\eta$ with G denoting the gas mass velocity, D the outer tube diameter and η the viscosity of the gas. G is referred to a nominal average free gas flow area which is chosen somewhat

* Waagner-Biro AG, Vienna.

Table I. Geometric and thermal data of the DRAGON steam generator units

<i>(a) Geometric data (one of six units)</i>	
Outer/inner diam of tubes	18/14 mm
Tube length:	
helix	approx. 4.3 m
total	approx. 7.4 m
Number of starts per helix	6, 7, 8, 9, 10, 11, 12 (63 total)
Angle of inclination:	
coils No. 1/4/7	17.3/16.2/15.6°
weighed average	16.0°
Coil (helix) diam	coils No. 1/4/7 245/395/545 mm
Circle of curvature diam	coils No. 1/4/7 269/428/587 mm
Helix to inner tube diam ratio	coils No. 1/4/7 17.5/28.2/38.9
Circle of curvature to tube id ratio	coils No. 1/4/7 19.2/30.6/42.0
Pitch of tube bank:	
transversal (in-line)	25 mm
longitudinal	40 mm
Lead, coils No. 1/4/7	240/360/480 mm
Number of turns, coils No. 1/4/7	5.32/3.33/2.41
Number of rows (in-line), average	30
Tube bundle nominal height:	
average	1 200 mm
over-all	1 300 mm
Gas flow area, gross (annulus)	0.2175 m ² (2.34 ft ²)
Free area coefficient:	
in-line transversal	0.28
staggered, diagonal	0.56
staggered, transversal	0.64
nominal average	0.46
Internal volume of pressure casing:	
excluding by-pass duct and valve	1.03 m ³ (36.4 ft ³)
gross	1.125 m ³ (39.7 ft ³)
Volume occupied by tube bundle, net (excluding gas by-pass duct and downcomers)	0.283 m ³ (10.0 ft ³)
Heat transfer area:	
gas-side, eff. total	16.3 m ² (175 ft ²)
steam/water-side, eff. total	12.7 m ² (137 ft ²)
Area density:	
gas-side	57.5 m ² /m ³ (17.5 ft ² /ft ³)
steam/water-side	44.8 m ² /m ³ (13.7 ft ² /ft ³)
<i>(b) Thermal and flow data, design load, gas-side, no by-pass</i>	
Thermal duty:	
working load	6 × 3.33 = 20 MW(th)
specified design load, per unit	3.4 MW(th)
Helium flow rate, per unit	3.57 lb/s (1.62 kg/s; 5 820 kg/h)
Helium temperatures, inlet/outlet	740 °C/335 °C
Helium working pressure, inlet	294 psia (20.7 atm)
Helium mass velocity (nominal average free flow area)	16.2 kg/s, m ²
Logarithmic mean temperature difference	291 °C
Reynolds number, log average	Re _t = 8650
Helium velocity, average	12.8 m/s (42.0 ft/s)
Gas-side heat transfer coefficient	857 kcal/m ² h °C (0.996 kW/m ² , °C)
<i>(c) Thermal and flow data, design load, steam/water side</i>	
Working pressure, steam outlet	229 psia (16.1 atm)
Water subcooling at inlet	1.5 °C
Mass velocity	1090 kg/s, m ² (224 lb/s, ft ²)
Exit steam fraction	approx. 17% sbw
Recirculation ratio (forced recirculation)	5.87
Steam/water flow rate, per unit	38 200 kg/h (84 200 lb/hr.)
Steam rate, per unit	6 500 kg/h (14 350 lb/hr.)
<i>(d) Heat fluxes:</i>	
Average heat flux:	
gas-side	179 500 kcal/m ² h (209 kW/m ²)
steam/water-side	230 500 kcal/m ² h (268 kW/m ²)
<i>(e) Power densities:</i>	
Heat transferred:	
per gross volume of casing	3.02 MW(th)/m ³ (0.0855 MW(th)/ft ³)
per net volume of tube bundle	12.0 MW(th)/m ³ (0.34 MW(th)/ft ³)
Rate of steam production:	
per gross volume of casing	5 770 kg/h, m ³ (360 lb/hr. ft ³)
per net volume of tube bundle	23 000 kg/h, m ³ (1435 lb/hr. ft ³)

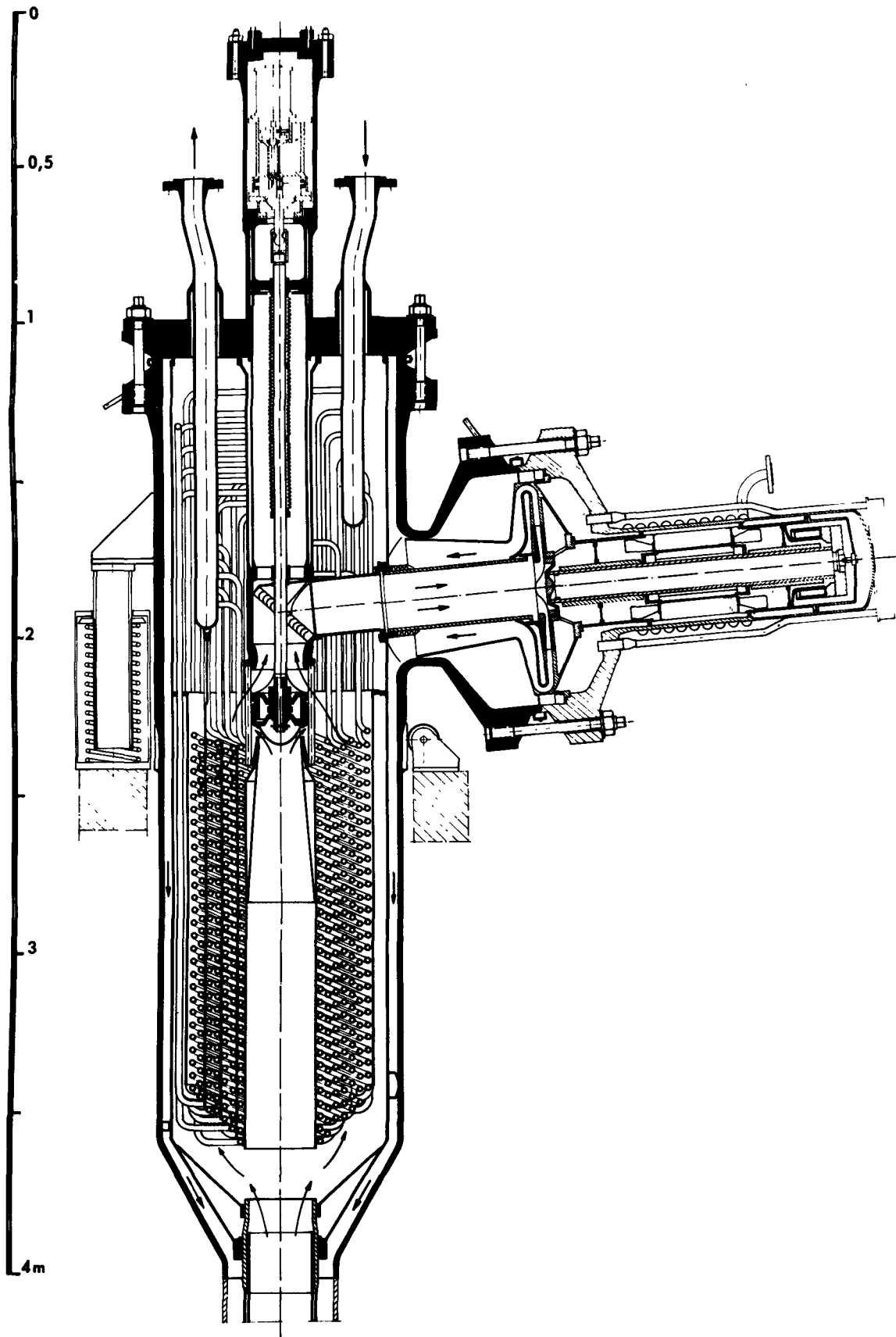


Figure 1. Sectional view of one of the six steam generator units (primary heat exchangers) for the OECD high temperature reactor project DRAGON at Winfrith, Dorset, England

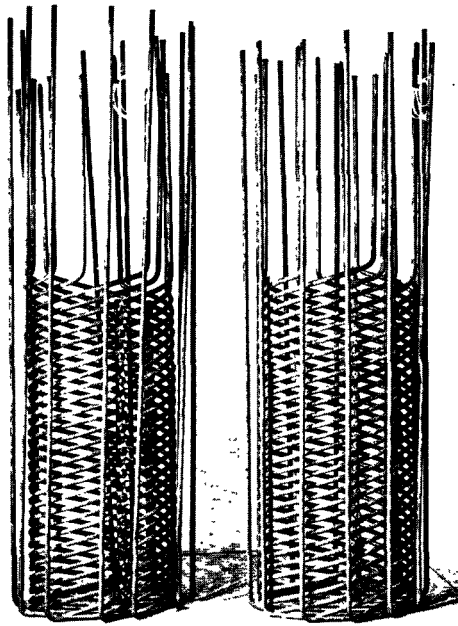


Figure 2. Two of the seven concentric multi-start helicoils of a DRAGON steam generator unit

arbitrarily as the arithmetic mean between the free-area of in-line and of staggered tube arrangement, the latter being based on transverse openings even if—as is the case in the DRAGON steam generators—minimum flow area for the staggered arrangement is in the diagonal openings (Table 1).

In Fig. 3, heat transfer test results have been plotted as j vs. Re_t . The best fit in the Reynolds number range above $Re_t = 2000$ is $m = 0.6$ and $a = 0.37$ and therefore

$$Nu_t = 0.37 Re_t^{0.6} Pr_t^{0.383};$$

or

$$j = 0.37 Re_t^{-0.4}.$$

Scatter of the experimental data is somewhat more pronounced in the range of Reynolds numbers from 900 to 1 800 indicating a transition of flow regimes and a validity limit for the above equations. The transition range corresponds to a load of about 10 to 20% under DRAGON conditions. No oscillations or instabilities of any kind could however be detected during the tests which were carried out with rising and falling Reynolds numbers.

The tube bundle was 30 rows deep (in-line) (Table 1), corresponding to 60 theoretical rows for the fully staggered tube arrangement. A correction for different row numbers is applied by using the following correlations for the row number correction factor which are based on available straight tube data [7] and were developed for use in computer calculations:

$$j_n = f_n j_\infty = \left(1 - \frac{a}{n} + \frac{b}{n^2} - \frac{c}{n^3}\right) j_\infty$$

where j_∞ denotes the asymptotic value of j and n the number of in-line rows. The coefficients for in-line

arrangement are $a = 0.759$; $b = 0.621$ and $c = 0.262$. For staggered arrangement

$$f_n' = 1 - \frac{a'}{n'} + \frac{b'}{(n')^2} - \frac{c'}{(n')^3}$$

with $a' = 0.712$; $b' = 0.042$ and $c' = -0.300$.

For the helical tube bundle with continuously changing tube arrangement as described above, we write $n' = 2n$ and we assume that

$$f_n'' = \frac{1}{2}(f_n + f_n') \\ = 1 - \frac{a}{2n} - \frac{a'}{4n} + \frac{b}{2n^2} + \frac{b'}{8n^2} - \frac{c}{2n^3} - \frac{c'}{16n^3}$$

which yields

$$f_n'' = 1 - \frac{a''}{n} + \frac{b''}{n^2} - \frac{c''}{n^3}$$

with

$$a'' = 0.5(a + 0.5a') = 0.558,$$

$$b'' = 0.5(b + 0.25b') = 0.316$$

and

$$c'' = 0.5(c + 0.125c') = 0.112.$$

We therefore obtain for $n = \infty$ and, for instance, $n = 10$ from the data for $n = 30$: $j_{30} = 0.37 Re_t^{-0.4}$; $j_\infty = 0.376 Re_t^{-0.4}$ and $j_{10} = 0.357 Re_t^{-0.4}$.

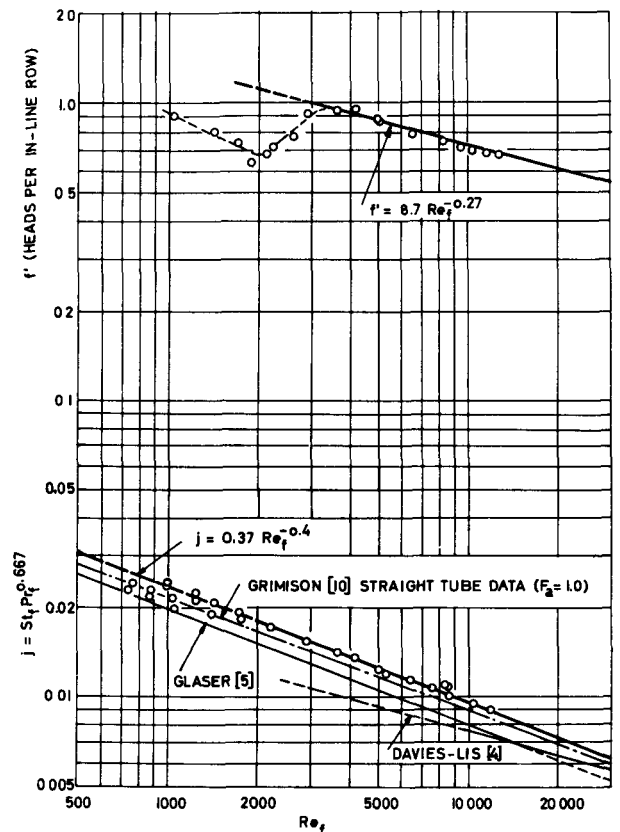


Figure 3. Gas-side heat transfer and pressure drop of flow across a bank of concentric multi-start helical tubes (prototype of DRAGON steam generators)

The local values of the heat transfer coefficients were derived from the average values as follows:

$$\begin{aligned} f_{n,\text{loc}} &= n \cdot f_n - (n-1)f_{n-1} \\ &= 1 - b \frac{1}{n(n-1)} + c \frac{2n-1}{n^2(n-1)^2} \end{aligned}$$

where b and c are the constants used above for in-line arrangements, for staggered arrangements (b' , c') or for the helicoils (b'' , c''). For $n = 1$, the equation leads to undefined values but there $f_{n,\text{loc}} = f_n$. For the tenth and following rows, $f_{n,\text{loc}}$ is practically 1.0.

Furthermore, a correction factor f_i for the departure from right angle cross flow resulting from the inclination of the tubes is introduced. Using values for bundles of straight tubes [8], the data were brought into an analytical form suitable for the computer and a correction for the effects of the helical component of the gas flow path was applied as follows [9]:

$$f_i = (\cos \beta)^{-0.6} \left[\left(1 - \frac{\alpha}{90} \right) \cos \alpha + \frac{\alpha}{1000} \sin \alpha \right]^{\alpha/235}$$

β is the angle between the direction of the helical gas flow and the bundle axis. $\beta = 0$ if left-handed and right-handed helices alternate in the radial direction. If all helices are either left-handed or right-handed, we assume $\beta = \epsilon(1 - \epsilon/90)$ as a first approximation. ϵ denotes the constant or nearly constant angle of inclination of the tubes measured against the plane normal to the helix axis and $\alpha = \epsilon + \beta$ (all angles in degrees).

For the DRAGON steam generator $\epsilon = 16^\circ$, $\beta = 13.2^\circ$, $\alpha = 29.2^\circ$ and $f_i = 0.9548$ and we finally obtain

$$j_n = 0.394 f_n f_i f_a Re_T^{-0.4}$$

after having added an arrangement factor which for the tested tube arrangement is 1.0 and which would allow to accommodate the formula to different tube arrangements [9].

In Fig. 3, results of the tests have been compared with the data of Davies and Lis [4] and Glaser [5]. They agree reasonably well, despite the different geometric conditions. In addition, it is evident that the foregoing correlation shows almost the same exponent of the Reynolds number and yields similar values as the formula of Grimison [10] for bundles of straight tubes.

Gas-side pressure drop

During the heat transfer tests, gas-side pressure drop measurements have also been carried out. Results are plotted in Fig. 3 as coefficient of friction f' (= number of velocity heads lost per in-line row) vs. Re_T . Pressure drop turned out to be somewhat higher than assumed from straight tube data. A transition zone is apparent between $Re_T = 2000$ and $Re_T = 3500$. Above $Re_T = 3000$, the friction coefficient can be described by the equation:

$$f' = 8.7 Re_T^{-0.27}$$

Steam/water-side pressure drop

Isothermal friction factors for flow inside a helical steel tube of 14 mm id, 245 mm coil diam, 240 mm lead and 257 mm diam of the circle of curvature—in fact one of the innermost coils of the DRAGON steam generator—were determined on a separate test rig. Water of ambient temperature was pumped through the tube. Reynolds numbers ranged from less than 200 to more than 200 000. A plot of the Fanning friction factor f vs. Re showed the smooth transition between the laminar and turbulent law mentioned in the literature [11; 12] for essentially plane coils. Data of the tests fit well, over the entire range of Reynolds numbers, the following correlation:

$$4f = 0.018 + \frac{64}{Re} + \frac{2.75}{\sqrt{Re + 3000}}$$

It should be noted that for $Re \rightarrow \infty$ the formula reduces to a constant value of f and for $Re \rightarrow 0$ it approaches the Hagen-Poiseuille law. It is easily shown that for the high Reynolds numbers as prevailing in the tubes of a high-pressure steam generator, the effect of helical curvature of the tubes on the tube friction factor and the difference of the friction factors between the innermost and outermost coils of a helical tube bundle can be accounted for by staggering the tube lengths somewhat, for instance by slightly increasing the inclination angle with decreasing diameter. Thus practically equal exit enthalpies are easily obtained.

Steam/water-side heat transfer

In steam generators of gas-cooled reactors, heat fluxes are rather high. For instance, in the steam generators of the DRAGON high temperature reactor, average heat flux on the steam/water-side of the tubes at design load is 268 kW/m², maximum heat flux is of the order of 500 kW/m². At such high heat fluxes, the steam/water-side heat transfer coefficient is of interest.

As a special study, prior to the experiments, previously described, the heat transfer of water flowing in the helical coils was investigated in order to provide a safe basis for the subsequent experiments. The transition between the laminar the turbulent law of heat transfer was found to be in the Reynolds number range of 13 000 to 15 000. This is about twice the figure expected from published data for essentially plane coils [11]. Gas-side heat transfer tests were therefore performed with water-side Reynolds numbers of at least 20 000, i.e., well above the transition zone.

As to the question of burn-out, not even for straight tubes are the multiplicity of parameters determining the onset of critical heat flux conditions and their complicated interdependence well understood at present despite a fair amount of recent literature on the subject [12]. Therefore, a separate research programme was carried out on the heat transfer characteristics in the two-phase flow region under forced-flow conditions. Part of this work has already been described elsewhere [13].

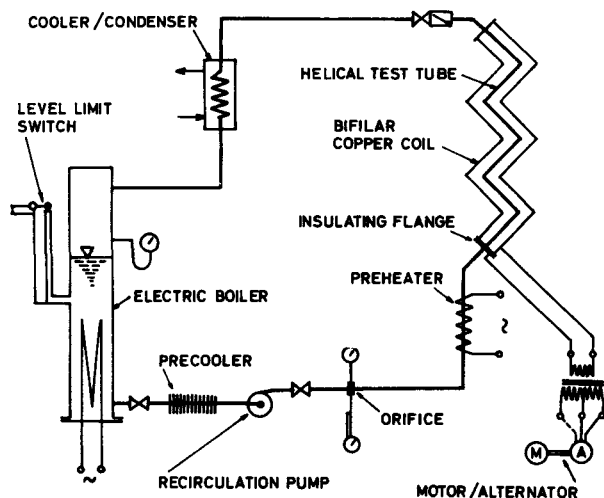


Figure 4. Flowsheet of test rig for boiling heat transfer experiments on helical tubes

Apart from tests under DRAGON working conditions, tests with very high heat fluxes were carried out and, in fact, several tubes ruptured by burn-out. Fracture always took place towards the exit and approximately in the horizontal plane. From temperature recordings it was concluded that onset of the boiling crisis, rise of wall temperature and rupture by burn-out must have taken place literally within a few seconds. By examination of samples at the Waagner-Biro metallurgical laboratory, a burn-out temperature of approximately 900°C or more was confirmed.

In a typical case, burn-out in an inclined tube of 14.0 mm id occurred at a heat flux of $1\,100\,000\text{ kcal/m}^2\text{h}$ ($1\,280\text{ kW/m}^2$), the pressure being 16 atm (228 psia; saturation temperature 200°C), the mass velocity $500\text{ kg/m}^2\text{, s}$ ($102.4\text{ lb/ft}^2\text{, s}$) and the exit steam quality 25% by weight. Since, in this instance, heat flux and minimum wall temperature at burn-out are known, $1\,100\,000:(900-200) = 1\,570\text{ kcal/m}^2\text{h}^{\circ}\text{C}$ ($1.83\text{ kW/m}^2\text{,}^{\circ}\text{C}$) would represent an upper limit of the burn-out heat transfer coefficient. The actual value was probably somewhat, and possibly much, lower. Initial rate of wall temperature rise of the 1 mm thick test tube at burn-out was therefore of the order of 250°C per second.

Further tests have been carried out on a separate test rig (Fig. 4) with helical tubes corresponding to the innermost coils of the DRAGON steam generator and under DRAGON design conditions as regards pressure, mass flow and exit steam qualities. Heat fluxes on the steam/water-side of the helical test tube so far ranged up to $430\,000\text{ kcal/m}^2\text{h}$ (500 kW/m^2) without any excessive wall temperature rise or burn-out occurring. This is about the maximum heat flux in the DRAGON steam generator where, however, it occurs only near tube inlet, at very low steam qualities. On the other hand, at the exit of the DRAGON steam generator

tubes, heat flux is of the order of only 125 kW/m^2 and therefore, at tube exit, the safety factor in terms of heat flux is more than 4.0. Wall temperature measurements have further shown that the boiling heat transfer coefficient is higher at the outer generatrix of the helical tube than at the inner one. Work is being continued.

CONCLUSIONS

Heat transfer characteristics of concentric multi-start helical tube bundles with essentially uniform inclination angle and, around the bundle perimeter, continuously changing tube pattern in cross-flow of gases, and characteristics of boiling heat transfer in helical tubes, were investigated. Tube bundles exhibiting these features have been provided for the steam generators of the DRAGON reactor experiment which are units of extreme power density. The helical tube arrangement of the particular type described appears to be promising for steam generators of future large gas-cooled reactors.

ACKNOWLEDGEMENT

Thanks are due to the Chief Executive of the OECD high temperature reactor project DRAGON for permission to publish those parts of the paper dealing with work carried out under the contract for design and supply of the DRAGON primary heat exchangers.

REFERENCES

1. Lamiral, M., and Lancel, M., *Pressure vessel and heat exchanger for EDFI*, Proc. of the 2nd International Conference on the Peaceful Uses of Atomic Energy P/1199, Vol. 7, p. 591, United Nations (1958).
2. Roux, J. P., and Bienvenu, C., Proc. IME, No. 15, 343-378 (1962).
3. OECD High temperature reactor project DRAGON, Annual Reports: 137-141 1959-1960; 35/36 1960-1961; 58-61, 1961-1962; 21 and 49, 1962-1963 ENEA, Paris (1961, 1962, 1963).
4. Davies, F. V., and Lis, J., J. Brit. Nuclear Energy Conf. 6, 314-323; 388; 412 (1961).
5. Glaser, H., Z. Verein Deutscher Ingenieure, Beiheft Verfahrenstechnik 112-125 (1938).
6. Chester, C. V., USAEC report ORNL-CF 57-9-33 (1957).
7. McAdams, *Heat Transmission*, McGraw-Hill, New York, 274-275 (1954).
8. Michejew, M. A., *Grundlagen der Wärmeübertragung*. Technik, Berlin 109 (1962).
9. Gilli, P. V., to be published in Trans. Amer. Nuclear Soc.
10. Grimison, E. D., Trans. ASME 59, 583-594 (1937).
11. e.g.: Seban, R. A., and McLaughlin, E. F., Int. J. Heat Mass Transfer 6, 387-395 (1963).
12. e.g.: Tippetts, F. E., Trans. ASME, Part C, J. Heat Transfer 86, 12-22 and 23-38 (1964).
13. Gilli, P. R., Verband der Graphischen Mitteilungen, No. 86, 288-300 (1963).

ABSTRACT—RÉSUMÉ—АННОТАЦИЯ—RESUMEN

A/519 Autriche

Caractéristiques de transfert de chaleur des faisceaux de tubes hélicoïdaux utilisés dans les générateurs de vapeur des réacteurs refroidis par un gaz

par P. V. Gilli

Des faisceaux de tubes hélicoïdaux sont utilisés dans les générateurs de vapeur de réacteurs du type à uranium naturel, refroidi au gaz carbonique, et du type à haute température, refroidi à l'hélium. Les générateurs de vapeur (échangeurs de chaleur primaires) du réacteur à haute température DRAGON de l'OCDE, conçus et réalisés par la S. A. Waagner-Biro en collaboration avec le projet DRAGON, sont très intéressants car ce sont des unités compactes d'une très grande densité de puissance. La chaleur transférée par unité de volume de faisceau de tubes s'élève à 12,0 MW(th)/m³ et par unité de volume du récipient sous pression à 3,02 MW(th)/m³. Les débits de vapeur par unité de volume sont 23 000 kg/h m³ et 5 770 kg/h m³ respectivement. Ces valeurs sont favorables en comparaison des générateurs classiques ou nucléaires existants qui utilisent un gaz pour le transfert de la chaleur.

La densité élevée du transfert de chaleur et de la production de vapeur des générateurs de vapeur DRAGON résulte, notamment, du nouvel arrangement compact des tubes. Chacune des six unités du générateur DRAGON se compose de sept cylindres concentriques formés de tubes d'évaporation hélicoïdaux dont la multiplicité augmente avec le diamètre du cylindre. Les angles d'inclinaison ainsi que les longueurs chauffées des tubes sont donc égaux malgré les grandes différences de diamètre des sept hélices, et la résistance à l'écoulement ainsi que l'écoulement en masse dans chaque tube sont égaux.

On a publié peu de données sur les caractéristiques de transfert de chaleur des tubes lisses hélicoïdaux multiples et rien sur l'influence du changement continu entre un arrangement de tubes en alignement et un arrangement avec décalage — ce qui caractérise la construction décrite; c'est pourquoi l'on a établi un programme expérimental concernant le transfert de chaleur « du côté gaz » ainsi que « du côté vapeur — eau ».

On a effectué des expériences concernant le transfert de chaleur « du côté gaz » dans le cadre du projet DRAGON. Les résultats peuvent être représentés dans le domaine au-delà de $Re_T = 2\,000$ par la formule ci-après:

$$St_T = 0,37 Re_T^{-0,4} Pr_T^{-0,667}$$

dans laquelle l'indice f se rapporte aux caractéristiques du gaz évaluées à la température moyenne du film pour la moyenne logarithmique de la surface de chauffe et où le terme de l'écoulement de masse dans le nombre de Reynolds se rapporte à une section du gaz nominale,

libre pour l'écoulement, adoptée comme moyenne arithmétique entre la section libre de l'arrangement en alignement et celle de l'arrangement avec décalage dans les ouvertures transversales. Un changement du régime d'écoulement est perceptible au-dessous de $Re_T = 2\,000$ mais on n'a observé aucune instabilité ou oscillation.

A cause du flux de chaleur élevé dans les générateurs du réacteur DRAGON (les valeurs maximales sont de l'ordre de grandeur de 500 kW/m²), le transfert de chaleur « du côté vapeur — eau » présente un intérêt particulier. On a mesuré des valeurs effectives du coefficient de transfert de chaleur à l'ébullition sur toute la longueur et sur la circonférence des tubes d'épreuve. Dans quelques cas on a déterminé aussi des conditions de caléfaction.

A/519 Австрия

Теплопередающие характеристики змеевиков трубных пучков, используемых в парогенераторах реакторов с газовым охлаждением

П. В. Гилли

Змеевиковые трубные пучки начинают использоваться в парогенераторах с газовым охлаждением на естественном уране. В качестве теплоносителя в таких реакторах используется углекислый газ или в реакторах высокотемпературного типа — гелий. Парогенераторы (теплообменники первичного контура) высокотемпературного реактора DRAGON, которые были разработаны и изготовлены фирмой «Вагнер — Биро» в сотрудничестве с персоналом проекта DRAGON, представляют особый интерес, поскольку они являются компактными установками с чрезвычайно высокой энергонапряженностью. Тепло, передаваемое в единице объема трубного пучка, составляет 12,0 Мвт/м³ (тепл.), а в единице внутреннего объема корпуса — 3,02 Мвт/м³ (тепл.). Паропроизводительность единицы объема составляет 23 000 кг/ч · м³ и 5770 кг/ч · м³ соответственно. Эти значения выше, чем в других существующих в настоящее время парогенераторах на обычных или атомных электростанциях, где в качестве греющей среды используются газы.

Высокие величины тепловых потоков и удельных паропроизводительностей парогенераторов реактора DRAGON обусловлены наряду с другими причинами новым компактным расположением трубок. Все шесть парогенераторов реактора DRAGON состоят из семи концентрично расположенных цилиндрических многозаходных змеевиков, причем число захо-

дов в змеевиках увеличивается с их диаметром. Поэтому углы наклона так же, как и обогреваемая длина трубок во всех змеевиках сохраняются равными, несмотря на большую разницу в диаметрах змеевиков. Таким образом, гидравлическое сопротивление и расход во всех трубках одинаковы.

Вообще очень мало данных опубликовано по теплообмену для змеевиковых пучков с небольшим углом наклона трубок и совсем нет данных по влиянию непрерывного перехода от коридорного расположения трубок к шахматному, являющемуся характерной особенностью описанной конструкции. В связи с этим приводятся экспериментальные исследования теплообмена как в газовом, так и в паро-водяном пространствах таких парогенераторов.

Эксперименты по теплопередаче от газа были выполнены при участии персонала проекта DRAGON. Результаты, полученные для области, для которой $Re = 2000$, можно описать формулой

$$St_f = 0,37 Re_f^{-0,4} \cdot Pr_f^{-0,667},$$

где индекс f относится к свойствам газа при средней температуре пограничного слоя газа, перепад температур в котором принимается равным среднелогарифмической разности между температурами поверхности и газа. Скорость в критерии Рейнольдса отнесена к номинально свободной проходной площади для газа, определенной как среднее арифметическое из свободной площади при коридорном расположении трубок и свободной площади при расположении их в шахматном порядке. Изменение характера режима течения происходит при $Re_f = 2000$, однако при этом никаких нестабильностей или колебаний не наблюдалось.

Благодаря высокому тепловому потоку в парогенераторах экспериментального реактора DRAGON (максимальные значения порядка 500 кВт/м^2) особый интерес представляет теплообмен в паро-водяном пространстве. Действительные значения коэффициента теплоотдачи при кипении были измерены по длине и по периметру исследованных трубок. Для некоторых случаев были определены условия возникновения кризиса.

A/519 Austria

Características de transferencia de calor de haces helicoidales de tubos para generación de vapor en reactores refrigerados por gas

por P. V. Gilli

En los generadores de vapor de reactores refrigerados por gas del tipo de uranio natural y CO_2 y del tipo de alta temperatura y helio se suelen emplear agrupaciones helicoidales de tubos. Los generadores de vapor del proyecto DRAGON, en cuyo diseño y

construcción ha colaborado la Waagner Biro A. G., tienen particular interés porque son unidades compactas de densidad de potencia sumamente elevada. El calor transferido por volumen de tubos alcanza $12,0 \text{ MW(t)/m}^3$, y $3,02 \text{ MW(t)/m}^3$ de volumen de intercambiador. La producción de vapor por unidad de volumen es, respectivamente, $23\,000 \text{ kg/h m}^3$ y $5\,770 \text{ kg/h m}^3$. Estos valores son bastante más elevados que los que se encuentran en otros generadores, sean tradicionales o nucleares, que emplean gas como medio de transferencia de calor.

La elevada densidad de transferencia de calor y de producción de calor de los hervidores DRAGON se debe, entre otras razones, a la disposición compacta, en cierto modo original, de los tubos. Cada una de las seis unidades de generación de vapor del reactor DRAGON consta de siete cilindros concéntricos de tubos evaporadores dispuestos según hélices de filetes múltiples, cuyo número aumenta con el diámetro de la hélice. En esta forma, los ángulos de inclinación y las longitudes de calentamiento de los tubos son iguales a pesar de las diferencias de diámetro entre las siete hélices. Del mismo modo, la resistencia al gas y el caudal por tubo son iguales.

Se han publicado muy pocos datos sobre las características de transferencia de calor de grupos sencillos de tubos helicoidales, y ninguno sobre los efectos del cambio continuo entre las disposiciones en línea y alternada de los tubos, que es una característica del generador descrito. Por este motivo se inició un programa experimental sobre la transferencia de calor en el lado gas y en el lado vapor-agua, de cuyos resultados informa la memoria.

Los experimentos de transferencia de calor en el lado gas se efectuaron con la colaboración del proyecto DRAGON. Para un número de Reynolds superior a $Re_f = 2\,000$, los resultados se pueden describir con la fórmula siguiente:

$$St_f = 0,37 Re_f^{-0,4} Pr_f^{-0,667}$$

donde el subíndice f se refiere a las propiedades del gas a la temperatura media de película correspondiente a la media logarítmica de la superficie de transferencia de calor, y donde el término que figura como velocidad másica en el número de Reynolds se refiere a una sección libre nominal de fluido tomada como la media aritmética entre las secciones libres de la disposición en línea y la disposición alternada de tubos, considerados transversalmente. Por debajo de $Re_f = 2\,000$ se hace patente una transición en el régimen del fluido, pero no se observaron inestabilidades ni oscilaciones.

Debido a los elevados flujos térmicos en los generadores de vapor del reactor DRAGON (los valores máximos son del orden de 500 kW/m^2), interesa especialmente la transferencia de calor del lado vapor-agua. Los valores efectivos del coeficiente de transferencia de calor por ebullición se midieron en toda la longitud y perímetro de los tubos ensayados. En algunos casos se determinaron condiciones de recalentamiento destructivo.

A method for the calculation of three-dimensional flux and temperature distributions in a Magnox reactor, and comparison with experimental measurements taken at Latina power station

By R. Negrini,* M. Paoletti Gualandi,* G. Ciancio,** A. Del Buono,**
T. Marzullo*** and B. Zaffiro***

The high capital cost of nuclear power plants gives a great incentive to produce the maximum output from the plants during operation: this means, in practice, to reach and maintain the maximum reactor power, within the safety limits, other conditions being equal. To this end, difficult problems must be solved and optimised during reactor operation. For the natural-uranium/graphite/CO₂ Latina reactor, the main routine operating problems are as follows:

Safety analysis. It is known that the fuel element temperatures must be limited, during operation, for safety and endurance reasons. The existing core instrumentation does not allow the monitoring of the temperature in every fuel channel because of their large number, characteristic of this type of reactor; it is therefore necessary to perform calculations which allow the temperatures of unmonitored fuel elements to be evaluated, with a certain degree of confidence.

Absorber cycle. Continuous handling of steel absorbers inside the core will be carried out in order to control the long term reactivity variation. It is, therefore, necessary to define, when required, steel absorber charging programmes, which, apart from controlling the desired amount of reactivity, allows the best neutron flux and temperature distribution in the reactor to be maintained.

To solve the above problems, it is necessary to evaluate the spatial distribution of neutron flux and fuel element temperature under various reactor operating conditions. The available nuclear codes to calculate three-dimensional distribution of neutron fluxes in a multi-region core are not suitable for application to gas/graphite reactors because of their large dimensions and the large number of singularities which must be taken into account. It has therefore been decided to produce a suitable method of calculation, based upon a combination of two 2-dimensional multi-region nuclear codes: the FTD2 [1] and the PDQ [2].

* SNAM, Div. AGIP Nucleare.

** CNEN, Div. Sicurezza e Controlli.

*** ENEL-SIMEA.

From the information it gives, the method of calculation produced has been called FATE, i.e., Flux and Temperature Evaluation. Comparison with the commissioning and initial operating experimental results of the Latina reactor, described in this report, proved the adequacy of the method for the desired purposes, and safety analysis and absorber pattern programming has already been performed for the Latina reactor, using the method of calculation described.

DESCRIPTION OF THE FATE CALCULATION METHOD

As previously stated, the 2-dimensional nuclear codes chosen to perform the calculation are the FTD2 and the PDQ-02. These two codes solve numerically the two-group diffusion equations of a multi-region core: the numerical solution is obtained by substituting finite difference equations for the differential equations.

The PDQ code was preferred to other similar codes because one can cover the vertical section of the reactor with a variable mesh sufficiently fine for our need (about 5 000 mesh points, for IBM 704). For this reason, such a code is particularly suitable for reproducing the axial distribution.

The FTD2 code was chosen because it is specially written to represent the horizontal section of a gas/graphite reactor, cell by cell, taking into account every singularity, both in the central and in interstitial positions. For this reason, such a code is particularly suitable for giving the distribution of neutron flux and temperatures in a horizontal section of the core.

The basic concept of FATE is to utilise the FTD2 code, suitably modified to calculate correctly, for every channel of the reactor, the following quantities:

- (a) Relative neutron fluxes, at a given height of the reactor;
- (b) Channel gas outlet temperature;
- (c) Fuel element can temperature, at a specific height of the reactor.

It was thought that a correct evaluation of such quantities could be obtained by the FTD2 code, if the radial variation of the axial flux form was known and suitably introduced into the FTD2 code. The axial information needed is derived from a PDQ (r, z) calculation. A detailed explanation of the combination of the two calculations is contained in the following sections.

Calculation of the neutron flux distributions

The diffusion equations of the FTD2 code are as follows:

$$\begin{aligned} -D_{MR} \left(\frac{\partial^2 \phi}{\partial x^2} + \frac{\partial^2 \phi}{\partial y^2} \right) + \left(\frac{D_{MR}}{L_R^2} + \alpha^2 D_{MZ} \right) \phi &= \frac{D_{FR}}{L_{SR}^2} \psi, \\ -D_{FR} \left(\frac{\partial^2 \psi}{\partial x^2} + \frac{\partial^2 \psi}{\partial y^2} \right) + \left(\frac{D_{FR}}{L_{SR}^2} + \alpha^2 D_{FZ} \right) \psi \\ &= \lambda K_\infty \frac{D_{MR}}{L_R^2} \phi, \end{aligned}$$

where:

D_{MR}, D_{FR} : radial diffusion coefficients, thermal and fast, respectively

D_{MZ}, D_{FZ} : axial diffusion coefficients, thermal and fast, respectively

ϕ, ψ : neutron fluxes, thermal and fast respectively

L_R^2, L_{SR}^2 : radial diffusion areas, thermal and fast respectively

K_∞ : infinite multiplication constant

α^2 : axial buckling

λ : eigenvalue.

It is important to note that the axial components of the thermal and fast leakages are, respectively:

$$\alpha^2 D_{MZ} \phi \quad \text{and} \quad \alpha^2 D_{FZ} \psi,$$

where the axial buckling α^2 is considered the same for the two neutron groups and constant through the reactor. This approximation was not considered acceptable, because the presence of partially inserted control rods in particular regions of the core causes accountable variation of α^2 through the reactor.

With a PDQ run in r, z geometry, which gives the axial flux distribution through the core, the values of the axial buckling at a given height \bar{z} in the reactor can be evaluated:

$$\alpha_M^2(\tau, \bar{z}) = \frac{\partial^2 \phi(\tau, \bar{z})}{\partial z^2} / \phi(\tau, \bar{z}), \quad \text{and}$$

$$\alpha_F^2(\tau, \bar{z}) = \frac{\partial^2 \psi(\tau, \bar{z})}{\partial z^2} / \psi(\tau, \bar{z}).$$

In order to introduce into the FTD2 the above values of the axial buckling and to overcome the FTD2 limitation which accepts only one value of α^2 , fictitious diffusion coefficients D'_{MZ} and D'_{FZ} have been derived from the following equations:

$$\alpha^2 D'_{MZ} \phi = \alpha_M^2 D_{MZ} \phi; \quad \alpha^2 D'_{FZ} \psi = \alpha_F^2 D_{FZ} \psi.$$

With this modification, the FTD2 is suitable to give correct results of the relative flux distribution through the core at a given height \bar{z} .

Calculation of channel gas outlet temperatures

The gas outlet temperature from a typical reactor channel is calculated by the FTD2. The equation used is the following:

$$T_{2,i} = T_1 + \frac{B}{M_i} p_i,$$

where $T_{2,i}$: channel gas outlet temperature

T_1 : channel gas inlet temperature

$1/B$: gas specific heat

M_i : channel gas mass flow

p_i : channel thermal power.

The channel power p_i is assumed in the FTD2 to be proportional to the thermal flux $\phi_i(\bar{z})$, at a given height, and is calculated by the following equation:

$$p_i = \frac{\gamma_i \phi_i(\bar{z})}{\sum_j \gamma_j \phi_j(\bar{z})} P,$$

where P : reactor total power

γ_i : number of fissions per unit flux.

This assumption was not considered acceptable because of the large variation in the axial flux form across the core. In FATE, this situation has been taken into account by re-defining γ_i as the channel fission rate for unit flux at a given height \bar{z} in the reactor:

$$\gamma_{i,\bar{z}} = \frac{\int_0^H \Sigma_{fi}(z) \phi_i(z) dz}{\phi_i(\bar{z})}$$

where H : active height of the core

$\Sigma_{fi}(z)$: fission macroscopic cross section.

The $\gamma_{i,\bar{z}}$ values are derived from the same PDQ calculation mentioned in the previous section. With this modification, FTD2 is suitable to give correct evaluation of the channel powers and gas outlet temperatures.

Calculation of the fuel element can temperatures

The fuel element can temperature of a typical channel in the reactor is calculated, by the FTD2, with the use of the following equation:

$$T_{S,i} = T_1 + K_i (T_{2,i} - T_1).$$

In order to give a correct evaluation of the can temperature at a given height \bar{z} in a channel, taking into account the axial rating distribution, the factor K_i is defined, in FATE, in the following way:

$$\begin{aligned} K_{i,\bar{z}} &= \frac{T_{S,i,\bar{z}} - T_{g,i,\bar{z}}}{T_{2,i} - T_1} + \frac{T_{g,i,\bar{z}} - T_1}{T_{2,i} - T_1} = \frac{\Sigma_{fi}(\bar{z}) \cdot A}{\gamma_{i,\bar{z}} \cdot St_i \cdot a} \\ &+ \frac{\int_0^{\bar{z}} \Sigma_{fi}(z) \phi_i(z) dz}{\int_0^H \Sigma_{fi}(z) \phi_i(z) dz}, \end{aligned}$$

where:

$T_{s,i,z}$: fuel element can temperature, at a given height z

$T_{g,i,z}$: gas temperature, at a given height z

A : channel area

a : heat transfer perimeter

St_i : channel Stanton number.

The $K_{i,z}$ values are derived from the same PDQ calculation mentioned previously.

Auxiliary calculations

The accuracy of the results of calculations for the evaluation of flux and temperature distribution in a power reactor depends, obviously, upon the correct solution of other problems, the main ones being:

(a) Correct evaluation of fuel lattice physical parameters;

(b) Correct evaluation of the physical parameters of singularities (i.e. control rods, absorbers, empty channels);

(c) Accurate representation of singularities, when these have to be smoothed out with the surrounding medium, for code requirements;

(d) Accurate evaluation of channel gas mass flows and Stanton numbers.

As far as the fuel lattice parameters are concerned, a calculation method correlated with experimental results produced in England, under the British Industries Collaborative Exponential Programme [3], was used. Some modifications, such as corrections for temperature effects and for neutron spectrum change in the neighbourhood of the reflector, were introduced to take into account the Latina reactor experimental results.

Lattice cells containing control rods and empty channels are represented in the FTD2 with lattice parameters; these parameters were obtained by smoothing out the heterogeneous structure in such a way as to maintain the cell boundary conditions [4]. Supercell technique was used in the PDQ calculation to smooth out, over appropriate regions, the absorbers and control rods fully or partially inserted into the core [4]. The channel mass flow distribution derived from commissioning measurements was used, while Stanton versus Reynolds curves derived from

rig experiments were correlated with reactor operating results.

Finally, it is worth while to mention that, in order to speed up the preparation of FTD2 input data, an IBM 704 computer programme was produced, which, handling the PDQ output, gives the values of $\alpha_M^2(r, z)$, $\alpha_F^2(r, z)$, $\gamma_{i,z}$ and $K_{i,z}$.

COMPARISON WITH THE COMMISSIONING AND INITIAL POWER OPERATING EXPERIMENTAL RESULTS OF THE LATINA REACTOR

A certain number of experimental checks were carried out during the commissioning and initial operation of the Latina reactor, before using the FATE method of calculation for operating purposes. The experimental data used for comparison with the theoretical predictions include:

(a) Flux distribution measurements carried out during commissioning both with and without absorbers and control rods loaded into the core;

(b) Channel gas outlet and can temperature distribution measurements during initial operation of the reactor.

The details of the commissioning experimental techniques are described in another paper of this Conference [5]. The experiments used for comparison are listed hereunder:

(a) Jo reactor commissioning experiment: radial macroscopic flux distribution measurement without absorbers and control rods in the core;

(b) A1 reactor commissioning experiment: radial and axial macroscopic flux distribution measurement with absorbers and control rods loaded into the core;

(c) A2 reactor commissioning experiment: radial and axial fine flux distribution measurement with absorbers and control rods loaded into the core;

(d) Initial power operation experiment: channel outlet gas temperature and can temperature distribution measurement with the reactor at power.

In Table 1 the comparison between the measured and calculated values are presented. Explanatory notes on each of the above experiments are contained in the following sections.

Table 1. Comparison of FATE results with experimental measurements

Reactor condition	Reactivity		Radial flux standard deviation (%)	Axial flux standard deviation (%)	Gas outlet temperature standard deviation	Can temperature standard deviation
	Theoretical mN	Experimental mN				
Jo	+34	critical	±4.58	—	—	—
A ₁	-37	critical	±4.17	±1.7 + ±4.4	—	—
A ₂	-37	critical	±1.13; 1.64	±1.8 + ±3.9	—	—
Initial power operation	+96	critical	—	—	±6 °C	±8.5 °C

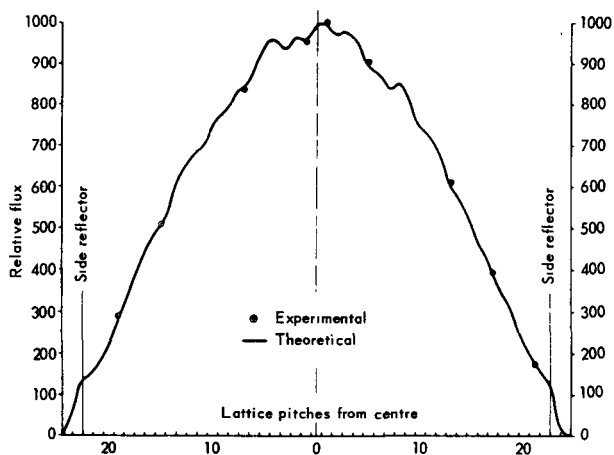


Figure 1. Jo radial flux distribution—SW/NE diameter

Jo reactor commissioning experiment

The reactor was fully loaded, with no absorbers or control rods in the core, the only singularities being the empty channels and the steel support struts of the neutron sources in the bottom half of two interstitial channels. The reactor was critical poisoned with air at a balance pressure of 504.6 cm Hg and ambient temperature.

The radial flux distribution has been measured in 115 channels at a height corresponding to the middle of the seventh fuel element in the channel. It is seen from Table 1 that the agreement between the theoretical and experimental results of flux distribution and reactivity is satisfactory.

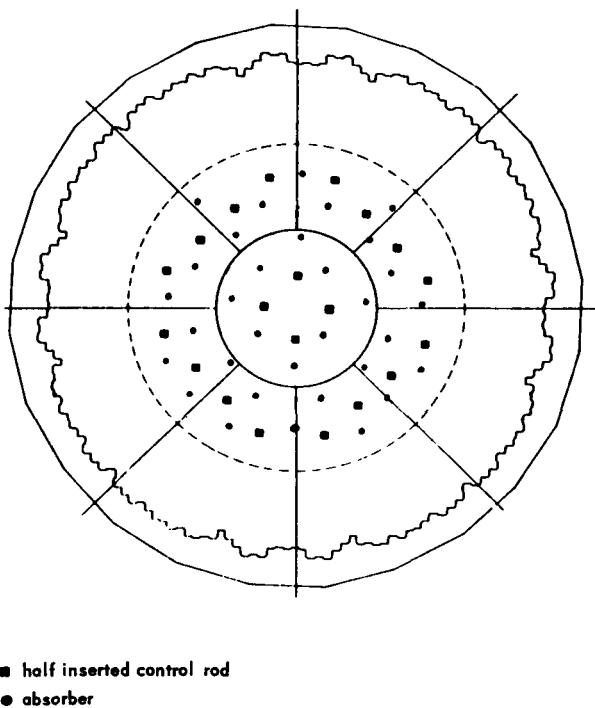


Figure 2. A1/A2 commissioning experiment; plan view of reactor core

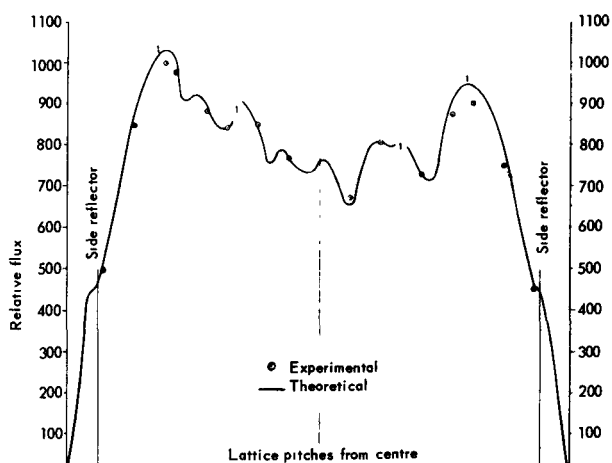


Figure 3. A1 radial flux distribution, NW/SE diameter

A1 reactor commissioning experiment

In Fig. 1 a typical radial flux distribution is shown.

This experiment differs from the previous one due to the loading into the reactor of 32 interstitial absorbers and 20 half-inserted sector control rods, as shown in Fig. 2.

The radial macroscopic flux distribution has been measured in 141 channels at the same height as in the previous experiment. In 12 channels, relatively far from the half-inserted control rods, the axial flux distribution has also been measured. The standard deviation of the differences between theoretical and experimental flux values is $\pm 4.17\%$ for the radial distribution, whereas it ranges from a minimum of $\pm 1.7\%$ in one channel and a maximum of $\pm 4.4\%$ in another channel for the axial distribution. This shows good agreement between experimental values and theoretical predictions.

In Fig. 3 a typical radial flux distribution is shown. The big dips shown are due to the absorbers and control rods loaded into the central region of the reactor.

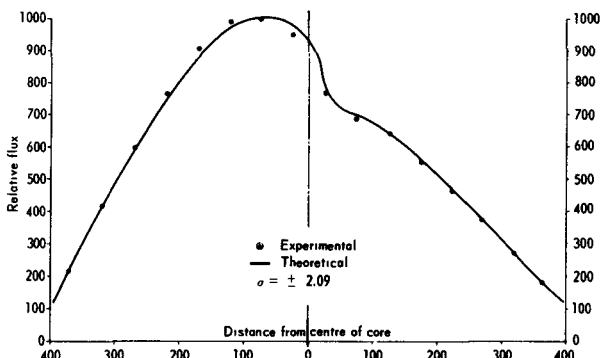


Figure 4. A2 axial flux distribution in a channel adjacent to a half-inserted control rod

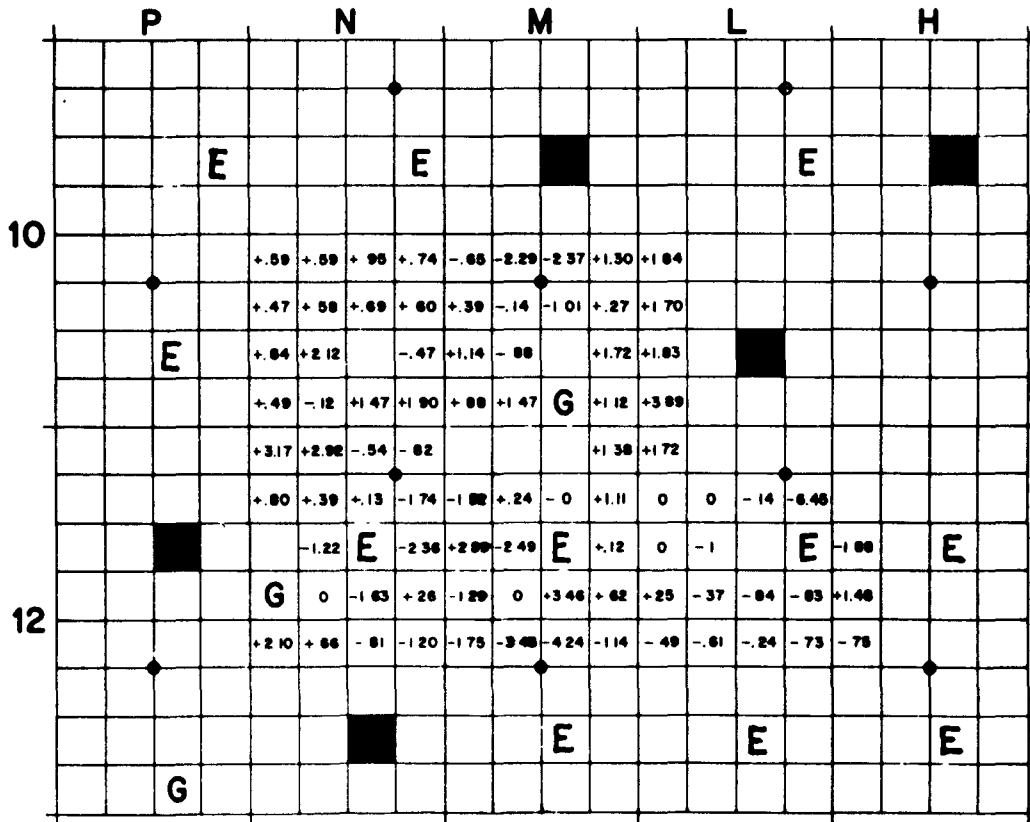
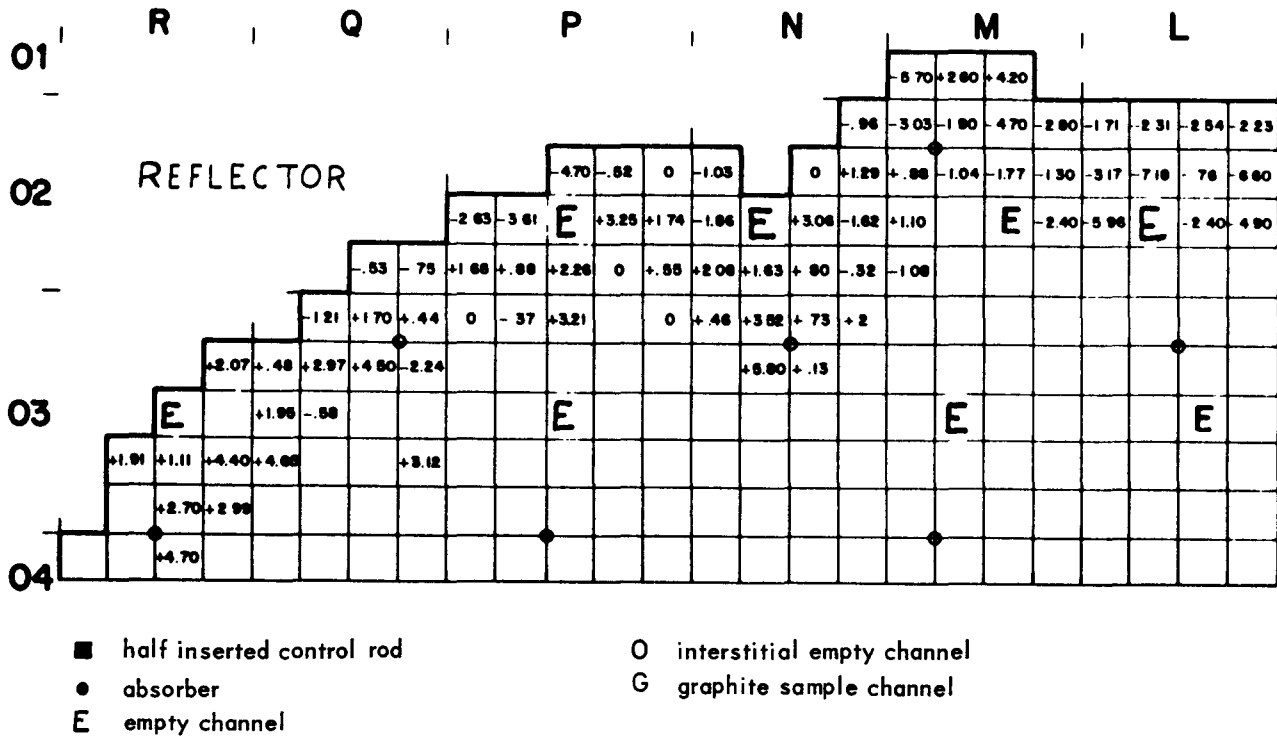


Figure 5. A2 distribution of % differences in the neighbourhood of the reflector, and of singularities in the central region

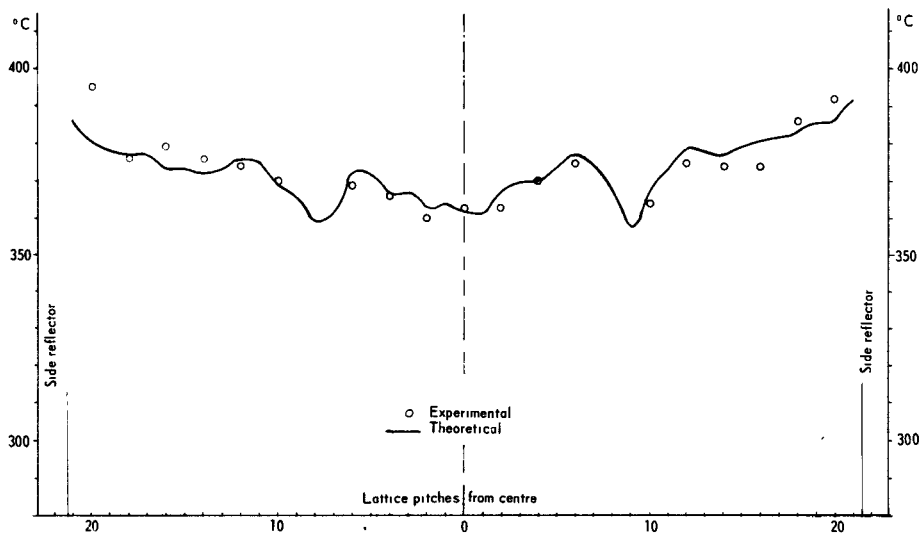


Figure 6. Radial gas outlet temperature distribution, SW/NE diameter

A2 reactor commissioning experiment

This experiment was carried out to measure the fine flux distribution in particular regions of the core. The reactor was in the same conditions as in the previous A1 experiment. The measurements made were:

- (i) Axial flux distribution in 7 channels near a half-inserted control rod;
- (ii) Radial flux fine structure in the neighbourhood of the reflector;
- (iii) Radial flux fine structure in the neighbourhood of various singularities in the central region of the reactor.

In Fig. 4 the axial flux distribution in a channel adjacent to a half-inserted control rod is shown. In Fig. 5 the percentage differences between theoretical and experimental flux values in the two radial flux fine structure measurements are given. The standard deviation of axial flux distributions varies between $\pm 1.8\%$ and $\pm 3.9\%$; the standard deviations of the two radial fine flux plots mentioned above are $\pm 1.13\%$ and $\pm 1.64\%$, respectively. This good agreement shows the adequacy of the calculation method to reproduce also the flux distribution around singularities.

Initial power operation experiment

The reactor conditions during this experiment were:

Thermal power	570 MW (80%)
Mean inlet gas temperature . . .	183 °C
Mean outlet gas temperature . . .	368 °C

Twenty-one absorbers and 20 partially inserted sector control rods were loaded into the core. The outlet gas temperatures were measured with thermo-

couples in 302 channels; the fuel element can temperatures were measured with thermocouples on the eighth fuel element in 75 channels. Comparison between experimental and theoretical results has given the following standard deviation:

Channel gas outlet temperature . . .	± 6 °C
Fuel element can temperature	± 8.5 °C

In Fig. 6 a typical gas temperature distribution through the reactor is shown. The results show that this calculation method can reproduce the temperature conditions of the reactor in operation and consequently is suitable for solving operational problems.

APPLICATION TO OPERATION FOR SAFETY ANALYSIS

The comparison between theoretical and experimental results has been done by normalizing theoretical values by a simple constant.

It has been generally found, as a consequence, that percentage errors are not necessarily normally distributed; nevertheless the error distribution can become normal if the normalizing function is a more complex one.

We found that by fitting the theoretical/experimental value ratio distribution with a development in terms of polynomials, the standard deviation is sensibly reduced and the errors tend to be normally distributed.

Such a result allows us to perform a statistical analysis so that we can determine the degree of safety for any operating condition, in terms of probability that a given maximum can temperature will be reached.

REFERENCES

1. Enderby, J. A., *FTD2—A two-dimensional flux and temperature distribution programme for thermal reactors*, UKAEA report TRG 46(R), Risley (1961).
2. Bilodeau, G. G., Cadwell, W. R., Dorsey, J. P., Fairey, J. G., and Varga, R. S., *PDQ—An IBM-704 code to solve the two-dimensional few-group neutron-diffusion equations*, WAPD-TM-70, Pittsburgh, Pa., Westinghouse Electric Corporation (1957).
3. *British Industries Collaborative Exponential Programme*, UKAEA report AEEW-R235 (Part I, III), Winfrith (1963).
4. Ciancio, G., Del Buono, A., Marzullo, T., Negrini, R., Paoletti Gualandi, M., Passarini, C., and Zaffiro, B., *Determinazione della reattività e della distribuzione del flusso nel reattore di Latina—Confronto con i risultati sperimentali di «commissioning»* Convegno di Fisica del Reattore, Milano, Società Lombarda di Fisica (Novembre 1963).
5. Bertini, A., Calcagno, M., Gualtieri, G., Lesnoni, G., Negrini, R., and Zaffiro, B., *Latina Power Station: Commissioning and initial operating experience*, P/865, Vol. 5, these proceedings.

ABSTRACT—RÉSUMÉ—АННОТАЦИЯ—RESUMEN

A/552 Italie

Méthode pour calculer les distributions tridimensionnelles de flux et de la température dans un réacteur au Magnox et comparaison avec les mesures faites à la centrale de Latina par R. Negrini et al.

La complète connaissance de la distribution de la température dans le cœur d'un réacteur de puissance dans n'importe quelles conditions de fonctionnement est essentielle pour le contrôle.

Il est aussi essentiel, en vue des évaluations économiques, de prévoir les perturbations qui pourraient survenir, pour une certaine distribution de température, à la suite du remplacement des absorbeurs rendu nécessaire par les changements de la réactivité à long terme, afin de maintenir la distribution optimale de la puissance dans les canaux.

Les informations nécessaires ne peuvent pas être fournies uniquement par les mesures, étant donné que, en raison de limitations pratiques, le nombre des thermocouples installés n'est qu'une fraction de celui qui serait nécessaire. Par conséquent, on doit mettre au point une méthode valable pour prévoir les puissances des canaux ainsi que la distribution de la température.

Il s'agit d'un problème à trois dimensions, étant donné que la présence des absorbeurs et des barres de contrôle, partiellement insérés dans le cœur crée des discontinuités et provoque des distorsions radiale, azimutale et axiale de la distribution du flux de neutrons.

Aucun des programmes à trois dimensions multiradiaux et multiaxiaux actuellement disponibles ne peut être appliqué aux réacteurs refroidis au gaz étant donné leurs grandes dimensions.

Les auteurs, pour résoudre le problème, ont développé une méthode de calcul qui est une combinaison appropriée de deux programmes à deux dimensions pour le calculateur IBM-704: FTD-2 et PDQ, qui sont basés tous les deux sur l'hypothèse d'un flux constant dans la troisième dimension.

Afin d'éliminer la limitation intrinsèque de ces deux programmes, les auteurs ont employé le programme PDQ pour obtenir la variation radiale d'un certain

nombre de paramètres qui représentent les formes du flux axial à une hauteur déterminée.

Ces informations, employées comme il convient dans le programme FTD-2, permettent de calculer correctement les distributions en x et y du flux à une hauteur déterminée, ainsi que les températures du gaz à la sortie du réacteur et les distributions tridimensionnelles de la température des gaines du combustible.

Cette méthode de prévision des distributions tridimensionnelles de la température et du flux a été vérifiée en la comparant avec les résultats expérimentaux obtenus à la centrale nucléaire de Latina pendant les essais de mise en service et le fonctionnement normal. L'accord a été satisfaisant.

En outre, les auteurs présentent une proposition d'application de cette méthode au contrôle du fonctionnement des réacteurs au Magnox refroidis au gaz sur la base des analyses des températures du gaz et des gaines.

A/552 Италия

Метод расчета трехмерных распределений потока и температур в магноксовом реакторе и сравнение с измерениями, произведенными на атомной электростанции в Латине

Р. Негрини et al.

Чтобы управлять энергетическим реактором, необходимо иметь полное представление о распределении температур в его активной зоне в любых рабочих условиях.

Для обеспечения экономичности необходимо поддерживать оптимальное распределение мощности по каналам. Для этого, в свою очередь, необходимо знать изменения распределения температур, которое вызывается перераспределением поглотителей при длительном изменении реактивности.

Необходимые данные нельзя получить экспериментальным путем, поскольку из-за практических ограничений установленное число

термонар недостаточно для этого. Поэтому необходимо разработать надежный метод предсказания распределения мощности и температур.

Это трехмерная проблема, поскольку присутствие дискретных поглотителей и управляющих стержней, частично введенных в активную зону, вызывает радиальные, азимутальные и осевые искажения распределения потока нейтронов.

Имющиеся в настоящее время трехмерные много радиальные, многоосевые программы нельзя применять для расчета реакторов с газовым охлаждением ввиду их больших размеров.

Авторы приступили к решению этой проблемы путем разработки расчетного метода, который является соответствующей комбинацией двух двумерных программ счетно-решающего устройства типа IBM-704, программы FTD-2 и программы PDQ, которые составлены исходя из предположения, что поток имеет постоянную форму в третьем измерении.

С целью преодоления присущей этим двум программам ограниченности авторы использовали программу PDQ для получения радиального изменения нескольких параметров при определенной форме осевого потока на данной высоте.

Эта информация, должным образом обработанная и включенная в программу FTD-2, дает возможность получить с помощью этой программы двумерное распределение (x, y) потока на данной высоте, а также температуры газа на выходе и трехмерное распределение температуры оболочки.

Этот трехмерный метод предсказания распределения потока и температур был проверен путем сравнения с результатами, полученными экспериментальным путем во время пуска и эксплуатации атомной электростанции в Латине; совпадение данных было удовлетворительным.

Кроме того, внесено предложение использовать этот метод для определения работоспособности магноксовых реакторов с газовым охлаждением посредством анализа температур газа и оболочки.

distribución de temperaturas en el núcleo para cualquier condición de operación.

Por razones económicas, es también necesario predecir la perturbación de una distribución determinada de temperaturas, producida por la modificación de los absorbentes que se utilizan para mantener la distribución óptima de potencia en los canales para compensar las variaciones lentas de reactividad durante la operación del reactor.

La información necesaria no puede obtenerse experimentalmente, ya que por razones de orden práctico sólo se puede introducir en el núcleo una fracción del total de los termopares necesarios para realizar la medida. Por este motivo se ha desarrollado un método de predecir las distribuciones de temperatura y sus variaciones.

Resulta un problema tridimensional por la existencia de absorbentes discontinuos y de las barras de control, parcialmente introducidas en el núcleo, que producen distorsiones en la distribución neutrónica axial, acimutal y radial.

Los programas de cálculo tridimensionales que existen actualmente no se pueden aplicar a los reactores refrigerados por gas, ya que son reactores de grandes dimensiones.

Los autores resuelven el problema desarrollando un método de cálculo que esencialmente es una combinación de dos programas bidimensionales para el computador IBM 704: los programas FTD2 y PDQ en los que se supone una distribución de flujo constante en la tercera dimensión.

Para salvar la limitación de estos dos programas los autores utilizan el código PDQ para obtener una variación radial de parámetros relacionados con las distribuciones axiales de flujo a una altura determinada.

Esta información, convenientemente manejada e introducida en el código FTD2, permite obtener las distribuciones de flujo según las direcciones x e y a una determinada altura, así como la temperatura de salida del gas y la distribución tridimensional de temperaturas en la vaina del elemento combustible empleado.

Los resultados de este método han sido comparados con los datos experimentales obtenidos en el reactor nuclear de potencia Latina: se ha obtenido una concordancia satisfactoria.

Además, este método puede ser aplicado al control de la operación de los reactores Magnox refrigerados por gas, analizando la temperatura del gas y de las vainas de los elementos combustibles.

A/552 Italia

Método para calcular la distribución tridimensional del flujo y la temperatura de un reactor Magnox y comparación con los datos experimentales tomados en la central de potencia Latina

por R. Negrini *et al.*

Para controlar un reactor de potencia es esencial tener un conocimiento lo más completo posible de la

Метод моделирования на аналоговых вычислительных машинах нестационарных тепловых процессов в газоохлаждаемых энергетических реакторах

В. Б. Нестеренко, В. М. Шадский *

ВВЕДЕНИЕ

Для разработки комплексных систем автоматического регулирования, исследования аварийных и пусковых режимов атомных энергетических установок в последнее время все чаще используют электронные вычислительные машины дискретного или непрерывного действия¹⁻³. Использование электронных вычислительных машин затруднено тем, что уравнения объектов регулирования (в частности, реактора, теплообменных аппаратов) есть уравнения в частных производных.

Вычислительные машины дискретного действия позволяют решать уравнения в частных производных. Существенным недостатком этих машин является сложный и длительный процесс программирования задачи. Вторым недостатком дискретных машин следует считать то, что их трудно применять для исследований при сопряжении с реальными элементами системы регулирования. В отличие от них аналоговые вычислительные машины характеризуются простотой подготовки и обработки машинных уравнений и легко сопрягаются с реальными элементами систем регулирования. Однако серийные АВМ (например, МН-7, ЭМУ-8, ЭМУ-10, МН-10, МН-14, МН-8, МНБ-1 и др.) созданы для решения обыкновенных дифференциальных уравнений, поэтому необходимо найти метод преобразования уравнений в частных производных по трем переменным в обыкновенные нелинейные дифференциальные уравнения.

МЕТОД МОДЕЛИРОВАНИЯ НА АВМ НЕСТАЦИОНАРНЫХ ТЕПЛОВЫХ ПРОЦЕССОВ В ГАЗООХЛАЖДАЕМЫХ РЕАКТОРАХ

Обозначения

T_m, T_r — текущая средняя по сечению температура твэла и газа;

* Институт тепло- и массообмена Академии наук БССР, г. Минск.

q_{vi} — тепловой поток на единицу объема;
 c_p, γ_r, V_r — теплоемкость, удельный вес и объем газа в реакторе;
 c_m, γ_m, V_m — теплоемкость, удельный вес и объем твэла;
 a — приведенный коэффициент теплопередачи;
 τ — время;
 G — расход газа;
 n — число членов ряда разложения;
 0 — номинальные значения;
 z — координата по высоте реактора. Начало системы координат принято в центре активной зоны;
 c_p — среднее по высоте реактора значение величины;
 z_p — значение величины на входе реактора;
 z — значение величины на выходе реактора;
 N_T — тепловая мощность реактора;
 \bar{N} — относительная мощность реактора;
 l — высота активной зоны;
 h — эффективные добавки торцовых отражателей;
 F, Π — поверхность теплообмена твэлов, периметр твэлов;
 S_m, S_r — площадь поперечного сечения по твэлам и газу.

Известно, что нестационарная теплопередача в твэлах реактора в общем виде может быть представлена уравнениями в частных производных по трем переменным: радиус твэла, координаты по длине и время.

Преобразование этих уравнений в обыкновенные дифференциальные уравнения обычно производится приближенными методами, в которых расчетная схема передачи тепла представлена через среднеинтегральные по сечению температуры твэлов и газа. При этих преобразованиях принимается ряд приближений и допущений.

После осреднения температур твэлов и газа по радиусу процесс теплообмена в реакторе описывается дифференциальными уравнениями в частных производных по двум переменным

$$\frac{\partial T_m}{\partial \tau} = \frac{q_{vi} V_m}{c_m \gamma_m V_m} - \frac{\alpha F}{c_m \gamma_m V_m} (T_m - T_r), \quad (1)$$

$$\frac{\partial T_r}{\partial \tau} = \frac{\alpha F}{c_p \gamma_r V_r} (T_m - T_r) - \frac{c_p G}{c_p \gamma_r V_r} \cdot \frac{\partial T_r}{\partial z}. \quad (2)$$

Необходимо найти метод определения параметров по длине реактора. Осреднение темпе-

ратур по длине реактора может быть представлено зависимостью средней температуры газа и температур входа и выхода

$$T_{r\text{ ср}} = \frac{T_{2p} + T_3}{2}.$$

В этом случае для получения приемлемой точности решения активную зону реактора или теплообменника надо разбить на такое число участков по длине, чтобы в пределах участка можно было считать изменение температур линейным. Однако метод конечных разностей нельзя рекомендовать для исследования динамики атомной энергетической установки, так как в этом случае системы уравнений нестационарной теплоотдачи в теплообменниках и в реакторе занимают большую часть блоков машин.

Наиболее простым и часто используемым методом осреднения температур по длине реактора при решении задач нестационарного теплообмена на аналоговых вычислительных машинах является замена системы с распределенными параметрами системой с сосредоточенными параметрами^{1,2}. Такой метод приемлем при небольших отклонениях параметров от их номинальных величин, а в случае изменений расхода газа, тепловой мощности реактора и температуры газа на входе точность решения этим методом оказывается недостаточной. При представлении теплообменных аппаратов системой уравнений с сосредоточенными параметрами в случае глубоких изменений переменных (запуск, прогрев двигателя, аварийные режимы и др.) искажается длительность переходного процесса, из рассмотрения выпадает ряд особенностей процессов теплообмена.

Ниже излагается метод осреднения температур газа по длине реактора, позволяющий получить приемлемую точность моделирования с меньшим числом операционных усилителей, чем в случае разбиения активной зоны на участки при применении метода конечных разностей⁴.

ГАЗООХЛАЖДАЕМЫЙ РЕАКТОР С ТВЭЛАМИ СТЕРЖНЕВОГО ТИПА

На рис. 1 представлена расчетная схема активной зоны реактора с ТВЭлами стержневого типа.

Нестационарный теплообмен между газом, текущим по каналу, и стенкой канала при наличии в стенке внутренних источников тепла переменной интенсивности обычно изучается при следующих допущениях:

1. Не учитывается недогрев газа в торцовых отражателях.

2. Не учитываются за малостью перетоки тепла в стенке вдоль канала.

3. Экспериментальные коэффициенты теплоотдачи установившегося течения применяются для переходных процессов.

4. Тепловыделение по длине твэла изменяется по косинусоиде.

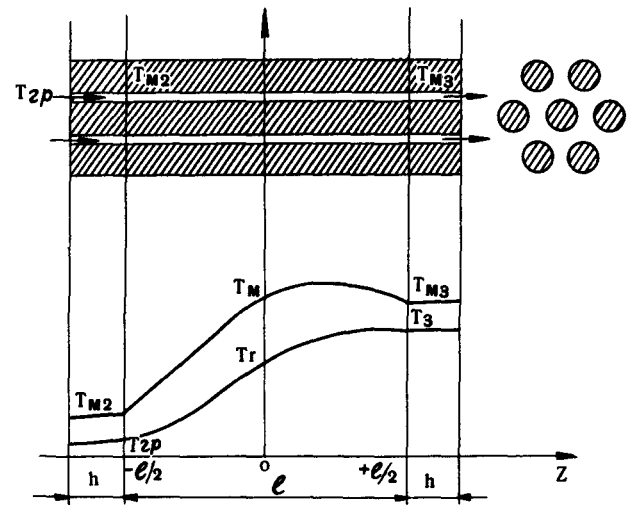


Рис. 1. Расчетная схема активной зоны реактора

При таких допущениях процесс нестационарного теплообмена в твэлах реактора описывается следующей системой:

$$c_m \gamma_m S_r \frac{\partial T_m}{\partial \tau} = q_{v0} S_m \left(\cos \pi \frac{z}{l+2h} \right) \bar{N} - \alpha \Pi (T_m - T_r), \quad (1a)$$

$$c_p \gamma_r S_m \frac{\partial T_r}{\partial \tau} + c_p G \frac{\partial T_r}{\partial z} = \alpha \Pi (T_m - T_r). \quad (2a)$$

Начало отсчета по длине принято в центре канала.

Начальные и граничные условия

$$\begin{aligned} z = -l/2, \quad T_r(\tau, -l/2) &= T_{2p0} \text{ при } \tau = 0, \\ z = l/2, \quad T_r(\tau, l/2) &= T_{30} \text{ при } \tau = 0, \\ T_r(\tau, -l/2) &= T_{2p}. \end{aligned}$$

Проинтегрируем уравнения (1а), (2а) в пределах $-l/2, +l/2$

$$\begin{aligned} c_m \gamma_m S_m \frac{d}{d\tau} \int_{-l/2}^{l/2} T_m(\tau, z) dz &= \\ &= q_{v0} S_m \bar{N} \int_{-l/2}^{l/2} \cos \pi \frac{z}{l+2h} dz - \\ &- \alpha \Pi \left(\int_{-l/2}^{l/2} T_m dz - \int_{-l/2}^{l/2} T_r dz \right), \quad (3) \end{aligned}$$

$$\begin{aligned} c_p \gamma_{r\text{ ср}} S_r \frac{d}{d\tau} \int_{-l/2}^{l/2} T_r dz &= \alpha \Pi \left(\int_{-l/2}^{l/2} T_m dz - \int_{-l/2}^{l/2} T_r dz \right) - \\ &- c_p G (T_3 - T_{2p}), \quad (4) \end{aligned}$$

$\frac{1}{l} \int_{-l/2}^{l/2} T_r(\tau, z) dz = T_{r\text{ ср}}$ — среднее значение температуры газа по длине канала,

$$\frac{1}{l} \int_{-l/2}^{l/2} T_m(\tau, z) dz = T_{m \text{ ср}} - \text{средняя температура}$$

твэлов по длине канала и т. д.

С учетом принятых обозначений уравнения (1а) и (2а) можно переписать в виде

$$\frac{dT_{m \text{ ср}}}{d\tau} = \frac{2q_{\text{в0}}V_m}{c_m\gamma_m V_m} \cdot \frac{l+2h}{\pi l} \left(\sin \pi \frac{l/2}{l+2h} \right) \bar{N} - \frac{\alpha F}{c_m\gamma_m V_m} (T_{m \text{ ср}} - T_{\Gamma \text{ ср}}), \quad (3 \text{ а})$$

$$\frac{dT_{\Gamma \text{ ср}}}{d\tau} = \frac{\alpha F}{c_p\gamma_{\Gamma \text{ ср}} V_{\Gamma}} (T_{m \text{ ср}} - T_{\Gamma \text{ ср}}) - \frac{c_p G}{c_p\gamma_{\Gamma \text{ ср}} V_{\Gamma}} (T_3 - T_{2\text{р}}). \quad (4 \text{ а})$$

Таким образом, для средних значений температуры газа $T_{\Gamma \text{ ср}}$ и стенки $T_{m \text{ ср}}$ получены нелинейные обыкновенные дифференциальные уравнения. Для их решения могут быть использованы аналоговые вычислительные машины.

Необходимо установить зависимость между средней температурой $T_{\Gamma \text{ ср}}$ и температурами газа на входе $T_{2\text{р}}$ и выходе T_3 . Для этого к интегралу вида $\int_{-l/2}^{l/2} T_{\Gamma}(\tau, z) dz$ применим метод интегрирования по частям в пределах $-l/2, +l/2$.

В результате последовательного интегрирования интеграл может быть представлен в виде бесконечного ряда

$$T_{\Gamma \text{ ср}} = \frac{1}{l} \int_{-l/2}^{l/2} T_{\Gamma}(\tau, z) dz = \frac{z}{l} T_{\Gamma} - \frac{z^2}{2l} \cdot \frac{\partial T_{\Gamma}}{\partial z} + \frac{z^3}{6l} \cdot \frac{\partial^2 T_{\Gamma}}{\partial z^2} - \frac{z^4}{24l} \cdot \frac{\partial^3 T_{\Gamma}}{\partial z^3} + \frac{z^5}{120l} \cdot \frac{\partial^4 T_{\Gamma}}{\partial z^4} - \dots \Big|_{-l/2}^{l/2}. \quad (5)$$

Бесконечный ряд (5) можно представить общим членом ряда

$$T_{\Gamma \text{ ср}} = \sum_1^{\infty} \left(\frac{z^n}{n!} \right) \cdot \frac{\partial^n T_{\Gamma}}{\partial z^n} (-1)^{n+1}. \quad (5 \text{ а})$$

Для ряда этого вида равномерная сходимость имеет место в случае, если ряд $\sum_1^{\infty} \frac{z^n}{n!}$ сходится равномерно на множестве z , а функция $\frac{\partial^n T_{\Gamma}}{\partial z^n}$ при любых z и n образует монотонную последовательность и при любых z и n ограничена

$$\left| \frac{\partial^n T_{\Gamma}}{\partial z^n} \right| \leq K.$$

Но степенный ряд $\sum_1^{\infty} \frac{z^n}{n!}$ сходится $5-7$ при любом z (радиус сходимости $R = \infty$).

Функция $T_{\Gamma}(\tau, z)$ в пределах интегрирования ряда $-l/2, +l/2$ непрерывна. Ввиду конечной величины теплового потока и средней температуры газа [интеграл (5)] производные по координате ограничены. Следовательно, бесконечный ряд (5) является равномерно сходящимся рядом.

Поэтому решение задачи может быть представлено в виде нескольких членов разложения $T_{\Gamma \text{ ср}}$ в ряд.

а. Один член ряда разложения.

$$T_{\Gamma \text{ ср}} = \frac{z}{l} T_{\Gamma} \Big|_{-l/2}^{l/2} = \frac{1}{2} (T_{2\text{р}} + T_3), \quad (5 \text{ б})$$

откуда

$$T_3 = 2T_{\Gamma \text{ ср}} - T_{2\text{р}}.$$

Получим систему уравнений

$$\frac{dT_{m \text{ ср}}}{d\tau} = \frac{2q_{\text{в0}}V_m}{c_m\gamma_m V_m} \cdot \frac{l+2h}{\pi l} \left(\sin \pi \frac{l/2}{l+2h} \right) \bar{N} - \frac{\alpha F}{c_m\gamma_m V_m} (T_{m \text{ ср}} - T_{\Gamma \text{ ср}}), \quad (3 \text{ а})$$

$$\frac{dT_{\Gamma \text{ ср}}}{d\tau} = \frac{\alpha F}{c_p\gamma_{\Gamma \text{ ср}} V_{\Gamma}} (T_{m \text{ ср}} - T_{\Gamma \text{ ср}}) - \frac{c_p G}{c_p\gamma_{\Gamma \text{ ср}} V_{\Gamma}} (T_3 - T_{2\text{р}}), \quad (4 \text{ а})$$

$$T_3 = 2T_{\Gamma \text{ ср}} - T_{2\text{р}}. \quad (6)$$

б. Два члена ряда разложения.

$$T_{\Gamma \text{ ср}} = \frac{z}{l} T_{\Gamma} - \frac{z^2}{2l} \cdot \frac{\partial T_{\Gamma}}{\partial z} + \dots \Big|_{-l/2}^{l/2} = \frac{1}{2} (T_{2\text{р}} + T_3) - \frac{l}{8} \left[\left(\frac{\partial T_{\Gamma}}{\partial z} \right)_3 - \left(\frac{\partial T_{\Gamma}}{\partial z} \right)_{2\text{р}} \right]. \quad (5 \text{ в})$$

Значения величин $l \left(\frac{\partial T_{\Gamma}}{\partial z} \right)_3$, $l \left(\frac{\partial T_{\Gamma}}{\partial z} \right)_{2\text{р}}$ получим из уравнения (2а)

$$l \left(\frac{\partial T_{\Gamma}}{\partial z} \right)_3 = \frac{\alpha F}{c_p G} (T_{m3} - T_3) - \frac{c_p \gamma_{\Gamma 3} V_{\Gamma}}{c_p G} \cdot \frac{dT_3}{d\tau},$$

$$l \left(\frac{\partial T_{\Gamma}}{\partial z} \right)_{2\text{р}} = \frac{\alpha F}{c_p G} (T_{m2} - T_{2\text{р}}) - \frac{c_p \gamma_{\Gamma 2} V_{\Gamma}}{c_p G} \cdot \frac{dT_{2\text{р}}}{d\tau},$$

$$T_{\Gamma \text{ ср}} = \frac{1}{2} (T_{2\text{р}} + T_3) - \frac{1}{8} \left[\frac{\alpha F}{c_p G} (T_{m3} - T_3 - T_{m2} + T_{2\text{р}}) - \frac{c_p \gamma_{\Gamma 3} V_{\Gamma}}{c_p G} \left(\frac{dT_3}{d\tau} - \frac{\gamma_{2\text{р}}}{\gamma_3} \cdot \frac{dT_{2\text{р}}}{d\tau} \right) \right],$$

откуда

$$\frac{dT_3}{d\tau} = \frac{\gamma_{2\text{р}}}{\gamma_3} \frac{dT_{2\text{р}}}{d\tau} + 8 \frac{c_p G}{c_p \gamma_3 V_{\Gamma}} \left(T_{\Gamma \text{ ср}} - \frac{T_{2\text{р}} + T_3}{2} \right) + \frac{\alpha F}{c_p \gamma_3 V_{\Gamma}} (T_{m3} - T_3 - T_{m2} + T_{2\text{р}}).$$

Получим систему уравнений

$$\frac{dT_{m \text{ ср}}}{d\tau} = \frac{2q_{\text{в0}}V_m}{c_m\gamma_m V_m} \cdot \frac{l+2h}{\pi l} \left(\sin \pi \frac{l/2}{l+2h} \right) \bar{N} - \frac{\alpha F}{c_m\gamma_m V_m} (T_{m \text{ ср}} - T_{\Gamma \text{ ср}}), \quad (3 \text{ а})$$

$$\frac{dT_{\Gamma \text{ cp}}}{d\tau} = \frac{\alpha F}{c_p \gamma_{\Gamma \text{ cp}} V_{\Gamma}} (T_{\text{м cp}} - T_{\Gamma \text{ cp}}) - \frac{c_p G}{c_p \gamma_{\Gamma \text{ cp}} V_{\Gamma}} (T_3 - T_{2\text{p}}), \quad (4 \text{ a})$$

$$\frac{dT_3}{d\tau} = \frac{\gamma_{2\text{p}}}{\gamma_3} \frac{dT_{2\text{p}}}{d\tau} + 8 \frac{c_p G}{c_p \gamma_3 V_{\Gamma}} \left(T_{\Gamma \text{ cp}} - \frac{T_{2\text{p}} + T_3}{2} \right) + \frac{\alpha F}{c_p \gamma_3 V_{\Gamma}} (T_{\text{мз}} - T_3 - T_{\text{мз}} + T_{2\text{p}}), \quad (7)$$

$$\frac{dT_{\text{мз}}}{d\tau} = \frac{q_{\text{в0}} V_{\text{м}}}{c_{\text{м}} \gamma_{\text{м}} V_{\text{м}}} \left(\cos \pi \frac{l/2}{l+2h} \right) \bar{N} - \frac{\alpha F}{c_{\text{м}} \gamma_{\text{м}} V_{\text{м}}} (T_{\text{мз}} - T_3), \quad (8)$$

$$\frac{dT_{\text{мз}}}{d\tau} = \frac{q_{\text{в0}} V_{\text{м}}}{c_{\text{м}} \gamma_{\text{м}} V_{\text{м}}} \left(\cos \pi \frac{l/2}{l+2h} \right) \bar{N} - \frac{\alpha F}{c_{\text{м}} \gamma_{\text{м}} V_{\text{м}}} (T_{\text{мз}} - T_{2\text{p}}). \quad (9)$$

в. Три члена ряда разложения

$$T_{\Gamma \text{ cp}} = \frac{z}{l} T_{\Gamma} - \frac{z^2}{2l} \cdot \frac{\partial T_{\Gamma}}{\partial z} + \frac{z^3}{6l} \cdot \frac{\partial^2 T_{\Gamma}}{\partial z^2} - \dots \Big|_{-l/2}^{+l/2}. \quad (5 \text{ г})$$

Вторые производные по температуре газа определяются из уравнения (2а)

$$\frac{\partial^2 T_{\Gamma}}{\partial z^2} = \frac{\alpha \Pi}{c_p G} \left(\frac{\partial T_{\text{м}}}{\partial z} - \frac{\partial T_{\Gamma}}{\partial z} \right) - \frac{c_p \gamma_{\Gamma} S_{\Gamma}}{c_p G} \cdot \frac{\partial^2 T_{\Gamma}}{\partial z \partial \tau}.$$

В силу того, что функция $T_{\Gamma}(\tau, z)$ непрерывна, имеет всевозможные частные производные (причем все они также непрерывны) и определена в открытой области $-l/2, +l/2$, справедливо соотношение

$$\frac{\partial^2 T_{\Gamma}}{\partial z \partial \tau} = \frac{\partial^2 T_{\Gamma}}{\partial \tau \partial z}.$$

Обозначим

$$l \left[\left(\frac{\partial T_{\Gamma}}{\partial z} \right)_{2\text{p}} + \left(\frac{\partial T_{\Gamma}}{\partial z} \right)_3 \right] = T'_{\Gamma z};$$

$$l \left[\left(\frac{\partial T_{\text{м}}}{\partial z} \right)_{2\text{p}} + \left(\frac{\partial T_{\text{м}}}{\partial z} \right)_3 \right] = T'_{\text{мз}},$$

где величины $T'_{\Gamma z}$, $T'_{\text{мз}}$ теперь являются функциями от τ . После подстановки пределов интегрирования в уравнение (5г) и несложных преобразований получаем

$$T_{\Gamma \text{ cp}} = \frac{1}{2} (T_{2\text{p}} + T_3) - \frac{1}{8} \left[\frac{2\alpha F}{c_p G} (T_{\text{мз}} - T_3) - 2 \frac{c_p \gamma_{\Gamma \text{ cp}} V_{\Gamma}}{c_p G} \cdot \frac{dT_3}{d\tau} - T'_{\Gamma z} \right] + \frac{1}{48} \left[\frac{\alpha F}{c_p G} (T'_{\text{мз}} - T'_{\Gamma z}) - \frac{c_p \gamma_{\Gamma \text{ cp}} V_{\Gamma}}{c_p G} \cdot \frac{dT'_{\Gamma z}}{d\tau} \right]. \quad (5 \text{ д})$$

Получаем систему уравнений

$$\frac{dT'_{\text{мз}}}{d\tau} = - \frac{\alpha F}{c_{\text{м}} \gamma_{\text{м}} V_{\text{м}}} (T'_{\text{мз}} - T'_{\Gamma z}), \quad (10)$$

$$\frac{dT'_{\Gamma z}}{d\tau} = 12 \frac{dT_3}{d\tau} + \frac{c_p G}{c_p \gamma_{\Gamma \text{ cp}} V_{\Gamma}} \left[48 \left(\frac{T_{2\text{p}} + T_3}{2} \right) - T_{\Gamma \text{ cp}} + \frac{1}{8} T'_{\Gamma z} \right] -$$

$$- \frac{\alpha F}{c_p \gamma_{\Gamma \text{ cp}} V_{\Gamma}} [12 (T_{\text{мз}} - T_3) - (T'_{\text{мз}} - T'_{\Gamma z})], \quad (11)$$

$$\frac{dT_3}{d\tau} = - \frac{\gamma_{2\text{p}}}{\gamma_3} \frac{dT_{2\text{p}}}{d\tau} + \frac{\alpha F}{c_p \gamma_3 V_{\Gamma}} (T_{\text{мз}} - T_3 + T_{\text{мз}} - T_{2\text{p}}) -$$

$$- \frac{c_p G}{c_p \gamma_{\Gamma \text{ cp}} V_{\Gamma}} T'_{\Gamma z}, \quad (12)$$

$$\frac{dT_{\Gamma \text{ cp}}}{d\tau} = \frac{\alpha F}{c_p \gamma_{\Gamma \text{ cp}} V_{\Gamma}} (T_{\text{м cp}} - T_{\Gamma \text{ cp}}) - \frac{c_p G}{c_p \gamma_{\Gamma \text{ cp}} V_{\Gamma}} (T_3 - T_{2\text{p}}), \quad (4 \text{ а})$$

$$\frac{dT_{\text{м cp}}}{d\tau} = 2 \frac{q_{\text{в0}} V_{\text{м}}}{c_{\text{м}} \gamma_{\text{м}} V_{\text{м}}} \cdot \frac{l+2h}{\pi l} \left(\sin \pi \frac{l/2}{l+2h} \right) \bar{N} - \frac{\alpha F}{c_{\text{м}} \gamma_{\text{м}} V_{\text{м}}} (T_{\text{м cp}} - T_{\Gamma \text{ cp}}), \quad (3 \text{ а})$$

$$\frac{dT_{\text{мз}}}{d\tau} = \frac{q_{\text{в0}} V_{\text{м}}}{c_{\text{м}} \gamma_{\text{м}} V_{\text{м}}} \left(\cos \pi \frac{l/2}{l+2h} \right) \bar{N} - \frac{\alpha F}{c_{\text{м}} \gamma_{\text{м}} V_{\text{м}}} (T_{\text{мз}} - T_3), \quad (8)$$

$$\frac{dT_{\text{мз}}}{d\tau} = \frac{q_{\text{в0}} V_{\text{м}}}{c_{\text{м}} \gamma_{\text{м}} V_{\text{м}}} \left(\cos \pi \frac{l/2}{l+2h} \right) \bar{N} - \frac{\alpha F}{c_{\text{м}} \gamma_{\text{м}} V_{\text{м}}} (T_{\text{мз}} - T_{2\text{p}}). \quad (9)$$

Аналогичные системы уравнений могут быть записаны для четырех, пяти и т. д. членов ряда разложения.

РЕЗУЛЬТАТЫ ЭЛЕКТРОННОГО МОДЕЛИРОВАНИЯ УРАВНЕНИЙ НЕСТАЦИОНАРНОГО ТЕПЛОБМЕНА

Предложенная выше методика позволяет описать нестационарный процесс теплообмена в аппарате с различной точностью в зависимости от взятого числа членов ряда разложения. Большее число членов ряда предполагает и более точное математическое описание процесса, однако мы получаем систему дифференциальных уравнений высокого порядка, что приводит к резкому увеличению аппаратуры для моделирования. С целью выбора оптимального числа членов ряда разложения на аналоговых вычислительных машинах типа МНБ-1 было проведено исследование нестационарных процессов теплообмена в газоохлаждаемом реакторе при различных внешних возмущениях в случае одного, двух и трех членов ряда разложения. Кинетика реактора при этом описывалась известными уравнениями¹ с учетом шести групп запаздывающих нейтронов

$$\frac{dn}{d\tau} = \frac{\Delta K - \beta}{l^*} n - \sum_1^6 \lambda_i C_i,$$

$$\frac{dC_i}{d\tau} = - \lambda_i C_i + \frac{\beta_i}{l^*} n,$$

где n — плотность нейтронов;

ΔK — реактивность;

β_i — доля запаздывающих нейтронов i -ой группы в общем числе нейтронов;

λ_i — постоянная распада источника i -ой группы запаздывающих нейтронов;

C_i — концентрация ядер — излучателей запаздывающих нейтронов;

l^* — среднее время жизни нейтронов.

Для газоохлаждаемого реактора были приняты эффективное время жизни $l^* = 10^{-5}$ сек и нулевой температурный коэффициент как по топливу, так и по замедлителю.

Проверка предложенного метода выполнена для газоохлаждаемого реактора атомной энергетической установки тепловой мощности 50 Мвт с твэлами стержневого типа. Теплоноситель — азот. Состав твэлов — $\text{UO}_2 + \text{BeO}$, замедлитель — BeO , покрытия твэлов — нержавеющая сталь.

Для газоохлаждаемого реактора атомной энергетической установки $N_T = 50 \text{ Мвт}$ произведена оценка точности представления зависимости $T_{г\text{ср}}$ через входную и выходную температуры и их производные по координате z с помощью различного числа членов ряда разложения $T_{г\text{ср}}$ в стационарном и нестационарном случаях.

Оценку погрешности усеченного ряда достаточно точно можно произвести первым опущенным членом этого ряда.

В стационарном случае точность разложения в ряд зависимости $T_{г\text{ср}}$ через температуры входа, выхода и их производные может быть оценена по номинальному режиму. Как показали расчеты, в стационарном случае достаточную точность обеспечивают два члена разложения в ряд (ошибка составляет 1—3%).

Нестационарные режимы газоохлаждаемого реактора $N_T = 50 \text{ Мвт}$ исследовались на аналоговых вычислительных машинах типа МНБ-1 при представлении $T_{г\text{ср}}$ через температуры входа и выхода различным числом членов ряда разложения и методом конечных разностей.

Вычислительная машина МНБ-1 представляет установку блочного типа. Операционные усилители машины имеют автоматическую стабилизацию нулевого уровня (канал модуляция-демодуляция) и соответственно малый дрейф на выходе (40—60 мкв за 10 мин). Частотная характеристика усилителя в режиме инвертирования линейна до частоты 1000 гц. Постоянные коэффициенты задаются компенсационным способом с погрешностью 0,2%. Статическая погрешность регистрирующего прибора составляет — 0,5%.

На АВМ МНБ-1 для названного газоохлаждаемого реактора рассмотрены отдельные по каждому параметру скачкообразные и синусоидальные возмущения при различном числе членов ряда разложения в уравнениях нестационарной теплопередачи реактора с целью определения границ применимости предложенного метода и необходимого числа членов ряда. Полученные результаты иллюстрируются рис. 2—6.

На рис. 2 показано изменение температуры газа на выходе реактора при скачкообразном уменьшении на 100° температуры газа на входе. Два и три члена ряда разложения дают практически одинаковые значения забросов температуры газа на выходе реактора. Один член ряда разложения при таком типе возму-

щений приводит к пятикратному превышению забросов температуры газа на выходе реактора.

На рис. 3, 4 представлено изменение нейтронной мощности реактора и выходной температуры газа при скачкообразном уменьшении весового расхода газа через реактор до $G = 0,25G_0$. Забросы температуры газа T_3 на выходе реактора при двух и трех членах ряда разложения практически совпадают. При одном члене ряда разложения $T_{г\text{ср}}$ заброс температуры газа на выходе реактора завьшается в 1,4—1,5 раза.

При сбросе стержней аварийной защиты ($\Delta K = -0,015$) и постоянных весовом расходе газа и температуре газа на входе в реактор кривые переходного процесса для всех переменных ($n, T_{м\text{ср}}, T_3, T_{г\text{ср}}$) хорошо совпадают друг с другом в случае одного, двух и трех членов разложения $T_{г\text{ср}}$ в ряд.

Рис. 5 иллюстрирует изменение средней температуры металла для этого случая. При возмущениях по реактивности возможно описание нестационарного теплообмена в реакторе уравнением с одним членом разложения $T_{г\text{ср}}$ в ряд через температуры входа и выхода.

После выявления отдельного влияния возмущений $\Delta G, \Delta T_{2p}, \Delta K$ для оценки точности представления уравнений нестационарной теплоотдачи одним, двумя или тремя членами разложения в ряд изучены динамические характеристики газоохлаждаемого реактора при комплексе возмущений:

- 1) глубоком изменении тепловой мощности реактора ($\Delta K \approx -0,005$),
- 2) скачкообразном уменьшении весового расхода газа через реактор $\Delta G = -0,75 G_0$,
- 3) постоянной, скачкообразно уменьшающейся на 100° или увеличивающейся на 50° температуре газа на входе в реактор.

Результаты моделирования показали, что при таких комплексных возмущениях представление зависимости $T_{г\text{ср}}$ через T_{2p} и T_3 одним членом ряда разложения дает существенное (в 1,5—2 раза) завьшение забросов температуры газа на выходе и занижение длительности переходного процесса по сравнению с действительными значениями в 1,3—1,5 раза.

Два члена ряда разложения $T_{г\text{ср}}$ через T_{2p} и T_3 и их производные по координате z обеспечивают достаточную точность решения при нестационарных режимах в реакторе (ошибка составляет 3—4%).

Эта же система при названном комплексе возмущений была решена численно методом конечных разностей. Результаты такого решения являются критерием правильности моделирования уравнений нестационарного теплообмена при различном числе членов разложения $T_{г\text{ср}}$ в ряд. При методе конечных разностей твэл реактора по длине разбивается на несколько участков и в пределах каждого участка принимается линейный профиль температур.

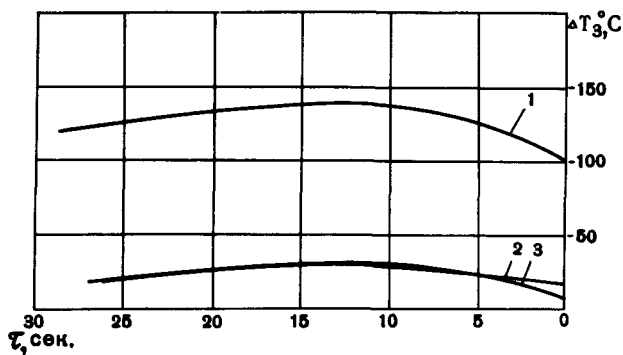


Рис. 2. Изменение температуры газа на выходе при изменении температуры на входе скачком на 100° (1, 2, 3—число членов ряда разложения)

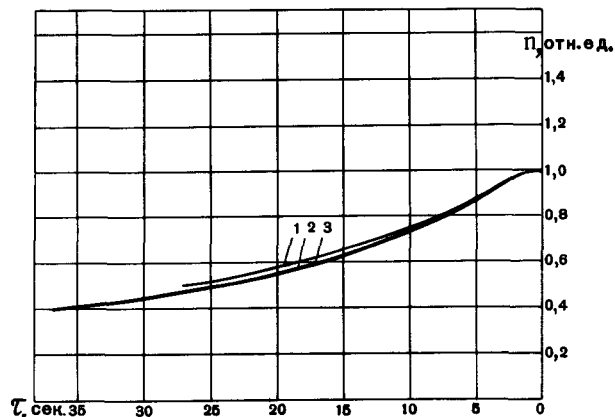


Рис. 3. График нейтронной мощности при изменении расхода газа скачком до $G=0,25G_0$ (1, 2, 3—число членов ряда разложения)

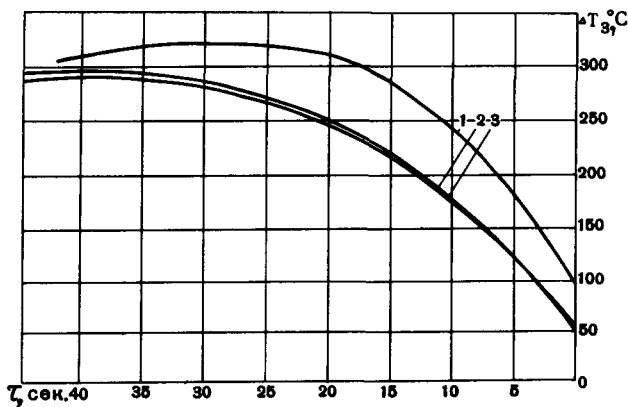


Рис. 4. График выходной температуры газа при изменении расхода газа скачком до $G=0,25G_0$ (1, 2, 3—число членов ряда разложения)

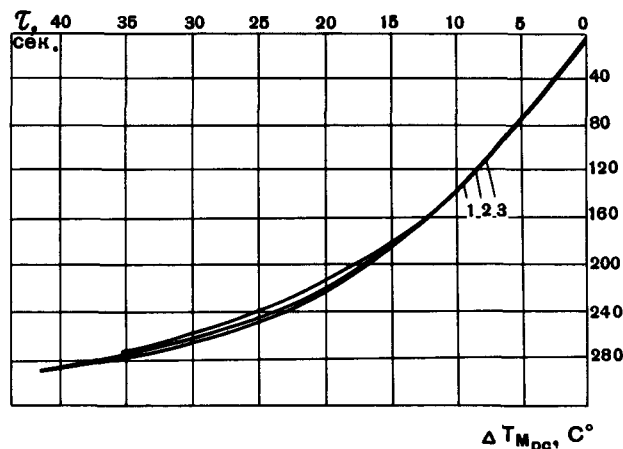


Рис. 5. График средней температуры металла при сбросе стержней аварийной защиты ($\Delta K=-0,015$) (1, 2, 3—число членов ряда разложения)

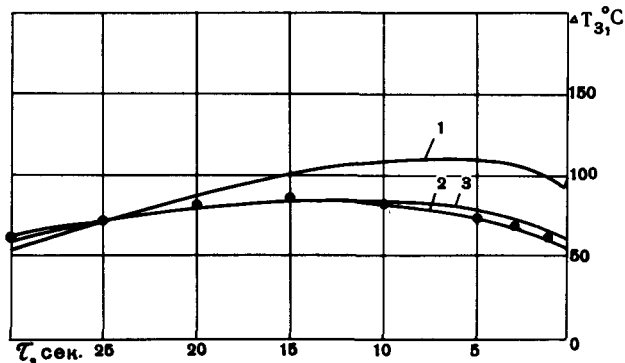


Рис. 6. График выходной температуры газа при одновременном изменении расхода и реактивности ($G=0,75 G_0$, $\Delta K=-0,005$) (1, 2, 3—число членов ряда разложения)

Число участков, на которые разбивается канал по длине, выбирается из требуемой точности решения (два, четыре, шесть участков). Результаты моделирования показали, что разделение твэла по длине на четыре участка

обеспечивает достаточную точность решения (погрешность не превышает 1—3%).

На рис. 6 нанесены точки контрольного численного решения методом конечных разностей, которые хорошо совпадают с кривыми решения для двух и трех членов ряда разложения.

ЗАКЛЮЧЕНИЕ

Разработанный метод моделирования на аналоговых вычислительных машинах нестационарных тепловых процессов в газоохлаждаемых реакторах учитывает распределенность параметров по длине реактора представлением среднеинтегральной температуры газа через температуры газа на входе и на выходе и их производные в виде нескольких членов ряда разложения.

Предложенный метод проверен при глубоких раздельных и комплексных возмущениях по расходу газа, тепловой мощности и температуре газа на входе реактора. Для газоохлаждаемого реактора энергетической установки достаточ-

ную точность решения обеспечивают два члена ряда разложения (погрешность не превышает 3—4%).

Проведено сравнение с другим способом моделирования — методом конечных разностей, который был контрольным, и показано, что предложенный метод экономнее, чем метод конечных разностей (реактор описывается пятью дифференциальными уравнениями против восьми при методе конечных разностей).

Разработанный метод моделирования динамических характеристик реактора может быть использован при изучении характеристик установки при прогреве, запуске, изменении мощности и аварийном расхолаживании.

Метод может быть эффективно использован при изучении динамических характеристик ре-

генератора, холодильника и других теплообменных аппаратов атомных энергетических установок.

ЛИТЕРАТУРА

1. Л а н ц о ш. Практические методы прикладного анализа. М., Физматгиз, 1961.
2. Г. М. Ф и х т е н г о л ь д. Курс математического анализа. Т. 1. М., Физматгиз, 1960.
3. В. Л. Д а н и л о в и др. Математический анализ, ряды. М., Физматгиз, 1961.
4. Н. А. Ш у л ь ц. Регулирование энергетических ядерных реакторов. М., Изд-во иностр. лит., 1957.
5. Дж. Б о у э н, Е. М е й с т е р с. Управление ядерными реакторами. М., Атомиздат, 1960.
6. Р. Б а с с а р д, Р. Д е л а у э р. Ракеты с атомным двигателем. М., Изд-во иностр. лит., 1960.
7. Б. Я. К о г а н. Электронные моделирующие устройства и их применение для исследования систем автоматического регулирования. М., Физматгиз, 1957.

ABSTRACT—RÉSUMÉ—АННОТАЦИЯ—RESUMEN

A/719 Byelorussian SSR

A method of simulating transient thermal processes in gas-cooled reactors using analogue computers

By V. B. Nesterenko and V. M. Shadsky

The analogue computers are used more often for the transient investigation with power change, heating, starting-up and reactor shut-down cooling. The use of these computers deteriorated as the transient heat transfer in reactor is described by partial differential equations.

Digital computers permit partial equations to be solved. The difficulty of direct connections of these computers with the real control system elements as well as complicated and laborious programming and programme arrangement is a considerable obstacle to their application for engineering calculations.

As the preparation of equation solutions is simple, it is not difficult to link the analogue computers with the real elements of control systems.

However serial analogue computers (MN-7, EMU-8 EMU-10, MN-8, MN-10, MN-14, MN-6) are designed to solve usual differential equations. Therefore the method for transformation of partial equations into ordinary non-linear differential equations is necessary.

This paper offers an effective and simple transformation method of partial equations into ordinary differential ones which take into account parameter distributions along the reactor length by the presentation of the average-integral on the length gas temperature in terms of inlet and outlet temperatures and their derivatives in the form of a series.

The method has been checked during vigorous discontinuous and sinusoidal disturbances both separate and simultaneous of the gas-flow-rate, reactor neutron flux and inlet gas temperature.

Two terms of above series provide good accuracy of the solution (error is not more than 3—4 per cent).

The method proposed is compared with finite difference method, taken as a reference one and it is shown that this method is more economic than the finite difference one (the reactor is described by five differential equations rather than by eight using the finite difference method).

The method may be effectively used for the dynamic characteristic study of a reactor, refrigerator and other heat exchangers of nuclear power plants.

This method may be used for the dynamic characteristic study of a gas-cooled reactor with energy change, heating-up, starting-up and reactor shut-down cooling.

A/719 RSS de Biélorussie

Méthode de simulation au moyen de calculateurs analogiques des processus thermiques transitoires dans les réacteurs de puissance refroidis par un gaz

par V. B. Nesterenko et V. M. Shadsky

Pour étudier les processus transitoires d'échange de chaleur lors d'une modification de la puissance et pendant le chauffage, la mise en marche et le refroidissement dû à l'arrêt d'urgence du réacteur, on utilise de plus en plus fréquemment des calculateurs électroniques analogiques. L'emploi de ces machines est rendu difficile par le fait que l'échange de chaleur non stationnaire dans un réacteur s'exprime par des équations différentielles aux dérivées partielles.

Les calculateurs électroniques numériques permettent de résoudre les équations aux dérivées partielles. Ce qui empêche avant tout de les employer pour des calculs techniques c'est la difficulté d'établir une liaison directe entre ces appareils et les dispositifs de réglage ainsi que la complexité de l'élaboration et de la mise au point des programmes.

Etant donné la simplicité du traitement que doivent subir les équations en vue de leur solution, il n'est

guère difficile d'établir une liaison entre les calculateurs analogiques à fonctionnement continu et les éléments des systèmes de réglage. Toutefois, les calculateurs analogiques de série (MN-7, EMU-8, EMU-10, MN-8, MN-10, MN-14 et MN-6) sont conçus pour résoudre les équations différentielles ordinaires. C'est pourquoi il faut une méthode permettant de transformer les équations aux dérivées partielles en équations différentielles non linéaires ordinaires.

Le mémoire propose à cet effet une méthode simple et efficace qui tient compte de la répartition des paramètres le long du réacteur, en utilisant la moyenne-intégrale de la température du gaz sur la longueur du réacteur représentée en fonction des températures d'entrée et de sortie du gaz et de leurs dérivées sous forme de séries.

La méthode a été vérifiée lors de fortes perturbations discontinues et sinusoidales, séparées ou simultanées, du débit de gaz, de l'énergie du flux neutronique du réacteur et de la température d'entrée du gaz. Deux termes de la série en question permettent d'obtenir une solution assez précise (l'erreur ne dépasse 3 à 4 %).

La méthode proposée a été comparée à la méthode des différences finies utilisée comme méthode de contrôle; elle est plus économique que cette dernière (le réacteur est décrit par cinq équations différentielles, alors qu'en appliquant la méthode des différences finies, il en faudrait huit).

On peut appliquer cette méthode avec succès à l'étude des caractéristiques dynamiques d'un réacteur, d'un refroidisseur et des divers appareils d'échange thermique employés dans les centrales nucléaires, ainsi qu'à l'étude des caractéristiques dynamiques d'un réacteur refroidi par un gaz, lors d'une modification de la puissance et pendant le chauffage, la mise en marche et le refroidissement dû à un arrêt d'urgence du réacteur.

A/719 RSS de Bielorussia

Método para el estudio en calculadoras analógicas del efecto de los procesos térmicos transitorios en los reactores de potencia con refrigerante gaseoso

por V. B. Nesterenko y V. M. Shadsky

Para el estudio de los procesos transitorios de intercambio de calor, durante las variaciones de potencia, el calentamiento la puesta en marcha y la extracción del calor residual en caso de parada de urgencia del reactor se utilizan cada vez más las calculadoras analó-

gicas electrónicas. El empleo de estas máquinas tropieza con la dificultad de que el proceso transitorio de intercambio de calor en un reactor se expresa por ecuaciones diferenciales en derivadas parciales.

Las calculadoras electrónicas digitales permiten resolver las ecuaciones en derivadas parciales. La principal dificultad para el empleo de estas máquinas en los cálculos de ingeniería, aparte el complejo y laborioso proceso de programación y depuración del programa, es la dificultad de acoplarlas directamente con los elementos reales de los sistemas de regulación.

Por la sencillez de la preparación de las ecuaciones para su resolución, las calculadoras analógicas de funcionamiento continuo se acoplan fácilmente con los elementos reales o con los sistemas de regulación. Sin embargo, las calculadoras analógicas de serie (MN-7, EMU-8, EMU-10, MN-8, MN-10, MN-14 y MN-6) están proyectadas para la resolución de ecuaciones diferenciales ordinarias. Por consiguiente, es necesario un método de transformación de las ecuaciones en derivadas parciales en ecuaciones diferenciales no lineales ordinarias.

En la memoria se propone un método eficaz y sencillo para la transformación de las ecuaciones en derivadas parciales en ecuaciones diferenciales ordinarias, que tien en cuenta la distribución de los parámetros a lo largo del reactor, utilizando la media integral de la temperatura del gas en función de las temperaturas de entrada y salida del gas y sus derivadas desarrolladas en serie.

Se ha comprobado el método en el case de perturbaciones intensas, separadas o simultáneas, discontinuas y sinusoidales, del caudal de gas, de la densidad neutrónica en el reactor y de la temperatura del gas a la entrada. Con dos términos de la serie indicada se obtiene una solución con bastante precisión (el error no pasa del 3-4 %).

Se ha comparado el método propuesto con el método de las diferencias finitas utilizado como partón, y se ha visto que es más económico que éste (el reactor está determinado por 5 ecuaciones diferenciales frente a 8 en el método de diferencias finitas).

Se puede utilizar el método eficazmente para el estudio de las características dinámicas de un reactor, de un refrigerante y de otros sistemas de intercambio de calor de las centrales nucleoelectricas, así como para estudiar las características dinámicas de un reactor de refrigerante gaseoso, correspondientes a las variaciones de potencia, el calentamiento, la puesta en marcha y la extracción del calor residual del reactor en caso de parada de urgencia.

Thermal and irradiation performance of experimental fuels operating in steam-water mixtures

By A. D. Lane and J. G. Collier*

Reactors moderated by heavy water and fuelled with natural uranium have been developed in Canada to the stage where they offer excellent prospects for economic power generation. Pressurized heavy water is used to cool the fuel in the 20 MW(e) NPD** station [1] which has been in operation over two years and the 200 MW(e) Douglas Point Station CANDU [2] where construction is now nearing completion. Organic liquids and evaporating light water are alternative coolants that may have economic and technical advantages for future reactors [3].

Various reactor concepts using evaporating light water as the coolant have been considered [3]. The main advantages of light-water cooling are:

(a) Steam generated in the reactor core can be used directly as the working fluid in a turbine. This results in higher thermodynamic efficiencies and in the elimination of the heat exchangers between the primary and secondary circuits;

(b) Light water is a common, inexpensive material with a long and satisfactory record as a power reactor coolant. A great wealth of experience in the mechanical, chemical and metallurgical fields is available through previous work for conventional and nuclear power plants.

However, neutron economy dictates a minimum hold-up of light water in the core. For this reason, studies have been carried out on a steam/water mixture in which the water is dispersed as a fog [4]. This program has included optimization studies and mechanical design, as well as in- and out-reactor experimentation.

More recently, this work has been extended to cover the system where light water is introduced into the fuel channel as a liquid and evaporated to a high steam quality.*** Future development of the light-water fog and boiling designs is seen in the once-through system in which the water is almost totally evaporated in the fuel channel. In this manner the amount of circulating water would be significantly reduced with a comparable cost reduction.

* Chalk River Nuclear Laboratories, Atomic Energy of Canada Limited.

** Nuclear Power Demonstration.

*** "Quality" is a measure of the steam content of the flow and is defined as the ratio of the mass of vapour flowing past a given point to the total mass flow.

THERMO-HYDRAULIC CONDITIONS FOR STEAM/WATER FLOW

A convenient diagram for depicting most of the possible thermohydraulic régimes in upward vertical flow is reproduced as Fig. 1. This shows a single tube fed with sub-cooled water and producing superheated steam. The walls are subjected to a constant heat flux, so that the mixture quality increases linearly with length. The change from bubble or froth flow to the annular and liquid-dispersed flow regions via slug and churn flow is essentially a phase inversion. In the liquid dispersed region, heat transfer can occur both by evaporation of the superheated liquid film from its free surface and by nucleation in the film itself.

The change from the liquid dispersed region to the liquid deficient region (dry-out) is considered to be the point of complete evaporation of the protective water film which takes place at qualities well below 100% at high heat fluxes. This transition is accompanied by a sharp decrease in the local heat transfer coefficient and an appreciable rise in the wall temperature. It should be noted, however, that the consequences of the dry-out transition at moderate and high qualities, differ substantially from those accompanying DNB* (or burn-out) in a low quality boiling system where steam blanketing usually results in the melting or rupture of the heating surface. As we shall see later, the dry-out condition does not necessarily lead to catastrophic failure of the heating surface. This fact is of considerable importance since the heat flux at which dry-out occurs decreases sharply with increasing quality [5]. To obtain an economic reactor system, it is necessary to operate the fuel element as close to the dry-out point as practicable. Inadvertent excursions into the liquid deficient régime beyond the dry-out point might be tolerated under transient or accident conditions, if it could be established that such excursions did not reduce the life of the fuel element.

The present work is restricted to the liquid dispersed flow (fog) and the liquid deficient regions. A steam/water mixture of the desired proportions is formed at the test channel inlet by spraying water into slightly superheated steam. The distribution of steam and water in the channel when formed in this manner

* DNB Departure from nucleate boiling.

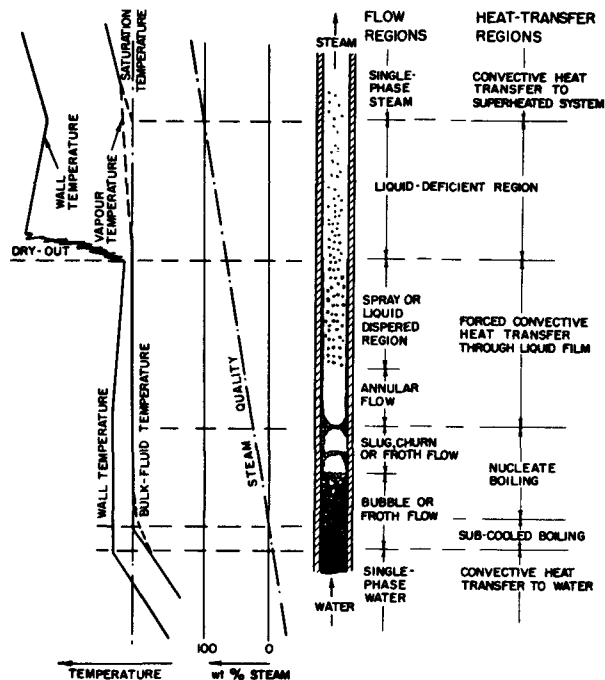


Figure 1. Thermo-hydraulic régimes in vertical upward flow

differs from that obtained by the evaporation of sub-cooled water.

The qualitative picture presented in Fig. 1 is in the main valid for more complex flow channel geometries although the quantitative relationship between the major variables may differ markedly from those for a heated tubular conduit. For example, in the present experiments with an internally heated annulus, the presence of a thick parasitic water film on the unheated outer wall of the channel considerably reduces the steam quality at dry-out.

Program

This work is aimed at establishing the feasibility of fog and once-through reactors from the view point of the fuel coolant combination. Feasibility problems exist in three main areas.

Thermodynamics and hydrodynamics

Satisfactory fuel channel designs must be developed to attain the high heat fluxes required for an economic system. This requires the study of heat transfer and hydrodynamics under conditions and in geometries that are outside the range of present experience.

Sheathing materials

Zircaloy-2 and other zirconium-base alloys are being used successfully as sheathing materials in pressurized-water reactors, and zirconium-base alloys have been assumed in conceptual designs of fog and once-through reactors. However, the economic advantages of these would be lost should these alloys prove unsuitable. Experiments were directed to their oxidation and hydriding behaviour in fog coolant and under liquid deficient conditions at various temperatures.

Coolant chemistry

Satisfactory methods for the chemical control of oxygen production and of crud* deposition are required. In the Canadian pressurized-water reactors, crud deposition is minimized by adding lithium hydroxide to maintain the coolant in an alkaline condition (pH 10). However, lithium hydroxide is non-volatile, and since its deposition could enhance fuel sheath corrosion [6], it has been replaced in two phase systems by ammonia. Coolant chemistry and crud deposition were thus studied in the irradiations as a function of ammonia additions.

Experimental facilities

The experiments were carried out in two almost identical high-pressure steam-water loops [7, 8]. The operation of both loops is quite flexible and a variety of cooling modes, covering pressurized water, boiling water, fog and superheated steam is possible.

In-reactor loop (X4)

The test section of the in-reactor loop is located in the NRX reactor. A schematic flow diagram is shown as Fig. 2. The steam and water flows are individually metered before entering the mixer where the water is injected into the steam through small orifices. The high quality fog leaving the test section passes to a separator, and the separated steam and water flows are measured. Chemical control is maintained by a purification system, using a by-pass flow from the boiler to the pump inlet.

Out-reactor loop (FLARE)

Electrically heated elements are used in this loop to simulate the fuel to be tested in X4. Electrical heaters of the same dimensions and heating capacity as the fuel elements were fabricated by a commercial

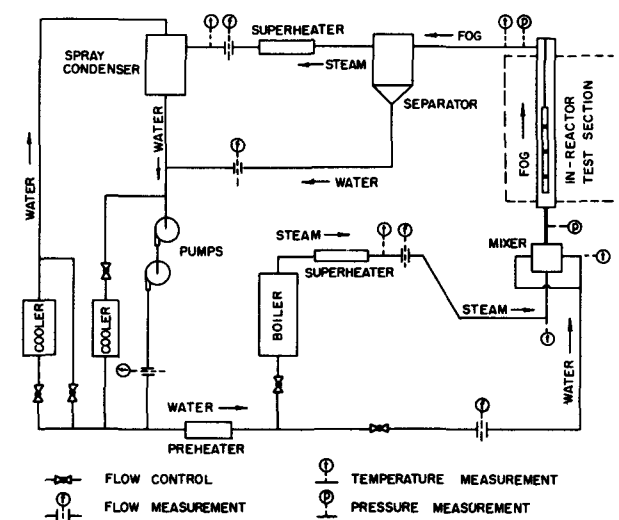


Figure 2. X4 steam and fog loop: simplified flow sheet

* Insoluble compounds (principally iron oxides) which deposit on heat-transfer surfaces.

manufacturer* and instrumented with thermocouples. [7].

Thermo-hydrodynamic experiments

A study has been made—mostly in FLARE—of the effects of detailed geometrical changes of the test element upon the dry-out heat flux. This study has included:

(a) the effect of varying heated length (25, 50, 75 and 100 cm);

(b) the effect of an upstream unheated section or fairing of varying length (0–100 cm) attached to the heater element;

(c) the effect of small axial gaps (0–0.65 cm) and radial misalignments (0–0.1 cm) between elements;

(d) the effect of two heated lengths (50 cm) separated by unheated sections and gaps (up to 4.0 cm).

The consequences of operation in the liquid deficient régime have been studied and methods for predicting the surface temperature in this régime examined. All experiments have been carried out at 70 kgf/cm², the operating pressure chosen for current reactor design studies.

Upstream fairing

As an example of this work, the study of the effect of an upstream unheated section has been chosen. The test-channel arrangement is shown in Fig. 3. The dry-out heat flux for a heated length (L_H) of 50 cm and an exit quality of 50 wt% steam is shown in Fig. 4 as a function of the upstream fairing length (L_1). The effect of this variable is considerable; the dry-out heat flux increases approximately 2.4 times as the fairing length is increased from zero to 100 cm.

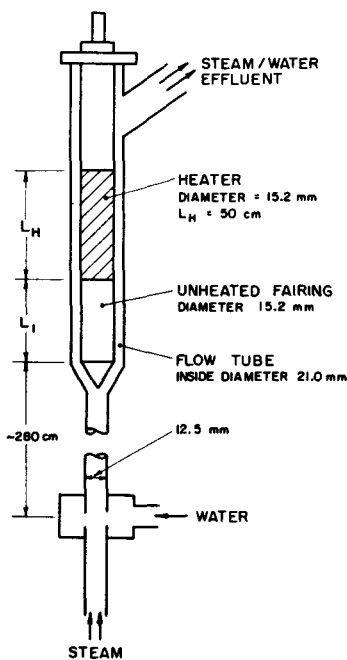


Figure 3. Test section

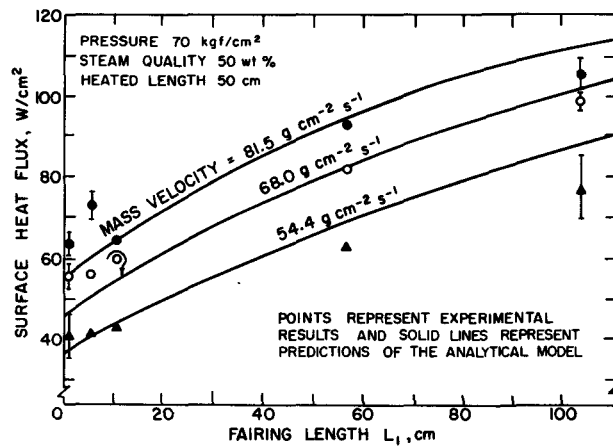


Figure 4. The effect of unheated length on the dry-out heat flux

Analytical model

A simple analytical model has been used to interpret these results and those from other parts of the program. In this example it is postulated that a liquid film is formed on the unheated fairing which is transferred to the heated section by shear forces and is then removed by evaporation and entrainment over the heated length. This model has been used to predict dry-out heat flux curves for the fuel strings used in the irradiation program. The full black lines on Fig. 4 show the prediction of the model in this particular example.

Surface temperatures

A number of tests have been carried out to examine the behaviour of the surface temperature below, at, and above the dry-out point. Figure 5 shows the surface temperature as a function of time during a dry-out experiment. At the start the test element power, and heat flux, is being increased until indications of dry-out are noted (incipient dry-out). The power is then adjusted to allow a small temperature oscillation ($\sim 5^\circ\text{C}$) and a set of readings is taken. At the end of this period a slight increase in the test element power ($\sim 2\%$) resulted in a sharp increase in surface temperature ($\sim 100^\circ\text{C}$) i.e., the dry-out point. Continued operation here gave very large temperature oscillations, despite no recorded changes in the steady-state value of the heat flux, quality or flow. It would appear that there is an alternate wetting and drying out of the surface. A further increase in power ($\sim 7\%$) gives a further rise in surface temperature (up to 512°C). However, in this case there are no oscillations and the surface now appears to be dry. The temperature at this point lies mid-way between the estimates based on other workers' results [9, 10]. All the characteristics described above can be seen in the records of the in-reactor dry-out and liquid deficient experiments.

Irradiation experiments

Five irradiation experiments were undertaken. The main purpose of each was to obtain information on a

* Canadian Chromalox Ltd., Toronto.

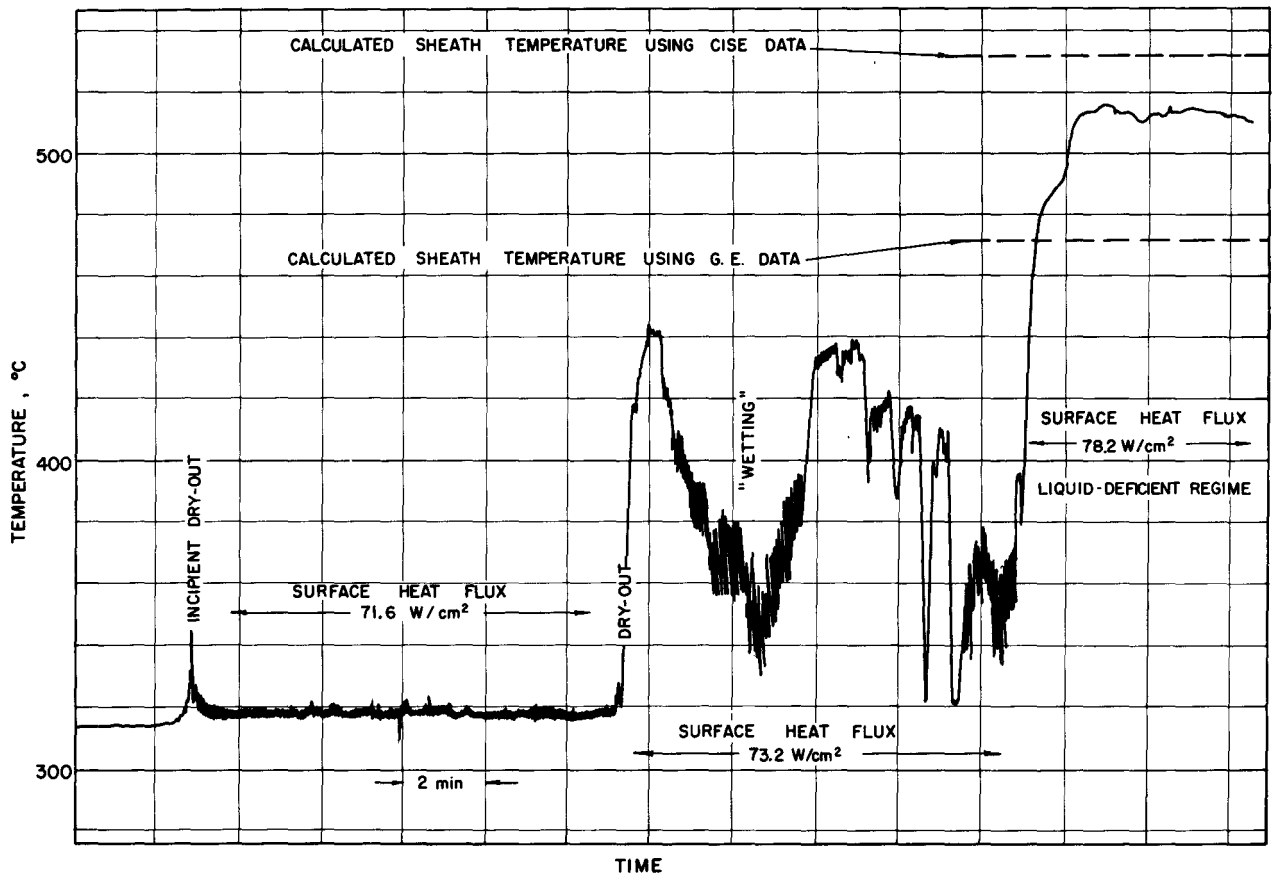


Figure 5. Typical sheath-temperature plot obtained from FLARE in dry-out test

specific aspect of the work. However each irradiation also provided some data in most areas of interest.

For each irradiation, fuel elements were assembled into strings similar to that shown in Fig. 8, but not necessarily with the same number or arrangement of

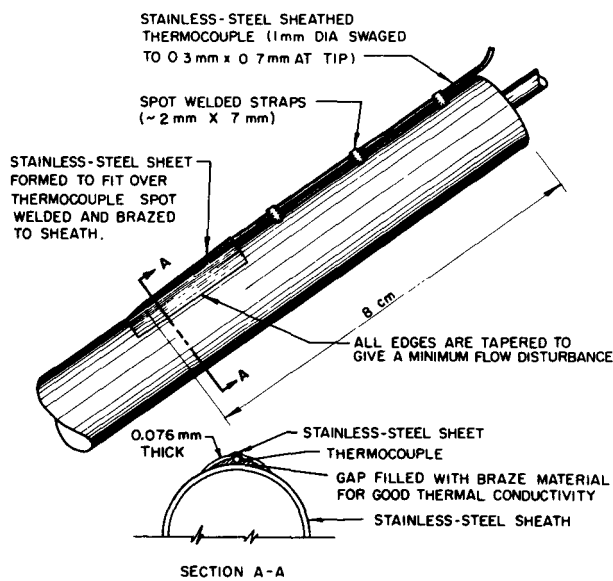


Figure 6. Attachment of sheath thermocouple (developed by Canadian General Electric Company Limited)

elements. An unheated fairing was included at the bottom of each string to establish a water film and enhance the dry-out heat flux of the assembly. The elements were attached to one another by two types of connector: one provided a smooth undisturbed surface from one element to the next, while the other provided an abrupt discontinuity to shed the water film. (Shedding the water film lowers the dry-out heat flux and thus promotes dry-out on downstream elements.) A number of the strings irradiated in this program contained special fuel elements with two thermocouples attached to their stainless steel sheaths. The thermocouples were mounted between the outside of the fuel element sheath and a piece of thin stainless steel sheet which was brazed and welded to the element (Fig. 6). These instrumented elements were used to indicate incipient dry-out and to measure the sheath temperatures attained in the liquid deficient region. The response of these thermocouple assemblies at dry-out was very similar to that shown in Fig. 5.

The following fuel irradiations have been undertaken in this part of the program, and some of the pertinent results from them have been summarized in Table 1:

(a) The first, designated as 421, was intended primarily to commission the loop and develop techniques for the remainder of the irradiation program [11];

(b) The second irradiation (422) was undertaken

Table I. Summary of irradiations

Specimens			Irradiation conditions in fog							Results				
Exp't	Identification	Material	Time h	Rating		Temperature		NH ₃ mg/kg	Steam quality wt%	Crud deposition		Net hydrogen mg/kg	Oxide thickness μm	Residual bow mm
				$f\lambda d\theta^a$ W/cm	Q/A W/cm ²	Nominal °C	Peak °C			μg Fe/cm ²	μm			
421	EPE	Zircaloy-2	385	36	100	295	N/R ^e	0.1 to 20	20-30	200	1.2	Uniform 20		0.25
	EPP	Zr-2½%Nb	1 570	34	95	295	295	Varied between 0 and 10	25-27	40	0.25	Nil	1-2	0.2
422 III ^b	EPM Top	Zircaloy-2	1 570	31	85	295	295		0 and 10	23-25	160	1.0	~20	1-6 with pits N/R
	EPM Bottom	Zircaloy-2	1 570	18	50	290	290	18-20		140	0.9	Nil		
	FZA Top	Zircaloy-2	770	21	58	380	~400	59 (dry) ~56	4	0.02	>200	<1-50 with pits	}2.5	
	FZA Bottom	Zircaloy-2	770	22	62	290	290		5	0.03	~50	<1-17 with pits		
423	FZB Top	Zircaloy-2	770	20	55	290	290	3-5	~55	6	0.04	N/R	N/R	}1.0
	FZB Bottom	Zircaloy-2	770	13	35	290	290		~52	4	0.02	N/R	N/R	
	FZM	Zr-2½%Nb	770	23	63	290	290	~50	6	0.04	N/R	N/R	0.2	
	FZH Top	Zircaloy-2	35½ ^c	32	88	~600	~700	41 (dry) 36	N/R	N/R	500-6 000	10-370 with pits	}N/R	
	FZH Bottom	Zircaloy-2	35½	32	88	295	295		19	0.12	<10	<1-7 with pits		
424 I	FZL	Zr-2½%Nb	35½	30	84	295	295	3-5	35	15	0.95	<10	None visible	N/R
	FZJ Top	Zircaloy-2	35½	29	80	295	290	34	3	0.02	<10	N/R	}N/R	
	FZJ Bottom	Zircaloy-2	35½	19	53	290	290	30	18	0.11	N/R	N/R		
	FZD Top	Zircaloy-2	51½ ^d	25	70	~430	<700	41 (dry) 36	N/R	N/R	1 000-4 000	<1-100 with pits	}N/R	
	FZD Bottom	Zircaloy-2	51½	25	70	295	295		4	0.02	<500	<1-40 with pits		
424 II	FZE Top	Zircaloy-2	51½	22	62	295	295	3-5	36	2	0.01	<10	N/R	}1.4
	FZE Bottom	Zircaloy-2	51½	15	42	290	290		33	3	0.02	N/R	N/R	
	FZN	Zr-2½%Nb	51½	16	45	290	290	32	4	0.02	N/R	N/R	0.1	
424 III	FZF Top	Zircaloy-2	110	25	68	460	~550	3-5	58 (dry)	4	0.02	100-400	<1-40 with pits	}1.5
	FZF Bottom	Zircaloy-2	110	24	66	295	295		54	5	0.03	Nil	None visible	

^a $f\lambda d\theta$ is a convenient measure of the heat rating of UO₂. For further details see reference [14].

^b Phases I and II failed prematurely and their failures have no bearing on the data presented.

^c Defected after irradiation of 34 hours in fog.

^d Defected after irradiation of 48½ hours in fog.

^e N/R = Not recorded.

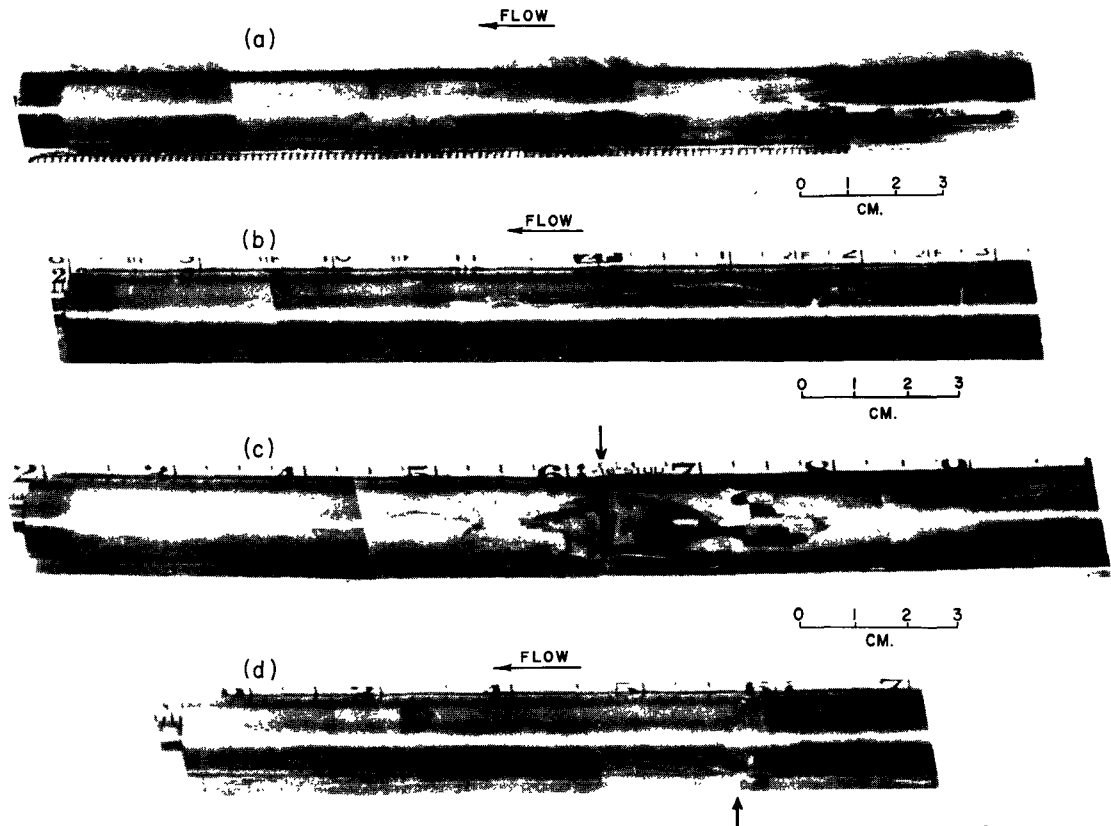


Figure 7. (a, b) 423 FSA and 424 III FZF, irradiated in dry-out; (c, d) Opposite sides of 424 II FZD, showing effect of thermal distortion
 For details of irradiations see Table 1, but note heavy white corrosion in (c) and its absence in (d); it is estimated that the side shown in (c) approached 700 °C while that in (d) ran at ~430 °C

principally to provide corrosion and hydriding data for fuel clad in Zircaloy-2 and $Zr-2\frac{1}{2}\%Nb$;

(c) The third irradiation (423) provided corrosion and hydriding data for Zircaloy-2 when operating in the liquid deficient region at temperatures up to ~400 °C. The conditions of this test were those that would be expected near the outlet end of a coolant channel in a fog or once-through reactor if an inadvertent dry-out occurred at that location.* The liquid deficient condition was detected during this experiment by sheath thermocouples, and dry-out was encouraged by the use of discontinuous couplings in the fuel string (cf. Fig. 8). Figure 7(a) is a post irradiation photograph of an element which operated in the liquid deficient region;

(d) The fourth and fifth irradiations (424 Phases I and III) provided corrosion and hydriding data for Zircaloy-2 when operating in the liquid deficient region at temperatures up to ~700 °C and ~550 °C respectively. These conditions were representative of the conditions near the centre of a fog-cooled or once-through reactor coolant channel. The expected temperature in the first of these two irradiations was

so high that it was considered a time-to-failure experiment.*

The fuel string used in 424 Phase I is shown in Fig. 8 along with the anticipated operating conditions. From this figure it is evident that elements 1, 2 and 3 should have been operating in a liquid deficient condition; however, examination of these elements after irradiation indicated that element 3 and the bottom portion of element 2 were probably wet during most of the irradiation. Similar effects were also observed in 423 and 424 Phase III. This phenomenon is not completely understood, nor is it accounted for by the analytical model. Figure 7(b) shows an element that operated dry in the fifth irradiation.

In addition to the stated primary objectives of the various irradiations, a large amount of ancillary information was also obtained.

(a) Two premature fuel failures (422 Phase II and 424 Phase II) appear to have been caused by a thermal distortion mechanism brought on by partial dry-out. In both cases large temperature differentials (up to 300 °C) were measured by thermocouples located at the same elevation but on opposite sides of an

* This is the most probable location for a dry-out in either of these reactor types.

* It is desirable to know the time-to-failure of fuel at various locations in a reactor channel under continuous dry-out conditions.

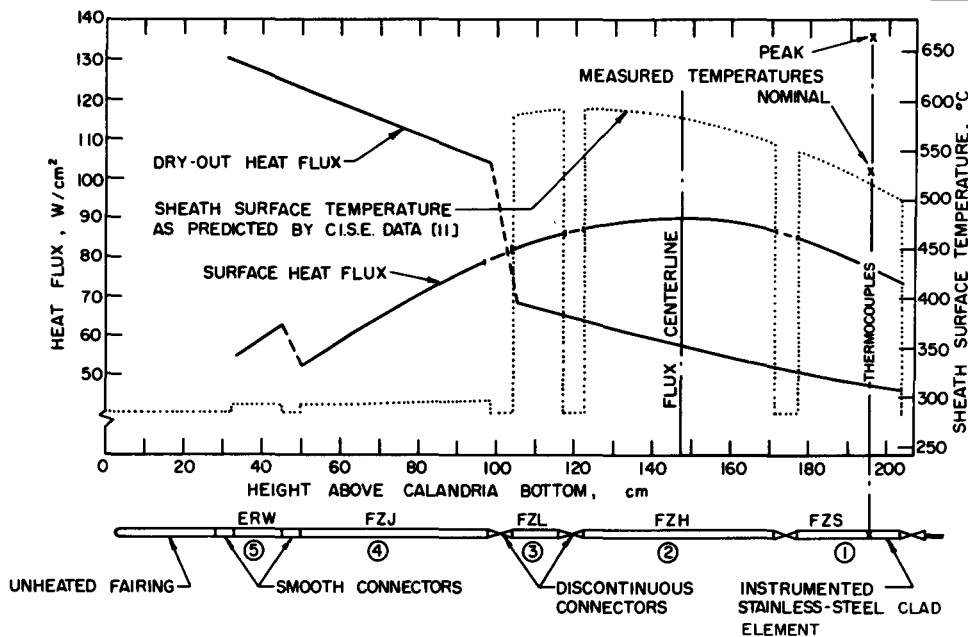


Figure 8. Fuel string and operating conditions for the time-to-failure irradiation (424 I)
Except for FZS, all elements are clad in zirconium base alloys

instrumented fuel element, and both followed the sequence of events depicted in Fig. 9. It is believed that the large temperature differential caused by a dry-out at high heat flux on only one side of an element induced a thermal bow. This bow reduced the steam phase velocity over the hot side of the element causing its temperature to rise even further. Figure 7(c, d) shows the effects of such a bow where it is estimated that the sheath temperature approached $700^{\circ}C$.

(b) None of the fuel elements failed catastrophically, and all were removed intact. In general, the signals from the fuel defects were similar to those observed with small defects in pressurized water. However, no fuel was operated for more than ~ 3 h in a defected condition.

(c) The elements which operated for appreciable periods with normal fog cooling (EPE, EPM and EPP in Table 1) exhibited the anticipated metal wastage by corrosion. The hydrogen pick-up in the two Zircaloy-2 clad elements is approximately that anticipated, while that in the $Zr-2\frac{1}{2}\%Nb$ clad element is less than expected. Small surface pits were noticed on a number of Zircaloy-2 clad elements. Although this pitting is unusual, similar pits were also observed on some unheated corrosion specimens irradiated with the fuel strings [12].

(d) Elements subjected to extended dry-out at high temperatures showed great variations in metal wastage and hydrogen content. These variations were evident along the length of the sheaths as well as around the circumference, and may well be associated with the thermal distortion mechanism described above.

(e) It was found that the addition of ammonia reduced the radiolytic oxygen content (at $10 \text{ mg NH}_3/\text{Kg}$ of coolant, oxygen was $< 0.005 \text{ cm}^3/\text{kg}$ of steam) [13]. Also the steady-state nitrate concentration became less as the ammonia concentration was increased. The coolant chemistry aspects of these irradiations are discussed more fully in another paper [13].

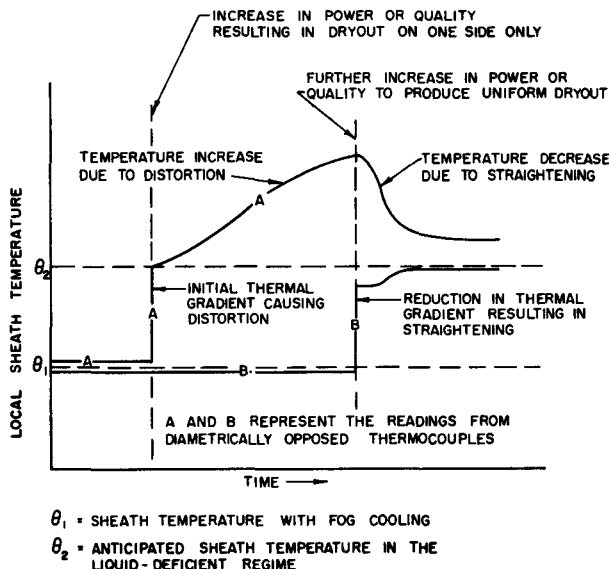


Figure 9. Thermal distortion mechanism

DISCUSSION

The out-reactor heat transfer experiments and the analytical model developed to interpret these measurements have clearly demonstrated the importance of the thin water film over the heating surface in fog cooling. Any point on the heated surface may receive liquid by two processes. Firstly, liquid is transported to the surface by turbulent diffusion of water droplets dispersed in the steam phase. Secondly, water is carried to the point by the flow of the surface film. In many of these experiments the major contribution

was by the second of the two mechanisms. This observation has considerable practical significance in the design of fuel assemblies for power reactors. Clearly, any impedance or disruption of the water film caused by structural members of the assembly will sharply reduce the dry-out heat flux. An example of this point is the performance of the different types of connector used in the irradiations. In future experiments, efforts will be made to increase the contribution made by the first process, that of turbulent diffusion of water droplets.

The combination of the effects of obstructions and of thermal distortion presents a design problem if bundle-type fuel assemblies* are to be used with fog coolant. An attempt must be made to keep such bundles free from discontinuities over the entire length of the fuel channel. The coolant conditions or heat flux must be adjusted to compensate for any unavoidable obstructions.

The program presented here has used only strings of single elements both for simplicity and because of an interest in using similar elements in a bundle-type assembly with fog coolant. However, future parts of the program will investigate other types of assembly.

It was anticipated that the Leidenfrost point** might have a marked effect on the deposition of crud. At sheath temperatures in excess of the Leidenfrost point the fuel sheath would not be wetted by impinging water droplets and it was felt that solids would not be deposited. So far, unfortunately, insufficient data have been collected to definitely establish this.

It has been postulated that a time-to-failure can be estimated for Zircaloy-clad fuel irradiated continuously in the liquid deficient state. Such an estimate would simply be the time required to corrode through a major part of the sheath thickness as predicted from known corrosion rates, estimated surface temperatures, and an allowance for the insulation properties of the corrosion-product film. This model predicts a rapidly increasing rate of sheath penetration with time (as the thickness of the corrosion-product layer increases). It was hoped that the dry-out irradiations would substantiate or refute this model. For example, if there were appreciable erosion of the corrosion-product film, the rate of sheath penetration would not increase as rapidly as predicted by the model. Unfortunately, local surface temperatures were not known to sufficient accuracy during the fourth and fifth irradiations (424 I and II) to be able to substantiate the model via measurements of the corrosion-product film thicknesses, as the corrosion rate of Zircaloy-2 changes very rapidly with temperature between 600 and 700 °C. However the relative thickness of the oxide and parent metal in these elements indicated that there had been no appreciable erosion of the oxide film.

* A bundle of single elements (in general 19 elements).

** The Leidenfrost point represents the conditions above which entrained droplets of water impinging on a dry surface will not wet that surface (approximately 500 °C at 70 kgf/cm²) [11].

CONCLUSIONS

These conclusions are drawn from the experimental programs:

(a) Out-reactor heat transfer experiments show the importance of the surface liquid film in fog cooling. A simple analytical model developed to interpret and correlate these measurements [7] was equally successful when applied to the results of in-reactor dry-out experiments. [11].

(b) Experiments in the liquid deficient region, where the dry-out heat flux has been exceeded, have been carried out both in- and out-reactor. The behaviour of the surface temperature and the peak values reached are generally in agreement with the findings of the workers at CISE [10].

(c) The program has demonstrated that thermocouples attached to the outside of a fuel element sheath can be effective in detecting incipient dry-out.

(d) Corrosion and hydrogen pick-up rates in both Zircaloy-2 and Zr-2½%Nb fuel sheaths are acceptably low when cooled by fog at the conditions of interest for fog cooled or once-through reactors for periods up to 1 600 h, provided the sheath surface remains wet. The pits observed in Zircaloy-2 require further investigation.

(e) There can be severe problems due to thermal distortion in slender fuel assemblies when subjected to nonuniform dry-out conditions. It is also noted that this distortion mechanism will be of particular importance in the design of bundle type fuel assemblies.

(f) Oxygen production by radiolytic decomposition of the coolant can be reduced to a very low level by adding 10 ppm NH₃ to the fog.

(g) The crud deposition on fuel surfaces cooled by fog with ammonia additions is only slightly greater than from lithiated water at pH 10 [13]. Crud deposition does not appear to be a cause of fuel failures in dry-out.

(h) The time-to-failure of Zircaloy-2 clad fuel under high temperature dry-out conditions, simulating those at the centre of a fog-cooled once-through reactor channel, is approximately 30 h. Fuel operating at conditions approximating those at the outlet of such a channel was not defected in 700 h of operation in the liquid-deficient region. The mode of failure in dry-out is not catastrophic but gradual, even under very severe conditions.

ACKNOWLEDGEMENTS

The authors would like to acknowledge the contributions and assistance of many individuals at CRNL, in the Canadian General Electric Company Limited and in the Canadian Westinghouse Company Limited, particularly: E. E. Winter, S. B. Dalgaard, E. O. Moeck, I. P. L. Macdonald, G. A. Wikhammer, R. J. Chenier, W. R. Leach, A. H. Smith, E. R. C. Ayers, R. S. Flemons (CGE), and K. T. Bates (Westinghouse).

The irradiation experiments were undertaken as part of a joint program between Atomic Energy of Canada Limited and the UK Atomic Energy Authority. A special acknowledgement is made to the following

UKAEA staff for their contributions and assistance: I. E. Oldaker, V. C. Orpen and J. E. LeSurf.

REFERENCES

1. Woodhead, L. W., and Brown, W. M., *Performance and problems of NPD*, P/008. Vol. 5, these Proceedings.
2. Douglas Point Nuclear Generating Station, Atomic Energy of Canada Limited report AECL-1596 (1962); also Nuclear Energy, 74-77 (1962).
3. Pon, G. A. *et al.*, *Prospective Heavy-Water Moderated Power Reactors*, P/010, Vol. 5, these Proceedings.
4. Pon, G. A., *Canad. Nuclear Tech.*, 1, 34-38 (Fall 1961).
5. Bennett, A. W. *et al.*, UKAEA AERE report R-3804 (1961).
6. Anderson, W. K., and McGoff, M. J., USAEC report KAPL-2203 (1962).
7. Collier, J. G. *et al.*, Atomic Energy of Canada Limited report AECL-1788 (1963).
8. Geary, N. R., and Horsman, J. C., Atomic Energy of Canada Limited report AECL-1692 (1963).
9. Polomik, E. E. *et al.*, publication 62 WA-136 Amer. Soc. Mech. Eng., New York (1962).
10. *A research program in two-phase flow*, Centro Informazioni Studi Esperienze, Milano (1963).
11. Collier, J. G. *et al.*, Atomic Energy of Canada Limited report AECL-1819 (1963).
12. Thomas, W. R. *et al.*, *Irradiation Experience with Zircaloy-2*, P/021, Vol. 9, these Proceedings.
13. Rae, H. K. *et al.*, *Experience with the Chemistry of Water in Moderator and Coolant Systems*, P/020, Vol. 9, these Proceedings.
14. Robertson, J. A. L. *et al.*, *J. Nuclear Materials*, 7, 225-262 (1962).

ABSTRACT—RÉSUMÉ—АННОТАЦИЯ—RESUMEN

A/16 Canada

Comportement à la chaleur et sous irradiation de combustibles expérimentaux dans des mélanges vapeur-eau utilisés comme caloporteurs par A. D. Lane et J. G. Collier

Le mélange vapeur-eau (brouillard) est capable de transporter de grandes quantités de chaleur; de plus, il n'exige pas une puissance de pompage excessive et n'introduit pas de grandes quantités de matière absorbante de neutrons à l'intérieur du cœur du réacteur. Avant d'employer le brouillard dans les réacteurs de puissance, il faudra continuer les recherches pour obtenir plus de renseignements portant sur: a) les propriétés thermiques et hydrodynamiques des systèmes à brouillard; b) les matériaux de gainage du combustible utilisables avec le brouillard; c) la chimie des systèmes à brouillard pour diminuer la corrosion et les dépôts.

On a employé des cartouches chauffées par effet Joule pour simuler le combustible et on a exécuté des expériences de laboratoire pour:

i) mesurer le flux de chaleur d'«assèchement» dans une file de cartouches (l'assèchement est le point où le film d'eau disparaît de la surface de transfert et le coefficient de transmission de chaleur tombe soudainement);

ii) déterminer les coefficients de transmission de chaleur pour des flux de chaleur dépassant celui de l'«assèchement»;

iii) déterminer l'effet de longueur des cartouches et celui dû à l'insertion de parties non chauffées.

On a effectué cinq irradiations de cartouches refroidies au brouillard à l'intérieur d'une boucle du réacteur NRX. Dans la première, on a mesuré le début de l'assèchement et on a montré que des

thermocouples superficiels pouvaient indiquer son apparition.

La seconde irradiation a duré 75 jours et a fourni des données sur la corrosion et sur l'absorption de l'hydrogène pour des gaines complètement mouillées, fabriquées à partir de deux alliages différents à base de zirconium.

On a entrepris les trois irradiations suivantes pour déterminer les taux de corrosion et d'hydruration des alliages de zirconium, lorsqu'on travaille à des flux de chaleur de 60, 70 et 90 W/cm² (au-delà de l'assèchement). On a trouvé que, pour le flux le plus élevé, il fallait 30 h environ pour atteindre le point de rupture. Cela se compare bien avec les prévisions obtenues à partir de taux de corrosion en dehors du réacteur, compte tenu du fait que le film de corrosion est un isolant. On a trouvé que les défauts se formaient graduellement sans produire de ruptures catastrophiques. La température des gaines s'est élevée à 670 °C durant des périodes prolongées. Dans chacune de ces trois irradiations, certaines cartouches avaient une surface sèche; d'autres, une surface mouillée. Le passage d'une zone mouillée à une zone sèche a été réalisé en interrompant l'écoulement du film d'eau par une discontinuité de surface. Les essais ont indiqué qu'il pouvait y avoir un problème de distorsion thermique dans la cartouche si sa gaine était partiellement sèche; cela peut rapprocher le point de rupture.

Lors des essais, on a fait varier le contenu de vapeur à la sortie entre 27 et 63 % (poids), et le débit unitaire de 107 à 136 g cm⁻² s⁻¹ à une pression constante de 70 kgf/cm². En général, les valeurs à l'assèchement obtenues à partir des expériences d'irradiation et des essais de laboratoire concordent entre elles, et avec celles déduites par le calcul de l'écoulement des films liquides le long de surfaces de transfert de chaleur.

A/16 Канада

Работоспособность опытного топлива, подвергающегося тепловому и радиационному воздействию в пароводяных смесях

А. Д. Лейн, Дж. Г. Колье

Паро-водяные смеси (туман) способны переносить большие количества тепла из реактора. При этом они не требуют затраты чрезмерных количеств энергии на перекачку, а также не требуют внесения в активную зону реактора больших количеств материала, поглощающего нейтроны. Прежде чем использовать туман в энергетических реакторах, следует провести исследования в трех областях:

- тепловые и гидродинамические свойства систем с туманом;
- материалы покрытий топлива, пригодные для использования в тумане;
- химия систем с туманом и возможности уменьшения коррозии и отложений.

Для проведения исследований использовались элементы, нагреваемые электрическим током. Это давало возможность моделировать тепловые режимы работы элементов в лабораторных условиях. Целью этих опытов было:

- измерить «высушку» тепловых потоков для топливных стержней («высушка» представляет собой такой тепловой поток, при котором исчезает водяная пленка с теплопередающей поверхности и коэффициент теплопередачи внезапно падает);
- определить коэффициенты теплопередачи для тепловых потоков ниже предела «высушки»;
- определить эффективность наличия тепловыделяющих элементов различной длины и наличия прогретых и непрогретых секций.

Было проведено пять облучений топлива, охлаждаемого туманом, в контуре Национального исследовательского экспериментального канадского реактора NRX. При первом облучении экспериментально исследовалось начало «высушки»; было обнаружено, что поверхностная термопара, установленная на поверхности тепловыделяющего элемента, может указывать на начало этого процесса.

Второе облучение проводилось в течение 75 дней и дало данные относительно коррозии и наводороживания полностью увлажненных оболочек топлива, изготовленных из двух различных сплавов с циркониевой основой.

Последующие три облучения проводились для того, чтобы определить коррозию и степень гидрирования циркониевых сплавов при эксплуатации их ниже предела «высушки» при тепловых потоках в 60, 70 и 90 $вт/см^2$. Было определено, что время до разрушения при наи-

высших из этих тепловых потоков должно быть равно приблизительно 30 ч. Это значение вполне совпадает с предсказаниями, полученными при определении скорости коррозии, проведенном во вне реакторных экспериментах, если дополнительно учесть время, необходимое для отделения коррозионной пленки. Было установлено, что образование дефектов происходит постепенно и не приводит к катастрофическим разрушениям. Во время этих опытов температура оболочки длительное время поддерживалась на уровне $670^\circ C$. В каждом из этих трех случаев облучения лишь некоторые тепловыделяющие элементы в канале имели сухие поверхности, а остальные имели увлажненные поверхности способствовало то, что поток водяной пленки обрывался вместе с разрывом поверхности. Опыты указали на возможную проблему тепловой деформации тепловыделяющего элемента в том случае, когда лишь часть его оболочки остается сухой, — это явление ускоряет разрушение.

Опыты по облучению проводились при влажности пара на выходе в пределах от 27 до 63% и при скоростях переноса массы от 107 до 136 $г/см^2 \cdot сек$. Все эти опыты проводились при давлении 70 $кг/см^2$. В целом результаты «высушки», полученные в экспериментах по облучению и в лабораторных опытах, хорошо согласуются друг с другом, а также и с теми результатами, которые были выведены на основе определения потоков жидкостных пленок на теплопередающих поверхностях.

A/16 Canadá

Características térmicas e irradiatorias de combustibles experimentales en mezclas de vapor y agua

por A. D. Lane y J. G. Collier

Las mezclas de vapor y agua (niebla) son capaces de transmitir grandes cantidades de calor generado por un reactor; además no exigen una potencia de bombeo excesiva ni introducen grandes cantidades de material absorbente de neutrones en el cuerpo del reactor. Para poder utilizar la niebla en los reactores de potencia, será menester proseguir las investigaciones a fin de obtener datos complementarios sobre: a) las propiedades térmicas e hidrodinámicas de los sistemas de niebla; b) los materiales de revestimiento del combustible apropiados para su empleo en niebla; c) la química de los sistemas de niebla, a fin de reducir al mínimo la corrosión y los depósitos.

Se han utilizado elementos calentados por efecto Joule que simulaban el combustible, en experimentos de laboratorio realizados para:

- i) medir los flujos térmicos de «deseccación» en haces de elementos combustibles (la «deseccación» es el punto en que la película de agua desaparece de

la superficie de transmisión y el coeficiente de transmisión térmica disminuye repentinamente);

ii) determinar los coeficientes de transmisión de calor para flujos térmicos superiores al de desecación;

iii) determinar los efectos resultantes de utilizar elementos de diferentes longitudes y de calentar unas secciones y otras no.

En un circuito del reactor NRX se han llevado a cabo cinco irradiaciones de combustible refrigerado con niebla. En la primera irradiación, se determinó el comienzo de la desecación y se demostró que pares termoelectrónicos instalados en la superficie pueden indicar una desecación incipiente.

La segunda irradiación duró 75 días y proporcionó información sobre la corrosión y la absorción de hidrógeno en el revestimiento de combustibles completamente humedecidos, elaborados con dos aleaciones distintas a base de zirconio.

Las tres irradiaciones siguientes se realizaron con el fin de determinar el índice de corrosión y de formación de hidruros en aleaciones de zirconio para flujos térmicos, superiores al de desecación, de 60, 70 y 90 W/cm². Se ha comprobado que con el flujo más elevado se requieren unas 30 h para alcanzar el punto de ruptura. Ello concuerda satisfactoriamente con las predicciones basadas en los índices de corrosión fuera

del reactor, teniendo en cuenta el efecto aislante de la película de corrosión. Se ha advertido que la formación de defectos es gradual sin rupturas graves. En el curso de estos ensayos, se han observado temperaturas del revestimiento de hasta 670 °C, durante periodos prolongados. En cada una de estas tres irradiaciones, la superficie de algunos elementos combustibles del haz permaneció seca, mientras que la del resto de los elementos era húmeda. La transición de una zona seca a una húmeda se favoreció interrumpiendo el movimiento de la película de agua por una discontinuidad superficial. Los ensayos indicaron la posible existencia de un problema de distorsión térmica de los elementos combustibles cuando sólo una parte del revestimiento está seco; ello puede acelerar la aparición de averías.

Los ensayos de irradiación se han efectuado en un intervalo de 27 a 63 por ciento en peso de vapor en la salida y caudales unitarios de 107 a 136 g cm⁻² s⁻¹ a una presión constante de 70 kgf/cm². En general, los resultados de desecación proporcionados por los experimentos de irradiación y los ensayos de laboratorio concuerdan satisfactoriamente entre sí y con los previstos por cálculo del movimiento de la película de líquido a lo largo de las superficies de transmisión térmica.

Améliorations apportées au transfert thermique des combustibles nucléaires par l'application du procédé «Vapotron»

par J. D. Le Franc*, H. Bruchner**, P. Domenjoud*** et R. Morin****

Quelques difficultés concernant l'amélioration des réacteurs à eau bouillante, en vue d'une meilleure rentabilité, sont en liaison étroite avec les phénomènes d'extraction de la chaleur de combustible et avec les régimes de stabilité de l'écoulement du fluide de refroidissement.

Plusieurs artifices, portant généralement sur les caractéristiques de l'écoulement ou sur celles du fluide de refroidissement, ont été expérimentés ou sont en cours d'étude. Les facteurs d'amélioration procurés par ces divers moyens ne dépassent généralement pas 1,3.

Par contre, l'application aux réacteurs nucléaires à eau bouillante du procédé Vapotron, dont l'efficacité est maintenant incontestée dans le domaine du refroidissement des tubes électroniques de puissance, pourrait apporter une augmentation plus sensible du transfert thermique entre combustible et fluide de refroidissement, tout en conservant une grande sécurité de fonctionnement.

Un second point qui ne sera pas développé dans la présente communication concerne la possibilité de modifier ou de reculer l'apparition de certains types d'instabilités de l'écoulement du fluide de refroidissement, du fait même de la structure de grappes à gaines «vapotronisées».

Enfin, les caractéristiques thermiques des échangeurs de chaleur à changement d'état métaux liquides/eau, employés dans les réacteurs rapides, pourraient être largement améliorées par l'utilisation de ce procédé.

LE PRINCIPE DE L'EFFET VAPOTRON *****

Les procédés usuels d'échange de chaleur entre un métal chauffé et un liquide à l'ébullition utilisent systématiquement des surfaces isothermes.

Il s'agira, par exemple, des tubes d'un échangeur-évaporateur, de l'anode d'un tube électronique qui reçoit le faisceau d'électrons ou des gaines transmettant la puissance d'un combustible nucléaire au fluide réfrigérant porté à l'ébullition (eau légère ou lourde, fluide organique, métal liquide...).

* Compagnie française Thomson-Houston

** Allgemeine Elektrizitäts-Gesellschaft

*** Alsthom

**** EURATOM

***** Vapotron: marque déposée CFTH

Dans ces conditions, on impose à l'interface paroi-liquide, soit une température, soit un flux thermique, soit une fonction de ces deux grandeurs. Il en résulte un point de fonctionnement bien défini sur la courbe caractéristique de l'échange considéré, représentée sur la figure 1 (courbe de Nuki-Yama).

L'installation est toujours conçue pour que ce point de fonctionnement soit situé sur la branche AC de cette courbe. On connaît, en effet, les dommages qui peuvent survenir s'il advient que le flux augmente au-delà de la valeur $(\phi/A)_C$ et la température de paroi au-delà de la valeur définie par $\Delta\theta_F$.

La technique du Vapotron est, au contraire, basée sur l'utilisation de surfaces d'échange essentiellement non isothermes.

Dans ce but, la paroi d'échange est agencée au moyen de corrugation ou dents, pour présenter des zones «froides» et des zones «chaudes» entre lesquelles s'établit un gradient stable dans le temps de température, pouvant s'étendre sur une centaine de degrés Celsius ou même davantage.

La figure 2 représente un élément combustible usuel (a) et un élément combustible muni d'une gaine

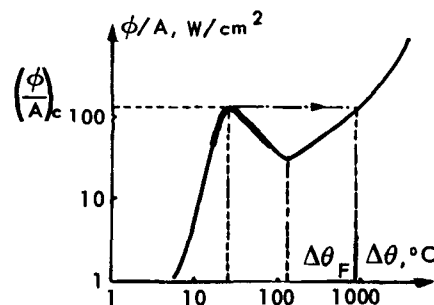


Figure 1. Courbe de Nuki-Yama

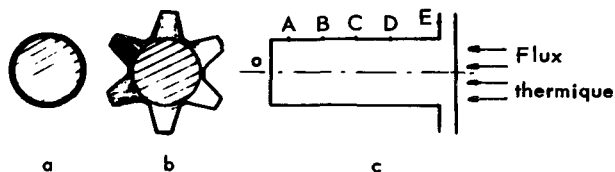


Figure 2. Éléments de combustible usuel et type Vapotron
a: gaine classique; b: gaine Vapotron; c: dent élémentaire

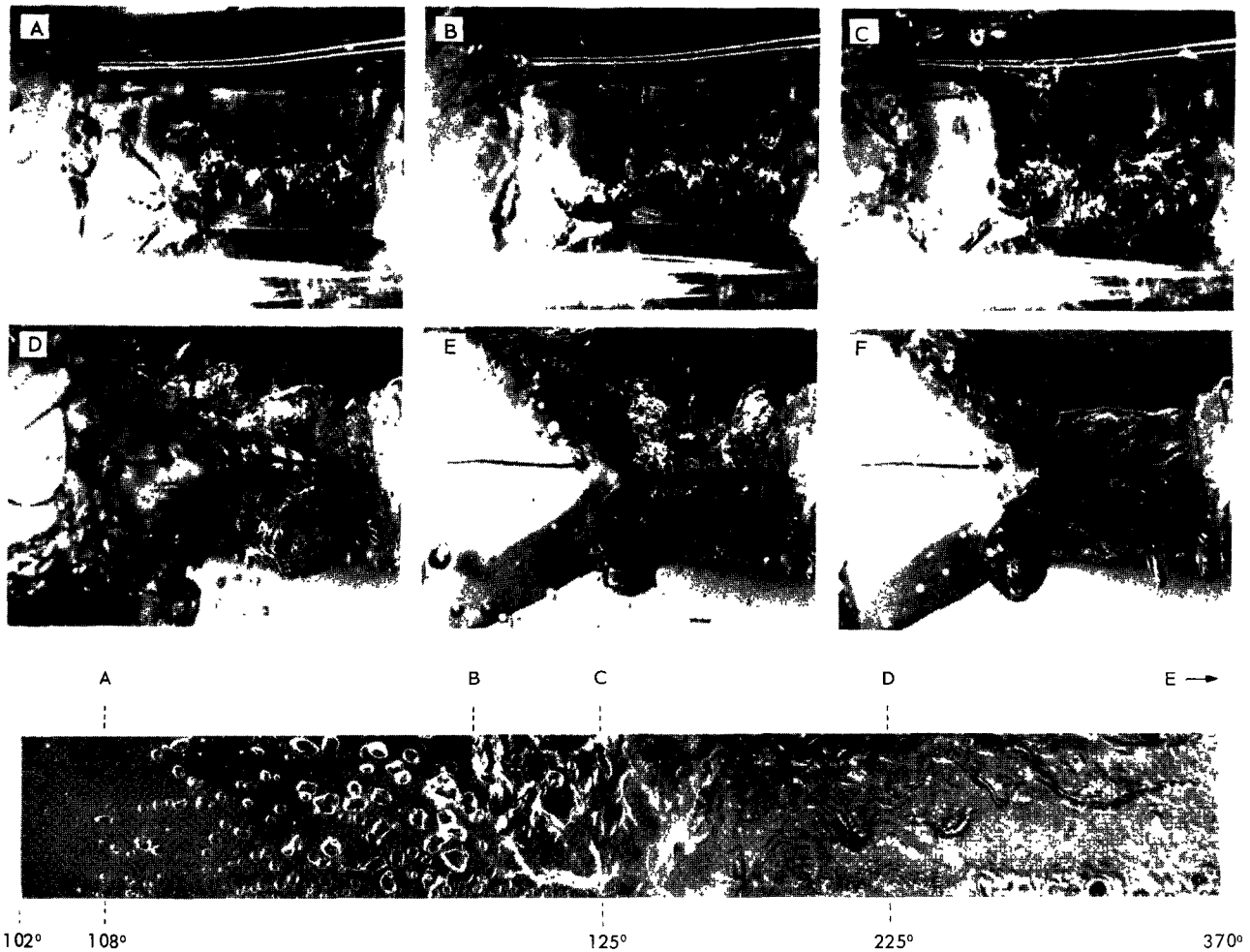


Figure 3. Effet Vapotron sur échantillon en cuivre

type Vapotron (b), c'est-à-dire d'une gaine munie d'un certain nombre de dents.

Pour analyser ce phénomène complexe qui constitue l'effet Vapotron, considérons un élément dissipatif représenté (figure 2) sous la forme d'une ailette massive dont les dimensions ont été déterminées en fonction de la conductivité du métal, de telle sorte que le gradient désiré de température s'établisse en fonctionnement entre sa base (chaude) et son extrémité (froide) en présence du liquide qui la baigne.

Imaginons que la puissance thermique dégagée dans le combustible, donc le flux thermique qui se présente à la base de cette dent, augmente progressivement.

Lorsque la température du métal aura légèrement dépassé la température de saturation, l'ébullition va apparaître au point E, qui est le point chaud, puis intéresser progressivement les points D, C, B et A.

Lorsque la température de E aura atteint la température critique, une zone de film correspondant à la branche dite ou réputée « instable » de la courbe I va se manifester puis s'étendre vers le point D, puis C.

Enfin, la puissance augmentant encore, la vaporisation pelliculaire apparaît en E et intéresse graduellement la surface qui se trouve entre les dents.

L'effet Vapotron est alors caractérisé par la coexistence stable des quatre phénomènes fondamentaux (figure 3): *a*) convection à l'extrémité de la dent (entre O et A); *b*) ébullition nucléée (entre A et B) et ébullition nucléée avec coalescence (entre B et C); *c*) zone dite « instable » (entre C et D), et *d*) vaporisation pelliculaire (entre D et E).

Si la puissance est augmentée jusqu'à ce que la température du point O atteigne la valeur critique, l'ébullition disparaît à la pointe; la dent se trouve entourée complètement d'un film de vapeur. C'est alors la caléfaction généralisée correspondant à un régime de température élevé.

On voit immédiatement que les dimensions de la dent ne peuvent pas être quelconques. Pour que le gradient soit stable, il est nécessaire que l'impédance thermique entre la base chaude qui reçoit le flux thermique et l'extrémité froide soit adéquate. L'efficacité du système est d'autant plus grande que cette pointe joue davantage son rôle de soupape et permet à la chaleur de trouver une voie plus facile qu'en E, D ou C, encombrés par la vapeur. Il existe donc, pour un échange donné, une relation entre les paramètres géométriques (longueur, épaisseur, intervalle entre les

dents) et la conductivité thermique du métal. Il est nécessaire que cette relation se trouve vérifiée pour que l'échange ait son efficacité maximale.

Tandis que toutes les techniques classiques mettant en œuvre l'ébullition sont tenues par deux impératifs confirmés par de nombreux essais: garder une bonne marge de sécurité vis-à-vis du flux critique, et renoncer à toute extension locale de la surface d'échange (qui, cessant d'être isotherme, perdrait de l'efficacité), on constate que la technique Vapotron a renversé ces deux limites: sur une surface de contact multipliée, par exemple par cinq, elle intègre tous les régimes d'ébullition, jusqu'à la pointe de flux comprise, ainsi que tous les régimes (tout aussi efficaces) situés sur la branche descendante de la courbe, régimes qui sont stabilisés par la continuité du gradient de température.

A cet accroissement très important d'efficacité et de stabilité en régime normal, le Vapotron joint une inertie thermique capable d'éviter un départ en caléfaction au cours d'une brève surcharge et, le cas échéant, d'étaler un régime de caléfaction sur une zone très large de températures permettant d'éviter la destruction.

QUELQUES PROBLÈMES POSÉS PAR L'ADAPTATION DU VAPOTRON AUX RÉACTEURS NUCLÉAIRES BWR

On voit combien la notion de prix de revient de l'énergie produite est liée à celle de puissance spécifique.

Dans les réacteurs à eau bouillante (BWR), un des phénomènes qui limitent la puissance spécifique du réacteur est la caléfaction.

La destruction d'un ou plusieurs barreaux ayant évidemment des conséquences très graves, des marges de sécurité très importantes sont prises qui limitent actuellement le flux thermique évacué par la gaine à environ 100 W/cm² (pour une pression de fonctionnement qui est habituellement de 70 kgf/cm²).

De plus UO₂, utilisé généralement comme combustible, a malheureusement une conductivité thermique médiocre. Il en résulte un gradient de température élevé à l'intérieur du barreau, et, si la puissance dissipée est trop importante, la température centrale peut atteindre, ou même dépasser, la température de fusion de l'oxyde (2 800 °C).

Ces considérations introduisent une autre limitation au flux thermique maximal admis sur la face externe des gaines.

Il se trouve actuellement que les travaux des métallurgistes sur UO₂ ont conduit à en améliorer les propriétés thermiques. En outre, il a été prouvé que la fusion du combustible au cœur du barreau ne conduisait pas à des conséquences trop fâcheuses; le résultat est que la balle est maintenant chez les thermiciens, qui s'efforcent d'apporter une solution au problème du transfert de la chaleur entre la gaine et le fluide.

Problèmes neutroniques

Les gaines Vapotron présentent un volume plus important que les gaines usuelles isothermes. Ce

facteur est naturellement défavorable, car, bien que les sections efficaces de capture neutronique de ces métaux soient relativement faibles, cette masse métallique provoque néanmoins une capture parasite.

Le problème fondamental de l'adaptation du Vapotron aux réacteurs bouillants est donc de diminuer le volume de la gaine, en conservant bien entendu les avantages apportés par une structure anisotherme.

De plus, la présence d'un volume variable de vapeur, dans des régions bien définies interférant avec la présence des dents elles-mêmes, modifie la répartition du flux de neutrons.

Problèmes thermiques

Les métaux de gainage les plus utilisés dans les réacteurs à eau sont l'aluminium, l'acier inoxydable et le Zircaloy-2, ces deux derniers pour les réacteurs à eau bouillante. Leurs propriétés comparées à celles du cuivre sont les suivantes:

Aluminium:	$\sigma_c = 0,2$ barn;
Acier inoxydable:	$\sigma_c = 3,0$ barns;
Zircaloy-2:	$\sigma_c = 0,2$ barn;
Cuivre:	$\sigma_c = 3,6$ barns;
$\Sigma_c = 1,2 \cdot 10^{-2}$ cm ⁻¹ ;	$K = 0,49$ cal
$\Sigma_c = 0,23$ cm ⁻¹ ;	$K = 0,04$ cal
$\Sigma_c = 7 \cdot 10^{-3}$ cm ⁻¹ ;	$K = 0,03$ cal
$\Sigma_c = 0,28$ cm ⁻¹ ;	$K = 0,94$ cal

σ_c étant la section efficace de capture neutronique, Σ_c la section macroscopique et K la conductivité thermique à 100 °C.

On voit que les métaux « nucléaires » ont une conductivité thermique beaucoup plus faible que celle du cuivre. Dans quelles limites cette diminution de la conductivité influe-t-elle sur les performances du système Vapotron ?

La pression de fonctionnement des réacteurs bouillants étant de l'ordre de 70 kg/cm², on pouvait penser que l'influence favorable de la pression compenserait la médiocrité des caractéristiques thermiques, et que, en définitive, on retrouverait pour ces pressions des performances identiques à celles qui étaient déjà bien connues pour des Vapotrons en cuivre travaillant à la pression atmosphérique. Cet espoir s'est, en effet, trouvé largement réalisé.

ESSAIS SUR DENTS ÉLÉMENTAIRES

Afin d'essayer de mieux comprendre le phénomène complexe de l'effet Vapotron et de vérifier l'influence des caractéristiques dimensionnelles des dents en liaison avec la conductivité du métal, quelques études portant sur des éléments individuels de protubérances Vapotron ont été réalisées sous la pression atmosphérique.

Les résultats importants de ces études ont été de deux types:

a) Détermination de la loi d'échange thermique reliant les flux locaux à l'écart de température de la

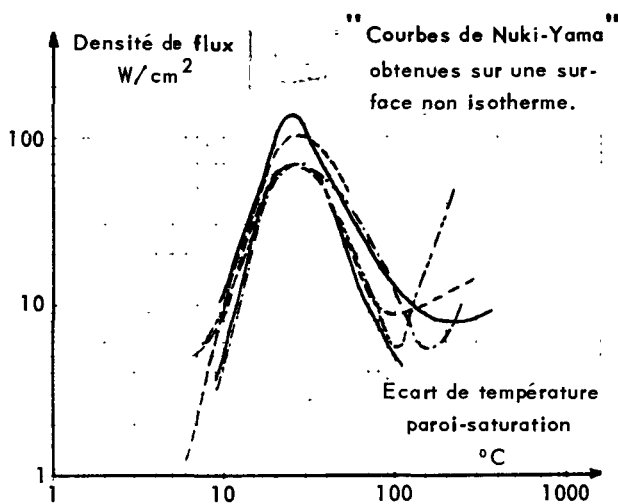


Figure 4. Loi d'échange sur paroi non isotherme

paroi par rapport à celle du liquide dans le cas d'une surface anisotherme,

b) Mise en évidence par l'expérience du dimensionnement des protubérances dans le rapport des conductivités thermiques des métaux constitutifs de la paroi chauffante.

La détermination de la loi d'échange sur paroi non isotherme a été faite sur un bloc d'argent de grandes dimensions. L'argent a été choisi, d'une part à cause de sa grande conductivité qui permet de « dilater » les phénomènes thermiques et de les rendre accessibles à la mesure avec plus de précision, d'autre part à cause de son inoxydabilité dans les conditions de l'expérimentation. Les modifications de l'état de surface entraînent en effet des modifications du coefficient local de transfert thermique. Les résultats obtenus sont illustrés par la figure 4.

Il faut noter l'accord assez bon de ces résultats avec ceux obtenus sur fils, plaques ou tubes isothermes par d'autres auteurs.

Toutefois, il est bon de remarquer que les effets des canaux qui séparent deux protubérances Vapotron peuvent avoir un effet très sensible sur l'allure de ces résultats et que les courbes de la figure 4 ne permettent pas de juger de cette influence. Une étude est actuellement en cours pour connaître l'importance de ce facteur. Des densités de flux thermiques, définies par rapport à la section de la base de la protubérance, supérieures à 800 W/cm^2 , ont pu être atteintes à 70 kg/cm^2 sur des dents en acier inoxydable de $3 \times 1,7 \text{ mm}$, sans constituer pour autant des valeurs critiques. Seule la conception du dispositif d'essais a limité l'expérimentation vers les flux plus élevés.

Nous avons vérifié expérimentalement la loi de dimensionnement des dents par l'utilisation du rapport des conductivités thermiques.

Ce résultat n'était pas évident a priori, car une étude théorique ne fait intervenir ni la dynamique de la production de la vapeur (naissance, croissance, acheminement des bulles) et les différents paramètres s'y rapportant (tension superficielle, viscosité), ni la

variation de la conductivité thermique avec la température.

On pouvait donc craindre de ne pas obtenir la stabilisation du gradient (caractéristique de l'effet Vapotron) à la pression atmosphérique, lorsque les dimensions de l'échantillon deviennent faibles par rapport aux dimensions des bulles, par exemple. Or, les résultats obtenus prouvent que ces craintes n'étaient pas justifiées, et que, même avec une réduction importante des dimensions dans le cas d'un métal de conductivité relativement basse, l'effet Vapotron est conservé, toutes conditions de fonctionnement restant identiques par ailleurs (pression, température de saturation, *pool boiling*).

ESSAIS SUR GAINES VAPOTRON DE SECTION RÉELLE

Les résultats précédemment décrits ont été obtenus, d'abord sur les dents élémentaires, puis avec un dispositif de chauffage dont le principe se rapprochait davantage d'un processus à température imposée qu'à flux imposé. Or, le cas de barreaux de combustible est différent. Le flux thermique est imposé par le dégagement de puissance produit dans l'oxyde d'uranium mais cette puissance conditionne également la température.

C'est pourquoi deux dispositifs ont été réalisés pour l'étude d'éléments de gainage sous basse et haute pression. Le combustible est simulé par une résistance de graphite cylindrique chauffée par effet Joule sous basse tension.

Notons que ce dispositif original simule plus fidèlement la dissipation thermique nucléaire que la méthode classique utilisée pour tous les essais hors pile relatés dans la littérature, qui consiste à se servir de la gaine elle-même comme résistance électrique.

Essais à basse pression, en *pool boiling*

La puissance effectivement transmise par l'échantillon est calculée par la confrontation des résultats de mesures électriques et calorimétriques.

Un certain nombre de profils de gaines ont été définis d'une manière plus ou moins approchée à partir des résultats exposés précédemment et tenant compte du diamètre usuel des « crayons » de combustible dans les réacteurs à eau bouillante. Quelques profils réalisés en acier inoxydable sont donnés sur la figure 5.

Des expériences ont été réalisées et l'on constate que l'effet Vapotron peut se manifester à la pression atmosphérique sur un profil aussi simple que le triangle équilatéral.

Quelques résultats donnant les flux maximaux admissibles en fonction de la pression sont donnés



Figure 5. Profils de gaines Vapotron

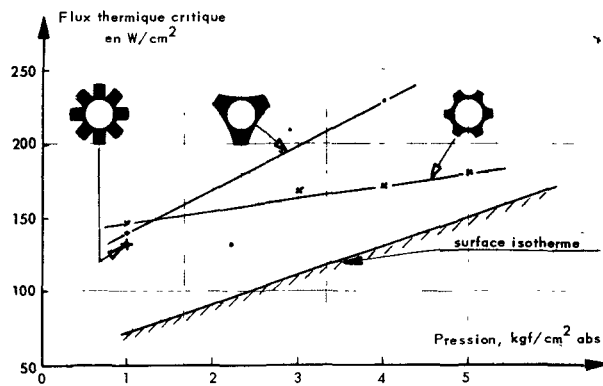


Figure 6. Flux critique en *pool boiling* sur éléments courts de gaines Vapotron, à basse pression

sur la figure 6, pour des profils Vapotron et un profil isotherme.

Dans tout ce qui suit, la densité de flux thermique est calculée par rapport à une surface d'échange équivalente définie de la manière suivante: c'est la surface extérieure d'un élément de combustible cylindrique qui comporterait la même masse de combustible et la même masse de gainage que l'élément Vapotron considéré.

Essais à haute pression, en convection forcée

Les essais sur des éléments de gainage courts ont permis de préparer les expériences sur une boucle de transfert thermique dont la puissance est d'environ 100 kW et qui permet de tester, sous 70 kgf/cm², des barreaux de 50 cm de longueur active. La cellule d'essais est représentée sur la figure 7. La réalisation d'un tel dispositif a nécessité la mise au point d'un grand nombre de procédés et tours de main technologiques.

Mesures

a) Mesure des températures de paroi de la gaine

Une mise en œuvre originale de thermocouple pour la mesure des températures de surface a été développée par la CFTH. Elle permet de connaître ces paramètres avec une bonne reproductibilité (figures 8 et 9).

b) Mesure des températures du fluide dans la cellule d'essais

Trois paramètres sont enregistrés:

- Température à l'entrée de la cellule d'essais,
- Température à la sortie de la cellule d'essais,

Sous-saturation du fluide à l'entrée de la cellule d'essais, mesurée directement par deux couples montés en différentiel placés, l'un à la sortie de la cellule (correspondant à la température de saturation), l'autre à l'entrée de la cellule donnant la température du liquide à l'entrée.

c) Mesure des pressions et des débits

- Pressions statiques à l'entrée et à la sortie,
- Perte de charge dans la cellule d'essais,
- Débit dans la cellule d'essais.

Appareillage de visualisation

On observe la gaine et le phénomène complexe de l'effet Vapotron pendant les essais sous pression par télévision en circuit fermé, ce qui permet un grandissement de 10. L'éclairage est assuré par des lampes immergées sous la pression de 70 kg/cm².

Sécurité

Les hautes températures atteintes au cours des essais nous ont obligés à aménager un système de détection préventive des points chauds accidentels. Celui-ci comprend une détection de défaut d'isolement et un détecteur optique à cellule photorésistive sensible au rouge naissant (0,84 micron).

Résultats

Au cours des essais préliminaires nous avons eu l'occasion de photographier, hors cellule d'essais, une gaine Vapotron de section carrée qui avait fonctionné sous une pression de 26 atmosphères et avec un flux voisin de 200 W/cm². Les zones correspondantes aux différents processus d'ébullition mis en œuvre par l'effet Vapotron étaient bien délimitées par les aspects différents de dépôts que nous observions lors de ces essais préliminaires. La figure 10 montre cette gaine.

Différents types de gaines vapotronisées ont été réalisés (figure 11). Afin de faire des comparaisons valables entre les efficacités de ces différents types, nous avons maintenu la valeur de la section droite de chacune de ces gaines constante. La différence porte donc uniquement sur la distribution de la matière autour d'un alésage comportant le combustible de diamètre constant.

D'un autre côté, nous comparons ainsi des gaines de surface d'échange équivalente, de même valeur. Cette surface d'échange est définie plus haut.

Initialement, le problème posé était de comparer les coefficients d'échange obtenus sur des gaines isothermes et des gaines vapotronisées dans des conditions similaires d'utilisation. Toutefois, une manière de présentation des résultats, devenue classique au cours de ces dernières années dans les travaux concernant les réacteurs bouillants, consiste à donner les valeurs du flux de caléfaction en fonction de certains paramètres thermodynamiques ou hydrodynamiques (titre en masse à la sortie du canal d'écoulement, enthalpie à l'entrée, etc.).

En régime isotherme, le flux maximal utilisable est une fraction faible (50%) du flux de caléfaction. Dans le régime Vapotron, on n'est pas limité par la proximité du flux de caléfaction, mais par la température que peut supporter la gaine pour des raisons technologiques. A cette température limite correspond un flux limite d'utilisation que nous appellerons flux maximal admissible en régime Vapotron.

La correspondance bi-univoque entre la température de fond de dents et le flux dissipé apparaît sur la figure 12 et correspond à un gainage acier inoxydable à 70 kg/cm².

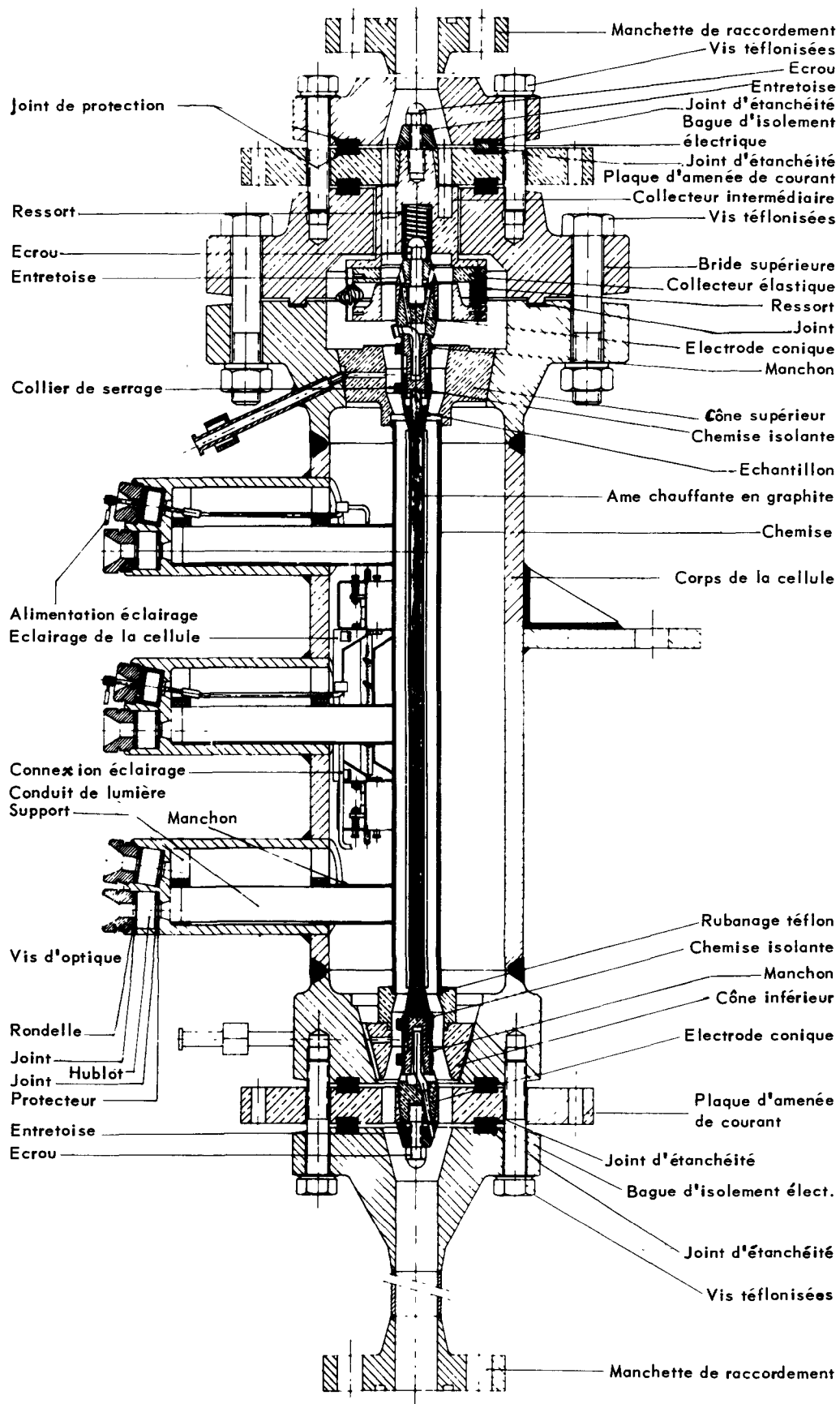
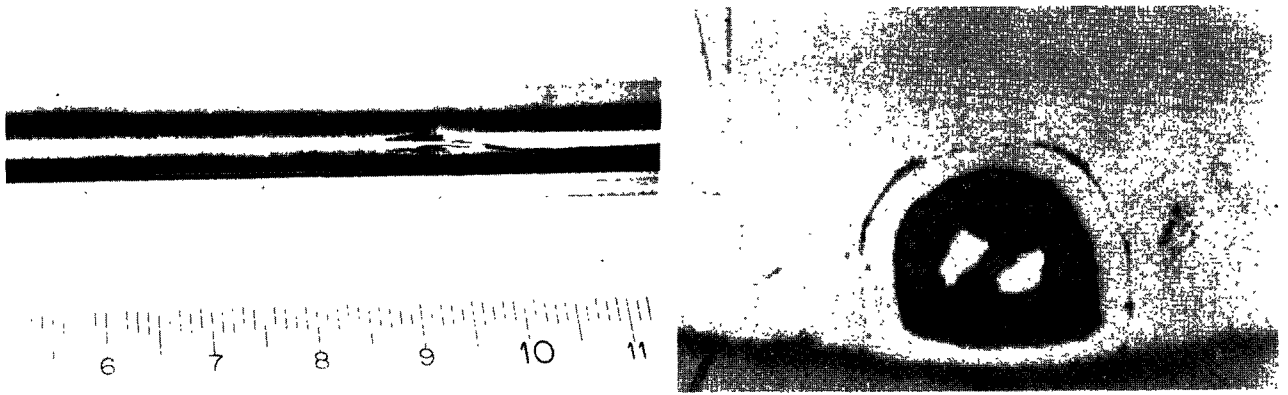


Figure 7. Cellule d'essais de 100 kW sous 70 bars



Figures 8 et 9. Thermocouple de gaine

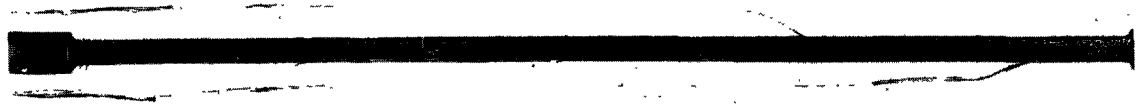


Figure 10. Gaine après essai

La figure 13 concrétise les résultats et représente:

a) *En régime isotherme*

Des flux de caléfaction en fonction des titres vapeur en sortie avec, comme paramètre, le débit massique. Il est à noter que les réacteurs en fonctionnement travaillent à 50% en dessous de cette valeur. Nous avons porté les points correspondant aux flux maximaux des BWR de Dresden, Garigliano et Pathfinder.

b) *En régime Vapotron dans le même système de coordonnées*

Nous avons porté les points expérimentaux correspondant à des régimes thermiques stables Vapotron. Des limitations accidentelles dues essentiellement au système de chauffage « réaliste » mais difficile à mettre en œuvre à ce régime de puissance sont apparues au début des expérimentations. Le lieu des points représentatifs des flux maximaux admissibles tels que définis ci-dessus et qui limite la zone du plan où l'on peut travailler est situé largement au-delà des points expérimentaux obtenus. Ces résultats confirment largement les possibilités du procédé Vapotron en BWR. Leur extension est en cours d'expérimentation.

PERTE NEUTRONIQUE

Sur le plan neutronique, il est certain que le procédé Vapotron, en augmentant le volume de gainage du combustible, affecte négativement le bilan neutronique. Il est cependant aisé de montrer que la perturbation alors introduite n'est pas déterminante et qu'au contraire la perte de réactivité peut être considérée comme faible.

En effet, supposons que dans un cœur identique à celui du réacteur de Garigliano nous remplaçons chacun des barreaux de combustible par un barreau muni de gaine Vapotron, en admettant que le volume

de gaine en Zircaloy supplémentaire alors introduit est équivalent à un doublement de l'épaisseur initiale, la perte de réactivité Δk_{eff} calculée pour un cœur froid à 20 °C est

$$\Delta k_{\text{eff}} = 0,036$$

Dans ces conditions, si l'on décidait de compenser cette perte de réactivité par une augmentation de l'enrichissement du combustible, il faudrait alors passer de l'enrichissement moyen de 2,02% à un enrichissement moyen voisin de 2,3%.

Notons que ces valeurs, pourtant faibles, doivent être considérées comme des limites supérieures, puisque, suivant notre hypothèse, le volume supplémentaire de gaine entraîne une modification du rapport vol. H₂O/vol. UO₂, qui s'écarte ainsi notablement de la valeur optimale, et que de plus le doublement de l'épaisseur de gaine que nous avons admis constitue une hypothèse pessimiste.

CONCLUSION

Dans ces conditions, étant donné que dans les réacteurs bouillants l'on utilise d'ores et déjà des enrichissements différents dans le cœur, que l'on admet de changer les matériaux de structure mécanique du cœur (Zircaloy ou inox) au cours de l'utilisation d'une charge d'éléments combustibles pendant laquelle la perte de réactivité est bien supérieure à celle calculée ci-dessus, il semble que l'économie neutronique puisse fort bien s'accommoder de l'utilisation de la gaine Vapotron.

L'application du Vapotron aux réacteurs nucléaires peut être envisagée sous des angles différentes.

Il est concevable, en particulier, de réaliser des barreaux de combustible de plus faible diamètre, ce

A Coûts en % →	FORME N°	PLAN N°	SECTION en cm ²	VOLUME DE GAINÉ Pour longueur utile de 49,2 cm, en cm ³	VOLUME DE GAINÉ rapporté au volume de la forme n° 1	PÉRIMÈTRE en cm	SURF D'ÉCHANGE en cm ²	RAPPORT r $r = \frac{\text{Surface d'échange}}{\text{Surf int de gainé}}$ (Surf. interne de la gainé de 49,2 cm utilisé 154,49 cm ²)	RAPPORT R $R = \frac{\text{Surface d'échange}}{\text{Surf d'éch forme 1}}$
	1	8310984	0,2714	13,35	1,000	3,642	179,18	1,160	1,000
	2	8314800	0,5142	25,30	1,900	4,560	224,35	1,452	1,253
	3		0,6716	33,04	2,475	5,505	270,85	1,752	1,512
	4		0,6196	30,48	2,285	4,386	215,79	1,395	1,205
	5		0,8600	42,31	3,170	5,634	277,19	1,793	1,545
	6	8310885 ^A	0,6711	33,01	2,462	5,592	275,13	1,780	1,533
	7	8310985 ^A	0,6646	32,70	2,450	10,80	531,36	3,435	2,965
	8	8310986 ^A	0,6470	31,83	2,385	8,585	422,38	2,732	2,355
	9	8314806	0,9032	44,45	3,330	5,925	291,51	1,886	1,626
	10	8314807	0,6647	32,70	2,450	4,644	228,48	1,478	1,275

Figure 11. Quelques types de gainés « vapotronisées »

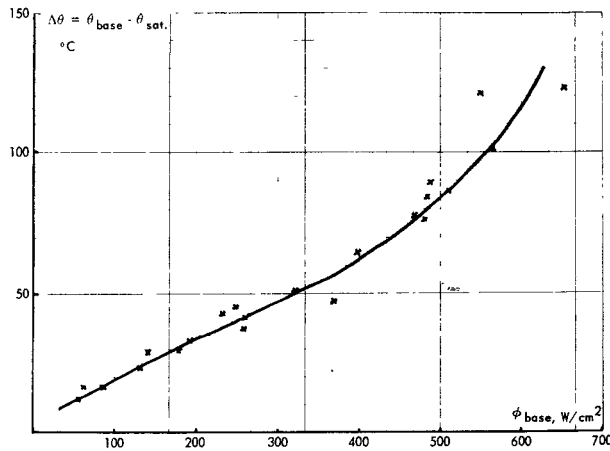


Figure 12. Echantillon comportant 2 dents séparées par un canal de largeur 2 mm
Matière: acier inoxydable; dimensions d'une dent: $3 \times 1,7 \times 20$ mm; pression: 70 bars abs

qui permettrait, tout en conservant la même température maximale au centre du combustible, d'extraire de chaque barreau un flux thermique notablement plus élevé avec une plus grande sécurité.

Une autre possibilité, a priori encore plus séduisante semble-t-il, consisterait, tout en conservant des barreaux de diamètres identiques à ceux utilisés actuellement (12 mm), à extraire un flux thermique légèrement plus élevé (20% par exemple) avec une sécurité beaucoup plus grande et très probablement la possibilité de fonctionner avec un titre vapeur plus élevé.

Enfin, la possibilité d'extraire un flux thermique nettement plus élevé que dans le cas des gaines isothermes permet d'envisager de tirer tout le profit possible de l'utilisation d'autres combustibles plus réfractaires ou plus conducteurs.

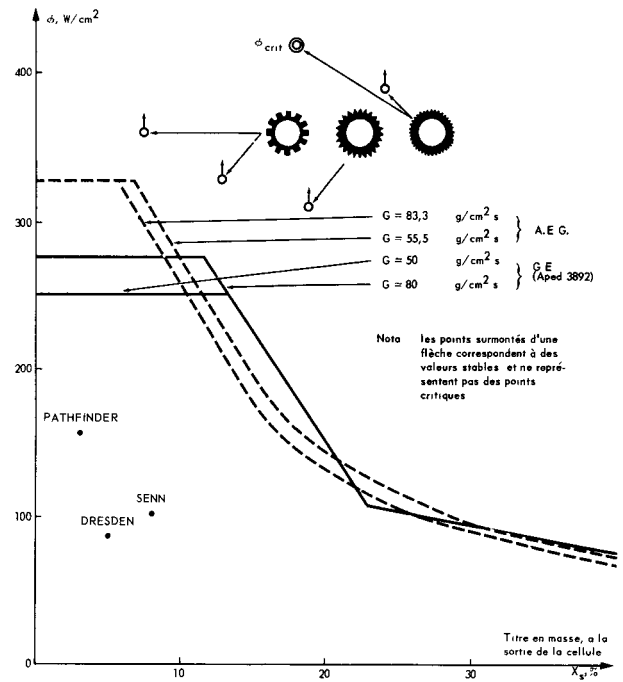


Figure 13. Comparaison de quelques points obtenus sur gaines Vapotron avec des courbes de flux critiques publiées par différents auteurs; pression ≈ 70 atm

REMERCIEMENTS

Ces travaux de recherches ont été effectués dans le cadre de l'accord Euratom - Etats-Unis, par une équipe CFTH - Alstom - AEG.

Ils n'auraient pas été possibles sans les conseils et avis éclairés de MM. Beurtheret, Lemaigen, Level de Curnieu et Matricon, et sans les efforts de tous les participants dirigés par M. Douguet, auxquels nous exprimons ici notre reconnaissance.

ABSTRACT—RÉSUMÉ—АННОТАЦИЯ—RESUMEN

A/96 France

Improvement introduced into the thermal transfer of nuclear fuels by the "Vapotron" process

By J. D. Le Franc *et al.*

The authors mainly deal with boiling water reactors (BWR) where the extraction of heat from the fuel is at present limited by the burn-out phenomenon. Knowing the outstanding performance of the Vapotron process in cooling high-powered electronic tubes, the authors present the first results from a number of experimental studies on the possible application of this process to BWRs.

In the first part of the paper, the principle of the Vapotron effect is briefly discussed. The second part is a presentation of the main problems arising from the

adaptation of the Vapotron process to nuclear reactors of the BWR type.

The third part, in fuller detail, gives an account of the experiments:

Here the authors describe first the results obtained on cans of this type, in various testing facilities designed to reproduce the thermodynamic conditions of a reactor. It will be seen that the performances achieved promise exchange coefficients much higher than those generally accepted. The very great increase in safety will also be illustrated allowing in particular an up-rating of the burn-out conditions.

They explain how such a system can be made to fit into the present concept of reactors in which the heat transfer is chiefly achieved by boiling, what essential differences it would cause in their structure, taking into account the technological requirements, and finally they indicate a balance sheet explaining the

main advantages of the *Nuclear Vapotron system* particularly on technical grounds.

A/96 Francia

A/96 Франция

Улучшение теплоотвода от ядерного топлива в результате применения метода VAPOTRON

Ж. Д. Ле Фран et al.

Авторы рассматривают реакторы с кипящей водой, в которых отвод тепла ограничивается явлением кризиса кипения. Отмечая отличительные характеристики метода Vapotron в области охлаждения электронных трубок мощности, авторы сообщают первые результаты экспериментов по применению метода Vapotron к реакторам с кипящей водой.

В первой части доклада описан принцип эффекта Vapotron. Во второй части изложены основные проблемы, связанные с применением принципа Vapotron к ядерным реакторам типа BWR.

Третья часть доклада наиболее подробна. В ней изложено описание экспериментов. Авторы излагают результаты, полученные на оболочках такого типа в различных опытных установках, сконструированных с целью воспроизведения термодинамических условий в реакторе. Полученные результаты позволяют ожидать, что коэффициенты теплоотдачи будут более высокими, чем те, которые обычно принимались. Авторы считают также, что надежность сильно возрастает; это позволяет, в частности, предотвратить возникновение условий кризиса.

Дается объяснение тому, как подобная система может сочетаться с современной концепцией кипящих реакторов и какие конструктивные отличия потребуются для ее применения с учетом технологических требований. В заключение авторы приводят итоговые данные, которые раскрывают технические преимущества системы «ядерный Vapotron».

Aplicación del procedimiento «Vapotron» para mejorar la transferencia térmica de los combustibles nucleares

por J. D. Le Franc et al.

Los autores consideran fundamentalmente los reactores de agua hirviendo en los cuales la extracción de calor del combustible queda actualmente limitada por el temible fenómeno del calentamiento. Conociendo los notables rendimientos del procedimiento Vapotrón en la esfera del enfriamiento de los tubos electrónicos de potencia, presentan los primeros resultados de un conjunto de estudios experimentales encaminados a aplicar ese procedimiento a los reactores de agua hirviendo.

En la primera parte de la memoria se expone sucintamente el principio del efecto Vapotrón. En la segunda parte se presentan los principales problemas que plantea la adaptación del procedimiento Vapotrón a los reactores nucleares de agua en ebullición.

En la tercera parte, que es la más extensa, se exponen los experimentos realizados.

Los autores presentan en primer término los resultados obtenidos con revestimientos de este tipo en diversas instalaciones de ensayo encaminadas a reproducir las condiciones termodinámicas que reinan en los reactores. Se observará que los rendimientos obtenidos permiten contar con coeficientes de intercambio muy superiores a los comúnmente admitidos. Los autores estiman asimismo que aumenta la seguridad lo que permite, especialmente, extender los límites de las condiciones de calentamiento.

Los autores explican cómo es posible incorporar tal dispositivo al concepto moderno de los reactores en los cuales la transferencia térmica se efectúa principalmente por ebullición, y cuáles serían las diferencias fundamentales que se introducirían en la estructura de los mismos, teniendo en cuenta los requisitos tecnológicos. Para terminar, presentan un cuadro comparativo en el que se ponen de manifiesto las ventajas que ofrece el procedimiento *Vapotron nucléaire* (Vapotrón nuclear) sobre todo en el plano técnico.

Critical heat flux considerations in the thermal and hydraulic design of water-cooled nuclear reactors

By S. Levy,* J. Batch** and J. Casterline***

The critical heat flux (CHF) condition is an important thermal and hydraulic limit in water-cooled nuclear reactors. Its importance comes from the fact that it is usually associated with a rapid deterioration of the heat transfer process and is accompanied by temperature oscillations and a temperature rise which can be detrimental to the integrity of fuel elements. The occurrence of CHF is illustrated in Fig. 1 which shows the temperature in a vertical heated rod as a function of the heat transfer rate to the coolant [1]. Temperature traces are shown for three different steam/water mixtures and they all exhibit three different modes of heat transfer. At low heat flux, evaporation occurs at the heated surface (nucleate boiling) or at the liquid film/vapor core interface. Evaporation is characterized by very high heat transfer coefficients and surface temperatures just above saturation. As more heat is transferred to the coolant, CHF occurs when the first substantial temperature rise or oscillation is recorded. As the heat flux increases further, the heated rod temperature continues to rise and oscillate. The oscillations first increase, pass through a maximum, and finally decrease. This is the transition boiling region where segments of the heated rod are covered intermittently by water and steam. Beyond this region, film boiling prevails; the heated surface is covered with steam, and its temperature is well above saturation.****

The pattern in Fig. 1 is typical of that found in water-cooled nuclear reactors, but the occurrence of CHF, the magnitude of the transition boiling temperature oscillations, and the film boiling temperatures will vary from one design condition to another. This paper is concerned with three aspects of CHF in water-cooled nuclear reactors: (a) the experimental measurement of CHF, (b) its analytical or empirical prediction, and (c) the application of these measurements or predictions to reactor design.

* General Electric Company, San Jose, California.

** Hanford Atomic Products Operation, Richland, Washington.

*** Columbia University, New York.

**** The terminology of CHF transition boiling and film boiling has appeared widely in pool boiling literature. It is used here because, in contrast to "departure from nucleate boiling" or "boiling crisis", it covers instances where evaporation at an interface rather than boiling prevails. It also makes no claim about the consequences of the phenomena as implied in the term "burnout".

EXPERIMENTAL MEASUREMENT OF THE CRITICAL HEAT FLUX

Extensive investigations of CHF have been made. Early studies performed in the United States used circular or rectangular geometries. These have been summarized by De Bortoli *et al.* [2].

Similar investigations, some very recent, have been performed in the USSR [3], Italy [4], Sweden [5], and the UK [6]. We shall be concerned here with the latest test results reported in the US in circular, rectangular, annular, and multirod geometries.

Before examining the data, two comments are in order about the methods of measurements:

(a) Various techniques have been used to detect the onset of CHF. Some use continuous temperature recordings as shown in Fig. 1; others rely upon a specified unbalance in the electrical resistance of the heated rod; others terminate the test when the heated rod temperature reaches a prescribed value. Figure 1 shows that all the methods would give approximately the same answer as long as the first temperature rise or oscillation is substantial, (i.e., at high CHF values). Different results, however, will be obtained for the bottom trace of Fig. 1. For this reason, it is important, as done here, to report the method used to detect CHF.

(b) Unstable test loop conditions are known to have a detrimental effect on CHF [3, 7, 8]. While unstable conditions can occur with subcooled water at the inlet of the test section, they have been reported mostly in tests where the inlet coolant was a low velocity steam and water mixture. Such systems have large preheaters and mixing sections which introduce large compressible volumes in the loop. This results in a "soft" hydraulic flow system where the driving force for flow is not strong enough to prevent flow fluctuations. Results obtained under such unstable conditions will not be discussed here.

Internally cooled tubular test sections

Three studies have been reported recently in the US. During 1963 and early 1964, a comprehensive investigation of CHF in uniformly heated vertical circular tubes was undertaken at Columbia University [9]. A total of 416 test points were obtained which covered the following conditions: pressure, 500 to 1 500 psig; mass velocity, 0.5 to 13×10^6 lb/h-ft²;

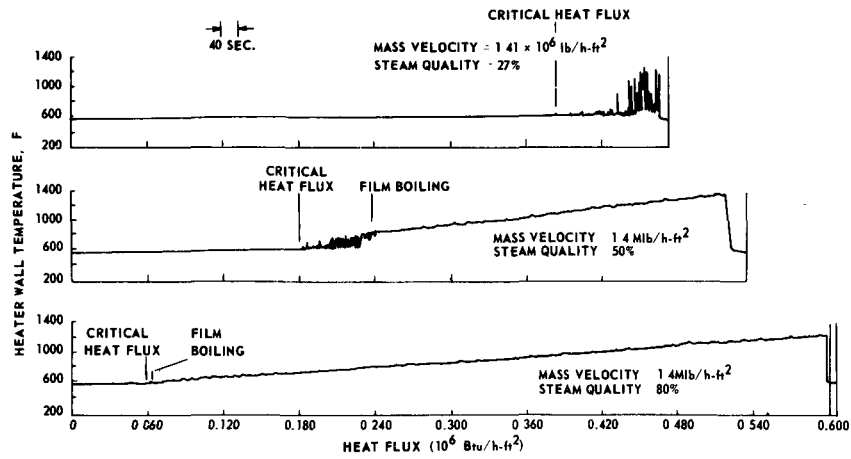


Figure 1. Temperature history at critical heat flux condition at 1000 psia

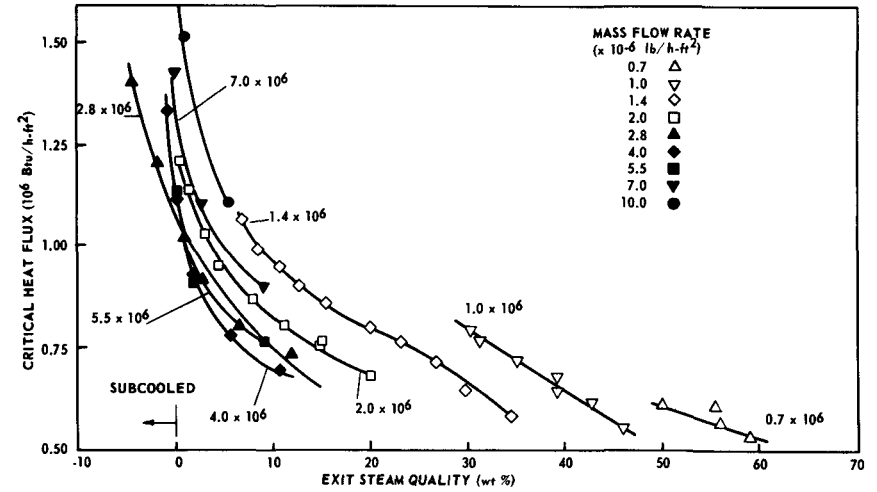


Figure 2. Critical heat flux condition in tubular test sections
Inside tube diameter 0.504 in,
Heated length 76 in,
Pressure 1000 psia

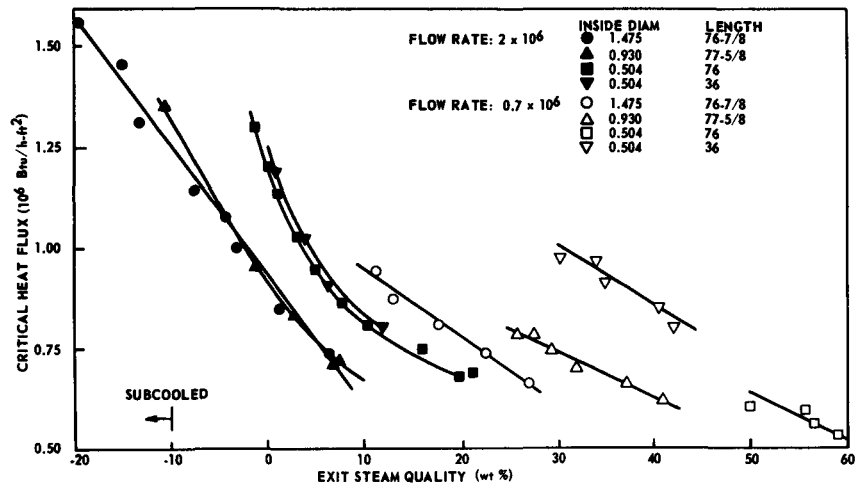


Figure 3. Effects of diameter upon critical heat flux in tubular test sections, pressure 1000 psia

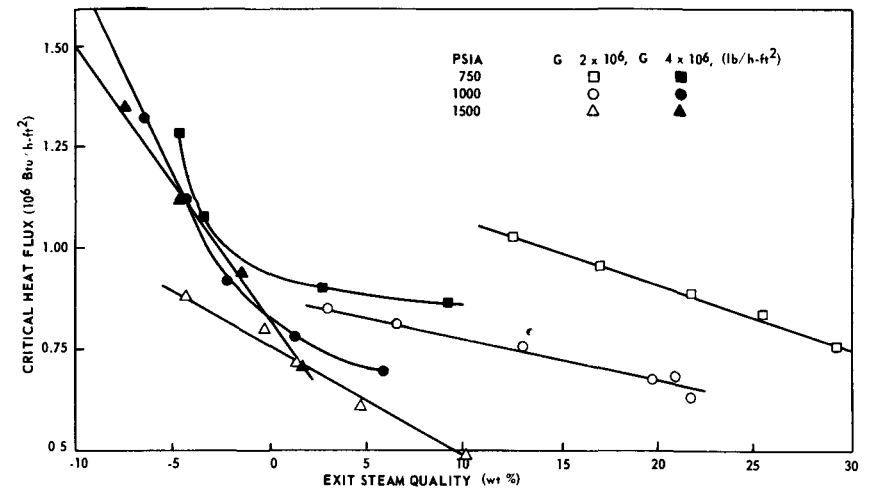


Figure 4. Effects of pressure upon critical heat flux in tubular test sections,
id 0.504 in, heated length 76 in

diameter, 0.245 to 1.5 in; length, 24 to 77 in; and exit conditions, 100 °F subcooled to 60% steam quality by weight. The method used to detect CHF was based on a Wheatstone bridge, where one leg of the bridge was composed of the heater rod. A bridge signal of definite magnitude was selected to correspond to the onset of CHF. This signal gives a rise of 50 to 100 °F in the heated tube temperature.

Typical test results are plotted in Figs. 2, 3 and 4. The data fall into two distinct regions: a subcooled, low steam quality region, and an annular flow high steam quality region. The two regions are separated by exit conditions of 5 to 10% steam quality.

In the subcooled, low steam quality region CHF increases as the mass flow rate increases (Figs. 2, 3 and 4). The effect of length is very small and the effect of diameter is slight, and causes a decrease in critical heat flux with increasing diameter (Fig. 3). There appears to be no pressure effect for subcooled coolant conditions, and a slight decrease in CHF with increasing pressure at low steam quality (Fig. 4).

In the annular flow high steam quality region, CHF decreases with increased mass flow rate (Figs. 2, 3 and 4). For the same mass flow rate and exit steam quality, the effects of heated length are slight, and CHF decreases with increasing diameter (Fig. 3) and pressure in the range 750 to 1 500 psia (Fig. 4). As the mass flow rate is increased, the effects of length, diameter, and pressure are reduced.

A second interesting study of CHF in a circular tube has been performed at Hanford [10]. Tests were performed in a 0.820 in (0.44 in id) Inconel tube heated uniformly over a 12 ft length. Both vertical and horizontal orientations were investigated. Sheathed thermocouples, spot-welded to the outer surface of the tube at 1 ft intervals along the length were used to detect the onset of CHF. In about one-third of the 64 tests performed, CHF occurred at various locations upstream from the outlet end. Upstream CHF conditions were observed only at mass velocities above 5×10^6 lb/h-ft². The upstream data points reported at 1 500 psig are shown in Fig. 5 together with the corresponding exit test conditions. Test points obtained for the more normal case of CHF conditions at the outlet end are also plotted for comparison. No clear explanation for this phenomenon can be given at this time except for the fact that it occurred only when the flow rate was very high and the coolant was close to or at saturation conditions at the inlet to the test section.

A third investigation of CHF has been reported by Babcock and Wilcox [11]. Tests were conducted at 2 000 psia in vertical pipes with varying axial heat flux distributions. The tests reveal that a nonuniform heat flux distribution gives a lower CHF value than does a uniformly heated tube.

Rectangular test sections

Eighty CHF runs have been made recently at 1 000 psia in a rectangular test section [12]. The

tests were performed in vertical channels $0.5 \times 2.10 \times 37$ in and $0.25 \times 2.10 \times 37$ in. The channels were uniformly heated only on the large sides of the rectangle and were equipped with windows to observe the flow structure up to and including the CHF point. Most of the test results are in the annular flow, high steam quality region and exhibit trends similar to those described for the Columbia University tubular test sections.

Annular test sections

Three experimental studies have been reported recently in the US. The first one was performed by Columbia University [13] to evaluate the performance of the Heavy Water Components Test Reactor (HWCTR) driver fuel assembly. Tests were conducted in two uniformly internally-heated vertical annular test sections 2.90 in od and 2.25 in id and 24 and 40 in long. The study was carried out at 500 and 1 000 psia with inlet water velocities of 5 to 20 ft/s and exit conditions of 4 to 120 °F subcooling. The CHF condition was detected by a Wheatstone bridge circuit and corresponds to a temperature rise of at least 50 °F. Mean lines through the data points are shown in Fig. 6. A few General Electric test results [14] are also plotted for comparison. At coolant velocities of 10, 15, and (to a lesser degree) 20 ft/s, severe loop vibrations and coolant inlet pressure fluctuations were experienced at Columbia University at 500 psia and about 30 °F exit subcooling. When vibrations occurred, the CHF values were as much as 15% below the dotted curves in Fig. 6. Several runs were also made with helium in the coolant. No effect of helium concentration on CHF was observed, even up to helium concentrations slightly in excess of saturation at the outlet of the test section.

The second of the reported annular studies is a systematic investigation carried out by General Electric Company [14]. A total of 610 data points were obtained in a uniformly, internally-heated, vertical annulus with flow upwards. The tests covered the following conditions: inside heated diameter, 0.375 to 0.540 in; outside unheated diameter, 0.555 to 1.250 in; hydraulic diameter, 0.180 to 0.875 in; heated length, 29 to 108 in; pressure, 600 to 1 450 psia; mass flow rate, 0.14 to 6.2×10^{-6} lb/h-ft²; and exit conditions, slightly subcooled to 62% steam quality by weight. The CHF was detected by a resistance bridge which becomes unbalanced when the resistance of the top 12 in of the heated rod changes. No point was considered valid unless the temperature rose simultaneously at one or more thermocouple locations. The CHF conditions reported in this study correspond to an increase in surface temperature of at least 50 °F.

Typical results are plotted in Figs. 7, 8 and 9. In many respects, the trends are similar to those described for circular tubes. There are again two distinct regions with opposite flow rate behavior, (Figs. 6, 7, 8 and 9) but the separation between them has moved toward the region of subcooled exit

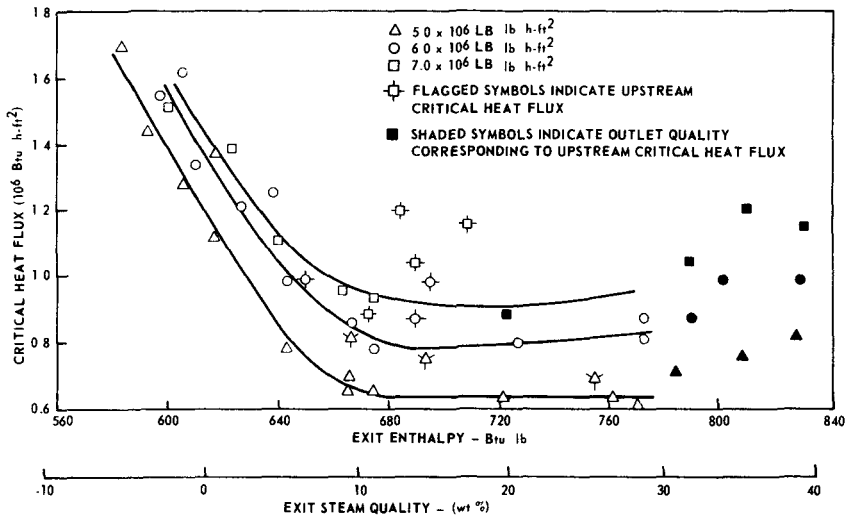


Figure 5. Upstream critical heat flux conditions in tubular test sections, pressure 1 500 psig

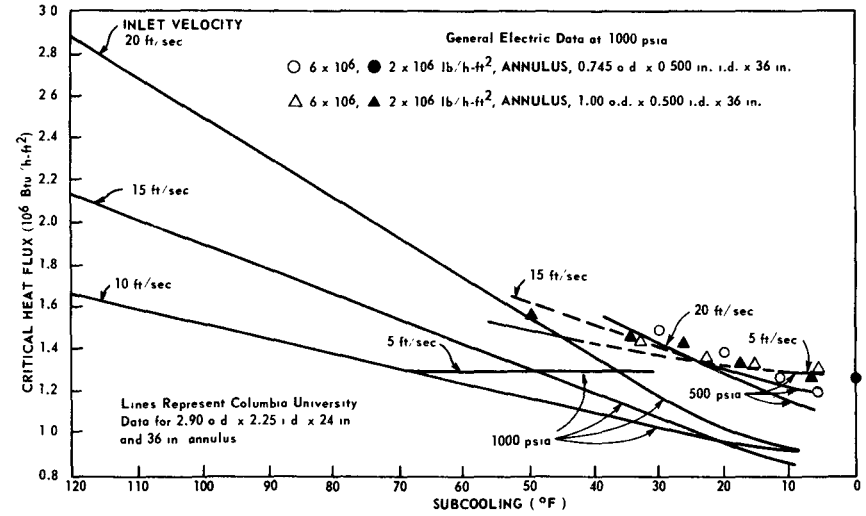


Figure 6. Critical heat flux in internally heated annular test sections with subcooled water conditions

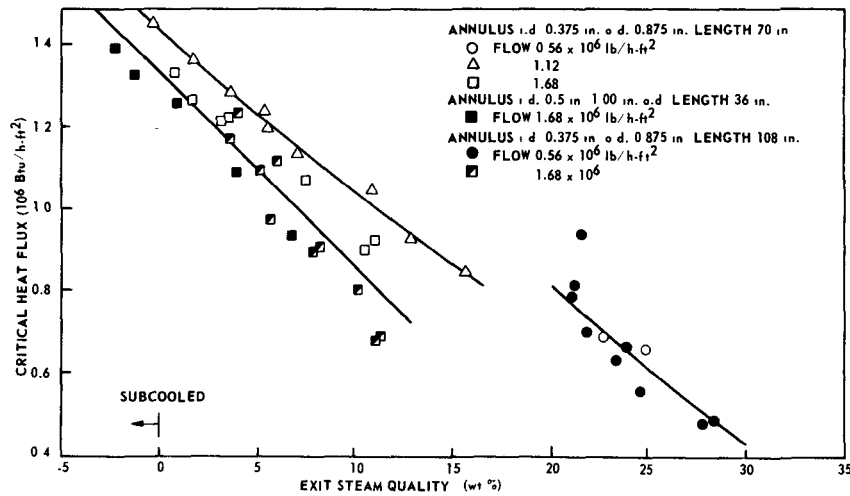


Figure 7. Critical heat flux in internally heated annular test sections, pressure 1 000 psia

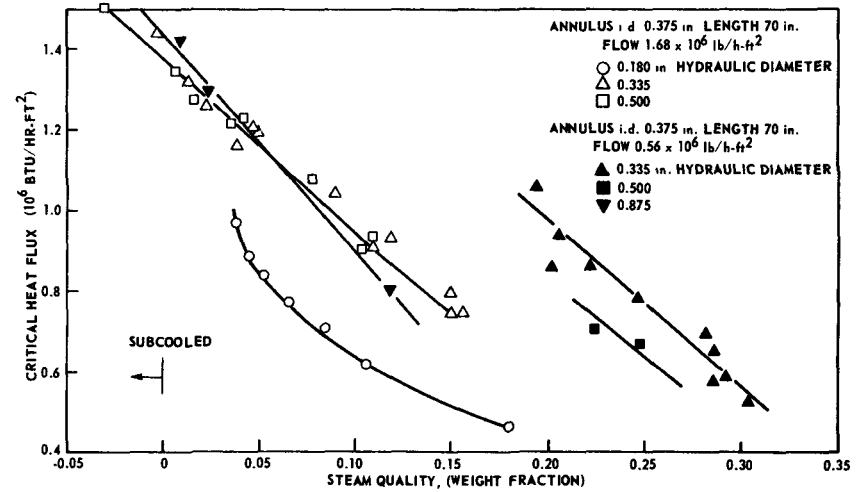


Figure 8. Effects of hydraulic diameter upon critical heat flux in internally heated annular test sections at 1 000 psia

conditions. In the subcooled region, CHF increases as the mass flow rate increases or as the pressure decreases from 1 000 to 500 psia (Fig. 6). According to the data of reference [14], the effects of channel size appear negligible.

In the annular flow, high steam quality region, CHF increases as the mass flow rate decreases (Figs. 7, 8 and 9). The effect of flow is reduced as the mass flow rate becomes high and it reverses itself beyond 2.0×10^6 lb/h-ft². For the same mass flow rate and exit steam quality, CHF decreases with increasing pressure from 600 to 1 400 psia (Fig. 9). The effects of heated length are negligible (Fig. 7), and CHF exhibits a maximum with respect to hydraulic diameter; it decreases for hydraulic diameters below 0.25 in and above 0.4 to 0.5 in (Fig. 8).

The effects of nonuniform heat generation in an internally-heated annular geometry have also been investigated [15]. A total of 48 data points was obtained with a cosine and a chopped cosine heat flux distribution. The tests gave CHF values identical to those for uniform heating if the local conditions of heat flux and steam quality prevailing at the CHF point were used.*

The third study of CHF in annular flow was performed by Allis Chalmers [16]. A few points were obtained in a uniformly internally-heated vertical annulus at 600 psig. Some of the points (plotted in Fig. 9) agree reasonably well with the General Electric results. A full comparison, however, is not possible because the inlet subcooling was kept small in most tests, and the variation in exit steam quality at a given flow is limited.

An interesting conclusion about the performance of circular and annular geometries can be drawn by comparing the data in Figs. 2 and 7. The two sets of results were selected purposely because they have about identical system pressure, heated length, and hydraulic diameter. It is observed that for the same mass flow rate and exit steam quality, the CHF values are lower for the annular than the tubular geometry. This is especially true at high steam quality and can be traced to an increased shear stress and increased steam concentration at the core tube wall of the annulus. A tube, due to its radial symmetry, does not exhibit any nonuniformity in shear stress or steam quality distribution. On the other hand, an annular flow geometry is known in single phase flow

to have a higher shear stress on the core tube wall than on the outer wall. Furthermore, the annulus used in Fig. 7 is only internally heated and the steam concentration is highest at the core tube wall because steam formed there does not mix immediately with the coolant flowing along the outer wall. The above hypotheses have been checked with "rough" liner tests [14]. Rings 1 in apart and extending 0.080 in into the stream were attached to the unheated surface of the annulus. The rings interrupt the flow and increase the shear stress on the unheated wall. Water normally accumulating there is forced toward the heated surface, and the CHF values increase, approaching those obtained in tubes.

Multirod test sections

Multirod sections have been operated in the US by Westinghouse [17], General Electric [1, 18, 19], Columbia University [20, 21], and Hanford [22-24]. The test conditions covered and the number of CHF points reported are shown in Table 1.

A summary description of the test sections, including their geometry, method of spacing, heat flux distribution, and CHF detection technique is given in Table 2. Considerable variations are seen to exist which make it difficult to compare the experimental results. Still, some common trends do emerge, and they are presented in Figs. 10, 11 and 12.

Figure 10 illustrates typical effects of flow upon CHF. It shows data obtained at 1 000 psia at Columbia University in a 6 ft, 19-rod test section (labeled C-6 in Table 2). In Fig. 10, the heat flux in the hottest test rod is plotted against the average exit steam quality. Two distinct regions again are seen to exist; a low steam quality region where CHF increases with mass flow rate, and a high steam quality, annular flow region where the reverse trend prevails. The two regions are separated by steam qualities of 15 to 20%, and the transition point between them moves to higher steam qualities as the rod-to-rod clearance and the flow rate are reduced (Fig. 11).

Figure 11 illustrates the effects of rod-to-rod spacing. Test results are plotted for two vertical test sections (C-3 and C-7) and two horizontal test sections (H-2 and H-3) with widely differing rod-to-rod pitch.** Mean curves are drawn at two constant flow rates through the experimental points of peak heat flux versus average exit steam quality. For both

* This does not agree with the results obtained in a circular tube by Swenson *et al.* [11]. The data reported in reference [11] must, however, be reviewed with suspicion since their uniform heat flux results are only 50% of those given in reference [2].

** These two sections were operated at slightly different pressures (1 000 vs. 1 200 psi), and the pressure effect is assumed negligible.

Table 1

	Pressure (psia)	Mass flow rate (10^6 lb/h-ft ²)	Exit coolant conditions	No. of test points
Westinghouse Electric Corp	2 000	0.4 and 0.9	18-26% steam	2
General Electric Company	1 000-1 400	0.18-1.9	1-90% steam	117
Columbia University	1 000-1 200	0.5-4.0	1-55% steam	136
Hanford	1 000-1 200	0.5-5.0	177 °F sub to 50% steam	157

Table 2. Descriptions of experimental multirod test sections

Designation	No. of rods	Heater rod od (in)	Heated length (in)	Spacing between outer rod and housing channel (in)	Spacing method	Heat flux distribution	Housing tube configuration	Critical heat flux detection	Flow direction
Bettis-1	9	0.413	9.25	0.060		<i>Westinghouse Electric Corporation</i>			
					9 rods welded at top and bottom to flange. Each flange has sixteen 0.247 in holes for flow	Uniform	1.47 in square shroud	Physical failure of test section	Vertical Up
						<i>General Electric Company</i>			
APED-1	2	7/16	30	0.120	Horizontal cylinders spaced 9 in apart extend from rods and channel	Uniform	Rectangular channel 0.79 in × 1.295 in 0.79 in sides rounded on 0.648 in radius	Thermocouples detect first temperature rise or oscillation	Vertical Up
APED-2	4	7/16	36 & 48	0.135	Horizontal cylinders spaced 11 in apart extend from rods and channel	1 rod 1.0/3 rods 0.9	1.332 square shroud with rounded corners	Thermocouples terminate test at 900 °F temp.	Vertical Up
APED-3	9	0.375	18	0.140 to 0.150	3 sapphire cylinders around each rod retained between plates at each end of heated section. Rulon spacers on 4 rods 10 in upstream of end of heated section	1 corner rod 1.0/1 outer rod 1.0/ center rod 1.0/6 rods 0.8	1.85 in square channel with 0.22 in rounded corners	Resistance unbalance & thermocouple temp. rise of at least 100 °F	Vertical Up
APED-4	9	0.375	18	0.120 to 0.130		1 corner rod 1.22/1 outer rod 1.0/ center rod 1.0/6 rods 0.8	1.85 in square channel with 0.22 in rounded corners	Resistance unbalance & thermocouple temp. rise of at least 100 °F	Vertical Up
						<i>Columbia University</i>			
C-1	7	0.550	36	0.089	0.083 wire wrapped on 6 rods on a 10 in pitch	Outer rods 1.0/center rods 0.965	1.994 in tube with ceramic segments to simulate infinite rod array	Resistance unbalance on center rod	Vertical
C-2	7	0.550	36	0.089	6 ceramic ferrule spacers 0.179 in od × 0.092 in × 0.5 in at midlength positions		1.994 in tube with ceramic segments to simulate infinite rod array	Resistance unbalance on center rod	Vertical Up
C-3	19	0.550	36	0.100	0.083 wire wrapped on 12 rods on a 10 in pitch. Bundle wire wrapped with 0.083 in wire on 10 in pitch	Outer rods 1.0/inner rods 0.871 center rod 0.806	3.195 in tube	Resistance unbalance & temperature recordings	Vertical Up
C-4	19	0.550	36	0.100		10 outer rods 0.445/5 inner rods 0.387/center rod 0.358/3 hot rods 1.0	3.195 in tube	Physical failure of test section	Vertical Up
C-5	19	0.550	36	0.100		Outer rods 1.0/inner rods 0.854/ center rod 0.807	3.195 in tube	Resistance unbalance and/or temperature recordings corresponding to temp. rise of at least 50 °F	Vertical Up
C-6	19	0.550	72	0.100		Outer rods 1.0/inner rods 0.806/ center rod 0.766	3.195 in tube		Vertical Up
C-7	12	0.440	17	0.022	0.022 wire wrapped on 12 rods on a 6 in pitch	Uniform	60° parallelogram made of contoured asbestos-phenolic to match curvature of heated rods	Vertical Up	
C-8	12	0.440	17	0.022		10 outer rods 0.379/2 center rods 1.0		Vertical Up	
C-9	12	0.440	17	0.022		10 outer rods 0.645/2 center rods 1.0		Vertical Up	
						<i>Hanford Atomic Products Operation</i>			
H-1	19	0.564	18.5	0.112	0.074 in wire wrapped on 12 rods on a 10 in pitch	Outer rods 1.0/inner rods 0.83/ center rod 0.83	3.25 in tube	Thermocouples imbedded in enamel-coated copper cylinders; temperature rise of at least 50 °F	Vertical Up
H-2	19	0.629	19.5	0.060	0.015 in wire wrapped on 12 rods on a 10 in pitch	Uniform	3.25 in tube		Horizontal
H-3	19	0.587	19.5	0.101	0.050 in wire wrapped on 12 rods on a 9 in pitch	Uniform	3.25 in tube		Horizontal
H-4	19	0.587	76.0	0.101	0.050 in wire wrapped on 12 rods on a 9 in pitch	Uniform	3.25 in tube		Horizontal
H-5	19	0.587	19.5	0.105	Ceramic warts 0.57 in long, 0.17 in wide, 0.048 in thick placed 6.25 in from each end of heated length	Uniform	3.25 in tube		Horizontal
H-6	19	0.564	19.5	0.110	Ceramic warts 0.375 in long, 0.10 in wide, 0.074 in thick placed 6.25 in from each end of heated length	Outer rods 1.0/inner rods 0.83/center rod 0.785	3.25 in tube		Vertical Up

SESSION 1. 10 P/224 S. LEVY et al.

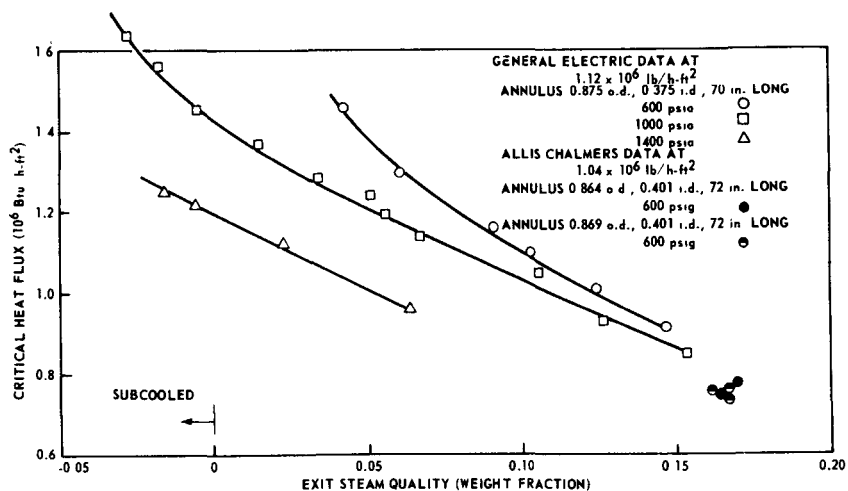


Figure 9. Effects of pressure upon critical heat flux in internally heated annular test sections

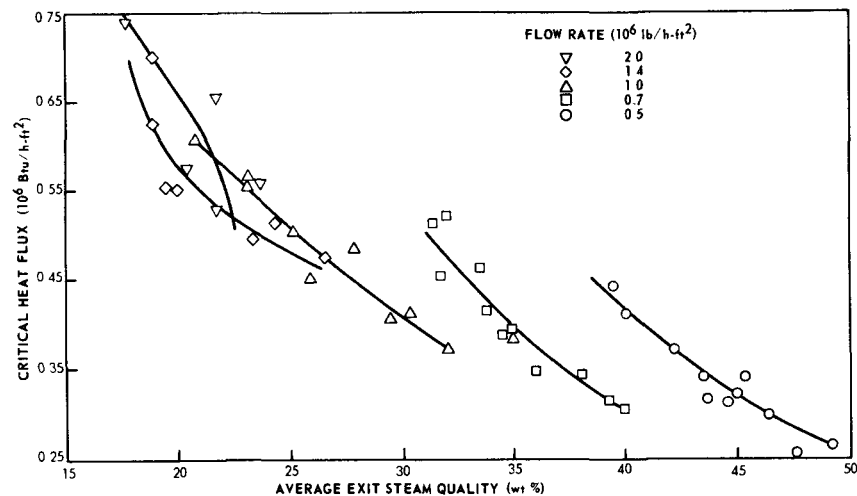


Figure 10. Typical critical heat flux data in multirod test sections, pressure \approx 1000 psia, test section C-6

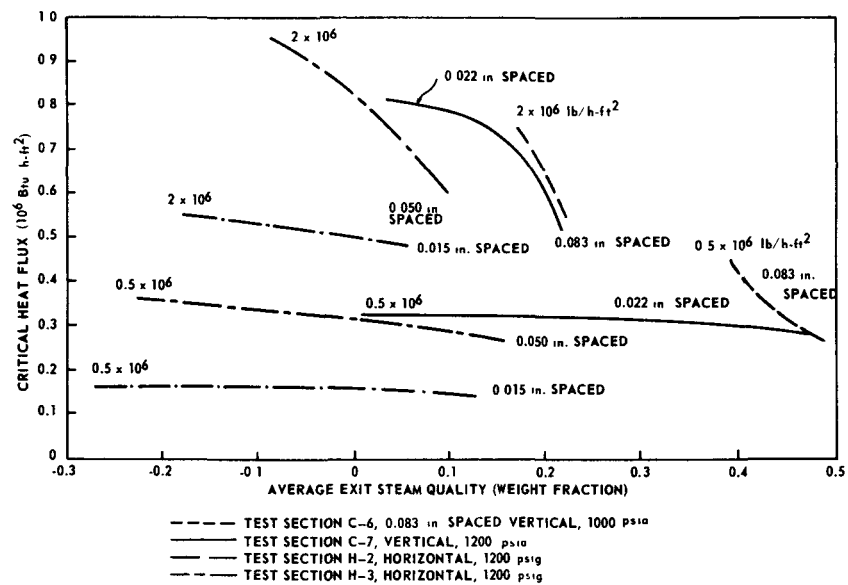


Figure 11. Effects of rod-to-rod spacing upon critical heat flux in multirod test sections

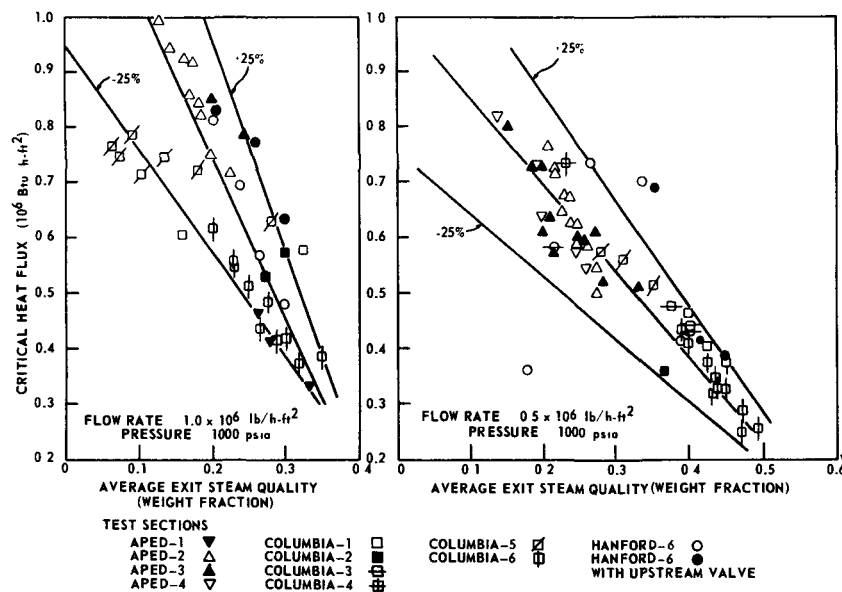


Figure 12. Available critical heat flux data in multirod test sections

the vertical and horizontal test sections, CHF decreases sharply when the rod-to-rod spacing* is reduced by a factor of 3 to 4. The effects are substantial at low mass flow rates where, for a very tight rod lattice, the CHF curve becomes independent of steam quality. The effects of rod spacing decrease as the flow rate becomes high and tend to disappear for vertical upward flow. It is observed that for small rod-to-rod spacing, the Columbia vertical data fall well above the Hanford horizontal results. One reason for this is that in the Hanford test sections, a large gap was left between the outer rods and the housing wall. This caused the inner flow channels (where CHF occurred) to be at higher enthalpies than the bulk values reported in Fig. 11. A further comparison of data for similar rod arrangements (H-1, H-6 and C-6) would show close agreement between Hanford and Columbia results.

The multirod test sections were spaced by both wires and ferrules. A comparison of test results obtained in test sections C-1 and C-2, and H-1 and H-6, would show the two spacing systems to be about equivalent, with the wire wrap results slightly (10%) above the ferrule data. The wire spacer is expected to improve mixing of the coolant, but its presence on the heated surfaces disturbs the liquid film flow along the rods more than the ferrules do. These two effects appear to compensate each other. Similar investigations of various spacers at General Electric [25] have shown that the ideal spacer is one which has minimum contact with the heated rods, yet can provide mixing of the coolant and particularly mixing of the water flowing along unheated walls.

Figure 12 is a plot of all the available multirod data for vertical upward flow at 1 000 psia and mass flow rates of 0.5 and 1.0×10^6 lb/h-ft². The results are shown in terms of CHF values in the hottest rod versus average exit steam quality. The data include substantial variations in heated length, rod-to-rod distance, heat flux distribution, and methods of spacing. A remarkable feature of Fig. 12 is that the effects of all these variations are small or self-compensating. Comparison of Fig. 12 with Figs. 2 and 7 also shows that multirod data fall below the corresponding tubular test points and agree more closely with the measurements in annular test sections.

A proposed explanation for the last result above is as follows. The test data in Fig. 12 were obtained with relatively uniform rod power generation. In some test sections the outer rod-to-channel clearance was small (equal to or less than the rod-to-rod spacing), and CHF first occurred on the rods facing an unheated channel. This matches the conditions in an internally heated annulus, and the multirod and annular data should agree. In the other test sections, the clearance between the outer rods and the flow channel was relatively large, and CHF occurred on an inner rod. However, in this case, the values of bulk enthalpy reported for CHF are lower than the local enthalpy

* As discussed later, this effect diminishes for rod-to-rod spacing in excess of 0.073 in (Fig. 12).

at the inner rods. This would shift the CHF data to the left or to lower values.

In a few test sections (C-8 and C-9), the heat generation in the inner rods was increased enough to have CHF occur in the inner rods rather than at its normal location (i.e., rods facing the unheated channel). It was found that for the same average exit steam quality, CHF on an inner rod was 30% higher in test section C-8 and 50% higher in test section C-9 than it would have been for an outer rod in the same uniformly heated test section. These values are closer to, but still below the circular pipe data. It is suspected that increased heat generation in the central rods leads to increased flow resistance in the interior flow passages and more coolant is diverted to the periphery of the bundle. This, in turn, lowers and raises the point at which the inner and outer rods respectively would normally reach the critical condition.

It is clear from the above discussion that, while the performance of multirod test sections can be estimated by curves of the type shown in Fig. 12, CHF in multirod geometries will be understood only when the flow, coolant enthalpy, and shear distribution and their interaction with geometry and heat flux can be predicted.

ANALYTICAL AND EMPIRICAL CORRELATIONS OF THE CRITICAL HEAT FLUX

Several correlations of CHF have been proposed for forced convection flow of water. Some of these have been used in reactor design and include: (a) the correlations of Jens-Lottes [26], Bernath [27], and Gambill [28] for subcooled exit conditions; (b) the equations of De Bortoli *et al.* [2], Bettis [29], Macbeth [30], and Wilson and Ferrell [31], for pipe and rectangular channels; (c) the correlation of Tong *et al.* [32] for circular, rectangular and multirod geometries; (d) the predictions of Tippetts [12] and Becker and Person [33] for circular, rectangular, and annular flow excluding subcooled conditions; (e) the limit lines of Janssen and Levy [34], drawn below annular test data.

Most of the above correlations are empirical. In the subcooled region only the equation of Gambill which utilizes a superposition-type solution can make any, if a slight, claim to theoretical grounds. In the steam quality region, only the correlations of Tippetts and Becker and Person are based upon theoretical considerations.** These two models, together with the earlier models of Isbin [36] and Goldmann [37], assume that the diffusion of liquid droplets to the wall, or liquid film, is the dominant mechanism and supplies the bulk of liquid to be evaporated.***

** Collier *et al.* [35] proposed a similar model for steam/water mixtures entering the test section.

*** Grace [38] has questioned this postulate. He reviewed test data obtained in air/liquid film flow conditions and concluded that the film flow rate was substantial and that the removal of liquid by evaporation and entrainment from the film would determine the CHF condition.

Some of the above correlations are evaluated in Figs. 13 and 14. Figure 13 compares the correlations with two sets of data obtained at Columbia University in tubular test sections. The Columbia results were selected because they were not used previously in formulating the correlations. It is seen that none of the correlations are satisfactory. The equations of Macbeth show the most consistent behavior of the empirical equations, while the theoretical equations of Tippets are the most acceptable.

Figure 14 compares the correlations of references [2, 29, 31, 32 and 34] with the experimental data in Fig. 12.* The correlating curves are based upon the geometry of the test section APED-2 (48 in long) which gave data points close to the mean line of Fig. 12. It is seen that the limit lines of reference [34] are much more acceptable than in Fig. 13. None of the correlations are satisfactory even though the equations of references [2, 29, 31] do not fall too far from the data. Deviation of the correlations from test results is not entirely unexpected because the correlations do not consider the complex shear stress and coolant enthalpy distribution that exists in a multirod bundle.**

The importance of one of these variables can be, for instance, demonstrated by calculating the ratio of coolant enthalpy rise in a local channel to the bulk enthalpy rise. Such computations were made for the Hanford 19-rod test sections (H-1 to H-6) which have three types of flow passages: 12 internal "triangular" passages, 6 internal "square" passages, and 12 external "triangular" passages. As might be expected, an imbalance exists between the mass flow rate and the heat input in the three types of flow passages and the 12 internal triangular passages were found to have the greatest ratio of heat input to mass flow rate. The ratio of the enthalpy rise in these "hot" passages to the bulk enthalpy rise was calculated for two cases. In the first case, no mixing was assumed to take place; in the second case, mixing was allowed to occur at the location of flow blockage by the wires or ferrules. Flow from the blocked passage was interchanged with bulk coolant in the proportion of the area blocked to the total area of the flow passage. The calculated ratios of the enthalpy rise in the "hot" passages to the bulk enthalpy rise ranged from 2.29 to 4.46 for no mixing, and from 1.33 to 3.54 with mixing.

In both cases considered, the computed ratios were substantially above one and they can be expected to grossly affect the proposed correlations. It is interesting to note that satisfactory correlation of the data from test sections H-1 to H-6 was obtained when

* The correlation of reference [32] is valid for heated/wetted perimeter ratio of 0.88 to 1.0. Its application to the APED-2 geometry is an extrapolation below the prescribed value of 0.88.

** Tippets [12] accounts for poor mixing in an internally heated annular test section by changing one of his empirical constants. Becker [39] accounts for it by multiplying the heat flux in circular tubes by the ratio of heated perimeter to total wetted perimeter.

the computed mixing factors were introduced in the equations of reference [32].

CRITICAL HEAT FLUX AND REACTOR DESIGN

The availability of CHF data or correlations does not by itself permit the evaluation of a specific reactor design with respect to CHF. It is clear that to predict CHF margins in a given reactor core, one must also be able to know or calculate all the variables entering the prediction: fuel geometry, system pressure, local flow rate, coolant enthalpy, and heat flux distribution. The uncertainties associated with these variables and their interaction with CHF design lines are discussed briefly in reference [40]. Let it suffice to state here that they can be just as important as the uncertainties in CHF correlations.

All water-cooled nuclear reactors are being designed to avoid CHF. The margin they operate below CHF has usually been set arbitrarily. More recently, investigations have been performed to assess the need or the size of this margin. The first extensive experimentation was performed at General Electric [41]. Heated rods were operated beyond CHF with forced convection flow of high pressure, steam/water mixtures. Film boiling coefficients were found to be large enough to not "burn out" the heated rods. Similar results have been reported by CISE [42] and Columbia University [20]. A more detailed investigation of operation beyond CHF is in progress at General Electric [1]. Typical results obtained in an electrically heated two-rod geometry (APED-1) are shown in Fig. 15. Figure 15 is a plot of the heater wall temperature in terms of the heat flux and steam quality prevailing at that point. The constant temperature lines are obtained by cross plotting many temperature traces of the type given in Fig. 1.

The existence of three modes of heat transfer is again noted in Fig. 15. The evaporation region falls below the CHF line; film boiling occurs above the curve marked limit of stable film boiling; and the transition region falls between the two curves. Since the surface temperature oscillates in the transition region, only the maximum temperature is shown in Fig. 15, and the oscillations can range all the way from the shown value to saturation temperature. Figure 15 shows that operation beyond CHF is possible, especially at the higher steam quality values.

The above results have been confirmed by a recent in-reactor test performed by General Electric [44].*** The purpose of the test was to investigate the consequences of operating a fuel rod beyond CHF under more extreme conditions than those anticipated in typical boiling water reactors. The test was performed at 1000 psia in a loop in the General Electric Test Reactor. The test assembly consisted of 4 fuel rods arranged in parallel. Two of the rods were clad with stainless steel, the other two with Zircaloy. Each fuel

*** Results of a similar experiment at higher flow and lower heat flux have been reported [43].

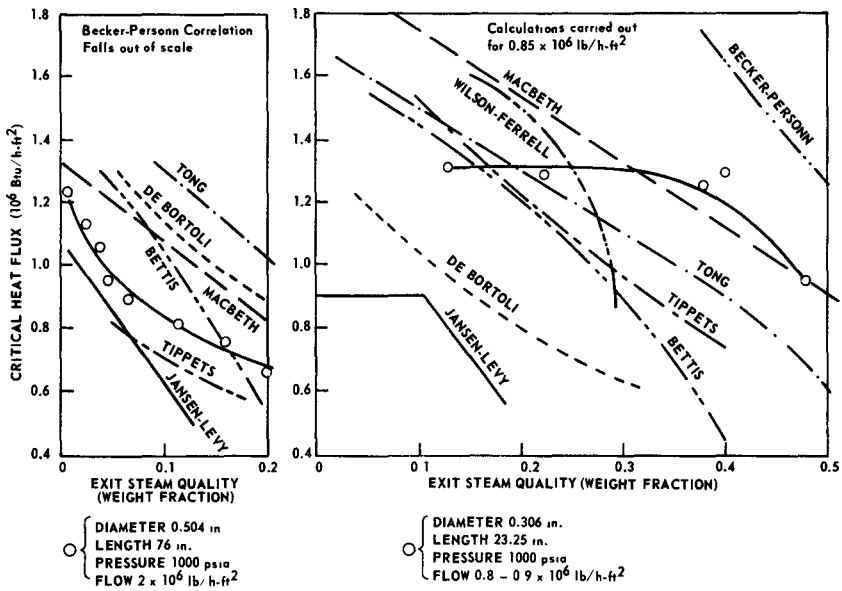


Figure 13. Comparison of correlations with critical heat flux data in tubular test sections

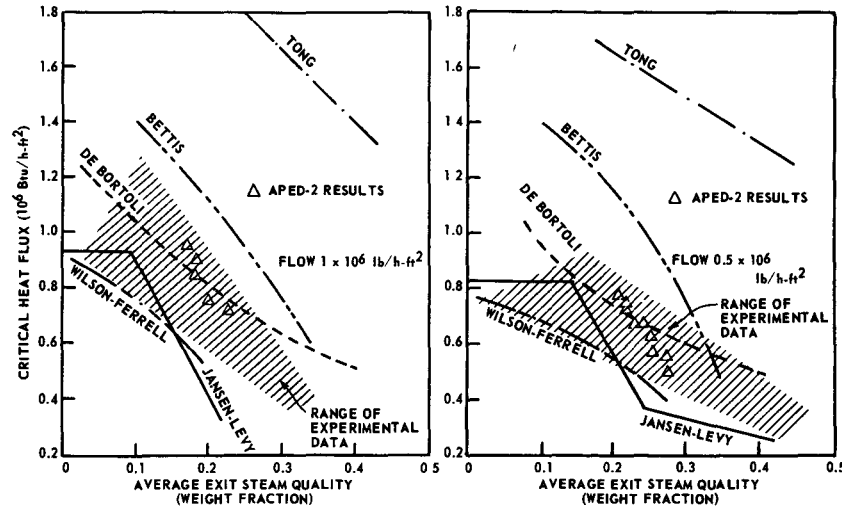


Figure 14. Comparison of correlations with critical heat flux data in multirod test sections at 1000 psia

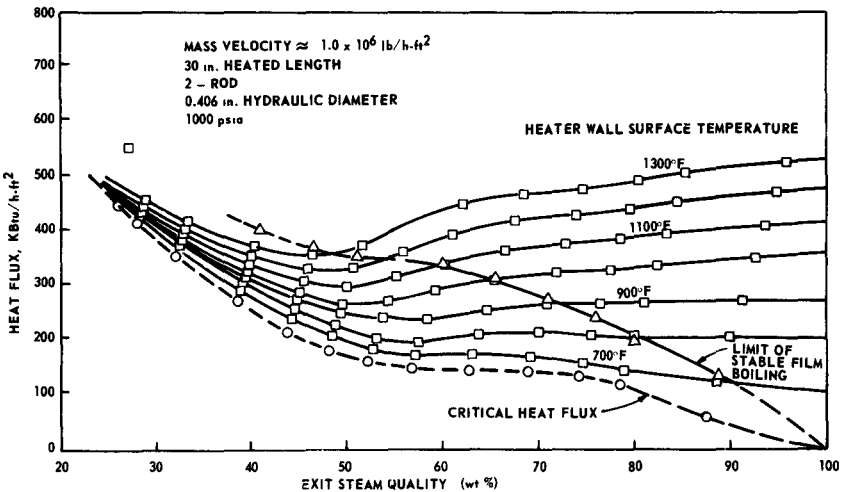


Figure 15. Operation in transition and film boiling regimes



Figure 16. Picture of fuel rod after operation well beyond the critical heat flux

rod (9/16 in od) was contained within a process tube (0.717 in id). The process tubes were equipped with thermocouples at various axial positions. The thermocouples were designed so that, should the fuel rod overheat, they would show a rise in temperature due to radiation heat transfer from the fuel to the process tube. The CHF condition was approached by stepwise reduction of the flow rate of subcooled water entering the test section. During the last two step reductions in flow, the attainment of conditions beyond CHF in the hottest stainless-steel-clad fuel rod was indicated by sudden temperature rises and subsequent increases in fission gas release.

The operating conditions prior to termination of the test have been calculated, based upon gamma scans of the fuel rods. The computations show that the overheated rod operated at a peak heat flux of 600 000 Btu/h-ft², a mass flow rate of 0.33×10^6 lb/h-ft², and a steam quality of about 35%. Good correspondence between out-of-pile and in-reactor measurements of CHF was found to exist. Hot cell examination of the hottest fuel rod revealed that it had a clad defect which reached the melting point of stainless steel (2 650 °F). This compares with a temperature of 2 100 °F calculated from the film boiling correlation of reference [41] or slightly above the 20% spread of the correlation. The defected rod and its sectioned process tube are shown in Fig. 16. The picture shows that the defect is localized and that, under even the severe test conditions employed, the defect was not serious and that operation of the rod was possible for several minutes before and after fission gases were released. It has also been established from grain growth of the clad material that a large area of the rod upstream and downstream of the defect operated well beyond CHF. This means that the stainless-steel-clad rod sustained heat fluxes slightly below 600 000 Btu/h-ft² at a flow rate of 0.33×10^6 lb/h-ft² and a steam quality of 35% (corresponding to temperatures below 2 500 °F) without failure. Present water-cooled reactor designs operate at conditions combining lower peak heat fluxes and/or higher flow rates. Should CHF occur in such reactors, the resulting clad temperatures would be much lower than those observed in the test and the consequences would not be serious.

CONCLUSIONS

(a) Considerable CHF data have been accumulated in simplified geometries. The test results have established the important variables and their roles.

(b) Results for CHF in multirod geometries are being accumulated. General trends and approximate estimates of CHF can be inferred from the early tests.

(c) Available correlations of CHF are not satisfactory, especially for complex geometries. Understanding of shear stress and coolant enthalpy distribution is needed to improve the correlations.

(d) Operation beyond CHF is feasible and the

consequences of sustaining a CHF condition in present water-cooled nuclear reactors would not be serious.

ACKNOWLEDGEMENTS

J. Hench, E. Janssen, J. Kervinen, E. Polomik, E. Quinn and T. Sorlie of APED, San Jose, were responsible for the APED work described here. Portions of this work were carried out under USAEC Contract AT(04-3)-189, P. A. 11 and 34. The Hanford work was carried out by the General Electric Company under USAEC Contract AT(45-1)-1350, and the contributions of D. E. Fitzsimmons, G. M. Hesson and E. D. Waters are gratefully acknowledged. The Columbia University work was carried out under Contract AT(04-3)-187, Tasks X, XIII, and XV. R. Biderman, S. Kokolis, J. Griffel, and B. Matzner made substantial contributions to the investigations reported here.

REFERENCES

- Hench, J. E., GEAP-4492 (1964). Also Quinn, E. P., GEAP-4487 and GEAP-4390 (1963).
- De Bortoli, R. A., Green, S. J., Letourneau, B. W., Troy, M., and Weiss, A., WAPD-188 (1958).
- Aladyev, I. T. et al., *International Developments in Heat Transfer, Part II*, 237 (1961).
- Silvestri, M., *International Developments in Heat Transfer, Part II*, 341 (1961). Also CISE, *A Research Program in Two-Phase Flow* (1963).
- Becker, K. M., Aktiebolaget Atomenergi, R4-163, RPL-121 (1962) and R4-173, RPL-659 (1963). Also Becker, K. M., and Hornborg, G., ASME Paper No. 63-HT-27.
- Lee, D. H., and Obertelli, J. D., UKAEA report AEEW-R 213 (1963).
- Lowdermilk, W. H., Lanzo, C. D., and Siegel, B. L., NACA TN-4382 (1958).
- Levy, S., and Beckjord, E. S., ASME Paper 60-HT-27.
- Matzner, B., and Griffel, J., Columbia University (MRP-XIII), April to December 1963 reports.
- Waters, E. D., Anderson, J. K., Thorne, W. L., and Batch, J. M., HW-73902 Rev. (1962).
- Swenson, H. S., Carver, J. R., and Karakala, C. R., ASME Paper No. 62-WA-297.
- Tippets, F. E., GEAP-3766 (1962). Also Journal of Heat Transfer, 86 (1964).
- Matzner, B., MRP-XIII (August 1962).
- Janssen, E., Kervinen, J. A., GEAP-3899 (1963). Also Janssen, E. et al., AMSE Paper No. 63-WA-149.
- Janssen, E., and Kervinen, J. A., GEAP-3755 (1963).
- Neusen, K. F., and Kangas, G. J., Report No. ACNP-62028 (1962).
- Green, S. J., Mauer, G. W., and Weiss, A., ASME Paper No. 62-HT-43.
- Hench, J. E., GEAP-4358 (1963).
- Polomik, E. E., and Quinn, E. P., GEAP-3940 (1962).
- Matzner, B., and Neill, J. S., USAEC report DP-857 (1963).
- Matzner, B., Columbia University, Task XV, Topical report 2 (1963) and 3 (1964).
- Waters, E. D., Hesson, G. M., Fitzsimmons, D. E., and Batch, J. M., HW-77303 (1963).
- Hesson, G. M., and Batch, J. M., HW-80391 (1964).
- Hesson, G. M., Fitzsimmons, D. E., and Batch, J. M., HW-80523 (1964).
- Hench, J. E., Personal Communication.

26. Jens, W. H., and Lottes, P. A., ANL-4627 (1951).
27. Bernath, L., AICHE Preprint 110, Third National Heat Transfer Conference (1959).
28. Gambill, W. R., AICHE Preprint 17, Fifth National Heat Transfer Conference (1962).
29. Bettis Progress Reports, WAPD-MRP-92 and 93 (1962).
30. Macbeth, R. V., UKAEA report AEEW-R-256 (1963).
31. Wilson, R. H., and Ferrell, J. K., BAW-168 (1961).
32. Tong, L. S., Currin, H. B., and Thorp, A. G., II, *Nucleonics* 21, 43 (1963).
33. Becker, K. M., and Personn, P., Aktiebolaget Atomenergi, AE-113 (1963).
34. Janssen, E., and Levy, S., APED-3892 (1962).
35. Collier, J. G. *et al.*, AICHE Preprint 37, Sixth National Heat Transfer Conference (1963).
36. Isbin, H. S. *et al.*, *Journal of Heat Transfer* 83, 149 (1961).
37. Goldmann, K. *et al.*, *Journal of Heat Transfer* 83, 158 (1961).
38. Grace, J. M., Ph.D. Thesis, University of Minnesota (1963).
39. Becker, K. M., and Hernborg, G., ASME Paper No. 63-HT-25.
40. Levy, S., and Bray, A. P., *Nuclear News*, 3 (1963).
41. Polomik, E. E., Levy, S., and Sawochka, S. G., *Journal of Heat Transfer*, 86, 81 (1964).
42. Bertoletti, S. *et al.*, CISE 36 (1961).
43. Collier, J. G. *et al.*, Studsvik Symposium, CRFD-1164 (1963).
44. Sorlie, T., Levy, S., Lyons, M., and Boyden, J., APED report in preparation.

ABSTRACT—RÉSUMÉ—АБСТРАКТ—RESUMEN

A/224 Etats-Unis d'Amérique

Flux thermique critique dans l'étude thermique et hydraulique des réacteurs nucléaires refroidis à l'eau

par S. Levy *et al.*

Le flux thermique critique constitue l'une des plus importantes limites thermiques et hydrauliques pour les réacteurs nucléaires refroidis à l'eau. Son apparition correspond à une détérioration rapide du processus de transfert de chaleur et s'accompagne d'oscillations de température qui peuvent endommager les éléments de combustible. Trois aspects de flux thermique critique dans les réacteurs nucléaires refroidis à l'eau sont envisagés dans le mémoire. Ce sont: a) la mesure expérimentale de la condition de flux thermique critique, b) sa prédiction analytique ou empirique, et c) l'application de ces mesures ou de ces prédictions à la conception des réacteurs nucléaires.

Des mesures récentes faites sur des géométries simplifiées, circulaires, rectangulaires et annulaires, sont passées en revue et analysées. Les données expérimentales correspondent à un domaine étendu des différents facteurs, par exemple: pressions comprises entre 35 et 105 kg/cm² (500 et 1 500 psia), débits compris entre 50 et 6 500 kg/hm² (0,1 et 13 · 10⁶ livres par heure par pied carré), diamètre hydraulique compris entre 0,46 et 3,8 cm (0,18 et 1,5 pouce), longueur chauffée comprise entre 60 et 670 cm (24 et 262 pouces), et divers modes de chauffage. On identifie et on décrit les paramètres principaux et leur effet sur la condition de flux thermique critique. La comparaison des résultats obtenus pour diverses géométries simplifiées et des chiffres obtenus précédemment permet de mettre en évidence les principales causes d'incertitude restantes, c'est-à-dire les effets des surfaces non chauffées, de la distribution du flux thermique, du petit diamètre hydraulique et des caractéristiques spéciales des essais en boucle.

On donne les résultats d'essais avec des assemblages

de 4, 7, 9, 12 et 17 barreaux. On identifie et on discute les effets dus au débit, à la pression dans le système, à l'écartement entre barreaux, à la distribution inégale du chauffage et à la longueur chauffée. Le rôle important des dispositifs d'écartement des barreaux et leur contribution, heureuse ou malheureuse, sont mis en évidence. La comparaison des résultats obtenus avec plusieurs barreaux et des résultats correspondants obtenus avec des géométries simplifiées montrent que l'anneau chauffé intérieurement et la géométrie circulaire représentent respectivement les limites inférieures et supérieures des résultats obtenus avec plusieurs barreaux.

On décrit ensuite de récentes corrélations empiriques et des prédictions analytiques des conditions de flux thermique limite. Les corrélations de Gambill, Green, Macbeth et Tong, et les prédictions analytiques de Becker, Collier, Grace, Isbin et Tippets sont indiquées. On signale les principaux points de désaccord entre les diverses relations proposées. La plupart des corrélations semblent s'appliquer seulement dans un domaine limité de géométrie et de conditions d'essai.

On discute l'application de ces résultats expérimentaux et de ces prédictions à l'étude des réacteurs. On passe d'abord en revue les autres sources d'incertitude pour l'étude et les calculs de fonctionnement, telles que la distribution de la puissance, du débit et de l'enthalpie du fluide de refroidissement. Ensuite on évalue les marges de sécurité nécessaires en fonction de l'état actuel de la connaissance des conditions de flux thermique critique et des conséquences qu'aurait un fonctionnement au delà de ce flux critique. Les résultats d'essais récents avec une géométrie à un et deux barreaux sont décrits. Les oscillations de température et l'ébullition en film qui se produisent au-delà des conditions de flux thermique critique sont indiquées. On décrit également un essai en pile avec un élément de combustible fonctionnant au-delà du flux thermique critique. Ces résultats montrent que, si la conception et l'exploitation répondent aux conditions nécessaires, les conséquences du fonctionnement au-delà du flux thermique critique peuvent être prédites et ne posent pas de problème sérieux.

A/224 США

Значение критического теплового потока при термогидравлических расчетах атомных реакторов с водяным охлаждением

С. Леви *et al.*

Критический тепловой поток является одним из самых важных гидрометрических и термических параметров ядерных реакторов с водяным охлаждением. Его образование обусловлено быстрым ухудшением процесса теплообмена и сопровождается температурными колебаниями и резким повышением температуры, что может привести к повреждению тепловыделяющих элементов. В настоящем докладе рассматриваются три проблемы, связанные с критическим тепловым потоком в атомных реакторах с водяным охлаждением: а) экспериментальное измерение критического теплового потока; б) предопределение его аналитическим или экспериментальным путем; в) применение результатов этих измерений в расчетах атомных реакторов.

Дается обзор и анализ результатов последних измерений при упрощенной геометрии, например круговой, кольцевой и прямоугольной в широких интервалах значений переменных величин: абсолютное давление 35—105 *атм*, расход теплоносителя от 48 до 6350 *кг/см² · ч*, гидравлический диаметр 4,57—38,1 *мм*, длина нагрева 60—665,5 *см*, а также различные способы нагрева. Выявлены и описаны важнейшие параметры и их влияние на критический тепловой поток. Сравняются параметры различных упрощенных геометрий и приводятся результаты ранее полученных исследований, с тем чтобы выявить остальные важные неопределенные параметры, такие как влияние холодной поверхности, распределение теплового потока, малый гидравлический диаметр и специфические характеристики петлевых испытаний.

Представлены результаты опытов с топливными сборками из четырех, семи, девяти, двенадцати и девятнадцати стержней. Определяются и обсуждаются эффекты скорости потока теплоносителя, давления в системе, расстояния между стержнями, неравномерного распределения температуры, а также длины нагрева. Подчеркивается важная роль межстержневых дистанционирующих прокладок и их положительное или отрицательное влияние. Сравнение данных, полученных в случае многостержневыхборок, с соответствующей упрощенной геометрией показывает, что сборки с кольцевой и круговой геометрией являются соответственно нижним и верхним пределами полученных данных.

Также рассматриваются корреляции, недавно полученные Гамбиллом, Гринном, Макбетом и Тонгом, и аналитические предсказания критических тепловых потоков Беккера, Колльера, Грейса, Исбина и Типпетса. Отмечены наиболее важные расхождения между различными предложенными корреляциями. Найдено, что большинство корреляций применимо только для ограниченного числа геометрий и условий опыта.

Обсуждаются возможности применения полученных результатов исследований и предсказаний в расчетах ядерных реакторов. Сначала дается краткий обзор таких источников неопределенностей в расчетах конструкции или рабочих условий, как мощность, режим потока теплоносителя и распределение его теплосодержания. Затем оцениваются требуемые пределы конструкции с учетом современных данных о критическом тепловом потоке и последствиях его превышения. Описаны недавно полученные результаты испытанийборок одно- и двухстержневой геометрии. Приводятся коэффициенты температурных колебаний и пленочного кипения в условиях превышения критического теплового потока. Также описывается испытание реактора с топливным стержнем, работающим в условиях превышения критического теплового потока. Эти результаты показывают, что при соблюдении соответствующих расчетных и эксплуатационных условий превышение критического теплового потока в процессе эксплуатации не приведет к серьезным последствиям, и их можно предвидеть.

A/224 Estados Unidos de América

Consideraciones acerca del flujo térmico crítico en el diseño térmico e hidráulico de los reactores nucleares refrigerados por agua

par S. Levy *et al.*

El régimen de flujo térmico crítico es uno de los límites térmicos e hidráulicos más importantes en los reactores nucleares refrigerados por agua. Su aparición está asociada con una alteración rápida del proceso de transmisión de calor y se acompaña de oscilaciones de la temperatura y una elevación rápida de la misma que puede ser perjudicial para la integridad de los elementos combustibles. Esta memoria trata de tres aspectos del régimen de flujo térmico crítico en los reactores nucleares refrigerados por agua. Estos aspectos son: а) medida experimental del régimen de flujo térmico crítico, б) su predicción analítica o empírica, в) aplicación de estas medidas o predicciones al proyecto de reactores nucleares.

Se revisan y analizan medidas recientes realizadas con geometrías simplificadas tales como la circular, rectangular y anular. Los datos de los ensayos comprenden un amplio intervalo de variables, a

saber, presiones absolutas de 500–1 500 psia (34–102 atmósferas), velocidades másicas de $0,1$ a 13×10^6 lb/h ft² (0,0135–1,75 kg/cm²s), diámetros hidráulicos de 0,18 a 1,5 pulgadas (0,45 a 3,8 cm), longitudes calentadas de 24 a 262 pulgadas (60 a 665 cm) y diversas formas de calentamiento. Se identifican y describen los principales parámetros y sus efectos sobre el régimen de flujo térmico crítico. La comparación de los resultados correspondientes a las diversas geometrías simplificadas, juntamente con otros datos obtenidos previamente, se utiliza para identificar las mayores fuentes de incertidumbre que todavía quedan, tales como los efectos de la superficie no calentada, la distribución del flujo térmico, el pequeño diámetro hidráulico y características especiales del circuito de prueba.

Se describen ensayos con estructuras de cuatro, siete, nueve, doce y diecinueve barras. Se determinan y discuten los efectos de la velocidad másica, presión del sistema, espaciado entre barras, distribución desigual de calentamiento y longitud calentada. Se insiste en el importante papel de los espaciadores entre barras y sus contribuciones potenciales, positivas o negativas. La comparación de los datos de barras múltiples con los resultados correspondientes de geometrías simplificadas muestra que el anillo calentado interiormente y la geometría circular actúan como límites inferior y superior, respectivamente, de los resultados de barras múltiples.

Se describen a continuación las recientes correlaciones empíricas y predicciones analíticas de regímenes

de flujo térmico crítico. Se señalan las correlaciones de Gambill, Green, Macbeth y Tong, y las predicciones analíticas de Becker, Collier, Grace, Isbin y Tippets. Se observan discrepancias importantes entre las diversas relaciones propuestas. Se encuentra que la mayoría de las correlaciones se aplican solamente en un intervalo limitado de geometrías y de condiciones de ensayo.

Se discute la aplicación de los anteriores resultados experimentales y predicciones para el proyecto de reactores nucleares. En primer lugar se revisan brevemente otras fuentes de incertidumbre en los cálculos de proyecto o funcionamiento, tales como la potencia, el caudal y distribución de la entalpía del refrigerante. A continuación, se consideran los coeficientes de seguridad que necesita el proyecto, de acuerdo con el estado actual de los conocimientos sobre el régimen del flujo crítico máximo y de las consecuencias del funcionamiento por encima de este flujo crítico. Se describen los resultados de pruebas recientes para una geometría de una y dos barras; se obtuvieron en ellas oscilaciones de temperatura y coeficientes de ebullición en película correspondiente a flujos térmicos superiores al crítico. Se describe también una prueba de un reactor con una barra de combustible que trabaja por encima del flujo térmico crítico. Estos resultados muestran que, bajo condiciones apropiadas de proyecto y funcionamiento, las consecuencias de trabajar más allá del flujo térmico crítico son predecibles y no graves.

Особенности теплообмена в ядерных реакторах, охлаждаемых несжимаемыми жидкостями

В. С. Осмачкин

ВВЕДЕНИЕ

Современные ядерные энергетические реакторы являются высокофорсированными тепловыми аппаратами. Из-за жестких ограничений допустимых температур теплоносителя, поверхности и сердечника тепловыделяющего элемента нужно знать поле температур в активной зоне реактора с высокой степенью надежности.

Основная задача теплового расчета реактора состоит в том, чтобы доказать с хорошей гарантией, что опасные температуры теплоносителя, покрытия и сердечника элемента не возникают ни при каких режимах работы реактора.

Специфика теплофизических задач, возникающих при проектировании современных ядерных реакторов, определяется конструкцией активной зоны. Для большинства энергетических ядерных реакторов, охлаждаемых несжимаемыми жидкостями, активная зона представляет собой компактный набор топливных сборок, выполненных в виде пучков цилиндрических тепловыделяющих элементов, заключенных в защитные чехлы. Для расчета распределения температур поверхности тепловыделяющих элементов нужно знать характер течения теплоносителя и скорость теплоотдачи в такой сложной геометрии. Компактность активной зоны и значительная неравномерность тепловыделения в реакторе требуют учитывать продольные изменения коэффициента теплоотдачи.

Эти задачи рассмотрены в настоящем докладе.

ПРОЦЕССЫ ПЕРЕНОСА В ТУРБУЛЕНТНОМ ПОТОКЕ НЕСЖИМАЕМОЙ ЖИДКОСТИ

Движение теплоносителей, используемых в современных ядерных реакторах, как правило, является турбулентным. Теоретическое описание процессов в турбулентном потоке весьма сложно. Хаотичность, неупорядоченность турбулентного движения требует применения статистических методов описания процессов. Однако такой подход реализовать очень трудно. Поэтому практическая гидродинамика пошла

по пути создания полуэмпирических феноменологических теорий. Сущность этих теорий состоит в том, что на основе некоторой модели процессов турбулентного обмена предлагаются связи между характеристиками пульсационного и осредненного движения. Весьма широкое распространение получила теория пути перемешивания Прандтля, согласно которой пульсации скорости в плоском канале можно представить в виде

$$u' \sim l_y \frac{dU}{dy},$$

где l_y — длина пути перемешивания, имеющая смысл характерного расстояния, проходимого пульсациями с сохранением «индивидуальности».

Для компонент тензора турбулентных касательных напряжений в плоском канале эта теория дает формулы вида

$$\tau_{xy} = \rho l_y^2 \left(\frac{dU}{dy} \right)^2.$$

Получим более четкую формулировку гипотезы Прандтля.

Воспользуемся уравнениями для пульсационных составляющих скорости

$$\begin{aligned} \frac{\partial u'_i}{\partial t} + U_k \frac{\partial u'_i}{\partial x_k} + u'_k \frac{\partial U_i}{\partial x_k} = -\frac{1}{\rho} \frac{\partial p'}{\partial x_i} + \\ + \nu \frac{\partial^2 u'_i}{\partial x_k^2} + \frac{\partial}{\partial x_k} (\overline{u'_i u'_k} - u'_i u'_k) \end{aligned} \quad (1)$$

и представим их в виде интегральных уравнений.

Для этого введем функцию Грина, определяемую уравнением

$$\frac{\partial V_0}{\partial t} + (U \nabla) V_0 - \nu \Delta V_0 = -\delta(\bar{r} - \bar{r}') \delta(t - t') \quad (2)$$

и необходимыми граничными условиями.

Функция V_0 описывает распределение скорости в потоке движущейся жидкости при мгновенном локализованном возмущении.

Тогда уравнения (1) можно записать в виде

$$\begin{aligned} u'_i(\bar{r}, t) = \int V_0(\bar{r}, \bar{r}', t, t') \times \\ \times \left[\frac{1}{\rho} \frac{\partial p'}{\partial x_i} + u'_k \frac{\partial U_i}{\partial x_k} - \frac{\partial}{\partial x_k} (\overline{u'_i u'_k} - u'_i u'_k) \right] d\bar{r}' dt'. \end{aligned} \quad (3)$$

Такая форма записи уравнения (1) позволяет применить метод последовательных приближений. В первом приближении в уравнении (3) пренебрежем всеми нелинейными членами, а также пульсациями давления.

Тогда

$$u_i(\bar{r}, t) \simeq \int u_k' \frac{\partial U_i}{\partial x_k} V_0(\bar{r}, \bar{r}', t, t') d\bar{r}' dt'. \quad (4)$$

Если размеры области пространства, где вероятность V_0 отлична от нуля, малы по сравнению с размерами области, где происходит существенное изменение осредненных значений скорости, то уравнение (4) можно упростить. Разложив градиент средней скорости в ряд Тэйлора около точки \bar{r} и ограничиваясь двумя членами разложения, получим приближенные формулы для пульсационных составляющих скоростей в виде

$$u_i(\bar{r}, t) \simeq \frac{\partial U_i}{\partial x_k} \int u_k'(\bar{r}', t') V_0(\bar{r}, \bar{r}', t, t') d\bar{r}' dt' + \frac{\partial^2 U_i}{\partial x_k \partial x_l} \int |\bar{r} - \bar{r}'|_l u_k'(\bar{r}', t') \times V_0(\bar{r}, \bar{r}', t, t') d\bar{r}' dt'. \quad (5)$$

В ядре потока, вблизи оси симметрии потока первые производные осредненной скорости малы. Поэтому пульсационные составляющие скорости определяются значениями вторых слагаемых равенства (5), то есть зависят от вторых производных средней скорости. Наоборот, вдали от оси симметрии потока велики первые слагаемые равенства. В этой области

$$u_i(\bar{r}, t) \simeq \frac{\partial U_i}{\partial x_k} \int u_k'(\bar{r}', t') V_0(\bar{r}, \bar{r}', t, t') d\bar{r}' dt' = l_k \frac{\partial U_i}{\partial x_k} \quad (6)$$

Отметим, что величина

$$l_k(\bar{r}, t) = \int u_k'(\bar{r}', t') V_0(\bar{r}, \bar{r}', t, t') d\bar{r}' dt'$$

имеет размерность длины и характеризует размер области, которая является «поставщиком» пульсаций скорости.

Пользуясь этими выражениями, можно уточнить вид функции Грина, чтобы учесть турбулентную диффузию пульсаций скорости.

Определив коэффициент турбулентной диффузии пульсаций с помощью равенства

$$D = \frac{u_i' u_k' - u_i' u_k'}{\frac{\partial u_i'}{\partial x_k}} \quad (7)$$

и введя функцию Грина второго приближения с помощью уравнения

$$\frac{\partial V}{\partial t} + (U \nabla) V - \nabla D \nabla V - \nu \Delta V = -\delta(\bar{r} - \bar{r}') \delta(t - t'), \quad (8)$$

получим формулы для пульсаций скорости второго приближения

$$u_i(\bar{r}, t) \simeq \int u_k' \frac{\partial U_i}{\partial x_k} V(\bar{r}, \bar{r}', t, t') d\bar{r}' dt', \quad (9)$$

или вблизи стенки

$$u_i(\bar{r}, t) \simeq \frac{\partial U_i}{\partial x_k} \int u_k'(\bar{r}', t') V(\bar{r}, \bar{r}', t, t') d\bar{r}' dt'. \quad (10)$$

С помощью этого соотношения можно вычислить приближенные значения составляющих тензора турбулентных касательных напряжений

$$\overline{u_j u_i'} = \lim_{\theta \rightarrow \infty} \frac{1}{2\theta} \cdot \frac{\partial U_i}{\partial x_k} \int_{-\theta}^{\theta} u_j(\bar{r}, t) \times \int u_k'(\bar{r}' t') V(\bar{r}, \bar{r}', t, t') d\bar{r}' dt'. \quad (11)$$

Поскольку функция Грина зависит только от разности $\tau = t - t'$, то формулу (11) можно записать в более удобной форме

$$\begin{aligned} \overline{u_j u_i'} &= \frac{\partial U_i}{\partial x_k} \int_0^{\infty} d\tau \lim_{\theta \rightarrow \infty} \frac{1}{2\theta} \int_{-\theta}^{\theta} u_j(\bar{r}, t) \times \\ &\times dt \int u_k'(\bar{r}', t - \tau) V(\bar{r}, \bar{r}', \tau) d\bar{r}' = \\ &= \frac{\partial U_i}{\partial x_k} \int_0^{\infty} d\tau \int \overline{u_j(\bar{r}, t) u_k'(\bar{r}', t - \tau)} V(\bar{r}, \bar{r}', \tau) d\bar{r}' = \\ &= \frac{\partial U_i}{\partial x_k} \int_0^{\infty} K_{jk}(\bar{r}, \tau) d\tau = \nu_{jk}^i \frac{\partial U_i}{\partial x_k}. \quad (12) \end{aligned}$$

Величина $\nu_{jk}^i(\bar{r}) = \int_0^{\infty} K_{jk}(\bar{r}, \tau) d\tau$ является компонентой тензора турбулентной вязкости. В лагранжевой системе координат функция $\int V(\bar{r}, \tau) d\bar{r}$ приближенно равна $e^{-\kappa\tau}$, где $\kappa = \frac{\alpha(\nu + D)}{l^2}$, α — константа; l — характерный размер области. Тогда для случая однородной изотропной турбулентности

$$\nu^i = \int_0^{\infty} \overline{u'(t) u'(t - \tau)} e^{-\kappa\tau} d\tau. \quad (13)$$

Это равенство совпадает с определением коэффициента турбулентной диффузии по Тэйлору^{1,2}.

Аналогичным образом, пользуясь уравнениями для пульсаций температуры

$$\frac{\partial T'}{\partial t} + U_k \frac{\partial T'}{\partial x_k} + u_k' \frac{\partial T}{\partial x_k} = a \frac{\partial T'}{\partial x_k^2} + \frac{\partial}{\partial x_k} (u_k' T' - u_k T') \quad (14)$$

и вводя функцию Грина с помощью уравнения

$$\frac{\partial W_0}{\partial t} + (U \nabla) W_0 - a \Delta W_0 = -\delta(\bar{r} - \bar{r}') \delta(t - t'), \quad (15)$$

можно получить интегральное уравнение для пульсаций температуры в виде

$$T'(\bar{r}, t) = \int W_0(\bar{r}, \bar{r}', t, t') \times \\ \times \left[u'_k \frac{\partial T}{\partial x_k} - \frac{\partial}{\partial x_k} (\overline{u'_k T'}) - u'_k T' \right] d\bar{r}' dt'. \quad (16)$$

В первом приближении

$$T'(\bar{r}, t) \simeq \int u'_k \frac{\partial T}{\partial x_k} W_0(\bar{r}, \bar{r}', t, t') d\bar{r}' dt' \quad (17)$$

или при тех же предположениях, что и при выводе формулы (5)

$$T'(\bar{r}, t) \simeq \frac{\partial T}{\partial x_k} \int u'_k(\bar{r}', t') W_0(\bar{r}, \bar{r}', t, t') d\bar{r}' dt' + \\ + \frac{\partial^2 T}{\partial x_k \partial x_l} \int |\bar{r} - \bar{r}'| u'_k(\bar{r}', t') W_0(\bar{r}, \bar{r}', t, t') d\bar{r}' dt'.$$

В области недалеко от стенки

$$T'(\bar{r}, t) \simeq \frac{\partial T}{\partial x_k} \int u'_k(\bar{r}', t') W_0(\bar{r}, \bar{r}', t, t') d\bar{r}' dt' = \\ = l_k^T \frac{\partial T}{\partial x_k}, \quad (18)$$

где l_k^T — аналог длины перемешивания для пульсаций температуры.

Так же как и в равенстве (7), можно приближенно учесть турбулентную диффузию пульсаций температуры, введя коэффициент турбулентной диффузии

$$D^T = \frac{\overline{u'_k T'} - u'_k T'}{\frac{\partial T'}{\partial x_k}}. \quad (19)$$

Тогда функция Грина второго приближения определяется уравнением

$$\frac{\partial W}{\partial t} + (U \nabla) W - \nabla D^T \nabla W - a \Delta W = \\ = -\delta(\bar{r} - \bar{r}') \delta(t - t'), \quad (20)$$

а пульсации температуры будут иметь вид

$$T'(\bar{r}, t) \simeq \frac{\partial T}{\partial x_k} \int u'_k(\bar{r}', t') W(\bar{r}, \bar{r}', t, t') d\bar{r}' dt'. \quad (21)$$

Составляющие вектора турбулентного потока тепла равны

$$\overline{u'_i T'} = \lim_{\vartheta \rightarrow \infty} \frac{1}{2\vartheta} \frac{\partial T}{\partial x_k} \int_{-\vartheta}^{\vartheta} u'_i(\bar{r}, t) \times \\ \times dt \int u'_k(\bar{r}', t') W(\bar{r}, \bar{r}', t, t') d\bar{r}' dt. \quad (22)$$

Поскольку W зависит от разности $\tau = t - t'$, то

$$\overline{u'_i T'} = \frac{\partial T}{\partial x_k} \int_0^{\infty} d\tau \lim_{\vartheta \rightarrow \infty} \frac{1}{2\vartheta} \int_{-\vartheta}^{\vartheta} u'_i(\bar{r}, t) \times \\ \times dt \int u'_k(\bar{r}', t - \tau) W(\bar{r}, \bar{r}', \tau) d\bar{r}' = \\ = \frac{\partial T}{\partial x_k} \int_0^{\infty} K_{ik}^T(\bar{r}, \tau) d\tau = a_{ik}^T \frac{\partial T}{\partial x_k}, \quad (23)$$

где

$$K_{ik}^T(\bar{r}, \tau) = \int \overline{u'_i(\bar{r}, t) u'_k(\bar{r}', t - \tau) W(\bar{r}, \bar{r}', \tau) d\bar{r}'}$$

Величина $a^t(\bar{r}) = \int_0^{\infty} K^T(\bar{r}, \tau) d\tau$ имеет смысл

коэффициента турбулентной теплопроводности.

Конкретный вид функции Грина $V(\bar{r}, t)$ и $W(\bar{r}, t)$ зависит от геометрии задачи.

В простейшем случае, когда можно пренебречь зависимостью коэффициентов уравнений (8) и (20) от координат, то есть когда область возмущений мала по сравнению с областью существенных изменений осредненных параметров потока, функции Грина можно найти с помощью преобразования Фурье.

При этом функция Грина для скорости

$$V(\bar{r} - \bar{r}', t - t') = \\ = \frac{1}{2\sqrt{\pi}(\nu + D)(t - t')^3} e^{-\frac{|\bar{r} - \bar{r}' - U \cdot (t - t')|^2}{4(\nu + D)(t - t')}}. \quad (24)$$

Функция Грина для температуры W имеет тот же вид, но вместо ν , D стоят a , D^T .

Приближенные построения, описанные выше, можно использовать для создания каких-либо, полуэмпирических схем расчета характеристик турбулентного потока.

Однако практические расчеты удобно проводить по более грубой схеме.

Рассмотрим стабилизированное течение жидкости в круглой трубе. Уравнение движения жидкости имеет вид

$$\frac{1}{\xi} \frac{d}{d\xi} \xi(\nu + \nu^t) \frac{dU}{d\xi} = \frac{R^2}{\rho} \frac{dP}{dz} = -2 \frac{\tau_w}{\rho} R. \quad (25)$$

Считая коэффициент турбулентной вязкости известной функцией координат, после двукратного интегрирования получим

$$U(\xi) = \frac{\tau_w R}{\rho \nu} \int_{\xi}^1 \frac{\xi d\xi}{1 + \frac{\nu^t}{\nu}}. \quad (26)$$

Введя известные обозначения

$$\nu_*^2 = \frac{\tau_w}{\rho}, \quad \frac{\nu_* R}{\nu} = \eta_0, \quad \xi = \frac{r}{R},$$

получим

$$\left. \begin{aligned} \varphi(\xi) &= \frac{U(\xi)}{\nu_*} = \eta_0 \int_{\xi}^1 \frac{\xi d\xi}{1 + \frac{\nu^t}{\nu}}, \\ \omega(\xi) &= \frac{U(\xi)}{U} = \frac{\int_{\xi}^1 \frac{\xi d\xi}{1 + \frac{\nu^t}{\nu}}}{\int_0^1 \frac{\xi^3 d\xi}{1 + \frac{\nu^t}{\nu}}}, \\ \text{Re} &= \frac{2UR}{\nu} = 2\eta_0^2 \int_0^1 \frac{\xi^3 d\xi}{1 + \frac{\nu^t}{\nu}}. \end{aligned} \right\} \quad (27)$$

Коэффициент сопротивления ζ равен

$$\zeta = \frac{8\tau_w}{\rho U^2} = \frac{8}{\left(\frac{U}{v_*}\right)^2} = F(\text{Re}). \quad (28)$$

Зная функцию $\frac{v^t}{v} = f(\xi, \eta_0)$, можно рассчитать все характеристики потока. Удачную зависимость для v^t предложил Рейхардт³

$$\frac{v^t}{v} = 0,4 \left(\eta - 11 \operatorname{th} \frac{\eta}{11} \right), \quad \eta = \frac{v_* y}{v} = \eta_0 (1 - \xi). \quad (29)$$

Согласно этой формуле коэффициент турбулентной вязкости изменяется в вязком слое как $\frac{v^t}{v} \sim y^3$, а при $\eta \gg 11$ $\frac{v^t}{v} \sim 0,4 \cdot \eta$.

Поскольку в турбулентном ядре профиль скорости описывается формулой

$$\varphi = 2,5 \ln \eta + 5,5, \quad (30)$$

коэффициент турбулентной вязкости должен изменяться в ядре потока по закону

$$\frac{v^t}{v} = \frac{1 - \frac{\eta}{\eta_0}}{\frac{d\varphi}{d\eta}} = \frac{\xi}{\frac{d\varphi}{d\eta}} = 0,4\eta\xi. \quad (31)$$

Поэтому естественно скорректировать формулу Рейхардта и определять коэффициент турбулентной вязкости формулой вида

$$\begin{aligned} \frac{v^t}{v} &= 0,4 \left(\eta - 11 \operatorname{th} \frac{\eta}{11} \right) \xi = \\ &= 0,4 \left[\eta_0 (1 - \xi) - 11 \operatorname{th} \frac{\eta_0 (1 - \xi)}{11} \right] \cdot \xi. \end{aligned} \quad (32)$$

Расчеты профиля скорости, основанные на формулах (27) и (32), представлены на рис. 1.

На рис. 2 показана зависимость коэффициента сопротивления ζ от числа Re .

Расчет коэффициента стабилизированной теплоотдачи сводится к вычислению известного интеграла Лайона

$$\begin{aligned} \frac{1}{\text{Nu}} &= 2 \int_0^1 \frac{d\xi}{\xi \left(1 + \frac{at}{a} \right)} \left[\int_0^\xi \omega(\xi) \xi d\xi \right]^2, \\ \frac{at}{a} &= \frac{at}{v^t} \frac{v^t}{v} \cdot \frac{v}{a} \simeq \text{Pr} \cdot \frac{v^t}{v}. \end{aligned} \quad (33)$$

Положив турбулентное число Прандтля равным единице и используя формулу (32), мы вычислили числа Нуссельта и коэффициенты теплоотдачи в интервале $0 < \text{Pr} \leq 100$, $5 \cdot 10^3 < \text{Re} < 10^6$. Результаты расчетов представлены на рис. 3, 4.

На рисунках проведено сравнение результатов расчетов с известными аппроксимационными уравнениями. Из этого сопоставления видно, что аппроксимация турбулентной вязкости по формуле (32) обеспечивает хорошее качество расчетов.

ЛОКАЛЬНАЯ ТЕПЛОТДАЧА В КАНАЛЕ РЕАКТОРА

Как известно, коэффициент теплоотдачи слабо зависит от вида граничного условия. Однако в ядерных реакторах, где тепловыделение существенно изменяется по длине канала, необходимо учитывать зависимость коэффициента теплоотдачи от скорости изменения тепловой нагрузки.

Рассмотрим процесс теплообмена в прямолинейном круглом канале. Пусть тепловая нагрузка $q(z)$ изменяется по длине произвольным образом. Выясним, какая скорость изменения тепловой нагрузки по длине канала может привести к заметным изменениям локального коэффициента теплоотдачи и локального температурного напора?

Рассмотрим сначала идеальный случай δ -образного теплоподвода в канале, то есть случай, когда тепло подводится на бесконечно малом элементе длины. Как изменяется профиль температуры вниз по потоку теплоносителя?

Очевидно, что в области действия источника тепла температура пристенных слоев жидкости много больше температуры ядра потока. Однако с течением времени при движении жидкости в канале слои жидкости перемещаются и температура жидкости выравнивается. Длина, на которой происходит выравнивание температуры, характеризует скорость стабилизации температурного профиля. Функцию, описывающую изменение температурного напора по длине канала, назовем функцией влияния тепловыделения и обозначим через $G(z)$.

Локальное значение температурного напора определим равенством

$$(T_w - \bar{T}) c \gamma \bar{U} S = \frac{\Pi}{2} \int_{-\infty}^z q(z') G(z - z') dz' \quad (34)$$

или

$$\frac{1}{\text{St}} = \frac{T_w - \bar{T}}{\frac{q(x)}{c \gamma \bar{U}}} = \int_{-\infty}^x f(x') G(x - x') dx', \quad (35)$$

где

$$f(x') = \frac{q(x')}{q(x)}; \quad x = \frac{z}{R}.$$

Если тепловыделение имеет δ -образный характер, то есть $f(x) = \delta(x)$, то

$$\frac{T_w - \bar{T}}{q} \cdot c \gamma \bar{U} = G(x).$$

Функцию $G(x)$ можно пронормировать условием $\int_0^\infty G(x) dx = A$ и характеризовать длиной

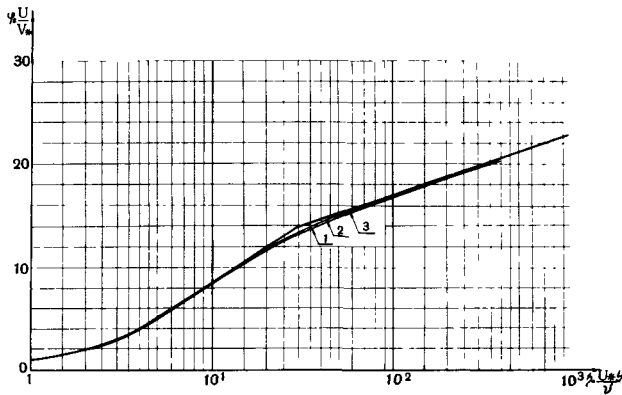


Рис. 1. Профиль скорости жидкости в трубе:
 1 — $Re=10^4$; 2 — $Re=10^5$; 3 — аппроксимация $\varphi=\eta$, $\eta < 5$;
 $\varphi=5 \ln \eta - 3,05$, $5 < \eta < 30$; $\varphi=2,5 \ln \eta + 5,5$, $\eta > 30$

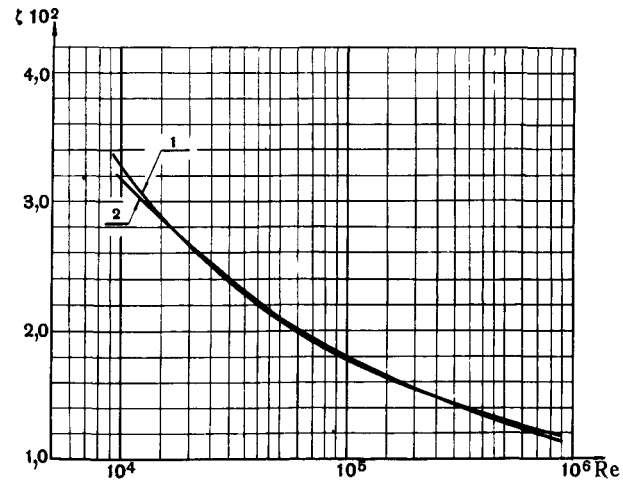


Рис. 2. Зависимость коэффициента сопротивления ζ от числа Re в трубе:
 1 — расчет по формулам (27), (28), (32);
 2 — $\zeta = \frac{0,3164}{Re^{0,25}}$ и $\zeta = \frac{1}{(1,82 \lg Re - 1,64)^2}$

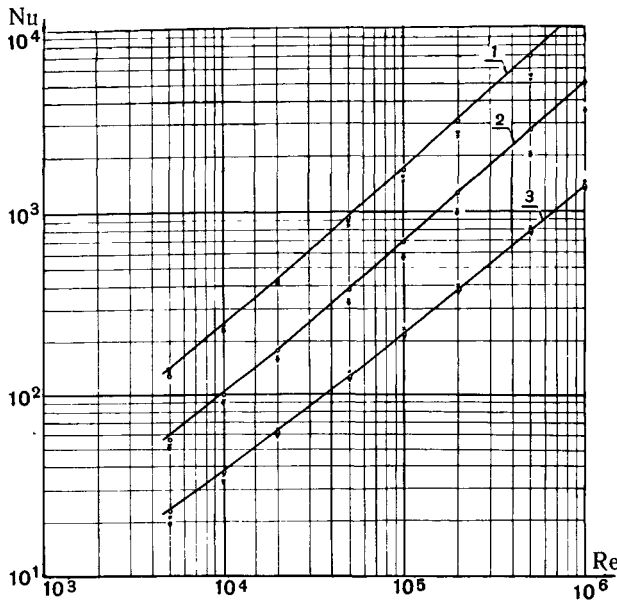


Рис. 3. Зависимость $Nu=f(Re, Pr)$ при течении в трубах жидкостей с $Pr > 1$:

1 — $Pr=100$; 2 — $Pr=10$; 3 — $Pr=1$; \times — $Nu=0,023 Re^{0,8} Pr^{0,4}$ [4]; ∇ — $Nu=0,021 Re^{0,8} Pr^{0,43}$ [5];

$$\circ - Nu = \frac{\zeta}{8} \cdot \frac{Re Pr}{12,7 \sqrt{\frac{\zeta}{8} (Pr^{2/3} - 1) + 1,07}}$$

где $\zeta = \frac{1}{(1,82 \lg Re - 1,64)^2}$ [6]

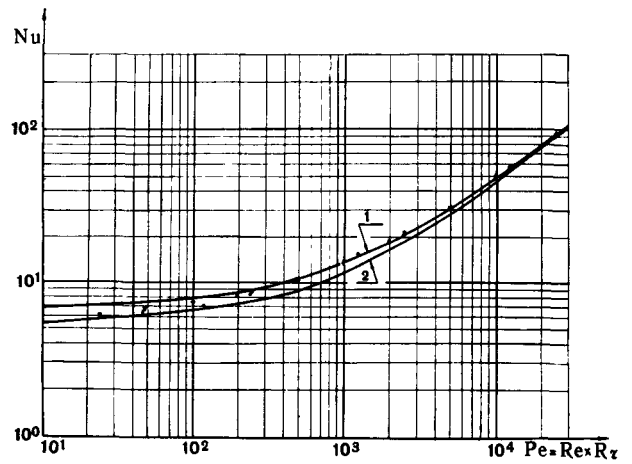


Рис. 4. Зависимость $Nu=f(Pe)$ при течении жидких металлов:

1 — $Nu = 7 + 0,025 Pe^{0,8}$; 2 — $Nu = 5,5 + 0,025 Pe^{0,8}$;
 ∇ — $Pr=0,005$; \times — $Pr=0,01$; \circ — $Pr=0,025$;
 Δ — $Pr=0,05$

релаксации $L = \frac{1}{A} \int_0^{\infty} xG(x) dx$, а также более высокими пространственными моментами $\bar{x}^n = \frac{1}{A} \int_0^{\infty} x^n G(x) dx$. Моменты функции влияния можно найти с помощью Фурье-преобразования. Пусть

$$\begin{aligned} \tilde{G}(p) &= \int_0^{\infty} e^{-px} G(x) dx \simeq \int_0^{\infty} G(x) dx - \\ &- p \int_0^{\infty} xG(x) dx + \frac{p^2}{2} \int_0^{\infty} x^2 G(x) dx - \dots \\ &\dots = A \cdot \left[1 - pL + \frac{p^2}{2} \bar{x}^2 \dots \right]. \end{aligned} \quad (36)$$

Тогда

$$\begin{aligned} A &= \tilde{G}(p) \Big|_{p \rightarrow 0}, \quad L = -\frac{1}{A} \cdot \frac{d\tilde{G}(p)}{dp} \Big|_{p \rightarrow 0}, \\ \bar{x}^2 &= \frac{1}{A} \cdot \frac{d^2 \tilde{G}(p)}{dp^2} \Big|_{p \rightarrow 0} \text{ и т. д.} \end{aligned} \quad (37)$$

Если на расстояниях порядка L функция $f(x)$ изменяется слабо, то можно произвести разложение этой функции в ряд Тэйлора, и тогда

$$\begin{aligned} \frac{1}{St(x)} &= \frac{T_w - \bar{T}}{q(x)} = \int_0^{\infty} f(x-x') G(x') dx' = \\ &= f(x) \int_0^{\infty} G(x) dx - \frac{df}{dx} \int_0^{\infty} xG(x) dx + \dots \\ \dots &= A \left[f(x) - L \frac{df}{dx} + \dots \right] \simeq Af(x-L). \end{aligned} \quad (38)$$

Таким образом, локальный коэффициент теплоотдачи определяется условиями теплоподвода на расстоянии L вверх по потоку.

Как мы увидим позднее, нормирующий множитель A равен обратной значению числа Стантона после термической стабилизации.

В связи с этим

$$\frac{1}{St(x)} \simeq \frac{1}{St_0} \cdot f(x-L). \quad (39)$$

Отсюда следует, что, используя формулы для коэффициента стабилизированной теплоотдачи в случае произвольного изменения теплоподвода по длине канала, мы занимаем значение коэффициента теплоотдачи при росте тепловыделения и завышаем при уменьшении тепловой нагрузки вдоль канала*. Последнее обстоятельство имеет существенное значение для водородных реакторов, где в выходной части активной зоны возможно возникновение поверхностного кипения. Оценки температуры стенки тепловыделяющих элементов и опреде-

ление возможности возникновения поверхностного кипения, выполненные по обычным формулам теплоотдачи, могут быть излишне оптимистичными.

Конечно, степень корректности подобных оценок зависит от скорости изменения тепловой нагрузки вдоль канала. Если в разложении (38) можно пренебречь членом $L \frac{df}{dx}$, то есть $L \frac{d \ln f(x)}{dx} \ll 1$, то влияние непостоянства тепловой нагрузки на коэффициент теплоотдачи мало. Иначе говоря, если относительные изменения тепловой нагрузки на длинах порядка длин релаксации L малы, то влиянием изменений нагрузки на коэффициент теплоотдачи можно пренебречь.

Для расчета локального коэффициента теплоотдачи при любом законе изменения тепловыделения по длине канала нужно знать функции влияния $G(x)$. Функцию влияния $G(x)$ и ее характерные параметры можно найти из решения уравнения энергии в потоке теплоносителя.

Это уравнение для условий течения жидкости в круглой трубе имеет вид

$$\begin{aligned} \frac{1}{\xi} \frac{\partial}{\partial \xi} \xi \left(1 + \frac{a^t}{a} \right) \frac{\partial T}{\partial \xi} &= \frac{U(\xi)}{a} R \frac{\partial T}{\partial x} = \\ &= \omega(\xi) \frac{Pe}{2} \frac{\partial T}{\partial x}, \end{aligned} \quad (40)$$

а граничное условие

$$\frac{dT}{d\xi} \Big|_1 = \frac{q(x)}{\lambda} R. \quad (41)$$

Решение уравнения (40) можно получить с помощью конечного интегрального преобразования по собственным функциям уравнения Штурма — Лиувилля

$$\frac{1}{\xi} \frac{d}{d\xi} \xi \left(1 + \frac{a^t}{a} \right) \frac{dY_n}{d\xi} + \beta_n^2 \omega(\xi) Y_n = 0 \quad (42)$$

с граничным условием $\frac{dY_n}{d\xi} \Big|_1 = 0$. При более общем граничном условии $\frac{dY_n}{d\xi} \Big|_1 = \kappa Y_n(1)$, можно решать более сложные задачи.

Пользуясь ортогональностью функций Y_n , то есть равенством

$\int_0^1 \xi \omega(\xi) Y_n Y_m d\xi = 0$ при $n \neq m$, можно любую функцию, заданную на интервале $(0,1)$, разложить в ряд

$$\theta(\xi, x) = \sum_n \frac{Y_n(\xi)}{\int_0^1 \xi \omega(\xi) Y_n^2 d\xi} \int_0^1 \xi \omega(\xi) \theta(\xi, x) Y_n(\xi) d\xi. \quad (43)$$

* Можно показать, что такая ситуация имеет место и при нестационарных процессах, когда $q = \text{const } f(t)$.

Если обозначить

$$\tilde{\theta}_n(x) = \int_0^1 \xi \omega(\xi) \theta(\xi, x) Y_n(\xi) d\xi, \quad (44)$$

то равенство

$$\theta(\xi, x) = \sum_n \frac{Y_n(\xi) \tilde{\theta}_n(x)}{\int_0^1 \xi \omega(\xi) Y_n^2 d\xi} \quad (45)$$

можно рассматривать как формулу обращения интегрального преобразования с конечными пределами.

Применив интегральное преобразование вида (44) к уравнению (40), то есть умножив уравнение на функцию $Y_n(\xi)$ и интегрируя от нуля до единицы, получим уравнение

$$\frac{Pe}{2} \cdot \frac{d\tilde{T}_n}{dx} = Y_n(1) \cdot \frac{q(x)R}{\lambda} - \beta_n^2 \tilde{T}_n, \quad (46)$$

решением которого является равенство

$$\tilde{T}_n(x) = Y_n(1) \frac{1}{c\gamma\bar{U}} \int_{-\infty}^x q(x') e^{-\frac{2}{Pe} \beta_n^2 (x-x')} dx'. \quad (47)$$

Профиль температуры в канале в соответствии с формулой (45) определяется рядом

$$T(\xi, x) = \frac{1}{c\gamma\bar{U}} \sum_n \frac{Y_n(\xi) Y_n(1)}{\int_0^1 \xi \omega Y_n^2 d\xi} \times \\ \times \int_{-\infty}^x q(x') e^{-\frac{2}{Pe} \beta_n^2 (x-x')} dx'. \quad (48)$$

Температурный напор у поверхности равен

$$T_w - \bar{T} = \frac{1}{c\gamma\bar{U}} \sum_n \frac{Y_n^2(1)}{\int_0^1 \xi \omega Y_n^2 d\xi} \times \\ \times \int_{-\infty}^x q(x') e^{-\frac{2}{Pe} \beta_n^2 (x-x')} dx', \quad (49)$$

а локальное значение обратного числа Стантона

$$\frac{1}{St(x)} = \frac{T_w - \bar{T}}{q(x)} = \int_{-\infty}^x \left[\sum_n \frac{Y_n^2(1)}{\int_0^1 \xi \omega Y_n^2 d\xi} \times \right. \\ \left. \times e^{-\frac{2}{Pe} \beta_n^2 (x-x')} \right] f(x') dx'. \quad (50)$$

Таким образом, функция влияния тепловыделения, введенная ранее, имеет вид

$$G(x) = \sum_n \frac{Y_n^2(1)}{\int_0^1 \xi \omega Y_n^2 d\xi} e^{-\frac{2}{Pe} \beta_n^2 x}. \quad (51)$$

Если граничное условие уравнения соответствует постоянной нагрузке $q = \text{const}$, то локальное число Стантона равно

$$\frac{1}{St(x)} = \frac{Pe}{2} \sum_{n \neq 0} \frac{Y_n^2(1)}{\beta_n^2 \int_0^1 \xi \omega Y_n^2 d\xi} \left(1 - e^{-\frac{2}{Pe} \beta_n^2 x} \right). \quad (52)$$

При $x \rightarrow \infty$ теплоотдача стабилизируется и

$$\frac{1}{St(x)} \Big|_{x \rightarrow \infty} = \frac{1}{St_0} = \frac{Pe}{2} \sum_{n \neq 0} \frac{Y_n^2(1)}{\beta_n^2 \int_0^1 \xi \omega Y_n^2 d\xi}. \quad (53)$$

Вычисляя моменты функции $G(x)$ по формулам (37), можно показать, что

$$\left. \begin{aligned} A &= \int_0^\infty G(x) dx = \frac{Pe}{2} \sum_{n \neq 0} \frac{Y_n^2(1)}{\beta_n^2 \int_0^1 \xi \omega Y_n^2 d\xi} = \frac{1}{St_0}, \\ L &= St_0 \int_0^\infty x G(x) dx = \\ &= St_0 \left(\frac{Pe}{2} \right)^2 \sum_{n \neq 0} \frac{Y_n^2(1)}{\beta_n^4 \int_0^1 \xi \omega Y_n^2 d\xi} \end{aligned} \right\} \quad (54)$$

Ограничиваясь в разложении (36) первыми двумя членами, то есть

$$\tilde{G}(p) \approx \frac{1}{St} (1 - pL) \approx \frac{1}{St_0} \cdot \frac{1}{1 + pL}, \quad (55)$$

получим приближенное представление функции $G(x)$ в виде

$$G(x) = \frac{1}{St_0} \cdot \frac{1}{L} e^{-\frac{x}{L}}. \quad (56)$$

Это позволяет рассчитывать локальное число Стантона при любом законе теплоподвода по формуле

$$\frac{1}{St(x)} = \frac{1}{St_0} \cdot \frac{1}{L} \int_{-\infty}^x f(x') e^{-\frac{x-x'}{L}} dx'. \quad (57)$$

В частности при $q = \text{const}$ на участке тепловой стабилизации

$$\frac{1}{St(x)} = \frac{1}{St_0} \left(1 - e^{-\frac{x}{L}} \right). \quad (58)$$

В такой форме следует обрабатывать данные о теплоотдаче на участке тепловой стабилизации. Длину тепловой стабилизации можно считать равной трем длинам релаксации. Это соответствует отлнчию $\frac{St}{St_0}$ от единицы на 5%.

Для практических расчетов локальных значений коэффициента теплоотдачи при сложной зависимости закона тепловыделения нужно знать систему собственных функций $Y_n(\xi)$. Расчеты этих функций и их собственных значений были выполнены по программе, составленной А. И. Кулешовым и Е. Д. Беляевой

на электронно-вычислительной машине. Зависимость коэффициента турбулентной теплопроводности $\frac{a^t}{a} \simeq \text{Pr} \frac{\nu^t}{\nu}$ от координат вычислялась по формуле (32), а профиль скорости $\omega(\xi)$ — по формуле (27). В табл. 1 собраны результаты расчетов длин тепловой стабилизации.

Таблица 1. Значения длин тепловой стабилизации $\frac{l}{d} = \frac{3}{2} L$.

Re	Pr=0,01			Pr=0,025		Pr=1,0
	10 ⁴	5·10 ⁴	10 ⁵	10 ⁴	10 ⁵	10 ⁴
$\frac{l}{d}$	2,43	8,5	12,8	5,01	14,2	13,7

На рис. 5 проведено сопоставление экспериментальных данных В. И. Субботина⁷ по теплоотдаче на участке тепловой стабилизации при течении жидких металлов с результатами расчетов. Длины тепловой стабилизации, полученные в этих опытах, хорошо согласуются с расчетом.

Продольное изменение локального значения числа Nu при синусоидальном теплоподводе показано на рис. 6.

Из этого графика видно, что число Nu на спадающей части синусоиды меньше стабилизированного значения на 20—40%.

ГИДРАВЛИЧЕСКОЕ СОПРОТИВЛЕНИЕ И ТЕПЛОТДАЧА ПРИ ПРОДОЛЬНОМ ОБТЕКАНИИ ПУЧКА СТЕРЖНЕЙ

Тепловыделяющие сборки ядерных реакторов часто выполняются в виде пучков цилиндрических стержней. Расчеты гидравлического сопротивления и теплоотдачи в таких каналах обычно проводятся по формулам, полученным при течении жидкости в трубах. Считается, что гидравлический диаметр, определяемый как $d_r = \frac{4S}{\Pi}$, достаточно хорошо учитывает специфику геометрии канала. Однако в ряде экспериментальных работ было показано⁸, что гидравлический диаметр не является универсальным характерным размером и не может обеспечить однозначного описания опытных данных для решеток стержней.

Поэтому желательно выполнить теоретические расчеты сопротивления и теплообмена в такой геометрии.

Полное решение уравнений движения и энергии при турбулентном течении жидкости в таких сложных геометрических условиях можно провести только численно. При этом

возникают известные трудности, связанные с неопределенностью характеристик турбулентного потока в таких условиях. Поэтому целесообразно проводить расчеты приближенно, но опираясь на разумное описание свойств турбулентного потока.

Таким приближенным методом для расчета может служить известный в нейтронной физике метод ячейки Вигнера—Зейдца, когда реальная ячейка решетки стержней заменяется некоторой симметричной цилиндрической ячейкой. Очевидно, что такой прием пригоден только для раздвинутых пучков, когда можно пренебрегать азимутальной зависимостью касательных напряжений и температурных напоров по окружности стержней. Расчеты теплоотдачи в такой симметризованной геометрии при течении жидких металлов проводились Двайером и Ти, а также Фридландером и Бониллой⁹.

Гидравлическое сопротивление решетки стержней

Рассмотрим течение теплоносителя в кольце, образованном поверхностью стержня и границей ячейки.

Интегрируя дважды уравнение движения (25) с использованием граничных условий, получим распределение скорости в кольце в виде

$$U(\xi) = -\frac{R^2}{2\mu} \cdot \frac{dp}{dz} \int_{\xi_0}^{\xi} \frac{(1-\xi^2) d\xi}{\xi \left(1 + \frac{\nu^t}{\nu}\right)}, \quad \xi_0 = \frac{r}{R}. \quad (59)$$

Средняя скорость в кольце

$$\bar{U} = -\frac{R^2}{2\mu} \frac{dp}{dz} \int_{\xi_0}^1 \frac{(1-\xi^2)^2 d\xi}{\xi \left(1 + \frac{\nu^t}{\nu}\right)}. \quad (60)$$

Задав распределение турбулентной вязкости, можно рассчитать профиль скорости и закон сопротивления

$$\zeta = \frac{8\tau_w}{\gamma \bar{U}^2} = \frac{8}{\varphi^2},$$

где

$$\varphi = \frac{\bar{U}}{v_*} = \frac{\eta_0}{(1-\xi_0)} \cdot \frac{\xi_0}{(1-\xi_0)^2} \int_{\xi_0}^1 \frac{(1-\xi^2)^2 d\xi}{\xi \left(1 + \frac{\nu^t}{\nu}\right)}. \quad (61)$$

Величина $\eta_0 = \frac{v_*(R-\varrho)}{\nu}$ является характерным динамическим параметром турбулентного потока. Число Рейнольдса, рассчитанное по гидравлическому диаметру, определяется фор-

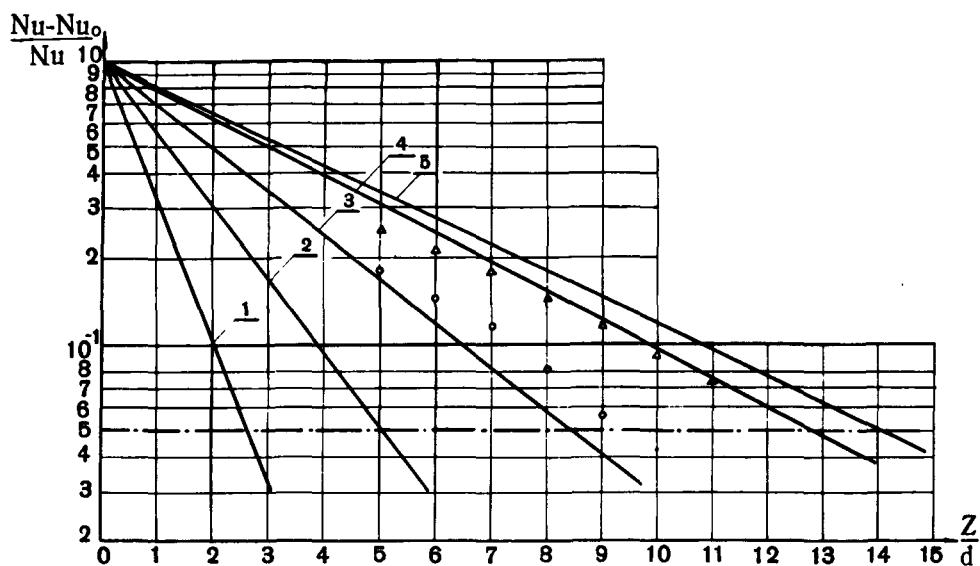


Рис. 5. Сравнение расчетных и экспериментальных данных по теплоотдаче на начальном тепловом участке при течении жидких металлов в трубах: эксперимент \circ — $Re=500$; Δ — $Re=1000$; расчет 1 — $Re=9,67 \cdot 10^3$ $Pr=0,01$; 2 — $Re=9,67 \cdot 10^3$ $Pr=0,025$; 3 — $Re=5 \cdot 10^4$ $Pr=0,01$; 4 — $Re=10^5$ $Pr=0,01$; 5 — $Re=10^5$ $Pr=0,025$

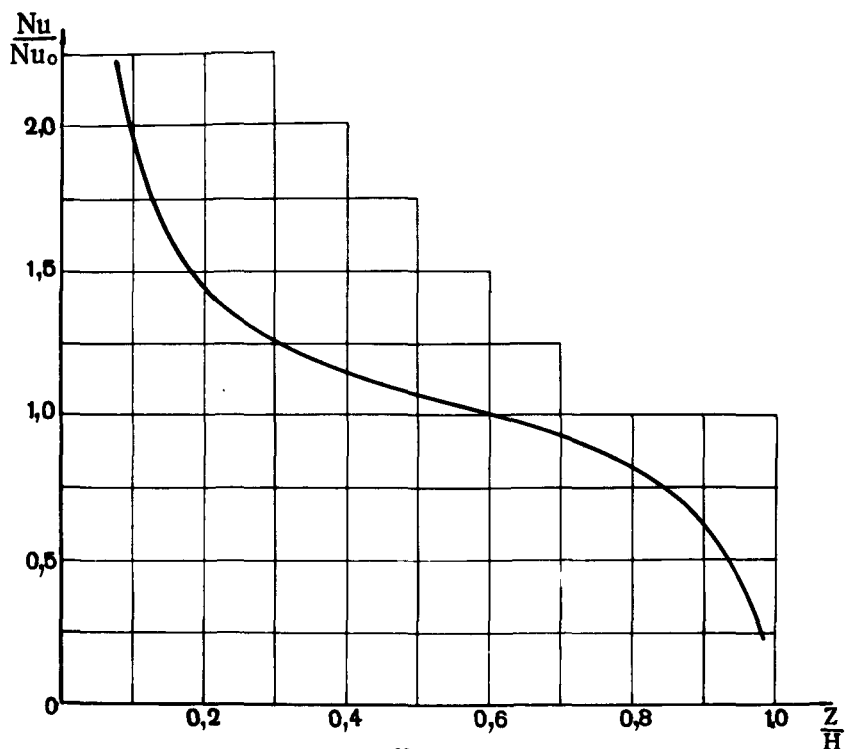


Рис. 6. Зависимость $\frac{Nu}{Nu_0}$ от относительной длины канала при синусоидальном теплоподводе:

$$Re=10^4; Pr=1,0; \frac{H}{d}=50$$

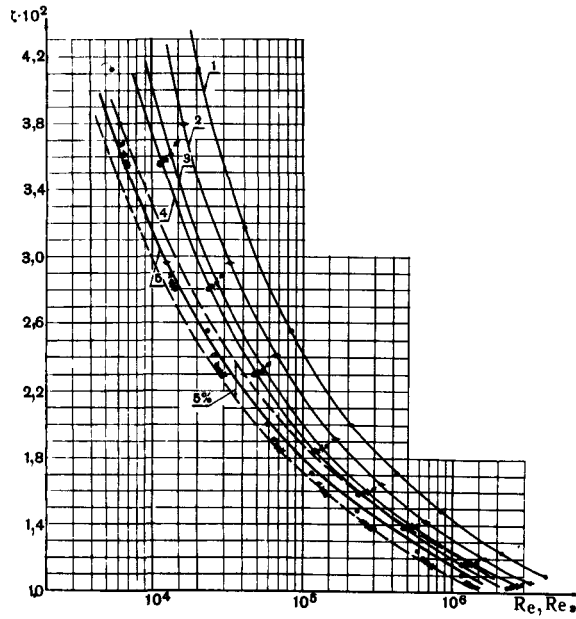


Рис. 7. Зависимость $\zeta = f(Re)$ и $\zeta = f(Re_0)$ для пучка стержней:

1 — $\circ \varepsilon = 0,1$; 2 — $\circ \varepsilon = 0,2$; 3 — $\circ \varepsilon = 0,4$; 4 — $\circ \varepsilon = 0,6$;

$\circ \varepsilon = 0,3$; $\circ \varepsilon = 0,5$; $\circ \varepsilon = 0,7$ $\delta - \zeta = \frac{1}{(1,82 \lg Re - 1,64)^2}$

Точки слева относятся к $Re_0 = Re \cdot \chi$ $\chi = \frac{2\varepsilon}{(1-\varepsilon)^2} \left[\frac{\varepsilon}{2} - \frac{3}{2} \frac{\ln \varepsilon}{1-\varepsilon} \right]$;

ρ — радиус стержня; R — радиус ячейки; $\varepsilon = \frac{\rho^2}{R^2}$

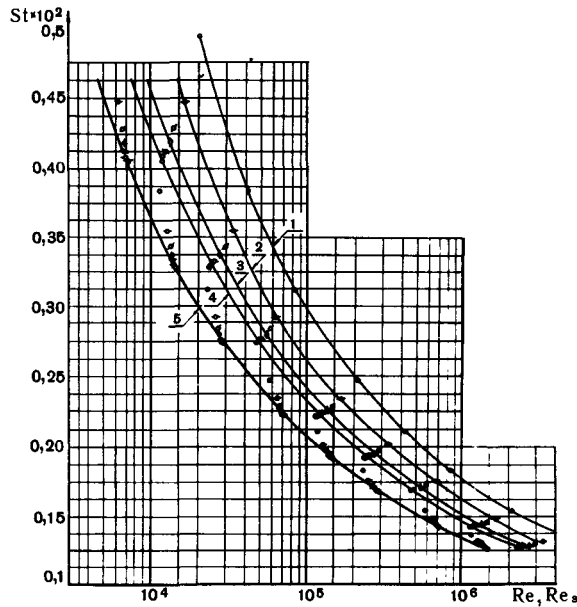


Рис. 8. Расчет теплоотдачи при продольном обтекании пучков стержней для $Pr = 1$:

1 — $\circ \varepsilon = 0,1$; 2 — $\circ \varepsilon = 0,2$; 3 — $\circ \varepsilon = 0,4$; 4 — $\circ \varepsilon = 0,6$;

$\circ \varepsilon = 0,3$;

$\circ \varepsilon = 0,5$; $\circ \varepsilon = 0,7$; $\delta - St = \frac{\zeta}{8} \cdot \frac{1}{12,7 \sqrt{\frac{\zeta}{8} (Pr^{2/3} - 1) + 1,07}}$

Точки слева относятся к Re_0

мулой

$$\text{Re} = \frac{\bar{U} \cdot d_r}{\nu} = \frac{2\eta_0^2}{(1-\xi_0^2)(1-\xi_0)^2} \int_{\xi_0}^1 \frac{(1-\xi^2)^2 d\xi}{\xi \left(1 + \frac{\nu^t}{\nu}\right)} \quad (62)$$

При ламинарном течении вдоль пучка стержней можно провести точные расчеты гидравлического сопротивления. Однако эти расчеты весьма сложны. Если воспользоваться равенствами (60) и (61), положив $\nu^t = 0$, то

$$-\frac{dp}{dz} = \frac{\bar{U}}{R^2} \left(\frac{\varepsilon}{2} - \frac{3}{2} - \frac{\ln \varepsilon}{1-\varepsilon} \right) = \zeta \cdot \frac{\gamma \bar{U}^2}{2g d_r}, \quad (63)$$

где

$$\zeta = \frac{64}{\bar{U} d_r \chi}; \quad \chi = \frac{2\varepsilon}{(1-\varepsilon)^2} \left(\frac{\varepsilon}{2} - \frac{3}{2} - \frac{\ln \varepsilon}{1-\varepsilon} \right);$$

$$\varepsilon = \frac{\pi \rho^2}{\pi R^2} = \xi_0^2. \quad (64)$$

Назовем величину $d_r \cdot \chi = d_a$ эффективным диаметром. При таком определении характерного диаметра закон сопротивления пучка совпадает с законом сопротивления для трубы, то есть

$$\zeta = \frac{64}{\text{Re}_a}, \quad \text{Re}_a = \text{Re} \cdot \chi. \quad (65)$$

Когда $\varepsilon \rightarrow 1$, $\chi \rightarrow \frac{2}{3}$ и $\zeta \rightarrow \frac{96}{\text{Re}}$ как для плоского канала.

Для расчета гидравлического сопротивления пучка стержней нужно знать закон изменения турбулентной вязкости в сечении. Можно полагать, что распределение турбулентной вязкости в решетке стержней описывается формулой вида

$$\frac{\nu^t}{\nu} = 0,4 \left[\eta_0 \frac{\xi - \xi_0}{1 - \xi_0} - 11 \text{th} \frac{\xi - \xi_0}{11(1 - \xi_0)} \right] \frac{1 - \xi}{1 - \xi_0}. \quad (66)$$

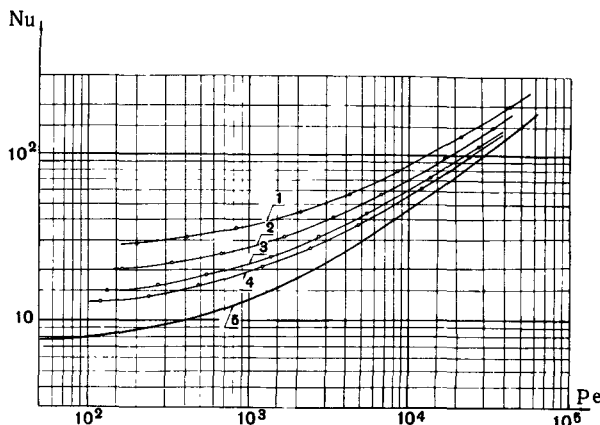


Рис. 9. Зависимость $Nu = f(Pe)$ при течении жидкого металла с $Pr = 0,01$ вдоль пучка стержней:

1 — $\varepsilon = 0,1$; 2 — $\varepsilon = 0,2$; 3 — $\varepsilon = 0,4$; 4 — $\varepsilon = 0,6$;
5 — $Nu = 7 + 0,025 Pe^{0,8}$.

Числа Nu и Pe рассчитаны по гидравлическому диаметру

Располагая формулами (61), (62), (66), можно вычислить коэффициент сопротивления ζ как функцию числа Рейнольдса Re и плотности решетки ε . Результаты таких расчетов показаны на рис. 7. Видно, что коэффициент ζ не является однозначной функцией числа Re , что и было отмечено в экспериментах.

Если число Рейнольдса определить по эффективному диаметру d_a

$$\text{Re}_a = \text{Re} \cdot \chi, \quad (67)$$

то расхождение зависимости $\zeta = f(Re)$ по параметру ε существенно уменьшается (см. рис. 7). Эти результаты позволяют заключить, что эффективный диаметр является лучшей геометрической характеристикой решетки стержней, чем гидравлический диаметр. Это, однако, справедливо лишь для раздвинутых пучков.

Коэффициент теплоотдачи при продольном обтекании пучка стержней

Для расчета теплоотдачи в пучках также можно пользоваться методом эквивалентной ячейки.

Интегрируя уравнение энергии (40) в кольце при соответствующих граничных условиях, получим формулу для расчета числа Нуссельта

$$\frac{1}{Nu} = \frac{2\xi_0^2}{(1-\xi_0^2)^3} \int_{\xi_0}^1 \frac{d\xi}{\xi \left(1 + \text{Pr} \cdot \frac{\nu^t}{\nu}\right)} \left(\int_{\xi}^1 \xi \omega(\xi) d\xi \right)^2. \quad (68)$$

Расчеты теплоотдачи в пучке проводились с использованием профиля скорости, определенного формулой (59) и зависимости турбулентной вязкости от координат по формуле (66).

Результаты расчетов представлены на рис. 8, 9, 10. Так же как и для коэффициента сопротивления ζ , число Нуссельта, рассчитанное

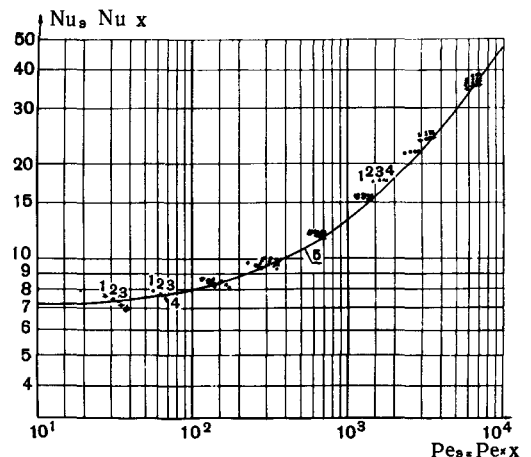


Рис. 10. Зависимость $Nu_a = f(Pe_a)$ при продольном обтекании пучка стержней жидкими металлами:

1 — $\varepsilon = 0,1$; 2 — $\varepsilon = 0,2$; 3 — $\varepsilon = 0,4$; 4 — $\varepsilon = 0,6$;
5 — $Nu_a = 7 + 0,025 Pe_a^{0,8}$; —○— $Pr = 0,005$; —○— $Pr = 0,01$;
△ — $Pr = 0,025$; × — $Pr = 0,05$

по гидравлическому диаметру, не является однозначной функцией числа Рейнольдса.

Если ввести эффективный диаметр, то расхождение зависимостей

$$Nu = f(Re), St = f(Re)$$

существенно уменьшается. При этом расчетные точки с разбросом 10—16% располагаются около критериальных зависимостей, полученных для труб. Этот результат также говорит о том, что обработку данных по теплоотдаче в пучках следует проводить по эффективному диаметру, а не по гидравлическому.

ОБОЗНАЧЕНИЯ

- a — коэффициент температуропроводности
 p — давление
 Π — периметр теплоотдачи
 R — радиус трубы, ячейки
 $u = U + u'$ — скорость потока
 $t = T + T'$ — температура
 \bar{S} — проходное сечение
 t, τ — время
 x, y, z — координаты
 \vec{r} — вектор r
 $\gamma = \frac{Q}{g}$ — удельный вес
 $\delta(t)$ — дельта-функция
 μ — вязкость
 ρ — плотность жидкости, радиус стержня в пучке
 ν — кинематическая вязкость
 $\varepsilon = \frac{Q^2}{R^2}$ — «плотность» решетки стержней
 ξ — безразмерная радиальная координата

- $\eta = \frac{v_* y}{\nu}$ — безразмерное расстояние от стенки
 ζ — коэффициент гидравлического сопротивления
 τ — касательное напряжение
 Nu, Re, St, Pe, Pr — критерии Нуссельта, Рейнольдса, Стантона, Пекле, Прандтля

ИНДЕКСЫ

- w — стенка
 t — турбулентный
 0 — стабилизированное значение
 $'$ — пульсационная составляющая скорости или температуры
 $\bar{\quad}$ — (черта) знак осреднения

ЛИТЕРАТУРА

1. Turbulent flows and heat transfer, editor C. C. Lin, Princeton University press (1959).
2. Taylor. Proc. London Math. Soc., 20, 196 (1921).
3. Reichardt. Zeitschrift angewandte Math. Mech, 3, № 7 (1951).
4. J. Knudsen, D. Katz, Fluid dynamics and heat transfer, New York (1958).
5. М. А. Михеев. Основы теплопередачи, ГЭИ (1956).
6. Б. С. Петухов, В. В. Кириллов. Теплоэнергетика, № 4 (1958), а также Б. С. Петухов, Е. А. Краснощекоев, В. С. Протопопов. Int. developments in heat transfer, part 3, № 67, p. 569 (1961).
7. В. И. Субботин, Атомная энергия, 13, № 2 (1962).
8. В. И. Субботин, Атомная энергия, 9, № 4 (1960).
9. International developments in heat transfer, pt. 3, № 62, 526 (1961).

ABSTRACT—RÉSUMÉ—АННОТАЦИЯ—RESUMEN

A/326 USSR

Specific (heat exchange) features in non-compressible liquid-cooled reactors

By V. S. Osmachkin

The paper gives the results of a theoretical study of specific features of heat exchange processes in the channels of non-compressible liquid-cooled reactors.

The author discusses the possibilities of extending Prandtl's hypothesis about turbulent transfer coefficients to arbitrary flows. Approximate equations for rate and temperature pulsations in an arbitrary liquid flow are derived from formulae written as integral equations describing the transfer of rate and temperature pulsation components. A mathematical analysis of "mixing lengths" introduced by Prandtl is presented.

The author considers the problem of stabilized heat transfer and hydraulic resistance in the reactor channels. The approximation of the turbulent viscosity coefficient is proposed used to calculate stabilized heat transfer and hydraulic resistance in tubes and for

streamline flows parallel to rod bundles. The results of calculations in a broad range of Reynolds and Prandtl numbers are in good agreement with the available experimental data. The use of the hydraulic diameter for heat transfer and hydraulic resistance calculations is shown to be invalid for the case of streamline flows parallel to bundles of rods. A new method is suggested for determining the equivalent diameter of rod bundles which makes it possible to apply the tube flow formulae for calculating the heat transfer and hydraulic resistance coefficients in rod bundles.

The paper presents calculations of heat transfer in circular tubes in the initial thermal region and in the sinesection thermal loop. Relaxation length values for the temperature curve are given which help determine heat transfer for an arbitrary thermal loop.

The author discusses the problems of critical thermal loads during surface boiling of heat-transfer agents in the reactor channels and the mechanism responsible for a heat-exchange critical point. An analytical expression is developed for critical thermal loads for tube flows below boiling point. The derived equation agrees with the experimental data.

A/326 URSS

A/326 URSS

Propriétés particulières des échanges de chaleur dans les réacteurs nucléaires refroidis par des liquides incompressibles

par V. S. Osmachkin

Ce mémoire est consacré à l'examen théorique des problèmes particuliers relatifs aux processus d'échange de chaleur dans les canaux des réacteurs nucléaires refroidis par des liquides incompressibles.

On examine la possibilité d'étendre l'hypothèse de Prandtl sur les coefficients de transfert turbulent au cas d'un écoulement quelconque. On obtient, à partir des équations sur le transfert des composantes pulsatoires de la vitesse et de la température, exprimées sous forme d'intégrales, des formules approximatives des pulsations de la vitesse et de la température dans un écoulement quelconque de liquide. On donne une interprétation analytique des « longueurs de mélanges » introduites par Prandtl.

On étudie la question relative au transfert de chaleur stabilisé et à la résistance hydraulique dans les canaux des réacteurs. A partir de l'approximation proposée du coefficient de viscosité turbulente on calcule le transfert de chaleur stabilisé et la résistance hydraulique en présence d'un écoulement dans les tubes et d'une circulation le long des faisceaux de barreaux. Ces calculs, faits pour un grand intervalle des nombres de Reynolds et de Prandtl, concordent bien avec les données expérimentales. Il est montré que l'utilisation du diamètre hydraulique pour le calcul de l'échange de chaleur et de la résistance hydraulique ne doit pas être faite lorsque la circulation se fait le long des faisceaux. On propose une nouvelle détermination du diamètre équivalent des faisceaux de barreaux permettant de calculer les coefficients de transfert de chaleur et de résistance hydraulique dans les faisceaux de barreaux d'après des formules relatives à la circulation dans les conduits.

On donne les résultats des calculs du transfert de chaleur dans les conduits tubulaires dans la région thermique initiale et en présence d'un apport de chaleur sinusoïdal. On introduit les longueurs de relaxation du profil de température qui permettent de calculer le transfert de chaleur pour un apport de chaleur quelconque.

On discute les questions relatives aux charges thermiques critiques dans le cas de l'ébullition superficielle des caloporteurs dans les canaux des réacteurs. On étudie le mécanisme de l'apparition de la crise de l'échange thermique. On obtient une formule théorique pour les charges thermiques critiques lorsque le liquide circulant dans les conduits n'est pas porté jusqu'à la température d'ébullition. Cette formule décrit bien les résultats expérimentaux.

Particularidades del intercambio de calor en los reactores nucleares refrigerados por líquidos incompresibles

por V. S. Osmachkin

El objeto de la memoria es el estudio teórico de las particularidades de los procesos de intercambio de calor en los canales de los reactores nucleares refrigerados por líquidos incompresibles.

Se analizan las posibilidades de extender la hipótesis de Prandtl acerca de los coeficientes de transporte turbulento al caso de una corriente cualquiera. Partiendo de las ecuaciones del transporte para las componentes pulsantes de la velocidad y de la temperatura, expresadas en forma de ecuaciones integrales, se obtienen fórmulas aproximadas para las pulsaciones de la velocidad y de la temperatura en una corriente cualquiera de líquido. Se da una interpretación analítica de las « longitudes de mezcla » introducidas por Prandtl.

Se considera el problema de la transferencia de calor estabilizada y de la resistencia hidráulica en los canales de los reactores. Basándose en la aproximación propuesta para el coeficiente de viscosidad turbulenta, se han calculado la transferencia de calor estabilizada y la resistencia hidráulica para la corriente en tubos y para el movimiento longitudinal en haces de barras. Los cálculos, que se han efectuado para un amplio intervalo de números de Reynolds y de Prandtl, concuerdan bien con los datos experimentales conocidos. Se demuestra que no se debe emplear el diámetro hidráulico en el cálculo del intercambio de calor y de la resistencia hidráulica cuando la circulación se efectúa a lo largo de los haces. Se propone una nueva definición del diámetro equivalente de un haz de barras, definición que permite calcular los coeficientes de transferencia de calor y de resistencia hidráulica en haces de barras utilizando las fórmulas obtenidas para la circulación en tubos.

Se presentan los resultados de cálculos de la transferencia de calor en tubos redondos en la zona térmica inicial y para conducción sinusoïdal del calor. Se introducen las longitudes de relajación de la distribución de temperatura, que permiten calcular la transferencia de calor para una conducción de calor cualquiera.

Se examinan los problemas de las cargas térmicas críticas en el caso de la ebullición superficial del refrigerante en los canales de los reactores. Se estudia el mecanismo que determina la criticidad en el intercambio de calor. Se obtiene una fórmula teórica para las cargas térmicas críticas en una circulación en tubos que no se lleva a la temperatura de ebullición del líquido. Dicha fórmula describe bien los resultados experimentales.

The transient heat transfer from hollow cylindrical fuel elements in boiling superheated conditions

By A. Jannussis*

The temperature distribution on a hollow cylindrical fuel cell can be obtained by applying the transient Fourier differential equation of heat conduction, neglecting the axial heat flow and assuming only slow pressure variations, i.e., operation where the saturation temperature is nearly constant.

The cell configuration considered has the fissionable material in the form of a cylindrical annulus covered inside and outside by a metallic cladding. Cooling is accomplished by the flow of boiling water over the outside of the element and by the passage of superheated steam through the inner cylinder (Fig. 1).

The advantage of a hollow cylindrical element when used in power reactors, especially for nuclear superheating, is that the maximum temperature becomes lower than in slabtype elements.

For the solution of the Fourier equation, the Laplace transform of the relative change of the heat flux through the fuel element surface and the relative change of the power will be used** [1].

To determine the temperature of the contacting surfaces between cladding and fuel layers, as well as cladding and cooling medium, it is necessary to know the transient temperature distribution in the cladding

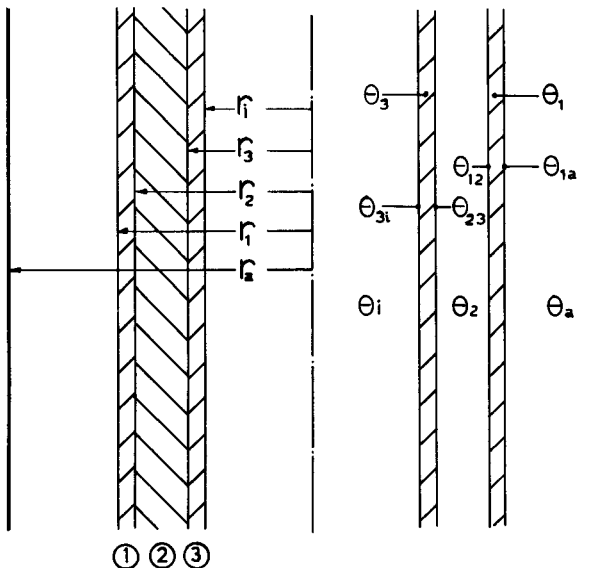


Figure 1. Cell configuration

* Nuclear Research Centre Democritus.

** A similar approach for the solution has been used by A. Kirchenmayer; his model, however, consisted of a solid rod.

layers $\Theta_1(t, r)$ and $\Theta_3(t, r)$, and in the fuel region $\Theta_2(t, r)$. These temperatures are the solutions of the following differential equations with the boundary conditions as indicated for each region:

(a) Outer shell ($r_1 \leq r \leq r_2$):

$$\partial\Theta_1/\partial t = a_c^2 \Delta\Theta_1,$$

where:

$$-\lambda_c(d\Theta_1/dr)_{r=r_1} = \alpha_a(t)[(\Theta_1)_{r=r_1} - \Theta_a],$$

$$(\Theta_1)_{r=r_2} = \Theta_{12}$$

and

$$-\lambda_c(d\Theta_1/dr)_{r=r_2} = -\lambda_B(d\Theta_2/dr)_{r=r_2} \quad (1)$$

(b) Fuel element ($r_2 \leq r \leq r_3$):

$$\partial\Theta_2/\partial t = a_B^2 \Delta\Theta_2 + W(t)/\rho_B c_B,$$

where

$$(\Theta_2)_{r=r_2} = \Theta_{12} \text{ and } (\Theta_2)_{r=r_3} = \Theta_{23} \quad (2)$$

(c) Inner shell ($r_3 \leq r \leq r_1$):

$$\partial\Theta_3/\partial t = a_c^2 \Delta\Theta_3,$$

where

$$\lambda_c(d\Theta_3/dr)_{r=r_1} = \alpha_i(t)[(\Theta_3)_{r=r_1} - \Theta_i],$$

$$(\Theta_3)_{r=r_3} = \Theta_{23}$$

and

$$\lambda_c(d\Theta_3/dr)_{r=r_3} = \lambda_B(d\Theta_2/dr)_{r=r_3}, \quad (3)$$

where a_B^2 , a_c^2 are the thermal diffusivities in fuel element and cladding respectively, λ_B , λ_c their thermal conductivities, and ρ_B and c_B are the fuel element density and specific heat, respectively.

The power variation $W(t)$ is assumed to be small, thus it can be expressed as:

$$W(t) = W_0(1 + y(t)) \text{ where } y(t) \ll 1 \quad (4)$$

The numbers $\alpha_i(t)$ and $\alpha_a(t)$ represent the heat transfer coefficients from the inner and the outer shell to the cooling media, respectively.

STEADY STATE

The case of steady state for the problem considered, has been completely solved by Aoki [2]; the solution is as follows:

$$\Theta_1 = \Theta_{12} - (\Theta_{12} - \Theta_a/A) \ln r/r_2,$$

where

$$A = \lambda_c/a_a \cdot 1/r_1 + \ln r_1/r_2 \quad (5)$$

$$\Theta_2 = \frac{W_0}{4\lambda_B \ln r_2/r_3} \left(r_2^2 \ln \frac{r}{r_3} + r_3^2 \ln \frac{r_3}{r} - r^2 \ln \frac{r_2}{r_3} \right) + \left(\Theta_{23} \ln \frac{r_2}{r} - \Theta_{12} \ln \frac{r}{r_3} \right) \cdot \frac{1}{\ln r_2 - \ln r_3} \quad (6)$$

$$\Theta_3 = \Theta_{23} - \Theta_{23} - \Theta_1/B \ln r_3/r$$

where

$$B = \lambda_c/a_i \cdot 1/r_1 + \ln r_3/r_1. \quad (7)$$

The contact temperatures Θ_{12} , Θ_{23} are given by the expressions:

$$\Theta_{12} = M_1 W_0 + M_2 \Theta_a + M_3 \Theta_1$$

and

$$\Theta_{23} = N_1 W_0 + N_2 \Theta_a + N_3 \Theta_1, \quad (8)$$

where:

$$M_1 = \frac{(J_2 + L)I_1 + LI_2}{J_1 J_2 + LJ_1 + LJ_2} \quad N_1 = \frac{LJ_1 + (J_1 + L)I_2}{J_1 J_2 + LJ_1 + LJ_2}$$

$$M_2 = \frac{J_1 J_2 + LJ_1}{J_1 J_2 + LJ_1 + LJ_2} \quad N_2 = \frac{LJ_1}{J_1 J_2 + LJ_1 + LJ_2}$$

$$M_3 = \frac{LJ_2}{J_1 J_2 + LJ_1 + LJ_2} \quad N_3 = \frac{J_1 J_2 + LJ_2}{J_1 J_2 + LJ_1 + LJ_2}, \quad (9)$$

and

$$I_1 = 1/2(r_2^2 - E/2D), \quad I_2 = 1/2(E/2D - r_3^2),$$

$$L = \lambda_B/D, \quad D = \ln r_2/r_3,$$

$$AJ_1 = \lambda_c, \quad AJ_2 = \lambda_c, \quad E = r_2^2 - r_3^2 \quad (10)$$

SOLUTION OF THE TIME-DEPENDENT EQUATIONS

The differential equations (1), (2) and (3) in cylindrical geometry, when using the Laplace transform and taking into consideration the steady state case, take the following form:

$$s\bar{\Theta}_1(s, r) - \Theta_1(0, r) = (a_c^2/s) \Delta(s\bar{\Theta}_1(s, r) - \Theta_1(0, r)),$$

$$s\bar{\Theta}_2(s, r) - \Theta_2(0, r) = (a_B^2/s) \Delta(s\bar{\Theta}_2(s, r) - \Theta_2(0, r)) + W_1 \bar{y}(s), \quad (11)$$

and

$$s\bar{\Theta}_3(s, r) - \Theta_3(0, r) = (a_c^2/s) \Delta(s\bar{\Theta}_3(s, r) - \Theta_3(0, r)),$$

where: $\Delta = (1/r)(d/dr)[r(d/dr)]$; $\bar{\Theta}(s, r)$ represents, in general, the Laplace transformed function; $\Theta(0, r)$ is the steady state solution; and $W_1 = W_0/\rho_B c_B$. In order to apply the Laplace transform, for the boundary conditions we put in general:

$$\Theta_j(t, r) = \Theta_j(0, r) + \delta\Theta_j(t, r). \quad (12)$$

Thus, after the transformation, we have

$$\bar{\Theta}_j(s, r) = \Theta_j(0, r)/s + \delta\bar{\Theta}_j(s, r) \quad (13)$$

Taking into consideration (12) and the steady state case, the boundary conditions for the three equations become:

$$-\lambda_c((d/dr)\delta\bar{\Theta}_1(s, r))_{r=r_1} = \alpha_a(\delta\bar{\Theta}_1(s, r)_{r=r_1} - \delta\bar{\Theta}_a(s)) + \delta\bar{\alpha}_a(s)(\Theta_1(0, r)_{r=r_1} - \Theta_a),$$

$$\delta\bar{\Theta}_1(s, r)_{r=r_2} = \delta\bar{\Theta}_{12}(s, r)_{r=r_2},$$

$$-\lambda_c((d/dr)\delta\bar{\Theta}_2(s, r))_{r=r_2} = -\lambda_B((d/dr)\delta\bar{\Theta}_2(s, r))_{r=r_2},$$

$$\delta\bar{\Theta}_2(s, r)_{r=r_2} = \delta\bar{\Theta}_{12}(s, r)_{r=r_2},$$

$$\delta\bar{\Theta}_2(s, r)_{r=r_3} = \delta\bar{\Theta}_{23}(s, r)_{r=r_3},$$

$$\delta\bar{\Theta}_3(s, r)_{r=r_3} = \delta\bar{\Theta}_{23}(s, r)_{r=r_3}, \quad (14)$$

$$\lambda_c((d/dr)\delta\bar{\Theta}_3(s, r))_{r=r_3} = \lambda_B((d/dr)\delta\bar{\Theta}_2(s, r))_{r=r_3},$$

and

$$\lambda_c((d/dr)\delta\bar{\Theta}_3(s, r))_{r=r_1} = \alpha_i(\delta\bar{\Theta}_3(s, r)_{r=r_1} - \delta\bar{\Theta}_i(s)) + \delta\bar{\alpha}_i(s)(\Theta_3(0, r)_{r=r_1} - \Theta_i).$$

Second order products of the form $\delta\bar{\Theta} \cdot \delta\bar{\Theta}_i$ have been neglected.

The solution of Eqs. (11) can be obtained in terms of the modified Bessel functions. These are:

$$s\delta\bar{\Theta}_1(s, r) - \Theta_1(0, r) = A_1 I_0(\Omega_1 r) + B_1 K_0(\Omega_1 r),$$

$$s\delta\bar{\Theta}_2(s, r) - \Theta_2(0, r) = A_2 I_0(\Omega_2 r) + B_2 K_0(\Omega_2 r) + W_1 \bar{y}(s),$$

and

$$s\delta\bar{\Theta}_3(s, r) - \Theta_3(0, r) = A_3 I_0(\Omega_1 r) + B_3 K_0(\Omega_1 r), \quad (15)$$

where:

$$\Omega_1 = \sqrt{(s/a_c^2)} \quad \text{and} \quad \Omega_2 = \sqrt{(s/a_B^2)}. \quad (16)$$

The coefficients A_j , B_j ($j = 1, 2, 3$) and the contact temperature functions $\delta\bar{\Theta}_{12}(s, r)$, $\delta\bar{\Theta}_{23}(s, r_3)$ verify the linear system of equations:

$$A_1[\alpha_a I_0(\Omega_1 r_1) + \lambda_c \Omega_1 I_1(\Omega_1 r_1)] + B_1[\alpha_a K_0(\Omega_1 r_1) - \lambda_c \Omega_1 K_1(\Omega_1 r_1)] = s\alpha_a \delta\bar{\Theta}_a(s) - s\delta\bar{\alpha}_a(s)(\Theta_1(0, r_1) - \Theta_a),$$

$$A_1 I_0(\Omega_1 r_2) + B_1 K_0(\Omega_1 r_2) = s\delta\bar{\Theta}_{12}(s, r_2),$$

$$A_1 \lambda_c \Omega_1 I_1(\Omega_1 r_2) - B_1 \lambda_c \Omega_1 K_1(\Omega_1 r_2) = A_2 \lambda_B \Omega_2 I_1(\Omega_2 r_2) - B_2 \lambda_B \Omega_2 K_1(\Omega_2 r_2),$$

$$A_2 I_0(\Omega_2 r_2) + B_2 K_0(\Omega_2 r_2) = s\delta\bar{\Theta}_{12}(s, r_2) - W_1 \bar{y}(s),$$

$$A_2 I_0(\Omega_2 r_3) + B_2 K_0(\Omega_2 r_3) = s\delta\bar{\Theta}_{23}(s, r_3) - W_1 \bar{y}(s),$$

$$A_3 \lambda_c \Omega_1 I_1(\Omega_1 r_3) - B_3 \lambda_c \Omega_1 K_1(\Omega_1 r_3) = A_2 \lambda_B \Omega_2 I_1(\Omega_2 r_3) - B_2 \lambda_B \Omega_2 K_1(\Omega_2 r_3),$$

$$A_3 I_0(\Omega_1 r_3) + B_3 K_0(\Omega_1 r_3) = s\delta\bar{\Theta}_{23}(s, r_3), \quad \text{and}$$

$$A_3[\alpha_i I_0(\Omega_1 r_i) - \lambda_c \Omega_1 I_1(\Omega_1 r_i)] + B_3[\alpha_i K_0(\Omega_1 r_i) + \lambda_c \Omega_1 K_1(\Omega_1 r_i)] = s\alpha_i \delta\bar{\Theta}_i(s) - s\delta\bar{\alpha}_i(s)(\Theta_3(0, r_i) - \Theta_i). \quad (17)$$

The above system of the eight non-homogeneous linear equations can be easily solved because of symmetry; the solution being in the form:

$$\begin{aligned} s\delta\bar{\Theta}_{12}(s, r_2) &= \frac{P_i}{P_a P_1 - Q_a Q_1} M_a - \frac{Q_a}{P_a P_1 - Q_a Q_1} M_i, \\ s\delta\bar{\Theta}_{23}(s, r_3) &= \frac{Q_i}{P_a P_1 - Q_a Q_1} M_a - \frac{P_a}{P_a P_1 - Q_a Q_1} M_i, \\ A_1 &= \frac{K_0(\Omega_1 r_2) \mu_a - [\alpha_a K_0(\Omega_1 r_1) - \lambda_c \Omega_1 K_1(\Omega_1 r_1)] \times s\delta\bar{\Theta}_{12}(s, r_2)}{\alpha_a X_{00}(\Omega_1 r_1, \Omega_1 r_2) + \lambda_c \Omega_1 X_{10}(\Omega_1 r_1, \Omega_1 r_2)}, \\ B_1 &= -\frac{I_0(\Omega_1 r_2) \mu_a - [\alpha_a I_0(\Omega_1 r_1) + \lambda_c \Omega_1 I_1(\Omega_1 r_1)] \times s\delta\bar{\Theta}_{23}(s, r_2)}{\alpha_a X_{00}(\Omega_1 r_1, \Omega_1 r_2) + \lambda_c \Omega_1 X_{10}(\Omega_1 r_1, \Omega_1 r_2)}, \\ A_2 &= \frac{K_0(\Omega_2 r_2) - K_0(\Omega_2 r_3)}{X_{00}(\Omega_2 r_2, \Omega_2 r_3)} W_1 \bar{y}(s) \\ &+ \frac{K_0(\Omega_2 r_3) s\delta\bar{\Theta}_{12}(s, r_2)}{X_{00}(\Omega_2 r_2, \Omega_2 r_3)} - \frac{K_0(\Omega_2 r_2) s\delta\bar{\Theta}_{23}(s, r_3)}{X_{00}(\Omega_2 r_2, \Omega_2 r_3)}, \\ B_2 &= -\frac{I_0(\Omega_2 r_2) - I_0(\Omega_2 r_3)}{X_{00}(\Omega_2 r_2, \Omega_2 r_3)} W_1 \bar{y}(s) \\ &- \frac{I_0(\Omega_2 r_3) s\delta\bar{\Theta}_{12}(s, r_2)}{X_{00}(\Omega_2 r_2, \Omega_2 r_3)} + \frac{I_0(\Omega_2 r_2) s\delta\bar{\Theta}_{23}(s, r_3)}{X_{00}(\Omega_2 r_2, \Omega_2 r_3)}, \\ A_3 &= \frac{K_0(\Omega_1 r_3) \mu_i - [\alpha_i K_0(\Omega_1 r_1) + \lambda_c \Omega_1 K_1(\Omega_1 r_1)] \times s\delta\bar{\Theta}_{23}(s, r_3)}{\alpha_i X_{00}(\Omega_1 r_1, \Omega_1 r_3) - \lambda_c \Omega_1 X_{10}(\Omega_1 r_1, \Omega_1 r_3)}, \\ \text{and} \\ B_3 &= -\frac{I_0(\Omega_1 r_3) \mu_i - [\alpha_i I_0(\Omega_1 r_1) - \lambda_c \Omega_1 I_1(\Omega_1 r_1)] \times s\delta\bar{\Theta}_{12}(s, r_2)}{\alpha_i X_{00}(\Omega_1 r_1, \Omega_1 r_3) - \lambda_c \Omega_1 X_{10}(\Omega_1 r_1, \Omega_1 r_3)}, \end{aligned} \quad (18)$$

where we put for brevity:

$$\begin{aligned} \mu_a &= s[\alpha_a \delta\bar{\Theta}_a(s) - \bar{\delta}\bar{\Theta}_a(s)(\Theta_1(0, r_1) - \Theta_a)], \\ \mu_i &= s[\alpha_i \delta\bar{\Theta}_i(s) - \bar{\delta}\bar{\Theta}_i(s)(\Theta_3(0, r_3) - \Theta_i)], \\ X_{k,n}(x, u) &= I_k(x)K_n(u) - (-)^{k+n} I_n(u)K_k(x); \end{aligned}$$

$k, n = 0, 1,$

$$\begin{aligned} P_a &= \frac{X_{10}(\Omega_2 r_2, \Omega_2 r_3)}{X_{00}(\Omega_2 r_2, \Omega_2 r_3)} \\ &+ \frac{\lambda_B \Omega_2}{\lambda_c \Omega_1} \cdot \frac{\alpha_a X_{10}(\Omega_1 r_2, \Omega_1 r_1) + \lambda_c \Omega_1 X_{11}(\Omega_1 r_1, \Omega_1 r_2)}{\alpha_a X_{00}(\Omega_1 r_1, \Omega_1 r_2) + \lambda_c \Omega_1 X_{10}(\Omega_1 r_1, \Omega_1 r_2)}, \\ P_i &= \frac{X_{10}(\Omega_2 r_3, \Omega_2 r_2)}{X_{00}(\Omega_2 r_2, \Omega_2 r_3)} \\ &- \frac{\lambda_B \Omega_2}{\lambda_c \Omega_1} \cdot \frac{\alpha_i X_{10}(\Omega_1 r_3, \Omega_1 r_1) - \lambda_c \Omega_1 X_{11}(\Omega_1 r_1, \Omega_1 r_3)}{\alpha_i X_{00}(\Omega_1 r_1, \Omega_1 r_3) - \lambda_c \Omega_1 X_{10}(\Omega_1 r_1, \Omega_1 r_3)}, \\ Q_a &= \frac{X_{10}(\Omega_2 r_2, \Omega_2 r_2)}{X_{00}(\Omega_2 r_2, \Omega_2 r_3)}, \quad Q_i = \frac{X_{10}(\Omega_2 r_3, \Omega_2 r_3)}{X_{00}(\Omega_2 r_2, \Omega_2 r_3)}, \\ M_a &= -W_1 \bar{y}(s) \frac{X_{10}(\Omega_2 r_2, \Omega_2 r_2) - X_{10}(\Omega_2 r_2, \Omega_2 r_3)}{X_{00}(\Omega_2 r_2, \Omega_2 r_3)} \\ &+ \frac{\lambda_B \Omega_2}{\lambda_c \Omega_1} \cdot \frac{X_{10}(\Omega_1 r_2, \Omega_1 r_2)}{\alpha_a X_{00}(\Omega_1 r_1, \Omega_1 r_2) + \lambda_c \Omega_1 X_{10}(\Omega_1 r_1, \Omega_1 r_2)} \mu_a, \\ \text{and} \\ M_i &= W_1 \bar{y}(s) \frac{X_{10}(\Omega_2 r_3, \Omega_2 r_3) - X_{10}(\Omega_2 r_3, \Omega_2 r_2)}{X_{00}(\Omega_2 r_2, \Omega_2 r_3)} \\ &+ \frac{\lambda_B \Omega_2}{\lambda_c \Omega_1} \cdot \frac{X_{10}(\Omega_1 r_3, \Omega_1 r_3)}{\alpha_i X_{00}(\Omega_1 r_1, \Omega_1 r_3) - \lambda_c \Omega_1 X_{10}(\Omega_1 r_1, \Omega_1 r_3)} \mu_i \end{aligned}$$

Similar combinations of the modified Bessel functions appear in the calculation of the thermal utilization factor of a reactor and have been studied in detail by Kirchenmayer [1].

After the determination of the coefficients and the contact temperature between fuel element and cladding, we can find the maximum temperature in the fuel element, as well as the surface temperatures between cladding and cooling medium.

REFERENCES

1. Kirchenmayer, A., *Atomkernenergie*, 3, 337 (1958).
2. Aoki, S., *Atomkernenergie*, 7, 52 (1962).

ABSTRACT—RÉSUMÉ—АННОТАЦИЯ—RESUMEN

A/569 Grèce

Transfert thermique en régime transitoire d'une matière fissile de forme cylindrique creuse sous conditions d'ébullition surchauffée

par A. Jannussis

En négligeant le transfert axial de chaleur et en supposant de petites variations de la pression (température de saturation presque constante), le flux thermique d'un cylindre de combustible creux peut être obtenu à l'aide de l'équation de Fourier de la conductivité thermique.

La configuration de la cellule est la suivante: la

matière fissile de forme cylindrique est comprise entre deux couches de métal (gaine). A travers le cylindre intérieur passe de la vapeur surchauffée tandis que la surface extérieure de la gaine est en contact avec de l'eau bouillante.

Afin d'obtenir la variation relative du flux thermique à travers la surface de l'élément de combustible et la variation relative de la puissance, nous employons la transformation de Laplace.

Pour pouvoir déterminer la température de la surface de contact entre gaine et combustible et celle de la surface de contact entre gaine et réfrigérant, il est nécessaire de connaître les distributions de la température dans la gaine $\Theta_1(t, r)$ et $\Theta_3(t, r)$, et dans l'élément de combustible $\Theta_2(t, r)$. Ces températures sont des solutions des équations différentielles

suivantes, avec les conditions aux limites appropriées:

a) Gaine extérieure ($r_1 \leq r \leq r_2$)

$$\frac{\partial \Theta_1}{\partial t} = a_c^2 \Delta \Theta_1,$$

$$\text{où } -\lambda_c \left(\frac{d\Theta_1}{dr} \right)_{r=r_1} = \alpha_a(t) [(\Theta_1)_{r=r_1} - \Theta_a],$$

$$(\Theta_1)_{r=r_2} = \Theta_{12} \text{ et } -\lambda_c \left(\frac{d\Theta_1}{dr} \right)_{r=r_2} = -\lambda_B \left(\frac{d\Theta_2}{dr} \right)_{r=r_2} \quad (1)$$

b) Élément de combustible ($r_2 \leq r \leq r_3$)

$$\frac{\partial \Theta_2}{\partial t} = a_B^2 \Delta \Theta_2 + \frac{W(t)}{\rho_B c_B},$$

$$\text{où } (\Theta_2)_{r=r_2} = \Theta_{12} \text{ et } (\Theta_2)_{r=r_3} = \Theta_{23} \quad (2)$$

c) Gaine intérieure ($r_3 \leq r \leq r_1$)

$$\frac{\partial \Theta_3}{\partial t} = a_c^2 \Delta \Theta_3,$$

$$\text{où } \lambda_c \left(\frac{d\Theta_3}{dr} \right)_{r=r_1} = \alpha_i(t) [(\Theta_3)_{r=r_1} - \Theta_i],$$

$$(\Theta_3)_{r=r_3} = \Theta_{23} \text{ et } \lambda_c \left(\frac{d\Theta_3}{dr} \right)_{r=r_3} = \lambda_B \left(\frac{d\Theta_2}{dr} \right)_{r=r_3} \quad (3)$$

(a_B^2 , λ_B), (a_c^2 , λ_c) sont les diffusivités et conductivités thermiques de la matière fissile et de la gaine respectivement; ρ_B , c_B sont la densité et la chaleur spécifique de l'élément de combustible.

La variation de puissance $W(t)$ étant supposée petite, nous pouvons écrire:

$$W(t) = W_0(1 + y(t)), \text{ où } y(t) \ll 1 \quad (4)$$

Les fonctions $\alpha_1(t)$ et $\alpha_a(t)$ représentent les coefficients de transfert de chaleur de la gaine intérieure et extérieure au milieu réfrigérant, respectivement.

En appliquant la transformation de Laplace aux équations (1), (2) et (3), nous obtenons les solutions suivantes, qui font intervenir les fonctions de Bessel modifiées:

$$s\delta\bar{\Theta}_1(s, r) - \Theta_1(0, r) = A_1 I_0(\Omega_1 r) + B_1 K_0(\Omega_1 r)$$

$$s\delta\bar{\Theta}_2(s, r) - \Theta_2(0, r) = A_2 I_0(\Omega_2 r) + B_2 K_0(\Omega_2 r) + \frac{W_0}{\rho_B c_B} \bar{y}(s) \quad (5)$$

$$s\delta\bar{\Theta}_3(s, r) - \Theta_3(0, r) = A_3 I_0(\Omega_1 r) + B_3 K_0(\Omega_1 r)$$

$\bar{\Theta}(s, r)$ représente la transformée de Laplace de $\Theta(t, r)$, et $\Theta(0, r)$ est la solution stationnaire qui a été obtenue par Aoki. De plus, nous avons posé: $\Omega_1 = (s/a_c^2)^{1/2}$ et $\Omega_2 = (s/a_B^2)^{1/2}$. Les coefficients A_1 , B_1 , A_2 , B_2 et A_3 , B_3 sont des fonctions explicites des paramètres connus.

О нестационарной теплопроводности кольцевых цилиндрических тепловыделяющих элементов, охлаждаемых кипящей водой и паром

А. Джаннусис

Величина теплового потока из кольцевого цилиндрического тепловыделяющего элемента может быть просто вычислена из решения нестационарного дифференциального уравнения теплопроводности Фурье, если пренебречь аксиальным тепловым потоком и считать, что колебания давления малы, то есть температура насыщения почти постоянна.

Рассматриваемый элемент состоит из делящегося материала в форме цилиндрического кольцевого канала, покрытого внутри и снаружи металлической оболочкой. Отвод тепла осуществляется за счет кипения воды снаружи элемента и перегрева пара внутри.

Для решения уравнения Фурье воспользуемся методом преобразования Лапласа для относительного изменения теплового потока на поверхности тепловыделяющего элемента и относительного изменения мощности.

Для определения температуры контактирующих поверхностей покрытия и топлива, а также покрытия и охлаждающей среды необходимо знать распределение нестационарных температур в покрытиях $\Theta_1(t, r)$ и $\Theta_3(t, r)$ и в топливе $\Theta_2(t, r)$. Эти температуры являются решениями следующих дифференциальных уравнений с граничными условиями, указанными для каждой зоны:

a) Внешняя оболочка ($r_1 \leq r \leq r_2$)

$$\frac{\partial \Theta_1}{\partial t} = a_c^2 \Delta \Theta_1,$$

$$\text{где } -\lambda_c \left(\frac{d\Theta_1}{dr} \right)_{r=r_1} = \alpha_a(t) [(\Theta_1)_{r=r_1} - \Theta_a],$$

$$(\Theta_1)_{r=r_2} = \Theta_{12} \text{ и } -\lambda_c \left(\frac{d\Theta_1}{dr} \right)_{r=r_2} = -\lambda_B \left(\frac{d\Theta_2}{dr} \right)_{r=r_2}. \quad (1)$$

b) Тепловыделяющий элемент ($r_2 \leq r \leq r_3$)

$$\frac{\partial \Theta_2}{\partial t} = a_B^2 \Delta \Theta_2 + \frac{W(t)}{\rho_B c_B},$$

$$\text{где } (\Theta_2)_{r=r_2} = \Theta_{12} \text{ и } (\Theta_2)_{r=r_3} = \Theta_{23}. \quad (2)$$

c) Внутренняя оболочка ($r_3 \leq r \leq r_1$)

$$\frac{\partial \Theta_3}{\partial t} = a_c^2 \Delta \Theta_3, \text{ где } \lambda_c \left(\frac{d\Theta_3}{dr} \right)_{r=r_1} = \alpha_i(t) [(\Theta_3)_{r=r_1} - \Theta_i],$$

$$(\Theta_3)_{r=r_3} = \Theta_{23} \text{ и } \lambda_c \left(\frac{d\Theta_3}{dr} \right)_{r=r_3} = \lambda_B \left(\frac{d\Theta_2}{dr} \right)_{r=r_3}. \quad (3)$$

где a_B^2 , a_c^2 — коэффициенты теплопроводности в топливе и покрытии соответственно, λ_B , λ_c — коэффициенты теплопроводности, ρ_B и c_B — удельный вес и удельная теплоемкость топлива.

Изменения тепловыделения $W(t)$ предполагаются небольшими, и поэтому их можно представить в виде модифицированных функций Бесселя:

$$W(t) = W_0 [1 + y(t)], \quad (4)$$

где $y(t) \ll 1$. Числа $\alpha_i(t)$ и $\alpha_a(t)$ — коэффициенты теплоотдачи от внутренней и внешней оболочки к охлаждающим средам.

Применив преобразование Лапласа к уравнениям (1), (2) и (3), решив их, получим следующие выражения:

$$\begin{aligned} s\delta\bar{\Theta}_1(s, r) - \Theta_1(0, r) &= A_1 I_0(\Omega_1 r) + B_1 K_0(\Omega_1 r); \\ s\delta\bar{\Theta}_2(s, r) - \Theta_2(0, r) &= A_2 I_0(\Omega_2 r) + B_2 K_0(\Omega_2 r) + \\ &+ \frac{W_0}{\rho_B c_B} \bar{y}(s), \end{aligned} \quad (5)$$

$$s\delta\bar{\Theta}_3(s, r) - \Theta_3(0, r) = A_3 I_0(\Omega_1 r) + B_3 K_0(\Omega_1 r),$$

где $\bar{\Theta}(s, r)$ означает функцию, преобразованную по Лапласу, $\Theta(0, r)$ является распределением температур в стационарном состоянии, как оно дано Аоки. Кроме того $\Omega_1 = \sqrt{s/a_c^2}$ и $\Omega_2 = \sqrt{s/a_c^2}$.

Коэффициенты A_1, B_1, A_2, B_2 и A_3, B_3 выражены как определенные функции известных параметров.

A/569 Grecia

Transmisión de calor en régimen transitorio de elementos combustibles cilíndricos huecos en condiciones de ebullición recalentada

por A. Jannussis

La transmisión de calor de una celda combustible cilíndrica hueca se puede obtener aplicando la ecuación diferencial de conductividad térmica de Fourier correspondiente al caso transitorio, despreciando el flujo axial de calor y admitiendo únicamente variaciones lentas de presión, es decir, operando en la zona cuya temperatura de saturación es aproximadamente constante.

Se considera que la configuración de la celda tiene el material fisible en forma de un anillo cilíndrico cubierto en el interior y exterior por una vaina metálica. La refrigeración se efectúa fluyendo agua hirviendo por el exterior del elemento y haciendo pasar vapor recalentado a través del cilindro interior.

Para resolver la ecuación de Fourier, se utilizará la transformada de Laplace del cambio relativo del flujo térmico a través de la superficie del elemento combustible y del cambio relativo de potencia.

Para determinar la temperatura de las superficies de contacto entre las capas combustibles y las vainas, así como entre la envoltura y medio refrigerador, se necesita conocer la distribución transitoria de temperatura en las capas de la vaina $\Theta_1(t, r)$ y $\Theta_3(t, r)$, y en la región del combustible $\Theta_2(t, r)$. Estas temperaturas son las soluciones de las siguientes ecuaciones diferenciales con las condiciones de contorno que se indican para cada región:

a) Vaina exterior ($r_1 \leq r \leq r_2$)

$$\frac{\partial \Theta_1}{\partial t} = a_c^2 \Delta \Theta_1$$

$$\text{donde } -\lambda_c \left(\frac{d\Theta_1}{dr} \right)_{r=r_1} = \alpha_a(t) [(\Theta_1)_{r=r_1} - \Theta_a],$$

$$(\Theta_1)_{r=r_2} = \Theta_{12} \text{ y } -\lambda_c \left(\frac{d\Theta_1}{dr} \right)_{r=r_2} = -\lambda_B \left(\frac{d\Theta_2}{dr} \right)_{r=r_2} \quad (1)$$

b) Elemento combustible ($r_2 \leq r \leq r_3$)

$$\begin{aligned} \frac{\partial \Theta_2}{\partial t} &= a_B^2 \Delta \Theta_2 + \frac{W(t)}{\rho_B c_B} \text{ donde } (\Theta_2)_{r=r_2} \\ &= \Theta_{12} \text{ y } (\Theta_2)_{r=r_3} = \Theta_{23} \end{aligned} \quad (2)$$

c) Vaina interior ($r_3 \leq r \leq r_1$)

$$\begin{aligned} \frac{\partial \Theta_3}{\partial t} &= a_c^2 \Delta \Theta_3 \text{ donde } \lambda_c \left(\frac{d\Theta_3}{dr} \right)_{r=r_1} \\ &= \alpha_i(t) [(\Theta_3)_{r=r_1} - \Theta_i], \end{aligned}$$

$$(\Theta_3)_{r=r_3} = \Theta_{23} \text{ y } \lambda_c \left(\frac{d\Theta_3}{dr} \right)_{r=r_3} = \lambda_B \left(\frac{d\Theta_2}{dr} \right)_{r=r_3} \quad (3)$$

donde a_B^2, a_c^2 son los coeficientes de difusión térmica en el combustible y la vaina, respectivamente, λ_B, λ_c sus coeficientes de conductividad térmica, y ρ_B y c_B son la densidad del elemento combustible y su calor específico, respectivamente.

Se admite que la variación de potencia $W(t)$ es pequeña, así que puede expresarse como:

$$W(t) = W_0 [1 + y(t)] \text{ donde } y(t) \ll 1 \quad (4)$$

Los números $\alpha_i(t)$ y $\alpha_a(t)$ representan los coeficientes de transmisión de calor de las capas interior y exterior a los medios refrigeradores respectivamente.

Cuando se aplica la transformación de Laplace a las ecuaciones (1), (2) y (3), se obtienen las siguientes soluciones en términos de las funciones de Bessel modificadas:

$$\begin{aligned} s\delta\bar{\Theta}_1(s, r) - \Theta_1(0, r) &= A_1 I_0(\Omega_1 r) + B_1 K_0(\Omega_1 r), \\ s\delta\bar{\Theta}_2(s, r) - \Theta_2(0, r) &= A_2 I_0(\Omega_2 r) \\ &+ B_2 K_0(\Omega_2 r) + \frac{W_0}{\rho_B c_B} \bar{y}(s), \end{aligned} \quad (5)$$

$$s\delta\bar{\Theta}_3(s, r) - \Theta_3(0, r) = A_3 I_0(\Omega_1 r) + B_3 K_0(\Omega_1 r),$$

donde $\bar{\Theta}(s, r)$ representa, en general, la función transformada de Laplace, y $\Theta(0, r)$ es la solución para el caso estacionario, dada por Аоки. Además, $\Omega_1 = \sqrt{s/a_c^2}$ y $\Omega_2 = \sqrt{s/a_c^2}$. Los coeficientes A_1, B_1, A_2, B_2 y A_3, B_3 se expresan como funciones explícitas de parámetros conocidos.

Boiling heat transfer and burn-out mechanism in boiling-water cooled reactors

By K. Torikai, M. Hori, M. Akiyama, T. Kobori and H. Adachi*

Nomenclature

A : total area of the heating surface, (m²)
 A_l : liquid fraction in fluid
 A_v : void fraction in fluid
 ΔA_v : void fraction difference between wall and bubble
 C_p : specific heat, (kcal/kg °C)
 D : diam, (m)
 d : diam, (m)
 G : mass transfer rate, (kg/m²s)
 g : gravity acceleration, (m/s²)
 g_c : unit conversion factor, (9.8 m/s²)
 i : interval of slug bubbles, (m)
 k_l : thermal diffusivity, (m²/s)
 L : latent heat, (kcal/kg)
 l_0 : length of pipe, (m)
 l_1 : mixing length of liquid in turbulence, (m)
 l_v : mixing length of vapour in turbulence, (m)
 q : heat flux, (kcal/m²s or kcal/m²h)
 q' : heat flux on the bubble contact area, (kcal/m²s or kcal/m²h)
 q_{BO} : burn-out heat flux, (kcal/m²s or kcal/m²h)
 R : radius, (m)
 R_b : bubble radius, (m)
 R_c : radius of bubble dry contact area, (m)
 R_e : Reynolds number
 s : slip ratio of velocity
 T : temperature, (°C)
 ΔT_{sat} : superheat degree, (°C)
 ΔT_{sub} : subcooling degree, (°C)
 t : time, (s or m/s)
 u : velocity, (m/s)
 u_b : bubble growth velocity, (m/s)
 u_m : average flow velocity, (m/s)
 u_{mo} : inlet average velocity, (m/s)
 v' : difference from mean velocity in y direction
 y : length, (m)
 γ : specific weight, (kg/m³)
 δ : thickness of liquid film, (m)
 δ' : decrease of thickness of liquid film, (m)
 δ_b : maximum thickness of liquid film, (m)
 η : viscosity, (kg s/m²)
 λ : friction factor of 2 phase flow
 λ_l : thermal conductivity of liquid (kcal/m °C s)
 λ_0 : fluid flow friction factor in smooth pipe
 λ_r : fluid flow friction factor in rough pipe

σ : surface tension, (kg/m)
 τ : shearing stress in fluid, (kg/m²)
 subscripts:
 l: liquid
 v: vapour

HEAT TRANSFER MECHANISM OF BOILING

It is generally believed that the area of contact between bubbles and heating surface hinders heat transfer. On the other hand, Bankoff [1] and Moore [2] assumed that the boiling bubbles do not present a dry but a wet contact with the heating surface through a thin layer of liquid. But this has not been proved, and the idea has remained purely a hypothesis. The authors have undertaken experiments [3] on the adhesion of bubbles on the heating surface with the use of an electro-conductive glass plate, such as that used in a previous experiment on boiling heat transfer under gamma rays (1959) [4]. The test section of the glass plate is coated with a thin film (thickness about 6μ) of SnO₂ (1 cm wide, 30 Ω /cm), as shown in Fig. 1.

The experimental procedure was as follows: First, a part of the glass surface was covered with a thin film, leaving the remaining part dry. At this stage before heating, a photograph was taken from below (Fig. 2). From the resulting photograph—Fig. 3(a)—the dry (a) and wetted (b) parts are clearly distinguishable: The dry part (a) presents incompletely reflected light from the rough (irregularity about 2μ) glass surface, while the wet part (b) registers completely reflected light from the smooth surface. The glass plate is then heated by passing direct current through the conductive film, and again photographed from below—Fig. 3(b). This photograph shows that there are two kinds of areas of bubble adhesion: (a) a part of contact through a thin water layer, and (b) a part of dry direct contact of vapour on the heating surface. Figure 4 relates the ratio between aggregate area of bubble adhesion and total heating surface to bulk water temperature, and shows that at constant heat flux the ratio increases with water temperature. With water temperature as parameter, the ratio increased with heat flux, as shown in Fig. 5.

It is seen also from Fig. 5 that the dry contact part is relatively small compared to the aggregate adhesion area, and even at burn-out flux the ratio is only about 50% (not 100%). Figure 6 illustrates the growth rates

* Japan Atomic Energy Research Institute Tokai-mura.

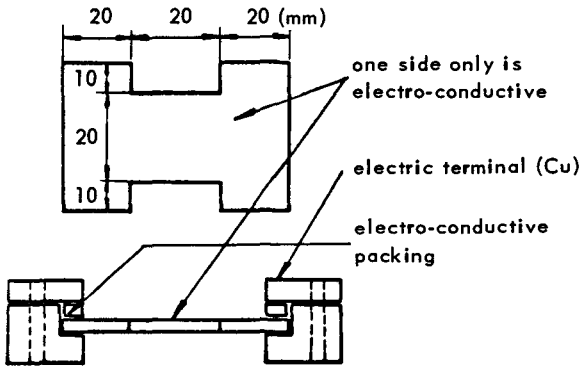


Figure 1. Test piece of electro-conductive glass

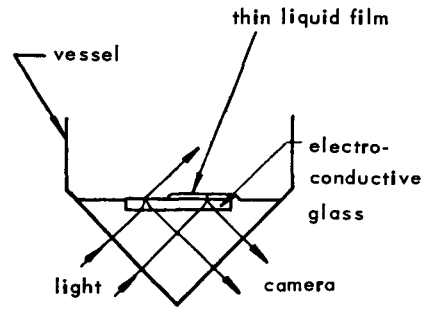


Figure 2. Method of observation of boiling bubble from below



Figure 3. (Above) Photograph from below in non-boiling condition. (a) Dry part; (b) Wet part (thin, liquid film). (Below) Photograph from below in boiling on the horizontal electro-conductive glass. 1: Initial bubbles; 2: During detachment; 3: Dry part; 4: Thin liquid layer. Heat flux: 4×10^5 kcal/m²h. Water temperature 100 °C

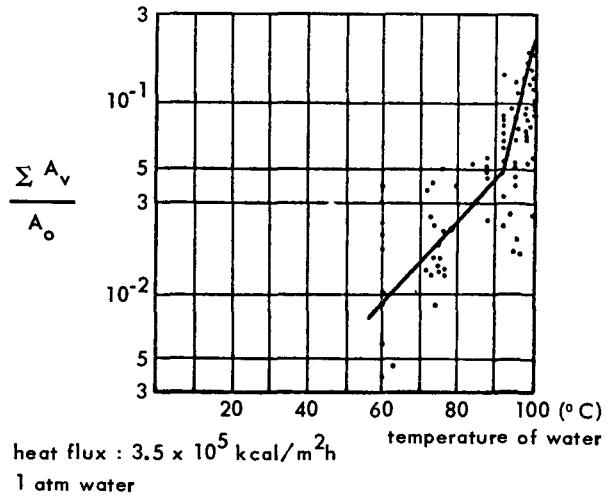
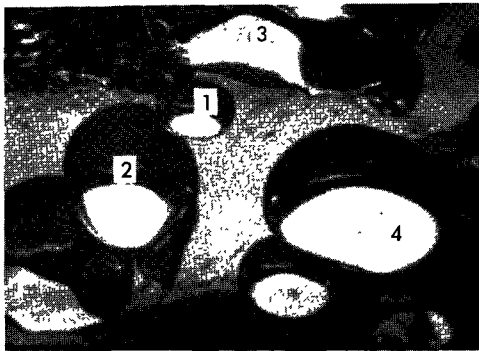


Figure 4. Ratio of bubbles contact area per unit of heating surface ($\Sigma Av/A_o$)

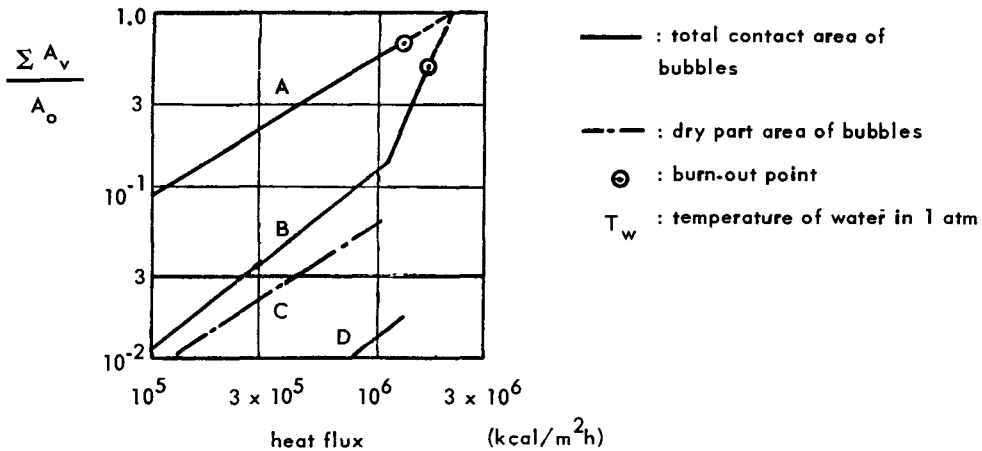


Figure 5. Ratio of bubbles contact area per unit heating surface ($\Sigma Av/A_o$). Curve A: $T_w = 100$ °C; B: $T_w = -70$ °C; c: $T_w = -100$ °C; D: $T_w = -70$ °C

of the aggregate adhesion area and that of dry contact.

We now consider the mechanism of the formation of a thin liquid layer [5]. During bubble growth, the shape of the bubble is roughly a hemisphere due to the inertia of the liquid surrounding the bubble, but as bubble growth rate slows down, the bubble gradually changes to spherical form. In the neighbourhood of the heating surface, the velocity of liquid moved by the bubble is not very large compared to bubble growth rate, and liquid viscosity acts to reduce the velocity to zero at the heating surface, where the thin liquid layer is formed (Fig. 7).

Assuming that: (a) liquid velocity within the thin layer is linear in the direction of layer thickness; (b) liquid flow within the layer is laminar; (c) bubble shape is a hemisphere; (d) layer thickness is determined by the diameter of bubble adhesion area; and (e) layer thickness is zero only at the centre point of bubble adhesion, we obtain as equations of continuity and motion in the thin liquid layer

$$\frac{\partial(2\pi R_u \delta)}{\partial R} = -2\pi R \frac{\partial \delta}{\partial t} \quad (1)$$

$$\frac{2\sigma}{R_b} (1 + K_\delta) = \frac{\eta u}{\delta \frac{\partial \delta}{\partial R}} \quad (2)$$

where

$$\frac{2\sigma}{R_b} K_\delta = \frac{\gamma_e}{g_e} \left(R_b \frac{du_b}{dt} + \frac{3}{2} u_b^2 \right) + 4\eta \frac{u_b}{R_b}$$

If ΔT_{sat} is not very high, $1 \doteq \sqrt{1 + K_\delta}$ (e.g., if $\Delta T_{\text{sat}} = 15^\circ\text{C}$, $\sqrt{1 + k_\delta} = 1.2$, with water of 1 atm and 100°C).

Then

$$\delta^2 \frac{\partial^2 \delta}{\partial R^2} + 2\delta \left(\frac{\partial \delta}{\partial R} \right)^2 + \frac{\delta^2}{R} \frac{\partial \delta}{\partial R} \doteq - \frac{\eta R_b}{2\sigma(1 + k_\delta)} \cdot \frac{\partial \delta}{\partial t}$$

of which a solution is

$$\delta = \delta_b \frac{R}{R_b}, \quad \delta_b = R_b \sqrt{\left(\frac{\eta u_b}{2\sigma(1 + k_\delta)} \right)} \quad (3)$$

If the bubble is not very small, the liquid layer temperature can be regarded equal to the liquid saturation temperature, so that heat conduction in the liquid layer is expressed as

$$\begin{aligned} q' &= \frac{1}{\pi R_b^2} \int_0^{R_b} \frac{\lambda_{\text{sat}}^{\Delta T}}{\delta} 2\pi R \cdot dR \\ &= \frac{2\sqrt{2}\lambda_1 \Delta T_{\text{sat}}}{R_b} \sqrt{\left(\frac{\delta}{\eta u_b} \right)} \sqrt{1 + k_\delta} \end{aligned} \quad (4)$$

from which u_b , q' and δ_b can be calculated (results shown graphically in Fig. 8).

The decrease of thickness of liquid layer by vaporization into the bubble was roughly calculated by the authors [6]:

$$\gamma_e L \frac{d\delta'}{dt} = \frac{\lambda_e^{\Delta T}}{\delta - \delta'} dt \quad (5)$$

$$\delta = \delta' \doteq \sqrt{\left(\frac{2\lambda_e}{\gamma_e L} \right)} \sqrt{(\Delta T_{\text{sat}} \cdot t)} \quad (6)$$

From Eq. (3) the dry contact area is given by

$$\pi R_c^2 \doteq \pi R_b^2 \frac{2\lambda_e}{g_e L} \Delta T_{\text{sat}} \cdot t \quad (7)$$

Calculated values from this equation are represented graphically in Fig. 6, and agree well with measured data. Heat conduction through the aggregate adhesion area can be obtained by simple calculation (dotted line in Fig. 9).

A comparison in Fig. 9 between the dotted line representing heat through the adhesion area and the solid line for total heat flux shows that boiling heat transfer is mainly assured by heat conduction through the thin liquid layer between adhering bubble and heating surface.

EXPERIMENT TO PROVE THE NEW BOILING HEAT TRANSFER MECHANISM

It is known from Moore's experiments that boiling surface temperature changes rhythmically with bubbling, but what directly causes this variation has so far not been made clear. The authors [7] performed an experiment on boiling heat transfer with a heated platinum wire 0.1 mm diam, in which they measured the oscillation of surface temperature by means of high speed camera and oscillograph, while photographing at the same time the boiling vapour and air bubbles. The results are illustrated in Fig. 10 where bubble generation and platinum wire temperature appear registered on the same picture. Figure 11 represents changes in time of bubble diam and ΔT_{sat} decrease versus time, as obtained from Fig. 10, and from these two figures it is seen that: (a) surface temperature changes little prior to bubble generation; (b) decrease of ΔT_{sat} is apparently proportional to the length of contact between bubble and wire; and (c) the drop of ΔT_{sat} at the moment of detachment of bubble from wire is smaller than during bubble growth.

Since the heat capacity of the thin platinum wire is extremely small, the heat transfer coefficient at every instance may be obtained by measuring ΔT_{sat} . When the wire temperature is higher than liquid saturation temperature, the wire temperature is affected by air bubbles as in the case of boiling bubbles. Above all, boiling heat transmission is not so much affected by the agitation caused by the generation and detachment of bubbles around the heating surface as by the formation and vaporization of liquid layers between bubbles and heating surface.

BURN-OUT MECHANISM IN POOL BOILING

In the boiling heat transfer experiments with a glass plate described earlier, the authors observed that: (a) even under high heat flux, boiling bubbles are generated and detach themselves in the normal pattern usually associated only with low heat flux; (b) at times bubbles may coalesce just on the heating surface at a stage where the growth rate has slowed down, as shown in Fig. 12; (c) more often the bubbles coalesce after

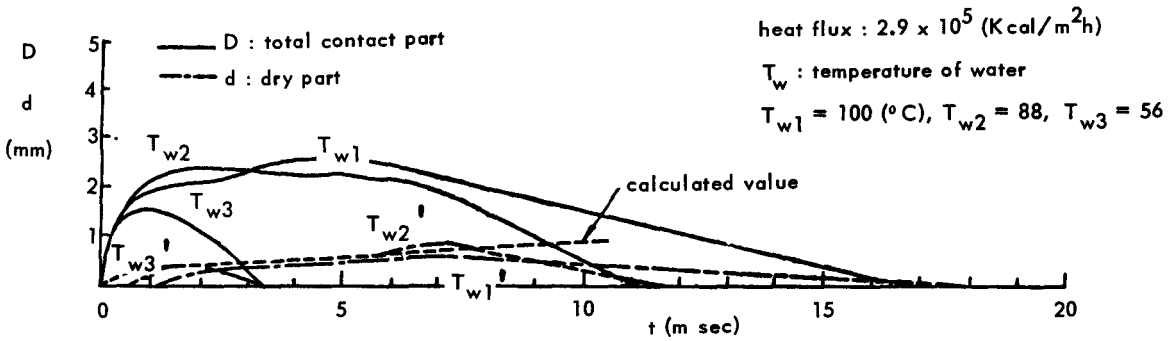


Figure 6. Relation of diameter in total contact part of bubbles and diameter in dry part of bubbles



Figure 7. Contact part of bubble on the heating surface

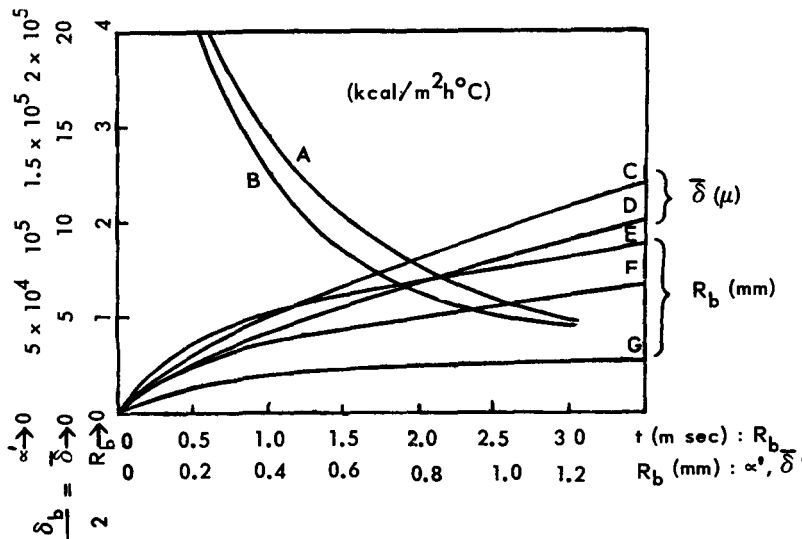


Figure 8. Heat transfer (q') and thickness (δ_b) of bubble contact part and bubble growth (R_b). Curve A: $\gamma \Delta T_{sat} = 5^\circ\text{C}$; B: $\Delta T_{sat} = 10^\circ\text{C}$; C: $\Delta T_{sat} = 10^\circ\text{C}$; D: $\Delta T_{sat} = 5^\circ\text{C}$; E: $\Delta T_{sat} = 10^\circ\text{C}$; F: $\Delta T_{sat} = 5^\circ\text{C}$; G: $\Delta T_{sat} = 5^\circ\text{C}$

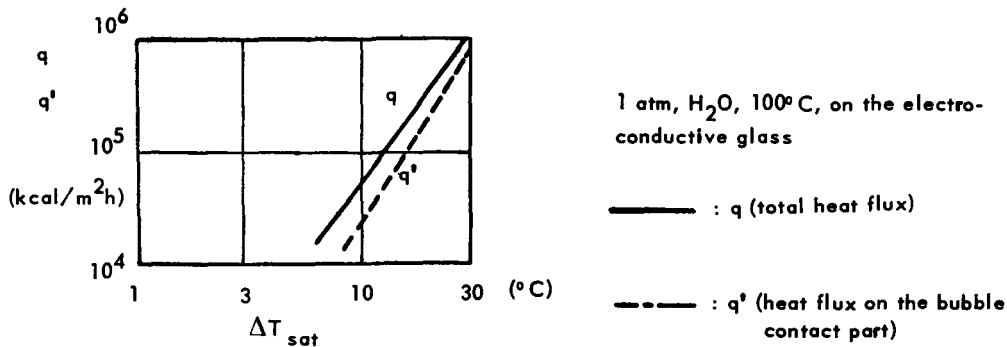
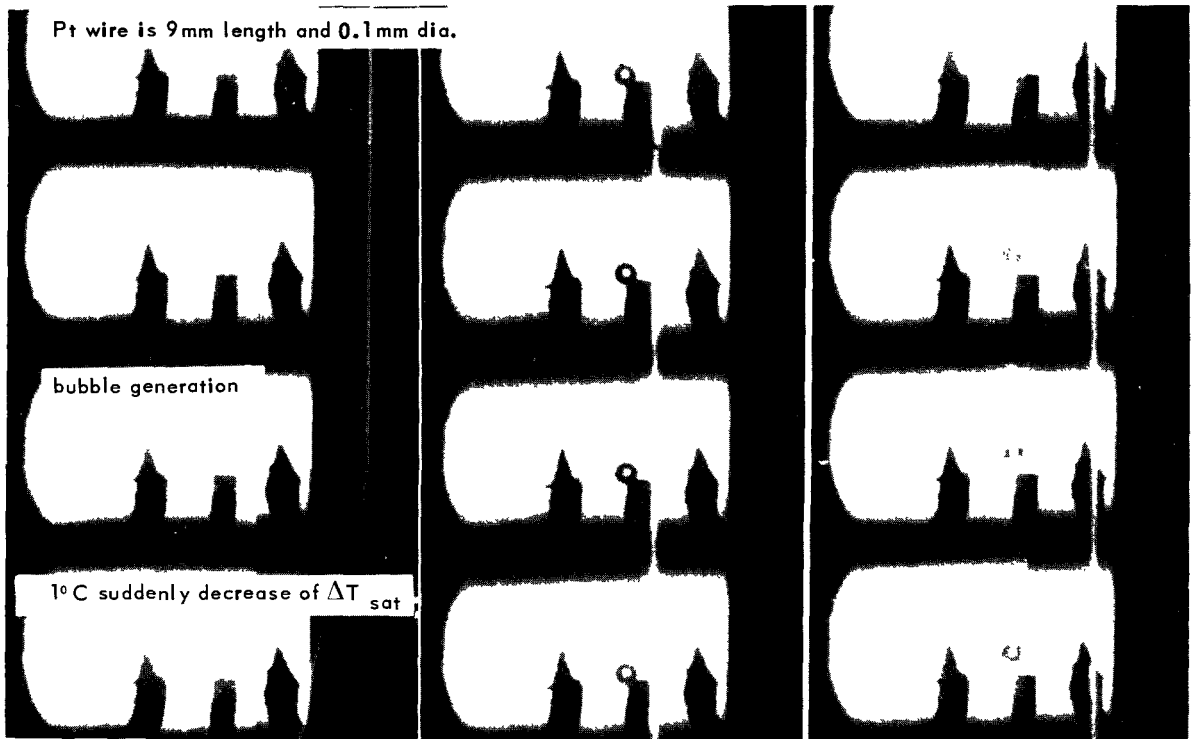


Figure 9. Relation of boiling heat flux and ΔT_{sat}



each interval is 40 parts

speed : 1 msec per 4 parts

$q = 5.4 \times 10^5 \text{ kcal/m}^2\text{h}$

Figure 10. Photographs of bubble growth and oscillograph of decrease of ΔT_{sat} by high pressure speed camera

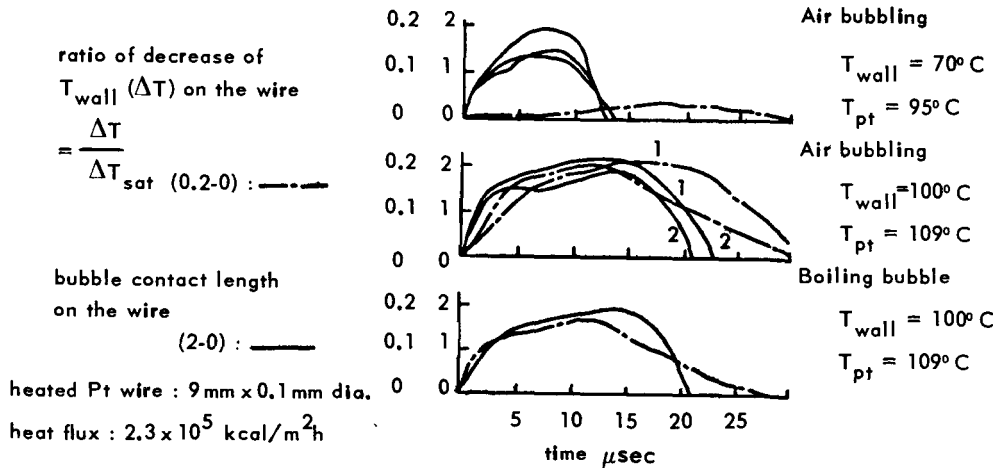


Figure 11. Relation of bubble contact length and ratio of decrease of ΔT_{sat} of the heated Pt wire

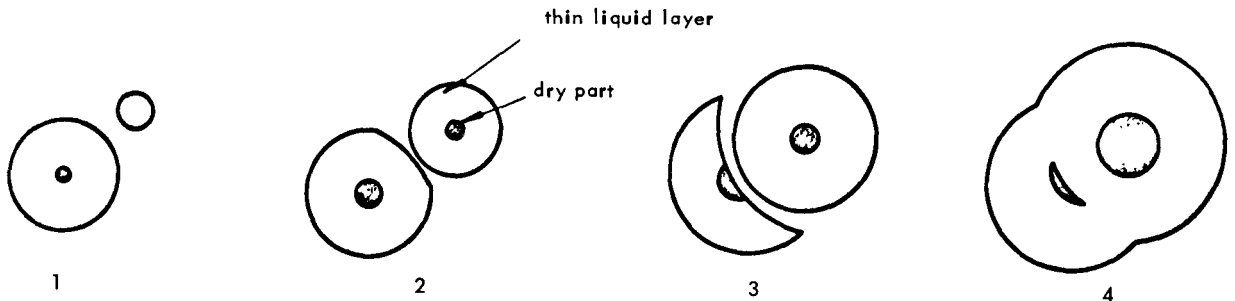


Figure 12. Process of boiling bubbles collaboration on the heating surface

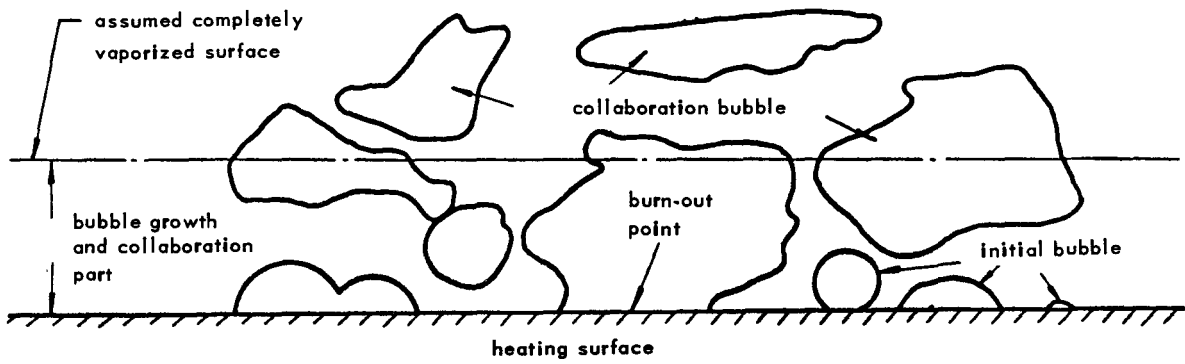


Figure 13. Schematic figure of high heat flux boiling from side

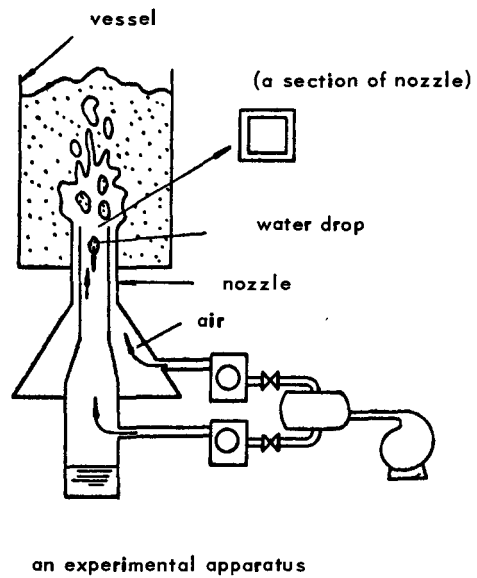
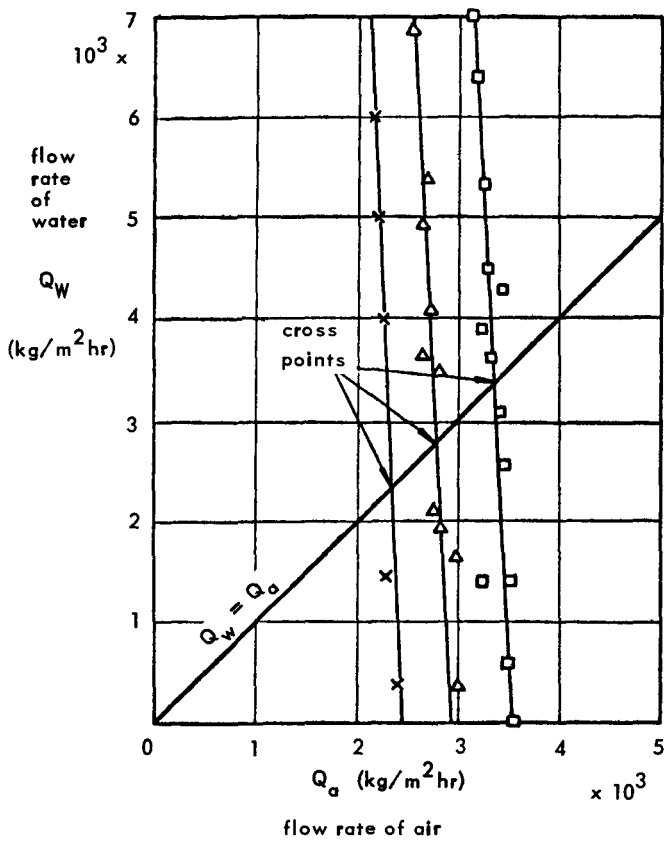


Figure 14. An experiment of counter flow of water and air

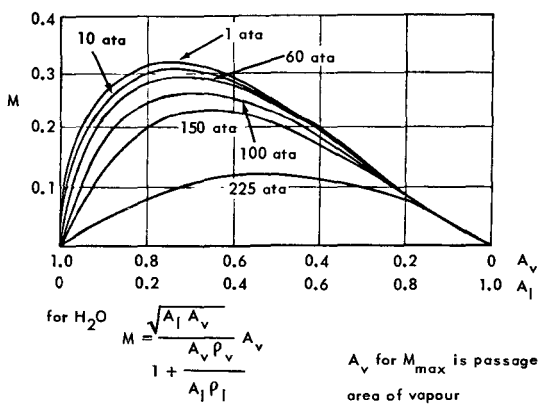


Figure 15. Relation of passage area of fluid and M

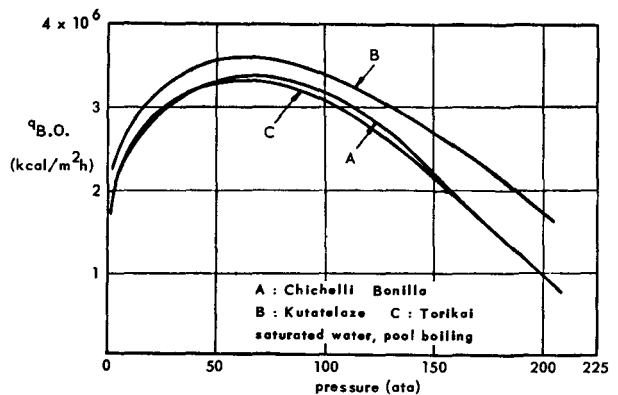


Figure 16. Relation of burn-out heat flux and pressure

detachment from the heating surface, as shown in Fig. 13, and constitute new bubbles, more similarly to the case of film boiling; and (d) even in the region of nucleated boiling, some amount of film boiling conducive to burn-out is produced when the heating surface is covered by agglomerated bubbles for periods longer than bubble generating time, as in Fig. 13. Thus burn-out in pool boiling is induced by the motion of the aggregate bubbles. The authors [8] analysed and studied the motion of vapour and water in pool boiling over a horizontal heating surface by simulation to a counter-flow movement between vapour generated by boiling and liquid necessary for boiling, in a manner such as produced by flooding.

The experiment was carried out on a counter-flow produced between air and water in the vicinity of the axis of the inner barrel of a double-walled nozzle such as shown in Fig. 14. The figure also gives experimental results, and points are indicated therein where the characteristic curves of water and air flows cross the curve of equal flow of air and water, marking the limiting points for counter-flow. The points correspond to the flow of vapour generated from the heating surface at burn-out heat flux. Below these cross points enough water would not be available to sustain the vaporization. From the results of this experiment the burn-out heat flux equation was derived.

$$q_{BO} = 0.43 \cdot g_c^{\frac{1}{2}} \cdot g^{\frac{1}{2}} \gamma^{\frac{1}{2}} L \{ \sigma (\gamma_e - \gamma_v) \}^{\frac{1}{2}} M \max \quad (8)$$

It will be noted that while this equation has not been obtained from an actual boiling heat transfer experiment, it has the same form as the equation derived from the boiling experiment by Kutateladze [9], with the difference that Eq. (8) possesses a term for M_{\max} representing the maximum value of M in Fig. 15. A_v of the same figure, for obtaining M_{\max} is the ratio of the vapour passage area to the total heating surface. Equation (8) has been compared with a large number of data from actual boiling experiments, especially those by Cichelli and Bonilla [10], as shown in Fig. 16, and as a result it is concluded that the limiting conditions of counter-flow between vapour and water in boiling constitute a major factor in burn-out.

BURN-OUT MECHANISM IN FORCED CONVECTION

The authors [11] considered that in the case of forced convection, as in the case of pool boiling, burn-out is caused by shortage at the heating surface of water necessary for boiling. In a vertical heating surface the generated vapour is diffused* by turbulence of the flow as well as by the ejection of bubbles from the heating surface by the inertia of bubble growth, as described by Isshiki [12]. The authors introduced a new variable mixing length l (the actual value of which is quite similar for both material diffusion and momentum transfer), with which each phase in the

* Diffusion in the sense that vapour moves from near the heating surface toward the main flow.

two-phase flow was analysed as in the case of uniform flow:

$$\left. \begin{aligned} \tau_l &= \gamma_l l \frac{\partial u_e}{\partial y} V_l' \frac{1}{g_c} \\ \tau_v &= \gamma_v l_v \frac{\partial u_v}{\partial y} V_v' \frac{1}{g_c} = p_v l_v s \frac{\partial u_e}{\partial y} V_v' \frac{1}{g_c} \\ \tau &= \tau_l A_l + \tau_v A_v = \lambda \frac{u_m^2}{8} \gamma \frac{1}{g_c} \end{aligned} \right\} \quad (9)$$

From the continuity of vapour and liquid,

$$\left. \begin{aligned} G_l &= \gamma_l l \frac{\partial A_l}{\partial y} V_l \\ -G_l &= G_v = G = \gamma_v l_v \frac{\partial A_v}{\partial y} V_v' = -\gamma_v l_v \frac{\partial A_l}{\partial y} V_v' \end{aligned} \right\} \quad (10)$$

Therefore

$$\gamma_l l V_l' = \gamma_v l_v V_v = \gamma l_v' = \frac{\lambda \cdot \frac{u_m^2}{8}}{\left(\frac{\partial u_l}{\partial y} \right) (A_l + S A_v)} \quad (11)$$

From Eqs. (10) and (11):

$$G = \gamma l \left(\frac{\partial A_l}{\partial y} \right) V' = \lambda \frac{u_m^2}{8} \cdot \frac{1}{A_l + S A_v} \cdot \frac{\left(\frac{\partial A_l}{\partial y} \right)}{\left(\frac{\partial u_l}{\partial y} \right)} \quad (12)$$

If $\left(\frac{\partial A_l}{\partial y} \right) / \frac{\partial u_l}{\partial y} = \Delta A_v / u_m$ and $s = 1$,

$$G(L + C_p T_{\text{sub}}) = q = u_m \gamma l \frac{\lambda}{8} \Delta A_v (L + C_p \Delta T_{\text{sub}}) \quad (13)$$

If $\Delta A_v = 1 - \bar{A}_v$ and q assumes its maximum value, i.e., the burn-out heat flux q_{BO} , the heating surface is completely covered by a vapour curtain. Here λ is an unknown factor. The authors [13] devised an experimental facility for measuring λ with forced circulation boiling under maximum conditions of 225 ata pressure, 340°C and 300 l/min flow, with pumping head up to 10 ata. The results of experiment, as represented in Fig. 18, indicate that λ is not very different from the friction coefficient λ_0 in uniform flow, and particularly in the case of high flow rate, it assumes the value λ_r related to the case of a rough pipe.

The next unknown factor is A_v . In the presence of subcooling, Poletavkin [14] has given the equation for void in boiling forced circulation above 7 atm. Using this to calculate the burn-out heat flux with subcooling and also, from Eq. (13) we obtained the results given in Fig. 19, which agree well with experimental data on burn-out. The agreement would be further improved by the insertion of true values of λ instead of the λ_r used here in all cases, but truly applicable only to high flow rate. The calculation of burn-out heat flux under saturation conditions, however, is not simple, since in such cases the void fraction follows the two-phase flow pattern, which is not yet clearly understood.

In forced circulation boiling, oscillations are often experienced in the vapour generation rate, pressure

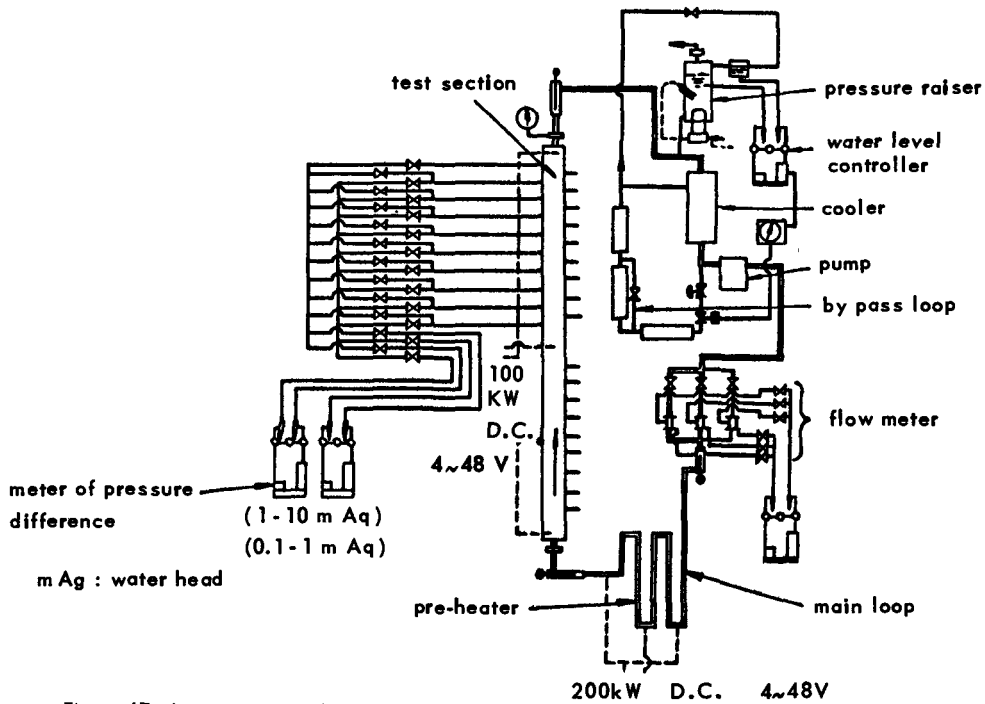


Figure 17. An experimental apparatus for fluid flow resistance in forced circulation boiling

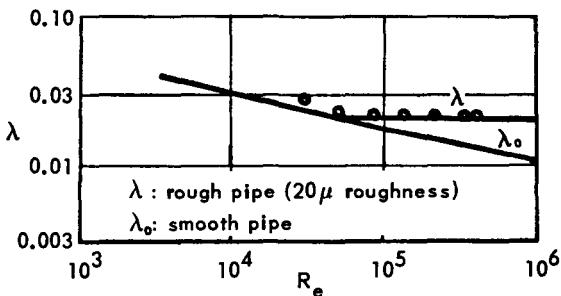


Figure 18. Fluid flow friction factor in boiling

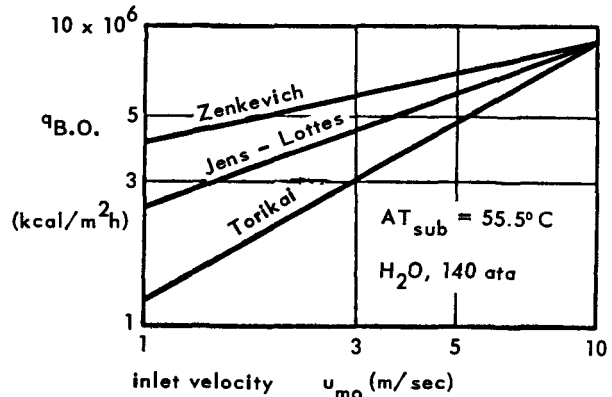


Figure 19. Burn-out heat flux in forced circulation at subcooling

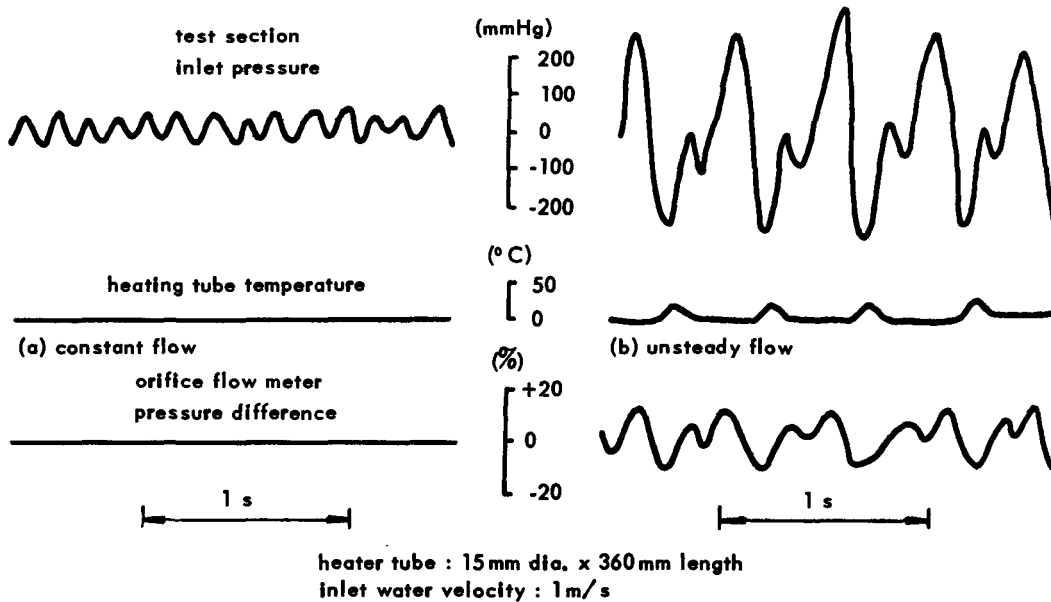


Figure 20. Two types of two-phase flow oscillation in forced circulation boiling

and flow rate. The authors [15] observed this oscillating phenomenon with an apparatus at atmospheric pressure, which could reveal a stronger effect of void than at high pressure. For the experiment, the authors also developed a new type of void meter [16] incorporating two electro-magnetic flow meters, one each at the inlet and outlet of the test section.

The oscillographic records of the experiment (Fig. 20) indicate that oscillations of pressure occur even under constant flow with low void, not to mention the case where there are oscillations in flow rate, when large oscillations of pressure of several cycles per second are observed.

The oscillations are particularly violent in the case of slug flow, and the authors [17] conducted separate experiments, which determined that the distance between slug bubbles were regular and could be expressed by

$$i = \frac{l_0}{n + \frac{1}{2}}, \quad n = 1, 2, 3. \quad (14)$$

Under boiling conditions the slug bubbles collapsed from subcooling at the test section outlet [18]. It was observed [19] also that the resulting shock waves, propagating at the speed of sound, caused other bubbles to collapse in their turn in succession as they encountered the waves. It was, however, found that with constant flow and low void, no oscillations occurred at the heating surface which were so great as to cause burn-out. This means that the foregoing analysis of burn-out heat flux is also applicable to the case of constant flow and low void.

ACKNOWLEDGEMENTS

The authors wish to express their appreciation of the useful discussion on the present work provided by

Prof. H. Tachibana, as well as of the valuable collaboration by Mr. T. Yamazaki.

REFERENCES

1. Bankoff, S. G. *et al.*, Jet Propulsion Lab., Memo 20-137 (1956).
2. Moore, F. D., and Mesler, R. B., Amer. Inst. Chem. Eng., 7, No. 4, 620/624 (1961).
3. Torikai, K., and Yamazaki, T., Preprint of Meeting of Nuclear Power Engineering held by JSME, 2/7 (1963).
4. Torikai, K., Akiyama, M., and Yamazaki, T., Proceedings of the 3rd Symposium on Atomic Energy, 365/368 (1959).
5. Torikai, K., Preprint of Meeting of Heat Transfer held by JSME 89/92 (1963).
6. Torikai, K., and Yamazaki, T., Preprint of Meeting of Nuclear Power Engineering held by JSME, 17/20 (1964).
7. Torikai, K., and Yamazaki, T., Preprint of Meeting of Heat Transfer held by JSME, 85/88 (1963).
8. Torikai, K., Preprint of Annual Meeting held by JSME, Heat Transfer part No. 25, 77/80 (1960).
9. Kutateladze, S. S., AEC report, AEC-tr-3770 (1951).
10. Cichelli, M. J., and Bonilla, C. F., Amer. Inst. Chem. Eng. J., 41, 755/787 (1945).
11. Torikai, K., Proposed Paper for AESJ (1961).
12. Isshiki, N., and Tamaki, H., Journal of JSME, 65, No. 525, 1393/1403 (1962).
13. Torikai, K., Hori, M., and Yamazaki, T., Journal of AESJ, 2, No. 1, 671/681 (1961).
14. Poletavkin, P. G. *et al.*, UKAEA report AERE. Lib/Trans. 804 (1958).
15. Torikai, K., Hori, M., and Ouchi, Y., Preprint of 1962 National Nuclear Congress, Tokyo, 202 (1962).
16. Kobori, T., Hori, M., Ouchi, Y., and Kikuchi, A., Preprint of Meeting of Nuclear Engineering held by AESJ, No. 19, 19 (1963).
17. Adachi, H., and Torikai, K., Preprint of Meeting of Nuclear Power Engineering held by JSME, 5/8 (1964).
18. Akiyama, M., Preprint of Meeting of Nuclear Power Engineering held by JSME, 15/21 (1963).
19. Hori, M., and Ouchi, Y., Preprint of Meeting of Nuclear Power Engineering held by JSME, 9/13 (1963).

ABSTRACT—RÉSUMÉ—АННОТАЦИЯ—RESUMEN

A/580 Japan

Transfert de chaleur à l'ébullition et mécanisme de caléfaction dans les réacteurs à eau bouillante

par K. Torikai *et al.*

Depuis 1956 des recherches expérimentales et théoriques ont été faites à l'Institut de recherches nucléaires du Japon, sur le transfert de chaleur et l'écoulement du fluide de refroidissement dans les réacteurs à eau bouillante.

Le phénomène de caléfaction, un des plus importants problèmes de l'évacuation de la chaleur des réacteurs refroidis par un liquide, est discuté dans ce rapport. On y a étudié les causes de la caléfaction et le flux de chaleur de caléfaction dans ses relations avec le taux élevé de transfert de chaleur de l'eau bouillante ainsi que le phénomène de l'écoulement à deux phases.

Durant les études d'ébullition en piscine, on a

cherché à déterminer le taux d'accroissement des bulles avec un faible flux de chaleur: les valeurs obtenues lors des expériences ont été les mêmes que celles données par les études théoriques. Pour un flux de chaleur élevé, on a observé le comportement des bulles et les variations de température à la surface de chauffe avec le temps, grâce à un réchauffeur de verre transparent conducteur d'électricité. On a trouvé que l'adhérence des bulles à la surface chauffante avait tendance à augmenter plutôt qu'à réduire le taux de transfert de chaleur. On en conclut que la caléfaction dans les piscines bouillantes est causée non par le fait que la surface chauffante est couverte de bulles, mais par le mouvement de bulles combinées et agrandies près de cette surface. Cela a ouvert la possibilité de prévoir le flux de chaleur de caléfaction dans le cas de l'ébullition en piscine, à partir d'une analyse du mouvement des bulles, et les résultats prévus ont été confirmés par les expériences.

On a également effectué des expériences sur la caléfaction pour les canaux d'écoulement du fluide de refroidissement. Aux valeurs proches de la caléfaction, le flux, la pression, le taux d'émission de vapeur et la vitesse d'écoulement ont présenté, à l'observation, un phénomène d'oscillation. Grâce à une analyse de ces phénomènes, il a été établi que la capacité thermique du réchauffeur et les caractéristiques d'écoulement des boucles, comme les caractéristiques des pompes, étaient également des facteurs importants, influençant la caléfaction. L'oscillation de l'écoulement a été étudiée plus à fond, à la fois expérimentalement et théoriquement, du point de vue du phénomène de l'écoulement à deux phases.

A/580 Япония

Теплопередача при кипении и кризис теплообмена в реакторах, охлаждаемых кипящей водой

К. Торикан *et al.*

С 1956 года в Японском исследовательском институте по атомной энергии проводятся экспериментальные и теоретические исследования по теплоотдаче и гидродинамике в реакторах, охлаждаемых кипящей водой.

В этом докладе обсуждается кризис теплообмена, представляющий собой одну из самых важных проблем теплоотдачи в кипящих реакторах. Исследовались причины возникновения кризиса теплообмена и критических тепловых нагрузок и их связи с коэффициентом теплоотдачи к кипящей воде и структурой двухфазного потока.

При изучении кипения в большом объеме исследовалась скорость роста пузырей при низкой тепловой нагрузке; экспериментальные данные хорошо согласуются с теорией. Для высоких тепловых нагрузок применение прозрачного стеклянного электропроводного нагревателя позволило вести наблюдения за режимом пузырей и за изменениями температуры поверхности нагрева. Было установлено, что сцепление пузырей на поверхности нагрева проявляет тенденцию к увеличению при уменьшении скорости теплоотдачи. Отсюда делается вывод, что кризис теплообмена при кипении в большом объеме вызывается не тем, что поверхность нагрева покрывается пузырями, а создается движением больших пузырей около этой поверхности. Это открыло возможность предсказывать критические тепловые нагрузки в большом объеме на основании анализа движения пузырей. Предсказанные результаты были подтверждены опытом.

Также проводились эксперименты по определению критических тепловых нагрузок в каналах. При нагрузках, близких к критическим, были проведены наблюдения за изменениями давления, скорости парообразования и расхода,

которые имели колебательный характер. Из анализа опытных данных было установлено, что теплоемкость обогревателя, гидродинамические характеристики контура и насоса являлись важными факторами, влияющими на значение критической нагрузки. В дальнейшем были исследованы экспериментально и теоретически нульсация расхода с точки зрения явления двухфазного потока.

A/580 Japan

Transmisión de calor y mecanismo del quemado destructivo en los reactores refrigerados por agua en ebullición

por K. Torikai et al.

Desde 1956, la transmisión de calor y la hidráulica de los reactores refrigerados por agua en ebullición se han estudiado teórica y experimentalmente en el Instituto de Investigaciones Nucleares del Japón.

Se discute en esta memoria el fenómeno del quemado destructivo, que es uno de los problemas más importantes de transmisión de calor en los reactores de agua en ebullición. Se han estudiado las causas del quemado destructivo y los flujos de calor durante el mismo, en cuanto se relacionan con la elevada capacidad de transmisión de calor del agua en ebullición así como con el fenómeno del flujo en dos fases.

Durante los estudios de ebullición en tanque abierto, se investigó la velocidad de crecimiento de las burbujas para flujos de calor bajos: los valores experimentales se aproximan bastante a los teóricos. A flujos elevados de calor se observaron, gracias a un dispositivo calefactor transparente de vidrio conductor, el comportamiento de las burbujas y la variación de la temperatura en la superficie calefactora. Se encontró que la adherencia de las burbujas a la superficie calefactora tendía a aumentar, en vez de a reducir, la transmisión del calor. Se deduce la conclusión, por consiguiente, de que la causa del quemado destructivo en tanques abiertos no es el que la superficie calefactora se cubra de burbujas, sino el movimiento en las proximidades de la superficie de las burbujas agrupadas y agrandadas. Ello permite predecir el flujo de calor durante el quemado destructivo en tanques abiertos mediante el análisis del movimiento de las burbujas; los resultados predichos fueron confirmados por la experiencia.

Se llevaron también a cabo experimentos de quemado destructivo en canales de refrigeración. Se observó que cerca del flujo crítico la presión, la producción de vapor y la velocidad del fluido se convertían en fenómenos oscilatorios. Al analizar dichos fenómenos, se estableció que la capacidad calorífica del elemento calefactor y las propiedades hidráulicas del circuito, tales como las características de las bombas, eran también factores importantes que afectaban al quemado destructivo. Las oscilaciones del caudal del refrigerante se estudiaron más a fondo, tanto teórica como prácticamente, desde el punto de vista del flujo de fluidos en dos fases.

The mechanism of nucleate boiling

By C. J. Rallis and H. H. Jawurek*

Before the full potential of boiling as a means of heat transfer can be realised it is necessary to have an understanding of its basic mechanism. Particularly is this the case in nuclear reactor applications where systems are complex and the risk of failure must be kept low. General design equations for the rate of heat transfer under such conditions are not currently available due to inadequate knowledge of the fundamental processes involved.

This paper reports work aimed at the elucidation of these fundamentals, and reviews the contributions made by the Boiling Heat Transfer Group at the University of the Witwatersrand.

An attempt was made to approach the problem in a direct manner. Only the simplest case of boiling, that is, nucleate boiling under saturated pool conditions, is dealt with. A thorough treatment of this case is considered a prerequisite to a more advanced study of boiling.

NOMENCLATURE

- A : heat transfer area, (ft²)
 D_d : equivalent spherical bubble diameter at departure, (ft)
 \bar{D}_{da} : arithmetic mean of D_d
 f : bubble frequency, s^{-1} or h^{-1}
 f_i : bubble frequency of individual source, s^{-1} or h^{-1}
 \bar{f} : mean of f_i
 \bar{f}_a : arithmetic mean of f_i
 $\bar{f}\bar{V}_d$: arithmetic mean of products of $f_i V_{di}$
 G_d : mass velocity of vapour in departing bubbles, (lb_m/h ft²)
 n : number of bubble sources on heat transfer surface
 $N = n/A$: bubble source concentration, (ft⁻²)
 N^o : nucleation site concentration, (ft⁻²)
 P_L : liquid pressure, atm.
 $(q/A), (q/A)_{tot}$: total heat flux, (Btu/h ft²)
 $(q/A)_{LH}$: latent heat transport, defined by Eq. (1), (Btu/h ft²)
 $(q/A)_{NC}$: natural convection flux, (Btu/h ft²)
 r_{max} : mouth radius of largest potentially active cavity, (ft)
 r_{max}^* : mouth radius of largest active cavity, (ft)

- r_{min}^* : mouth radius of smallest active cavity, (ft)
 T_{sat} : saturation temperature of liquid, (°R)
 T_w : heater wall temperature, (°R)
 ΔT_{sat} : ($T_w - T_{sat}$), (°R)
 V_d : bubble volume at departure, (ft³)
 V_{di} : bubble volume at departure for a particular source, (ft³)
 \bar{V}_d : mean of V_{di}
 \bar{V}_{da} : arithmetic mean of V_{di}
 v_v : specific volume of vapour, (ft³/lb_m)
 δ : limiting thermal boundary layer thickness, (ft)
 λ_v : latent heat of vaporization, (Btu/lb_m)
 ρ_v : vapour density, (lb_m/ft³)
 σ : surface tension, lb_f/ft

Latent heat transport

During saturated boiling, heat may be considered to leave a surface via two components: the first is transferred to the liquid by convection, later to manifest itself in bubble growth after departure and in evaporation at the free liquid surface; the second causes formation and growth of bubbles up to the point of their departure. The latter component is termed latent heat transport, and is defined as

$$(q/A)_{LH} = \rho_v \lambda_v \sum_{i=1}^n f_i V_{di} / A \quad (1)$$

with properties evaluated at the saturated state corresponding to the liquid pressure.

For many years it was generally held that in nucleate boiling, whether sub-cooled or saturated, the contribution of the latent heat transport to the total flux was negligible. Gunther and Kreith [1], also Rohsenow and Clark [2], had shown this to be the case in sub-cooled boiling. The latter, as well as many subsequent workers, considered these results to be equally applicable to saturated boiling. This view has resulted in a plethora of mechanisms and correlations for the rate of heat transfer, all based on the convective component alone. Adequate reviews of these have been published [3, 4].

This application of findings on sub-cooled boiling to saturated boiling was, in the absence of experimental justification, considered an unacceptable extrapolation. In consequence a programme was initiated to investigate the contribution of latent heat transport in saturated pool boiling, the first results of which were

* Department of Mechanical Engineering, University of the Witwatersrand, Johannesburg.

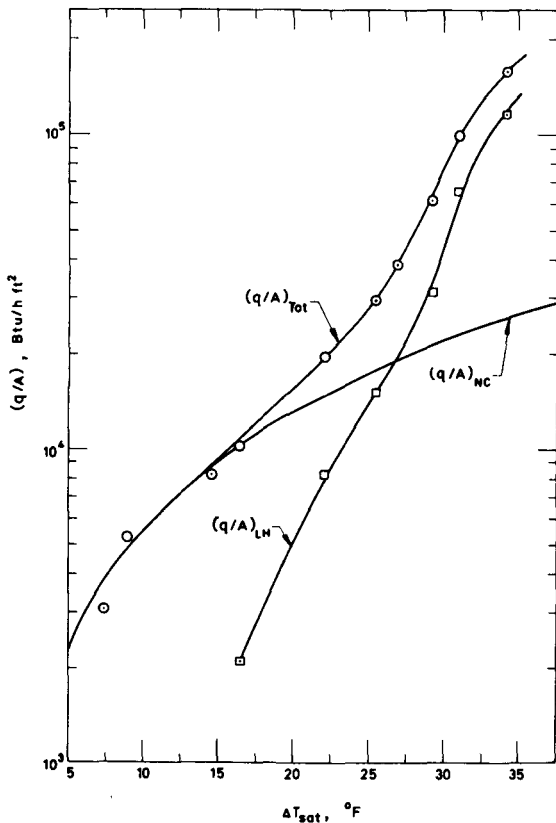


Figure 1. Boiling curve for water also showing latent heat transport and extrapolated natural convection curve

published in 1961 [5]. These preliminary results showed that, for water boiling at atmospheric pressure, latent heat transport was at no stage negligible, and appeared to be the sole contributor at the peak flux. Data on ethanol showed the same trend.

Subsequently these studies were continued after refining the apparatus and experimental techniques [6]. Boiling took place from an electrically heated nickel wire of 0.02 in diam, immersed in a stagnant pool of water at saturation point and at atmospheric pressure. Electrical and thermometric measurements allowed the determination of (q/A) and ΔT_{sat} . Motion pictures of the test section and bubbles provided measurements of bubble departure volume, V_d , and bubble frequency, f .

In the flux range investigated, vapour emanation occurred in the form of discrete bubbles (isolated or coalesced on the surface). Continuous vapour columns or jets, as observed on flat plates even at moderate fluxes, were absent. The number of bubble sources was defined as the number of surface localities from which bubbles departed. At low fluxes, in the regime of isolated bubbles, the number of nucleation sites equals the number of bubble sources; at higher fluxes, however, where lateral coalescence of bubbles occurs, this ceases to be valid.

The resulting boiling curve, $\log(q/A)$ against ΔT_{sat} , and the latent heat transport, as calculated from Eq. (1), are shown in Fig. 1. The natural convection curve

is correlated and extrapolated by an equation of the form $(q/A)_{\text{NC}} = \text{const. } \Delta T_{\text{sat}}^{\frac{1}{2}}$. The percentage contribution of latent heat transport to the total flux is plotted against total flux in Fig. 2. This contribution increases smoothly with flux; at the peak flux (not measured but about 4 to 6×10^5 Btu/h.ft²) it alone might represent the total flux.

It was stated earlier that convection (natural and bubble-induced) and latent heat transport together account for the total flux, other mechanisms being considered inoperative or negligible. This view is substantiated as follows: with respect to disturbance of the thermal boundary layer, the area of influence of one bubble source is small, corresponding to approximately two bubble diameters [7]. Thus, in the region of very low bubble source concentration, the convection mechanism may be roughly approximated by one of undisturbed natural convection. Thus, for the first two low-flux determinations shown in Fig. 2, the percentage convection contribution is obtained from extrapolated natural convection data. The sum of the contribution from latent heat transport and convection is close to 100 per cent within the estimated experimental error bounds. It is felt that the small discrepancy is due to the neglect of bubble-induced convection.

Evidently the two main contributions to the total flux require further investigation. Many workers appear to be dealing with the convection component. Our group has, to date, tended to concentrate attention on the rather neglected latent heat transport component.

By definition, a study of this involves investigations into (a) bubble departure volume and frequency, and (b) bubble source concentration, i.e. nucleation and coalescence. These inevitably also have a bearing on any bubble-induced convection mechanism.

The remainder of this paper reports studies into (a) and (b).

Bubble frequency and departure volume

Consider boiling with discrete bubble formation (i.e. no continuous vapour jets) on a surface of area A

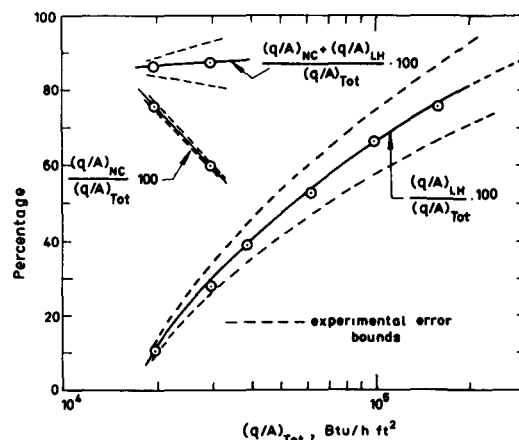


Figure 2. Latent heat transport and convection as percentages of total heat flux

having n bubble sources. At a particular flux and pressure the bubble frequency and successive departure volumes for a particular source i (where $i = 1, 2, \dots, n$) are not constant. The variation is generally not large, but is significant. Let f_i and V_{di} be the mean values, over a period of time, of bubble frequency and departure volume of a source i . Different sources produce bubbles with different values of f_i and V_{di} , which are statistically distributed about means.

It has been general practice to report frequency and volume data in terms of arithmetic means of f_i and V_{di} , i.e. as \bar{f}_a and \bar{V}_{da} . Data indicate that at a fixed pressure both \bar{f}_a and \bar{V}_{da} are flux independent except in the vicinity of the peak flux. The resulting relation

$$\bar{f}_a \cdot \bar{V}_{da} = \text{const.} \quad (2)$$

is well known.

However, the purpose of studying bubble frequencies and volumes is to determine the mass velocity of departing vapour, G_d , fundamentally defined as

$$G_d = \sum_{i=1}^n (f_i V_{di}) \rho_v / A \quad (3)$$

since the actual latent heat transport is given by

$$(q/A)_{LH} = G_d \lambda_v \quad (4)$$

This mass velocity is also required for any formulation of a bubble Reynolds number, to be used if correlation based solely on a convection mechanism is to be attempted.

G_d can also be expressed in terms of mean frequencies and departure volumes, \bar{f} and \bar{V}_d :

$$G_d = (n/A) \bar{f} \cdot \bar{V}_d \rho_v = \sum_{i=1}^n (f_i V_{di}) \rho_v / A \quad (5)$$

Clearly Eq. (5) permits any definition of one of the two parameters \bar{f} and \bar{V}_d ; the definition of the other is then fixed. Thus it is possible to derive a consistent mean \bar{V}_d if \bar{f} is chosen as the arithmetic mean, and vice versa. The use of both as arithmetic means is not permissible if the equality in Eq. (5) is to be maintained. This matter has been considered in detail elsewhere [8]. It is preferable not to separate f and V_d , but

rather to define the mean product

$$\bar{fV} = \sum_{i=1}^n (f_i V_{di}) / n \quad (6)$$

and hence G_d as

$$G_d = (n/A) \bar{fV}_d \rho_v = \sum_{i=1}^n (f_i V_{di}) \rho_v / A \quad (7)$$

The product $\bar{f}_a \bar{D}_{da}$ or $\bar{f}_a \bar{V}_{da}$ which is flux independent finds no application in boiling work. The product \bar{fV}_d , however, varies with flux as shown in Fig. 3.

Theoretical work, mainly of a hydrodynamic nature, is necessary to predict the variation of fV_d with physical properties, flux and pressure.

An additional outcome of the fV_d study has been the finding that, at fixed flux and pressure, each bubble source on the surface exhibits the same value of the product $f_i V_{di}$ within reasonable statistical scatter, i.e.

$$f_i V_{di} = \text{const.} \quad (8)$$

See Fig. 4. It is felt that the scatter is due to shortcomings of the ciné technique which did not allow the establishment of a good time average for each determination of $f_i V_{di}$. Even so, correlation coefficients ranging from 0.83 to 0.92 were obtained for five different flux settings, with the sixth low-flux determination of somewhat irregular patch boiling yielding 0.67. The correlation coefficients can be considered significant, since the underlying f_i and V_{di} data were reasonably normally distributed.

The significance of the foregoing is that with boiling on a surface, each source over a period of time produces the same mass of vapour; that is, if $f_i V_{di}$ is a good time average, then

$$f_i V_{di} = \bar{fV}_d \quad (9)$$

The deeper significance of this behaviour is being studied.

Bubble sources and nucleation

Nucleation proceeds from vapour entrapped in microscopic surface cavities. This has been demonstrated both analytically and experimentally [9, 10, 11, 12]. Evidence of this was also obtained by Dutkiewicz [13] in 1958 using two liquids—ethanol and water—having markedly different boiling curves. When the heating wire, after prolonged boiling with ethanol, was transferred into water and re-tested, the boiling curve initially approximated or coincided with the ethanol boiling curve. This pretreatment effect decreased with time and vanished after about six hours of boiling. Correspondingly similar behaviour was observed when the order of testing liquids was reversed.

Nucleation may be assumed to take place from surface cavities of conical geometry. Griffith and Wallis [10] have shown that, with respect to nucleation, a cavity may be adequately characterised by specifying the mouth radius only. Mouth radii of potentially active cavities will have some frequency distribution. Clearly, the size distribution is all important in determining the shape of the boiling curve. An

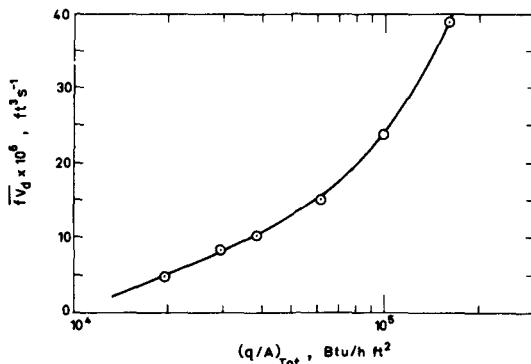
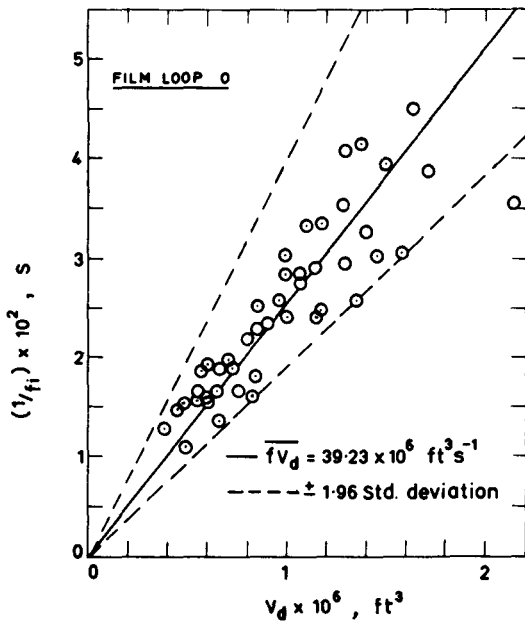
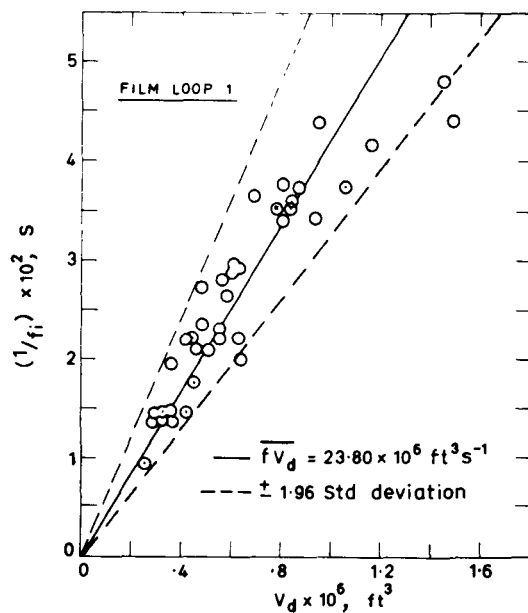


Figure 3. Variation of mean product of bubble frequency and departure volume with heat flux



(a)



(b)

Figure 4. (a) Relationship between bubble frequency and volume at departure. (b) Relationship between bubble frequency and volume at departure

approximate method is outlined whereby this distribution may be obtained from macroscopic measurements.

Consideration is limited to "smooth" surfaces, namely, to conditions where the largest cavity on the surface (of mouth radius r_{\max}) is always active, that is,

$$r_{\max}^* = r_{\max} = \text{const.} \quad (10a)$$

This is equivalent to saying that the limiting thickness of the thermal boundary layer, δ , which is flux and pressure dependent, must at all stages be large enough

to contain the vapour nucleus of the largest cavity, that is

$$\delta > r_{\max} \quad (10b)$$

It is now necessary to obtain a nucleation criterion, that is, an equation relating cavity mouth radius and wall superheat, ΔT_{sat} . Such an equation exists for nucleation in a constant temperature field only. For nucleation in a variable temperature field, such as exists near a heating surface, no satisfactory criterion has been developed. However, as long as the limitations of Eq. (10) are satisfied, the constant temperature field expression may be used as an approximation. Nucleation may then be characterized by

$$r_{\min}^* = 2\sigma T_w v_v / \lambda_v \Delta T_{\text{sat}} \quad (11)$$

The derivation of this equation is well known [10]. The choice of wall temperature, T_w , and the evaluation of physical properties at T_w are substantiated at a later stage.

According to Eq. (11) the largest potentially active cavity will nucleate first, smaller and smaller cavities only becoming active as ΔT_{sat} is raised. Thus, since the largest cavity remains active as ΔT_{sat} increases, a plot of \mathcal{N} , the number of nucleation sites per unit area, against r_{\min}^* will result in the cumulative cavity size distribution for the surface under study. Differentiation with respect to r_{\min}^* yields the frequency distribution.

To illustrate and to substantiate this approach, the data of Fig. 5 are employed. Figure 5 is the customary representation of bubble source concentration data. Before the onset of coalescence the nucleation site (active cavity) concentration, \mathcal{N} , equals the bubble source concentration N . After coalescence this relation ceases to hold. High-flux \mathcal{N} data are rather difficult to obtain. The water data of Fig. 5 show the result of an examination of ciné films of the bubble field. It is seen that the relation

$$(q/A) = \text{const. } \mathcal{N}^{0.5} \quad (12)$$

holds for the entire range, irrespective of coalescence. This finding should facilitate future experiments considerably, since it permits the visual determination of a few N or \mathcal{N} values in the region of isolated bubbles and allows extrapolation to high concentrations using Eq. (12). This work, incidentally, also shows that the number of pin-holes per unit area in Gaertner and Westwater's plating runs [14] is, in fact, the nucleation site concentration.

Values of nucleation site concentration to be employed in the determination of the \mathcal{N} versus r_{\min}^* distribution were obtained from the smoothed and extrapolated data of Fig. 5. Corresponding ΔT_{sat} values were read from the smoothed boiling curves, that is, in the case of water from Fig. 1; r_{\min}^* values were calculated using Eq. (11). The resulting cumulative and frequency distributions of cavity mouth radii of the nickel surface employed in the water run are presented in Fig. 6. The low cavity-radius part of the distribution was not obtained since the boiling

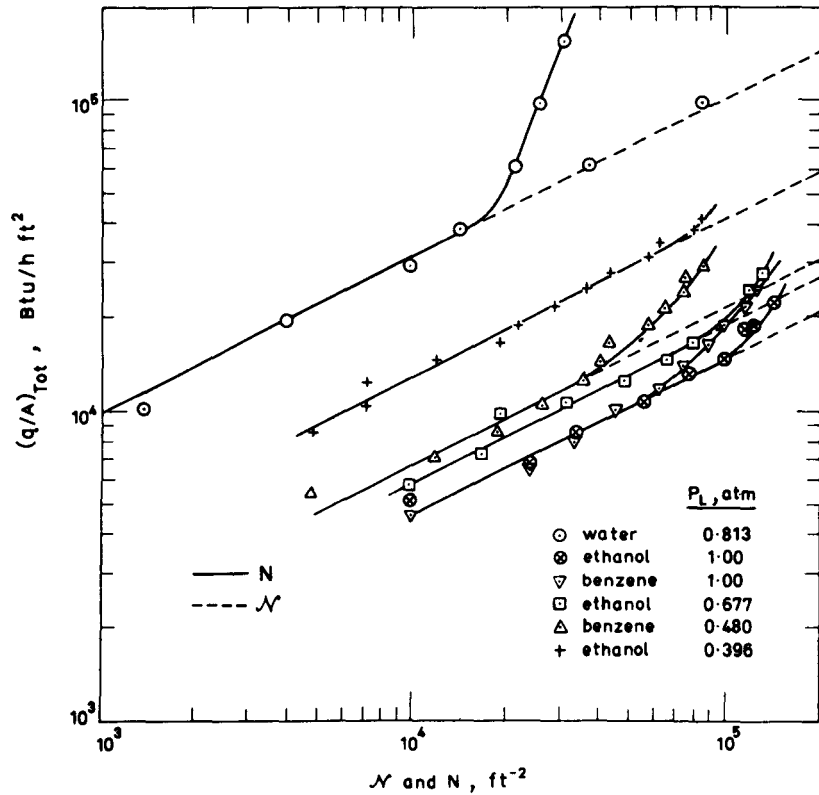


Figure 5. Variation of nucleation site concentration (N') and bubble source concentration (N) with heat flux

curve was not determined in the close vicinity of burn-out.

It was felt that a test to determine the quantitative-ness of the postulated potentially active cavity size distribution was necessary. Since visual examination of the surface microstructure appeared unprofitable, an indirect test was devised. This consisted of conducting boiling tests with different liquids at different

pressures on the same surface, and of determining the cavity size distribution for each run in the manner described above. If the resulting distributions were approximately the same, some trust could be placed in the method. N' measurements and boiling curves for ethanol and benzene at atmospheric and sub-atmospheric pressures were obtained from these tests and are recorded in Figs. 5 and 8 and also in reference [15]. Great care was exercised to avoid "hysteresis" and to achieve reproducibility. Details of the experimental procedure are given elsewhere [15]. The resulting cumulative distributions, N' against r_{min}^* , are shown in Fig. 7. The curves, though not coinciding, show reasonable agreement. Considering the roughness of the approximations involved and the difficulty of obtaining reproducible boiling curves, this result is encouraging.

At this point the choice of T_w as the appropriate temperature in Eq. (11) and the evaluation of physical properties at T_w may be justified. The procedure of obtaining the distributions of Fig. 7 was repeated twice—once using T_{sat} in Eq. (11) and once using $(T_w + T_{sat})/2$. The maximum deviation of the distributions was obtained when using T_{sat} and the minimum when using T_w . That is, nucleation could be best described as a process occurring in a constant temperature field T_w . This implies that the thickness of the thermal boundary layer is considerably larger than a vapour nucleus, and that the limitations of Eq. (10) are satisfied.

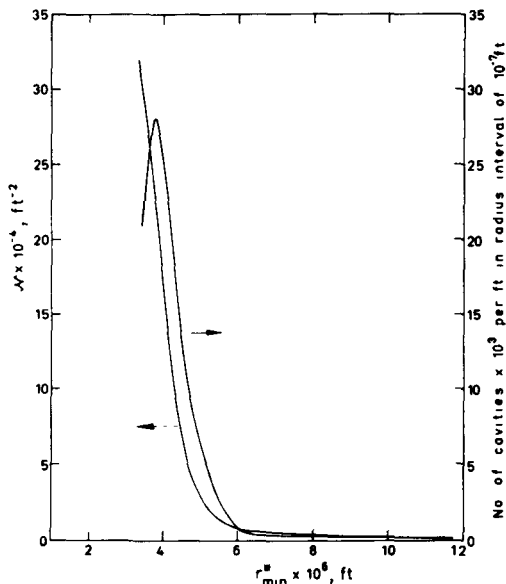


Figure 6. Nucleation cavity size distribution for nickel surface

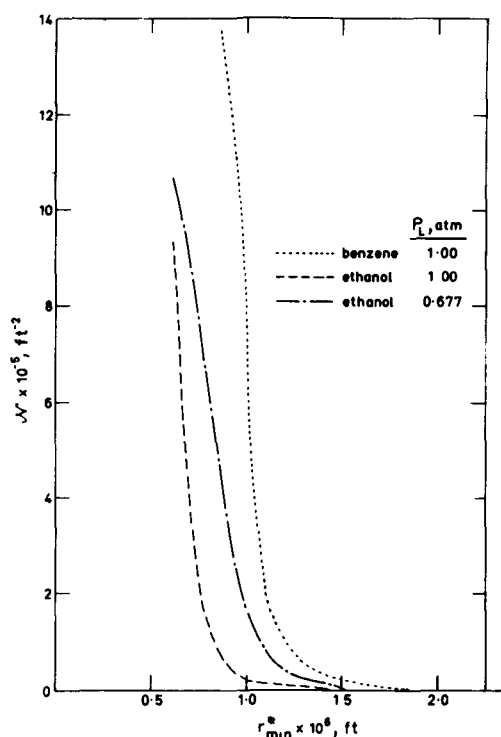


Figure 7. Cumulative cavity size distribution for platinum surface

Determinations similar to those of Fig. 7 were also obtained by Griffith and Wallis [10]. Their work may be considered as further evidence of the general validity of this method of determining the size range of potentially active cavities on a heating surface.

It is clear that the approach outlined above requires considerable refinement. The effect of variation in the thickness of the thermal boundary layer requires special attention.

The next step would appear to be the determination of the cavity size distributions of different types of surface and the establishment of some general trends.

A further phenomenological test of the validity of the nucleation mechanism embodied in Eq. (11) suggested itself. The effect of pressure in Eq. (11) is such as to permit, to a rough approximation [6, 16], the use of

$$r_{\min}^* = \text{const.} / \Delta T_{\text{sat}} P_L \quad (13)$$

Thus, if the pressure and the wall superheat are reduced in a boiling system, r_{\min}^* increases. During operation at a particular low pressure, the situation arises where $r_{\min}^* = r_{\max}^*$ in the middle region of a boiling curve. With the range of active cavity sizes now equal to zero, nucleation, and hence nucleate boiling, must cease or otherwise proceed by some mechanism other than the normal one. At some even lower pressure the value of ΔT_{sat} required for normal nucleation will exceed that associated with the peak flux; below this pressure the normal nucleate regime should be altogether absent.

To test the foregoing it is necessary to conduct boiling runs at various low pressures with a particular

surface-liquid combination. Such tests were performed [15] at saturation temperature, care being once again taken to avoid "hysteresis" and to achieve reproducibility. The results are presented in Fig. 8.

During run E.1 (1.0 atm) and run E.2 (0.677 atm) the well-known boiling curves were traced. This also applies to run E.3 (0.396 atm) in the high flux range. At low flux, run E.3 exhibited a highly unusual change in direction. This behaviour appeared to be associated with the cessation of the normal mechanism of nucleation. Inspection of Fig. 5, in which the N versus (q/A) data for this run are reported, shows that no dramatic change in the bubble source concentration occurred at this point. However, nucleation seemed to become unstable; bubbles no longer emanated from fixed sources in column formation, but appeared to be formed at points shifting about on the surface. This effect was particularly noticeable in run E.4 (0.294 atm) where bubble-producing sources jumped around on the surface in a rapid and apparently random manner.

A curve similar to that for run E.3 has been obtained by van Stralen [17] for the boiling of a solution of whey in water at a pressure of 0.132 atm. Boiling as in run E.4 does not appear to have been hitherto reported.

The phenomena of runs E.3 and E.4 cannot be attributed to "hysteresis effects" or "temperature overshoot" since: (a) runs were performed at decreasing flux; (b) the test procedure used in obtaining runs E.3 and E.4 was identical to that adopted for the stable runs E.1 and E.2; and (c) this instability did not die away with time. In fact on one occasion during operation in the unstable region, even though the bubble pattern remained irregular, the flux was maintained at the same setting for over an hour; in the same run at higher flux no irregularity was observed.

Run E.5 (0.136 atm) illustrates the complete cessation of nucleation. At a flux slightly higher than that of the last point recorded, the surface burst into film boiling. The nucleate regime was entirely absent. Van Stralen [18] and Lienhard and Schrock [19] have observed the same phenomenon.

Run E.6 (1.0 atm) is a satisfactory check on reproducibility.

Similar results to the above were also obtained for benzene.

As a result of this cessation of normal nucleation at low pressures only three stable boiling runs were obtained with ethanol and benzene and these were the only ones that could be analysed to give the cumulative cavity size range distribution on the heating surface, see Fig. 7.

Tests at reduced pressure, such as those described above, provide powerful evidence of the correctness of the proposed nucleation mechanism.

Suggested method of correlating results

Evidently the total heat flux during saturated nucleate boiling is made up of two components—latent

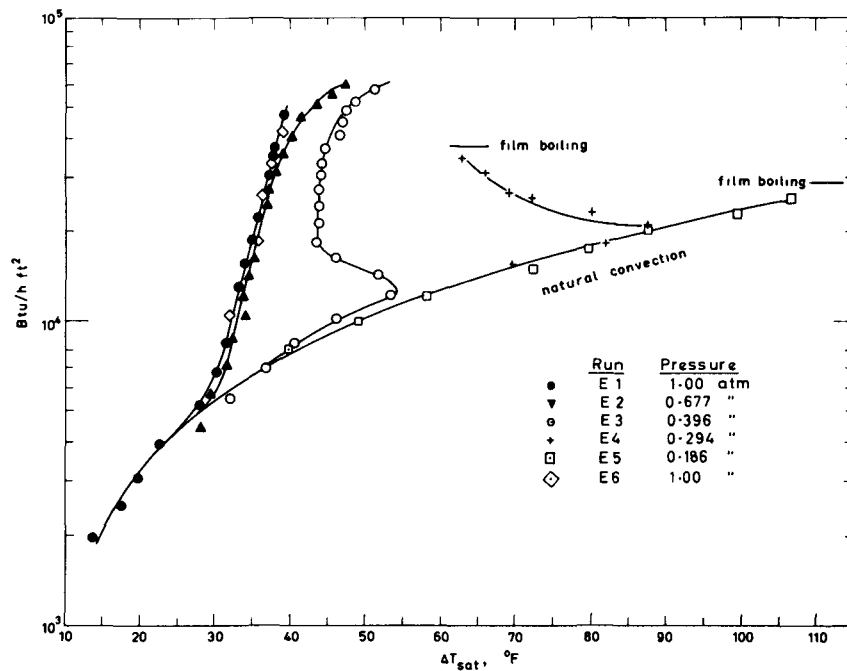


Figure 8. Boiling curves for ethanol showing unstable nucleate boiling and absence of the nucleate regime at low pressure

heat transport and convection. Clearly both these are dependent on N , f and V_d . However, their relative contributions to the total flux vary throughout the nucleate boiling region. At the low-flux end the convection component predominates, whereas at the high-flux end latent heat transport is the controlling factor. Thus no single equation based on either of these components alone can be expected to work. Each component must be correlated separately.

The total flux and latent heat transport are directly measurable. The difference between them should then be correlated using the appropriate convection mechanism. This aspect of the problem is currently receiving attention.

CONCLUSIONS

(a) Latent heat transport and convection together account for the total flux in saturated nucleate boiling.

(b) Latent heat transport is at all stages significant; it is probable that at burn-out it alone represents the total flux.

(c) The mean product $f\bar{V}_d$, if defined correctly, increases throughout the flux range.

(d) At fixed flux and pressure the product fV_d is the same for each bubble source within reasonable statistical scatter.

(e) The relationship between heat flux, (q/A) , and the number nucleation sites per unit area, \mathcal{N} ,

$$(q/A) = \text{const. } \mathcal{N}^n$$

where $n \simeq 0.5$ holds up to high fluxes, irrespective of

coalescence. After the onset of coalescence the number of bubble sources, N , increases more slowly with flux, n assuming values as high as 2.6.

(f) Nucleation from each surface cavity may be approximately characterized by

$$r_{\min}^* = 2\sigma T_w v_v / \lambda_v \Delta T_{\text{sat}}$$

provided that the thermal boundary layer thickness is greater than the mouth radius of the largest cavity, that is $\delta > r_{\max}$.

(g) If the limitation $\delta > r_{\max}$ is satisfied, then a plot of \mathcal{N} against r_{\min}^* approximately represents the cumulative cavity size distribution for the surface under study; from this the cavity size frequency distribution can be calculated.

(h) The nucleation criterion (in term (g) above) can yield predictions on the size range of active cavities. These have been verified by experiments and lead to the following general conclusions:

(i) the effect of lowering the pressure on a boiling system is such as to decrease the size range of active cavities;

(ii) for a particular surface-liquid combination a definite low pressure exists, below which the boiling curve exhibits instability;

(iii) this threshold is reached when the size range of cavities active in the normal sense becomes zero. Beyond this threshold there exists a hitherto unrecognized regime of unstable nucleate boiling;

(iv) in this unstable regime nucleation and boiling proceed by mechanisms other than the normal;

(v) at even lower pressures the nucleate regime is altogether absent.

SUMMARY

Experimental and analytical work elucidating the mechanism of saturated nucleate boiling has thus been reported. The bulk of this work deals with latent heat transport, $(q/A)_{LH}$, which is shown to contribute significantly to the total flux. The study of $(q/A)_{LH}$ involved investigations into:

- (a) *Bubble departure*. The interrelation between bubble frequency and departure volume was dealt with.
- (b) *Bubble source concentration*. This involved a study of surface characterization and bubble coalescence. A method was developed by which the size distribution of potentially active nucleation cavities on a surface could be obtained from macroscopic measurements. A nucleation criterion was adopted, which was tested against and confirmed by experimental results showing:
- (i) the existence of a regime of unstable nucleate boiling at low pressure; and
 - (ii) the complete absence of nucleate boiling at even lower pressure.

Suggestions for future work were made. A rational approach to the general correlation of nucleate boiling heat transfer was outlined.

REFERENCES

1. Gunther, F. C., and Kreith, F., *Photographic study of bubble formation in heat transfer to subcooled water*, in Heat Transfer and Fluid Mechanics Institute, ASME 113-138 (1949).
2. Rohsenow, W. M., and Clark, J. A., *Trans. ASME* 73 609/620 (1951).

3. Zuber, N., and Fried, E., *J. Amer. Rocket Soc.* 32 1332/1341 (1962).
4. Zuber, N., *Int. J. Heat Mass Transfer* 6 53/78 (1963).
5. Rallis, C. J., Greenland, R. V., and Kok, A., *South African Mech. Engin.* 10 171/186 (1961).
6. Rallis, C. J., and Jawurek, H. H., *Latent heat transport in saturated nucleate boiling*. Provisionally accepted, *Int. J. Heat Mass Transfer*.
7. Hsu, Y. Y., and Graham, R. W., *An Analytical and experimental study of the thermal boundary layer and ebullition cycle in nucleate boiling*. NASA report TN-D-594, Lewis Research Centre, Cleveland, Ohio (1961).
8. Jawurek, H. H., *South African Mech. Engin.* 13 47/48 (1963).
9. Bankoff, S. G., *Trans. ASME* 79 735/740 (1957).
10. Griffith, P., and Wallis, J. D., *Chem. Engin. Progr. Symp. Ser.* 56 No. 30 49/65 (1960).
11. Bankoff, S. G., *Amer. Inst. Chem. Engrs. J.* 4 24/26 (1958).
12. Clark, H. B., Strenge, P. S., and Westwater, J. W., *Chem. Engin. Progr. Symp. Ser.* 55 No. 29 103/110 (1959).
13. Dutkiewicz, R. K., *South African Mech. Engin.* 7 231/246 (1958).
14. Gaertner, R. F., and Westwater, J. W., *Chem. Engin. Progr. Symp. Ser.* 56 No. 30 39/48 (1960).
15. Jawurek, H. H., *Nucleation during boiling with special reference to its cessation at low pressure*. M.Sc. thesis in Chem. Engin. University of Cape Town, Rondebosch, South Africa (1962).
16. Séméria, R. L., *Quelques résultats sur la mécanique de l'ébullition*. VII Journées de l'Hydraulique, Soc. Hydro-technique de France, Question II, Rapport No. 3, Paris (1962).
17. Van Stralen, S. J. D., *British Chem. Engin.* 6 834 (1961).
18. Van Stralen, S. J. D., *Chem. Engin. Sci.* 5 290/296 (1956).
19. Lienhard, J. H., and Schrock, V. E., *J. Heat Transfer* C85 261/272 (1963).

ABSTRACT—RÉSUMÉ—АННОТАЦИЯ—RESUMEN

A/600 Afrique du Sud

Le mécanisme de l'ébullition nucléée

par C. J. Rallis et H. H. Jawurek

Avant de pouvoir reconnaître toutes les possibilités que présente l'ébullition comme moyen de transfert de chaleur, il est nécessaire d'en comprendre le mécanisme de base. Ce mémoire constitue une tentative d'aborder simplement et directement ce problème. Nous ne traitons que du cas d'ébullition le plus simple, à savoir l'ébullition nucléée dans les conditions de liquide saturé. Nous considérons l'examen de ce cas simple comme la condition préalable de toute étude plus approfondie de l'ébullition.

Pendant de nombreuses années, le transfert de chaleur latente défini par

$$(q/A)_{LH} = \rho_v \lambda_v \sum_{i=1}^n f_i V_{di}/A = N f \bar{V}_d \rho_v \lambda_v$$

a été considéré comme une contribution négligeable au flux total de chaleur dans toutes les conditions

d'ébullition nucléée. Les résultats expérimentaux concernant l'ébullition nucléée, à saturation, que nous donnons ci-dessous, indiquent que le rapport $(q/A)_{LH}/(q/A)_{Tot}$ augmente régulièrement lorsque le flux augmente, et tend vers l'unité lorsque $(q/A)_{Tot}$ tend vers la caléfaction. Le transfert de chaleur latente ainsi que la convection expliquent le flux total de l'ébullition de liquide saturé.

La plus grande partie du mémoire traite des paramètres qui entrent dans la formulation de $(q/A)_{LH}$. Ils doivent inévitablement influencer n'importe quel mécanisme de convection créé par des bulles.

Les deux paramètres les plus importants entrant dans la formule $(q/A)_{LH}$ sont: a) la concentration des sources de bulles, N , qui dépend essentiellement de la surface, et b) le taux moyen de la circulation de masse de chaque source, $f \bar{V}_d \rho_v$, de nature essentiellement hydrodynamique. Cependant, ces deux paramètres sont étroitement liés entre eux.

Les résultats expérimentaux montrent: a) que la moyenne arithmétique $f \bar{V}_d$ augmente avec le flux;

b) que, pour un flux particulier, le produit fV_d est à peu près le même pour chaque source de bulles.

Le terme N , concentration des sources de bulles, est de la plus grande importance du point de vue de la corrélation du transfert de chaleur, par le fait qu'il entre tant dans la formulation de transfert de chaleur latente que dans celle de la convection comme nombre de sources qui contribuent à la circulation du liquide. Dans la région des bulles isolées, la concentration des sources de bulles, N , est identique à la concentration des points de nucléation, N^0 ; pour des flux plus élevés, ce n'est plus le cas, car la vapeur de plusieurs noyaux peut s'assembler pour former une seule bulle. Le rapport

$$(q/A)_{\text{Tot}} = \text{const. } N^n$$

où $n \simeq 0,5$ est confirmé pour l'ébullition de l'eau à la pression atmosphérique et pour les composés organiques à diverses pressions basses.

En utilisant ce rapport ainsi qu'une équation caractérisant la nucléation à partir d'une cavité, une courbe d'ébullition étant donnée, nous avons pu arriver à la distribution des dimensions de cavités de nucléation potentiellement actives; cela signifie qu'une surface peut être caractérisée par rapport à la nucléation. Nous présentons des données tant sur N^0 que sur N , et par conséquent sur la coalescence.

L'analyse utilisant l'équation de nucléation indique que cette dernière et par suite l'ébullition nucléée ne peuvent continuer indéfiniment à des pressions toujours plus basses; pour une combinaison surface-liquide donnée, il existe une pression au-dessous de laquelle la nucléation ne peut se poursuivre normalement. Des expériences de confirmation montrent que cette pression marque le seuil d'un régime d'ébullition nucléée instable, non reconnu jusqu'ici. A une pression inférieure, le régime nucléé est entièrement absent.

Bien qu'elle en soit encore à son début, l'étude dont nous rendons compte ici démontre comment on pourrait obtenir une corrélation rationnelle du transfert de chaleur pour l'ébullition nucléée.

A/600 ЮАР

Механизм образования зародышей при кипении

К. Дж. Рэллис, Г. Г. Джоурек

Прежде чем осуществлять процесс интенсивного кипения как средства теплопередачи, необходимо понять основной механизм кипения. Этот доклад представляет собой попытку просто и доходчиво объяснить эту проблему. В докладе рассматривается только простейший случай, а именно кипение с образованием зародышей в сосуде с насыщенным паром. Рассмотрение этого простейшего случая является необходимым условием для более детального исследования процесса кипения.

В течение многих лет скрытую теплопередачу, определяемую уравнением

$$(q/A)_{\text{ЛН}} = P_v \lambda_v \sum_{i=1}^n f_i v_{di} / A = N f \bar{v}_d P_v \lambda_v,$$

рассматривали как незначительную часть общего теплового потока, образующегося при всех условиях кипения с образованием зародышей. Результаты экспериментального исследования образования зародышей при кипении в сосуде с насыщенным паром, приведенные в данном докладе, указывают на то, что отношение $(q/A)_{\text{ЛН}} / (q/A)_{\text{общ}}$ неизменно увеличивается с увеличением потока, стремясь к 1, по мере того как $(q/A)_{\text{общ}}$ стремится к величине, соответствующей кризису кипения. Скрытая теплопередача и конвекция вместе объясняют сущность потока при насыщенном кипении.

Значительное место в данном докладе отведено рассмотрению параметров в уравнении $(q/A)_{\text{общ}}$. Это, безусловно, должно иметь отношение к любому механизму, описывающему конвекцию вследствие пузырькового кипения.

Двумя наиболее важными параметрами, входящими в $(q/A)_{\text{ЛН}}$ являются: а) концентрация источника пузырьков N , которая главным образом зависит от поверхности, и б) средняя скорость потока массы от каждого источника $f v_d \rho_u$, которая по своей природе в основном определяется гидродинамикой. Однако оба эти параметра взаимосвязаны.

Результаты экспериментов показывают, что а) среднеарифметическое произведение $f v_d$ увеличивается с увеличением потока и б) при данном потоке произведение $f v_d$ приблизительно одинаково для каждого источника пузырьков.

Параметр N , концентрация источника пузырьков, имеет первостепенное значение, так как он позволяет определить соотношение величин теплопередачи, которая описывается уравнением в виде скрытого переноса тепла и в виде уравнения конвекции, куда оно входит как число источников, вызывающих поток жидкости. Что касается отдельных пузырьков, концентрация источника пузырьков N идентична концентрации среды, в которой происходит образование зародышей N . При более высоких скоростях потока эта идентичность больше не имеет места, так как пар от нескольких зародышей может слипаться и образовывать только один пузырек. Отношение $(q/A)_{\text{общ}} = \text{const } N^h$, где $h \simeq 0,5$, является справедливым для кипения воды при атмосферном давлении и для органических жидкостей при низких давлениях.

С помощью этого отношения и уравнения, характеризующего явление образования зародышей из полости, а также с помощью приведенной кривой кипения найдено возможным установить диапазон размеров полостей, потенциально активных в отношении образования зародышей: то есть можно охарактеризовать поверхность в отношении образования зародышей.

Приведены данные об N , N и, следовательно, о сипании.

Анализ уравнения, описывающего условия образования зародышей, указывает на то, что процессы образования зародышей и, следовательно, процессы образования зародышей кипения не могут протекать бесконечно при все уменьшающихся давлениях. Для данного случая поверхность — жидкость давление настолько мало, что процесс образования зародышей не может протекать обычным порядком. Опыты, поставленные с целью подтверждения этого положения, показывают, что это давление является пороговым для пока еще неизвестного режима неустойчивого кипения с образованием зародышей. При меньшем давлении механизм образования зародышей вообще отсутствует.

Хотя механизм этого явления находится лишь на начальной стадии изучения, в докладе приведены кривые, показывающие, при каких корреляциях теплопередачи можно получить рациональные величины кипения с образованием зародышей.

A/600 Sudafrica

El mecanismo de ebullición por núcleos

por C. J. Rallis y H. H. Jawurek

Antes de apreciar por entero las posibilidades de la ebullición como proceso de transferencia de calor, es preciso comprender su mecanismo básico. Este artículo intenta tratar el problema de un modo sencillo y directo. Únicamente se estudia el caso más sencillo de ebullición, es decir, la ebullición por núcleos en condiciones de saturación. Se considera que este caso es un paso previo a cualquier estudio más profundo de la ebullición.

Durante muchos años se ha supuesto que el transporte de calor latente, definido por

$$(q/A)_{cl} = p_v \lambda_v \sum_{i=1}^n f_i V_{di}/A = N f \bar{V}_d p_v \lambda_v$$

no contribuye apreciablemente al flujo total de calor para todas las condiciones de ebullición por núcleos. Los resultados experimentales sobre ebullición por núcleos a saturación, que se exponen en el presente artículo, indican que la relación $(q/A)_{cl}/(q/A)_{Tot}$ aumenta continuamente al aumentar el flujo y tiende a la unidad cuando $(q/A)_{Tot}$ tiende hacia el quemado. Transporte de calor latente y convección dan cuenta del flujo total en el caso de ebullición saturada.

La mayor parte de este artículo trata de los parámetros que entran en la fórmula para $(q/A)_{cl}$. Inevitablemente, éstos deben influir también sobre cualquier mecanismo de convección inducido por burbujas.

Los dos parámetros más importantes que entran en $(q/A)_{cl}$ son: *a*) la concentración de fuentes de burbujas, N , que depende fundamentalmente de la superficie, y *b*) el ritmo medio de flujo de masa de cada fuente, $f \bar{V}_d \rho_v$, que esencialmente es de naturaleza hidrodinámica. Sin embargo, ambos parámetros están relacionados entre sí.

Los resultados experimentales demuestran que *a*) la media aritmética del producto $f \bar{V}_d$ crece con el flujo y *b*) para un flujo determinado, el producto $f \bar{V}_d$ es aproximadamente el mismo para cada fuente de burbujas.

El término N , la concentración de fuentes de burbujas, es de fundamental importancia desde el punto de vista de la correlación de transferencia de calor, puesto que entra en la formulación para el transporte de calor latente así como en la de corrección a través del número de fuentes que inducen flujo de líquido. En la región de burbujas aisladas, la concentración de fuentes de burbujas, N , es idéntica a la concentración de lugares de nucleación N' ; para flujos más altos, esto ya no se aplica puesto que el vapor de varios núcleos puede soldarse y formar una sola burbuja. Se confirma la relación $(q/A)_{Tot} = \text{const. } N^n$ con $n \approx 0,5$ para ebullición de agua a la presión atmosférica y de orgánicos a varias presiones bajas.

Usando esta relación y una ecuación que caracteriza la formación de núcleos a partir de una cavidad y dada una curva de ebullición, se encuentra que es posible calcular la distribución de tamaños de las cavidades de formación de núcleos potencialmente activos. Se presentan datos sobre N' y N y por lo tanto sobre la fusión de burbujas.

Mediante la ecuación de formación de núcleos se demuestra que este proceso y por tanto la ebullición por núcleos no puede desarrollarse indefinidamente a presiones cada vez más bajas; para una determinada combinación superficie-líquido existe una presión por bajo de la cual el mecanismo de formación de núcleos en el sentido normal no puede tener lugar. Los experimentos confirman que esta presión marca el umbral de un régimen de ebullición por núcleos inestable hasta ahora no reconocido. A presiones inferiores el régimen de ebullición por núcleos está totalmente sustente.

El estudio que aquí se presenta, aunque todavía en las primeras fases de desarrollo, ilustra las líneas que deben seguirse para obtener una correlación racional de transferencia de calor a través de la ebullición por núcleos.

Boiling from a liquid interface

By M. Novaković and M. Stefanović*

Boiling from a liquid surface is an interesting phenomenon which could be used in new apparatuses for heat transfer and for the investigation of boiling phenomena under conditions approaching to ideal. This investigation was made with the aim of studying boiling from an almost ideal surface and determining heat transfer coefficients. To correlate the results with the physical parameters investigations were made of the nucleation of water, ethyl alcohol, benzene and n-pentane.

The problem of heat transfer between immiscible liquids has been little studied, especially in the case of one liquid boiling. L. Trefethen [1] studied nucleation from the interface of two liquid phases but he did not measure heat fluxes and heat transfer coefficients. K. F. Gordon, T. Singh and E. Y. Weisman [2] measured heat transfer between a mercury surface and boiling water, methyl and ethyl alcohol. They found that for a superheated mercury surface with $\Delta t = 4-57^\circ\text{C}$ one obtains a heat flux $q = 4\,060 - 298\,000 \text{ kcal/m}^2\text{h}$ and the heat transfer coefficient $\alpha = 976 - 8\,800 \text{ kcal/m}^2\text{h }^\circ\text{C}$ in which case the dependence of heat flux on the superheated mercury surface is $q = C\Delta t^n$ where n is constant for water ($n = 1.43$) and ethyl alcohol ($n = 1$), while it decreases for methyl alcohol from $n = 2.2$ to $n = 1$. The study of the same problem of boiling heat transfer from a liquid interface was started in this laboratory some time ago and results for water and alcohol are published [5].

EXPERIMENTAL TECHNIQUE

The experimental vessel (Fig. 1) consisted of a glass cylinder connected to a steel bottom by means of a rubber ring. The connection was made at a relatively cold place and the mercury was isolated from the rubber by a water interspace. The vessel was covered with a stainless steel top with an opening for air, an opening for water and mercury, and a micrometer screw travelling thermocouple. The steam was conducted by a glass pipe inserted in the top. The pipe had double walls, the inner diameter being 35 mm. Between these walls an electric heater was placed to prevent condensing of the vapour within the pipe and returning of the condensate into the experimental vessel.

The thin mercury layer above the convex middle part of the bottom was heated by an electric heater spirally wound round the lower part of the copper column (bed), 56 mm in diameter. Thus boiling from the surface of the vessel was avoided as it was kept at a temperature below the boiling point. The upper front surface of the column is tightly silver soldered to the thin steel bottom (0.3 mm thick) which was finely finished. Starting from the steel bottom, seven horizontal holes for thermocouples were made (1.6 mm diam.) at every 10 mm along the length of the copper column up to the axis. The heat flux through the steel bottom and the temperature of its upper surface were determined from measured temperature distributions in the copper. The whole copper column with the heater and thermocouples was insulated. The influence of the ends was also avoided by extracting vapour through the outlet glass pipe from the central part only. The outlet pipe had a smaller diameter than the copper column. In the mercury layer temperatures were measured with a chromel-mercury travelling thermocouple. A single 0.3 mm diameter chromel wire was inserted into a capillary tube with a 1 mm outer diameter so that only 0.5 mm of the end of the wire was free from glass. The position of this tube, which projected horizontally into the mercury layer, could be adjusted by a micrometer screw so that vertical temperature traverses could be made. The mercury in a pvc hose was led from the vessel to the cold junction where a mercury-chromel contact was made and kept in melting ice. Thermocouple emfs were measured by the zero method.

The apparatus was set on three legs whose height could be adjusted by a screw bolt thus enabling the steel bottom to be brought into the horizontal position. This position was checked with a spirit level in two normal directions.

The mercury layer thickness above the steel bottom was determined by a "comb" fixed to the periphery of the bottom. The tooth points of the comb were arranged at different calibrated heights. The mercury layer thickness was adjusted so that its free surface touched the corresponding tooth point by slight lifting and lowering of a communicating vessel.

To reduce heat losses (dissipation of heat flux) thinner mercury layers were used. However, the mercury layer would break if it were thinner than a certain value. The average thickness of the stable mercury layer was about 5 mm for boiling water and

* Boris Kidrič Institute of Nuclear Sciences, Beograd-Vinča.

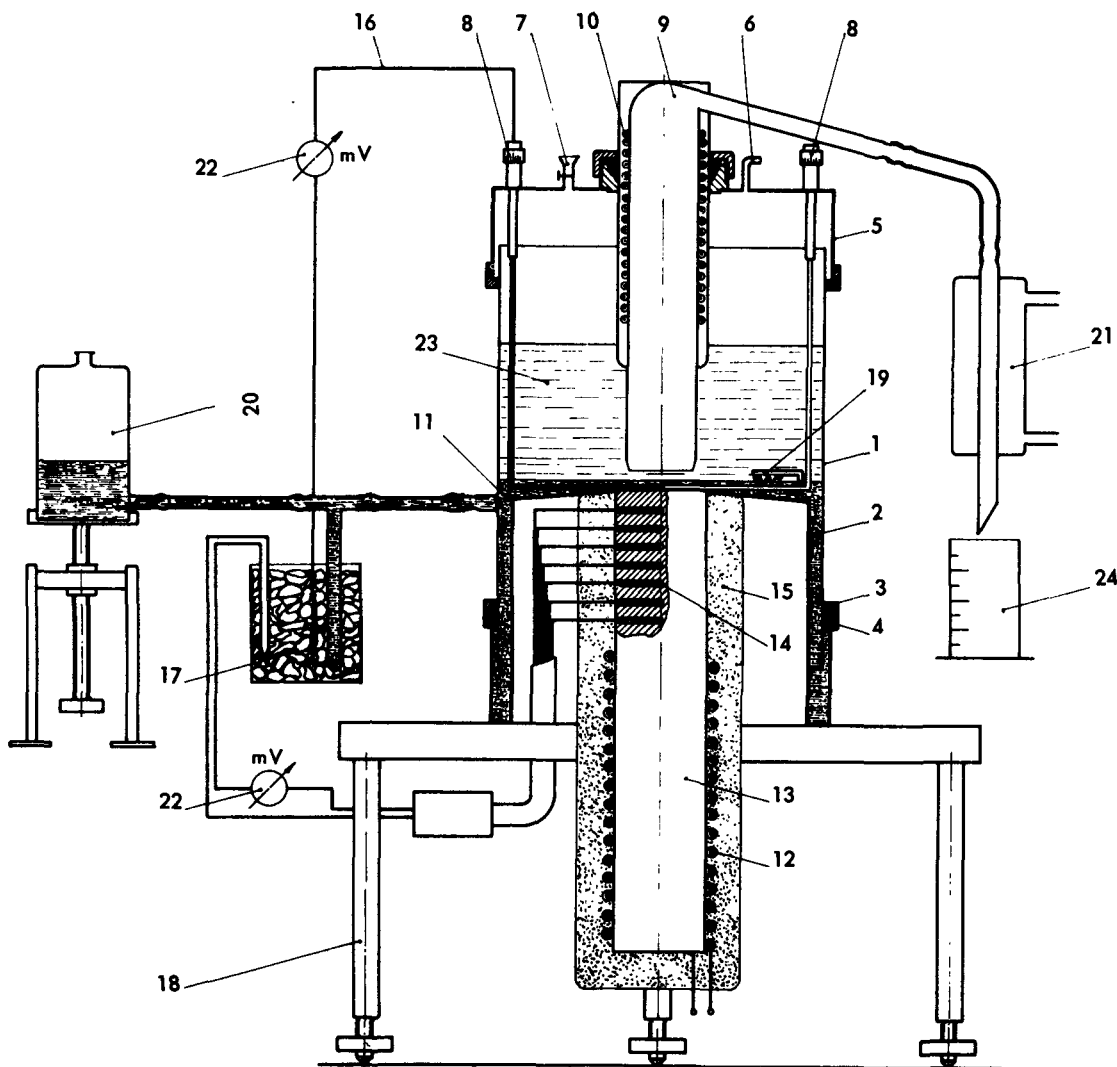


Figure 1. Experimental apparatus

- | | |
|--|--|
| 1. Glass cylinder (boiling vessel) | 12. Electric heater |
| 2. Steel bottom | 13. Copper column |
| 3. Rubber ring | 14. Thermocouple holes in the copper column |
| 4. Water | 15. Thermal insulation |
| 5. Steel top | 16. Chromel wire of the chromel-mercury thermocouple |
| 6. Opening for communication with the atmosphere | 17. Cold point of the thermocouples |
| 7. Opening for water and mercury | 18. Stand |
| 8. Micrometer screws for adjustment of thermocouples | 19. "Comb" |
| 9. Glass pipe conducting steam out of the glass cylinder | 20. Communicating vessel |
| 10. Electric heater in the glass cylinder | 21. Condenser |
| 11. Mercury | 22. Instruments for measuring emf |
| | 23. Boiling liquid |
| | 24. Measuring glass for the condensate |

about 3 mm for boiling alcohol, benzene and n-pentane. The thickness increased with an increase of heat flux. The last experiments were performed with a 5 mm mercury layer for all liquids. For this mercury layer thickness, heat losses from the steel bottom to the surface of the mercury heating surface were determined by comparing the heat flux obtained on the basis of the condensate and the temperature gradient in the copper column for all the four liquids. The flux varied from $q = 9.75 \times 10^3$ kcal/m²h to $q = 1.15 \times 10^5$ kcal/m²h and superheating from $\Delta t =$

9.5 °C to $\Delta t = 46$ °C. The ranges of these variables for particular liquids are given below:

water	$9.5 < \Delta t < 23$
alcohol	$23 < \Delta t < 46$
benzene	$22.4 < \Delta t < 40.9$
N-pentane	$18.6 < \Delta t < 36.6$

$1.5 \times 10^4 < q < 1.15 \times 10^5$
$1.1 \times 10^4 < q < 7 \times 10^4$
$1.66 \times 10^4 < q < 6.47 \times 10^4$
$9.75 \times 10^3 < q < 4.65 \times 10^4$

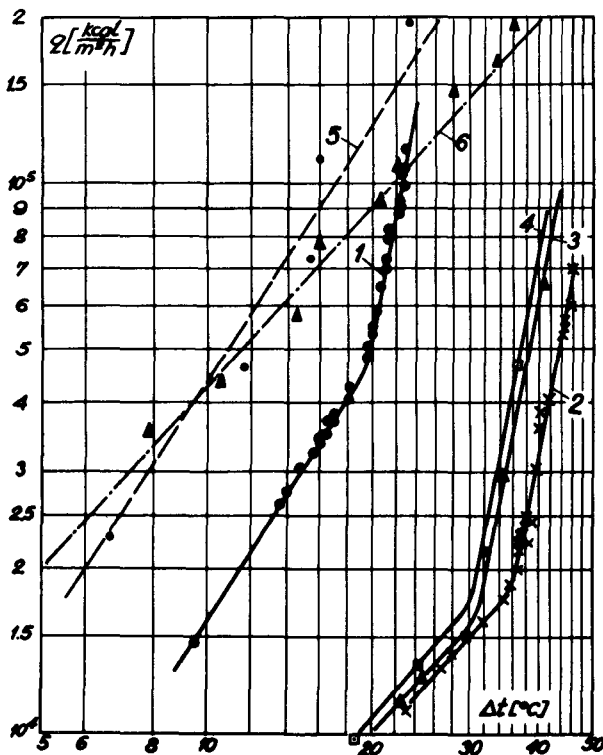


Figure 2. Dependence of heat flux on heating

1. Results for water (Novaković and Stefanović)
2. Results for alcohol (Novaković and Stefanović)
3. Results for benzene (Novaković and Stefanović)
4. Results for pentane (Novaković and Stefanović)
5. Results for water of K. F. Gordon *et al.*
6. Results for alcohol of K. F. Gordon *et al.*

No measurements were made at smaller heat fluxes because of the difficulty of getting the system into a stationary state. No measurements were made either at higher fluxes because the strong boiling prevented exact temperature measurement in the mercury layer.

The boiling heat flux was determined by measuring the condensate at set time intervals and was calculated on the basis of the test surface covered by a glass pipe opening ($A = 9.5 \text{ cm}^2$) and was checked by the copper temperature gradient. The temperature of the heating mercury surface was determined by extrapolating the temperature distributions in the mercury layer.

THE EXPERIMENTAL RESULTS AND OBSERVATIONS

Nucleation took place at preferred points, called nucleation centres, from which bubbles were released at almost regular intervals similarly as from solid surfaces. Even at constant flux these centres formed by sudden breaking out of a new bubble followed by characteristic crackling. This bubble grew much faster and its size when it escaped was bigger than that of bubbles appearing at a centre already formed. Below the centre a very slight concavity of the mercury was observed. Unlike boiling from solid surfaces nucleation centres are mobile.

The results of measurements are plotted as the dependence of heat flux on superheating (Fig. 2).

The broken line on the graph (Fig. 2) shows the results reported by Gordon *et al.* [2]. It can be seen that in our experiments higher superheating was obtained for the same fluxes in the measured range.

In the graphs one can easily discern two boiling regions similar to those with solid surfaces, one in which the ratio $dq/d(\Delta t)$ is smaller (convective boiling) and the other with a much higher ratio (developed bubble boiling). The slopes of the lines representing results for bubble boiling are the same for all the four liquids. It is of interest to note that the slopes of broken lines showing Gordon's results [2] coincide with slopes obtained for convection boiling.

It is evident from the graph that the results for bubble boiling show a linear dependence on a log-log graph, i.e., they have the form

$$\alpha = Cq^n \quad (1)$$

A similar dependence can be obtained by cross plotting for other pairs of parameters ($q, \Delta t$ and $\alpha, \Delta t$). From the experimental results, using the method of least squares, the following values for the constants in Eq. (1) are obtained: $n = 0.81$ for the four liquids; C is different for each of the four liquids.

Comparing our experimental relation with those based on Kutateladze's [3], Kruzilin's* [3] and Rohsenow's** [4] well-known boiling equations, it

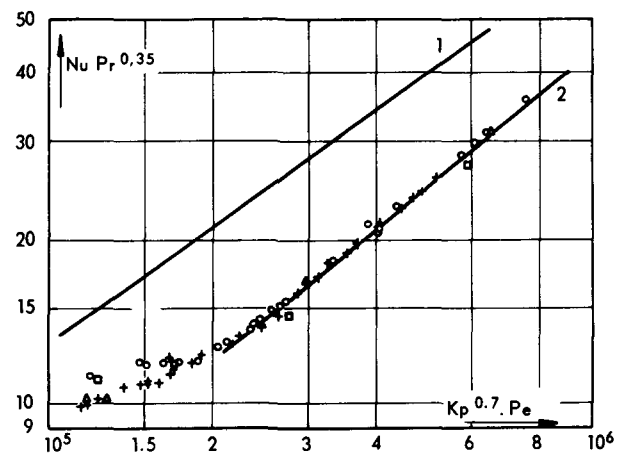


Figure 3. Dimensionless boiling equations

Experimental results for boiling from the mercury surface (Novaković and Stefanović)

- + : Water
- Δ : Benzene
- : Alcohol
- : Pentane

1. Kutateladze's equation
2. Equation of Novaković and Stefanović [4]

* Kruzilin's equation: $Nu = 0.082Pr^{-0.5}Pe^{0.7}Kf^{0.377}$.

** Rohsenow's equation:

$$C(t_p - t_s)/r_s = C_1[(q/\mu r_s)\sqrt{(\sigma)(\gamma' - \gamma'')}]^{0.35}Pr^{1.7}$$

or

$$Nu = C_1Pr^{1.35}Pe^{1.35}$$

is clear that Kutateladze's equation of the form:

$$Nu = A Pr^{n_1} \times Pe^{n_2} \times Kp^{n_3}, \quad (2)$$

correlates our results best for all fluids.

The graph in Fig. 3 shows our experimental results in dimensionless forms and the dependences obtained on the basis of Kutateladze's equation

$$Nu = 7 \times 10^{-4} Pr^{0.35} Pe^{0.7} Kp^{0.7}. \quad (3)$$

The curve of Kutateladze's correlation is less steep than ours but it gives somewhat bigger values for heat transfer coefficients in the range investigated. This was taken into account by a slight adjustment of the exponent n_2 and the constant A in Eq. (2). By the least squares method the values of the exponent n_2 and of the constant A were found ($n_2 = 0.81$, $A = 2 \times 10^{-4}$), so that our dependence has the following form:

$$Nu = 2 \times 10^{-4} Pr^{-0.35} Pe^{0.81} Kp^{0.7}. \quad (4)$$

The results differ by about $\pm 3\%$.

From the graph in Fig. 3 it is evident that the beginnings of bubble boiling for all the liquids investigated

have shown a certain regularity. In other words, bubble boiling starts when the values of the criteria $Kp^{0.7} \times Pe^{0.81}$ are approximated:

$$Kp^{0.7} \times Pe^{0.81} \approx 6.25 \times 10^4 \quad (5)$$

$$\text{or} \quad Nu \times Pr^{0.35} \approx 12.5. \quad (6)$$

SOME OBSERVATIONS AND RESULTS BASED ON THE PHOTOGRAPHS TAKEN WITH A HIGH-SPEED CINE-CAMERA

Photographs of the appearance and development of bubbles were taken with a high-speed cine-camera (6 000 frames per second) for the heat flux values ranging from $q = 25 \times 10^3$ to $q = 50 \times 10^3$.

Figure 4 presents the preliminary results for the development of several typical bubbles. It is apparent that the diameter of the bubble increases with time and that with an increasing flux the development rate of the bubble also increases.

Figure 5 shows the time τ_0 for which bubbles remain on the heating surface as a function of the diameter d_0 of the bubble at separation for various fluxes. For our values of the heat flux and boiling conditions the values lie within the range $2 \text{ mm} < d_0 < 6 \text{ mm}$; $50 \text{ s}^{-3} > \tau_0 > 20 \text{ s}^{-3}$. The graph also illustrates that with increasing flux the time τ_0 for which bubbles remain on the surface is shortened while d_0 increases. Thus bubbles escaping with a larger diameter d_0 remained a shorter time on the heating surface, i.e., their τ was shorter. These results are not in agreement with observations of Fritz, Ende and Jakob for solid surfaces. This can be explained by different physical conditions of the boiling (a considerably higher superheating of the heating surface for the same heat fluxes). The results shown in Fig. 5 indicate that a good many films should be taken in order to give a round correlation.

CONCLUSION

The results of these measurements are reproducible and conclusive. The scattering of results is slight because of improved measuring techniques and careful avoidance of secondary effects. The results obtained for the four liquids correlated with equation (4) are in good agreement. There is a considerable disagreement between the results of our investigations and those of K. F. Gordon [2]. In our opinion the disagreement originates in the experimental conditions. Our results concern only boiling heat transfer from a liquid interface, i.e., from a mercury surface. We think that because of boiling at the meniscus between the glass shield of the experimental vessel and the place where the thermocouple penetrates into the free mercury surface, smaller superheating was obtained (at the same heat fluxes) as reported by Gordon *et al.* This was also experimentally supported. By inserting thermocouple wires into the mercury surface of the experimental apparatus, the heat flux was

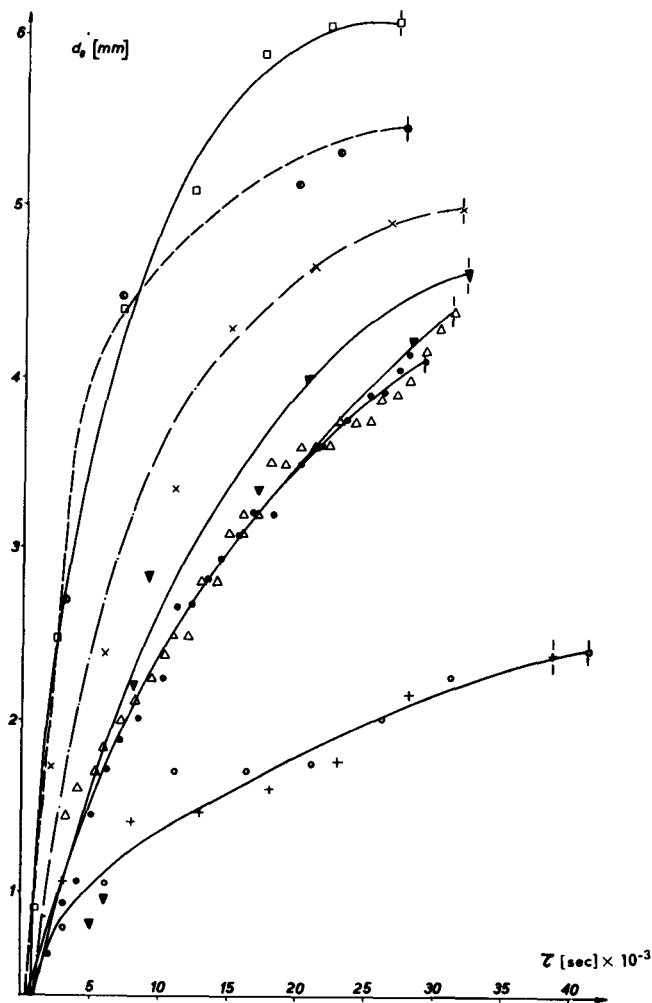


Figure 4. Diagram of bubble growth. The moments of the departure of a bubble from the heating surface are marked by vertical lines

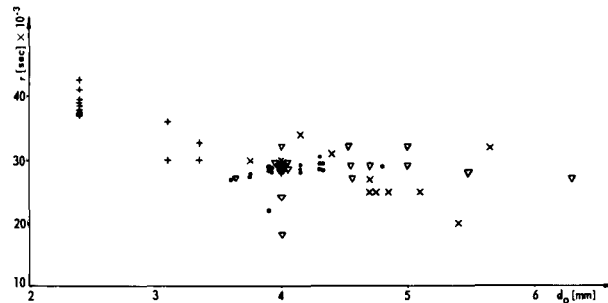


Figure 5. The time for which bubbles remain on the heating surface as a function of the bubble diameter at separation
 + : $q \approx 25.10^3$ (kcal/m²h) o : $q \approx 30.10^3$ (kcal/m²h)
 x : $q \approx 40.10^3$ (kcal/m²h) ∇ : $q \approx 50.10^3$ (kcal/m²h)

increased by 50%–100% (at the expense of redistribution) resulting in a diminished mercury surface superheating for 5°C to 10°C depending on the experimental conditions.

In our opinion this method of heat transfer is of great interest and our work has only touched on this problem. Further work on this is in progress in our laboratory. An analysis of the dynamics of vapour bubbles by taking their photographs with a high-speed cine-camera is in progress. Several preliminary photographs taken [5] and our observations helped us to see and understand the problems and the extent of this analysis which would give a good deal of information for further theoretical interpretation of the boiling phenomenon.

At higher heat fluxes the surface of the liquid metal becomes wavy. In this way the effective surface of heat transfer between two immiscible liquids becomes larger, thus enabling an increase of heat flux.

It is of some interest to compare the efficiency of the boiling heat transfer from a solid surface with or without a liquid metal. In a general case the addition of a liquid metal leads to an increase in the temperature of the solid surface for the given flux. Nevertheless, the increase of the temperature of the heating solid surface can be advantageous for solid surface temperatures exceeding those corresponding to burn-out heat fluxes. It should be noted that at these temperatures heat fluxes are expected to increase with the liquid metal layer. In other words it is possible to correct the dependence of heat flux on the preheating of the solid heating surface by varying the thickness of the liquid metal layer and its physical parameters and to obtain a more favourable dependence, an easier control as a result of greater temperature variation with the changing heat flux, and possibly, to achieve a higher burn-out of heat fluxes.

A very interesting heat transfer range is to be found at solid surface temperatures exceeding the liquid metal boiling point. Here the liquid metal layer boils from the solid surface and it condenses into the boiling liquid above the liquid metal.

Such a complex mechanism of heat transfer can be

achieved in a nuclear reactor or in the secondary heat exchangers for the reactor system.

NOMENCLATURE

T_s (°K):	absolute saturation temperature
t_s (°C):	saturation temperature
t_p (°C):	temperature of the heating surface
$\Delta t = t_p - t_s$ (°C):	liquid superheat temperature difference
q (kcal/m ² h):	heat flux density
α (kcal/m ² h °C):	heat transfer coefficient
P_s (kg/m ²):	saturation pressure
r_s (kcal/kg):	latent heat of vaporization
C (kcal/kg °C):	specific heat of the liquid at constant pressure
σ (kg/m):	surface tension
γ' (kg/m ³):	specific weight of the liquid
γ'' (kg/m ³):	specific weight of the vapour
λ (kcal/mh °C):	thermal conductivity of the liquid
a (m ² /h):	thermal diffusivity
ν (m ² /h):	kinematic viscosity of the liquid
μ (kg/m h):	viscosity of the liquid
Nusselt's number:	$Nu = \alpha \sqrt{[\sigma/(\gamma' - \gamma'')]/\lambda}$
Pecklet's number:	$Pe = q \sqrt{[\sigma/(\gamma' - \gamma'')]/r_s \gamma'' a}$
Kutateladze's number:	$Kp = P_s / \sqrt{[\sigma(\gamma' - \gamma'')]}$
Kruzilin's number:	$Kt = (r_s \gamma'')^2 / ACT_s \gamma' \times \sqrt{[\sigma(\gamma' - \gamma'')]}$

REFERENCES

1. Trefethen, L., *J. Appl. Phys.* 28,923 (1957).
2. Gordon, K. F., Singh, T. and Weisman, E. Y., *Internat. J. Heat Mass Transfer*, 3, 90 (1961).
3. Kutateladze, C. C., in *Osnovi teorii teploobmena*, Mashgiz, Moskva, 332 (1962).
4. Rohsenow, W. M. and Choi, H. Y., *Heat mass and momentum transfer*, Prentice-Hall, Inc., Englewood Cliffs, New Jersey, 223 (1961).
5. Novaković, M. and Stefanović, M., *Internat. J. Heat Mass Transfer* (July 1964).

ABSTRACT—RÉSUMÉ—АННОТАЦИЯ—RESUMEN

A/699 Yougoslavie

Ébullition d'un liquide à la surface d'un autre liquide

par M. Novaković et M. Stefanović

Les auteurs présentent les résultats d'une étude sur le transfert de chaleur dans le cas de l'ébullition d'un liquide sur une surface parfaitement lisse (interface liquide-liquide). De cette manière, on élimine la rugosité superficielle.

Ils décrivent un appareil original qui supprime les effets secondaires (par exemple, l'ébullition sur une surface solide). Ils ont utilisé la surface horizontale du mercure comme surface de chauffe à partir de laquelle quatre liquides ont été portés à ébullition à la pression atmosphérique. La surface du liquide (interface) a été maintenue dans un état de grande propreté par une méthode expérimentale spéciale. Les liquides utilisés étaient l'eau, l'alcool éthylique, le benzol et le n-pentane, qui ont tous des points d'ébullition compris entre 35 et 100 °C.

Les auteurs présentent les résultats des mesures du flux de chaleur d'ébullition q , de la surchauffe de la surface du liquide de chauffage Δt et du coefficient de transfert de chaleur correspondant α . La surchauffe de la surface de chauffage (liquide) était plus élevée qu'en cas d'ébullition sur une surface solide.

On distingue nettement deux régions d'ébullition, malgré leur ressemblance visuelle: l'ébullition par convection et l'ébullition par nucléation; les conditions de passage de l'un des deux genres d'ébullition à l'autre sont indiquées. Le coefficient de transfert de chaleur en fonction de la différence de température (surchauffe superficielle) pour les deux régions peut être représenté par la formule:

$$\alpha = C(\Delta t)^n$$

dans laquelle C est une constante qui dépend des paramètres physiques des liquides portés à ébullition et n une constante pour tous les liquides bouillants dans la région d'ébullition par nucléation.

Si, pour tous les liquides étudiés, on établit une corrélation entre les résultats obtenus en ce qui concerne le transfert de chaleur, d'une part, et les propriétés physiques du liquide considéré, d'autre part, ces résultats peuvent être représentés par la formule sans dimension suivante:

$$Nu = A(Pr, Pe, Kp)$$

dans laquelle les variables Nu , Pr , Pe et Kp sont des nombres sans dimension qui dépendent des paramètres des bulles.

Les auteurs donnent les résultats d'une étude préliminaire sur le mécanisme de nucléation faite au moyen d'une caméra rapide (6 000 images par seconde). Ils ont constaté que la fréquence des bulles augmente avec l'augmentation du diamètre de

celles-ci au moment où elles se séparent, alors que c'est le phénomène opposé que l'on constate dans les expériences d'ébullition à partir de surfaces solides. Les auteurs discutent les possibilités de nouvelles études détaillées au moyen de la photographie rapide.

A/699 Югославия

Кипение с жидких поверхностей раздела

М. Новакович, М. Стефанович

В настоящей работе приводятся результаты исследования теплопередачи при кипении с гладкой горизонтальной поверхности раздела «жидкость — жидкость». В этих условиях влияние шероховатости поверхности нагрева исключается.

Описана оригинальная аппаратура, с помощью которой проводилось исследование и на которой отсутствуют побочные эффекты. Поверхностью нагрева являлась горизонтальная поверхность ртути, на которой кипели различные жидкости при атмосферном давлении. Чистота жидкой поверхности раздела поддерживалась с помощью специальной экспериментальной методики. Исследовалось кипение четырех жидкостей: воды, этилового спирта, бензола и *n*-пентана с точками кипения между 35 и 100° С.

Приведены результаты измерения теплового потока q на поверхности нагрева, перегрева Δt поверхности нагрева и соответствующего коэффициента теплопередачи a при кипении. Установлен факт большей степени перегрева жидкой поверхности, чем в случае кипения с твердых шероховатых поверхностей.

Четко различаются два визуально сходных режима: конвекционное и пузырьковое кипение. Показано, при каких условиях один режим переходит в другой. Коэффициент теплопередачи как функция перегрева поверхности ртути для обоих режимов выражается как

$$a = C(\Delta t)^n,$$

где C — постоянная, зависящая от физических параметров кипящих жидкостей, а n — постоянная величина для всех кипящих жидкостей в режиме пузырькового кипения.

Результаты по теплопередаче для всех жидкостей скоррелированы с физическими параметрами кипящих жидкостей и представлены как

$$Nu = A(Pr, Pe, Kp),$$

где переменные Nu , Pr , Pe и Kp являются без-

размерными критериями, зависящими от параметров пузырьков.

Даны предварительные результаты полученные с помощью ускоренной киносъемки (6000 кадров в секунду). Найдено, что частота пузырька растет с увеличением диаметра пузырька при отрыве, что противоположно экспериментальным результатам при кипении с твердых поверхностей.

A/699 Yugoslavia

Ebullición desde una superficie de separación entre dos líquidos

par M. Novaković y M. Stefanović

El artículo presenta los resultados de una investigación de transmisión de calor por ebullición desde una superficie, idealmente suave, de separación entre dos líquidos. De esta forma se elimina la rugosidad de la superficie.

Se describe un aparato original que elimina efectos colaterales (v.g., ebullición desde una superficie sólida). Se usó una superficie horizontal de mercurio como superficie de calentamiento para hacer hervir cuatro líquidos a la presión atmosférica. La superficie de separación se conservó en un alto grado de limpieza por un procedimiento experimental especial. Los líquidos a hervir fueron: agua, alcohol etílico, benceno y n-pentano, cuyas temperaturas de ebullición van de 35 °C a 100 °C.

Se dan los resultados de las medidas del flujo de calor por ebullición q , supercalentamiento Δt de la superficie líquida de calentamiento y el coeficiente de transmisión de calor α correspondiente. Se observó que el supercalentamiento era mayor que en el caso de ebullición a partir de superficies sólidas.

Se distinguen claramente dos regiones de ebullición, similares a la vista, la ebullición convectiva y la ebullición por núcleos; se indican las condiciones de paso de una clase de ebullición a la otra. El coeficiente de transmisión de calor puede representarse en función de la diferencia de temperatura (supercalentamiento de la superficie) para ambas regiones por la relación $\alpha = C(\Delta t)^n$ donde C es una constante que depende de parámetros físicos de los líquidos en ebullición y n una constante para todos los líquidos hirvientes en la región de ebullición por núcleos.

Los resultados de transmisión de calor para todos los líquidos se relacionan con las propiedades físicas de los mismos y se representan en la expresión sin dimensiones: $Nu = A(Pr, Pe, Kp)$, donde las variables Nu , Pr , Pe y Kp son números sin dimensiones basados en parámetros de burbuja.

Se da cuenta de un estudio preliminar del mecanismo de formación de núcleos con cámara rápida de cine (6 000 fotos/s). Se observó que la frecuencia de las burbujas aumenta con el diámetro de las burbujas que emigran, que es precisamente lo contrario de los resultados experimentales sobre ebullición a partir de superficies sólidas. Se analizan las posibilidades de nuevos estudios detallados usando cámara rápida de cine.

Basic heat transfer and hydrodynamics studies in two-phase flow

By M. Silvestri, N. Adorni, S. Bertoletti, I. Casagrande, L. Cravarolo, G. P. Gaspari, A. Hassid, C. Lombardi, E. Pedrocchi and G. Peterlongo*

INTRODUCTION

This paper describes the experimental work on heat transfer and hydrodynamics with two-component mixtures and with steam-water mixtures flowing vertically upwards, which has been underway at CISE since 1958 [1]. This work is aimed at paving the way for the use of steam-water mixtures as a coolant for power reactors. The available knowledge on steam-water mixtures was extended towards the range of high outlet qualities and high specific mass flowrate.

A closed loop designed for room temperature operation and pressure up to 25 kg/cm² was used to perform experiments with two-component mixtures in adiabatic flow [2]. The test section, whose length is 400 cm, is fed separately with gas and liquid. The mixer is of the annular slot type, with gas entering on the run side. Suitable gas blowers were designed and built [3].

The experimental range was as follows:

Temperature:	16 to 40 °C
Pressure:	up to 22 kg/cm ²
Gas phase:	argon, nitrogen
Gas density:	3 to 40 × 10 ⁻³ g/cm ³
Gas viscosity:	1.8 to 2.2 × 10 ⁻⁴ poise
Liquid phase:	water, ethyl alcohol
Liquid viscosity:	0.7 to 1.2 × 10 ⁻² poise
Surface tension:	72 and 23 dyn/cm
Specific mass flowrate:	30 to 300 g/cm ² s
Quality:	0 to 1

Annular dispersed flow was mainly studied but other flow patterns were also studied, though to a less extent. Most of the experiments were performed with round tubes of 1.5 and 2.5 cm diam.

More complicated geometries were however studied but in less detail:

Annular conduits: rod 1 and 1.5 cm diam; tube 2.5 cm id.

Cluster: 7 rods 1 cm diam; tube 4.6 cm id.

The steam-water measurements were performed using two open loops of different sizes [4, 5]. In both cases the test line is pressurized by means of a control valve discharging into the atmosphere without heat

recovery; pressure in the test line is usually automatically controlled at the downstream end of the test section. Heating is obtained by Joule effect by passing a direct current through the metallic wall of the test section. The test section is preceded by an adiabatic section having the same cross-section geometry (calming length).

The largest number of experiments were made with a large calming length directly connected to a once-through boiler. In other cases the calming length was short and was either preceded by a throttling valve or by a mixing device separately fed with steam and water.

The range of physical variables explored was:

Pressure	40 to 90 kg/cm ² ;
Specific mass flowrate	100 to 400 g/cm ² s;
Inlet quality	-0.5 to 1.

A very large number of experiments were performed with tubular test sections covering the following range:

Heated length	2 to 400 cm;
Diam	0.5 to 2.5 cm;
Axial power distribution uniform; rectangular, obtained by an intermediate non-heated length; linearly increasing or decreasing, chopped cosine.	

Annuli and to some extent clusters were also tested; when necessary, reference is made to these measurements, which are still in progress; in particular, the influence of transverse obstacles (spacers) was studied in this case.

Non-conventional instrumentation and measurement techniques briefly described in the following sections were developed; in particular, the following may be mentioned: sampling probes [2, 6, 7], instruments for the direct measurement of the shear stress at the wall [8, 9], a method for the measurement of the liquid holdup [10, 11], differential thermocouples for heat transfer measurements [12], heat transfer crisis detectors [4, 5, 6].

This work was performed under contracts with the European Atomic Energy Community (Euratom).

By the end of this programme it is possible that the behaviour of steam-water mixtures is understood to such an extent that reliable orientative reactor

* CISE—Centro Informazioni Studi Esperienze, Segrate (Milan).

studies can be undertaken. Obviously, however, a number of specially designed experiments reproducing particular configurations and conditions will eventually be necessary during the development of a new reactor concept.

NOMENCLATURE

- D : equivalent diam
 D_e : outer diam in an annulus
 D_i : inner diam in an annulus
 G : average specific mass flowrate over the cross section (gas + liquid)
 G^+ : specific mass flowrate of one phase (gas or liquid)
 H : enthalpy
 L : length
 L_{sat} : saturation length $\left(= L \frac{W_{sat}}{W} \right)$
 P : pressure
 Q : total volume flowrate (gas + liquid)
 s : film thickness
 S : slip ratio
 U : actual linear velocity of one phase (gas or liquid)
 v^+ : flowrate specific volume of the mixture $\left(= \frac{1}{\rho^+} \right)$
 W : total power input to the heated section at the crisis
 W_{sat} : saturation power $(= X_0 \Gamma H_{gl} = W_{1,sat} + W_{2,sat} + \dots)$
 $W_{1,sat}$: power input over L_{sat} to the particular surface where the crisis is made to set on
 $W_{2,sat}, \dots$: power inputs over L_{sat} to surfaces different from that where the crisis is made to set on
 X : gas quality (by weight) $\left(= \frac{\text{average } G_g^+}{G} \right)$
 or $\frac{H - H_l}{H_{gl}}$ with steam-water mixtures
 X_v : gas quality (by volume)
 y : distance from the wall of the conduit
 α : gas volume fraction
 γ : surface tension
 Γ : total mass flowrate
 ΔP : pressure drop
 $\Delta \theta_F$: inner wall to bulk temperature difference
 μ : viscosity
 ρ : density
 ρ^+ : flow rate density $(= X_v \rho_g + (1 - X_v) \rho_l)$
 $\bar{\rho}$: actual density of the mixture $(= \alpha \rho_g + (1 - \alpha) \rho_l)$
 τ : wall shear stress
 ϕ : heat flux

Subscripts

- f: friction
 g: gas
 gl: gas minus liquid

- HT: in heat transfer conditions
 in: inlet
 l: liquid
 o: outlet

Phase and velocity distribution in annular-dispersed flow

The phase distribution is characterized by a continuous liquid film upon any wettable surface in contact with the two phases; the liquid volume fraction decreases from the surface towards the core, where the gas phase is the continuous one and the liquid is resolved into small droplets. The transition between the liquid film and the core is not well defined due to the irregular nature of the film surface; however, an approximated value of the extension of the film region can be given by the so-called electrical film thickness, which is obtained through the measurement of the electrical resistance of the liquid film: due to waves on the film surface and to the presence of a gas bubble inside the film itself, the electrical thickness is supposed to be an underestimated value.

The phase and velocity profiles over the conduit cross section were investigated in round tubes by means of two different kinds of sampling probes. The central region was investigated by means of a small cylindrical probe (0.2 cm id) [2, 6] which could also be used as a Pitot tube which measures directly the local values of G_1^+ , G_g^+ and of the impact pressure. The local values of U_g , U_l and $(1 - \alpha)$ (that is of the slip ratio) were evaluated through an analytical procedure based on the observation of the different behaviour of the two phases in proximity of an obstacle [6, 13].

The region adjacent to the wall was investigated, not by taking the electrical film thickness, but by means of a very different sampling probe [7]. In this case the values of the velocity and liquid volume fraction were evaluated assuming locally $S = 1$ over the region investigated (this is not in contrast with the results obtained over the core).

Typical profiles of the measured quantities (G_1^+ and G_g^+), detected with a two-component mixture under conditions which are supposed to be very close to fully developed flow, are reported in Fig. 1, where the evaluated quantities (U_g , $(1 - \alpha)$) are also indicated. The G_1^+ profile presents a minimum in correspondence with the axis of the conduit; the maximum value is always very near to the wall, well within the film region. The $(1 - \alpha)$ profile, as could be expected shows the liquid volume fraction continuously increasing towards the wall; the value $(1 - \alpha) = 1$ was never observed even at the minimum wall distance permitted by the probe (0.013 cm). No discontinuity in $(1 - \alpha)$ is observed by passing from the core to the film region.

The U_g profiles are very similar to, but sharper than, those existing in single-phase flow. The apparent wall roughness, due to the irregularities of the film-core

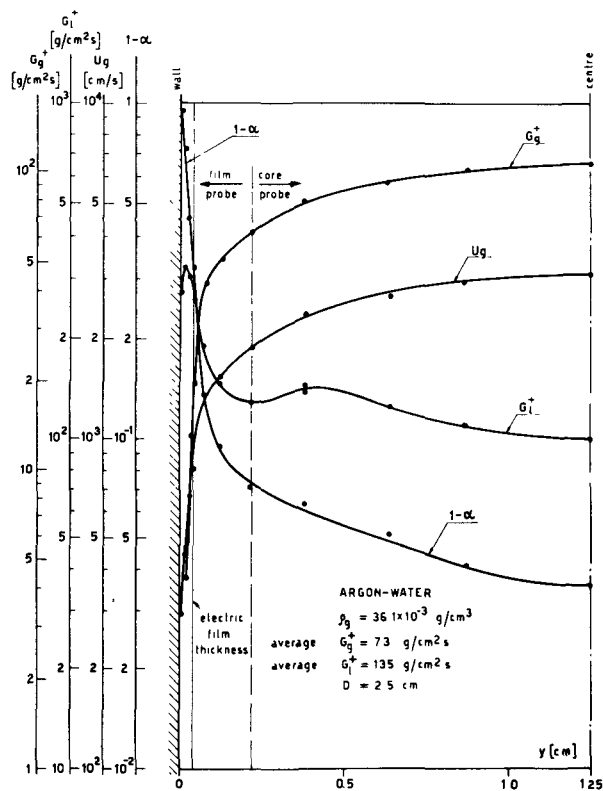


Figure 1. Typical phase and velocity distribution in a round duct

interface, and the damping of the turbulence, due to the droplets, might account for this.

Two remarks can be made [14]:

(a) The local values of the slip ratio seem to be close to one (1 to 1.5) over the whole cross section, and tend to increase near the wall. The higher values of the over-all slip ratio should be attributed therefore only to the higher liquid concentration in the low velocity region.

(b) The local values of the void fraction are rather large (0.4 to 0.2) even at wall distances much lower than the electrical film thickness. So one must suppose that small bubbles are present in the film region, which therefore is not to be considered as an all-liquid region, but the region in which, in contrast with the core, the liquid phase is the continuous one.

The phase and velocity distribution in the core region were investigated also with steam-water mixtures both under adiabatic and heat transfer conditions. The results are qualitatively the same, but the heat transfer seems to increase the liquid concentration in a zone of the core close to the film region.

For the electrical film thickness with two-component mixtures in adiabatic flow, which possibly is the easiest quantity to measure, an attempt was made to find out an empirical correlation, just in order to describe the influence of the main parameters involved.

For round tubes, the expression [13, 15, 16]:

$$s = f(X, G, \gamma) \rho_g^{0.55} D^{0.8}$$

was found to fit the experimental data ($\pm 10\%$) over the investigated range ($s = 0.02$ to 2 mm), but a simple

analytical form of the function $f(X, G, \gamma)$ adequate over the whole range was not found: qualitatively one can say that, for constant γ , s decreases with increasing X and G and, for constant X and G , with decreasing γ ; the last effect is marked in the range of the highest values of X and G .

The film thickness was measured also in the case of more complicated geometries, such as annuli [15] or clusters [17]. For annuli, the film thickness on the external wall can be given in the following form:

$$s_e = s_{e0} \left(\frac{D_e - D_i}{D_e} \right)^{0.45}$$

where s_{e0} is the thickness corresponding to $D_i = 0$ (with the same value of D_e). The film thickness on the internal wall is always lower than s_e (by a factor 1.5 to 3) and it was not possible to establish a dependence on D_i and D_e .

With clusters, at the highest liquid flowrate, the film thickness may vary even to a marked extent from rod to rod, probably due to the entrance effects, which in this case extend over a greater distance.

An important parameter, related to the heat transfer properties of the two-phase mixtures, is the liquid flowrate in the film region (Γ_F). This quantity, under adiabatic conditions, was evaluated in a first approximation from the G_1^+ profiles on the basis of the electrical film thickness.

For a single round tube (2.5 cm id), the following correlation was found to hold ($\pm 10\%$) [14]:

$$\frac{\Gamma_F}{\pi D \mu_1} = 5.3 (s^+)^{1.1} \quad (20 \leq s^+ \leq 300)$$

(where $s^+ = \frac{s\sqrt{\tau\rho_1}}{\mu_1}$), independently of γ , ρ_g and, at least within the narrow range investigated, of μ_1 , μ_g and ρ_1 ; the influence of the diameter was not investigated. According to this correlation, all other things being equal, Γ_F decreases with increasing X , while the trend is non-monotonic with G . For the same values of X and G , Γ_F is practically independent of ρ_g , but decreases markedly with decreasing γ .

Pressure drop

The pressure difference between two sections of a conduit results from the contribution of (a) the resistance undergone by the fluid against its motion, (b) the action of gravity and (c) the variation of the kinetic energy, or momentum, of the fluid. In two-phase flow these factors have a different significance depending on whether we consider the energy or the momentum balance of the fluids [6, 18, 19].

In the first case they are represented by: the energy lost in irreversibilities, proportional to the total volume flowrate ($Q \Delta P_f$); the potential energy due to gravity, proportional to the flowrate density (ρ^+); and the variation of the kinetic energy. In the second case they are represented by: the shear stress on the wall; the actual density of the mixture ($\bar{\rho}$); and the momentum variation. We call frictional pressure drop, or

pressure loss, the quantity ΔP_f which appears in the energy equation of two-phase flow and is directly related to the pumping power.

In adiabatic flow it is relatively easy to separately evaluate the single contributions in the measured pressure drop. In fact with a conduit of uniform cross section, and with a negligible variation of the gas density and of the phase and velocity distribution in the flow direction, the contribution of the energy or momentum variation can be neglected. As a consequence, the knowledge of the flowrate density, according to the energy equation, makes it possible to compute immediately the pressure loss; on the other hand, as will be seen later on, if a direct measurement of the shear stress can be performed, the actual density of the mixture can also be evaluated.

In annular dispersed flow ΔP_f increases monotonously with quality up to $X \simeq 0.7$; above this value, and depending on the physical properties of the two phases, ΔP_f may reach a maximum for low specific mass flowrates. The influence of the various parameters was separately studied and, in the range of monotonic variation, brought to the following empirical correlation, which is valid in fully developed flow for round tubes, annuli and clusters (within $\pm 20\%$) [15, 16, 19]:

$$\frac{\Delta P_f}{L} = K \frac{G^{1.4} \gamma^{0.4}}{D^{1.2}} \left(\frac{1}{\rho^+} \right)^n \quad (\text{CGS units})$$

where $K = 0.112$ and $n = 0.75$.*

It may be observed that the dependence on the equivalent diameter is the same, while the exponent of G is lower than in single-phase flow. The influence of viscosity of both phases was found to be negligible, whereas that of the surface tension is relatively marked [21].

The shear stress on the wall was measured directly with a special device. The principle consists in measuring, in addition to the pressure gradient, the force balancing a small sleeve of the same internal dimensions as the conduit, and which can slide along the flow direction [8, 9]. Shear stress data for round tubes are correlated through the following empirical relationship:

$$\tau = 9.1 \times 10^{-3} \frac{\gamma^{0.4}}{D^{0.3}} G^{1.5} X^{0.7} \frac{1}{\rho_g^{0.9}} \quad (\text{CGS units})$$

It is worth mentioning that the influence of μ_1 and μ_g does not appear in the correlation. Although this was not investigated, it can be inferred nevertheless that it should be negligible, since both ΔP and $\bar{\rho}$ do not depend on these parameters.

Under heat transfer conditions the contribution of the energy of momentum variation is in many cases a substantial fraction of the total pressure drop. Unfortunately this contribution is not simple enough to evaluate, and therefore an empirical correlation

(in graphical form) of the total pressure drop was elaborated for round tubes in the form [20]:

$$\frac{\Delta P_{HT}}{\Delta P_0} = f \left[\left(\frac{\Delta v^+}{v_0^+} \right) / \frac{L}{D} \right]$$

where ΔP_0 is the total adiabatic pressure drop and v_0^+ the flowrate specific volume corresponding to the outlet conditions, while Δv^+ is the variation of the flowrate specific volume over the length L . In many practical cases the ratio $\frac{\Delta P_{HT}}{\Delta P_0}$ is close to one. The approximation is better with positive inlet quality but it is still reasonably correct if the two-phase flow exists along most of the conduit.

Liquid volume fraction

Four different methods were used to measure directly or to evaluate, in adiabatic conditions, the liquid volume fraction, and the related quantities (mean density and over-all slip ratio), which are based on the following principles:

Measurement of the variation of the hold-up in the liquid line [10] for given flow conditions**;

Measurement of the shear stress on the wall and of the pressure drop, in those cases in which the momentum variation along the flow direction is negligible [7, 8];

The integration of the phase distribution profiles over the conduit cross section [13, 22];

The integration of the profiles of the quantity of matter given by the β -ray attenuation measurements [6, 23].

The values of the liquid volume fraction given by these methods agree within $\pm 10\%$, that is, actually, within the accuracy of the measurements. This gives a certain confidence about the reliability of methods and results.

The experimental data (22) show that the difference between the values of $(1 - \alpha)$ and of $(1 - X_v)$ depends, as would be expected, on the flow pattern. In the region of bubble flow (that is, roughly, for $(1 - X_v) > 0.65$) these values are nearly identical, while in annular-dispersed flow (roughly $(1 - X_v) < 0.15$) they generally are appreciably different, and their difference depends on the other parameters.

With argon-water mixtures in round tubes at various pressures the following correlation gives an approximation better than 10% ($(1 - X_v) > 0.01$) [22]:

$$\frac{1 - \alpha}{1 - X_v} = \frac{3.45}{(1 - X_v)^{0.2} G^{0.3} \rho_g^{0.2} D^{0.25}} \quad (\text{CGS units})$$

It may be noted that the Martinelli-Lockhart [24], Martinelli-Nelson [25], and Hughmark [26] correlations do not take into consideration G and D , while Marchaterre [27] gives a dependence on G very close to that indicated by the CISE data.

* In the more restricted range explored with steam-water mixtures (round tubes) the best fitting values of K and n are respectively 0.087 and 0.86 [20].

** This method was also used for liquid volume fraction measurements with heat transfer in a small loop operating at a pressure of 10 kg/cm^2 [11].

The role played by μ_g and μ_l was not established with accuracy, but it can be said [22], and agreed by other authors, that it is inferior to that of the other parameters and probably very moderate. The influence of ρ_l was not investigated. The influence of γ is difficult to precise within the range investigated. From a qualitative point of view $(1 - \alpha)$ decreases with decreasing γ , but this effect is less important in correspondingly high values of $(1 - \alpha)$. As an example, a comparison is made between the results obtained in a round tube, 2.5 cm id, using alternatively water ($\gamma = 72$ dyn/cm) and alcohol ($\gamma = 23$ dyn/cm) as the liquid phase. In annular dispersed flow we have a good approximation ($(1 - \alpha)_{\text{water}} > 0.05$):

$$(1 - \alpha)_{\text{alcohol}} = (1 - \alpha)_{\text{water}} - 0.03$$

(at the same $1 - X_v$)

In the region $0.15 < (1 - X_v) < 0.65$ the respective influence of the various parameters is qualitatively the same as in annular-dispersed flow, and decreases quantitatively going towards the upper limit.

A limited number of experiments in adiabatic conditions were performed also in a cluster geometry [17]. The values of the ratio $\frac{1 - \alpha}{1 - X_v}$, for the same G , X and physical properties, are not too different from the values obtained with a round tube 1.5 cm id.

Heat transfer

Heat transfer measurements [12, 28] were made by means of differential thermocouples; the junctions of one differential thermocouple were installed respectively on the external wall of the heated section (hot junction) and on the external wall of an adiabatic section of the test line (cold junction).

The readings of such thermocouples were reduced, after calibration in single-phase flow, to the temperature difference $\Delta\theta_F$ between the bulk temperature and the temperature of the heated wall in contact with the coolant, in correspondence with the hot junction. The accuracy of measurements was adequate for the detailed observation of the heat transfer mechanisms in two-phase flow.

Figure 2 gives an example of the behaviour of $\Delta\theta_F$ versus ϕ at the outlet of a heated tube for constant inlet conditions. Up to a given threshold (dropdown threshold = ϕ_D) $\Delta\theta_F$ is affected by two distinct hysteresis effects: with the first one, when ϕ reaches up to or above ϕ_D , the representative point will follow a path such as A, B, A'; with the second one, if ϕ remains lower than ϕ_D , the path will be along A, α , β .

The observations permit one to state tentatively that in typical cases of liquid film heat transfer, as with steam-water mixtures, even at relatively low quality, free-surface evaporation is the predominant heat transfer mechanism. For a given value of the heat flux the description of the film (of its free surface, in particular) can correspond to any point in a determined

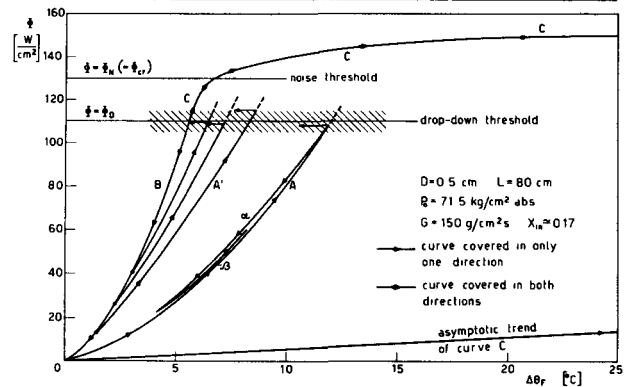


Figure 2. Typical trend of the wall-to-bulk temperature difference versus heat flux near the outlet

range of metastable structural states and the particular structure in existence strongly reflects on heat transfer. Moreover, whereas curves A, A', etc., depend both on inlet conditions and on the history of the heat flux variations, curve B is independent of these parameters within the accuracy of the experiments. Above a determined value of the heat flux (ϕ_D), only one stable structure of the film can exist, and the representative point follows curve C; curves C branch off from curve B at heat flux levels which depend on inlet conditions.

The structure of the film along curves C is characterized by locally and occasionally thinner patches; for a given power input the film temporarily dries out over these patches and then reforms or tends to reform; in such conditions (noise threshold) heat transfer is affected by a very characteristic noise. The noise first sets on at the outlet of the heated section and progressively reaches upstream for increasing power inputs.

If the heat flux is increased above the noise threshold, the wall is progressively freed of water. When this is achieved, heat transfer involves two steps: convection to steam which becomes effectively superheated; evaporation of droplets in superheated steam. One may imagine that droplets carried in the bulk become progressively incapable of entering into contact with the wall.

Moreover, the behaviour of heat transfer after fast ramp power rises has been studied. It was found that for values of the specific mass flowrate, at least up to 200 g/cm²s, such power rises can cause for short periods premature and exasperated crises (premature patch dry-out of the liquid film) even for values of the heat flux inferior to the noise threshold. Heat flux rapidly rising from zero to a given value renders the metastable states of the liquid film more unstable.

Heat transfer crisis

Sharp transitions between different evaporative heat transfer mechanisms are described as heat transfer crises. The noise onset observed in the present heat transfer experiments corresponds to this description, since in particular both $\overline{\Delta\theta_F}$ (time average of $\Delta\theta_F$) and the noise amplitude increase rapidly with the power input from the noise threshold onwards [12, 28].

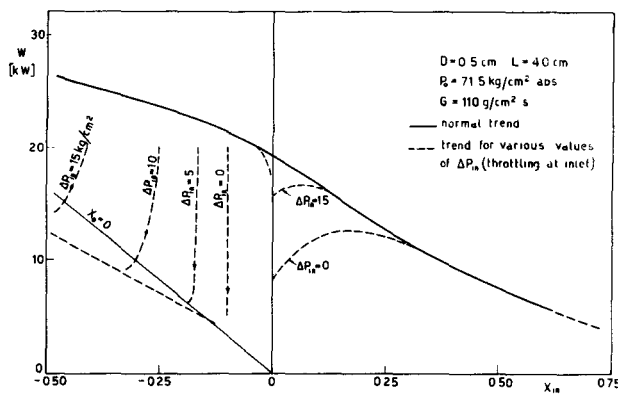


Figure 3. Typical trend of the critical power versus inlet quality

The available evidence suggests that the noise onset is due to the disruption of the liquid film wetting the heated surface, and therefore this phenomenon will be described as film disruption crisis.

Experimentally [4, 5] the noise threshold is detected by a differential thermocouple similar to those used for heat transfer measurements, the hot junction of which was installed on the external wall of the heated surface close to the outlet. The test section was furthermore provided with two distinct power tripping devices: an electrical circuit with a system of relays sensitive to the change of the electrical resistance, and therefore of the temperature of a small portion of the heated surface near the outlet, and a microswitch held open by a low melting point metallic strip in close contact with the heated wall. These devices could be used both to detect the crisis and as safety devices.

In an ideal case, the critical power, in particular conditions defined by the heated length, cross-section geometry, specific mass flowrate and absolute pressure, when plotted versus inlet quality (Fig. 3) is seen to decrease monotonously for increasing X_{in} and tends to zero for X_{in} tending to unity; the trend is approximately linear for $X_{in} \leq 0$.

As this work progressed, a correlation using the outlet parameters was found to fit satisfactorily the experimental data obtained with round tubes, uniform heat flux, $X_{in} \gg 0$ [6].

The normal trend of the critical power versus inlet quality can be affected by very marked disturbances [29]. In a first approximation, to describe data relevant to this normal trend in the case of upward flow in vertical channels with constant cross section, without transverse obstacles, including separately heated surfaces as outer tube and rod in an annulus, the following parameters are found [29, 30] sufficient: cross-section geometry; absolute pressure; specific mass flowrate; length of the section between the point where $X = 0$ and the outlet of the heated section (saturation length L_{sat}); power input one L_{sat} to the particular surface where the crisis is made to set on ($W_{1,sat}$).

In the case of $X_{in} > 0$, L_{sat} should be extrapolated as $L_{sat} = L \frac{W_{sat}}{W}$: actually [31], all other conditions

being equal, the critical power input is very largely independent of the heat flux distribution for $X_{in} > 0$, although this is not valid any more above a given value (for instance 5) of the ratio of maximum to average heat flux.

The adequacy of these parameters to describe the crisis, and the fact that the onset of the crisis in two separately heated surfaces cooled by the same flow are independent phenomena actually suggest that, once two-phase flow is established, heat transfer is essentially governed by the amount of water flowing close to the heated wall which should, moreover, be little influenced by the water flowing in the bulk or close to other surfaces.

The disturbances affecting the normal trend of data and the limits of the field in which L_{sat} and $W_{1,sat}$ are adequate parameters are discussed now:

(a) In the case of $X_{in} < 0$, the heat flux should not be such that the situation at any point over the cross section could be very far from thermodynamic equilibrium.

(b) For $X_{in} < 0$ strong pressure pulsations may occur when the power input is such that the outlet quality X_0 is near zero; they may end by a heat transfer crisis probably due to the onset of film boiling. These pulsations depend on the characteristics of the test line; for instance the introduction of a concentrated pressure drop immediately upstream of the heated section influences markedly the trend of the phenomenon (see dotted lines in Fig. 3).

(c) For small positive values of X_{in} especially in the lower range of the flowrates a strong perturbation is generally found which still leaves unaltered the characteristics of the film disruption crisis. The perturbed trend may be due to slug flow and may be brought closer to normal by a concentrated pressure drop at inlet (see dotted lines in Fig. 3).

(d) For $X_{in} > 0$ the extrapolated saturation length can be relevant to the observed phenomenon only if the actual inlet phase distribution is not too different from that resulting from ebullition over ($L_{sat} - L$) with a heat flux equal to the average over L . This explains the strong effect of inlet conditions found with short test sections [32].

(e) For high inlet linear velocities, when the liquid film is thinnest, discrepancies between data obtained with different test sections of the same geometry may be due to roughness or, more generally, to small-scale geometrical imperfections of the heated wall.

(f) If spacers or other obstacles are present, providing bridges over the gap between heated surfaces or heated and non-heated surfaces, the crisis is no longer an independent phenomenon for each surface; the same may be expected for very small gaps between distinct surfaces. No interaction between distinct surfaces has, however, been found for gaps down to 0.15 cm.

For the normal trend of data the film disruption crisis correlation should have the form:

$$F(\text{cross-section geometry, } P, G, W_{1,sat}, L_{sat}) = 0$$

However, it may also be convenient to look for formulae using system-describing parameters (for instance L , W , X_{in}); such formulae should be implicitly equivalent to the expression $F = 0$ [29].

REFERENCES

- Silvestri, M., Finzi, S. et al. *Gas-liquid and vapour-liquid mixtures as cooling agents*, Proceedings of the Second International Conference on the Peaceful Uses of Atomic Energy, P/1367, Vol. 7, p. 819, United Nations (1958).
- Adorni, N., Cravarolo, L., Giorgini, A., Hassid, A., and Pedrocchi, E., *Design and construction of a high pressure facility for hydrodynamics experiments on two-phase flow—Instrumentation—Preliminary tests in single and two-phase flow*, CISE report R-75 (1963).
- Adorni, N., and Cravarolo, L., *Development of a high pressure blower*, Energia Nucleare, 10 (10), 548 (1963).
- Adorni, N., Alessandrini, A., Bertolotti, S., Gaspari, G. P., Lombardi, C., Peterlongo, G., Soldaini, G., and Zavattarelli, R., *Description of a loop for heat transfer experiments with steam-water mixtures (Part I) and of pressure drop measurements in adiabatic conditions (Part II)*, CISE report R-62 (1962).
- Adorni, N., Alessandrini, A., Peterlongo, G., Ravetta, R., *Large-scale experiments on heat transfer and hydrodynamics with steam-water mixtures; Description of the experimental plant*, CISE report R-79 (1963).
- A research programme in two-phase flow*, CISE report (January 1963).
- Adorni, N., Alia, P., Cravarolo, L., Hassid, A., and Pedrocchi, E., *An isokinetic sampling probe for phase and velocity distribution measurements in two-phase flow near the wall of the conduit*, CISE report R-89 (1963).
- Adorni, N., Cravarolo, L., Hassid, A., Pedrocchi, E., and Silvestri, M., *Measurement of shear stress on the wall of a conduit and its application to the void fraction determination in two-phase flow*, Review of Scientific Instruments, 34 (8), 937 (1963).
- Cravarolo, L., Giorgini, A., Hassid, A., and Pedrocchi, E., *A device for the measurement of shear stress on the wall of a conduit—its application in the mean density determination in two-phase flow—Shear stress data in two-phase adiabatic vertical flow*, CISE report R-82 (1964).
- Alia, P., Cravarolo, L., Hassid, A., Pedrocchi, E., and Silvestri, M., *A volume displacement method for the measurement of the liquid volume fraction in two-phase adiabatic flow*, CISE report R-92 (1964).
- Schrock, V. E., Angelino, G., Possa, G., and van Erp, J. B., *Density measurements in a boiling channel*, Energia Nucleare, 10 (10), 525 (1963).
- Bertolotti, S., Lombardi, C., and Silvestri, M., *Heat transfer to steam-water mixtures*, CISE report R-78 (1964).
- Cravarolo, L., Hassid, A., and Pedrocchi, E., *Phase and velocity distribution in two-phase adiabatic annular-dispersed flow*, CISE report R-109 (1964).
- Cravarolo, L., and Hassid, A., *Phase and velocity distribution in two-phase adiabatic dispersed flow*, CISE report N-98 (1963). Presented at the European Atomic Energy Society Symposium, Studsvik (October 1963).
- Adorni, N., Casagrande, I., Cravarolo, L., Hassid, A., Pedrocchi, E., and Silvestri, M., *Further investigations in adiabatic dispersed two-phase flow: Pressure drop and film thickness measurements with different channel geometries—Analysis of the influence of geometrical and physical parameters*, CISE report R-53 (1963).
- Casagrande, I., Cravarolo, L., Hassid, A., and Pedrocchi, E., *Adiabatic dispersed two-phase flow: Further results on the influence of physical properties on pressure drop and film thickness*, CISE report R-73 (1963).
- Alia, P., Cravarolo, L., Hassid, A., and Pedrocchi, E., *Two-phase adiabatic vertical upflow: A preliminary study of a cluster geometry*, CISE report R-108 (1964).
- Casagrande, I., and Cravarolo, L., *Some remarks on the power consumption and pressure loss in adiabatic vertical two-phase flow*, Energia Nucleare, 9 (1), 36 (1962).
- Alia, P., Cravarolo, L., Hassid, A., and Pedrocchi, E., *Pressure drop in two-phase adiabatic vertical upflow*, CISE report R-107 (1964).
- Gaspari, G. P., Lombardi, C., and Peterlongo, G., *Pressure drops in steam-water mixtures. Round tubes—vertical upflow*, CISE report R-83 (1964).
- Cravarolo, L., Hassid, A., and Pedrocchi, E., *Some remarks on the Martinelli-Nelson pressure loss correlation in two-phase flow*, Energia Nucleare, 10 (7), 395 (1963).
- Alia, P., Cravarolo, L., Hassid, A., and Pedrocchi, E., *Liquid volume fraction in adiabatic two-phase vertical upflow—Round conduit*, CISE report R-105 (1964).
- Cravarolo, L., Hassid, A., and Villani, S., *A beta-ray attenuation method for density measurements of liquid-gas mixtures in adiabatic flow*, Energia Nucleare, 8 (12), 751 (1961).
- Lockhart, R. W., and Martinelli, R. C., *Proposed correlation of data for isothermal two-phase, two-component flow in pipes*, Chem. Eng. Progr., Vol. 45, No. 1 (1949).
- Martinelli, R. C., and Nelson, D. B., *Prediction of pressure drop during forced circulation boiling of water*, Transaction of the ASME (August 1948).
- Hughmark, G. A., and Pressburg, B. S., *Holdup and pressure drop with gas-liquid flow in a vertical pipe*, Amer. Inst. Chem. Eng. Journal, 7 (4), (1961).
- Marchaterre, J. F., and Høglund, B. M., *Correlation for two-phase flow*, Nucleonics (August 1962).
- Bertolotti, S., and Lombardi, C., *Heat transfer of steam-water mixtures at 70 kg/cm² in round tubes*, CISE report N-97 (1963). Presented at the European Atomic Energy Society Symposium, Studsvik (October 1963).
- Heat transfer crisis with steam-water mixtures*, CISE report R-99 (1964). (Report in preparation.)
- Bertolotti, S., Lombardi, C., and Peterlongo, G., *Qualitative remarks on the nature of the heat transfer crisis with steam-water mixtures*, Energia Nucleare, 11 (5), 268 (1964).
- Bertolotti, S., Gaspari, G. P., Lombardi, C., and Zavattarelli, R., *Critical heat flux data for fully developed flow of steam-water mixtures in round vertical tubes with non uniform axial power distribution*, CISE report R-74 (1963).
- Alessandrini, A., Peterlongo, G., and Ravetta, R., *Large-scale experiments on heat transfer and hydrodynamics with steam-water mixtures: Critical heat flux and pressure drop measurements in round vertical tubes at the pressure of 51 kg/cm² abs*, CISE report R-86 (1963).

ABSTRACT—RÉSUMÉ—АННОТАЦИЯ—RESUMEN

A/867 Italie

Etudes de base sur le transfert de chaleur et l'hydrodynamique dans les écoulements à deux phases

par M. Silvestri *et al.*

Ce mémoire présente un examen général du travail expérimental effectué au CISE dans le domaine du transfert de chaleur et de l'hydrodynamique des écoulements à deux phases en convection forcée. Nous y indiquons les principaux résultats obtenus de même que certaines corrélations des données expérimentales.

Les principaux points abordés sont les suivants:

- a) Distribution de phase et de vitesse.
- b) Chute de pression;
- c) Fraction volumique de liquide;
- d) Mécanisme du transfert de chaleur;
- e) Crise du transfert de chaleur.

Les expériences ont été effectuées sur des conduits verticaux en écoulement ascendant; le régime annulaire-dispersé a été principalement étudié.

Les expériences de transfert de chaleur ont été exécutées avec des mélanges eau-vapeur à haute pression (50 à 90 kg/cm²).

Mais la plus grande partie des résultats concernant la distribution de phase et de vitesse et la fraction volumique de liquide a été obtenue avec des mélanges à deux constituants en conditions adiabatiques à la température ambiante (jusqu'à 22 kg/cm² de pression); cependant, quelques expériences ont été effectuées avec transfert de chaleur.

Les mesures de chutes de pression ont été effectuées dans toutes les conditions citées plus haut, avec et sans transfert de chaleur.

On a concentré les recherches principalement à des tubes cylindriques; cependant d'autres géométries plus compliquées, telles que des espaces annulaires et des grappes, ont fait l'objet de quelques expériences.

L'influence des conditions hydrodynamiques à l'entrée et de la distribution axiale de puissance a été aussi étudiée.

Les conditions expérimentales avec les mélanges à deux constituants ont été les suivantes:

- Phase gazeuse: argon, azote
- Phase liquide: eau, alcool éthylique
- Température: 16 à 40 °C
- Pression: jusqu'à 22 kg/cm²
- Débit massique spécifique: 30 à 300 g/cm²s
- Titre: 0 à 1

Conduits cylindriques { diamètre: 1,5 à 2,5 cm
longueur: 120 à 350 cm

Avec les mélanges eau-vapeur, les domaines étudiés ont été suivants:

- Pression: 50 à 90 kg/cm²
- Débit massique spécifique: 100 à 400 g/cm²s
- Titre à l'entrée: 0,5 à 0,1

Titre à la sortie: supérieur à zéro

Conduits cylindriques { diamètre: 0,5 à 2,5 cm
longueur chauffée: 2 à 400 cm

Ce travail a été exécuté sous contrat avec la Communauté européenne de l'énergie atomique (EURATOM).

A/867 Италия

Основные исследования теплопередачи и гидродинамики в двухфазном потоке

M. Сильвестри *et al.*

Дается общий обзор экспериментальной работы, проделанной в Информационном центре экспериментальных исследований в области теплопередачи и гидродинамики двухфазного потока при вынужденной конвекции. Приводятся основные результаты и некоторые корреляции экспериментальных данных. Основными вопросами являются следующие:

- a) фаза и распределение по скоростям;
- b) падение давления;
- c) объемная доля жидкости;
- d) теплопередача;
- e) кризис теплопередачи.

Эксперименты проводились с потоком, направленным вверх по вертикальным трубопроводам; был исследован главным образом режим кольцеобразно рассеянного потока.

Данные по теплопередаче были получены на паро-водяных смесях при высоком давлении (50 ÷ 90 кг/см²).

Большая же часть данных о фазе и распределении по скоростям, а также по объемной доле жидкости была получена на двухкомпонентных смесях в адиабатических условиях при комнатной температуре (давление до 22 кг/см²); однако лишь ограниченное количество экспериментов было проведено с теплопередачей.

Измерения падения давления проводились во всех экспериментальных условиях, указанных выше, как с теплопередачей, так и без нее.

Для большинства экспериментов применялись круглые трубы; частично были исследованы более сложные геометрии, такие, как кольцеобразная и в виде пучка. Было также изучено влияние гидродинамических условий на входе в трубопровод и осевое распределение тепловой мощности.

Условия экспериментов на двухкомпонентных смесях были следующими:

Газообразная фаза: аргон, азот
 Массовый удельный расход: $30 \div 300 \text{ г/см}^2 \cdot \text{сек}$

Жидкостная фаза: вода, этиловый спирт
 Качество: $0 \div 1$

Температура: $16 - 40^\circ \text{C}$

Круглые трубы
 Диаметр: $1,5 \div 2,5 \text{ см}$
 Длина: $120 \div 350 \text{ см}$

Давление: до 22 кг/см^2

На паро-водяных смесях исследовался диапазон

Давление: $50 \div 90 \text{ кг/см}^2$
 Массовый удельный расход: $100 \div 400 \text{ г/см}^2 \cdot \text{сек}$
 Диаметр: $0,5 \div 2,5 \text{ см}$

Качество на входе: $-0,5 \div 1$
 Длина нагрева:

Качество на выходе: выше нуля
 $2 \div 410 \text{ см}$

Эта работа была проделана по контрактам, заключенным с Европейским сообществом по атомной энергии (Евратом).

A/867 Italia

Estudios básicos sobre transmisión de calor e hidrodinámica en flujo bifásico

por M. Silvestri et al.

Se presenta un repaso general del trabajo experimental realizado en el CISE acerca de la transmisión de calor y la hidrodinámica del flujo bifásico en convección forzada. Se señalan los resultados principales y se dan algunas correlaciones de los datos experimentales.

Los puntos principales son los siguientes:

- Distribución física y de velocidades;
- Caída de presión;
- Fracción de volumen de líquido;
- Transmisión de calor;
- Crisis de la transmisión de calor.

Los experimentos se realizaron en conductos verticales con flujo ascendente y sobre todo se estudió el régimen de flujo anularmente disperso.

Se recogieron datos de transmisión de calor en mezclas agua-vapor con alta presión. (40 a 90 kg/m^2).

En cambio, la mayor parte de los datos referentes a la distribución de las fases y velocidades, así como acerca de la fracción de volumen líquido, se recogieron a temperatura ambiente (presión hasta de 22 kg/cm^2) con mezclas de dos componentes en condiciones adiabáticas; no obstante se realizó un cierto número de experimentos con transmisión de calor.

Las medidas de caída de presión se llevaron a cabo en todas las condiciones experimentales citadas más arriba, con y sin transmisión de calor.

La mayoría de las experiencias se hicieron con tubos redondos aunque también se investigaron hasta cierto punto geometrías más complicadas, como anillos y haces.

También se estudió la influencia de las condiciones hidrodinámicas a la entrada del conducto y la de la distribución axial de potencia.

He aquí las condiciones experimentales para mezclas de dos componentes:

Fase gaseosa: argón, nitrógeno
 Fase líquida: agua, alcohol etílico

Temperatura: 16 a 40°C
 Presión: hasta 22 kg/cm^2
 Caudal específico másico: 30 a $300 \text{ g/cm}^2\text{s}$
 Calidad: 0 a 1

Tubos redondos:
 Diámetro $1,5$ a $2,5 \text{ cm}$
 Longitud 120 a 350 cm

Con mezclas agua-vapor, la zona explorada fué:

Presión: 40 a 90 kg/cm^2
 Caudal específico másico: 100 a $400 \text{ g/cm}^2\text{s}$
 Calidad de entrada: $-0,5$ a 1
 Calidad de salida: mayor de cero

Tubos redondos:
 Diámetro $0,5$ a $2,5 \text{ cm}$
 Longitud caldeada 2 a 400 cm

Este trabajo se realizó bajo contrato con la European Atomic Energy Community (EURATOM).

Liquid-metal heat transfer

By O. E. Dwyer* and R. N. Lyon**

For heat transfer to or from a fluid flowing in a channel, integral equations of the type first developed by Lyon [1], and based on a generalization of the von Kármán [2] approach, have found considerable use in the liquid-metal heat transfer field. These equations, for the conditions of uniform heat flux and fully established flow, are based on the assumption of independence of physical properties with transverse temperature variation, which is usually permissible for liquid metals. Equations of this type have been written for: (a) round pipes [1], (b) infinite parallel plates, with heat transfer from one plate only [3], (c) concentric annuli with heat transfer from the inner wall only [4], (d) the same, with heat transfer from the outer wall only [4], (e) in-line flow through rod bundles having equilateral triangular spacing and a P/D ratio greater than 1.3 [5], and (f) in-line flow through rod bundles having square spacing and a P/D ratio greater than 1.7 [6]. In all of these equations, the eddy diffusivity of heat transfer ϵ_H is represented by the product $\psi\epsilon_M$, where ϵ_M is the eddy diffusivity of momentum transfer, and ψ is the ratio of the two diffusivities.

ϵ_M and its effect on Nusselt number

Figure 1 shows a number of possible ϵ_M profile curves for turbulent flow through an annulus. All are identical over the radial distances between the walls and the radii of maximum ϵ_M . Between these radii, four different types of profiles are shown, all of which have been used or recommended in the past. Type (a) has been used by Knudsen and Katz [7], (b) is similar to the measured profiles of Page *et al.* [8] for the flow of air in narrow channels, (c) is typical of profiles calculated by means of the correlation of Rothfus, Walker, and Whan [9], and (d) is similar to the early predictions of von Kármán [2] for turbulent flow in pipes. The equality of the ϵ_M maxima is in accordance with the correlation of Rothfus *et al.*, which is based upon the premise that the radius of maximum velocity for turbulent flow in annuli is the same as that for laminar flow in annuli.

The uncertainty of the ϵ_M profile in the region of maximum linear velocity is mostly the result of its being indeterminate at r_m , the radius of maximum velocity. However, there seems to be increasing evidence that the shape of the ϵ_M profile is closer to

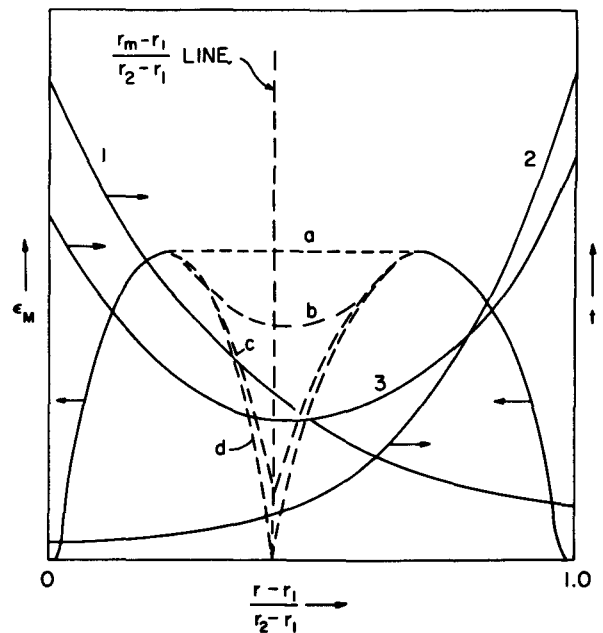


Figure 1. Typical ϵ_M and temperature profiles for heat transfer to a liquid metal flowing in an annulus

Curves a, b, c, and d represent different types of ϵ_M profile curves; while curves 1, 2, and 3 represent cases of heat transfer from inner wall only, outer wall only and from both walls with equal fluxes, respectively. r_1 , r_2 and r_m represent inner radius, outer radius, and radius of maximum velocity, respectively

that represented by curve (b), with the value at r_m roughly $\frac{3}{4}$ of the maximum value. Curves similar to those in Fig. 1 apply to pipes, parallel plates, and in-line flow through rod bundles. For pipes, only the right portion of the figure applies; for parallel plates, the curves would look similar to those shown except r_m would be at the mid-transverse point; and for rod bundles, only the left portion of the figure applies.

The effect of ϵ_M profile shape on the calculated heat transfer coefficient can be quite significant depending upon flow rate, geometry and, in the case of annuli and parallel plates, whether the heat transfer is unilateral or bilateral. The numbers in Table 1 represent the ratio of the heat transfer coefficient calculated using profile (b) to that using profile (c). For some cases, the effect is nil; for others, it is appreciable. In a given case, the relative magnitude of the effect can be judged by comparing the ϵ_M and temperature curves in Fig. 1. The higher the slope of the temperature curve, the greater the effect. For a

* Brookhaven National Laboratory, Upton, New York.

** Oak Ridge National Laboratory, Oak Ridge, Tennessee.

Table 1. Effect of ϵ_M -profile shape on heat transfer coefficient for heat transfer to liquid metals under conditions of uniform heat flux and fully established flow

Typical case	ratio, Coefficient based on ϵ_M profile (b) / Coefficient based on ϵ_M profile (c)		
	$\bar{\psi}Pe = 10^2$	$\bar{\psi}Pe = 10^3$	$\bar{\psi}Pe = 10^4$
(1) Pipes	1.00	(1.00)	(1.01)
(2) Parallel plates, heat flow from one plate only .	1.01	1.04	1.08
(3) Parallel plates, equal heat fluxes from both plates	1.00	1.00	1.01
(4) Annuli, $y = 2$, heat flux from inner wall only .	1.02	1.06	1.11
(5) Annuli, $y = 2$, heat flux from outer wall only .	1.00	1.01	(1.03)
(6) Annuli, $y = 2$, equal heat fluxes from both walls, h_1	1.00	0.99	0.93
(7) Annuli, $y = 2$, equal heat fluxes from both walls, h_2	1.00	1.01	1.04
(8) Rod bundles, $P/D = 1.5$, equilateral triangular array, in-line flow . .	1.00	(1.01)	(1.04)

Note: h_1 and h_2 refer to heat transfer from inner and outer walls, respectively.

given case, the greater the flow rate, the greater will be the effect also, owing to the greater contribution of eddy conductivity in the heat transfer process.

Case 6 in Table 1 is interesting in that the ratios of the coefficients are less than 1.0 for $Pe = 10^3$ and $Pe = 10^4$. This means that the higher the eddy conductivity, the lower the heat transfer coefficient. The apparent paradox is explained by the fact that the higher the eddy, and therefore the total, conductivity, the less the temperature gradient, and also the stream temperature, in the outer portion of the annulus, for the same inner wall temperature. The strong weighting influence of the flow in the peripheral cross-sectional area lowers the average bulk temperature and, therefore, lowers the coefficient for the inner wall.

Determination of ψ and its effect on Nusselt number

There have been many attempts to produce a satisfactory analytical method for evaluating ψ . Since 1958, four such attempts have been published by workers in the US. These methods, all based upon some modification of Prandtl's [10] mixing-length theory, are listed in Table 2; and there given, for

Table 2. Analytical relationships for evaluating the diffusivity ratio

Year	Author(s)	Ref.	Function of	No. of empirical constants
1958	Lykoudis & Touloukian . .	10	Pr	1
1960	Azer & Chao	11	Re, Pr, y	2
1963	Dwyer	12	$Pr, \epsilon_M/\nu$	3
1963	Schrock <i>et al.</i>	13	$Pr, \epsilon_M/\nu$	1

each method, are the variables upon which ψ depends and the number of empirical constants used. Dwyer's [13] basic equation contained three constants, but instead of going to the trouble of evaluating them, he presented a second equation having two empirical constants, which expressed $\bar{\psi}$, which is ψ averaged across the flow area, as a function of Pr and $(\epsilon_M/\nu)_{max}$, the maximum value of ϵ_M/ν across the flow area. This equation is given in the next section.

There have been three papers published in the US that present experimental values of ψ for mercury flowing in round tubes; that of Isakoff and Drew [15] in 1951, that of Brown *et al.* [16] in 1956, and that of Schrock *et al.* [14] in 1963. Some of the results of these workers, together with results calculated by the analytical methods mentioned above, are shown in Fig. 2. The Dwyer curves are based upon his original equation for ψ , but the constants used in it are preliminary values recently obtained at Brookhaven. The equation as used here, therefore, is

$$\psi = \frac{0.2/Pr - 2}{(\epsilon_M/\nu)^{0.9}} \tag{1}$$

where, Pr represents Prandtl number and ν , the kinematic viscosity. The ψ profile, as evaluated by the equation of Lykoudis and Touloukian [11], would be a horizontal straight line having a value of 0.35 at all Reynolds numbers.

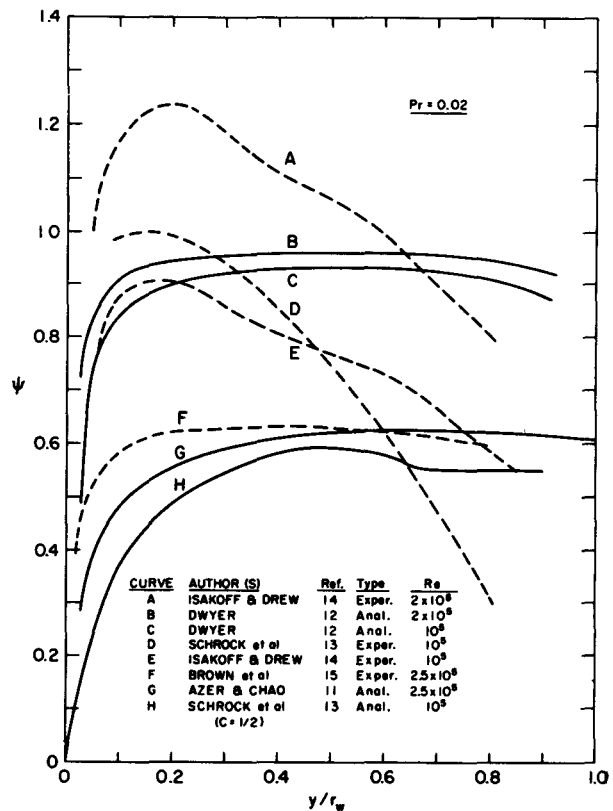


Figure 2. Experimental values of diffusivity ratio obtained with mercury flowing through round pipes, compared with values calculated by various proposed methods. Here, y represents distance from wall, and r_w the pipe radius

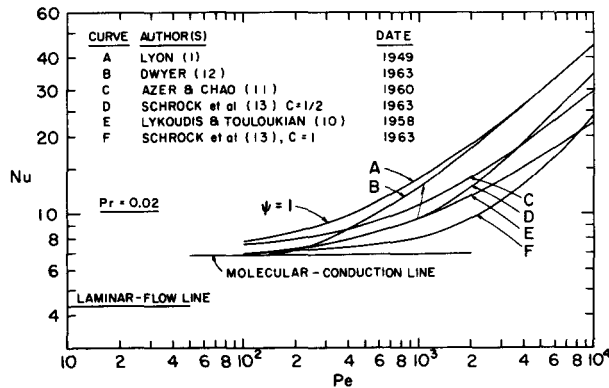


Figure 3. Comparison of theoretical curves representing liquid-metal heat transfer for flow in round tubes, under conditions of constant wall heat flux and fully established turbulent flow

The outstanding feature of Fig. 2 is the lack of agreement between the various curves. However, the experimental curves tend to fall sharply as the center line of the pipe is approached, whereas the analytical curves are rather flat, which would appear more reasonable. The experimental curves, moreover, show large differences in magnitude. So do the analytical curves, but this is simply a question of the arbitrary choices of the empirical constants. The conclusion is that further, more accurate experimental measurements are necessary before the correct shape of the typical ψ profile can be reasonably established. Such measurements are very difficult to make.

The four equations for estimating ψ are also compared in Fig. 3 where the theoretical equation for pipes, already referred to, is plotted on a Nusselt number (Nu) vs. Peclet number (Pe) graph. The curve for $\bar{\psi} = 1$ is shown for reference. Here again, we see large differences between the curves. Curve B seems most reasonable because (a) it agrees more closely with recently published experimental results, (b) it merges with the molecular-conduction curve at low Peclet numbers, and (c) it merges with the curve for $\psi = 1$, at high Peclet numbers. On the latter point, it is believed that when the Reynolds number reaches 300 000 or above, depending on Prandtl number, $\bar{\psi}$ reaches unity. Moreover, there are indications that $\bar{\psi}$ may even exceed unity beyond this critical flow rate.

There have been several sets of experimental data on channel-flow liquid-metal heat transfer published in both the US and the USSR in recent years for flow through pipes, annuli, and rod bundles, which show Nusselt numbers exceeding those calculated on the assumption that $\bar{\psi} = 1$ when the Peclet number exceeds about 5 000. Besides the possibility that, at high flow rates, $\bar{\psi}$ may exceed unity, there are other possible explanations for this observation, such as the use of wrong ϵ_M profile curves and low friction factor curves, but these do not appear so plausible. More experimental work on the effects of turbulence on heat and momentum transfer in liquid metals is required before this present anomaly is cleared up.

Theory vs. experiment for channel flow

The theoretical equations already mentioned for channel flow can be represented to within about $\pm 5\%$ error by semi-empirical equations of the type

$$Nu = \alpha + \beta(\bar{\psi}Pe)^\gamma \quad (2)$$

for $10^2 \leq Pe \leq 10^4$. Both Nu and Pe are based upon the standard equivalent diameter. This equation, with a given set of constants, is satisfactory for practically all liquid metals, i.e. $0.005 \leq Pr \leq 0.03$. For practical purposes, it is recommended that $\bar{\psi}$ be evaluated by the convenient equation recently published in reference [13].

$$\bar{\psi} = 1 - \frac{1.82}{Pr(\epsilon_M/\nu)_{\max}^{1.4}} \quad (3)$$

for flow through pipes, parallel plates, annuli, and rod bundles. For heat transfer to liquid metals flowing through tubes and between parallel plates, α , β , and γ are simple constants; for flow through annuli, they are usually functions of Y (the ratio of outer to inner radius); and for in-line flow through rod bundles, they are usually functions of P/D , the pitch:diameter ratio. Table 3 summarizes this information for a large number of cases. The values given in this table are based on the conditions of uniform heat flux, fully established velocity and temperature profiles, and ϵ_M profile type (b).

It has become increasingly evident that, in the case of liquid metals, eddy conduction does not contribute to convective heat transfer at the low end of the turbulent flow regime. The Reynolds number at which eddy conduction begins to operate depends on the Prandtl number and channel geometry. Figure 4 shows some typical curves for three different channels at $Pr = 0.02$. The critical Peclet numbers for pipes, the annulus, and the rod bundle are approximately 150, 300, and 700, respectively. They correspond to Reynolds numbers of 7 500, 15 000, and 35 000 respectively. Figure 4 also shows the laminar lines for the three cases. It will be noticed that in the case of the annulus, there is very little difference between the laminar and molecular-conduction turbulent Nusselt numbers. This is almost true for the rod bundle case also. It means that for both cases an appreciable advance into the turbulent regime is necessary, before the heat transfer coefficients become much greater than those for laminar flow.

Equation (2), with constants from Table 3 and $\bar{\psi}$ evaluated by Eq. (3), will now be compared with recently published experimental results in the US for three channel-flow geometries: pipes, annuli, and rod bundles. The only pipe-flow results published since 1958 are those of Baker and Sesonske [20]. These results are shown in Fig. 5 where it is seen that the agreement between predicted and experimental results is very good. Also, the only annulus flow results are those of Baker and Sesonske. These results are shown in Fig. 6 where the agreement is not as good as in Fig. 5. Over much of the Peclet range covered, the experimental points fell about 15%

Table 3. Summary of empirical constants for use in Equation (2) for various geometries, under conditions of uniform heat fluxes and fully established velocity and temperature profiles

Flow through	Conditions of heat transfer	Nusselt No.	y	α	β	γ	Ref.
1. Round pipes		Nu	—	7.0	0.025	0.8	1
2. Annuli	Heat transfer from inner wall only	Nu_1	1-7	$4.82 + 0.697y$	0.0222	$0.758y^{0.058}$	16
	Heat transfer from outer wall only	Nu_2	1-7	$5.54 - 0.023y$	0.0189 $+0.00316y$ $+0.0000867y^2$	$0.758y^{-0.0204}$	16
	Equal heat fluxes from both walls	Nu_1	1.5	11.80	0.0726	0.701	17
			2.0	15.30	0.0855	0.704	
			3.0	27.00	0.1095	0.707	
		Nu_2	1.5	8.23	0.0418	0.733	17
			2.0	7.55	0.0415	0.736	
			3.0	7.08	0.0414	0.739	
	Heat transfer from both walls, with $t_1 = t_2$ at any axial position	Nu_1	1.5	10.40	0.0603	0.708	17
			2.0	11.05	0.0613	0.718	
3.0			12.52	0.0647	0.732		
1.5			8.92	0.0462	0.721		
2.0			8.58	0.0432	0.731		
	Nu_2	2.0	8.16	0.0403	0.741	17	
		3.0	8.16	0.0403	0.741		
3. Parallel plates	Heat transfer from one plate only	Nu	—	5.60	0.01905	0.775	2
	Equal heat fluxes from both plates	Nu	—	9.49	0.0596	0.688	2
4. In-line flow between rod bundles equilateral triangular spacing		Nu	$P/D = 1.3-3.0$	6.66	0.0155	0.86	18
				$+ 3.126(P/D)$ $+ 1.184(P/D)^2$			
5. In-line flow between rod bundles having square spacing		Nu	$P/D = 1.7-10.0$	7.0	$0.0275(P/D)^{0.27}$	0.8	19
				$+ 4.24(P/D)^{1.52}$			

above the predicted curve. Nu vs. Pe curves obtained from Eqs. (2) and (3) are found, however, to be in good agreement with experimental results on annuli recently published by Petrovichev [21] and Subbotin *et al.* [22] in the USSR.

The experimental results in Figs. 5 and 6 were obtained simultaneously on a stainless steel double-pipe exchanger, and the individual coefficients were calculated from measured over-all temperature differences. This procedure involves an assumption as to the relative magnitudes of the individual coefficients before they can be calculated.

The rod-bundle (or tube bank) geometry is frequently encountered in the design of nuclear reactors and their associated heat-exchange equipment. In recent years, three semi-empirical equations have been published in the US for estimating heat transfer coefficients for in-line flow between rod bundles having equilateral triangular spacings under conditions of uniform heat flux and fully established velocity and temperature profiles. These equations were by Dwyer and Tu [5] in 1960, Friedland and Bonilla [6] in 1961, and Maresca and Dwyer [19] in 1963. The last equation is represented by Eq. (2) with the functions for α , β , and γ listed in Table 3. All three equations were

developed by approximating the hexagonal flow area, associated with each rod, by a circle of the same area and assuming an annulus model. This is a valid assumption for P/D ratios above 1.3. The three equations apply at least in the P/D range 1.3 to 3.0 and the Peclet number range 10^2 to 10^4 .

The Maresca-Dwyer equation is compared with recent experimental results in Fig. 7. Some published results of Nimmo and Dwyer [23] are shown for mercury flowing through a 13-rod bundle of 0.500-in rods; and some results of Kalish and Dwyer [24] are shown, for flow of NaK through a 19-rod bundle. In each case, surface temperatures were measured by thermocouples embedded just below the surface; and the rods, all electrically heated, had nickel-plated copper sheaths. The agreement between the experimental points for both liquid metals and the predicted curve is quite good.

Cross flow through rod bundles and tube banks

In the design of conventional shell-and-tube liquid-metal heat exchangers, one must estimate heat transfer coefficients for flow at various angles across the tube banks. Since 1958, there have been one experimental and two analytical cross-flow studies in the US.

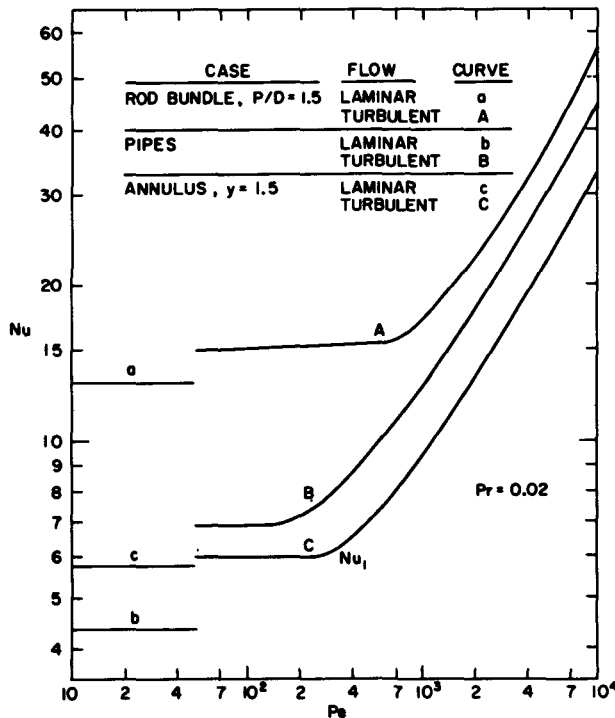


Figure 4. Typical curves for heat transfer to liquid metals flowing through various-shaped channels under conditions of uniform heat flux and fully established velocity and temperature profiles. In the case of the annulus curves, the heat transfer is from the inner wall only

Rickard, Dwyer and Dropkin [25] measured heat transfer rates to mercury flowing at right angles through a bank of staggered rods having an equilateral triangular spacing with a P/D ratio of 1.38. They correlated their results by the empirical equation

$$Nu = 4.03 + 0.228(Pe)^{0.67} \quad (4)$$

In that study, the condition of uniform heat flux was closely approached, the Peclet number was varied from 400 to 4 000, and only the test rod was heated. In Eq. (4), Nu is based on the average temperature difference from surface to bulk mercury, and Pe is

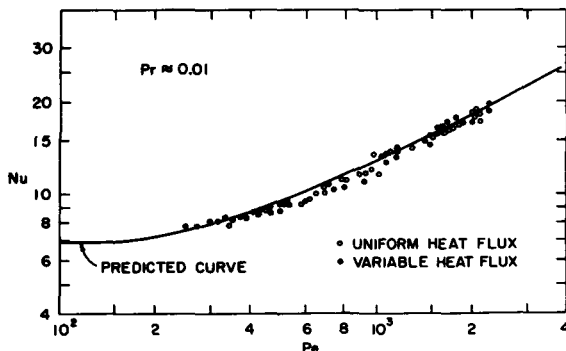


Figure 5. Comparison of predicted and experimental results for heat transfer to NaK flowing in round tube under fully established conditions. The predicted curve is based upon Eqs. (2) and (3). The experimental results are due to Baker and Sesonske

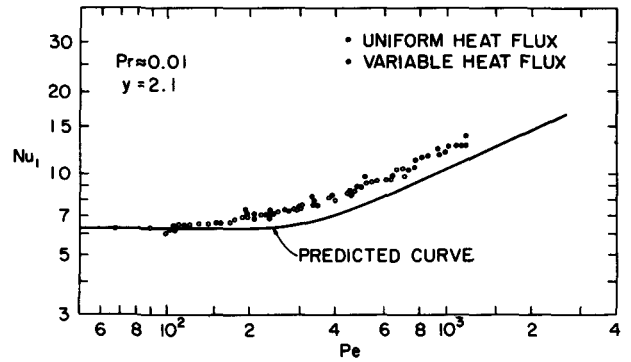


Figure 6. Comparison of predicted and experimental results for heat transfer to NaK flowing in an annulus under fully established conditions. The predicted curve is based upon Eqs. (2) and (3). The experimental results are due to Baker and Sesonske

based upon the average velocity through the minimum flow area.

Hsu [26] recently proposed a theoretical equation for estimating tube-average Nusselt numbers, in the intermediate Peclet number range, for liquid metals in cross-flow through rod bundles, or tube banks. It is

$$[Nu]_{90^\circ} = 0.958(\phi_1/D)^{1/2}(Pe)^{1/2} \quad (5)$$

where Pe is based upon the average up-stream velocity of the liquid metal before entering the rod bundle, and ϕ_1 is the unit velocity potential at the rear stagnation point of a rod. Tabulated values of the ratio ϕ_1/D , which is a unique function of the P/D ratio and rod spacing, were given by the author for both square and equilateral triangular arrays. Hsu's equation represents a further development of a similar study published earlier by Cess and Grosh [27]. Both studies were based on the assumptions of inviscid flow, no interaction between the thermal boundary layers of adjacent rods, and absence of eddy conduction. The main difference between the

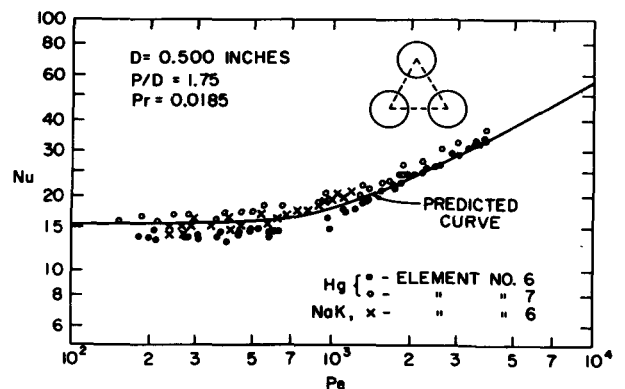


Figure 7. Heat transfer to liquid metals flowing in-line through unbaffled rod bundles under conditions of uniform heat flux and fully established turbulent flow. The data points for the mercury were taken on test elements 6 and 7 about one year apart, both of which were wetted by the mercury

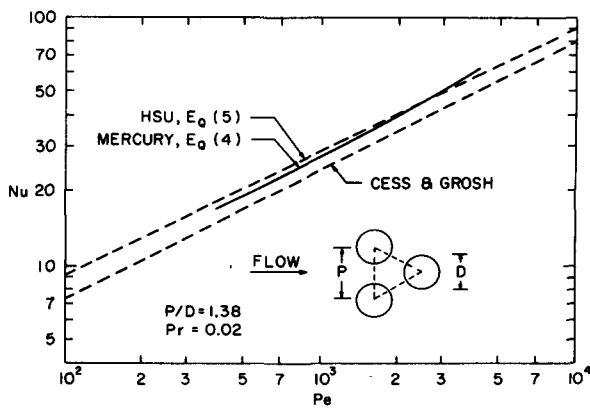


Figure 8. Heat transfer to liquid metals in 90° cross flow through rod bundles or tube banks under conditions of uniform heat flux. Comparison between experimental results of Rickard *et al.* [25] with theoretical predictions of Hsu [26] and Cess and Grosh [27]

two studies was that Cess and Grosh used a conducting-sheet analogy to determine values of the ratio ϕ_1/D , whereas Hsu determined this quantity by using a complex analytical function originally developed by Howland and McMullen [28]. A comparison of Eqs. (4) and (5) is shown in Fig. 8, along with the earlier Cess-Grosh prediction. The agreement between the experimental results and Hsu's equation is very good. Both were based upon a uniform stream temperature approaching the rod, which is taken as the bulk temperature in evaluating $[Nu]_{90^\circ}$. In an actual exchanger this is not the case, but the effect of the difference is expected to be very slight. Both theoretical curves in the figure are based on a cosine-type temperature distribution around the rod, which was established earlier by the experimental results of Hoe, Dropkin, and Dwyer [29].

Cross flow and parallel flow are the two limiting cases of the general type of shell-side flow existing in a shell-and-tube heat exchanger. To estimate tube-average heat transfer coefficients under conditions of oblique flow across a particular tube in a tube bank, Hsu [30] has assumed that the heat transfer conditions are the same as 90° flow across an elliptical-shaped tube in a bank of such tubes. The shape of the ellipse is determined by an imaginary plane cutting across the circular tubes in such a way that a second plane passing through the axis of the tube intersects the first plane at right angles and in a line parallel to the flow stream. According to Hsu, Nusselt numbers for oblique flow can be well approximated by the equation

$$[Nu]_\theta = 0.958(\phi_1/D)^{\frac{1}{2}}(Pe)^{\frac{1}{2}} \left[\frac{\sin \theta + \sin^2 \theta}{1 + \sin^2 \theta} \right]^{\frac{1}{2}} \quad (6)$$

where $\theta = 90^\circ$ for normal cross flow and approaches zero for parallel flow. In this equation, the characteristic length term in both Nu and Pe is the od of the tubes, and the velocity in Pe is on a tube-free basis as in Eq. (5). According to Eq. (6), as the flow angle of the liquid metal through the tube bank changes from 90 to 75 to 60 and to 45° , the tube-average heat transfer coefficient drops by 1.9, 3.9, and 10.3%, respectively.

Eq. (6) becomes less and less reliable as θ falls more and more below 45° .

For flow across single tubes, the value of ϕ_1/D in both Eqs. (5) and (6) becomes 2.00.

Asymmetry effects

Geometrical asymmetry has been known to have a deleterious effect on average heat transfer rates to or from liquid metals flowing in annuli and through staggered rod bundles. The reason this effect is so pronounced with liquid metals is that the bulk of the temperature drop through the flowing fluid is not in the region very close to the wall, as it is in the case of ordinary fluids. Local coefficients in the region of least clearance are depressed more than those in the region of greatest clearance are increased, the result being that the average coefficient for the device drops.

In recent years, there have been three studies carried out at Brookhaven which have shed light on the effects of geometrical asymmetry on liquid-metal heat transfer. In a study of heat transfer to mercury flowing in-line through a rod bundle, Friedland *et al.* [31] attributed to bowing of the rods the fact that in some cases their measured coefficients fell as much as 50% below those obtained when the rods were known to be straight. Snyder [32] analyzed slug-flow liquid-metal heat transfer in an eccentric annulus under the following conditions: heat transfer from the inner wall only, no circumferential variation of inner wall temperature, constant heat flux per unit length of annulus, and fully established temperature profiles. For an r_2/r_1 ratio of 1.94, he found the average slug-flow Nusselt number to decrease by about 11 and 24% as the eccentricity increased from 0 to 20, and to 40%, respectively. Average turbulent-flow Nusselt numbers for this same annulus were estimated to decrease roughly 28, 19, and 6% at Peclet numbers of 10^2 , 10^3 , and 10^4 , respectively, when the eccentricity was increased from 0 to 50%.

In a current analytical study of heat transfer to liquid metals flowing through eccentric annuli, Yu [33] has found that small amounts of eccentricity have a very marked effect on the average heat transfer coefficient under the following conditions: heat transfer from the inner wall only, uniform heat flux, and fully established turbulent flow. For example, for an annulus having a r_2/r_1 ratio of 1.5, at a Peclet number of 1 700, the average coefficient decreased about 59% as the eccentricity was increased from 0 to 15%.

The more uniform the heat flux and the lower the flow rate, the greater will be the reduction in the average coefficient for a given amount of asymmetry. But, under actual conditions, the circumferential temperature variation caused by asymmetry tends to produce circumferential heat flow in the rod or tube wall, causing departure from the condition of uniform heat flux and thereby tending to mitigate the effect of the asymmetry.

The possibility of the reduction of average heat transfer coefficients in heat exchange equipment by the appearance of geometrical asymmetries presents

problems to the designer. However, in conventional baffled shell-and-tube heat exchangers having a small amount of parallel flow, the problem is not believed to be serious. On the other hand, for certain other geometrical designs, it can be quite serious.

Boiling liquid-metal heat transfer

This is important in civilian power reactor technology for two reasons: (a) it is relevant to the matters of safety analysis and hot-spot evaluation, and (b) it is essential in the consideration of water-liquid metal dual-cycle systems for electrical power generation.

In a theoretical study, Chen [34] has proposed a superposition approach for estimating convective boiling coefficients in round vertical tubes with net vapor generation. For the micro-convective contribution—that due to bubble growth—he proposes a relationship derived from the Forster-Zuber [35] pool boiling theory; while for the macro-convective contribution—that due to stream flow—he uses a modification of the Lyon-Martinelli [1] equation. Comparison of Chen's predicted results with recent experimental results published by the General Electric Co. [36] and by Hoffman and Krakoviak [34] is given in Fig. 9. The term X_{tt} is the conventional Martinelli two-phase flow parameter, and h_L represents the liquid-phase coefficient at the same liquid Reynolds number. Some of the scatter in the results may be attributable to the large super-heat sometimes required to nucleate bubbles in liquid-metals.

Subcooled forced-convection burnout, or critical heat flux, with sodium is being investigated at Atomic International [37]. As yet, no clear correlation between critical heat flux and flow rate has been observed for flow rates ranging from 0.37×10^6 to 1.2×10^6 lb/hr-ft² (50 to 163 g/s-cm²). The critical flux was found to decrease from 1.5×10^6 to 0.47×10^6

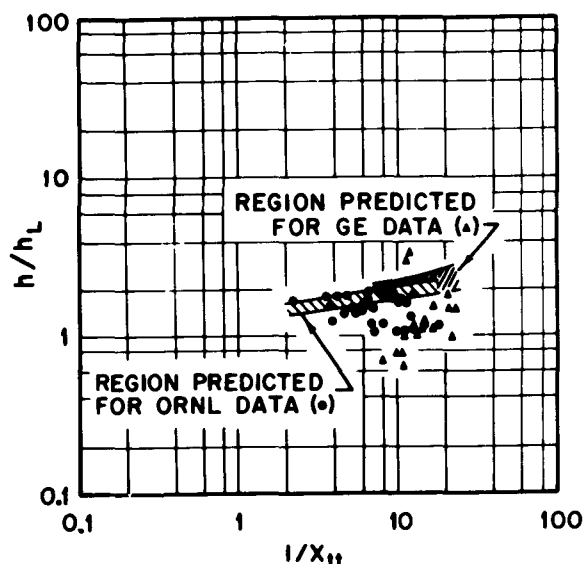


Figure 9. Comparison of Chen's [34] correlation with ORNL data on convective boiling of potassium and General Electric data on convective boiling of sodium

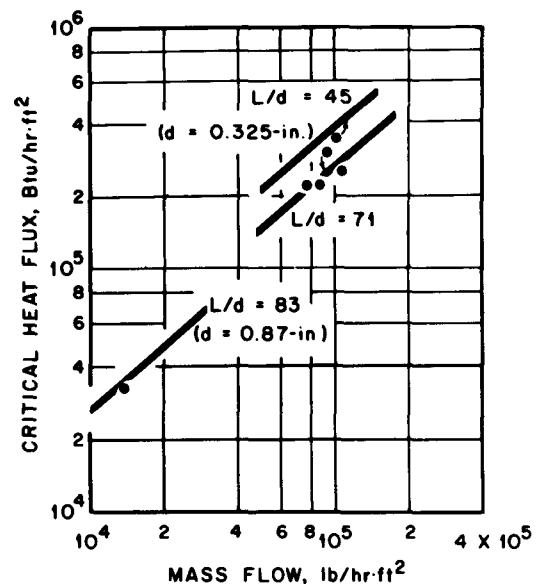


Figure 10. Comparison of Hoffman's [34] burnout-heat-flux results for potassium with correlation of Lowdermilk et al. [38] for water

$$(1 \text{ Btu} = 0.271 \text{ cal/hr-cm}^2,$$

and

$$1 \text{ lb/hr-ft}^2 = 1.356 \times 10^{-4} \text{ gm/s-cm}^2)$$

Btu/hr-ft² (4.07×10^5 to 1.27×10^5 cal/hr-cm²), as pressure increased from 0.15 to 0.34 atm.

Burnout heat flux tests for potassium, with net vapor generation and forced convection, have been reported by Hoffman [34]. The results for two stainless steel tubes are shown in Fig. 10. The solid lines are predictions based on the correlation of Lowdermilk, Lanzo, and Siegel [38] for water. The good agreement between the results is presumably due to the similarity of pertinent physical properties for the two different liquids.

REFERENCES

1. Lyon, R. N., Chem. Eng. Progr., 47 75/79 (1951).
2. von Kármán, T., Trans. A.S.M.E., 61 705/710 (1939).
3. Dwyer, O. E., Heat Transfer to Liquid Metals Flowing Turbulently Between Parallel Plates, to be published in Nuclear Sci. Eng.
4. Dwyer, O. E., and Tu, P. S., Nuclear Sci. Eng., 15 58/68 (1963).
5. Dwyer, O. E., and Tu, P. S., Chem. Eng. Progr. Symposium Series No. 30, 56 183/193 (1960).
6. Friedland, A. J., and Bonilla, C. F., Amer. Inst. Chem. Engineers J., 7 107/112 (1961).
7. Knudsen, J. G., and Katz, D. L., Fluid Dynamics and Heat Transfer. McGraw-Hill Book Co., New York 453/454 (1958).
8. Page, F., Corcoran, W. H., Schlinger, W. G., and Sage, G. H., J. Ind. Eng. Chem., 44 419/424 (1952).
9. Rothfus, R. R., Walker, J. E., and Whan, G. A., Amer. Inst. Chem. Engineers J., 4 240/245 (1958).
10. Prandtl, L., Physik. Z., 29 487/489 (1928).
11. Lykoudis, P. S., and Touloukian, Y. S., Trans. A.S.M.E., 80 653/666 (1958).
12. Azer, N. Z., and Chao, B. T., Int. J. Heat Mass Transfer 1 121/138 (1960).

13. Dwyer, O. E., Amer. Inst. Chem. Engineers J., 9, 261/268 (1963).
14. Schrock, S. L., Buyco, E. H., and Sesonske, A., *Eddy Diffusivity Ratios for Mercury Flowing in a Tube* paper presented at the 6th National Heat Transfer Conf., Boston (August 11-14, 1963).
15. Isakoff, S. E., and Drew, T. B., *Proceedings of the General Discussion on Heat Transfer*, London Conf., I. Mech. E. and A.S.M.E., 405/409 (1951).
16. Brown, H. E., Amstead, B. H., and Short, B. E., Trans. A.S.M.E., 79 279/285 (1957).
17. Dwyer, O. E., Nuclear Sci. Eng., 17 336/344 (1963).
18. Dwyer, O. E. and Tu, P. S., *Bilateral Heat Transfer to Liquid Metals Flowing in Annuli* to be published in Nuclear Sci. Eng.
19. Maresca, M. W., and Dwyer, O. E., *Heat Transfer to Mercury Flowing In-Line Through a Bundle of Circular Rods*. Trans. A.S.M.E., Series C, J. of Heat Transfer, 86, 180/186 (1964).
20. Baker, R. A. and Sesonske, A., Nuclear Sci. Eng., 13, 283/288 (1962).
21. Petrovichev, V. I., Atomnaya Energiya 7 366/369 (1959).
22. Subbotin, V. I., Ushakov, P. A., and Sviridenko, I. P., Atomnaya Energiya 9 310/312 (1960).
23. Nimmo, B., and Dwyer, O. E., *Heat Transfer to Mercury Flowing In-Line Through a Rod Bundle*, submitted to Journal of Heat Transfer, A.S.M.E.
24. Kalish, S. and Dwyer, O. E., *Heat Transfer to NaK Flowing In-Line Through a Bundle of Circular Rods* (to be published).
25. Rickard, C. L., Dwyer, O. E., and Dropkin, D., Trans. A.S.M.E., 80 646/652 (1958).
26. Hsu, C. J., *Analytical Study of Heat Transfer to Liquid Metals in Cross-Flow Through Rod Bundles*, to be published in Int. J. Heat Mass Transfer.
27. Cess, R. D., and Grosh, R. J., Trans. A.S.M.E., 80 677/682 (1958).
28. Howland, R. C. J., and McMullen, B. W. Cambridge Phil. Soc., 32 402/415 (1936).
29. Hoe, R. J., Dropkin, D., and Dwyer, O. E., Trans. A.S.M.E., 79 899/907 (1957).
30. Hsu, C. J., unpublished work, Brookhaven National Lab., Upton, New York, USA.
31. Friedland, A. J., Dwyer, O. E., Maresca, M. W., and Bonilla, C. F., *Proceedings of 1961-1962 Intern. Heat Transfer Conf.*, Boulder, Colorado, and London, England, A.S.M.E., New York, N.Y. 526/534 (1961).
32. Snyder, W. T., Amer. Inst. Chem. Engineers J., 9, 503/506 (1963).
33. Yu, W. S., and Dwyer, O. E., *Heat Transfer to Liquid Metals Flowing Turbulently in Eccentric Annuli* (to be published).
34. *Proceedings of the 3rd High-Temperature Liquid-Metal Heat Transfer Technology Meeting*. USAEC report ORNL 3605 (Sept. 4-6, 1963).
35. Forster, H. K., and Zuber, N., Amer. Inst. Chem. Engineers J., 531/535 (1955).
36. Longo, J., Editor, *Alkali Metals Boiling and Condensing Investigations*, Quarterly Progress Reports 2 and 3, Space Power and Propulsion Section, General Electric Co. (April 1963).
37. Lurie, H., and Jarrett, A. A., Progress Report for Oct.-Dec., 1963, on Boiling Studies for Sodium Reactor Safety, Atomics International (see also R. C. Noyes, ref. 34).
38. Lowdermilk, W. H., Lanzo, C. D., and Siegel, B. L., *Investigation of Boiling Burnout and Flow Stability for Water Flowing in Tubes*, Nat. Adv. Comm. Aero. Technical Note 4382 (Sept. 1958).

ABSTRACT—RÉSUMÉ—АННОТАЦИЯ—RESUMEN

A/225 Etats-Unis

Transfert de chaleur par métaux liquides

par O. E. Dwyer et R. N. Lyon

Cette communication résume les résultats obtenus récemment dans l'étude du transfert de chaleur par métaux liquides, en indique l'importance, en s'attachant particulièrement à l'application aux centrales nucléaires refroidies par des métaux liquides. Elle ne comprend que les résultats pertinents obtenus aux Etats-Unis de 1958 à 1963 inclus. Dans la seconde moitié de cette période de six ans, on a publié plus d'informations sur le transfert de chaleur par métaux liquides que dans m'importe laquelle des périodes de trois ans précédentes. La tendance aux Etats-Unis a été de faire des études d'analyse fondamentale et des études expérimentales sur des systèmes simples, bien définis et contrôlés plutôt que des mesures de transfert de chaleur sur des installations prototypes d'échange de chaleur.

Pour le transfert de chaleur par métal liquide à une seule phase, on dispose de nouvelles formules théoriques et semi-empiriques qui permettent de prédire le coefficient de transfert de chaleur, dans différentes conditions d'écoulement dans des canaux et pour

l'écoulement sur des corps immergés. Dans la première catégorie, les cas étudiés ont été les espaces annulaires, les plaques parallèles et les écoulements rectilignes dans des grappes de barreaux (ou de tubes); dans la seconde catégorie, les sphères et l'écoulement perpendiculaire à des cylindres de section circulaire ou elliptique. Ces derniers cas représentent une bonne approximation des écoulements sous divers angles au travers des barreaux dans une grappe de barreaux (ou de tubes dans un faisceau de tubes).

Pour l'écoulement dans un canal, les équations théoriques des nombres de Nusselt contiennent le terme ψ , rapport de la diffusivité tourbillonnaire du transfert de chaleur à celle du transfert de moment, tandis que les équations semi-empiriques contiennent le terme $\bar{\psi}$, valeur moyenne efficace de ψ . L'évaluation de ces rapports est l'un des problèmes principaux dans la prédiction des coefficients de transfert de chaleur. On comprend mieux maintenant la forme générale d'une courbe typique représentant le nombre de Nusselt en fonction du nombre de Peclet pour un écoulement en canal. Pour les écoulements dans des parties annulaires ou entre plaques parallèles, l'évaluation de la diffusivité par tourbillons dans la zone transversale de vitesse linéaire maximale pose un autre problème. Quelques progrès ont aussi été

réalisés dans ce domaine, qui n'est heureusement important que dans les conditions proches de l'échange de chaleur unilatéral aux grandes vitesses d'écoulement.

Parmi les observations intéressantes obtenues ces dernières années sur le transfert de chaleur par métaux liquides, on peut citer: *a*) la variation pratiquement nulle du coefficient de transfert de chaleur avec l'écoulement en canal pour un intervalle considérable en régime turbulent, *b*) l'effet très prononcé d'une dissymétrie géométrique sur les coefficients de transfert de chaleur local et moyen, *c*) l'indication que $\bar{\psi}$ est supérieur à 1 pour les grands débits, *d*) l'influence principale sur $\bar{\psi}$ de ϵ_M/ν , rapport entre la diffusivité tourbillonnaire du transfert de moment et la viscosité cinématique, et *e*) la forte influence, dans les transferts de chaleur bilatéraux pour des écoulements turbulents annulaires ou entre plaques parallèles, sur les coefficients de transfert de chaleur des flux de chaleur relatifs provenant des deux surfaces. Le problème du « mouillage » et l'aspect associé de la pureté des métaux liquides sont discutés brièvement.

Il y a eu une forte expansion de la recherche sur le transfert de chaleur par métaux liquides à deux phases aux Etats-Unis au cours des deux dernières années, mais il est encore trop tôt pour discuter des résultats obtenus. Cette communication résume les résultats récents et présente l'état des connaissances sur des sujets tels que l'ébullition en masse, le flux thermique critique, l'ébullition et la condensation à convection forcée.

A/225 США

Жидкометаллические теплоносители

Э. Дуайер, Р. Н. Лайон

В этом докладе суммируются результаты и подчеркивается значение последних достижений в области изучения жидкометаллических теплоносителей; для ядерных энергетических установок. В докладе анализируются данные, полученные по этому вопросу в США в 1958—1963 годах. Во второй половине этого шестилетнего периода было опубликовано больше работ по жидкометаллическим теплоносителям, чем в течение любого предыдущего трехлетнего периода. В США аналитико-теоретические и экспериментальные исследования интенсивности теплообмена ведутся предпочтительно на простых, хорошо отрегулированных и точно контролируемых системах, а не на прототипных установках.

В настоящее время для определения коэффициентов теплоотдачи при использовании жидкометаллического теплоносителя в различных условиях течения как для случая движения теплоносителя внутри каналов, так и для случая наружного омывания тел различной формы разработаны новые теоретические и полумпирические зависимости. В первом случае

для условий потока в канале рассматривались кольцевые щели, параллельные пластины и параллельное движение вдоль пучка стержней (или трубок), а во втором случае рассматривались шары и поперечное омывание цилиндров круглого и эллиптического сечения. Последние могут рассматриваться как хорошее приближение потоков, направленных под различными углами к пучку стержней (или трубок).

При движении в канале теоретические зависимости для критерия Нуссельта содержат величину $\bar{\psi}$ являющуюся показателем соотношения между турбулентной составляющей переноса тепла и составляющей переноса тепла за счет изменения количества движения, в то время как полумпирические уравнения содержат величину $\bar{\psi}$ являющуюся действительным средним значением для ψ .

Главная задача при определении коэффициентов теплоотдачи состоит в оценке этих соотношений. В настоящее время мы имеем лучшее представление об общей форме кривой зависимости критерия Нуссельта от числа Пекле для движения в канале. При потоках через кольцевые щели и между параллельными пластинками возникает еще одна задача — оценка коэффициента турбулентной диффузии в поперечной области максимальной линейной скорости. Некоторые успехи были достигнуты также и в этом случае. Однако эта задача является трудной только при условиях, приближающихся к одностороннему теплопереносу в потоках высокой интенсивности.

Среди интенсивных наблюдений, сделанных за последние годы в связи с изучением жидкометаллических теплоносителей, были установлены следующие факты:

a) высокое постоянство коэффициента теплоотдачи при движении потока в канале на большом расстоянии по каналу; *b*) резко выраженное влияние геометрической асимметрии на местный и средний коэффициенты теплоотдачи; *c*) указание на то, что значение величины ψ превышает 1 при очень высоких скоростях потока; *d*) высокая зависимость ψ от ϵ_M/ν — отношения турбулентной составляющей переноса тепла к кинематической вязкости; *e*) при двухстороннем теплопереносе в турбулентном потоке через кольцевые щели и параллельные пластины наблюдается сильная зависимость коэффициентов теплоотдачи от относительных тепловых потоков, исходящих от обеих поверхностей. Кратко рассматриваются проблемы «смачиваемости» и связанные с ней проблемы чистоты жидких металлов.

В течение последних двух лет объем работы в США в области изучения двухфазных жидкометаллических теплоносителей увеличился во много раз. Тем не менее сейчас еще слишком рано оценивать результаты этой работы. В данном докладе суммируются новейшие результаты и уровень наших знаний по таким во-

просам, как кипение в большом объеме, критические явления при кипении, кипение в условиях принудительной конвекции и конденсация.

A/225 Estados Unidos de América

Transferencia de calor líquido – metal

por O. E. Dwyer y R. N. Lyon

Se resume e indica el significado de progresos recientes en el estudio de la transferencia térmica líquido – metal, haciendo resaltar las aplicaciones al proyecto de plantas nucleares de potencia, refrigeradas por metal líquido. El documento trata solamente de la información pertinente procedente de los Estados Unidos durante los años 1958 – 1963. En la segunda mitad de este período se ha publicado más información sobre el tema, que durante cualquier intervalo igual de tiempo precedente. La tendencia en los Estados Unidos ha sido preferir la realización de estudios fundamentales, analíticos y experimentales en sistemas controlados bien definidos, a la medida de la velocidad de transferencia térmica en prototipos de intercambiadores de calor.

Se dispone actualmente de nuevas expresiones teóricas y semiempíricas de transferencia térmica en fase simple líquido – metal, que permiten obtener los coeficientes de transmisión de calor en distintas condiciones de flujo, tanto a través de canales, como alrededor de cuerpos sumergidos. En el primer grupo, se han estudiado los casos de anillos, placas paralelas, y flujo en haces de barras o tubos: en el segundo, esferas y flujo normal a cilindros de sección transversal circular y elíptica. Estos últimos casos pueden aceptarse como buenas aproximaciones de los que comprenden flujos a ángulos variables con barras en haces de barras (o tubos en un banco de tubos).

En el flujo canalizado, las ecuaciones teóricas para los números de Nusselt contienen el término ψ , la razón de la difusividad turbulenta de la transferencia

de calor, a la de cantidad de movimiento, mientras que las ecuaciones semiempíricas contienen el término $\bar{\psi}$ que es el valor medio de ψ .

El problema mayor en la predicción de coeficientes de transmisión de calor, es la evaluación de estas razones. Se dispone actualmente de un conocimiento más preciso sobre la forma general de la curva del número de Nusselt en función del número de Peclet para flujo canalizado. Otro problema, en el caso de flujo en anillos y placas paralelas, es el cálculo de la difusividad turbulenta en la región transversal de velocidad lineal máxima. Se han conseguido aquí también ciertos progresos pero, afortunadamente, el problema sólo es importante en condiciones próximas a la transferencia unilateral de calor con velocidades de flujo altas.

Entre los puntos interesantes, observados durante los últimos años, en transferencia de calor líquido – metal, destacan: a) la independencia esencial de los coeficientes de transmisión de calor del flujo en el canal, aun bastante dentro del régimen turbulento, b) un efecto muy pronunciado de disimetría geométrica, en coeficientes de transmisión de calor, locales y medios, c) indicios de que $\bar{\psi}$ es mayor que la unidad para velocidades de flujo muy altas, d) fuerte dependencia de $\bar{\psi}$ del ϵ_M/ν , razón de difusividad turbulenta de transferencia de cantidad de movimiento, a viscosidad cinemática, y e) la dependencia marcada de los coeficientes de transmisión de calor, en transferencia bilateral para flujos turbulentos en anillos y entre placas, de los flujos de calor relativos de las dos superficies. Se discutirán brevemente los problemas del « mojado » y el asociado de pureza líquido – metal.

En los dos últimos años ha tenido lugar en los Estados Unidos un incremento considerable en la investigación de la transferencia de calor en sistemas bifásicos metal – líquido, pero es prematuro esperar ya resultados de este cúmulo de trabajos. En este artículo se resumirán los resultados recientes, y se presentará el estado de nuestro conocimiento sobre temas como piscinas en ebullición, flujo térmico crítico, ebullición con convección forzada y condensación.

Теплосъем в элементах реакторов с жидкометаллическим охлаждением

В. И. Субботин, П. А. Ушаков, П. Л. Кириллов, М. Х. Ибрагимов, М. Н. Ивановский, Е. В. Номофилов, Д. М. Овечкин, Л. Н. Сорокин, В. П. Сорокин

Данный доклад содержит результаты некоторых исследований теплообмена жидких металлов, полученные в Физико-энергетическом институте.

ТЕПЛОБМЕН ПРИ ТЕЧЕНИИ ЖИДКИХ МЕТАЛЛОВ В ТРУБАХ

Одна группа опытных данных по теплообмену в трубах располагается около кривой, построенной по формуле

$$Nu = 5 + 0,025 \cdot Re^{0,8}, \quad (1)$$

другая располагается существенно ниже. Причиной этого различия является термическое сопротивление между стенкой и жидким металлом (R_k). Чтобы исключить его влияние, данные по измерению профиля температуры жидких металлов были представлены в виде следующих формул¹:

$$T^+ = y^{++}, \quad 0 < y^{++} < 1 \quad (2)$$

$$T^+ = 1,87 \ln(y^{++} + 1) + 0,065y^{++} - 0,36, \quad (3)$$

$$1 < y^{++} < 11,7 \quad (4)$$

$$T^+ = 2,5 \cdot \ln y^{++} - 1, \quad y^{++} > 11,7$$

Здесь

$$T^+ = \frac{t \cdot \rho \cdot c_p \cdot \sqrt{\frac{\tau}{\rho}}}{q}; \quad y^{++} = \frac{y \sqrt{\frac{\tau}{\rho}}}{\nu} \cdot Pr.$$

Уравнение (2) очевидно; (4) описывает кривую, осредняющую опытные данные, а (3) подобрано так, чтобы на границах зон $y^{++} = 1$ и $y^{++} = 11,7$ были равны значения T^+ и производные $\partial T^+ / \partial y^{++}$.

Зависимость (4) является недостаточно точной для вычисления коэффициентов турбулентного обмена. В центре потока распределение температуры в действительности имеет примерно параболический характер. Однако это различие не оказывает большого влияния на результаты расчета коэффициентов теплообмена. После интегрирования уравнений получается формула (1). Путем измерения температуры стенки и распределения температуры

в потоке жидких металлов было установлено, что контактное термическое сопротивление в основном определяется количеством окислов и других примесей, сконцентрированных вблизи стенки, и зависит от диаметра трубы и скорости теплоносителя примерно таким же образом, как и толщина ламинарного подслоя. Данные по контактным термическим сопротивлениям для разных жидких металлов обобщаются в безразмерных координатах $\frac{R_k \lambda_f}{d} \div Re$.

В результате измерения полей температуры в потоках различных теплоносителей были определены коэффициенты турбулентного переноса тепла². При анализе опытных данных для ртути, воды и воздуха установлено, что коэффициенты турбулентного переноса тепла не зависят от числа Pr (рис. 1). Получены следующие формулы:

$$\frac{\varepsilon_a}{\nu} = 2,04 \cdot 10^{-3} \cdot Re \left[1 + \left(\frac{r}{r_0} \right)^2 - 2 \left(\frac{r}{r_0} \right)^3 \right] - [0,329 + 8,36 \cdot 10^{-7} Re] \cdot y^+ \cdot e^{-0,0833 \cdot y^+}, \quad (5)$$

$$Nu = 7,24 - \frac{9,5}{\lg Re} + 0,0153 \cdot Re^{0,82} \cdot Pr^n, \quad (6)$$

где $n = 0,58 - 0,18 \cdot \text{th}(0,8 \lg Pr)$ для $10^4 < Re < 5 \cdot 10^5$ и $< 0 < Pr < 10$.

Было установлено, что величина $\varepsilon = \frac{\varepsilon_a}{\nu}$ изменяется по радиусу трубы и зависит² от числа Re.

Путем измерения турбулентных пульсаций температуры в потоках воды и ртути установлено, что амплитуды пульсаций температуры в фиксированной точке подчиняются нормальному закону распределения.

Коэффициент корреляции R_r между пульсациями в двух точках $r_1 - r_2$ уменьшается от 1 до нуля с увеличением расстояния между точками ($r_2 - r_1$) от нуля до 10 (см. рис. 1). Характерный масштаб турбулентности в радиальном направлении L_r слабо меняется в области $0 < \frac{r}{r_0} < 0,9$ и быстро уменьшается по мере приближения к стенке. Максимальное

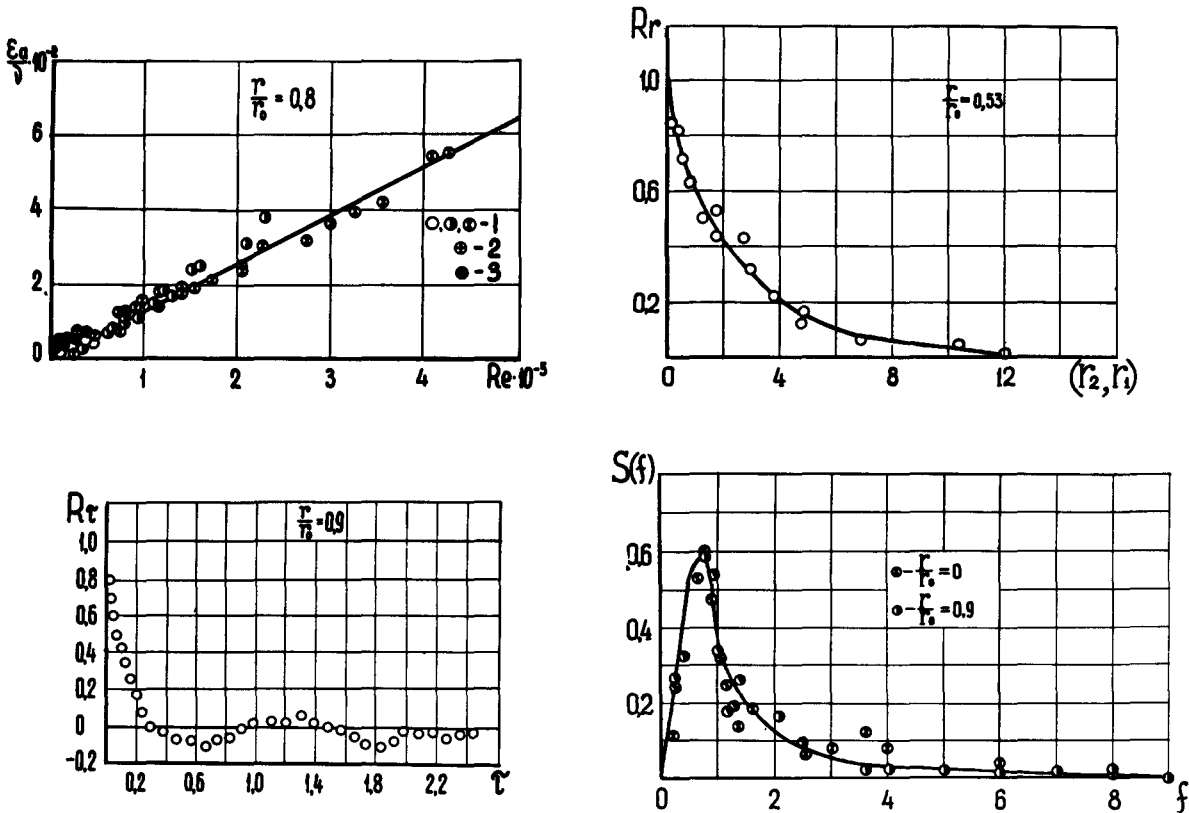


Рис. 1. Коэффициенты турбулентного переноса тепла, корреляции и спектральная функция:

1—для жидких металлов; 2, 3—для воды и воздуха. R_c —для воды при $Re = 17 \cdot 10^5$; R_r —для ртути при $Re = 10^5$; $S(f)$ —для ртути

значение L_r равно $0,1 \cdot r_0$ при $\frac{r}{r_0} \approx 0,7$. Характерные масштабы турбулентности в осевом направлении значительно больше, чем в радиальном, то есть турбулентные вихри сильно вытянуты вдоль потока жидкости.

Коэффициент корреляции R_c является функцией параметра сдвига по времени τ и не зависит от начала отсчета времени (см. рис. 1). Таким образом, функция, описывающая пульсации температуры в фиксированной точке турбулентного потока, является стационарной случайной функцией.

Плотность спектральной функции $S(f)$ имеет максимум при частоте $\sim 0,8$ гц и быстро убывает по мере увеличения частоты возмущения. Почти всю энергию ($\sim 98\%$) переносят турбулентные возмущения, имеющие частоту < 10 гц (см. рис. 1). Среднее время жизни возмущения составляет $\sim 0,1$ сек при $Re = 10^5$.

Опыты показали, что длина начального участка тепловой стабилизации для жидких металлов зависит от числа Re более сильно, чем для обычных жидкостей².

ТЕМПЕРАТУРНОЕ ПОЛЕ ПУЧКОВ ЦИЛИНДРИЧЕСКИХ ТЕПЛОВЫДЕЛЯЮЩИХ ЭЛЕМЕНТОВ

В работе участвовали А. В. Жуков, В. Д. Таланов, Ю. И. Орлов, Б. Н. Габрианович.

Распределение температуры по периметру цилиндрических тепловыделяющих элементов определяется геометрией решетки пучка, свойствами и режимом течения жидкости, а также свойствами тепловыделяющих элементов.

Анализ дифференциальных уравнений и соответствующих граничных условий для тепловыделяющих стержней с защитной оболочкой приводит к следующей зависимости для области стабилизированного теплообмена:

$$T_f = \frac{t_w - \bar{t}_w}{qR_2} \lambda_f = f\left(\frac{S}{d_2}; \varphi; Re; Pr; M_k\right). \quad (7)$$

Свойства тепловыделяющего элемента в общем случае характеризует параметр

$$M_k = \frac{\lambda_f}{\lambda_w} \cdot \frac{1 + m\xi^{2k}}{1 - m\xi^{2k}}, \quad (8)$$

где $m = \frac{\lambda_w - \lambda_0}{\lambda_w + \lambda_0}$ ($-1 \leq m \leq 1$); λ_f , λ_w , λ_0 — теплопроводности жидкости, оболочки и тепловыделяющего элемента;

$\xi = \frac{R_1}{R_2}$ — отношение внутреннего радиуса оболочки к внешнему;

k — номера гармоник ряда Фурье, в виде которого представлена ³ функция (7).

В зависимости от их тепловых свойств тепловыделяющие элементы можно разделить на следующие группы, соответствующие предельным значениям M_k .

1-я группа. На внутренней поверхности оболочек ($r = R_1$) выполняется условие $q \approx \text{const}$ по периметру, если $\lambda_w \gg \lambda_0$,

$$M_k \approx \frac{\lambda_f}{\lambda_w} \cdot \frac{1 + \xi^{2k}}{1 - \xi^{2k}}. \quad (9)$$

Для тонкостенных оболочек ($\frac{R}{\delta_2} \ll 1$)

$$M \approx \frac{\lambda_f R_2}{\lambda_w \delta} \quad (10)$$

здесь ($\delta = R_2 - R_1$).

2-я группа. На внутренней поверхности оболочек выполняется условие $t \approx \text{const}$, если $\lambda_w \ll \lambda_0$

$$M_k \approx \frac{\lambda_f}{\lambda_w} \cdot \frac{1 - \xi^{2k}}{1 + \xi^{2k}}. \quad (11)$$

Для тонкостенных оболочек

$$M \approx \frac{\lambda_f \delta}{\lambda_w R_2}. \quad (12)$$

3-я группа. Элементы с оболочками эквивалентны тепловыделяющим стержням с теплопроводностью λ_w при большой толщине оболочек ($\xi^{2k} \ll 1$) или когда теплопроводности элементов и оболочек равны ($\lambda_0 = \lambda_w$; $m = 0$),

$$M \approx \frac{\lambda_f}{\lambda_w}. \quad (13)$$

4-я группа. Элементы с оболочками эквивалентны тепловыделяющим стержням с теплопроводностью λ_0 при тонких оболочках ($\frac{\delta}{R^2} \ll 1$),

$$M \approx \frac{\lambda_f}{\lambda_0}. \quad (14)$$

Приведенная классификация цилиндрических тепловыделяющих элементов помогает выбрать методы их теплового моделирования в лабораторных условиях. В качестве моделей использовались трубки с равномерным теплоподводом на внутренней поверхности, создаваемым электронагревателями. Такими трубками легко имитировать тепловыделяющие элементы 1-й, 2-й групп с тонкостенными оболочками (10), (12) и элементы 3-й, 4-й групп (13), (14). Моделирование элементов 1-й и 2-й групп с достаточно толстостенными оболочками осуществить трудно, так как условия моделирования (8), (9), (11) при произвольных зна-

чениях k сводятся к требованию выполнения условий

$$\frac{\lambda_f}{\lambda_w} \approx \text{idem}, \quad \frac{\lambda_w}{\lambda_0} \approx \text{idem}, \quad \xi = \text{idem}.$$

Если заранее известно, какая из гармоник (k) дает наибольший вклад в температурное поле, можно воспользоваться приближенным моделированием. Например, для треугольной решетки основная гармоника $k \approx 6$:

$$\left(\frac{\lambda_f}{\lambda_w} \cdot \frac{1 + \xi^{12}}{1 - \xi^{12}} \right)_{\text{мод}} \approx \left(\frac{\lambda_f}{\lambda_w} \frac{1 + m \xi^{12}}{1 - m \xi^{12}} \right)_{\text{наг}}. \quad (15)$$

Температурные поля макетов тепловыделяющих элементов исследовались на пучках, состоящих из семи (треугольная решетка) или девяти (квадратная решетка) электрообогреваемых трубок и фигурного вытеснителя. Температура жидкости измерялась на выходе из всех ячеек. За расчетную температуру принималась температура жидкости около центрального стержня. Такая методика исследований была проверена опытами с пучком из 37 обогреваемых трубок. Толщина стенок трубок была достаточно большой. Поэтому трубки можно было считать эквивалентными сплошным стержням.

На ртути ($\text{Pr} = 0,022 \div 0,025$) и воде ($\text{Pr} = 2,4 \div 4,8$) исследовались плотные пучки из нержавеющей стали ($\frac{\lambda_w}{\lambda_f} = 1,85$ и 24 соответственно). В опытах с эвтектическим сплавом Na—K ($\text{Pr} = 0,022 \div 0,024$) использовались плотные пучки из нержавеющей стали ($\frac{\lambda_w}{\lambda_f} = 0,69$) и меди ($\frac{\lambda_w}{\lambda_f} = 16,3$).

Распределения температуры и теплового потока по периметру стержней (толстостенных трубок) плотных пучков показаны на рис. 2. Распределение теплового потока было найдено из решения задачи теплопроводности для стержня

$$\frac{q}{q} \approx 1 - \sum_k k \frac{A_k}{M_k} \quad (16)$$

при

$$T_j = \sum_k A_k \cos k \varphi. \quad (17)$$

Приведенные на рис. 2 данные для жидких металлов усреднены в интервале $80 < \text{Re} < 550$. В этом интервале неравномерность температуры для Na—K уменьшается с ростом Re примерно на 30%, а для ртути — на 10%. Данные для воды усреднены в интервале $10^4 < \text{Re} < 2 \cdot 10^4$, в котором профиль температуры изменяется незначительно.

Значения Pr и λ_w/λ_f для воды и жидких металлов сильно отличаются друг от друга. Однако неравномерности температуры и тепловых потоков отличаются не очень сильно. Характерно, что при теплоосъеме водой неравномерность температуры наименьшая.

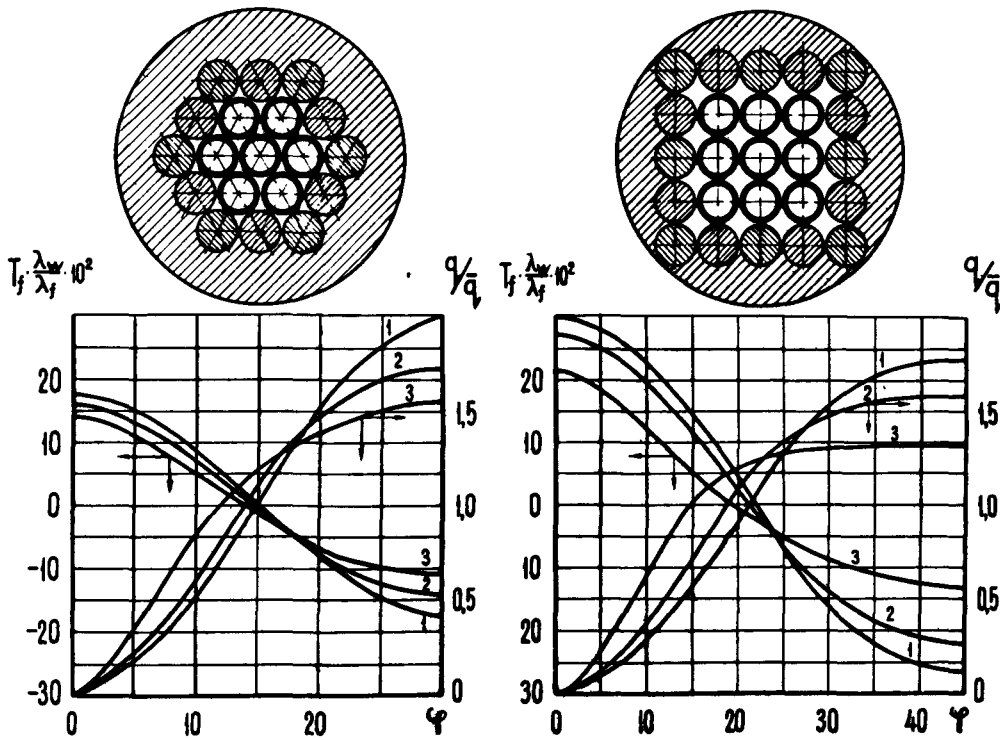


Рис. 2. Распределение температуры и тепловых потоков по периметру стержней плотных пучков: 1, 2, 3—для ртути ($\frac{\lambda_w}{\lambda_f}=1,85$), сплава Na—K ($\frac{\lambda_w}{\lambda_f}=0,69$) и воды ($\frac{\lambda_w}{\lambda_f}=24$) соответственно

На основании рассмотренных данных, аналитических расчетов и результатов других опытов можно констатировать следующее. Безразмерная неравномерность температуры для тепловыделяющих стержней без оболочки примерно пропорциональна λ_f/λ_w . Для толстостенных трубок величина T_f слабо зависит от толщины стенок трубок.

Для тонкостенных трубок величина T_f относительно слабо зависит от λ_w/λ_w . Следовательно, T_f слабо зависит и от толщины стенок трубок, так как изменение относительной теплопроводности эквивалентно изменению относительной толщины стенки трубки [см. формулы (10) и (12)].

При увеличении относительного шага стержней в пучке влияние параметра M_k уменьшается. Так, уже при $\frac{S}{d_2}=1,1$ неравномерность температуры по периметру стержней примерно в пять раз меньше, чем в плотной упаковке. Поэтому при $\frac{S}{d_2}>1,1$ параметр M_k можно исключить из уравнения (7) и для большинства случаев не учитывать неравномерность температуры по периметру стержней.

Опытные данные для плотных упаковок с треугольной решеткой аппроксимируются фор-

мулой (рис. 3)

$$Nu=0,15 \left(\frac{\lambda_w}{\lambda_f}\right)^{0,02} \cdot Pe^{0,3+0,04 \sqrt{\lambda_w/\lambda_f}}, \quad (18)$$

$$Pr \ll 1; 80 < Pe < 600; 0,69 < \frac{\lambda_w}{\lambda_f} < 16,3.$$

Данные для плотных квадратных решеток приведены в работе ³.

Опытами установлено, что при одинаковых диаметрах стержней и одинаковых скоростях жидкого металла коэффициенты теплоотдачи практически не зависят от шага стержней. Коэффициенты теплоотдачи к жидким металлам в пучках с треугольной решеткой описываются формулой (см. рис. 3)

$$Nu=0,58 \left(\frac{d_r}{d_2}\right)^{0,55} \cdot Pe^{0,45}, \quad (19)$$

$$80 < Pe < 4000; 1,1 < \frac{S}{d_2} < 1,5.$$

Характерный размер — гидравлический диаметр ячейки. На рис. 3 приняты следующие обозначения:

$$\psi = \frac{Nu}{\left(\frac{\lambda_w}{\lambda_f}\right)^{0,02} \cdot Pe^{0,3+0,04 \sqrt{\lambda_w/\lambda_f}}} \text{ для плотной упаковки}$$

$$\text{и } \psi = \frac{Nu}{\left(\frac{d_r}{d_2}\right)^{0,55} \cdot Pe^{0,45}} \text{ для пучков с } \frac{S}{d_2} > 1.$$

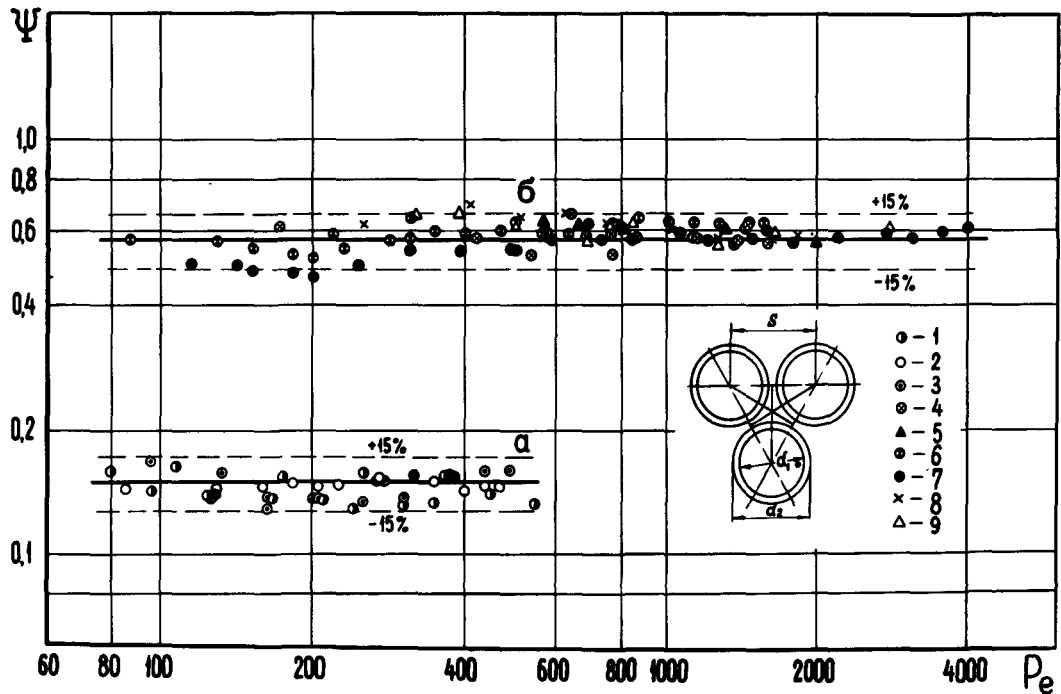


Рис. 3. Теплоотдача в пучках стержней. Плотные пучки (а): 1, 2, 3 — для $\frac{\lambda_w}{\lambda_f} = 0,69; 1,85$ и $16,3$ соответственно.

Раздвинутые пучки (б):

4, 5, 6, 7, 8, 9 — для $\frac{S}{d_2} = 1,1; 1,15; 1,2; 1,3; 1,4$ и $1,5$ соответственно

Особенности теплообмена в пучках наблюдаются также и при теплосъеме водой. Стабилизированные значения средних по периметру чисел Nu при течении воды в плотных пучках стержней с треугольной и квадратной решетками описываются формулой

$$Nu \approx 0,01 Re^{0,8} \cdot Pr^{0,43} \quad (20)$$

$400 < Re < 50\,000.$

Характерный размер — гидравлический диаметр. Разброс точек относительно осредняющей линии не превышает $\pm 15\%$.

В настоящее время по теплообмену при продольном обтекании водой и воздухом пучков стержней с $\frac{S}{d_2} > 1$ накоплен определенный фактический материал. Большинство данных для воды, в том числе и результаты, полученные авторами на воде для пучков с $\frac{S}{d_2} = 1,1; 1,2; 1,4; 1,5$, согласуются с формулой Вейсмана

$$Nu = c Re^{0,8} \cdot Pr^{\frac{1}{3}}, \quad (21)$$

где для треугольной решетки с $1,1 < \frac{S}{d_2} < 1,5$

$$c = 0,026 \frac{S}{d_2} - 0,006.$$

Данные по теплоотдаче к воздуху более противоречивы. Часть из них согласуется с формулой для круглых труб, другая часть не согласуется ни с формулой для круглых труб, ни с формулой (21).

Имеющиеся данные для жидких металлов и обычных жидкостей показывают, что применение формул, полученных в опытах с круглыми трубами, для расчета температурного поля пучков стержней (с использованием гидравлического диаметра) может привести во многих случаях к серьезным ошибкам.

СРЕДНИЕ КОЭФФИЦИЕНТЫ ТЕПЛОТДАЧИ В КОЖУХОТРУБНЫХ ТЕПЛООБМЕННИКАХ

В работе участвовали М. Я. Суворов и А. М. Колотвин.

Средние коэффициенты теплоотдачи в семи-трубных теплообменниках были получены для сплава Na—K. Внутри трубок протекал натрий. В опытах измерялись средние коэффициенты теплопередачи от натрия к сплаву натрий — калий.

По найденным коэффициентам теплопередачи и рассчитанным по формуле (1) коэффициентам

теплоотдачи в трубах определялись средние коэффициенты теплоотдачи в межтрубном пространстве. В интервалах $1,1 < \frac{S}{d_2} < 1,4$; $60 < \frac{l}{d_r} < 260$; $200 < Re < 1200$ опытные данные с точностью $\pm 10\%$ аппроксимируются формулой

$$Nu = 8 \left[\frac{d_r}{l} + 0,027 \left(\frac{S}{d_2} - 1,1 \right) \right] \cdot Pe^{0,6}. \quad (22)$$

Зависимость $Nu = f(Re)$ в теплообменниках более сильная (степень $\sim 0,6$), чем в пучках стержней (степень $\sim 0,45$), а стабилизация теплообмена наступает при больших l/d_r .

Числа Nu для теплообменников и обогреваемых пучков (19)–(22) сильно отличаются друг от друга по следующим причинам. Средние коэффициенты теплоотдачи в теплообменниках учитывают влияние участков тепловой стабилизации и относятся к случаю непостоянного по длине теплового потока. Однако для больших l/d_r влиянием этих участков можно пренебречь, а эффект от неравномерности теплового потока невелик.

Главная причина заключается в сильном влиянии необогреваемой обечайки на температурное поле жидкости в теплообменнике. При определении коэффициентов теплопередачи в теплообменнике используются значения средних смешанных температур потоков жидкостей, которые существенно отличаются от локальных. Вследствие того что температура теплоносителя непостоянна по сечению теплообменника, различные ряды трубок имеют разную интенсивность теплообмена. Указанный эффект уменьшается с увеличением числа трубок крайне медленно.

Предполагая, что температура жидкости в трубках теплообменника примерно постоянна (это близко к условиям опытов), коэффициенты теплоотдачи постоянны по длине трубок, теплообмен между ячейками отсутствует, можно получить формулу

$$\frac{Nu_1}{Nu_2} \approx \frac{8nl Nu_1}{d_r N Pe \ln \left[(1-\mu) \exp(-A_1) + \mu \exp(-A_{II}) \right] + R\alpha_1}, \quad (23)$$

где Nu_1 — число Нуссельта для центральной зоны пучка тепловыделяющих элементов;

Nu_2 — среднее число Нуссельта для межтрубного пространства теплообменника;

n, N — соответственно число трубок и ячеек в теплообменнике;

μ — доля периферийных ячеек (ячеек, образованных крайними трубками и обечайкой);

R — термическое сопротивление между греющей жидкостью и внешней поверхностью трубок;

$$\alpha_1 \equiv \frac{Nu_1 \cdot \lambda_f}{d_r}; \quad A \equiv \frac{kPl}{C_p \gamma v};$$

l, k, P, v — длина, коэффициент теплопередачи, периметр теплообмена, объемный расход

теплоносителя для центральной (индекс I) и периферийной (индекс II) зон теплообменника; при $n \rightarrow \infty \frac{Nu_1}{Nu_2} \rightarrow 1$.

Приближенные расчеты по формуле (23) дают результаты, качественно согласующиеся с опытными данными. Оказалось, что с ростом числа Pe разница между Nu_1 и Nu_2 уменьшается, причем $Nu_1 > Nu_2$. Отсюда вытекает интересный вывод: зависимость $Nu_1 = f(Re)$ должна быть более слабой, чем зависимость $Nu_2 = f(Re)$, что и наблюдается в опытах.

Рассмотренные выше результаты экспериментов и расчетов показывают, что полученные в опытах с теплообменниками данные нельзя непосредственно использовать для расчета пучков тепловыделяющих элементов реакторов.

ТЕПЛООБМЕН ПРИ КИПЕНИИ ЖИДКИХ МЕТАЛЛОВ И КОНДЕНСАЦИИ ИХ ПАРОВ

В исследовании теплообмена при кипении жидких металлов участвовали А. А. Ивашкевич, А. П. Кудрявцев. Опыты проводились с натрием, кипящим на горизонтальной поверхности в условиях свободной конвекции. Поверхность теплообмена диаметром 38 мм была расположена на одном уровне с дном бака. Теплоподвод осуществлялся путем электронной бомбардировки теплопередающей стенки.

Натриевый пар конденсировался в охлаждаемом потоком воздуха конденсаторе, расположенном в верхней части бака. Давление паров натрия измерялось датчиком компенсационного типа с индукционным «нуль-прибором» (чувствительность ~ 1 мм рт. ст.).

При измерениях коэффициентов теплоотдачи теплопередающая стенка в ряде случаев была выполнена трехслойной. В цилиндрическую чашечку из нержавеющей стали под вакуумом заливалась медь. Поверхность меди после механической обработки покрывалась тонким слоем никеля (~ 20 мк). В отдельных опытах никелевое покрытие разрушилось и натрий контактировал непосредственно с медью. В других случаях теплопередающая стенка была двухслойной (нержавеющая сталь — медь). При этом натрий кипел на поверхности из нержавеющей стали.

Температура стенки измерялась двумя термомпарами, залитыми в слое меди. Распределение температуры в натрии и паре измерялось подвижной термопарой.

При исследовании критических тепловых потоков теплопередающая стенка изготовлялась или из жаропрочного сплава на никелевой основе, или из молибдена.

Для периодической очистки натрия от окислов холодильником-ловушкой и отбора проб натрия методом вакуумной дистилляции был предусмотрен замкнутый циркуляционный контур.

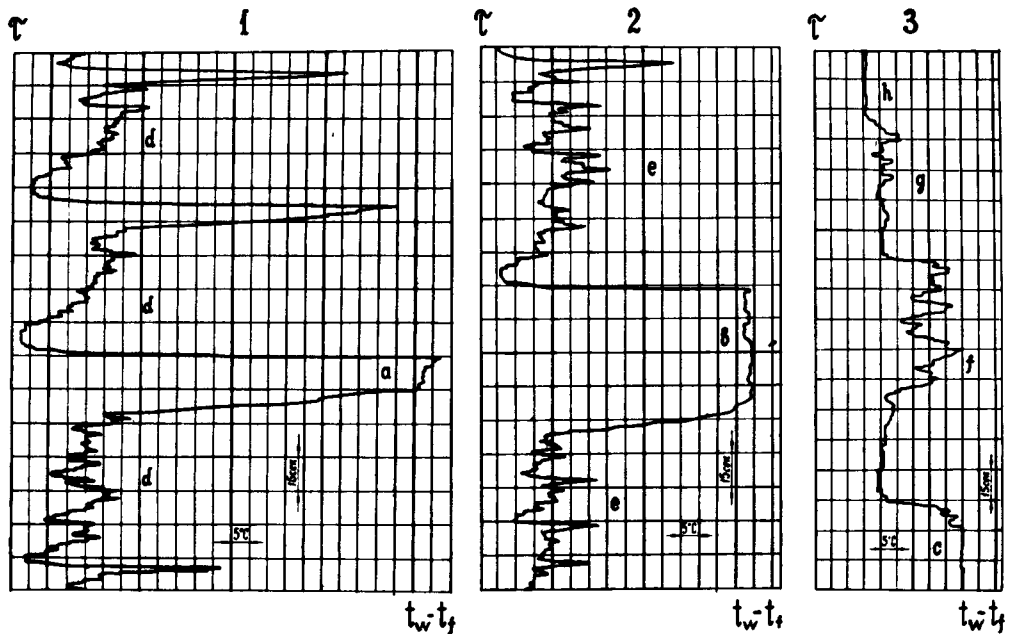


Рис. 4. Изменение во времени температуры стенки при кипении натрия:

1, 2, 3—для $q=1,4 \cdot 10^6$; $0,82 \cdot 10^6$; $0,47 \cdot 10^6 \frac{\text{ккал}}{\text{м}^2 \cdot \text{ч}}$ и $t_S=710$; 690 ; 800°C соответственно

Исследования показали, что на поверхностях из нержавеющей стали и никеля натрий может быть сильно перегрет по отношению к термодинамически равновесной температуре t_S (до 100°C и выше). Натрий во всем объеме оказывается также сильно перегретым. В этом случае кипение на поверхности теплообмена отсутствует даже при больших тепловых потоках ($\sim 10^6 \text{ ккал/м}^2 \cdot \text{ч}$), тепло от стенки отводится теплопроводностью и конвекцией, а со свободной поверхности натрия происходит испарение. Разница температур натрия и паров при этом достигает значительной величины. Такой режим существовал иногда десятки часов.

Установлено, что для натрия существуют два режима кипения: устойчивое и неустойчивое. Устойчивое кипение сопровождается относительно малыми пульсациями температуры стенки. Неустойчивое кипение характеризуется большими пульсациями температуры стенки (до 100°C и выше). При неустойчивом кипении частота пульсаций температуры ниже, чем при устойчивом. На поверхностях из никеля и стали наблюдались оба режима кипения. На медных поверхностях кипение было всегда устойчивым. Оба режима могут существовать длительное время. Перепад температуры на свободной поверхности натрия резко уменьшается при переходе от естественной конвекции к неустойчивому кипению и становится незначительным при развитом кипении.

Различные режимы кипения были также замечены при просвечивании кипящего слоя натрия рентгеновскими лучами.

На рис. 4 приведены характерные зависимости температуры теплоотдающей стенки от времени, записанные быстродействующим потенциометром ЭПП-09. Участки диаграмм *a*, *b*, *c* соответствуют теплоосъему без кипения. В конце этих участков резко снижаются температура натрия и температурный напор «стенка — жидкость» вследствие вскипания натрия. Переходный процесс сопровождается сильными ударами и повышением давления в баке. Участки *d*, *e*, *f* соответствуют неустойчивому, а участки *g*, *h* — устойчивому кипению натрия.

Полученные в опытах значения коэффициентов теплоотдачи приведены на рис. 5 ($\alpha \text{ ккал/м}^2 \cdot \text{ч} \cdot ^\circ \text{C}$, $q \text{ ккал/м}^2 \cdot \text{ч}$). Там же нанесены литературные данные по теплоосъему при кипении натрия на трубках ^{4,5} и при кипении сплава Na—K на плоской поверхности ⁶. Опытные данные на рис. 5 можно качественно разбить на три группы. Первая группа соответствует случаю, когда тепло от стенки отводится конвекцией и теплопроводностью, а кипение отсутствует. Опытные точки этой группы располагаются вблизи линии, построенной по формуле $\alpha = 100q^{1/2} \text{ ккал/м}^2 \cdot \text{ч} \cdot ^\circ \text{C}$. Эта формула описывает данные, полученные на той же установке в условиях, когда кипение заведомо отсутствовало ($t_w \ll t_S$).

Вторая группа опытных данных соответствует развитому кипению. Линия, осредняющая эти данные, аппроксимируется формулой

$$\alpha \approx 4q^{2/3} \text{ ккал/м}^2 \cdot \text{ч} \cdot \text{°C} \quad (24)$$

Между интенсивностью пульсаций и расслоением на рис. 5 опытных данных по теплоотдаче при развитом кипении существует определенная связь: чем меньше пульсации температуры, тем выше значения коэффициентов теплоотдачи (сравните рис. 4 и 5).

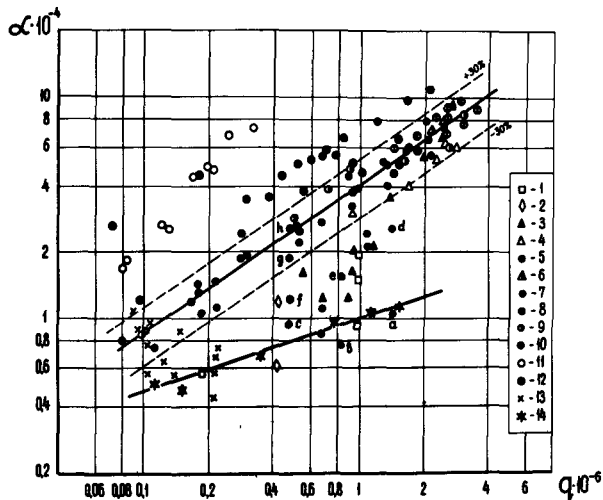


Рис. 5. Теплоотдача при кипении натрия:

1, 2, 3—никелевая поверхность; $t_s = 600, 650$ и 700°C ; 4, 5, 6, 7—медная поверхность, $t_s = 700, 750, 800$ и 850°C ; 8, 9, 10—поверхность из нержавеющей стали; $t_s = 700, 800$ и 850°C соответственно. 11, 12, 13—данные работ ^{4,5,6}; 14—для свободной конвекции ($t_s = 500^\circ\text{C}, P = 1 \text{ ат}$)

Третья группа опытных данных, соответствующая неустойчивому кипению натрия, располагается в промежутке между двумя первыми группами.

В исследованном интервале изменения параметров зависимость $\alpha = f(P_s)$ оказалась слабой.

Значения критических тепловых потоков при кипении натрия в условиях свободной конвекции (рис. 6) описываются формулой

$$q_{кр} = (1,5 + 1,3P_s \cdot 10^6 \text{ ккал/м}^2 \cdot \text{ч}; \quad 0,015 < P_s < 1, 2 \text{ ат}. \quad (25)$$

С формулой (25) согласуются данные работы⁵. Характерно, что кризис кипения наступает раньше, если ему предшествует неустойчивое кипение натрия. Например, при $P_s \approx 0,35 \text{ ат}$ значения $q_{кр}$ для развитого и неустойчивого кипения отличаются приблизительно на 70% (точки a, b на рис. 6).

Было проведено исследование процесса конденсации «неподвижного» калиевого пара на плоской стенке из нержавеющей стали. По-

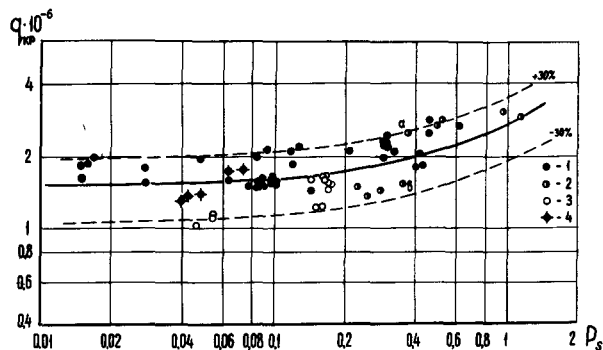


Рис. 6. Критические тепловые потоки при кипении натрия: 1, 2, 3—для поверхностей из жаропрочного сплава, молибдена и нержавеющей стали соответственно; 4—данные работы ⁵

верхностью конденсации являлся лист фольги 0,2 мм, напаянный серебряным припоем на массивный медный параллелепипед. Термопары были заделаны в медь.

За 20 мин конденсации при 450°C калий полностью смочил стенку, и конденсация стала пленочной. Пары калия при освещении белым светом имели яркую голубовато-зеленую окраску.

Коэффициенты теплоотдачи были гораздо меньше рассчитанных с учетом лишь термического сопротивления пленки конденсата. Это может быть вызвано контактным термическим сопротивлением на стенке и термическим сопротивлением на границе «пар — конденсат»,

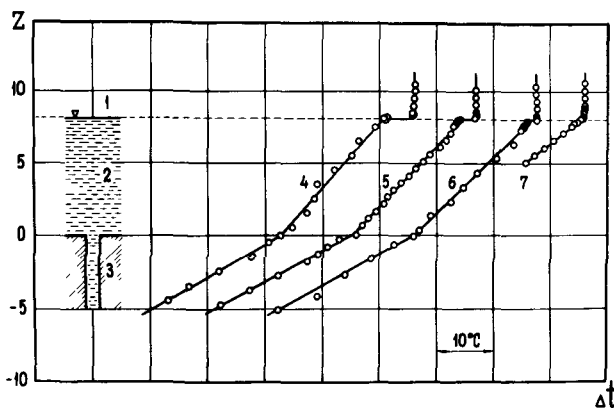


Рис. 7. Распределение температуры в калиевом паре, конденсате и стенке конденсатора:

1, 2, 3—пар, конденсат и стенка; 4, 5, 6, 7—для температуры пара 345, 364, 383 и 640°C

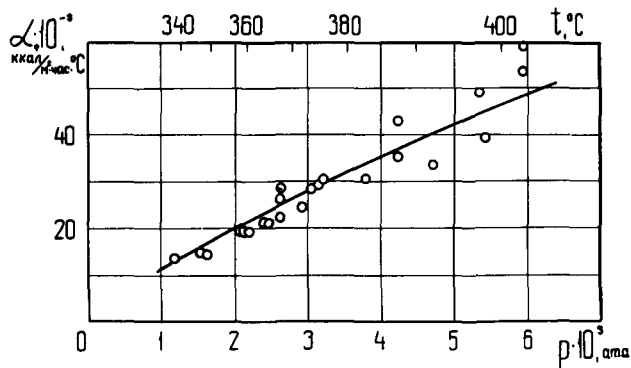


Рис. 8. Коэффициенты теплоотдачи при конденсации паров калия:

1—опытные данные; 2—расчет

связанным с фазовым переходом или с присутствием в паре неконденсирующихся газов.

Для исследования влияния указанных факторов были произведены измерения подвижной термопарой распределений температуры в калиевом паре, конденсате и стенке. На верхнем торце конденсатора была сделана ванночка глубиной 8 мм, которая заполнялась конденсатом. Измерения температурного поля стенки производились путем погружения подвижной термопары в узкую (0,95 мм) вертикальную щель, выфрезерованную в стенке конденсатора. Измерения показали, что контактное термическое сопротивление между стенкой из

нержавеющей стали и конденсатом калия отсутствует.

При низких давлениях между паром и конденсатом обнаруживается «скачок» температуры, который уменьшается с ростом давления (рис. 7). Величина «скачка» температуры согласуется с расчетом по газокинетической теории, если при этом коэффициент конденсации принят равным единице и учтена поправка на относительную скорость пара по направлению к поверхности конденсации⁷ (рис. 8).

Как показывают предварительные опыты, значения коэффициентов теплоотдачи при конденсации паров калия в горизонтальной круглой трубе примерно те же, что и при конденсации на плоской поверхности. Возникающая в процессе конденсации в трубе паров калия радиальная составляющая скорости влияет на гидравлическое сопротивление.

ЛИТЕРАТУРА

1. П. Л. Кириллов. «Атомная энергия», 13, вып. 5, 481 (1962).
2. В. И. Субботин, М. Х. Ибрагимов, Е. В. Номофилов. «Атомная энергия», 13, вып. 2, 155 (1962) и 14, вып. 4, 414 (1963). «Теплоэнергетика», № 6, 70 (1963).
3. В. И. Субботин, П. А. Ушаков, А. В. Жуков, Б. Н. Габрианович, В. Д. Таланов и И. П. Свириденко. «Атомная энергия», 9, вып. 6, 461 (1960) и 13, вып. 2, 162 (1962).
4. R. Lyon, A. Fost, A. Katz, Chem. Eng. Progress, symposium series, vol. 51, No 7, 41 (1955).
5. R. C. Noyes. Trans ASME, series C, No 2, 125 (1963).
6. N. Madison, C. Bonilla, Chem. Eng. Progress, symposium series, vol. 56, No 30, 251 (1960).
7. Р. Я. Кучеров и Л. Э. Рикенглаз. Докл. АН СССР, 133, № 5, 1130 (1960).

ABSTRACT—RÉSUMÉ—АННОТАЦИЯ—RESUMEN

A/328 USSR

Heat transfer from fuel elements of liquid metal-cooled reactors

By V. I. Subbotin *et al.*

Notwithstanding definite progress in the theoretical context, experimental studies on heat transfer to liquid metals remain for the present the main research methods.

This paper gives new data on heat transfer to liquid metals obtained in recent years from the development of liquid metal-cooled reactors.

As a result of temperature gradient measurements in the flow of sodium, sodium-potassium alloy, lithium and mercury, a general equation for temperature distribution in different liquid metals has been obtained. Turbulent flow heat transfer coefficients in tubes have been determined, together with some statistical properties of turbulent flow.

In studying the free convection effect it has been observed that the MacAdams rule is not applicable to liquid metals.

In this paper the problems of heat transfer from plate-type fuel elements are considered. These elements are characterized by a large heat transfer surface. Analytical calculations and experimental studies have revealed some specific features of heat transfer in channels of rectangular cross section. Data have been obtained relating heat transfer and temperature distribution to the channel geometry, and to the thicknesses and thermal conductivities of both fuel layer and cladding etc.

The problems of heat removal where liquid metals flow through bundles of cylindrical fuel elements have been examined. Empirical formulae for calculations relating to such systems are given. The temperature distribution in bundles of fuel elements is also shown to depend on their physical properties (thermal conductivity, dimensions etc.).

It has been shown that the "equivalent hydraulic diameter" cannot apply in generalizing heat transfer data for liquid metals in channels of complicated cross section.

Fuel elements are classified according to their thermal properties and the possibility of thermal simulation under laboratory conditions. Methods of thermal simulation with cylindrical fuel elements are described.

Experimental results for liquid metals are compared with corresponding results for water. A note is made of the inadequate explanation concerning the use of hydraulic diameter as the characteristic value for bundles through which water or ordinary liquids flow.

A method has been studied for the approximate calculation of temperature distribution in a bundle of cylindrical elements, based on the analysis in the liquid of a uniform velocity flow (laminar flow). In certain cases these results give a sufficiently accurate physical picture.

This paper presents the results of work on determining mean heat transfer coefficients in shell-and-tube heat exchangers of the "liquid metal-liquid metal" type having different lattice pitches and different lengths of tubes. It is shown that mean heat transfer coefficients in heat exchangers and in fuel element bundles must differ from each other.

Investigation of the pressure drop in fuel element bundles has brought to light certain properties inherent in these systems (e.g., a significant decrease in pressure drop coefficients with tightly packed bundles, etc.).

A substantial number of heat transfer experiments where the liquid metal flows perpendicularly through tube bundles has enabled the mean heat transfer coefficient to be calculated. However, pulsation amplitudes of temperature at the heat transfer surface, reaching 40–60% of the average temperature head, cast a doubt on the safety of lengthy operation of certain systems mentioned.

The results of experimental heat transfer studies are given, made by altering the overall conditions. Investigations of burn-out heat fluxes and heat transfer coefficients when sodium is boiling under free convection conditions have revealed some important properties of liquid metal boiling.

Condensation processes of potassium vapours have been studied using a flat vertical wall. Visual observations and photographs have shown the features of the change from droplet to film condensation.

A/328 URSS

Transfert de chaleur sur les éléments de combustible des réacteurs à refroidissement par métaux liquides

par V. I. Subbotin *et al.*

Malgré les réalisations certaines dans le domaine de la théorie, ce sont les études expérimentales du

transfert de chaleur par les métaux liquides qui constituent encore les méthodes principales d'investigation.

Ce mémoire contient de nouvelles données relatives à l'échange de la chaleur par les métaux liquides obtenues au cours des dernières années grâce au développement des réacteurs à refroidissement par métaux liquides. Les expériences faites sur le sodium, l'alliage sodium-potassium, le lithium, le mercure pour la mesure des gradients de température ont permis d'établir une seule formule pour le profil de la température dans le métal liquide, de déterminer les coefficients du transfert turbulent de la chaleur dans des conduits tubulaires et d'évaluer certaines caractéristiques statistiques de l'écoulement turbulent.

On a remarqué en examinant l'influence de la convection naturelle que la loi de Mac Adams ne s'applique pas aux métaux liquides.

Ce mémoire examine les questions de l'évacuation de la chaleur des éléments de combustible en forme de plaques ayant une surface importante d'échange thermique. Des calculs analytiques et des recherches expérimentales ont montré une série de propriétés spécifiques d'échange thermique, propres aux canaux à section rectangulaire et ont permis d'obtenir des données pour la détermination de la relation qui lie le transfert de chaleur et le champ de température avec la géométrie du canal, l'épaisseur et la conductivité thermique de la couche productrice de chaleur et de l'enveloppe de protection, etc.

On étudie les questions de l'évacuation de la chaleur lorsque les métaux liquides circulent le long de faisceaux d'éléments de combustible cylindriques. On donne des formules empiriques pour le calcul de tels systèmes.

On montre que le champ de température des faisceaux d'éléments de combustible est également déterminé par les caractéristiques (dimensions et conductivité) de ces éléments.

On démontre que le diamètre hydraulique équivalent ne peut être appliqué pour généraliser les données relatives à l'échange de chaleur par les métaux liquides dans des canaux de forme compliquée.

On classe les barreaux combustibles du point de vue de leurs propriétés thermophysiques et de la simulation thermique. On décrit les méthodes de simulation thermique des éléments de combustible cylindriques.

Les valeurs obtenues pour les métaux liquides sont comparées aux valeurs correspondantes obtenues pour l'eau. On note l'explication insuffisante du problème concernant l'utilisation du diamètre hydraulique en tant que grandeur caractéristique pour les faisceaux le long desquels circule l'eau ou d'autres liquides ordinaires.

On étudie la méthode de calcul approximatif du champ de température des éléments cylindriques en faisceaux en prenant pour base l'analyse du courant du liquide à vitesse uniforme sur la section (courant plat). Ces résultats donnent, dans certains cas, une image physique suffisamment juste.

Ce mémoire indique les résultats de recherche sur les coefficients moyens de transfert de chaleur dans les échangeurs "métal-métal" à tubulures de pas et de longueurs différents. Il est montré que les coefficients moyens de transfert de chaleur doivent être différents dans les échangeurs de chaleur et dans les faisceaux d'éléments sous forme de barreaux.

Des recherches sur la résistance hydraulique des faisceaux de barreaux ont permis de mettre en évidence certaines caractéristiques particulières à de tels systèmes (baisse brutale des coefficients de résistance des faisceaux compacts et autres relations).

Un nombre suffisant d'expériences sur le transfert de chaleur lorsque l'écoulement des métaux liquides perpendiculaire au faisceau de tubes permet de calculer le coefficient moyen de transfert de chaleur. Cependant les amplitudes de pulsation de la température de la surface d'échange de chaleur qui atteignent 40 à 60 % de la contrainte thermique moyenne, amènent un doute en ce qui concerne la sécurité d'un fonctionnement prolongé certains des systèmes mentionnés.

Des recherches expérimentales ont été consacrées aux problèmes d'échange de chaleur lorsque l'état d'agrégation varie. Des expériences de mesures des charges thermiques critiques et du transfert de chaleur lors de l'ébullition du sodium dans les conditions de convection naturelle ont montré une série de propriétés importantes de l'ébullition des métaux liquides (pulsations de la température, instabilité, différents régimes d'ébullition, etc.).

Les processus de condensation des vapeurs de potassium ont été étudiés dans des expériences avec une paroi verticale plate. Des observations visuelles et des photographies ont montré les particularités du passage de la condensation en gouttes à la condensation en film.

A/328 URSS

Transferencia de calor en los elementos de combustible de reactores refrigerados por metales líquidos

por V. I. Subbotin *et al.*

A pesar de los claros progresos en el campo teórico, las investigaciones experimentales relativas a la transferencia de calor por metales líquidos siguen constituyendo el más importante método de estudio.

En la memoria se presentan nuevos datos acerca del intercambio de calor con metales líquidos obtenidos en los últimos años gracias al desarrollo de los reactores refrigerados por dichos líquidos. Los experimentos realizados con sodio, con aleación sodio-potasio, con litio y con mercurio, para determinar los gradientes de temperatura, permitieron establecer una fórmula única para la curva de distribución de la temperatura en un metal líquido, determinar los coeficientes de transferencia turbulenta

del calor en tubos circulares, y también estimar algunas características estadísticas de la corriente turbulenta.

Al estudiar la influencia de la convección natural se advirtió que la conocida ley de MacAdams no es aplicable a los metales líquidos.

En la memoria se consideran algunas cuestiones relacionadas con la extracción de calor en el caso de placas de combustible con aletas. Los cálculos teóricos y las investigaciones experimentales pusieron de manifiesto particularidades específicas del intercambio de calor, típicas para canales de sección rectangular, y proporcionaron datos para determinar la relación funcional que existe entre la transferencia de calor y la distribución de temperatura, la geometría del canal, el espesor y la conductibilidad térmica de la capa productora de calor y de la vaina, etc.

Se estudia el problema de la extracción del calor cuando los metales líquidos circular a lo largo de haces de elementos combustibles cilíndricos, y se presentan fórmulas empíricas para el cálculo de tales sistemas.

Se muestra que la distribución de temperaturas en los haces de elementos combustibles viene determinada también por ciertas propiedades de los elementos (las dimensiones y la conductibilidad).

Se demuestra que el concepto de diámetro hidráulico equivalente no es aplicable a la generalización de los datos relativos al intercambio de calor con metales líquidos en canales de forma complicada.

Se clasifican los elementos combustibles en forma de barra desde el punto de vista de sus propiedades físico-térmicas y de la preparación práctica de modelos térmicos. Se describen métodos de construcción de modelos térmicos de los elementos combustibles cilíndricos.

Los datos obtenidos para metales líquidos se comparan con datos relativos al agua. Se hace notar que es insuficiente la explicación relativa a la aplicabilidad del concepto de diámetro hidráulico como magnitud característica de los haces a lo largo de los cuales circula agua y otros líquidos ordinarios.

Se examina un método aproximado de cálculo de la distribución de temperaturas en elementos cilíndricos que constituyen un haz, método basado en el análisis de la corriente de un líquido con velocidad uniforme en todos los puntos de cada sección transversal (corriente plana). Estos resultados, en algunos casos, proporcionan una imagen suficientemente fiel del proceso físico.

En el informe se presentan los resultados de un estudio sobre los coeficientes medios de transferencia de calor en los intercambiadores "metal-metal", con pasos diferentes de la red de tubos y distinta longitud. Se demuestra que los coeficientes medios de transferencia de calor en los intercambiadores y en los haces de elementos combustibles en forma de barra deben ser diferentes.

Las investigaciones acerca de la resistencia hidráulica de los haces de barras permitieron poner de manifiesto algunas particularidades propias de dichos sistemas

(disminución brusca de los coeficientes de resistencia de los haces compactos, etc.).

Un número suficiente de experimentos relativos a la transferencia de calor, cuando la corriente de los metales líquidos es perpendicular al haz de tubos, permite calcular el coeficiente medio de transferencia de calor. Sin embargo, las amplitudes de pulsación de la temperatura de la superficie de intercambio de calor, que alcanzan entre el 40 % y el 60 % del valor medio, inspiran temor en relación con la seguridad de funcionamiento en caso de un trabajo prolongado en algunos de dichos sistemas.

Se han estudiado experimentalmente los problemas

de intercambio de calor cuando tienen lugar cambios de fase. Medidas experimentales de los flujos térmicos críticos y de los coeficientes de transferencia de calor cuando hierve el sodio en condiciones de convección natural pusieron de manifiesto toda una serie de características esenciales de la ebullición de metales líquidos (pulsaciones de la temperatura, inestabilidad regímenes diversos de ebullición, etc.).

Los procesos de condensación de los vapores de potasio se estudiaron en experimentos con una pared vertical plana. Las observaciones visuales y las fotografías revelaron detalles del paso de la condensación en gotas a la pelicular.

Some theoretical problems of heat conduction in reactor fuel elements

By J. Schmid*

Problems of heat conduction in fuel elements of cylindrical geometry are solved in cases where the thermal conductivity, the heat-transfer coefficient and the contact resistance are dependent on temperature. In the calculation we consider an arbitrary distribution of heat sources over the cross section, and variable boundary conditions along the circumference. We neglect heat conduction in the direction of the z -axis.

NOTATION

r, ϕ : polar co-ordinates (m), (rad)
 R : radius of the boundary of two media (m)
 t : temperature ($^{\circ}\text{C}$), ($^{\circ}\text{K}$)
 λ : thermal conductivity (kcal/mh $^{\circ}\text{C}$)
 q : density of heat sources (kcal/m 3 h)
 ρ : contact resistance (m 2 h $^{\circ}\text{C}$ /kcal)
 α : heat-transfer coefficient (kcal/m 2 h $^{\circ}\text{C}$)

SOLUTION OF THE HEAT CONDUCTION EQUATION IN CYLINDRICAL GEOMETRY

The heat conduction equation in cylindrical geometry

$$-\left[\frac{1}{r} \frac{\partial}{\partial r} \left(r \lambda \frac{\partial t}{\partial r} \right) + \frac{1}{r^2} \frac{\partial}{\partial \phi} \left(\lambda \frac{\partial t}{\partial \phi} \right) \right] = q(r, \phi) \quad (1)$$

is modified by means of the equation (similarly as in ref. [1])

$$\lambda(t) = \lambda_0 + \lambda_1(t) \quad (2)$$

where

$$\lambda_0 = \lambda(t_0) \lambda_1(t) = \lambda(t) - \lambda(t_0)$$

and where t_0 is a suitably selected reference temperature. After insertion into (1) we obtain equation

$$\begin{aligned} & -\lambda_0 \left[\frac{\partial^2 t}{\partial r^2} + \frac{1}{r} \frac{\partial t}{\partial r} + \frac{1}{r^2} \frac{\partial^2 t}{\partial \phi^2} \right] \\ & = q(r, \phi) + \lambda_1(t) \left[\frac{\partial^2 t}{\partial r^2} + \frac{1}{r} \frac{\partial t}{\partial r} + \frac{1}{r^2} \frac{\partial^2 t}{\partial \phi^2} \right] \\ & \quad + \frac{d\lambda_1}{dt} \left[\left(\frac{\partial t}{\partial r} \right)^2 + \frac{1}{r^2} \left(\frac{\partial t}{\partial \phi} \right)^2 \right]. \quad (3) \end{aligned}$$

We assume that the influence of non-linearities (i.e., the second and third term on the right-hand side of Eq. (3)) is small, and a solution of the equation is sought by means of the iteration process.

The zero approximation $t^{(0)}(r, \phi)$ for the function

$t(r, \phi)$ is obtained from the equation

$$\frac{\partial^2 t^{(0)}}{\partial r^2} + \frac{1}{r} \frac{\partial t^{(0)}}{\partial r} + \frac{1}{r^2} \frac{\partial^2 t^{(0)}}{\partial \phi^2} = -q^{(0)}, \quad (4a)$$

where

$$q^{(0)} = \frac{1}{\lambda_0} q(r, \phi), \quad (5a)$$

and further approximations are obtained by solving equation

$$\frac{\partial^2 t^{(m)}}{\partial r^2} + \frac{1}{r} \frac{\partial t^{(m)}}{\partial r} + \frac{1}{r^2} \frac{\partial^2 t^{(m)}}{\partial \phi^2} = -q^{(m)}, \quad (m = 1, 2, 3, \dots), \quad (4b)$$

where

$$\begin{aligned} q^{(m)} = \frac{1}{\lambda_0} \left\{ q(r, \phi) - \lambda_1(t^{(m-1)}) q^{(m-1)} + \frac{d\lambda}{dt} \Big|_{t=t^{(m-1)}} \right. \\ \left. \times \left[\left(\frac{\partial t^{(m-1)}}{\partial r} \right)^2 + \frac{1}{r^2} \left(\frac{\partial t^{(m-1)}}{\partial \phi} \right)^2 \right] \right\}. \quad (5b) \end{aligned}$$

Equation (4) is solved by Fourier's method. Expanding the sources into a Fourier series and assuming the solution in the form

$$t^{(m)}(r, \phi) = \sum_{n=0}^{\infty} (c_n^{(m)}(r) \cos n\phi + s_n^{(m)}(r) \sin n\phi)$$

differential equations for functions $f_n(r)$ are obtained of the form

$$\begin{aligned} {}^l f_n''(r) + \frac{1}{r} {}^l f_n'(r) - \frac{1}{r^2} n^2 {}^l f_n(r) = -{}^l q_n^{(m)}(r) \\ l = \begin{cases} c(n = 0, 1, 2, \dots) \\ s(n = 1, 2, 3, \dots) \end{cases} \end{aligned}$$

All these equations are solved by means of the method of integration factors [2].

The solution of Eqs. (4) takes the form

$$\begin{aligned} t^{(m)}(r, \phi) = A_0^{(m)} + B_0^{(m)} {}^l q r + c Z_0^{(m)} \\ + \sum_{n=1}^{\infty} [(A_n^{(m)} r^n + B_n^{(m)} r^{-n} + c Z_n^{(m)}) \cos n\phi \\ + (C_n^{(m)} r^n + D_n^{(m)} r^{-n} + s Z_n^{(m)}) \sin n\phi], \quad (6) \end{aligned}$$

where

$$\begin{aligned} {}^l Z_n^{(m)} = -r^n \int_{r_0}^r r'^{-(2n+1)} \int_{r_0}^{r'} (r'')^{n+1} {}^l \bar{q}_n^{(m)}(r'') dr'' dr' \\ l = \begin{cases} c(n = 0, 1, 2, \dots) \\ s(n = 1, 2, 3, \dots) \end{cases} \end{aligned}$$

and where ${}^l \bar{q}_n^{(m)}(r)$ are Fourier coefficients of function $q^{(m)}$.

Equations (5) and (6) are rewritten using matrix

* Institute of Nuclear Research, Řež near Prague.

symbols in a more convenient form. The series (6) for $t^{(m)}(r, \phi)$ may be written as the product of matrix S and vector $\vec{T}^{(m)}$,

$$t^{(m)}(r, \phi) = S \cdot \vec{T}^{(m)},$$

where

$$S = [1, \cos \phi, \sin \phi, \cos 2\phi, \sin 2\phi, \dots]$$

$$T^{(m)} = {}_1M\vec{C}^{(m)} + \vec{Z}^{(m)} \quad (7)$$

vector $\vec{C}^{(m)}$ containing integration constants of the order $A_0^{(m)}, B_0^{(m)}, A_1^{(m)}, B_1^{(m)}, C_1^{(m)}, D_1^{(m)}, \dots$, vector $\vec{Z}^{(m)}$ has the components ${}^cZ_0^{(m)}, {}^cZ_1^{(m)}, {}^sZ_1^{(m)}, \dots$, and the matrix ${}_1M$ takes the following form

$${}_1M = \begin{pmatrix} 1 & \lg r & 0 & 0 & 0 & 0 & 0 & 0 & 0 & 0 & \dots \\ 0 & 0 & r & r^{-1} & 0 & 0 & 0 & 0 & 0 & 0 & \\ 0 & 0 & 0 & 0 & r & r^{-1} & 0 & 0 & 0 & 0 & \\ 0 & 0 & 0 & 0 & 0 & 0 & r^2 & r^{-2} & 0 & 0 & \\ 0 & 0 & 0 & 0 & 0 & 0 & 0 & 0 & r^2 & r^{-2} & \\ \vdots & & & & & & & & & & \end{pmatrix} \quad (8)$$

For the derivations $\frac{\partial t^{(m)}}{\partial r}$ and $\frac{1}{r} \frac{\partial t^{(m)}}{\partial \phi}$ we obtain

$$\left. \begin{aligned} \frac{\partial t^{(m)}}{\partial r} &= S({}_2M\vec{C}^{(m)} + \vec{Z}'^{(m)}) = S\vec{T}_r^{(m)} \\ \frac{1}{r} \frac{\partial t^{(m)}}{\partial \phi} &= S\vec{T}_\phi^{(m)} \end{aligned} \right\} \quad (9)$$

matrix ${}_2M$ (or rather vector $Z'^{(m)}$) being the derivation of matrix ${}_1M(\vec{Z}^{(m)})$ and

$$\vec{T}_\phi^{(m)} = \frac{1}{r} \begin{pmatrix} 0 \\ C_1^{(m)}r + D_1^{(m)}r^{-1} + {}^sZ_1^{(m)} \\ -(A_1^{(m)}r + B_1^{(m)}r^{-1} + {}^cZ_1^{(m)}) \\ \vdots \\ \vdots \end{pmatrix}$$

The product of two Fourier series having the coefficients a_n, b_n and v_n, w_n , i.e., the product $S\vec{A} \cdot S\vec{V}$, where vectors \vec{A} and \vec{V} include Fourier coefficients a_n, b_n and v_n, w_n , may be written as:

$$SK_a\vec{V}$$

Matrix K_a contains the coefficients a_n, b_n , its form being

$$K_a = \frac{1}{2} \begin{pmatrix} 2a_0 & a_1 & b_1 & a_2 & b_2 & a_3 & b_3 & \dots \\ 2a_1 & 2a_0 + a_2 & b_2 & a_1 + a_3 & b_1 + b_3 & a_2 + a_4 & b_2 + b_4 & \\ 2b_1 & b_2 & 2a_0 - a_2 & -b_1 + b_3 & a_1 - a_3 & -b_2 + b_4 & a_2 - a_4 & \\ 2a_2 & a_1 + a_3 & -b_1 + b_3 & 2a_0 + a_4 & b_4 & a_1 + a_5 & b_1 + b_5 & \\ 2b_2 & b_1 + b_3 & a_1 - a_3 & b_4 & 2a_0 - a_4 & -b_1 + b_5 & a_1 - a_5 & \\ 2a_3 & a_2 + a_4 & -b_2 + b_4 & a_1 + a_5 & -b_1 + b_5 & 2a_0 + a_6 & b_6 & \\ 2b_3 & b_2 + b_4 & a_2 - a_4 & b_1 + b_5 & a_1 - a_5 & b_6 & 2a_0 - a_6 & \\ \vdots & & & & & & & \\ \vdots & & & & & & & \\ \vdots & & & & & & & \end{pmatrix} \quad (10)$$

We next determine Fourier coefficients for function $\lambda_1^{(m-1)}(r, \phi)$. We expand $\lambda_1^{(m-1)}(t)$ in the vicinity of the point $t = t_0$ into a Taylor series, of the form

$$\lambda_1^{(m-1)}(t) = a_0(t - t_0) + a_1(t - t_0)^2 + a_2(t - t_0)^3 + \dots$$

and insert in it the series for $t^{(m-1)}(r, \phi)$. Vector $\vec{\lambda}_1^{(m-1)}$, containing Fourier coefficients for function $\lambda_1^{(m-1)}(r, \phi)$, takes the form

$$\vec{\lambda}_1^{(m-1)} = \left(\sum_{j=0}^{\infty} a_j K_{V^{(m-1)}}^j \right) \vec{U}^{(m-1)}, \quad (11)$$

where

$$\vec{U}^{(m-1)} = \vec{T}^{(m-1)} - \vec{T}_0; \vec{T}_0 = t_0 \vec{I}; \vec{I} = \begin{pmatrix} 1 \\ 0 \\ 0 \\ \vdots \\ \vdots \end{pmatrix}.$$

By means of the same procedure we obtain the following expression for Fourier coefficients of function $d\lambda_1/dt$

$$\vec{\lambda}_2^{(m-1)} = \vec{a}_0 + \left(\sum_{j=1}^{\infty} (j+1)a_j K_{V^{(m-1)}}^j \right) \vec{U}^{(m-1)}, \quad (12)$$

where

$$\vec{a}_0 = a_0 \vec{I}.$$

The vector of Fourier coefficients of function $\vec{q}^{(m)}$ may be written in the form

$$\vec{q}^{(m)} = \vec{q}^{(0)} + \frac{1}{\lambda_0} [-\vec{K}_{\sigma^{(m-1)}} \vec{\lambda}_1^{(m-1)} + (\vec{K}_{T_r^{(m-1)}}^2 + \vec{K}_{T_\phi^{(m-1)}}^2) \vec{\lambda}_2^{(m-1)}]. \quad (13)$$

From the nuclear fuel point of view, the temperature dependence of the thermal conductivity in the form

$$\lambda(t) = b_0 + b_1 v = b_2 v^2 + \dots, v = \frac{1}{t - t_0} \quad (14)$$

is very important. By a similar procedure, we obtain the following expression for vector $\vec{q}^{(m)}$:

$$\vec{q}^{(m)} = \vec{q}^{(0)} - \frac{1}{\lambda_0} \left\{ \vec{K}_{\sigma^{(m-1)}} \left[\sum_{j=1}^{\infty} b_j \vec{K}_{V^{(m-1)}}^{j-1} \right] + (\vec{K}_{T_r^{(m-1)}}^2 + \vec{K}_{T_\phi^{(m-1)}}^2) \left[\sum_{j=1}^{\infty} j b_j \vec{K}_{V^{(m-1)}}^j \right] \right\} \vec{V}^{(m-1)}, \quad (15)$$

where

$$\vec{V}^{(m-1)} = \vec{K}_{U^{(m-1)}} \vec{I}.$$

We may now determine $t^{(0)}(r, \phi)$ from Eq. (4a); vector $\vec{q}^{(1)}$ from expressions (13) or (15); function $t^{(1)}(r, \phi)$ by solving Eq. (4b) for $m = 1$, etc.

For the calculation itself, it is best to divide the region of variable r into a number of sections and to calculate the vectors $\vec{q}^{(m)}(r_i)$ numerically.

BOUNDARY CONDITIONS

In the next chapter we shall deal with solutions of boundary problems for an annular region, consisting of an arbitrary number of annuli. Therefore, we will now give the external boundary conditions on the surface of the annular region. Relations will be given for the internal and external surface of the annular region together (if two signs appear in the formulae, the upper one is valid for the internal radius and the lower one for the external radius). We will further give the inner (fourth) boundary condition for the boundary of two media.

Central arrangement

First boundary condition

The first boundary condition requires the fulfilment of the equation

$$t(R, \phi) = F_1(\phi) \quad (16)$$

where $F_1(\phi)$ is a given function. When we expand function $F_1(\phi)$ into a Fourier series, substituting into (16) series (6) for $t^{(m)}(r, \phi)$, we may write out algebraic equations for individual functions of argument ϕ and write the boundary condition thus

$${}_1M\vec{C}^{(m)} = {}_1\vec{F}^{(m)} \quad (17)$$

where

$${}_1\vec{F}^{(m)} = \vec{A}_1 - \vec{Z}^{(m)}$$

and where vector \vec{A}_1 includes Fourier coefficients of function $F_1(\phi)$.

Second boundary condition

The second boundary condition takes the form of

$$\pm \lambda(t) \frac{\partial t}{\partial r} \Big|_{r=R} = G(\phi). \quad (18)$$

We rewrite Eq. (18), using relation (2), to give

$$\pm \lambda_0 \frac{\partial t^{(m)}}{\partial r} \Big|_{r=R} = G(\phi) \mp \lambda_1(t^{(m-1)}) \frac{\partial t^{(m-1)}}{\partial r} \Big|_{r=R}. \quad (18')$$

After conversion to the matrix form, we obtain

$${}_2M\vec{C}^{(m)} = {}_2\vec{F}^{(m)} \quad (19)$$

where

$${}_2\vec{F}^{(m)} = \frac{1}{\lambda_0} [\pm \vec{B} - \lambda_0 \vec{Z}'^{(m)} - \vec{K}_{\lambda_1^{(m-1)}} \vec{T}'^{(m-1)}]$$

and where vector \vec{B} includes Fourier coefficients of function $G(\phi)$.

Third boundary condition

The third type of boundary condition is written as follows:

$$\pm \lambda(t) \frac{\partial t}{\partial r} \Big|_{r=R} = \alpha(\phi, t, t_R)[t(R, \phi) - t_R(\phi)]. \quad (20)$$

Assuming that function $\alpha(\phi, t, t_R)$ may be modified to the form

$$\alpha(\phi, t, t_R) = \Phi(\phi)[1 + F(t, t_R)] \quad (21)$$

we may write boundary condition (20), using relation (2), as

$$\begin{aligned} & \mp \lambda_0 \frac{\partial t^{(m)}}{\partial r} \Big|_{r=R} + \Phi(\phi)[t^{(m)}(R, \phi) - t_R(\phi)] \\ & = -\Phi(\phi) F(t^{(m-1)}, t_R) \\ & \times [t^{(m-1)}(R, \phi) - t_R(\phi)] \pm \lambda_1(t^{(m-1)}) \frac{\partial t^{(m-1)}}{\partial r} \Big|_{r=R} \end{aligned} \quad (20')$$

After conversion to the matrix form, we obtain

$${}_3M\vec{C}^{(m)} = {}_3\vec{F}^{(m)} \quad (22)$$

where

$$\left. \begin{aligned} {}_3M &= K_{\alpha} {}_1M \mp \lambda_0 {}_2M \\ {}_3\vec{F}^{(m)} &= K_{\alpha}(\vec{T}_R - \vec{Z}^{(m)}) \pm \lambda_0 \vec{Z}'^{(m)} \\ &\quad - K_{\alpha}(K_{T^{(m-1)}} - K_{T_R})\vec{F}^{(m-1)} \pm K_{T_r^{(m-1)}}\vec{\lambda}_1^{(m-1)}. \end{aligned} \right\} \quad (23)$$

We assume the dependence of α on temperature is given by relation

$$\alpha = \alpha_0 \left(\frac{t}{t_R} \right)^{-k}$$

or

$$\alpha = \Phi(\phi)[1 + C_0 w + c_1 w^2 + \dots]$$

where

$$w = \frac{t - t_R}{t_R} {}_1c_{j-1} = \left(\frac{-k}{j} \right), \quad (j = 1, 2, 3).$$

Vector $\vec{F}^{(m-1)}$ is then given by the expression

$$\vec{F}^{(m-1)} = \left(\sum_{j=1}^{\infty} c_{j-1} K_{\vec{w}^{(m-1)}} \right) \vec{W}^{(m-1)},$$

where

$$\vec{W}^{(m-1)} = K_{T_R}^{-1}(\vec{T}^{(m-1)} - \vec{T}_R).$$

Fourth boundary condition

The boundary conditions on the boundary of two concentric annular regions may be written in the following form (1: inner annulus, 2: outer annulus)

$$\left. \begin{aligned} t_2(R, \phi) &= t_1(R, \phi) + \lambda_1(t_1)\rho_1(\phi, t_1, t_2) \frac{\partial t_1}{\partial r} \Big|_{r=R} \\ - \lambda_2(t_2) \frac{\partial t_2}{\partial r} \Big|_{r=R} &= -\lambda_1(t_1) \frac{\partial t_1}{\partial r} \Big|_{r=R} \end{aligned} \right\} \quad (24)$$

Combining the expression

$$\rho_1(\phi, t_1, t_2) = \Psi(\phi)[\rho_{01} + \rho_{11}(t_1, t_2)]$$

with Eqs. (24) we obtain

$$\begin{aligned}
 t_2^{(m)}(R, \phi) &= t_1^{(m)}(R, \phi) + \lambda_{01}\rho_{01} \Psi(\phi) \frac{\partial t_1^{(m)}}{\partial r} \Big|_{r=R} \\
 &+ \{\lambda_{01}\rho_{11}(t_1^{(m-1)}, t_2^{(m-1)}) + \lambda_{11}(t_1^{(m-1)}) \\
 &\times [\rho_{01} + \rho_{11}(t_1^{(m-1)}, t_2^{(m-1)})]\} \Psi(\phi) \frac{\partial t_1^{(m-1)}}{\partial r} \Big|_{r=R} \\
 &\times \lambda_{02} \frac{\partial t_2^{(m)}}{\partial r} \Big|_{r=R} = \lambda_{01} \frac{\partial t_1^{(m)}}{\partial r} + \lambda_{11}(t_1^{(m-1)}) \frac{\partial t_1^{(m-1)}}{\partial r} \Big|_{r=R} \\
 &- \lambda_{12}(t_2^{(m-1)}) \frac{\partial t_2^{(m-1)}}{\partial r} \Big|_{r=R} \quad (25)
 \end{aligned}$$

The dependence of integration constants of annulus 2 on integration constants of annulus 1 may be expressed as

$$\vec{C}_2^{(m)} = {}_4M_{1,2} \vec{C}_1^{(m)} + {}_4\vec{F}_{1,2}^{(m)}, \quad (26)$$

where

$${}_4M_{1,2} = {}_4M'_{1,2} + \Delta_{1,2}$$

$${}_4\vec{F}_{1,2}^{(m)} = {}_4\vec{F}'_{1,2}^{(m)} + \vec{\delta}_{1,2}^{(m)} + R_1 \vec{P}^{(m-1)} + R_2 \vec{Q}^{(m-1)}$$

and where

$${}_4M'_{1,2} = \begin{matrix} & N_0 & & & \\ & & N_1 & & \\ & & & N_1 & \\ & & & & N_2 \\ & & & & & N_2 \end{matrix}$$

$$\begin{matrix} {}_4\vec{F}'_{1,2}^{(m)} = & {}^cG_0 & & & \\ & {}^cG_1 & & & \\ & {}^sG_1 & & & \\ & {}^cG_2 & & & \\ & {}^sG_2 & & & \\ & \vdots & & & \\ & \vdots & & & \\ & \vdots & & & \end{matrix}$$

$$N_0 = \begin{pmatrix} 1 & 2\bar{\lambda} \lg R \\ 0 & \lambda_{01}/\lambda_{02} \end{pmatrix}$$

$$N_n = \begin{pmatrix} \bar{\lambda} & \bar{\lambda} R^{-2n} \\ \bar{\lambda} R^{2n} & \bar{\lambda} \end{pmatrix}$$

$${}^cG_0 = \begin{pmatrix} {}^cZ_0^{(m)} - {}^cZ_0^{(m)} - \left[{}^cZ_0'^{(m)} \frac{\lambda_{01}}{\lambda_{02}} - {}^cZ_0'^{(m)} \right] R \lg R \\ \left[{}^cZ_0'^{(m)} \frac{\lambda_{01}}{\lambda_{02}} - {}^cZ_0'^{(m)} \right] \end{pmatrix}$$

$${}^iG_n = \frac{1}{2} \begin{pmatrix} R^{-n} \left[{}^iZ_n^{(m)} - {}^iZ_n^{(m)} + \left({}^iZ_n'^{(m)} \frac{\lambda_{01}}{\lambda_{02}} - {}^iZ_n'^{(m)} \right) \frac{R}{n} \right] \\ R^n \left[{}^iZ_n^{(m)} - {}^iZ_n^{(m)} - \left({}^iZ_n'^{(m)} \frac{\lambda_{01}}{\lambda_{02}} - {}^iZ_n'^{(m)} \right) \frac{R}{n} \right] \end{pmatrix}$$

$$\bar{\lambda} = \frac{1}{2}(1 + \lambda_{01}/\lambda_{02}), \bar{\lambda} = \frac{1}{2}(1 - \lambda_{01}/\lambda_{02}), l = c, s.$$

$$\Delta_{1,2} = \frac{1}{2} \lambda_{01} \rho_{01} R_1 K_{\psi 2} M$$

$$\vec{\delta}_{1,2}^{(m)} = \frac{1}{2} \lambda_{01} \rho_{01} R_1 K_{\psi 1} \vec{Z}'^{(m)}$$

$$\vec{P}^{(m-1)} = \left\{ \lambda_{01} K_{\rho_{01}^{(m-1)}} + \rho_{01} K_{\lambda_{11}^{(m-1)}} \times \left[I + \frac{1}{\rho_{01}} K_{\rho_{11}^{(m-1)}} \right] \right\} K_{\psi} \vec{T}_{r_1}^{(m-1)}$$

$$\vec{Q}^{(m-1)} = K_{\lambda_{11}^{(m-1)}} \vec{T}_{r_1}^{(m-1)} - K_{\lambda_{12}^{(m-1)}} \vec{T}_{r_2}^{(m-1)}$$

$$R_1 = \frac{1}{2} \begin{matrix} \sigma_0 & & & & \\ & \sigma_1 & & & \\ & & \sigma_1 & & \\ & & & \sigma_2 & \\ & & & & \sigma_2 \\ & & & & & \vdots \\ & & & & & & \nu_0 \\ & & & & & & \nu_1 \\ & & & & & & \nu_1 \\ & & & & & & \nu_2 \\ & & & & & & \nu_2 \\ & & & & & & \vdots \end{matrix}$$

$$R_2 = \frac{R}{2\lambda_{02}}$$

$$\sigma_0 = \begin{pmatrix} 2 \\ 0 \end{pmatrix}, \quad \sigma_n = \begin{pmatrix} R^{-n} \\ R^n \end{pmatrix},$$

$$\nu_0 = \begin{pmatrix} -2 \lg R \\ R \end{pmatrix}, \quad \nu_n = \begin{pmatrix} \frac{1}{n} R^{-n} \\ \frac{1}{n} R^n \end{pmatrix}$$

Eccentric arrangement

We derive an expression for the temperature $t(\bar{r}, \phi')$ on a circle of radius R , moved in the direction

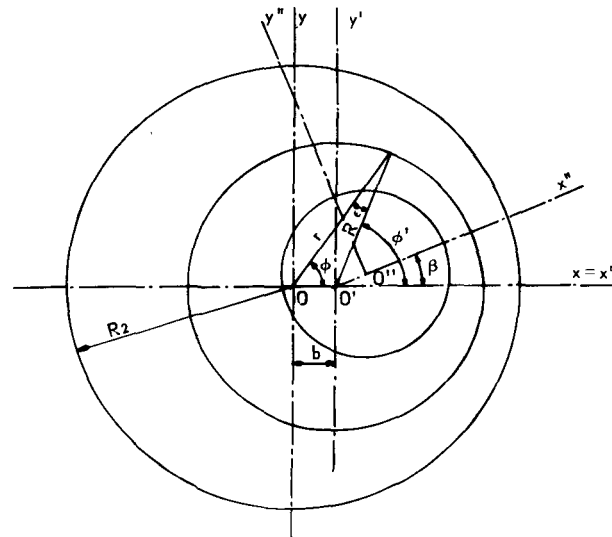


Figure 1. Eccentric arrangement

of axis x by a value b (Fig. 1). We insert the following expressions into the series for $t(r', \phi)$ in the form of (6)

$$\left. \begin{aligned} \cos \phi' &= \chi(\cos \phi + e) & \sin \phi' &= \chi \sin \phi \\ \cos \epsilon &= \chi(1 - e \cos \phi) & \sin \epsilon &= \chi e \sin \phi \\ r &= R/\chi \end{aligned} \right\} \quad (27)$$

where

$$\chi = \frac{1}{\sqrt{(1 - 2e \cos \phi + e^2)}} e = \frac{b}{R}$$

Considering that eccentricity is small, we expand expressions (27) according to the binomial theorem and we leave in the expressions only linear terms for eccentricity e . After rearrangement we obtain for the course of the temperature this expression (for $n \leq 3$)

$$\begin{aligned} t(\bar{r}, \phi') &= t(R, \phi) = A_0 + B_0(\lg r + e \cos \phi) \\ &+ {}^cZ_0 + e \cos {}^cZ_0 \\ &+ V_1 \cos \phi + X_1 \sin \phi + e/2[(W_1 + V_1) \\ &+ (W_1 - V_1) \cos 2\phi + (Y_1 - X_1) \sin 2\phi] \\ &+ V_2 \cos 2\phi + X_2 \sin 2\phi \\ &+ e[(W_2 + V_2) \cos \phi + (Y_2 + X_2) \sin \phi \\ &+ (W_2 - V_2) \cos 3\phi + (Y_2 - X_2) \sin 3\phi] \\ &+ V_3 \cos 3\phi + X_3 \sin 3\phi \\ &+ \frac{3}{2}e[(W_3 + V_3) \cos 2\phi \\ &+ (Y_3 + X_3) \sin 2\phi] \end{aligned}$$

where

$$\begin{aligned} V_n &= A_n R^n + B_n R^{-n} + {}^cZ_n(R) \\ X_n &= C_n R^n + D_n R^{-n} + {}^sZ_n(R) \\ W_n &= A_n R^n - B_n R^{-n} + \frac{1}{n} {}^cZ_n \\ Y_n &= C_n R^n - D_n R^{-n} + \frac{1}{n} {}^sZ_n \end{aligned}$$

and where

$${}^cZ_n = R {}^cZ_n'(R), \quad {}^sZ_n = R {}^sZ_n'(R).$$

Similarly we may obtain derivations $\partial t/\partial r$ and $\partial t/\partial \phi$.

Boundary conditions for the eccentric region may be defined similarly as in the previous section. The derivative in Eqs. (18) and (20), and on the left-hand side of condition (24), must be replaced by the derivative of the form

$$\lambda(t) \left[\frac{\partial t(r', \phi')}{\partial r} \Big|_{r=\bar{r}} \cos \epsilon - \frac{1}{\bar{r}} \frac{\partial t(\bar{r}, \phi')}{\partial \phi} \sin \epsilon \right].$$

Rotation of the co-ordinate system

When several eccentric regions occur in a given system, the co-ordinate system has to be rotated by an angle of β (Fig. 1). The transformation takes the form of

$$\vec{C} = \vartheta \vec{C}' + \vec{F}^0 \quad (28)$$

where

$$\vartheta = \begin{pmatrix} 1 & & & & 0 \\ & 1 & & & 0 \\ & & h_1 & & H_1 \\ & & & h_2 & \vec{F}^0 = \frac{1}{2} H_2 \\ & & & & \vdots \\ & & & & \vdots \\ & & & & \vdots \end{pmatrix}$$

$$h_n = \begin{pmatrix} \cos n\beta & & \sin n\beta & & \\ & \cos n\beta & & \sin n\beta & \\ -\sin n\beta & & & & \\ & -\sin n\beta & & & \cos n\beta \end{pmatrix}$$

$$R^{-n} \left[\left({}^cZ_n + \frac{R}{n} {}^cZ_n' \right) (\cos n\beta - 1) + \left({}^sZ_n + \frac{R}{n} {}^sZ_n' \right) \sin n\beta \right]$$

$$R^n \left[\left({}^cZ_n - \frac{R}{n} {}^cZ_n' \right) (\cos n\beta - 1) + \left({}^sZ_n - \frac{R}{n} {}^sZ_n' \right) \sin n\beta \right]$$

$$H_n = R^{-n} \left[\left({}^sZ_n + \frac{R}{n} {}^sZ_n' \right) (\cos n\beta - 1) - \left({}^cZ_n + \frac{R}{n} {}^cZ_n' \right) \sin n\beta \right]$$

$$R^n \left[\left({}^sZ_n - \frac{R}{n} {}^sZ_n' \right) (\cos n\beta - 1) - \left({}^cZ_n - \frac{R}{n} {}^cZ_n' \right) \sin n\beta \right]$$

SOLUTION OF BOUNDARY PROBLEMS

Let us now determine the temperature distribution for an annular region, composed of L layers. Taking for a basis of calculation the integration constants of the first zone (i.e., the nearest one to its beginning) and eliminating gradually integration constants of intermediate layers, we obtain

$$\vec{C}_i^{(m)} = {}_4M_{1,i} \vec{C}_1^{(m)} + {}_4\vec{F}_{1,i}^{(m)}, \quad (29)$$

where

$$\begin{aligned} {}_4M_{1,i} &= {}_4M_{i-1,i} \cdot {}_4M_{i-2,i-1} \\ &\quad \cdot {}_4M_{i-3,i-2} \cdots \cdot {}_4M_{2,3} \cdot {}_4M_{1,2} \\ {}_4\vec{F}_{1,i}^{(m)} &= {}_4M_{i-1,i} \{ {}_4M_{i-2,i-1} [{}_4M_{i-3,i-2} (\cdots) \\ &\quad + {}_4\vec{F}_{i-3,i-2}^{(m)}] + {}_4\vec{F}_{i-2,i-1}^{(m)} \} + {}_4\vec{F}_{i-1,i}^{(m)}. \end{aligned}$$

Outer boundary conditions on radii R_0 and R_L have been given.

We thus obtain a system of equations

$$\left. \begin{aligned} {}_{k_0}M_1 \vec{C}_1^{(m)} &= {}_{k_0}\vec{F}_1^{(m)} \\ {}_{k_L}M_L \vec{C}_L^{(m)} &= {}_{k_L}\vec{F}_L^{(m)} \\ \vec{C}_L^{(m)} &= {}_4M_{1,L} \vec{C}_1^{(m)} + {}_4\vec{F}_{1,L}^{(m)} \end{aligned} \right\} \quad (30)$$

($k = 1, 2, 3$ according to the type of boundary condition). Eliminating vector $\vec{C}_L^{(m)}$, we may determine vector $\vec{C}_1^{(m)}$ from the expression

$$\vec{C}_1^{(m)} = M^{-1} \vec{F}^{(m)}, \quad (31)$$

where

$$M = \begin{pmatrix} k_0 M_1 \\ k_L M_L \cdot 4 M_{1,L} \end{pmatrix} \quad \vec{F}^{(m)} = \begin{pmatrix} k_0 \vec{F}_1^{(m)} \\ k_L \vec{F}_L^{(m)} - k_L M_L \cdot 4 \vec{F}_{1,L}^{(m)} \end{pmatrix}$$

The procedure for the solution will therefore be as follows: we determine the zero approximation for $\vec{C}_1^{(0)}$ from the given equations, neglecting all non-linearities, i.e., $\lambda_1 = 0$. By means of relations (29) we determine the other vectors $\vec{C}_i^{(0)}$. Then using zero approximations, we calculate non-linearities for all equations required and determine the first approximation. We proceed similarly for all other approximations.

In the case when the dependence of λ in temperature is very small, but the dependence of ρ and α on temperature is strong, it may be found suitable to hasten the calculation by calculating more iterations for boundary conditions for one iteration step of Eq. (4).

Note: Where the boundary condition of the second type is applicable to both surfaces, the functions G_0 and G_L must fulfil condition

$$R_0 \int_0^{2\pi} G_0(\phi) d\phi + R_L \int_0^{2\pi} G_L(\phi) d\phi = \int_0^{2\pi} \int_{R_0}^{R_L} q(r, \phi) r dr d\phi.$$

APPLICATIONS

Example I

Let us estimate the convergence of the iteration procedure for a circular cylinder with constant heat

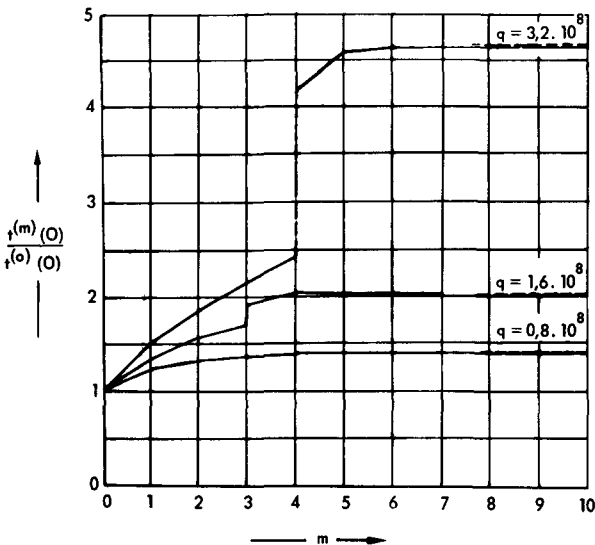


Figure 2. Maximum temperature on the axis of an element of circular cross section for individual iterations. Aitken's method was used every time after several iterations to estimate the resulting value ($\lambda = c/t$, $c = 3\,092$ kcal/mh, $R = 10$ mm)

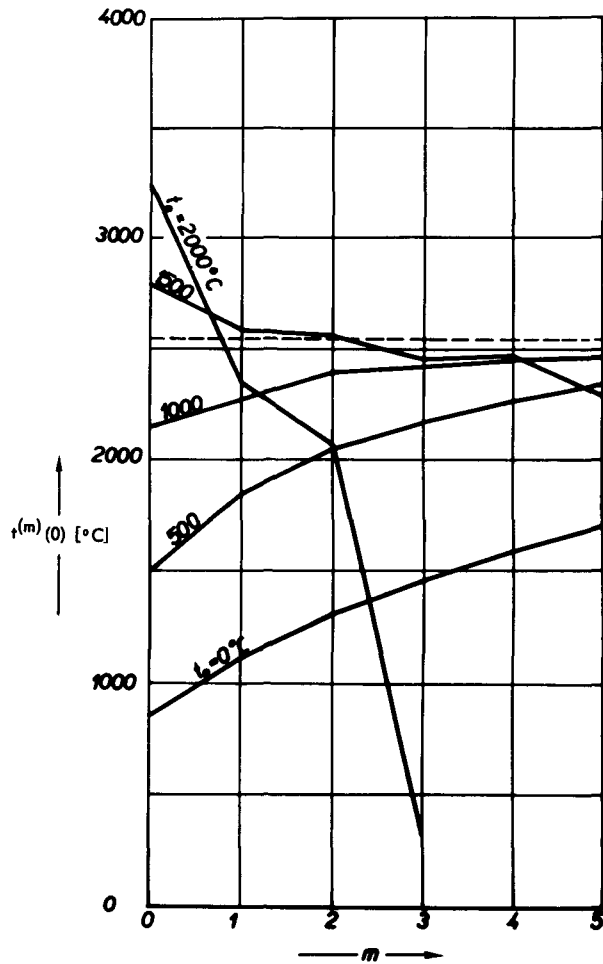


Figure 3. Maximum temperature on the axis of an element of circular cross section for individual iterations for various values of $\lambda(t_0)$ ($q = 1.6 \times 10^8$ kcal/m²h, $\lambda = c/t$, $c = 3\,092$ kcal/mh, $R = 10$ mm)

sources and for the first type boundary condition, independent of the angle ϕ (we assume $t_R = 0^\circ\text{C}$). For this case, the equation (6) may be modified to the form

$$t^{(m)} = A_0 + cZ_0^{(0)} - \int_0^r \frac{\lambda_1^{(m-1)}(r')}{\lambda_0} t'^{(m-1)}(r') dr' \quad (32)$$

For the dependence of thermal conductivity on temperature in the form of

$$\lambda = c/t \quad t[^\circ\text{K}]$$

a calculation has been performed for various heat load values. It appears that the iteration procedure in this case is convergent for arbitrary values of q , even though for large temperature differences the number of iterations will increase. On Fig. 2, the temperature on the cylinder axis is plotted as a function of the number of iteration steps. To obtain convergence more rapidly, Aitken's method was used every time after several iterations to estimate the resulting values.

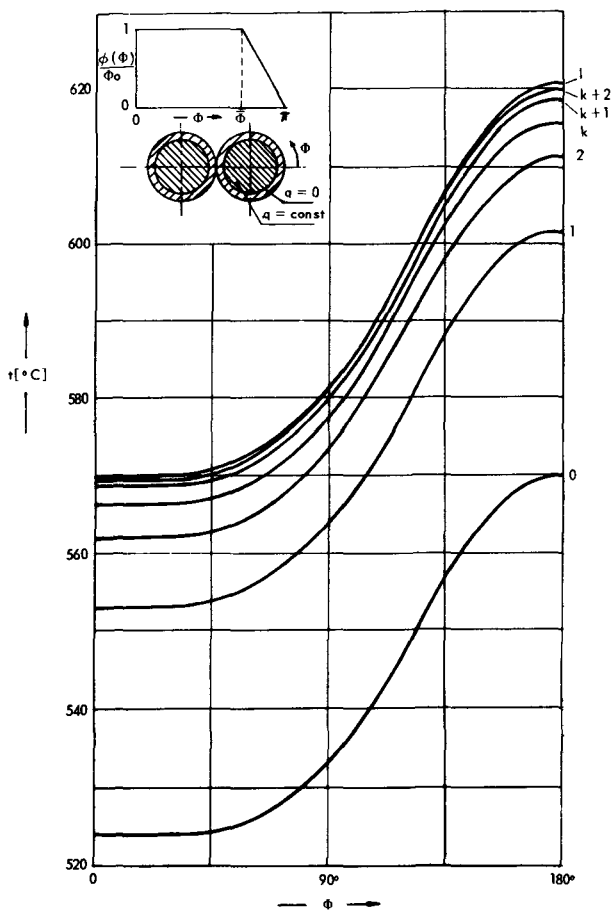


Figure 4. Plot of surface temperature of the fuel-element rod (0: surface temperature when neglecting the influence of temperature on α ; 1, 2, ...: surface temperature in individual iterations; l : resulting course ($R_1 = 4$ mm, $R_2 = 5$ mm, $\phi_0 = \alpha_0 = 4\,000$ kcal/m²h °C, $\lambda_1 = 20$ kcal/mh °C, $\lambda_2 = 138$ kcal/mh °C, $\rho = 10^{-4}$ m²h °C/kcal, $q = 3.75 \times 10^8$ kcal/m³h)

By analysis of expression (32) it is possible to show that in the given case the method will evidently

converge for the case

$$\left| \frac{\lambda_1^{(m-1)}}{\lambda_0} \right|_{\max} \leq k < 1.$$

From this point of view it is therefore necessary to be careful in selecting the value of λ_0 , i.e., t_0 . Figure 3 shows the character of convergence for various values of t_0 for one case. A similar calculation has been carried out for other dependences of λ on temperature.

This example was chosen because of the possibility to solve it easily, using the method by Kirchhoff [3]. This method, for some special cases of temperature dependence of the thermal conductivity, gives the results in a closed form. Our case (i.e., $\lambda = c/t$) is one of them. On Figs. 2 and 3, the results of the method described in this paper (full line) are compared with that of the method by Kirchhoff (dashed line).

Example 2

The second example deals with the temperature distribution in a fuel rod with cladding, for the case of irregular cooling due to the contact of two rods. The chosen course of $\Phi(\phi)$ is shown in Fig. 4, and the dependence of α on temperature is considered in the form

$$\alpha(\phi, t, t_R) = \Phi(\phi) \left(\frac{t}{t_R} \right)^{-0.55}$$

The course of the surface temperature for individual iterations is plotted in Fig. 4. After the second iteration was used, Aitken's method was the next step (on the figure denoted by k). The final course is denoted by l .

REFERENCES

1. Crank, J., *The Mathematics of Diffusion*, Oxford (1956).
2. Morse, M., and Feshbach, H., *Methods of Theoretical Physics*, New York (1953).
3. Carslaw, H. S., and Jaeger, J. C., *Conduction of Heat in Solids*, Oxford (1959).

ABSTRACT—RÉSUMÉ—АННОТАЦИЯ—RESUMEN

A/527 Tchécoslovaquie

Quelques problèmes théoriques de transfert de chaleur dans les éléments de combustible de réacteurs

par J. Schmid

Le mémoire donne la solution d'un problème de limite de transfert de chaleur que posent les éléments de combustible d'un réacteur nucléaire lorsque la conductivité thermique dépend de la température.

Les conditions aux limites non linéaires sont du type où le coefficient de transfert de chaleur ou la résistance de contact à l'interface de deux milieux

dépendent de la température. En admettant que la contribution de la partie non linéaire soit négligeable, on peut trouver la solution par un procédé d'itération dont on peut attendre, dans ces conditions, des résultats convergents.

Si la conductivité thermique, le coefficient de transfert de chaleur et la résistance de contact sont indépendants de la température, la première étape du procédé d'itération consistera simplement à résoudre l'équation correspondante dans une géométrie cylindrique pour les conditions aux limites données.

Cette méthode a été appliquée à certains problèmes de calcul des caractéristiques de canaux chauds.

Некоторые теоретические проблемы теплопроводности в тепловыделяющих элементах ядерных реакторов

Й. Шмидт

Решается краевая задача теплопроводности в тепловыделяющих элементах ядерных реакторов, когда коэффициент теплопроводности зависит от температуры. Нелинейные граничные условия относятся к типу, когда коэффициент теплопередачи или контактное тепловое сопротивление на границе двух сред зависят от температуры. Принимая, что нелинейность мала, можно найти решение методом итераций, причем можно предположить, что здесь мы имеем сходящийся случай.

Если коэффициент теплопроводности, теплопередачи и контактное сопротивление не зависят от температуры, достаточно найти решение соответствующего уравнения в цилиндрической геометрии для данных граничных условий как первую ступень процесса итерации.

Этот метод был применен для решения некоторых проблем при расчете горячего канала.

Algunos problemas teóricos de transmisión del calor en elementos combustibles de reactores

por J. Schmid

Se resuelve un problema de contorno de transmisión de calor en elementos combustibles de reactores con conductibilidad térmica dependientes de la temperatura. Las condiciones de contorno no lineales son de tipos con coeficiente de transmisión del calor dependiente de la temperatura o con resistencia de contacto en la superficie de separación de dos medios dependiente de la temperatura. Suponiendo pequeña la contribución de los términos no lineales puede obtenerse la solución mediante un proceso iterativo que, en este caso, es de esperar que converja.

Si son independientes de la temperatura la conductibilidad térmica, el coeficiente de transmisión del calor y la resistencia de contacto, basta hallar la solución de la ecuación correspondiente en geometría cilíndrica, con las condiciones de contorno dadas, como primer paso del proceso iterativo.

El método ha sido aplicado a algunos problemas del cálculo de factores de canales calientes.

The optimum reactivity control of a multi-zone nuclear reactor in relation to the maximum output of the power station

By J. Schmid and V. Stach*

Nuclear power reactors are equipped with a control system for the compensation of a considerable excess of reactivity. The actual reactivity excess, however, is comparatively low during the steady state operation of the reactor, particularly in the case of continuous refuelling. Therefore the question arises of how to exploit a given compensation system of a reactor when at a steady state. Because the compensation by control rods is always connected with loss of the reactor output, the minimum loss of the electrical output of the reactor is considered as the criterion for the best choice of the compensation.

These considerations do not apply when the macroscopic neutron flux distribution and the spatial variation of the output is influenced by the insertion of the control rods, which is the case for the build-up of a poisoned zone. They are intended for a reactor for which the macroscopic flux distribution is determined by the design of a multi-zone core without any relation to the control system.

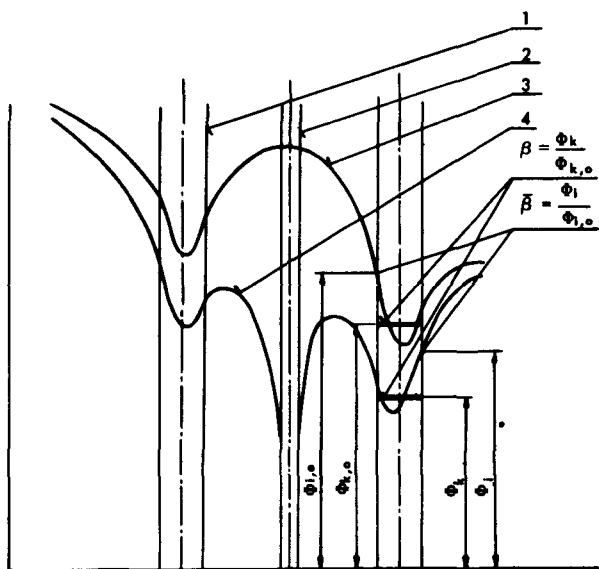


Figure 1. Influence of a control rod on an adjacent channel
1: Fuel element; 2: Control rod; 3: Original unperturbed neutron flux; 4: Flux perturbed by an inserted control rod

* The Nuclear Research Institute of the Czechoslovak Academy of Science, Řež by Prague.

In such a reactor, a control rod inserted into the core causes a local flux perturbation resulting in the lowering of both mean output and its spatial distribution in neighbouring experimental channels. It is not possible, however, to compensate for this reduction, at least not by increasing the output of more distant experimental channels beyond the nominal level, because such a reactor design includes a number of experimental channels which restrict the output.

The effect of an inserted control rod on a neighbouring experimental channel is shown in Fig. 1, where, as well as in the following figure, the fuel element is considered as an assembly consisting of a number of fuel pins. The influence of the rod on the fuel assembly output is characterized by the parameters β and $\tilde{\beta}$. β represents the ratio of the mean neutron flux in the fuel assembly after the insertion of the control rod to the mean value of the unperturbed flux. $\tilde{\beta}$ denotes the ratio of the maximum value of the neutron flux in the fuel assembly after the insertion of the control rod to the original maximum value. It was possible to express the parameter β for the particular system under consideration by the relation [1]:

$$\beta = 1 - \kappa \frac{\Phi_a}{\Phi_{k,0}},$$

where Φ_a and $\Phi_{k,0}$ are the values of the macroscopic neutron flux distribution in the position of the regulating rod and in the position of the experimental channel prior to the perturbation, κ is an empirical constant. For the determination of $\tilde{\beta}$ it is necessary to carry out a more detailed analysis of the neutron flux distribution in the fuel element (see Fig. 2). In the actually treated case it was possible to express the perturbed neutron flux distribution as follows:

$$\Phi(\rho, \phi) = \Phi_0(\rho) \left[1 + f \frac{\rho}{\rho_{max}} \cos \alpha \right]$$

where $\Phi_0(\rho)$ is the flux variation in the unperturbed fuel assembly, f is an empirical constant; the meaning of the remaining quantities can be clearly seen in the figure. For the fuel assembly located at any position in the core, the neutron flux is influenced by macroscopic perturbation of the flux (the perturbation is represented by the reactor boundary) and by a control

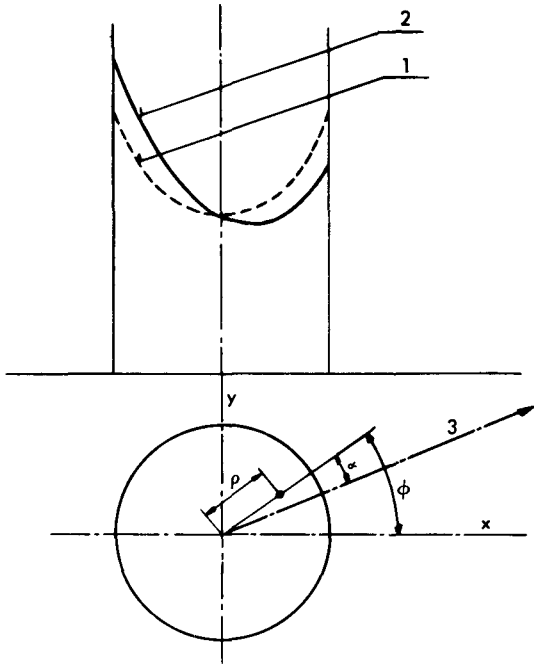


Figure 2. Neutron flux distribution in the fuel assembly
 1: Undisturbed flux; 2: Perturbed flux;
 3: Direction of the perturbation

rod. The neutron flux variation in the fuel assembly influenced by both perturbations can be expressed as:

$$\Phi(\rho, \phi) = \Phi_0(\rho) \left[1 + \frac{\rho}{\rho_{max}} (f_1 \cos \alpha_1 + f_2 \cos \alpha_2) \right].$$

The value of f_1 can be estimated from the macroscopic variation of neutron flux in the reactor; f_2 has been found experimentally [1]:

$$f_2 = c - \sqrt{\left(a + b \frac{\Phi_a}{\Phi_{k,0}} \right)}$$

where a, b, c , are empirical constants. By simple analytical operations maximum values of $\Phi(\rho, \phi)$ for the cases with and without control rod respectively, and therefore the value of β , can be determined.

The quantity β fixes the depression of the thermal output of the experimental channel, β specifies the depression of maximum temperature in the fuel assembly by the relation:

$$t_{max} = t_0 + \beta(t_{max,0} - t_0).$$

The quantity β has a significance in such cases, i.e., where it is possible to modify the flow rate of the coolant through the channel in order to exploit the fuel pin maximum permissible temperature and when this step can reduce the loss of the reactor output.

For a partially inserted control rod, only a part of the neighbouring channel is influenced by the perturbation. According to the experimental results [2], it is possible to set up the longitudinal variation of the neutron flux in a perturbed channel from the unperturbed and perturbed cosine-like variations with the exception of the region of one or two diffusion lengths of the lattice around the end of the control rod (see

Fig. 3). For the estimation of the output, temperature and the flow rate variations, the actual variation has been extrapolated up to the position at the end of the rod.

The reactivity of a partially inserted control rod varies with the insertion depth according to the relation:

$$\frac{\delta_k(h)}{\delta_k(\bar{H})} = \frac{\int_0^{h+L} \Phi^2(z) dz}{\int_0^{\bar{H}+L} \Phi^2(z) dz},$$

where \bar{H} is the maximum insertion depth of the rod (smaller than the core height); L is the diffusion length of the lattice.

The thermal output of a perturbed channel depends on h as follows

$$\begin{aligned} \frac{N_{T,k}(h)}{N_{T,k}(0)} &= \frac{\int_{\Delta/2}^{H-\Delta/2} \Phi_k(z) dz}{\int_{\Delta/2}^{H-\Delta/2} \Phi_{k,0}(z) dz} \\ &= \frac{(1 + \beta) \cos \frac{\pi \Delta}{2H} + (1 - \beta) \cos \frac{\pi}{H} \left(h + \frac{\Delta}{2} \right)}{2 \cos \frac{\pi \Delta}{2H}} \end{aligned}$$

where H is the extrapolated reactor height, $\Delta/2$ is the extrapolation length.

The relative thermal output loss of the perturbed channel is

$$\begin{aligned} \gamma_T(h) &\equiv 1 - \frac{N_{T,k}(h)}{N_{T,k}(0)} \\ &= \frac{1}{2} (1 - \beta) \left[1 - \frac{\cos \frac{\pi}{H} \left(h + \frac{\Delta}{2} \right)}{\cos \frac{\pi \Delta}{2H}} \right]. \end{aligned}$$

The ratio of $\frac{\gamma_T(h)}{\gamma_T(\bar{H})}$ and $\frac{\delta_k(h)}{\delta_k(\bar{H})}$, which represents the normalized value of the relative thermal output loss related to the compensated reactivity is denoted as μ_T . The plot of $\mu_T(h)$ is shown in Fig. 4. The change of the thermal efficiency of the power station caused by the depressed outlet temperature of the perturbed channel will not be great and the variation of the

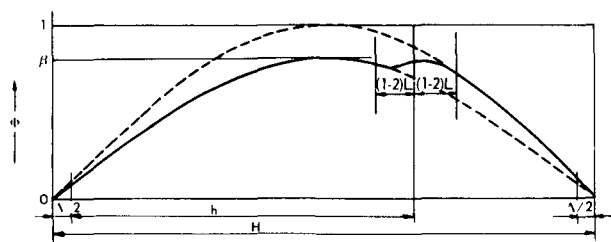
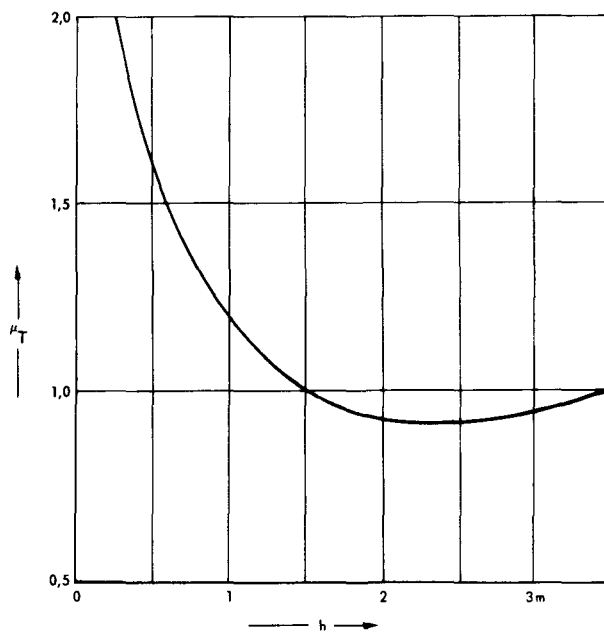


Figure 3. Neutron flux distribution in an adjacent channel at a partially inserted control rod

Figure 4. Plot of μ_T against h

normalized value of the relative electrical output loss μ_E will differ only slightly from μ_T .

For the case of long-term reactivity compensation at steady working state, one can consider the adjustment of the coolant flow rate to the depressed output in perturbed channels and to evaluate the gain of the electrical output which can be reached in this way. Three different cases of heat removal conditions depending on the insertion depth of the control rod arise when the coolant flow rate in the channel is lowered (see Fig. 5, the direction of the coolant flow being the same as that of the insertion of the control rod):

(a) the perturbation does not reach the position in the fuel channel where originally there was the maximum fuel element temperature; (b) the end of the control rod is inserted closely to the original point of the maximum temperature; (c) the end of the control rod is inserted sufficiently beyond the original point of maximum temperature.

For the maximum temperature of the fuel pin for case (a) we get, on the basis of well-known relations, the following relation:

$$t_{\max} = t_0 + \frac{G_{i,0} t_{i,v,0} - t_0}{G_i} \frac{1}{2 \cos \frac{\pi \Delta}{2H}} \times \left\{ \bar{\beta} \cos \frac{\pi \Delta}{2H} + (1 - \bar{\beta}) \cos \frac{\pi}{H} \left(h + \frac{\Delta}{2} \right) + \sqrt{\left(1 + \left[\frac{2\vartheta}{t_{i,v,0} - t_0} \left(\frac{G_i}{G_{i,0}} \right)^{0.2} \cos \frac{\pi \Delta}{2H} \right]^2 \right)} \right\}.$$

The above-mentioned relation refers to the maximally loaded cell of the fuel element; $t_{i,v,0}$ is the coolant outlet temperature from the most highly loaded cell at the normal operational state, t_0 is the coolant

inlet temperature, ϑ is the maximum temperature difference between the surface of the fuel pin and the coolant in this cell at the normal operational state, and G_i and $G_{i,0}$ are the flow rates in the cell at modified and normal régime respectively.

If we require the maximum temperature to remain equal to the maximum allowed temperature of the fuel pin while inserting the control rod, we get for the flow rate the equation

$$\left(\frac{G_i}{G_{i,0}} \right) = \frac{t_{i,v,0} - t_0}{t_{\max,0} - t_0} \frac{1}{2 \cos \frac{\pi \Delta}{2H}} \times \left\{ \bar{\beta} \cos \frac{\pi \Delta}{2H} + (1 - \bar{\beta}) \cos \frac{\pi}{H} \left(h + \frac{\Delta}{2} \right) + \sqrt{\left(1 + \left[\frac{2\vartheta}{t_{i,v,0} - t_0} \left(\frac{G_i}{G_{i,0}} \right)^{0.2} \cos \frac{\pi \Delta}{2H} \right]^2 \right)} \right\}.$$

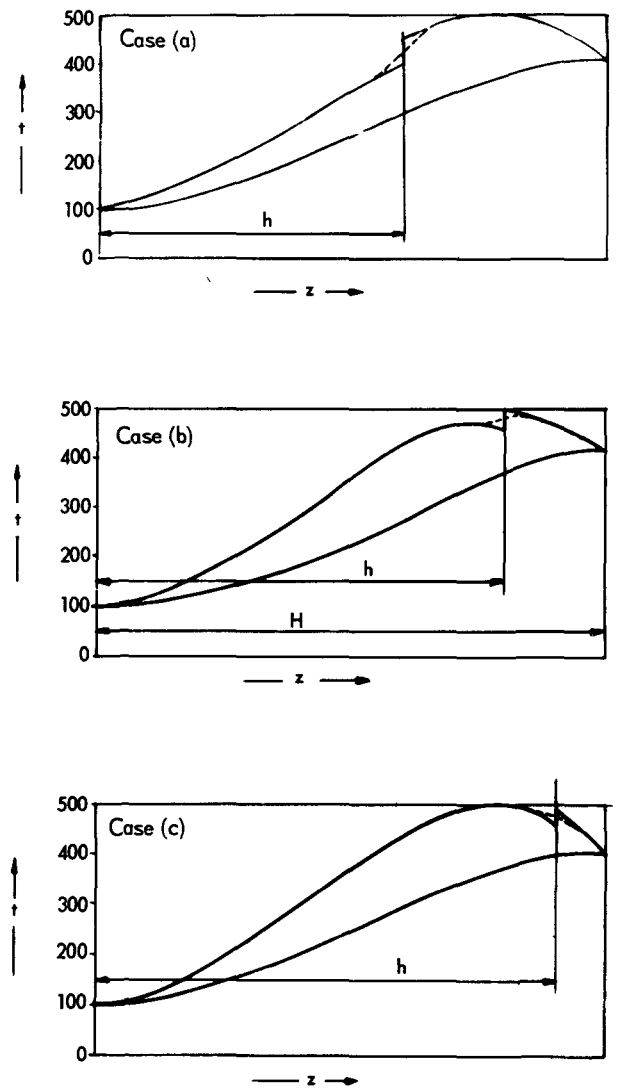


Figure 5. Various cases of the heat removal conditions from the perturbed channel, when modifying the coolant flow rate. The directions of both the flow and the rod insertion coincide

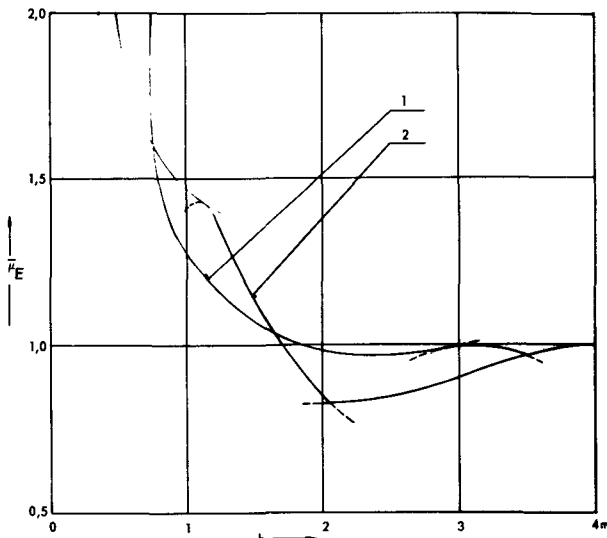


Figure 6. Plot of $\bar{\mu}_E$ against h

The direction of the flow and of the rod insertion: 1: coincident; 2: opposite

Similarly, we get equations for the flow rate modification, for cases (b) and (c):

$$\left(\frac{G_i}{G_{i,0}}\right)_b = \frac{t_{i,v,0} - t_0}{t_{max,0} - t_0} \frac{1}{2 \cos \frac{\pi \Delta}{2H}} \times \left\{ \bar{\beta} \left[\cos \frac{\pi \Delta}{2H} - \cos \frac{\pi}{H} \left(h + \frac{\Delta}{2} \right) \right] + \frac{2\vartheta}{t_{i,v,0} - t_0} \left(\frac{G_i}{G_{i,0}} \right)^{0.2} \cos \frac{\pi \Delta}{2H} \cdot \sin \frac{\pi}{H} \left(h + \frac{\Delta}{2} \right) \right\},$$

and

$$\left(\frac{G_i}{G_{i,0}}\right)_c = \frac{t_{i,v,0} - t_0}{t_{max,0} - t_0} \frac{1}{2 \cos \frac{\pi \Delta}{2H}} \times \left\{ \bar{\beta} \cos \frac{\pi \Delta}{2H} + (1 - \bar{\beta}) \cos \frac{\pi}{H} \left(h + \frac{\Delta}{2} \right) + \sqrt{1 + \left[\frac{2\vartheta \bar{\beta}}{t_{i,v,0} - t_0} \left(\frac{G_i}{G_{i,0}} \right) \cos \frac{\pi \Delta}{2H} \right]^2} \right\}.$$

With a good approximation we can put $G_i/G_{i,0} = G_k/G_{k,0}$ where G_k and $G_{k,0}$ are the flow rates through the fuel element and in the case under consideration we can estimate the normalized value of the relative electrical output loss related to the compensated reactivity, which we shall denote $\bar{\mu}_E$.

In an analogous way we get the function $\bar{\mu}_E(h)$ for the case when the control rod is inserted in the direction opposite to that of the coolant flow. The results are shown in Fig. 6.

Figures 4 and 6 clearly show that in the case of no control of the coolant flow rate through the perturbed channel the optimum insertion depth of the control rod is in the range of $\frac{1}{2}$ to $\frac{3}{4}$ of the core height. If control of the coolant flow rate is applied, then for the coincident direction of both the insertion of the rod

and the coolant flow, $\bar{\mu}_E$ is nearly constant in the range of more than all the second half of the rod lift. The direction of the rod insertion and the coolant flow being opposite to each other, $\bar{\mu}_E$ possesses a distinct minimum in about the half of the core height.

The temperature of the gas at the outlet of the perturbed channel $t_{k,v}$ depends on the insertion depth, when the flow rate is adjusted, according to the relation

$$t_{k,v} = t_0 + (t_{k,v,0} - t_0) [1 - \gamma_T(h)] \frac{G_{k,0}}{G_k},$$

where $t_{k,v,0}$ is the outlet temperature at the nominal régime of the channel. The plot is shown in Fig. 7. for the case when the direction of both the rod insertion and the coolant flow coincide.

For the selection of the core radius on which the regulating rod is to be inserted, a parameter is used which equals the ratio of the output loss to the compensated reactivity. If both the numerator and the denominator of this ratio are normalized with respect to the position of the control rod in the centre of the core, then for a uniform arrangement clearly holds $\nu = \Phi(0)/\Phi(r)$, where $\Phi(0)$ is the neutron flux in the centre of the core, $\Phi(r)$ is the flux in the place where the rod is inserted.

For the core composed of zones with different fuel assemblies, we have $\nu = (N_i/N_0) \times (\Phi(0)/\Phi(r))$ where N_i/N_0 is the ratio of the fuel assembly output of the i th zone to that of the central zone respectively, when in the same neutron flux. The functions ν_T and ν_E are plotted in Fig. 8.

The relative thermal output loss of the reactor due to the insertion of the control rods can be expressed as,

$$\tau = \frac{N_{R,T,0} - N_{R,T}}{N_{R,T,0}} = \frac{\sum_{j=1}^m \sum_{i=1}^n N_{k,T,0,i} \cdot \gamma_{ij}}{\sum_{i=1}^n N_{k,T,0,i}}$$

where n is the number of experimental channels in the reactor, m is the number of inserted rods, $N_{R,T}$ is the thermal output of the reactor. A similar expression can be written for the relative change of the total

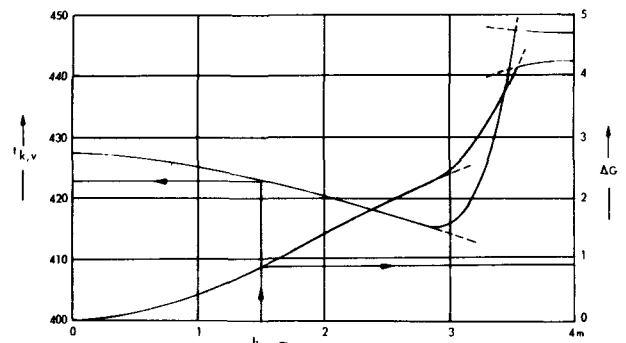


Figure 7. Plots of the change of the coolant flow rate and of the outlet temperature from the influenced fuel assembly versus the insertion depth of the control rod

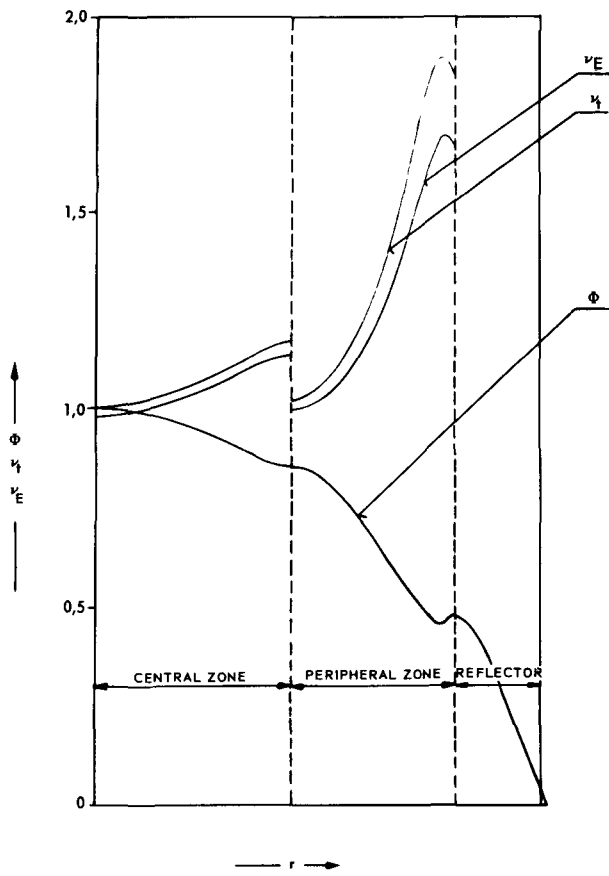


Figure 8. Variation of ν_T and ν_E

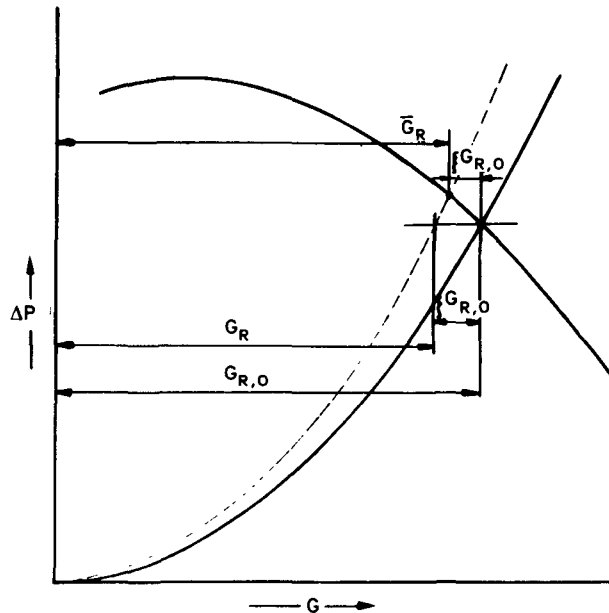


Figure 9. Displacement of the operation point when changing the flow rate in perturbed channels

coolant flow rate ξ . The coolant outlet temperature will be given by the relation,

$$t_{R,v} = t_0 + (t_{R,v,0} - t_0) \frac{1 - \tau}{1 - \xi}$$

where $t_{R,v,0}$ is the coolant outlet temperature in the

reactor without the perturbation. Using the given relation between the coolant parameters and the efficiency of the power station η , we can write for relative electrical output loss ϵ_0 ,

$$\epsilon_0 \equiv \frac{N_{R,E,0} - N_{R,E}}{N_{R,E,0}} = 1 - (1 - \tau) \frac{\eta}{\eta_0}$$

Changing the flow rate of the coolant through the perturbed channels, the performance curve of the primary circuit will be also changed and the operation point on the performance curve of the circulators will be shifted as shown by the diagram in Fig. 9. The over-all electric output change is

$$\epsilon = 1 - (1 - \epsilon_0) \frac{1 - \xi}{1 - \xi}$$

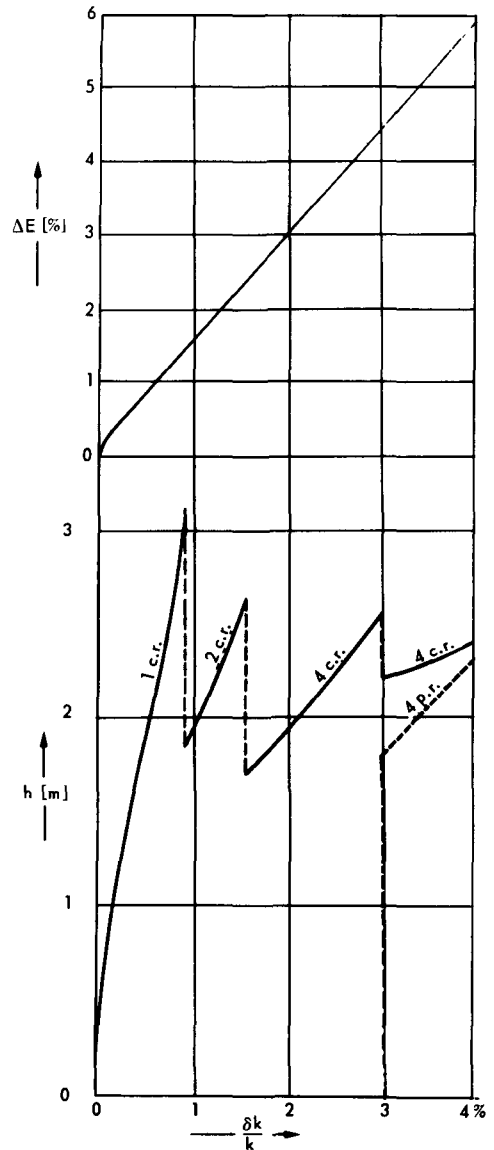


Figure 10. Electrical output loss of the reactor and the optimum mode for insertion of the control rods in dependence on the compensative reactivity value (Full lines 1, 2, and 4 denote the cases of insertion of one, two and four central control rods respectively; dashed line 4 denotes the case of insertion of four rods in the outer zone of the core)

For the given case, the problem of the minimum reactor output loss by reactivity compensation has been treated according to the foregoing method. The result is shown in Fig. 10.

REFERENCES

1. Belkin, V. F., and Švedov, O. V., The thermal neutron flux distribution in channels of a heavy-water reactor (in Russian). ITEF, Moscow (1961).
2. Belkin, V. F., and Iljičev, P. I., Personal communication.

ABSTRACT—RÉSUMÉ—АННОТАЦИЯ—RESUMEN

A/776 Tchécoslovaquie

Compensation optimale de réactivité dans un réacteur à plusieurs zones en vue de la production maximale d'énergie

par J. Schmid et V. Stach

Les réacteurs des centrales nucléaires ont un excédent de réactivité relativement important pendant leur fonctionnement avec chargement en continu, particulièrement avec des éléments de combustible neufs. Pour compenser cet excédent de réactivité, il faut utiliser des barres absorbantes qui affectent de façon importante la puissance du réacteur. Le but de cette communication est de définir les conditions permettant de minimiser la perte de production de la centrale, c'est-à-dire de déterminer l'ordre et la profondeur d'insertion des barres de compensation.

Les calculs s'appliquent à un réacteur à eau lourde refroidi par gaz. Ce type de réacteur dispose d'un nombre relativement faible de canaux expérimentaux. On admet que les barres de compensation n'affectent que les quatre canaux immédiatement voisins (réseau carré) et que le réacteur ainsi que les distances entre barres d'absorption sont assez grands pour que les interférences entre les barres insérées soient négligeables.

On donne les formules fondamentales qui permettent de déterminer la puissance thermique d'un canal expérimental donné en fonction de la profondeur d'insertion de la barre absorbante voisine. On résout le problème dans le cas d'un débit de gaz constant dans le canal, et dans le cas du débit qui permet de conserver la température maximale autorisée pour l'élément combustible. On résout ce second cas dans deux conditions différentes: barre de compensation insérée du côté de l'entrée du gaz de refroidissement ou du côté de la sortie de ce gaz.

La communication donne les relations qui permettent de déterminer l'effet des barres de compensation sur la puissance thermique et électrique du réacteur pour des débits de gaz contrôlés ou non contrôlés dans les canaux individuels.

La dernière partie du mémoire aborde le problème de la compensation optimale d'un excédent de réactivité donné. On donne des fonctions qui caractérisent la perte de production électrique relative en fonction de l'efficacité relative de la barre absorbante. A l'aide de ces fonctions on peut déterminer la profondeur optimale d'insertion des barres d'absorption et l'ordre optimal d'insertion des barres dans un réacteur à plusieurs zones.

A/776 Чехословакия

Оптимальная компенсация реактивности многозонального реактора и максимальная мощность электростанции

И. Шмид, В. Стах

Реакторы ядерных электростанций при эксплуатации с непрерывной перегрузкой тепловыделяющих элементов и особенно при эксплуатации со свежими тепловыделяющими элементами имеют довольно большой запас реактивности. Для компенсации этого запаса вводится ряд компенсирующих стержней, которые сильно влияют на мощность реактора. Целью настоящей работы явилось определение условий (определение порядка и глубины введения отдельных компенсирующих стержней), при которых потери мощности электростанции будут минимальны.

Расчеты касаются тяжеловодного реактора с газовым охлаждением. У этого типа реактора число экспериментальных каналов относительно невелико. В работе авторы исходили из предположения, что компенсирующие стержни влияют только на четыре технологических канала, которые находятся в непосредственном соседстве с ними (квадратная решетка), и из предположения, что реактор и соответственно расстояние между введенными поглощающими стержнями настолько велики, что можно пренебречь интерференцией вводимых стержней.

Приведены основные соотношения для определения тепловой мощности данного экспериментального канала в зависимости от глубины введения поглощающего стержня, находящегося рядом с этим каналом. Проблема решалась для случая, когда расход газа через канал не меняется и когда он имеет величину, достаточную для того, чтобы температура тепловыделяющего элемента не поднималась выше максимально допустимой. Второй случай решался для двух различных условий, а именно: для случая введения компенсирующих стержней со стороны входа теплоносителя и для случая введения их со стороны выхода теплоносителя.

Кроме того, приведены соотношения для определения влияния компенсирующих стержней на тепловую и электрическую мощность реактора для случая нерегулируемого и регулируемого расхода газа через отдельные каналы.

Последняя часть работы посвящена вопросу, каким способом можно оптимально компенсировать данный запас реактивности.

Введены функции, характеризующие относительную убыль электрической мощности, отнесенную к относительной эффективности поглощающего стержня. По виду этих функций можно определить, во-первых, оптимальную глубину введения поглощающего стержня и, во-вторых, оптимальный порядок, в котором надо вводить стержни у многозонального реактора.

A/776 Checoslovaquia

El control óptimo de la reactividad en un reactor de varias zonas en relación con la producción máxima de la central

por J. Schmid y V. Stach

Los reactores de las centrales nucleoelectricas tienen un exceso de reactividad relativamente grande en los casos de funcionamiento con carga continua, sobre todo en el caso de elementos combustibles frescos. Para compensar este exceso de reactividad hay que emplear cierto número de barras absorbentes que perturban considerablemente el nivel de potencia del reactor. En esta memoria se estudian las condiciones en las que se minimizan las pérdidas de potencia,

determinando la secuencia y profundidad de inserción de las barras compensadoras.

Los cálculos se refieren a un reactor de agua pesada refrigerado por gas. Este tipo de reactor tiene un número relativamente pequeño de canales experimentales. En esta memoria se supone que las barras compensadoras afectan solamente a los cuatro canales más próximos (se trata de una red cuadrada) y que tanto el reactor como la distancia entre las barras son lo suficientemente grandes como para hacer despreciables los efectos de interferencia.

Se dan las relaciones que permiten la determinación de la potencia térmica de un canal experimental en función de la profundidad de inserción de la barra absorbente vecina. El problema se resuelve para el caso de un flujo constante de gas y para un flujo tal que la temperatura máxima permisible del elemento combustible se mantenga fija. Este último caso se resuelve suponiendo que la barra compensadora se inserte, bien en la dirección de entrada del refrigerante o bien en la salida.

Asimismo se dan relaciones para determinar el efecto de las barras compensadoras sobre la producción térmica y eléctrica del reactor para los casos de flujo de gas controlado en cada canal individual.

La última parte de la memoria trata el problema de la compensación óptima del exceso dado de reactividad. Se introducen unas funciones que caracterizan la pérdida relativa de producción eléctrica relacionándola con la eficiencia relativa de la barra absorbente. Mediante estas funciones se pueden determinar la profundidad y la secuencia óptimas de inserción de la barra absorbente en un reactor de varias zonas.

Heat transfer

Chairman: P. J. Nowacki (Poland)

Paper P/580 (presented by K. Torikai)

DISCUSSION

S. S. KUTATELADZE (USSR): Although the convective heat transfer processes in the type of reactor which we are discussing are closely bound up, even in the case of liquid metals, with turbulent transfer phenomena, no sufficiently accurate methods have been evolved for determining turbulent transfer coefficients in the range of finite Reynolds numbers. It has however been possible—and this is an important point—to obtain for flows with “diminishing” viscosities ($\mu \rightarrow 0$), i.e., for $Re \rightarrow \infty$, a series of asymptotic solutions free from empirical constants. New asymptotic solutions can also be obtained for various important cases of boiling heat transfer.

Thus, apart from my equation for q_{BO} under boiling conditions and free convection—quoted in the paper by Mr. Torikai—it is also possible to obtain a formula for very high liquid flow speeds— ω_0 and $T \ll T''$:

$$q_{BO} = \phi^*(1 - \phi^*) \frac{C_f}{2} r \omega_0 \sqrt{\gamma' \gamma''} \left(1 + C \sqrt{\frac{\gamma''}{\gamma'}} \frac{C_D \Delta T}{r} \right)$$

Where ϕ^* = steam content of zone adjacent to wall
 C_f = friction coefficient
 r = latent heat of boiling
 C = constant

The remaining symbols are the normally accepted ones.

Formula [13] in Torikai's paper is close to this solution when $Cp\Delta T \gg r$.

I should like also to draw attention to the fact that, as far as the analogy between boiling and bubbling is concerned, Torikai's experimental results are in principle similar to the results obtained by ourselves in the USSR and also by Spalding in England.

Another problem which needs to be borne in mind is the molecular weight of the gas.

Paper P/326 (presented by N. I. Buleev)

DISCUSSION

O. E. DWYER (United States of America): I would like to compliment Dr. Osmachkin on this informative paper. I was particularly interested in his treatment of the case of in-line flow of liquid metals through un baffled rod bundles. A few years ago, we produced an analytical solution to this problem, at the Brookhaven National Laboratory, in which we assumed that the radial velocity distribution, with respect to a given rod, was the same as that in the inner portion of an

annulus having the same inner radius, the same radius of maximum velocity and the same average velocity through the inner portion. It seemed that this was preferable to basing the velocity distribution on that for flow in pipes. I have made a spot check which shows that Figure 9 in Dr. Osmachkin's paper is in rather good agreement with Eq. [2] in paper P/225*, if one uses the constants in Table 3 of that paper and assumes $\bar{\psi} = 1$. The constants are based on the annulus model.

At low Pe numbers, we believe that Nu is almost independent of Pe . At a pitch: diam ratio of 1.7 for example, we have concluded that below $Pe \approx 700$, the eddy contribution to total heat transfer is negligibly small, leaving molecular conduction as the dominant mechanism.

Above $Pe \approx 700$, eddy conduction becomes increasingly important, until at $Pe \approx 10^4$, it is close to unity. Thus, the higher the Peclet number, the greater the accuracy required in determining ν_T .

Paper P/16 (presented by A. D. Lane)

DISCUSSION

H. S. ISBIN (United States of America): Have you carried out sufficient tests to enable you to summarize the effects of eccentric positioning of the test sections?

A. D. LANE (Canada): No, we have not. We do however hope to do some work on spacing.

H. S. ISBIN (United States of America): When you estimate radiation heat transfer from the oxidized Zircaloy sheath, what values do you use for the emissivity of the surfaces?

A. D. LANE (Canada): We have not tried to estimate radiation from oxidized Zircaloy sheaths during irradiation, for two reasons. First of all, in the case where thermal bowing occurred and appreciable corrosion resulted, the temperatures were estimated from thermocouple readings on stainless steel elements subjected to similar conditions and also from an examination of the extent of the sheath corrosion. Secondly, in normal operation the temperature of the surroundings, i.e., the test section, was the same inside and outside the reactor and in general little below the fuel-sheath temperature.

V. I. SUBBOTIN (USSR): I have one comment to make in connection with this paper. Burn-out does not occur in the same way at high and at low pressures, and at high pressures there is no great increase in the

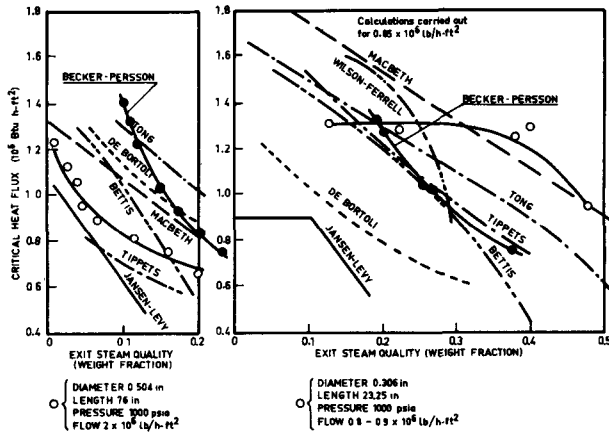


Figure 1. Comparison of correlations with critical heat-flux data in tubular test sections

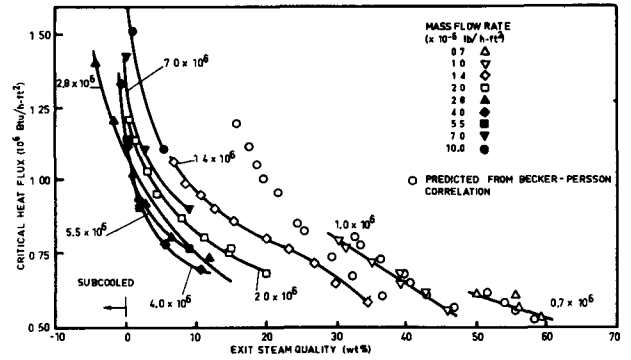


Figure 2. Critical heat-flux condition in tubular test sections
Inside tube diameter: 0.504 in; heated length: 76 in; pressure: 1 000 psia

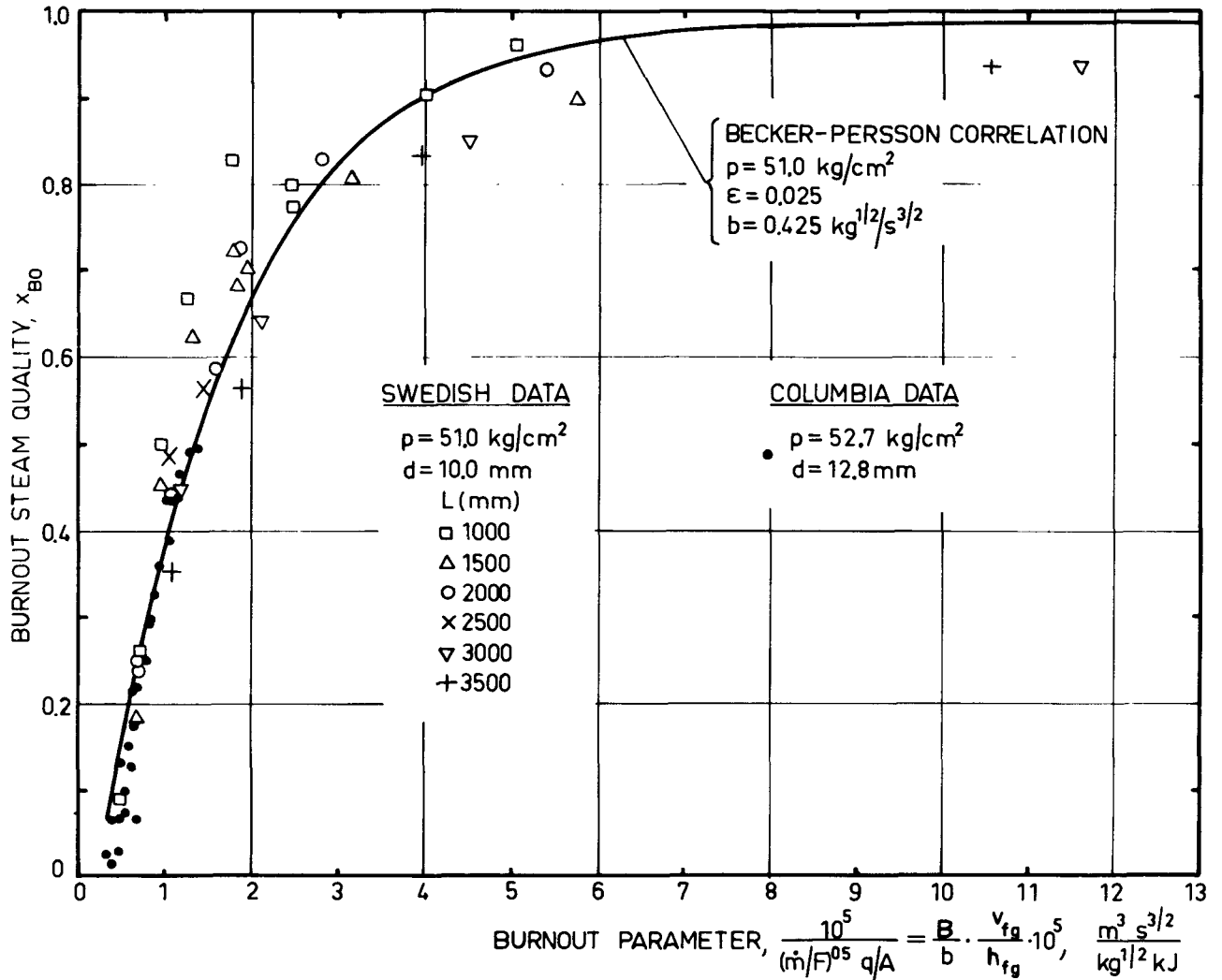


Figure 3. Comparison of experimental and predicted burn-out conditions

temperature of the heat-producing wall when burn-out occurs. It seems to me that in a number of cases this could be a source of error in experimental determinations of q_{BO} .

Paper P/224

DISCUSSION

K. M. BECKER (Sweden): Figure 13 in the paper compares different correlations with two selected sets of the Columbia data. It seems from this comparison as if the Becker-Persson correlation is rather inadequate from the point of view of predicting burn-out conditions. We have, however, shown, in a paper (K. M. Becker, *Report in progress*, AB Atomenergi, Studsvik, Sweden) to be published in October or November 1964, that this correlation predicts the burn-out heat fluxes for about 3 000 Swedish burn-out measurements to within ± 5 per cent in the following ranges of variables:

$$\begin{aligned} 2.7 < p < 91 \text{ kg/cm}^2 \\ 100 < G < 3\,500 \text{ kg/m}^2 \text{ s} \\ 35 < q/A < 600 \text{ W/cm}^2 \\ 0.05 < X < 1.00 \\ 4 < d < 13 \text{ mm} \\ 600 < L < 3\,500 \text{ mm} \end{aligned}$$

I think I can explain why our correlation looks so bad in Figure 13. The correlation, which is based on the Vanderwater-Isbin flow model, contains two constants, ϵ and b , which represent the entrainment and droplet diffusion rates and which have to be determined from experimental data. When our paper on the correlation was written about between 18 months and two years ago, the Swedish burn-out studies only covered measurements up to 40 kg/cm^2 , and the constants ϵ and b above this pressure had to be determined from foreign data. In the case now discussed, where the pressure is $1\,000 \text{ psia}$, ϵ and b were determined by means of the CISE data (K. M. Becker and P. Persson, *An Analysis of Burn-out Conditions for Flow of Boiling Water in Vertical Round Ducts*, ASME paper No. 63-WA-51). To obtain these data, steam-water mixtures were applied to the inlet of the test section. As we pointed out in our paper, the correlation cannot for this reason be considered reliable at this pressure when it is applied to predict burn-out in ducts with sub-cooled inlet conditions.

The new paper I mentioned contains new ϵ and b values which can be used at the higher pressures.

Figure 1 shows Figure 13 in Levy's paper after insertion of the correct values for ϵ and b in the Becker-Persson correlation.

It will be seen that the agreement between the Columbia data and our correlation is now satisfactory. This fact can be brought out even more clearly if use is made of some of the data presented in Figure 2 in Levy's paper. A comparison is given in Figure 2.

The increasing scatter at low steam qualities is to be expected in view of the fact that the correlation is

based on the *climbing* film flow model. If, however, b is also made a function of the steam quality, the scatter shown in Figure 2 at low steam qualities can be reduced appreciably.

Finally, in Figure 3 our correlation is applied to the Swedish data and the Columbia data for a pressure of about 50 kg/cm^2 .

It will be observed that here too there is excellent agreement between the two sets of data and our correlation.

Paper P/93 (presented by J. Villeneuve)

DISCUSSION

W. M. CAMPBELL (Canada): In Canada we also have been studying fouling, but our results appear to be different from those presented in this paper. There may not, however, be any real disagreement.

The process we use is as follows. The coolant is carefully treated with Attapulugus clay and filtered to remove all particulates (organic and inorganic); those components which promote organic fouling are essentially absent.

Under these conditions we have found, as described in paper P/15*, that chlorine promotes mass-transfer iron fouling, and that the form of the chlorine is very important. Trichlorethylene, for example, is a more effective promoter than chlorodiphenyl. We feel that the chlorine compound which is added has to break down to form an active chlorine compound, so far unidentified. Thus, if a stable chlorine compound is used in tests, the wrong conclusion could be drawn regarding the effect of chlorine.

I submit that in the case described in paper P/93 the effect has been masked by the fairly high organic fouling impurity and the stability of the organic chlorine compound added.

I would also draw attention to one of our X-7 loop tests which showed almost no fouling on fuel-element surfaces maintained at $450\text{--}500^\circ\text{C}$ for 82 days ($0.1 \mu\text{g/cm}^2 \text{ h}$).

J. VILLENEUVE (France): I agree that chlorine has different effects depending on the form in which it is found in the circuit. In our circuit we used an OM2 terphenyl produced from the polymerization of a benzene that had been chlorinated by mistake. The substance involved was thus a combined chlorine that has no effect on fouling. With time, however, it must have combined with the iron in the circuit and fouling has now occurred through transfer.

In our experiments, we have always found that there is a clearly defined threshold at 500°C . Above this temperature, one finds local pyrolysis which produces a film consisting of a soft product that sticks to the heating wall.

L. S. DZUNG (Switzerland): What was the range of the Prandtl numbers for the cooling media used in this experiment?

J. VILLENEUVE (France): The Prandtl numbers varied between 5 and 12.

L. S. DZUNG (Switzerland): I note that the correlation formula used in this paper has the same structure as the classical correlation first suggested by Colburn in 1930. I should be interested to know how your formula in fact compares with the classical one. It seems to me that the mechanism of heat transfer depends mainly on the physical properties of the medium, which are characterized by the Prandtl number and the Reynolds number. The chemical properties are not very much involved. The formula in the paper should therefore also apply to media other than organic liquids provided the Prandtl number is within the appropriate range.

J. VILLENEUVE (France): The correlation we find is different from the classical ones, e.g., that of Colburn—in that the exponent of the Reynolds number is 0.9. As has already been pointed out, e.g. in reference [1] of the paper, the exponent of the Reynolds number increases with the Prandtl number. By using the semi-theoretical calculation of Martinelli for our case, we obtain a value of 0.9 for the exponent.

Paper P/53 (presented by P. Lévêque)

DISCUSSION

R. F. S. ROBERTSON (Canada): We in Canada are very interested in the mechanism proposed by Lévêque in this paper. Our evidence suggests that a concept based on the combination of a pure radiolysis which is independent of LET and temperature and a pyrolysis which is independent of dose rate may perhaps be an over-simplification. In the case of the capsule irradiations carried out in the NRX reactor—mentioned in our paper P/15—we have found for both ortho- and meta-terphenyl that the yields as a function of temperature are nearly the same at dose rates of 0.1 and 0.3 W/g. Dr. Lévêque's mechanism would not predict this result. We do agree, however, that, in meta-terphenyl at least, the pyrolysis rate of radiolysed material is significantly higher than that of unirradiated material. Our results indicate that fast neutrons are more damaging than γ rays and that G_n/G_γ is about 3 for temperatures below 375° C.

Papers P/225 (presented by O. E. Dwyer) and P/328 (presented by V. I. Subbotin)

(It was agreed that these papers should be discussed together.)

DISCUSSION

L. S. DZUNG (Switzerland): Firstly, I wish to congratulate the authors of paper P/225, which provides us with a most complete summary on the information available on heat transfer with media of low Prandtl number.

My comment refers to Figure 1 in which, for some curves, the eddy diffusivity ϵ_M has a cusp in the portion of the channel between two walls. Now this portion is characterized by a zero-velocity gradient, i.e., the flow is locally homogeneous. Thus, physically the eddy

diffusivity should also have zero gradient, i.e., there should be no cusp. I wonder if Mr. Dwyer has any comment on this point.

O. E. DWYER (United States of America): The eddy diffusivity of momentum transfer at a given transverse point in the flow channel depends primarily on the shearing stress and the slope of the velocity profile at that point. Since, at the radius of maximum velocity, these are zero, it is impossible to evaluate the diffusivity at this point. However, the ϵ_M versus $(r - r_1)/(r_2 - r_1)$ curve for an annulus should be differentiable at all points and should also have zero slope at the radius of maximum velocity. Curve (b) in Figure 1, the one preferred by the authors, satisfies these requirements. There is adequate experimental evidence to indicate that profile (a) in Figure 1 is very unlikely. Moreover, a fairly uniform velocity profile in the central portion of the annulus does not mean that the eddy diffusivity of momentum in that region also has to be uniform.

P. GILLI (Austria): I would like to make a comment and to ask one question on Mr. Dwyer's paper. I should like to refer particularly to the heat transfer of liquid metals in cross-flow through tube bundles, which might represent the case of a heat exchanger or of a steam generator for a nuclear power plant with a liquid-metal cooled reactor.

I would suggest that it is possible to combine the two formulae quoted by the author for the Nusselt number in cross-flow, that is the empirical equation [Eq. (4)] by Rickard, Dwyer and Dropkin (Ref. [25] of the paper) and the theoretical formula [Eqs. (5) and (6)] by Hsu.* Each of these formulae exhibits interesting features. Equation (4) shows a constant figure—4.03—in addition to the power function of the Peclet number and thus obviously takes account of molecular conductance. The formula has, however, been obtained for one particular tube arrangement only. On the other hand Eqs. (5) and (6)—thanks to ϕ_1 , the unit-velocity potential difference between forward and rear stagnations points of the tube—are valid for different tube arrangements but do not take account of molecular conductance. Thus the Nusselt number according to this formula becomes zero for a Peclet number of zero.

It would not be difficult to combine the two formulae. We would have to change the coefficient 0.958 in Eqs. (5) and (6), or else this coefficient and the exponent of the Peclet number and of ϕ_1/D , in such a way that, by adding the constant 4.03, Nu was in line with the experimental results. One way this could be achieved would be to reduce the coefficient by about 10 to 20%. Alternatively, it would be possible in Eq. (4) to substitute the function ϕ_1/D and a suitably chosen coefficient for the coefficient 0.228. Thus a more general and more satisfactory formula would be achieved for the cross-flow of liquid metals through tube bundles, which would also be valid for small Peclet numbers and for various tube arrangements.

Now to my question, which relates to the values of

* Int. J. Heat Mass Transfer, Vol. 7, pp. 431–446 (April 1964).

ϕ_1/D tabulated in the paper by Hsu to which I have already referred. These values of ϕ_1/D refer to square in-line and to equilateral triangular tube arrangements only. Have values of ϕ_1/D for more general tube arrangements been calculated by the Hsu method at the Brookhaven National Laboratory or elsewhere?

O. E. DWYER (United States of America): Eq (4) is an empirical equation based upon experimental results for a single rod bundle, one having a P/D of 1.38. It gives a Nu versus Pe curve, the slope of which increases with Pe . However, Eqs. (5) and (6) having been based on the assumption of inviscid flow, give straight lines on a Nu versus Pe plot. Thus, Eqs. (4) and (5) deviate in the low Pe range. It is evident therefore that Eqs. (5) and (6) do not apply at the Peclet extremes as well as Eq. (4) does. A modification of Eq. (5), consistent with the characteristics of Eq. (4), as Dr. Gilli suggests, would be appropriate for estimating cross-flow heat transfer coefficients for conditions differing from those on which Eqs. (4) and (5) were based.

With reference to the existence of ϕ_1/D values, I know of none other than those published in refs. [27] and [30].

If I may now comment on the other paper, we in the United States know that Dr. Subbotin and his colleagues at the Institute of Physics and Energetics in the USSR have performed very extensive and splendid work in recent years in the field of liquid-metal heat transfer. Their results have contributed much to our present knowledge of the subject. It has been reassuring to us working in the same field in the United States to see from time to time that there was substantial agreement in several areas of independent research in both countries.

To improve our knowledge of liquid-metal heat transfer, more information is required on the nature of the eddy contribution to the total heat transfer mechanism; a more accurate means of predicting the eddy diffusivity of heat transfer is also needed. In this connection, the work described by Dr. Subbotin in connection with the measurement and correlation of local temperature fluctuations in the flowing metal stream is very significant.

Dr. Subbotin and his co-workers have studied extensively the important problem of heat transfer from rod bundles, with both closed and open packing, to in-line flow of liquid metals. In their Eqs. (18) and (19), which are based upon experimental results for these two cases respectively, the Nusselt number is shown to have the same dependence on the Peclet number throughout the whole Peclet range covered. This is at variance with results obtained at Brookhaven on staggered rod bundles with both mercury and NaK (as shown by the results plotted in Figure 7 of paper P/225), as long as good thermal contact exists between the flowing metal and the heat transfer surface.

I think that, at Peclet numbers in the low turbulence range, Eq. (19) in Dr. Subbotin's paper will probably yield Nusselt numbers below those for molecular conduction only; this could only be explained by the

absence of good thermal contact at the rod surfaces, under such flow conditions.

V. I. SUBBOTIN (USSR): The results of Mr. Dwyer's experiments on heat transfer from rod bundles to in-line flow are in good agreement with ours at $Pe > 500$. At $Pe < 500$, there are divergences which increase as the Pe numbers become smaller. One of the reasons for this divergence may be the axial heat flows, the values for which increase as the Pe numbers become smaller.

It is difficult to explain the divergence by contact phenomena. In our experiments, purity was systematically controlled and impurities were never higher than 10^{-3} wt%. A comparison between our experiments and Mr. Dwyer's leads to the conclusion that we must have had some fouling on the heat-producing wall.

N. I. BULEEV (USSR): I should like to raise a question to which little attention has been paid in the literature on hydraulics and heat transfer in channels.

When we compare the results of theoretical calculations relating to turbulent viscosity and temperature conductivity coefficients with experimental data we are not in fact comparing identical concepts.

The expressions $p\epsilon_M \frac{\partial \omega}{\partial r}$ and $p\epsilon_H \frac{\partial T}{\partial r}$ where $\epsilon_M = l_1^2 \left| \frac{\partial \omega}{\partial n} \right|$ and $\epsilon_H = l_r^2 \left| \frac{\partial \omega}{\partial n} \right|$, which appear in the initial expressions for heat movement and flow, are only the main components of the turbulent stress and turbulent heat flow. In this sense the initial theoretical equations are approximate.

In the case of experimental data, however, when results are based on measured velocity and temperature profiles, full values are obtained for turbulent stresses and heat flows.

If, in experimental work, we represent the values obtained for $\overline{pn'\omega'}$ and $\overline{pn'T'}$ in the form $p\epsilon_M^*(\partial\omega/\partial r)$ and $p\epsilon_H^*(\partial T/\partial r)$, and we then find the values ϵ_M^* , ϵ_H^* (formal values) and the ratio $\epsilon_H^*/\epsilon_M^*$, then these values will not have exactly the same significance as ϵ_M , ϵ_H and ϵ_H/ϵ_M and may differ from them by more than ten per cent.

In my view, when we investigate the values, ϵ_M , ϵ_H and ϵ_H/ϵ_M , it is essential to use some single theoretical model for the momentum and heat turbulent transfer.

V. I. SUBBOTIN (USSR): When making calculations, the traditional practice is to take the value of the turbulent viscosity coefficient (ϵ_r) and then, on the basis of whatever value is used for the turbulent Prandtl number (ϵ), to find the coefficient of turbulent thermal conductivity (ϵ_a). This approach was understandable in the days when experiments were being carried out on the measurement of velocity fields and there were no reliable experiments on the measurement of temperature fields. At the present time however it is possible to find ϵ_a directly and to substitute it into the corresponding expressions.

O. E. DWYER (United States of America): In most

cases, velocity profiles can be predicted with considerably greater accuracy than temperature profiles; and since one can now convert ϵ_M values to ϵ_H values, for channel flow, with some confidence, I accordingly feel that the $\epsilon_M \rightarrow \epsilon_H \rightarrow Nu$ route is more often preferred for estimating heat transfer coefficients in most new situations.

Paper P/135 (presented by C. Cunningham)

DISCUSSION

J. PELCE (France): Very similar work has been going on at the CEA laboratories, but, in our case, the emphasis has been on elements with herringbone finning. We have been trying to solve the same problems and we have been using the same methods.

We have been doing a fair amount of work on thermal characteristics and pressure drops for a wide variety of finning arrangements with a view to working out formulae suitable for use in reactor optimization calculations. Details of this work are available if anyone should be interested in having them.

We have also made detailed studies of the thermal behaviour of the cans chosen for particular reactors such as EDF2 and EDF3. Particular attention has been paid to the thermal peculiarities of whole sets of cans, arranged to simulate actual pile geometry, at rated operation (with special emphasis on the problem of angular displacement between elements). We have also studied the influence of low flows for cases of upward (EDF3) and downward (EDF4) gas streams, and also the geometries of deformed cans.

All these tests were performed on full-size or over-size models. Our conclusions are very largely in line with those set forth in papers P/135 and P/136. Information on our results is contained in CEA reports 2469 and 2470.

In connection with paper P/135, I have two questions. First, in the experiments described did the gas flow up or down? And could you give us some idea of the accuracy of your results? Secondly, have you carried out detailed investigations with cans possessing more than four sectors?

C. CUNNINGHAM (United Kingdom): The results of low flow tests reported in the paper relate to upward flow. It is impossible to give a precise answer on the question of accuracy. Inasmuch as it is possible to generalize, the standard deviation in our heat-transfer tests can be put at about 2%. As for your second question, we have not carried out detailed investigations on herringbone elements with more than four sectors.

W. L. GRANT (South Africa): Figures 1E and 2E indicate the variation of heat transfer with relative element orientation. Is this variation the same for both vertical and horizontal fuel-element channels?

C. CUNNINGHAM (United Kingdom): We have not carried out any orientation tests in vertical channels. In all our other tests at high Reynolds numbers, however, we have not been able to detect differences due to channel altitude—this is readily understandable as buoyancy effects are insignificant.

Paper P/719 (presented by V. B. Nesterenko)

DISCUSSION

Y. EL-MESHAD (United Arab Republic): Mr. Nesterenko, could you tell us about the possibility of using your averaging technique (a) when taking into consideration the cladding material or for multilayer fuel elements in general, and (b) when taking into consideration the axial heat flow along the fuel material?

V. B. NESTERENKO (USSR): By using methods of approximation, it is possible to allow for the thermal resistance of the fuel can in the heat-transfer coefficient we quoted. In this investigation no account was taken of the heat flow along the element in the case of gas, because of the smallness of the quantity involved.

Paper P/552 (presented by R. Negrini)

There was no separate discussion of this paper.

Compte rendu de la séance I. 10

Transfert de chaleur

Président: P. J. Nowacki (Pologne)

Mémoire P/580 (présenté par K. Torikai)

DISCUSSION

S. S. KUTATELADZE (URSS): Les processus de transfert de chaleur par convection dans le type de réacteur qui nous occupe sont étroitement liés, même

dans le cas des métaux liquides, à des phénomènes de transfert turbulent, mais aucune méthode d'une précision satisfaisante n'a été élaborée pour déterminer les coefficients de transfert turbulent pour des nombres de Reynolds d'un intervalle fini. Cependant on a pu — et ceci est important — obtenir pour des écoulements de

viscosités « décroissantes » ($\mu \rightarrow 0$), c'est-à-dire pour $Re \rightarrow \infty$, une série de solutions asymptotiques indépendantes de constantes empiriques. De nouvelles solutions asymptotiques peuvent aussi s'obtenir pour divers cas importants de transfert de chaleur à l'ébullition.

Ainsi, outre mon équation pour q_{BO} dans les conditions d'ébullition et de convection libre — mentionnée dans le mémoire de M. Torikai — il est possible également d'obtenir une formule pour de très grandes vitesses ω_0 d'écoulement liquide et $T \ll T''$:

$$q_{BO} = \phi^*(1 - \phi^*) \frac{C_t}{2} r \omega_0 \sqrt{\gamma' \gamma''} \left(1 + C \sqrt{\frac{\gamma''}{\gamma'}} \frac{C_p \Delta T}{r} \right)$$

où ϕ^* = teneur en vapeur dans la région de la paroi

C_t = coefficient de frottement

r = chaleur latente de vaporisation

C = constante

Les autres symboles ont leur signification habituelle.

La formule 13 du mémoire de M. Torikai est voisine de cette solution quand $C_p \Delta T \gg r$.

Je voudrais aussi attirer l'attention sur le fait que, pour tout ce qui concerne l'analogie entre ébullition et bouillonnement, les résultats des expériences de Torikai sont dans leur principe semblables aux résultats obtenus par nous-mêmes en URSS ainsi que par Spalding en Angleterre.

Une autre considération qu'il faut garder présente à l'esprit est la masse moléculaire du gaz.

Mémoire P/326 (présenté par N. I. Buleev)

DISCUSSION

O. E. DWYER (Etats-Unis d'Amérique): Je voudrais féliciter M. Osmachkin de sa communication si instructive. J'ai surtout été intéressé par la méthode qu'il emploie dans le cas de l'écoulement longitudinal de métaux liquides à travers des grappes de barreaux nus. Voilà quelques années, nous avons donné de ce problème, au Laboratoire national de Brookhaven, une solution analytique, dans laquelle on assimilait la distribution radiale des vitesses, par rapport à un barreau donné, à celle dans la zone intérieure d'un anneau de même rayon intérieur, de même rayon de vitesse maximale et de même vitesse moyenne dans la zone intérieure; cela valait mieux, semble-t-il, que de prendre pour distribution fondamentale des vitesses celle de l'écoulement dans des tuyaux. J'ai fait une vérification qui montre que la figure 9 du mémoire de M. Osmachkin est en assez bon accord avec l'équation 2 du mémoire P/225, si l'on utilise les constantes du tableau 3 de ce mémoire et si l'on suppose $\bar{\varphi} = 1$. On a choisi les constantes en se fondant sur le modèle annulaire.

A de faibles valeurs du nombre Pe , nous pensons que Nu est presque indépendant de Pe . A une valeur repère, rapport de diamètre de 1,7 par exemple, nous avons conclu qu'au-dessous de $Pe \approx 700$, la part du tourbillon dans le transfert de chaleur total était

négligeable, ce qui donnait à la conduction moléculaire le rôle prédominant.

Au-dessus de $Pe \approx 700$, l'importance de la conduction tourbillonnaire s'accroît de plus en plus, jusqu'à $Pe \approx 10^4$, où elle est proche de l'unité. Ainsi, plus le nombre de Péclet est élevé, plus il faut de précision dans la détermination de ν_T .

Mémoire P/16 (présenté par A. D. Lane)

DISCUSSION

H. S. ISBIN (Etats-Unis d'Amérique): Avez-vous fait assez d'essais pour pouvoir donner une idée des effets de l'excentrement des sections d'essais ?

A. D. LANE (Canada): Non, nous n'en avons pas fait assez. Mais nous espérons bien faire quelques études sur l'espacement.

H. S. ISBIN (Etats-Unis d'Amérique): Dans votre évaluation du transfert de chaleur rayonnée par la gaine de Zircaloy oxydée, quelles valeurs prenez-vous pour l'émissivité des surfaces ?

A. D. LANE (Canada): Nous n'avons pas cherché à évaluer le rayonnement des gaines de Zircaloy oxydées pendant l'irradiation, cela pour deux raisons. Tout d'abord, dans le cas où la chaleur produit un cintrage causant une corrosion sensible, on évaluait les températures à partir de lectures de thermocouples placés sur des éléments d'acier inoxydable soumis aux mêmes conditions, ainsi qu'à partir d'un examen de l'étendue de la corrosion de la gaine. En second lieu, en marche normale, la température du milieu ambiant, c'est-à-dire de la section d'essai, était la même à l'intérieur et à l'extérieur du réacteur, et elle était en général peu inférieure à la température de la gaine du combustible.

V. I. SUBBOTIN (URSS): J'ai une remarque à faire concernant ce mémoire. La caléfaction ne se produit pas de la même manière à haute et à basse pression, et à haute pression il n'y a guère d'augmentation de température de la paroi chauffante quand se produit la caléfaction. Il me semble que, dans bien des cas, cela pourrait être une source d'erreur dans les déterminations expérimentales de q_{BO} .

Mémoire P/224

DISCUSSION

K. M. BECKER (Suède): La figure 13 du mémoire compare différentes relations avec deux ensembles de valeurs choisies de Columbia. D'après cette comparaison, il semble que la relation de Becker-Persson est assez mal adaptée au point de vue de la prévision des conditions de caléfaction. Cependant, nous avons montré dans un mémoire (K. M. Becker, rapport à paraître, A. B. Atomenergi, Studsvik, Suède) qui sera publié en octobre ou novembre 1964 que cette relation permet de prévoir les flux thermiques de caléfaction dans quelque 3 000 mesures faites en

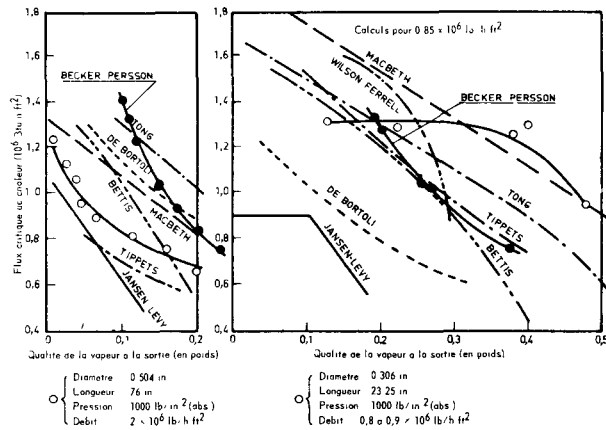


Figure 1. Comparaison des corrélations avec les données sur le flux critique de chaleur pour des sections d'essai tubulaires

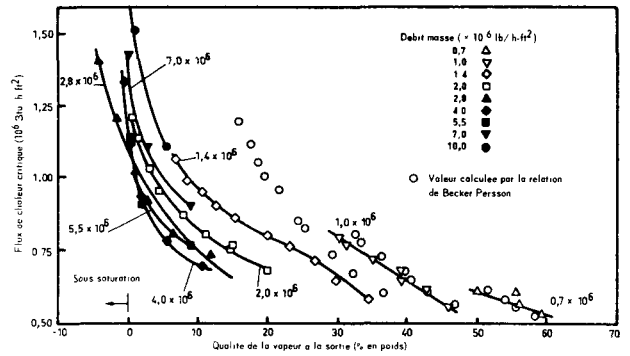


Figure 2. Conditions de flux de chaleur critique dans les sections tubulaires d'essai

Diamètre intérieur du tube: 0,504 in; longueur chauffée: 76 in; pression: 1 000 lb/in² (abs.)

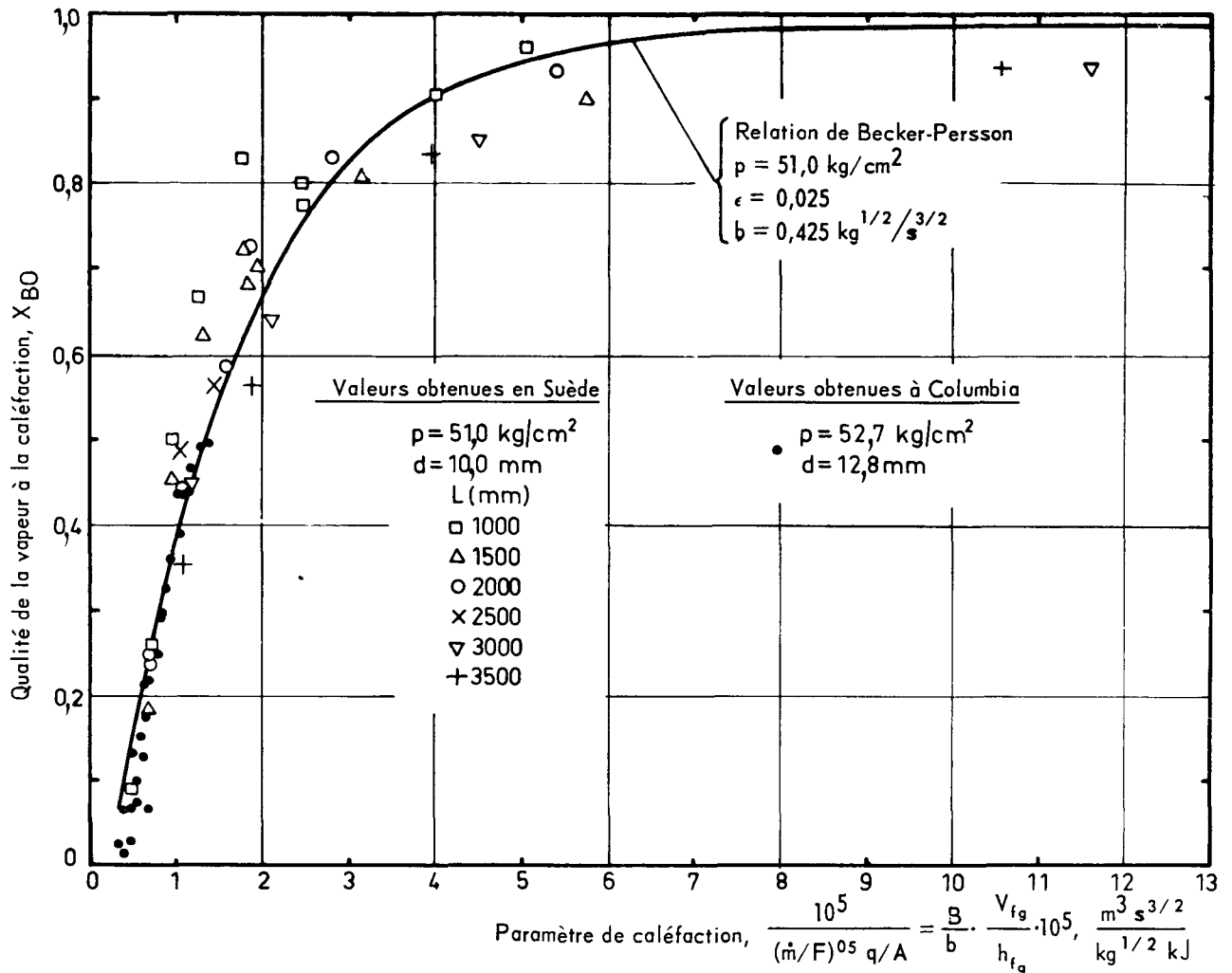


Figure 3. Comparaison des conditions de caléfaction expérimentales et calculées.

Suède à $\pm 5\%$ près dans les intervalles suivants des variables:

$$2,7 < p < 91 \text{ kg/cm}^2$$

$$100 < G < 3\,500 \text{ kg/m}^2 \text{ s}$$

$$35 < q/A < 600 \text{ W/cm}^2$$

$$0,05 < X < 1,00$$

$$4 < d < 13 \text{ mm}$$

$$600 < L < 3\,500 \text{ mm}$$

Je crois pouvoir expliquer pourquoi notre relation se présente si mal sur la figure 13. La relation, qui est basée sur le modèle d'écoulement de Vanderwater-Isbin, contient deux constantes, ϵ et b , qui représentent les vitesses de diffusion d'entraînement et de gouttelettes et que l'on doit déterminer à partir de données expérimentales. Quand nous avons écrit le mémoire sur la corrélation, il y a environ dix-huit mois à deux ans, les études faites en Suède sur la caléfaction ne recouvraient que des mesures ne dépassant pas 40 kg/cm^2 ; et les constantes ϵ et b pour des pressions supérieures avaient dû être déterminées à partir de données de l'étranger. Dans le cas qui nous occupe, où la pression (absolue) est de 1 000 livres par pouce carré (69 bars), ϵ et b ont été déterminées au moyen des données de la CISE (K. M. Becker et P. Persson, *An Analysis of Burn-out Conditions for Flow of Boiling Water in Vertical Round Ducts*, ASME paper No. 63-WA-51). Pour obtenir ces données, on introduisait des mélanges eau-vapeur à l'admission de la section d'essai. Comme nous l'avons fait ressortir dans notre mémoire, on ne peut en conséquence, pour cette pression, faire confiance à la corrélation lorsqu'elle s'applique à la prévision de la caléfaction dans des conduites avec sous-refroidissement aux conditions d'admission.

Le nouveau mémoire que je signale contient de nouvelles valeurs de ϵ et de b , valables aux pressions supérieures.

La figure 1 représente la figure 13 du mémoire de Levy après introduction des valeurs correctes de ϵ et de b dans la relation de Becker-Persson.

On verra que l'accord entre les valeurs de Columbia et notre relation est dès lors satisfaisant. Cela est illustré de manière encore plus nette si l'on utilise quelques-unes des valeurs présentées à la figure 2 du mémoire de Levy. La comparaison est faite à la figure 2.

L'augmentation de la dispersion pour de basses teneurs en vapeur est à prévoir, vu que la relation est basée sur le modèle d'écoulement de film *ascendant*. Mais si l'on rend aussi b fonction de la teneur en vapeur, la dispersion représentée à la figure 2 pour de basses teneurs en vapeur peut être beaucoup réduite.

Enfin, dans la figure 3, notre relation est appliquée aux valeurs suédoises et aux valeurs de Columbia pour une pression d'environ 50 kg/cm^2 .

On observera là encore un excellent accord entre les deux ensembles de valeurs et notre corrélation.

Mémoire P/93 (présenté par J. Villeneuve)

DISCUSSION

W. M. CAMPBELL (Canada): Au Canada aussi nous avons étudié l'encrassement, mais nos résultats diffèrent, en apparence, de ceux présentés dans ce mémoire. Peut-être, cependant, n'y a-t-il pas réellement désaccord.

La méthode que nous utilisons est la suivante. Le réfrigérant est soigneusement traité à l'argile *Attapulgus* et filtré pour éliminer toutes les particules (organiques et inorganiques); les constituants qui causent l'encrassement organique sont essentiellement absents.

Dans ces conditions, nous avons trouvé, comme l'expose le mémoire P/15, que le chlore provoque un encrassement ferrugineux avec transfert de masse et que l'état du chlore est très important. Le trichloréthylène, par exemple, agit davantage que le chlorodiphényle. Nous pensons que le composé chloré, après addition, se dissocie pour former un composé chloré actif, non encore identifié. Ainsi, si l'on emploie un composé chloré stable dans des essais, on risque de tirer des conclusions fausses sur l'influence du chlore.

Je suggère que, dans le cas étudié au mémoire P/93, l'effet a été masqué par la concentration assez élevée de l'encrassement organique et par la stabilité du composé chloré organique que l'on ajoutait.

Je voudrais aussi attirer l'attention sur l'un de nos essais en boucle X-7, qui indiquait un encrassement presque nul à la surface d'éléments de combustible maintenus à $450-500^\circ\text{C}$ pendant 82 jours ($0,1 \mu\text{g/cm}^2 \text{ h}$).

J. VILLENEUVE (France): Je conviens que le chlore peut avoir des effets différents selon la forme sous laquelle il se trouve dans le circuit. Dans notre boucle, nous utilisons un terphényle OM2 additionné de produits provenant d'un benzène qui avait été craqué en présence de chlore par erreur. Le chlore était donc sous forme combinée et nous n'avons pas vu d'encrassement sur la paroi chauffante. Cependant, sous l'effet de la température, le chlore combiné a formé probablement des chlorures ferreux avec le fer doux placé dans notre boucle, et un encrassement est alors apparu par transport moléculaire.

Il semble que, dans les conditions de nos essais, il y ait un seuil assez net aux environs de 500°C . Au-dessus de cette température, on voit très rapidement se former une boue adhérente, mais assez molle, sur la paroi chauffante.

L. S. DZUNG (Suisse): Quelle était la gamme des nombres de Prandtl du milieu réfrigérant dans cette expérience?

J. VILLENEUVE (France): Le nombre de Prandtl variait entre 5 et 12.

L. S. DZUNG (Suisse): Je remarque que la relation utilisée dans ce mémoire a la même forme que la relation classique proposée en premier lieu par Colburn en 1930. Je voudrais savoir dans quelle mesure votre formule ressemble à la formule classique. Il me

semble que le processus de transfert thermique dépend essentiellement des propriétés physiques du milieu, qui sont caractérisées par le nombre de Prandtl et par le nombre de Reynolds. Les propriétés chimiques n'interviennent que peu. La formule de ce mémoire devrait donc s'appliquer aussi à des milieux autres que des liquides organiques, à condition que le nombre de Prandtl soit dans la gamme convenable.

J. VILLENEUVE (France): La formule que nous trouvons diffère des formules classiques, telles que celle de Colburn, en particulier par l'exposant du nombre de Reynolds, qui est 0,9. Comme on l'a déjà montré, par exemple dans la référence (1) du mémoire, l'exposant du nombre de Reynolds augmente avec le nombre de Prandtl. En utilisant le calcul semi-théorique de Martinelli pour ce cas, nous retrouvons l'exposant 0,9.

Mémoire P/53 (présenté par P. Lévêque)

DISCUSSION

R. F. S. ROBERTSON (Canada): Nous autres, Canadiens, sommes très intéressés par le mécanisme que propose M. Lévêque dans son mémoire. Nos constatations suggèrent qu'un schéma fondé sur la combinaison d'une radiolyse pure, indépendante du TEL et de la température, et d'une pyrolyse indépendante du taux d'irradiation, est peut-être un excès de simplification. Dans le cas des irradiations d'ampoules faites dans le réacteur NRX — signalées dans notre mémoire P/15 — nous avons trouvé que, pour l'ortho comme pour le méta-terphényle, les vitesses en fonction de la température étaient presque les mêmes à des taux d'irradiation de 0,1 et de 0,3 W/g. Le mécanisme décrit par M. Lévêque ne permet pas de prévoir ce résultat. Cependant, nous convenons tout à fait que, du moins pour le méta-terphényle, la vitesse de pyrolyse d'un matériau radiolysé est sensiblement plus grande que celle d'un matériau non irradié. Nos résultats montrent que les neutrons rapides causent plus de dégâts que les rayons gamma et que G_n/G_γ est voisin de 3 aux températures inférieures à 375 °C.

Mémoires P/225 (présenté par O. E. Dwyer) et P/328 (présenté par V. I. Subbotin)

(Il été décidé que ces deux mémoires seraient discutés ensemble)

DISCUSSION

L. S. DZUNG (Suisse): Tout d'abord, je tiens à féliciter les auteurs du mémoire P/225, qui nous fournit un résumé tout à fait complet des connaissances en matière de transfert thermique dans des milieux ayant de faibles nombres de Prandtl.

Ma remarque concerne la figure 1, où, sur quelques courbes, la diffusivité turbulente ϵ_M présente un point de rebroussement dans la région du canal entre deux parois. Ainsi cette région est caractérisée par un gradient de vitesse nul, c'est-à-dire que l'écoulement est localement homogène. Donc, pour des raisons de physique, la diffusivité turbulente devrait aussi avoir

un gradient nul, c'est-à-dire qu'il ne devrait pas y avoir de rebroussement. Je me demande si M. Dwyer peut commenter quelque peu cette question.

O. E. DWYER (Etats-Unis d'Amérique): La diffusivité turbulente du transfert de quantité de mouvement en un point donné perpendiculairement à l'écoulement dans le canal dépend d'abord de l'effort de cisaillement et de la pente du profil de vitesse en ce point. Puisque, au rayon de vitesse maximale, ceux-ci sont nuls, il est impossible d'évaluer la diffusivité en ce point. Cependant, la fonction ϵ_M de $(r - r_1)/(r_2 - r_1)$ pour un anneau devrait avoir une dérivée en chaque point, et la courbe devrait aussi avoir une pente nulle au rayon de vitesse maximale. La courbe (b) de la figure 1, celle que préfèrent les auteurs, remplit ces conditions. L'expérience donne de bonnes raisons de croire que le profil (a) de la figure 1 est très improbable. En outre, un profil de vitesses bien uniforme dans la région centrale d'un anneau ne signifie pas que la diffusivité turbulente de la quantité de mouvement dans cette région doit aussi être uniforme.

P. GILLI (Autriche): Je voudrais faire une remarque et poser une question sur le mémoire de M. Dwyer. Je désirerais me reporter spécialement aux échanges thermiques de métaux liquides en écoulement transversal à travers des faisceaux de tubes, ce qui peut représenter le cas d'un échangeur de chaleur ou celui d'un générateur de vapeur pour une centrale nucléaire avec réacteur refroidi par un métal liquide.

Je voudrais suggérer la possibilité de combiner les deux formules citées par l'auteur pour le nombre de Nusselt en écoulement transversal, c'est-à-dire l'équation empirique [éq. (4)] de Rickard, Dwyer et Dropkin (référence [25] du mémoire) et la formule théorique [éq. (5) et (6)] de Hsu*. Chacune de ces formules présente des caractéristiques intéressantes. Dans l'équation (4) figure une constante, 4,03, plus une fonction de puissance du nombre de Péclet, ce qui manifestement tient compte de la conductance moléculaire. Cependant, la formule n'a été établie que pour une disposition particulière de tubes. D'autre part, les équations (5) et (6) — grâce à ϕ_1 , la différence potentielle de vitesse unitaire entre les points stationnaires en avant et en arrière du tube — sont valables pour diverses dispositions de tubes, mais ne tiennent pas compte de la conductance moléculaire. Ainsi, d'après cette formule, le nombre de Nusselt s'annule lorsque le nombre de Péclet s'annule.

Il ne serait pas difficile de combiner ces deux formules. Il faudrait changer le coefficient 0,958 des équations (5) et (6), ou bien ce coefficient et l'exposant du nombre de Péclet et celui de ϕ_1/D , de telle manière que, en ajoutant la constante 4,03, Nu soit ajusté aux résultats des essais. Une méthode pour y parvenir serait de réduire les coefficients d'environ 10 à 20%. On pourrait encore, dans l'équation (4), remplacer la fonction ϕ_1/D et trouver un coefficient convenablement choisi au lieu du coefficient 0,228. Ainsi, on

* Int. J. Heat Mass Transfer, Vol. 7, pp. 431-446 (avril 1964).

arriverait à une formule plus générale et plus satisfaisante pour les écoulements transversaux de métaux liquides à travers des faisceaux de tubes, qui serait valable aussi bien pour de faibles nombres de Péclet et pour diverses dispositions de tubes.

Voici maintenant ma question, qui porte sur les valeurs de ϕ_1/D mises en tableau dans le mémoire de Hsu que j'ai déjà cité. Ces valeurs de ϕ_1/D ne se rapportent qu'à des dispositions de tubes parallèles en carré ou en triangle équilatéral. Des valeurs de ϕ_1/D pour des dispositions de tubes plus générales ont-elles été calculées par la méthode de Hsu au Laboratoire national de Brookhaven ou ailleurs ?

O. E. DWYER (Etats-Unis d'Amérique): L'équation (4) est une équation empirique fondée sur les résultats d'essais pour un seul faisceau de barres ayant un P/D de 1,38. Elle donne une courbe représentant Nu en fonction de Pe , dont la pente croît avec Pe . De leur côté, les équations (5) et (6), établies en supposant l'écoulement non visqueux, donnent des droites pour le tracé de Nu en fonction de Pe . Ainsi les équations (4) et (5) donnent des valeurs notablement différentes dans la gamme des faibles valeurs de Pe . C'est pourquoi il est évident que les équations (5) et (6) ne s'appliquent pas aussi bien que l'équation (4) aux valeurs extrêmes du nombre de Péclet. Une modification de l'équation (5), compatible avec les caractéristiques de l'équation (4), telle que la suggère M. Gilli, conviendrait à la détermination des coefficients d'échanges thermiques en écoulement transversal pour des conditions différentes de celles qui ont servi à établir les équations (4) et (5).

En ce qui concerne les valeurs de ϕ_1/D , je n'en connais pas d'autres que celles publiées dans les références [27] et [30].

Si je puis maintenant commenter l'autre mémoire, nous savons aux Etats-Unis que M. Subbotin et ses collègues de l'Institut de physique et d'énergétique de l'URSS ont réalisé des travaux remarquables et très complets dans le domaine du transfert thermique par métaux liquides. Leurs résultats ont largement contribué à notre connaissance actuelle du sujet. Il était rassurant pour nous, qui travaillions dans le même domaine aux Etats-Unis, de voir de temps à autre qu'il y avait un large accord dans plusieurs branches de recherches suivies indépendamment dans les deux pays.

Pour améliorer notre connaissance des transferts thermiques par métaux liquides, il faut davantage de renseignements sur la nature de la contribution des turbulences dans le mécanisme complet des transferts thermiques; il faut aussi une méthode plus précise pour calculer la diffusivité turbulente du transfert de chaleur. De ce point de vue, les travaux décrits par M. Subbotin à propos des mesures et des relations des fluctuations locales de température dans le courant de métal ont une très grande importance.

M. Subbotin et ses collaborateurs ont fait une étude complète du grand problème des transferts thermiques de grappes de barres, avec assemblage soit fermé soit ouvert, dans un écoulement parallèle de métaux

liquides. Dans leurs équations (18) et (19), tirées de résultats expérimentaux pour ces deux cas, le nombre de Nusselt est donné par la même fonction du nombre de Péclet dans toute la gamme de ce dernier nombre qui a été étudiée. Cela s'écarte des résultats obtenus à Brookhaven sur des grappes de barreaux en quinconce avec du mercure et du NaK (illustré par les résultats représentés graphiquement à la figure 7 du mémoire P/225) tant que le contact thermique est bon entre le courant de métal et la surface d'échange de chaleur.

Je pense que, pour les nombres de Péclet du domaine de faible turbulence, l'équation (19) du mémoire de M. Subbotin donnerait sans doute des nombres de Nusselt inférieurs à ceux obtenus avec la conduction moléculaire seule; cela ne pourrait s'expliquer que par un défaut de contact thermique à la surface des barreaux dans un tel écoulement.

V. I. SUBBOTIN (URSS): Les résultats des expériences de M. Dwyer sur les transferts thermiques de grappes de barreaux dans un écoulement longitudinal sont en bon accord avec les nôtres pour $Pe > 500$. Lorsque $Pe < 500$ il y a des divergences qui croissent à mesure que Pe décroît. L'une des raisons de ce désaccord est peut-être la propagation longitudinale de la chaleur, dont la valeur augmente lorsque les nombres de Péclet diminuent.

Il est difficile d'expliquer le désaccord par des phénomènes de contact. Dans nos essais, la pureté était contrôlée systématiquement et les impuretés ne dépassaient jamais $10^{-3}\%$ en poids. Une comparaison entre nos résultats et ceux de M. Dwyer mène à la conclusion que nous avons dû avoir quelque encrassement sur la paroi chauffante.

N. I. BULEEV (URSS): Je voudrais soulever une question à laquelle on n'a guère prêté attention dans la littérature sur l'hydraulique et les transferts thermiques dans des canaux.

Lorsqu'on compare les résultats de calculs théoriques concernant les coefficients de viscosité turbulente et de conductivité thermique avec les données expérimentales, on ne compare pas en fait les mêmes choses.

Les expressions $\rho \epsilon_M \frac{\partial \omega}{\partial r}$ et $\rho \epsilon_H \frac{\partial T}{\partial r}$, où $\epsilon_M = l_1^2 \left| \frac{\partial \omega}{\partial r} \right|$ et $\epsilon_H = l_T^2 \left| \frac{\partial \omega}{\partial r} \right|$, qui figurent dans les expressions initiales du mouvement thermique et de l'écoulement, ne sont que les composantes principales de l'effort turbulent et du flux thermique turbulent. En ce sens, les équations théoriques initiales sont approchées.

Par contre, dans le cas des données expérimentales, comme les résultats proviennent des mesures de profils de vitesses et de températures, ce sont les valeurs complètes que l'on obtient pour les efforts et les flux thermiques turbulents.

Si, dans les expériences, on met les valeurs obtenues pour $\overline{pr'\omega'}$ et $\overline{pr'T'}$ sous la forme $\rho \epsilon_M^* (\partial \omega / \partial r)$ et $\rho \epsilon_H^* (\partial T / \partial r)$, d'où l'on tire les valeurs ϵ_M^* , ϵ_H^* (par définition de ces valeurs) et le rapport $\epsilon_H^* / \epsilon_M^*$, ces

valeurs n'auront pas exactement le même sens que ϵ_M , ϵ_H et ϵ_H/ϵ_M , et n'en seront qu'approchées — à quelques douzaines d'unités pour cent.

A mon avis, quand on recherche les valeurs ϵ_M , ϵ_H et ϵ_H/ϵ_M , il est essentiel d'utiliser un seul modèle théorique pour le moment et le transfert thermique turbulent.

V. I. SUBBOTIN (URSS): Dans les calculs, la tradition est de prendre la valeur du coefficient de viscosité turbulente (ϵ_T), puis, à partir de la valeur, quelle qu'elle soit, utilisée pour le nombre de Prandtl en turbulence (ϵ), de déterminer le coefficient de conductivité thermique turbulente (ϵ_a). Cette méthode se comprenait au temps où les expériences portaient sur les mesures de champs de vitesses et où il n'y avait pas d'expérience sûre pour la mesure de champs de température. Aujourd'hui, cependant, il est possible de trouver ϵ_a directement et d'introduire sa valeur dans les expressions correspondantes.

O. E. DWYER (Etats-Unis d'Amérique): La plupart du temps, les profils de vitesses peuvent se calculer avec une précision bien meilleure que les profils de températures; et comme on peut maintenant traduire avec quelque confiance les valeurs ϵ_M en valeurs ϵ_H , pour l'écoulement dans un canal, je crois donc plus souvent préférable le chemin $\epsilon_M \rightarrow \epsilon_H \rightarrow Nu$ pour évaluer les coefficients de transfert thermique dans la plupart des situations nouvelles.

Mémoire P/135 (présenté par C. Cunningham)

DISCUSSION

J. PELCE (France): Des travaux tout à fait semblables ont été menés dans les laboratoires du CEA, mais, pour nous, l'effort a porté sur des éléments avec ailettes en chevrons. Cependant, le but poursuivi et les méthodes utilisées sont tout à fait semblables.

Nous avons eu le souci d'étudier les caractéristiques thermiques et les pertes de charges d'un grand nombre de dispositions d'ailettes, en vue d'établir une formulation utilisable dans les calculs d'optimisation de réacteurs. La documentation sur ces travaux est à la disposition de tous les intéressés.

Nous avons aussi étudié dans le détail le comportement thermique des gaines choisies pour des réacteurs donnés, comme EDF2 et EDF3. Nous avons prêté une attention particulière aux singularités thermiques sur des trains de gaines simulant au mieux la géométrie en pile, en régime nominal (nous avons étudié en particulier les décalages angulaires entre éléments). Nous avons aussi étudié l'influence des faibles débits en courants gazeux ascendants (EDF3) et descendants (EDF4), ainsi que l'influence de déformations d'ailettes.

Tous ces essais ont été effectués sur maquette à l'échelle réelle ou à une échelle plus grande. Nos conclusions sont, dans l'ensemble, conformes à celles exposées dans les mémoires P/135 et P/136. Bon

nombre de nos résultats sont donnés dans les rapports CEA n^{os} 2469 et 2470.

A propos du mémoire P/135, je voudrais poser deux questions. D'abord, dans les essais à faible débit, le courant était-il ascendant ou descendant, et de plus, avec quelle précision estimez-vous connaître vos résultats? Deuxièmement, avez-vous fait les mêmes études détaillées sur des gaines à plus de quatre secteurs?

C. CUNNINGHAM (Royaume-Uni): Les résultats des essais à faible débit mentionnés dans le mémoire sont pour un courant ascendant. Il est impossible de bien répondre à la question de la précision. Dans la mesure où l'on peut généraliser, l'écart type dans nos essais de transferts thermiques peut se placer autour de 2%. Pour répondre à votre seconde question, je dirai que nous n'avons pas fait d'étude détaillée d'éléments à chevrons avec plus de quatre secteurs.

W. L. GRANT (Afrique du Sud): Les figures 1 E et 2 E montrent les variations du transfert thermique avec l'orientation relative des éléments. Ces variations sont-elles les mêmes pour les deux dispositions, verticale et horizontale, des canaux d'éléments combustibles?

C. CUNNINGHAM (Royaume-Uni): Nous n'avons fait aucun essai d'orientation dans des canaux verticaux. Cependant, dans tous nos autres essais avec nombres de Reynolds élevés, nous n'avons pu voir de différence due à la hauteur des canaux, ce qui se comprend aisément car les effets de poussée sont sans importance.

Mémoire P/719 (présenté par V. B. Nesterenko)

DISCUSSION

Y. EL-MESHAD (République arabe unie): Je voudrais demander à M. Nesterenko de nous indiquer s'il est possible d'utiliser sa méthode de moyenne, a) en tenant compte du matériau de gainage ou, en général, pour des éléments combustibles à plusieurs couches, et b) en tenant compte de la propagation de la chaleur suivant l'axe le long du matériau combustible?

V. B. NESTERENKO (URSS): Avec des méthodes d'approximation, on peut tenir compte de la résistance thermique de la gaine du combustible dans le coefficient de transfert thermique que nous mentionnons. Dans cette étude, on n'a pas tenu compte de la propagation de la chaleur le long de l'élément dans le cas d'un gaz, à cause de la faible valeur de la grandeur en question.

Mémoire P/552 (présenté par R. Negrini)

DISCUSSION

Ce mémoire n'a pas fait l'objet d'une discussion distincte.

Теплообмен

Председатель: П. Е. Новаски (Польша)

Доклад Р/580 (представил К. Торикаи)

ДИСКУССИЯ

С. С. КУТАТЕЛАДЗЕ (СССР): Хотя процессы конвективного теплообмена в тех реакторах, которые мы обсуждаем, тесно связаны даже в случае жидких металлов с процессами турбулентного переноса, не было разработано никаких достаточно точных методов для определения коэффициентов турбулентного переноса в пределах конечных чисел Рейнольдса. Однако представлялось возможным — и это очень важно — получить для потоков с «исчезающей» вязкостью ($\mu \rightarrow 0$), то есть для $Re \rightarrow \infty$, ряд асимптотических решений, свободных от эмпирических констант. Новые асимптотические решения могут также быть получены для различных важных случаев теплообмена при кипении.

Так, не говоря уже о моем уравнении для $q_{\text{крит}}$ при кипении в большом объеме, приведенном в докладе г-на Торикаи, можно также получить формулу для очень высоких скоростей потока жидкости ω_0 и $T \leq T''$:

$$q_{\text{крит}} = \varphi^* (1 - \varphi^*) \frac{C_f}{2} r \omega_0 \sqrt{\gamma' \gamma''} \left(1 + C \sqrt{\frac{\gamma''}{\gamma'}} \frac{C_p \Delta T}{r} \right),$$

где φ^* — паросодержание вблизи стенки; C_f — коэффициент трения; r — скрытая теплота парообразования; C — постоянная. Остальные обозначения общепринятые.

Уравнение (13) в докладе г-на Торикаи близко к этому решению для $C_p \Delta T \gg r$.

Что касается аналогии между кипением и барботажем, то я хотел бы обратить внимание на то, что экспериментальные результаты, полученные г-ном Торикаи, в принципе подобны результатам, полученным нами в СССР, а также Сполдингем в Великобритании.

Другой проблемой, которую следует иметь в виду, является молекулярный вес газа.

Доклад Р/326 (представил Н. И. Булеев)

ДИСКУССИЯ

О. Е. ДВАЙЕР (США): Я хотел бы выразить удовлетворение обстоятельным докладом д-ра

Осмачкина. Особенно интересно описание продольного обтекания жидкими металлами пучков стержней. Несколько лет назад в Брукхейвенской национальной лаборатории мы получили аналитическое решение этой задачи, в котором мы предположили, что радиальное распределение скоростей по отношению к данной стержню было тем же, что и во внутренней части кольцевого зазора, имеющего тот же внутренний радиус, тот же радиус максимума скорости и ту же среднюю скорость во внутренней части. Казалось, что это было предпочтительнее, чем основывать профиль скоростей на распределении скоростей при течении в трубах. На этом заседании я сделал сопоставление, которое показывает, что рис. 9 в докладе д-ра Осмачкина довольно хорошо согласуется с уравнением 2 в докладе Р/225, если использовать константы из табл. 3 этого доклада и принять $\bar{\psi} = 1$. Константы основаны на кольцевой модели.

При низких числах Re , мы полагаем, что Nu почти не зависит от Re . При отношении шага к диаметру, например, 1,7 мы пришли к выводу, что при ниже $Re \approx 700$ вклад турбулентности в полную теплопроводность пренебрежимо мал, так что основным процессом остается молекулярная теплопроводность.

Выше $Re \approx 700$ вклад турбулентности становится все более важным, достигая при $Re \approx 10^4$ значения, близкого к единице. Таким образом, чем выше число Пекле, тем с большей точностью надо определять ν_T .

Доклад Р/16 (представил А. Д. Лейн)

ДИСКУССИЯ

Х. С. ИСБИН (США): Проводили ли Вы опыты, которые позволили бы Вам определить влияние эксцентрического расположения экспериментальных участков?

А. Д. ЛЕЙН (Канада): Нет. Однако мы наеемся провести исследования по дистанционированию.

Х. С. ИСБИН (США): Когда Вы оцениваете передачу тепла излучением от окисированных циркуловых покрытий, какие значения излучательной способности поверхностей Вы используете?

А. Д. ЛЕЙН (Канада): Мы не пытались оценить излучение оксидированных циркалоевых покрытий по двум причинам. Прежде всего, в случае, когда происходил изгиб за счет термических напряжений и наблюдалась заметная коррозия, температуры определялись по показаниям термопар на элементах из нержавеющей стали, помещенных в подобные условия, а также путем обследования степени коррозии покрытия. Во-вторых, при нормальной работе температура окружения экспериментального участка была одинакова внутри и вне реактора и немного ниже температуры топливного покрытия.

В. И. СУББОТИН (СССР): У меня есть одно замечание в связи с этим докладом. Пережог не происходит одинаковым образом при высоких и при низких давлениях. При высоких давлениях не происходит большого увеличения температуры тепловыделяющей стенки при пережоге. Мне кажется, что в ряде случаев это могло бы быть источником ошибки при экспериментальном определении $q_{\text{крит}}$.

Доклад Р/224

ДИСКУССИЯ

К. М. БЕККЕР (Швеция): На рис. 13 доклада показано сравнение разных расчетных формул с данными, полученными в Колумбийском университете. Из этого сопоставления представляется, что формула Беккера—Перссона неудовлетворительна с точки зрения предсказания условий кризиса теплообмена. В статье (К. М. Беккер АВ Atomenergi Studsvik, Швеция), которая должна быть опубликована в октябре — ноябре 1964 г., мы показали, что эта формула предсказывает с точностью в $\pm 5\%$ критические тепловые потоки для приблизительно 3000 экспериментов по кризису теплообмена, осуществленных в Швеции, при следующих изменениях параметров:

$$\begin{array}{r} 2,7 < p < 91 \text{ кг/см}^2 \\ 100 < G < 3500 \text{ кг/см}^2 \cdot \text{сек} \\ 35 < q/A < 600 \text{ вт/см}^2 \\ 0,05 < X < 1,00 \\ 4 < d < 13 \text{ мм} \\ 600 < L < 3500 \text{ мм} \end{array}$$

Полагаю, что смогу объяснить, почему расчеты по нашей формуле выглядят так плохо на рис. 13.

Наше рассмотрение, основанное на модели Вандеруотера — Исбина, включает в себя две константы ϵ и b , которые представляют скорости поперечного перемещения и диффузии капель и должны определяться из экспериментальных данных. Когда наша работа была написана (около двух лет назад), имевшиеся в Шве-

ции данные по критическим нагрузкам были получены в опытах только до 40 кг/см^2 , и константы ϵ и b были определены с использованием данных CISE (К. М. Беккер и Р. Перссон, Анализ критических тепловых нагрузок для потока кипящей воды в вертикальных круглых каналах, представлен в ASME № 63-WA-51). Для того чтобы получить эти данные, на вход экспериментального участка подавалась паро-водяная смесь. Как мы уже отмечали в нашей работе, расчетная формула не может считаться надежной, когда ею пользуются для определения условий кризиса в каналах с недогревом воды на входе. Упомянутая мной работа содержит новые значения ϵ и b , которыми можно пользоваться при более высоких давлениях.

На рис. 1 представлены данные из рис. 13 доклада Леви после подстановки правильных значений ϵ и b в формулу Беккера — Перссона.

Можно заметить, что согласие между данными Колумбийского университета и расчетом по нашей формуле теперь вполне удовлетворительное. Это можно показать еще более ясно, если использовать некоторые данные, представленные на рис. 2 в докладе Леви. Сравнение дано на рис. 2.

Надо ожидать повышенного разброса при малом паросодержании из-за того, что формула основана на модели жидкой пленки, движущейся по стенке канала. Если предположить, что b зависит от паросодержания, то разброс, показанный на рис. 2 при низком паросодержании, может быть заметно уменьшен.

Наконец, на рис. 3 наша формула сравнивается с шведскими данными и данными Колумбийского университета для давления около 50 кг/см^2 .

Можно заметить, что здесь также наблюдается прекрасное согласие между экспериментальными данными и расчетами по нашей формуле.

Доклад Р/93 (представил Ж. Вильнёв)

ДИСКУССИЯ

В. М. КЭМПБЕЛЛ (Канада): Мы в Канаде также изучали образование загрязнений теплоотдающих поверхностей, но наши результаты отличаются от изложенных в докладе. Однако на самом деле несоответствия нет. Мы используем следующий процесс.

Теплоноситель тщательно обрабатывают адсорбирующей глиной Attapulgis и фильтруют для того, чтобы удалить все механические примеси (органические и неорганические); компоненты, способствующие органическому загрязнению, по существу отсутствуют.

При этих условиях мы нашли, как это и описано в докладе Р/15, что Si способствует загрязнению теплоотдающих поверхностей посредством переноса продуктов его взаимодейст-

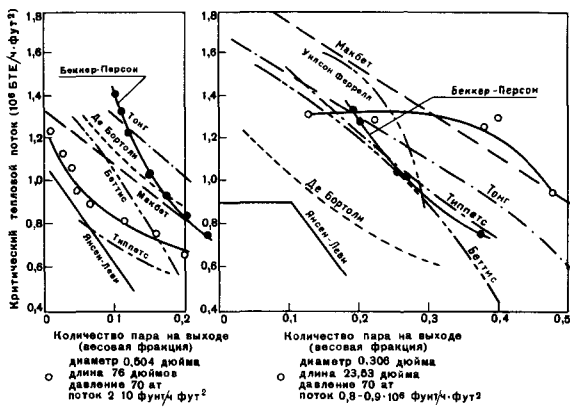


Рис. 1. Сравнение метода корреляций с данными по критическому тепловому потоку в опытном отрезке трубы. Расчеты выполнены для потока $0,85 \cdot 10^6 \text{ фунт/ч} \cdot \text{фут}^2$

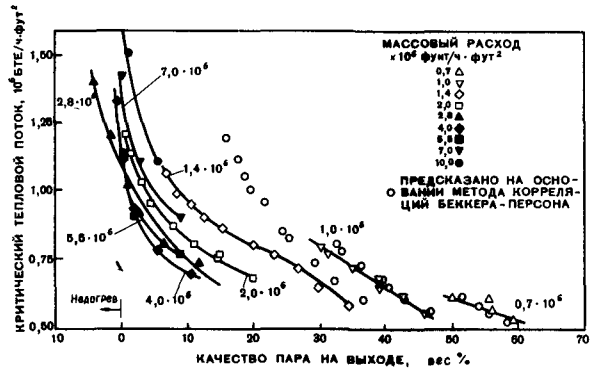


Рис. 2. Условия критического теплового потока в опытном отрезке трубы. Внутренний диаметр трубы 0,504 дюйма, длина трубы в состоянии нагрева 76 дюймов, давление 70 ат

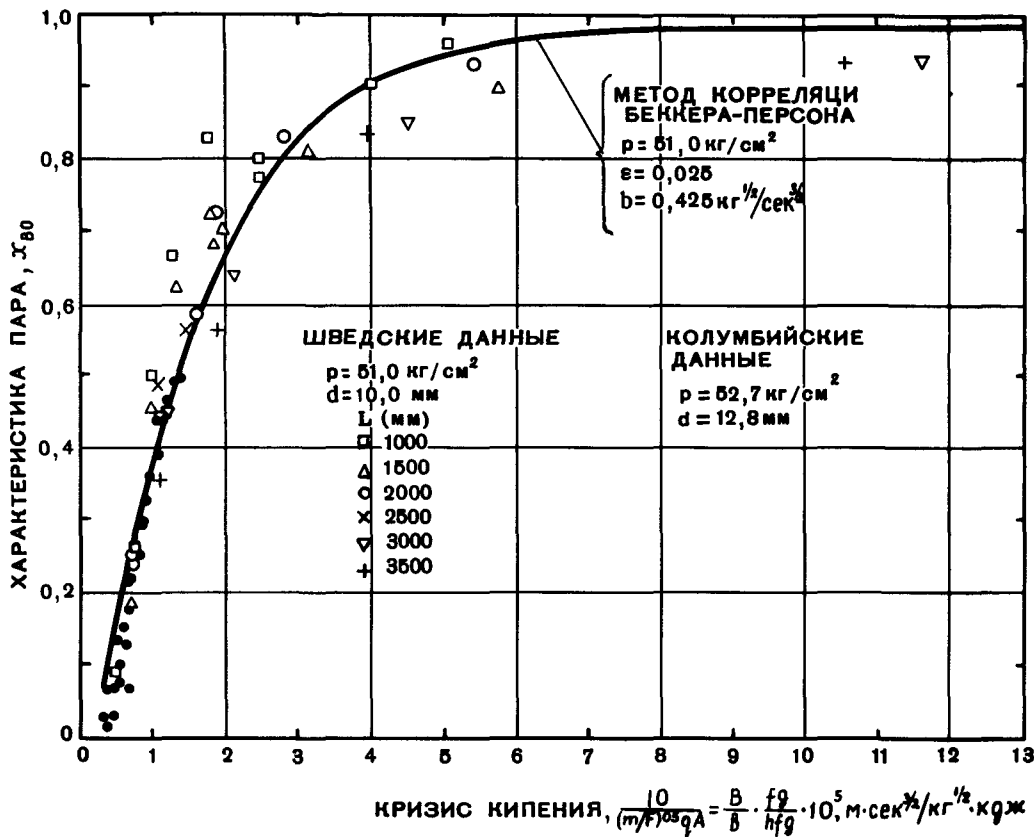


Рис. 3. Сравнение экспериментальных и расчетных данных по условиям кризиса кипения

вия с железом в контуре и что форма, в которой Cl присутствует, очень важна. Например, треххлористый этилен более эффективно способствует развитию процесса, чем хлористый дифенил. Нам кажется, что добавляемое соединение Cl должно разлагаться, образуя «активное» хлористое соединение, до сих пор не опознанное. Так, если в опытах используется стабильное хлористое соединение, о действии Cl может быть сделан неправильный вывод.

Я полагаю, что в случае, описанном в докладе P/93, результат опыта было трудно выявить из-за наличия весьма высокого органического загрязнения и из-за стабильности добавляемого органического соединения Cl.

Я хотел бы также обратить внимание на один из наших опытов, проведенных на реакторной петле X-7, при котором не было обнаружено почти никакого загрязнения на поверхностях тепловыделяющих элементов, работавших при температуре 450—500° C в течение 82 дней (0,1 мг/см² · ч).

Ж. ВИЛЬНЁВ (Франция): Я согласен, что Cl оказывает различное влияние в зависимости от того, в какой форме он находится в контуре. В нашем контуре мы использовали терфенил-ОМ2, полученный в результате полимеризации бензола, хлорированного по ошибке. Таким образом, использовавшееся вещество содержало связанный Cl, который не влияет на образование загрязнений. Однако через некоторое время должно последовать его соединение с Fe в контуре и загрязнение посредством переноса. В наших экспериментах мы всегда находили ярко выраженный порог при 500° C, выше этой температуры происходит местный пиролиз, в результате которого образуется пленка, состоящая из мягкого вещества, удерживающегося на нагреваемой стенке.

Л. С. ДЗУНГ (Швейцария): В каком диапазоне находились числа Прандтля для охлаждающих сред в этом эксперименте?

Ж. ВИЛЬНЁВ (Франция): Число Прандтля изменялось от 5 до 12.

Л. С. ДЗУНГ (Швейцария): Я вижу, что формула, приведенная в этом докладе, имеет ту же структуру, что и классическое соотношение, впервые предложенное Колборном в 1930 году. Мне было бы интересно узнать, чем в самом деле Ваша формула отличается от классической. Мне кажется, что механизм теплопередачи зависит главным образом от физических свойств среды, которые характеризуются числами Прандтля и Рейнольдса. Химические свойства не играют большой роли. Поэтому формула в докладе должна быть применимой к средам, отличным от органических жидкостей, если только число Прандтля лежит в соответствующих пределах.

Ж. ВИЛЬНЁВ (Франция): Найденная нами формула отличается от классических, например от формулы Колборна, тем, что показатель сте-

пени при числе Рейнольдса равен 0,9. Как уже отмечалось (см. ссылку¹ в докладе), показатель степени при числе Рейнольдса увеличивается при увеличении числа Прандтля. Воспользовавшись полутеоретическим расчетом Мартинелли для нашего случая, мы получили для показателя степени значение 0,9.

Доклад P/53 (представил П. Левек)

ДИСКУССИЯ

Р. Ф. С. РОБЕРТСОН (Канада): Мы в Канаде очень интересуемся механизмом, предложенным Левеком в этом докладе. У нас есть основания полагать, что представления, основанные на комбинации чистого радиолиза, не зависящего от ЛПЭ, температуры, пиролиза и от мощности дозы, может быть примитивным упрощением. В случае облучения капсул, проведенного на реакторе NPX (упомянутом в нашем докладе P/15), мы нашли как для орто-, так и для метатерфенила, что выходы реакций как функция температуры почти одинаковы для мощностей доз 0,1 и 0,3 вт/г. Механизм, предложенный д-ром Левеком, не смог бы предсказать такой результат. Однако мы согласны, что по крайней мере в случае метатерфенила, подвергнутого радиолизу, скорость пиролиза значительно выше скорости пиролиза без облучения. Наши результаты указывают, что быстрые нейтроны обладают более сильной разрушающей способностью, чем γ -частицы и G_n/G_γ равно примерно 3 при температурах ниже 375° C.

Доклады P/225 (представил О. Е. Двайер) и P/328 (представил В. И. Субботин)

(Эти доклады обсуждались совместно)

ДИСКУССИЯ

Л. С. ДЗУНГ (Швейцария): Во-первых, я хочу поздравить авторов доклада P/225, наиболее полно подводящего итог всем сведениям, касающимся теплоотдачи к жидкостям с низким числом Прандтля.

Мое замечание относится к рис. 1, на котором для некоторых кривых график турбулентной вязкости ϵ_M имеет выгиб на участке между двумя стенками. Поскольку этот участок характеризуется нулевым градиентом скорости, то поток локально однороден. Таким образом, физически турбулентная вязкость также должна иметь на этом участке производную, равную нулю, то есть не должно быть никакого выгиба на графике. Интересно узнать мнение г-на Двайера по этому поводу.

О. Е. ДВАЙЕР (США): Турбулентная вязкость в заданной точке поперечного сечения канала зависит главным образом от полного касательного напряжения и от крутизны профиля скорости в этой точке. Так как для радиуса, где скорость максимальна, эти величины равны нулю, нельзя определить турбулентную вязкость в этой точке. Однако кривая зависимости ϵ_M от $(r - r_1/r_2 - r_1)$ для кольцевого зазора должна быть дифференцируема во всех точках и должна иметь первую производную, равную нулю, для радиуса, где скорость максимальна. Кривая b на рис. 1, с которой авторы предпочитают работать, удовлетворяет этим требованиям. Имеется достаточно экспериментальных доказательств, указывающих на то, что профиль a на рис. 1 очень маловероятен. Кроме того, упрощенный профиль скорости в центральной части кольцевого зазора не означает, что турбулентная вязкость в этой области также должна слабо изменяться.

П. ГИЛЛИ (Австрия): Я хотел бы сделать замечание и задать вопрос по докладу г-на Двайера. Я хотел бы особенно остановиться на теплоотдаче к жидким металлам при поперечном обтекании пучков труб, что может соответствовать теплообменнику или парогенератору для атомной электростанции с реактором, охлаждаемым жидким металлом. Мне кажется возможным объединить обе формулы, приведенные автором для числа Нуссельта в случае поперечного обтекания, а именно эмпирическое уравнение [уравнение (4)] Риккарда, Двайера и Дропкина (ссылка ²⁵ в докладе) и теоретическую формулу [уравнения (5) и (6)], приводимую Хсю*. У каждой из этих формул есть интересные особенности. Уравнение (4) использует постоянное число 4,03 в добавление к степенной функции от числа Пекле и, таким образом, очевидно, учитывает молекулярную теплопроводность. Однако эта формула была получена только для одного конкретного расположения труб. С другой стороны, из-за введения Φ_1/D разности потенциалов скоростей между точками набегания и застоя уравнения (5) и (6) справедливы для разных расположений труб, но не учитывают молекулярную теплопроводность. Так, число Нуссельта, согласно этой формуле, обращается в нуль при нулевом значении числа Пекле.

Нетрудно объединить обе формулы. Пришлось бы заменить коэффициент 0,958 в уравнениях (5) и (6) или же этот коэффициент и показатель степени числа Пекле и Φ_1/D таким образом, чтобы при добавлении константы 4,03 Nu согласовывался с результатами экспериментов. Одним из способов осуществления этого было бы

снижение коэффициента примерно на 10—20%. Другим возможным способом была бы подставка в уравнение (4) функции Φ_1/D и подходящим образом выбранного коэффициента вместо коэффициента 0,228. Таким образом, была бы получена более общая и более удовлетворительная формула для случая поперечного обтекания жидкими металлами пучков труб, которая также была бы справедливой для малых чисел Пекле и для различного расположения труб.

Теперь по поводу моего вопроса, относящегося к значениям Φ_1/D , вычисленным в докладе Хсю, на который я уже ссылался. Эти значения Φ_1/D относятся только к случаям расположения труб в узлах квадратной и треугольной решеток. Были ли в Брукхейвенской национальной лаборатории или где-либо еще вычислены по методу Хсю значения Φ_1/D для других решеток?

О. Е. ДВАЙЕР (США): Уравнение (4) представляет собой эмпирическое соотношение, основанное на результатах экспериментов с одним пучком труб, а именно характеризующимся величиной P/D , равной 1,38. Оно дает кривую зависимости Nu от Pe , у которой наклон возрастает с Pe . Однако, поскольку уравнения (5) и (6) основываются на предположении о невязком потоке, они дают прямую линию на графике зависимости Nu от Pe . Таким образом, уравнения (4) и (5) дают разные результаты в области низких Pe . Поэтому очевидно, что уравнения (5) и (6) не могут применяться при крайних значениях Пекле, в отличие от уравнения (4). Видоизмененное уравнение (5), согласующееся с характеристиками уравнения (4), могло бы, как предлагает д-р Гилли, быть использовано для определения коэффициентов теплопередачи при поперечном течении в условиях, отличающихся от условий, для которых были получены уравнения (4) и (5). Что касается существования значений Φ_1/D , я знаю только те, что были опубликованы в работах ^{27, 30}.

Что касается другого доклада, то следует заметить, что мы в США знаем, что д-р Субботин и его сотрудники в Физико-энергетическом институте в СССР провели в последние годы обширную и качественную работу в области теплоотдачи к жидким металлам. Полученные ими результаты явились ценным вкладом в наши современные знания по этому вопросу.

Для нас, работающих в той же области в США, было важно отмечать время от времени, что существует значительное согласие в исследованиях, проводившихся в обоих странах независимо друг от друга.

Для того чтобы углубить наши знания о теплоотдаче в жидких металлах, надо иметь больше сведений о природе турбулентного переноса и его вклада в суммарный механизм теплоотдачи, также нужен более точный способ расчета турбулентной вязкости. Поэтому очень важной

* По сообщению Гилла, доклад Хсю был опубликован в журнале Int. J. Heat Mass Transfer, 7, No. 4, 431—446 (1964).

является работа, описанная д-ром Субботиным по измерениям корреляций флуктуаций локальной температуры в потоке жидкого металла.

Д-р Субботин и его сотрудники глубоко изучили важную проблему передачи тепла от пучков труб к потоку жидких металлов при продольном обтекании как плотных, так и раздвинутых пучков. В их уравнениях (18) и (19), основывающихся на результатах экспериментов соответственно для этих двух случаев, показано, что число Нуссельта одинаково зависит от числа Пекле во всем исследованном диапазоне Пекле. Это не согласуется с результатами, полученными в Брукхейвене для пучков труб, расположенных в шахматном порядке как для ртути, так и для NaK (что видно из результатов, приведенных на рис. 7 доклада Р/225), если только существует хороший тепловой контакт между текущим металлом и теплоотдающей поверхностью.

Я думаю, что для чисел Пекле, соответствующих слабой турбулентности, уравнение (19) в докладе д-ра Субботина, возможно, даст числа Нуссельта меньшие, чем при учете только молекулярной теплопроводности; при таких условиях потока это может быть объяснено только отсутствием хорошего теплового контакта на поверхности стержней.

В. И. СУББОТИН (СССР): Результаты экспериментов г-на Двайера по теплопередаче при продольном обтекании пучков стержней находятся в хорошем согласии с нашими при $Re > 500$. При $Re < 500$ видны расхождения, которые увеличиваются с уменьшением чисел Re . Одной из причин для этого расхождения могут быть аксиальные перетечки тепла, которые увеличиваются с уменьшением чисел Re .

Трудно объяснить расхождение плохим тепловым контактом. В наших экспериментах чистота систематически проверялась и загрязнения никогда не превышали 10^{-3} вес. %. Сравнение наших экспериментов с опытами г-на Двайера позволяет все же сделать заключение о том, что, должно быть, у нас были загрязнения на теплоотдающей стенке.

Н. И. БУЛЕЕВ (СССР): Я хотел бы затронуть вопрос, которому до сих пор уделялось мало внимания в литературе, по гидравлике и теплопередаче в каналах.

Когда мы сравниваем результаты теоретических вычислений, относящихся к коэффициентам турбулентной вязкости и температуропроводности, с экспериментальными данными, мы в действительности не сравниваем одинаковые понятия. Выражения $re_M \frac{\partial \omega}{\partial r}$ и $re_H \frac{\partial T}{\partial r}$, где

$\epsilon_M = l_v^2 \frac{\partial \omega}{\partial n}$ и $\epsilon_H = l_r^2 \frac{\partial \omega}{\partial n}$, которые фигурируют в начальных выражениях для переноса тепла и количества движения, являются только главными составляющими турбулентного напряжения и турбулентного потока тепла. В этом смы-

сле исходные теоретические уравнения являются приближенными. Однако в случае экспериментальных данных, когда результаты основаны на измеренных распределениях скорости и температуры, для турбулентных напряжений и тепловых потоков получаются полные значения.

Если в экспериментальной работе мы представим значения, полученные для величин $\overline{r\omega' \omega'}$ и $\overline{r\omega' T'}$, в форме $re_M^* \frac{\partial \omega}{\partial r}$ и $re_H^* \frac{\partial T}{\partial r}$ и затем находим значения ϵ_M^* , ϵ_H^* (формальные значения) и отношение $\epsilon_H^*/\epsilon_M^*$, тогда эти величины не будут иметь точно то же значение, что и ϵ_M , ϵ_H и ϵ_H/ϵ_M и могут отличаться от них на более чем $10^0/0$. По-моему, когда мы исследуем значения ϵ_M , ϵ_H и ϵ_H/ϵ_M , очень важно пользоваться какой-нибудь одной теоретической моделью для турбулентного переноса импульса и тепла.

В. И. СУББОТИН (СССР): Обычно на практике при вычислениях берут значение коэффициента турбулентной вязкости (ϵ_t) и затем, на основе каждого конкретного значения турбулентного числа Прандтля (ϵ), находят коэффициент турбулентной теплопроводности (ϵ_a). Такой подход был понятен в те дни, когда в опытах измерялись поля скоростей и не было надежных экспериментов по измерению полей температур. Однако в настоящее время можно находить непосредственно ϵ_a и подставлять эту величину в соответствующие выражения.

О. Е. ДВАЙЕР (США): В большинстве случаев распределения скоростей могут быть предсказаны со значительно большей точностью, чем распределения температур, и, так как можно довольно уверенно перевести значения ϵ_M в значения ϵ_H , я поэтому думаю, что последовательность $\epsilon_M \rightarrow \epsilon_H \rightarrow Nu$ более подходит для определения коэффициентов теплоотдачи в большинстве вновь встречающихся случаев.

Доклад Р/135 (представил К. Каннингэм)

ДИСКУССИЯ

Ж. ПЕЛС (Франция): Очень похожая работа проводится в лабораториях Комиссариата по атомной энергии Франции, но в нашем случае основное внимание уделялось элементам с оребрением в форме шипов. Мы старались разрешить те же проблемы и использовали те же методы. Мы много работали над изучением тепловых характеристик и перепадов давления для самых различных видов оребрения, стараясь получить формулы, пригодные для использования в расчетах по оптимизации реакторов. Если кто-нибудь заинтересуется детальным описанием этой работы, он сможет его получить.

Мы также провели подробные опыты по изучению тепловых характеристик оболочек, выбранных для конкретных реакторов, таких как EDF-2 и EDF-3.

Исключительное внимание уделялось особенностям тепловых свойств полных сборок, размещенных в том же порядке, что и в реакторе при работе на номинальных параметрах (причем, особенно тщательно изучалась проблема углового смещения элементов). Мы также изучали влияние малых скоростей потоков для случаев с восходящим (EDF-3) и нисходящим (EDF-4) потоками газа, а также формы деформированных оболочек.

Все эти опыты проводились на моделях в натуральную величину или увеличенных моделях. Наши выводы в значительной степени согласуются с выводами, приведенными в докладах P/135 и P/136. Сведения о наших результатах содержатся в докладах P/2469 и P/2470 Комиссариата по атомной энергии Франции.

В связи с докладом P/135 я хочу задать два вопроса. Во-первых, в описанных опытах газ двигался вверх или вниз? А также не могли бы Вы указать нам примерную точность Ваших результатов? Во-вторых, проводили ли Вы подробные исследования с оболочками, имеющими более чем четыре сектора?

К. КАННИНГЭМ (Соединенное Королевство): Результаты опытов с низкими потоками, описанные в докладе, относятся к восходящему потоку. Точный ответ на вопрос о точности дать нельзя. В той степени, в какой можно дать такой ответ, исходя из общих рассуждений, среднее квадратичное отклонение в наших опытах по передаче тепла может быть оценено примерно в 2%. Что касается Вашего второго вопроса, то мы не проводили подробных исследований

элементов с оребрением в виде шипов, имеющими более чем четыре сектора.

В. Л. ГРАНТ (ЮАР): Рис. 1Е и 2Е показывают изменение теплопередачи в зависимости от относительной ориентации элемента. Является ли это изменение одинаковым как для вертикального, так и для горизонтального канала?

К. КАННИНГЭМ (Соединенное Королевство): Мы не проводили никаких опытов по ориентации элементов в вертикальных каналах. Однако во всех других наших опытах при высоких числах Рейнольдса мы не смогли заметить различия из-за различного положения по высоте канала. Это легко понять, ибо влияние плавучести несущественно.

Доклад P/719 (представил В. Б. Нестеренко)

ДИСКУССИЯ

И. ЭЛЬ-МЕСХАД: Г-н Нестеренко, не могли бы Вы рассказать нам о возможности использования вашего способа усреднения: а) при учете оболочки или в общем для многослойных твэлов и б) при учете аксиального потока тепла по топливу?

В. Б. НЕСТЕРЕНКО (СССР): Используя приближенные методы, можно внести поправку на термическое сопротивление оболочки твэла в приведенный нами коэффициент теплопередачи. В этом исследовании применительно к течению газа поток тепла вдоль элемента не учитывался из-за его малости.

Доклад P/552 (представил Р. Негрини)

Этот доклад отдельно не обсуждался.

Acta de la Sesión I. 10

Transmisión de calor

Presidente: P. J. Nowacki (Polonia)

Documento P/580 (presentado por K. Torikai)

DISCUSIÓN

S. S. KUTATELADZE (URSS): Aun cuando los procesos de transmisión de calor por convección, en el tipo de reactor que estamos discutiendo, están muy relacionados, incluso en el caso de los metales líquidos, con los fenómenos de transferencia turbulenta, no se ha desarrollado ningún método suficientemente preciso para determinar los coeficientes de transmisión de calor en régimen turbulento, en el intervalo de valores finitos del número de Reynolds. Sin embargo (y esto tiene importancia) se ha podido obtener, para flujos de viscosidad «decreciente» ($\mu \rightarrow 0$), es decir, para $Re \rightarrow \infty$, una serie de soluciones asintóticas en las que no intervienen constantes empíricas. Se pueden obtener también otras soluciones asintóticas para diversos casos importantes de transmisión de calor con ebullición.

De esta manera, además de mi ecuación para q_{BO} en régimen de ebullición y convección libre, citada en la memoria del Sr. Torikai, también se puede obtener una fórmula para el caso de flujo de líquidos a velocidades muy grandes ω_0 y $T \ll T''$:

$$q_{BO} = \phi^*(1 - \phi^*) \frac{C_f}{2} r \omega_0 \sqrt{\gamma' \gamma''} \left(1 + C \sqrt{\frac{\gamma''}{\gamma'}} \frac{C_p \Delta T}{r} \right)$$

donde ϕ^* = fracción de vapor de la región adyacente a la pared

C_f = coeficiente de rozamiento

r = calor latente de ebullición

C = constante

Los demás símbolos son los adoptados normalmente.

La fórmula (13) de la memoria de Torikai es parecida a esta solución cuando $C_p \Delta T \gg r$.

Me gustaría también llamar la atención sobre el hecho de que, en lo que se refiere a la analogía entre la ebullición y el burbujeo, los resultados experimentales de Torikai son, en principio, semejantes a los resultados que hemos obtenido nosotros en la URSS y también a los obtenidos por Spalding en Inglaterra.

Otra cuestión que hay que tener en cuenta es el peso molecular del gas.

Documento P/326 (presentado por N. I. Buleev)

DISCUSIÓN

O. E. DWYER (Estados Unidos de América): Querría felicitar al Dr. Osmachkin por esta memoria

tan informativa. Me ha interesado particularmente su tratamiento del caso de flujo lineal de metales líquidos por haces de barras sin deflectores. Hace unos años obtuvimos una solución analítica de este problema, en el Laboratorio Nacional de Brookhaven, para la cual suponíamos que la distribución radial de velocidades respecto a una barra determinada, era la misma que en la parte interior de una región de sección anular que tuviese el mismo radio interior, el mismo radio de velocidad máxima y la misma velocidad media para toda la parte interior. Parecía que esto era preferible a tomar como base de la distribución de velocidades la correspondiente al flujo en tuberías. He hecho una comprobación que indica que la figura 9 de la memoria del Dr. Osmachkin concuerda bastante bien con la ec. (2) del documento P/225 si se utilizan las constantes de la tabla 3 de dicha memoria y se supone $\bar{\psi} = 1$. Las constantes están basadas en el modelo anular.

Creemos que, para números de Peclet pequeños, Nu casi no depende de Pe . Para un valor del cociente paso/diámetro de 1,7, p. ej., hemos llegado a la conclusión de que, por debajo de $Pe \approx 700$, la contribución de la turbulencia a la transmisión total de calor es despreciable, quedando la conducción molecular como el mecanismo preponderante.

Por encima de $Pe \approx 700$, la contribución de la conducción turbulenta va siendo cada vez más importante, hasta que para $Pe \approx 10^4$ es próxima a la unidad. Así, cuanto mayor es el número de Peclet, tanto mayor es la precisión con que es necesario determinar ν_T .

Documento P/16 (presentado por A. D. Lane)

DISCUSIÓN

H. S. ISBIN (Estados Unidos de América): ¿Han realizado Vds. un número de ensayos suficiente para permitirles resumir los efectos de la situación excéntrica de las secciones de ensayo?

A. D. LANE (Canadá): No. Sin embargo, esperamos efectuar algunos ensayos sobre el espaciado.

H. S. ISBIN (Estados Unidos de América): Cuando Vds. evalúan la transmisión de calor por radiación de la vaina de zircaloy oxidada, ¿qué valores utilizan para la emisividad de las superficies?

A. D. LANE (Canadá): No hemos intentado evaluar la radiación de calor de las vainas de zircaloy oxidado durante la irradiación, por dos razones. En primer lugar, en el caso en que, a causa de la temperatura, se

producía arqueamiento que daba lugar a una corrosión apreciable, se estimaban las temperaturas mediante termopares colocados en elementos de acero inoxidable sometidos a unas condiciones semejantes, y también mediante el examen de la magnitud de la corrosión de las vainas. En segundo lugar, en funcionamiento normal, la temperatura de las proximidades, es decir, de la sección de ensayo, era igual dentro y fuera del reactor y, en general, muy poco inferior a la temperatura de la vaina del combustible.

V. I. SUBBOTIN (URSS): Voy a hacer un comentario en relación con esta memoria. El quemado destructivo no se produce de la misma manera a presiones altas que a presiones bajas; a presiones altas no hay gran aumento de temperatura de la pared productora de calor cuando se produce dicho quemado. Me parece que, en algunos casos, esto podría ser una causa de error en la determinación experimental de q_{BO} .

Documento P/224

DISCUSIÓN

K. M. BECKER (Suecia): La figura 13 de la memoria presenta una comparación de diferentes correlaciones con dos conjuntos seleccionados de los datos de Columbia. A juzgar por esta comparación, parece que la correlación de Becker-Persson es poco adecuada para la predicción de las condiciones de quemado destructivo. Sin embargo, hemos mostrado en una memoria (K. M. Becker, *Report in progress*, AB Atomenergi, Studsvik, Suecia) que se va a publicar en octubre o noviembre de 1964, que con esta correlación se determinan los flujos térmicos de quemado destructivo correspondientes a unas 3 000 mediciones suecas, con un error comprendido entre ± 5 por ciento, dentro de los siguientes intervalos de variación:

$$\begin{aligned} 2,7 < p < 91 \text{ kg/cm}^2 \\ 100 < G < 3\,500 \text{ kg/m}^2 \text{ s} \\ 35 < q/A < 600 \text{ W/cm}^2 \\ 0,05 < X < 1,00 \\ 4 < d < 13 \text{ mm} \\ 600 < L < 3\,500 \text{ mm} \end{aligned}$$

Creo que puedo explicar por qué nuestra correlación parece tan mala en la figura 13. La correlación, que está basada en el modelo de flujo de Vanderwater-Isbin, contiene dos constantes, ϵ y b , que representan las velocidades de arrastre y de difusión de las gotitas, y que han de determinarse a partir de datos experimentales. Cuando escribimos nuestra memoria sobre dicha correlación, hace año y medio o dos años, los estudios sobre quemado destructivo en Suecia abarcaban mediciones hasta 40 kg/cm^2 solamente, y había que determinar las constantes ϵ y b para presiones más elevadas a partir de datos extranjeros. En el caso que estamos tratando, en el cual la presión es 70 kg/cm^2 , se utilizaron los datos de CISE para determinar ϵ y b (K. M. Becker y P. Persson, *An Analysis*

of Burn-out Conditions for Flow of Boiling Water in Vertical Round Ducts, ASME paper No. 63-WA-51). Para obtener dichos datos se introdujeron mezclas agua-vapor por la entrada de la sección de ensayo. Como indicábamos en nuestra memoria, por esta razón no se puede considerar la correlación como fidedigna, a esta presión, si se aplica para predecir el quemado destructivo en conductos con la entrada en condiciones de subenfriamiento.

La nueva memoria que he mencionado contiene nuevos valores de ϵ y b que pueden utilizarse a presiones más altas.

La figura 1 muestra la figura 13 de la memoria de Levy después de introducir los valores de ϵ y b correctos en la correlación de Becker-Persson.

Se observará que la concordancia entre los datos de Columbia y nuestra correlación es ahora satisfactoria. Se puede aclarar este hecho aún más utilizando algunos de los datos presentados en la figura 2 de la memoria de Levy. Se presenta una comparación en la figura 2.

El aumento de la dispersión para bajas calidades del vapor es de esperar, dado que la correlación está basada en el modelo de flujo de película *ascendente*. Sin embargo, si se considera que b es también función de la calidad del vapor, la dispersión que muestra la figura 2 para bajos títulos del vapor puede reducirse apreciablemente.

Por último, en la figura 3 se aplica nuestra correlación a los datos suecos y a los de Columbia para una presión de unos 50 kg/cm^2 .

Se observará que también en este caso es excelente la concordancia entre los dos conjuntos de datos y nuestra correlación.

Documento P/93 (presentado por J. Villeneuve)

DISCUSIÓN

W. M. CAMPBELL (Canadá): En el Canadá también hemos estado estudiando el percutimiento, pero nuestros resultados, al parecer, son diferentes de los presentados en esta memoria, aunque podría no haber una verdadera discordancia.

El procedimiento que utilizamos es el siguiente: se trata el refrigerante cuidadosamente con arcilla de Attapulgus y se filtra para eliminar todas las partículas (orgánicas e inorgánicas); los componentes que promueven el percutimiento orgánico están esencialmente ausentes.

En estas condiciones, hemos encontrado que, como se describe en el documento P/15, el cloro promueve el percutimiento con hierro por transporte de materia, y que la forma en que se encuentra el cloro es muy importante. Por ej., el tricloroetileno es más eficaz, como promotor, que el clorodifenilo. Tenemos la impresión de que el compuesto de cloro que se añade tiene que descomponerse para formar un compuesto clorado «activo», hasta ahora no identificado. Por consiguiente, si se emplea en los ensayos un compuesto de cloro estable, se podría deducir una conclusión errónea en relación con el efecto del cloro.

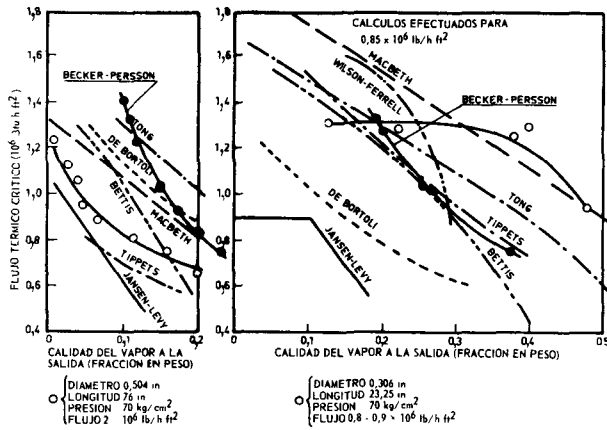


Figura 1. Comparación de correlaciones con datos de flujo térmico crítico en secciones de ensayo tubulares

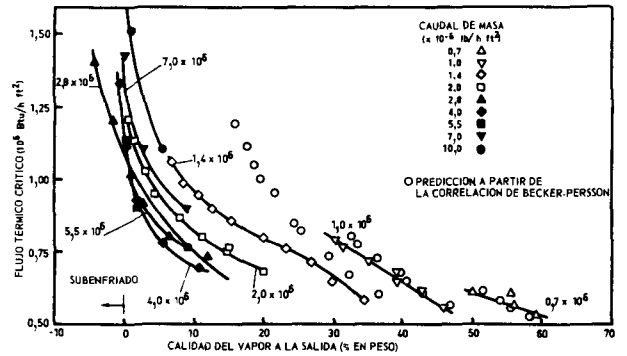


Figura 2. Condición de flujo térmico crítico en secciones de ensayo tubulares
Diametro interior del tubo: 0,504 in; longitud en caliente: 76 in; presión: 70 kg/cm²

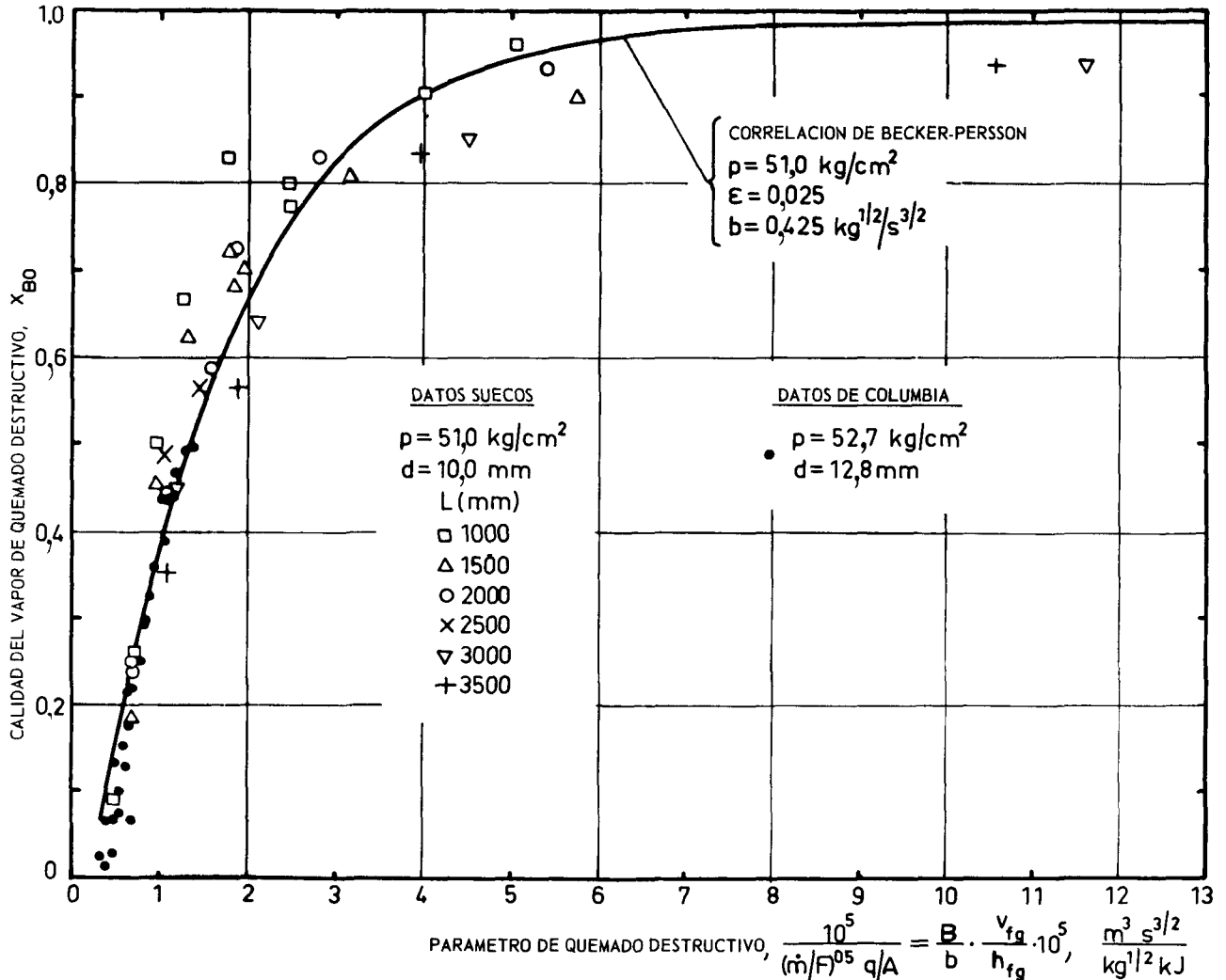


Figura 3. Comparación de las condiciones de quemado destructivo experimentales y teóricas

Opino que, en el caso descrito en el documento P/93, el efecto ha sido enmascarado por el notable percutimiento orgánico y por la estabilidad del compuesto orgánico de cloro añadido.

También me gustaría que se prestase atención a uno de nuestros ensayos en el circuito X-7, que casi no mostraba percutimiento en la superficie de los elementos combustibles mantenidos a 450–500 °C durante 82 días (0,1 $\mu\text{g}/\text{cm}^2 \text{ h}$).

J. VILLENEUVE (Francia): Estoy de acuerdo en que el cloro produce distintos efectos según la forma en que se encuentre en el circuito. En nuestro circuito hemos usado trifenilo OM2 producido por polimerización de un benceno que se había clorado por equivocación. La sustancia utilizada era, por tanto, un cloro combinado que no produce efecto ninguno sobre el percutimiento. Sin embargo, con el tiempo debe haberse combinado con el hierro del circuito y ahora se ha producido percutimiento por transferencia.

En nuestros experimentos hemos observado siempre que hay un umbral claramente definido, a 500 °C. Por encima de esta temperatura se observa pirolisis local que produce una película formada por un producto blando que se adhiere a la pared caliente.

L. S. DZUNG (Suiza): ¿Qué intervalo de números de Prandtl de los refrigerantes han utilizado en este experimento?

J. VILLENEUVE (Francia): El número de Prandtl variaba entre 5 y 12.

L. S. DZUNG (Suiza): Observo que la correlación utilizada en esta memoria tiene la misma estructura que la correlación clásica propuesta originalmente por Colburn en 1930. Me interesaría saber en qué difiere su ecuación de la clásica. Me parece que el mecanismo de transmisión de calor depende principalmente de las propiedades físicas del medio, que están caracterizadas por el número de Prandtl y el número de Reynolds. Las propiedades químicas no influyen mucho. Por tanto, la ecuación de la memoria debería ser aplicable a otros medios, además de los líquidos orgánicos, siempre que el número de Prandtl esté dentro del intervalo apropiado.

J. VILLENEUVE (Francia): La correlación que hemos obtenido difiere de la clásica, es decir, la de Colburn, en que el exponente del número de Reynolds es 0,9. Como se ha indicado ya, p. ej., en la referencia [1] de la memoria, el exponente del número de Reynolds aumenta con el número de Prandtl. Aplicando a nuestro caso el método de cálculo semiteórico de Martinelli obtenemos el valor 0,9 para el exponente.

Documento P/53 (presentado por P. Lévêque)

DISCUSIÓN

R. F. S. ROBERTSON (Canadá): En el Canadá nos interesa mucho el mecanismo propuesto por Lévêque en esta memoria. Nuestros resultados experimentales indican que un concepto basado en la combinación de una radiolisis pura, que es independiente de LET y de la temperatura, y una pirolisis que es indepen-

diente de la intensidad de la dosis puede ser una simplificación excesiva. En el caso de las irradiaciones en cápsula realizadas en el reactor NRX (mencionadas en nuestro documento P/15) hemos encontrado que, tanto si se trata del orto como del meta-trifenilo, la descomposición en función de la temperatura es casi la misma para dosis de 0,1 y 0,3 W/g. El mecanismo del Dr. Lévêque no permitiría prever este resultado. Sin embargo, estamos de acuerdo en que, al menos en el caso del meta-trifenilo, la velocidad de la pirolisis del material que ha experimentado la radiolisis es significativamente mayor que la correspondiente al material sin irradiar. Nuestros resultados indican que los neutrones rápidos producen más deterioro que los rayos γ y que G_n/G_γ es aproximadamente 3 para temperaturas inferiores a 375 °C.

Documentos P/225 (presentado por O. E. Dwyer) y P/328 (presentado por V. I. Subbotin)

(Se había decidido que ambos documentos se discutirían a la vez)

DISCUSIÓN

L. S. DZUNG (Suiza): En primer lugar, deseo felicitar a los autores del documento P/225, que nos proporciona un resumen muy completo de la información disponible sobre la transmisión de calor con medios de número de Prandtl pequeño.

Mi comentario se refiere a la figura 1, en la cual, en algunas de las curvas, la difusividad turbulenta ϵ_M tiene un máximo en la porción del canal comprendido entre dos paredes. Esta porción se caracteriza por ser cero el gradiente de velocidad, es decir, el flujo es localmente homogéneo. Por tanto, físicamente, la difusividad turbulenta debería tener también gradiente nulo, es decir, no debería haber ningún máximo. ¿Querría el Dr. Dwyer hacer algún comentario sobre esta cuestión?

O. E. DWYER (Estados Unidos de América): La difusividad turbulenta de la transferencia de la cantidad de movimiento en un punto dado de una sección transversal del canal depende primordialmente de la tensión tangencial y de la pendiente del perfil de velocidad en ese punto. Puesto que, para el radio correspondiente a la velocidad máxima, ambos son nulos, es imposible evaluar la difusividad en dicho punto. Sin embargo, la curva de ϵ_M en función de $(r - r_1)/(r_2 - r_1)$ para un conducto de sección anular, debe ser diferenciable en todos sus puntos y tener una pendiente nula en el radio correspondiente a la velocidad máxima. La curva (b) de la figura 1, que es la que prefieren los autores, satisface estos requisitos. Hay resultados experimentales adecuados que indican que el perfil (a) de la figura 1 es muy poco probable. Además, un perfil de velocidad bastante uniforme en la porción central del conducto anular no significa que la difusividad turbulenta de la cantidad de movimiento en dicha región haya de ser también uniforme.

P. GILLI (Austria): Me gustaría hacer un comentario y una pregunta sobre la memoria del Sr. Dwyer. Me

refiero particularmente a la transmisión de calor de metales líquidos, en corrientes cruzadas, a haces de tubos, que podría representar el caso de un cambiador de calor o de un generador de vapor de una central nuclear con un reactor refrigerado por metal líquido.

Sugiero que es posible combinar las dos fórmulas citadas por el autor, relativas al número de Nusselt en corrientes cruzadas, es decir, la ecuación empírica [ec. (4)] de Rickard, Dwyer y Dropkin (ref. [25] de la memoria) y la fórmula teórica [ecs. (5) y (6)] de Hsu*. Cada una de estas fórmulas tiene sus particularidades interesantes. La ec. (4) muestra una cantidad constante (4,03) además de la función exponencial del número de Peclet, con lo que, evidentemente, tiene en cuenta la conducción molecular. Sin embargo, la fórmula se refiere únicamente a una disposición particular de los tubos. Por otra parte, las ecs. (5) y (6) (gracias a ϕ_1 , la diferencia de potencial, para la velocidad unitaria, entre los puntos de remanso anterior y posterior del tubo) son válidas para diferentes distribuciones de los tubos pero no tienen en cuenta la conducción molecular. Por tanto, el número de Nusselt, según esta fórmula, es nulo para un número de Peclet igual a cero.

No sería difícil combinar las dos fórmulas. Habría que cambiar el coeficiente 0,958 de las ecs. (5) y (6), o si no, este coeficiente y el exponente del número de Peclet y de ϕ_1/D , de forma que, sumando la constante 4,03, Nu estuviese de acuerdo con los resultados experimentales. Un modo de conseguir esto sería reducir el coeficiente en un 10 a un 20 por ciento. También sería posible sustituir, en la ec. (4), el coeficiente 0,228 por la función ϕ_1/D y un coeficiente adecuado. De esta forma se obtendría una fórmula más general y más satisfactoria para el flujo cruzado de metales líquidos por haces de tubos, que también sería válida para valores pequeños del número de Peclet y para diversas disposiciones de los tubos.

En cuanto a mi pregunta, se refiere a los valores de ϕ_1/D tabulados en la memoria de Hsu a la que ya he hecho referencia. Estos valores de ϕ_1/D se refieren a distribuciones de tubos en cuadro y en triángulo equilátero solamente. ¿Se han calculado valores de ϕ_1/D para distribuciones más generales de tubos, por el método de Hsu, en el Laboratorio Nacional de Brookhaven o en algún otro sitio?

O. E. DWYER (Estados Unidos de América): La ec. (4) es una ecuación empírica basada en resultados experimentales para un solo haz de tubos, que tiene $P/D = 1,38$. Da una curva de Nu en función de Pe cuya pendiente crece con Pe . Sin embargo, las ecs. (5) y (6), que se basan en la hipótesis de flujo no viscoso, dan líneas rectas al representar Nu en función de Pe . Así pues, las ecs. (4) y (5) se desvían para valores pequeños de Pe . Por lo tanto, es evidente que las ecs. (5) y (6) no son tan buenas para valores extremos de Pe como la ec. (4). Una modificación de

la ec. (5), de conformidad con las características de la ec. (4), como sugiere el Dr. Gilli, sería apropiada para calcular coeficientes de transmisión de calor en corrientes cruzadas en condiciones distintas de las que sirvieron de base para las ecs. (4) y (5).

En cuanto a la existencia de valores de ϕ_1/D , no conozco más que los publicados en las referencias [27] y [30].

Ahora desearía hacer un comentario sobre la otra memoria. En los Estados Unidos sabemos que el Dr. Subbotin y sus colegas del Instituto de Física y Energía han realizado en la URSS un trabajo muy extenso y magnífico, durante estos últimos años, en el campo de la transmisión de calor en metales líquidos. Sus resultados han contribuido mucho a nuestro conocimiento actual de este tema. Ha sido muy tranquilizador para los que trabajamos en el mismo campo, en los Estados Unidos, el ver, de vez en cuando, que había una concordancia sustancial en varias zonas de investigación independiente en ambos países.

Para mejorar nuestro conocimiento de la transmisión de calor en metales líquidos, se necesita más información sobre la naturaleza de la contribución turbulenta al mecanismo de transmisión de calor en su conjunto; también se necesita un medio más preciso para calcular la difusividad turbulenta de la transmisión de calor. En este sentido, el trabajo descrito por el Dr. Subbotin, relativo a la medición y a la correlación de las fluctuaciones de las temperaturas locales en la corriente metálica, es muy significativo.

El Dr. Subbotin y sus colaboradores han estudiado ampliamente el importante problema de la transmisión de calor de haces de tubos, tanto con haces muy juntos como espaciados, a metales líquidos con flujo lineal. En sus ecs. (18) y (19), que se basan en resultados experimentales para estos dos casos, respectivamente, se muestra que el número de Nusselt depende de la misma manera del número de Peclet en todo el intervalo de éste que se ha estudiado. Esto difiere de los resultados obtenidos en Brookhaven con haces de barras en triángulo equilátero, tanto con mercurio como con NaK (como indican los resultados presentados en la figura 7 del documento P/225), mientras exista un buen contacto térmico entre el metal que fluye y la superficie de transmisión de calor.

Creo que, para números de Peclet correspondientes al intervalo de poca turbulencia, la ec. (19) de la memoria del Dr. Subbotin, probablemente dará números de Nusselt menores que los correspondientes a la conducción molecular únicamente; esto sólo puede explicarse por no haber buen contacto térmico en la superficie de las barras en estas condiciones de flujo.

V. I. SUBBOTIN (URSS): Los resultados de los experimentos del Sr. Dwyer sobre transmisión de calor de haces de barras con flujo lineal concuerdan bien con los nuestros para $Pe > 500$. Para $Pe < 500$ hay desviaciones que aumentan a medida que dis-

* Int. J. Heat Mass Transfer, vol. 7, págs. 431-446 (abril 1964).

minuye Pe . Una de las razones de dicha desviación puede ser el flujo de calor axial, cuyo valor aumenta al disminuir el número de Peclet.

Es difícil explicar dicha diferencia mediante fenómenos de contacto. En nuestros experimentos se controlaba la pureza sistemáticamente; las impurezas nunca fueron superiores a 10^{-3} por ciento en peso. La comparación de nuestros experimentos con los del Sr. Dwyer da como conclusión que se nos ha debido percudir algo la pared caliente.

N. I. BULEEV (URSS): Desearía plantear una cuestión a la que se ha prestado poca atención en las publicaciones sobre hidráulica y transmisión de calor en tuberías.

Si comparamos con los datos experimentales los resultados de cálculos teóricos relativos a la viscosidad turbulenta y a la conductividad térmica, en realidad no estamos comparando dos conceptos idénticos.

Las expresiones $p_{\epsilon_M} \frac{\partial \omega}{\partial r}$ y $p_{\epsilon_H} \frac{\partial T}{\partial r}$, en las cuales $\epsilon_M = l_1^2 \left| \frac{\partial \omega}{\partial n} \right|$ y $\epsilon_H = l_1^2 \left| \frac{\partial \omega}{\partial n} \right|$, que aparecen en las expresiones iniciales de paso del calor y flujo, son sólo los componentes principales del esfuerzo turbulento y del flujo térmico turbulento. En este sentido, las ecuaciones teóricas iniciales son aproximadas.

En el caso de los datos experimentales, en cambio, cuando los resultados se basan en las medidas de los perfiles de velocidad y temperatura, se obtienen los valores totales de los esfuerzos y de los flujos térmicos turbulentos.

Si en el trabajo experimental representamos los valores obtenidos para $\overline{pn'\omega'}$ y $\overline{pn'T'}$ en la forma $p_{\epsilon_M}*(\partial\omega/\partial T)$ y $p_{\epsilon_H}*(\partial T/\partial r)$, y encontramos los valores ϵ_M^* , ϵ_H^* (valores formales) y la razón $\epsilon_H^*/\epsilon_M^*$ estos valores no tendrán exactamente el mismo significado que ϵ_M , ϵ_H y ϵ_H/ϵ_M y pueden diferir de éstos en mas del 10 por ciento.

En mi opinión, cuando investigamos los valores ϵ_M , ϵ_H y ϵ_H/ϵ_M es esencial utilizar algún modelo teórico único para la transferencia turbulenta de cantidad de movimiento y de calor.

V. I. SUBBOTIN (URSS): La forma tradicional de realizar el cálculo es tomar el valor del coeficiente de viscosidad turbulenta (ϵ_T) y después, basándose en el valor que se utilice para el número de Prandtl turbulento (ϵ), hallar el coeficiente de conductividad térmica turbulenta (ϵ_a). Este procedimiento era comprensible en los tiempos en que se realizaban experimentos para la medición de campos de velocidad y no había experimentos fidedignos para la medición de campos de temperatura. En cambio actualmente es posible determinar ϵ_a directamente y sustituirlo en las expresiones correspondientes.

O. E. DWYER (Estados Unidos de América): En la mayoría de los casos se pueden determinar teóricamente los perfiles de velocidad con una precisión considerablemente mayor que los de temperatura, y puesto que ahora se pueden transformar los valores de ϵ_M en valores de ϵ_H , para el flujo en tuberías, con

cierta confianza, creo que el camino $\epsilon_M \rightarrow \epsilon_H \rightarrow Nu$ se prefiere con más frecuencia para estimar coeficientes de transmisión de calor en la mayoría de las situaciones nuevas.

Documento P/135 (presentado por C. Cunningham)

DISCUSIÓN

J. PELCE (Francia): Se han desarrollado un trabajo muy similar en los laboratorios del CEA, pero, en nuestro caso, se ha prestado mayor atención a los elementos con aletas en espigón. Hemos intentado resolver los mismos problemas y hemos utilizado los mismos métodos.

Hemos trabajado bastante sobre las características térmicas y las caídas de presión correspondientes a una gran variedad de disposiciones de las aletas, con miras a la obtención de fórmulas adecuadas para los cálculos de optimización de reactores. Los detalles de este trabajo están a la disposición de quien esté interesado en ellos.

También hemos estudiado con detalle el comportamiento térmico de las vainas elegidas para reactores concretos, como EDF2 y EDF3. Se ha prestado particular atención a las peculiaridades térmicas de conjuntos completos de vainas, dispuestas de modo que simulasen la geometría real del reactor, en las condiciones nominales de funcionamiento (dando especial importancia al problema del desplazamiento angular entre elementos). Hemos estudiado también la influencia de flujos pequeños en casos de corrientes gaseosas en sentido ascendente (EDF3) y descendente (EDF4), así como de las geometrías de vainas deformadas.

Todos estos ensayos fueron realizados con modelos de tamaño natural o mayor. Las conclusiones a que hemos llegado están, en gran parte, de acuerdo con las expuestas en los documentos P/135 y P/136. Los informes CEA 2469 y 2470 contienen información sobre nuestros resultados.

En relación con el documento P/135, deseo hacer dos preguntas. Primera: en los experimentos descritos, ¿el flujo gaseoso era ascendente o descendente? y ¿podría Vd. darnos una idea de la precisión de sus resultados? Segunda: ¿ha realizado Vd. investigaciones detalladas con vainas que tuviesen más de cuatro sectores?

C. CUNNINGHAM (Reino Unido): Los resultados de los ensayos de pequeños caudales descritos en la memoria se refieren a flujo ascendente. Es imposible dar una respuesta precisa a la pregunta sobre la precisión. Hasta donde es posible generalizar, puede decirse que la desviación típica de nuestros ensayos de transmisión de calor es aproximadamente 2 por ciento. En cuanto a su segunda pregunta, no hemos realizado investigaciones detalladas con elementos de aletas en espigón que tengan más de cuatro sectores.

W. L. GRANT (Sudáfrica): Las figuras 1E y 2E indican la variación de transmisión de calor en función de la orientación relativa de los elementos. ¿Es esta variación igual en los canales de elementos combustibles horizontales y verticales?

C. CUNNINGHAM (Reino Unido): No hemos realizado ningún ensayo de orientación en canales verticales. Sin embargo, en todos los demás ensayos con número de Reynolds elevado, no hemos podido detectar diferencias debidas a la altura del canal; lo que es fácilmente comprensible porque los efectos de empuje ascensional son insignificantes.

Documento P/719 (presentado por V. B. Nesterenko)

DISCUSIÓN

Y. EL-MESHAD (República Árabe Unida): Sr. Nesterenko, ¿podría Vd. hablarnos de la posibilidad de usar su técnica de promediar: *a*) cuando se tiene

en cuenta el material de la vaina o, en general, cuando los elementos constan de varias capas, y *b*) cuando se tiene en cuenta el flujo de calor axial a lo largo del material combustible?

V. B. NESTERENKO (URSS): Utilizando métodos aproximados, es posible tener en cuenta la resistencia térmica de la vaina del combustible en el coeficiente de transmisión de calor que hemos citado. En nuestra investigación no se tuvo en cuenta el flujo de calor a lo largo del elemento en el caso del gas, a causa de la pequeñez de la cantidad de que se trata.

Documento P/552 (presentado por R. Negrini)

No hubo discusión de esta memoria.

Session I.11

HYDRAULIC PROBLEMS OF REACTOR ENGINEERING

LIST OF PAPERS

		Page
	Water cooling	
P/55	Quelques aspects fondamentaux de l'ébullition dans les réacteurs nucléaires <i>Some fundamental aspects of boiling in nuclear reactors</i>	H. Mondin <i>et al.</i> 247
P/95	La technique des écoulements diphasés tourbillonnaires dans les réacteurs à eau <i>Technique for vortex type two-phase flow in water reactors</i>	C. Foure <i>et al.</i> 255
P/230	Fluid dynamics, stability, and vapor-liquid slip in boiling reactor systems	P. A. Lottes <i>et al.</i> 263
P/231	Helical, forced-flow heat transfer and fluid dynamics in single and two-phase systems	H. F. Poppendiek, W. R. Gambill 274
P/232	Critical flow phenomena in two-phase mixtures and their relationships to nuclear safety	H. S. Isbin <i>et al.</i> 286
P/327	Критические тепловые потоки при вынужденном течении воды <i>Burn-out heat fluxes under forced water flow</i>	Г. В. Алексеев <i>et al.</i> G. V. Alekseev <i>et al.</i> 295
P/329	Теоретическая модель турбулентного обмена в трехмерном потоке жидкости <i>Theoretical model of turbulent transfer in three-dimensional fluid flow</i>	Н. И. Булеев 305 N. I. Buleev
P/589	Heat transfer and hydraulic stability in boiling-water reactors	M. Bogaardt <i>et al.</i> 316
P/607	Hydrodynamic instability and dynamic burn-out in natural circulation two-phase flow. An experimental and theoretical study	K. M. Becker <i>et al.</i> 325
P/801	Two-phase flow investigations for a marine boiling water reactor	E. Kjelland-Fosterud <i>et al.</i> 338
	Gas cooling	
P/50	Etudes aérodynamiques et thermiques de gaines d'éléments combustibles refroidis par gaz <i>Aerodynamic and thermal studies of cans of gas cooled fuel elements</i>	P. Gelin, J. P. Milliat 347

LIST OF PAPERS

(Continued)

	<i>Page</i>
P/524 The influence of an electric field on the heat transfer to CO ₂ coolant at high and low pressure in a nuclear reactor	F. Berger, L. Derian 355
General	
P/698 Heat transfer intensification by use of the longitudinally variable pressure gradient	Z. Zarić 364

Quelques aspects fondamentaux de l'ébullition dans les réacteurs nucléaires

par H. Mondin, P. Lavigne, et R. Semeria*

La connaissance des phénomènes liés à l'ébullition est indispensable pour les projets de tous les réacteurs refroidis par liquide.

Si l'ébullition est prévue en régime de fonctionnement normal, il est nécessaire de connaître les pertes de charge en double phase et le taux volumique de vapeur.

Dans tous les cas, il faut pouvoir évaluer la marge de sécurité entre le régime à puissance maximale permise et le niveau d'apparition de phénomènes critiques pouvant résulter d'accidents divers: augmentation de la puissance, diminution du débit ou de la pression. L'importance économique de ces problèmes est considérable, car une meilleure détermination du niveau de puissance dangereux entraînera une réduction des coefficients de sécurité et, du même coup, un abaissement important du prix de l'électricité d'origine nucléaire ou une augmentation de l'efficacité des réacteurs de recherche.

Ces phénomènes critiques sont: la caléfaction (*burn-out*), la redistribution de débit, et les instabilités hydrodynamiques. Les deux derniers phénomènes peuvent entraîner la caléfaction.

Toutes ces questions ont été l'objet de très nombreuses études, particulièrement aux Etats-Unis, mais pendant plusieurs années les résultats obtenus par des méthodes empiriques ont été extrêmement dispersés et parfois incohérents, ce qui montre l'extrême complexité des problèmes étudiés. Tous les chercheurs dans le domaine de l'ébullition en ont conclu qu'il était nécessaire, pour y voir clair, d'entreprendre des études fondamentales des mécanismes élémentaires, locaux ou globaux, qui étaient la cause des manifestations observées.

Au Service des transferts thermiques du Centre d'études nucléaires de Grenoble, ces études ont commencé en 1959. Elles peuvent se diviser en études d'observations de l'ébullition par cinématographie ultra-rapide et strioscopie, et en études des phénomènes globaux: perte de pression, caléfaction, oscillations de débit.

Le présent mémoire se borne à indiquer seulement quelques aspects nouveaux qui mettent en évidence des mécanismes élémentaires. Ces aspects sont très divers. Parfois il s'agit de phénomènes directement

observés, parfois de modèles inédits en accord raisonnable avec l'expérience et qui, par leur commodité, facilitent la compréhension d'aspects plus complexes dans lesquels on les inclut.

OBSERVATION DE L'ÉBULLITION

La structure d'un écoulement diphasé est caractérisée par sa granulométrie, dont un paramètre essentiel dans un canal chauffant est la granulométrie pariétale. Dans le cas de l'ébullition nucléée, ceci conduit à l'étude des populations de germes générateurs de bulles, puis à celle des dimensions des bulles soit isolées, soit agglomérées en coalescences, en fonction de paramètres tels que le flux calorifique (ou la température de paroi), la pression, la température et la vitesse d'écoulement du fluide.

Population de germes générateurs de bulles

Les expériences antérieures avaient permis de préciser l'influence du flux calorifique, ainsi que d'indiquer le rôle de la nature du métal, de l'état de la surface et de son vieillissement.

L'influence de la pression n'avait été étudiée que jusqu'à 5 atmosphères environ, par Kutadeladze et Zisina-Molozhen.

Le dénombrement des colonnes de bulles issues de la surface chauffée permet d'accéder à la population de germes à condition d'éviter leur agglomération; pour cela, on utilise un fil chauffant d'autant plus fin que la pression est plus élevée (de 0,3 mm à la pression atmosphérique jusqu'à 0,01 mm à 100 atmosphères). Dans de l'eau à la température de saturation on obtient sur des fils de platine les formules empiriques suivantes [1]:

$$N/A = (1,2/100)\phi^2 \times p^1 \quad 1 < p < 100 \text{ atm}$$

$$\Delta T_{\text{sat}} = 10 \times \phi^{0,25} \times p^{-0,23} \quad \phi < 100 \text{ W/cm}^2$$

Le tableau 1 explicite les symboles utilisés.

On en déduit qu'à une pression donnée, N/A varie comme ΔT_{sat}^8 . Si on considère le rayon critique minimal R_c pour qu'un germe s'amorce

$$R_c = \frac{2\sigma T_{\text{sat}} \left(\frac{1}{\rho_v} - \frac{1}{\rho_l} \right)}{\xi \times \Delta T_{\text{sat}}}$$

on déduit que N/A varie comme R_c^{-8} à pression constante.

* Commissariat à l'énergie atomique. Avec la collaboration de S. Fabrega et P. Vernier.

Tableau I. Symboles utilisés

c_p	chaleur spécifique (<i>heat capacity</i>)
D	diamètre
g	accélération de la pesanteur (<i>acceleration of gravity</i>)
G	vitesse massique (<i>mass velocity</i>)
\mathcal{L}	chaleur de vaporisation (<i>latent heat of vaporization</i>)
N/A	population de germes actifs par cm^2 (<i>population of active sites</i>)
P	pression (<i>pressure</i>)
R	rayon (<i>radius</i>)
T	température
V	vitesse (<i>velocity</i>)
X	qualité: rapport du débit masse vapeur au débit masse total (<i>quality</i>)
γ	glissement (<i>slip ratio</i>)
ΔP	chute de pression (<i>pressure drop</i>)
ΔT_{bat}	surchauffe de paroi (<i>wall super heat</i>) = $T_p - T_{\text{sat}}$
$\Delta T, \Delta T_{\text{sub}}$	sous-saturation (<i>subcooling</i>) = $T_{\text{sat}} - T_1$
ρ	masse spécifique (<i>density</i>)
σ	tension superficielle (<i>surface tension</i>)
τ	qualité thermodynamique déduite du bilan thermique
ϕ	densité de flux calorifique (<i>heat flux</i>)
α	taux volumique de vapeur (<i>void fraction</i>)
<i>Indices</i>	
l	liquide
p	paroi (<i>wall</i>)
sat	saturation (<i>saturation</i>)
v	vapeur

Pour un R_c minimum donné, N/A varie comme $p^{-5,16}$, ce qui montre que l'augmentation de la pression rend inactifs les germes de grande dimension.

Granulométrie des bulles isolées

On a étudié le diamètre de décrochage d'une bulle quittant la paroi chauffante en fonction de la pression [2] (fig. 1). Sur la même figure est portée la courbe donnée par la formule de Fritz et Ende avec un angle de contact de 45° . Cette formule, qui est satisfaisante pour des bulles en équilibre et que nous avons

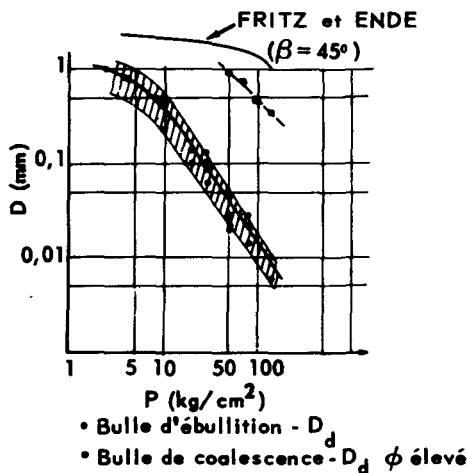


Figure 1. Diamètre de décrochage des bulles en fonction de la pression

vérifiée jusqu'à 50 kg/cm^2 , ne prédit pas le diamètre de départ des bulles d'ébullition isolées, pour lesquelles les forces de gravité $(\rho_1 - \rho_v)gv$, v étant le volume de la bulle, restent petites devant les forces de tension superficielle. On est alors conduit à supposer que ces dernières sont faibles ou nulles dans la première phase de croissance (0,01 s environ) et que la force qui maintient la bulle sur la paroi est une force d'inertie, dont le terme prépondérant F' est ici de la forme $(dM'/dt)(dR/dt)$, M' étant la masse virtuelle. D'où

$$F' = -k\rho_v(3/R)(dR/dt)^2 \quad k \geq 0,5$$

Nous avons vérifié que par l'égalité:

$$F' = (\rho_1 - \rho_v)gv$$

soit, pratiquement, $(dR/dt)^2(1/R) = C^{\text{te}}$, il est possible d'expliquer la rapide diminution du diamètre de départ de la bulle avec la pression.

Dans un canal, la force d'entraînement de l'écoulement fait d'abord glisser la bulle le long de la paroi, mais on a observé jusqu'à 140 kg/cm^2 que la dimension des bulles isolées sur la paroi restait du même ordre que celle mesurée en vase.

Le domaine de ces bulles isolées est cependant très limité. L'expérience montre qu'en vase et à la saturation, le phénomène d'agglomération devient nettement observable au-dessus de flux calorifiques de 15 W/cm^2 et ceci quelle que soit la pression ($p < 140 \text{ kg/cm}^2$). En canal, la limite de coalescence est fonction de la sous-saturation, de la vitesse et de la géométrie du canal; elle peut, aux faibles vitesses et faibles sous-saturations, être inférieure à celle observée en vase pour la même sous-saturation.

Coalescence des bulles

Le domaine des bulles isolées est limité pratiquement au début de l'ébullition aussi bien en vase qu'en canal. On observe que le régime le plus étendu est celui des coalescences qui se forment aux dépens des bulles précédentes.

En vase, à la saturation et à haute pression (50 à 140 kg/cm^2), les bulles isolées imposent leur granulométrie jusqu'à 15 W/cm^2 environ. Entre 15 et 70 W/cm^2 , bulles isolées et coalescences donnent une courbe granulométrique à deux maxima, puis, au-delà de 70 W/cm^2 , on n'observe plus de bulles isolées au-dessus de la paroi: les coalescences imposent définitivement leur granulométrie. En vase, la dimension des coalescences diminue avec la pression (fig. 1) et augmente lentement avec le flux calorifique [2].

En convection forcée à haute pression, on a observé l'ébullition en sous-saturation sur une plaque chauffante placée dans l'axe d'un canal rectangulaire transparent ($V < 4 \text{ m/s}$, $\Delta T_{\text{sub}} < 50^\circ\text{C}$, $p = 80 \text{ kg/cm}^2$): les bulles isolées ne sont observables que dans un très petit domaine en début d'ébullition, puis les coalescences forment une couche double phase atteignant plusieurs millimètres d'épaisseur.

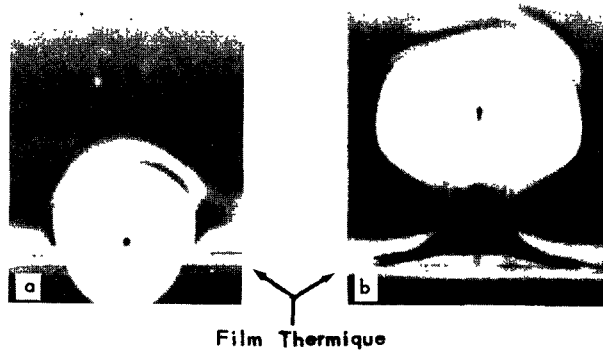


Figure 2. Détachement d'une bulle

(Fil chauffant 0,3 mm horizontal) a: Naissance de la bulle; b: Entraînement après décrochage

Perturbation du film thermique par l'ébullition (bulles isolées)

On observe le film thermique par une méthode strioscopique (*Schlierenphotography*) et en cinématographie ultra-rapide [3].

Les mécanismes observés sur des tubes, des fils et des rubans verticaux ou horizontaux placés dans un vase sont très divers selon les conditions de l'ébullition [4-5].

Ebullition en vase à la saturation:

L'examen des films montre nettement deux mécanismes:

a) Mécanisme de Forster-Greif: la bulle, en explosant sur la paroi, soulève le film thermique en une calotte la coiffant (fig. 2), et elle l'emporte dans son mouvement ascensionnel.

b) Mécanisme d'entraînement (drift): la bulle, se détachant de la paroi, entraîne derrière elle du fluide en partie prélevé au film thermique. Cet effet a été étudié par Sir Darwin et Lighthill en fluide parfait infini, mais la présence du plan a pour effet d'élargir la perturbation due au mouvement de la bulle. Ce mécanisme facilite la reconstitution du film thermique et permet d'expliquer des «temps de contact» (temps séparant le départ d'une bulle de la naissance de la suivante) quasi nuls.

Ebullition en vase avec sous-saturation

a) Aux faibles sous-saturations, la bulle se détache et se condense pendant son ascension; les deux mécanismes précédents subsistent, mais il faut tenir compte d'un effet d'accélération de la bulle dû à sa condensation et lié à la variation de la masse apparente M' avec (dR/dt) ; on a mesuré [6] la vitesse ascensionnelle de bulles de vapeur injectées dans de l'eau faiblement sous-saturée (2°C environ) et mesuré des accélérations dépassant 20 g prévisibles par la théorie (fig. 3).

La bulle ayant disparu, le fluide chaud accéléré forme un panache turbulent s'épanouissant dans le fluide. La formation d'un jet fluide à partir de la disparition d'une bulle en mouvement est signalée par Birkhof.

b) Aux fortes sous-saturations, les bulles ne se détachent pas de la paroi dans la phase visible de la

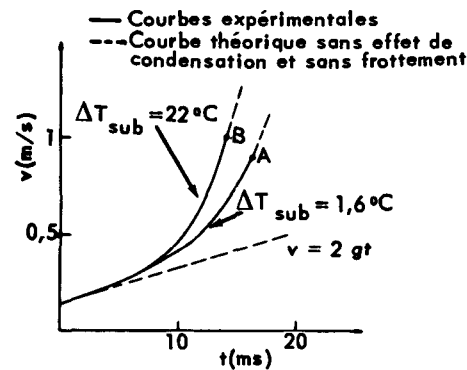


Figure 3. Vitesse ascensionnelle de bulles se condensant

condensation; la perturbation du film thermique a essentiellement lieu après la disparition de la bulle; du point de condensation est expulsée une bouffée d'eau chaude prélevée au film thermique; projetée dans le fluide froid, elle peut soit rester sous forme d'une sphérule diffusant lentement, soit plus généralement former un champignon turbulent s'épanouissant rapidement à quelques diamètres de bulle de la paroi (fig. 4).

Pré-ébullition

Lorsque la température de paroi atteint la température de saturation, on peut observer sur certains points de la surface, avant la formation visible de bulles de vapeur, des jets d'eau chaude perpendiculaires à la paroi, soit quasi continus, soit pulsés à grande fréquence: la vibration des germes à la limite de leur stabilité permet d'expliquer la présence de ces jets.

En conclusion, l'étude strioscopique montre l'extrême variété des mécanismes mis en jeu, la seule notion commune reste la population de germes, qui doit donc être le paramètre prépondérant dans les formules d'échange thermique en ébullition. L'exploitation des résultats obtenus est en cours et l'étude se poursuit en régime de convection forcée.

PERTE DE PRESSION EN DOUBLE PHASE

Passage de la simple phase à la double phase dans un canal chauffant

Le calcul des pertes de pression par accélération, élévation et frottement dans un écoulement eau-vapeur exige en toute rigueur la connaissance complète

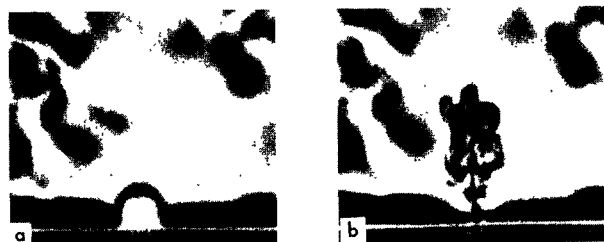


Figure 4. Evanouissement d'une bulle à la paroi a: Naissance; b: Panache après condensation

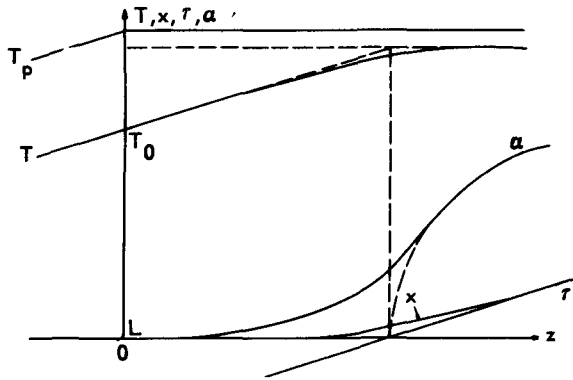


Figure 5. Evolution des paramètres hydrothermiques dans un canal chauffant

de la répartition des deux phases en chaque section (qualité et taux volumique en particulier). Dans un canal chauffant, on peut, en supposant l'équilibre thermodynamique réalisé en chaque section, calculer une qualité thermodynamique \mathcal{E} : cette hypothèse d'une diffusivité transversale infinie s'est avérée satisfaisante pour les qualités élevées ou les faibles puissances de chauffage. Par contre, elle est insuffisante dans la zone d'apparition de l'ébullition (ébullition en sous-saturation ou à faible qualité) car elle ne rend pas compte de la présence d'une quantité importante de vapeur près de la paroi chauffante, donc d'une qualité réelle X plus élevée que τ . En conséquence, on a utilisé un modèle simple [7] permettant de calculer X depuis le début d'ébullition L défini par la cote prise comme origine ($z = 0$) où $T_p = T_{\text{sat}}$, et se raccordant pratiquement pour les qualités élevées à la courbe $\tau(z)$ (fig. 5). On en déduit le taux volumique réel α en supposant ici le glissement égal à 1. Le modèle consiste à comparer en chaque section la vitesse de condensation à la vitesse de formation de la vapeur.

La vitesse de condensation dm/dt de la masse de vapeur m est proportionnelle à m et à la sous-saturation moyenne dans la section z : $\Delta T_z = T_{\text{sat}} - T$.

$dm/dt = Km \Delta T_z$, K sera le seul paramètre du modèle à déterminer expérimentalement en fonction de la géométrie et de la pression.

La masse de vapeur dn fournie par une longueur dz de canal pendant l'unité de temps est:

$$dn = \left[1 - \frac{\Delta T_z}{\Delta T_L} \right] \phi / \ell + dz, \text{ avec } \Delta T_L = T_{\text{sat}} - T_0$$

A partir de ces deux équations et du bilan thermique, on obtient la relation entre X et τ :

$$dX/d\tau = 1 - (A + BX)(X - \tau) \quad \text{avec } X = 0 \\ \text{pour } \tau = 1/A \text{ au point } L$$

où

$$A = \ell / (C_p \Delta T_L) \text{ et } B = (K\rho_1 \times S\ell^2) / (\mathcal{P}\phi C_p) \\ \text{avec } \mathcal{P} = \text{périmètre chauffant.}$$

Cette équation de Ricatti généralisée, dont la solution est obtenue analytiquement ou numériquement, a permis de corrélérer de façon satisfaisante les

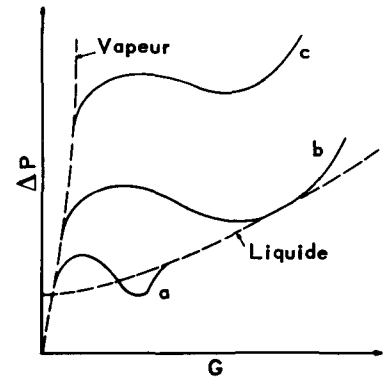


Figure 6. Courbes en S à basse pression

pertes de pression par frottement dans un canal rectangulaire à haute pression [8], ceci sans singularité particulière au début F de l'ébullition franche ($\tau = 0$).

Perte de pression globale. Courbes en S

Afin de prévoir le débit de refroidissement de canaux de réacteur, et en particulier le phénomène de «redistribution de débit», on a coutume de tracer les courbes dites «en S», donnant la perte de pression totale ΔP entre les extrémités du canal chaud en fonction du débit spécifique G . Nous voulons attirer l'attention sur deux particularités de ces courbes, rencontrées pour des réacteurs à basse pression (fig. 6) [9].

Pour des canaux larges, l'ébullition peut, à son début, alléger la colonne fluide sans beaucoup accroître le frottement, donc diminuer ΔP par rapport à l'écoulement sans ébullition (courbe a). A pression d'entrée donnée, la pression aval diminue rapidement lorsque la vitesse augmente. On peut alors observer une vaporisation du liquide dans toute sa masse (*flash boiling*) (courbe b). Le fonctionnement sans vaporisation peut être impossible (courbe c), par exemple dans le cas de canaux longs et étroits.

ÉCHAUFFEMENT CRITIQUE (*burn-out*)

Pour contribuer aux efforts qui sont faits dans le domaine de la thermique des réacteurs pour comprendre ce phénomène très complexe, nous apportons quatre remarques:

a) Influence de la longueur totale

Pendant plusieurs années, on a cherché l'influence de la longueur du canal chauffant. Or, on peut démontrer [10] que, lorsque l'eau est en simple phase à l'entrée du canal, on peut toujours ajuster la sous-saturation en fonction de la longueur, de manière à obtenir des états physiques identiques aux mêmes distances de la sortie de plusieurs canaux de longueurs différentes. On en déduit que la longueur n'intervient pas dans une corrélation utilisant les paramètres de sortie. Les résultats expérimentaux obtenus par de nombreuses équipes montrent que cette propriété

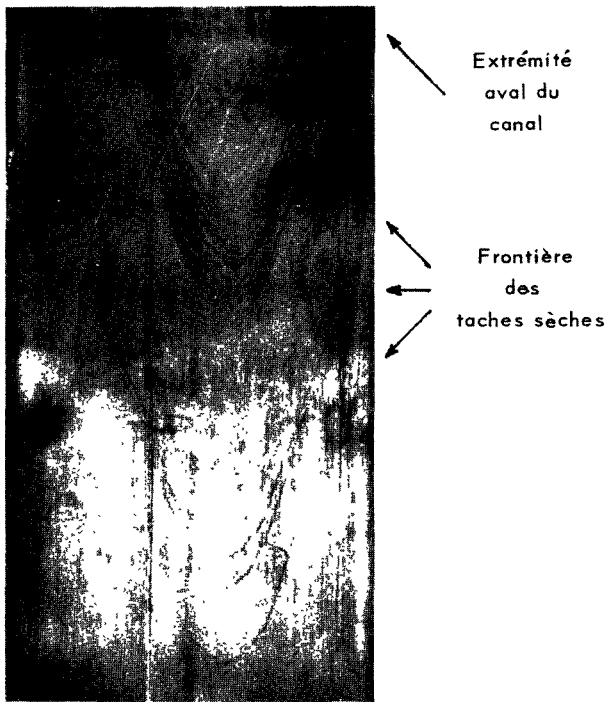


Figure 7. Photographie des frontières de taches sèches formées dans les conditions critiques

peut être généralisée pourvu que l'enthalpie d'entrée reste inférieure à l'enthalpie de saturation.

b) Comparaison du *burn-out* en régime établi et du *burn-out* induit par des oscillations de débit

Dans beaucoup de cas, l'échauffement critique est la conséquence du déclenchement d'oscillations de débit. Dans ce cas, la qualité de vapeur à la sortie est déphasée par rapport au débit massique spécifique à la sortie, et il est indispensable de faire le calcul de ce déphasage pour comparer les conditions critiques dans ce cas avec celles obtenues en régime établi.

Le calcul montre que, en régime de débit oscillant, le *burn-out* en chauffage uniforme se produit pour des flux nettement inférieurs à ceux que l'on obtiendrait avec les mêmes combinaisons de qualité et de vitesse massique à la sortie les plus défavorables en régime établi. On en déduit que le film liquide à la paroi, qui caractérise les écoulements à qualité élevée, est moins stable en régime transitoire.

c) Forme des taches sèches

Sur des canaux rectangulaires et à haute pression (80 et 140 atm), pour des qualités de sortie élevées, on a découvert que les taches sèches caractérisant le *burn-out* laissent sur la paroi du canal des traces de forme parabolique (fig. 7), ce qui permet de vérifier certaines théories sur la formation de ces taches sèches.

d) Echauffement critique en régime transitoire à faible pression et en sous-saturation

Dans le domaine des réacteurs de type piscine à hautes performances, le *burn-out* est à craindre lors

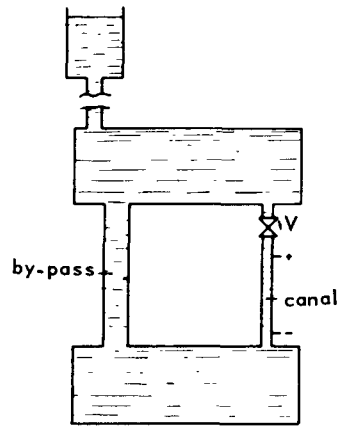


Figure 8. Boucle d'étude des conditions critiques pendant une inversion de débit (schéma)

d'une inversion de débit dans un canal, par arrêt des pompes en particulier. La boucle hors pile d'étude de ce phénomène (fig. 8) permet de déterminer le flux critique pour différents canaux.

Le régime d'essai en transitoire consiste à ouvrir la vanne V au-dessus du canal et simultanément à appliquer le flux ϕ . On estime qu'il y a flux critique ϕ_c lorsque la température augmente dangereusement.

On observe des phénomènes très complexes: l'écoulement est pulsé à une période de l'ordre de la seconde avec expulsion et injection de liquide aux deux extrémités (*chugging*). L'influence du diamètre intérieur du tube D_i et du métal en fonction de la sous-saturation inférieure est montrée en fig. 9 et en fig. 10. On y compare ce type de *burn-out* avec celui correspondant au régime permanent: vanne ouverte, le flux est augmenté progressivement, ce qui permet d'obtenir une convection naturelle en double phase favorisée

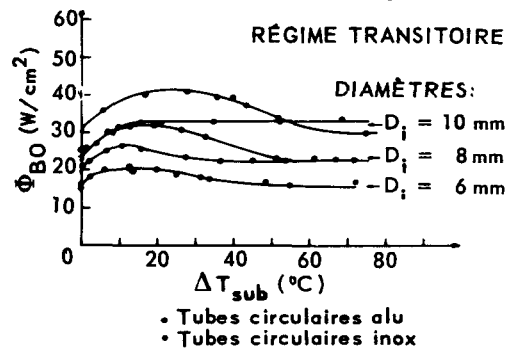


Figure 9. Influence du diamètre et du métal

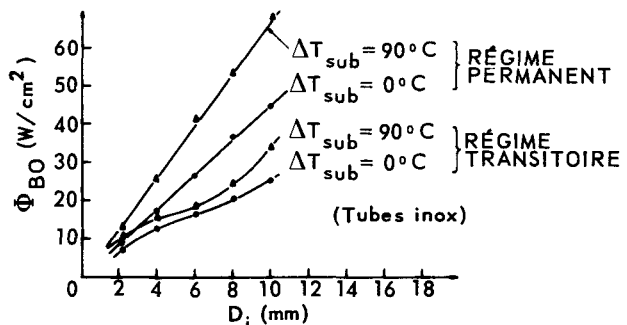


Figure 10. Influence du régime et de la sous-saturation

par la cheminée (*riser*) surmontant le canal, l'écoulement restant pulsé.

En transitoire, le *burn-out* apparaît avant l'extrémité supérieure du tube chauffant, car de l'eau plus froide est aspirée de la cheminée vers le canal; le flux critique augmente alors avec la sous-saturation de l'eau surmontant le canal, conséquence logique de l'écoulement fortement pulsé.

OSCILLATION DE DÉBIT DANS UN CANAL BOUILLANT

Une étude effectuée sous contrat EURATOM [9] avait pour but de déterminer les frontières d'apparition et la forme des oscillations de débit dans un canal bouillant de section circulaire, chauffé uniformément et fonctionnant à pression modérée (1 et 8 atm abs.), avec une perte de pression imposée constante entre les extrémités. La convection naturelle est également possible.

Voici quelques résultats de cette étude:

a) Le seuil d'apparition des oscillations est le même que celui de leur disparition et est indépendant du choix du paramètre que l'on fait varier pour franchir la frontière;

b) On a montré par le calcul et vérifié expérimentalement que les oscillations en convection naturelle étaient un cas particulier d'oscillations à convection forcée correspondant à une perte de pression imposée égale au poids d'eau. Il y a donc continuité parfaite entre les seuils et les périodes dans les deux types de convection;

c) La période au voisinage de seuil est approximativement indépendante du freinage à l'entrée du canal et de la longueur de la cheminée (*riser*). Elle varie comme l'inverse de la vitesse moyenne du liquide dans la zone bouillante;

d) On a des seuils d'oscillation aussi bien pour des qualités de sortie légèrement négatives (ébullition locale) que pour des qualités de sortie élevées;

e) La forme des oscillations au voisinage du seuil se présente sous deux aspects principaux:

1. *Type de relaxation* (fig. 11): l'amplitude atteint sa valeur de régime dès la première oscillation et chaque perturbation a une durée constante;

2. *Type progressif* (fig. 12): l'amplitude atteint



Figure 11. Oscillation de débit du type à relaxation dans un canal bouillant

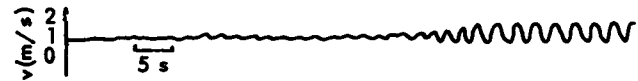


Figure 12. Oscillation de débit du type progressif dans un canal bouillant

lentement sa valeur de régime après un grand nombre d'oscillations régulières.

L'étude générale des systèmes oscillants montre que l'on peut passer du premier type au second par augmentation des termes «dissipatifs», c'est-à-dire ici de la perte de pression par frottement, ce qui est conforme aux résultats expérimentaux.

CONCLUSION

Les quelques aspects nouveaux de l'ébullition et des phénomènes connexes qui ont été exposés constituent une contribution qui peut paraître petite en comparaison de l'extrême complexité des problèmes qui se posent aux projeteurs de réacteurs refroidis par liquide.

Mais si on rassemble tous les résultats analogues obtenus dans le domaine de l'ébullition depuis cinq ans, on constate que des progrès considérables ont été réalisés, qui justifient l'orientation vers les études fondamentales prise par les chercheurs pendant cette période. Malgré la simplicité et le faible prix des moyens expérimentaux mis en œuvre, l'effort de réflexion entrepris, valorisé par une excellente collaboration internationale, s'est avéré extrêmement fructueux.

BIBLIOGRAPHIE

1. Semeria, R., Comptes rendus des VII^{es} Journées de l'hydraulique, tome 1, 90-97 Société hydrotechnique de France, Paris (1962).
2. Semeria, R., Comptes rendus Acad. Sc. 256, 1227-1330, Paris (1963).
3. Behar, M., Semeria, R., La houille blanche, 687-691 (octobre 1963).
4. Behar, M., Semeria, R., Comptes rendus Acad. Sc., 257 2801-2803, Paris (1963).
5. Behar, M., *Ebullition et strioscopie*, film 16 mm, Centre d'études nucléaires de Grenoble (1964).
6. Jansen, F., Comptes rendus Acad. Sc. (en publication), Paris.
7. Lavigne, P., Rapport CEA 2365 (1963).
8. Delayre, R., et Lavigne, P., Symposium de Studsvik (octobre 1963).
9. Fabrega, S., Rapport final n° 1—Contrat EURATOM 076-61-12-RDF (1963).
10. Mondin, H., Symposium de Studsvik (octobre 1963).

ABSTRACT—RÉSUMÉ—АННОТАЦИЯ—RESUMEN

A/55 France

Some fundamental aspects of boiling in nuclear reactors

By H. Mondin *et al.*

The main results obtained at Grenoble during the last four years in the field of boiling mechanisms and related phenomena in nuclear reactors are reported.

Observation of boiling

By the use of photography and high-speed cinematography (8 000 frames per second maximum), boiling in a vessel or a tube was observed up to 140 kg/cm². The populations of bubble-generating seeds (sites) were counted, and a correlation giving their number per unit of surface area as a function of the thermal flux and the pressure was established. The diameter of the bubbles breaking off from the wall was studied up to 140 kg/cm²; three types of bubble have been shown to exist:

(a) Those in equilibrium, their diameter following the formula of Fritz and Ende;

(b) Bubbles formed by boiling, the diameters of which decrease rapidly with the pressure (1/100 mm to 100 kg/cm²);

(c) The coalescences which appear in saturated liquid above 15 W/cm², their proportions being independent of the pressure.

Photographic observations were made of the movements of the thermal film associated with the generation of the seeds, at the initiation and condensation of the bubbles; the mechanisms responsible for the highly efficient heat transfer could thus be defined.

Pressure losses in two-phase flow

A physical model of the continuous variation of the free space content in a boiling channel has been proposed by means of which the pressure losses can be calculated without invoking a break in the coefficient of friction when free boiling begins. Agreement between theory and experiment is satisfactory. The various forms which total pressure loss in a boiling tube may present as a function of flowrate have been studied. Special features are observed at very low and very high speeds.

Burn-out

Under steady operating conditions, it is shown that in a uniformly heated channel the burn-out flux as a function of output rate is generally independent of the length. When burn-out is a result of output oscillation, the conditions of burn-out are compared with those obtained under steady conditions. The burn-out flux following uniform "no-flow" heating has been studied in a channel containing still water. The flux reaches a maximum at conditions below saturation.

Output oscillations

Using a low pressure (8 atm) loop, the influence of various parameters on the periods of output oscillations

in a boiling channel on the thresholds at which they appear, was studied. Some new aspects of this complex phenomena were observed and are reported.

A/55 Франция

Некоторые фундаментальные аспекты кипения в ядерных реакторах

X. Мондин *et al.*

Приводятся основные результаты, полученные в Гренобле за четыре года в результате изучения механизмов кипения и смежных явлений в ядерных реакторах.

Наблюдение за кипением

С помощью фотографии и сверхскоростной кинематографии (максимум 8000 снимков в секунду) проводилось наблюдение за кипением в сосуде или канале при давлениях до 140 кг/см².

Было подсчитано число центров (мест) образования пузырьков и получено соотношение, устанавливающее их количество на единицу поверхности в зависимости от теплового потока и давления.

Диаметр отделяющихся от стенки пузырьков изучался при давлениях до 140 кг/см². Выявлены три типа пузырьков:

- пузырьки в состоянии равновесия, когда их диаметр соответствует формуле Фрица и Энде;
- пузырьки при кипении, когда их диаметр быстро уменьшается с увеличением давления (0,01 мм до 100 кг/см²);
- слияние пузырьков в жидкости при поверхностном тепловыделении сверх 15 Вт/см², когда их размеры не зависят от давления.

Были проведены стрископические наблюдения за движениями тепловой пленки, связанной с зарождением центров образования пузырьков в начале процесса и конденсацией, — таким путем удалось уточнить механизмы, регулирующие перенос тепла.

Потери давления в двухфазном потоке

Создана модель постоянного изменения коэффициента пустотности в кипящем канале, позволяющая рассчитывать потери давления без разрыва коэффициента трения в начале свободного кипения. Согласие теории с экспериментом удовлетворительное.

Были изучены эффекты полного падения давления при кипении в канале в зависимости от режима. Особенности наблюдались при очень малых и очень больших скоростях.

Кризис кипения

Отмечается, что при установившемся режиме в канале с равномерным нагревом критический тепловой поток как функция мощности не зависит от длины этого канала.

Когда кризис является следствием колебания мощности, то условия кризиса сравниваются с условиями, полученными на установившемся режиме.

Изучается критический тепловой поток, получаемый в результате равномерного нагрева в канале с неподвижной водой. Поток как функция недогрева имеет максимум. Исследуется влияние геометрии и природы металла.

Колебания мощности

На контуре с низким давлением (8 ат) выяснялось влияние различных параметров на периоды колебаний мощности в кипящем канале и на пороги их появления.

Некоторые новые аспекты этого сложного явления наблюдались и описаны в докладе.

A/55 Francia

Algunos aspectos fundamentales de la ebullición en los reactores nucleares

por H. Mondin *et al.*

Se indican los principales resultados que desde hace cuatro años se vienen obteniendo en Grenoble en materia de mecanismos de ebullición y de fenómenos conexos en los reactores nucleares.

Observación de la ebullición

Se ha observado, por fotografía y cinematografía ultrarrápidas (máximo de 8 000 imágenes por segundo), la ebullición en recipientes o en canales hasta 140 kg/cm².

Se han contado las poblaciones de gérmenes (*puntos*) generadores de burbujas y se ha establecido una correlación que expresa su número por unidad de superficie en función del flujo térmico y de la presión.

Se ha estudiado hasta 140 kg/cm² el diámetro de las

burbujas que se desprenden de las paredes; se han observado tres tipos de burbujas:

a) Las burbujas en equilibrio, cuyo diámetro satisface la fórmula de Fritz y Ende;

b) Las burbujas de ebullición, cuyo diámetro disminuye rápidamente con la presión (0,01 mm a 140 kg/cm²);

c) Las coalescencias que aparecen en líquido saturado por encima de 15 W/cm² y cuya proporción es independiente de la presión.

Por visualización estrioscópica se observan los movimientos de la película térmica asociados al comienzo de la formación de los gérmenes, al iniciarse y al condensarse las burbujas. De este modo se han podido aclarar los mecanismos determinantes de la excelente transmisión de calor.

Pérdidas de presión en circulación bifásica

Se ha preparado un modelo de variación continua del índice de vacío en un canal de ebullición, que permite calcular las pérdidas de presión sin discontinuidad del coeficiente de rozamiento al principio de la ebullición franca. La comparación con los resultados experimentales es satisfactoria.

Se han estudiado las diversas formas que puede presentar la pérdida total de presión en un canal de ebullición, en función del caudal. Se observan particularidades a velocidades muy bajas y muy elevadas.

Calefacción

En régimen estable, se demuestra que en un canal uniformemente calentado, el flujo de calefacción en función del título de salida es en general independiente de la longitud.

Cuando la calefacción es consecuencia de la oscilación del caudal, se comparan las condiciones de calefacción con las obtenidas en régimen estable.

Se ha estudiado el flujo de calefacción a raíz de un calentamiento uniforme "en escalón" en un canal que contenía agua estancada. El flujo presenta un máximo en función del grado de no saturación. Se ha examinado la influencia de la geometría y de la naturaleza del metal.

Oscilaciones de caudal

En un circuito de baja presión (8 atm) se ha investigado la influencia de diversos parámetros sobre el período de las oscilaciones de caudal en un canal en ebullición y sobre los umbrales a que éstas aparecen.

Se han observado algunos aspectos nuevos de este complejo fenómeno.

La technique des écoulements diphasés tourbillonnaires dans les réacteurs à eau

par C. Foure, C. Moussez et D. Eidelman*

INTRODUCTION

Si on superpose au mouvement de translation du fluide qui s'écoule le long d'une paroi un mouvement de rotation, le champ de forces centrifuges provoque une modification de la répartition des températures et vitesses qui doit être, en principe, favorable à l'échange de chaleur.

Des expériences de base [1] ont montré qu'il en était bien ainsi en écoulement à phase unique et les gaines polyzonales ou à chevrons, d'un emploi quasi généralisé dans les réacteurs à gaz, font application de ce procédé en provoquant les écoulements de rotation secondaires par les ailettes attachées à la gaine [2, 3]. On peut également provoquer ces rotations par des jets auxiliaires répartis [4]. Lorsqu'il s'agit d'un liquide susceptible de passer au moins momentanément en phase vapeur, les résultats sont quelquefois spectaculaires en ce qui concerne le flux critique, pour peu que l'on consente à une perte de charge élevée [5].

L'objet des travaux entrepris par notre société depuis 1960 dans le cadre de contrats EURATOM-USAEC est de définir une technique faisant appel à des écoulements hélicoïdaux accolés, adaptables aux types de géométrie et aux conditions de fonctionnement en usage dans les réacteurs nucléaires refroidis par eau bouillante, d'assembler les données nécessaires pour aborder un avant-projet, particulièrement sur les pertes de charge, fractions de vide et flux critique et atteindre en même temps une compréhension suffisante des phénomènes mis en cause.

L'intérêt s'est concentré sur le type de réacteur nucléaire refroidi par eau bouillante le plus courant qui utilise le même fluide pour le ralentissement des neutrons et dont le cœur est généralement constitué de faisceaux de barreaux combustibles cylindriques verticaux assemblés en maille carrée, entre lesquels circule, de bas en haut, le mélange eau-vapeur. Il était donc important de montrer l'efficacité d'un tourbillon engendré dans le canal unitaire délimité par quatre barreaux et la compatibilité d'un ensemble d'écoulements tourbillonnaires unitaires associés. Le mélange est mis en rotation par des bandes vrillées introduites dans chaque canal unitaire, occupant ou non la totalité de sa section droite.

Dans des essais préliminaires sur des géométries simples (canaux cylindriques circulaires, annulaires et rectangulaires), on constate, par visualisation d'un mélange eau-air, le rassemblement de la phase légère dans l'axe des vrilles et la compatibilité d'existence des tourbillons unitaires associés (fig. 1).

Parallèlement aux essais thermiques de détermination du flux critique, ont été étudiées les chutes de pression du mélange à deux phases centrifugé ainsi que la «fraction de vide» ou fraction de volume total de mélange occupé par la vapeur. La connaissance de cette dernière grandeur dans les canaux du réacteur est importante puisqu'elle définit la capacité modératrice du mélange.

Types d'expérimentations

Les essais ont porté sur la comparaison entre les écoulements droits et tourbillonnaires, et les trois grandeurs principales pour lesquelles des corrélations ont été recherchées sont, comme on l'a déjà exposé, la fraction de vide, la chute de pression et le flux critique. Les installations permettant d'effectuer ces expériences sont de deux types: *a*) une installation non thermique à cycle semi-ouvert, et *b*) des installations thermiques, boucle en circuit fermé.

Configuration du canal

La section d'essais se compose de quatre barreaux ϕ 14 mm (chauffants dans les essais thermiques) centrés aux sommets d'un carré de 19 mm de côté introduits dans un canal dont les limites toujours inertes thermiquement simulent la présence des barreaux adjacents aux barreaux centraux (fig. 2a). L'ensemble représente une portion interne d'un assemblage de barreaux combustibles et délimite neuf canaux unitaires de forme cruciforme dans lesquels les bandes vrillées sont introduites. D'un canal unitaire à ceux qui l'entourent, le sens de rotation des tourbillons est inversé.

Cette géométrie a été étudiée hydrodynamiquement sans et avec vrilles «circulaires» et «cruciformes» et thermiquement sans et avec vrilles «cruciformes» seulement. Les bandes vrillées sont définies par leur demi-pas réduit y , longueur nécessaire pour une rotation de 180° exprimée en multiple de la largeur de la bande. Cette dernière est dite «circulaire» lorsque sa largeur est constante; elle est alors inscrite à l'intérieur

* Division atomique de la Société nationale d'étude et de construction de moteurs d'aviation.

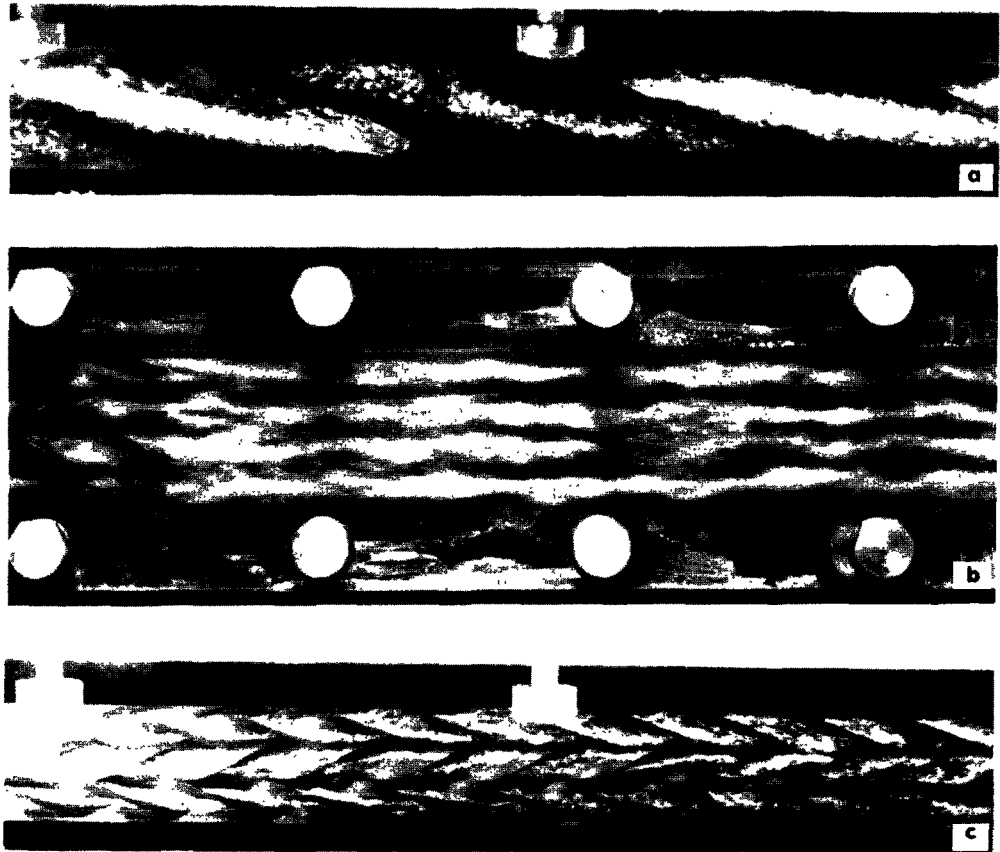


Figure 1. Visualisation de l'écoulement montrant le rassemblement de la phase gazeuse au voisinage des axes des vrilles
 a: Tube circulaire (1 bande vrillée); b: Canal rectangulaire (4 bandes vrillées); c: Canal annulaire (6 bandes vrillées autour d'un barreau axial)

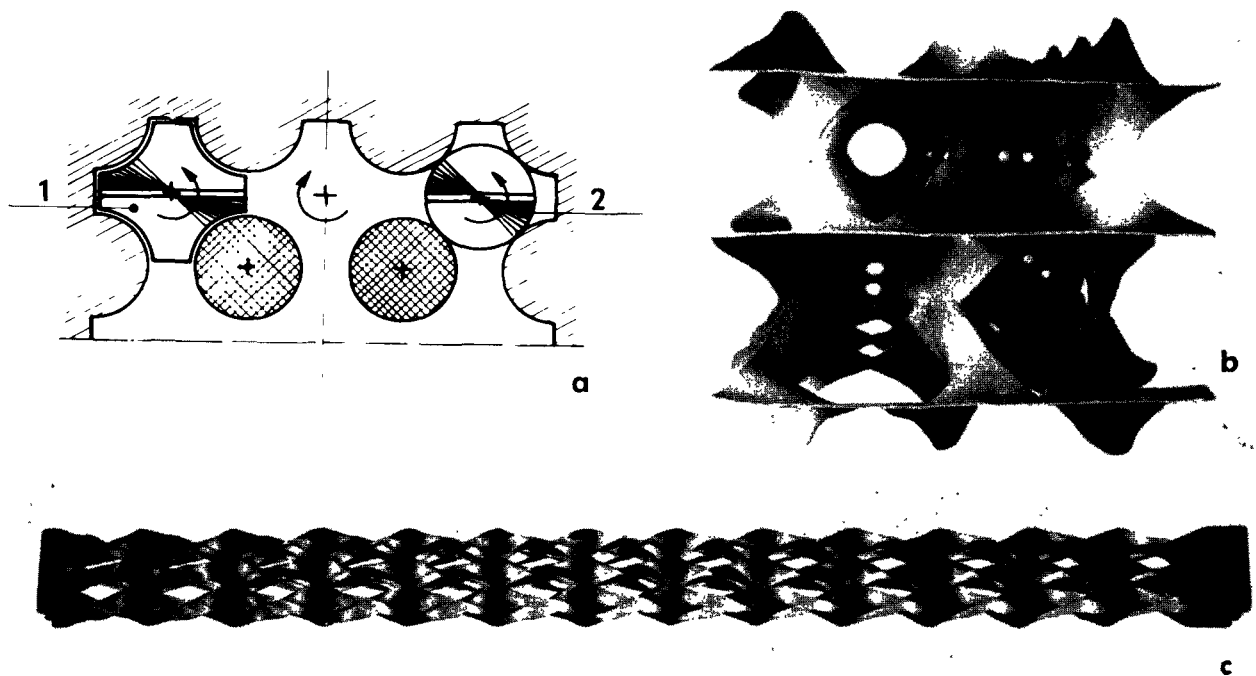


Figure 2. Vrilles
 a: Vrille cruciforme (1), vrille circulaire (2); b: Vue en bout d'un assemblage de vrilles cruciformes;
 c: Vue latérale du même assemblage

d'un canal unitaire et tangente aux barreaux par points.

Les vrilles dites « cruciformes » ont une largeur évolutive comprise entre le pas de la maille et la distance entre deux barreaux située sur une diagonale. C'est la première cote qui est prise comme largeur de référence. La vrille est tangente aux barreaux sur toute sa développée et vue en bout, elle occupe la totalité du canal unitaire (fig. 2b et 2c).

Après quelques essais préliminaires, un demi-pas égal à 3 a été choisi pour tous les travaux. Ce demi-pas correspond environ à la limite technologique d'obtention de vrilles d'épaisseur comprise entre 0,4 et 0,7 mm.

ESSAIS HYDRODYNAMIQUES

Les conditions d'expérimentation portent sur le mélange air-eau à des pressions comprises entre 1 et 5 bars. On recherche la chute de pression en écoulement à deux phases et la fraction de vide pour des vitesses caractéristiques de l'eau comprises entre 0,25 et 4 m/s et des titres en masse de 0 à 30%.

Mesures

Les chutes de pression sont mesurées à la paroi.

La fraction de vide moyenne est obtenue par deux méthodes:

a) La première, qui a été mise au point pour ces essais, consiste à mesurer la vitesse moyenne du liquide en y incorporant une brève injection d'un traceur électrolytique (eau + sel) [6]. Le passage du traceur est détecté dans deux plans, l'un à l'entrée, l'autre à la sortie de la section d'essais, par deux électrodes isolées l'une de l'autre et mises sous tension. Au passage du sel on constate un défaut d'isolement, signal reçu par un oscillographe électro-optique avec enregistrement sur bande photographique. La connaissance de la vitesse de la phase liquide seule, jointe à celle des débits-masses respectifs de l'eau et de l'air, permet de déterminer la fraction de vide.

b) Dans le but de recouper les résultats de la méthode de la bouffée conductrice, la fraction de vide a été également mesurée par absorption des rayons gamma. La fraction de vide globale s'obtient à partir d'enregistrements (fig. 3) réalisés section d'essais vide, remplie d'eau ou parcourue par le mélange eau-air.

Résultats

En général, les résultats sont en assez bon accord avec les courbes de Martinelli [7, 8] correspondant à la pression atmosphérique et ceci pour toutes les configurations. L'accord paraît d'ailleurs substantiellement meilleur lorsqu'on s'intéresse à des écoulements giratoires induits par des vrilles. La figure 4a illustre les résultats de chutes de pression portés dans le diagramme (ϕ , X).

On constate:

a) Sans vrilles: un écart maximum par rapport à la courbe de Martinelli de 30% et un effet de la vitesse débitante;

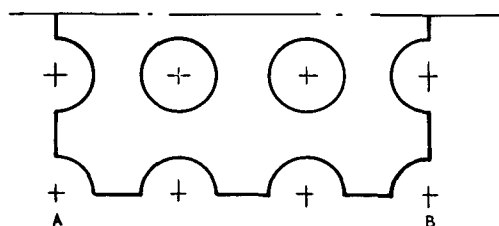
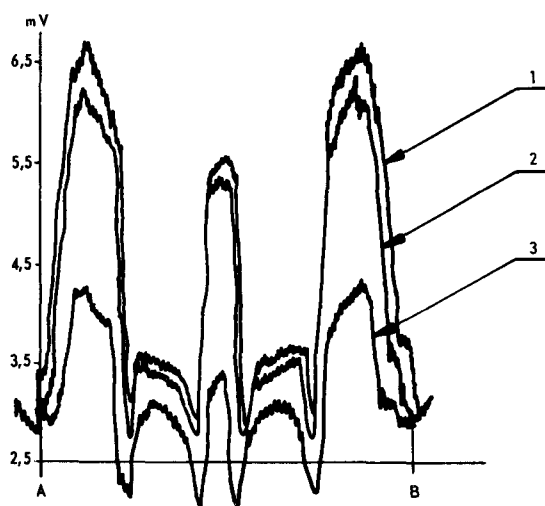


Figure 3. Enregistrement gammamétrique
1: Air; 2: Mélange air-eau; 3: Eau

b) Avec vrilles: un écart inférieur à 10% sans effet de vitesse.

La figure 4b donne les résultats correspondants pour la fraction de vide α . Les écarts avec la courbe de Martinelli, sans et avec vrilles, sont alors respectivement de 20 et 10%.

La comparaison des résultats obtenus par les deux méthodes est généralement bonne. La moyenne quadratique des écarts dans les deux expériences, avec et sans vrilles, est de l'ordre de 6%. En fait, les écarts maximaux varient de 14 à -12%, valeurs obtenues dans le cas d'essais à très faibles ou très fortes fractions de vide, c'est-à-dire aux faibles titres pour la méthode du traceur et aux titres élevés pour la méthode gammamétrique où la sensibilité des méthodes n'est pas satisfaisante.

Signalons que pour chaque mesure la dispersion intrinsèque est inférieure à 5%. On peut trouver une relation simple [9] entre ϕ et α de la forme

$$\phi = K(1 - \alpha)^{-p}$$

avec $p = 0,91$ et $K = 1,1$ sans vrilles, $K = 0,95$ avec vrilles pour $y = 3$. Dans cette représentation la dispersion constatée est de $\pm 15\%$.

ESSAIS THERMIQUES

On recherche le flux critique d'ébullition en faisant croître la puissance fournie par effet Joule aux quatre barreaux de la section d'essais pour des conditions d'entrée de l'écoulement définies (débit, titre). Les

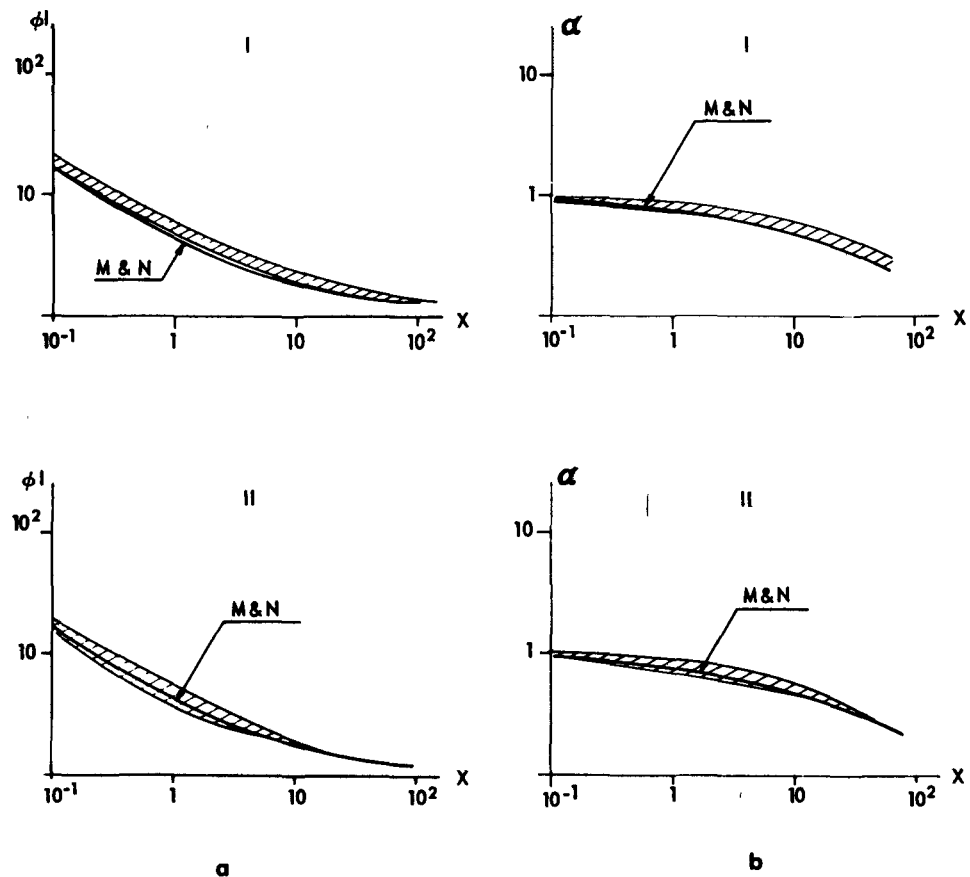


Figure 4. Chute de pression et fraction de vide. Comparaison des résultats SNECMA avec les courbes de Martinelli et Nelson (repérées M et N)
Mélange eau-air à la pression atmosphérique, titre $x \leq 29\%$; Vitesse de l'eau seule comprise entre 0,25 et 4 m/s; I: sans vrilles, II: avec vrilles; a: Facteur de frottement; b: Fraction de vide

installations utilisées comprenaient deux boucles à circulation forcée, l'une fonctionnant au voisinage de la pression atmosphérique, l'autre à 70 bars reproduisant les conditions de fonctionnement d'un réacteur nucléaire.

Un détecteur de crise a été mis au point afin d'éviter la destruction systématique des tubes chauffants à chaque point de mesure. L'élément sensible est constitué par un tube en pyrex sur lequel est enroulé un fil de constantan de 8/100 de mm, à raison de deux spires par mm. En cuivrant, sur toute la longueur de l'enroulement, des zones limitées par des génératrices du cylindre, on réalise huit rangées de couples thermoélectriques cuivre-constantan. Une sur deux des génératrices est isolée par un revêtement de ciment réfractaire, l'autre—dite sensible—est en regard de la surface chauffante à préserver.

Une augmentation de température, assez rapide, de la surface de chauffe agit par rayonnement sur les couples nus sans influencer les couples protégés thermiquement. Ces derniers jouent le rôle de soudures froides pour l'ensemble du système. La multiplicité des couples en série permet de détecter, rapportées à chaque couple, des variations de température très faibles. Pour protéger les éléments chauffants de la section à quatre barreaux, un détecteur est introduit

dans chaque tube générateur de puissance. Le signal obtenu permet, par l'intermédiaire d'un montage électronique, de couper l'alimentation électrique de la section d'essais.

Résultats

A la pression atmosphérique

Conditions expérimentales: titres d'entrée variant de -3 à $+2\%$; vitesses de 0,25 à 1,5 m/s; flux critiques inférieurs à $2\,500\text{ kW/m}^2$.

L'évolution du flux critique en fonction du débit surfacique est représentée sur la figure 5a pour une section d'essais avec et sans vrilles. On remarquera qu'à débit donné l'introduction des bandes vrillées permet d'atteindre des flux 35 à 50% supérieurs aux flux réalisés en l'absence de tout dispositif de centrifugation. De plus, la crise, pour un flux donné, apparaît à un débit nettement plus faible pour les écoulements giratoires. Le rapport entre le débit avec écoulement droit et celui avec écoulements tourbillonnaires atteint 2.

A 70 bars

Conditions expérimentales: titres d'entrée variant de -6 à 15% ; vitesse de 0,25 à 1,5 m/s; flux critiques inférieurs à $2\,500\text{ kW/m}^2$.

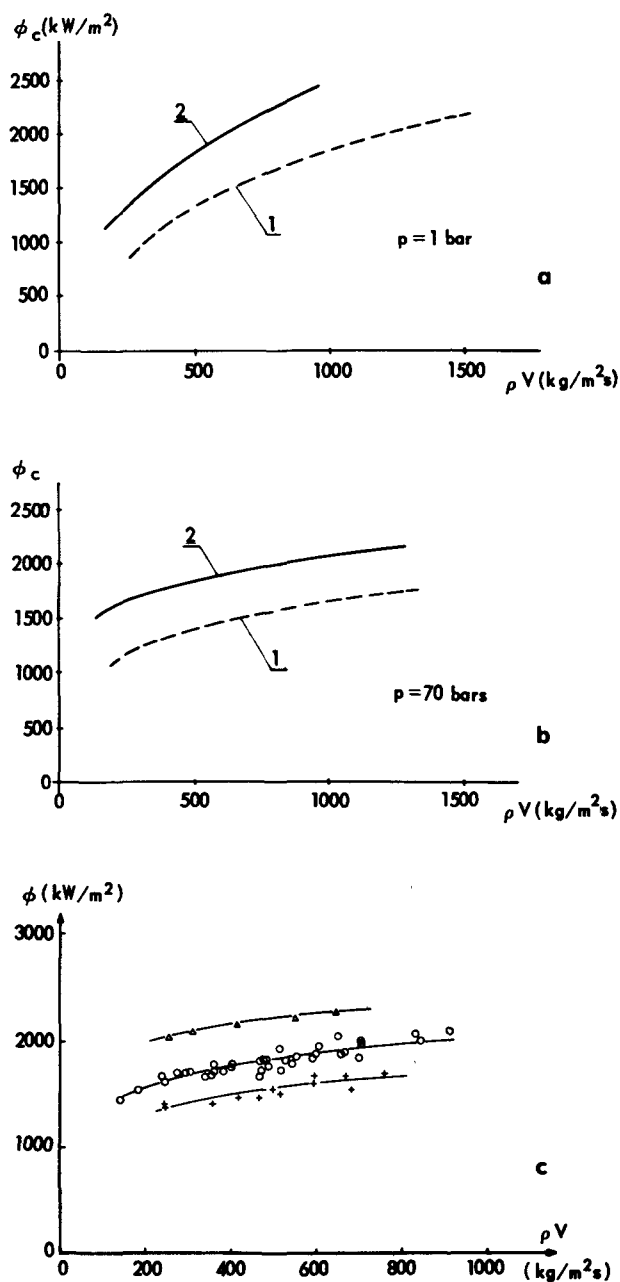


Figure 5. Flux critique en fonction du débit surfacique
Entrée à la saturation, sans vrilles: 1, avec vrilles cruciformes: 2, a: Résultats à 1 bar; b: Résultats à 70 bars; c: Effets de la rugosité à 70 bars; 0: Tubes du commerce; +: Tubes polis; Δ : Tubes grenailés

La figure 5b montre que l'augmentation du flux critique par introduction des vrilles est moindre. Sur cette figure, par souci de clarté, n'ont été tracés que les résultats correspondant aux écoulements pour lesquels la saturation est atteinte à l'entrée de la section d'essais.

Aux deux niveaux de pression considérés, il a pu être constaté une stabilité accrue de l'écoulement diphasé lorsque les sections d'essais sont équipées de vrilles.

Il est apparu qu'aussi bien sans vrilles qu'avec vrilles les flux critiques obtenus évoluaient d'une

première limite à une limite supérieure de 50% environ après un certain temps de fonctionnement de la boucle à 70 bars. Il a été constaté que dans le même temps un mince dépôt se formait sur les barreaux chauffants en inconel à partir, semble-t-il, des pièces en alliage léger simulant les barreaux avoisinants.

Après nickelage de ces pièces, afin d'éviter ce phénomène, les essais furent repris avec des barreaux présentant les états de surface suivants:

Barreau commercial: CLA 0,75 μ

Barreau poli: CLA 0,2 μ

Barreau grenailé: CLA 4,7 μ

La figure 5c représente les flux critiques obtenus avec vrilles en fonction du débit surfacique avec entrée à saturation et pour les trois types de rugosité. On voit que par rapport au barreau commercial les barreaux polis font perdre environ 20% et les barreaux grenailés font gagner 20%.

D'autres travaux ont été publiés ou sont en cours sur ce sujet [10-12]. Il est possible que la rugosité ne joue un rôle favorable que tant que son échelle n'est pas trop grande par rapport à l'épaisseur du film liquide.

APPLICATION A UN RÉACTEUR BOUILLANT

Un ensemble d'études devant permettre la définition d'un avant-projet de réacteur bouillant adapté à l'utilisation rationnelle des avantages thermiques alloués par l'écoulement tourbillonnaire a été entrepris.

L'influence de l'introduction des vrilles sur le facteur de multiplication infini k_∞ d'un réseau de réacteur bouillant type a d'abord été déterminée. Le réacteur type choisi est celui de la SENN. Les courbes de la figure 6 montrent l'évolution du k_∞ en fonction de l'enrichissement en ^{235}U pour diverses épaisseurs de vrilles en Zircaloy et suivant que le réacteur est chaud ou froid. Un calcul analogue a été fait pour des vrilles en acier inoxydable. On voit que l'enrichissement initial supplémentaire nécessaire pour retrouver le même k_∞ à chaud est faible. Pour un enrichissement initial $\alpha = 2,1\%$, les valeurs de α nécessaires sont les suivantes:

	Zircaloy			Acier inoxydable		
e (cm)	0,04	0,06	0,08	0,04	0,06	0,08
α (%)	2,135	2,15	2,17	2,32	2,45	2,57

On a vu que l'introduction de vrilles dans un réseau augmente le flux critique calorifique. Le réseau d'un réacteur à écoulement tourbillonnaire pourra être constitué avec des barreaux combustibles de diamètre inférieur. Considérons les caractéristiques du réseau à k_∞ maximal de deux réseaux isotropes indéfinis (sans boîtiers ni barres de contrôle):

	Rayon du barreau (cm)	Pas de réseau (cm)	Puissance volumique kW/l	Puissance massique $\text{(kW/kg de } \text{UO}_2\text{)}$
Sans vrilles ...	1,394	0,626	2,51	25,9
Avec vrilles en Zircaloy (0,4 mm d'épaisseur)	1,361	0,464	1,93	42,8
				12,4
				22,5

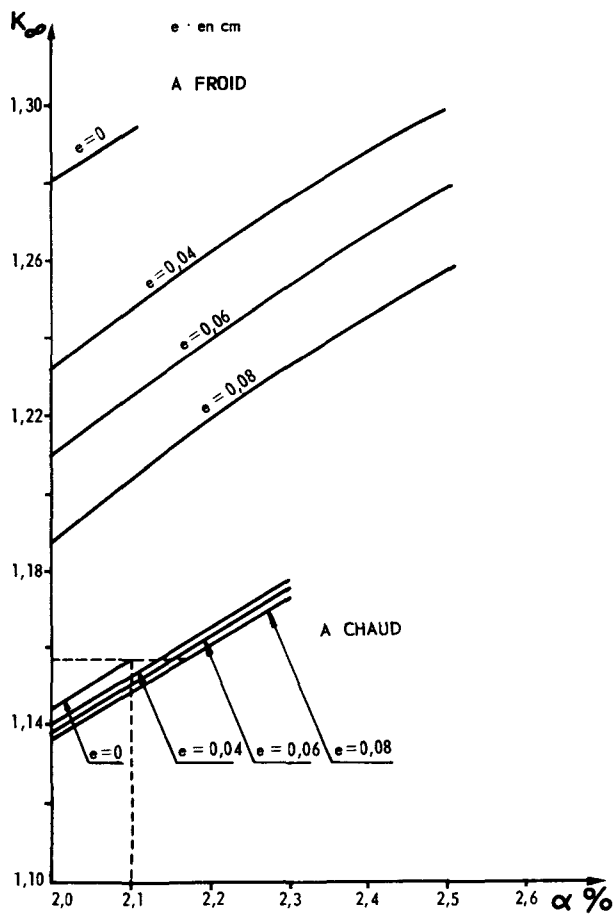


Figure 6. k_{α} en fonction de l'enrichissement α pour différentes épaisseurs de vrilles en Zircaloy-2

Pour une puissance totale à extraire donnée, on obtiendra un cœur beaucoup plus compact par

l'utilisation des vrilles sans avoir à augmenter la longueur totale de barreaux combustibles. Aussi l'investissement initial en combustible sera plus faible. Cependant cela signifie que pour un taux de combustion admissible donné, la rotation des barreaux combustibles devra être accélérée. Une étude économique tenant compte du coût de cette rotation et de l'introduction de vrilles d'une part, du gain sur le combustible immobilisé ainsi que sur le prix de première installation par diminution de la taille d'autre part, devrait fournir des indications précises sur l'intérêt des écoulements tourbillonnaires par vrilles dans les réacteurs bouillants.

Soulignons que les valeurs des rayons déterminées sont des valeurs minimales compatibles avec l'extraction d'un flux de chaleur surfacique donné.

La figure 7 montre deux configurations de cœur à vrilles envisagées: un réacteur à vrilles dérivé du type à boîtiers et un réacteur à vrilles dans lequel on a supprimé les boîtiers.

Pour un réacteur fournissant 450 MW(th), on est conduit à un cœur de 120 assemblages de 100 barreaux chacun et une hauteur active de 2,36 m. Le diamètre du cœur, suivant la solution, serait compris entre 2,10 m et 2,50 m.

Dans le premier cas, le boîtier est constitué par une enveloppe ondulée fixée sur le paquet de vrilles constituant l'élément structural de l'ensemble. L'ondulation des tôles permet l'existence des vrilles, même aux frontières du boîtier, donc le refroidissement par tourbillon des barreaux de rive. La barre de contrôle de forme cruciforme est constituée par l'assemblage rigide des tubes contenant le poison et de diamètre extérieur voisin de celui des barreaux combustibles (fig. 7a).

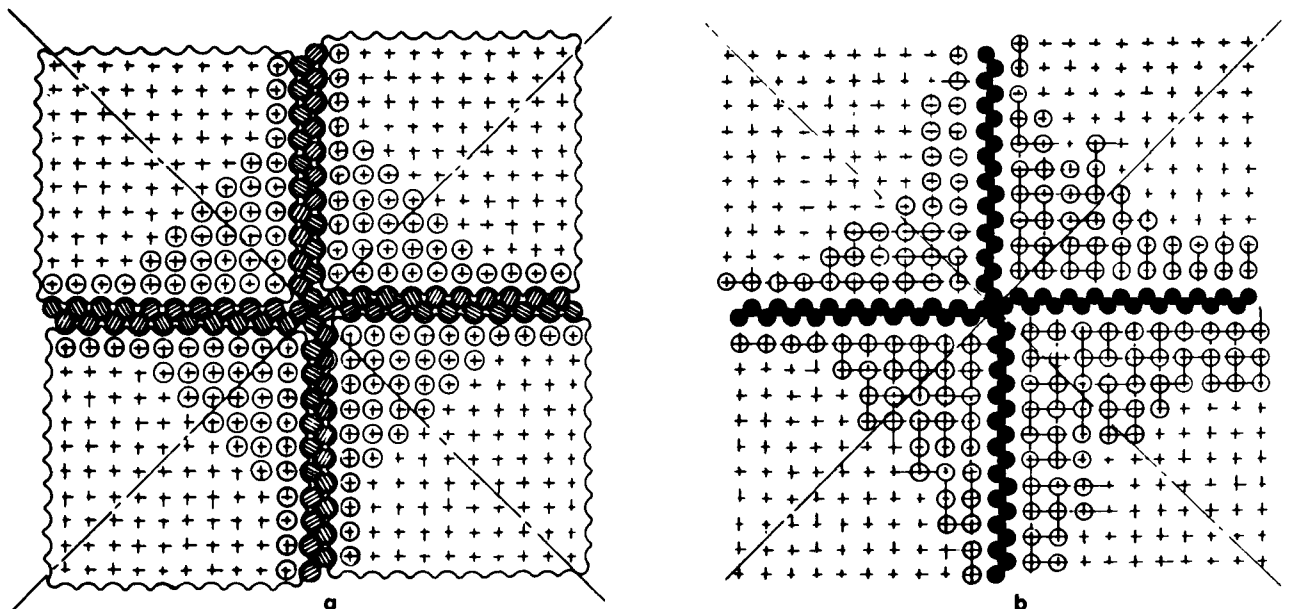


Figure 7. Détail du réseau à vrilles
a: Avec boîtiers ondulés; b: Sans boîtiers

Pour un réseau sans boîtiers, les vrilles formeraient toujours l'élément structural de l'assemblage combustible. Les barres de contrôle seraient constituées de barreaux cylindriques fixés à un poussoir cruciforme, les barreaux coulissant dans des tubes guides placés à demeure dans le réacteur et de diamètre extérieur identique à celui des barreaux combustibles (fig. 7b).

L'application de cette technique n'est pas limitée aux réacteurs nucléaires refroidis et modérés par eau bouillante. On peut l'envisager pour tous les réacteurs refroidis par liquides bouillants ou brouillards, qu'ils soient thermiques hétérogènes à modérateur eau lourde ou graphite, ou homogènes avec mélange ou alliage hydrure métallique-combustible métallique ou qu'ils soient à spectre de neutrons rapides. On notera également que cette technique prend un intérêt particulier si le réacteur doit opérer dans un champ de gravité d'orientation variable (navire) ou nul (vaisseau spatial).

BIBLIOGRAPHIE

1. Kreith, F., et Margoulis, D., Applied Scientific Research, Sect. A, Vol. 8, No. 6, 457-473 (1959).
2. Ritz, H. L., *Cartouche active cloisonnée à ailettes hélicoïdales*, Actes de la deuxième Conférence internationale sur l'utilisation de l'énergie atomique à des fins pacifiques, P/48; vol. 4, Nations Unies (1959).
3. Pelcet J., François, S., et Housseaux, O., Rapport CEA 2.469.
4. Mihail A., et Foure, C., Journées de la transmission de la chaleur IFCE, SFT, Paris (1961).
5. Gambill, W. R., et Grenne, N. D., Chem. Eng. Prog. 54, 68-76 (1958).
6. Foure, C., VII^{es} Journées de l'hydraulique, SHF, Paris (1962).
7. Martinelli, R. C., et Nelson, D. B., Trans. ASME, vol. 70, 695-702 (1948).
8. Lockhart, R. W., et Martinelli, R. C., Chem. Eng. Prog., vol. 45 (1949).
9. Mondin, H., VII^{es} Journées de l'hydraulique, SHF, Paris (1962).
10. Durant, W. S., et Mirshak, S., DP 380 (1959).
11. Janssen, E., Levy, S. et Kervinen, J. A., ASME 63 WA 149 (1963).
12. Quinn, E. P., GEAP-4487 (1964).

ABSTRACT—RÉSUMÉ—АННОТАЦИЯ—RESUMEN

A/95 France

Technique for vortex type two-phase flow in water reactors

By C. Foure et al.

This report is based on work which has been carried out for the most part under a contract with the EURATOM/USA Joint Committee.

In the first place it has been shown that the longitudinal vortices which are contiguous and coherent can be produced and preserved in channels having different cross sections, in particular those occurring in boiling water nuclear reactors where the fuel elements are placed at the nodes of a square lattice. Each elementary vortex is produced by a spiral metallic strip placed in the channel.

The pressure drop and the proportion of voids during two-phase flow have been determined as a function of the main parameters which can apparently be regrouped in the form proposed by Martinelli and his co-workers.

By means of these twisted strips it has been possible to increase the heat transferred to a boiling water flow by 25 to 40 per cent for the same pumping power, depending on whether one operates at 70 bars or at atmospheric pressure. Apart from their role of flow guides, these strips joined together can become part of the core structure.

The calculation of K_{∞} for a typical boiling-water reactor fitted with spiral vanes shows that the extra enrichment required to compensate for the presence of the material of the strip is very small (below 0.1% for Zircaloy strips 0.4 mm thick).

A boiling-reactor core designed to make best use of the spiral strips could operate at a power per unit volume greater (by at least 50%) than that of a reactor without these spirals. An economic study will show the advantages of this type of modification.

A/95 Франция

Техника двухфазных вихревых потоков в водных реакторах

К. Фуре et al.

Этот доклад основывается на работе, которая большей частью была проведена по контракту с Евратомом и Объединенным комитетом США.

Вначале показано, что продольные, расположенные рядом когерентные вихри могут быть созданы и сохранены в каналах с переменным поперечным сечением и, в частности, в сечениях, которые имеются в ядерных кипящих реакторах, где тепловыделяющие элементы расположены в гнездах решетки с квадратной ячейкой. Каждый элементарный вихрь вызывается витой металлической лентой, закрепленной в соответствующем подканале.

Падение давления и пустотный коэффициент при двухфазном потоке определялись в зависимости от основных параметров, которые, видимо, можно сгруппировать по формуле, предложенной Мартинелли и его сотрудниками.

С установлением витых лент подогрев кипящего водяного потока может быть увеличен на

25—40% при той же мощности прокатки, если работа ведется при давлении около 70 бар или около атмосферного давления. Эти соединенные между собой ленты помимо своей функции распределителя потока могут выполнять конструктивные функции.

Расчет k_{∞} для кипящего реактора с витыми лентами показывает, что дополнительное обогащение, необходимое для компенсации поглощения нейтронов материалом витков, должно быть очень небольшим (ниже 0,1% для витков из циркония толщиной 0,4 мм).

Активная зона кипящего реактора, в которой используются витые ленты и спроектированная наилучшим образом, могла бы работать на более высокой плотности энерговыделения (по крайней мере на 50% выше), чем реактор без витков.

Экономическое исследование выявит выгодные условия применения этого метода.

A/95 Francia

La técnica de la circulación bifásica turbulenta en los reactores de agua

por C. Foure et al.

Esta memoria se basa en trabajos realizados en su mayor parte bajo contrato del Comité Conjunto EURATOM/USA.

Se trata preferentemente de demostrar que se pueden establecer y mantener torbellinos longitudi-

nales apareados y coherentes en canales de distintas secciones, en especial en las de los reactores nucleares de agua en ebullición, donde los elementos combustibles están situados en los nudos de un enrejado de malla cuadrada. Cada torbellino elemental está producido por una cinta metálica enroscada dentro del subcanal de que se trate.

Se han determinado la caída de presión y la proporción de vacíos en régimen de circulación bifásica, en función de parámetros principales que parecen poder reagruparse en la forma dada por Martinelli y sus colaboradores.

Por medio del artificio de las cintas enroscadas, pueden aumentarse los flujos de calor aplicables a una corriente de agua en ebullición de un 25 a un 40%, a la misma potencia de bombeo, según se trabaje en las proximidades de los 70 bares o de la presión atmosférica. Aparte su función como parrilla de circulación, estas cintas acopladas entre sí, pueden jugar un papel en la estructura del núcleo.

El cálculo de k_{∞} en un reactor de agua hirviendo dotado de estas cintas en espiral demuestra que el enriquecimiento adicional necesario para compensar la presencia de los materiales absorbentes de las cintas es muy reducido (inferior al 0,1% en el caso de cintas en Zircaloy de 0,4 mm de espesor).

Un núcleo de reactor de agua en ebullición concebido para utilizar al máximo las cintas enroscadas podría funcionar a una potencia global superior, al menos en un 50%, a la de un reactor sin estas cintas y del mismo volumen.

Un estudio económico decidirá la importancia del interés de los reactores que hagan aplicación de esta técnica.

Fluid dynamics, stability and vapor-liquid slip in boiling reactor systems

By P. A. Lottes,* W. H. Cook,** K. F. Neusen,*** R. W. Wright,****
S. M. Zivi,**** and N. Zuber*****

This paper presents a few of the highlights of two-phase flow research relative to boiling reactors in the United States. Recent studies in two-phase flow have been summarized by members of the United States and the Euratom community [1]. Work at Oak Ridge National Laboratory, while not directed at boiling power plants, is very important. Their studies covering low pressure high power density research reactor systems are discussed in the Euratom report. Similarly, some of the latest General Electric efforts relative to boiling power plants are given in the same report. A recent summary [2] covers approximately the last fifteen years of the literature and lists 2 843 abstracts in the field of two-phase flow and heat transfer.

EXAMPLES OF GENERAL FLUID DYNAMIC STUDIES

The work at ANL is closely related to some of the university efforts through the recently formed Association of Midwest Universities (AMU). This organization in co-operation with ANL has sponsored two-phase flow research relative to boiling reactor systems at the graduate student and post-doctorate level. The work prior to the ANL-AMU joint program was restricted to the steady state flow of boiling water in natural circulation systems at pressures up to 600 psia (41 atm) [3, 4].

Slip ratio studies have been made in both vertical and horizontal systems. Vertical air-water systems were previously reported [5]. Richardson [6] studied flow patterns, pressure drop, and slip ratio in horizontal systems. He concluded: (a) that the frictional pressure drop could be correlated in terms of local liquid velocity; (b) slip is strongly related to quality or weight flow fraction of gas, with no observable effect of mass flow rate; (c) an apparent negative loss coefficient exists, based on contraction losses, which would seem to indicate that the reduction in liquid flow area at the contraction was less than the reduction in gas flow area. A later study by Voigt [8] on a vertical air-water

system contains a more complete coverage of losses resulting from a change in area.

Fohrman [7] studied the effect of viscosity on slip ratio in horizontal systems using glycerine in water to vary the viscosity. An increase in viscosity by a factor of 500 produced an apparent increase in the slip ratio by a factor of about 6.5, a result contrary to expectations. The results can be rationalized by using the slip model proposed by Bankoff [9], who proposed that the apparent slip ratio based on an over-all mass balance may be greater than unity, even though the local value of slip ratio at any point in the stream may be equal to unity. Fohrman's work confirms Bankoff's model since an increase in viscosity could alter the shape of the velocity and density profiles in the direction that would indicate an apparent increase in slip. If a larger percentage of the bubbles were forced to flow at a higher local velocity (in the center of the channel), the over-all effect would be an apparent increase in slip.

Measurements of density and liquid velocity profiles have been attempted by Neal [10] to confirm this behavior. He used a movable probe in a flowing stream of mercury and nitrogen. Whenever the probe pierced a bubble, the current flow through the probe was interrupted. By examining the traces recorded during the experiment, Neal was able to determine local density distributions. Attempts to measure local liquid velocity distributions were only partially successful. Nassos has extended Neal's work to an air-water system [11].

Smissaert [12] studied slip in air-water, nitrogen-Freon 113, and nitrogen-mercury systems in natural circulation at atmospheric pressure and low liquid velocity (0 to 1 ft/s or 0 to 0.3 m/s). Generally slip ratios were directly proportional to the liquid surface tension and inversely proportional to the dynamic viscosity. The viscosity effect was opposite to the observation of Fohrman. Fohrman, however, was using much higher liquid velocities (4.5 to 19 ft/s or 1.4 to 5.8 m/s).

Vogrin [13] studied the flow of air-water mixtures through a horizontal converging-diverging nozzle. He concluded: (a) the pressure decreased past the nozzle throat for compressible type flow and remained constant for incompressible type flow; (b) the exit water velocities were constant and exit slip ratio increased as the gas flow rate was increased at a fixed

* Argonne National Laboratory, Argonne, Illinois.

** General Electric Company, San Jose, California.

*** Allis-Chalmers Manufacturing Company, Milwaukee, Wisconsin.

**** Space Technology Laboratories, Inc., Redondo Beach, California.

***** General Electric Company, Schenectady, New York.

liquid flow rate, and (*c*) the slip ratio approached unity at the high qualities (10 to 15%).

Petrick [14] studied vapor carryunder in both air-water systems and in EBWR. Data (Fig. 1) taken on an atmospheric pressure air-water loop covered a range of quality from 0.2×10^{-3} to 2.0×10^{-3} and downcomer velocities of 1 to 2.5 ft/s (0.3 to 0.76 m/s); included for comparison are a few test points from EBWR. Petrick also extensively studied bubble size distribution, bubble size versus bubble velocity relationships, phase distributions perpendicular to the flow direction, and down-flow slip ratios [14].

The present ANL-AMU projects include studies in the propagation of waves and pressure pulses in an air-water flow system, power-to-void transfer functions, forced convection boiling heat transfer for fluids through their critical property states, forced convection instability near the critical point, and the response of a boiling channel to power modulation.

There are many opinions concerning the choice of parameters when correlating slip data. Reactor designers at Argonne presently are using a graphical correlation developed by Marchaterre and Hoglund [15], as shown in Fig. 2. The curves are considered adequate for engineering use provided that the superficial velocities are greater than 0.8 ft/s (0.24 m/s). Data from a number of systems were compared and the resulting curves represented a best fit of the data.

THERMAL HYDRAULIC OSCILLATIONS

During the past five years, the stability of two-phase flow systems with heat addition has been studied extensively. A critical review of the effort and results preceding this period is reported in [16]. In-pile [17-21] and numerous out-of-pile experiments have been carried out with water [22-30] and other liquids [31, 32] at pressures from atmospheric up to the thermodynamic critical point [33]. There has been a significant analytical effort to elucidate the phenomenon [21, 22, 23, 30, 31, 33-44].

In-pile experiments (GEAP)

An extensive series of power stability tests have been conducted in the VBWR to predict the transient response and stability of power producing BWR's [21]. Both natural and forced circulation coolant flow were studied over a wide range of flows and power outputs:

Forced circulation

Power1, 15, 20, 26 MW(th)
Flow2 600 to 20 000 gpm
Pump head0 to 290 ft
Core bypass leakage % core flow0 to 400

Natural circulation

Power9 to 20 MW(th)
-----------------	-----------------

Theoretical analyses of the dynamic responses were used to guide the experimental parametric study. An average parameter control system analysis technique

was used that included the reactor kinetics, the fuel thermal response, the thermal-hydraulic response, and the void reactivity response.

The results of this investigation can be summarized as follows:

(a) Reactor stability theory [21] predicts the stability characteristics of the VBWR well for the natural circulation operation of the plant (Fig. 3). Forced circulation operation conditions are predicted equally well for systems whose flow velocities in the two-phase region are not too far removed from natural circulation. This theory is believed adequate for any boiling water reactor having characteristics similar to the VBWR.

(b) The most significant parameters affecting the absolute stability of the VBWR reactor are the void coefficient of reactivity, and the condition of system hydraulics. Other parameters, such as pressure and fuel time response, can have sizeable effects in some reactor systems.

(c) A system analysis, as described in [21], is much more reliable than intuitive treatment for high flow forced circulation systems.

(d) Operational noise cannot be used as a measure of absolute stability.

(e) Rod oscillator tests have provided significant and quantitative absolute stability data; steady state noise and transient response have not. Rod oscillator tests should be conducted on every boiling water reactor which has significant design differences from those for which there is absolute stability data.

Hydraulic stability loop experiments

Out-of-pile experiments have been conducted at different system pressures with water (and other liquids) flowing through various geometries [22-30].

Experiments [18, 20, 28] have been conducted in a natural circulation loop to investigate the steady-state response, the power impulse response and power oscillation response of various parameters. For two-phase flow transients in channels, it was concluded that (a) undamped and (self-excited) oscillatory responses are easily obtained by parametric changes and small disturbances; (b) the pressure in the heater rises in response to power oscillations without a change in pressure difference across the channel (the fluid in the heater acts as a capacitance under these circumstances); (c) intermediate subcooling operation showed flow responses which were less stable than higher or lower subcooling runs, and (d) the frequency dependent theory is not, at present, in a form well suited to prediction of transients.

Other experiments show the effect of system geometry and loop characteristics, nucleating characteristics of the heating surface, mass flow rate, two-phase pressure drop, system pressure, power, flow and pressure oscillations, subcooling, and parallel ducts [22-33].

Figure 4 illustrates the effect of subcooling and of mass flow rate on the frequency and amplitude of oscillations at constant heat flux, system geometry and

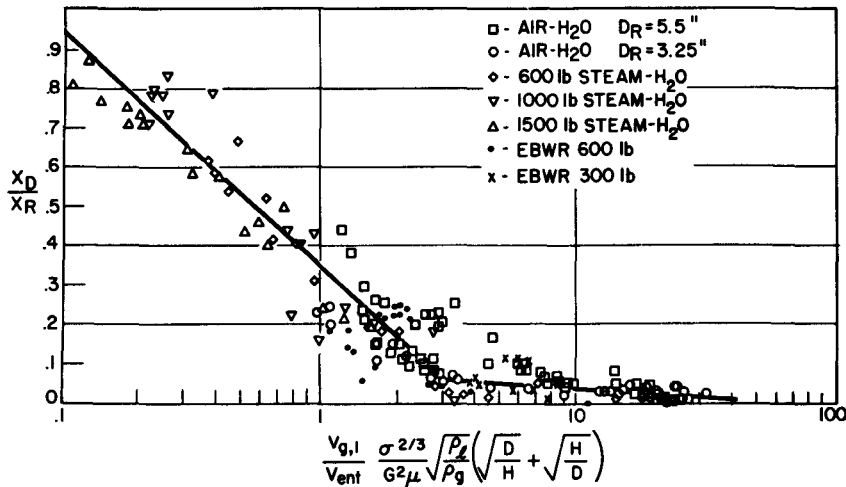


Figure 1. Correlation of ANL carryunder data

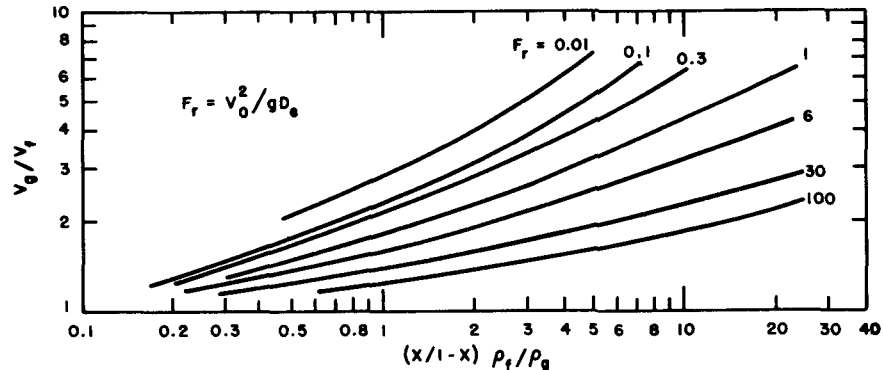


Figure 2. Correlation of velocity ratios as a function of Froude-number and the volumetric flow rate of each phase

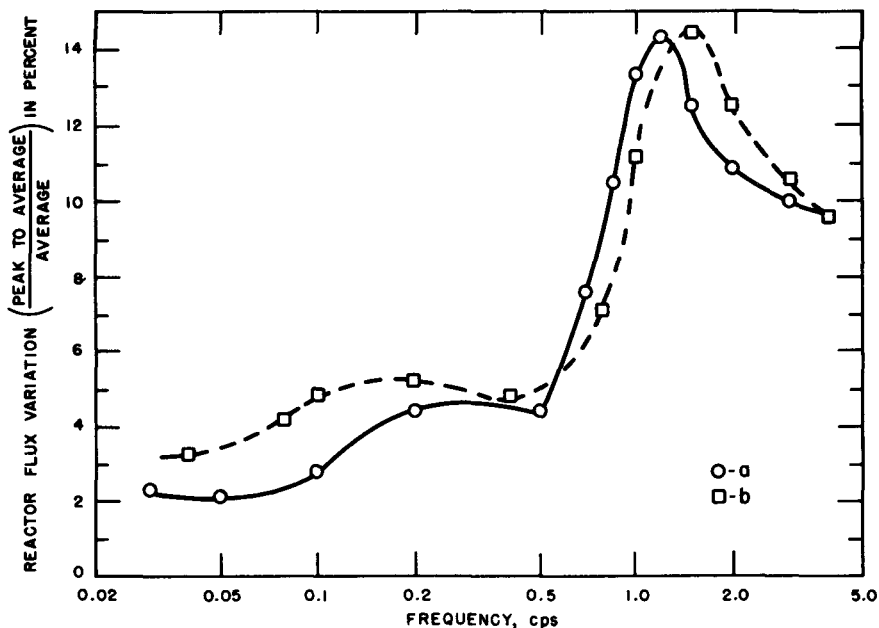


Figure 3. Reactor power transfer function comparison of prediction with experiment
 a: 15-18 test series 15 MW(th) natural circulation; b: Pretest analysis No. 17, 20 MW(th),
 4 675 gpm core flow, parallel flow channel hydrodynamics (hottest consumers channel)
 (reproduced from [21])

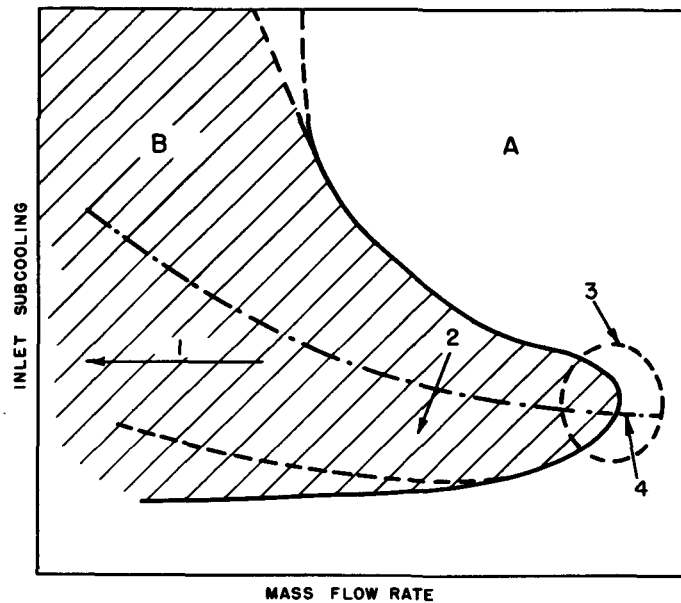


Figure 4. Schematic representation of stability map showing paths of experiments and other qualitative information at constant heat flux, system geometry, and condenser pressure
 A: Stable; B: Unstable; 1: Increasing period of oscillation;
 2: Decreasing period of oscillation; 3: Nature of closure unknown;
 4: Maximum amplitude (reproduced from [32])

condenser pressure [32]. These results (and others like these) are important because they definitively indicate that no flat statement concerning the effect of a single parameter can be made. Statements like increasing the subcooling induces instability and similar ones have often been made in the literature. Figure 4 indicates that such statements are, at best, only partially correct and generally misleading because the effect of a parameter can be evaluated only if the region and mode of variation is specified. Whether the region of oscillation is open (as indicated in Fig. 4) or closed has not been determined. Some results indicate that it may be closed [38].

Analytical investigations

Analytical investigations have been conducted by formulating appropriate models or by considering the conservation laws for the mixture.

Several mechanisms leading to an oscillatory behavior of a loop have been identified and have been verified by subsequent experiments performed with pentane [31].

The time dependent equations describing the conservation of mass, momentum and energy for the two-phase mixture and of energy for the metal have been programmed on computers together with boundary conditions at the metal-fluid interface [23, 33, 34, 38-44]. The analyses differ from each other in the assumptions made with respect to the two-phase flow pressure drop, void fraction, and boundary conditions in the low quality and subcooled boiling region. Values predicted by these analyses agree well with experimental data on a particular system obtained over a restricted range of parameters. Two results appear of special interest. One analysis [41] demonstrates a distinct progression of enthalpy waves through the mixture whereas another [42-44] shows that at least one mode of instability, which depends on the heat flux density, is generated in the low quality and the subcooled boiling region. This analytical result, which seems supported by some experimental data, suggests that non-uniform heating along the test section could be used as a means of increasing the total power output of the system while still maintaining stable operation.

The transient response of an adiabatic two-phase (bubbling) system which makes use of kinematic waves has been analyzed [45]. The comparison of predicted values with experimental data shows that changes in void concentrations are propagated through the two-phase mixture by means of kinematic waves [45]. The propagation of these waves and, therefore, the transient response of the two-phase mixture depends on the two-phase flow regime. The application of the kinematic wave theory to a study of diffusion in two-phase media is also discussed [45].

Conclusions

The experimental and analytical investigations have identified several mechanisms that may lead to an oscillatory behavior of a two-phase flow loop. The oscillation and instabilities are generated by

phenomena in the boiling section only or originate as a consequence of an interaction between the boiling section and the rest of the system.

Well-instrumented experiments coupled with analytical investigations are being performed at several laboratories to establish the mechanism, domain, and characteristics of oscillations. These investigations should permit prediction of the onset of oscillations for various liquids (water, liquid metals and cryogenic fluids) as functions of system geometry, pressure, and operating characteristics.

SPERT 1A REACTOR STUDIES (STL)

Stability studies

Boiling water reactor stability studies at TRW Space Technology Laboratories (STL) have attempted to explain the power oscillations observed in the SPERT 1A reactor [46]; therefore, most of the loop experiments on steam-void dynamics at STL have utilized the geometry of a SPERT 1A moderator-coolant channel at atmospheric pressure. A single rectangular coolant channel was formed between two electrically heated aluminum walls and two unheated edge strips [47]. The rectangular channel was mounted in a loop which could be operated either with convection or with the flow fixed at a constant magnitude by a discharge-throttled centrifugal pump. The void fraction exhibited large local fluctuations, even under nominally steady-state conditions. During power input modulation, the detection of the small amplitude coherent response of the void fraction, required cross-correlating the void signal with the imposed power. Detailed results have been presented in previous publications [47, 49, 50, 51, 52].

The hydrodynamics of the SPERT 1A reactor were simulated for divergent power oscillations with the tank water at saturation at the free surface by operating the laboratory loop under natural circulation with 100 °C (212 °F) water temperature at the test-section inlet and 120 cm (3.94 ft) of hydrostatic head above the inlet.

Figure 5 illustrates two void fraction responses, one for natural circulation and one for forced circulation, both with the same steady-state flow $V = 44.5$ cm/s (1.45 ft/s). The position of the void fraction response measurement was approximately midway along the boiling length, where the steady-state void fraction was about 50 per cent. The phase lag of the void fraction response was reported in [51], with 180° lag being attained at 1 cycle/s in the natural circulation case, and at 0.8 cycle/s in the forced circulation case. The peak in the void response is attributed to the response of the void fraction to the inlet flow variation. The flow response itself is approximately proportional to the time derivative of the total void volume response to power modulation [51]. Thus, a feedback interaction between the void volume and the flow produces the difference between the natural circulation and the forced flow-power-void transfer function.

The void fraction response measurements for natural circulation have been combined with the known zero-power reactor kinetics transfer function and the measured void coefficient of reactivity of the SPERT 1A reactor to compute the stability of the reactor under the conditions where power oscillations occurred [53]. These calculations for 500 W in the laboratory channel, and 500 kW in the reactor, show a feedback-loop phase-shift of 180° at a frequency of 0.95 cps, where the feedback loop gain is about 1.7. Thus by the Nyquist criterion of feedback loop stability, the reactor should be decidedly unstable as a result of reactivity feedback at 500 kW power, with an oscillation frequency of 0.95 cps. The threshold of reactivity-feedback instability would be expected to occur at a power level somewhat below 500 kW. This result is in agreement with the observed spontaneous power oscillations in the reactor [46], which arose at a power level of about 400 kW and with a frequency of 1 cps. The natural circulation flow and void fraction were quite stable in the laboratory channel at 500 W power, indicating that a hydrodynamic instability was not the cause of the reactor power oscillations.

As the steady-state power level is increased in the laboratory experiment, the peak in the natural circulation void fraction response to power modulation becomes very pronounced, and its frequency increases as illustrated in Fig. 6. The void fraction responses for both natural and forced circulation are shown, along with the response at 500 W natural circulation. As the steady-state power level is increased to 1 000 W without modulation, undamped coherent hydrodynamic oscillations occur at a frequency of 1 cps. The resonance peak in the natural circulation void fraction response is the result of the void-flow feedback interaction, and the threshold of hydrodynamic oscillations appears to correspond to the operating conditions for which the feedback loop becomes unstable [51, 52].

Pressure pulse studies

R. W. Wright [54, 55] has conducted experiments at STL related to the generation of pressure pulses in rapid power excursions in water-moderated metal plate reactors. The BORAX 1 reactor was destroyed in a power excursion with an initial period of $2.5 \mu\text{s}$ which produced a pressure pulse in excess of 6 000 psi (410 atm) [56]. The $3.2 \mu\text{s}$ destructive excursion in the SPERT 1D reactor produced a pressure pulse between 3 000 psi (204 atm) and 4 000 psi (272 atm) with a rise time of less than $0.5 \mu\text{s}$, but delayed about $15 \mu\text{s}$ after peak power [57]. In the laboratory experiment for the production of pressure pulses by the rapid heating of a surface in contact with water, a nominal 700°C ($1\,260^\circ\text{F}$) temperature rise was produced in the stainless steel heated element in $150 \mu\text{s}$ by electrical resistance heating. The ratio of heat transfer surface to pipe cross sectional area was about 30, as compared with a ratio of heat transfer surface to pressure relief area of about 20 for BORAX 1, assuming that pressure relief occurred radially outward in the reactor. The

ratio of heated surface to adjacent water volume was about the same in the laboratory experiment as in the reactor. The rate of temperature rise was about ten times as great as in the BORAX 1 destructive excursion.

In the experiment, heating transients with a 700°C ($1\,260^\circ\text{F}$) rise produced peak pressures of about 800 psi (54.5 atm). These results show that multi-thousand psi pressure pulses cannot be generated thermally in geometries similar to the unmolten BORAX 1 and SPERT 1 cores. At the time of the pressure pulse in each of the reactor destructive transients, large portions of the aluminum alloy reactor fuel plates were molten; whereas, in the laboratory experiment, the stainless steel heated surface remained solid. If the surface area of the reactor fuel were augmented as a consequence of melting, greater heat transfer surface would be required in the laboratory experiment, and high pressures would be expected.

Following the initial high pressure pulse, the pressure fell through ambient to a vacuum of about 10 psig (0.7 atm). After about $20 \mu\text{s}$, a sharp 150 psi (10 atm) pressure pulse occurred followed again by vacuum and a continued series of pulses. The vacuum is considered to be the effect of vapor blanketing of the heated element after the initial pressure pulse. The blanketing insulated the heated element from the virtually unheated bulk water, and vapor condensation on the cold water interface produced the vacuum. This process gave the inertial water column about 10 g downward acceleration to re-contact the heated surface. The magnitudes of the impact pressure pulses and the periods between them were consistent with this interpretation.

VAPOR-LIQUID SLIP IN BOILING REACTOR SYSTEMS (EXAMPLES FROM ALLIS-CHALMERS)

Void fractions in a round unheated duct

A basic study of void fractions in a large unheated duct is being conducted at Allis-Chalmers under the Euratom program. The study *Investigation of Vapor Volume Fraction and Slip Velocity* is providing a good basis for understanding the two-phase flow parameters associated with varying flow patterns that occur over a wide range of velocity and average void fraction. Superficial liquid velocities from (and including) zero to 20 ft/s (6.1 m/s) and average void fractions ranging from 0.10 to 0.90 are being studied.

Void fraction profiles are being obtained for each of the flow conditions tested [58]. A sample profile is given in Fig. 7 for 600 psig (42 atm) and 2.5 ft/s (0.76 m/s) superficial liquid velocity. A characteristic of the gamma attenuation technique is that individual points in the profile represent the average void fraction along the beam path, which means an average along a chord for a circular duct.

The relatively simple geometry of this study provides an opportunity to check on models that describe the void fraction distribution. Chordal void fraction profiles were calculated for the exponential model

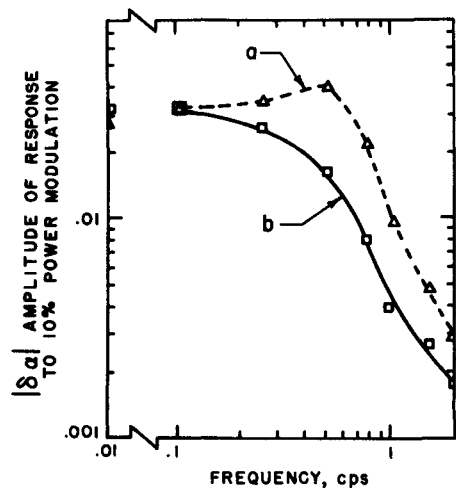


Figure 5. The effect of forced flow on the amplitude of void fraction response to 10% power modulation, at one atmosphere pressure
 a: Natural circulation, 500 W;
 b: Forced flow, 500 W

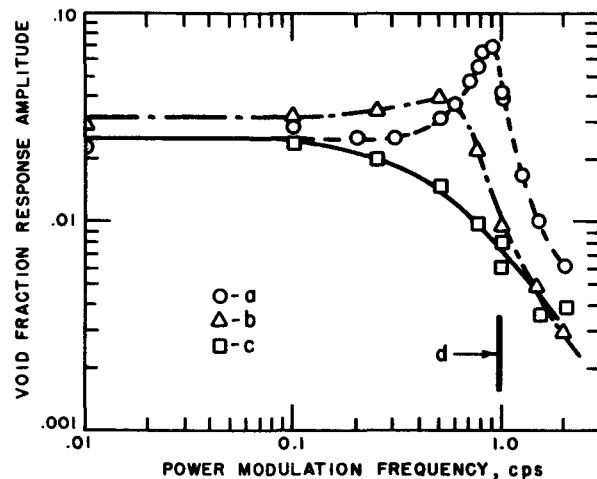


Figure 6. Amplitude of steam void fraction response to 10% amplitude power modulation, at one atmosphere pressure
 a: Natural circulation 940 W 12" from inlet; b: 500 W 18" from inlet; c: Forced circulation 940 W 12" from inlet; d: Frequency of hydrodynamic oscillations at 1 000 W

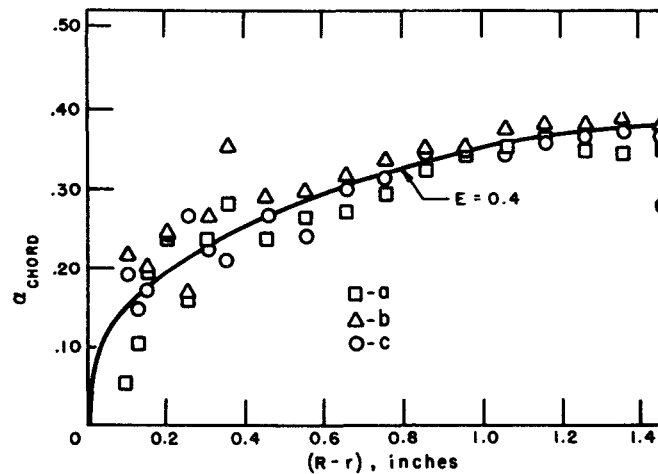


Figure 7. Sample chordal void fraction profile for round unheated duct
 a: 2 feet from inlet; b: 3 feet from inlet; c: 4 feet from inlet

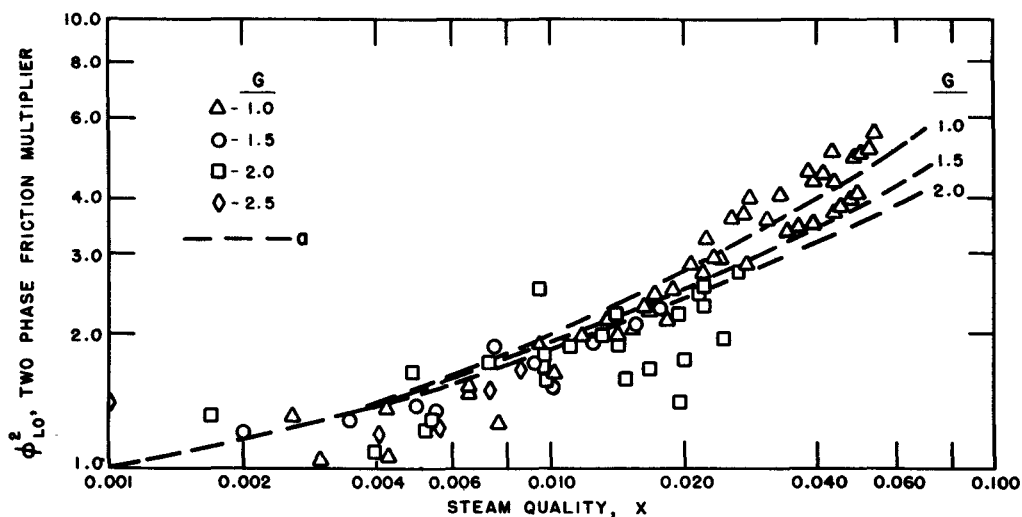


Figure 8. Boiling friction losses as a function of quality and mass velocity (G , in 10^6 lb/hr ft²)
 a: Modified Martinelli correlation

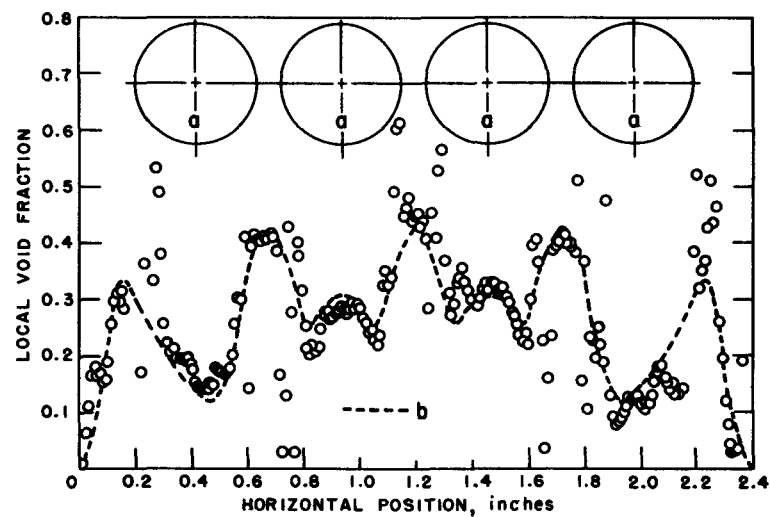


Figure 9. Typical void fraction distribution for vertical upflow in heated 16-rod test section for $R_g = 0.278$, $x = 0.0082$, $G = 1.23 \times 10^6$ lb/hr ft², $\theta = 158\,000$ Btu/hr ft²
 a: Pin row location; b Mean curve from superposition averaging

suggested by Bankoff [9]. The curve labeled $E = 0.4$ in Fig. 7 was calculated from:

$$\alpha = \alpha_{\max} \left[1 - \frac{r}{R} \right]^E$$

In this example $E = 0.4$ seemed to give the best fit of the data points.

Steam volume fraction in a bubbling two-phase mixture

Experiments were performed in an 18-in-diam vertical channel to determine the steam volume fraction as a function of superficial steam velocity for a mixture with no liquid flow [59]. Volume fraction values were determined from differential pressure measurements. The range of test variables was: system pressure 800–2000 psig (54–137 atm) and superficial steam velocity 0.30–4.2 ft/s (9.1 to 128 cm/s).

Multi-rod pressure drop and void fraction study

With the ever increasing application of parallel rod arrays in reactor fuel elements, the importance of extending the two-phase flow technology to that geometry becomes apparent. Established correlations and theories have relied heavily on round tube or rectangular channel studies for their experimental basis. Additional supporting evidence on rod bundles is needed to determine whether or not these correlations apply to the multi-rod case. Pressure drop and void fraction investigations have been made for a heated 16 rod array (4 × 4) duplicating the design of the Pathfinder reactor [60, 61].

Friction factors, loss coefficients and vapor volume fractions were measured.

Following a check of the rod bundle pressure drop during single-phase flow, boiling pressure drop data were taken over a wide range of power and flow conditions.

Values of ϕ_{Lo}^2 the two-phase friction multiplier are plotted in Fig. 8 as a function of steam quality x and mass velocity G .

For comparison purposes, curves depicting the modified Martinelli correlation [5, 62] are also plotted in Fig. 8. Agreement of the data with the correlation predictions is generally within $\pm 25\%$. The original Martinelli-Nelson correlation [63] allowed for no flow effects and would correspond to a value of $G = 1.25 \times 10^6$ lb/hr-ft² (170 g/scm²). While agreement with this value is about $\pm 25\%$, some effect of flow is evident. Either the original or modified forms of the Martinelli correlation using the equivalent diameter will predict the boiling friction losses on rod bundles over the range of qualities tested.

Local void fractions in the 16-rod array were determined at the flow condition and axial location of interest. The results of the void fraction traverses indicate that the void profile within a rod bundle is definitely not flat as is often assumed in making neutron flux calculations. A typical plot of local void fraction versus horizontal position is shown in Fig. 9. The circular symbols are all data points and the dashed line is an average arrived at by superimposing

all the data from symmetrical positions on one plot. The void fraction goes to zero at the unheated wall which encloses the bundle. More interesting is the apparent tendency for the vapor to collect in the spaces between rods. This result is in agreement with earlier air-water results in a 4 × 9 rod array [64]. Another noteworthy effect is the lower void fractions on the rods adjacent to the wall. This would indicate that the effect of the wall extends into the bundle even though the rods were uniformly heated.

SUMMARY

Fundamental studies in fluid dynamics, stability, and vapor-liquid slip in boiling reactor systems are continuing in the United States at an increasing rate.

Sufficient information is available to estimate boiling reactor performance. Final operating limits of boiling reactor power plants, however, are still based upon full scale tests.

University studies are generally very fundamental, with emphasis on studying the mechanisms of two-phase flow. Industrial studies are engineering rather than fundamental, and usually refer to a specific reactor design.

Steady state experiments have provided much useful design information. The transient studies which include such tests as flow instability, transfer function experiments, etc., have likewise provided useful information. Flow oscillations in boiling systems, however, are not completely understood. Much more theoretical and experimental work is required on the general problem of flow stability in order to optimize and increase power density of boiling systems.

REFERENCES

1. Euratom, USAEC, EUR 352.e (1963).
2. *Kepple, R. R., and Tung, T. V., ANL-6734 (1963).
3. *Marchaterre, J. E., *et al.*, ANL-5735 (1960).
4. *Hoglund, B. M., *et al.*, ANL-5760 (1961).
5. Lottes, P. A., *et al.*, Proceedings of the Second International Conference on the Peaceful Uses of Atomic Energy, P/1983, Vol. 7, p. 784, United Nations (1958).
6. *Richardson, B. L., ANL-5949 (1958).
7. *Fohrman, M. J., ANL-6256 (1960).
8. Voigt, D. K. O., to be published.
9. Bankoff, S. G., Journal of Heat Transfer 82 (Series C, No. 4), 265–272 (1960).
10. *Neal, L. G., ANL-6625 (1963).
11. *Nassos, G. P., ANL-6738 (1963).
12. *Smissaert, G. E., ANL-6755 (1963).
13. *Vogrin, J. A., ANL-6754 (1963).
14. *Petrick, M., ANL-6581 (1962).
15. Marchaterre, J. F., and Hoglund, B. M., Nucleonics 20 (8), 142–146 (1962).
16. Anderson, R. P., and Lottes, P. A., *Progress in Nuclear Energy, Ser. IV, 4, Technology, Engineering and Safety*, Pergamon Press, N.Y., 3/28 (1961).
17. *Cook, W. H., *et al.*, GEAP-3794 (1961).
18. *Howard, C. L., *et al.*, GEAP-4159 (1962).
19. *Howard, C. L., *et al.*, GEAP-4383 (1963).

20. *Howard, C. L., *et al.*, GEAP-4481 (1963).
21. *Members of Engr. Dept., GEAP-3971 (1964).
22. *Quandt, E. R., WAPD-T-1134 (1960), also in Chemical Engr. Progress Monograph and Symposium Series, No. 32, 111-126.
23. *Christensen, H., ANL-6385 (1961).
24. *McGowan, E. J., and Bodoia, J. R., WAPD-BT-27 (1962).
25. *Zivi, S., *et al.*, RWD-RL-167 (1960).
26. *Zivi, S., *et al.*, RWD-RLM-236 (1961).
27. *Hodde, J. A., *et al.*, GEAP-3935 (1962).
28. *Howard, C. L., *et al.*, GEAP-4159 (1963).
29. *Howard, C. L., *et al.*, GEAP-4301 (1963).
30. *Anderson, R. P., *et al.*, ANL-6653 (1963), also in Chemical Engr. Progress Monograph and Symposium Series, 59 (No. 41) 96/103 (1963).
31. Wallis, G. B., and Healsey, J. H., ASME Transactions, J. of Heat Transfer, 83, 363/369 (1961).
32. Gouse, S. W., and Andrysiak, C. D., ASME Multi-Phase Flow Symposium, N. J. Lipstein, Ed., ASME, N.Y. 84/89 (1963).
33. *Harden, D. G., ANL-6710 (1963).
34. Fleck, J. A., J. Nuclear Energy, Part A, 11 114/130 (1960).
35. Akcasu, A. Z., Nuclear Sci. Eng. 10, 337/345 (1961).
36. Hansen, P. D., Microtech. Report No. 195 (1961).
37. Stenning, A. H., ASME Paper No. 62-WA-155 (1962).
38. *Garlid, K., *et al.*, ANL-6381 (1961).
39. Meyer, J. E., Nuclear Sci. Eng. 10, 269/277 (1961).
40. *Meyer, J. E., and Williams, J. S., WAPD-BT-25, 47/72 (1962).
41. Meyer, J. E., and Rose, R. P., ASME Trans. J. of Heat Transfer, 85, 1/9 (1963).
42. *Jones, A. B., KAPL-2170 (1961).
43. *Jones, A. B., KAPL-2208 (1962).
44. *Jones, A. B., KAPL-2290 (1963).
45. *Zuber, N., and Hench, J., 62-GL-111 (1962).
46. *Forbes, S. G., *et al.*, IDO-16309 (1956).
47. *Kemp, R. F., *et al.*, RWD-RL-167 (1959).
48. Ball, W. P., *et al.*, Trans. Amer. Nuclear Soc. 1 (2) 59 (1958).
49. *Morse, A. L., *et al.*, RWD-RL-190 (1960).
50. *Brown, W. W., *et al.*, STL-6112 (1961).
51. *Zivi, S. M., *et al.*, STL-6212 (1962).
52. Wright, R. W., and Zivi, S. M., Trans. Amer. Nuclear Soc., 6 (1), 108 (1963).
53. *Nyer, W. E., *et al.*, IDO-16285 (1956).
54. Wright, R. W., Trans. Amer. Nuclear Soc., 6, 2, 338/339 (1963).
55. *Wentz, *et al.*, STL-6312 (1963).
56. *Dietrich, J. R., AECD-3668 (1954).
57. Miller, R. W., *et al.*, Trans. Amer. Nuclear Soc. 6 (1) 138/139 (1963).
58. *Neusen, K. F., *et al.*, ACNP-64002 (1964).
59. *Wilson, J. F., *et al.*, ACNP-63028 (1963).
60. Sher, N. C., *et al.*, Paper presented at 55th Annual Meeting of Amer. Inst. Chem. Eng., Preprint No. 158 Chicago (1962).
61. Kangas, G. J., and Neusen, K. F., ACNP-63002 (1963).
62. *Lottes, P. A., *et al.*, ANL-6063 (1959).
63. Martinelli, R. C., and Nelson, D. B., Trans. Amer. Soc. Mech. Engrs. 70, 695/702 (1948).
64. Condon, R. A., and Sher, N. C., Nuclear Sci. Eng. 14, 327/338 (1962).

* USAEC report.

ABSTRACT—RÉSUMÉ—АБХОТАЦІЯ—RESUMEN

A/230 Etats-Unis d'Amérique

Dynamique des fluides, stabilité et glissement liquide-vapeur dans les réacteurs à eau bouillante

par P. A. Lottes *et al.*

Le mémoire passe en revue les progrès récents dans l'étude de l'écoulement à deux phases, réalisés dans les laboratoires nationaux, les universités et l'industrie.

Au Laboratoire national d'Argonne, on a étudié la perte de charge et le rapport de glissement dans l'écoulement à deux phases dans des tuyères, les rapports de glissement dans les écoulements horizontaux et verticaux, l'effet de la viscosité du liquide sur le rapport de glissement, le glissement dans les systèmes à deux composants et aux faibles débits, les problèmes de l'entraînement de la vapeur et quelques méthodes instrumentales choisies pour la mesure des coefficients de vide.

La General Electric Company a étudié la prévision des vides dans des systèmes à bouillonnement, l'ébullition en écoulement horizontal, les réponses en régimes stationnaire et transitoire des systèmes comprenant des vides, la propagation des ondes cinématiques dans les mélanges à deux phases, la

stabilité d'écoulement des systèmes bouillants et la séparation de la vapeur.

En ce qui concerne la stabilité des systèmes bouillants, on passe en revue les expériences de stabilité d'écoulement en circulation naturelle, effectuées dans l'industrie et dans diverses universités. On tire deux conclusions de cet examen: a) les instabilités d'écoulement peuvent avoir pour origine soit la partie bouillante du système, soit les parties extérieures, soit encore les interactions entre la partie bouillante et le reste du système; b) on ne peut parler du début de l'instabilité d'écoulement sans préciser avec soin la région de fonctionnement du système, et sans définir la direction d'évolution des variables du système.

Les deux principaux domaines étudiés par Allis-Chalmers, pour l'hydraulique du cœur de réacteur, sont la perte de charge et la fraction de volume de vapeur (coefficient de vide). Les études de perte de charge faites à 600 psi (42 kg/cm²) dans le cadre du projet du réacteur Pathfinder ont montré que la géométrie à barreaux parallèles pouvait être traitée au moyen des relations de perte de charge à deux phases telles qu'elles ont été établies. Une étude étendue des coefficients de vide dans des conditions d'écoulement semblables à celles que l'on trouve dans

les conduites verticales est poursuivie au titre du programme de l'EURATOM. Une étude limitée des coefficients de vide dans la géométrie à barreaux parallèles a été faite pour Pathfinder. En relation avec le programme de séparation de vapeur, des mesures du coefficient de vide ont aussi été faites sur des mélanges à deux phases dégageant des bulles. Ces données portent sur des pressions allant de 300 à 2 000 psi (21 à 140 kg/cm²) et avec des diamètres de cuve de 4 à 36 pouces (10 à 90 cm).

Les études des laboratoires de technologie spatiale sur la stabilité des réacteurs à eau bouillante ont porté notamment sur la mesure en laboratoire de la fonction de transfert puissance-vide dans un canal simulé refroidi à l'eau du SPERT 1A. Ces mesures de fonction de transfert avec circulation naturelle ont montré que l'oscillation de puissance divergente observée dans le réacteur SPERT 1A à 97 °C peut s'expliquer par une instabilité de contre-réaction de réactivité, et non par une instabilité purement hydrodynamique. Quand la puissance de ce canal augmente et s'approche du seuil d'instabilité hydrodynamique, un pic de résonance se produit dans la fonction de transfert à 1 Hz, fréquence à laquelle une oscillation hydrodynamique finit par se produire. La résonance montre que la variation du vide en fonction de la modulation de puissance est dominée par une interaction entre l'écoulement à l'entrée et le vide de vapeur, et que lorsque cette interaction de contre-réaction devient instable il se produit une oscillation hydrodynamique spontanée.

On a essayé de reproduire au laboratoire les impulsions de pression destructrices qui se sont produites dans les excursions des réacteurs SPERT 1 et BORAX 1. Un chauffage électrique transitoire produisait des élévations de la température de surface de 700 °C en 150 μ s pour un élément en acier inoxydable chauffé dans une géométrie qui reproduisait les cœurs métalliques non fondus de SPERT 1 et BORAX 1. L'ordre de grandeur des impulsions de pression produites par transfert de la chaleur à l'eau était d'environ 800 psi (56 kg/cm²), très inférieur à ce qui avait été observé dans les excursions des réacteurs. Des lectures négatives de pression (vide) suivent l'apparition de vapeur dans ces transitoires thermiques.

A/230 США

Гидродинамика, стабильность и паро-жидкостное скольжение в кипящих реакторных системах

П. А. Лоттс et al.

Рассматриваются новейшие достижения правительственных лабораторий, университетов и частных предприятий в изучении двухфазного потока. В Аргоннской национальной лаборатории исследовались перепад давления и коэффици-

циенты скольжения двухфазного потока сквозь сопла, а также в горизонтальных и вертикальных потоках, влияние вязкости жидкости на коэффициент скольжения, скольжение в двухкомпонентных системах, скольжение в потоках с малой весовой скоростью, проблемы выноса пара и некоторые методы и приборы для измерения доли парового пространства.

На фирме «Дженерал электрик» велись работы по таким вопросам, как расчет парового пространства в барботажных системах, кипение в горизонтальных потоках, стационарное состояние и переходные характеристики систем парового пространства, распространение кинематических волн в двухфазных смесях, стабильность потоков в кипящих системах и изучение проблемы сепарации пара.

В связи с изучением стабильности кипящих систем в докладе рассматриваются достижения как в промышленности, так и в разных университетах по стабильности кипения в условиях естественной конвекции. При этом было сделано два вывода: а) нестабильность потока может возникать либо из-за испарительных участков системы, либо из-за внешних ее частей, либо в результате взаимодействия между испарительным участком и остальными участками системы; б) невозможно точно определить момент наступления неустойчивости потока, до тех пор пока не будет тщательно определена область работы системы, а также направление изменения переменных параметров системы.

Два основных вопроса, изученные фирмой «Аллис-Чалмерс» в связи с гидравликой активной зоны реактора, включали: потери напора и долю парового объема, то есть объема парового пространства. Исследование потери напора при давлении 42,2 кг/см² в связи с проектом Пасфайндерского реактора показало, что гидравлическое сопротивление при продольном омывании пучка стержней можно рассчитывать по известным зависимостям для потери напора в двухфазном потоке. Усиленное изучение доли объема парового пространства в условиях, подобных встречающимся в потоках в подъемных стойках, ведется в рамках программы Евратома. Ограниченные исследования доли объема парового пространства в условиях омывания пучков параллельных стержней были проведены также в связи с проектом Пасфайндерского реактора. При исследовании сепарации пара были проведены измерения доли объема парового пространства в двухфазных барботирующих смесях. Эти данные охватывают диапазон давлений от 21 до 140 кг/см² и емкости диаметром от 10 до 91,4 см.

Изучение стабильности водяных кипящих реакторов фирмой «Спейс технолоджи лабораториз» проводилось путем лабораторных измерений функции переноса энергии — пространство в технологическом канале с водяным теплоносителем модели SPERT-1A. Эти измерения функции переноса при естественной конвекции

показали, что энергетические колебания, наблюдавшиеся в реакторе при температуре 97°C , могут быть объяснены скорее неустойчивостью обратной связи по реактивности, чем чисто гидродинамической неустойчивостью. Когда энергетический уровень этого канала повышался до порога гидродинамической неустойчивости, резонансный максимум в функции переноса развивался при частоте 1 *гц*. При этой частоте появляются гидродинамические колебания. Появление резонанса указывает на то, что ответная реакция парового пространства на изменения частоты энергетического уровня поддается взаимодействию входящего потока с паровым пространством и что, когда влияние этой обратной связи становится неустойчивым, начинается самопроизвольное гидродинамическое колебание.

Сделана попытка имитировать в лаборатории разрушительные импульсы давления, которые возникали при колебании режима работы реакторных установок SPERT-1 и BORAX-1. Быстрый электрический нагрев вызывал за 150 *мксек* подъем температуры поверхности нагревательного элемента из нержавеющей стали до 700°C , геометрия которого моделирует нерасплавленные металлические активные зоны SPERT-1 и BORAX-1. Величина импульсов давления, созданных теплоотдачей к воде, составляла $56,2 \text{ кг/см}^2$, что намного ниже импульсов давления, наблюдаемых в реакторе во время колебаний рабочего режима. Отрицательное манометрическое давление (т. е. вакуум) получается вследствие явления парового обволакивания во время таких переходных тепловых процессов.

A/230, Estados Unidos de América

Динамика де флюидос, естаблльдад и десльза- мьенто ллькльдо-ватор ен лос реаторос де агуа ен ебульсьон

пор P. A. Lottes et al.

Se revisan los últimos progresos de los estudios de flujo en dos fases efectuados en los laboratorios del Gobierno, universidades e industria.

Los estudios efectuados en Argonne National Laboratory abarcan la pérdida de carga y relación de deslizamiento en el flujo de dos fases a través de boquillas, relación de deslizamiento en flujos horizontales y verticales, efecto de la viscosidad del líquido sobre la relación de deslizamiento, deslizamiento en sistemas de dos componentes, deslizamiento a bajas velocidades másicas, problemas de arrastre de nieblas y varias técnicas de instrumentación seleccionadas para la medida de las fracciones de huecos.

El trabajo presentado por la General Electric Company trata de problemas tales como la predicción

de huecos en sistemas con burbujas, ebullición en flujo horizontal, respuesta de los sistemas con huecos en régimen estacionario y transitorio, propagación de ondas cinéticas en mezclas de dos fases, estabilidad del flujo de sistemas en ebullición y estudios de separación vapor-agua.

Por lo que se refiere a la estabilidad de los sistemas de ebullición, se presenta una revisión de los experimentos sobre la estabilidad de flujo con circulación natural, efectuados en las industrias y en varias universidades. Dos conclusiones se deducen de esta revisión: a) las inestabilidades del flujo pueden surgir de las secciones en ebullición, de los componentes externos del sistema, o de una interacción entre la sección de ebullición y el resto del sistema; b) no se pueden establecer afirmaciones definitivas relativas al comienzo de la inestabilidad del flujo a menos que se especifique cuidadosamente la zona de funcionamiento del sistema y se detalle también el sentido de cambio de las variables del mismo.

Los dos campos principales investigados por Allis-Chalmers con vistas a la hidráulica de núcleos de reactores son la caída de presión y la fracción en volumen de vapor de agua (fracción de huecos). Los estudios sobre caídas de presión realizados a 600 libras por pulgada cuadrada, para el reactor Pathfinder, mostraron que la geometría de barras paralelas podía tratarse con las correlaciones establecidas para la caída de presión en dos fases. Se está efectuando un amplio estudio, comprendido en el programa de EURATOM, sobre las fracciones de huecos en condiciones de flujo análogas a las que se encuentran en las «chimeneas». Se ha efectuado para el Pathfinder un estudio parcial de fracciones de huecos en geometrías de barras paralelas. En relación con el programa de separación de vapor, se tomaron también medidas de la fracción de huecos en mezclas de dos fases con burbujas. Estos datos cubrieron un intervalo de presiones desde 300 hasta 2 000 libras por pulgada cuadrada y diámetros de vasija desde 4 hasta 36 pulgadas.

Los estudios efectuados en el Space Technology Laboratories sobre la estabilidad de reactores de agua en ebullición han incluido medidas de laboratorio de la función de transferencia potencia-huecos, en un canal simulado del SPERT 1A con agua como refrigerante. Estas medidas de la función de transferencia con circulación natural mostraron que las oscilaciones de potencia divergentes observadas en el reactor SPERT 1A a 97°C se pueden explicar como una inestabilidad por realimentación de reactividad, no como una inestabilidad puramente hidrodinámica. Cuando se incrementa en este canal el nivel de potencia aproximándose al umbral de la inestabilidad hidrodinámica, se desarrolla un pico de resonancia en la función de transferencia a 1 c/s, frecuencia a la cual llegaría a ocurrir una oscilación hidrodinámica. La resonancia indica que la respuesta de los huecos a la modulación de potencia llega a quedar dominada por la interacción entre el flujo de entrada y los huecos del vapor, y cuando esta interacción de realimentación

llega a ser inestable ocurre una oscilación hidrodinámica espontánea.

Se intentó reproducir en el laboratorio los impulsos de presión destructivos que se presentaron en los ensayos de divergencia de los reactores SPERT 1 y BORAX 1. Mediante calentamiento eléctrico transitorio se ocasionaron, en 150 microsegundos, incrementos de temperatura en la superficie de 700 °C en un elemento de acero inoxidable con una geo-

metría que reproducía los núcleos metálicos no fundidos de los reactores SPERT 1 y BORAX 1. La magnitud de los impulsos de presión producidos por el calor transmitido al agua fueron de cerca de 800 libras por pulgada cuadrada, lo cual es mucho menos que lo que se había observado en los ensayos de divergencia del reactor. En estos estados térmicos transitorios, al recubrimiento de vapor sigue una presión negativa (vacío).

Helical, forced-flow heat transfer and fluid dynamics in single and two-phase systems*

By H. F. Poppendiek** and W. R. Gambill***

This paper investigates the influence of superposed, rotational motion on forced-flow heat transfer and fluid dynamics in single and two-phase systems. Helical flow may be developed by forcing a fluid through a tube that contains a continuous twisted divider, a helical guide vane located only at the tube wall, or tangential entrance ducts. Heat transfer and fluid friction data available for single and two-phase systems are presented and analytical interpretations are discussed which assist in explaining the heat and momentum transport characteristics.

A number of studies reported in the literature have shown that heat transfer in single and two-phase forced-flow systems can be significantly improved by superposing a rotational velocity component on the axial flow [1, 2, 3]. Generally the consequences of the superposed rotational flow are (a) to increase the eddy diffusivities of the circulating fluids, (b) to generate free convection currents in single phase systems under conditions of wall heat addition, (c) to redistribute the phases in two-phase systems as a result of the centrifugal forces, and (d) to increase fluid friction. The effectiveness of a helical-flow system depends on specific temperature and flow rate limitations which define a given cooling task.

Several applications of helical-flow cooling in nuclear reactor and heat exchange systems can be envisioned. Poor convective heat transfer to gases can be improved without changing the system geometry or coolant axial flow rate by superposing a strong rotational velocity component on the axial flow. Another application relates to forced-flow boiling heat transfer. In linear or nonhelical flow, boiling heat transfer conductances are often low in the exit region of a boiler tube where fog flow exists. The conductances may be low even in the initial region of the boiler tube if vapor films develop at the tube wall. Helical flow, however, forces liquid layers against the tube wall in the low quality region, thereby yielding more effective heat transfer. Similarly, in the high vapor quality fog flow region, centrifugal forces increase the number of liquid droplets in the vapor layers near the tube wall, thus increasing the evaporative heat transfer.

An additional and specific example of how superposed rotational flow can improve heat transfer relates to a heterogenous, circulating fuel reactor. Consider a reactor system in which fluid fuel flows through one or more tubes in the core. A representative radial volumetric heat flux distribution in the fuel for this system is a modified Bessel function (maximum flux value at the tube wall and a minimum value at the tube centre). Under these circumstances, large radial fuel temperature differences (high wall temperatures) result unless external wall cooling is employed [4]. Such high wall temperatures can be reduced without external wall cooling by superposing an appropriate rotational velocity component on the axial flow. This flow pattern creates an axial velocity profile whose shape approximates the Bessel function volumetric heat source distribution in the fuel. Under these conditions, a desirable, nearly uniform radial fuel temperature distribution results [5].

ANALYTICAL INTERPRETATIONS OF HEAT TRANSFER AND FLUID FRICTION

Single-phase systems

The increased heat transfer in single-phase helical-flow systems results primarily from increased fluid turbulence and free convection (under conditions of wall heat addition). Exact analytical descriptions of the heat and momentum transfer in helical flow systems are difficult to obtain because of the complex geometries and fluid flow patterns involved. It is possible, however, to examine the relative importance of some of the transport mechanisms and develop idealized mathematical models which can be used to characterize single-phase helical flow systems.

Momentum transfer

A number of fluid dynamics analyses applicable to helical or rotational flow can be found in the literature. An interesting study has been reported by Smithberg and Landis [6] for single-phase flow in a tube with a twisted divider. An approximate pressure drop expression is derived which accounts for axial and tangential flow and vortex mixing. The predicted results are in good agreement with several sets of experimental data. Flow instability in curvilinear flow systems and superposed natural convection processes

* With contributions by N. D. Greene.**

** Geoscience Ltd., Solana Beach, California.

*** Oak Ridge National Laboratory, Oak Ridge, Tenn.

further complicate the transport processes in helical flow. For example, the early work of Wattendorf [7] demonstrated that the turbulence level in fluid layers contiguous to the concave wall of a curved channel system was significantly greater than that for linear flow; this increase was explained on the basis of Rayleigh's flow instability criterion. The classical analysis of Schmidt and Beckman [8] defines the free convection process in a vertical heated plate system. Fluids having high volumetric expansion coefficients and low kinematic viscosities with large wall heat addition develop free convection patterns under helical flow conditions, thereby increasing the fluid friction.

A simplified expression for the isothermal friction factor in the turbulent flow regime can be derived by considering only gross flow features. A large fraction of a fluid flowing in a tube exists in an annular region near the wall. If the fluid flows helically through the tube the effective flow length has been increased by the ratio of the helical path at the tube wall per unit of axial distance $(1 + (\pi D/p)^2)^{1/2}$. Similarly the resultant fluid velocity [20] in the annular region near the wall has increased approximately by the same ratio. If these quantities are substituted into the pressure drop equation, a group of terms results which is defined as the friction factor for helical flow; this function is based on the flow length, equivalent diameter, and mean fluid velocity for an axial flow system and is given by the relation

$$\frac{\zeta_h}{\zeta_l} = \left[1 + \left(\frac{\pi}{p/D} \right)^2 \right]^{1.5} \frac{D_l}{D_h} \quad (1)$$

This equation is compared to experimental adiabatic helical flow friction data in a subsequent section.

Heat transfer

Several heat transfer analyses applicable to helical or rotational flow can be found in the literature. For example, Kreith [9] used the Wattendorf data to calculate heat transfer conductances in curved channels. Smithberg and Landis [6] derive an expression for convective heat transfer in a tube with a twisted divider; the effect of free convection on the over-all heat transfer was not included.

An expression for the turbulent Nusselt modulus for helical flow (excluding free convection) can be derived on the same bases given for the friction factor relation, Eq. (1). The ratio of helical to linear flow Nusselt moduli for ordinary liquids and gases is

$$\frac{Nu_{forced}}{Nu_l} = \left[1 + \left(\frac{\pi}{p/D} \right)^2 \right]^{0.4} \left(\frac{D_h}{D_l} \right)^{0.8} \quad (2)$$

Free convection heat transfer expressions for idealized natural convection cells in a horizontal fluid layer under unstable temperature gradient conditions have been derived. Typical power law Grashof-Prandtl modulus equations result that are similar to the experimental expressions for turbulent free convection from horizontal cylinders. The relative importance of free convection to forced convection in turbulent

helical flow with wall heat addition can be estimated by the expression,

$$\frac{Nu_{free}}{Nu_l} = 7.1 \frac{(\beta \Delta t)^{1/3}}{Re_l^{0.13} Pr^{0.07}} \left(\frac{\pi}{p/D} \right)^{2/3} \left(\frac{D_l}{D_h} \right)^{2/3} \quad (3)$$

Eq. (3) is based on a one-third power Grashof-Prandtl relation and is valid only for ordinary liquids and gases. The acceleration field in the Grashof modulus is given by the ratio of the square of the tangential fluid velocity in the boundary layer to the tube radius. Also, the ratio of the tangential to linear velocity has been expressed in terms of the pitch to diameter ratio. The comparison made in Eq. (3) implies that free convection can be superposed in a forced convection system. It is clear that the complicated simultaneous processes are only approximately additive. The sum of Eqs. (2) and (3), Nu_h/Nu_l , is compared to experimental helical flow data in a subsequent section.

Two-phase systems

The increased heat transfer in two-phase helical flow systems results primarily because of the favorable distribution of the two phases in the boiler tube. In the initial, low vapor quality region of the tube, the liquid layers are forced against the heat transfer wall. In the exit, high vapor quality region of the tube, the liquid droplets are similarly held by the centrifugal forces in an annular region contiguous to the heat transfer wall.

Momentum transfer

A number of fluid dynamics models have been developed which aid in the description of two-phase, helical-flow phenomena [10]. One frictional pressure drop relation has been derived for flow in a tube with a circular cross section and for both phases in the viscous flow regime. The flow cross section of the fluid contiguous to the wall is an annulus and the cross section of the inner fluid is circular. The frictional pressure drop solution has been evaluated for (a) a gaseous annulus with a liquid core (linear flow film boiling) and (b) a liquid annulus with a gaseous core (wetted-wall linear flow or helical flow boiling). Similar annular flow analyses were made for viscous-turbulent and turbulent-turbulent flow regimes. A typical frictional pressure drop graph for the viscous-turbulent case for small ratios of annulus to core mass flow rates is shown in Fig. 1. Some preliminary comparisons have been made of this model with experimental helical-flow water-air pressure drop data; for low annulus to core mass flow rate ratios, the calculated curve was found to have a magnitude and distribution similar to that of the experimental curve. Another analysis dealt with two-phase flow in curved channels (idealized rectangular cross section). Viscous-viscous flow was considered first. The force balance and viscous shear stress equations for curvilinear flow were utilized in the derivation. It is of practical interest to evaluate the fluid dynamics in boiling systems in which the helical flow was created only by tangential entrance ducts rather than by a twisted

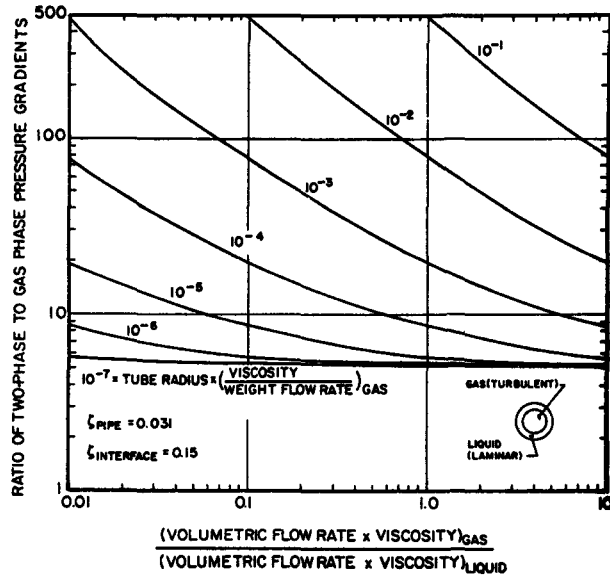


Figure 1. Annular viscous-turbulent two-phase frictional pressure gradient solution

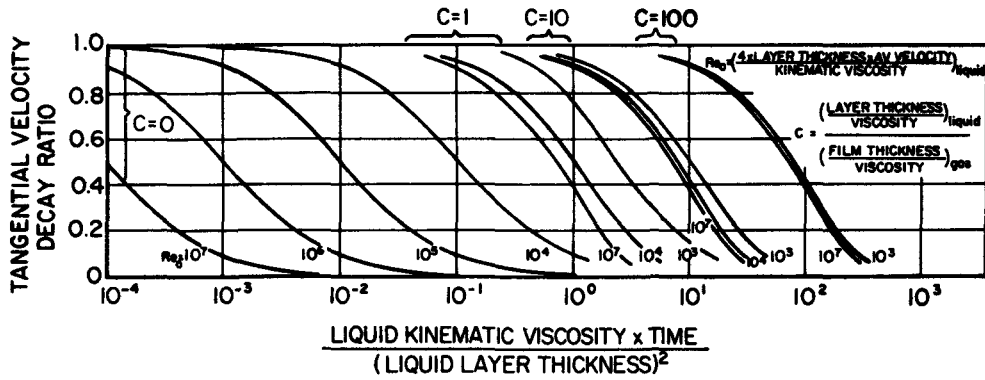


Figure 2. Dimensionless tangential velocity decay function of turbulent liquid layers rotating in stationary tube

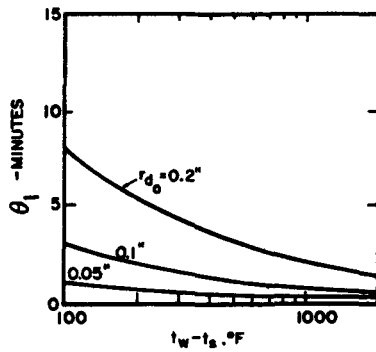


Figure 3. Water droplet vaporization lifetimes for idealized film boiling

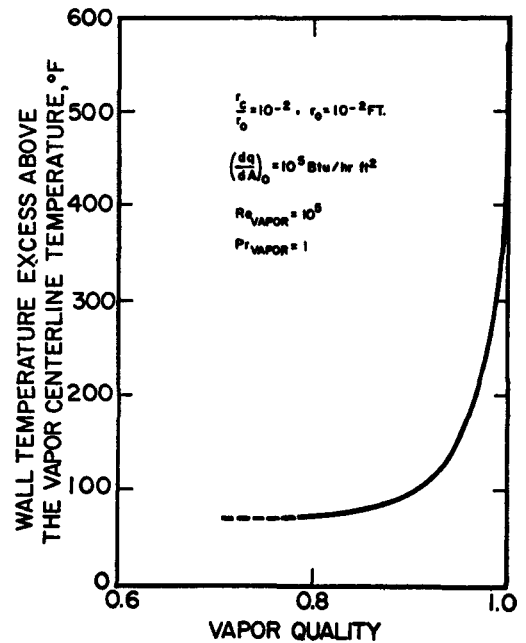


Figure 4. Wall superheat versus vapor quality calculated using fog flow heat transfer model

divider. Consequently, the velocity decay of thin, unconstrained, rotating liquid layers separated from a stationary tube wall by a gas film has been studied [11]. A transient flow analysis of the two-phase system was made by equating tangential shear and friction forces. The thickness of the gas layer was postulated to be small in comparison to the liquid layer. A set of four simultaneous equations was solved for viscous-viscous and turbulent-viscous flow regimes. The results for the case of a turbulent liquid layer and a viscous gas film are shown in Fig. 2.

Heat transfer

Several heat transfer models have been developed which aid in the description of forced, helical flow boiling. One analysis hypothesizes that a liquid film exists adjacent to the boiler tube wall [11]. Heat transfer through the superheated liquid layer occurs by conduction or eddy transfer and vaporization takes place at the liquid-vapor interface. The momentum transfer equations for annular flow referenced in the previous section are used with the liquid film heat transfer equation for either uniform wall-heat-flux or uniform wall-temperature boiler tube conditions. The simultaneous solution of these equations by numerical methods yield local information on the vapor qualities, wall temperatures, or heat fluxes as well as frictional and acceleration pressure drops.

A number of researchers have studied heat transfer to drops and in fog flow [11, 12, 13, 14, 35]. Consider the vaporization of a stationary, saturated liquid droplet on a hot horizontal surface at a uniform temperature [11]. The drop is suspended above the hot surface by an issuing vapor film beneath the drop. The latent heat transfer during vaporization is equated to heat conduction from the hot surface through the vapor film to the drop. The weight of the drop is equated to an integrated vapor film pressure force; the pressure distribution includes a variable vapor velocity with radius as a result of mass addition with radius. The vapor film thickness and weight flow rate can be obtained from a simultaneous solution of the heat transfer and force equations. The droplet lifetime can be obtained by integrating an equation that relates the vapor flow rate to the derivative of the droplet weight with respect to time. For disk-shaped drops whose height and width are equal, the resulting vaporization lifetime equation for fully established film boiling is,

$$\theta_1 = \frac{30\zeta^{1/5}}{7(160)^{1/5}} \frac{\gamma_1^{4/5} L^{3/5} r_{d,0}^{7/5}}{\gamma_v^{1/5} (t_w - t_s)^{3/5} k_v^{3/5} a^{1/5}} \quad (4)$$

Computed results for water are shown in Fig. 3. As the gravitational field increases, both the film thickness and drop lifetime decrease, thereby increasing the heat transfer to the drop. As the gravitational field increases, the droplet population increases at the wall and the total heat transfer is further increased. Studies have indicated that the results for stationary droplets are equally applicable to droplets in motion in practical systems. Thus it is clear that a radial gravitational

field is advantageous in increasing the heat flux in the high quality region of a boiler tube.

Some researchers have suggested that as a drop collides with the heat transfer surface in a boiler tube, the drop is completely vaporized and this process is the prime heat transfer mechanism. Experimental evidence indicates, however, that total vaporization on impact is not completely dominant. It seems probable that droplet vaporization takes place at all radial positions in the vapor; there is no doubt, however, that evaporation is greater near the wall than in the core region of the tube. Therefore, heat transfer in fog flow can be thought of as forced convection with a volume heat sink. The equations that define the model are,

$$u \frac{\partial t}{\partial x} = \frac{\partial}{\partial r} \left[(a + \epsilon) r \frac{\partial t}{\partial r} \right] - \frac{Sr}{\gamma_v c_{p,v}}, \quad (5)$$

$$\text{where} \quad S = \frac{3\gamma_v c_{p,v} \epsilon (t - t_s)}{r_o^2 \left(\frac{r_c}{r_o} \right)^3 \left(\frac{r_o}{r_d} - \frac{r_o}{r_c} \right)} \quad (6)$$

The heat sink, S , is defined by a number of postulates. A droplet is surrounded by a region of influence called a cell. Within the cell, heat is transferred from superheated gas at the outer region of the cell to the saturated liquid drop; heat is transferred by an eddy transport process when the cell is located in the turbulent core of the pipe and by conduction when the cell is located near the heat transfer wall. Simultaneous with the heat transfer process, mass is transferred from the droplet surface to the outer regions of the cell by diffusion. A heat transfer analysis of this idealized energy transfer process yields an expression for the heat sink given by Eq. (6). The heat sink is proportional to an eddy diffusivity and the local superheat and inversely proportional to the cube of the ratio of cell radius to pipe radius and the first power of the ratio of the pipe radius to the drop radius. Figure 4 shows calculated wall and centerline temperature differences as a function of quality for specific conditions shown in the graph; a uniform wall heat flux and volume heat sink with radius was postulated. Note the rapid increase in the radial temperature difference as the quality increases from 0.8 to 1.0 where the value for gaseous convection is reached. The droplet radii used in these calculations are uniquely determined by the relation between quality and the liquid-vapor fraction. Some available linear flow water boiling data show features similar to the calculated curve in Fig. 4.

EXPERIMENTAL HEAT TRANSFER AND FLUID FRICTION DATA AND SOME PREDICTED RESULTS

Single-phase systems

Momentum transfer

Available helical flow friction factor data have been converted to a common basis and plotted in Fig. 5. The mean experimental results shown were generally

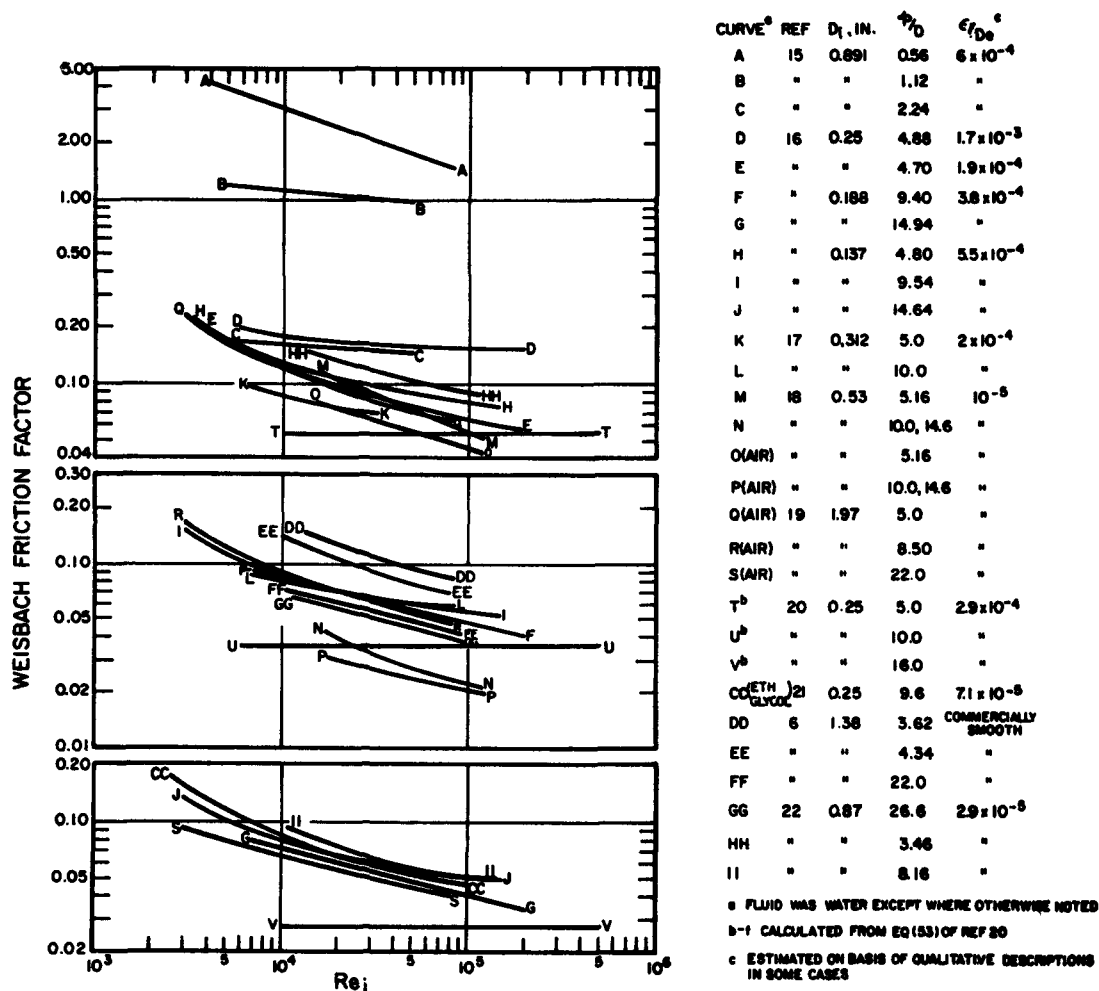


Figure 5. Helical flow friction factor versus Reynolds modulus

obtained under adiabatic conditions. Accurate ORNL friction data [16] were obtained with multiple, axially spaced pressure taps machined by an electrical discharge method through the tube wall at circumferential locations midway between opposing divider edges. The surface roughness conditions and pitch to diameter ratios are also shown in Fig. 5. The insert used in the tube of [15] was composed of polished aluminum with an anodized surface. Experimental adiabatic helical to linear friction factor ratios as a function of pitch to diameter ratio for $10^4 < Re_i < 10^5$ are shown in Fig. 6 together with the adiabatic prediction Eq. (1). Definitive nonadiabatic friction data are not available. However, it is clear that they would fall substantially above the adiabatic values. Flow decay experiments were conducted in a long, empty, transparent, plastic tube in which thin liquid layers were allowed to flow in vortex fashion [10]. The vectorial directions of the flow layers were measured as a function of axial distance down the tube. From these studies experimental velocity decay data were obtained. The results were in good agreement with values predicted by the velocity decay model described.

Heat transfer

Helical-flow forced convection data obtained for heating water, air, and ethylene glycol are plotted in Fig. 7. The free convection effect can be observed by comparing the wall cooling data (E') with corresponding wall heating measurements (D). Quantitative measurements of surface condition were not generally reported, but it was indicated that some tubes were hydraulically smooth [18, 19, 22], and, the others were slightly rough. When electrical wall heating was used, heat generation in the swirl generators was negligible (<1%). The insert of [15] consisted of a spiral flight wrapped around a small-diameter rod coincident with the tube axis, which allowed use of very tight twist ratios. Additional heat-transfer data are reported by Fleming [23], Stonecypher [24], and Tatom [25]. Data for heating isopropylated Santowax in swirl flow have been obtained by Judd [26], and Koch [19] also used spaced-propeller swirl generators in air heating experiments. Four USSR helical-flow references were noted [27, 28, 29, 30]. Experimental helical to linear Nusselt modulus ratios as a function of pitch to diameter ratio for $10^4 < Re_i < 10^5$ are shown in Fig. 8 together with an analytical prediction, Eqs. (2) and (3).

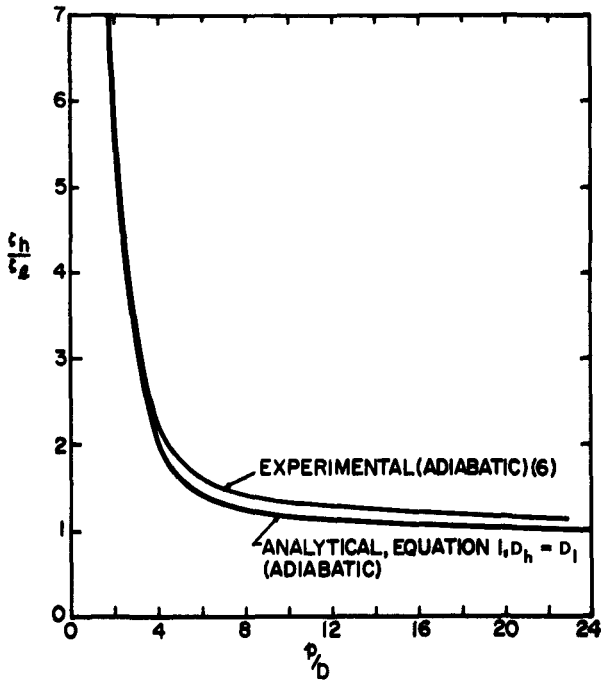


Figure 6. Helical to linear flow friction factor ratio versus pitch to diameter ratio

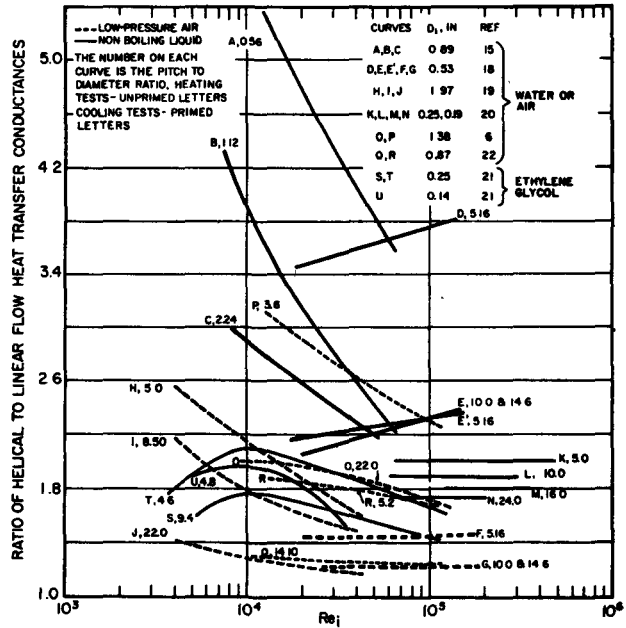


Figure 7. Helical flow heat transfer conductances versus Reynolds modulus

Two-phase flow

Momentum transfer

Local boiling [20, 25] and saturation boiling [12, 31] pressure drop measurements are available. Saturation boiling pressure drop measurements for mercury flow in a vertical tube with a twisted divider were also obtained [32]. The results are shown in dimensionless form in Fig. 9 together with experimental and predicted linear flow data; the predicted curve was based

on a simple slug flow model [11]. Helical flow predictions are currently being evaluated.

Evans [33] found in air-water tests with no heat addition that coiled wires were not as efficient in rotating the core flow and in keeping bubbles from the wall as were twisted dividers.

Heat transfer

Figure 10 shows the performance improvement resulting from the swirl motion of saturated Freon [34].

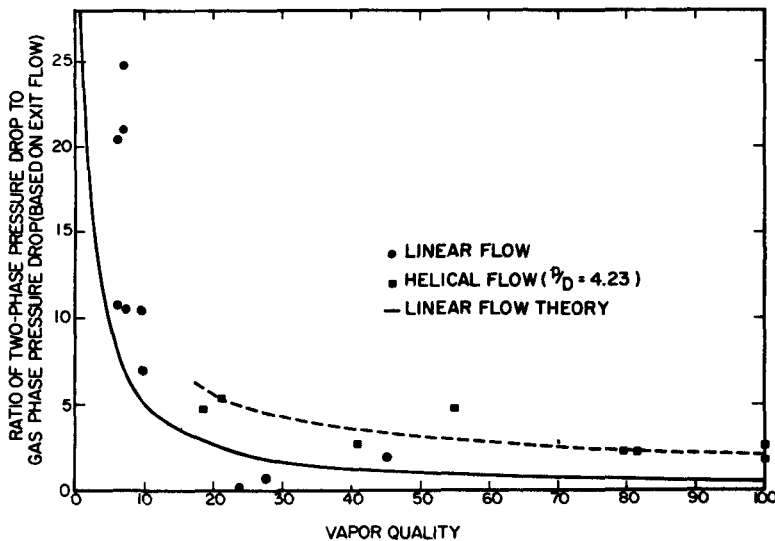


Figure 8. Helical to linear flow Nusselt modulus ratio versus pitch to diameter ratio

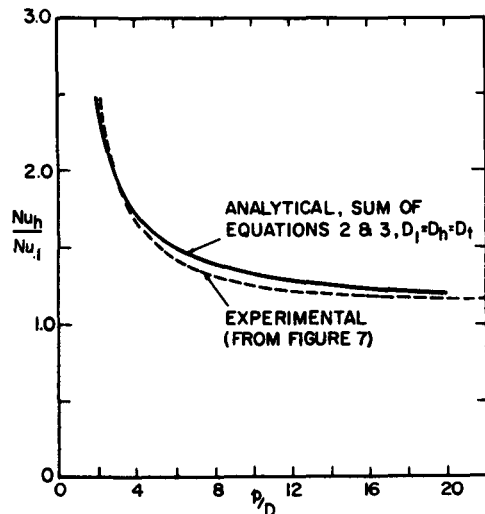


Figure 9. Helical and linear flow frictional pressure drop data versus mercury vapor quality

The fractional vaporization at a given temperature difference is larger for the helical flow. Tatom [25] found that helical flow local boiling conductances were greater than axial flow values with water for a given heat flux. At a given pressure loss or pumping power, however, the helical flow and axial flow heat transfer conductances were approximately equal. Blatt and Adt [31], as well as Gido and Koestel [12], found that the effect of helical flow was more pronounced in film boiling than in nucleate boiling. With Freon 11 at a wall-bulk temperature difference of 300 °F, the helical flow film boiling conductance was approximately three times larger than that for axial flow. In the nucleate-boiling region, Blatt and Adt concluded that high coefficients were obtained under all conditions with Freon 11 when swirl flow was imposed, but that with water this was true only under subcooled conditions or at low vapor qualities.

A recent comparison was made [21] of both water and ethylene glycol pool and forced-convection boiling data (axial and swirl flow) with Kutateladze's proposed boiling correlation [35]. The data generally fall ~50% above the average line suggested by Kutateladze, after a one-eighth power gravity ratio is empirically introduced to bring the swirl data into better agreement with the pool and axial-flow boiling data. Water burn-out heat fluxes as large as 54.8×10^6 Btu/h ft² have been attained with tangential entrance ducts [1] and 37.4×10^6 Btu/h ft² with full-length twisted dividers [20]. Figure 11 shows a graph of six sets of helical flow burn-out data for water; the fluxes are as much as 2.6-fold larger than the corresponding values for axial flow. This increase is a function of pumping power dissipation per unit surface area or centrifugal intensity. Kutateladze's equation for the burn-out heat flux under saturated pool-boiling conditions [35] indicates that the pool boiling burn-out flux should vary with the fourth root of the local acceleration. This variation, which is of considerable importance in space-vehicle nuclear

reactors operating in a reduced-gravity environment, has been substantially confirmed experimentally by Costello and Adams [36], Ivey [37], and Morozkin *et al.* [38] in rotating pool experiments. Foure *et al.* [39] extended previous studies made with water to the two-phase condition and to annular geometries at low pressures and velocities. Again the heat transfer was improved. Further, it was noted that the helical flow significantly improved the boiling flow stability, probably because the slug-flow regime was suppressed.

An apparatus was constructed and used to measure vaporization lifetimes of water and mercury droplets on a horizontal hot surface [11]. The experimental water data fell approximately 25% above values predicted with Eq. (4). Experimental mercury data fall approximately 10% below the predicted values (see Fig. 12).

Boiling mercury heat transfer data obtained in linear and helical flow were reported by Gido and Koestel [12]. A small diameter wire helix having a pitch to diameter ratio of 3.9 was inserted in contact with the inner wall of a heated tube. The swirl wire increased the heat transfer conductance in the film boiling region by a factor of about 2.5, but an attempt to correlate the data with vapor qualities was not successful. Boiling sodium heat transfer measurements in a tube with a twisted divider having a pitch to diameter ratio of 9.45 were obtained by the General Electric Co. [42]. In general, the conductances increased several fold between zero and about 20% vapor quality and then decreased to a value (at 50% vapor quality) that was an order of magnitude lower than the entrance conductance. It is believed that the increasing conductance variation in the initial region of the boiler tube supports the liquid annulus heat transfer model described in the previous section. Heat transfer conductances increase as liquid layer thicknesses decrease.

Boiling mercury heat transfer measurements in a tube with twisted dividers having various pitch to

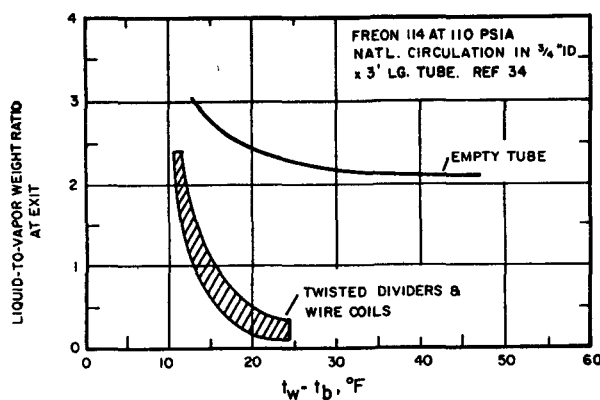


Figure 10. Liquid-to-vapor weight ratio versus wall-bulk temperature difference for boiling Freon in a vertical tube

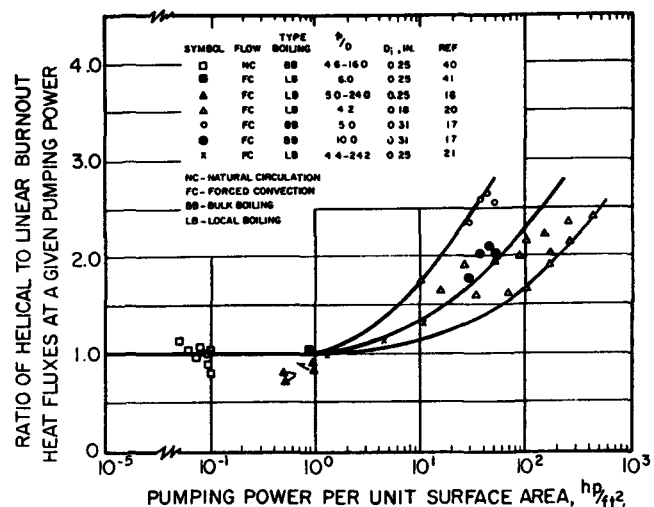


Figure 11. Variation of the ratio of helical to linear flow burn-out heat fluxes at constant pumping power

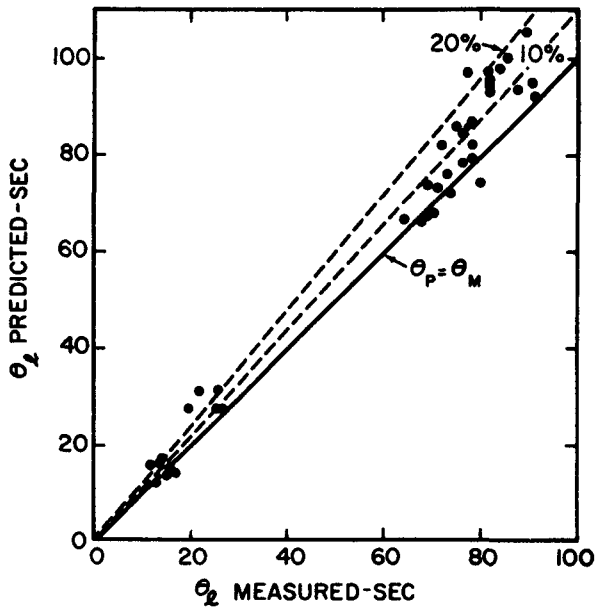


Figure 12. Measured and predicted mercury droplet lifetimes

diameter ratios have also been obtained [11, 32]. Figure 13 compares experimental helical flow data for a pitch to diameter ratio of 4.23 with experimental linear flow measurements and predicted functions. Note that the experimental and predicted data for linear flow are in general agreement; comparisons for helical flow have only been made at 0% and 100% vapor qualities. Some of the interesting conductance variations in the low and high vapor quality regions for helical flow can be explained with the aid of liquid annulus and fog flow models discussed previously. Note that helical flow heat transfer is again superior to that for linear flow over the entire quality range. The helical flow data are about two orders of magni-

tude above the linear flow values in the low quality region for the conditions shown.*

CONCLUSIONS

In the helical flow of liquids or gases, the heat transfer conductances and pressure drops were found to increase with the magnitude of the rotational fluid flow component. The results also depend on the specific fluid velocity profiles and wall heat addition. The heat transfer conductances and pressure drops in two-phase flow systems were also found to increase with the rotational fluid flow component. However, the functional variation was found to be more complicated because of the various ways in which the two phases can distribute themselves.

Heat and momentum transfer in helical single-phase flow can be predicted by accounting for free and forced convection mechanisms. Free convection is controlled by the acceleration field produced by the velocity field of the rotating fluid and the magnitude of the wall heat addition. Forced convection is normally increased by the relatively larger vectorial fluid velocities. In two-phase or boiling systems, the acceleration forces in helical flow control the spacial distribution of liquid films and droplets in boiler tubes; the corresponding heat transfer and fluid friction can be estimated with idealized transport models.

From the experimental heat and momentum transfer data, it can be shown that the ratio of Stanton modulus to the friction factor for helical single and two-phase flow is not a unique function as in the case of linear single-phase flow. Generally, for single

* The Pratt and Whitney Aircraft Div. and the AiResearch Co. have also conducted helical flow boiling liquid metal experiments; the results have not been compared in detail but are in general agreement with the Geoscience data.

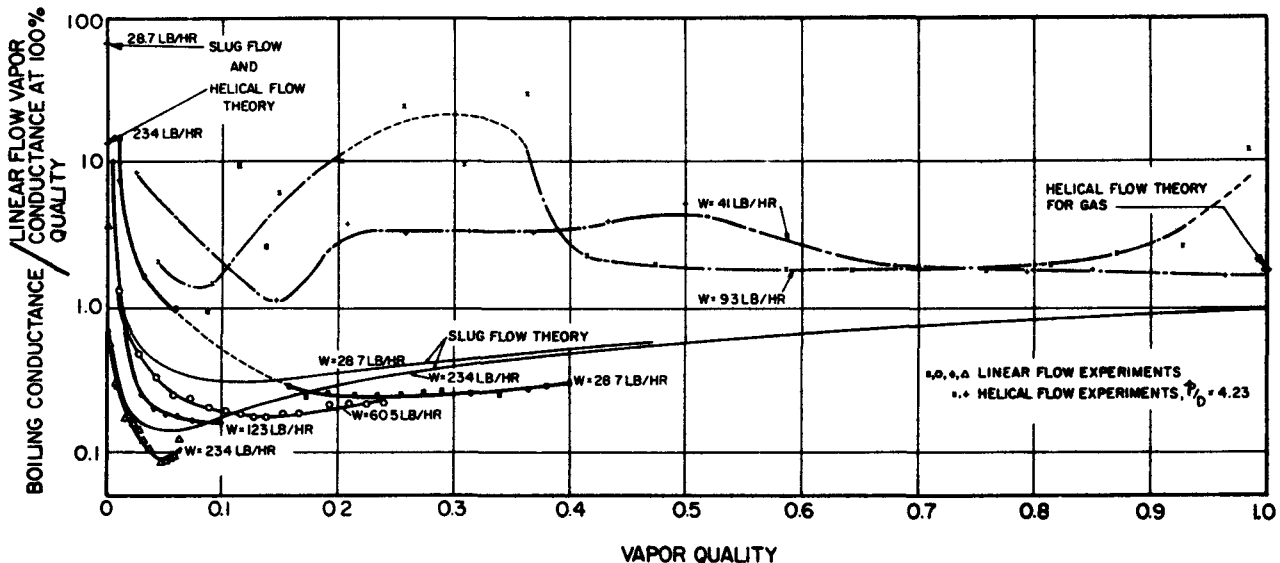


Figure 13. Normalized boiling heat transfer conductances for mercury flow in tubes versus vapor quality

phase systems the Stanton-friction factor ratio for helical flow is less than the corresponding ratio for linear flow. A wide range of ratios are believed possible, with the ratios depending on the character of the velocity structure, phase distribution, turbulence promotion, and wall heat addition.

The heat transfer per unit pumping power (effectiveness) of helical flow depends on a number of system conditions. In single phase flow for a constant geometry, radial fluid temperature difference and axial flow rate, helical flow effectiveness is generally inferior to linear flow. In single phase flow for a constant geometry and radial temperature difference but variable axial flow rate, helical flow effectiveness can be superior to linear flow. If the geometry and difference between the maximum wall temperature and coolant inlet temperature are held fixed, either linear or helical flow could be more effective. In two-phase flow, the effectiveness of helical flow is generally superior to that for linear flow; thus, excessive wall superheat temperatures can be reduced and exit vapor qualities increased in helical flow.

NOMENCLATURE

a : acceleration of gravity or thermal diffusivity of vapor
 $c_{p,v}$: heat capacity of vapor
 $\frac{dq}{dA}$: heat flux
 D : inner tube diameter
 D_e : equivalent diameter
 D_h, D_l : equivalent diameter for helical and linear flow systems, respectively
 D_t : equivalent diameter for tangential flow in a tube
 k_v : thermal conductivity of vapor
 L : latent heat of vaporization
 p : helix pitch (based on 360 degrees)
 r : radial distance
 r_c : cell radius
 r_d : droplet radius
 $r_{d,o}$: initial droplet radius
 r_o : inside radius of boiler tube
 S : droplet heat sink
 t : local vapor temperature
 t_b : bulk temperature
 t_s : saturation temperature
 t_w : wall temperature
 u : local vapor velocity
 x : axial distance
 β : volumetric expansion coefficient of the coolant
 Δt : wall-fluid temperature difference
 ζ : Weisbach friction factor
 ζ_h, ζ_l : Weisbach friction factors for helical and linear flow systems, respectively
 ϵ : eddy diffusivity of vapor and surface roughness
 θ_1 : droplet evaporation lifetime

γ_l, γ_v : liquid and vapor weight densities, respectively
 Nu_{forced} : forced convection Nusselt modulus for helical flow system
 Nu_{free} : free convection Nusselt modulus for helical flow system
 Nu_h : Nusselt modulus for a helical flow system
 Nu_l : forced convection Nusselt modulus for linear flow system
 Pr : Prandtl modulus
 Re_l : Reynolds modulus for linear flow system
 Re_i : Reynolds modulus based on inside tube diameter and linear or axial coolant flow rate

REFERENCES

- Gambill, W. R., and Greene, N. D., Chem. Eng. Prog., 54, 10, 68 (1958).
- Evans, S. I., and Sarjant, R. J., J. Inst. Fuel, 24, 216 (Sept. 1951).
- Gambill, W. R., and Greene, N. D., US Patent, No. 2 950 604.
- Poppendiek, H. F., and Palmer, L. D., Nuclear Sci. Eng., 3, 1, 85 (1958).
- Poppendiek, H. F., and Greene, N. D., US Patent, No. 3 136 700 (9 June 1964).
- Smithberg, E., and Landis, F., ASME, J. Heat Trans., 86, 39 (Feb. 1964).
- Wattendorf, F. L., Proc. Roy. Soc. A., 148, 565 (1935).
- Schmidt, E., and Beckmann, W., Tech. Mech. Therm., 1, 341 and 391 (1930).
- Kreith, F., Heat Trans. and Fluid Mech. Inst. 111, Stanford Univ. Press (1953).
- Poppendiek, H. F., Greene, N. D., MacDonald, F. R., Wright, H. R., Sabin, C. M., and Thompson, A. S., Geoscience Report 10 (AEC Contract AT(04-3)-409), TID-18028 (GLR-10), (Sept. 1961-Aug. 1962).
- Poppendiek, H. F., Greene, N. D., MacDonald, F. R., Sabin, C. M., Livett, R. K., and Thompson, A. S., (AEC Contract AT(04-3)-409), (GLR-15) (Sept. 1962-Aug. 1963).
- Gido, R. G., and Koestel, A., NAA-SR-6309, TRW Report ER-4833 (Oct. 1962).
- Goldman, K., Firstenberg, H., and Lombardi, C., Trans. ASME, J. Heat Trans., 83, Series C, 2, 158.
- Stein, R. P., Crane, M., Firstenberg, H., Hankel, R., and Israel, S., United Nuclear Corp., Report UNC 5008-I, NYO-9844-I (1962).
- Greene, N. D., Convair Aircraft Report ERR-SD-024 (1960).
- Gambill, W. R., and Bundy, R. D., ORNL (unpublished data) 1962.
- Viskanta, R., Nuclear Sci. Eng., 10, 202 (1961).
- Kreith, F., and Margolis, D., Appl. Sci. Research, 8, Sec. A, 457 (1959).
- Koch, R., VDI Forschungsheft, 469, 1 (1958), also AEC-TR. 3875.
- Gambill, W. R., Bundy, R. D., Wansbrough, R. W., Chem. Eng. Prog. Symp. 57, 32, 127 (1961).
- Gambill, W. R., and Bundy, R. D., Amer. Inst. Chem. Engineers J., 9, 55 (1963).
- Seymour, E. V., Trans. Inst. Chem. Engineers, 41, 159 (1963).
- Fleming, Jr., J. D., PhD. Thesis, Sch. of Chem. Engr., Ga. Tech., Dissertation Abstracts, 19, 79 (1959).
- Stonecypher, T. E., PhD. Thesis, Sch. of Chem. Engr. Ga. Tech., Dissertation Abstracts, 21, 89 (1961).

25. Tatom, F. B., MS Thesis, Sch. of Mech. Engr., Auburn Univ. (1962).
26. Judd, R. L., Canadian General Electric Co., Tech. Rept R61-CAP-44 (1961).
27. Goldshtik, M. A., Akad. Nauk SSSR, Otdel. Tech. Nauk. 12, 24 (1958), also AEC-TR-4832.
28. Zhukauskas, A. A., Heat Trans. and Therm. Sim., 201 Academy of Sciences, USSR Press, Moscow (1959).
29. Yermolin, V. K., Izvest. Akad. Nauk SSSR, 1, 55 (1960).
30. Ibragimov, M. Kh., Nomofilov, E. F., and Subbotin, V. I., Teploenergetika, 8, 7, 57 (1961), in Russian.
31. Blatt, T. A., and Adt, Jr., R. R., ASME Paper No. 63-WA-42, Meeting held in Philadelphia, Pa., (1963).
32. Geoscience Ltd., AEC Progress Report 21 (Dec. 1963-Feb. 1964).
33. Evans, D. G., NASA TM X-725 (1963).
34. Allen, C. F., AEC R & D Report K-1487 (Oct. 19, 1961).
35. Kutateladze, S. S., 2d Ed., Ch. 10, Moscow-Leningrad (1949, 1952); AEC Trans. 3770 (1959).
36. Costello, C. P., and Adams, J. M., Paper 30, Part II, 255, ASME, International Heat Transfer Conference at Boulder, Colo. and Westminster, London (1961).
37. Ivey, H. S., UKAEA Report AEEW-R99 (Sept. 1961).
38. Morozkin, V. I., *et al.*, High Temperature, 1, 1, 88 (1963).
39. Foure, C., Rosuel, A. H., Sourieux, G., Special Report 5, EURAEC-146 (1961).
40. Gambill, W. R., and Bundy, R. D., USAEC Report ORNL-3026 (20 Dec. 1960).
41. Goldmann, K., NDA 2-79 (25 June 1958).
42. Longo, J., General Electric Co., Quarterly Progress Reports 2, 3, and 4, Contract NAS 3-2528 (April and July 1963).

ABSTRACT—RÉSUMÉ—АННОТАЦИЯ—RESUMEN

A/231 Etats-Unis d'Amérique

Transfert de chaleur hélicoïdal en circulation forcée et dynamique des fluides des systèmes à une et deux phases

par H. F. Poppendiek et W. R. Gambill

Le mémoire étudie l'influence d'un mouvement de rotation superposé sur le transfert de chaleur en circulation forcée et sur la dynamique des fluides dans les systèmes à une et deux phases. On peut créer un écoulement hélicoïdal en faisant passer le fluide dans un tube contenant une séparation continue courbée ou un guide hélicoïdal placé uniquement le long de la paroi du tube. Dans ces conditions l'écoulement est complètement ou partiellement dirigé par les guides. On peut également créer un écoulement hélicoïdal dans un tube en introduisant le fluide par des orifices d'entrée tangentiels. L'écoulement résultant est un écoulement rotationnel en décroissance, non commandé, superposé à un écoulement axial constant.

De nombreux chercheurs ont mesuré les caractéristiques de transfert de chaleur et de frottement de fluide pour des gaz et des liquides en écoulement hélicoïdal dans des tubes. En général, les conductances de transfert de chaleur et les coefficients de frottement ou les pertes de charges croissent en même temps que la composante d'écoulement rotationnel. Les profils de vitesse spécifique du fluide et l'importance de l'apport de chaleur de la paroi influencent également les résultats expérimentaux. On a également des mesures de transfert de chaleur à deux phases ou à l'ébullition et des mesures de frottement de liquide pour des métaux liquides et des liquides ordinaires en écoulement hélicoïdal dans des tubes. De nouveau, on a observé que les conductances de transfert de chaleur et les coefficients de frottement ou les pertes de charge augmentent avec l'importance de la composante d'écoulement rotationnel comme dans le cas de l'écoulement à une phase; cependant, la fonction de

variation est plus compliquée en raison des différentes possibilités de distribution des deux phases dans le tube.

On peut prédire les transferts de chaleur et de quantité de mouvement dans l'écoulement hélicoïdal à une phase en tenant compte des mécanismes de convection libre et forcée qui existent dans l'écoulement courbe. Le terme de convection libre dans un fluide donné est sous la dépendance du champ d'accélération produit par le champ de vitesses du fluide en rotation et de l'importance de l'apport de chaleur à la paroi. Le terme de convection forcée en écoulement hélicoïdal pour un fluide donné est défini par le niveau de turbulence, généralement élevé à cause des vitesses vectorielles du fluide relativement grandes et de l'incitation géométrique à la turbulence. Dans les systèmes à deux phases ou en ébullition, les forces d'accélération dans l'écoulement hélicoïdal déterminent la distribution spatiale des films liquides et des gouttelettes dans les tubes bouilleurs, ainsi que le transfert de chaleur correspondant et le frottement de fluide. Dans la région de vapeur de basse qualité d'une chaudière, les forces centrifuges dans l'écoulement rotationnel obligent le liquide à rester au contact de la paroi des tubes, ce qui conduit à un échange de chaleur plus efficace. Dans la zone d'écoulement en brouillard de vapeur de haute qualité, les forces centrifuges augmentent la densité des gouttelettes liquides dans les couches de vapeur contiguës à la paroi des tubes, augmentant ainsi de façon marquée l'échange de chaleur assurant l'évaporation dans cette zone importante. On peut estimer la perte de charge due au frottement dans un tube avec écoulement à deux phases à l'aide de modèles mathématiques simplifiés si les phases sont distribuées selon des conformations simples. On a pu analyser la dynamique des fluides pour des écoulements hélicoïdaux forcés et non forcés dans des tubes. Les modèles mathématiques de transfert de chaleur et de dynamique des fluides ont servi à prévoir les performances de systèmes d'écoulement hélicoïdal à une et deux phases.

Ces résultats sont en bon accord avec le comportement expérimental.

On a montré expérimentalement que le rapport du module de Stanton au coefficient de frottement pour un écoulement hélicoïdal à une et deux phases n'était pas une fonction unique comme dans le cas d'un écoulement linéaire à une seule phase. On pense qu'une gamme étendue de rapports peut exister en fonction du caractère de la distribution des vitesses de l'écoulement rotationnel, de la distribution des phases, de l'importance de la turbulence et de l'apport de chaleur de la paroi. Quelques aspects de la variation du rapport entre le transfert de chaleur et la puissance de pompage peuvent être expliqués analytiquement.

A/231 США

Теплообмен в условиях вынужденного движения спирального потока и гидродинамика одно- и двухфазных систем

Х. Ф. Поппендик, В. Г. Гамбилл

В настоящем докладе исследуется влияние дополнительного вращательного движения на теплообмен и гидродинамику в вынужденном потоке одно- и двухфазной систем. Спиральный поток может быть осуществлен путем подачи жидкости через трубку со встроенной непрерывной спирально завитой вставкой или с винтообразным направляющим ребром, расположенным только у стенки трубы. В этих условиях форма потока всецело или частично определяется формой направляющих. Спиральный поток в трубе может быть также получен принудительной подачей потока через тангенциальные входные патрубки. В результате создается поток с уменьшающимся по мере течения вращательным движением, накладывающимся на постоянную осевую составляющую потока.

Ряд исследователей измеряли интенсивность теплообмена и гидравлическое сопротивление при спиральном движении газов и жидкостей в трубах. В общем было установлено, что интенсивность теплообмена и коэффициенты трения или потеря напора увеличиваются с ростом вращательной составляющей движущегося потока. Профили скоростей потока выбранной жидкости, величина тепловой добавки, вносимой стенкой, также влияют на экспериментальные результаты. Имеются также данные по теплообмену при наличии двухфазного потока или в случае кипения, а также данные по гидравлическому сопротивлению жидких металлов и обычных жидкостей при их спиральном

движении в трубках. Оказалось, что коэффициенты теплоотдачи и потери напора увеличиваются с ростом вращательной составляющей потока, как это было в случае однофазного потока. Однако функциональная зависимость более сложна ввиду возможности различного распределения обеих фаз в трубе.

Перенос тепла и количества движения в спиральном однофазном потоке может быть предопределен в случае учета механизмов естественной и вынужденной конвекции, которые существуют в криволинейных потоках. Член естественной конвекции для данной жидкости зависит от поля ускорения, созданного полем скорости вращающейся жидкости, и от количества тепла, принимаемого от стенки. Член вынужденной конвекции в спиральном потоке для данной жидкости определяется уровнем турбулентности, который обычно довольно высок вследствие сравнительно высоких векторных скоростей жидкостей и геометрического увеличения турбулентности. В двухфазных или кипящих системах силы ускорения спирального потока определяют распределение жидкостных пленок и капель в испарительных трубках, а также соответствующий теплообмен и гидравлическое сопротивление. В зоне низкокачественного пара котла центробежные силы вращающегося потока неизменно принуждают жидкость прилегать более плотно к стенкам трубок, что приводит к более эффективному теплообмену. В зоне насыщенного пара-тумана центробежные силы увеличивают плотность жидких капель в слоях пара, примыкающих к стенке трубы, тем самым значительно увеличивая теплообмен при испарении в этой важной зоне. Потери напора, вызванные трением в трубке с двухфазным потоком, могут быть оценены посредством идеализированных математических моделей, если распределение фаз не сложно. Сделан анализ гидродинамики для ограниченного и неограниченного спирального потока в трубках. Использовались такие математические модели переноса тепла и гидродинамики, которые позволили предопределить характеристики спиральных одно- и двухфазных потоков. Эти результаты в общем согласуются с экспериментальными данными.

Экспериментально установлено, что отношение числа Стантона к коэффициенту трения при спиральном одно- и двухфазном потоке не является однозначной функцией, как в случае прямолинейного однофазного потока. Предполагают, что возможен широкий диапазон этих отношений в зависимости от характера структуры скоростей спирального потока, распределения фаз, усиления турбулентности и перехода тепла от стенки. Некоторые виды изменения величины отношения интенсивности теплообмена к мощности на перекачку могут быть объяснены аналитически.

A/231 Estados Unidos de América

Intercambio de calor en un flujo forzado helicoidal y dinámica de fluidos en sistemas de una y dos fases

por H. F. Poppendiek y W. R. Gambill

Este trabajo investiga la influencia del movimiento rotatorio provocado en el intercambio de calor por flujo forzado y la dinámica del fluido en sistemas de una y dos fases. Un flujo helicoidal puede provocarse forzando un fluido a través de un tubo que contenga un tabique continuo retorcido o un álabe guía en hélice colocado solamente en la pared del tubo. En estas circunstancias las configuraciones del flujo están coartadas completa o parcialmente por las guías del flujo. También puede producirse flujo helicoidal en un tubo forzando la entrada del fluido por conductos tangenciales. El régimen de flujo que resulta no está coartado y se presenta un flujo rotatorio discretamente superpuesto a una componente axial constante.

Varios investigadores han medido el intercambio calorífico y las características de rozamiento de gases y líquidos sometidos a un flujo helicoidal en tubos. En general se encontró que las conductancias para el intercambio calorífico y los coeficientes de rozamiento o caídas de presión aumentaban con la magnitud de la componente rotatoria del flujo fluido. También influían en los resultados experimentales las distribuciones de velocidades específicas del fluido y las cantidades de calor aportadas por las paredes. Se dispone también de medidas de intercambio calorífico y rozamiento fluido para sistemas de dos fases o en ebullición en metales líquidos y líquidos ordinarios sometidos a flujo helicoidal en tubos. Asimismo se halló que las conductancias de intercambio calorífico y los coeficientes de rozamiento o caídas de presión aumentaban con la magnitud de la componente rotatoria del flujo fluido, como pasaba con el flujo de una sola fase; no obstante, la función de variación es más complicada debido a las distintas formas en que las dos fases pueden distribuirse en el tubo.

Teniendo en cuenta los mecanismos de convección libre y forzada que existen en las configuraciones curvilíneas del flujo se puede predecir el intercambio

de calor y de impulso en el flujo helicoidal en fase simple. Para un fluido dado el término de convección libre se rige por el campo de aceleración producido por el campo de velocidad del fluido rotatorio y por el valor del aporte calorífico de la pared. El término de convección forzada, para un fluido dado, en flujo helicoidal lo define el nivel de turbulencia que normalmente es grande debido a que las velocidades vectoriales del fluido son relativamente grandes y a que provoca turbulencia geométrica. En sistemas en ebullición o de dos fases, las fuerzas de aceleración en el flujo helicoidal rigen la distribución espacial de las películas líquidas y de las gotitas en los tubos de las calderas y sus correspondientes intercambios calorífico y rozamiento del fluido. En la región de baja calidad de vapor de una caldera, las fuerzas centrífugas del flujo rotatorio obligan al líquido a acercarse a la pared del tubo con lo que se mejora el intercambio calorífico. En la región en que el flujo es húmedo, de alta calidad de vapor, las fuerzas centrífugas aumentan la densidad de las gotas líquidas en las capas de vapor próximas a la pared del tubo, con lo que aumenta sensiblemente el intercambio calorífico por evaporación en esta importante región. La caída de presión por rozamiento en un tubo por el que fluyen dos fases se puede estimar con ayuda de modelos matemáticos ideales si las fases se distribuyen en figuras sencillas. Se han hecho análisis dinámicos del fluido para flujo helicoidal, coartado o no coartado, en tubos. Los modelos matemáticos de intercambio calorífico y dinámica de fluidos se han usado para predecir el funcionamiento de sistemas de flujo helicoidal de una y dos fases. En general estos resultados concuerdan con el comportamiento experimental.

Se encontró experimentalmente que, la razón del módulo de Stanton al coeficiente de rozamiento para flujo helicoidal de una o dos fases no era función unívoca, como en el caso del flujo lineal de una sola fase. Parece ser que puede haber una amplia gama de razones según sean la estructura de velocidades del flujo rotatorio, la distribución de las fases, la promoción de turbulencia y el aporte de calor de la pared. Algunos aspectos de la variación de la razón entre intercambio de calor y potencia de bombeo pueden explicarse analíticamente.

Critical flow phenomena in two-phase mixtures and their relationships to nuclear safety

By H. S. Isbin,* H. K. Fauske,** M. Petrick,** C. H. Robbins,***
R. V. Smith,**** S. A. Szawlewicz***** and F. R. Zaloudek*****

Containment systems are provided for nuclear safety to protect the public and local area from fission product releases. In addition to the fuel cladding, items which also function as fission product barriers are the primary cooling system piping and vessels, and the reactor containment. The integrity of the barriers is further safeguarded through additional devices such as the core spray systems, neutron poison injection systems, emergency condensers, reactor enclosure cooling systems, and systems for closing valves in containment penetration lines such as coolant piping and ventilation ducts. In the event of a break in the primary coolant system with loss of coolant, pressures and temperatures throughout the reactor and containment will change, and the barriers and emergency cooling systems must operate as intended. This paper is concerned with the status of the art on the estimation of the liquid coolant loss rate in postulated failures. Although coolant loss rate has little effect on maximum pressure build-up for dry capsule containment, it is important in pressure suppression and pressure relief type containment. The rate of coolant loss will determine the time in which emergency cooling systems must start to operate to prevent fuel melting, poison injection and the rapidity with which isolation valves must close.

The purpose of this paper is to focus attention on the current status of the available analyses and experimental programs which relate to the evaluation of the rate of coolant flow through apertures, including orifices and tubes. For a given aperture and state of the fluid, correlations and predictive methods are sought for the discharge rates. The release of liquid coolants, with accelerating flows through breaks, to lower pressure regions introduces the complexities of metastability producing superheated liquids which may or may not undergo extensive nucleation and vaporization. Models, experimental verifications and applications are presented for critical two-phase flow. Conditions for two-phase critical flow are readily achieved by flows from pipes. The more general

problems of two-phase flow through apertures, including orifices, nozzles and short tubes, are noted and references are made to models that attempt to take into account the non-equilibrium conditions of the liquid and vapor flows. Also included are brief descriptions and current results from experimental programs designed to present scaled versions of reactor installation as well as experiments designed to learn more about the two-phase flow phenomena.

CRITICAL TWO-PHASE FLOW

With single-phase flow, the maximum mass flow rate of a fluid discharging from an opening into an enlarged downstream section is no longer dependent upon the downstream pressure. The fluid velocity at the opening is just large enough to prevent the propagation of pressure impulses from the downstream side to the upstream side. The single-phase maximum flow rate is called the critical or sonic flow and various conditions may be used to derive the appropriate analytical definitions. Gas-liquid, two-phase flows also exhibit maximum discharges, almost independent of the downstream pressure [1]. Although the individual phase velocities may be considerably smaller than the corresponding sonic velocities [2], the two-phase flow must accommodate itself in such a way as to minimize the influence of the much lower downstream pressure effects. Excellent summaries of the experimental investigation on two-phase critical flow are available [2, 3, 4, 5], and in this section we examine and compare models and data for the critical discharge of steam-water mixtures from pipes. The models serve to define the maximum discharge rate with the critical conditions of pressure and quality at the opening or end of pipe. The difficulties in calculating the pressure drops in the piping leading to the opening are discussed in references [4, 6, 7], and trial-and-error evaluations are usually required for relating the critical flow rates with the upstream conditions.

Models

In all models considered in this section, the following assumptions are made: (a) the two-phase discharge is from a constant-area duct or has been expanded in

* University of Minnesota, Minneapolis, Minnesota.

** Argonne National Laboratory, Argonne, Illinois.

*** General Electric, APED, San Jose, California.

**** National Bureau of Standards, Boulder, Colorado.

***** US Atomic Energy Commission, Washington, D.C.

***** General Electric, HAPO, Richland, Washington.

an ideal nozzle such that both phases are at the same static pressure and is local equilibrium; (b) the velocity of each phase is uniform at the exit, and the flow is steady.

Although the assumptions neglect departure from phase equilibrium and neglect entrainment, the models, nevertheless, do represent practical limits for predicting the critical flows.

Homogeneous flow. Two-phase flow with each phase at the same velocity leads to the homogeneous (or equilibrium) model. The mixture specific volume is given by

$$v = v_f + xv_{fg} \quad (1)$$

The momentum and continuity equations with the restraint that the change in mass flow rate with respect to pressure is zero at constant entropy define the critical mass flow rate as

$$G^2 = -g_c \left(\frac{\partial p}{\partial v} \right)_s \quad (2)$$

The form of the equation is identical to that for the single-phase criterion.

Annular-flow models. The annular-flow model utilizes a two-phase flow pattern with the vapor flowing in the core and the liquid flowing in the annulus at the wall. Again, the continuity and momentum equations may be combined to yield Eq. (2) for the critical mass rate with the following definition for the mixture specific volume:

$$v = \frac{x^2 v_g}{\alpha} + \frac{(1-x)^2 v_f}{1-\alpha} \quad (3)$$

where α represents the "void" fraction, or fraction of the cross-sectional area for flow occupied by the vapor.

A variety of methods has been used to estimate the void fraction. Existing two-phase void correlations involving the Martinelli data and Armand data [3] have been modified to provide the values of α to be used with Eq. (2). Experimental data on void fractions appropriate for critical flows have not yet been determined, and there is good evidence to indicate that data and correlations obtained at lower flow rates are not adequate [2]. The most thoroughly tested method for estimating the void fraction for critical flows is the Fauske method [2]. A second and recent innovation is due to Levy [8]. Other approaches which utilize the energy balance are noted in later sections.

In the methods noted, the partial derivative $(\partial p/\partial v)$ is evaluated at constant entropy and the references noted should be consulted for the procedural details. Comparisons may also be made by carrying out the evaluation at constant enthalpy (Fauske method). The differences are generally not significant. Qualities usually used for the presentation of predicted flow rates with critical pressure and quality are the values obtained from an energy balance with the kinetic energy terms being well approximated by the homogeneous model.

Fauske method. In addition to the assumptions noted at the start of this section, the following requirement is made a part of the model: (c) the pressure gradient attains a finite, maximum value for a given flow rate and quality:

$$\left| \frac{dp}{dl} \right|_{G,x} = \{\text{Maximum}\}_{\text{finite}} \quad (4)$$

The critical flow is attained when the flow rate no longer increases with decreasing static pressure, $(dG/dp) = 0$. At the critical condition, the maximization of the flow is achieved by varying the void fraction.

$$\frac{\partial}{\partial \alpha} \left[\frac{\text{Rate of momentum}}{\text{gain by convection}} \right] = 0 \quad (5)$$

The resulting slip ratio is $K = u_g/u_f = (V_g/v_f)^{1/2}$, and the void fraction is

$$\alpha = \left[1 + \frac{1-x}{x} \left(\frac{v_f}{v_g} \right)^{1/2} \right]^{-1} \quad (6)$$

Levy method [8]. The momentum and continuity equations for the two-phase flow, neglecting the head and frictional losses, may be used to determine a specific relationship between quality and void fraction. Starting with an initial condition of $x = 0$, $\alpha = 0$, the following equation is obtained:

$$x = \frac{\alpha(1-2\alpha) + \alpha \sqrt{\{(1-2\alpha)^2 + \alpha[(2\rho_f/\rho_g)(1-\alpha)^2 + \alpha(1-2\alpha)]\}}}{(2\rho_f/\rho_g)(1-\alpha)^2 + \alpha(1-2\alpha)} \quad (7)$$

No additional assumptions are needed to determine the critical flow rate using Eqs. (2) and (3).

Minimum kinetic energy model. Starting with a simplified energy balance and relating the two-phase flow to an upstream stagnation condition, h_0 and s_0 :

$$h_0 = h_f + xh_{fg} + E_K \quad (8)$$

$$E_K = \frac{G^2}{2g_c J} [K(1-x)v_f + xv_g]^2 \left(x + \frac{1-x}{K^2} \right) = \frac{G^2}{2g_c J} \phi(K, x, p) \quad (9)$$

For isentropic flow, $x = (s_0 - s_f)/s_{fg}$, and thus $\phi(K, x, p)$ and in turn, G , become functions of only K and p . Minimizing the specific kinetic energy, $(\partial E_K/\partial K) = 0$, leads to the slip ratio $K = (v_g/v_f)^{1/2}$ [9]. The concept of minimum kinetic energy flow has also been presented by Zivi [10]. Other investigators, including Ryley in 1952 [11], have independently suggested that $K = (v_g/v_f)^{1/2}$. A detailed comparison of models and data is given by Moody [9], and for convenience, reference will be made to the Moody model.

Applications

Steam-Water. The predictions of the Fauske, Levy, and Moody models for steam-water flows are presented in Figs. 1, 2, and 3. Detailed comparisons of experimental data for critical steam-water flows are given in references [2, 3, 8, 9]. The differences between

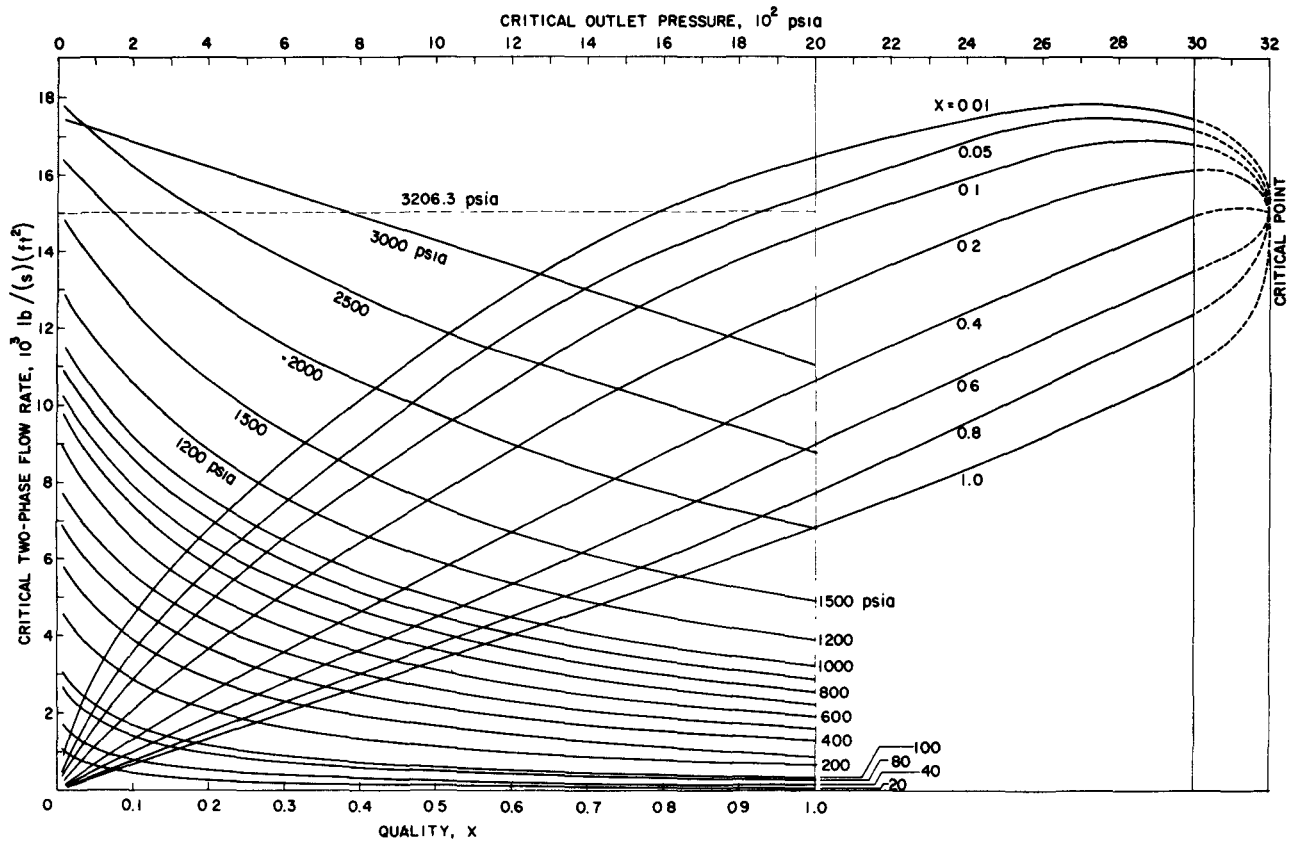


Figure 1. Predictions of critical steam-water flow rates with the Fauske model

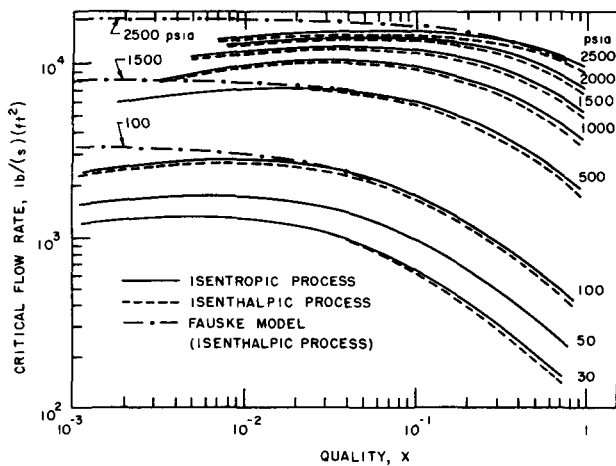


Figure 2. Predictions of critical steam-water flow rates with the Levy model [8]. Also shown are comparisons with the Fauske model for $P = 100, 500, \text{ and } 2500$ psia

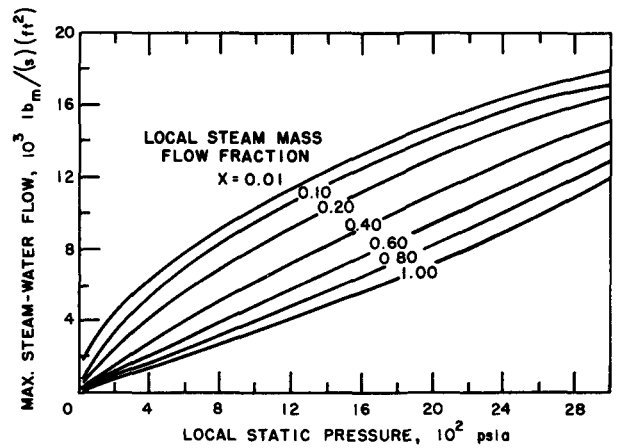


Figure 3. Predictions of critical steam-water flow rates with the Moody model [9]

models are surprisingly small and all three methods appear to correlate well the experimental data, with the Fauske model exhibiting the best comparisons. The Moody model yields mass flow values which are consistently higher than the Fauske results except for low qualities. In regions of low and decreasing quality, the Levy and Moody models yield maximum flow rates, whereas the Fauske model leads to increasing flow rates. Experimental data at the low qualities are not available for distinguishing these effects. The predicted critical mass flow is particularly sensitive to

changes in slip ratio or void fraction at the low qualities.

The experimental values for the critical flows for steam-water mixtures from pipes exceed the values predicted by the homogeneous model. As the quality is decreased, the deviations from the homogeneous model become more pronounced. For example, the experimental values are far greater than the predicted values at low qualities and low pressures. The homogeneous model predictions for critical steam-water flows are presented in Fig. 4. Detailed comparisons

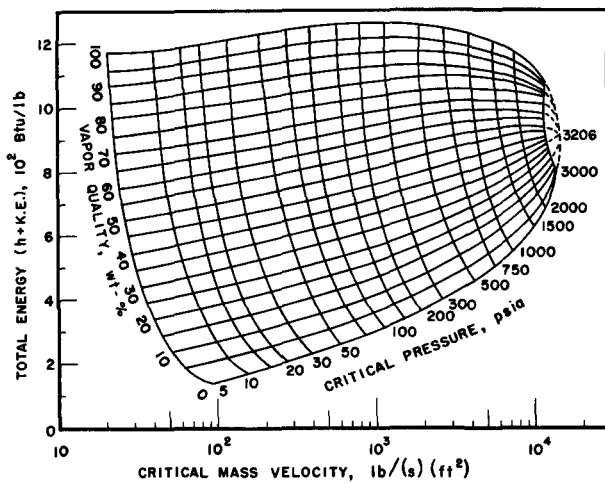


Figure 4. Predictions of critical steam-water flow rates with the homogeneous model

of the homogeneous model with experimental data and with other models are given in references [1, 2, 3].

Liquid metals. The Fauske method has been applied for estimating the two-phase critical flow of mercury, caesium, rubidium, potassium, sodium, and lithium [9]. Experimental data for comparing the predictions of the Fauske method or other models are not available.

Cryogenic fluids. The use of models to obtain upper and lower limits is necessary for situations in which insufficient data are available for guidance. Smith [4] has prepared a detailed literature survey on critical two-phase flow with special applications of models for hydrogen, nitrogen, oxygen, and several refrigerants.

TWO-PHASE FLOW THROUGH APERTURES

A variety of phenomena occurs for the flow of fluids through apertures with initial starting conditions of saturated or nearly saturated liquids [4, 12, 13, 14, 15]. For example, it is well recognized that flows of saturated liquids through sharp-edged orifices behave as single-phase fluids and no flashing occurs at the orifice opening. As the physical size of the aperture is increased permitting longer contact times in traversing the opening, nucleation and vaporization increase. The breaking up of the metastable liquid jet in the aperture has not been studied sufficiently to provide adequate guidance for the development of models predicting critical flows. Apertures include nozzles and short tubes. For sufficiently long tubes, the assumption that the phases are in close approach to equilibrium appears to be adequate and the critical flow models discussed in the previous section may be applied.

Although some success has been achieved in characterizing the metastable flow conditions for specific geometries, analyses without resort to experimental data do not yet appear possible. Table 1 illustrates approaches which have been used:

Table 1

Conditions	Comment	Reference
Flow of superheated water in short tubes.	One-dimensional, nonequilibrium, homogeneous, two-phase flow theory. Experimental parameters required to fit growth rates for the vapor nuclei sites.	Simpson and Silver (1962) [14]
Reservoir of saturated water, sharp-edged orifice in tank wall as the aperture.	(a) Solutions for the flow of two-phase equilibrium, compressible, homogeneous fluids; (b) solutions for metastable flow; (c) two-phase, growing bubble, homogeneous flow. Solutions (b) and (c) each introduce a single parameter to characterize the model.	Isbin and Gavalas (1962) [16]
Flow of flashing water through short tubes (including orifices of various lengths) and nozzles.	(a) Surface tension models developed by Burnell, and Kinderman and Wales; (b) Surface evaporation model by Bailey and Pasqua. Empirical constants are required for all models.	For current review, see Zaloudek (1963) [15] and Smith (1963) [4]

EXPERIMENTAL PROGRAMS

Most of the investigations on the flow of flashing fluids through apertures, as summarized in references [4, 13], were motivated by the needs of industrial applications involving steam-power plants, refrigeration, and in a variety of chemical processing plants. A series of recent and current experimental programs has evolved to study more specifically the designs for nuclear reactor containment. A brief account of the programs is given in Chapter 12 of the *Reactor Containment Handbook*, ORNL (1964). Large scale engineering safety tests are noted in reference [17].

MSA Research Corporation blowdown tests [18]

Apertures used were orifices having a 1.5-in diameter and lengths of 0.5, 1.5, and 12 in. The blowdown rate of water was measured from a 518 gallon vessel with water at the orifice inlet subcooled approximately 100 °F. The observed flow rates were somewhat lower than the predictions based upon the Burnell correlation, and also lower than the predictions of the orifice equation using the saturation pressure as the pressure in the throat of the orifice.

Pacific Gas and Electric Co. tests for Humboldt and Bodega Bay

Tests have been run by the Pacific Gas and Electric Company which simulate loss of reactor coolant due to pipe breaks for the Humboldt Bay and Bodega Bay nuclear plants. The Humboldt test facility consisted basically of a pressure vessel with a nozzle at the bottom connected to an air-filled tank simulating

the pressure suppression system dry well; the dry well was then connected by piping to the suppression chamber pool. In testing, the pressure vessel was first partially filled with water and heated to a pressure of 1 250 psig. Instrumentation measured the initial volume of water in the reactor vessel and transient pressures in various parts of the system simulating the dry well and suppression chamber. The pressure vessel had a total volume of 55.8 ft³ and the nozzle at the bottom of the pressure vessel leading to the orifice was 6 in in diameter and 9 in long. Calculations indicate that the point of critical flow was the orifice. The diameters of the sharp-edged orifices ranged from 0.30 to 3.28 in.

The tests in support of the Bodega Bay pressure suppression containment were similar to the Humboldt tests with the simulated reactor vessel having a volume of 80 ft³ with an inside diameter of 27 in. Tests were run with flow nozzles as well as with sharp-edged orifices. Diameters ranged from 0.906 to 5.12 in.

In all tests performed, the average and not the instantaneous discharge rates were measured. Data for Humboldt and Bodega tests are available in references [19, 20, 21]. Evaluation of the Humboldt and Bodega results yields some interesting indications and conclusions:

(a) The average flow rate was about the same through sharp-edged orifices and the two nozzle shapes used, indicating that critical flow in the aperture is controlling.

(b) The size of the orifice or nozzle relative to the pressure vessel diameter has an important effect on the average flow rate. Figure 5 is a plot of average mass flow rate (lb/s-ft² of break) vs the ratio of break diameter to vessel diameter. Mass flow rates are high with small openings and lower with large openings, and this phenomenon may be related to the entrapment and sweeping out of the steam bubbles produced in the vessel with outflows through the larger openings.

(c) The blowdown behavior of the Humboldt and Bodega vessels was very similar although one was about 50% bigger in diameter and volume than the

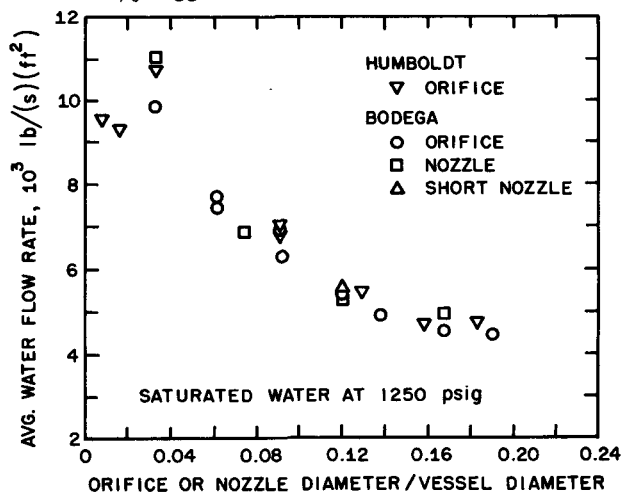


Figure 5. Average mass flow discharge rates in Humboldt and Bodega tests

other. This tends to indicate that reduced scale tests can be used to predict loss of coolant from large reactor vessels, provided the information indicated in item (b) is available for a sufficient range of conditions, including effects of initial pressure.

(d) Average vessel discharge rate was not affected significantly if the water in the vessel was subcooled initially by not more than about 30–40 °F. Beyond this amount of subcooling the average discharge rate increased as the initial subcooling was increased.

General Electric HAPO tests

Choking can occur at the entrance of a pipe with the flow of subcooled water depressurizing to the saturation pressure. Experiments [15] were performed to study the flashing of initially compressed (subcooled) water through short lengths of pipe with length/diameter ratios of up to 20, and upstream pressures from 115 to 1 800 psia. Flow rates associated with upstream choking were accurately predictable by conventional nozzle equations using single-phase contraction coefficients and assuming the lower pressure to be the saturation value.

For very short pipes ($L/D < 6$) with abrupt entrances, the flow patterns and critical flow rates were influenced by either a free or submerged discharge condition. With a submerged discharge, such pipes were observed to be subject only to the upstream choking mentioned above, and the downstream pressure would be equal to or greater than the saturation pressure. With a free discharge, the hot water was observed to separate from the wall of the pipe at the entrance and flow detached from the walls in a metastable stream. With such flow patterns, choking occurred at the exit of the pipe when the downstream pressure was low enough to cause sufficient vaporization in the nonequilibrium stream. Critical flow rates under these circumstances were in fair agreement with the semi-empirical correlations of Burnell [22], Kinderman and Wales [23], and Bailey [24].

Programs are under way to extend the available steam-water critical discharge data to higher temperatures and pressures than presently available in literature. In preliminary phases of this investigation [25], experiments have been performed to determine the maximum discharge rates from a 1 000-gallon, 2 500-psi pressure vessel through one-half in diameter flow passages with water temperatures up to 550 °F. Correspondence of the observed critical mass velocity with values predicted by the Fauske theory has been observed at critical pressures as high as 600 psia. In this program, experiments are to be performed to determine the critical discharge characteristics of pipe sizes up to 4 in and to investigate critical flow in various valves, elbows, and tees discharging directly to atmosphere.

University of Minnesota tests

Whereas a variety of blowdown and transient tests has been made to study specific design applications,

there is need to study in a more detailed fashion the two-phase flows through apertures. The University of Minnesota facility provides measurements of the instantaneous flow rates and thrusts for the discharge of saturated water through apertures. Measurements of the static pressure profiles in the immediate vicinity of the opening as well as in the aperture provide additional guides for analysis. The pressure vessel (16 in id) is suspended by a load cell and flexible fittings are provided for piping connections. A second load cell is mounted diametrically opposite the aperture and serves to record the thrusts produced by the discharge. Saturated water up to 250 psig is prepared by boiling the water and venting steam prior to each run.

Measurements of the static pressure within the aperture (short orifices with uniform and tapered lengths) indicate an almost uniform pressure, at least over half the length. Use of this back pressure with the usual orifice equation for single phase liquid flow accurately predicts the mass flow rate. As yet no tests have been made to simulate any reactor core structure in the vicinity of the aperture, and the conclusion to date is that no flashing occurs within the vessel. The extent of the flashing within the aperture itself is under investigation. Models are being examined which might adequately account for the pressures within the aperture, mass flow rates, thrusts, postulated conditions of the metastable liquid jets, and influence of aperture geometry. The critical flow phenomenon within the short-length apertures differs from that observed for flows from pipes in which phase equilibrium conditions are closely approximated.

AMU-ANL containment tests

The Argonne National Laboratory (ANL) and the Associated Midwest Universities (AMU) have co-

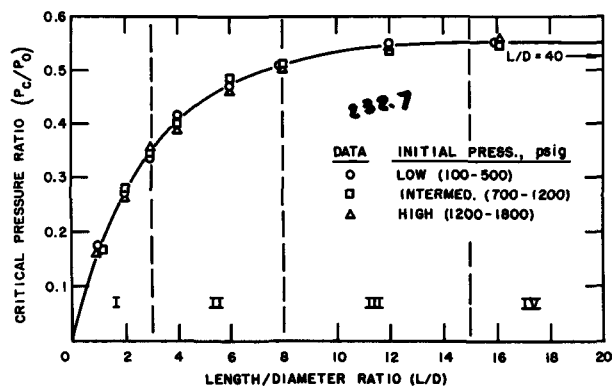


Figure 7. AMU-ANL critical pressure ratio vs length/diameter ratio for 0.25 in id tube

operated in carrying out advanced research programs involving nuclear reactor heat transfer and fluid flow. The AMU-ANL containment test facility is capable of handling the discharge of saturated water at pressures up to 2 000 psia. The pressure vessel has a volume of 35 ft³ and is instrumented with pressure and differential pressure transducers (to provide the flow measurement rates), thermocouples, and electronic recorders such that both steady state and transient measurements can be made.

The results of preliminary tests with a 0.25 in id tube are presented in Figs. 6 and 7. Discharge rates vs initial pressure P_0 , for saturated water in the vessel, are presented in Fig. 6 with length of test section to diameter (L/D) ratio as the parameter. Pressure profiles were measured and extrapolated to the exit of the tube so as to obtain the critical exit pressure, P_c . In Fig. 7, the ratio P_c/P_0 is plotted vs length to diameter ratio, and a single curve is adequate to represent the results. The critical pressure ratio remains constant for $L/D = 15$ to $L/D = 40$, decreases slowly between $L/D = 15$ and $L/D = 8$, decreases more rapidly as L/D ratio approaches zero. Effects of diameter have not yet been investigated. For a tube with $L/D \approx 0$, or a sharp-edged orifice, the mass flow rate for an initially saturated liquid can be evaluated using the incompressible flow equation for the orifice:

$$G = 0.61\sqrt{2g_c(P_0 - P_b)(144)/v} \quad (10)$$

where P_b is the downstream ambient pressure.

For short tubes, $L/D < 3$, Eq. (10) is used with P_b being replaced by the exit critical pressure, P_c . The metastable flow for short tubes is similar to that found in the Freon tests [26]. In region II of Fig. 7, the flow rates are smaller than would be predicted by use of $\Delta P = P_0 - P_c$, indicating that the use of the orifice equation would require a pressure higher than the exit critical pressure. The violent breakup of the metastable liquid jet probably accounts for the high pressure fluctuations (± 50 psi) observed in the test sections. With increasing L/D ratios, region III of Fig. 7, pressure profiles are stable, and it is believed that the degree of metastability is rapidly decreasing as L/D approaches 15. This is also indicated by

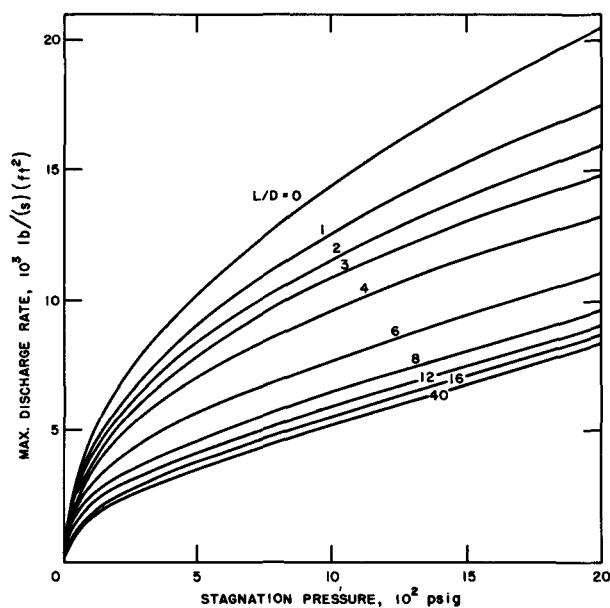


Figure 6. AMU-ANL maximum discharge rates vs stagnation pressure for 0.25 in id tube

smaller reductions in the flow rates for increasing L/D ratio compared to region II. The boundary between region II and III is not well defined at present and more detailed analysis of the data may show that the two regions are not separable. In region IV, $L/D = 16$ to 40, the critical pressure ratio attains a constant value of 0.55. The discharge rates measured for $L/D = 12$ to 40 can be evaluated closely by the Fauske method and similar models using the measured critical pressure and calculated quality. These results provide an indication of the required L/D value necessary to approach the conditions of phase equilibrium and the applicability of the annular flow models.

The tests in progress, including measurements of void fractions at the tube exit, are designed to explore more fully the two-phase critical flow structure, and to extend the correlations and models.

Cryogenic Engineering Laboratory (NBS, Boulder, Colorado)

One of the USA-NASA projects for space vehicle engines is NERVA, which proposes to use a reactor as the energy source and hydrogen as the working fluid. Two-phase, critical mass flows of hydrogen will be investigated.

SUMMARY

Reactor containment and emergency cooling systems are designed to cope with the transient and maximum pressure buildups arising from loss of coolant accidents. The expulsion of the coolant from pipe and vessel breaks in high pressure water systems will involve metastable and two-phase flow phenomena, including what is called the maximum, critical, or choking two-phase flow rate. This paper has focused attention on the model studies and empirical evaluations of the critical coolant loss rates through apertures such as orifices, nozzles, and tubes.

The model studies have served to bracket upper and lower limits for the critical discharge of steam-water mixtures from pipes. The lower limit is provided by the homogeneous model. The deviations of the homogeneous model from the experimental results have been well verified. Three different models, Fauske, Levy, and Moody, yield critical mass flow rates in good agreement with the experimental results. Further work needs to be done to ascertain the differences in the predictions at low qualities, and measurements of the void fractions at critical flow will provide a discerning test for the models.

The discharge of saturated water through short length apertures involves metastable liquid jets and the breakup of the jets. Adequate predictive models have not yet been developed. The critical discharge through short tubes and nozzles can be predicted on the basis of the orifice equation for single-phase liquid flows, provided the pressure drop is related to the pressure within the aperture. Current experimental studies are attempting to characterize the important parameters.

Summary results are presented for blowdown tests of specific reactor designs, including some insight on methods for scaling tests. The current status of the coolant discharge studies for reactor containment programs is briefly described.

NOMENCLATURE

- E_K : kinetic energy of two-phase flow per unit mass
 G : mass flow rate
 g_c : Newton's constant
 h : specific enthalpy; h_0 , h_l , h_{lg} ; stagnation, liquid, liquid to vapor
 J : mechanical equivalent of heat
 K : slip ratio, u_g/u_l ; $K: (v_g/v_l)^{1/2}$ Fauske method; $K_M(v_g/v_l)^{1/2}$ Moody method
 l : length in flow direction
 p : pressure; P_c : critical pressure; P_0 : pressure in vessel; P_b : downstream pressure
 L/D : ratio of length of test section to diameter
 s : specific entropy; s_0 , s_l , s_{lg} : stagnation, liquid, liquid to vapor
 u : velocity; u_g , u_l : gas, liquid
 v : mixture specific volume; v_l , v_g , v_{lg} : saturated liquid, vapor, liquid to vapor
 x : quality, mass fraction vapor in flow mixture
 α : "void fraction," fraction of cross-sectional area for flow occupied by vapor
 $\phi(K, x, p)$: $[K(1-x)v_l + xv_g]^2[x + (1-x)/K^2]$, function of K, x, p

REFERENCES

1. Isbin, H. S., Moy, J. E., and Da Cruz, A. J. R., Amer. Inst. Chem. Eng. Journal, 3, 361/365 (1957).
2. Pacific Gas and Electric Co., Preliminary Hazards Summary Report, Bodega Bay Atomic Power Unit Number 1, USAEC report ANL-6633 (1962).
3. Fauske, H. K., USAEC report ANL-6779 (1963).
4. Smith, R. V., National Bureau of Standards Technical Note 179, Supt. of Documents, U.S. Govt. Printing Office, Washington, D.C. (1963).
5. Zaloudek, F. R., USAEC report HW-68934 Rev. (1961).
6. Fauske, H. K., Nuclear Sci. and Eng., 17, 1/7 (1963).
7. Isbin, H. S., Fauske, H., Grace, T., and Gracia, I. Jr., Symp. Two-phase Fluid Flow, Inst. of Mech. Eng., London (1962).
8. Levy, S., USAEC report GEAP-4395 (1963).
9. Moody, F. J., USAEC report APED-4378 (1963).
10. Zivi, S. M., ASME Paper No. 63-HT-16 (1963).
11. Ryley, D. J., Engineer, 193, 363/367 (1962).
12. Friedrich, Hans, Energie, 10, No. 5, 175/185 (1958); Energie, 12, No. 10, 3/11 (1960); and Vetter, G., Energie, 14, No. 1, 3/11 (1962).
13. Isbin, H. S., Mosher, D. R., and Moen, R. H., USAEC report AECU-2994 (1954).
14. Simpson, H. C., and Silver, R. S., Symp. Two-Phase Fluid Flow, Inst. Mech. Eng., London (1962).
15. Zaloudek, F. R., USAEC report HW-77594 (1963).
16. Isbin, H. S., and Gavalas, G. R., Proceedings of the 1962 Heat Transfer and Fluid Mechanics Institute, Stanford University Press (1962).

17. Wilson, T. R., Hauge, O. M., and Matheney, G. B., USAEC report IDO-16833 Rev. 1 (1963).
18. Arker, A. J., and Kaufman, R. A., USAEC report KAPL-M-AJA-3 (1960). See also MSAR 59-130 (1959) and MSAR-60-81 (1960).
19. Barton, D. B., Ashworth, C. P., Janssen, Earl, and Robbins, C. H., ASME Paper 61-WA-222, 1/19 (1961).
20. Ashworth, C. P., Barton, D. B., and Robbins, C. H., Nuclear Eng., 7 (75), 313/321 (1962).
21. Pacific Gas and Electric Co., Preliminary Hazards Summary Report, Bodega Bay Atomic Power Unit Number 1, USAEC report NP-12476 (1962).
22. Burnell, J. G., Engineering, 164, 572/576 (1947).
23. Kinderman, W. J., and Wales, E. W., Trans. ASME, 79, 183/190 (1957).
24. Bailey, J. F., Trans. ASME, 73, 1109/1116 (1951).
25. Zaloudek, F. R., USAEC report HW-80535 (1964).
26. Fauske, H. K., and Min, T. C., USAEC report ANL-6667 (1963).

ABSTRACT—RÉSUMÉ—АННОТАЦИЯ—RESUMEN

A/232 Etats-Unis d'Amérique

Les phénomènes d'écoulement critique dans les mélanges à deux phases et leur influence sur la sûreté nucléaire

H. S. Isbin *et al.*

L'expulsion du réfrigérant lors d'une rupture de canalisation ou de cuve d'un système à eau sous pression élevée entraîne des phénomènes d'écoulement métastable et à deux phases y compris les écoulements critiques ou les étranglements. Les enveloppes de sécurité et les systèmes de refroidissement de secours doivent être prévus pour faire face aux élévations de pression transitoires et maximales et à la vitesse de perte du réfrigérant.

Les débits calculés pour l'expulsion du réfrigérant sans vaporisation du liquide sont nettement supérieurs à ceux calculés pour un écoulement homogène à deux phases. On a pu établir un certain nombre de modèles analytiques pour prévoir l'écoulement critique à deux phases dans des ouvertures comprenant des orifices, des tuyères et des canalisations. On sait également que la nature et l'emplacement de la rupture ont une influence sur le type d'écoulement du réfrigérant et, par conséquent, sur le choix du modèle. On indique les débits critiques prédits par les divers modèles pour des réfrigérants tels que l'eau, les fluides cryogènes et les métaux liquides.

La littérature traitant des phénomènes d'écoulement à deux phases représente un aspect important des connaissances nécessaires pour évaluer les problèmes en question; cependant, seules des expériences relativement récentes apportent les données nécessaires à l'étude de cas concrets. Les résultats expérimentaux disponibles pour les écoulements critiques à deux phases dans des canalisations sont exposés et comparés avec les prédictions des modèles analytiques. La discussion comprend des conclusions sur les mérites et les possibilités d'utilisation des modèles. Des essais d'expulsion de réfrigérant ont été effectués afin d'établir des critères pour la prédiction des écoulements à deux phases; ces résultats sont également discutés et comparés avec les prédictions.

Un exposé de l'état actuel des programmes relatifs à la sûreté des réacteurs nucléaires comprend une brève description des études sur les pertes de réfrigérant actuellement en cours aux Etats-Unis. Les

résultats préliminaires se rapportent à l'étude de l'état du fluide à l'intérieur de la cuve (mesures de pression et de vide), à la distribution des pressions dans les sections et dans des ouvertures des canalisations, aux variations des rapports L/D pour les sections de sortie, et à la mesure des vides à la position critique de sortie. Presque tous les essais en cours utilisent l'eau comme fluide avec des pressions allant jusqu'à 2 000 psig (140 kg/cm²). La suite des programmes d'essai avec utilisation de fluides cryogènes permettra d'obtenir des renseignements sur les phénomènes d'écoulement critique à deux phases intéressant les applications nucléaires spatiales. L'utilisation de fréon donne des résultats visuels et quantitatifs.

Pour chaque ensemble de conditions décrivant un accident par perte de réfrigérant, on indique les problèmes qui restent à résoudre pour prédire les vitesses d'écoulement et on estime approximativement les limites d'erreur. On décrit un programme destiné à mettre en évidence les effets intégrés d'un accident par perte de réfrigérant.

A/232 США

Критические потоки двухфазных смесей и их влияние на безопасность реактора

Г. С. Исбин *et al.*

Выброс теплоносителя через разрывы труб или корпуса в реакторах с водяным охлаждением под высоким давлением может вызвать метастабильные и двухфазные потоки, включая критические потоки. Для того, чтобы справиться с резким кратковременным подъемом давления и быстрой потерей теплоносителя, предусмотрены специальные контейнеры и охлаждательные устройства на случай такой аварии.

По расчетам, скорость выбрасываемого теплоносителя без испарения жидкости значительно выше расчетной скорости для двухфазного гомогенного потока. Вследствие этого были разработаны различные аналитические модели, чтобы предопределить размеры критического двухфазного потока через любые отверстия, включая дыры, сопла и трубы. Установ-

лено, что характер и местоположение прорыва влияет на тип утечки теплоносителя и, следовательно, на выбор модели. Для таких теплоносителей, как вода, криогенные жидкости и расплавленные металлы, приводятся критические скорости потока, установленные разными моделями.

Литература о явлениях, связанных с двухфазными потоками, содержит важные данные, необходимые для понимания и оценки этих проблем, однако только сравнительно недавние опыты полностью выяснили понятия, необходимые для анализа практических случаев. Представлены имеющиеся экспериментальные данные относительно критического двухфазного потока в трубах, эти данные сравнены с расчетными на основании теоретических моделей. Обсуждение включает выводы относительно достоинств и применимости этих моделей. Проведены опыты с выбрасыванием теплоносителя, с тем чтобы установить критерии конструкции для предупреждения двухфазных потоков; полученные результаты обсуждены и сравнены с расчетными.

В разделе о современном состоянии проблем ядерной безопасности в США кратко описываются исследования утечки теплоносителя. Предварительные результаты включают исследование состояния жидкости внутри корпуса реактора (измерение давления и парового пространства), распределение давления в отверстии, и в участках труб, колебания показаний теческатора в участках, где происходят выбрасывания, и измерение парового пространства в состоянии критической утечки. Почти во всех опытах в качестве рабочей среды использовалась вода при давлении в системе $140,6 \text{ кг/см}^2$. Дальнейшее проведение испытаний с использованием криогенных жидкостей даст сведения о критических явлениях двухфазного потока в связи с применением ядерной энергии в космическом пространстве. Применение фреона позволяет получить как визуальные, так и количественные результаты.

При любом сочетании условий, описывающих аварийную потерю теплоносителя, неразрешенными остаются вопросы определения скорости утечки, но доклад делает некоторую оценку вероятного предела погрешности. Описана программа, имеющая целью показать совокупность результатов аварии, приводящей к потере теплоносителя.

A/232 Estados Unidos de América

Fenómenos de flujo crítico en las mezclas de dos fases y sus relaciones con la seguridad nuclear

por H. S. Isbin et al.

La expulsión del refrigerante por roturas de tuberías o de depósitos en los sistemas de agua a alta presión

lleva consigo fenómenos de flujo metastable y de dos fases, incluso flujos críticos. Los sistemas de contención y de refrigeración de emergencia deben proyectarse para hacer frente a la evolución dinámica y al máximo alcanzado por la presión, y a la velocidad de pérdida del refrigerante.

Los caudales calculados para la expulsión del refrigerante sin que ocurra vaporización del líquido son mucho mayores que los correspondientes a un flujo homogéneo con dos fases. Por lo tanto se ha establecido una serie de modelos analíticos para predecir flujos críticos con dos fases a través de aberturas tales como orificios, toberas y tuberías. Se reconoce también que la naturaleza y la posición de la rotura tiene influencia sobre el tipo de flujo y, por tanto, sobre la elección del modelo adecuado. Se indican los caudales críticos predichos mediante el uso de varios modelos para refrigerantes tales como agua, líquidos criogénicos y metales líquidos.

La bibliografía que existe sobre los fenómenos de flujo en dos fases constituye un aspecto importante de los conocimientos necesarios para la evaluación de los problemas implicados. Sin embargo, sólo después de experimentos relativamente recientes, se cuenta con los fundamentos necesarios para la evaluación de casos prácticos. Se presentan los resultados experimentales de que se dispone para flujo crítico en dos fases en tuberías y se comparan con las predicciones de los modelos analíticos. La discusión incluye una crítica de los méritos y aplicabilidad de cada uno. Se han hecho ensayos de expulsión de refrigerante (blowdown) para establecer criterios válidos para la predicción de los caudales de dos fases. También se discuten estos resultados y se comparan con las predicciones.

Al presentar el estado actual de los programas de seguridad de reactores nucleares se describen brevemente los estudios de descarga de refrigerante que se están efectuando en los Estados Unidos. Los resultados preliminares comprenden investigaciones del estado del fluido dentro del recipiente (medidas de la presión y de la fracción de huecos), distribución de la presión en la abertura y en secciones de la tubería, variaciones de la relación L/D para las secciones de descarga y medidas de la fracción de huecos en el punto de descarga crítica. Casi todos los ensayos en curso de ejecución emplean agua a presiones de hasta 2 000 libras por pulgada cuadrada (140 atmósferas). La ampliación posterior de los programas experimentales con líquidos criogénicos proporciona información sobre los fenómenos de flujo crítico para aplicaciones espaciales. El uso de freon proporciona resultados visuales y cuantitativos.

Para unas condiciones dadas, que definan un accidente de pérdida de refrigerante, se indican algunos problemas, todavía no resueltos, que existen para predecir las velocidades de descarga, con una cierta idea de los márgenes de error. Se describe un programa elaborado para mostrar los efectos globales de un accidente de pérdida de refrigerante.

Критические тепловые потоки при вынужденном течении воды

Г. В. Алексеев, Б. А. Зенкевич, О. Л. Песков, О. В. Ремизов,
Н. Д. Сергеев, В. И. Субботин

К настоящему времени имеется значительное количество работ, посвященных изучению кризиса кипения при вынужденном течении недогретой воды и пароводяной смеси в круглых трубах и каналах иной геометрии.

Однако анализ всех этих работ не дает возможностей составить достаточно четкое представление об основных закономерностях, которым подчиняется кризис кипения.

Систематизация имеющегося материала затруднена тем, что исследования, проведенные при вынужденном течении воды в трубах, несмотря на большое количество работ, не охватывают режимных параметров в достаточном количестве их сочетаний. Поэтому нельзя проследить изменение степени влияния каждого из параметров на критический тепловой поток $q_{кр}$ по мере изменения других параметров. А работ, проведенных на каналах отличной от труб геометрии, крайне мало.

Настоящий доклад посвящен анализу опытных данных по кризису кипения при вынужденном течении недогретой воды и пароводяной смеси в трубах в сопоставлении с данными, полученными для внешнего обтекания одиночной трубы в симметричном кольцевом зазоре трубы, расположенной по оси квадратного канала и внешнем продольном омывании пучков труб.

Анализ опытных данных базируется на результатах многолетних систематических исследований, проведенных авторами. Установки для проведения опытов и их методика ничем не отличались от общепринятых и здесь не описываются. Описание их приводилось, например, в работах ¹⁻³.

КРИЗИС КИПЕНИЯ В ТРУБАХ

Основные закономерности

Приводимые ниже результаты частично использовались в ранее опубликованных работах ^{1, 4, 6}. Однако для настоящего доклада они существенно дополнены, уточнены и расширены по параметрам. Наиболее важным и интересным является вопрос об основных

закономерностях, которым подчиняется кризис кипения. Вопрос этот в сущности сводится к изучению влияния на $q_{кр}$ режимных параметров: давления, скорости течения и энтальпии жидкости в зоне кризиса.

На рис. 1 приведены графические зависимости критического теплового потока от массовой скорости воды W_2 с параметрами ее на линии насыщения в зоне кризиса. Отклонения от параметров, соответствующих линии насыщения, составляли в отдельных опытах не более $1 \div 1,5^\circ \text{C}$ в сторону недогрева и 0,5 вес.% в сторону паросодержания (по расчетам теплового баланса).

Анализ кривых по давлениям * показывает, что $q_{кр}$ находится в обратной зависимости от давления во всем интервале, при этом с увеличением массовой скорости потока воды зависимость от давления уменьшается. Графики также показывают, что влияние скорости на $q_{кр}$ неоднозначно и зависит от давления и величины самой скорости.

Влияние энтальпии воды на $q_{кр}$ иллюстрируется графиками на рис. 2. На этих графиках видно, что значения $q_{кр}$ находятся в обратной зависимости от энтальпии воды (в зоне кризиса) и при этом влияние энтальпии воды увеличивается с возрастанием скорости воды. При одной и той же относительной энтальпии характер кривых меняется с изменением давления, а при постоянном давлении характер кривых зависит от энтальпии воды. Неоднозначность влияния скорости течения воды на $q_{кр}$ при давлениях 196 и 392 н/см² имеет место и в области недогретой воды.

Таким образом, обнаруженное впервые авторами в 1956 г. неоднозначное влияние скорости воды на $q_{кр}$ в области пароводяной смеси ⁵ имеет место в более широком интервале параметров.

Резюмируя анализ графических зависимостей, можно сделать следующее заключение: степень влияния каждого из режимных параметров в отдельности зависит от сочетания

* Всюду указано абсолютное давление.

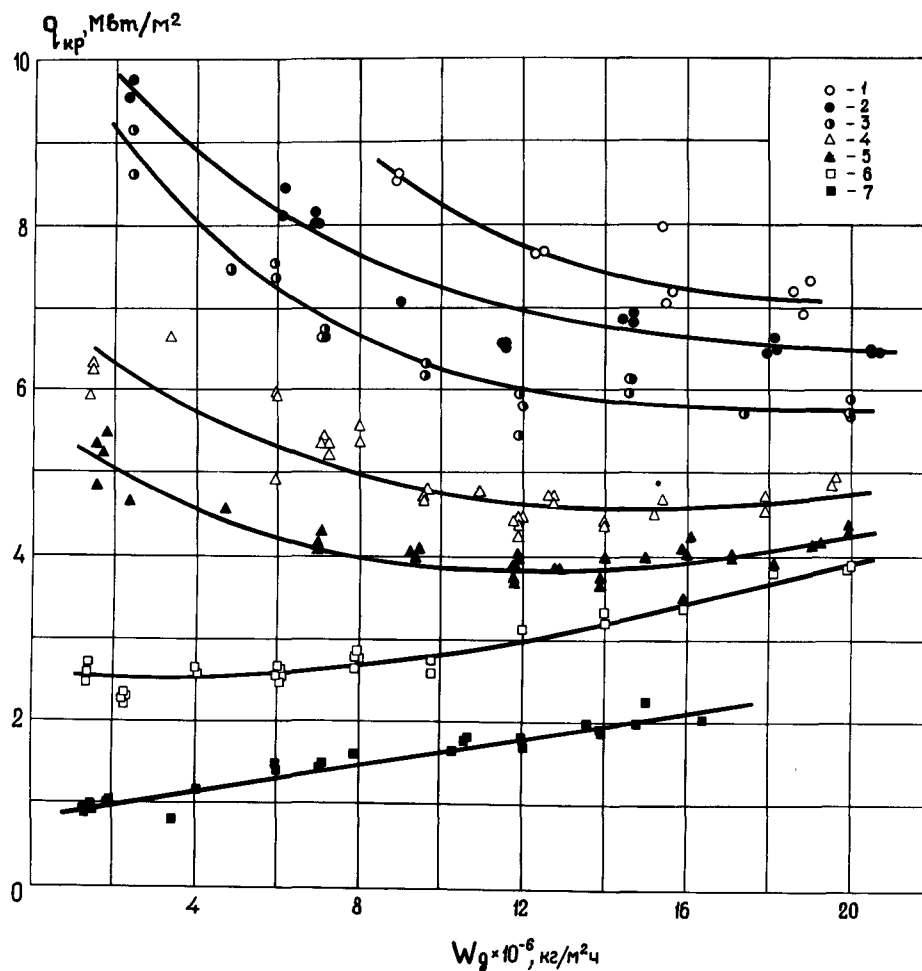


Рис. 1. $q_{кр}$ на линии насыщения для труб:

1, 2, 3, 4, 5, 6, 7—соответствуют давлениям 196; 294; 392; 784; 981; 1373; 1962 н/см^2

с другими параметрами. Так, например, влияние скорости течения воды на $q_{кр}$ зависит от значений фиксированных при этом давления и энталпии.

Влияние побочных факторов

Представляет интерес влияние на кризис и побочных факторов, таких как, например, обогреваемой длины и диаметра трубы, а также неравномерности концентрации теплового потока по внутренней поверхности трубы.

Опытные данные, которыми иллюстрировались основные закономерности кризиса кипения в настоящем докладе, получены на трубах с внутренним диаметром 8—9 мм и обогреваемой длиной от 100 до 2100 мм.

Анализ опытных данных в сопоставлении с литературными данными показывает, что влияние обогреваемой длины трубы на $q_{кр}$ в указанных пределах не имеет места в области недогретой воды, а при длине $l \geq 200$ мм и в области пароводяной смеси. Следует заметить, что до сих пор имелись в виду опытные

данные, полученные на экспериментальной установке, в циркуляционном контуре которой отсутствовали пульсации потока воды, возникающие в случае наличия генератора пульсаций (конденсатор и др.). Однако в работе ⁷ отмечается сильное влияние обогреваемой длины на $q_{кр}$ при наличии пульсаций в контуре. При этих условиях чем больше обогреваемая длина трубы, тем меньше $q_{кр}$. Влияние это в некоторых случаях оценивается сотнями процентов.

Авторами ¹ было обнаружено, что для интервала давления 1373 ÷ 1962 н/см^2 в области недогретой воды внутренний диаметр трубы ($d_{вн} = 4 \div 12$ мм) на $q_{кр}$ не влияет. Последнее было подтверждено опытами А. П. Орнатского ⁸ на недогретой воде при $P = 245$ н/см^2 , которые показали значительное увеличение $q_{кр}$ при уменьшении $d_{вн}$ с 4 до 1 мм, но также и отсутствие влияния в интервале $d_{вн} = 4 \div 6$ мм.

Однако в опытах В. Е. Дорошука и Ф. П. Ландман ⁹ при $P = 490 \div 1665$ н/см^2 обнаружено

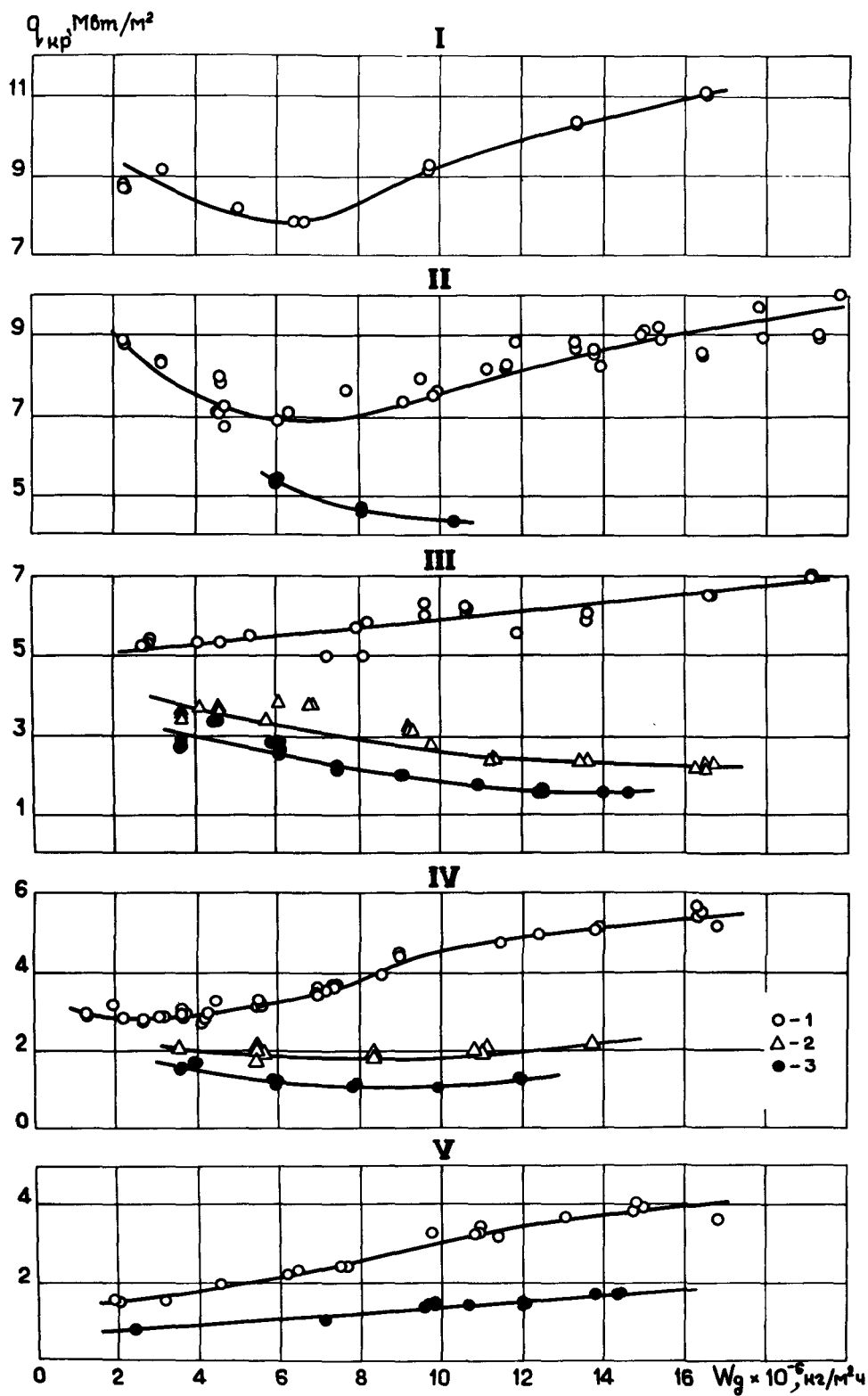


Рис. 2. $q_{кр}$ при различных энтальпиях для труб:

1, 2, 3—соответствуют относительной энтальпии -0,1; 0,1; 0,2. I, II, III, IV, V—соответствуют давлениям 196; 392; 981; 1373; 1765,8 н/см^2

влияние $d_{\text{вн}}$ на $q_{\text{кр}}$ во всем интервале $d_{\text{вн}} = 3 \div 8$ мм, как в области недогретой воды, так и еще более в области пароводяной смеси.

Сильное влияние $d_{\text{вн}}$ на $q_{\text{кр}}$ для пароводяной смеси обнаружено и Р. А. Рыбиным¹⁰ при $P=981$ н/см², $W_g = (3 \div 20) \cdot 10^6$ кг/м²·ч, весовых паросодержаниях x до 0,35 в интервале $d_{\text{вн}} = 2 \div 10$ мм.

Опыты авторов доклада подтвердили наличие влияния $d_{\text{вн}}$ на $q_{\text{кр}}$ в области пароводяной смеси при $P=981$ и 1373 н/см², $W_g = 6 \cdot 10^6$ и $10 \cdot 10^6$ кг/м²·ч, $x=0 \div 0,4$ в интервале $d_{\text{вн}} = 4,8 \div 12$ мм.

Однако вопрос о влиянии $d_{\text{вн}}$ на $q_{\text{кр}}$ требует дополнительного подробного изучения.

Весьма важным и интересным является изучение влияния на кризис кипения неравномерности концентрации теплового потока по поверхности тепловыделения. Неравномерность концентрации теплового потока, например, в твэлах активной зоны ядерного реактора может иметь место по крайней мере в двух случаях:

- а) неравномерности концентрации делящегося материала по объему твэла;
- б) в твэлах сложной конфигурации при наличии ребер, которые так же, как и тело твэла,

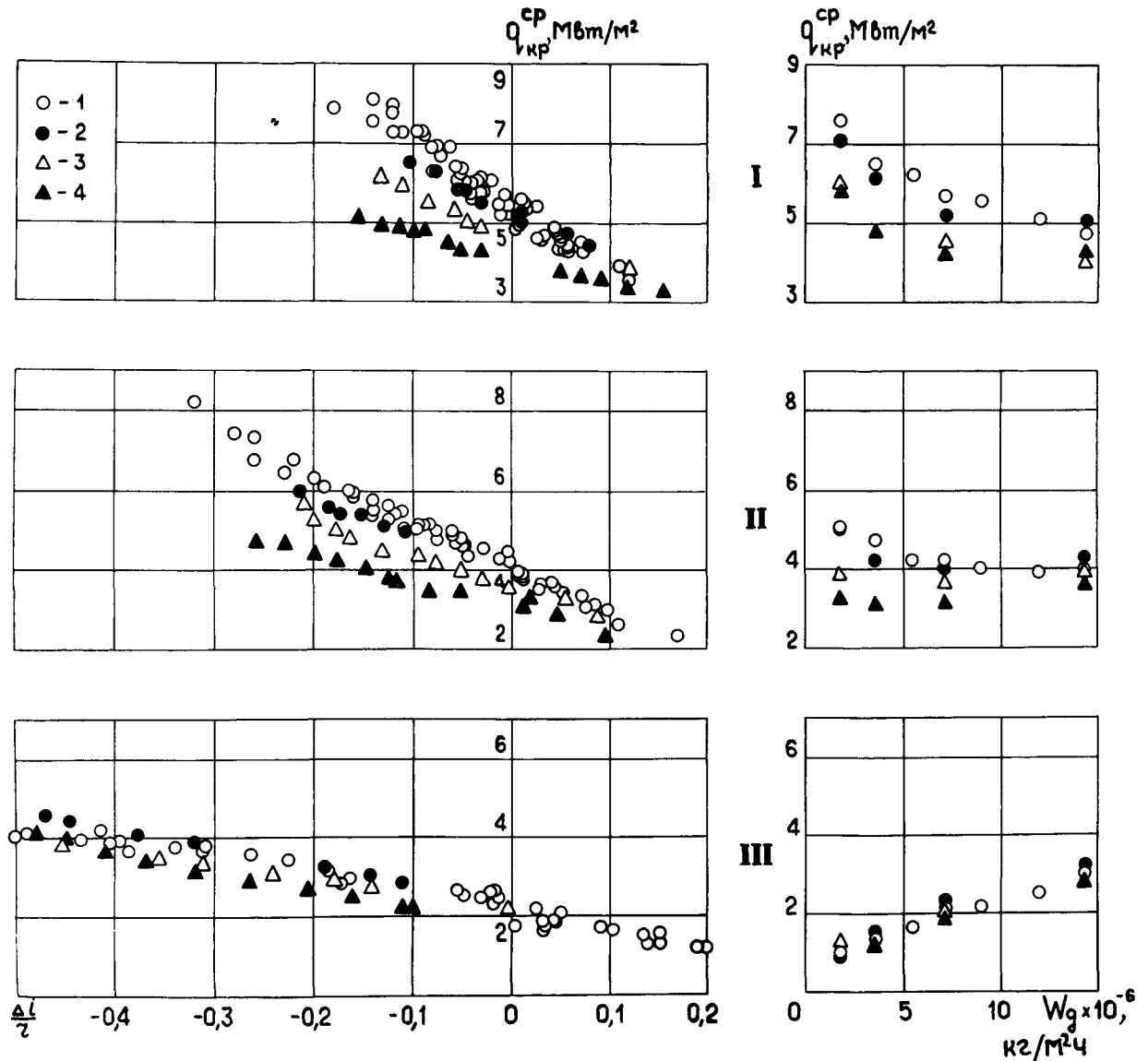


Рис. 3. Влияние неравномерности концентрации теплового потока на $q_{\text{кр}}$ в круглых трубах:

1, 2, 3, 4 — соответствуют значениям $q_{\text{кр}}^{\text{макс}}/q_{\text{кр}}^{\text{ср}}$ 1; 1,12; 1,28; 1,50. I, II, III — соответствуют давлениям 588; 981; 1765,8 н/см². Все зависимости $q_{\text{кр}} = f(W)$ даны для $\frac{\Delta i}{r} = 0$, а зависимости для массовой скорости $7,2 \cdot 10^6$ кг/м²·ч

заполнены активным материалом. При этом ребра в местах сопряжения с телом твэла, как правило, имеют закругления, в которых и возникают концентрации теплового потока.

Если оценивать степень неравномерности концентрации теплового потока на теплоотдающей поверхности отношением $q_{кр}^{макс}/q_{кр}^{ср}$, где $q_{кр}^{ср}$ — средний критический тепловой поток по всей поверхности тепловыделения, а $q_{кр}^{макс}$ — максимальный локальный критический тепловой поток, то в первом случае оно практически может быть невелико и вряд ли будет превышать с учетом растечек тепла ^{1, 2}; во втором случае это отношение зависит от радиуса закругления между ребром и телом твэла и может достигать 2 ÷ 3. В последнем случае на значение $q_{кр}$ может оказать влияние гидродинамика потока воды при наличии ребер на твэле.

Для изучения влияния неравномерности концентрации теплового потока на $q_{кр}$ в чистом виде были проведены опыты на круглых трубах с $d_{вн} = 10$ мм длиной 400 мм и с эксцентриситетом (три значения) между наружной и внутренней поверхностями. Для трех значений эксцентриситета отношение $q_{кр}^{макс}/q_{кр}^{ср}$, найденное по эяграмм теплового потока *, составляло 1,12; 1,28 и 1,50.

На рис. 3 представлены опытные данные, показывающие влияние неравномерности концентрации теплового потока на $q_{кр}$ в сравнении с опытами на равномерно обогреваемой трубе. Из графиков видно, что чем больше $q_{кр}^{макс}/q_{кр}^{ср}$, тем ниже средний критический тепловой поток. При этом локальный максимальный критический тепловой поток, как можно заключить по опытным данным на рис. 3, в области больших недогрева примерно равен $q_{кр}$ для равномерно обогреваемой трубы, а по мере уменьшения недогрева и перехода к пароводяной смеси $q_{кр}^{макс}$ становится больше $q_{кр}$ для равномерно обогреваемой трубы. Кроме того, влияние концентрации зависит от режимных параметров потока воды, а именно: в области недогретой воды влияние больше, в области пароводяной смеси — меньше. С повышением давления влияние неравномерности концентрации теплового потока падает, так же как, видимо, и с увеличением скорости потока воды.

Следует отметить, что в работе ¹¹ опыты при давлениях 255; 981 и 1765,8 н/см² в области недогретой воды и пароводяной смеси показали, что при $q_{кр}^{макс}/q_{кр}^{ср} = 1,8$ $q_{кр}$ примерно равно для равномерно обогреваемой трубы.

Если неравномерность концентрации теплового потока по поверхности тепловыделения обусловлена неравномерностью концентрации активного материала по объему твэла (горя-

чие пятна»), то при практически возможных в этом случае значениях $q_{кр}^{макс}/q_{кр}^{ср}$ влиянием этого фактора можно пренебречь, имея в виду, что максимальный рабочий тепловой поток в реакторе выбирается с запасом относительно $q_{кр}$, как правило, не менее 2. Только при значениях $q_{кр}^{макс}/q_{кр}^{ср} > 1,2$ (закругления у основания ребер) с этим фактором необходимо считаться.

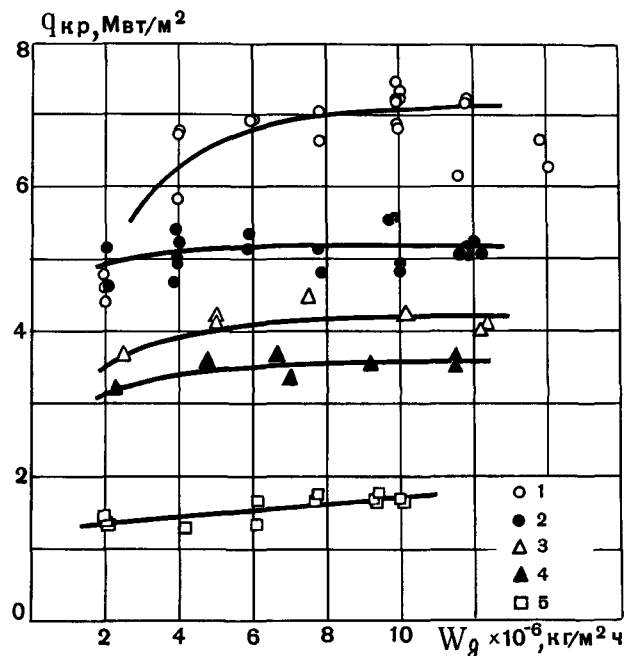


Рис. 4. $q_{кр}$ на линии насыщения для кольцевого зазора:

1, 2, 3, 4, 5 — соответствуют давлениям 392; 784; 981; 1274; 1962 н/см²

КРИЗИС КИПЕНИЯ ПРИ ВНЕШНЕМ ПРОДОЛЬНОМ ОБТЕКАНИИ ТРУБ

Авторы проводили исследования по кризису кипения при внешнем обтекании водой односторонней трубы в симметричном кольцевом зазоре. Опыты были проведены при ширине кольцевого зазора 1,5 мм на трубе-нагревателе с $d = 12$ мм; обогреваемая длина 200 мм. На рис. 4 изображены скоростные зависимости $q_{кр} = f(W_g)$ для интервала давлений 392 ÷ 1962 н/см² с параметрами воды на линии насыщения в зоне кризиса.

Как видно, степень влияния скорости воды на критические тепловые потоки изменяется от положительного значения до нулевого (приблизительно). Скоростные зависимости для недогретой воды и пароводяной смеси при давлениях 392; 784 и 981 н/см² следует тому же закону (рис. 5).

На рис. 6 представлены опытные данные в виде зависимостей $q_{кр} = f(W_g)$ для случая внешнего обтекания трубы, расположенной по оси

* Эяграммы теплового потока построены по результатам расчета численным методом с учетом растечек тепла.

квадратного канала, а на рис. 7 при внешнем продольном омывании пучков труб.

Из сравнения зависимостей $q_{кр} = f(W_g)$ следует, что для тех интервалов параметров, где для труб с внутренним охлаждением влияние скорости потока на $q_{кр}$ неоднозначно, для труб с внешним охлаждением отрицательное влияние скорости не имеет места.

С точки зрения опубликованных к настоящему времени теорий кризиса кипения при вынужденном течении жидкости ¹²⁻¹⁴ такая принципиальная разница в закономерностях влияния скорости течения на $q_{кр}$ для случаев внутреннего и внешнего охлаждения труб совершенно не объяснима. Видимо, в цитированных теоретических работах наиболее существенные черты явления кризиса не нашли отражения.

Есть еще одно отличие закономерностей кризиса кипения при внутреннем и внешнем охлаждении труб. Как отмечалось выше, обогреваемая длина при внутреннем охлаждении не влияет на $q_{кр}$, по крайней мере при $l \geq 200$ мм и $d_{вн} = 8-9$ мм. Однако опыты при внешнем охлаждении одиночной трубы в кольцевом зазоре показали, что влияние длины канала проявляется вполне отчетливо (рис. 8).

Авторами проведено исследование критических тепловых потоков при наличии тепловыделения на обеих поверхностях, образующих кольцевой канал. Критический режим создавался, как правило, на одной теплоотдающей поверхности, в то время как с другой поверхности нагрева подводился дополнительный тепловой поток определенной величины. В части опытов кризис кипения наблюдался на обеих поверхностях одновременно. Установлено, что при давлениях $981 \div 1472$ н/см² и закрепленных параметрах на выходе из канала критические тепловые потоки в кольцевом канале с двухсторонним подводом тепла выше, чем в случае одностороннего обогрева, причем критические тепловые потоки на одной теплоотдающей поверхности возрастают с увеличением дополнительного теплового потока от другой поверхности. Это можно объяснить тем, что при одинаковых условиях на выходе из канала энтальпия части потока теплоносителя, влияющая на момент возникновения кризиса на одной теплоотдающей поверхности, будет меньше, чем средняя энтальпия на выходе из канала за счет дополнительного подвода тепла от другой поверхности.

Значение энтальпии в зоне кризиса можно определить из уравнения теплового баланса для кольцевого канала, вычитая из общего приращения энтальпии на выходе ее приращение за счет дополнительного подвода тепла. В этом случае сравнение опытных данных для кольцевых каналов с односторонним и двухсторонним подводом тепла приводит к совпадающим результатам.

РАСЧЕТНЫЕ РЕКОМЕНДАЦИИ

Недогретая вода в трубах

Во многих опубликованных работах предлагаются рекомендации для вычисления $q_{кр}$ при недогретой воде. Эти рекомендации получены на основании обработки разрозненных опытных данных, заимствованных из литературных источников. Поэтому не было проведено детального анализа частных зависимостей, а именно такой анализ является непременным условием надежности расчетных рекомендаций. Вследствие этого при оценке влияния скорости течения воды на $q_{кр}$ не могла быть учтена неоднозначность влияния скорости. Влияние скорости оценено, хотя и переменное, но положительной степенью.

Сопоставление этих расчетных рекомендаций с опытными зависимостями в широком диапазоне параметров показало их полную непригодность при тех сочетаниях режимных параметров, когда влияние скорости течения воды на $q_{кр}$ отрицательно. В работе ⁵ неоднозначное влияние скорости воды $q_{кр}$ было учтено посредством переменной степени, которая является функцией давления и энтальпии воды в зоне кризиса. Авторы рекомендуют для вычисления $q_{кр}$ одну из модификаций этого уравнения:

$$K = K_1^{0,65} (110 - 240K_2) [1 + 0,75 \times \times 10^5 / (7,4 \cdot 10^3 W)^{1,1+2K_1-0,3K_2}] \cdot 10^{-5},$$

где

$$K = \frac{q_{кр}}{r} \sqrt{\frac{v}{\sigma W_g}}; \quad K_1 = \frac{Y''}{Y'}; \quad K_2 = \frac{\Delta i}{r}.$$

Пределы применений уравнения: $P = 294 \div 2060$ н/см²; $W_g = 1 \div 15$ м/сек; $\Delta t_n = 2 \div 200^\circ$; $d_{вн} = 8 \div 10$ мм; $l \geq 100$ мм.

Пароводяная смесь в трубах

Для вычисления $q_{кр}$ при вынужденном течении пароводяной смеси в трубах с учетом влияния внутреннего диаметра трубы предлагается следующая эмпирическая формула:

$$q_{кр} = 46,5 W_g^n (1-x)^m \left(\frac{Y'}{Y''}\right)^{2,2} \times \times \left(1 + \frac{8 \cdot 10^9}{W_g^k}\right) \cdot \frac{2,71}{d_{вн}^{0,48}} \text{ вт/м}^2,$$

где

$$n = 0,56 - 0,0189 \frac{Y'}{Y''}; \quad m = 0,7 \frac{Y'}{Y''} - 0,40;$$

$$K = 1,13 + 3,6 \frac{Y''}{Y'} - 0,45x.$$

Пределы применения формулы: $P = 981 \div 1962$ н/см²; $W_g = (4 \div 18) \cdot 10^8$ кг/м²·ч; $x = 0 \div 0,4$; $d_{вн} = 4 \div 12$ мм; $l \geq 200$ мм.

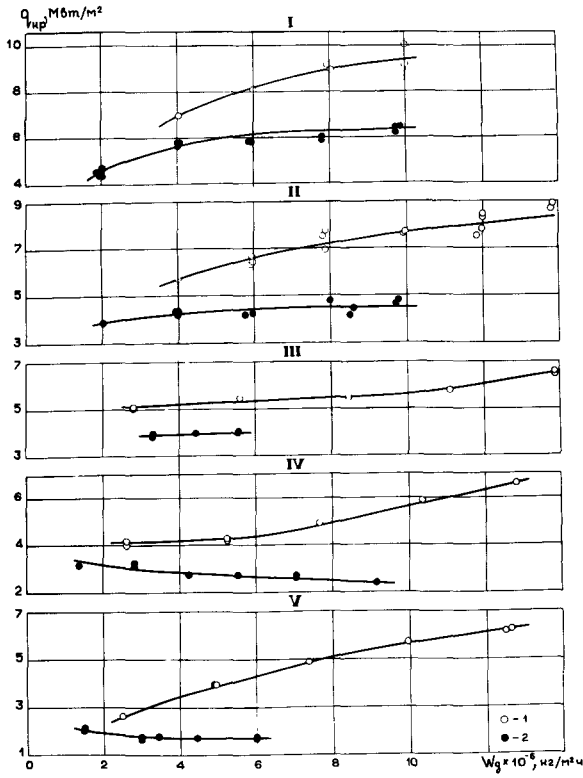


Рис. 5. $q_{кр}$ при различных энтальпиях для кольцевого зазора:

1 — недогрев 40° ; 2 — $\frac{\Delta i}{r} = 0,1$. I, II, III, IV, V — соответствуют давлениям 392; 784; 981; 1470; 1765,8 н/см²

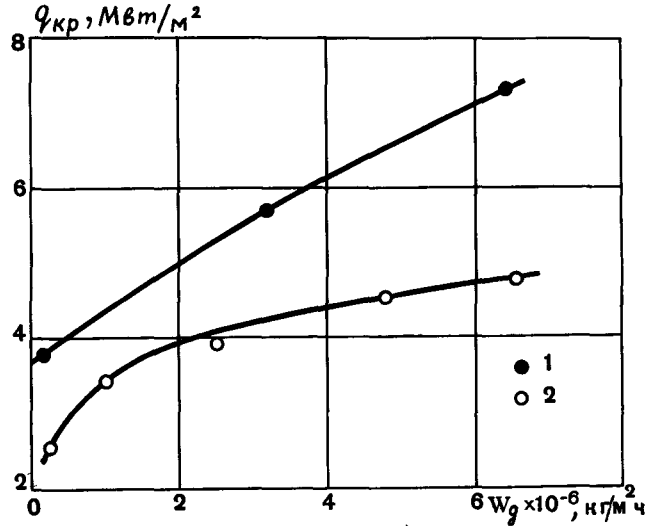


Рис. 6. $q_{кр}$ при внешнем обтекании трубы, расположенной по оси квадратного канала размером $1,6 \times 16,6$ мм, $d_{вн} = 12$ мм, $l = 200$ мм:

1 — $P = 294$ н/см², $\Delta t_H = 10^\circ$; 2 — $P = 981$ н/см², $\Delta t_H = 5^\circ$

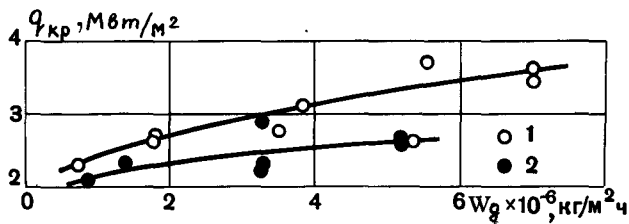


Рис. 7. $q_{кр}$ при продольном омывании пучков из 7 труб $5 \times 0,25$ мм, треугольная решетка с шагом 6,5 мм:

1 — $P = 981$ н/см², $\frac{\Delta i}{r} = 0,2$

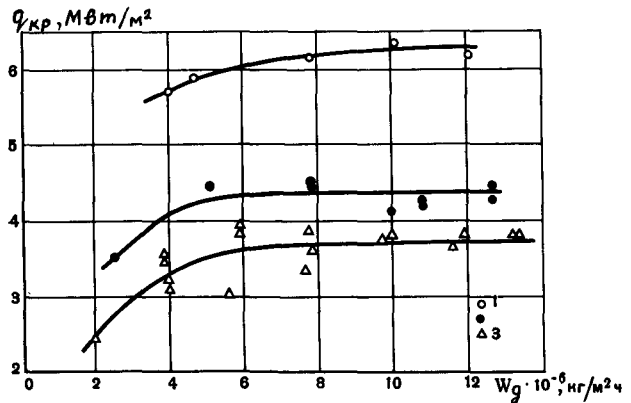


Рис. 8. $q_{кр}$ на линии насыщения при внешнем охлаждении одиночной трубы в кольцевом зазоре для различной обогреваемой длины, $P = 981$ н/см²:

1, 2, 3 — соответствуют обогреваемой длине 100; 200 и 400 мм

Для невысоких давлений в последнее время авторами получена следующая эмпирическая формула:

$$q_{кр} = [1,46 \cdot 10^{-4} r^{1,72} (1-x)^{-2} - 0,116 W_g] \frac{2,71}{d_{вн}^{0,48}} \text{ вт/м}^2,$$

где $m = 3,48 - 0,54 (r/4,18 \cdot 10^6)$.

Пределы применения формулы: $P = 392 \div 981 \text{ н/см}^2$; $W_g = (2 \div 18) \cdot 10^6 \text{ кг/м}^2 \cdot \text{ч}$; $x = 0 \div 0,4$; $d_{вн} = 4 \div 12 \text{ мм}$; $l \geq 200 \text{ мм}$.

Внешнее обтекание одиночной трубы в симметричном кольцевом зазоре

К настоящему времени имеется еще недостаточно опытных данных по $q_{кр}$ для кольцевых зазоров, особенно по изучению влияния побочных факторов (обогреваемая длина, диаметр трубы, ширина кольцевого зазора), поэтому преждевременно было бы предлагать расчетные рекомендации для широкого интервала параметров с учетом влияния побочных факторов. Вследствие этого ниже приводится только эмпирическая формула для вычисления $q_{кр}$ для воды с параметрами на линии насыщения

$$q_{кр} = 5,14 \cdot 10^{-3} \gamma' \frac{W}{0,25 + W} \text{ вт/м}^2.$$

Пределы применения формулы: $P = 392 \div 1962 \text{ н/см}^2$; $W = 2 \div 7 \text{ м/сек}$; $l = 200 \text{ мм}$.

Ширина кольцевого зазора 1,5 мм при диаметре трубы-нагревателя 12 мм.

ОБОЗНАЧЕНИЯ

$q_{кр}$, вт/м^2 — критический тепловой поток
 P , н/см^2 — абсолютное давление
 W_g , $\text{кг/м}^2 \cdot \text{ч}$ — массовая скорость потока воды
 W , м/сек — линейная скорость воды в зоне кризиса
 γ' , кг/м^3 — плотность воды на линии насыщения
 γ'' , кг/м^3 — плотность пара на линии насыщения
 r , дж/кг — скрытая теплота испарения воды
 σ , н/м — коэффициент поверхностного натяжения на границе пар—вода

ν , $\text{м}^2/\text{ч}$ — коэффициент кинематической вязкости воды на линии насыщения

$\Delta t_{н}$, град — недогрев воды до температуры насыщения в зоне кризиса

$\frac{\Delta i}{r}$ — относительная энтальпия (отрицательна

для недогретой воды и положительна для паро-водяной смеси; в последнем случае численно равна весовому паросодержанию x в долях единицы)

Δi , дж/кг — теплота недогрева для недогретой воды (отрицательна) или теплота перегрева для паро-водяной смеси (положительна)

$d_{вн}$, мм — внутренний диаметр трубы

l , мм — обогреваемая длина экспериментального участка

ЛИТЕРАТУРА

1. Б. А. Зенкевич и В. И. Субботин. Атомная энергия, 3, 149 (1957).
2. Г. В. Алексеев, Б. А. Зенкевич и В. И. Субботин. Теплоэнергетика, № 10, 72 (1963).
3. Б. А. Зенкевич, В. И. Субботин и М. Ф. Троянов. Атомная энергия, 4, 370 (1958).
4. Б. А. Зенкевич и О. В. Ремизов. ИФЖ, 6, 112 (1963).
5. Б. А. Зенкевич. Атомная энергия, 6, 169 (1959).
6. О. Л. Песков, В. И. Субботин, Б. А. Зенкевич и Н. Д. Сергеев. Вопросы теплоотдачи и гидравлики двухфазных сред. Ред. С. С. Кутателадзе, ГЭИ, 44 (1961).
7. М. А. Стырикович, З. Л. Миропольский, М. Е. Шицман, И. Л. Мостинский, А. А. Ставровский и Л. Е. Факторович. Теплоэнергетика, № 5, 81 (1960).
8. А. П. Орнатский. Теплоэнергетика, № 6, 67 (1960).
9. В. Е. Дорошук, Ф. П. Ланцман. Теплоэнергетика, № 8, 73 (1963).
10. Р. А. Рыбин. ИФЖ, 6, 15 (1963).
11. З. Л. Миропольский и И. Л. Мостинский. Теплоэнергетика, № 11, 64 (1958).
12. С. С. Кутателадзе. Основы теории теплообмена. М., Машгиз, 1962.
13. H. S. Ishin et al. Trans. of the ASME, Series «C» J. of Heat Transfer, 83, No. 2, 149 (1961).
14. Jan Po Shang. Trans. of the ASME, Series «C» J. of Heat Transfer, 85, No. 2, 89 (1963).

ABSTRACT—RÉSUMÉ—АННОТАЦИЯ—RESUMEN

A/327 USSR

Burn-out heat fluxes under forced water flow

By G. V. Alekseev *et al.*

The paper reports the results of systematic research on burn-out for the case of forced water flow in channels of different geometries. The study has dealt with the main factors of burn-out, i.e., on the effect which fixed parameters have on q_{BO} : pressure, flow rate and enthalpy of the water.

On the basis of experiments carried out in tubes with forced water flow having saturation parameters, the

authors show that the effect of pressure on q_{BO} depends on the water flow rate. At high flow rates the effect of pressure is less than at flow rates. The effect of flow rate on q_{BO} is not simple since it is also dependent on the pressure and the magnitude of the flow rate.

The results of the experiments mentioned are given in the form of a family of curves for the expression $q_{BO} = f(W_g)$ for pressures from 20–200 atm(a). W_g is the mass flow. The analysis of graphs of $q_{BO} = f(W_g)$ obtained for different flow enthalpies and different pressures shows that q_{BO} is inversely proportional to enthalpy and that the effect of enthalpy increases with the flow rate. The shape of the $q_{BO} = f(W_g)$ curves

for a given pressure depends on the flow enthalpy and its change with pressure.

The authors show that the composite effect of flow rate on q_{BO} is also evident in the region of unsaturated water and not only in the region of steam-water mixture, as was previously believed. In short, the effect of each fixed parameter on q_{BO} depends on the values fixed for the other parameters.

The authors quote and analyse experimental burn-out data obtained with longitudinal flow outside individual tubes (annular spacing) and outside tube bundles for a pressure range of 40–200 atm(a) in the first case and from 30–100 atm(a) in the second case.

Apart from a quantitative difference in respect of the internal cooling of the tubes, burn-out in the case of external cooling of the tubes has its own qualitatively distinct properties. The difference is such that if, as mentioned above, the effect of the water flow rate in the tubes on q_{BO} is complex, it is always positive although variable in the case of externally cooled tubes.

From the point of view of existing burn-out theories in the case of the forced flow of a liquid, this difference, dependent on whether the cooling of the tubes is internal or external, is not explained.

A/327 URSS

Charges thermiques critiques dans le cas de l'écoulement forcé d'eau

par G. V. Alekseev *et al.*

Le mémoire rapporte les résultats de recherches systématiques sur la caléfaction dans le cas de l'écoulement forcé d'eau dans des canaux de différentes géométries. L'étude a porté sur les régularités principales caractéristiques de la caléfaction, c'est-à-dire sur l'influence qu'ont sur q_c les paramètres du régime: pression, vitesse d'écoulement et enthalpie de l'eau.

Se fondant sur des expériences effectuées pour l'écoulement forcé dans des conduites d'eau présentant les paramètres à la saturation, les auteurs montrent que l'influence de la pression sur q_c dépend de la vitesse d'écoulement de l'eau: aux vitesses élevées, l'influence de la pression est plus faible qu'aux vitesses réduites. L'influence de la vitesse sur q_c n'est pas simple car elle dépend de la pression et de la valeur de la vitesse elle-même.

Les résultats des expériences mentionnées sont donnés sous la forme d'un diagramme d'ensemble des relations $q_c = f(W_g)$ pour des pressions de 20 à 200 atm (abs) (W_g étant le débit-masse). L'analyse des courbes $q_c = f(W_g)$ établies pour différentes enthalpies du courant et différentes pressions montre que q_c est inversement proportionnel à l'enthalpie et que l'influence de l'enthalpie croît avec la vitesse de l'écoulement. L'allure des courbes $q_c = f(W_g)$ pour une pression donnée dépend de l'enthalpie du courant et change avec la pression.

Les auteurs montrent que l'influence composite de la vitesse d'écoulement sur q_c se manifeste également dans la région de l'eau sous-saturée et non pas

seulement dans celle du mélange vapeur-eau, ainsi qu'on le croyait auparavant. En résumé, l'influence de chacun des paramètres du régime sur q_c dépend des valeurs fixées des autres paramètres.

Les auteurs citent et analysent des données expérimentales sur la caléfaction, obtenues pour l'écoulement extérieur longitudinal sur des tubes isolés (espace annulaire) et sur des faisceaux de tubes, l'intervalle de pression étant de 40 à 200 atm (abs) dans le premier cas et de 30 à 100 atm (abs) dans le deuxième.

Outre une différence quantitative par rapport au refroidissement intérieur des tubes, la caléfaction dans le cas du refroidissement extérieur des tubes a ses propres régularités, qualitativement distinctes. La différence est que si, comme on l'a indiqué plus haut, l'influence de la vitesse d'écoulement de l'eau dans les tubes sur q_c est multiple, elle est toujours positive bien que variable dans le cas de tubes refroidis extérieurement.

Du point de vue des théories existantes de la caléfaction dans le cas de l'écoulement forcé d'un liquide, cette différence, suivant que le refroidissement des tubes est intérieur ou extérieur, n'est pas expliquée.

A/327 URSS

Cargas térmicas críticas en el caso de la circulación forzada de agua

por G. V. Alekseev *et al.*

La memoria da cuenta de los resultados de investigaciones sistemáticas efectuadas sobre el calentamiento en el caso de la circulación forzada de agua en canales de diferentes geometrias. El estudio se refiere a las regularidades principales características del calentamiento, es decir a la influencia que ejercen sobre q_c los parámetros del régimen: la presión, la velocidad de la corriente y la entalpía del agua.

A partir de experiencias realizadas respecto de la circulación forzada en tuberías de agua cuyos parámetros corresponden a la saturación, los autores demuestran que la influencia de la presión sobre q_c depende de la velocidad de la corriente del agua: para grandes velocidades, la influencia de la presión es menor que para pequeñas velocidades. La influencia de la velocidad sobre q_c no es simple porque depende de la presión y del valor de la propia velocidad.

Los resultados de las experiencias mencionadas se dan en forma de diagrama de conjunto de las relaciones $q_c = f(W_g)$ para presiones de 20 a 200 atm (a) (siendo W_g el caudal-masa). El análisis de las curvas $q_c = f(W_g)$ trazadas para diferentes entalpías de la corriente y diferentes presiones muestra que q_c es inversamente proporcional a la entalpía y que la influencia de ésta aumenta al crecer la velocidad de la corriente. La forma de las curvas $q_c = f(W_g)$ para una presión dada depende de la entalpía de la corriente y cambia con la presión.

Los autores demuestran que la influencia compuesta de la velocidad de la corriente sobre q_c también se

manifiesta en la región del agua subsaturada y no sólo en la de la mezcla vapor-agua, como se creía antes. En resumen, la influencia de cada uno de los parámetros del régimen sobre q_c depende de los valores de los demás parámetros.

Los autores citan y analizan datos experimentales sobre el calentamiento obtenidos para la circulación exterior longitudinal en tubos aislados (espacio anular) y en haces de tubos, siendo al intervalo de presiones de 40 a 200 atm (a) en el primer caso y de 30 a 100 atm (a) en el segundo.

Además de una diferencia cuantitativa con relación

a la refrigeración interior de los tubos, el calentamiento en el caso de la refrigeración exterior de los tubos presenta sus propias regularidades, cualitativamente distintas. La diferencia se debe a que, como se ha indicado antes, la influencia de la velocidad de la corriente del agua en los tubos sobre q_c es múltiple y es siempre positiva, a pesar de ser variable en el caso de tubos refrigerados exteriormente.

Desde el punto de vista de las teorías actuales del calentamiento en el caso de la circulación forzada de un líquido no se explica esa diferencia, según que la refrigeración de los tubos sea interior o exterior.

Теоретическая модель турбулентного обмена в трехмерном потоке жидкости

Н. И. Булеев

Содержанием настоящей работы является развитие методов расчета полей скорости и температуры в турбулентных потоках жидкости в каналах произвольной формы.

1. ОСРЕДНЕННЫЕ УРАВНЕНИЯ ТУРБУЛЕНТНОГО ДВИЖЕНИЯ

Запишем систему осредненных уравнений турбулентного движения в прямоугольной системе координат для несжимаемой жидкости.

Уравнение движения

$$\frac{\partial \bar{q} \bar{v}_k}{\partial t} + \sum_{i=1}^3 \frac{\partial}{\partial x_i} (\bar{q} \bar{v}_i \bar{v}_k) = -\frac{\partial \bar{P}}{\partial x_k} + \bar{q} \nu \Delta \bar{v}_k - \sum_{i=1}^3 \frac{\partial}{\partial x_i} (\overline{q v_i v_k}), \quad (1.1)$$

уравнение неразрывности

$$\sum_{k=1}^3 \frac{\partial}{\partial x_k} (\bar{q} \bar{v}_k) = 0, \quad (1.2)$$

уравнение притока тепла

$$\frac{\partial \bar{q} \bar{T}}{\partial t} + \sum_{i=1}^3 \frac{\partial}{\partial x_i} (\bar{q} \bar{v}_i \bar{T}) = \bar{q} k \Delta \bar{T} - \sum_{i=1}^3 \frac{\partial}{\partial x_i} (\overline{q v_i T'}). \quad (1.3)$$

Здесь v_1, v_2, v_3 — составляющие скорости по осям координат;

P — давление;

T — температура;

ρ — плотность жидкости;

ν — молекулярный кинематический коэффициент вязкости;

k — коэффициент температуропроводности.

Символ Δf означает трехмерный оператор Лапласа от функции f . Ради простоты записи уравнений (1.1)–(1.3) коэффициент вязкости $\mu = \rho \nu$ и коэффициент теплопроводности $\lambda = \rho k$ приняты постоянными.

После появления работы Рейнольдса¹, в которой были получены уравнения (1.1), (1.2),

дальнейшее развитие теории турбулентного обмена пошло по пути создания полуэмпирических теорий, в основу которых было положено понятие длины пути смешения молей, аналогичное понятию длины свободного пробега молекул в кинетической теории газов (см., например, обзор в монографии²).

Для исследования одномерных течений жидкости $w(x)$ широкое практическое применение приобрела полуэмпирическая аппроксимация турбулентного напряжения $\rho u'w'$ формулой Прандтля — Кармана³

$$-\rho u'w' = \rho \varepsilon \frac{\partial w}{\partial x}, \quad (1.4)$$

где $\varepsilon = l^2 \left| \frac{\partial w}{\partial x} \right|$,

причем l — есть некоторый масштаб турбулентности (длина пробега моля).

При $l = \kappa x$ и соответствующем выборе начала отсчета x формула Прандтля для коэффициента ε в большинстве случаев обеспечивала достаточно удовлетворительное решение гидродинамических задач.

Статистическая теория турбулентности развивалась позже (в 20–30-х годах). Однако при наличии серьезных теоретических достижений статистическая теория все же не смогла до настоящего времени выдать практически приемлемый алгоритм замыкания уравнений Рейнольдса.

В настоящей работе делается обобщение полуэмпирического подхода Прандтля — Кармана на случай произвольного трехмерного потока жидкости.

2. ТРЕХМЕРНАЯ МОДЕЛЬ ТУРБУЛЕНТНОГО ОБМЕНА В ПРОИЗВОЛЬНОМ ПОТОКЕ ЖИДКОСТИ

Турбулентное движение будем рассматривать как результат наложения неупорядоченных неустановившихся завихрений на некоторое основное статистически среднее движение. Каждое случайно возникшее и быстро исчезающее завихрение, имеющее, допустим, поперечный

размер $2l$, переносит порции жидкости с поперечным размером l на расстояния также порядка l .

Для удобства математического описания переносов количества движения и тепла, вызванных неупорядоченными движениями порций жидкости внутри нестационарных завихрений, будем представлять себе, что из окрестности каждой точки M потока, рассматриваемой в системе координат, движущейся со скоростью осредненного потока в точке M , вылетают во всех направлениях с одинаковой вероятностью порции жидкости («моли»). Введем понятие линейного масштаба турбулентности $L(M)$, отражающего характерный линейный размер нестационарных завихрений в окрестности переменной точки M потока жидкости. Будем считать, что характерный «диаметр» d молей, вылетающих из окрестности точки M , с точностью до некоторого постоянного множителя β тождествен масштаб L :

$$d = \beta L. \quad (2.1)$$

Продолжая следовать идее о локальном подобии, будем полагать, что модуль характерной скорости движения моля, «возникающего» в окрестности точки M , пропорционален модулю деформации поля скорости осредненного движения в точке M и характерному масштабу L в этой точке:

$$V' = \begin{cases} \mu L \left| \frac{\partial V}{\partial n} \right|, & \text{если } \frac{L^2}{v} \left| \frac{\partial V}{\partial n} \right| \geq \omega, \\ 0, & \text{если } \frac{L^2}{v} \left| \frac{\partial V}{\partial n} \right| < \omega, \end{cases} \quad (2.2)$$

где

$$\left| \frac{\partial V}{\partial n} \right|^2 = 2 \left(\frac{\partial \bar{u}}{\partial x} \right)^2 + 2 \left(\frac{\partial \bar{v}}{\partial y} \right)^2 + 2 \left(\frac{\partial \bar{w}}{\partial z} \right)^2 + \left(\frac{\partial \bar{v}}{\partial z} + \frac{\partial \bar{w}}{\partial y} \right)^2 + \left(\frac{\partial \bar{w}}{\partial x} + \frac{\partial \bar{u}}{\partial z} \right)^2 + \left(\frac{\partial \bar{u}}{\partial y} + \frac{\partial \bar{v}}{\partial x} \right)^2,$$

а μ и ω — безразмерные константы*.

Вид аппроксимационной формулы для характерного линейного масштаба L будет сформулирован позже.

Займемся теперь анализом турбулентных напряжений $\tau_{ik} = -\rho \overline{v_i v_k}$ и турбулентных тепловых потоков $q = c\rho \overline{v_i T}$, входящих в уравнения (1.1) и (1.3).

Выражения $\rho \overline{v_i v_k}$ и $c\rho \overline{v_i T}$ в какой-либо точке M есть соответственно осредненные потоки количества движения mv_k и тепла ctT , создаваемые составляющей пульсации скорости v'_i в положительном направлении оси x_i через единичную площадку, перпендикулярную оси x_i и движущуюся со скоростью осредненного потока в точке M .

Рассмотрим единичную площадку около некоторой точки M_0 внутри потока, ориентиру-

ванную перпендикулярно оси x_i и движущуюся со скоростью осредненного движения в точке M_0 (рис. 1). Через эту площадку могут пролетать моли из окрестностей различных точек потока. Пусть в какой-то момент времени

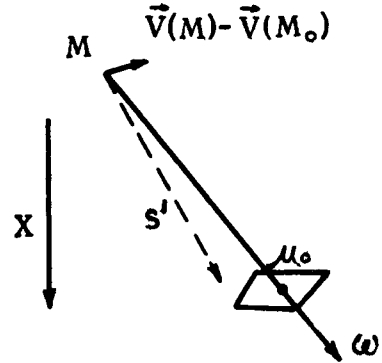


Рис. 1

t через точку M_0 пролетает со скоростью V^* моля, вышедший из окрестности точки M . Если бы моля двигался от точки M к точке M_0 без замедления, то его скорость V^* в момент прохождения через точку M_0 была бы в точности равна алгебраической сумме скорости осредненного движения \vec{V} в точке M и пульсационной скорости моля \vec{V}' , взятой в системе координат, движущейся с осредненным потоком в точке M . Пульсации же $v'_i(M_0)$ в момент прохождения моля через точку M_0 были бы равны соответственно

$$v'_i(M_0) = V'(M) \cos(s', x_i) + [\bar{v}_i(M) - \bar{v}_i(M_0)], \quad (2.4)$$

причем под s' здесь подразумевается направление вектора скорости V' в системе координат, движущейся с осредненным потоком в точке M (см. рис. 1).

В действительности же в результате взаимодействия моля с окружающей средой скорость моля изменяется в процессе его движения, и, следовательно, фактические пульсации $v'_i(M_0)$ будут отличны от вычисленных по формулам (2.4). Аналогичным образом температура рассматриваемого моля T^* в момент прохождения его через точку M_0 не будет равна его температуре в исходной точке M .

Введем гипотезу о взаимодействии движущегося моля с окружающей жидкостью. Уравнения изменения количества движения и притока тепла для движущегося объема запишем в виде*

* «Энергетическое соотношение» (2.2) по структуре аналогично выражению для удельной диссипации кинетической энергии ламинарного течения жидкости.

* Введение уравнений (2.5) является обобщением идей о взаимодействии движущегося моля с окружающей жидкостью, развивавшихся в работах ^{7,8}, и др.

$$\begin{aligned} dv_i^* &= \frac{3}{R} A_1 (\bar{v}_i - v_i^*) dt, \\ dT^* &= \frac{3}{R} A_2 (\bar{T} - T^*) dt. \end{aligned} \quad (2.5)$$

Здесь \bar{v}_i^* и T^* — составляющие скорости и температуры в движущемся объеме; \bar{v}_i и \bar{T} — значения этих функций в окружающей жидкости; R — «радиус» моля, связанный с масштабом $L(M)$ соотношением (2.1); A_1 и A_2 — некоторые коэффициенты, имеющие размерность $m/сек$.

В уравнениях (2.5) перейдем от независимой переменной t к переменной r , являющейся расстоянием движущегося моля от точки вылета M в системе координат, движущейся со скоростью осредненного потока жидкости в точке M :

$$dt = \frac{dr}{\bar{V}'}$$

Тогда уравнения (2.5) примут вид

$$\frac{dv_i^*}{dr} + P_1 v_i^* = P_1 \bar{v}_i, \quad \frac{dT^*}{dr} + P_2 T^* = P_2 \bar{T}, \quad (2.6)$$

где

$$P_1 = \frac{3A_1}{R\bar{V}'}, \quad P_2 = \frac{3A_2}{R\bar{V}'}. \quad (2.7)$$

Запишем приближенные решения уравнений (2.6), полагая в этих уравнениях коэффициенты P_1 и P_2 постоянными, а траекторию моля s от точки M к точке M_0 прямой линией.

В частности, решение для $v_i^*(r)$ при $r=s$, где $s=MM_0$, запишем в виде

$$v_i^*(s) = e^{-P_1 s} \left[\int_0^s P_1 \bar{v}_i e^{P_1 r'} dr' + v_i^*(0) \right], \quad (2.8)$$

где

$$v_i^*(0) = V'(M) \cos(s', x_i) + \bar{v}_i(M).$$

Представим скорость \bar{v}_i в окружающей жидкости на пути MM_0 в виде линейной функции расстояния r . Тогда на основании (2.8) получим

$$\begin{aligned} v_i^*(M_0) &= v_i^*(s) - \bar{v}_i(s) = V'(M) f_0 \cos(s', x_i) + \\ &+ [\bar{v}_i(M) - \bar{v}_i(M_0)] f_1, \end{aligned} \quad (2.9)$$

где

$$f_0 = e^{-P_1 s}, \quad f_1 = \frac{1}{P_1 s} (1 - e^{-P_1 s}).$$

Аналогичным образом получим выражение для пульсации температуры $T'(M_0)$ в момент прохождения рассматриваемого моля через точку M_0 :

$$T'(M_0) = [\bar{T}(M) - \bar{T}(M_0)] f_2,$$

$$\text{где } f_2 = \frac{1}{P_2 s} (1 - e^{-P_2 s}) = f_1(P_2 s). \quad (2.10)$$

Будем полагать, что разность скоростей осредненного движения $\bar{V}(M) - \bar{V}(M_0)$ на рас-

стоянии MM_0 порядка длины пробега моля по абсолютной величине значительно меньше абсолютной величины пульсационной скорости моля \bar{V}' .

При использовании выражений (2.9) и (2.10) потоки $\rho v_i'(M_0) v_k'(M_0)$ и $\rho v_i'(M_0) T'(M_0)$, создаваемые пульсацией скорости $v_i'(M_0)$ при прохождении моля из окрестности точки M через точку M_0 , запишем в виде

$$\begin{aligned} \rho v_i'(M_0) v_k'(M_0) &= F_{ik}(M, M_0) \simeq \rho V'^2(M) f_0^2 \times \\ &\times \cos(s, x_i) \cdot \cos(s, x_k) + \rho V'(M) f_0 f_1 [\bar{v}_k(M) - \\ &- \bar{v}_k(M_0)] \cos(s, x_i) + \rho V'(M) f_0 f_1 [\bar{v}_i(M) - \\ &- \bar{v}_i(M_0)] \cos(s, x_k), \end{aligned} \quad (2.11)$$

$$\begin{aligned} \rho v_i'(M_0) T'(M_0) &= E_i(M, M_0) \simeq \\ &\simeq \rho V'(M) f_0 f_2 [\bar{T}(M) - \bar{T}(M_0)] \cos(s, x_i). \end{aligned} \quad (2.12)$$

В выражениях (2.11), (2.12) отброшены произведения $[\bar{v}_i(M) - \bar{v}_i(M_0)] [\bar{v}_k(M) - \bar{v}_k(M_0)] f_2^2$ и $[\bar{v}_i(M) - \bar{v}_i(M_0)] \cdot [\bar{T}(M) - \bar{T}(M_0)] f_1 f_2$, как малые более высокого порядка, а $\cos(s', x_i)$ принят приближенно равным $\cos(s', x_i)$.

Для получения осредненных величин $\overline{\rho v_i v_k}$ и $\overline{\rho v_i T'}$ в точке M_0 необходимо, очевидно, правые части выражений (2.11), (2.12) проинтегрировать по окружающей пространственной области D с соответствующей весовой функцией $\varphi(M \rightarrow M_0)$, являющейся вероятностью прохождения через точку M_0 моля с центром из единичной окрестности произвольной точки M :

$$\overline{\rho v_i v_k} = \int_D F_{ik}(M, M_0) \varphi(M \rightarrow M_0) d\tau, \quad (2.13)$$

$$\overline{\rho v_i T'} = \int_D E_i(M, M_0) \varphi(M \rightarrow M_0) d\tau. \quad (2.14)$$

Спектр направлений движения молей, пересекающих точку M_0 , в системе координат, движущейся со скоростью осредненного течения жидкости в точке M_0 , будем считать приближенно изотропным.

Плотность вероятности $\varphi(M \rightarrow M_0)$ примем в виде сферически симметричного нормального закона распределения с дисперсией σ , пропорциональной масштабу турбулентности L в точке M_0 , а именно

$$\varphi(M \rightarrow M_0) = \frac{1}{4\pi\sigma^2} \sqrt{\frac{2}{\pi}} \frac{1}{\alpha L_0} e^{-\frac{1}{2} \cdot \frac{s^2}{(\alpha L_0)^2}}, \quad (2.15)$$

где L_0 — есть значение масштаба L в точке M_0 , а α — безразмерная константа.

Масштаб турбулентности $L(M)$, входящий в выражения (2.1), (2.2) и (2.15), в первом приближении отождествим с характерным рас-

стоянием точки M от стенок канала. Он определяется формулой

$$\frac{1}{L} = \frac{1}{\pi} \int_{\Omega} \frac{1}{l} d\omega, \quad (2.16)$$

где l — есть расстояние от точки M до стенки канала в направлении ω .

Во втором приближении масштаб $L(M)$ будем считать, кроме того, зависящим от локальных особенностей поля скорости осредненного течения (см. работу ⁴).

Для случая вынужденных течений жидкости в закрытых каналах будем считать достаточной аппроксимацию масштаба L формулой (2.16).

Вид функций $L(M)$, вычисленных по формуле (2.16) для сечений различных каналов, приведен в разд. 4. Здесь лишь отметим, что получаемые по формуле (2.16) значения масштаба L с точностью до постоянного множителя хорошо согласуются с экспериментальными оценками масштабов турбулентности (см. работы ^{5,6} и др.).

Итак, все функции, входящие в интегральные выражения (2.13) и (2.14), определены. Выражения (2.13) и (2.14) являются общими интегральными формулами для компонент тензора турбулентных напряжений и составляющих вектора турбулентного потока.

В целях упрощения использования полученных аппроксимаций для $\overline{\rho v_i v_k}$ и $\overline{\rho v_i T'}$ произведем некоторые дальнейшие преобразования выражений (2.13) и (2.14).

Разности функций v_i и T' в точках M и M_0 представим в виде разложения по осям координат по формуле

$$\psi(M) - \psi(M_0) \approx - \left(\frac{\partial \psi}{\partial s} \right)_0 \cdot s = \sum_{i=1}^3 \left(\frac{\partial \psi}{\partial x_i} \right)_0 \times s \cdot \cos(s, x_i), \quad (2.17)$$

где $\left(\frac{\partial \psi}{\partial s} \right)_0$ — значение производной $\frac{\partial \psi}{\partial s}$ в точке M_0 .

С учетом формул (2.2), (2.11), (2.12) и (2.17) выражения (2.13), (2.14) для $\overline{\rho v_i v_k}$ и $\overline{\rho v_i T'}$ запишем следующим образом:

$$-\overline{\rho v_i v_k} = -\rho \mathcal{P}_{ik} + \sum_{j=1}^3 \rho \varepsilon_m^{ij} \frac{\partial \overline{v_k}}{\partial x_j} + \sum_{j=1}^3 \rho v_m^{kj} \frac{\partial \overline{v_i}}{\partial x_j}, \quad (2.18)$$

$$-\overline{\rho v_i T'} = \sum_{j=1}^3 \rho \varepsilon_n^{ij} \frac{\partial \overline{T'}}{\partial x_j}, \quad (2.19)$$

где

$$\mathcal{P}_{ik}(M_0) = \mu^2 \int_D F^2(M) f_0^2 \varphi(M \rightarrow M_0) \cos(s, x_i) \times \cos(s, x_k) d\tau, \quad (2.20)$$

$$\varepsilon_m^{ij}(M_0) = \mu \int_D F(M) \cdot f_0 f_1 s \varphi(M \rightarrow M_0) \cdot \cos(s, x_i) \times \cos(s, x_j) d\tau, \quad (2.21)$$

$$\varepsilon_n^{ij}(M_0) = \mu \int_D F(M) \cdot f_0 \cdot f_2 s \cdot \varphi(M \rightarrow M_0) \times \cos(s, x_2) \cos(s, x_j) d\tau, \quad (2.22)$$

причем

$$F = \begin{cases} L \left| \frac{\partial V}{\partial n} \right|, & \text{если } \frac{L^2}{v} \left| \frac{\partial V}{\partial n} \right| \geq \omega, \\ 0, & \text{если } \frac{L^2}{v} \left| \frac{\partial V}{\partial n} \right| < \omega. \end{cases}$$

Выражения, стоящие под знаком Σ в формуле (2.18), имеют ту же структуру, что и прандтлевское напряжение для случая плоского потока. Слагаемые же типа \mathcal{P}_{ik} являются некоторым турбулентным аналогом статического давления в жидкости.

При решении практически необходимых задач система уравнений (1.1)–(1.3) и (2.18), (2.19) в каждом конкретном случае может быть значительно упрощена, исходя из заранее известных гидродинамических особенностей исследуемого потока жидкости и требуемой точности решения задачи.

В частности, уравнения движения (1.1) и притока тепла (1.3) для турбулентных течений жидкости в прямолинейных каналах вдали от входного сечения с учетом (2.18) и (2.19) и после отбрасывания несущественных членов можно записать в виде

$$0 = -\frac{1}{\rho} \cdot \frac{\partial P}{\partial z} + \frac{\partial}{\partial x} \left\{ (v + \varepsilon_m^x) \frac{\partial w}{\partial x} \right\} + \frac{\partial}{\partial y} \left\{ (v + \varepsilon_m^y) \frac{\partial w}{\partial y} \right\}, \quad (2.23)$$

$$w \frac{\partial T}{\partial z} = \frac{\partial}{\partial x} \left\{ (k + \varepsilon_n^x) \frac{\partial T}{\partial x} \right\} + \frac{\partial}{\partial y} \left\{ (k + \varepsilon_n^y) \frac{\partial T}{\partial y} \right\} + \frac{\partial}{\partial z} \left\{ (k + \varepsilon_n^z) \frac{\partial T}{\partial z} \right\}, \quad (2.24)$$

причем в выражениях для ε_m^{ij} и ε_n^{ij} (2.21)–(2.22)

$$\left| \frac{\partial V}{\partial n} \right| = \left| \frac{\partial w}{\partial n} \right| = \sqrt{\left(\frac{\partial w}{\partial x} \right)^2 + \left(\frac{\partial w}{\partial y} \right)^2}.$$

3. ЗНАЧЕНИЯ КОЭФФИЦИЕНТОВ

η , α , A_1 и A_2

Значения эмпирических коэффициентов μ , α , A_1 и A_2 , входящих в изложенную модель турбулентного обмена, установим на основании некоторых экспериментальных измерений моментов связи в турбулентном потоке, а также путем использования других эмпирических данных.

Прежде всего, для обеспечения согласия с экспериментальными данными результатов расчета по формуле (2.18) среднеквадратичных пульсаций скорости и касательных напряжений в турбулентных потоках жидкости следует положить

$$\mu = 1,7 \div 1,8, \quad \mu \alpha = 0,75. \quad (3.1)$$

Механизм взаимодействия молей с окружающей средой, описываемый уравнениями (2.5),

будем полагать двояким. Во-первых, движущийся моль обменивается с окружающей средой «субстанциями» v_i и T в результате молекулярной диффузии. Во-вторых, движущийся моль, представляя собой не твердое тело, а некий «бурлящий комок жидкости», обменивается с окружающей жидкостью «макрочастицами».

Поэтому коэффициенты A_1 и A_2 , входящие в уравнения (2.5), представим в виде суммы двух слагаемых, отражающих соответственно действие молекулярного механизма передачи субстанции и обмен «макрочастицами»:

$$A_1 = (b_1 + b_2) \frac{v}{R}, \quad A_2 = b_3 \frac{k}{R} + b_4 \frac{v}{R}, \quad (3.2)$$

где b_1, b_2, b_3, b_4 — некоторые безразмерные величины, причем b_1 и b_3 близки к единице. Следуя работе ⁴, примем

$$b_4 = b_2, \quad b_3 = b_1 \left(\frac{v}{k} \right)^{0,33}. \quad (3.3)$$

С учетом формул (3.2), (3.3), (2.1) и (2.2) аргументы функций f_0, f_1 и f_2 запишем следующим образом:

$$P_1 s = \frac{12\theta^2 (b_1 + b_2)}{\mu \alpha \gamma_*} \cdot \frac{s}{\alpha L},$$

$$P_2 s = \frac{12\theta^2 (b_1 D^{0,67} + b_2)}{\mu \alpha \gamma_*} \cdot \frac{s}{\alpha L}, \quad (3.4)$$

где

$$\gamma_* = \frac{L^2}{v} \cdot \left| \frac{\partial V}{\partial n} \right|, \quad D = \frac{k}{v}, \quad \theta = \frac{\alpha}{\beta}.$$

Эмпирические коэффициенты b_1 и b_2 будем считать ради простоты константами. Коэффициент θ , стоящий множителем при b_1 и b_2 , может быть введен в b_1 и b_2 , и поэтому будем считать его равным единице.

Следуя работе ⁴, примем

$$b_1 = 1, \quad b_2 = 4. \quad (3.5)$$

После некоторых пробных расчетов полей скорости и температуры в потоках жидкости в круглой трубе значения коэффициентов μ, α, b_1 и b_2 окончательно приняты равными $\mu = 1,8, \alpha = 0,42, b_1 = 0,9, b_2 = 3,8$ (3.6)

Критическое число ω принято равным 25.

4. РЕЗУЛЬТАТЫ РАСЧЕТА ПОЛЕЙ СКОРОСТИ И ТЕМПЕРАТУРЫ В ТУРБУЛЕНТНЫХ ПОТОКАХ ЖИДКОСТИ В ПРЯМОЛИНЕЙНЫХ КАНАЛАХ

Изложенная модель турбулентного обмена была использована для расчетов полей скорости и температуры в турбулентных потоках жидкости в круглой трубе, в кольцевых и плоских зазорах, в каналах с прямоугольным сечением и в ячейках решеток стержней.

При практическом решении уравнений типа (2.23) и (2.24) в этих задачах были исполь-

зованы некоторые упрощения выражений (2.21) и (2.22) для коэффициентов ϵ_M^{jj} и ϵ_H^{jj} .

Так, интегральные выражения для ϵ_M^{jj} и ϵ_H^{jj} по пространственной области D вокруг какой-либо рассматриваемой точки M_0 упрощены до интегралов по отрезку, параллельному оси x_j :

$$\epsilon_M^{jj}(M_0) = c L_0 \int_{-\infty}^{\infty} L \left| \frac{\partial w}{\partial n} \right| f_0(q \xi_j) \times \\ \times f_1(q \xi_j) G(\xi_j) d\xi_j. \quad (4.1)$$

$$\epsilon_H^{jj}(M_0) = c L_0 \int_{-\infty}^{\infty} L \left| \frac{\partial w}{\partial n} \right| f_0(q \xi_j) \times \\ \times f_1(\lambda q \xi_j) G(\xi_j) d\xi_j, \quad (4.2)$$

где

$$F = \begin{cases} L \left| \frac{\partial w}{\partial n} \right|, & \text{если } \gamma_* \geq 25, \\ 0, & \text{если } \gamma_* < 25, \end{cases}$$

$$\xi_j = \frac{x_j - (x_j)_0}{\alpha L_0}, \quad G(\xi) = \frac{1}{2} |\xi| e^{-1/2 \xi^2},$$

$$q = \alpha L_0 P_1 = \frac{75}{\gamma_*} \cdot \frac{L_0}{L}, \quad (4.3)$$

$$c = \sqrt{\frac{2}{\pi}} \frac{\mu \alpha}{3} = 0,20, \quad \lambda = 0,8 + 0,2 D^{0,67}.$$

Функция $L(M)$ в сечениях бесконечно протяженных прямолинейных каналов вычислялась по формуле (2.16), которая для таких каналов приводится к виду

$$1/L(M) = \frac{1}{2} \int_0^{2\pi} \frac{1}{l} d\varphi, \quad (4.4)$$

где $l(\varphi)$ — расстояние рассматриваемой точки M до периметра поперечного сечения канала в направлении φ .

Для канала (зазора) шириной $2b$ между двумя параллельными пластинами формула (4.4) дает (см. работу ⁴)

$$\frac{L}{b} = \left(1 - \frac{z}{2} \right) z, \quad (4.5)$$

где $z = \frac{y}{b}$, причем y есть расстояние рассматриваемой точки M от одной из пластин.

Нетрудно получить на основании (4.4) и формулу для масштаба $L(M)$ в сечении трубы радиуса a

$$\frac{L}{a} = \frac{1 - \xi^2}{2E(\xi, \pi/2)}, \quad (4.6)$$

где

$$\xi = \frac{r}{a}, \quad E(\xi, \varphi) = \int_0^{\varphi} \sqrt{1 - \xi^2 \sin^2 \alpha} d\alpha.$$

График функции $L(\xi)$ для круглой трубы приведен на рис. 2.

Как видно из рис. 2, длина пути смешения l , вычисленная Никурадзе ⁵⁺ по экспериментально измеренным профилям скорости в трубе,

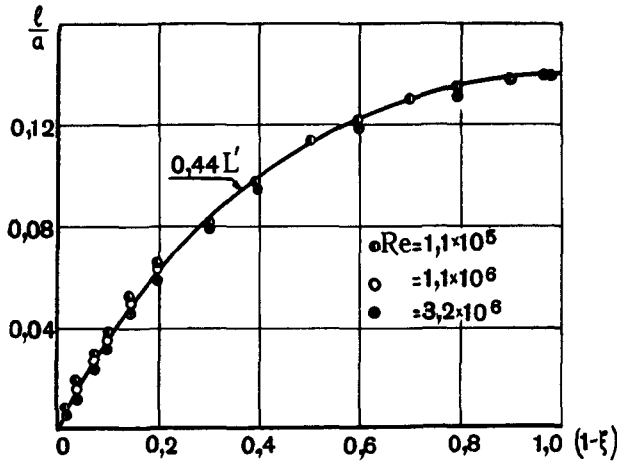


Рис. 2. Сопоставление функций L и l для круглой трубы ($L' = \frac{L}{a}$, $\xi = \frac{r}{a}$)

практически тождественна (с точностью до постоянного множителя) масштабу $L : l = 0,44L$.

Величину \tilde{a} , определяемую для произвольного канала формулой

$$\frac{1}{\tilde{a}} = \frac{1}{2\pi} \int_0^{2\pi} \frac{1}{l_c} d\varphi = \frac{1}{\pi L_c}, \quad (4.7)$$

где $l_c(\varphi)$ — расстояние от «центра» канала до стенки в направлении φ , будем называть эффективным радиусом канала и везде в дальнейшем использовать как характерный поперечный размер канала при составлении безразмерных гидродинамических характеристик потока.

В частности, для круглой трубы радиуса a согласно формуле (4.7) будем иметь $\tilde{a} = a$; для плоского зазора шириной $2b$ получим $\tilde{a} = \frac{\pi}{2} b$; для канала прямоугольного сечения со сторонами $2a$ и $2b$ ($b < a$)

$$\tilde{a} = \frac{\pi}{2} \frac{ab}{\sqrt{a^2 + b^2}}. \quad (4.8)$$

На рис. 3 и 7 представлены результаты расчета средней по сечению безразмерной скорости $u = \frac{w}{v_*}$ и коэффициента сопротивления $\zeta = \frac{8}{u^2}$ в круглой трубе и широком диапазоне изменения безразмерного динамического параметра $\Phi = \frac{av_*}{\nu}$, где a — радиус трубы, а $v_*^2 = \frac{a}{2} \frac{1}{\rho} \left| \frac{\partial P}{\partial z} \right|$. Число $Re = \frac{2a\tilde{a}v_*}{\nu}$ связано с Φ соотношением $Re = 2\tilde{U}\Phi$.

При $\Phi < 32$ ($Re < 500$) решение для \tilde{U} переходит в решение для ламинарного режима: $\tilde{U} = 0,25\Phi$.

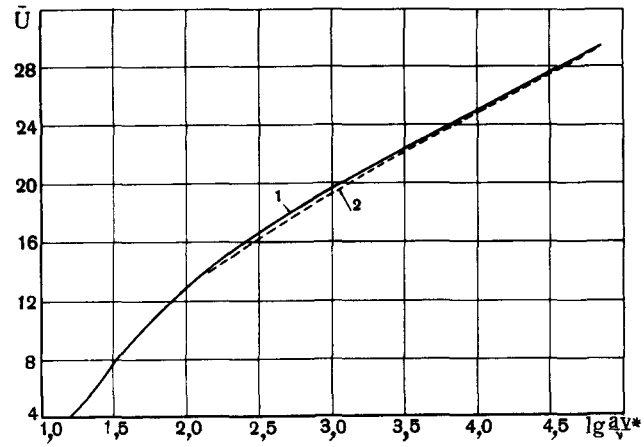


Рис. 3. Зависимость средней скорости \tilde{U} от динамического параметра Φ для круглой трубы: 1 — результаты расчета; 2 — экспериментальная кривая

На рис. 4 представлены рассчитанные профили скорости U по радиусу трубы. Построены общепринятые кривые $V = f\left(\frac{yv_*}{\nu}\right)$ для различных чисел Re , где y — есть расстояние от стенки. Картина разветвления кривых $U = f\left(\frac{yv_*}{\nu}\right)$ при различных числах Re , полученная на рис. 4, близка к разветвлению соответствующих

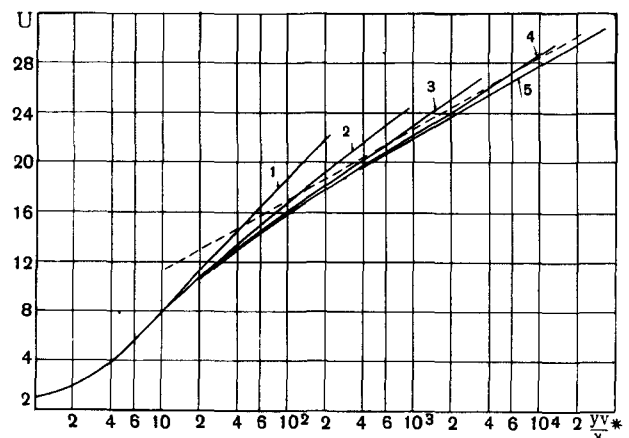


Рис. 4. Рассчитанные профили скорости $U(y)$ в круглой трубе при различных значениях чисел Re .

Кривые 1—5 соответствуют $Re = 6,9 \cdot 10^4$, $3,4 \cdot 10^4$, $1,6 \cdot 10^4$, $7,3 \cdot 10^3$, $3,2 \cdot 10^3$; пунктирная кривая — решение Прандтля:

$$U = 5,5 + 5,75 \lg \frac{yv_*}{\nu}$$

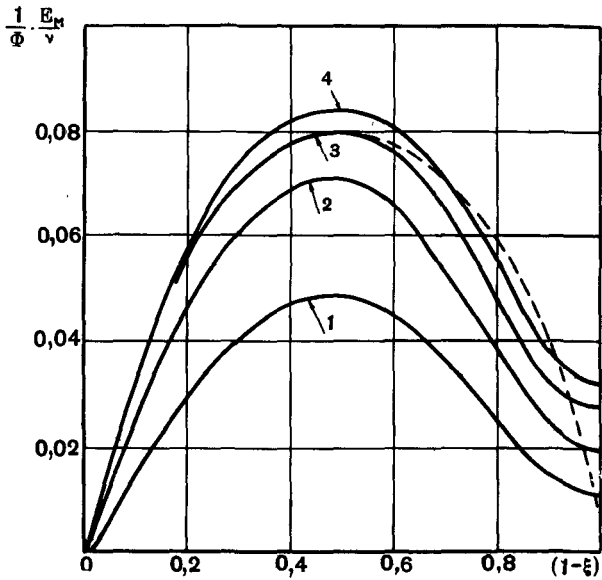


Рис. 5. Рассчитанные значения коэффициента турбулентной вязкости ϵ_m в потоке жидкости в трубе. Кривые 1—4 соответствуют $Re = 6,9 \cdot 10^3, 3,4 \cdot 10^4, 1,6 \cdot 10^5, 7,3 \cdot 10^5$; пунктирная кривая — экспериментальные данные⁵, относящиеся к числам $Re = 10^5 \div 10^6$

кривых, построенных по экспериментальным данным (см., например, работу⁹).

На рис. 5 представлены рассчитанные профили коэффициента турбулентной вязкости ϵ_m по сечению трубы при различных значениях чисел Re .

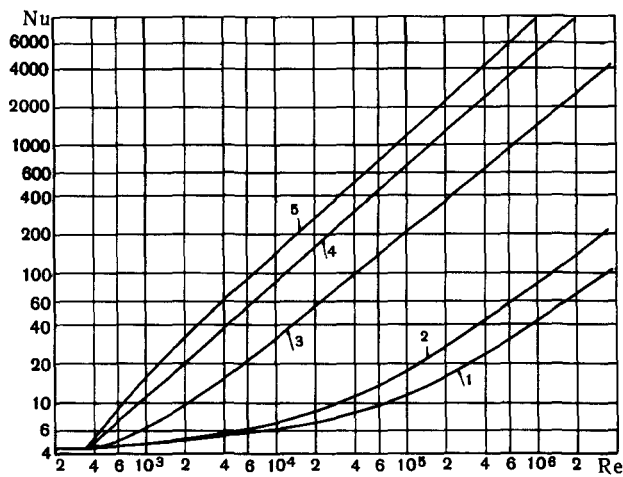


Рис. 6. Результаты расчета чисел Nu для потоков жидкостей в круглой трубе: 1 — $Pr = 0,010$; 2 — $Pr = 0,025$; 3 — $Pr = 1,0$; 4 — $Pr = 10$; 5 — $Pr = 100$

Как видно из рис. 3—5, результаты расчета поля скорости U в потоках жидкости в трубе хорошо согласуются с экспериментальными данными.

Отметим при этом, что учет условия (2.3) при расчете поля скорости (а также поля температуры в жидкостях с $Pr \leq 1$) оказался совершенно несущественным. Учет же условия (2.3) при расчете поля температуры в потоках жидкостей с $Pr \geq 1$ несколько снижает рассчитанные числа Nu и дает более резко выраженный переход решения для Nu к решению для ламинарного режима (при $Re \approx 400$).

На рис. 6 представлены результаты расчета чисел Nu для потоков различных жидкостей в круглой трубе при условии на стенке трубы: $q = \text{const}$, где q — плотность теплового потока. В интервале чисел Re от $3 \cdot 10^3$ до $3 \cdot 10^6$ представленные результаты расчета чисел Nu для потоков жидкостей в круглой трубе можно описать интерполяционной формулой

$$Nu = A + 3,90 (Re \cdot 10^{-3})^m Pr^n, \quad (4.9)$$

где

$$A = 2,5 + 1,3 \lg(1 + Pr^{-1}),$$

$$m = 0,918 - 0,051 \lg(1 + 10 Pr^{-1}),$$

$$n = 0,65 - 0,107 \lg(1 + 10 Pr).$$

Приведенные на рис. 6 результаты расчета достаточно хорошо согласуются с экспериментальными данными как для жидкостей с $Pr \leq 1$ (работы^{10,11} и др.), так и для жидкостей с большими числами Pr (работы^{11,12} и др.).

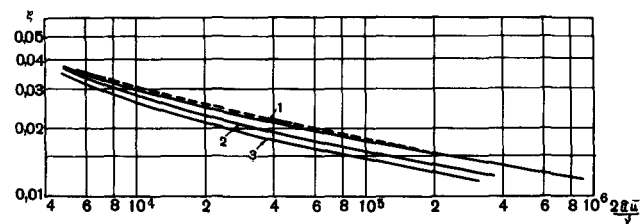


Рис. 7. Результаты расчета коэффициентов сопротивления ζ в кольцевых и плоских зазорах:

1 — круглая труба ($\theta = 0$); 2 — кольцевой зазор с $\theta = 0,5$; 3 — зазоры с $\theta = 0,8 \div 1,0$; пунктирная кривая — экспериментальные данные для круглой трубы

На рис. 7 представлены результаты расчета коэффициента сопротивления $\zeta = \frac{8}{\bar{U}^2}$ в кольцевых зазорах, образованных цилиндрами радиусов a_1 и a_2 ($a_1 < a_2$) при различных значениях динамического параметра $\Phi = \frac{\bar{a} v_*}{\nu}$ (или

числа $Re = \frac{2\bar{a}\bar{v}}{\nu}$ где $v_*^2 = \frac{\bar{a}}{2} \cdot \frac{1}{\rho} \left| \frac{\partial P}{\partial z} \right|$, $U = \frac{w}{v_*}$,
причем*

$$\bar{a} = \left[\frac{\pi}{4} + \left(1 - \frac{\pi}{4}\right) \left(1 - \frac{a_1}{a_2}\right)^2 \right] (a_2 - a_1). \quad (4.10)$$

Как видно из рис. 7, кривые для $\zeta = f(Re)$ в кольцевых зазорах при различных значениях параметра $\theta = a_1/a_2$ заключены между соответственными кривыми $\zeta = f(Re)$ для круглой трубы и плоского зазора.

При уменьшении Φ решение для \bar{U} в плоском зазоре в выбранных переменных приближается к формуле $U = 0,27\Phi$.

На рис. 9 приводится пример расчета поля скорости $U(x, y)$ в канале прямоугольного сечения с параметром $\gamma = \frac{a}{b} = 2$ при $\Phi = 888$. Здесь, как и везде в дальнейшем для произвольных каналов,

$$U = \frac{w}{v_*}, \quad v_*^2 = \frac{\bar{a}}{2} \cdot \frac{1}{\rho} \left| \frac{\partial P}{\partial z} \right|, \quad \Phi = \frac{\bar{a}v_*}{\nu}, \quad Re = \frac{2\bar{a}w}{\nu}, \quad \zeta = \frac{8}{U^2}$$

На рис. 8 представлены результаты расчета коэффициента сопротивления ζ в турбулентных

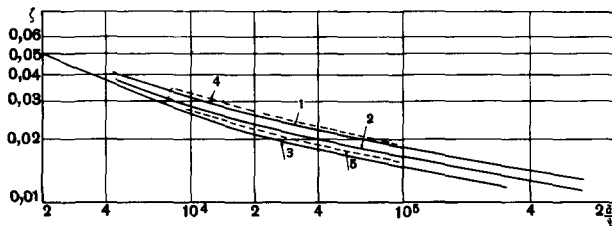


Рис. 8. Результаты расчета коэффициентов сопротивления ζ в каналах с прямоугольным сечением:

1 и 2 — соответствуют $\gamma = 1$ и $\gamma = 5$; 3 — плоский зазор; 4, 5 — результаты измерений¹⁵ при $\gamma = 1$ и $\gamma = 5 \div 10$

потоках жидкости в каналах с прямоугольным сечением при различных значениях отношения сторон сечения γ . При фиксированном значении числа Re коэффициент сопротивления ζ убывает с увеличением параметра γ .

На рис. 8 представлены для сопоставления результаты измерений коэффициентов сопротивления ζ в каналах с прямоугольным сечением¹⁵. Как следует из рис. 8, результаты расчета коэффициента сопротивления ζ в каналах с прямоугольным сечением достаточно хорошо согласуются с результатами измерений**.

* Формула (4.10) интерполяционная.

** Рассчитанные в работе¹⁵ значения коэффициента ζ для прямоугольных каналов с помощью графо-аналитического метода Дейслера-Тэйлора весьма близко согласуются со значениями ζ , полученными в настоящей работе.

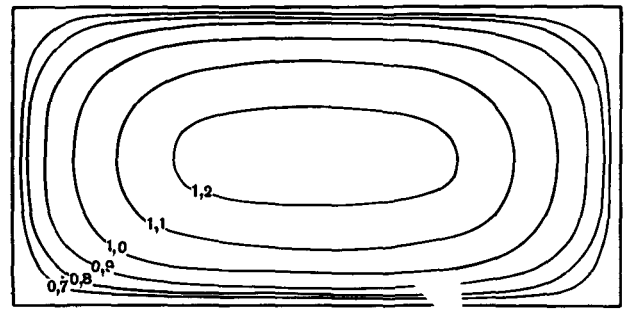


Рис. 9. Рассчитанное поле скорости $U(x, y)$ в канале с прямоугольным сечением ($\gamma = 2$, $Re = 3,4 \cdot 10^4$)

В связи с тем, что поле температуры в потоке жидкости в канале прямоугольного сечения определяется большим числом параметров, а именно: распределением источников тепла, конструкцией и теплопроводностью стенок канала, числом Rg для жидкости и числами Re и γ , нет необходимости заранее строить какие-либо обобщенные зависимости характеристик температурного поля от чисел Re , Rg и т. д. Расчет температурных полей с использованием уравнения (2.24) имеет смысл проделать лишь для конкретной конструкции ячейки теплообменного аппарата.

Приведем, наконец, некоторые результаты расчета полей скорости и температуры в турбулентных потоках жидкости в решетках стержней.

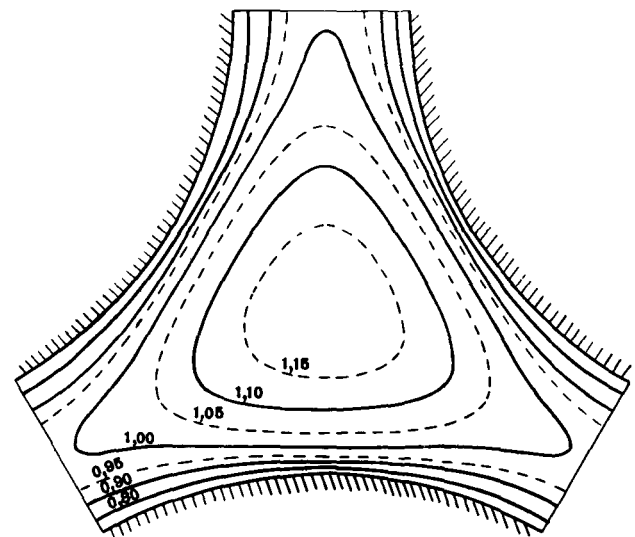


Рис. 10. Рассчитанное поле скорости $U(r, \varphi)$ в ячейке треугольной решетки стержней с относительным шагом $h = 1,2$, $Re = 2,48 \cdot 10^4$

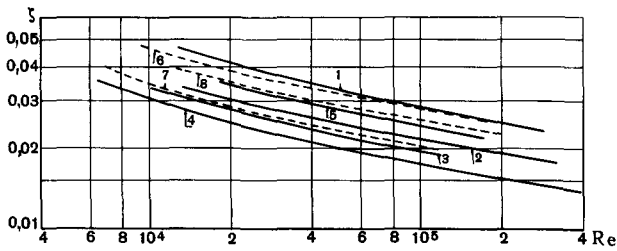


Рис. 11. Рассчитанные коэффициенты сопротивления ζ в ячейках треугольной и квадратной решеток стержней при различных значениях шага h :

1, 2, 3—треугольная решетка ($h=1,0$; 1,1; 1,2); 4—круглая труба; 5—ячейка квадратной решетки, ($h=1,0$); экспериментальные кривые: 6,7—треугольная решетка ($h=1,0^{14}$ и $h=1,2^{13}$); 8—квадратная решетка ($h=1,0^{14}$)

На рис. 10 дан пример расчета поля скорости в треугольной решетке стержней с относительным шагом $h=1,2$ при продольном ее обтекании.

На рис. 11 представлены результаты расчета коэффициентов сопротивления ζ в ячейках треугольных решеток в зависимости от чисел Re и шага решетки h . При выбранном здесь характерном поперечном размере канала \tilde{a} рассчитанные кривые $\zeta=f(Re, h)$ при различных значениях шага решетки h расположены в логической последовательности. При равных значениях числа Re коэффициенты сопротивления ζ возрастают с усилением «неправильности» формы сечения канала от круга. При использовании же в качестве определяющего поперечного размера канала гидравлического радиуса R' полученная обобщенная зависимость $\zeta'=f(Re', h)$ такой логической закономерности не имеет.

На рис. 11 приведены также результаты расчета коэффициента сопротивления ζ в ячейке квадратной решетки стержней с относительным шагом $h=1,0$. На этом же рисунке пунктирными кривыми 6—8 изображены результаты измерений коэффициентов сопротивления ζ в ячейках различных решеток, взятые из работ ¹⁴ и ¹³. Как видно из рис. 11, рассчитанные в настоящей работе коэффициенты сопротивления для решеток с относительным шагом $h=1,0 \div 1,2$ близко согласуются с результатами измерений.

На рис. 12 приведен пример расчета безразмерной температуры $\theta = \frac{\lambda_{ж}(T-T_c)}{2q_0R}$ на поверхности тепловыделяющего стержня в ячейке треугольной решетки с шагом $h=1,0$ при течении в этой ячейке жидкости с $Pr=0,025$. Число Re равно $5 \cdot 10^4$. Величина q_0 здесь означает тепловой

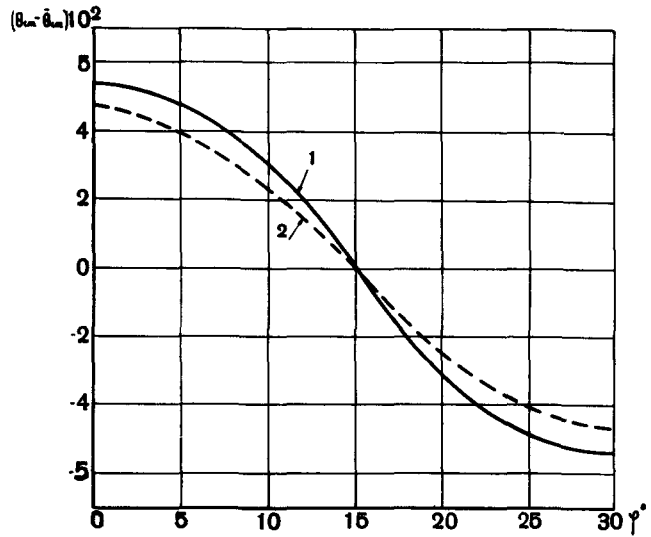


Рис. 12. Пример расчета безразмерной температуры $\theta = \frac{\lambda_{ж}(T-T_c)}{2q_0R}$ на поверхности теплопроводящего стержня в ячейке треугольной решетки с шагом $h=1,0$, $Pr = 0,025$, $Re = 5,10^4$:

1—результаты расчета; 2—результаты измерений¹⁶

поток в сечении стержня на окружности радиуса $r_0=0,773R$, где R — радиус стержня, а $\lambda_{ж}$ — теплопроводность жидкости. Условия задачи здесь соответствуют физическим условиям экспериментов ¹⁶. Пунктирная линия на рис. 12 изображает результаты измерений функции θ из работы ¹⁶. Как видно из рис. 12, результаты расчета температуры θ в указанных конкретных условиях достаточно хорошо согласуются с результатами измерений.

Итак, приведенные в настоящей работе результаты расчета полей скорости и температуры в потоках жидкости в различных каналах дают основание считать, что изложенная пространственная модель турбулентного обмена может быть использована для расчета гидравлических сопротивлений и температурного режима в ячейках теплообменников произвольной конструкции.

ЛИТЕРАТУРА

1. O. R e y n o l d s. Phil. Trans. of the Royal Society (1895).
2. Л. Г. Л о й д я н с к и й. Механика жидкостей и газа. М., 1959.
3. L. P r a n d t l. VDI, 77, No. 5 (1933).
4. Н. И. Б у л е в. В сб. «Теплопередача». М., Изд-во АН СССР, 1962.
5. I. N i k u r a d s e. Forshungsheft, 356 (1932).
6. М. Е. М и н с к и й. Докл. АН СССР, 28, № 8 (1940).

7. К. Д. Воскресенский, Е. С. Турилина. В сб. «Теплопередача и тепловое моделирование». М., Изд-во АН СССР, 1959.
8. R. G. Deissler. NACA, RM E52F05 (1951).
9. R. R. Rothfus and C. C. Monrad. Ind. and Eng. Chem. 47, No. 6 (1955).
10. В. И. Субботин и др. Инж.-физ. ж., № 4 (1963).
11. М. А. Михеев. Основы теплопередачи. М., 1956.
12. W. Buhne. Die Wärme, 61, No. 9 (1938).
13. В. М. Турнеау, R. E. Grimble and J. E. Zerbe. Trans. ASME, 79, No. 8 (1957).
14. В. И. Субботин и др. Атомная «энергия», 13, вып. 2 (1962).
15. I. P. Hartnett, I. C. Y. Koh, S. T. McComas. Trans. ASME, Ser. C, No. 1 (1962).
16. В. И. Субботин и др. «Атомная энергия», 9, вып. 6 (1960).

ABSTRACT—RÉSUMÉ—АННОТАЦИЯ—RESUMEN

A/329 USSR

Theoretical model of turbulent transfer in three-dimensional fluid flow

By N. I. Buleev

This paper discusses a kinetic three-dimensional model of turbulent transfer, which is explained in detail by the author. This model shows in a general form the stresses and additional turbulent thermal fluxes, by means of velocity and temperature distribution functions, which are expressions in the initial flow and heat transfer equations in the case of turbulent flow in a liquid. Thus a mathematical form and a solution to hydrodynamic and thermophysical problems can be given arising in any turbulent flow in a liquid.

The theoretical model developed has been tested by calculations of velocity and temperature distribution in turbulent liquid flows in a circular channel. Velocity and temperature distributions, pressure drop coefficients and the Nusselt number thus obtained agree well with available experimental data.

The results of calculations of velocity and temperature distribution are then discussed for a turbulent flow of liquids in channels of different cross section, e.g., annular, flat, rectangular, and in solid bar lattices. The results of these calculations are compared with experimental data.

The satisfactory agreement between the results of calculations and experimental data imply that the theoretical model in this paper allows the temperature conditions of a fuel element of whatever cross section to be evaluated with sufficient certainty.

The problem of the calculation of temperature distributions in a flow of turbulent liquid is formulated in the zone of thermal stability. Account is taken of longitudinal heat leakages along the walls of the channel as well as in the liquid. Results of the calculations of temperature distributions in the zone of thermal stability in the tube are given for different values of Re , Pr of the wall thickness and of the ratio between the thermal conductivities of the tube wall and the liquid.

The results given of the calculations of temperature distributions in the liquid flow, taking into account longitudinal heat leakages enable especially an estimate to be made of the possible evaluation errors from experimental methods of the Nusselt number for turbulent liquid flows.

In conclusion, the possibilities of some future generalizations in the theory and methods of calculation of hydrodynamic and thermal conditions in reactor cores are discussed in the paper.

A/329 URSS

Modèle théorique d'échange turbulent dans un écoulement de liquide à trois dimensions

par N. I. Buleev

Ce mémoire présente un modèle cinétique tridimensionnel de l'échange turbulent, qui a été élaboré par l'auteur. Ce modèle permet de représenter sous une forme générale, au moyen de fonctions des champs de vitesse et de température pris en moyenne, les tensions et les flux thermiques turbulents supplémentaires qui entrent dans les équations initiales du mouvement et de l'apport de chaleur pour le cas d'un écoulement turbulent du liquide. On peut ainsi donner une forme mathématique et une solution aux problèmes d'hydrodynamique et de thermophysique que pose un écoulement turbulent quelconque de liquide.

Le modèle théorique mis au point a été testé sur les calculs de champs de vitesse et de température dans des courants de liquides turbulents en conduit circulaire. Les champs de vitesse et de température, les coefficients de résistance et le nombre Nu ainsi obtenus concordent bien avec les données expérimentales dont on dispose.

On expose ensuite les résultats du calcul des champs de vitesse et de température dans des écoulements turbulents de liquides dans des canaux de formes différentes—annulaire, plate, rectangulaire—et dans des réseaux de barreaux. Les résultats de ces calculs sont comparés aux données expérimentales.

La concordance satisfaisante entre les résultats du calcul et les données expérimentales donne à penser que le modèle théorique exposé permet d'évaluer avec suffisamment de certitude le régime de température d'un élément de combustible à section de forme quelconque.

On formule le problème du calcul des champs de température dans un courant de liquide turbulent dans la zone de stabilisation thermique. On y tient compte des fuites longitudinales de chaleur le long des parois du canal comme dans le liquide. On donne les résultats du calcul des champs de température dans la zone de stabilisation thermique du tube pour différentes

valeurs de Re , Pr , de l'épaisseur de la paroi et du rapport entre les conductibilités thermiques des parois du tube et du liquide.

Les résultats présentés du calcul des champs de température dans un courant de liquide, en tenant compte des fuites longitudinales de chaleur, permettent en particulier d'estimer les erreurs possibles d'évaluation par des méthodes expérimentales du nombre Nu pour les écoulements turbulents de liquides dans des canaux.

En conclusion, on expose dans le rapport les possibilités de quelques généralisations futures de la théorie et des méthodes de calcul des régimes hydrodynamique et thermique dans les cellules des réacteurs.

A/329 URSS

Modelo teórico del intercambio turbulento en una corriente de líquido en tres dimensiones

por N. I. Buleev

En la memoria se expone un modelo cinético tridimensional del intercambio turbulento, elaborado por el autor. Dicho modelo permite, de manera general, representar las tensiones y los flujos térmicos turbulentos complementarios, que intervienen en las ecuaciones iniciales del movimiento y del aporte de calor para el caso de una corriente turbulenta de un líquido, como funciones de los campos de velocidad y de temperatura promediados. Como consecuencia, resulta posible la formulación matemática y la resolución del problema hidrodinámico y de física del calor que plantea una corriente turbulenta cualquiera de un líquido.

El modelo teórico desarrollado se ha probado calculando los campos de velocidad y de temperatura para corrientes de líquidos turbulentos en tubos

circulares. Los campos de velocidad y de temperatura, los coeficientes de resistencia y el número Nu así obtenidos concuerdan bien con los datos experimentales que se poseen.

Se exponen luego los resultados del cálculo de los campos de velocidad y de temperatura en las corrientes turbulentas de un líquido en canales de otras formas—anulares, planos, rectangulares—y en redes de barras. Los resultados del cálculo se comparan con los datos experimentales.

La concordancia bastante buena entre los resultados del cálculo y los datos experimentales hace esperar razonablemente que el modelo teórico expuesto permita calcular, con suficiente precisión, el régimen de temperaturas de un elemento combustible de sección de forma cualquiera.

Se formula el problema del cálculo de los campos de temperatura en una corriente de líquido turbulento en la zona de estabilización térmica. En este caso, se tienen en cuenta también las pérdidas longitudinales de calor tanto a lo largo de la pared del canal como en el líquido. Se presentan los resultados del cálculo de los campos de temperatura en la zona de estabilización térmica en un tubo para distintos valores de los números Re y Pr , del espesor de la pared y de la razón de la conductibilidad térmica de la pared del tubo a la del líquido.

Los resultados que se presentan del cálculo de los campos de temperatura en una corriente de líquido, teniendo en cuenta las pérdidas longitudinales de calor, permiten en particular estimar los posibles errores del cálculo por métodos experimentales del número Nu para corrientes turbulentas de un líquido en canales.

Finalmente, se exponen en el informe algunas posibilidades de generalización ulterior de la teoría y de los métodos de cálculo de los regímenes hidrodinámico y térmico en las celdas de los reactores.

Heat transfer and hydraulic stability in boiling-water reactors

By M. Bogaardt,* C. L. Spigt,* F. J. M. Dijkman* and N. Madsen**

In the laboratory for Heat Transfer and Reactor Engineering of the Technological University of Eindhoven (Netherlands) work is being carried out in the field of heat transfer by gases and by liquids. Part of this work has a direct bearing on nuclear reactors. In this report, reference is made only to the work carried out on heat transfer and stability in boiling-water reactors. This work is carried out under contract with the EURATOM USA Joint Research and Development Board.

The work on boiling-water reactors is done using a high pressure (40 atm) boiling loop as well as an atmospheric glass loop. Also, some fundamental research on the microscopic phenomena is performed in special equipment. The experimental work is backed-up by theoretical work, both of a fundamental and an applied character.

FUNDAMENTAL RESEARCH

Local temperature fluctuations during boiling

As is known, local temperature variations occur both in the liquid and in the heating surface during bubble formation and bubble growth. Such temperature fluctuations have been reported, for instance, by Hsu and Schmidt [1] and by Moore and Messler [2]. The present work was started in order to verify the rather startling observations by the latter authors.

The apparatus used consists of a horizontal stainless steel boiling plate in thermal contact with an electrically heated copper block, cast around a coiled Calrod resistance heating element. The vapour from the boiling liquid is condensed in a shell-and-tube heat exchanger and returned by gravity to the boiling pool.

The thermocouple used for the experiments consists of a flattened constantan wire, sandwiched between thin layers of Teflon (10 to 30 μ thick). This assembly is inserted through the stainless steel boiling plate, perpendicularly to the boiling surface.

Temperature dips varying from 5 to 17 °F have been observed and recorded over the greater part of the nucleate boiling range from 40 000 Btu/h ft² °F to near burn-out.

The temperature fluctuations vary irregularly from 5 to 17 °F, though there seems to be a slight trend for

the amplitude to decrease with increasing heat flux. The frequency of the dips increases very rapidly with increasing superheat. Some of the thermocouples registered the typical signal until very near burn-out.

An analogue model has been constructed according to the description of heat transfer and fluid motion [3] just mentioned, as shown in Fig. 1. The mathematical description seems to yield curves which resemble the temperature oscillograms closely.

Two-phase flow model

The aim of this study has been to provide a theoretical approach for an understanding of the steady and unsteady behaviour of vertical boilers. The following phenomena especially seem to have to form an essential part of any model:

- (a) The generation of bubbles on the boiling wall;
- (b) The agitation introduced in the flow by the boiling process;
- (c) The diffusion and growth of the bubbles in the flow;
- (d) The interrelationship between bubble distribution and velocity distribution;
- (e) The collapse and agglomeration of bubbles in combination with the existence of different flow régimes (bubble flow, slug flow, annular flow, etc.).

For a detailed description of the following analysis see Ref. [4]. The study has been restricted so far to the bubble régime. The case of a vertical, axially symmetric boiler has been considered. The general equations have been formulated for the unsteady case. This results in a set of simultaneous equations for the various unknowns as a function of the space and time co-ordinates. Much emphasis has been placed upon the correct representation, in the theory, of the following experimentally found facts:

(a) The large increase in frictional pressure drop due to the two-phase character of the flow.

(b) The large increase in heat transfer due to nucleate boiling. The theoretical model ascribes both effects to an increased turbulence level due to a relative movement of the bubbles with respect to the surrounding liquid. This increase in turbulence level is analogous to the turbulence in one-phase flow; however, the turbulence intensity may not be zero at the wall when nucleate boiling takes place.

After introducing dimensionless parameters it has been found that eight similarity parameters govern the solution of the exact equations.

* Technological University of Eindhoven.

** University of Rhode Island, USA.

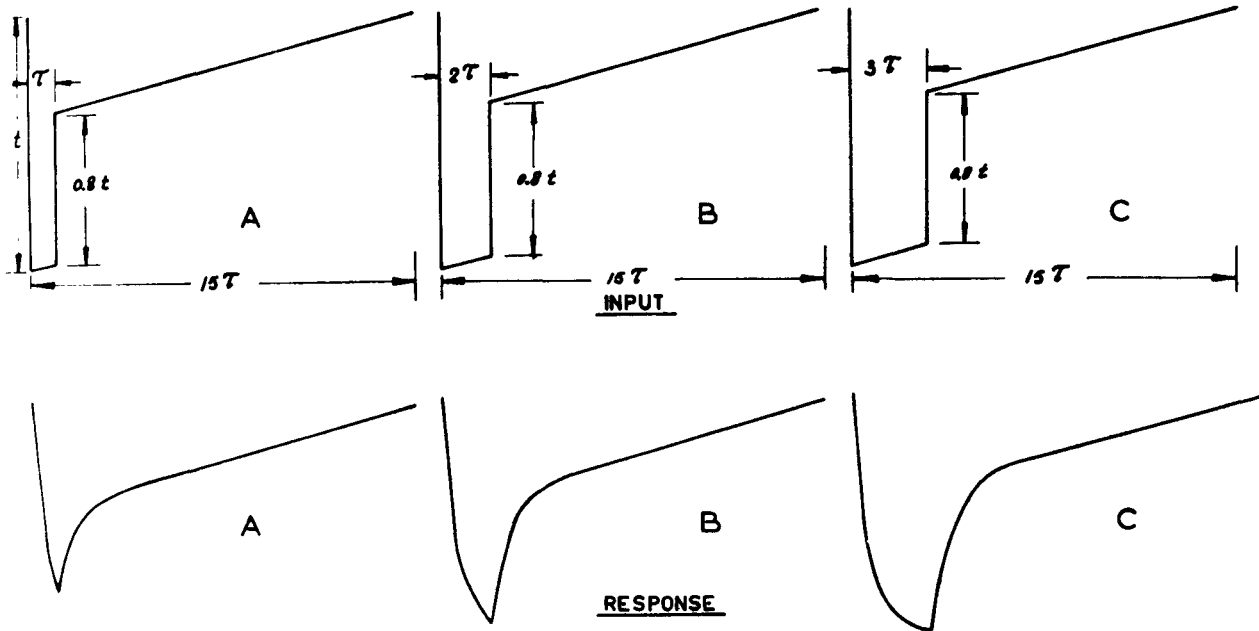


Figure 1. First order response to various inputs simulating the measured temperature dips at the heating surface

By the introduction of prescribed radial distributions the set of partial differential equations for the steady case is reduced to a set of ordinary differential equations that are solvable by numerical means without great difficulty.

At every point the quasi-homogeneous fluid is characterized by:

- (a) A dimensionless velocity ω of the liquid phase;
- (b) A velocity $\omega + \omega_s$ of the bubbles where ω_s is the local slip velocity of one bubble with respect to the surrounding fluid;
- (c) A dimensionless temperature v ;
- (d) A mean void ratio β averaged over-all bubble radii;
- (e) A void ratio distribution function b which is a function of the dimensionless bubble radius P ;
- (f) A pressure coefficient c_p .

Numerical solutions of the complete set of equations are at present being obtained.

STATIONARY CIRCULATION MODEL

A programme has been written to calculate the recirculation rate and void distribution along the height of a natural circulation boiling-water loop in steady state conditions. The programme has been divided into three parts:

(a) in which the velocity directly follows from the balance between the driving head and pressure losses. The onset of bulk boiling is taken to occur when the water temperature reaches the saturation temperature corresponding to the system pressure.

(b) in which the onset of boiling is taken to occur when the temperature is equal to the local saturation temperature. The introduction of a velocity dependent non-boiling length makes an iteration process necessary.

(c) in which local boiling effects are included. The subcooled boiling is calculated according to the description of R. W. Bowring [5]. The inclusion of subcooled boiling results in an increase of the non-bulk boiling length and in a change of the void distribution over the channel.

The model has been designed in such a way that the calculation goes successively through all three parts. In designing the model the possibility of easily substituting different heat flux distributions and correlations for the expansion loss, acceleration loss, slip-factor, two-phase friction loss and entrance loss has been provided for. Some results are shown and compared with experiments in Fig. 2.

LOOP EXPERIMENTS

Apparatus

The experiments are carried out in a pressurized boiling-water loop at 40 atm and in several atmospheric boiling glass loops. The pressurized loop has a

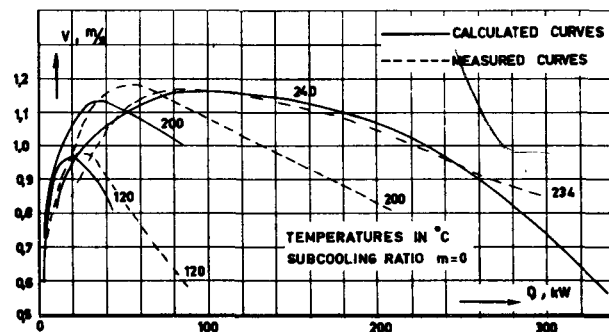


Figure 2. Comparison of steady state calculation with measured data

2 600 mm long vertical test section, an inlet subcooler, and a fast control 1 MW dc power supply. The heated dummy elements are surrounded by a shroud of 50, 60 or 70 mm diam. The steam is fed to a condenser at the top of the installation and is again returned to the downcomer. The loop is provided with pressure taps, Pitot tubes, burn-out detectors, thermocouples and a number of void-fraction meters along the height of the riser.

Methods

In the experiments the following quantities are measured or recorded as a function of power, pressure and subcooling:

Natural circulation rate. The natural circulation rate is measured using the pressure drop across the inlet, and the differential pressure, from a Pitot tube.

Void fraction. The void fraction measurements have been made using a radioactive method, in which a thulium γ -source is centrally placed inside the heating element, while four scintillation counters are grouped around the riser. The signals from the four counters are mixed and the sum is measured.

Impedance gauges are also applied to follow the fluctuations in void fractions and to measure the void distribution along the height.

Static pressure. The static pressure along the riser and downcomer is measured on multi-manometers together with Pitot tube signals. The absolute pressure is recorded by means of a specially developed capacitance void gauge.

Temperatures. The temperatures are measured using calibrated chromel-alumel thermocouples. For recording purposes fast response thermocouples are applied.

Burn-out detector. A burn-out detector is used as a safety device. The signal from this detector, which gives an indication of the temperature fluctuation present in the rod, is recorded.

All signals mentioned are recorded using an ultra-violet recorder. For a detailed analysis the signals from the inductive differential pressure gauges are recorded on a magnetic tape, as well as signals from the impedance void gauges, absolute pressure gauge, saturation temperature thermocouples and burn-out detector. In some programmes the analogue signals were converted to digital data and stored on a paper tape to feed the experimental data into a digital computer. A digital computer programme was written to compute the auto-correlation and the power density curves. The auto-correlation functions, cross-correlation functions and power spectra were also calculated by means of a special purpose analogue computer, ISAC. The experimental results obtained so far indicate that in many cases the onset of the hydraulic instabilities is quite sudden. In some cases, however, especially at higher pressures or with a riser with a larger hydraulic diameter, there is not an abrupt change from stable to unstable operations as a result of an incremental change of power, but rather an increasing lack of stability observed over a range of power inputs.

Experimental results

In Figs. 3 and 4 some of the results of measurements of flow rate and void fraction, as a function of power, pressure, subcooling and axial position, are given. The signals of the seven impedance void gauges and of the flow-rate and absolute pressure gauges during instabilities have been recorded, and some results are given in Fig. 5. They show relative phase-shifts between the signals and in the case of the void gauges a decreasing amplitude in void with increasing distance from the bottom of the shroud. The upper void gauge with the highest mean void fraction scarcely shows an unstable signal. This phenomenon has also been observed in the glass boiling-water loop. From this it follows that the pressure fluctuations are largest at the bottom of the shroud.

The experiments indicate that subcooling decreases the frequency of the fluctuations. The amplitude of the oscillations for the high subcooling case is larger than for the low subcooling case.

Root mean square values of power spectra obtained by digital calculations have been compared with those obtained by calculations in an analogous way. The agreement appears to be quite good.

For a series of pressures the onset of instabilities has been determined by plotting the root mean square values, taken at the instability frequency of the power spectra, of the flow rate, voidage and absolute pressure signals as a function of the power. The experiments have been continued until burn-out occurred. A rapid increase of the amplitude of the oscillations at lower temperatures can be observed (Fig. 6). At high temperatures the curves are far less steep.

The root mean square values of the power spectra taken at the instability frequency of the flow-rate signal and other signals at 160 °C are given as a function of power and subcooling temperature in Fig. 7. A subcooling temperature of 2.5 °C at the inlet gives a minimum power at which instabilities start.

TRANSFER FUNCTION MEASUREMENTS

As mentioned in the previous sections, transfer functions in the boiling channel have been made on the basis of noise analysis, auto and cross-correlations by means of a digital computer programme. In addition, transfer functions can be readily obtained by disturbing the boiling system by a sinusoidal input signal and analysing the required output signal by normal Fourier techniques. The Fourier analysis is necessary in order to be able to reject the noise in the output signal. In Fig. 8 an example of an experimental transfer function is presented.

BURN-OUT EXPERIMENTS

Burn-out and hydraulic stability experiments under natural convection were carried out at saturation temperatures of 230, 200, 180 and 140 °C with a 7-rod bundle test section in which the geometry was very close to a Halden boiling-water reactor second

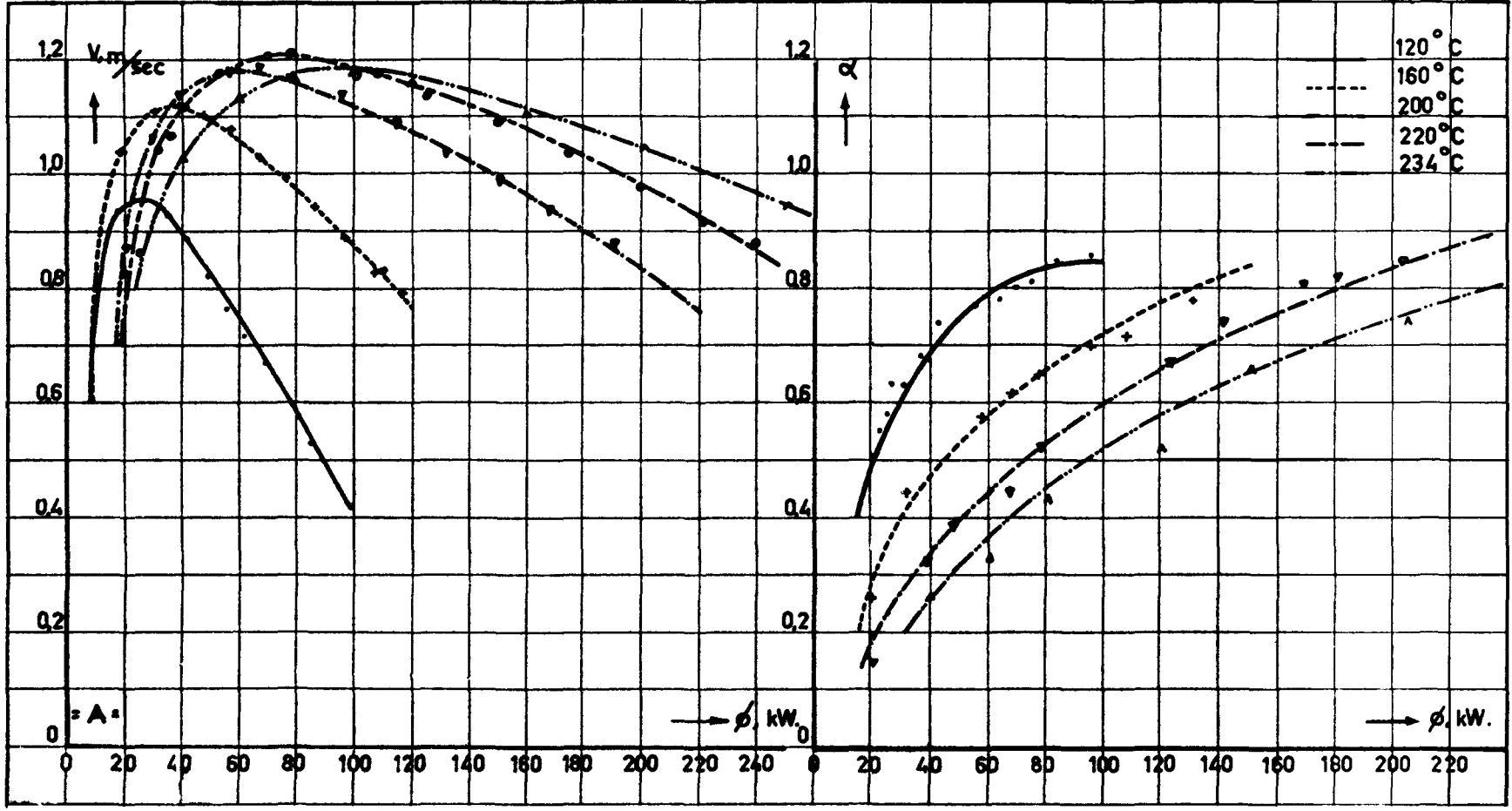


Figure 3. Results of steady state experiments in a natural circulation boiling loop
The circulation rate and void fraction as a function of channel power for different temperatures

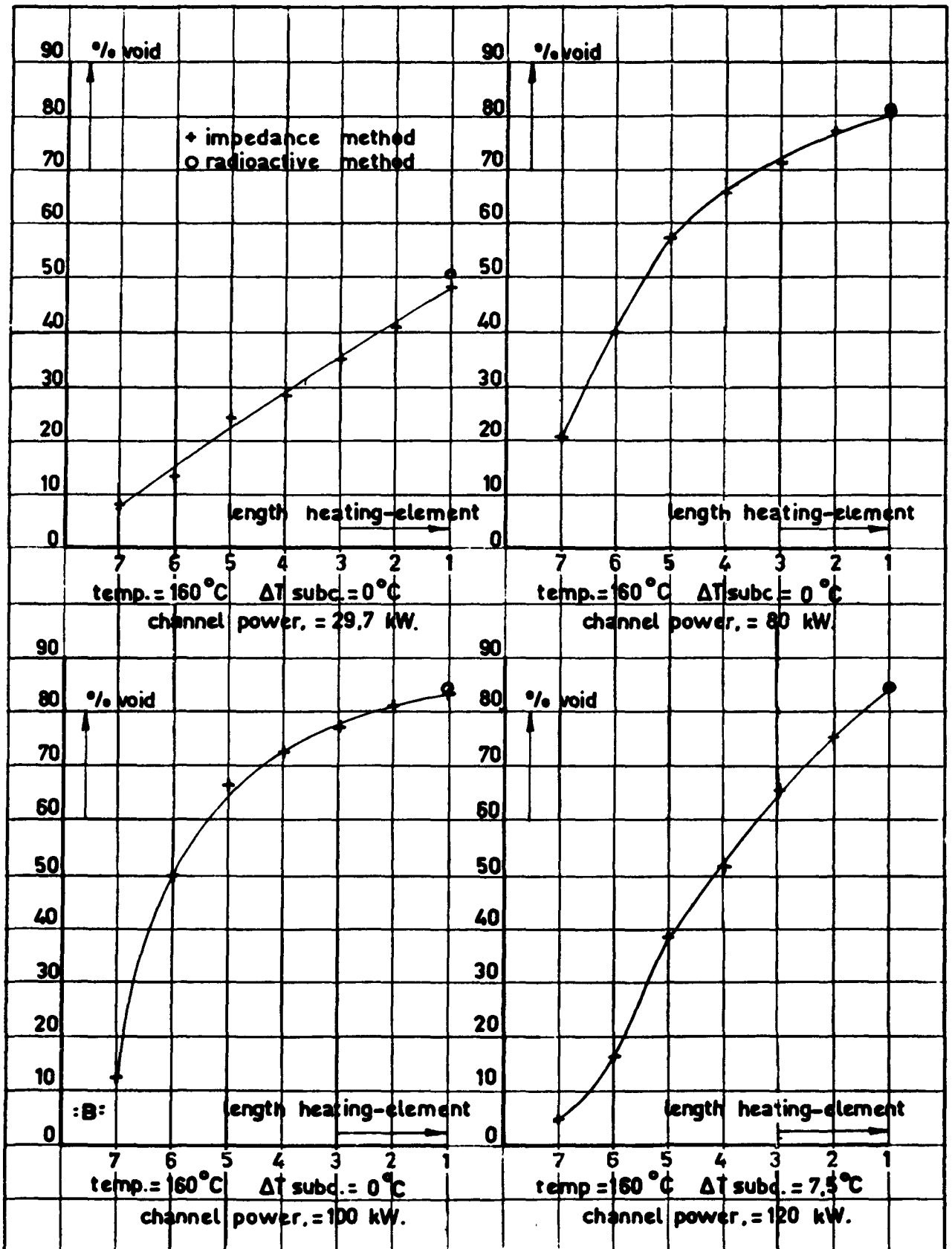


Figure 4. Results of steady state experiments in a natural circulation boiling loop
Void distribution along the riser

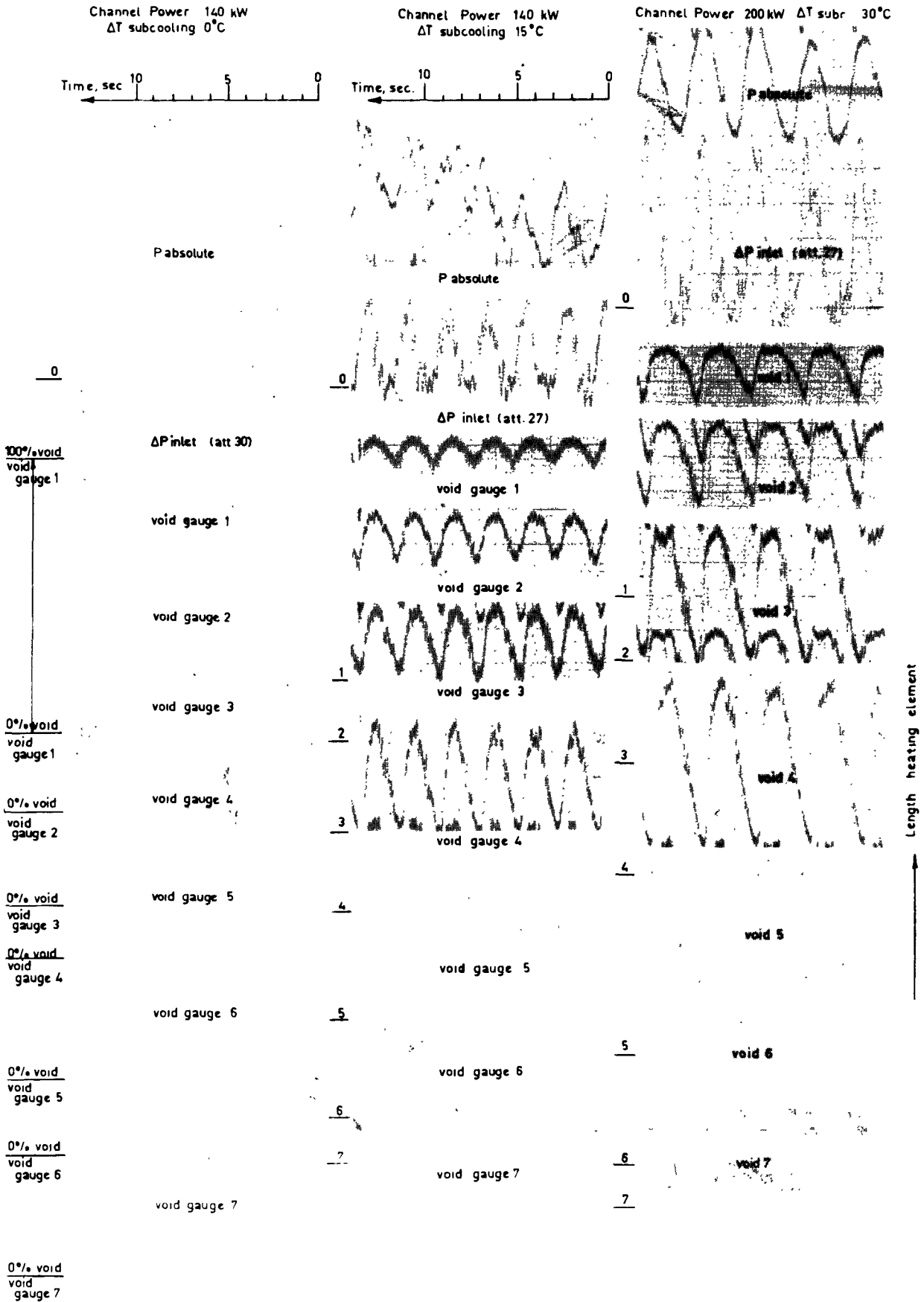


Figure 5. Signals from different quantities during hydraulic instabilities with and without subcooling

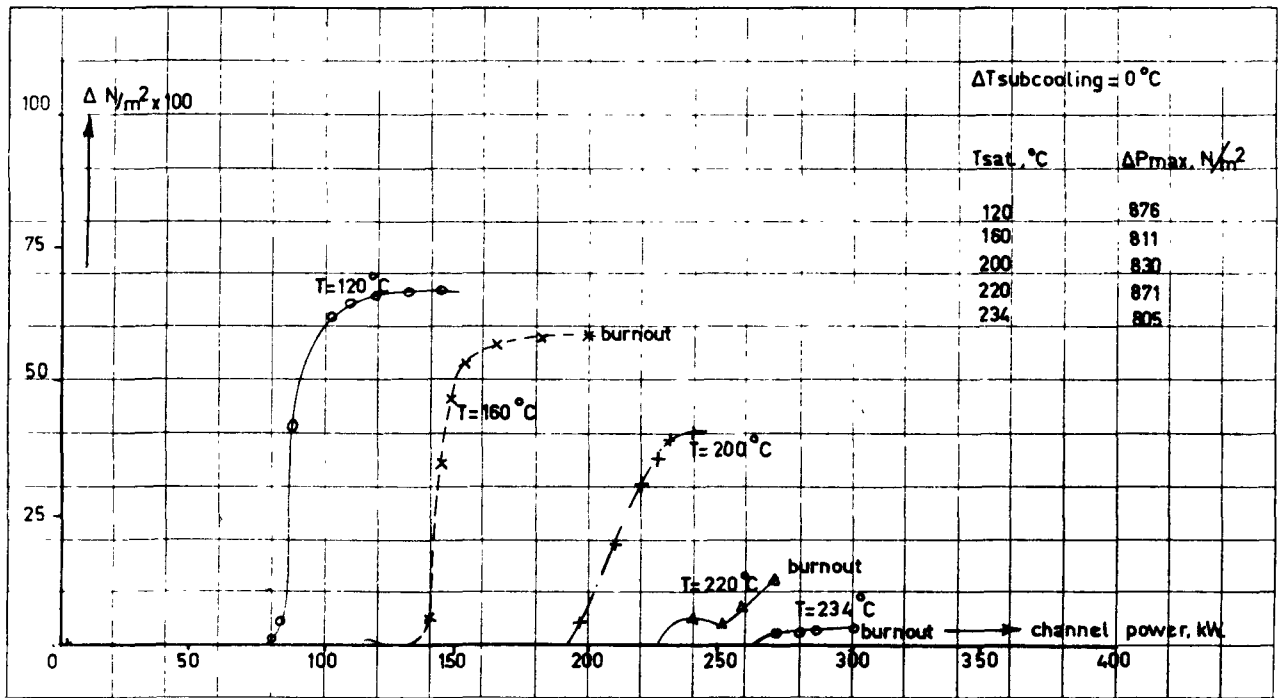


Figure 6. The root mean square values of the inlet pressure drop, taken at the instability frequency, as a function of power and pressure

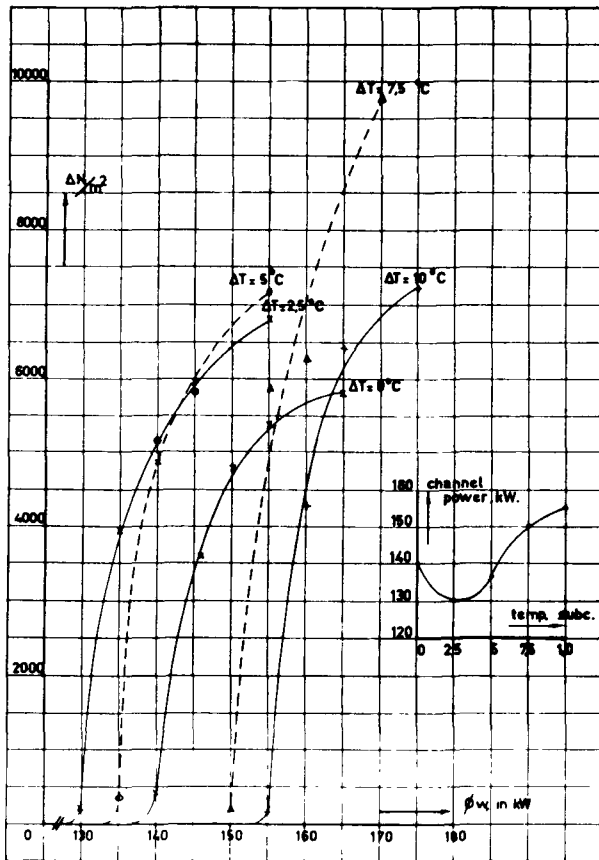


Figure 7. The root mean square values of the inlet pressure drop taken at the instability frequency, as a function of power and subcooling

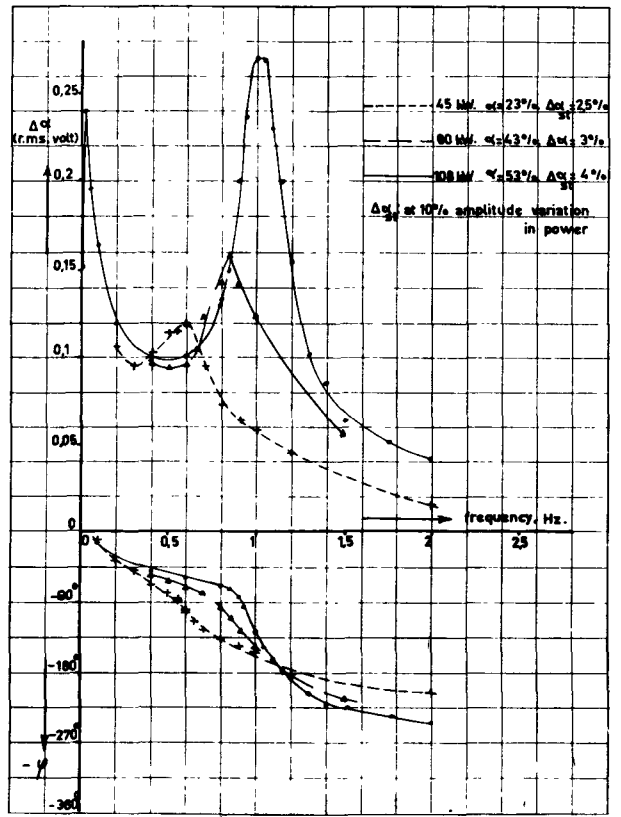


Figure 8. Measured transfer functions from power to void

charge fuel element. The inlet subcooling was varied. Local high heat fluxes to probe burn-out were obtained by the hot patch technique.

The majority of the burn-out trips occurred with the top half of the middle rod of the bundle overheating under conditions of noisy periodic flow oscillations.

An introductory series of experiments was carried out in which, due to a number of causes, no exact results were obtained. Nevertheless, a number of conclusions could be drawn from the experiments:

(a) By applying a hot patch with sharp edges, burn-out occurred at 200 °C at a channel power of 201 kW, whereas burn-out was not obtained even at a channel power of 472 kW with a streamlined hot patch. The implication of these results is that the shape of the patch influences the channel power at which burn-out occurs. It was shown that two types of burn-out could be clearly distinguished, i.e., heat flux burn-out, which occurs under stable flow conditions, and burn-out due to flow instabilities.

(b) It was found consistently that in the cases where stable flow burn-out occurred it did so at the upper of two equally-rated hot patches.

(c) At 140 °C unstable flow burn-out occurred in the lower hot patch of the outer rod and at 180 °C at the top of the heated section of the outer rod, not in the hot patch (about one-quarter of the channel upstream where the heat flux was 50% higher). This

suggests that the position of the burn-out point and the conditions under which it occurs are governed by a different mechanism than in stable flow and depend upon the dynamic characteristics of the channel.

The experiments were performed at temperatures of 140, 180, 200 and 230 °C. The series of experiments performed at 230 °C is the most complete, in that the subcooling was varied from 14 to 94 kW. In the range of low subcooling, no burn-out could be brought about due to power input limitations (600 kW), whereas at 94 kW subcooling a very sudden and extremely rapid burn-out occurred at a channel power of 550 kW.

REFERENCES

1. Hsu, S. T., and Schmidt, F. W., *Measured variations in local surface temperatures in pool boiling of water*, Paper 60-HT-32, A.M.S.E.-A.I.Ch.E. Heat Transfer Conference (1960).
2. Moore, F. D., and Messler, R. B., *The measurement of rapid surface temperature fluctuations during nucleate boiling of water*, Amer. Inst. Chem. Engineers J. 7, no. 4 (1961).
3. Semeria, R. L., *An experimental study of the characteristics of vapour bubbles*, Two-Phase Flow Symposium, London (1962).
4. Van der Walle, F., and Lamein, H. J., *On the hydrodynamic aspects of two-phase flows in vertical boilers, Part I and II*, Report WW 016-R 50 (1963).
5. Bowring, R. W., *Physical model, based on bubble detachment and calculation of steam voidage in the subcooled region of a heated channel*, Halden Project report, H.P.R. 10 (1962).

ABSTRACT—RÉSUMÉ—АННОТАЦИЯ—RESUMEN

A/589 Pays-Bas

Transfert de chaleur et stabilité hydraulique dans les réacteurs à eau bouillante

par M. Bogaardt *et al.*

Des recherches fondamentales se poursuivent actuellement au Laboratoire de transfert de chaleur et de génie nucléaire de l'Université technique d'Eindhoven sur l'échange de chaleur par formation de bulles et accroissement de la diffusivité thermique par suite de l'augmentation de la turbulence dans les couches limites.

Un modèle mathématique a été construit pour décrire la boucle de transfert de chaleur qui fonctionne sous une pression allant jusqu'à 40 atm, la puissance pouvant atteindre 600 kW et le sous-refroidissement à l'entrée 40 °C. Ce modèle est comparé avec les résultats expérimentaux fournis par la boucle.

Les conditions dans lesquelles apparaît l'instabilité d'écoulement sont examinées et la nature des instabilités dans la région allant jusqu'à la caléfaction est établie pour différentes valeurs de la pression et de la sous-saturation à l'entrée à l'aide d'une analyse des courbes de puissance spécifique.

Les caractéristiques dynamiques de la boucle sont étudiées à l'aide de l'analyse des fonctions de transfert.

La validité de la linéarisation appliquée est examinée et les fonctions de transfert obtenues sont comparées avec celles découlant de l'analyse du bruit.

Enfin, le mémoire rapporte les résultats d'une étude systématique de la caléfaction de grappes de barreaux, étude qui comprend l'analyse de l'instabilité d'écoulement qui précède la caléfaction.

A/589 Нидерланды

Теплообмен и гидравлическая стабильность в кипящих реакторах

М. Богардт *et al.*

В Лаборатории реакторной техники и процессов теплообмена Эйндховенского технологического университета ведутся фундаментальные исследования проблем отвода тепла за счет образования пузырьков и увеличения коэффициента теплопроводности вследствие увеличения турбулентности в пограничных слоях.

Построена действующая математическая модель теплопередающего контура под давлением до 40 ат, мощностью на входе до 600 кВт и разности температуры насыщения и температуры

теплоносителя на входе в реактор до 40° C. Модель сравнивается с экспериментальными результатами, полученными при эксплуатации контура.

Исследуется неустойчивость потока и характеризуется его природа в области критического теплового потока путем анализа кривых плотностей энерговыделения. В этом случае давление и недогрев в реакторе изменяются.

На основе анализа зависимостей теплообмена изучаются динамические характеристики контура. Обосновываются линейные изменения величин, получающиеся зависимости теплообмена сравниваются с зависимостями, полученными при анализе шумов.

Наконец, сообщаются результаты систематического изучения пережога пучков топливных стержней, включая анализ неустойчивости потока, предшествующего достижению критического теплового потока.

A/589 Países Bajos

Transmisión de calor y estabilidad hidráulica en reactores de agua hirviente

por M. Bogaardt *et al.*

Se están efectuando estudios fundamentales de laboratorio sobre la eliminación de calor por forma-

ción de burbujas y por aumento de la difusión térmica debida a un incremento de turbulencia en capas límites en el laboratorio de Transmisión de Calor y de Ingeniería de Reactores de la Technological University de Eindhoven.

Se ha establecido un modelo matemático del circuito de transmisión de calor que funciona a presiones de hasta 40 atm, potencias de hasta 600 kW y subenfriamientos de entrada hasta 40 °C. Los datos del modelo se comparan con los resultados obtenidos experimentalmente en el circuito.

Los autores estudian el comienzo de la inestabilidad del fluido y caracterizan la naturaleza de la misma en un intervalo que alcanza hasta el recalentamiento destructivo, analizando curvas de densidad de potencia. También en este caso varían la presión y el subenfriamiento de entrada del fluido.

Estudian las características dinámicas del circuito por análisis de funciones de transferencia. Discuten la validez de la simplificación lineal en que se basan y las funciones de transferencia resultantes se comparan con las obtenidas por análisis de ruidos.

Finalmente, la memoria informa sobre estudios sistemáticos del recalentamiento destructivo en conjuntos de barras, que incluyen el análisis de la inestabilidad del fluido que precede a aquel fenómeno.

Hydrodynamic instability and dynamic burn-out in natural circulation two-phase flow—an experimental and theoretical study

By K. M. Becker, S. Jahnberg, I. Haga, P. T. Hansson and R. P. Mathisen*

In recent years a research programme concerning the flow of steam-water mixtures in vertical heated channels has been in progress at AB Atomenergi in Sweden. During the first phases of this programme the steady forced circulation flow was studied, and measurements of pressure drop, void fractions, heat transfer coefficients and burn-out have been presented in a series of reports [1-6].

However, it has been observed by many investigators that strong hydrodynamic oscillations may under certain conditions develop in boiling loops. These oscillations may reduce the burn-out values considerably compared to conditions in steady flow. In nuclear boiling reactors such oscillations may also influence the total void volume and therefore the reactivity. The oscillations occur more readily under natural circulation than for forced circulation, and information permitting prediction of the onset of flow instabilities in the fuel elements, the nature of the flow and the burn-out conditions during oscillatory behaviour of the system are therefore of particular importance for the designer of boiling reactors with natural circulation.

A study of the flow in vertical heated channels during natural circulation was therefore included in our research programme. During this study both analytical and experimental techniques were used. The method of tackling the problem experimentally was to simulate the reactor fuel element by means of test sections which were electrically heated. It is desirable to carry out full-scale experiments, but since such experiments would be very time-consuming and difficult to analyze or interpret, it was decided to start the investigation by studying the flow in channels of the most simple geometry, such as round ducts, with the purpose of determining the influence on stability and dynamic burn-out of such basic parameters as static pressure, inlet subcooling, surface heat flux, mass velocity, test section diam, heated length and inlet and outlet throttling. However, a loop for studying full-scale rod clusters will soon be in operation. Theoretically, the problem has been approached by considering the basic conservation laws of energy, mass and momentum in one-dimensional form, and

reducing these equations to a set of partial differential equations which was possible to solve numerically by means of a Ferranti Mercury digital computer. One should note, however, that an important physical difference exists between a loop experiment and the conditions encountered in a reactor. When the flow oscillates in the reactor, the steam void fraction and the reactivity of the system become time dependent. The change of reactivity influences the power which again influences the void fraction. In the present analytical and experimental study this interaction between void fraction and power has been neglected as well as the hydrodynamic interaction between different channels.

One-dimensional analysis for onset of instability for two-phase flow in vertical heated channels

Basic equations and boundary conditions

For the present analysis one-dimensional flow is assumed. This implies that all radial gradients are neglected, and the conservation laws for mass, energy and momentum then become

Continuity equation

$$\frac{\partial}{\partial t} [\rho_f(1 - \alpha) + \rho_g\alpha] + \frac{\partial}{\partial z} [\rho_f v_f(1 - \alpha) + \rho_g v_g\alpha] = 0 \quad (1)$$

Energy equation

$$\frac{\partial}{\partial t} [\rho_f e_f(1 - \alpha) + \rho_g e_g\alpha] + \frac{\partial}{\partial z} [\rho_f v_f h_f(1 - \alpha) + \rho_g v_g h_g\alpha] = \frac{q_L}{F} \quad (2)$$

Momentum equation

$$\frac{\partial}{\partial t} [\rho_f v_f(1 - \alpha) + \rho_g v_g\alpha] + \frac{\partial}{\partial z} [\rho_f v_f^2(1 - \alpha) + \rho_g v_g^2\alpha] + \frac{\partial p}{\partial z} + g[\rho_f(1 - \alpha) + \rho_g\alpha] + \left(\frac{\partial p}{\partial z}\right)_0 \phi^2 = 0 \quad (3)$$

In addition to Eqs. (1, 2 and 3) two more equations are needed in order to describe the system completely

* AB Atomenergi, Stockholm and Studsvik.

† The nomenclature is found in [12] and [13].

in the two-phase flow region. These equations concern the multiplier, ϕ^2 , for computing the two-phase flow friction pressure gradient, and the relation between the void fraction, α , and the steam quality x . At present only empirical correlations based on experimental results are available. For the two-phase flow friction multiplier two correlations were used. The first was the Martinelli and Nelson [7] correlation, which was put in the mathematical form [8]

$$\phi^2 = 1 + ax^b \quad (4)$$

where a and b are functions of pressure only.

$$a = \frac{3\,900 - 19.6p}{6.75 + p} \quad b = 1.025 - 1.74 \times 10^{-3}p \quad (5)$$

The other was the correlation by Becker *et al.* [1]

$$\phi^2 = 1 + 2\,400 \left(\frac{x}{p}\right)^{0.96} \quad (6)$$

Also for computing the relation between void fraction and steam quality, two different correlations were used. The first was based on Martinelli and Nelson's results, which according to reference [8] can be expressed by an equation for the slip ratio

$$S = (1 + cx^3) \left(0.795 + 0.410 \frac{\rho_f}{w}\right) \quad (7)$$

where c is a pressure dependent parameter.

The other void fraction correlation was based on the momentum model by Levy [9], which in order to obtain a better agreement with experimental results was modified as described in reference [10].

Boundary condition

The boundary condition for Eqs. (1–3) is obtained by integrating the pressure drop over the heated channel

$$\Delta p = - \int_0^L \frac{\partial p}{\partial z} dz \quad (8)$$

Two cases leading to two versions of the flow model were considered.

Case 1

The pressure difference over the heated channel including inlet and outlet losses is prescribed and the boundary condition then becomes

$$\Delta p_0 = - \int_0^L \frac{\partial p}{\partial z} dz + \Delta p_{in} + \Delta p_{ce} \quad (9)$$

This version of the model is similar to the stability problem studied by Quandt [11].

Case 2

A complete natural circulation loop, including riser, steam separator, and downcomer will now be considered, and the boundary condition becomes

$$- \int_0^L \frac{\partial p}{\partial z} dz + \Delta p_{ce} - \int_L^{L+L_r} \frac{\partial p}{\partial z} dz + \Delta p_{re} + \Delta p_{in} = \Delta p_d \quad (10)$$

It can be shown that the pressure drop over the channel as well as the other pressure differences in Eq. (9) or (10) can be expressed in terms of inlet water acceleration, $\dot{v}_0(t)$, and properties describing the instantaneous state in the loop. Equation (9) or (10) will then give an explicit equation for $\dot{v}_0(t)$, which together with the continuity equation can be solved numerically.

The analysis is based upon the following assumptions:

(a) The pressure drop along the channel is small compared with the mean system pressure;

(b) The inlet fluid temperature is constant;

(c) The effect of subcooled boiling is neglected except for a small correction, which is applied to the frictional pressure drop in the nonboiling region as described in reference [10].

Assumption (a) permits the use of space and time independent values for density, internal energy and enthalpy for both phases of the fluid.

Assumption (b) is permissible if the transport time through the downcomer is large compared with the time constant associated with the instability.

Treatment of equations

The integration of the pressure gradient over the heated channel, using Eqs. (1)–(3), yields

$$- \int_0^L \frac{\partial p}{\partial z} dz = a_1(t) \frac{dv_0}{dt} + a_2(t) \quad (11)$$

where the details of the analysis and $a_1(t)$ and $a_2(t)$ are given in reference [12].

Calculating the pressure differences over the outer loop and applying the boundary condition, Eq. (9) or (10), one obtains:

$$- \int_0^L \frac{\partial p}{\partial z} dz = b_1(t) \cdot \frac{dv_0}{dt} + b_2(t) \quad (12)$$

The functions $b_1(t)$ and $b_2(t)$, which contain the inlet and outlet pressure losses, will be different for the two cases represented by Eqs. (9) and (10). For details of the calculation refer to [12].

Summary of differential equations

From Eqs. (11) and (12) the following expression is obtained for the inlet acceleration

$$\frac{dv_0}{dt} = \frac{b_2(t) - a_2(t)}{a_1(t) - b_1(t)} \quad (13)$$

Equation (13) together with the continuity equation

$$\frac{\partial \alpha}{\partial t} = \frac{1}{\rho_l - \rho_g} \cdot \frac{\partial w}{\partial z} \quad (14)$$

describes the transient flow in the loop. The equations can be solved numerically when initial conditions for the variables are known.

Initial conditions

As initial conditions for Eqs. (13) and (14), the steady state solution was chosen. This solution was

obtained from the same set of equations, neglecting all time derivatives and using an iterative method. Starting with an assumed value for v_0 , the pressure drops for the heated channel and the outer part of the loop were calculated. If the pressure balance was not satisfactory, a new value for v_0 was chosen and the procedure was repeated until a sufficient accuracy for the pressure drop balance was obtained.

Numerical solution of differential equations

The system of partial differential equations was solved numerically by a simple finite difference technique for both space and time co-ordinates, using a Ferranti Mercury digital computer.

The first sequence of the computer programme concerns the steady state flow. Utilizing this sequence a series of calculations was performed for different values of the heat input, but at fixed values for the pressure, inlet subcooling and liquid level. This enabled us to establish curves for the mass flow rate versus the power input. Then the transient flow response caused by a step increase of 1 per cent in $q_L(z, t)$ was calculated. Considering the inlet velocity, it appeared that the response was a transient with large oscillations. If the oscillation diverged the initial steady flow condition in the loop was considered unstable and if the oscillation decayed the initial flow was considered stable. Flow transients were calculated for some values of the power input, and the stability limit was determined as that power input where the oscillation in inlet velocity changed from decreasing to increasing amplitude.

Concerning the spatial variation of $q_L(z, t)$ there are at present two versions of the programme, one with $q_L(z, t)$ constant along the channel length, and one where $q_L(z, t)$ can be given a 3-step variation over the channel length, each of arbitrary length and magnitude.

Apparatus

The loop was designed for an operating pressure of 70 atg and constructed of stainless steel. The flowsheet of the loop is shown in Fig. 1 and for the details of the loop and its exact dimensions we refer to a previous report [13].

The test sections were 20, 30 and 36 mm inner diam stainless steel ducts and the heated lengths were 4 890 mm for the 20 and 36 mm ducts, and 4 420 mm for the remaining duct.

Instrumentation

The following quantities were measured:

- (a) Static pressure
- (b) Pressure drop over test section
- (c) Inlet and outlet water temperatures
- (d) Power input
- (e) Mass flow rate
- (f) Liquid level in the steam separator
- (g) Wall temperatures at 16 axial positions of the test section
- (h) Pressure drop over the throttle valve.

In order to determine the burn-out conditions, two burn-out detectors were installed. Concerning the details of the instrumentation we refer to reference [13].

Experimental procedures

Before starting a run, the loop was completely filled with desalinated water, and all ducts connecting instruments to the loop were degassed. Then a small amount of power was supplied to the test section. After noting the observations the power was slightly increased, and after about 15 min thermal equilibrium was obtained so that a new set of readings could be taken. As the power increased, the flow reached a maximum and then decreased. Ultimately the power reached a value where the flow became unstable and started to oscillate. Three cases are actually possible:

- (a) Diverging oscillations causing burn-out;
- (b) Stable oscillations;
- (c) Burn-out without oscillations.

In the second case, the amplitude of the oscillations increases, if one continues to increase the power, and burn-out will finally be obtained. In the third case, the flow is completely stable until burn-out is obtained, and one would expect the burn-out values to be identical with values obtained during steady state forced circulation.

Research programme and range of variables

An examination of the problem revealed that for a fixed geometry of the loop and the test section the critical power could be defined by the function

$$(q/A)_{Cr} = f(p, \Delta T_{sub}, H) \quad (15)$$

The mass velocity, m/F , and the steam quality x are not included since these parameters are determined when the parameters in Eq. (15) are fixed. In addition to the parameters in Eq. (15) it was decided also to study the effects of the test section diam and the effects of changing the geometry of the loop. The geometrical changes employed were throttling of the flow before or after the test section. The performance of the loop permitted the static pressure to be varied between 10 and 70 atm(g) the inlet subcooling between 2 and 16 °C and the liquid level between 5 635 and 5 935 mm above the reference level. Throttling of the flow before the test section was achieved by means of the throttle valve in the downcomer. Five positions of this valve were employed. Throttling of the flow after the test section was obtained by reducing the number of 8.2 mm holes in the riser exit—2, 3, 4 and 96 holes were used. In addition, a few runs were made with both inlet and outlet throttling. In order to reduce the number of runs, the effects of inlet subcooling, liquid level and throttling were only studied at a pressure of 50 atm (g) using the 20 mm test section. The total research programme consisted then of 39 runs.

Experimental results

The effects of pressure, inlet subcooling, liquid level, inlet throttling, outlet throttling and diameter were

Table I. Measured flow conditions at onset of instability and burn-out

Run No.	d mm	L_H mm	H mm	P atm(g)	ΔT_{sub} $^{\circ}\text{C}$	ζ_1	F_0/F	$(\dot{m}/F)_{C_r}$ kg/m ² s	$(Q/V)_{C_r}$ kW/l	x_{C_r}	$(\dot{m}/F)_{B_0}$ kg/m ² s	$(q/A)_{B_0}$ W/cm ²	x_{B_0}
1	20	4 890	5 835	10	50	0.55*	16.15	860	41.6	10.8	—	42.0	—
2	20	4 890	5 835	20	4.1	0.60*	16.15	885	61.6	17.1	500.00	51.5	52.6
3	20	4 890	5 835	30	3.2	0.65*	16.15	735	96.8	35.2	563.0	58.8	56.2
4	20	4 890	5 835	40	2.8	0.75*	16.15	725	120.0	46.5	630.0	67.0	60.0
5	20	4 890	5 835	50	2.1	0.80*	16.15	735	146.0	58.6	732.0	75.7	60.9
6	20	4 890	5 835	60	2.2	0.70*	16.15	812	158.0	57.3	805.0	80.5	61.4
7	20	4 890	5 835	70	2.4	0.65*	16.15	901	157.0	51.4	900.0	79.0	51.7
8	20	4 890	5 835	50	7.2	0.80*	16.15	856	121.0	40.0	796.0	67.5	48.4
9	20	4 890	5 835	50	11.0	0.80*	16.15	1 025	83.8	20.5	835.0	637.0	42.4
10	20	4 890	5 835	50	16.0	0.80*	16.15	1 140	68.0	13.1	910.0	57.2	32.8
11	20	4 890	5 635	50	2.0	0.80*	16.15	706	146.0	62.3	694.0	74.6	63.5
12	20	4 890	5 735	50	1.9	0.80*	16.15	732	146.0	58.9	720.0	75.0	61.6
13	20	4 890	5 935	50	2.0	0.80*	16.15	770	146.0	56.0	751.0	76.1	59.8
14	20	4 890	5 835	50	2.0	1.25	16.15	716	151.0	62.3	707.0	78.3	65.5
15	20	4 890	5 835	50	2.2	8.00	16.15	—	—	—	637.0	76.9	71.4
16	20	4 890	5 835	50	2.4	21.25	16.15	—	—	—	570.0	73.7	76.4
17	20	4 890	5 835	50	3.3	60.0	16.15	—	—	—	461.0	63.5	81.2
18	20	4 890	5 835	50	11.0	2.85	16.15	770.0	130.0	47.1	735.0	70.1	53.5
19	20	4 890	5 835	50	11.0	6.75	16.15	675.0	144.2	60.5	660.0	75.8	65.3
20	20	4 890	5 835	50	11.0	15.5	16.15	—	—	—	600.0	74.4	70.7
21	20	4 890	5 835	50	11.0	—	16.15	—	—	—	505.0	69.4	78.7
22	20	4 890	5 835	50	3.1	0.80*	0.655	582	97.6	49.1	459.0	61.0	78.2
23	20	4 890	5 835	50	3.0	0.80*	0.492	529	77.6	43.0	378.0	52.8	82.3
24	20	4 890	5 835	50	3.2	0.80*	0.328	615	21.8	9.6	395.0	32.3	47.9
25	30	4 420	5 365	10	10	0.59*	11.84	1 230	36.0	4.3	820.0	54.6	17.4
26	30	4 420	5 365	20	10	0.59*	11.84	1 025	80.0	15.9	820.0	80.9	29.3
27	30	4 420	5 365	30	10	0.66*	11.84	875	124.0	32.5	770.0	104.4	42.0
28	30	4 420	5 365	40	10	0.75*	11.84	843	160.5	—	823.0	124.7	49.4
29	30	4 420	5 365	50	10	0.80*	11.84	880	174.0	49.4	870.0	132.4	51.8
30	30	4 420	5 365	60	10	0.70*	11.84	Stable	Stable	Stable	952.0	132.0	48.7
31	30	4 420	5 365	50	10	5.0	11.84	—	—	—	825.0	133.1	55.0
32	30	4 420	5 365	50	10	11.2	11.84	—	—	—	760.0	131.4	59.1
33	30	4 420	5 365	50	10	69.0	11.84	—	—	—	565.0	111.0	67.5
34	36	4 890	5 835	10	8	1.18*	5.0	940.0	44.2	9.5	725.0	54.3	18.4
35	36	4 890	5 835	20	8	1.22*	5.0	770.0	89.4	28.4	755.0	84.1	30.3
36	36	4 890	5 835	30	7.9	1.37*	5.0	760.0	115.5	39.7	755.0	105.9	40.9
37	36	4 890	5 835	30	1.8	1.37*	5.0	**	**	**	836.0	115.5	31.2
38	36	4 890	5 835	30	4.0	1.37*	5.0	**	**	**	769.0	128.2	37.1
39	36	4 890	5 835	50	8	120.0	5.0	**	**	**	512.0	138.4	65.2

* Throttle valve fully open.

** Not recorded owing to instrumentation failure.

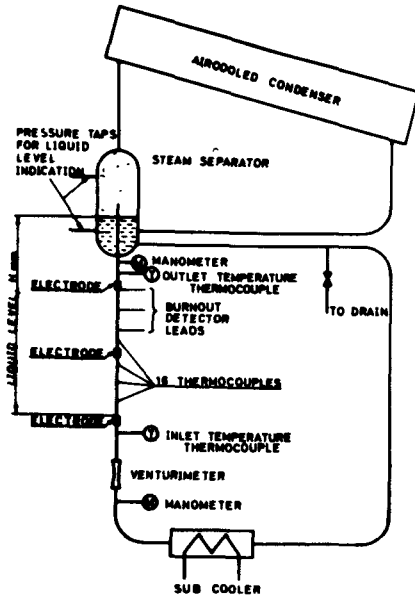


Figure 1. Flow diagram

studied separately, one of the parameters being varied, the remaining being kept constant. The major portion of the experimental programme was carried out using the 20 mm diam test section and in the following discussion the results concern this duct, unless otherwise stated. The measured flow conditions at the onset of instability and burn-out are given in Table 1.

Effect of pressure

The effect of pressure was studied regarding the case where the inlet subcooling was approximately 2°C, and where the liquid surface was 5 835 mm above the reference level. The results are shown in Fig. 2, where the measured mass velocities are plotted versus the surface heat flux. The power density, or the power per litre test section, is also indicated along the horizontal axis, since perhaps this parameter is of greater significance for the stability than the surface heat flux. The end point on each curve represents the last measurement of the series. A further increase of

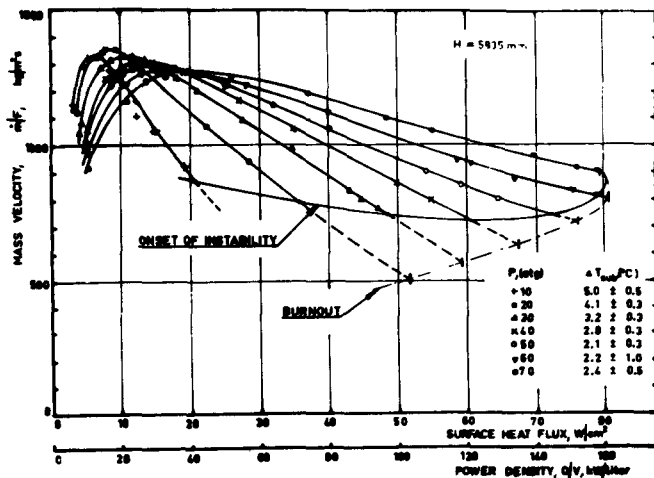


Figure 2. Effect of pressure

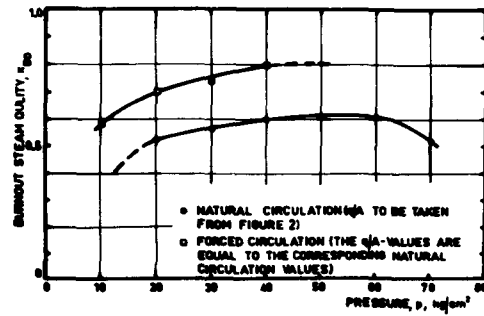


Figure 3. Comparison between natural and forced circulation burn-out data

the power caused the burn-out detector to react, indicating that burn-out conditions had been obtained in the test section. Curves representing the threshold of instability and the burn-out values are also given. Concerning the measurement of mass velocity after the onset of instability, there may be slight errors in the measured values, owing to the effects of fluid acceleration on the venturimeter readings. Only dotted curves are therefore shown in the oscillating flow regime.

It is observed that as the pressure increases, the threshold of instability increases and approaches the burn-out curve with which it coincides at approximately 65 atm(g). For higher pressures, burn-out is obtained direct without the flow passing through the oscillating regime. Further, one observes that the burn-out heat flux has a maximum value at a pressure of 65 atg. This is in agreement with the available information for steady state forced convection burn-out, where the maximum heat flux occurs at a pressure of between 40 and 75 atm(g) [14].

In order to compare the measured burn-out values with forced circulation burn-out conditions, the 20 mm test section was, on completion of the measurements, mounted in a forced circulation loop. This loop had a pump with a pressure head of 8 atg. It was therefore possible to apply heavy throttling of the flow before the test section, securing as far as one could detect stable operation of the loop. Unfortunately, the

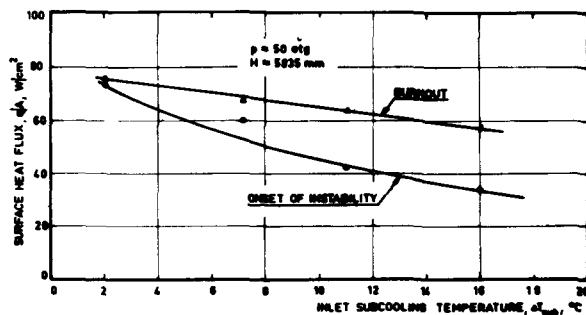


Figure 4. Effect of inlet subcooling on critical and burn-out heat fluxes

forced circulation loop had only a maximum operating pressure of 40 atg, so that the comparison could only be established up to this pressure.

The comparison in question is given in Fig. 3 in terms of the burn-out steam qualities. One should note that the forced circulation burn-out qualities were obtained by extrapolating from the measurements to the same heat fluxes as the natural circulation data. The comparison reveals that the forced circulation data are higher by a factor of about 1.3. It would have been of great interest to extend the forced circulation runs to 70 atm(g) where no flow oscillations were observed in the natural circulation loop. Such runs are now planned in our laboratory using a recently built high pressure loop.

Effect of inlet subcooling

The effect of inlet subcooling was studied at a pressure of 50 atg and a liquid level, H , of 5 835 mm in the steam separator. In Fig. 4 the heat fluxes at the onset of oscillations and at burn-out are plotted versus the inlet subcooling. It is observed that the stability of the flow is strongly reduced as the inlet subcooling increases. At 16 °C inlet subcooling a critical heat flux of 34 W/cm² was obtained compared with 73 W/cm² at 2 °C subcooling.

However, at very great subcooling temperatures it is possible that the critical power will start to increase with a further increase of the inlet subcooling, since a relatively large portion of the power is then used for just heating the water up to the saturation temperature. This behaviour is demonstrated in Fig. 5, where the critical power density at a pressure of 50 atm(g) is plotted versus the inlet subcooling. In the figure are also included the data obtained at 164 °C and 244 °C inlet subcooling with a 10 mm diam test section. These data were obtained during an earlier phase of the investigation before the steam separator was installed and have been discussed in reference [13]. A very large increase of the critical power density is observed at the highest subcoolings so that the value obtained at 244 °C inlet subcooling, is actually higher than the value corresponding to 2 °C subcooling. Our loop is now being modified so that the flow in the whole range of subcooling temperatures can be studied.

Effect of liquid level

The effect of the liquid level in the steam separator was studied in the case of 2.0 °C inlet subcooling and 50 atm(g) pressure. The maximum possible variation was 300 mm, and since this value is small compared with the length of the test section with the riser, only small variations of the measured critical and burn-out heat fluxes could be expected. The conclusions reached should therefore be treated with caution.

As shown in Fig. 17 of Ref. [13] we found that the burn-out heat flux increases slightly with increasing liquid level, while the critical heat flux remained constant. The corresponding critical steam qualities, however, decreased from 0.61 to 0.52 as the liquid level was changed from 5 635 mm to 5 935 mm.

Effect of inlet throttling

The effect of throttling before the test section was studied in respect of 50 atg pressure, 5 835 mm liquid level and ≈ 2.0 °C and ≈ 11.0 °C respectively inlet subcooling. The throttling of the flow through the throttle valve is indicated by means of the ζ_i -values for the throttle valve defined by the equation

$$\Delta p_i = \zeta_i \rho_f \frac{v^2}{2} \quad (16)$$

where v is the velocity of saturated water through the test section. The results obtained for 11 °C inlet subcooling are shown in Fig. 6.

It can be observed that as the throttling increases, the stability of the loop also increases and finally the flow is so stable that burn-out is obtained direct without preceding flow oscillations. With regard to the burn-out heat fluxes, these also increase with increasing inlet throttling until they reach a maximum whereafter they decrease with further throttling owing to the high steam qualities which are now encountered in the test section. This is more clearly demonstrated in Fig. 7, where the burn-out steam qualities are plotted versus the inlet throttling. The corresponding values for forced circulation are also indicated in the figure. The forced circulation points were obtained by extrapolation to 50 atm(g) from the measured values, which were obtained between 10 and 40 atm(g). As the pressure drop over the throttle valve increases, the measured burn-out steam qualities rapidly approach the values for forced circulation, indicating the absence of flow instabilities.

Effect of outlet throttling

The outlet throttling was varied by changing the number of 8.2 mm holes at the end of the riser. We found that as the outlet throttling increased, the critical and burn-out heat fluxes decreased, indicating that outlet throttling renders the flow more unstable. For the details of these results see Ref. [13].

Effect of test section diameter

The measurement with the 30 mm and 36 mm diam test section will only be discussed briefly, and as regards the details of these runs we refer to a report by Mathisen *et al.* [15].

Figure 8 shows the results of studying the effects of pressure, using the 30 mm test section. Generally, the curves reveal the same characteristic shapes as the curves for the 20 mm duct previously shown in Fig. 2. Owing to differences in heated length, inlet subcooling and the fact that the throttling effect of the outer loop is relatively greater when a 30 mm test section is used, a satisfactory quantitative comparison between the two sets of data cannot be established. Corresponding data obtained with the 36 mm test section are given in Fig. 9. A comparison between two sets of data obtained with the 20 and 36 mm ducts at almost identical values for the pressure, inlet subcooling and liquid level is presented in Fig. 10. The flow in the

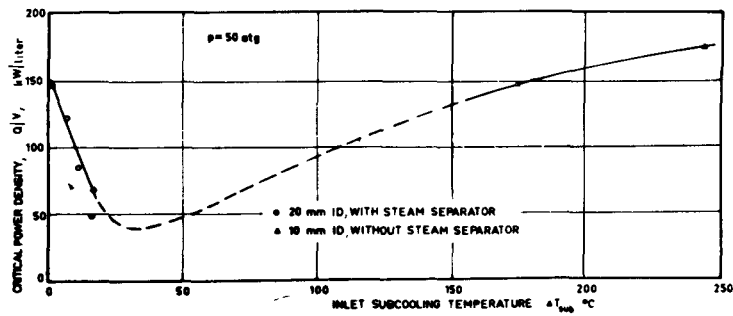


Figure 5. Effect of inlet subcooling on critical power density

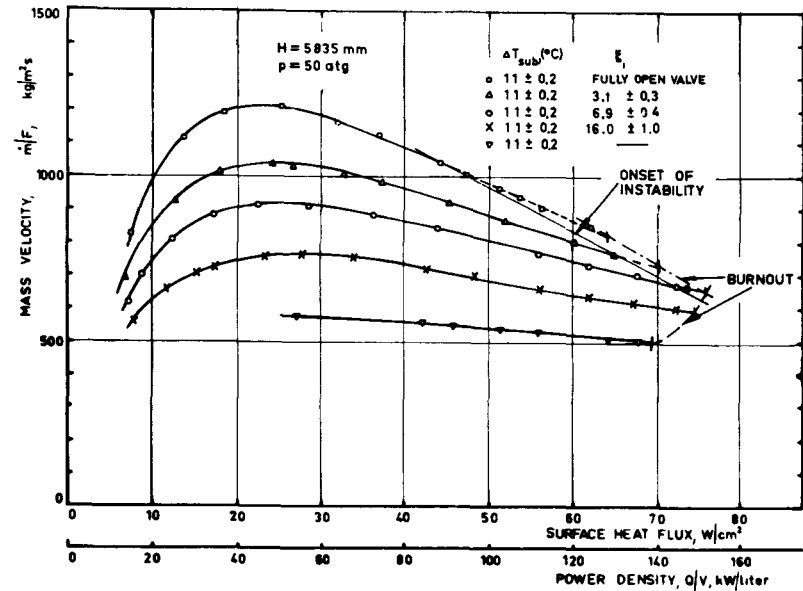


Figure 6. Effect of inlet throttling

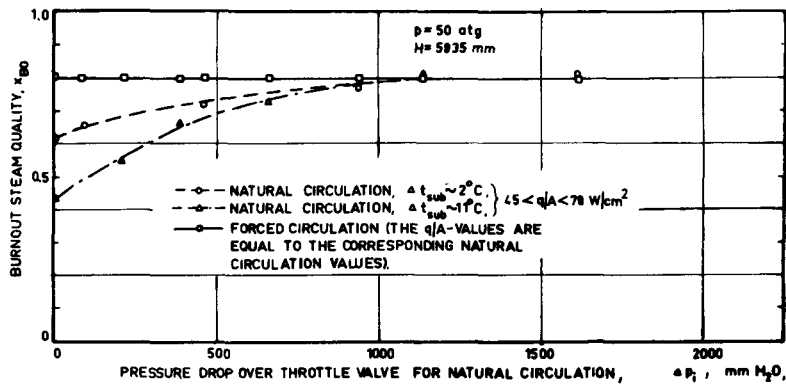


Figure 7. Effect of inlet throttling on burn-out

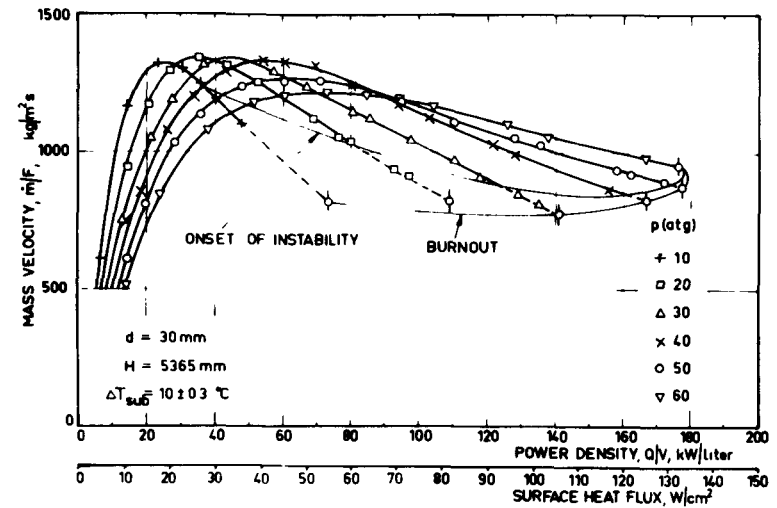


Figure 8. Effect of pressure

20 mm duct became unstable at a power density of 122 kW/l, while the flow in the 36 mm duct was still stable at a power density of 135 kW/l, which corresponded to the maximum possible operating power for the loop, or 675 kW. The theoretical value for the onset of instability, computed by means of analysis was in this case 154 kW/l. This seems to indicate that the stable power density increases with an increasing diam. However, this conclusion needs further experimental verification, since in the two cases, the relative effect of the throttling of the flow in the outer loop was different, a fact which may have helped to stabilize the flow in the 36 mm test section. Analytically, this diam effect was verified by means of the model previously presented.

Comparison between experimental and theoretical results

The experimental results described previously have been valuable in checking the theoretical flow model. Until now 12 cases of the measurements have been analyzed.

Figure 11 shows a comparison between the predicted and the measured mass velocities for the case of 2 °C inlet subcooling and no throttling. In the pressure range of 20 to 50 atm(g) the agreement between theoretical and measured mass velocities is rather good, the discrepancy being a maximum of 10 per cent and on the average only 3–4 per cent. For 10 atm(g) the theoretical values are about 15 per cent higher than those measured, but at 70 atm(g) the theoretical are about 15 per cent lower. The measured and the predicted thresholds of instability are also indicated in the figure. One should note that in the case of 70 atm(g), burn-out was obtained without any oscillations being observed. In this case the analysis predicts stable flow up to a steam quality of 1.0.

In Fig. 12 a summary of the experimental results is compared with the analysis. The data by Quandt [11] and by Spigt *et al.* for an annulus [16] and a 7-rod cluster [17] are also included. The present measurements and Quandt's data are in excellent agreement with the predictions, the deviations being less than 10 per cent. Spigt's data also agree reasonably with the analysis showing deviations up to 35 per cent. These deviations may perhaps be due to the pressure drop over the middle spacer in the test section, which was quite significant and had, for mathematical purposes, to be distributed uniformly along the test section when the theoretical model was applied.

Application to boiling heavy water reactors (BHWs)

In the present section the previously described analytical and experimental results will be applied to the assessment of the boiling channels in BHWs. One should then bear in mind that the present results were obtained for uniform power distribution, whereas in a reactor the power varies along the channel. Applying the theoretical model to the non-uniform case indicates that the shape of the power distribution along the channel may have a significant effect on the stability.

However, this has not yet been verified experimentally. Further, the knowledge about the effects of cross-section geometry cannot be considered sufficient for accurate predictions of the flow stability in fuel elements consisting of a large number of rods. The conclusions obtained in the present section should therefore be taken with caution.

The power output of the boiling channels in BHWs can be limited by one of the following four criteria.

- (a) Dynamic burn-out caused by hydrodynamic oscillations;
- (b) Static burn-out caused by excessive heat flux;
- (c) Void reactivity feed back instability;
- (d) Excessive UO_2 temperatures.

The first three of these criteria are affected by the problems discussed in this paper.

With regard to (a) the available experimental results are considered to give appreciable support to the theoretical model. When applying the model to reactor calculations, the pressure loss due to inertial damping in the downcomer is neglected, since this term is small when only one oscillating channel is considered. Since the model in the case of axially uniform heat flux distribution has given good agreement with experiments for round ducts, with lengths and hydraulic diameters typical for BHWs, as well as an annulus and a rod cluster, it is assumed to give reasonable results for the multi rod cluster fuel elements for BHWs. The model, however, predicts the instability threshold only and the additional power margin to burn-out is at present discounted. This may be a conservative approach since, due to larger nuclear fuel time constants a larger difference between the instability threshold and dynamic burn-out may exist in reactors than in loop experiments.

The void reactivity feedback problem is presently being treated in Sweden with models in which simplified versions of the model described in this paper are used to represent the hydraulic part of the problem, and the reactivity feed back is added. Later, the more complete hydraulics will be included in a new model.

By varying one parameter such as, for instance, the inlet throttling, the criteria determining the power limitation may change from dynamic burn-out to static burn-out. A detailed understanding of both phenomena is therefore essential, and a good design should allow the same safety margin with respect to both criteria.

The problem of static burn-out has been studied experimentally. This study comprised burn-out measurements in round ducts, annuli, 3-rod and 7-rod clusters, and with regard to the results refer to [3, 4, 5 and 18].

Influence of inlet throttling

Increasing the inlet throttling in the natural circulation loop at constant inlet subcooling, ΔT_{sub} , resulted in a gradual increase of the instability threshold and dynamic burn-out limit, until eventually

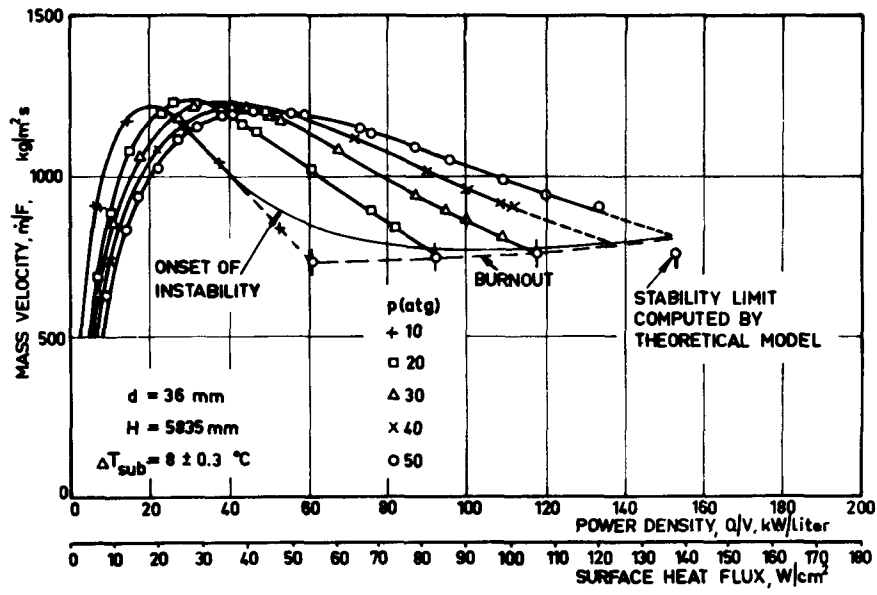


Figure 9. Effect of pressure

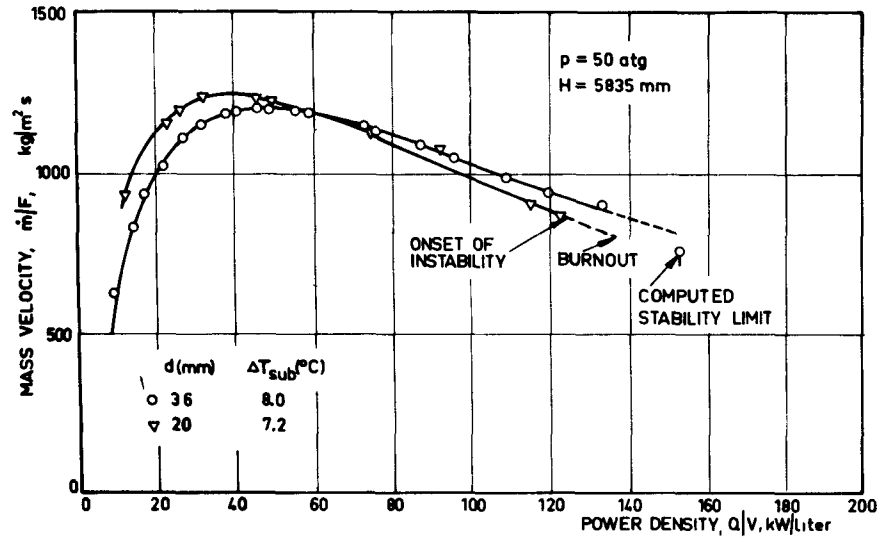


Figure 10. Effect of diameter

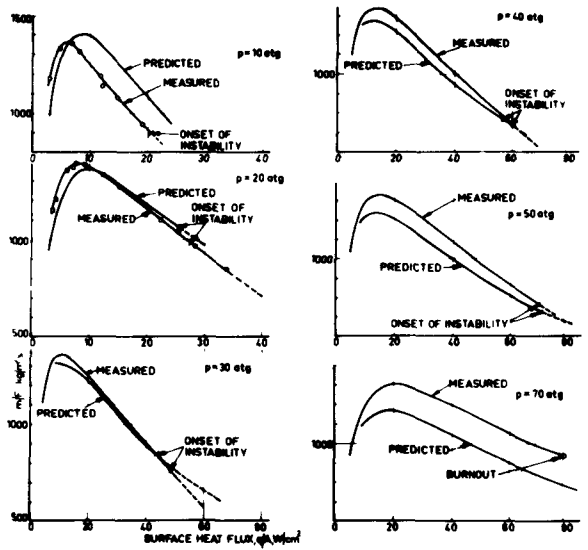


Figure 11. Comparison between analytical and experimental results

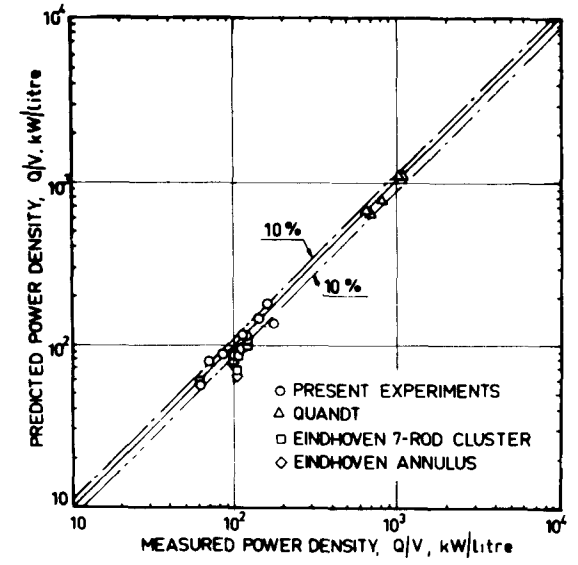


Figure 12. Comparison between measured and predicted critical power densities

the curves evened out and decreased slightly for the highest inlet throttlings applied. The burn-out curve for the same tube tested in forced circulation with large inlet throttling has a slight negative slope for the same range of mass velocities and steam qualities as the natural circulation experiment and gives eventually a point of intersection with the dynamic burn-out curve. It is therefore possible to make the two design criteria coincide by selecting an appropriate value for the inlet throttling. The reason for the nearly flat shape of the static burn-out curve when the flow is throttled is the fact that the decrease in burn-out flux resulting from an increase in quality is almost compensated by the increase in burn-out heat flux with decreasing velocity. For typical BHWs operating with a given feed water temperature, the degree of subcooling is also affected slightly by quality in accordance with the heat balance equations: $\dot{m}T_{tw}x + \dot{m}T_{sat}(1-x) = \dot{m}T_{in}$, thus

$$\Delta T_{sub} = x(T_{sat} - T_{tw}) \quad (17)$$

and this produces slightly larger variations in velocity for a given variation in quality, thus compensating to a still greater degree for the influence of quality. Under these conditions, the static burn-out flux is practically independent of quality over the range of practical interest. These conclusions are based on both the burn-out correlation by Becker and Persson [5] and the correlation by Macbeth [19]. An example on the importance of the inlet throttling for the design of reactor fuel elements is presented in Fig. 13, where for different values of the inlet throttling, the predicted mass velocities in a Marviken fuel element [20] are plotted versus the power. The intersection between the stability and the static burn-out curve gives a good indication about the magnitude of the inlet throttling, which is reasonable to apply.

Influence of equivalent heated diameter

According to the previously presented analytical and experimental results, the critical power density at given values for ΔT_{sub} and p increases slightly with an increase in the equivalent heated diameter, D_e , which is based on the heated part of the perimeter only. For a given cluster, with a certain number of rods, an increase in the rod spacing with the corresponding increase in shroud diameter would thus increase the stable channel power more than that proportional to D_e . An increase in D_e for constant x_{re} and \dot{m}/F is found to reduce the static burn-out heat flux according to both Swedish and American data. On the other hand, an increase in D_e under natural circulation would also produce a reduction in x_{re} whilst \dot{m}/F would not, according to the present measurements, be affected significantly. Analysing the influence of these changes on the static burn-out heat flux, it is found that the various factors almost exactly cancel over the range of interest. The static burn-out flux plotted against D_e for a given core height and number and diameter of rods gives thus a practically horizontal curve. Since the dynamic power limit increases with D_e , a point of intersection between the two limits can be found.

The equivalent heated diameter is therefore a valuable design parameter which together with the inlet throttling enables the engineers to design the reactor with the same safety margins against dynamic and static burn-out.

Influence of channel length

The analytical model indicates that a decrease in the boiling channel length increases the critical power density. For a predetermined reactor power and volume, a reduction in channel length also reduces $\dot{m}/F \times x_{re}$. Since the static burn-out heat flux is mainly a function of $\dot{m}/F \cdot x_{re}$ a reduction in channel length will increase the static burn-out heat flux.

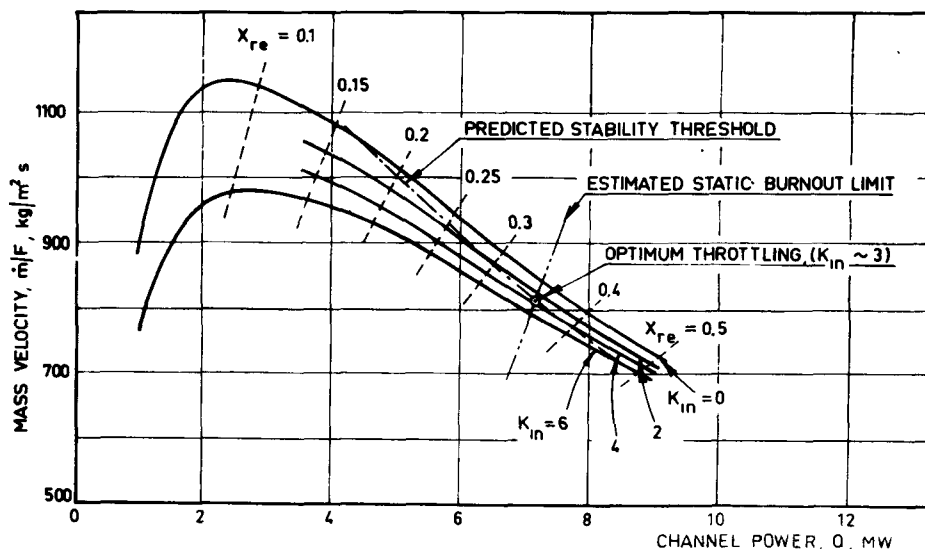


Figure 13. Effect of throttling in a Marviken boiling channel

However, the gain in power density is obtained at the expense of increased reactor vessel diameter and increased neutron leakage.

REFERENCES

1. Becker, K. M., Hernborg, G., and Bode, M., *An Experimental Study of Pressure Gradients for Flow of Boiling Water in a Vertical Round Duct* (Part 1, 2, 3 and 4), reports AE-69, AE-70, AE-85 and AE-86, AB Atomenergi, Stockholm (April 1961 to September 1962).
2. Rouhani, S. Z., and Becker, K. M., *Measurements of Void Fractions for Flow of Boiling Heavy Water in a Vertical Round Duct*, report AE-108, AB Atomenergi, Studsvik (February 1963).
3. Becker, K. M., et al., *Measurements of Burn-out Conditions for Flow of Boiling Water in Vertical Round Ducts* (Part 1 and 2), reports AE-87 and AE-114 (May 1963), AB Atomenergi, Studsvik (September 1962).
4. Becker, K. M., and Hernborg, G., *Measurements of Burn-out Conditions for Flow of Boiling Water in a Vertical Annulus*, ASME Paper No. 63-HT-25 (August 1963).
5. Becker, K. M., and Persson, P., *An Analysis of Burn-out Conditions for Flow of Boiling Water in Vertical Round Ducts*, ASME Paper No. 63-WA-51 (November 1963).
6. Becker, K. M., *Burn-out Conditions for Flow of Boiling Water in Vertical Rod Clusters*, Amer. Inst. Chem. Eng. Journal (March 1963).
7. Martinelli, R. C., and Nelson, D. B., *Prediction of Pressure Drop during Forced Circulation Boiling of Water*, Trans. ASME, Vol. 70, p. 695 (1948).
8. Lange, H., and Steinman, O., *Calculation of Pressure Drop in Ducts and Fuel Elements with Shroud*, report IPV-19, AB Atomenergi, Stockholm (1960).
9. Levy, S., *Steam Slip—Theoretical Prediction from Momentum Model*, Journal of Heat Transfer (May 1960).
10. Jahnberg, S., *Transients in Two-Phase Flow with One-Dimensional Model*, report RFR-197, AB Atomenergi, Stockholm (August 1962).
11. Quandt, E. R., *Analysis and Measurement of Flow Oscillations*, IV National Heat Transfer Conference, Buffalo (August 1960).
12. Jahnberg, S., *A One-Dimensional Model for Calculation of Non-Steady Two-Phase Flow*, Paper presented at the EAES Symposium on Two-Phase Flow, Steady State Burn-out and Hydrodynamic Instability, Studsvik (October 1963).
13. Becker, K. M., et al., *Measurements of Hydrodynamic Instabilities, Flow Oscillations and Burn-out in a Natural Circulation Loop*, report AE-131, AB Atomenergi, Stockholm (1964).
14. Collier, J. G., *Heat Transfer and Fluid Dynamic Research as Applied to Fog Cooled Power Reactors*, Atomic Energy of Canada Ltd., report AECL-1631 (June 1962).
15. Mathisen, R. P., et al., report in progress, AB Atomenergi, Studsvik (April 1963).
16. Spigt, C. L., et al., *The Onset of Hydraulic Instabilities in an Annular Channel*, report WW 016-R53, Technological University of Eindhoven (September 1963).
17. Spigt, C. L., and Bogaardt, M., *Some Burn-out and Instability Experiments on a 7-Rod Cluster*, report WW 016-R48, Technological University of Eindhoven (July 1963).
18. Becker, K. M., and Hernborg, G., *Measurements of Burn-out Conditions for Flow of Boiling Water in 3-Rod and 7-Rod Clusters*, report AE-153 AB Atomenergi, Studsvik (August 1964).
19. Macbeth, R. W., *Forced Convection Burn-out in Simple Uniformly Heated Channels. A Detailed Analysis of World Data*, Paper presented at the EAES Symposium on Two-Phase Flow, Steady State Burn-out and Hydrodynamic Instability, Studsvik (October 1963).
20. Margen, P. H., et al., *The Design of the Marviken Boiling Heavy Water Reactor with Nuclear Superheating*, P/603, Vol. 6, these proceedings.

ABSTRACT—RÉSUMÉ—АННОТАЦИЯ—RESUMEN

A/607 Suède

Instabilité hydrodynamique et caléfaction dynamique dans un courant à deux phases en circulation naturelle. Etude expérimentale et théorique

par K. M. Becker et al.

Il est présenté un modèle théorique permettant de prédire le seuil d'instabilité d'un courant à deux phases dans une boucle à circulation naturelle. Le modèle calcule le changement transitoire de courant causé par une perturbation en échelons de l'apport de chaleur, et est basé sur la loi de la conservation de masse, de quantité de mouvement et d'énergie sous forme unidimensionnelle. Des corrélations empiriques sont utilisées dans le modèle pour l'estimation des fractions de vide et des pertes de pression dans le courant à deux phases. Les équations sont résolues numériquement en une approximation de différences finies codée pour une calculatrice numérique. Il existe deux versions du modèle: l'une où la perte de pression totale dans le conduit est donnée, et l'autre

où la perte de pression totale est calculée d'après les caractéristiques de la boucle extérieure.

Une étude expérimentale de l'instabilité hydrodynamique et de la caléfaction dynamique dans un courant à deux phases a été effectuée dans une boucle à circulation naturelle dans la gamme de pressions entre 10 et 70 atm (eff.). Les sections d'essai étaient constituées par des conduits cylindriques d'un diamètre intérieur de 20, 30 et 36 mm et d'une longueur chauffée de 4 890 mm. Les résultats expérimentaux montrent que, dans les gammes soumises aux essais, la stabilité du courant croît pour une augmentation de pression et un accroissement de l'étranglement en amont de la section d'essais, mais décroît pour une augmentation du sous-refroidissement à l'entrée et un accroissement de l'étranglement en aval de la section d'essais. Une comparaison des caractéristiques de la vapeur de caléfaction en circulation naturelle avec les données correspondantes à la circulation forcée a montré que les premières données sont inférieures d'un facteur pouvant atteindre 2,5. Cependant, en appliquant l'étranglement à l'entrée du courant, on obtient des valeurs de caléfaction qui se

рapprochent des valeurs obtenues avec la circulation forcée et finissent par coïncider avec celles-ci.

Les résultats expérimentaux obtenus au cours des essais susmentionnés ainsi que les données fournies par d'autres sources ont été comparés avec les seuils de stabilité obtenus à l'aide du modèle théorique. Les comparaisons portaient sur la disposition circulaire, annulaire et en faisceaux des barreaux, et la concordance entre les limites de stabilité expérimentales et théoriques était excellente, les écarts étant en général inférieurs à 10%.

L'application des résultats expérimentaux et théoriques à l'estimation d'un réacteur à eau lourde bouillante est examinée. Il est montré d'une façon qualitative comment l'instabilité hydrodynamique et la caléfaction affectent l'optimisation des performances d'un réacteur.

A/607 Швеция

Гидродинамическая неустойчивость и динамика кризиса в условиях естественной циркуляции двухфазного потока. Экспериментальное и теоретическое исследование

К. М. Бекер et al.

Представлена теоретическая модель для предсказания порога неустойчивости двухфазного потока в петле с естественной циркуляцией. Эта модель позволяет рассчитывать возникновение неустановившегося потока из-за скачкообразного изменения количества поступающего тепла. Она основана на законах сохранения массы, количества движения и энергии в одномерной форме. Эмпирические зависимости использовались в этой модели для оценки доли пустот и перепадов давления в двухфазном потоке. Эти уравнения решаются численно в конечно-разностном приближении, запрограммированном для расчета на цифровой вычислительной машине. Существуют два варианта модели: в одном варианте общий перепад давления в канале задается заранее, а в другом — общий перепад давления рассчитывается по всему каналу, на основе данных, полученных в нижней камере.

Экспериментальные исследования гидродинамической неустойчивости и динамики кризиса в двухфазном потоке были выполнены в петле с естественной циркуляцией в диапазоне давлений от 10 до 70 ат. Рабочие участки представляли собой круглые трубы внутреннего диаметром 20, 30 и 36 мм и обогреваемой длиной 4890 мм. Экспериментальные результаты показали, что в исследованных пределах стабильность потока возрастает с увеличением давления и дросселирования перед рабочим участком и уменьшается с увеличением переохла-

ждения входящего потока и дросселирования после рабочего участка. Сравнение качества пара при кризисе в условиях естественной циркуляции с соответствующими данными при принудительной циркуляции показало, что в первом случае данные были ниже почти в 2,5 раза. Однако путем дросселирования потока на входе значения величин при кризисе приближались и окончательно совпадали с данными для принудительной циркуляции. Настоящие экспериментальные результаты, также как и данные из других источников, сравнивались с порогами стабильности, полученными с помощью теоретической модели. Эти сопоставления включали круглую, кольцевую геометрию и геометрию пучка стержней. Было найдено очень хорошее соответствие экспериментальных и теоретических пределов стабильности. Отклонения в основном составляли меньше 10%.

Обсуждается применение экспериментальных и теоретических результатов для оценки конструкции кипящего тяжеловодного реактора. Показано качественно, как гидродинамическая неустойчивость и кризис влияют на оптимизацию рабочих характеристик реактора.

A/607 Suecia

Inestabilidad hidrodinámica y grado de quemado dinámico en flujo a doble fase en circulación natural. Estudio experimental y teórico

por K. M. Becker et al.

Se presenta un modelo teórico para predecir el umbral de inestabilidad para flujo a doble fase en un circuito de circulación natural. El modelo permite calcular el transitorio de flujo originado por una perturbación tipo peldaño en la entrada de calor, y está basado en las leyes de conservación de masa, momento y energía, en forma unidimensional. En el modelo presentado se emplean correlaciones empíricas para estimar los porcentajes de vacíos y los descensos de presión del flujo de doble fase. Las ecuaciones se resuelven numéricamente en aproximación por incrementos finitos codificada para un computador digital. Existen dos versiones del modelo: una en que se especifica previamente la caída total de presión en el canal, y otra en la que aquella se calcula a partir de los datos de entrada.

Se ha llevado a cabo un estudio experimental de la inestabilidad hidrodinámica y del grado de quemado dinámico en flujo bifásico y en un circuito de circulación natural en la zona de presiones de 10 a 70 atm(g). Las secciones de ensayo fueron conductos circulares de 20, 30 y 36 mm de diámetro interior, y una longitud en caliente de 4 890 mm. Los resultados experimentales han demostrado que, dentro de los márgenes ensayados, la estabilidad del flujo aumenta

con la presión y con el grado de estrangulamiento antes de la sección de ensayo, pero disminuye al aumentar el subenfriamiento de entrada así como el estrangulamiento después de la sección de ensayo. Comparando las características vapor-grado de quemado en circulación natural con los datos correspondientes en circulación forzada, se advierte que los primeros fueron inferiores en un factor de hasta 2,5. Sin embargo, aplicando al flujo estrangulamiento en la entrada, los valores de quemado convergen y finalmente coinciden con los correspondientes a circulación forzada.

Estos resultados experimentales así como los datos disponibles de otras procedencias se han comparado

con los umbrales de estabilidad obtenidos por el modelo teórico. En el estudio comparativo se han incluido geometrías circular, anular y de agrupamiento de barras, y la concordancia entre los límites de estabilidad experimentales y teóricos fué muy satisfactoria, quedando generalmente las desviaciones comprendidas dentro de un intervalo menor del 10 por ciento.

Se estudia la aplicación de los resultados experimentales y teóricos en su contribución al diseño de los reactores de agua pesada en ebullición. Se demuestra cualitativamente cómo la inestabilidad hidrodinámica y el grado de quemado afectan a la optimización de las características del reactor.

Two-phase flow investigations for a marine boiling water reactor

By E. Kjelland-Fosterud, I. Bencze, B. Kierulf and O. R. Kolberg*

This paper describes research work done in support of a nuclear ship design project. The work has been concentrated on three aspects of the coolant flow, using three different experimental facilities. Work continues in two of these.

In a marine boiling water reactor the moderator density, and hence the reactivity of the core, is dependent upon the vertical accelerations due to ship motion. This dependence arises through the following mechanisms:

(a) The buoyancy force on the steam bubbles change, influencing the velocity of the steam bubbles relative to the water and perhaps also the changeover from one flow régime to another. This effect will alter the core void fraction, i.e., the volume fraction of vapour in the core even at constant power and circulation rate.

(b) The natural circulation driving head changes, so that the circulating mass of coolant will accelerate. The changes in circulation velocity which results depends upon the frequency of the vertical accelerations, the ratio of the natural circulation driving head to the total driving head, and upon the momentum of the circulating water. Variations in water velocity through the core will lead to variations in the rate of steam production, since the water is subcooled at entry to the reactor core, and also in the absolute steam velocity. Both effects cause void fluctuations.

(c) Incomplete separation in the upper plenum leads to entrainment of steam bubbles in the downcomer. The entrainment process, which is dependent upon vertical accelerations, will affect the natural circulation driving head, the subcooling at the core inlet, and, if subcoolers are fitted, cause deviations from the designed plant heat balance. Although the magnitude of these effects can be reduced by fitting forced circulation pumps, it might be more economical to dispense with these and rely on natural circulation alone or aided by a steam injector jet pump.

The research programme involves investigation of the effect of ship motion on the reactor core void fraction, investigation of the dynamic response of the coolant circuit to accelerations, and the effect of coolant circuit inertia and subcooling on this response, using a mobile loop called Yo-Yo. This loop

will later be used for carry-under investigations, and for checking the hydraulic loop of reactor dynamics models.

Carry-under is investigated qualitatively in a large-scale, atmospheric air-water rig called Cubox, which permits tests on rectangular risers and downcomers of different areas.

The steam injector jet pump has been investigated in a high pressure loop, simulating a section of the reactor core with riser and downcomer.

INVESTIGATION OF VARIABLE g -EFFECTS ON THE HYDRAULIC LOOP

Background

Calculations, using the accepted form of slip correlation for two-phase bubbly and slug flow, $S = C_1 + C_2/\sqrt{Fr}$, where C_1 and C_2 may be functions of void fraction, but not significantly of local water velocity, and Fr = local Froude number, indicate that the direct influence of changes in gravity on slip should be negligible at reactor conditions. It should, therefore, be permissible to use existing two-phase flow data, which have all been obtained on stationary rigs, in the reactor dynamic analysis.

The reactor coolant channels are short, and entrance effects and transition points between flow patterns might alter with g in such a way that significant changes in slip ratio would be found. The main purpose of this investigation was, however, only to confirm that the direct g -effect on slip was insignificant.

Apparatus

The rig consists of a natural circulation, 30 kW, 50 ata boiling loop mounted on a frame which can be oscillated vertically with a stroke of 10 m and a period of about 5 s. Figure 1 shows a photograph of the complete rig and Fig. 2 shows the loop arrangement diagrammatically.

The heating element is a 25 mm diam, 0.25 mm wall thickness, 1 200 mm long stainless steel tube which is rigidly mounted inside a pressure tube. The condenser, mounted on top of the steam dome, consists of 8 U-tubes, individually supplied through small bore valves with cooling water from a piston pump. The coolant passes from the pump to the

* Institutt for Atomenergi, Kjeller.

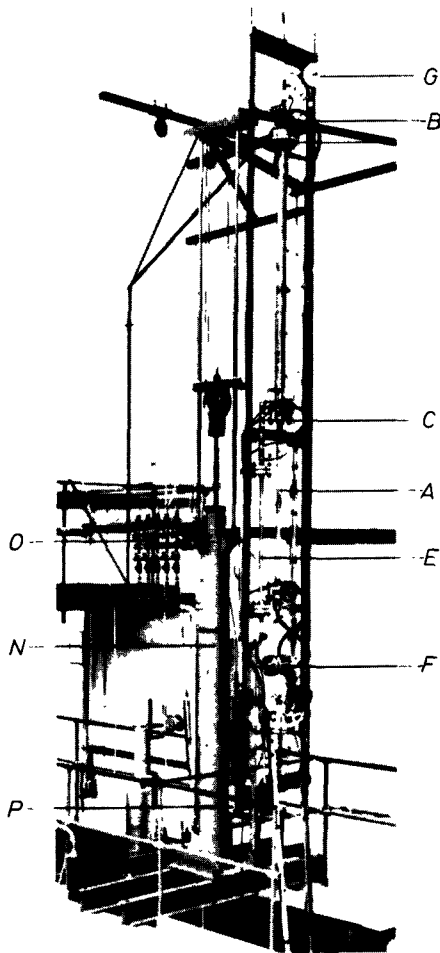


Figure 1. Yo-Yo. Arrangement of rig

- A HEATING SECTION
- B CONDENSER
- C SUBCOOLER
- D RISER
- E DOWNCOMER
- F FLOWMETER
- G PRESSURE GAUGE
- H-L IMPEDANCE VOID METERS
- M NIVEAU CONTROLLER
- N CYLINDER
- O AIR VALVES
- P CONTROL SYSTEM

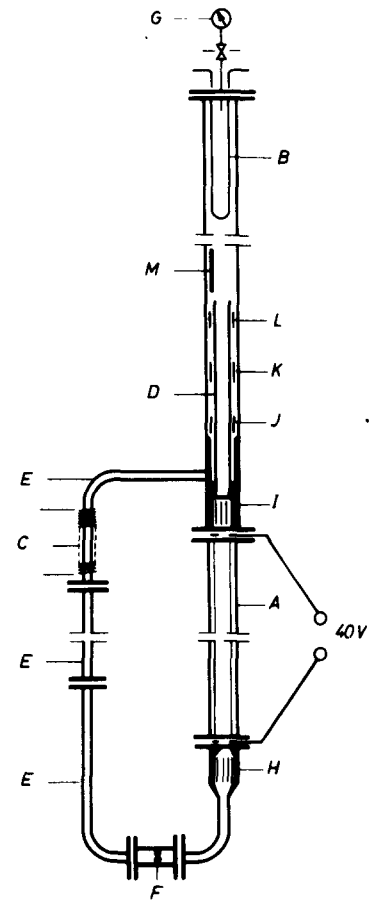


Figure 2. Yo-Yo. Diagram of loop

condenser through a small bore, high pressure rubber hose, and evaporates completely in the condenser. The exhaust is always superheated, and is discharged directly into the air. This arrangement is necessary to prevent changes in the rate of heat removal with loop position.

The subcooler consists of two parallel copper tubes tightly coiled round the downcomer and held by screw clips in contact with the downcomer. The heat transfer rate is kept low, and the cooling water flow rate is high, in order to prevent local boiling which might cause subcooling fluctuations with loop position.

The downcomer shown on the photograph is a 25 mm bore tube about 2 m long. For some of the tests this was replaced by a similar diameter tube of 6 m length, obtained by coiling a longer tube in the loop plane.

The loop is bolted to a frame which is guided by two steel wires secured to the roof and the floor of the laboratory. The loop is moved by a pneumatic cylinder through a 5:1 pulley and wire arrangement. The control system consists of 10 solenoid valves (5 for inlet and 5 for exhaust) controlled by micro-switches in connexion with a rotating cam.

Instrumentation

An impedance void meter is placed immediately above the heating element. It consists of an insulated tube mounted between an earthed central cylinder and the earthed pressure tube. The impedance between the insulated tube and earth depends on the void fraction of the flow, the conductivity of the water and strictly also on the flow pattern [2].

An identical reference meter was placed immediately below the heating element, in order to compensate for the change in conductivity with temperature and water purity. Sensors working on the same principle are mounted in the annulus surrounding the riser, and are used for measuring downcomer void fractions and water level. Circulation rate is sensed by a standard de Havilland Potter meter, pressure by a Bourdon precision gauge, and the acceleration by a Hottinger cell. All instrument signals, except the system pressure, are transmitted to a UV recorder. The circulation rate is calculated from the time interval between the Potter meter pulses, to avoid the damping caused by an integrator. Signals can also be stored on a tape recorder, from which they are fed into an analogue computer for comparison with a mathematical model of the loop dynamics [5].

Procedure

Tests have been run within the following ranges of variables:

Pressure between	10 ata and 50 ata
Power between	10 kW and 28.5 kW
Circulation rates between .	0.7 m/s and 1.0 m/s
Exit void fractions between	0.16 and 0.72
Subcooling has been either	0 or 5.4 kW.

Accelerations have always been between +2 *g* and +0.6 *g*, i.e., +1 *g* and -0.4 *g* from normal gravity, with a period of about 5 s. The gravity fluctuations were not sinusoidal.

In some of the tests, a downcomer giving three times the original single phase inertia was used in order to reduce the amplitudes of circulation oscillations. The changes in exit void fraction that were not produced by changes in circulation rate and quality should thus be revealed more clearly.

Some of the test results were analysed by comparing the measured circulation and void oscillations by the ones predicted by an analogue computer model. In this model the dependence of gravity variations on slip ratio is neglected [5].

The measured void fractions showed instantaneous fluctuations between 0 and 60–70% void. In order to obtain readable traces, it was necessary to damp out the void signal by introducing a filter with 1 s time constant. The error in amplitude and phase thus produced was compensated for by introducing a similar filter in the read-out from the computer.

Results and discussion

A representative extract of the results are plotted in Figs. 3–6.

If a strong dependence of gravity on slip had been present, buoyancy changes should have caused an increase in slip ratio with increasing gravity. This would tend to empty the channel of vapour, and liquid must stream from the downcomer to compensate. The measured amplitudes of void and circulation oscillations should be larger than predicted on the assumption of zero *g*-effect upon slip.

Figure 4 shows the prediction from the analogue computer model where any dependence of gravity on slip is neglected, compared with the experimental results. The disagreement, believed to be due to instrumentation errors and inaccuracies in the computer model, amounts to 0.05–0.1 in void fraction and 10–15% in circulation rate. The observed fluctuations are always smaller than those predicted by the computer.

It is therefore concluded that no significant unexpected effects can be present, and that the slip ratio is not significantly influenced by gravity variation. The actual value of the *g*-effect on slip cannot be found from these tests since it appears to be of the same order as the errors in the quality and circulation effect of the slip correlation used for the computer model.

The subcooler was positioned near the downcomer inlet in order to kill any vapour carry-under at an early stage. The presence of vapour in the downcomer would have reduced the natural circulation driving head. No carry-under was, however, produced in this loop because of low fluid velocity in the upper part of the downcomer. The only effect produced by the subcooler is amplification of the void and circulation fluctuations because of oscillations in outlet temperature from the constant power subcooler. This effect is illustrated on Fig. 6.

The inertia of the circulating water, which has an important influence on the dynamic behaviour of the hydraulic loop and hence on the reactor, can be varied by the designer within fairly wide limits. Figure 3 shows the effect of increasing the length of the water path in the downcomer by a factor of 3. The fluctuations in void and circulation are reduced by a factor of 1.5.

A schematic drawing of a possible application to a natural circulation reactor is shown on Fig. 7. The design, which incorporates a 60° spiral to increase the momentum of the water, should reduce the amplitude of circulation oscillations by a factor of 1.8 for a 10 s period sinusoidal *g*-oscillation, and by a factor of 2.8 for a 5 s period, on the assumption of zero subcooling and constant power. The effect on the complete reactor is described in [3].

Conclusions

The following conclusions have been drawn from the experiments:

- The error introduced by neglecting the direct *g*-effect upon slip is small. It should, therefore, be safe to assume that data from stationary rigs may be used with confidence in the design of natural circulation boiling water reactors for marine application;
- No effects have been found which indicate any sudden transition from one flow régime to another;
- No carry-under has been produced in this geometry where the water velocity in the upper part of the downcomer was 0.2 times the circulation velocity;
- A stabilizing effect may be achieved by increasing the single-phase inertia.

CARRY-UNDER INVESTIGATION

Background

Calculations using data from [1] indicate that low downcomer qualities can be obtained only when the downcomer velocity is low. The void fractions which are predicted, using data from the same source, are excessive, as long as any appreciable carry-under occurs at all, since the slip ratios approach zero as the downcomer velocity is reduced.

The correlations quoted in [1] suggest that two different modes of vapour separation operate. This investigation was aimed at providing a qualitative

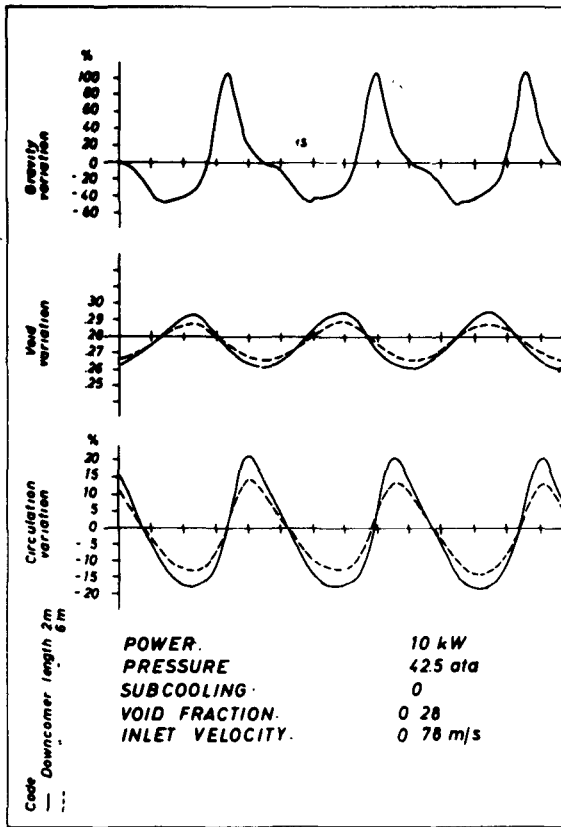


Figure 3. Yo-Yo. g-responses with long and short downcomer

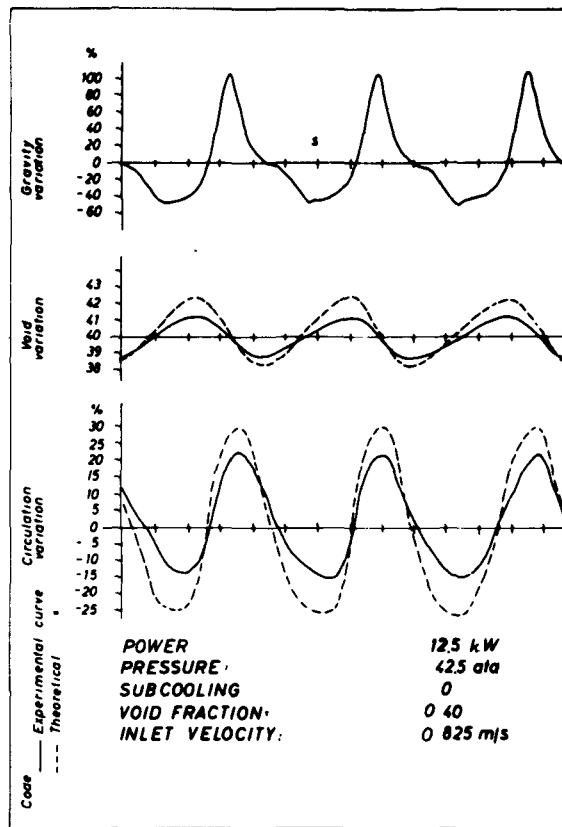


Figure 4. Yo-Yo. g-response. Comparison with analogue computer prediction

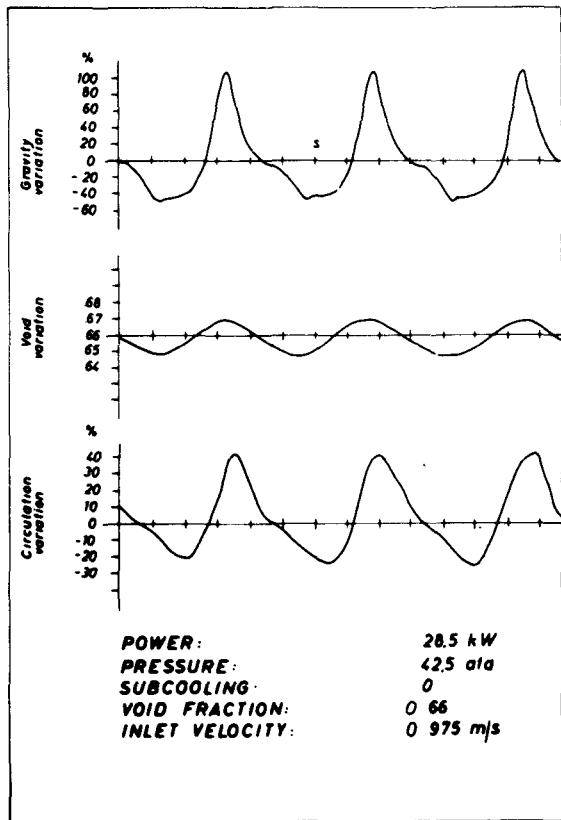


Figure 5. Yo-Yo. g-response at higher power

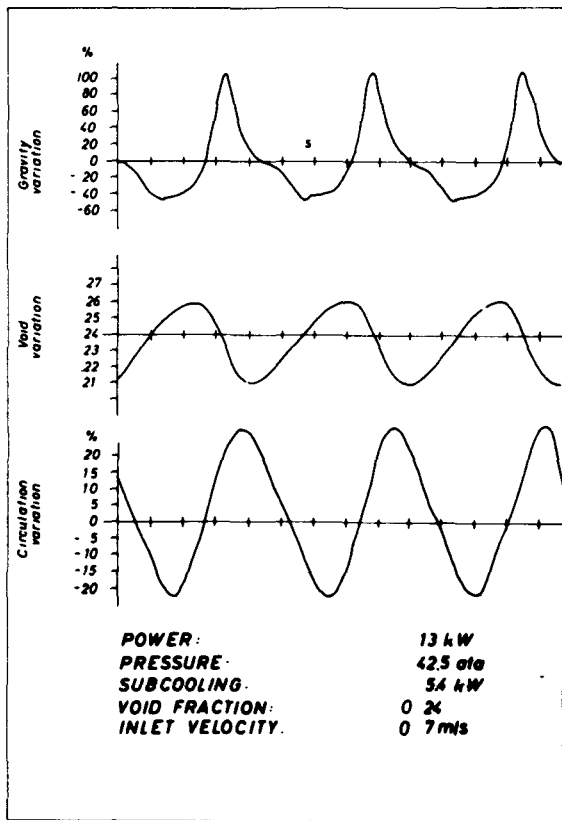


Figure 6. Yo-Yo. g-response with subcooling

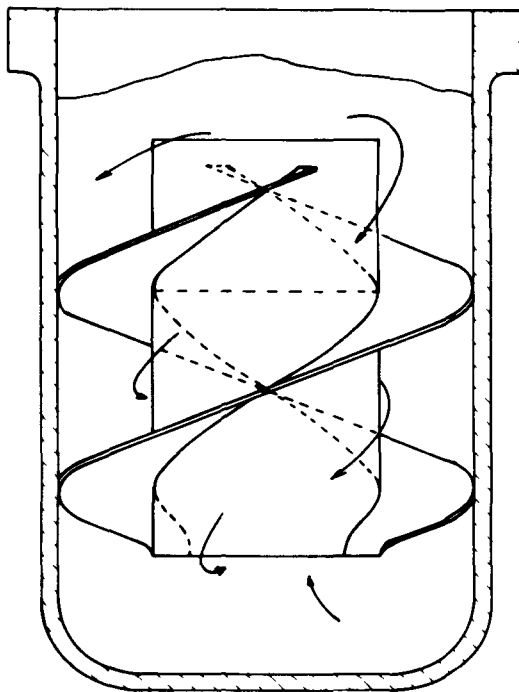


Figure 7. Reactor with spiral downcomer

picture of these processes, in order to check the correlations of [1].

Apparatus

The rig is shown in Fig. 8. The water is circulated by means of a variable pitch propeller driven by a 4 hp electric motor. Water is drawn from the separation chamber through the propeller to the riser. Air is supplied from a compressor through manifolds placed in the riser. The wall between the riser and downcomer can be moved, and the downcomer area in the tests reported here measured 0.34×0.9 m and the riser 0.2×0.9 m.

The air-water mixture flows from the downcomer along the bottom of the box and into the separation space, where full separation of the air takes place.

The air flow rate is measured by Rotameter, the water flow rate by a Pitot meter across the orifice at

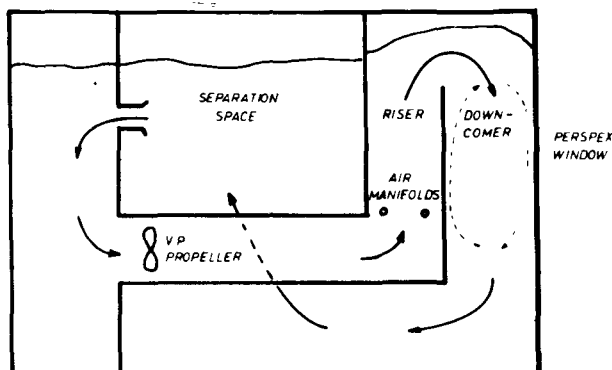


Figure 8. Cubox. Layout

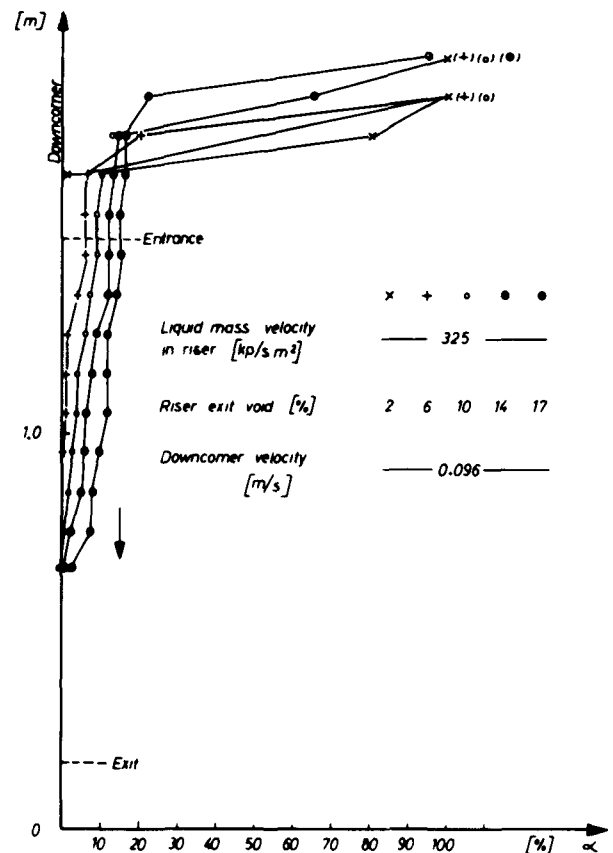


Figure 9. Cubox. Downcomer void profiles

the entrance to the well leading to the propeller duct. Void fraction is measured by an impedance meter working on the same principle as in Yo-Yo [2]. This probe was traversed to give the void fractions indicated in Figs. 9 and 10. The flow was assumed truly two-dimensional, and all traverses were done in the plane midway between the two long walls of the box.

Visual observations

When the rate of air supply is kept constant and the downcomer velocity is increased from zero, the following flow patterns are observed: At zero net downcomer flow turbulent eddies in the downcomer are induced by the riser turbulence, and the upper part of the downcomer becomes loaded with air bubbles. When the downcomer water velocity is increased, this air-carrying region becomes extended in length. The lower limit of the void region coincides with the lower limit of the eddy region. When the downcomer velocity is increased still further, the void region extends further down and eventually reaches the entrance to the separation space. The downcomer void fraction is then decreased, since the bubbles previously rising along the separation wall to the riser are now sucked into the separation space, and carry-under is high.

The void fraction in the high void region varies with riser conditions. When, at constant circulation rate, the air supply is shut off, the void fraction in

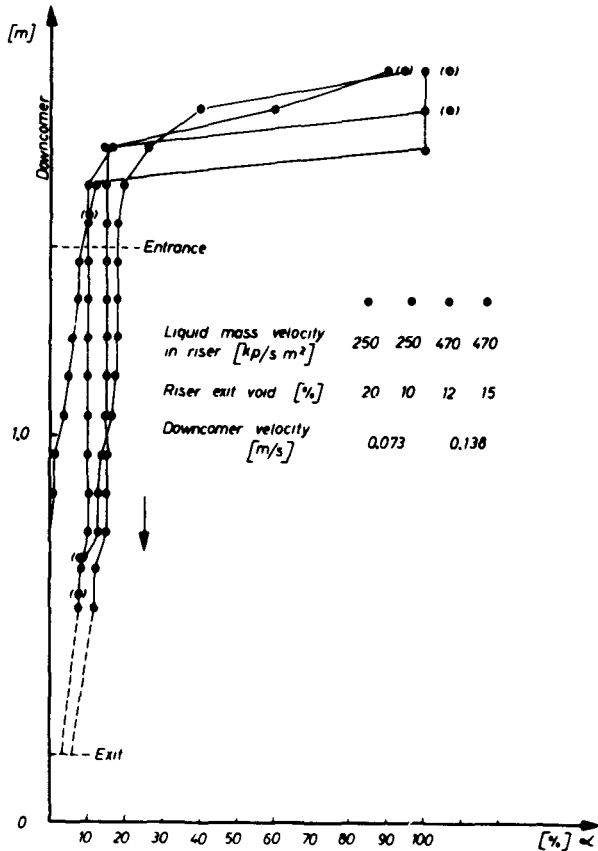


Figure 10. Cubox. Downcomer void profiles

the downcomer is reduced slowly, and occasionally very large bubbles being formed under the lower corner of the riser wall are broken up as they hit the horizontally flowing water from the riser. The rate of escape for any of these bubbles is small. When the air is turned on again, the steady state void fraction is reached in a few seconds.

The flow patterns are sensitive to water purity. When impurities are present, eddies rotating in the plane of the window appear, the void region extends further down and its lower boundary is diffused. Carry-under starts as soon as the circulation is started.

Reduction in the hydraulic diameter of the flow by a factor of 7, obtained by inserting partitions parallel to the riser wall, has no significant effect.

An increase in wall friction either on the window or the riser wall, by inserting a grid consisting of 20 mm high horizontal fins spaced 30 mm over a depth of 400 mm, had no effect.

Conclusions

- Carry-under starts when the downcomer water velocity exceeds a critical value;
- The void fractions calculated on the basis of data from [1] are unreliable at low downcomer velocities;
- The height of the downcomer is an important variable.

STEAM INJECTOR-JET PUMP

Introduction

A section of a boiling water reactor is shown on Fig. 11. A combined steam injector-jet pump, a number of which will be distributed around the reactor downcomer, is shown diagrammatically.

The condensate returned to the reactor from the steam turbine-condenser circuit is subcooled compared to the reactor pressure. In the ship reactor system chosen for analysis, the reactor pressure is $49 \times 10^5 \text{ N/m}^2$, and the condensate is preheated to 130°C . For a range of mass flows of steam and subcooled water inlet conditions, and appropriate design of inlet nozzles and mixing chamber, a low pressure is generated by the condensate in the mixing chamber. Steam will flow into the mixing chamber,

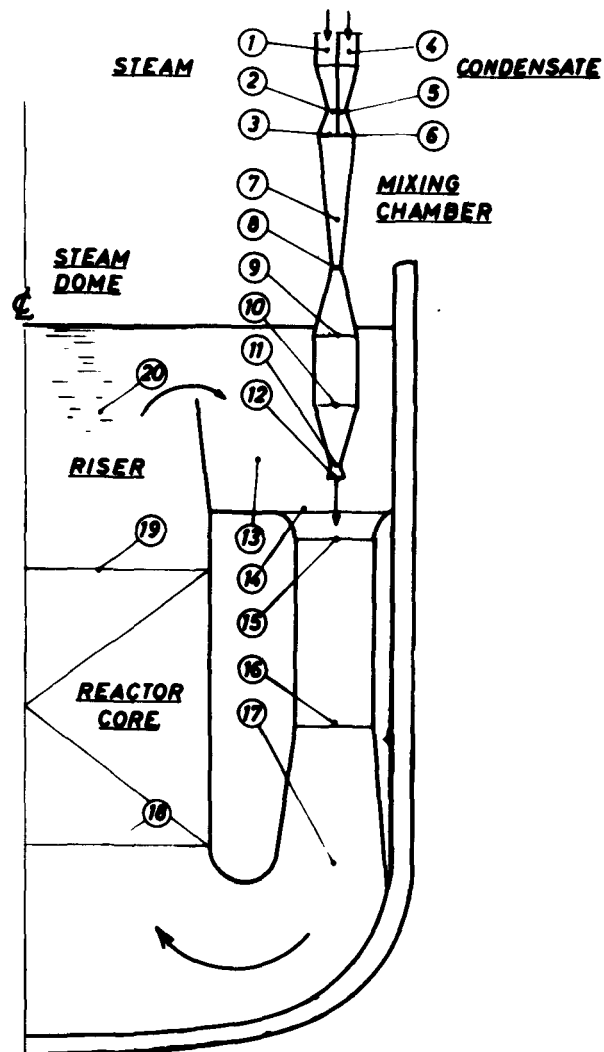


Figure 11. Steam injector as a reactor installation
 1-3: Steam or nearly saturated water inlet; 4-6: Subcooled water (condensate) inlet; 7: Mixing chamber; 8-9: Mixing chamber diffuser; 9-12: Jet nozzle elongation with a convergent-divergent nozzle; 13: Point with minimum velocity at entrance to the downcomer; 14: Point with maximum velocity at entrance to the downcomer; 15-17: Downcomer with diffuser; 18-20: Reactor core with riser

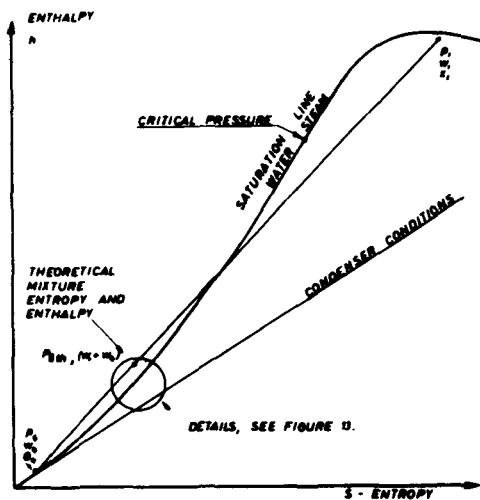


Figure 12. Theoretical mixing process

and part of the steam enthalpy can be converted to kinetic energy in a jet emerging from the mixing chamber. The jet can emerge from section 8 to 12 depending on the design.

This jet is used as an ordinary water jet pump to increase the circulation rate of the reactor coolant in the circuit 13 to 20.

The principal advantages of this system for forced circulation is no moving parts within the reactor, and no or negligible power used for circulation.

Theory

The process can best be illustrated with reference to the h - s diagrams in Figs. 12 and 13. Steam with conditions pressure p_1 and dryness fraction x_1 is mixed with subcooled water of pressure p_4 and temperature θ_4 . In a mixing process without losses,

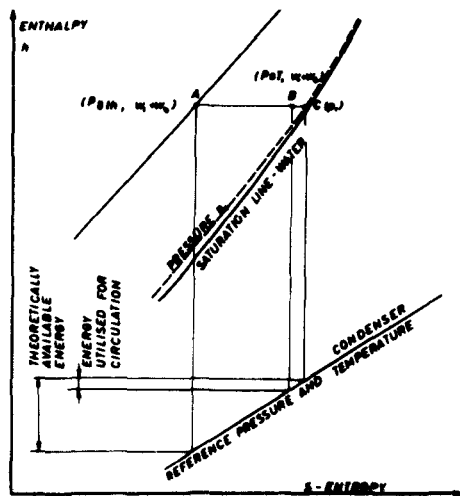


Figure 13. Theoretical mixing process. Details

the mixture conditions will be on the straight line joining these two points. The mass flow ratio W_1/W_4 will determine the point denoted A. The theoretical pressure at A is p_{8th} . The actual pressure, measured when the mixture kinetic energy is converted to pressure, is p_{8T} at point B, and C is given by the system pressure p_1 . A, B and C has the same enthalpy. The expression $(p_{8T} - p_1)/(p_{8th} - p_1)$ is defined as the efficiency of the steam injector.

Loop design

A high pressure loop, maximum 98×10^5 N/m², simulating a section of the reactor core, riser and downcomer with one injector installed, has been built and operated. A series of injector designs based on a theoretical analysis of mixing process, and on measurements, have been supplied:

Steam, max mass flow 0.13 kg/s, max pressure 60×10^5 N/m².

Subcooled water, max mass flow 0.28 kg/s, max pressure 83×10^5 N/m².

Results

The injector can be operated according to the theory indicated. With a loop pressure of 49×10^5 N/m², a subcooled water pressure above 63×10^5 N/m² was necessary to start the injector. With the injector operating, this pressure could be reduced as far as 30×10^5 N/m² before the injector stopped. With the enthalpy of the mixture $W_1 + W_4$ approaching that of saturated water at pressure p_1 , the injector stopped, as predicted by the theory. Efficiencies of 2-3% as defined above were obtained. The efficiency was reasonably constant with varying subcooled water temperature. $\theta_4 = 105^\circ\text{C}$ was the maximum temperature at which the injector operated.

The water jet pump circuit data are reasonably close to those predicted by conventional momentum exchange theory.

Conclusions

Stable operation over a wide range of inlet conditions can be expected. A considerable damping of nuclear power oscillations with g variations for a boiling water ship reactor can be expected [3]. A final optimization of injector design for operation at higher subcooled water temperature, endurance tests and parallel operation of injectors are still required.

REFERENCES

1. Petrick, M., *A Study of Vapour Carry-Under and Associated Problems*. USAEC report ANL-6581 (July 1962).
2. Orbeck, I., *Impedance Void Meter*. KR-32. Institutt for Atomenergi, Kjeller, Norway (Nov. 1962).
3. Christensen, H., *et al.*, *On the Behaviour of Boiling Water Ship Reactors*, p. 748, Vol. 6, these Proceedings.

ABSTRACT—RÉSUMÉ—АННОТАЦИЯ—RESUMEN

A/801 Norvège

A/801 Норвегия

Études d'écoulement à deux phases pour un réacteur marin à eau bouillante

par E. Kjelland-Fosterud et al.

Ce mémoire décrit un travail de recherche effectué dans le cadre d'un projet de réacteur nucléaire marin. Il est important de pouvoir prédire le comportement dynamique d'un réacteur à eau bouillante, utilisé en mer. Puisque seul le circuit hydraulique est affecté, il suffit de l'étudier expérimentalement et d'utiliser les résultats d'expérience comme vérification partielle d'un modèle mathématique de la dynamique de tout le réacteur.

Des essais ont été faits au moyen d'une boucle à circulation naturelle, de 30 kW à 50 atm(abs.), qui peut osciller verticalement. La course est de 10 m et les accélérations comprises entre 0,6 et 2,0 g.

Il est important de connaître la quantité de mouvement de l'eau qui circule, pour déterminer la réponse dynamique d'un réacteur à eau bouillante. On décrit un système permettant au constructeur de varier dans une large mesure l'inertie de l'eau à la descente. Les effets de cette construction sur le comportement dynamique du réacteur sont décrits dans le mémoire de H. Christensen et al. Les résultats indiquent qu'il n'est pas nécessaire d'avoir recours à de puissantes pompes de circulation.

Cependant, la circulation forcée améliore la stabilité d'un réacteur à eau bouillante. Au lieu de pompes classiques, il est proposé d'utiliser une pompe à jet combinée avec l'injection de vapeur, qui occasionne des frais négligeables par comparaison avec les pompes classiques. La théorie de l'injecteur est expliquée, et des résultats d'expérience, où une boucle ayant une pression maximale de 100 atm(abs.) et une puissance maximale de 300 kW fut utilisée, sont examinés. L'influence de l'injecteur sur la conception des réacteurs à eau bouillante et sur leur comportement est discutée.

Dans un réacteur utilisant la circulation naturelle ou par injecteur, celle-ci est fortement affectée par l'entraînement de vapeur à la descente, ce qui diminue la hauteur statique qui est cause de la circulation naturelle. Il est vraisemblable que l'entraînement de la vapeur vers le bas devra être fortement restreint dans ce type de réacteur.

L'entraînement de la vapeur a été étudié expérimentalement dans la boucle mobile décrite ci-dessus et dans des boucles air-eau à grande échelle. En considérant l'entraînement de vapeur comme faisant partie d'un problème d'écoulement à deux phases, il est apparu que les effets géométriques jouaient un rôle important. Ceux-ci furent étudiés et les résultats sont donnés.

Исследования двухфазного потока для судового кипящего реактора

Э. Кьелланд-Фостеруд et al.

В докладе описаны исследовательские работы, проводимые в обоснование проекта судового ядерного реактора. Важно иметь возможность предсказать динамическое поведение кипящего реактора на море. Поскольку влияние испытывает только гидравлическая схема, достаточно исследовать это экспериментально, используя экспериментальные результаты в качестве частичной проверки приемлемости математической динамической модели для всего реактора.

Были проведены испытания в петле при мощности 30 кВт и давлении 50 ат с естественной циркуляцией. Эта петля может колебаться вертикально. Размах 10 м, ускорение между 0,6 и 2 g.

Момент циркулирующей воды важен для динамической реакции кипящего реактора. Описана конструкция, которая дает проектировщикам свободу изменять инерцию воды в циркуляционной трубе в широких пределах. Влияние этой конструкции на динамическое поведение реактора описано в докладе Х. Христенсена и др. Результаты показывают, что нет необходимости в мощных циркуляционных насосах.

Однако принудительная циркуляция улучшает стабильность энергетического кипящего реактора. Вместо обычных насосов предлагается использовать комбинированный паровой инжектор — струйный насос, который требует пренебрежимо малых затрат по сравнению с обычными насосами. Будет изложена теория инжектора и приведены экспериментальные данные, полученные на петле с максимальным давлением 100 ат и максимальной мощностью 30 кВт. Обсуждается влияние инжектора на конструкцию кипящего реактора и его поведение.

В реакторе с естественной циркуляцией или с инжектором на циркуляцию влияет главным образом попадание пара в циркуляционную трубу, что уменьшает подпор естественной циркуляции. Поэтому представляется необходимым в таких реакторах ограничить попадание пара до очень малых величин.

Попадание пара было исследовано экспериментально в описанной выше подвижной петле, а также в больших воздушно-водяных петлях. Если рассматривать попадание пара как

аспект проблемы двухфазного потока, становится ясно, что важны геометрические эффекты. Они были исследованы, и в докладе приводятся результаты.

A/801 Noruega

Investigación sobre el flujo de dos fases para un reactor marino de agua en ebullición

por E. Kjelland-Fosterud *et al.*

La memoria describe el trabajo de investigación efectuado como base del proyecto de un reactor nuclear marino. Es importante poder predecir el comportamiento dinámico de un reactor de agua en ebullición en el mar. Puesto que el circuito hidráulico es el único afectado, es suficiente investigar éste experimentalmente, utilizando los resultados experimentales como una comprobación parcial de la validez de un modelo matemático dinámico para la totalidad del reactor.

Se han efectuado ensayos en un circuito de 30 kW y 50 atm(abs.) con circulación natural, y en el cual pueden llevarse a cabo oscilaciones verticales. El recorrido es de 10 m y las aceleraciones están comprendidas entre 0.6 g y 2 g.

La cantidad de movimiento del agua circulante es importante para la respuesta dinámica de un reactor de agua en ebullición. Se describe un diseño con el cual se da al proyectista libertad para variar la

inercia del agua en el tubo de bajada dentro de unos límites amplios. En la memoria presentada por H. Christensen *et al.* se describe el efecto de este diseño sobre el comportamiento dinámico del reactor. Los resultados indican que no son necesarias bombas de circulación potentes.

Sin embargo, la circulación forzada aumenta la estabilidad de un reactor de potencia de agua en ebullición. En lugar de bombas clásicas se propone el uso de una combinación de inyector de vapor y eyector, que exige desembolsos pequeños comparados con los de bombas convencionales. Se explicará la teoría del inyector, y se revisarán datos experimentales de un circuito con una presión máxima de 100 atm(abs.) y potencia máxima de 300 kW. Se discutirá la influencia del inyector sobre el diseño y comportamiento del BWR.

En un reactor que emplee circulación natural o circulación por inyector, la circulación está muy afectada por el arrastre del vapor dentro del tubo de bajada, lo cual reduce la carga de presión disponible para la circulación natural. Parece que este arrastre debe ser limitado a muy pequeños valores en estos reactores.

Se ha investigado el arrastre experimentalmente en el circuito móvil descrito anteriormente, y en unos circuitos a gran escala de aire-agua. Considerando el arrastre como un aspecto del problema del modelo de flujo de dos fases, se ha puesto en claro que son importantes los efectos geométricos. Se han investigado éstos y se dan los resultados.

Études aérodynamiques et thermiques de gaines d'éléments combustibles refroidis par gaz

par P. Gelin* et J. P. Milliat**

Les études aérodynamiques et thermiques de grappes ont été entreprises au CEA en 1959; celles des gaines à chevrons se sont développées au laboratoire de Chatou de l'EDF et au laboratoire de Saclay du CEA à la fin de l'année 1959. En 1962, une étude générale sur les corrugations a débuté au laboratoire de Saclay pour l'amélioration des grappes et s'est ensuite poursuivie dans les deux laboratoires pour le refroidissement interne des éléments combustibles annulaires. Pour la gaine interne de ces éléments, il est également prévu des ailettes longitudinales qui font actuellement l'objet d'essais systématiques au laboratoire de Saclay.

L'effort le plus important a porté sur les gaines à ailettes en chevrons et sur les combustibles en grappe. Les laboratoires du CEA et de l'EDF disposent maintenant de moyens d'essai puissants et, dans le domaine de leurs objectifs communs, ils travaillent en pleine collaboration.

Les moyens d'essai employés sont de deux types: installations fonctionnant à la pression atmosphérique pour l'étude principalement des phénomènes locaux tels que distributions de vitesse et de température dans l'écoulement, répartitions de température sur les parois chauffantes, et installations sous pression destinées d'abord à fournir les performances des éléments combustibles dans des conditions équivalentes à celles des réacteurs, mais utilisées aussi pour mesurer des singularités aérodynamiques et thermiques.

ÉTUDES DES COMBUSTIBLES EN GRAPPES

Les études expérimentales qui ont été développées pour les grappes ont eu pour objectif principal le réacteur EL4; c'est pour cette raison que l'on n'a réalisé que des maquettes de grappe à 19 éléments cylindriques lisses sauf pour quelques essais particuliers de perte de charge. Les buts poursuivis ont été les suivants:

a) Détermination des pertes de charge singulières dues aux pièces d'assemblage; évolution de celles-ci vers les dispositions à pertes de charge minimales;

b) Détermination de la distribution des coefficients d'échange de chaleur dans la section droite d'une grappe;

c) Disposition optimale des éléments de la grappe par un calcul de l'évolution des points chauds de gaine dans le canal;

d) Déformation des crayons sous l'effet des dilatactions thermiques différentielles en tenant compte d'une modification corrélative des coefficients d'échange.

Etudes des pertes de charge [1]

Les mesures de pertes de charge ont porté sur les maquettes de tous les éléments combustibles étudiés dont la conception s'est rapidement orientée vers une structure à pièces d'assemblage d'extrémité et entretoise intermédiaire. Les essais ont été réalisés sur une boucle à eau chaude; le nombre de Reynolds formé avec le diamètre hydraulique de la section droite a varié entre 40 000 et 500 000.

Un essai préalable a permis de s'assurer que le coefficient de frottement en longueur indéfinie d'un contour tel que celui de la figure 1 suivait, en fonction du nombre de Reynolds, sensiblement la même loi que celle d'un tube circulaire lisse.

La perte de charge singulière à la jonction des deux cartouches consécutives ainsi que celle de l'entretoise intermédiaire ont été déduites de la perte de charge d'un ensemble de 4 maquettes en supposant sur les éléments cylindriques un coefficient de frottement égal à celui que donne une grappe de longueur indéfinie. Ces pertes de charge singulières ont été rapportées à

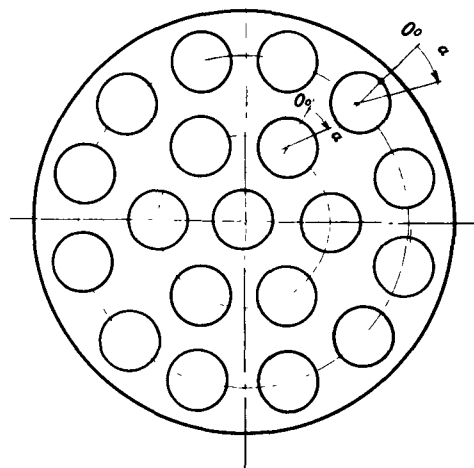


Figure 1. Section de grappe du type EL4

* Commissariat à l'énergie atomique.
** Electricité de France.

la pression dynamique formée avec la vitesse moyenne de l'eau dans une section droite courante et sont ainsi caractérisées par les coefficients ξ_g pour la jonction de deux cartouches et ξ_e pour l'entretoise. Accessoirement, on a déterminé de la même manière les coefficients ξ_0 et ξ_s relatifs respectivement à l'entrée et à la sortie du train de cartouches. Ces coefficients dépendent un peu du décalage angulaire de deux grappes successives et du nombre de Reynolds. Pour la grappe EL4, on a trouvé en moyenne $\xi_g = 0,62$; $\xi_e = 0,33$; $\xi_0 = 0,20$; $\xi_s = 0,54$ pour un nombre de Reynolds de 500 000.

Distribution des coefficients d'échange

La mesure directe d'une distribution de coefficients d'échange de chaleur dans la section droite d'une grappe est rendue très délicate par les effets de conduction dans les parois. Aussi, parallèlement à des essais d'échange de chaleur [2], on a réalisé des expériences de transfert de masse [3] dans lesquelles on dépose sur chaque élément de la grappe une couche de naphthalène qui est ensuite usinée avec une précision de 0,005 mm. Cette grappe est soumise à un écoulement d'air à la pression atmosphérique pendant un temps tel que l'épaisseur de sublimation soit en moyenne de 0,3 mm. Après essai, les cotes de chaque élément sont mesurées circonférentiellement et longitudinalement à 0,01 mm près; on en déduit ainsi la distribution correspondante du flux ϕ_m de matière évaporée que l'on associe à la concentration c de naphthalène dans la section droite de la grappe et la concentration saturante c_0 pour définir un coefficient d'échange h_m tel que $h_m = \phi_m / (c_0 - c)$ (par concentration, on entend la masse de naphthalène par unité de volume d'air). L'expérience montre que les courbes de distribution de h_m dans une section droite de la grappe évoluent en fonction de l'abscisse de cette section dans le canal mais tendent rapidement vers des profils stables. Par contre, d'un essai à l'autre, ces courbes ne

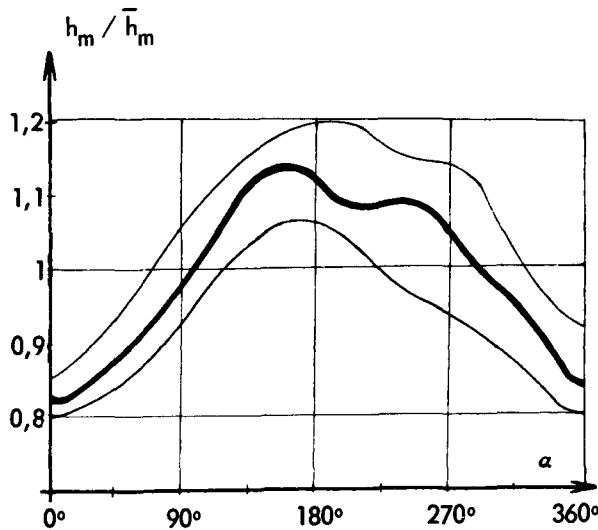


Figure 2. Variation circonférentielle relative du coefficient d'échange autour d'un élément périphérique de grappe

sont reproductibles qu'avec une certaine dispersion. La figure 2 donne, pour un élément périphérique de la grappe EL4, la courbe qui résulte de la moyenne de plusieurs essais ainsi que les deux courbes qui délimitent l'ensemble des points de mesure. La figure 3 donne la courbe moyenne d'un élément intermédiaire. Les variations de h_m mesurées sur l'élément central sont toujours restées très faibles (inférieures à $\pm 2\%$).

A l'aide du même montage expérimental, on a mesuré la distribution des vitesses dans une section droite de la grappe à une distance suffisante de la pièce d'assemblage amont pour que le régime dynamique soit établi. Grâce à un montage approprié, une sonde de pression totale de 0,5 mm de diamètre extérieur a permis de mesurer également près des parois la vitesse u en fonction de la distance y à la paroi dans une zone où la relation $u(y)$ est logarithmique. On a admis que les coefficients de cette relation étaient ceux de la loi:

$$\frac{u}{u_*} = 5,65 \log \frac{\rho u_* y}{\mu} + 4,9$$

dans laquelle u_* est la vitesse de frottement $\sqrt{\tau_0/\rho}$ formée avec l'effort tangentiel local τ_0 par unité de surface et la masse volumique ρ . De la mesure de u et y sur une normale à la paroi, on a déduit la valeur locale de u_* en chaque point du contour de la grappe. L'importance de la distribution des vitesses de frottement ressort de sa confrontation avec les résultats de transfert de masse et de transfert thermique. Ces derniers ont été obtenus sur une maquette à grande échelle constituée par 19 tubes d'acier inox de 60 mm de diamètre extérieur et de 3 mm d'épaisseur, chauffés par effet Joule et refroidis avec de l'air à la pression atmosphérique [2]; chacun de ces tubes était équipé d'un dispositif interne mesurant la température de paroi intérieure par déplacement angulaire de 15 en 15 degrés. A partir de ces mesures et par un calcul de conduction, on en a déduit la température de paroi t et la densité de flux de chaleur ϕ le long du contour extérieur de chaque tube dans une même section droite. En associant t et ϕ à la température moyenne $\bar{\theta}$ de l'air dans cette section, on en tire une distribution de coefficients d'échanges $h = \phi / (t - \bar{\theta})$ que l'on compare à celle des coefficients de sublimation forcée h_m et celle des vitesses de frottement u_* . La figure 4 donne un exemple de cette comparaison des valeurs de h , h_m et u_* rapportées à leurs valeurs moyennes \bar{h} , \bar{h}_m et \bar{u}_* pour un crayon externe de la grappe EL4. Les différences entre ces trois distributions peuvent s'expliquer qualitativement à partir des répartitions de vitesse et de température près des parois [3]; on aurait pu définir h et h_m d'une manière plus physique à partir des valeurs moyennes de la concentration c et de la température θ sur une normale à la paroi, mais on y a renoncé provisoirement à cause des difficultés de mesure. Dans la pratique, la courbe h_m/\bar{h}_m permet de calculer avec une précision suffisante la carte des températures dans un crayon. Comme le phénomène de conduction qui s'établit en pile dans une grappe ne peut pas être reproduit exactement hors pile, la

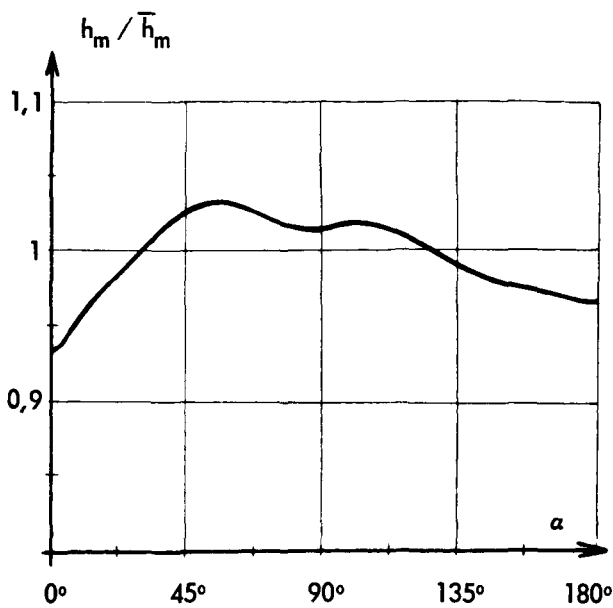


Figure 3. Variation circonférentielle relative du coefficient d'échange autour d'un élément intermédiaire de grappe

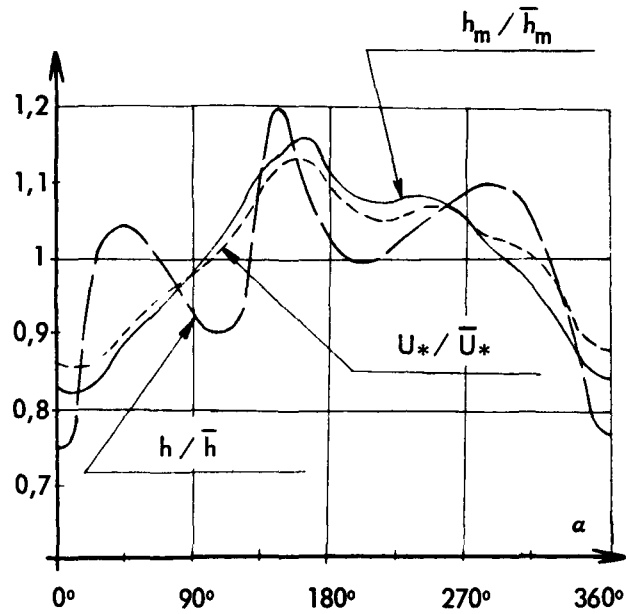


Figure 4. Comparaison des mesures pour un élément périphérique

distribution des températures dans le combustible et les gaines est calculée à partir des conditions aux limites d'échange de chaleur gaine-gaz et de la distribution des sources de chaleur telle qu'elle ressort d'expériences neutroniques. On peut ainsi déterminer la disposition des crayons qui permet d'extraire le maximum de puissance pour une température maximale de gaine donnée [4].

Déformation des crayons [4]

On a admis que les déformations réelles d'un crayon restaient inférieures à celles que prendrait isolément la gaine sous l'effet de ses seules contraintes thermiques en phase élastique. Pas ailleurs, toute déformation engendre une modification de la répartition des coefficients d'échange; cette modification elle-même peut tendre à accentuer les déformations et éventuellement conduire à une instabilité. C'est pourquoi une étude préalable d'évolution des coefficients d'échange en fonction du rapprochement de deux crayons voisins a été faite par l'analogie de transfert de masse et a permis de calculer en grandeur et en direction les flèches prises par les différents types de crayons; on a vérifié que ces flèches étaient stables [4].

ÉTUDE DES CORRUGATIONS [5]

Une première série d'essais a porté sur un écoulement dans un canal annulaire avec contour externe lisse et contour interne corrugué; ce dernier était chauffé électriquement avec un flux constant par unité de longueur. Par un calcul approprié, on corrige les résultats expérimentaux pour se ramener au cas où le contour externe est également chauffant, de telle sorte que le flux de chaleur radial le long de la ligne de vitesse maximale soit nul. On peut ainsi

définir un nombre de Margoulis, un coefficient de frottement et un nombre de Reynolds caractérisant intrinsèquement la surface corruguée. La mise en œuvre de ces expériences et leur dépouillement sont très longs, ce qui limite le nombre de types de surfaces étudiées. Par ailleurs, les corrugations offraient une perspective intéressante pour le refroidissement interne des éléments combustibles annulaires de la filière graphite-gaz, et l'installation d'essai ne permettait pas d'atteindre des nombres de Reynolds suffisamment grands. Aussi a-t-on réalisé à Saclay une deuxième série d'essais sur un autre montage comportant un tube circulaire refroidi intérieurement par du CO₂ sous pression et chauffé extérieurement par une circulation d'eau chaude dans des conditions telles que la température du tube évoluait très peu. Le tube était constitué par un assemblage soudé de plusieurs éléments corrugués intérieurement. Le Tableau 1

Tableau I. Mesures relatives aux corrugations internes

Type(a)	$R = 3 \cdot 10^5$		$R = 2 \cdot 10^6$	
	$10^3 f$	$10^3 \mathcal{M}$	$10^3 f$	$10^3 \mathcal{M}$
1	8,4	3,5	9,3	3,04
2	15,6	4,25	16,4	3,15
3	19,2	4,5	21,8	3,1
4	12,5	3,85	9	2,46
5	12,2	4,95	15,3	3,8

Note a:
 Type 1: Filetage à pas standard (hauteur 0,53 mm, pas 0,75 mm)
 Type 2: Filetage à pas carré (hauteur 0,2 mm, pas 1,4 mm)
 Type 3: Corrugations annulaires (hauteur 0,5 mm, pas 5 mm)
 Type 4: Ondulation approximativement sinusoïdale (profondeur 0,9 mm, pas 8 mm)
 Type 5: Corrugation orientée en chevron d'angle 20° avec l'écoulement et de profondeur 0,4 mm

donne, pour deux nombres de Reynolds R , le coefficient de frottement f et le nombre de Margoulis \mathcal{M} de quelques types étudiés.

Le laboratoire de Chatou (EDF) a fait quelques essais sur des tubes corrugués intérieurement en utilisant un chauffage externe à flux constant par effet Joule. Les résultats obtenus sont en excellent accord avec ceux du CEA à Saclay.

Dans leur ensemble, les résultats se prêtent bien aux corrélations préconisées par D. Dipprey et R. Sabersky [6].

GAINES À AILETTES LONGITUDINALES INTERNES

Des gaines à ailettes longitudinales internes ont été étudiées sur un tube de diamètre intérieur 50 mm et avec différentes surfaces d'échange. Pour un même nombre de Reynolds formé avec le diamètre hydraulique, le coefficient de frottement moyen sur le périmètre interne décroît lorsqu'on accroît le développement de la surface tandis que le rapport du nombre de Margoulis au coefficient de frottement décroît aussi mais semble tendre vers une valeur de l'ordre de 0,4 pour de grands développements (Rapport CEA à paraître).

ÉTUDES DES GAINES À AILETTES EN CHEVRONS

Les gaines à chevrons sont caractérisées par le fait que leurs ailettes sont disposées sur un nombre pair de secteurs d'une surface cylindrique, les ailettes de deux secteurs adjacents étant orientées symétriquement par rapport à la direction générale de l'écoulement. Ces gaines ont été étudiées pour équiper des tubes d'uranium de diamètre extérieur 40 et 43 mm, et comportent des ailettes hélicoïdales pour EDF2 et des ailettes planes pour EDF3, EDF4 et les projets suivants.

L'écoulement résulte de la symétrie géométrique: le gaz pénètre entre les ailettes près d'un plan de symétrie E, s'échauffe dans les sous-canaux formés par les espaces entre deux ailettes consécutives et s'échappe près du plan de symétrie S suivant pour décrire ensuite une trajectoire hélicoïdale et se réintroduire de la même manière entre les ailettes près du plan E. L'échauffement dans les sous-canaux crée sur la gaine, dans une section droite du canal, une succession de points chauds et de points froids: le recyclage du gaz crée sur une génératrice de la gaine une modulation de la température par rapport à une évolution moyenne. Si, en chaque point du contour intérieur de la gaine, on définit un coefficient d'échange h_0 par la température t_0 , la densité de flux de chaleur ϕ_0 en ce point et la température moyenne θ du gaz dans la section droite correspondante, on peut définir un nombre de Margoulis \mathcal{M}_0 tel que

$$\mathcal{M}_0 = \frac{h_0 s}{q C_p} = \frac{\phi_0 s}{(t_0 - \theta) q C_p}$$

où s , q et C_p sont respectivement la section de passage, le débit masse et la chaleur spécifique à pression constante du gaz.

Pour caractériser l'évolution circonférentielle et longitudinale de \mathcal{M}_0 , on considère sur le contour intérieur de la gaine les génératrices d'entrée G_E situées dans les plans de symétrie E d'entrée du gaz, les génératrices de sortie G_S dans les plans de symétrie S de sortie du gaz et les génératrices G_M dans les plans bissecteurs de deux génératrices G_E et G_S successives. Dans une section droite de la gaine, on constate alors expérimentalement que non seulement la moyenne $\bar{\mathcal{M}}_{0c}$ de \mathcal{M}_0 est très voisine de la moyenne des valeurs \mathcal{M}_{0G} que prend \mathcal{M}_0 sur les génératrices médianes G_M mais aussi que les différentes valeurs \mathcal{M}_{0G} sont pratiquement égales entre elles. Les valeurs \mathcal{M}_{0G} étant mesurées aisément, on a préféré rapporter la valeur minimale $\mathcal{M}_{0c \min}$ de \mathcal{M}_0 à une valeur \mathcal{M}_{0G} plutôt qu'à $\bar{\mathcal{M}}_{0c}$ pour définir le coefficient $f_c = \mathcal{M}_{0c \min} / \mathcal{M}_{0G}$ qui a été trouvé indépendant de l'abscisse de la section droite dans le canal.

Sur une génératrice médiane G donnée, on considère de même le rapport $f_1 = \mathcal{M}_{0G \min} / \bar{\mathcal{M}}_{0G}$ de la valeur minimale $\mathcal{M}_{0G \min}$ de \mathcal{M}_0 à la valeur moyenne $\bar{\mathcal{M}}_{0G}$ de \mathcal{M}_0 .

On constate également que f_1 ne dépend pas de la génératrice G_M choisie. Il en résulte que le nombre de Margoulis moyen $\bar{\mathcal{M}}_0$ sur toute la surface intérieure de la gaine est sensiblement égal à $\bar{\mathcal{M}}_{0G}$ et que la valeur minimale $\mathcal{M}_{0 \min}$ de \mathcal{M}_0 sur cette surface est donnée par $\mathcal{M}_{0 \min} = f_c f_1 \bar{\mathcal{M}}_{0G}$. C'est la valeur de $\mathcal{M}_{0 \min}$ qui est prise pour le calcul des points chauds de gaine dans un réacteur. Les références [7] et [8] donnent l'étude détaillée des singularités thermiques.

L'effort de traînée F qu'exerce l'écoulement sur une gaine et son canal est mesuré sur une longueur suffisante L ; on en déduit un coefficient de frottement global tel que: $F = f_0 \pi D_0 L (q^2 / 2 \rho s^2)$, où D_0 est le diamètre intérieur de la gaine (diamètre extérieur de l'uranium) et ρ la masse volumique moyenne sur la longueur L .

La traînée sur le canal est faible devant celle de la gaine, qui est due principalement à la variation de quantité de mouvement entre l'entrée et la sortie des sous-canaux. C'est ce que confirme l'expérience qui montre que f_0 ne dépend du nombre de Reynolds que pour les faibles valeurs de celui-ci et ne dépend pas du diamètre du canal, tout au moins dans la plage étudiée (90 à 120 mm pour un diamètre intérieur de gaine de 40 ou 43 mm). Dans la même plage, le diamètre du canal est également sans influence sensible sur le nombre de Margoulis $\bar{\mathcal{M}}_0$, ainsi d'ailleurs que sur les coefficients f_c et f_1 . Il en résulte que les coefficients $\bar{\mathcal{M}}_0$, f_0 et f_1 caractérisent la gaine indépendamment du diamètre du canal.

Méthodes d'essai

Trois méthodes ont été employées; elles sont décrites dans les références [7] et [8]; la première, dite à chauffage isotherme, consiste à chauffer intérieurement la gaine par un courant d'eau chaude avec un débit suffisant pour que la paroi intérieure de la gaine

soit presque isotherme. La gaine est refroidie extérieurement par un courant de CO_2 sous pression. La mesure des débits et des températures d'entrée et de sortie des deux fluides fournit un nombre de Margoulis moyen par un calcul simple. Le même montage d'essai sert à la mesure de f_0 . Cette méthode, rapide à mettre en œuvre, a été très développée au laboratoire de Saclay; compte tenu des remarques du paragraphe précédent, elle permet d'essayer un grand nombre de profils, dont les meilleurs sont étudiés plus en détails par la seconde méthode, dite à flux constant. Dans cette dernière, les gaines sont chauffées par effet Joule, soit à l'aide d'éléments constitués d'un tube d'acier inox isolé électriquement de la gaine par un dépôt rectifié de zircon (laboratoire du CEA), soit par un tube unique d'acier inox muni d'un isolant en tissu de verre (laboratoire de l'EDF). Les gaines sont équipées de thermocouples le long d'une génératrice médiane au moins, et, dans une ou plusieurs sections droites, sur les génératrices G_E , G_S et G_M . Tous ces thermocouples permettent d'accéder à la fois à \bar{M}_0 et aux coefficients f_c et f_1 .

Malgré le volume important de résultats locaux que la seconde méthode est susceptible de fournir, il s'est avéré nécessaire, pour la bonne compréhension des phénomènes physiques, d'étudier plus finement et plus complètement les singularités de température dans la gaine et l'évolution des vitesses et des températures dans l'écoulement. C'est pourquoi des essais ont été réalisés à grande échelle et à la pression atmosphérique pour des commodités expérimentales, tout en conservant la possibilité d'atteindre des nombres de Reynolds voisins de ceux du réacteur [7]. Le chauffage était à flux constant comme pour les essais sous pression. Ces trois méthodes ont donné des résultats très cohérents entre eux.

Représentation des résultats

Chaque gaine peut être caractérisée par ses coefficients f_0 , f_c et f_1 et par l'évolution de \bar{M}_0 en fonction d'un nombre de Reynolds \mathcal{R}_0 formé avec le diamètre intérieur de la gaine. Pour un nombre de Reynolds donné, des gaines qui présentent le même resserrement d'ailette et sensiblement la même surface par unité de longueur se prêtent bien à une représentation dans un diagramme (\bar{M}_0, f_0) car, en coordonnées logarithmiques, les points représentatifs se groupent autour d'une droite $\bar{M}_0^n/f_0 = \text{constante}$, avec n voisin de 3. Or, si l'on considère un canal de réacteur dont on adapte la section de passage pour que son débit et ses températures d'entrée et de sortie soient fixes, il en résulte que la puissance de soufflage à associer au canal seul est sensiblement proportionnelle à f_0/\bar{M}_0^3 . C'est pourquoi le rapport \bar{M}_0^3/f_0 a été pris comme critère de qualité. L'ensemble des résultats obtenus sur les gaines à chevrons figure dans les rapports annexés à la présente communication. Dans ce qui suit, on ne fera état que de ceux qui illustrent le mieux les remarques précédentes en présentant successivement:

a) les gaines à ailettes hélicoïdales (retenues pour le réacteur EDF2);

b) les gaines à ailettes planes (retenues pour les réacteurs EDF3 et EDF4).

Gainnes à ailettes hélicoïdales

Un grand nombre d'essais ont été effectués [7-9], en faisant varier le nombre d'ailettes (de 36 à 80), l'angle α d'inclinaison des ailettes par rapport à l'écoulement (de 36 à 80°) et le nombre de secteurs (de 4 à 8). Les résultats sont portés sur la figure 5 dans le diagramme (\bar{M}_0, f_0) pour $\mathcal{R}_0 = 7 \times 10^5$; on constate que les points se groupent autour d'une même courbe $\bar{M}_0^n/f_0 = \text{constante}$, pour un nombre d'ailettes donné.

Afin de rechercher des corrélations entre les différents paramètres géométriques propres aux ailettes en chevron une série d'essais particulièrement fructueux a été réalisée avec la méthode du chauffage isotherme [7]; on a fait varier l'angle α de 10 à 50° et le nombre de secteurs de 4 à 16, tout en conservant un même profil de sous-canal dans sa section droite et des épaisseurs d'ailettes voisines. La figure 6 donne les résultats dans le diagramme (\bar{M}_0, f_0) pour $\mathcal{R}_0 = 7 \times 10^5$. On constate que les points se groupent très bien autour d'une seule courbe $\bar{M}_0^n/f_0 = \text{constante}$.

Gainnes à ailettes planes [10, 11]

Les essais sur gainnes hélicoïdales montrèrent que, pour augmenter \bar{M}_0^n/f_0 , il convenait de développer encore la surface chauffante, ce qui a pu être réalisé par l'emploi de fraises-scies conduisant à des ailettes planes. Différents facteurs concourent à la limitation de la surface d'échange à partir d'un diamètre de base donné; aussi, toutes les gainnes étudiées diffèrent-elles plus par l'agencement des ailettes que par la section droite des sous-canaux; c'est ainsi que la distance ϵ entre les plans de symétrie de deux ailettes successives n'a guère varié qu'entre 1,5 et 2,2 mm; de ce fait, le nombre d'ailettes n'a pas varié beaucoup. Parallèlement, les hauteurs d'ailettes sont restées comprises entre 7 et 10 mm.

Par contre, une étude très poussée a été faite sur les paramètres géométriques suivants:

a) Angle α des ailettes avec la direction générale de l'écoulement (15 à 30°);

b) Profil longitudinal des ailettes et du fond du sous-canal, ce dernier pouvant être rectiligne, concave ou convexe;

c) Forme géométrique de la gaine au voisinage de ses plans de symétrie: implantation des centreurs (incorporés ou rapportés), utilisation des rainures longitudinales, etc.

On n'a pas recherché à nouveau à étudier d'une façon systématique le nombre de secteurs, qui a été principalement de 8, sauf pour quelques essais particuliers.

Pour un nombre de Reynolds \mathcal{R}_0 donné, dans le diagramme (\bar{M}_0, f_0) , les points représentatifs des gainnes se groupent dans une bande de $\pm 15\%$ autour d'une courbe $\bar{M}_0^n/f_0 = \text{constante}$ (n étant voisin de 3), ainsi que le montre la figure 7. Les coefficients de

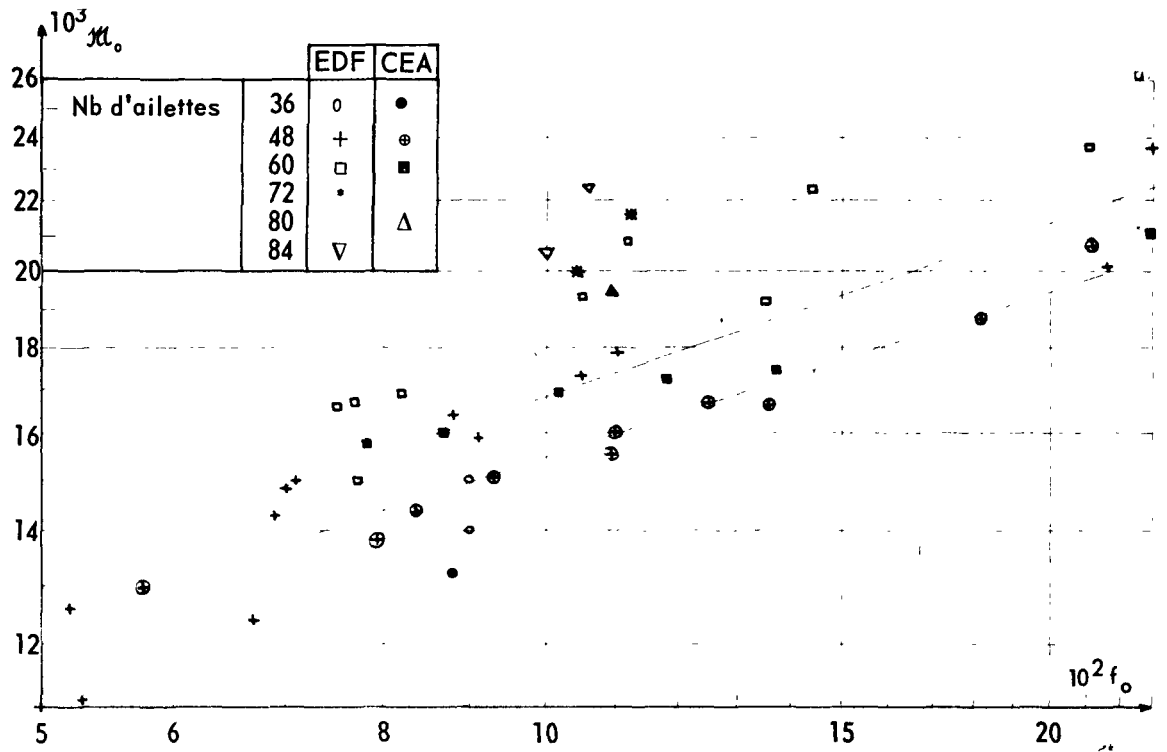


Figure 5. Gains à ailettes hélicoïdales: $R_0 = 7 \times 10^6$

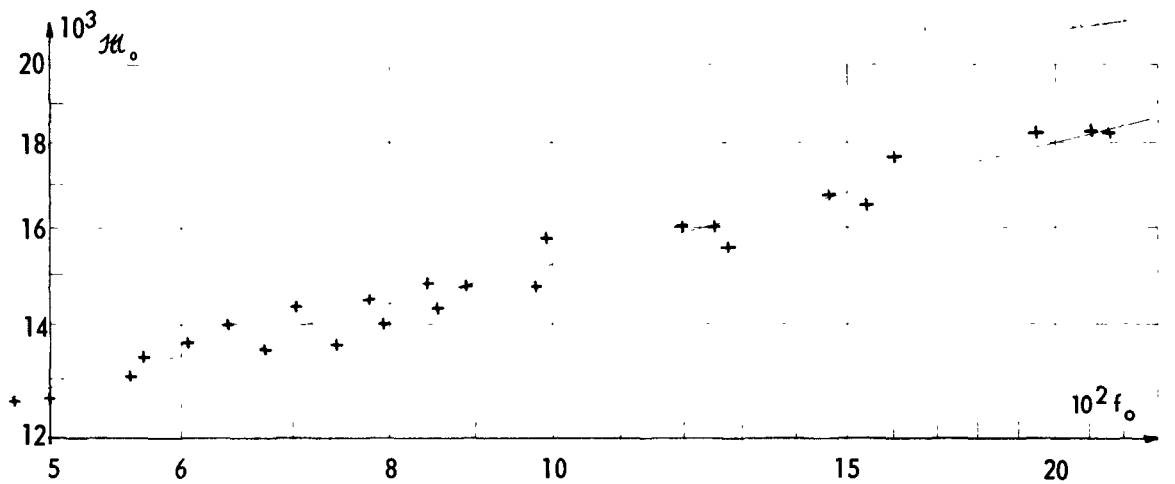


Figure 6. Gains à ailettes hélicoïdales (variation de α et du nombre de secteurs)

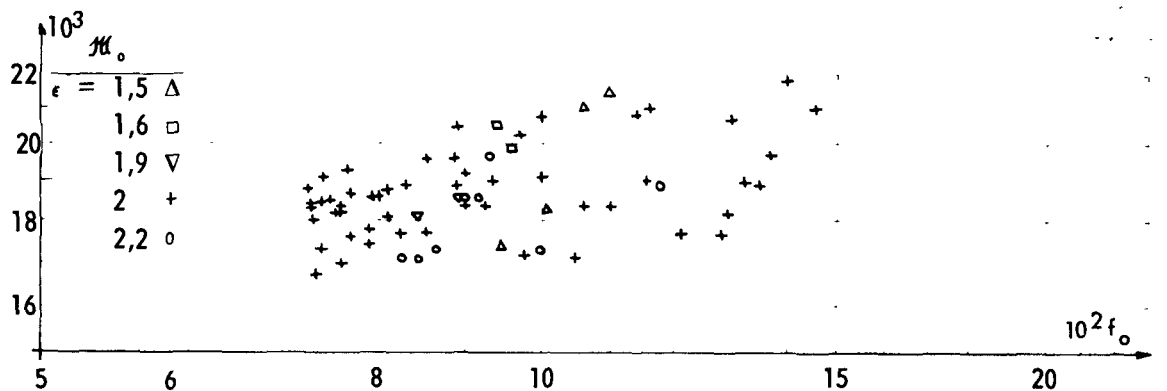


Figure 7. Gains à ailettes planes

singularité f_c et f_1 associés à ces gaines restent compris dans les intervalles suivants: $0,85 < f_c < 0,95$ et $0,90 < f_1 < 0,95$.

Synthèse des résultats expérimentaux [12]

Une formulation semi-théorique a été élaborée au CEA pour le calcul a priori des coefficients \bar{M}_0 et f_0 d'une gaine à chevrons. Cette formulation, qui regroupe bien les résultats obtenus sur les gaines à ailettes hélicoïdales, utilise des valeurs expérimentales de répartition de vitesse entre les ailettes et d'évolution de coefficient d'échange sur les parois de celles-ci.

CONCLUSION

Les résultats dont il est fait état dans la présente communication se caractérisent par leur qualité autant que par l'ampleur du travail qu'ils représentent. Leur validité peut être illustrée par le fait que, pour les gaines à chevrons, deux laboratoires très différents comme ceux de l'EDF à Chatou et du CEA à Saclay recoupent leurs valeurs numériques à 10% près. Tant pour les études de grappes que pour celles des gaines à chevrons, une des préoccupations constantes des expérimentateurs est d'orienter leurs travaux en s'affranchissant le plus possible d'un empirisme facile au bénéfice de la connaissance physique des phénomènes eux-mêmes.

BIBLIOGRAPHIE

1. Berriaud, C., *Etude des pertes de charge dans les grappes EL4*, Rapport CEA 2465.
2. Gasc, B., *Etude thermique de la grappe EL4 à la pression atmosphérique*, Rapport CEA 2466.

3. Geffroy, J., *Utilisation des transferts de masse et de quantité de mouvement pour l'étude des coefficients locaux d'échange de chaleur dans un élément de combustible en grappe*, Rapport CEA 2468.
4. Berriaud, C., Gargaud, J., Gasc, B., Geffroy, J., et Richardot, J., *Problèmes aérothermiques posés par l'étude d'une grappe*, Rapport CEA 2467.
5. Gargaud, J., et Paumard, G., *Amélioration du transfert de chaleur par l'emploi de surfaces corruguées*. Rapport CEA 2464.
6. *Heat and momentum transfer in smooth and rough tubes at various Prandtl numbers*, Technical Report 32-269, Jet Propulsion Laboratory, California Institute of Technology (juin 1962).
7. Pelce, J., François, S., Houseaux, O., et Pierre, B., *Etude expérimentale du transfert de chaleur et des pertes de charge des gaines à ailettes hélicoïdales en chevron*, Rapport CEA 2469.
8. Rodet, E., *Etude de l'écoulement d'un fluide dans un canal équipé de cartouches chauffantes à ailettes polyzonales ou chevrons*, Bulletin du Centre de recherches et d'essais de Chatou n° 4) (juin 1963).
9. Milliat, J. P., *Etude expérimentale de gaines à ailettes de type chevron*. Symposium of the Institution of Mechanical Engineers, Londres (novembre 1960) et The Journal of British Nuclear Energy Conference, vol. 6, n° 4 (octobre 1961).
10. Pierre, B., François, S., Liermann, J., Maillet, E., et Pelce, J., *Etude expérimentale du transfert de chaleur et des pertes de charge de gaines à ailettes planes en chevrons*, Rapport CEA 2470.
11. Milliat, J. P., *Etude expérimentale de gaines à ailettes chevrons pour réacteurs nucléaires refroidis au gaz*, Bulletin du Centre de recherches et d'essais de Chatou, n° 2 (octobre 1962).
12. Pelce, J., Malherbe, J., et Pierre, B., *Etude théorique et expérimentale du transfert de chaleur et des pertes de charge de gaines à ailettes en chevron: corrélations entre paramètres géométriques et aérothermiques*. Rapport CEA 2471.

ABSTRACT—RÉSUMÉ—АННОТАЦИЯ—RESUMEN

A/50 France

Aerodynamic and thermal studies of cans of gas cooled fuel elements

By P. Gelin and J. P. Milliat

Research on clusters was undertaken at the CEA in 1959, while studies on herring-bone cans were developed at the EDF laboratory at Chatou and the CEA laboratory at Saclay, at the end of 1959. In 1962, a general study on corrugations was begun at the Saclay laboratory with a view to improving the clusters, and continued later in both laboratories relative to the internal cooling of annular fuel elements. As these studies progressed, trial facilities were extended while experimental methods have improved constantly. At the present time, both laboratories, working in complete collaboration, have powerful means at their disposal.

Work on the clusters has been concerned chiefly

with pressure losses due to the assembly parts, and with the temperature variations around the elements of the cluster. In this way, we have been able to determine satisfactorily the hot points of the can, the deformations of the fuel elements and the conditions of stability of these deformations.

In the case of the herring-bone cans, studies have been directed to the evolution of performances as a function of the geometric parameters on the one hand, and to the special aerodynamic and thermal features caused by the fins and by interruptions of cartridge on the other hand. These studies have led to a very thorough knowledge of the cartridges chosen for the reactors EDF2 and EDF3, and now, open up very hopeful prospects for future reactors, particularly those fitted with annular elements; among the alternatives suitable for the inner surface of the annular element can, corrugations and longitudinal fins have been fairly extensively tested over a wide range of Reynolds number.

A/50 Франция

Аэродинамические и термические исследования оболочек тепловыделяющих элементов, охлаждаемых газом

П. Желен, Ж. П. Мийэ

Исследования пучков тепловыделяющих элементов были предприняты Комиссариатом по атомной энергии в 1959 году; в конце этого же года лаборатория фирмы «Электрисите де Франс» в Шату и лаборатория Комиссариата по атомной энергии в Сакле приступили к исследованию ребристых оболочек. В 1962 году в лаборатории Сакле началось общее исследование оболочек с рифлеными поверхностями, направленное на усовершенствование пучков элементов; затем оно было продолжено в обеих лабораториях с целью улучшения внутреннего охлаждения кольцевых тепловыделяющих элементов. В ходе выполнения этих исследований создавалось опытное оборудование и улучшались методы экспериментов. В настоящее время обе лаборатории, работающие в тесном контакте, располагают мощной экспериментальной базой.

При исследовании пучков особое внимание было уделено падениям нагрузки, обусловленным крепежными деталями и колебаниями температуры вокруг элементов пучка. Удалось также найти удовлетворительное решение проблемы теплонапряженных мест оболочки, деформации элементов и условий стабильности этих деформаций.

Исследования ребристых оболочек были посвящены изменениям характеристик в зависимости от геометрической формы ребер, а также аэродинамическим и термическим особенностям, обусловленным ребрами и прерывистостью тепловыделяющих элементов. В результате этих исследований было получено полное представление о тепловыделяющих элементах, предназначенных для реакторов EDF-2 и EDF-3, и в настоящее время намечены весьма обнадеживающие перспективы для тепловыделяющих элементов (особенно кольцевых) будущих реакторов. Представляют интерес результаты экспериментов, проведенных в широкой области

числа Рейнольдса, с кольцевыми тепловыделяющими элементами, имеющими внутреннюю оболочку с рифленой поверхностью и продольными ребрами.

A/50 Francia

Estudios Aerodinámicos y Térmicos de las Vainas de Elementos Combustibles Refrigerados por Gas

por P. Gelin y J. P. Milliat

Los estudios de haces de barras han sido llevados a cabo en el CEA en 1959, mientras que los de vainas con aletas longitudinales se han desarrollado en el Laboratorio de Chatou del EDF y en el Laboratorio de Saclay del CEA a finales del año 1959. En 1962 se ha comenzado en el Laboratorio de Saclay un estudio general sobre las corrugaciones para la mejora de los haces y se ha continuado después en los dos laboratorios para el enfriamiento interno de los elementos combustibles anulares. A medida que avanzaban estos estudios, se han ampliado los medios de pruebas, mientras los métodos experimentales no han cesado de mejorarse. Actualmente, los dos laboratorios, que trabajan en plena colaboración, disponen de poderosos medios.

Respecto a los haces de barras, el esfuerzo se ha dirigido sobre todo a las pérdidas de carga debidas a las piezas de ensambladura y a las variaciones de temperatura en torno a los elementos del haz. Así se ha llegado a determinar de un modo satisfactorio los puntos calientes de las vainas, las deformaciones de los elementos y las condiciones de estabilidad de estas deformaciones.

Respecto a las vainas con aletas longitudinales los estudios han versado, por un lado, sobre la evolución de las comprobaciones en función de los parámetros geométricos, y por otro, sobre las singularidades aerodinámicas y térmicas creadas tanto por las aletas como por las interrupciones del cartucho. Estos estudios han desembocado en un conocimiento muy completo de los cartuchos escogidos para los reactores EDF2 y EDF3, y abren ahora perspectivas muy alentadoras para los reactores futuros, en particular los equipados con elementos anulares; entre las soluciones convenientes para la envoltura interna del elemento anular, las contracciones y las aletas longitudinales han sido objeto de pruebas bastante extensas en un amplio margen del número de Reynolds.

The influence of an electric field on the heat transfer to CO₂ coolant at high and low pressure in a nuclear reactor

By F. Berger and L. Derian*

At the 1958 Geneva Conference we reported [1] the results of experiments showing that, by the application of an electric field, it is possible to increase the transfer of heat into a gaseous coolant partially ionized by radiation in a nuclear reactor. The experiments were carried out with electrically heated elements cooled with air at atmospheric pressure. An increase of the heat transfer into partially ionized air is attainable at substantially lower voltages than in un-ionized air [2, 3, 4, 5].

The effect of the electric field on the transfer of heat is caused by electroconvection, i.e., the flow of gas is affected by the motion of ions in the electric field. In un-ionized gas the effect can occur only with a large potential gradient which causes field ionization in the gas. The density of ions in the cooling gas of a nuclear reactor is relatively high, consequently the flow of gas and the transfer of heat can be influenced by electric fields of intensities too low to cause field ionization.

Since 1958 we have continued our work on this problem. A theoretical analysis of the influence of an electric field on the flow of a partially ionized gas has been carried out [6, 7]. This has improved the understanding of the mechanism of the process and has helped with the analysis of experimental data. Experiments for the determination of the influence of an electric field on the transfer of heat into air and into carbon dioxide at pressures up to 2 kp/cm² (kgf/cm²) were carried out in a reactor with the aid of an electrically heated model of a fuel element [8]. A similar series of experiments was carried out with a uranium fuel element and carbon dioxide at pressures up to 30 kp/cm² in a nuclear reactor. The cylindrical elements were 28 mm in diameter and the applied potential differences were such that field ionization was impossible. All experiments were carried out with direct fields. The results of these experiments form the subject of this paper.

After the 1958 Geneva Conference some experiments on the influence of an electric field on the transfer of heat into CO₂ in a nuclear reactor were carried out in France [9]. The experimental conditions were substantially different from ours. A thin (1.4 mm diam) electrically heated wire was used and con-

sequently the electric field was not homogeneous and at higher voltages corona discharges occurred. The French experiments, contrary to ours, were carried out with alternating electric fields. The results are not, therefore, directly comparable.

EXPERIMENTAL METHOD

Experiments at low pressures

The experiments were carried out in a low pressure closed-circuit reactor loop. A number of the elements of the loop consisted of those used previously in an open-circuit loop described in Ref. [1]. In particular we re-used the experimental channel, formed by a Field-type tube, and the heating element made of stainless steel (od 28 mm, length 485 mm), internally heated by an electric wire. The lower part of the channel, containing the heating element, was inserted into the core of the reactor VVR-S. The electric field was formed between the earthed heating element and the insulated lower part of the inner tube (id 41 mm), which was connected to an adjustable HT source. The flow of gas was obtained by a Roots pump. The surface temperature of the element was measured in three positions with Ni-NiCr thermocouples and the temperatures of the gas with Cu-constantan thermocouples. A detailed description of the experimental arrangement and apparatus is given in Ref. [8].

The experiments were carried out with CO₂ at pressures of 1, 1.5 and 2 kp/cm and with air at pressures of 1 and 2 kp/cm². The velocity of the gas was between 3 and 25 m/s, the reactor power was from 500 up to 2 500 kW of heat, and the potential difference between the electrodes 0–3 000 V. The mean temperature of the gas was 120–190 °C and the surface temperature of the element between 350 and 450 °C. The Reynolds number in the experimental channel was from 5×10^3 to 3.5×10^4 .

Experiments at high pressures

These experiments were carried out in a high pressure gas-cooled loop of the reactor VVR-S; this loop has been described elsewhere [10, 11 and 13]. A rod-type fuel element of natural uranium, clad with a magnesium alloy, was used. The diameter of the uranium core was 24 mm and its length 500 mm, while the

* Institute of Nuclear Research Řež, near Prague.

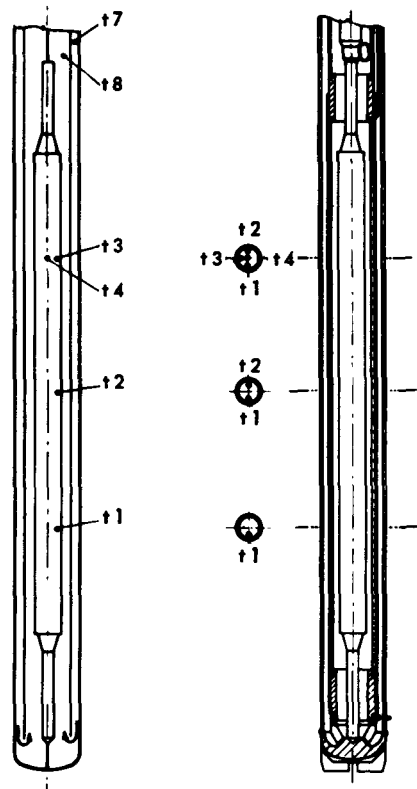


Figure 1 (left). Arrangement of thermocouples in the uranium fuel element.—Figure 2 (right). Design of the lower part of the experimental reactor loop channel

diameter of the clad element was 28 mm. The element was again placed vertically. Four vertical holes were drilled into the uranium. Magnesium tubes, closed at their bottom ends, were inserted into the holes and welded into the top lid of the element. Chromel-alumel thermocouples contained in flexible stainless steel tubes (1 mm diam) and insulated by powdered MgO were inserted into the magnesium tubes. Three thermocouples measured the temperatures at various depths near the surface of the uranium, while the fourth thermocouple measured the temperature on the axis of the uranium rod at the same depth as the uppermost surface thermocouple. The thermocouples were located inside the fuel element in order to avoid any possible effect of the thermocouples on the surface temperature and also to avoid any interference with the electric field between the fuel element and the outer electrode. The temperature of the gas at the points of entry and exit from the experimental area was measured with similar thermocouples. The placing of the thermocouples is shown schematically in Fig. 1.

The channel of the loop was again a Field tube. The external tube was made of stainless steel clad with aluminium, while the internal tube was made of aluminium. The lower part of the aluminium tube was insulated by quartz rings and a micanite coat, and formed the outer electrode. The high voltage was brought to the outer electrode by the aid of a cable with silicon-rubber insulation. The polarity

of the applied voltage could be reversed. The fuel element formed the second electrode and was earthed. The gap between the coaxial electrode was 6 mm. Details of the lower part of the experimental channel are shown in Fig. 2. The construction of the whole channel is described in detail in Ref. [12].

The source of high voltage consisted of four rectifiers connected in a Grätz circuit. The nominal voltage was 2×50 kV with an output current of 50 mA.

The experiments were carried out with carbon dioxide at pressures of 5 to 30 kp/cm², the reactor power was 500 to 2 000 kW, the gas velocities were 5 to 26 m/s, and the potential difference between the electrodes was from 0 to 30 kV. The maximum reactor power of 2 000 kW corresponds to a mean thermal neutron flux of 7.5×10^{12} n/cm²s in the fuel element and 9.2×10^{12} in the cooling gas. The heat output of the fuel element was 9.3 kW and its surface temperature was up to 400 °C. The temperature of the gas was 25–50 °C on entry and 45–100 °C on exit. The range of Reynolds numbers was from 6×10^4 to 6×10^5 .

EXPERIMENTAL RESULTS

Experiments at low pressures

The mean value of the heat transfer coefficient was evaluated for the upper part of the experimental section and thus the influence of the entrance section was eliminated. The heat transfer coefficient was calculated for the steady state before and after as well as during the application of the electric field. The heat output of the element was determined by the heat balance of the gas. A further check was obtained from the electrical input of the element. During the application of the electric field the heat balance of the gas includes the electric power dissipated in the HT circuit, which is not removed from the element. Consequently the thermal output of the element during the action of the field was considered equal to the output before and after the application of the field. The relative change of the heat transfer coefficient α is then $\alpha'/\alpha = \Delta t/\Delta t'$ where Δt is the difference in the mean temperature between the surface of the

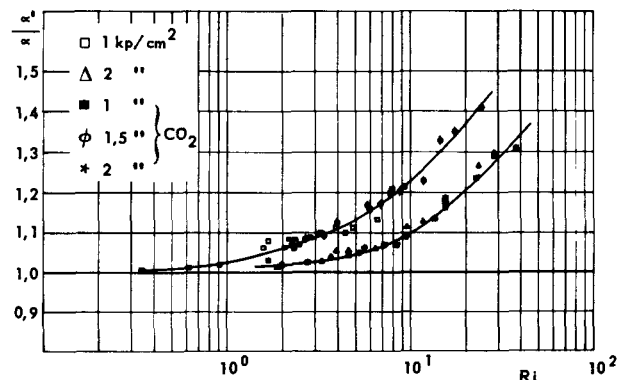


Figure 3. Relative increase in the mean heat — transfer coefficient for air and CO₂ at low pressures

element and the gas; the dashed letters refer to the values during the application of the field.

At these low pressures the electric field changed the value of the heat transfer coefficient only if the element acted as the cathode. A similar result was obtained previously [1].

Figure 3 shows the relative improvement of the heat transfer, i.e., the ratio α'/α , as a function of the modified Richardson criterion Ri . The significance of this criterion for the flow of gas in a transverse electric field was shown by Stach [6]. Under the present experimental conditions the influence of the electric field on the heat transfer is determined by processes in the diffusive layer near the cathode. With certain simplifying assumptions the following relations were derived for this layer [7]:

For unsaturated currents between the electrodes, $i < 0.6$;

$$Ri = \frac{e\phi_h n_0 h^2}{D_1 \rho w_s^2} \cdot \frac{i^2}{i + C_1 i^2} \sqrt{C_{0k}}. \quad (2)$$

For currents near saturation, $i > 0.7$;

$$Ri = \frac{e\phi_h n_0 h^2}{D_1 \rho w_s^2} i \left[1 + \frac{\frac{\lambda}{2} (1 + 3\mathcal{E})(1 - i)}{1 - \frac{4 - \lambda}{10} (1 - i)} \right] \quad (3)$$

where:

ϕ_h : potential difference between the electrodes

n_0 : ionization density

D_1 : diffusion constant for cations

ρ : density of the gas

w_s : mean velocity of the gas

h : width of the channel

$i = \frac{I}{I_M}$: degree of saturation of the current

I : electric current

$I_M = n_0 e V$: saturated current

V : volume of gas in the channel

$C_1, C_{0k}, \lambda, \mathcal{E}$: constants dependent upon gas parameters

It can be shown [8] that, for a given geometry of the experimental channel and approximately constant temperature of the gas, Eqs. (2) and (3) can be rewritten as:

$$i < 0.6: Ri = K \frac{\phi_h I_M}{w_s^2} \cdot \frac{i}{1 + C_1 i} \sqrt{C_{0k}} \quad (4)$$

$$i > 0.7: Ri = K \frac{\phi_h I_M}{w_s^2} i \left[1 + \frac{\frac{\lambda}{2} (1 + 3\mathcal{E})(1 - i)}{1 - \frac{4 - \lambda}{10} (1 - i)} \right] \quad (5)$$

where K is a constant for a given gas.

The method for the calculation of the degree of saturation of the current i and of the Richardson criterion is given in [8].

From Fig. 3 it is apparent that the experimental points for both gases at equal pressures fall on one

curve. It appears that the Richardson criteria as used here accounts well for the difference in the properties of the two gases but not for the different pressures. In the lower part of the curve the ratio of the relative increase α'/α for equal Ri is more than twice as large for 1 kp/cm² than for 2 kp/cm²:

$$[(\alpha' - \alpha)/\alpha]_{1\text{kp/cm}^2} = 2.33 [(\alpha' - \alpha)/\alpha]_{2\text{kp/cm}^2}$$

In the region of higher Ri this ratio decreases. At a pressure of 1.5 kp/cm² the values of α'/α do not lie between those for 1 and 2 kp/cm² as might be expected, but practically on the curve for 1 kp/cm². Similarly, the measured currents I at a pressure of 1.5 kp/cm² are higher than theoretically expected. The cause of this discrepancy might be the inaccuracy in the values of the recombination coefficient and the ionic mobilities at the given pressure.

The maximum increase in the heat transfer coefficient, 40%, was achieved in an experiment with CO₂ at a pressure of 1.5 kp/cm² and a reactor power $W_r = 2500$ kW, the voltage was 2.4 kV and the mean gas velocity 5.4 m/s. As shown in Fig. 3, the maximum possible increase in the heat transfer coefficient was never achieved. A further increase in Ri , caused particularly by increased voltage, might further increase α' .

Some experiments with CO₂ at low voltage (up to 1000 V) and small Reynolds numbers ($\sim 5 \times 10^3$) showed a negative effect, i.e., the heat transfer coefficient was decreased by the action of the electric field. This effect was small, i.e., up to 4% at a pressure 1.5–2 kp/cm² and only a few tenths % at 1 kp/cm². As the voltage is increased, the negative effect disappears and becomes positive. The negative effect presumably occurs when the stabilizing action of the electric field on the gas flow predominates over the disturbance of the cathode boundary layer caused by the field. The negative effect is not shown in Fig. 3.

Experiments at high pressure

From the experimental values obtained with the uranium fuel element and with CO₂ at high pressures, the local heat transfer coefficients were evaluated for the points at which the thermocouples were located in the fuel elements. The dependence of the effect on the distance from the point of entry of the cooling gas could thus be shown. The local values of α_x were determined under the following assumptions:

(a) The vertical distribution of the neutron flux remained unchanged when the experimental fuel element was inserted into the reactor core;

(b) The conduction of heat along the axis of the fuel element was negligible;

(c) The surface temperature of the cladding was equal to the temperature measured in the uranium near the surface.

Although these assumptions were not precisely fulfilled, small deviations from them could not seriously affect the results, because the relative change of the heat-transfer coefficients, caused by the action of the electric field, was evaluated. The specific heat

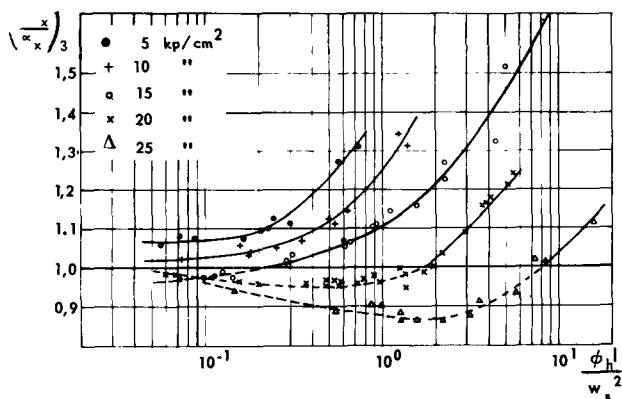


Figure 4. Relative change of the local heat-transfer coefficient at point 3; negative polarity of the fuel element

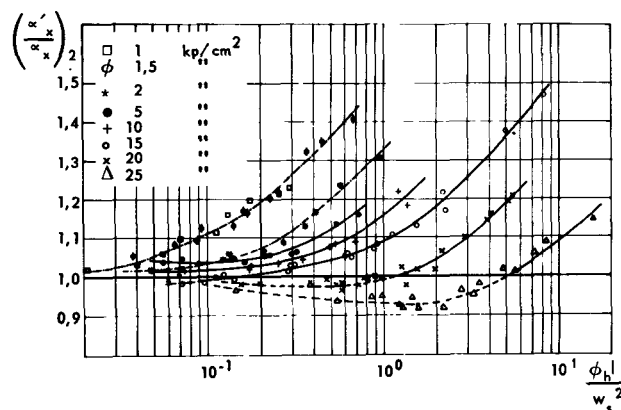


Figure 5. Relative change of the local heat-transfer coefficient at point 2; negative polarity of the fuel element

release in the three evaluated points as well as the corresponding gas temperatures could then be easily calculated from the known heat output of the element which was again determined from the heat balance, the known vertical distribution of the neutron flux and from the measured entrance and exit temperatures of the gas. The local heat transfer coefficients were then calculated with the aid of Eq. (1).

The current between the electrodes, at the applied pressures and potential differences, was far from saturation. This is shown by theoretical calculation as well as by the measured dependence of the current on the voltage. The exact evaluation of the Richardson criterion in the form given above is difficult in these cases for following reasons: the accuracy of the degree of saturation of the current, as determined either by calculation or by extrapolation of the experimental curve current vs. voltage, is low. Also, the values of the recombination coefficient and the ionic mobilities, as given in literature for the given range of pressures, are not very reliable.

It may be shown, however, that if we assume that the ionic mobilities and recombination coefficients are inversely proportional to the pressure (this supposition is approximately valid in the range of studied pressures), the values of C_1 and C_{0k} are independent of pressure, and Eq. (4) can be rewritten as:

$$Ri = K_1 \frac{\phi_h I}{w_s^2} \cdot \frac{1}{1 + C_1 i}, \quad (6)$$

where I is the measured current. Because C_1 is smaller than 1, and i is of the order of 0.1, we may write $C_1 i \ll 1$ and

$$Ri \approx (\phi_h I) / w_s^2 \quad (7)$$

Figures 4 and 5 show the change of the local heat transfer coefficients α'_x/α_x as a function of the value $\phi_h I / w_s^2$ again for the negative polarity of the fuel element. It is apparent, that at high pressures the ratio α'_x/α_x is at first smaller than 1, i.e., the electric field causes a decrease of heat transfer: after passing its minimum the value of α'_x/α_x grows and reaches values larger than 1—the heat transfer is increased. The higher the pressure of the gas, the higher are

values of $\phi_h I / w_s^2$ necessary to achieve the positive effect. At constant $\phi_h I / w_s^2$ the relative increase in heat transfer becomes smaller with increasing pressure. The maximum increase in α_x of over 60% was achieved at a pressure of 15 kp/cm²; the gas velocity was 7 m/s and the voltage 20 kV. However, the maximum possible increase in α_x was achieved at zero pressure. The attainable value $\phi_h I / w_s^2$ was limited by the gas velocity which was necessary for cooling the fuel element as well as by the voltage at which discharges in the channel occurred. The magnitude of the negative effect increases with increasing pressure; at 25 kp/cm² the maximum relative decrease in α_x was 12%.

The increase in the mean value of the heat transfer coefficient as found at low pressures is comparable—in view of the positions of the thermocouples—with the change of the local α_{x2} at point 2. The change of the mean α in CO₂ at pressures of 1 and 2 kp/cm² is therefore shown in Fig. 5 by dotted and dashed lines.

A comparison of Fig. 4 and 5 shows that the effect depends also on the position of the measured point. Both the positive and the negative effects are in most cases larger at point 3, near the gas exit, than at point 2, which was nearly at the middle height of the reactor core. This difference is still more evident from Fig. 6, where the ratio α'_x/α_x is given as a function of the applied voltage at a constant reactor power for all three measured points; the gas velocity appears as a parameter. The effect at point 1, which was nearest to the gas entry, is smallest. We suppose that the dependence of the effect on the position is caused by the influence of the entrance section upon the flow of gas as well as by the increasing concentration of ions in the gas along the channel. It is difficult to separate these two factors and define their relative importance. Figure 6 shows also the influence of the separate variables, i.e., the gas velocity and the voltage, on the change of the heat-transfer coefficient.

The dispersion of the measured values, which is apparent from Figs. 4 and 5, can be explained by the following reasons: at some experimental conditions (especially at high pressures) fluctuations were

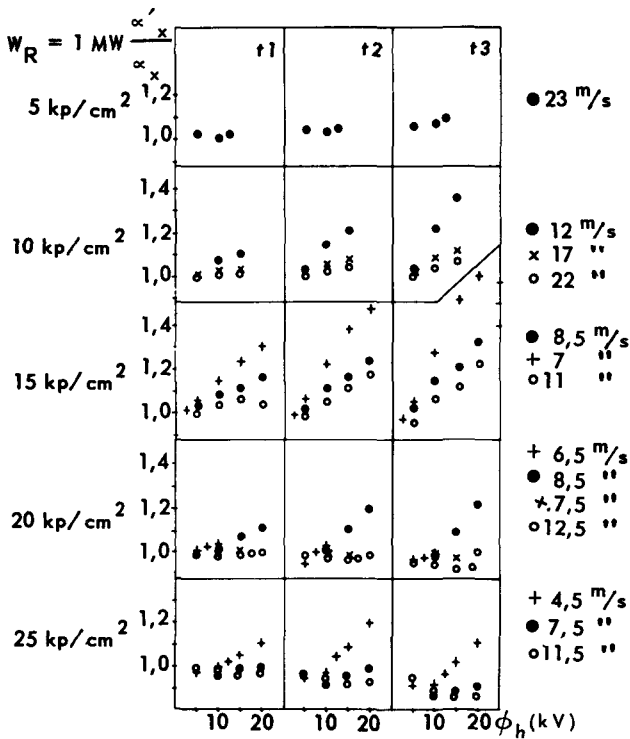


Figure 6. Relative change of the local α_x as a function of the applied voltage at different heights; negative polarity of the fuel element

caused by the simultaneous operation of two gas circulators (their rpm being not exactly equal) which decreased the accuracy of the determined gas velocities. A correction of the gas velocity, on the basis of the known thermal output of the fuel element, was made in those cases. This imperfection was removed later by including a second gas volume into the loop and by transferring the orifice to another position. Another probable reason for the dispersion of the measured values are the approximations made in the derivation of the criterion $\phi_h I / w_s^2$, where some factors, which may influence the effect in a low degree, were neglected. It is not clear yet whether the value $\phi_h I / w_s^2$, which resulted from an analysis of the influence of the field

on the gas flow near the electrode, is equally suitable for the region of negative effects. Dashed lines were therefore used on Figs. 4 and 5 in this region.

It was learned from these experiments that at higher pressures it is also possible to influence by an electric field the heat transfer from a fuel element, which acts as the anode. At atmospheric pressure no measurable effect was found with positive polarity of the fuel element. However, at 5 kp/cm² a negative effect, and at still higher pressures a positive effect, appears.

This can be explained by the fact, that much heavier (molecular) negative ions are originated in the gas at high pressures. These are similar to the positive ions and the character of the action of the field on the gas flow near the anode is therefore principally similar to its action near the cathode.

An analysis of the experimental results showed that the relative change of α_x —with positive polarity of the element—may well be expressed as a function of the expression $\phi_h I / w_s^{2.5}$; see Figs. 7 and 8. It is apparent from Fig. 7 that the dependence of the effect on the criterion $\phi_h I / w_s^{2.5}$ differs from that with negative polarity. At 6 kp/cm² only the negative effect appears and this grows steadily over the whole range of parameters. At 10 kp/cm² and higher pressures a positive effect appears; with the increase of the value $\phi_h I / w_s^{2.5}$, the effect at first increases, reaches a maximum and then decreases. The higher the pressure of the gas, the higher the maximum value of α'_x / α_x ; at pressures over 20 kp/cm² the maximum was not attained. The maximum increase in α_x during these experiments—over 50%—was achieved at a pressure of 20 kp/cm², a gas velocity of 6.8 m/s and a voltage of 20 kV. The maximum negative effect was 8% at 6 kp/cm².

A comparison of the results obtained with both polarities shows that at pressures up to 10 kp/cm² the increase in heat transfer (at equal values of $\phi_h I / w_s^2$) is substantially larger at negative polarity of the fuel element; on the other hand, at pressures from 20 kp/cm² upwards, the effect is larger with positive polarity.

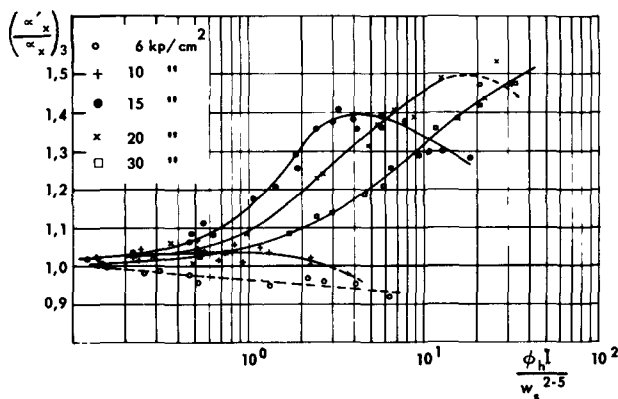


Figure 7. Relative change of the local α_x at point 3; positive polarity of the fuel element

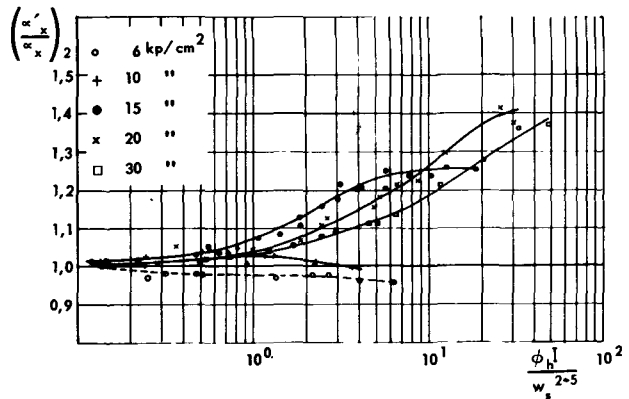


Figure 8. Relative change of the local α_x at point 2; positive polarity of the fuel element

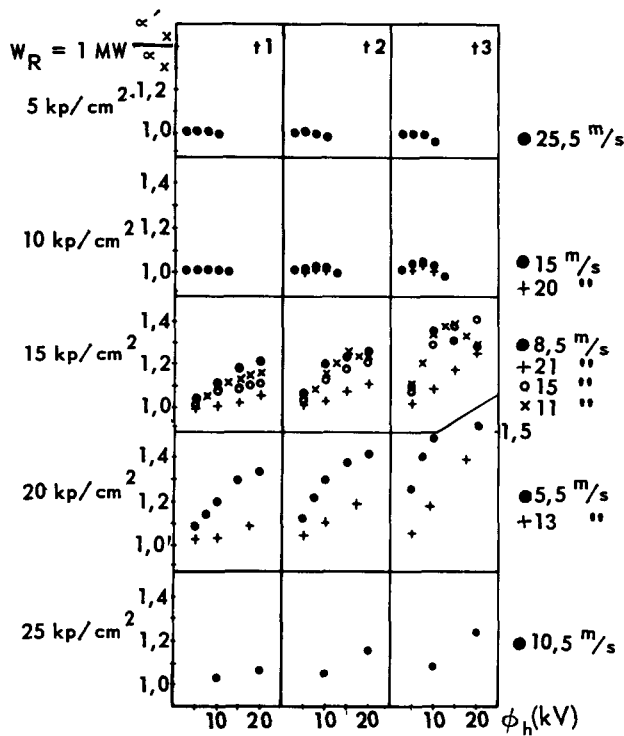


Figure 9. Relative change of the local α_x as a function of the applied voltage at different heights. Positive polarity of the fuel element

Figure 9 shows again the relative change of α_x'/α_x for all three measured points as a function of the applied voltage at constant reactor power and different gas velocities for the positive polarity of the fuel element.

With regard to the practical applications of the described phenomenon, the consumption of electric energy is important. The ratio of the consumed energy to the energy which can be gained by increasing the heat transfer depends substantially on the parameters of the gas and of the electric field. The dependence of the relative increase of α_x on the ratio of the consumed electrical output to the thermal power of the fuel element is shown for a few cases in Fig. 10. Apparently the potential gain of energy is in most cases substantially larger than the consumption of electric energy, though the effectiveness of the conversion of thermal into electrical energy must be considered.

The influence of the electric field on the pressure drop through the experimental section was not studied in these experiments. This effect was, however, studied during the following series of experiments, which were carried out at the time when this paper was being prepared. The preliminary results show no measurable effect of the pressure loss.

CONCLUSIONS

The influence of a direct current electric field on the heat transfer from a cylindrical fuel element to the CO_2 coolant at pressures up to 30 kp/cm^2 in a nuclear

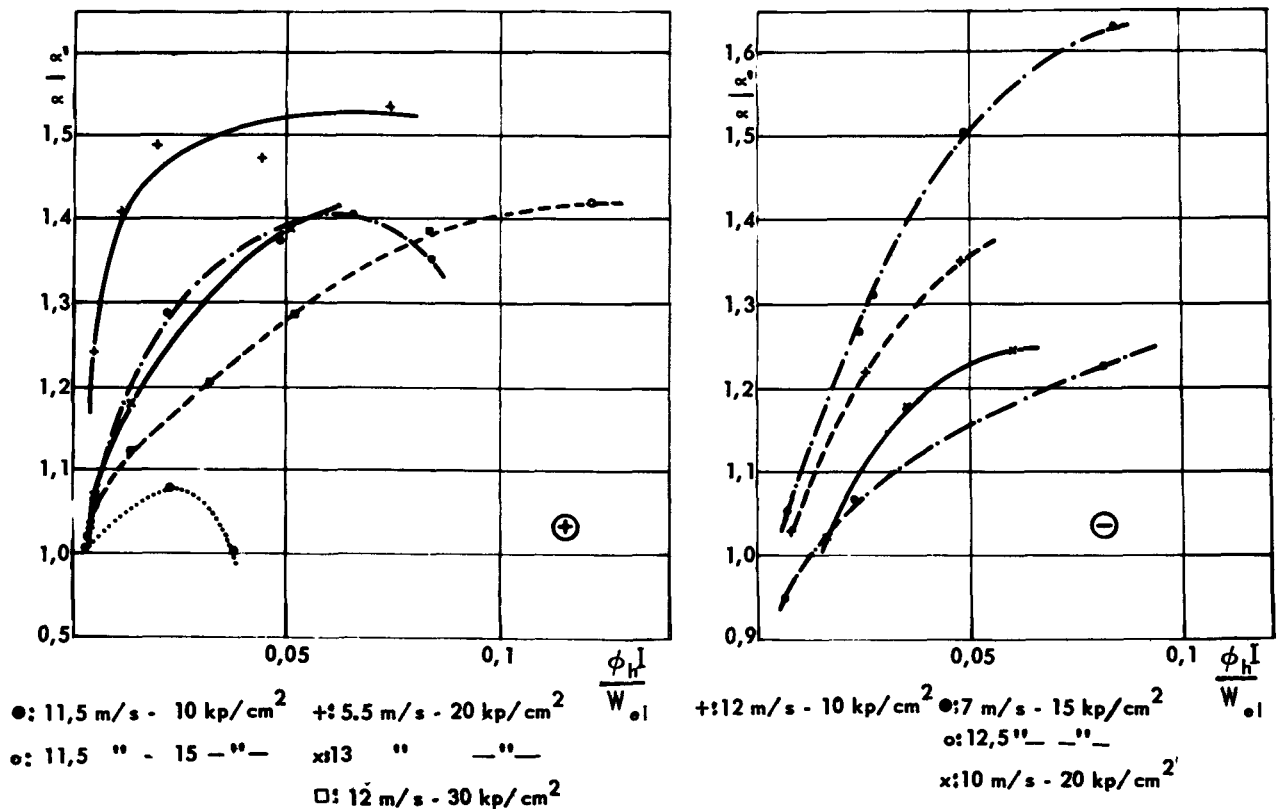


Figure 10. Correlation of the relative increase in α_x at point 3 vs. the ratio of consumed electrical input to the heat output of the fuel element for some cases at both polarities

reactor has been determined. It has been found that depending on the parameters of the gas and the electric field either an increase or a decrease in the heat transfer may be achieved at both polarities of the heat-transfer surface. At the conditions of these experiments the achieved increase in heat transfer was substantially larger than the achieved decrease. At pressures lower than 15 kp/cm² the increase of α was larger when the fuel element acted as the cathode; at higher pressures the increase was larger when it acted as the anode.

Further experiments are to be carried out at pressures up to 40 kp/cm² and in the course of these the effect of alternating fields at low frequencies will also be studied.

The reported results may be practically significant for gas-cooled power reactors as well as for those new methods of conversion of energy, where partially-ionized gases are used.

REFERENCES

1. Berger, F., and Stach, V., Proceedings of the Second International Conference on the Peaceful Uses of Atomic Energy, P/2486, Vol. 7, p. 751, United Nations (1958).

2. Senftleben, H., and Bültmann, E., *Zeitschr. f. Ph.* 136, 389 (1953).
3. Schmidt, E., and Leidenfrost, W., *Chemie-Ing. Techn.* 26, 35 (1954).
4. Ahsmann, G., and Kronig, R., *Appl. Sci. Res. A2*, 235 (1950).
5. Berger, F., and Stach, V., *Zeszyty problemowe nauki polskiej XIII*, 159 (1958).
6. Stach, V., *Int. J. Heat Mass Transfer* 5, 445 (1962).
7. Stach, V., *Práce ČVUT v Praze, VI, 1/2*, 297 (1961).
8. Berger, F., and Derian, L., *Práce ÚJV-ČSAV č.666/62-Report Inst. Nuclear Research; Řež near Prague* (1962).
9. Rapport CEA 2122, Centre d'Etudes nucléaires de Grenoble (1962).
10. Berger, F., and Peččík, E., *Jaderná energie* 8, 263 (1962).
11. Berger, F., Cihlář, A., and Peččík, E., *Jaderná energie* 9, 213 (1963).
12. Mašek, V., *Práce ÚJV-ČSAV 922/63, Report Inst. Nuclear Research; Řež near Prague* (1963).
13. Musilek, F., *et al.*, *A Review of Investigations and Experimental Utilization of the Research Reactor in the Institute of Nuclear Research of the Czechoslovak Academy of Sciences*, P/531, Vol. 7, these Proceedings.

ABSTRACT—RÉSUMÉ—АННОТАЦИЯ—RESUMEN

A/524 Tchécoslovaquie

Influence d'un champ électrique sur le transfert de chaleur aux pressions basses et élevées, dans un réacteur refroidi par l'anhydride carbonique

par F. Berger et L. Derian

Le gaz de refroidissement qui traverse le cœur d'un réacteur nucléaire est partiellement ionisé par les rayonnements. L'action d'un champ électrique peut provoquer un mouvement d'ions perpendiculaire au courant du gaz. Comme la concentration volumique des ions dans le gaz est relativement élevée, on peut modifier de cette façon l'ensemble du courant gazeux et plus particulièrement l'échange de chaleur entre le combustible et le gaz. A la deuxième Conférence de Genève, nous avons rendu compte de certaines expériences faites sur un modèle d'élément de combustible chauffé électriquement et refroidi par de l'air à la pression atmosphérique. Ces expériences ont démontré la possibilité d'intensifier l'échange de chaleur dans les réacteurs au moyen d'un champ électrique.

Depuis lors, un certain nombre d'expériences ont été effectuées dans le circuit, refroidi par un gaz, du réacteur tchécoslovaque VVR-S, d'abord sur un modèle chauffé électriquement et ensuite sur un élément à uranium en forme de barre. Les auteurs donnent les résultats de ces dernières expériences, dans lesquelles on a fait varier la pression de l'anhydride

carbonique de refroidissement de 5 à 30 kg/cm² et la tension entre les électrodes (l'une étant constituée par l'élément de combustible et l'autre par la paroi du canal) de 0 à 30 kV. En plus de l'influence de la pression et de l'intensité du champ électrique, on a étudié l'effet en fonction de la vitesse du gaz, de la densité d'ionisation du gaz, et de la polarité de la surface d'échange de chaleur. Les expériences ont permis d'élargir les connaissances antérieures et d'établir certains faits nouveaux.

On a établi notamment qu'au moyen d'un champ électrique continu, on peut obtenir aussi bien un accroissement (effet positif) qu'une diminution (effet négatif) du transfert de chaleur au gaz.

L'influence du champ électrique sur l'échange de chaleur entre l'élément de combustible et le gaz partiellement ionisé varie principalement selon que l'élément fonctionne comme cathode ou comme anode.

Lorsque la polarité de l'élément de combustible est négative, l'augmentation relative du transfert de chaleur est le plus élevée aux basses pressions. L'accroissement relatif du transfert de chaleur augmente lorsque croissent l'intensité du champ et la densité d'ionisation du gaz; il diminue lorsque croissent la vitesse et la pression du gaz. Aux pressions élevées, l'effet qui était positif devient négatif; la pression à laquelle ce changement se produit dépend des autres paramètres déterminants.

Pour une polarité positive de l'élément, on n'a observé aucune influence du champ électrique sur le transfert de chaleur à pression atmosphérique. Aux basses pressions (5 kg/cm²), l'effet est négatif. Lorsque

la pression augmente, l'effet peut devenir positif. A des pressions plus élevées (15 kg/cm² ou davantage), on peut obtenir une augmentation considérable du transfert de chaleur. L'accroissement relatif du transfert de chaleur augmente encore lorsque croissent l'intensité du champ et la densité de l'ionisation. Il diminue lorsque croît la vitesse du gaz, mais, contrairement à ce qui a été observé dans l'expérience antérieure, augmente (dans les limites des pressions étudiées) lorsque la pression croît.

L'accroissement relatif maximal du transfert de chaleur atteint au cours de ces expériences a été d'environ 50%. La diminution maximale (effet négatif) a été d'environ 15%. Les auteurs décrivent les expériences en détail, indiquent les variations de l'effet en fonction des paramètres principaux et donnent une interprétation de ce phénomène.

A/524 Чехословакия

Влияние электрического поля на теплопередачу теплоносителя CO₂ при высоких и низких давлениях в ядерном реакторе

Ф. Бергер, Л. Дериан

Газовый теплоноситель, протекающий через активную зону ядерного реактора, под воздействием облучения частично ионизируется. Воздействием электрического поля можно вызвать движение ионов перпендикулярно направлению газового потока. Поскольку концентрация ионов в газовом объеме относительно высока, можно этим способом воздействовать на весь газовый поток и особенно на теплопередачу от тепловыделяющего элемента к газу. На Второй Женевской конференции авторы сообщали об экспериментах с электрически нагреваемым макетом тепловыделяющего элемента, охлаждаемым воздухом при атмосферном давлении. Результаты этих экспериментов показали реальную возможность интенсификации теплопередачи посредством применения электрического поля в ядерных реакторах.

После этого была проведена серия экспериментов на газоохлаждаемой петле чехословацкого реактора ВВР-С вначале с электрически нагреваемым макетом, а затем с урановым тепловыделяющим элементом стержневого типа. В настоящем докладе приведены в основном результаты этих последних экспериментов, при которых давление охлаждающей углекислоты изменялось в пределах от 5 до 30 кг/см², а напряжение между электродами — урановым тепловыделяющим элементом и внутренней поверхностью канала — изменялось в пределах от 0 до 30 кВ. Наряду с исследованием влияния давления газа и напряженности электрического поля было исследовано воздействие скорости газа,

степени ионизации газа и полярности теплопередающей поверхности. В результате экспериментов были открыты некоторые новые факты, а также расширены сведения, полученные ранее.

Было установлено, что под действием электрического поля постоянного тока может иметь место как увеличение (положительный эффект), так и уменьшение (отрицательный эффект) интенсивности теплопередачи к газу.

Воздействие электрического поля на теплопередачу от тепловыделяющего элемента к частично ионизированному газу зависит главным образом от того, в качестве чего работает тепловыделяющий элемент — катода или анода.

При отрицательной полярности тепловыделяющего элемента относительное увеличение теплопередачи достигает наибольшего значения при низких давлениях. Значение относительного увеличения теплопередачи возрастает с увеличением напряженности поля и с ростом степени ионизации и понижается с повышением скорости и давления газа. При более высоких давлениях положительный эффект переходит в эффект отрицательный; уровень давления, при котором происходит это изменение характера эффекта, зависит от других определяющих параметров.

При положительной полярности тепловыделяющего элемента и при атмосферном давлении не было отмечено влияния электрического поля на теплопередачу. При низких давлениях газа (5 кг/см²) имеет место отрицательный эффект, который при дальнейшем повышении давления переходит в положительный. При более высоких давлениях (15 кг/см² и выше) может быть получено существенное повышение теплопередачи. Величина относительного повышения теплопередачи также растет с повышением напряженности поля и плотности ионизации и уменьшается с ростом скорости газа. В отличие от предыдущего случая эффект нарастает с ростом давления газа (в исследуемой области давлений).

Максимальное относительное увеличение теплопередачи, полученное при этих опытах, доходило до 50%. Максимальное понижение теплопередачи (отрицательный эффект) составляло около 15%. В докладе даны более подробное описание экспериментов, количественные зависимости эффекта от основных параметров и объяснение явления.

A/524 Checoslovaquia

La influencia de un campo eléctrico sobre la transmisión de calor al refrigerante CO₂ a presiones altas y bajas en un reactor nuclear por F. Berger y L. Derian

El gas refrigerante que circula a través del núcleo de un reactor nuclear está ionizado parcialmente a causa de la radiación. Se puede obtener un flujo de

iones perpendicular a la dirección de circulación del gas mediante la aplicación de un campo eléctrico. Cuando la concentración de iones en el volumen del gas es relativamente elevada, es posible afectar de esta forma a la totalidad de la corriente gaseosa y especialmente a la transmisión de calor de los elementos combustibles al gas. En la Segunda Conferencia de Ginebra informamos sobre los experimentos efectuados con un modelo de elemento combustible calentado eléctricamente y refrigerado por aire a la presión atmosférica. Se demostró con estos experimentos la posibilidad de aumentar la transmisión de calor en reactores nucleares mediante la aplicación de un campo eléctrico.

Desde entonces, se han ejecutado una serie de experimentos en el circuito refrigerado por gas del reactor checoslovaco VVR-S, primero con un modelo calentado eléctricamente y más tarde con un elemento combustible de uranio en forma de barra. Esta memoria da principalmente los resultados de estos últimos experimentos, en los cuales se cambió la presión del dióxido de carbono refrigerante desde 5 hasta 30 kgf/cm², y el voltaje entre los electrodos (uno de los cuales estaba formado por el elemento combustible de uranio y el otro por la pared del canal), se varió desde 0 a 30 kV. Además de la influencia de la presión y de la intensidad del campo eléctrico, se estudió la dependencia del efecto de la velocidad del gas, densidad de ionización del gas y la polaridad de la superficie cambiadora de calor. Los experimentos realizados sirvieron tanto para destacar algunos nuevos hechos como también para ampliar los conocimientos previos.

Se estableció que, por la acción de un campo eléctrico en corriente continua, se puede obtener un incremento (efecto positivo) y una disminución (efecto negativo) de la transmisión de calor al gas.

La influencia del campo eléctrico sobre la transmisión de calor desde el elemento combustible hacia el gas parcialmente ionizado, depende, principalmente, de si el elemento combustible trabaja como cátodo o como ánodo.

Con la polaridad negativa del elemento combustible el aumento relativo de la transmisión de calor es más elevado a bajas presiones. El valor del incremento relativo de la transmisión de calor crece al aumentar la intensidad del campo y al aumentar la densidad de la ionización del gas, mientras que disminuye al aumentar la velocidad del gas y la presión. A presiones más elevadas el efecto positivo cambia a efecto negativo; la presión a la cual ocurre este cambio depende de los otros parámetros determinantes.

Con polaridad positiva del elemento combustible, no se observó, a presión atmosférica, influencia del campo eléctrico sobre la transmisión de calor. Se presenta un efecto negativo a bajas presiones (5 kgf/cm²). El efecto se puede transformar en positivo por un aumento ulterior de la presión. A mayores presiones (15 kgf/cm² o mayores) se puede obtener un incremento considerable de la transmisión de calor. El valor del aumento relativo de transmisión de calor crece de nuevo al aumentar la intensidad del campo y la densidad de ionización, pero disminuye al aumentar la velocidad del gas. Sin embargo, contrariamente al caso anterior, aumenta (en el intervalo de presiones considerado) al aumentar la presión.

El aumento relativo máximo de la transmisión de calor alcanzado durante estos experimentos alcanzó cerca del 50%. La disminución máxima de la transmisión de calor (efecto negativo) fue de cerca del 15%. Se dará en esta memoria una descripción más detallada de los experimentos, de la magnitud de los efectos en función de los parámetros principales y una interpretación del fenómeno.

Heat transfer intensification by use of the longitudinally variable pressure gradient

By Z. Zarić*

The importance of achieving high rates of heat transfer from reactor fuel elements is generally recognized. In gas-cooled reactors, in particular, the increase of heat transfer rates directly affects plant energy costs. Up to now extended surfaces with magnesium cladding and surface roughening in the case of low conductivity cladding have been exclusively employed in obtaining moderately high heat fluxes in gas-cooled reactors. The main effect of finning is to increase the heat transfer surface per unit fuel length, but the heat transfer rates from the surface itself are still moderate owing to the inevitably poor aerodynamic design of these surfaces. Moreover, an increase in the heat transfer surface per unit fuel length results in a decrease of the heat transfer coefficients on the fin surface. Artificial surface roughening significantly increases heat transfer rates. For certain types of roughness the increase is almost threefold compared with the flow in smooth channels, with an accompanying increase of pressure losses by a factor of about eight [7, 14]. The present status of achieving high convection heat transfer rates cannot be qualified as satisfactory. Novel approaches and more basic research are needed to clarify the heat transfer mechanism in turbulent flows.

Very high convection heat transfer rates are found in flows across beds of spheres and tube banks. These high rates are partly attributed to the increase in the turbulence level occurring in such flows. However, the structure of turbulence in flows across tube banks is much more complex and the high heat transfer rates in them cannot be explained by the rise of turbulence intensity alone. Heat transfer rates in tube banks are strongly dependent on the pitch to diameter ratios, and in closely spaced rows they are almost double the rates in tube banks with higher pitch to diameter ratios [13]. When the longitudinal pitch to diameter ratio is less than unity flow passages exhibit a succession of contractions and expansions so that the longitudinal pressure gradient changes several times in sign and value. Smaller transversal pitch to diameter ratios lead to higher absolute values of the pressure gradient.

Adverse pressure gradient flows reveal some interesting features. Recently, Kline *et al.* [4, 5] investigating the flow in diffusers by a special visualization tech-

nique, have shown that a longitudinal vortex pattern, slightly inclined from the wall, is found in the viscous sublayer of the turbulent boundary layer. These vortices break up near the edge of the sublayer into a typical turbulent hash and promote a continual transport of fluid between wall layers and the outer portion of the flow. The angle at which the vortex system stands to the wall increases with the increase of the adverse pressure gradient and vortices break up a shorter distance downstream resulting in an increased number of break-ups. At a given value of the pressure gradient vortices begin to accumulate in larger transitory stalls which further promote fluid mixing in the boundary layer. Visual observations are in good agreement with a limited number of investigations of the turbulence characteristics of an adverse pressure gradient flow. Intensities of all fluctuating velocity components, turbulence rates of production and dissipation are greatly in excess of those for a zero pressure gradient flow [8, 10, 12].

The physical picture of the flow near the wall in an adverse pressure gradient indicates that the rate of heat transfer must increase in this case. Experimental data of heat transfer in adverse pressure gradient flows, however, are very scarce, particularly for the heat transferred from the surface to an incompressible fluid. Recently, Romanenko *et al.* [11] have investigated heat transfer from heated air to the walls of diffusers with aperture angles of 8 and 12°. Their data show that there is no similarity between velocity and temperature profiles and indicate an increase of the heat transfer rate with increasing pressure gradient.

In order to make a preliminary check of the validity of the presumed influence of an adverse pressure gradient on the rate of heat transfer, we measured local coefficients of heat transfer from the surface of heated cones placed in a tube to form annular diffusers [1]. Cones of 12 and 16° angles were investigated. Results have shown a significant increase of heat transfer coefficients, those of a 16° cone being as much as 60% higher compared to the flow in an annulus of constant cross section.

The present paper gives results of an experimental investigation of local heat transfer rates in two-dimensional channels composed in such a way as to form a succession of divergent and convergent passages. The geometrical parameters were chosen so that the flow in divergent sections of the channel

* Boris Kidrič Institute of Nuclear Sciences, Beograd-Vinča.

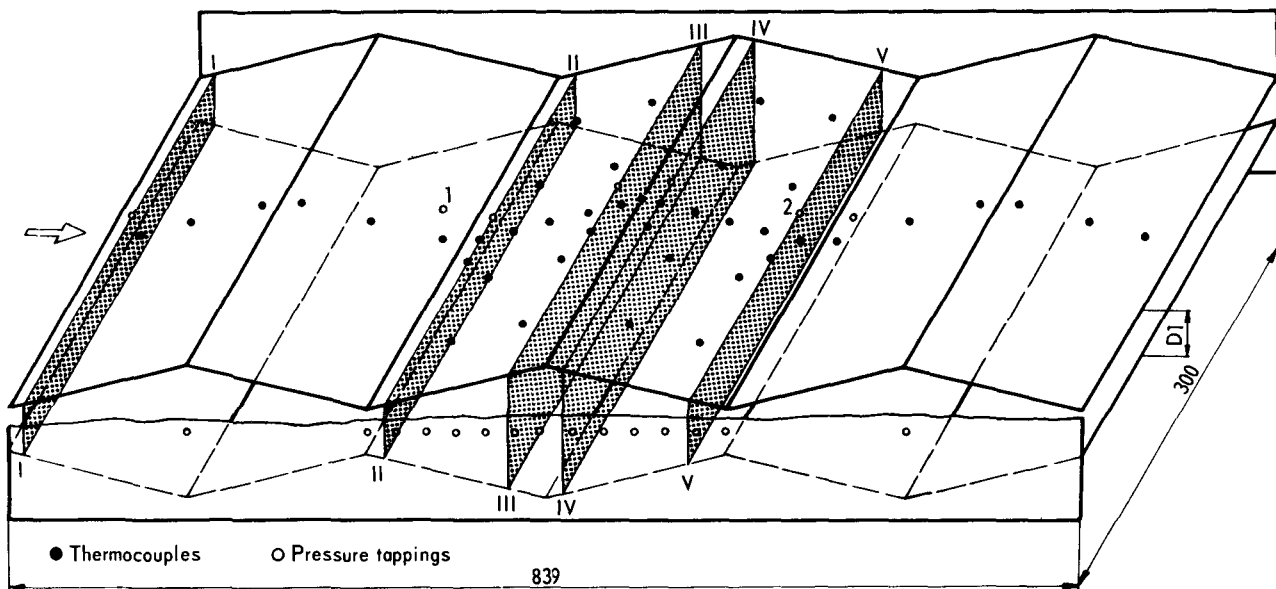


Figure 1. Diagram of the test section

would be approximately in the zone of the formation of transitory stalls according to Kline [4].

APPARATUS AND INSTRUMENTATION

The test section is schematically shown in Fig. 1. It consists of a rectangular channel formed by two profiled and two straight stainless steel plates. The profiled plates placed parallel to each other form a succession of six geometrically equal divergent and convergent sections, each 141 mm long and with an aperture angle of $16 \pm 1^\circ$. Two minimum distances between plates, namely 26.0 and 44.5 mm, were investigated, the length to throat width ratios of divergent sections being 5.4 and 3.15 respectively. The profiled plates were heated electrically by twelve individual heaters, a pair for each section. The heaters were made of resistance strips placed parallel to the plate width and isolated from it by a 1 mm thick mica sheet. Equally spaced strips were pressed to the plates by means of screws and pressing plates. The alternating current in the strips was adjusted to produce an approximately uniform heat flux of about 0.5 W/cm^2 on the inner plate surface. The test section was insulated from the surroundings by layers of glass wool and asbestos sheets.

Along the polished inside surface of the profiled plates thermocouples were embedded into grooves filled with tin. The thermocouple arrangement on one plate is shown in Fig. 1. To measure the static pressure distribution along the channel several holes of 1 mm diam were drilled normal to the plate surface. For the $L/D_1 = 3.15$ channel, fifteen additional pressure tappings were made along one of the side walls. In order to get a better insight into the flow regime, fluid velocity and temperature distributions were measured in four cross sections along the channel (II to V in Fig. 1). Velocity profiles were taken by total and static

pressure traversing probes displaced by micrometer screws. Temperature distributions were measured by 0.5 mm diam chromel-alumel thermocouples of the thermocoaxial type.

A geometrically identical but unheated channel with four divergent-convergent sections was placed upstream of the test section. The air inlet temperature was measured upstream of the apparatus. The air flow of up to 0.7 kg/s was supplied by a centrifugal blower. The air flow rate was measured by standard diaphragms. Thermocouple outputs were measured individually with a potentiometer accurate to about 0.2°C . Static pressure readings were taken by alcohol-filled U-tubes and pressure differences for velocity measurements by a Casella-type micromanometer. The heat flux was calculated from current and voltage drop readings on each individual heater.

RESULTS AND DISCUSSION

Measured velocity and temperature distributions in cross sections II to V are shown in Fig. 2 for the two L/D_1 ratios. The curve of the velocity distribution for the flow between parallel plates is also included [9]. Velocity profiles in cross sections III and IV, near the outlet from the divergent, and at the inlet of the convergent section, are characteristic of the flow with a moderately large adverse pressure gradient, but they do not show any indication of the flow separation. From Fig. 2 it is evident that an asymmetry exists in the velocity profile in cross section III of the $L/D_1 = 3.15$ channel indicating different flow conditions on opposite channel walls. In general, there is no similarity between the temperature and velocity profiles.

Local heat transfer coefficients along two central divergent-convergent sections are given in Fig. 3 for both L/D_1 ratios. It is seen that there is considerable scattering of experimental points relating to one cross

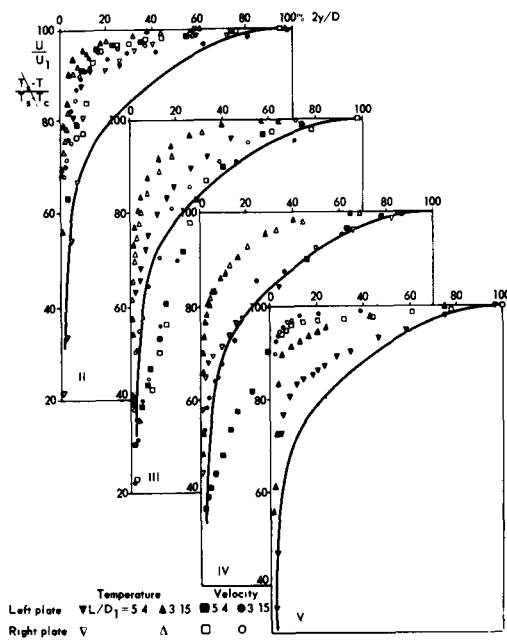


Figure 2. Velocity and temperature distributions

section which indicates certain three-dimensionality of the flow and different flow conditions existing at opposite walls. In case of the $L/D_1 = 3.15$ channel, the difference in flow conditions at opposite walls results in different heat transfer rates, those of the left plate being consistently higher than those of the right one. From the velocity distribution near the end of the divergent section (Fig. 2-III) it is seen that the flow along the left plate is closer to separation, thus affecting the heat transfer rates.

Distribution of the local values of Stanton number along the channel is given in Fig. 3 as the ratio of the Stanton number calculated from the experimental data and the Stanton number for constant cross section channels (St_0) for the same Reynolds number [6]. The value of the local Stanton number increases steadily along the divergent section. Near the outlet from this section a sharp increase is evident which can be explained by the formation of large transitory stalls in this zone. The pronounced maximum at the beginning of the convergent section, in the readjustment zone, is in accordance with the visualization studies of Kline *et al.* [5] who in such zones found that the flow picture in wall layers is similar to that associated with a large pressure gradient. For the lower pressure gradient channel local Stanton number values in the divergent section are somewhat lower than in the case of the $L/D_1 = 5.4$ channel. The maximum value at the beginning of the convergent section is, however, considerably lower which indicates a particularly strong influence of the pressure gradient and flow conditions on the heat transfer rate in this

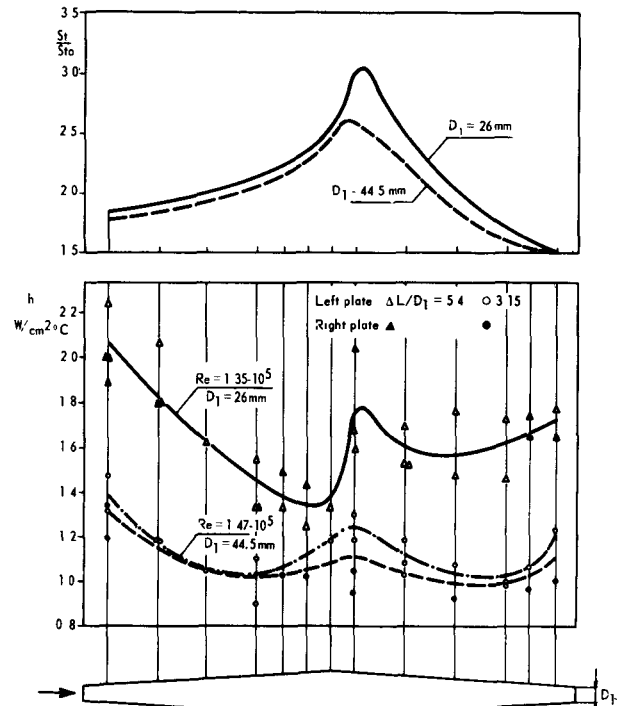


Figure 3. Variation of the local heat transfer coefficient and St number along the channel

zone. Along the convergent section the Stanton number decreases steadily in value but is still considerably greater than in the case of a zero pressure gradient flow. Thus it is seen that the high intensity turbulence produced in the divergent section has a significant influence on the rate of heat transfer in the convergent section. These findings are in accordance with those of Kestin *et al.* [3] who investigated the influence of turbulence on the transfer of heat from plates in an accelerated flow. The influence of the pressure gradient is even stronger than in the divergent section as can be seen in Fig. 3.

In Fig. 4 the average Stanton numbers calculated from the mean values of all heat transfer coefficients measured along the channel (h_b) and the average

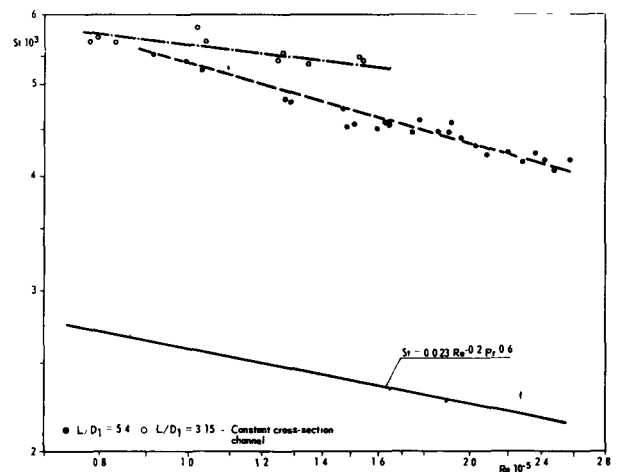


Figure 4. Average Stanton number vs. Reynolds number

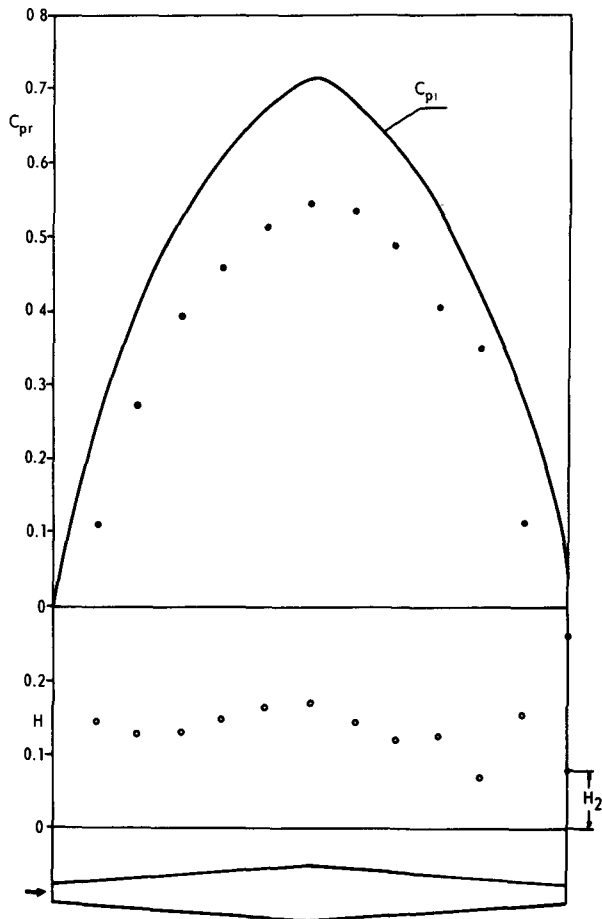


Figure 5. Variation of the static pressure recovery and pressure loss coefficients along the $L/D_1 = 3.15$ Channel, $Re = 1.94 \cdot 10^5$

distance between plates (D_a), are plotted against Reynolds number and compared with the curve for the constant cross section channel Stanton number [6]. Figure 4 shows that average Stanton number values for divergent-convergent channels are considerably higher than the corresponding values for zero pressure gradient flows.

Ideal and actual pressure recovery coefficients, C_{pi} and C_{pr} respectively, along the two central divergent-convergent sections are given in Fig. 5 for the $L/D_1 = 3.15$ channel, together with the pressure loss coefficient (H) variation. The pressure loss coefficient has a sharp rise at the beginning of the divergent section, increases steadily to a maximum value at the end of this section and then decreases slowly along the convergent section with a sharp drop at the end of this section. Decrease of the pressure loss coefficient in the convergent section is a consequence of the velocity redistribution with a corresponding transfer of the kinetic energy into the pressure energy. The pressure loss coefficient at the end of the convergent section (H_2) is taken as the coefficient of the pressure loss in a pair of divergent-convergent sections. For the $L/D_1 = 5.4$ channel, pressure loss coefficients (H_2) were calculated from pressure differences between two symmetrically located tappings near the end of the convergent

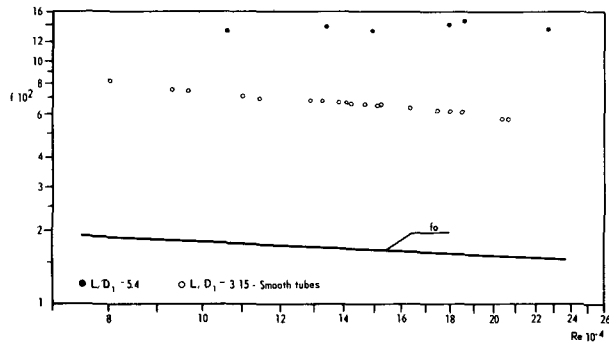


Figure 6. Friction factor vs. Reynolds number

section in the profiled plate (pressure tappings 1 and 2 in Fig. 1).

Friction factors f calculated on the basis of the average distance between the plates and the average flow velocity in the channel are plotted in Fig. 6 against Reynolds number for both L/D_1 ratios. The curve of the friction factor in smooth tubes (f_0), which holds approximately for the rectangular channels [2], is also plotted in Fig. 6.

CONCLUSION

The positive influence of the longitudinally variable pressure gradient on the convection heat transfer intensification has been confirmed by measurements of local rates of heat transfer in divergent-convergent channels of an aperture angle of 16° and the length to throat width ratios of 3.15 and 5.4. Along the adverse pressure gradient section, the values of the local Stanton number increase steadily. Intense turbulence produced in this section increases significantly the rate of heat transfer in the convergent section above the level of the zero pressure gradient channel flow. The average values of the Stanton number in the divergent-convergent channels tested are about twice those in a constant cross section channel. The increase in the pressure loss is significant but the pumping power in a constant cross section channel needed to obtain the same average heat transfer coefficient is still approximately twice that in a divergent-convergent channel with the same average distance between plates.

The experimental data presented show that the longitudinally variable pressure gradient can be successfully used to obtain qualitatively the same effect as regards the convective heat transfer rates as that produced by surface roughening for instance. The two geometries tested surely do not represent an optimal combination of geometrical parameters which influence the flow regime and heat transfer. From the results obtained it is not possible to get an insight into the influence of important parameters such as the aperture angle, the shape of the surface and the length of the divergent to the length of the convergent section ratio. Present experimental data show for instance a sharp increase in losses occurring at the beginning of the divergent section which might

possibly be avoided with a better design. It is also of interest to broaden the zone of maximum heat transfer rates at the end of the divergent section by an appropriate design of the plate shape. The work on testing other geometries of divergent-convergent channels is in progress. The work is also directed towards a better understanding of the flow and heat transfer mechanism in such channels.

ACKNOWLEDGEMENTS

The author would like to thank Professor A. Fortier of the Faculté des Sciences de Paris for his valuable help in the work and advice in defining the problem.

The author also wishes to thank Messrs M. Baotić, M. Stanković and R. Raiković who helped in constructing the apparatus and performing the measurements.

NOMENCLATURE

- B : Channel width
 C_{pi} : Ideal pressure recovery coefficient, $= 1 - (D_1/D)^2$
 C_{pr} : Actual pressure recovery coefficient,

$$= \frac{2(p - p_1)}{\rho u_1^2} + \frac{(T_b - T_{b1})}{T_{b1}} (D_1/D)^2$$

 c_p : Specific heat at constant pressure
 D : Distance between plates
 H : Pressure loss coefficient, $= C_{pi} - C_{pr}$
 h : Heat transfer coefficient, $= q/(T_s - T_b)$
 f : Friction factor, $= H_2(D_b/L) (D_b/D_1)^2$
 f_0 : Friction factor in smooth tubes, $= (2 \Delta p/\rho u^2) (D/L)$
 L : Length of sections measured along the plates
 p : Static pressure
 q : Heat flux at inner plate surface
 T : Absolute temperature
 u : Fluid velocity
 w : Mass flow

y : Distance from the wall

μ : Viscosity

ρ : Fluid density

Dimensionless numbers:

Re : Reynolds number, $= 2w/\mu B$

St : Stanton number, $= hDB/c_p w$

Subscripts:

a: Average along the channel

b: Bulk

c: Centre of the channel

s: Plate surface

1: Inlet divergent section

2: Outlet convergent section

REFERENCES

1. Afgan, N., and Zarić, Z., Bull. Boris Kidrič Inst. Nucl. Sci., 15 (1964).
2. Harnett, J. P., Koh, J. C. Y., and McComas, S. T., J. Heat Transfer 84C, 82 (1962).
3. Kestin, J., Maeder, P. F., and Wang, H. E., Intern. J. Heat Mass Transfer, 3, 133 (1961).
4. Kline, S. J., J. Basic Eng. 81D, 305 (1959).
5. Kline, S. J., and Runstadler, P. W., J. Appl. Mech 81, 166 (1959).
6. Knudsen, J. G., and Katz, D. L., Fluid Dynamics and Heat Transfer, McGraw Hill, New York, 406 (1950).
7. Malherbe, J., CEA-2283 (1963).
8. Milliat, J. P., Thèses, Fac. Sci. Univ. Grenoble (1956).
9. Pai, S. I., J. appl. Mech 20, 109 (1953).
10. Robertson, J. M., and Calehuff, G. L., Proc. ASCE, J. Hydraulics Div. 83, 1393 (1957).
11. Romanenko, P. N., Leontev, A. I., and Oblivin, A. N., Intern. J. Heat Mass Transfer 5, 541 (1962).
12. Ruetenik, J. P., and Corrsin, S., in 50 Jahre Grenzschichtforschung, Friedr. Vieweg & Sohn, Braunschweig, 446 (1955).
13. Tolubinski, V. I., and Legki, V. M., Teploenergetika 8, 53 (1961).
14. Walker, V., Nucl., Eng. 6 144 (1961).

ABSTRACT—RÉSUMÉ—АННОТАЦИЯ—RESUMEN

A/698 Yougoslavie

Intensification du transfert de chaleur par un gradient de pression longitudinal variable

par Z. Zarić

Pour les réacteurs nucléaires refroidis par un gaz, le problème consistant à trouver des moyens efficaces d'intensifier le transfert de chaleur est encore actuel, et les progrès dans ce domaine peuvent conduire à des améliorations significatives des caractéristiques du réacteur. Les moyens à présent utilisés, ailettes et surfaces rugueuses, sont encore peu efficaces.

On observe des taux très élevés de transfert thermique dans le cas d'écoulement de fluide normalement à des rangées de tubes très proches les uns des autres ou à travers des couches de particules sphériques. Dans les deux cas, on trouve une succession d'agrandissements et de rétrécissements de la section droite d'écoulement avec des variations importantes de gradient de pression longitudinal.

L'étude de l'écoulement d'un fluide dans un divergent montre que des tourbillons longitudinaux sont formés sur les parois et se rompent à la frontière de la couche limite, donnant ainsi un taux élevé de turbulence dans l'écoulement. Cet effet doit agir sur le transfert thermique. D'autre part, on a prouvé que

le degré de turbulence a une influence sur le transfert thermique dans les conduits convergent.

Sur la base de cette analyse, on a fait des expériences préliminaires sur le transfert de chaleur dans un divergent annulaire; elles ont montré un accroissement significatif des coefficients d'échange thermique par rapport à un écoulement sans gradient de pression. Les expériences ont été effectuées dans une installation à deux dimensions qui est décrite dans le mémoire. La partie où se faisaient les mesures se composait d'un canal rectangulaire avec deux parois profilées de manière à former une succession de sections convergentes et divergentes avec un demi-angle de 8° . Les parois profilées ont été chauffées électriquement et les températures locales aux parois ont été mesurées par de nombreux thermocouples le long du canal. On a mesuré dans quatre sections droites les répartitions des vitesses et des températures. On a aussi mesuré la distribution des pressions statiques le long du canal.

Les résultats expérimentaux montrent l'influence considérable du gradient de pression longitudinal sur l'intensité des échanges thermiques. Le nombre de Stanton, calculé pour la section droite locale, augmente le long du divergent jusqu'à être plus de deux fois celui qui correspond à l'écoulement sans gradient de pression. La turbulence intense créée dans la partie divergente se traduit par une augmentation marquée des coefficients d'échange thermique dans la partie convergente également. Les coefficients de perte de charge qui augmentent le long du divergent diminuent sensiblement dans le convergent, indiquant une récupération d'énergie de pression dans cette partie.

Les résultats cités, obtenus pour une seule géométrie, montrent que l'effet du gradient de pression peut être utilisé avec succès pour l'augmentation du transfert thermique dans le cas du refroidissement par un gaz. On s'occupe d'étudier les autres géométries afin de trouver les combinaisons optimales des paramètres ayant une influence sur le transfert de chaleur et l'écoulement du fluide.

A/698 Югославия

Интенсификация теплопередачи путем изменения продольного градиента давления

Ц. Царич

Проблема нахождения эффективных способов интенсификации переноса тепла в реакторах с газовым охлаждением все еще является актуальной, и успехи в этом направлении могут оказать значительное влияние на рабочие характеристики реактора. Используемые в настоящее время способы улучшения теплообмена, как, например, увеличение теплоотдающей по-

верхности или придание ей шероховатости, недостаточно эффективны.

Особенно интенсивный перенос тепла наблюдается в потоках, протекающих перпендикулярно сборкам тесно расположенных труб или же через слой сферических частиц. В обоих случаях наблюдаются чередующиеся расширения и сужения проходов для потока, сопровождающиеся значительными изменениями продольного градиента давления. Изучение жидкого потока в диффузорах показывает, что образование вдоль стенок продольных вихрей, которые разбиваются на краю граничного слоя, вызывает таким образом сильную турбулентность в потоке. Это явление должно оказывать влияние на интенсивность переноса тепла. С другой стороны, было доказано, что степень турбулентности влияет также на перенос тепла и в сужающихся проходах.

На основании вышеприведенных соображений было предпринято предварительное исследование переноса тепла в кольцевом диффузоре, которое показало значительное улучшение переноса тепла по сравнению с потоком без всякого градиента давления. Экспериментальные исследования были проведены на описанном в настоящем докладе двумерном устройстве. Испытательная зона состояла из прямоугольного канала, двум стенкам которого была придана такая форма, что они образовывали чередование расходящихся и сходящихся поверхностей с полууглом 8° . Стенки с этим профилем нагревались электрическим способом, и температура стенок в разных местах вдоль канала измерялась многочисленными термопарами. График скоростей и температур потока измерялся в четырех поперечных сечениях. Измерялось также распределение статического давления вдоль испытательной зоны.

Экспериментальные данные свидетельствуют о сильном влиянии противоположного градиента давления на интенсивность переноса тепла. Число Стантона в различных частях потока непрерывно увеличивается вдоль диффузора и увеличивается более чем в два раза по сравнению с потоком без градиента давления. Создаваемая в расходящейся части интенсивная турбулентность существенно влияет на интенсивность переноса тепла также и в сходящейся части. Коэффициент потери давления, сильно увеличивающийся вдоль диффузора, значительно падает в сходящейся части, что указывает на рекуперацию энергии давления в этой части.

Приводимые выше результаты, полученные только для одной геометрии, указывают на возможность успешного использования действия градиента давления для интенсификации переноса тепла охлаждающим газом. В настоящее время испытываются другие геометрические формы для нахождения оптимального сочетания параметров, влияющих на перенос тепла и на характер потока.

A/698 Yugoslavia

Intensificación de la transmisión de calor mediante el uso del gradiente de presión longitudinal variable

por Z. Zarić

Sigue planteado el problema de encontrar métodos efectivos para intensificar la transmisión de calor en reactores refrigerados por gas y los progresos en esta dirección pueden conducir a mejoras significativas en la operación de los reactores. Los métodos utilizados en la actualidad, a saber: superficies extendidas y superficies rugosas, no son todavía suficientemente efectivos.

Se han encontrado relaciones de transmisión de calor especialmente elevadas en fluidos que fluyen normalmente a un bloque de tubos poco espaciados y en lechos de partículas esféricas. En ambos casos se observan ensanchamientos y estrechamientos sucesivos en los tubos de flujo con grandes variaciones en el gradiente longitudinal de presión.

El estudio del flujo del fluido en difusores revela la formación de vórtices longitudinales que se rompen sobre el borde de la capa de separación produciendo un alto grado de turbulencia en la corriente. Este efecto debe influir sobre las relaciones de transmisión de calor. Por otra parte se ha comprobado que el grado de turbulencia influye sobre la transmisión de calor en canales convergentes.

Basándose en el análisis anterior se ha emprendido una investigación preliminar de la transferencia de calor en un difusor anular, la cual ha demostrado un aumento considerable en las relaciones de transferencia de calor en comparación con el flujo con un gradiente

de presión nulo. La investigación experimental se llevó a cabo en un dispositivo bidimensional que se describe en la memoria. La sección de prueba consistía en un canal rectangular con dos paredes, cuyo perfil formaba una sucesión de secciones divergentes y convergentes con un semiángulo de 8° . Estas paredes fueron calentadas eléctricamente y las temperaturas locales en ellas se midieron a lo largo del canal mediante varios termopares. Los perfiles de velocidad y temperatura en el fluido se midieron en cuatro secciones rectas. También se midió la distribución de presión hidrostática a lo largo de la sección de prueba.

Los datos experimentales indican una considerable influencia del gradiente de presión sobre la relación de transmisión de calor. El número de Stanton basado en el área de flujo local aumenta continuamente a lo largo del difusor hasta más del doble en comparación con el flujo sin gradiente de presión. La intensa turbulencia creada en la sección difusora influye también considerablemente sobre la relación de transmisión de calor en la sección convergente. El coeficiente de pérdidas de presión que aumenta a lo largo del difusor disminuye notablemente en la sección convergente indicando una recuperación de energía de presión en esta sección.

Los resultados anteriores, obtenidos para una sola geometría, demuestran que puede usarse con éxito el efecto del gradiente de presión para la intensificación de la transmisión de calor en los casos de refrigeración por gas. Se están probando otras geometrías a fin de encontrar una combinación óptima de parámetros que influirán en la transmisión de calor y en el flujo del fluido.

Hydraulic problems of reactor engineering

Chairman: N. A. Dollezhal (USSR)

Paper P/230 (presented by P. A. Lottes)

DISCUSSION

G. H. LATZKO (Netherlands): The paper gives an excellent review of the vast amount of experimental work being performed in this field in the United States. On the other hand, it does not provide the designer with any firm recommendation on the information to be used for calculating slip velocity and two-phase pressure drop. In this connection I should be interested to know how well the curves for slip shown in Fig. 2 correlate with the Bankoff slip model suggested elsewhere in the paper. Do abscissa and ordinate values refer to local channel conditions, and the Froude number to the channel inlet?

P. A. LOTTES (United States of America): There is good agreement between the slip curves shown and the Bankoff model. The choice of this particular figure is a matter of personal preference from the point of view of engineering. The values of abscissa and ordinate both refer to average, not local, conditions.

H. CHRISTENSEN (Norway): In the section of your paper dealing with in-pile experiments on power stability you state that "operational noise cannot be used as a measure of absolute stability". In paper P/589, the very opposite observation is made—namely, that in the case of a boiling loop, it is possible, on the basis of a noise power spectrum analysis, to obtain very good determination of the point of instability, except perhaps at the highest powers where burn-out follows quickly.

Do you think that this difference in the results obtained might possibly be due to the presence in the Vallecitos reactor of fuel elements of different ratings and perhaps different construction? Given this situation, the tendency towards instability with increasing powers could be gradual, with flow channels reaching instability one by one. This would make it impossible to define an exact point of instability.

P. A. LOTTES (United States of America): I think that the answer you suggest is the correct one. It is possible to have flow and void oscillations between parallel channels even though the *total* mass flow remains constant. In fact, Professor Gouse performed his experiments at MIT* along those very lines, namely with constant total mass-flow rate.

H. CHRISTENSEN (Norway): Results are given in the penultimate section of your paper for local void

measurements. Could you please describe the method of measurement?

P. A. LOTTES (United States of America): The attenuation of gamma rays was used to measure the void fractions in the rod-bundle experiment by Allis-Chalmers. A traverse was made in a direction perpendicular to the direction of flow.

E. KJELLAND-FOSTERUD (Norway): What is the estimated accuracy of the slip correlation shown in Figure 2?

P. A. LOTTES (United States of America): The estimated accuracy is $\pm 25\%$ for most of the data. A list of data, including ranges of test variables and percentage deviation from the correlation, is given in Ref. [15].

E. KJELLAND-FOSTERUD (Norway): Have you attempted to correct the Froude number to include the density ratio and the real pressure gradient, and have you tried to establish whether the correlation then describes the sort of slip ratios you find in Richardson's experiments on contractions?

P. A. LOTTES (United States of America): We have not corrected the Froude number to include the density ratio. The value of V_0 shown is the liquid velocity based on a situation where no vapour is present. It is equivalent to the total mass-flow rate divided by the liquid density.

S. S. KUTATELADZE (USSR): Nuclear technology has acted as a powerful stimulus to research on two-phase hydrodynamics. More and more experimental data are being accumulated, the results obtained are often contradictory and the whole field is becoming increasingly difficult to survey. In view of this situation, it seems to me that a special effort should be made to construct a number of physical-mathematical models which are fairly simple from the formal point of view but which are of general application.

In this connection I should like to draw attention to two important points. In the first place, a number of integral characteristics of two-phase flows (e.g. dp/dx) are in a first approximation conservative with regard to the structure of the mixture involved. Secondly, in a number of cases the stability characteristics are closely bound up with the structure of the mixture. In the latter case it can be shown that there is a criterion of the type

$$K = (W_{cr} \sqrt{\rho''}) / \sqrt[4]{g^2 \sigma (\rho' - \rho'')}$$

which represents the relationship between the kinetic energy of the light phase and the surface energy of the

* Ref. [32] of the paper.

phase separation. This makes it possible to construct a universal three-quadrant chart for the stability of different types of two-phase flows.

Some attempt to evolve a hydrodynamic theory for two-phase systems along these lines seems to me to be extremely desirable.

Paper P/327a (presented by V. I. Subbotin)

DISCUSSION

K. M. BECKER (Sweden): In connection with the effects of heated length on burn-out, measurements performed in Sweden agree with your finding that there is no length effect for round ducts. On the other hand, the length effect which Alekseev observed in annuli has not been confirmed by our measurements. In a recent report,* we have shown that burn-out in annuli of different lengths can be correlated to within $\pm 5\%$ in terms of $(q/A)_{BO}$, without any length term being included.

With regard to your measurements for dual heating in an annulus, I should like to mention a result quoted in a paper presented last year at the ASME-AICME Heat Transfer Conference in Boston,** viz. that when both walls were heated with the same heat flux, burn-out always occurred on the inner wall of the annulus. It was also reported in this paper that the outer wall could be overloaded up to 70% before burn-out occurred simultaneously on both walls. As indicated in the Swedish report mentioned above, we have found the same effect in a 3-rod cluster, where it was possible to overload the shroud about 50% compared to the rods before simultaneous burn-out on the shroud and the rods occurred.

I should be interested to know how much the outer wall of your annulus was overloaded when simultaneous burn-out on both cylinders occurred.

V. I. SUBBOTIN (USSR): Traditionally, the value of q_{BO} is treated as one of the original water parameters. In the case of annular channels, the total energy supplied affects the heat content of the original water. If account is taken of the proportion of heat supplied from each surface, then a comparison of experimental data for annular channels with one-surface and two-surface heat supply will yield congruent results.

H. S. ISBIN (United States of America): The authors are to be congratulated on presenting such a wealth of parametric investigations. The studies reported are extensive and detailed and must have required a considerable effort over a period of years. To enable the results of these labours to be more fully utilized it is to be hoped that a compilation of the experimental data will also be made available. It is recognized that the predictive models, as noted in your references,

* Becker, K. M., Hernborg, G., and Flinta, F. E., *Measurements of Burn-out Conditions for Flow of Boiling Water in Vertical 3-Rod and 7-Rod Clusters*, Report AE-153, Aktiebolaget Atomenergi, Stockholm, (August 1964).

** Becker, K. M., and Hernborg, G., *Measurements of Burn-out Conditions for Flow of Boiling Water in a Vertical Annulus*, ASME Paper No. 63-HT-25.

are of only limited value, but they can serve as useful tools in providing an insight into the mechanisms involved in the production of a heat transfer crisis.

I should be interested to hear what progress you have made in supplementing your empirical results with model descriptions of the phenomena producing the heat transfer crisis in the quality regions and in the subcooled regions.

V. I. SUBBOTIN (USSR): I think that it is too early to draw general conclusions from the work that has been done in the field of burn-out theory. What we really have to do is to build up a reliable body of facts and obtain information on what takes place on the hot wall before and at the time burn-out occurs. After that we shall be able to work on the theory.

H. S. ISBIN (United States of America): I have two further questions. First, have you carried out any visual studies of the burn-out crisis for steam/water systems under pressure? Secondly, in view of the need to extend burn-out studies to liquid-metal coolants, have you tried to adapt your steam/water results to burn-out tests with liquid metals? If so, what liquid systems were used?

V. I. SUBBOTIN (USSR): We have not been carrying out any visual studies to investigate the water boiling under pressure. As for your second question, I think it is rather risky to try to extrapolate q_{BO} data, computed for water, to liquid metals.

Paper P/50 (presented by P. Gelin)

DISCUSSION

G. J. BEALEY (United Kingdom): My questions relate to the performance of internally cooled surfaces, briefly referred to in your paper.

Since 1960 my company has been investigating the heat transfer performance of internally finned tubes with a view to their application to a highly rated magnox fuel element. Axial finning, helical fins and helical fins with axial splitters have all been tested for pressure drop and heat-transfer performance.

Our experience has been that, though adequate performance has been achieved at low Reynolds numbers and ratings, heat-transfer performance suffers a severe reduction as conditions more closely approach reactor values. For example, the Stanton number for one surface was reduced by a factor of 2.5 for an increase in rating from 2.5 to 10 kW/ft. The required rating was between 20 and 30 kW/ft. The explanation for this was that mixing between the gas in the flutes and in the main stream was poor. In our experience adequate mixing can only be achieved by devices which result in an unacceptable pressure loss.

We would therefore be particularly interested in having more details of the types of surfaces tested and the ratings and Reynolds numbers covered by the test.

P. GELIN (France): This of course raises a fundamental question, namely the influence of the heat flux on the heat-exchange coefficients.

At the CEA (Saclay) we have performed numerous tests with cans possessing a circular cross-section and lined with longitudinal fins. These cans were cooled internally by a stream of CO₂ at a pressure of 15 bars and heated on the outside by a stream of hot air moving at a velocity which made the external contour practically isothermal. The fins were arranged in a circle 50 mm in diameter. The number of fins varied between 24 and 50 and their height between 2.2 and 8.5 mm. The Reynolds number obtained with the diameter of 50 mm varied from 300 000 to 3 000 000 and the power per unit length from 5 to 20 kW/m.

Under these conditions it was found that the ratio between the average Margoulis number on the heating contour and the average friction coefficient on the heating contour was constant to within 10% over the whole range of variation of the Reynolds number. The friction coefficient used in this calculation was measured in isothermal flow.

These numerical values have been confirmed by the EDF Chatou laboratory, which carried out a constant-flow experiment on a 48-fin can that was practically identical to one of those we tested.

If in those tests the heat flux had been a sensitive independent parameter, the ratio between the Margoulis number and the friction coefficient would necessarily have varied considerably. This ratio

varied with the type of fins used, but remained between 0.25 and 0.45.

Paper P/524 (presented by F. Berger)

DISCUSSION

M. TROOST (United States of America): Have you made any comparison of your method of improving heat transfer with surface-roughening techniques? If so, is surface roughening more economical from the point of view of the energy required?

F. BERGER (Czechoslovakia): We have not made any direct comparison between the two methods of improving heat transfer. Surface roughening is technically easier but the additional pressure loss for an equal improvement in heat transfer is definitely lower when an electric field is applied. On the other hand, account also has to be taken of the consumption of electric energy in the H.T. circuit. The specific conditions of each individual case will therefore determine which method is more economical. I should perhaps emphasize that our work was primarily devoted to fundamental research into the influence of electric fields on heat transfer.

Paper P/232 (presented by H. S. Isbin)

There was no discussion of this paper.

Compte rendu de la séance I. 11

Problèmes hydrauliques de la technologie des réacteurs

Président: N. A. Dollezhal (URSS)

Mémoire P/230 (présenté par P. A. Lottes)

DISCUSSION

G. H. LATZKO (Pays-Bas): Le mémoire présente une excellente vue d'ensemble de la somme des travaux accomplis dans ce domaine aux Etats-Unis. Toutefois, il ne fournit aux ingénieurs chargés des projets aucune recommandation ferme sur les données à utiliser pour le calcul de la vitesse de glissement et de la perte de charge à deux phases. A ce propos, je serais heureux de savoir quel est l'accord entre les courbes pour le glissement données dans la figure 2 et le modèle de glissement de Bankoff proposé à un autre endroit du mémoire. Les abscisses et les ordonnées se rapportent-elles aux conditions locales dans le canal, et le nombre de Froude à l'entrée du canal?

P. A. LOTTES (Etats-Unis d'Amérique): Il existe un bon accord entre les courbes du glissement présentées et le modèle de Bankoff. Le choix de la figure est une question de préférence personnelle du point de vue du

technicien. Les abscisses et les ordonnées se rapportent aux conditions moyennes, et non locales.

H. CHRISTENSEN (Norvège): Dans la section de votre mémoire qui traite de l'expérience sur la stabilité de la puissance, effectuée en pile, vous dites que « le bruit en exploitation ne peut être utilisé comme mesure de stabilité absolue ». Dans le mémoire P/589, on indique le contraire, c'est-à-dire que, dans le cas d'un circuit bouillant, on peut, à partir d'une analyse du spectre de puissance de bruit, obtenir de très bonnes estimations du niveau d'instabilité, sauf peut-être aux puissances les plus élevées, où la caléfaction est proche.

Pensez-vous que ce désaccord entre les résultats obtenus puisse être dû à la présence dans le réacteur de Vallecitos d'éléments de combustible de performances différentes et peut-être de construction différent? Etant donné cette situation, la tendance à l'instabilité à mesure que la puissance croît pourrait être progressive, les canaux d'écoulement atteignant l'instabilité un à un.

Ceci rendrait impossible la définition d'un niveau exact d'instabilité.

P. A. LOTTES (Etats-Unis d'Amérique): Je pense que la réponse que vous proposez est la bonne. Il est possible d'avoir des fluctuations de débit et de vide entre des canaux parallèles, alors même que le débit massique *total* reste constant. En fait le professeur Gouse a effectué ses expériences au MIT* exactement selon ce principe, c'est-à-dire avec un débit massique total constant.

H. CHRISTENSEN (Norvège): Des résultats sont donnés à l'avant-dernier chapitre de votre mémoire pour des mesures de vide local. Pourriez-vous décrire la méthode de mesure?

P. A. LOTTES (Etats-Unis d'Amérique): C'est l'atténuation des rayons gamma qui a servi à mesurer le taux volumique de vapeur dans l'expérience d'Allis-Chalmers sur les grappes de barreaux. On faisait un pointage dans une direction perpendiculaire à celle de l'écoulement.

E. KJELLAND-FOSTERUD (Norvège): Quelle est la précision estimée de la relation de glissement donnée à la figure 2?

P. A. LOTTES (Etats-Unis d'Amérique): La précision est estimée à $\pm 25\%$ sur la plupart des chiffres. Une liste de chiffres, avec les gammes des variables des essais et l'écart en pourcentage par rapport à la relation est donnée dans la référence 15.

E. KJELLAND-FOSTERUD (Norvège): Avez-vous cherché à corriger le nombre de Froude pour y faire intervenir le rapport de densité et le gradient de pression réel, et avez-vous essayé d'établir si la relation rendait alors compte du genre de rapports de glissement trouvés dans les expériences de Richardson sur des contractions?

P. A. LOTTES (Etats-Unis d'Amérique): Nous n'avons pas corrigé le nombre de Froude pour y faire intervenir le rapport de densité. La valeur V_0 donnée est la vitesse du liquide, à partir d'une situation où la vapeur est absente. Elle est équivalente au débit massique total divisé par la densité du liquide.

S. S. KUTATELADZE (URSS): La technologie nucléaire a servi de puissant stimulant aux recherches d'hydrodynamique à deux phases. Les données expérimentales continuent à s'accumuler, les résultats obtenus sont souvent contradictoires, et il devient de plus en plus difficile d'avoir de tout ce domaine une vue d'ensemble. Devant cette situation, il semble qu'il faudrait un effort particulier pour élaborer un certain nombre de modèles physico-mathématiques qui seraient assez simples du point de vue formel mais qui auraient une grande généralité d'application.

A ce propos, je voudrais attirer votre attention sur deux choses importantes. Tout d'abord, un certain nombre de caractéristiques intégrales des écoulements à deux phases (par exemple $= dp/dx$) ne changent pas, en première approximation, avec la structure du

mélange étudié. Deuxièmement, dans un certain nombre de cas, les caractéristiques de stabilité sont étroitement liées à la structure du mélange. Dans ce deuxième cas, on peut montrer qu'il existe un critère du type

$$K = (W_{cr} \sqrt{\rho'}) / \sqrt{[g^2 \sigma (\rho' - \rho)]}$$

qui représente la relation entre l'énergie cinétique de la phase légère et l'énergie de la surface de séparation des phases. Ceci permet d'établir un diagramme ternaire universel pour la stabilité de divers types d'écoulements à deux phases.

Chercher à développer dans ce sens une théorie de l'hydrodynamique des systèmes à deux phases me paraît une chose tout à fait souhaitable.

Mémoire P/327a (présenté par V. I. Subbotin)

DISCUSSION

K. M. BECKER (Suède): A propos des effets de la longueur chauffée sur la caléfaction, des mesures faites en Suède concordent avec vos observations selon lesquelles la longueur est sans effet pour des canaux circulaires. D'autre part, l'effet de longueur observé par Alekseev dans des anneaux n'a pas été confirmé par nos mesures. Dans un rapport récent**, nous avons montré que la caléfaction dans des anneaux de diverses longueurs peut s'exprimer à $\pm 5\%$ près en fonction du $(q/A)_{BO}$, sans faire intervenir un terme longueur.

A propos de vos mesures de double chauffage d'un anneau, je voudrais signaler un résultat cité dans un mémoire présenté l'année dernière à la Conférence ASME-AICME sur les transferts thermiques, à Boston***, à savoir que, lorsque les deux parois sont chauffées avec des flux thermiques égaux, la caléfaction se produit toujours sur la paroi intérieure de l'anneau. On rapportait aussi dans ce mémoire que la paroi extérieure pouvait accepter une surcharge atteignant 70% avant que la caléfaction n'apparaisse en même temps sur les deux parois. Comme il est dit dans le rapport suédois déjà mentionné, nous avons trouvé le même effet avec une grappe de trois barreaux, où l'on pouvait créer sur la bouclier une surcharge d'environ 50% par rapport aux barreaux, avant l'apparition simultanée de la caléfaction à la fois sur le bouclier et sur les barreaux.

Je serais heureux de connaître la surcharge de la paroi extérieure de votre anneau à l'apparition de la caléfaction simultanément sur les deux cylindres.

V. I. SUBBOTIN (URSS): Comme on le fait habituellement, la valeur de q_{BO} est traitée comme l'un des paramètres de l'eau initiale. Dans le cas de canaux annulaires, l'énergie totale fournie influe sur la chaleur emmagasinée dans l'eau initiale. Si l'on tient

** Becker, K. M., Hernborg, G., et Flinta, F. E., *Measurements of Burn-out Conditions for Flow of Boiling Water in Vertical 3-Rod and 7-Rod Clusters*, rapport AE-153, Aktiebolaget Atomenergi, Stockholm, Suède (août 1964).

*** Becker, K. M., et Hernborg, G., *Measurements of Burn-out Conditions for Flow of Boiling Water in a Vertical Annulus*, rapport ASME No. 63-HT-25.

* Référence [32] du mémoire.

compte de la fraction de chaleur fournie par chaque surface, alors une comparaison des données expérimentales pour des canaux annulaires avec apport de chaleur par une ou par deux surfaces donnera des résultats congruents.

H. S. ISBIN (Etats-Unis d'Amérique): Il faut féliciter les auteurs d'avoir présenté une telle richesse de recherches paramétriques. Les études rapportées sont vastes et détaillées; elles ont dû exiger beaucoup d'efforts pendant plusieurs années. Pour permettre une utilisation plus complète des résultats de ces travaux, on doit espérer que l'on pourra disposer en outre d'un recueil des données expérimentales. On reconnaît que les modèles pour prévisions, signalés dans vos références, n'ont qu'une valeur limitée, mais ils peuvent servir d'instruments utiles pour comprendre les mécanismes mis en œuvre dans l'apparition d'un point critique dans les transferts thermiques.

Je serais heureux de savoir quels progrès vous avez faits pour compléter vos résultats empiriques par des modèles servant à décrire les phénomènes produisant la crise du transfert thermique dans les régions riches et dans les régions sous-saturées.

V. I. SUBBOTIN (URSS): Je pense qu'il est trop tôt pour tirer des conclusions générales des travaux faits dans le domaine de la théorie de la caléfaction. Ce que nous devons faire, en fait, c'est constituer un ensemble sûr de faits et recueillir des renseignements sur ce qui se passe sur la paroi chaude avant la caléfaction et à la caléfaction. Ensuite nous serons à même de travailler à la théorie.

H. S. ISBIN (Etats-Unis d'Amérique): J'ai encore deux questions à poser. Premièrement, avez-vous fait des études visuelles de la crise par caléfaction pour les systèmes eau-vapeur sous pression? Deuxièmement, vu la nécessité d'étendre les études de caléfaction à des réfrigérants métalliques liquides, avez-vous essayé d'adapter vos résultats pour eau-vapeur à des essais de caléfaction avec métaux liquides? Dans l'affirmative, quels systèmes liquides utilisez-vous?

V. I. SUBBOTIN (URSS): Nous n'avons fait aucune étude visuelle pour nos recherches sur l'eau bouillante sous pression. Quant à votre seconde question, je crois plutôt hasardeux de chercher à extrapoler les valeurs q_{BO} calculées pour l'eau à des métaux liquides.

Mémoire P/50 (présenté par P. Gelin)

DISCUSSION

G. J. BEALEY (Royaume-Uni): Mes questions portent sur les performances des surfaces refroidies intérieurement, mentionnées brièvement dans votre mémoire.

Depuis 1960, ma compagnie fait des recherches sur les capacités de transfert thermique de tubes munis d'ailettes à l'intérieur, en vue de leur application à un élément de combustible à Magnox à haut rendement. Ailettes longitudinales, ailettes hélicoïdales et ailettes hélicoïdales avec déflecteurs ont toutes subi des essais de perte de charge et d'échange thermique.

Bien que les performances atteintes soient convenables pour des nombres de Reynolds et des puissances spécifiques faibles, il résulte de nos travaux que les capacités d'échange thermique sont beaucoup réduites quand les conditions deviennent plus proches de celles qui se présentent dans les réacteurs. Par exemple, le nombre de Stanton pour une surface est divisé par 2,5 pour une augmentation de puissance spécifique de 2,5 à 10 kW par pied. La puissance spécifique voulue était entre 20 et 30 kW par pied. L'explication du fait est que le mélange entre le gaz dans les cannelures et dans le courant principal se fait mal. D'après notre expérience, un mélange convenable n'est réalisable qu'au moyen de dispositifs qui conduisent à une perte de charge inacceptable.

C'est pourquoi nous voudrions particulièrement avoir plus de détails sur les types de surfaces essayés et sur les puissances spécifiques et les nombres de Reynolds dans ces essais.

P. GELIN (France): Ceci soulève évidemment une question fondamentale, celle de l'influence du flux de chaleur sur les coefficients d'échange thermique.

Au CEA (Saclay) nous avons fait de nombreux essais avec des gaines à section circulaire munies d'ailettes longitudinales. Ces gaines étaient refroidies intérieurement par un courant de CO_2 sous une pression de 15 bars et chauffées à l'extérieur par un courant d'air chaud dont la vitesse était telle que la paroi extérieure était pratiquement isotherme. Les ailettes étaient disposées sur un cercle de 50 mm de diamètre. Le nombre d'ailettes variait entre 24 et 50, et leur hauteur entre 2,2 et 8,5 mm. Les nombres de Reynolds obtenus avec le diamètre de 50 mm variaient de 300 000 à 3 000 000, et la puissance par unité de longueur de 5 à 20 kW/m.

Dans ces conditions, on a trouvé que le rapport entre le nombre de Margoulis moyen sur la paroi chauffante et le coefficient de frottement moyen sur la paroi chauffante était constant dans des limites de 10% dans tout l'intervalle de variation du nombre de Reynolds. Le coefficient de frottement utilisé dans ce calcul était mesuré en écoulement isotherme.

Ces valeurs numériques ont été confirmées par le laboratoire de l'EDF à Chatou, qui a fait une expérience à écoulement constant sur une gaine à 48 ailettes, pratiquement identique à l'une de celles que nous avons testées.

Si dans ces essais le flux thermique avait été un paramètre indépendant sensible, le rapport entre le nombre de Margoulis et le coefficient de frottement aurait varié d'une manière considérable. Ce rapport dépendait du type d'ailettes, mais restait compris entre 0,25 et 0,45.

Mémoire P/524 (présenté par F. Berger)

DISCUSSION

M. TROOST (Etats-Unis d'Amérique): Avez-vous fait la comparaison entre votre méthode d'amélioration des transferts thermiques et les techniques de

corrugation de surface? Dans l'affirmative, la corrugation de surface est-elle plus économique du point de vue de l'énergie nécessaire?

F. BERGER (Tchécoslovaquie): Nous n'avons fait aucune comparaison directe entre les deux méthodes. La corrugation de surface est techniquement plus simple, mais le supplément de perte de charge à égalité d'amélioration des transferts thermiques est nettement plus faible si on applique un champ électrique. D'autre part, on a aussi tenu compte de la

consommation d'énergie électrique dans le circuit H.T. Ce sont donc les conditions propres à chaque cas particulier qui détermineront quelle méthode est la plus économique. Je dois peut-être souligner que l'objet de nos travaux était en premier lieu la recherche fondamentale sur l'effet des champs électriques sur le transfert thermique.

Mémoire P/232 (présenté par H. S. Isbin)

Ce mémoire n'a pas fait l'objet d'une discussion.

Протокол заседания I. II

Проблемы гидравлики в ядерных реакторах

Председатель: Н. А. Доллежал (СССР)

Доклад P/230 (представил П. А. Лоттс)

ДИСКУССИЯ

Г. Х. ЛАЦКО (Нидерланды): В докладе сделан отличный обзор большого количества экспериментальных работ, проведенных в США. С другой стороны, в нем не содержится каких-либо твердых рекомендаций, необходимых для расчета коэффициента проскальзывания или сопротивления при движении двухфазной смеси. Я хотел бы знать, насколько хорошо кривые для коэффициента проскальзывания, показанные на рис. 2 доклада, согласуются с результатами расчета по модели Бэнкова. Соответствуют ли значения на рисунке локальным параметрам потока, а число Фруда — параметрам на входе в канал?

П. А. ЛОТТС (США): Между кривыми, показанными на рисунке, и данными, рассчитанными на модели Бэнкова, имеется хорошее согласие. Выбор конкретных значений является делом личного вкуса. Значения величин по осям координат относятся к средним, а не локальным условиям.

Х. КРИСТЕНСЕН (Норвегия): В разделе Вашего доклада, посвященном внутриреакторным экспериментам по стабилизации мощности, Вы утверждаете, что «рабочий шум не может использоваться как мера абсолютной устойчивости». В докладе P/589 высказано противоположное мнение, а именно анализом спектральной плотности шума кипящей петли можно точно определить точку неустойчивости, за исключением, может быть, области высоких нагрузок, где быстро наступает кризис теплообмена.

Не считаете ли Вы, что отрицательные результаты получены вследствие различных конструкций и различного тепловыделения твэлов Вальеситосского реактора. В этом случае при увеличении мощности такая система постепенно приближается к неустойчивости и расход в каналах становится неустойчивым неодновременно. Это создает трудности в точном определении точки неустойчивости.

П. А. ЛОТТС (США): Я думаю, что Ваше объяснение совершенно правильно. Даже если полный расход остается постоянным, вполне возможны колебания расхода и паросодержания в параллельных каналах. Именно в таких условиях, то есть при постоянном полном расходе, проф. Гаус проводил свои эксперименты в Массачусетском технологическом институте (см. ссылку ³² доклада).

Х. КРИСТЕНСЕН (Норвегия): В предпоследнем разделе Вашего доклада приведены результаты измерений локальных паросодержаний. Не могли бы Вы описать метод измерений?

П. А. ЛОТТС (США): Для измерения истинных паросодержаний в пучке стержней применялся метод γ -просвечивания в направлении, перпендикулярном направлению движения потока.

Э. КЬЕЛЛАНД-ФОСТЕРУД (Норвегия): Какова точность коэффициента проскальзывания, представленного на рис. 2?

П. А. ЛОТТС (США): Для большинства данных точность $\pm 25\%$. Сводные данные, включая диапазон изменения параметров и относительное отклонение от предлагаемого обобщения, представлены в работе ¹⁵.

Э. КЬЕЛЛАНД-ФОСТЕРУД (Норвегия): Пытались ли Вы корректировать число Фруда, с тем

чтобы включить отношение плотностей и реальный градиент давления? Пытались ли Вы установить, что описанное Вами обобщение данных по коэффициенту проскальзывания приводит к уменьшению расслоения данных Ричардсона.

П. А. ЛОТТС (США): Мы не включали в число Фруда отношение плотностей. Значение V_0 является скоростью потока в сечении, где достигается температура насыщения. Она равна весовой скорости потока, деленной на удельный вес жидкости на линии насыщения.

С. С. КУТАТЕЛАДЗЕ (СССР): Атомная техника дала мощный стимул исследованиям в области гидродинамики. Накапливается все больший объем экспериментальных данных, подчас противоречащих друг другу. И все более затрудняется обзорение этих экспериментальных данных. Поэтому, на мой взгляд, надо обратить особое внимание на построение некоторых достаточно простых в формальном отношении, но общих по значению физико-математических модулей.

Здесь я хочу обратить внимание на два важных обстоятельства в этой области. Во-первых, ряд интегральных характеристик двухфазных потоков (например, $\frac{dP}{dx}$) консервативен относительно структуры фаз. Это позволяет использовать здесь некоторые общие соображения для построения соответствующих моделей.

Во-вторых, характеристики устойчивости систем в ряде случаев тесно связаны со структурой. Здесь вторая сторона картины этого сложного процесса. Можно показать, что в последнем случае существует критерий устойчивости

структуры типа $k = \frac{w_{\text{крит}}^2 \sqrt{\rho''}}{\sqrt{g^2 \sigma (\rho' - \rho'')}}}$, представ-

ляющий соотношение кинетической энергии легкой фазы и энергии граници поверхности раздела фаз, который позволяет построить достаточно универсальную, трехмерную карту устойчивости различных типов двухфазных потоков. Мне представляется, что эти два направления могут сыграть известную роль в обобщении того большого материала, который рассматривался на нашем сегодняшнем заседании.

Доклад Р/327 (представил В. И. Субботин)

К. М. БЕККЕР (Швеция): Результаты экспериментов, выполненных в Швеции, согласуются с Вашими данными о том, что при движении теплоносителя в круглых трубах обогреваемая длина не оказывает влияния на значения критических тепловых нагрузок. С другой стороны, наши опыты не подтверждают эффекта длины на критические нагрузки в кольцевых каналах, обнаруженного Алексеевым. В нашей работе *

мы показали, что критические тепловые нагрузки для кольцевых каналов различной длины могут быть описаны с точностью $\pm 5\%$ без включения каких-либо членов, содержащих обогреваемую длину канала.

В связи с Вашими измерениями критических нагрузок для кольцевых каналов, обогреваемых с двух сторон, я хотел бы напомнить о результатах, описанных в докладе, представленном на конференцию по теплоотдаче ASME — AICME в Бостоне **. Согласно нашим данным, при одинаковом обогреве обеих поверхностей кризис кипения всегда возникал на внутренней стенке канала. В этом докладе также сообщалось, что внешняя стенка может быть нагружена на 70% большим потоком тепла, прежде чем возникает кризис теплообмена на обеих поверхностях. Как указано в упомянутом выше шведском докладе, мы обнаружили аналогичный эффект в трехстержневом пучке, где было возможно нагрузить чехол на 50% большим тепловым потоком, чем поток тепла на поверхности стержней, прежде чем кризис возникал на поверхностях стержней и на чехле одновременно.

Мне интересно знать, насколько оказывалось возможным в Ваших экспериментах перегружать внешнюю поверхность кольцевых каналов для одновременного возникновения критических условий на обеих поверхностях.

В. И. СУББОТИН (СССР): Вообще величина $q_{\text{крит}}$ традиционно считается одним из исходных параметров для воды. В случае кольцевых каналов общая энергия влияет на теплосодержание исходной воды. Если учесть долю тепла, генерируемой на каждой поверхности, то сравнение экспериментальных данных для кольцевых каналов с одной и двумя поверхностями энерговыделения приведет к совпадению результатов.

Х. С. ИСБИН (США): Следует поздравить авторов, представивших столь ценные исследования. Для анализа этих широких и детальных экспериментов потребуются несколько лет напряженной работы. Будем надеяться, что для нас станет доступным полное описание экспериментальных данных. Это позволит полнее использовать результаты представленных работ. Понятно, что расчетные модели, как это следует из Вашего доклада, имеют еще ограниченное значение. Однако такие модели являются полезными средствами для проникновения в механизм кризиса теплообмена.

Мне было бы интересно услышать, насколько успешны попытки соединения эмпирических результатов с теоретическим описанием явлений, приводящих к кризису теплоотдачи при движении недогретой жидкости и паро-водяной смеси.

* К. М. Becker et al. Report AE-153, Ab Atomenergi, Stockholm, Sweden, Aug. 1964.

** К. М. Becker and G. Hernborg. ASME Paper No. 63-HT-25, 1963.

В. И. СУББОТИН (СССР): Я полагаю, что еще слишком рано делать общие выводы в отношении теории кризиса кипения. Все то, что мы действительно должны сделать, это накопить достаточное количество надежных фактов и выяснить механизм явления на горячей стенке до и во время кризиса кипения. Только после этого можно приступить к разработке теории процесса.

Х. С. ИСБИН (США): У меня есть еще два вопроса. Во-первых, проводили ли Вы визуальные наблюдения кризиса кипения в паро-водяных смесях под давлением? Во-вторых, имея в виду необходимость исследований критических нагрузок для жидкометаллических теплоносителей, пытались ли Вы сопоставлять Ваши данные по критическим нагрузкам для паро-водяных смесей и данные опытов с жидкими металлами? Если да, то какие использовались жидкие металлы?

В. И. СУББОТИН (СССР): Что касается визуальных наблюдений, то мы не проводили никаких визуальных исследований кризиса кипения под давлением.

В отношении второго вопроса, я думаю, что довольно опасно пытаться экстраполировать данные $q_{крит}$ для паро-водяных смесей и для жидких металлов.

Доклад Р/50 (представил П. Желин)

ДИСКУССИЯ

Г. Дж. БИЛИ (Соединенное Королевство): Мои вопросы относятся к качеству поверхностей, охлаждаемых внутри, упомянутых в Вашем докладе. С 1960 года с целью использования высоконапряженных магнетронных теплоотдающих элементов мы исследуем теплоотдачу труб с внутренним оребрением. Исследованы потери давления и теплоотдача в трубах с продольным или винтовым оребрением, а также с винтовым оребрением и продольными перегородками.

Наш опыт показывает, что, хотя при малых числах Рейнольдса и низких нагрузках достигаются удовлетворительные результаты, по мере приближения к реакторным параметрам происходит существенное уменьшение скорости теплоотдачи. Например, при увеличении тепловой нагрузки с 2,5 до 10 *квт/фут* число Стантона уменьшилось в 2,5 раза. Рабочие же нагрузки лежат между 20 и 30 *квт/фут*. Это объясняется тем, что перемешивание газа в пазухах и основного потока было недостаточным. По нашим данным, перемешивания можно добиться только в системах, имеющих недопустимо большие потери давления.

Поэтому мы особенно заинтересованы в получении более полного описания типов испытанных поверхностей, а также перекрытого оптимума диапазона чисел Рейнольдса и нагрузок.

П. ЖЕЛИН (Франция): Вопрос о влиянии теплового потока на коэффициент теплоотдачи, безусловно, имеет очень важное значение.

В Сакле мы провели многочисленные испытания труб с круглыми и продольными ребрами. Такие трубы изнутри охлаждались потоком углекислого газа при давлении 15 *бар*. Вдоль внешней образующей трубы двигался горячий воздух, скорость которого была достаточна для практической изотермичности внешнего контура. Внешний диаметр оребрения составлял 50 *мм*. Число ребер изменялось в пределах 25—50, высота ребер от 2,2 до 8,5 *мм*. Число Рейнольдса варьировалось от 300 000 до $3 \cdot 10^6$, а погонная тепловая нагрузка — от 5 до 20 *квт/м*.

При таких условиях было найдено, что отношение среднего по обогреваемому контуру значения числа Маргулиса и среднего коэффициента трения было постоянным с точностью до 10% во всем интервале изменения числа Рейнольдса. Коэффициент трения, использованный при расчетах, измерялся в условиях изотермического течения.

Эти результаты были подтверждены в лаборатории, где проводились эксперименты с 48 ребристыми трубами, которые практически идентичны с исследованными нами.

Если в таких опытах тепловой поток был независимым параметром, отношение числа Маргулиса и коэффициента трения значительно изменялось. Диапазон изменения этого отношения для исследованных типов ребер составлял 0,25—0,45.

Доклад Р/524 (представил Ф. Бергер)

ДИСКУССИЯ

М. ТРУСТ (США): Проводили ли Вы сравнение Вашего метода увеличения теплоотдачи с методом искусственной шероховатости? Если да, то не являлся ли последний метод более экономичным с точки зрения затрат энергии?

Ф. БЕРГЕР (Чехословакия): Мы не проводили прямого сопоставления методов увеличения теплоотдачи. Метод искусственной шероховатости технически более прост, но дополнительные потери давления в случае использования электрического поля определенно меньше, чем в первом случае при одинаковом улучшении теплоотдачи. С другой стороны, следует учесть потребление электрической энергии в контуре. Поэтому экономичность различных методов будет определяться конкретными условиями. Я должен подчеркнуть, что наша работа была посвящена в первую очередь фундаментальным исследованиям влияния электрического поля на скорость теплоотдачи.

Доклад Р/232 (представил Х. С. Исбин)

По этому докладу дискуссии не было.

Acta de la sesión 1.11

Problemas hidráulicos de la tecnología de reactores

Presidente: N. A. Dollezhal (URSS)

Documento P/230 (presentado por P. A. Lottes)

DISCUSIÓN

G. H. LATZKO (Países Bajos): Esta memoria es una excelente revisión de la gran cantidad de trabajo experimental que se realiza en los Estados Unidos en este campo. Por otra parte, no proporciona al proyectista ninguna recomendación firme sobre la información que debe usar para calcular la velocidad de deslizamiento y la pérdida de carga en flujo bifásico. Me interesaría conocer, en relación con esto, cómo se correlacionan las curvas para el deslizamiento, de la figura 2, con el modelo de deslizamiento de Bankoff que se menciona en otro lugar de la memoria. Los valores de abscisas y ordenadas ¿se refieren a condiciones locales del canal? y el número de Froude ¿a la entrada del canal?

P. A. LOTTES (Estados Unidos de América): Existe un buen acuerdo entre las curvas de deslizamiento expuestas y el modelo de Bankoff. La elección de esta cifra, en particular, es una cuestión de preferencia personal desde el punto de vista ingenieril. Los valores de abscisas y ordenadas se refieren ambos a condiciones medias y no locales.

H. CHRISTENSEN (Noruega): En la sección de su memoria que se refiere al experimento dentro del reactor sobre la estabilidad de la potencia, Vds. afirman que "el ruido en la operación no puede usarse como medida de la estabilidad absoluta". En el documento P/589 se hace la observación opuesta, o sea, que en el caso de un circuito de ebullición, es posible obtener determinaciones muy buenas del punto de inestabilidad basándose en el análisis del espectro ruido-potencia, excepto, quizás, para las potencias más altas, a las cuales la fusión se produce rápidamente.

¿Cree Vd. que esta diferencia de los resultados obtenidos puede ser debida a la presencia, en el reactor de Vallecitos, de elementos combustibles de diferentes densidades de potencia y quizás diferente construcción? Dada esta situación, la tendencia hacia la inestabilidad a potencias crecientes puede ser gradual, alcanzando los canales la inestabilidad uno a uno. Esto haría imposible definir un punto exacto de inestabilidad.

P. A. LOTTES (Estados Unidos de América): Creo que la explicación que Vd. sugiere es la correcta. Es posible tener oscilaciones de flujo y huecos entre

canales paralelos, aun cuando el caudal *total* permanezca constante. De hecho, el Prof. Gouse realizó sus ensayos en el MIT* con esta línea de trabajo, o sea con un caudal constante.

H. CHRISTENSEN (Noruega): En la sección penúltima de su memoria se dan resultados de medidas locales de huecos. ¿Puede Vd. describir el método de medida?

P. A. LOTTES (Estados Unidos de América): Se empleó la atenuación de rayos gamma para medir las fracciones de huecos en el experimento con haces de barras de Allis-Chalmers. Se hizo una exploración transversal en dirección perpendicular a la del flujo.

E. KJELLAND-FOSTERUD (Noruega): ¿Cuál es la exactitud estimada de la correlación de deslizamiento expuesta en la figura 2?

P. A. LOTTES (Estados Unidos de América): La exactitud estimada es $\pm 25\%$ para la mayor parte de los datos. En la referencia [15] se da una lista de datos, que incluye los intervalos de variación de las variables ensayadas y la desviación porcentual de la correlación.

E. KJELLAND-FOSTERUD (Noruega): ¿Han tratado Vds. de corregir el número de Froude para que incluya la relación de densidades y el gradiente real de presión? y ¿han intentado establecer si la correlación describe, entonces, la clase de relaciones de deslizamientos que se encuentran en los experimentos de Richardson sobre contracciones?

P. A. LOTTES (Estados Unidos de América): No hemos corregido el número de Froude para que incluya la relación de densidades. El valor de V_0 expuesto es la velocidad del líquido basada en una situación en que el vapor no está presente. Es equivalente al caudal total dividido por la densidad del líquido.

S. S. KUTATELADZE (URSS): La tecnología nuclear ha actuado como un poderoso estímulo para la investigación de la hidrodinámica de dos fases. Se están acumulando cada vez más datos experimentales, los resultados obtenidos son frecuentemente contradictorios y se hace cada vez más difícil revisar la totalidad del campo de trabajo. En vista de esta situación, me parece que debiera hacerse un esfuerzo especial para construir un número de modelos

* Ref. [32] de la memoria.

físico-matemáticos que fueran relativamente sencillos desde el punto de vista formal, pero que fueran de aplicación general.

A este respecto, me gustaría indicar dos puntos importantes. En primer lugar, en cierto número de características integrales del flujo bifásico (v.g. dp/dx) son conservadoras, en primera aproximación, con respecto a la estructura de la mezcla de que se trata. En segundo lugar, en algunos casos, las características de estabilidad están íntimamente ligadas a la estructura de la mezcla. En este último caso puede demostrarse que exists un criterio del tipo

$$K = (W_{cr} \sqrt{\rho'}) / \sqrt[4]{g^3 \sigma (\rho' - \rho'')}$$

que representa la relación entre la energía cinética de la fase ligera y la energía superficial de la separación de fases. Ello hace posible construir un gráfico universal de tres cuadrantes para la estabilidad de diferentes tipos de flujo bifásico.

Me parecen muy convenientes los intentos en este sentido, para desarrollar una teoría hidrodinámica de los sistemas bifásicos.

Documento P/327a (presentado por V. I. Subbotin)

DISCUSIÓN

K. M. BECKER: Con relación a los efectos de la longitud de calefacción sobre la fusión, las medidas realizadas en Suecia concuerdan con su conclusión de que no existe influencia del efecto de longitud para tubos redondos. Por otra parte, no se ha confirmado en nuestras medidas el efecto de longitud que observó Alekseev en canales anulares. En un trabajo reciente*, hemos demostrado que la fusión en canales anulares de diferentes longitudes, puede correlacionarse dentro de un error de $\pm 5\%$ sobre $(q/A)_{BO}$, sin incluir la longitud en ningún término.

Con respecto a sus medidas para calentamiento doble en un canal anular, quisiera mencionar un resultado que figura en el trabajo presentado el pasado año en la "Heat Transfer Conference" de ASME-AICME de Boston**, es decir que, cuando ambas paredes se calientan con el mismo flujo calorífico, la fusión se produce siempre en la pared interior del canal anular. También se informó en esa memoria que la pared exterior podía sobrecargarse hasta un 70% antes de que se produjera la fusión en ambas paredes. Como se indicaba en el informe sueco mencionado anteriormente, hemos encontrado el mismo efecto en un haz de 3 barras, en el que era posible sobrecargar el tubo envolvente en cerca del 50% con respecto a las barras, antes que se produjera la fusión simultáneamente en el tubo envolvente y en las barras.

Me interesaría saber cuánto se sobrecargó la

* Becker, K. M., Hernborg, G., y Flinta, F. E., *Measurements of Burn-out Conditions for Flow of Boiling Water in Vertical 3-Rod and 7-Rod Clusters*. Informe AE-153, Aktiebolaget Atomenergi, Estocolmo, Suecia. Agosto de 1964.

** Becker, K. M., y Hernborg, G., *Measurements of Burn-out Conditions for Flow of Boiling Water in a Vertical Annulus*, ASME Paper No. 63-HT-25.

pared exterior de su canal anular cuando se produjo la fusión simultánea en ambos cilindros.

V. I. SUBBOTIN (URSS): Tradicionalmente, el valor de q_{BO} se trata como uno de los parámetros originales del agua. En el case de canales anulares, la energía total suministrada afecta a la entalpía del agua original. Si se tiene en cuenta la proporción de calor suministrada desde cada superficie, entonces una comparación de datos experimentales para canales anulares con aporte de calor a una superficie y a dos superficies, arrojará resultados congruentes.

H. S. ISBIN (Estados Unidos de América): Hay que felicitar a los autores por la presentación de tal riqueza de investigaciones paramétricas. Los estudios presentados son extensos y detallados y deben haber requerido un esfuerzo considerable durante años. Para permitir que los resultados de estos trabajos sean utilizados más ampliamente, hay que esperar que también se haga asequible una compilación de los datos experimentales. Hay que reconocer, como Vd. nota en sus referencias, que los modelos de predicción tienen sólo un valor limitado, pero pueden servir como instrumentos útiles para poder comprender los mecanismos que intervienen en la producción de una crisis de transmisión de calor.

Me interesaría escuchar los progresos que Vds. hayan hecho para suplementar sus resultados empíricos con descripciones a base de modelos de los fenómenos que producen las crisis de transmisión de calor, en las regiones que contienen vapor y en las subenfriadas.

V. I. SUBBOTIN (URSS): Creo que es prematuro deducir conclusiones generales del trabajo realizado en el campo de la teoría de la fusión. Lo que realmente tenemos que hacer es construir un conjunto de hechos de garantía y obtener información sobre lo que tiene lugar en la pared caliente antes de la fusión y durante ella. Después, seremos capaces de ocuparnos de la teoría.

H. S. ISBIN (Estados Unidos de América): Tengo que hacer dos preguntas más. Primera ¿han realizado Vds. estudios visuales de la crisis de fusión para sistemas agua-vapor a presión? Segunda, en vista de la necesidad de extender los estudios de fusión a refrigerantes de metal líquido ¿han tratado de adaptar sus resultados sobre agua-vapor a ensayos de fusión con metales líquidos? En caso afirmativo ¿qué sistemas líquidos se emplearon?

V. I. SUBBOTIN (URSS): No hemos realizado estudios visuales para investigar la ebullición de agua a presión. Respecto a su segunda pregunta, creo que es bastante aventurado el tratar de extrapolar datos de q_{BO} obtenidos para agua, a metales líquidos.

Documento P/50 (presentado por P. Gelin)

DISCUSIÓN

G. J. BEALEY (Reino Unido): Mis preguntas se refieren al comportamiento de superficies calentadas

interiormente, a las que se refieren brevemente en su trabajo.

Mi compañía ha estado investigando desde 1960 el comportamiento a la transmisión de calor de tubos con aletas interiores, con vistas a su aplicación a elementos combustibles de magnox, de elevada densidad de potencia. Se han ensayado, respecto al comportamiento en pérdida de carga y transmisión de calor, aletas axiales, helicoidales, y helicoidales con tabiques separadores axiales.

Nuestra experiencia indica que la transmisión de calor sufre una reducción seria en cuanto las condiciones se aproximan más a las correspondientes al reactor, aunque se han obtenido rendimientos adecuados con números de Reynolds y densidades de potencia bajas. Por ejemplo, el número de Stanton para una superficie se redujo en un factor 2,5 para un aumento en la densidad de potencia de 2,5 a 10 kW/ft. El valor requerido estaba comprendido entre 20 y 30 kW/ft. La explicación de ello era que la mezcla del gas situado entre las aletas y el de la corriente principal era pobre. En nuestra experiencia, se puede obtener una mezcla adecuada sólo mediante artificios que producen una pérdida de carga inaceptable.

Estaríamos por tanto particularmente interesados en tener más detalles sobre los tipos de superficies ensayados y las densidades de potencia y números de Reynolds que abarcaban los ensayos.

P. GELIN (Francia): Esto plantea, desde luego, una cuestión fundamental: la influencia del flujo calorífico sobre los coeficientes de intercambio de calor.

Hemos realizado en el CEA (Saclay) muchos ensayos con vainas de sección recta circular y cubiertas de aletas longitudinales. Estas vainas estaban refrigeradas interiormente por una corriente de CO₂ a la presión de 15 bares y calentadas por el exterior con una corriente de aire caliente que se movía a tal velocidad que hacía el contorno exterior prácticamente isotérmico. Las aletas estaban dispuestas en un círculo de 50 mm de diámetro. El número de aletas variaba entre 24 y 50 y su altura entre 2,2 y 8,5 mm. El número de Reynolds obtenido con el diámetro de 50 mm variaba entre 300 000 y 3 000 000, y la potencia por unidad de longitud entre 5 y 20 kW/m.

En estas condiciones se encontró que la relación entre el valor medio del número de Margoullis del perímetro calefactor, y el coeficiente de rozamiento medio del perímetro calefactor, era constante, dentro de un 10%, para todo el intervalo de variación del número de Reynolds. El coeficiente de rozamiento usado en estos cálculos se midió en flujo isotérmico.

Estos resultados numéricos han sido confirmados por el laboratorio Chatou de EDF, el cual llevó a cabo un experimento de flujo constante con una vaina de 48 aletas que era prácticamente igual a una de las que nosotros ensayamos.

Si en estos ensayos el flujo calorífico hubiera sido un parámetro independiente importante, la relación entre el número de Margoullis y el coeficiente de rozamiento tendría que haber variado considerablemente. Esta relación variaba con el tipo de aletas empleado, pero permaneció entre 0,25 y 0,45.

Documento P/524 (presentado por F. Berger)

DISCUSIÓN

M. TROOST (Estados Unidos de América): ¿Han hecho Vds. comparaciones de su método para mejorar la transmisión de calor, con las técnicas de desbaste de la superficie? Si es así ¿es el desbaste de la superficie más económico desde el punto de vista de la energía requerida?

F. BERGER (Checoslovaquia): No hemos hecho ninguna comparación directa entre los dos métodos de mejorar la transmisión de calor. El desbaste de la superficie es técnicamente más fácil, pero la pérdida de carga adicional, para una mejora igual en la transmisión de calor, es definitivamente inferior cuando se aplica un campo eléctrico. Por otra parte, hay que tener también en cuenta el consumo de energía eléctrica en el circuito de A.T. Las condiciones específicas de cada caso determinarán, por tanto, qué método es más económico. Quisiera hacer resaltar que nuestro trabajo se dirigió principalmente a la investigación fundamental sobre la influencia de campos eléctricos sobre la transmisión de calor.

Documento P/232 (presentado por H. S. Isbin)

No hubo discusión de esta memoria.

Session 3.7

REACTOR PLANT EQUIPMENT

LIST OF PAPERS

		Page
<i>Control</i>		
P/126	Recent developments in the instrumentation and control of large gas-cooled reactors D. S. Hiorns <i>et al.</i>	385
P/229	Improvements in instrumentation for high-performance power reactors S. H. Hanauer	395
P/330	Система управления реакторами И. Я. Емельянов <i>et al.</i> <i>Control system of nuclear reactors</i> I. Y. Emelyanov <i>et al.</i>	404
P/518	Résultats pratiques et perspectives de l'utilisation de poison en solution dans les réacteurs à eau sous pression M. Plumier <i>et al.</i> <i>Practical results and prospects for the use of a soluble poison in the pressurised-water reactors</i>	413
<i>Pressure vessels</i>		
P/52	Les caissons en béton précontraint des réacteurs français de la filière uranium naturel – graphite – gaz carbonique G. Lamiral <i>et al.</i> <i>The prestressed concrete pressure-vessels of the French natural uranium-graphite-carbon dioxide gas sequence reactors</i>	422
P/140	The design and construction of prestressed concrete pressure vessels with particular reference to Oldbury nuclear power station A. Houghton Brown <i>et al.</i>	433
P/141	The design of prestressed concrete pressure vessels, with particular reference to Wylfa R. S. Taylor, A. J. Williams	446
P/144	Investigations to predict the performance of steel reactor pressure circuit components in service. C. H. A. Townley, E. Procter	456
P/227	Problems in the design and construction of large reactor vessels A. L. Gaines, L. Porse	464
P/331	Корпуса водо-водяных энергетических реакторов высокого давления В. В. Стекольников <i>et al.</i> <i>Vessels for power reactors cooled and moderated by water at high pressures</i> V. V. Stekolnikov <i>et al.</i>	473
P/522	Pressure vessel for the first Czechoslovak nuclear power station J. Hauer <i>et al.</i>	484
P/810	Design and manufacture of the reactor pressure vessels for the Ågesta and Marviken Power Stations and some future developments O. Hellström	498
<i>Control rods</i>		
P/809	Design, development and manufacture of control rod drives for heavy-water power reactors S. Ericsson, B. Ahlnäs	505

LIST OF PAPERS

(Continued)

		Page
	<i>Fuelling machinery</i>	
P/54	Les appareils de chargement et déchargement du combustible dans les réacteurs uranium naturel – graphite – gaz B. Saitcevsky, D. Gaussoit	512
	<i>Fuel loading and unloading devices for the natural uranium-graphite-gas sequence reactors</i>	
P/139	Experience with Bradwell and Latina on-load fuel handling equipment and its influence on future designs J. O. Joss <i>et al.</i>	522
P/808	Fuel handling equipment for the Ågesta D ₂ O moderated pressure vessel reactor G. Granelli <i>et al.</i>	532
	<i>Other components</i>	
P/51	Etude de structures nouvelles adaptées aux réacteurs graphite – gaz et eau lourde – gaz R. Martin, R. Roche	541
	<i>Study of new structures adapted to gas-graphite and gas-heavy-water reactors</i>	
P/94	Les circuits de gaz carbonique dans les centrales nucléaires E. Robert <i>et al.</i>	548
	<i>CO₂ circuits in nuclear power stations</i>	
P/137	Graphite core structures for large gas-cooled power reactors . . . P. C. Warner, M. A. Bayer	560
P/138	Gas circulators and their drives for large gas-cooled power reactors H. Bateman <i>et al.</i>	569
P/143	Some engineering problems of the SGHW 100 MW(e) prototype reactor N. Bradley <i>et al.</i>	579
P/228	Components for sodium reactors H. O. Monson <i>et al.</i>	588
P/592	Mild steel in primary circuits of water-cooled power reactors K. Videm	600
P/696	Special problems relating to monotube boilers in nuclear power stations J. Kägi, P. Doroszalai	609
P/728	Experience in the design, calculation and manufacture of power reactor components K. J. de Jong <i>et al.</i>	618
P/770	Apport de la réalisation d'une grande centrale nucléaire dans la conception et la construction des équipements pour réacteurs P. Klees, C. Gérard	627
	<i>The effect of the construction of a large nuclear power plant on the design and manufacture of reactor equipment</i>	
P/834	Strength problems of the flanged joint J. Kuchta	636
P/857	Some engineering studies conducted in introducing a British type reactor for the Tokai atomic power station T. Yoshioka <i>et al.</i>	642

Recent developments in the instrumentation and control of large gas-cooled reactors

By D. S. Hiorns,* T. O. Jeffries,** D. Moore,** H. Moores** and A. H. Weaving*

To simplify operational procedures, current British nuclear power stations use centralised control, made practicable by new methods of data presentation. Solid state equipment has been increasingly applied both here and to reactor safety circuits and control rod systems to improve reliability, and this paper reviews these developments.

CENTRALISED CONTROL

Why centralised control is adopted

Since 1960, all nuclear stations ordered by the Generating Board specify centralised control. Whilst the reliability of control equipment used in British power stations was high, it had been general practice to provide manual control to supplement auto control and to increase availability, in view of the large cost of plant outages (particularly of nuclear stations where it could amount to £10 000 per day). The associated instrumentation was usually duplicated by adopting multiple local control centres. Simple control systems were often adequate on local panels, with few controls per operator, so long as sufficient staff were available to man the panels but, with the increasing complexity of plant in the latest stations, the concept of local control centres is no longer adequate.

By efficient design of one centralised control area, and the adoption of new techniques of data presentation from extremely reliable equipment, the advantages of the earlier arrangement are retained, with economy in the number of staff. With this system the plant can be started, operated and shut down from the central control room, leading to reduce communication errors, wider interest for each operator and more efficient action under fault conditions.

Scope of the application of centralised control

Semi-automatic control in limited sequences is the method adopted for control of established plant operations on heat exchangers, gas circulators and the gas circuit auxiliary systems. Turbo-alternator start-up includes sequence start-up of auxiliaries and, in one station, computer controlled run-up to speed. Local

control is retained where the cost of control centralisation is not justified, as on isolating valves operated only for maintenance, and automatic ancillary plant, such as feed make-up.

The optimum start-up technique for large reactors with high irradiations is not sufficiently well established to permit automatic start-up. Reliance is placed on operator vigilance during criticality and increasing temperature phases, backed up by an automatic protective system. Data processing is required to give the operator the clearest display of plant conditions at these times.

MAIN CONTROL ROOM DESIGN

When control is centralised compactness must be maintained in spite of the additional functions introduced into the control room, otherwise the efficiency of control is lost and the essential aims are not achieved. Radical changes such as extensive use of auto control, basically new concepts of display of data which has already been processed, and the increased use of miniature equipment combine to achieve the objective. The size of control room is smaller than at earlier stations in spite of the additional information now available to the operators.

Control room manning on which design is based

Station operation is supervised by the Shift Charge Engineer, and his assistant will supervise the main

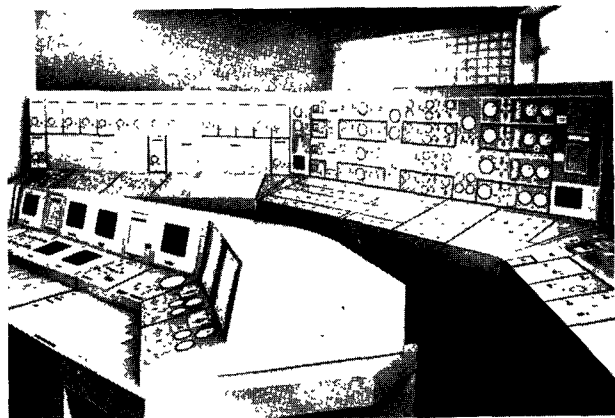


Figure 1. Mock-up of typical control room layout

* Central Electricity Generating Board, Design and Construction Department, London.

** English Electric Company Limited, Cambridge Road, Whetstone, near Leicester.

control room. A unit operator is in charge of each reactor assisted by plant operators and fuelling machine operators. The unit operator will be responsible for all main plant in normal operation and will bring the reactor through criticality and up to power. The plant operator starts up all conventional and nuclear plant sub-systems upon instructions from the unit operator and generally assists during normal operation.

Functional layout of control surfaces

The latest nuclear stations adopt a control room layout which is typified by the preliminary mock-up of the Wylfa nuclear power station (Fig. 1). The control desk in the foreground of the picture is the focal point of control for a reactor-turbine unit and where the Unit Operator is usually seated to supervise normal operation. Controls and indications for sub-systems and auxiliary system start-up are grouped on free-standing panels arranged in an arc and shown at the back of the picture. It will be noted that a distinction is made between normal power indicating instrumentation on the vertical surfaces of the panels and start-up controls on the semi-horizontal surfaces. Systems common to the two reactors are grouped separately on panels or a console adjacent to the Supervisor's administrative desk (not shown). Fuelling machine control is sited in a special area, which is an extension of the main station control area.

Under abnormal or fault conditions maximum automatic transfer to standby equipment is incorporated. The grouping of controls and indications for normal operation at the control desk provides, with few additions, efficient emergency control.

Radical changes in data presentation being adopted

The operator now demands only the information required for his current needs, and all other plant data is continuously monitored in the data processing system. Conventional indications could not be rearranged from minute to minute and demanded information is therefore displayed in tabular form on a series of suitably positioned cathode ray tubes, using alpha-numeric characters. Over 4 000 indications or statements of the condition of the plant are available to the operators on the tabular display system.

Future design trends in data presentation are concerned with adaptive displays for particular operations. A comprehensive analogue display, probably using cathode ray tubes, is being considered for comparative monitoring of many separate but similar measurements—for example, control rod positions—may be displayed as a histogram to show quickly the relative rod insertions.

With the display of only selected plant readings, abnormal conditions must be brought to the operator's attention. Individual faults are each displayed on cathode ray tubes but complex fault conditions, particularly when two abnormalities occur simultaneously, are analysed by the data processing system and the cathode ray tubes indicate the one or two

prime cause faults and actions which the operator should take.

The compact functional grouping of miniature controls

In recent years, lower voltage (often 50 V) miniature control equipment similar to that used in telephone practice, but of an even higher standard of reliability, has been used, operating into the main power circuits through interposing relays. The recent development of improved interposing relays has encouraged this tendency. More controls and indications of this type can be grouped on the panels and close proximity between each control and its associated indication is easily arranged.

Where a group of operations must be carried out during start-up, but operator decision is not required at each stage, the use of auto-sequence control results in the elimination of many controls and lamp indications, and reduces panel size and the cost of equipment and cabling.

DATA PROCESSING SYSTEM

Reliability is of first importance

To carry out the functions described above, the data processing system must be of the highest reliability. An availability of 99% has been practicable for some time in small data processing units and has been reported for on-line systems; even this high level of availability would be inadequate for the data processing system of a nuclear station if all the displayed data were lost for 1% of the time. Two approaches are therefore required to make the effect of faults less serious: firstly, sub-division and redundancy in the equipment, and secondly, increasing the reliability of the equipment supplied. The latter is achieved by using improved manufacturing methods and by adopting equipment which embodies solid state techniques where practicable, air conditioning, and is of proved reliability, rather than a new design.

Where a single fault can cause a complete system outage, as in the central computer system, redundancy is essential and both (a) the use of two computers with overlap for essential duties, and (b) the use of two computers with one computer carrying 100% of the station duty and the other acting as a standby, have been considered. Within cost limitations, (b) has advantages over (a) as the "essential duties" are dependent upon operating conditions of the plant at the time of fault. Using (b) with suitable changeover equipment, it should be possible to achieve availability factors of 99.9% including an allowance for non-availability of common equipment. Clearly it would be essential for the design of the common equipment to be simple and as reliable as possible and a check system would be required to monitor the operation of both the running and the standby computer. Failures in the running machine would initiate changeover to the standby, and failure of either machine would initiate alarms so that corrective action may be taken.

Periodically the check system on the running machine will be artificially failed, and changeover initiated, to check the equipment as a whole.

For the peripheral equipment, sub-division increases availability and both the analogue and digital scanners can be so divided that failure of a single component puts out of commission only one section (which is a small proportion of the whole) and vital signals can be fed to the data processor through more than one section of the scanner. Similar conditions apply to the magnetic drum stores, but for the display equipment the cathode ray tubes will be sufficient in number to provide alternative tubes in the event of failure of one. In the event of failure of the whole display system, use could be made of the logging printers, located near the main control room.

Other necessary features of the computer

Most of the inputs to the data processing system are either dictated in time by plant events, or are continuously varying signals, the value of which depend largely on their being available on operator demand. The data processing system must be fast enough, therefore, to handle the maximum number of inputs anticipated, without delay in meeting operator demands for information. In the design stages, a reasonable assumption is that not more than 60% of the "busy minute" should be occupied under worst operating conditions. A fast store is usually essential and must be adequate for storing the data processing and organising programmes, whilst bulk storage is invested in comparatively slow magnetic drums, the data being transferred in blocks to the fast store when required.

The effective speed of the data processor is very much related to the comprehensiveness of the order code, particularly where this includes "jump" and modification orders, and short machine instruction times; the required accuracy of data handling calls for a computer word length of greater than 12 bits.

An interrupt facility is vital with an on-line data processor of the size envisaged, enabling it to operate with many peripheral equipments, and provide priority for urgent actions.

Features of peripheral units

Analogue scanners must have adequate speed to carry out all scanning functions in the maximum time permissible, and a rate of about 100 points per second is possible. Where relays are required for low level inputs signals, consideration must be given to both reliability and life of the relays in view of the large number of operations required. The accuracy of the analogue scanner should be about 0.1% needing a 10 bit output from the analogue to digital converter. To eliminate interference from power cabling when low level signals are transmitted over considerable distances, the scanner must have high common mode and normal mode rejection. This can be achieved by the design of data amplifiers and filter networks and the avoidance of common mode to normal mode

conversion by the balancing of input cabling and cubicle wiring. All analogue input signals are checked for high and low alarm levels in order to detect both plant and equipment faults. The scanner must also be checked for proper operation at short intervals. The digital state scanner converts the alarm inputs into computer words, changes in which are interpreted by the data processor as new alarms or cancelled alarms.

A number of cathode ray tubes, mounted adjacent to the control positions, are required to display alpha-numeric information. The recurring frequency of writing must be sufficiently high to give a substantially flicker-free display, and provision made for data to be up-dated at 5 second intervals which is compatible with normal and fault rates-of-change of the variables monitored.

A variety of printing and typewriting equipment is required to provide routine logs and alarm print-out, and act as an independent standby to the display system just mentioned. Tape punching equipment provides output data where high speed operation, or suitability for subsequent processing, is specified. Instructions may be read into the system using a tape reading facility.

Application of the data processing equipment described

Table 1 lists the important design parameters for the data processing systems being built for the Wylfa nuclear power station.

The computer chosen was designed for on-line use and met the requirements for reliability, accuracy and speed described in the previous section. An interrupt system is provided and the data being worked upon and the organising programme are stored in the fast store. Two 100% central processing units are provided together with changeover facilities to achieve a very high reliability. Operation of the computers and the changeover facilities is regularly checked as previously described. In the event of total computer failure, sufficient conventional instruments and alarms are provided to permit continued running under steady conditions and a safe shutdown in the event of any fault.

The analogue scanner uses relays, operated by solid state drive circuits to select the inputs required, because of the low level of the many inputs from thermocouple signals, and the error introduced by solid state scanners. The inputs are checked for high or low levels and as the rates of change are normally slow a scanning interval of 30 s has been chosen as a compromise between fast relay operation with consequent wear, and the rate-of-change normally experienced. A state scanner checks plant alarm signals.

The computer examines the alarm input signals derived both from the state and the analogue scanners, and where a number of alarms arise simultaneously, these are analysed to show the basic cause of the fault. Upon receipt of an alarm, the system examines the state of other alarms which occupy a casual position

Table 1. Important parameters for a typical data processing system

<i>Computer</i>		
Number per station	2	
Word length	20 bits parallel	
Fast store capacity	4 096 words each	
Typical order	{ read—write cycle	10 μ s
	{ add, subtract transfer	22 μ s
	{ decimal to binary or reverse	70 μ s
<i>Magnetic drum</i>		
Capacity	3 of 100 000 words each	
Maximum access time	40 ms	
<i>Scanners</i>	2/station	
<i>Analogue section</i>		
Number of inputs	2 400	
Input level	30 mV (full scale)	
Scan speed	100 points/s max	
<i>State section</i>		
Number of inputs	1 200	
Scan repetition frequency	4 times/s	
<i>Tabular display</i>		
Number of display tubes per station	20	
Average number of characters/tube	680	
<i>Print out</i>		
5 typewriters for tabular display B.C.D. and log	10 characters/s	
4 strip printers for alarm and B.C.D.	5 lines/s	
2 tape punch machines	100 characters/s	
2 tape readers	500 characters/s	

relative to it. This process is repeated for each linked alarm until one is located for which no casual alarms exist, and the pattern so established is converted into a display of the main fault and the operator action required to correct it. Individual alarms are listed for the operator and are recorded for post-mortem analysis.

Burst cartridge detection is described in [2]. The system at Wylfa is in two parts. The group system which monitors gas from every reactor channel group each minute and the single channel system by which any individual channel can be monitored. In both cases, the signal from the monitor is examined by the computer for alarm conditions, compensating for signal variation at part load.

The single channel system requires complex control of selection valves which is dictated by computer programme. A routine scan of each reactor channel may be demanded and, in addition, single channels can be selected for continuous monitoring. In the event of a group system alarm, an automatic search by the single channel system of the channels in the group concerned is initiated, and the computer calculates the time available to discharge the faulty element in the channel in alarm.

An automatic turbine run-up facility is also available from the data processor. The turbine is brought into the condition for start-up using sequence control, after which the state of all equipment is checked by the computer. The turbine stop valve by-pass is opened sufficiently to accelerate the machine at pre-determined rates up to synchronous speed and important variables such as casing temperature, differential

expansion, speed and vibration are checked at short intervals. If any variable deviates from normal, the steam conditions and rotor speed are held constant to give a heat soaking. If an alarm condition is reached on any variable, the stop valves are tripped, thereby shutting down the turbine. The running up of the turbine is thus checked much more frequently and in much more detail than the operator could himself, and it is hoped that accidents such as bent shafts will be rendered impossible.

After an accident or fault, it is often difficult to determine the state of the plant before the trip. To avoid this, some 120 important variables are monitored at short intervals and the values recorded in a drum store. After, say, 20 min, the earliest readings are erased and more recent values are added. In the event of a fault, these values are not erased but are printed out for analysis.

Using an interrupt facility it is possible to use spare time on the data processor to perform off-line computing. This typically may be the analysis of B.C.D. data, calculations of station efficiency, or fuel economics.

SOLID STATE REACTOR SAFETY CIRCUITS

Reactor safety circuits

During normal operation a power reactor is controlled either by manual operation or by a number of automatic servo systems to obtain optimum power output within the safety limits of the reactor. Under minor fault conditions, the automatic control systems reduce the reactor power to safe values, but in addition

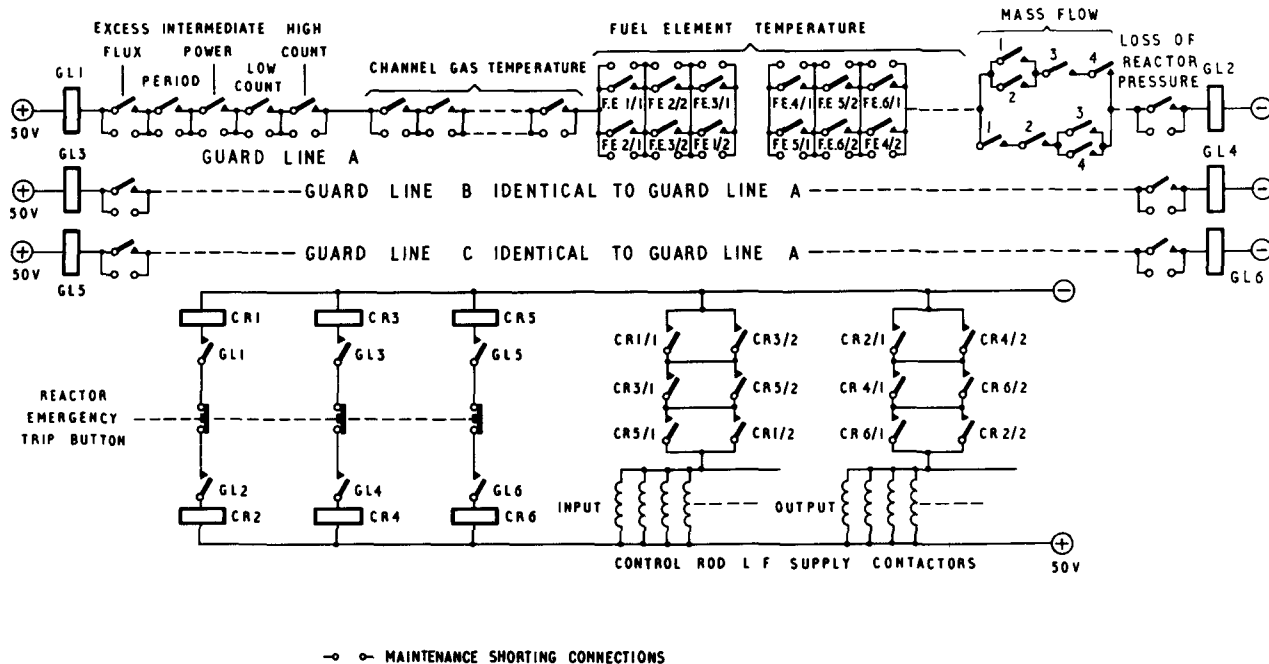


Figure 2. Typical arrangement of reactor safety circuits using relays

reactor safety circuits, which are entirely separate from all other control and monitoring systems, provide absolute protection for all fault conditions [2]. Power reactor safety circuits may be regarded as consisting of three stages: parameter monitoring equipments, which feed the guard lines or logic circuits, which in turn operate the control rod trip circuits. In the event of a reactor fault, the safety system is arranged to open the electrical feeds to the control rod actuators and allow the control rods to drop into the reactor under gravity.

A reactor protection system must be extremely reliable in its operation and as far as possible have a preferred mode of failure in the direction of safety. Up to the present time, in the United Kingdom all power reactor protection systems have employed electromagnetic relays in the guard lines and control rod trip circuits [3]. A typical arrangement of a relay protection system is illustrated in Fig. 2. The design of relay logic systems is well established, but to maintain confidence in the correct operation of the system, frequent periodic proof testing and maintenance are required. However, in spite of this testing and maintenance a relay might fail to operate when required to initiate a reactor trip.

Solid state switching devices

Solid state switching devices may be used to replace the relays in the guard lines and such a system requires virtually no maintenance. With careful design, a solid state system may be made inherently safer than the corresponding relay system by ensuring that (a) the system shall not rely upon a preferred mode of failure to produce a reactor trip, and (b) the logic in the system should not be performed by analogue adding of input signals. To satisfy these design

criteria, the system should be dynamic in its operation, being switched alternately between two states, and the system should fail in the direction of safety if the switching ceases.

Development work showed that the laddic satisfied these criteria in addition to the other basic safety requirements, and it was adopted. The laddic is a multi-aperture ferrite core, upon which logic may be performed, and a seven hole laddic is illustrated in Fig. 3. The operation of the laddic in its present form is described in [1] and may be summarised as follows: dc currents generated within the monitoring equipment are applied to the control windings, Fig. 3, (a, b, c) and the set (d) and reset windings (e) are pulsed alternately. When the dc currents are applied to the control windings, the alternating flux is forced into the outer path formed by the first and last rungs and the side rails, and hence the input flux links the output winding (f). Under these circumstances an output signal is present so long as the dc currents are applied. As soon as one or more of the control windings is

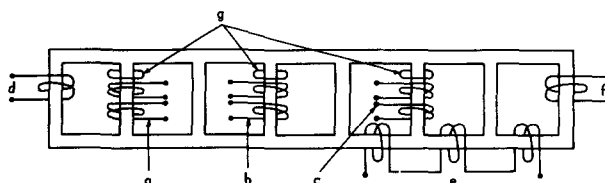


Figure 3. Arrangement of laddic core and windings

- a) } Control windings
- b) }
- c) }
- d: Set winding
- e: Reset winding
- f: Output winding
- g: Shorted turns

de-energized, the flux linkages collapse and the output disappears. A seven hole laddic driven in this manner behaves as a 3-input "and gate", that is, an output is present so long as all three control windings (a, b, c) are energized.

The original laddic was not proof against shorted turns in the control windings, but the present disposition of the reset windings, Fig. 3 (e), makes the laddic proof against all shorted turns [1].

The properties of shorted turns may be used now to reduce the control currents required, and permanently shorted turns, (g) in Fig. 3, are applied to the control rungs. The control windings are duplicated, and may be cross connected in pairs, and the laddic then behaves as a 2-out-of-3 gate or three 1-out-of-1 gates. A longer laddic may be made and cores with up to nineteen holes were tested, but longer laddics showed no particular advantage and the seven hole laddic was adopted for safety circuit applications.

The solid state safety system

The seven hole laddic illustrated in Fig. 3 forms the basic module of the guard lines, replacing the relays of Fig. 2. When coupling laddics together in order to build up a system, it is convenient to use the output of one to reset the next, and a single transistor with a series resistance in the collector circuit is used as an amplifier to overcome the signal attenuation within the laddic.

The relay guard lines of Fig. 2 are replaced by three chains of laddic modules, one of which is shown in Fig. 4. Each relay contact has been replaced by a control winding on a laddic. Two "set" supplies are used, and the connections are transposed as shown to eliminate any unsafe effects due to possible cracking within a core [1].

In the system developed, fourteen laddics are connected in series in each guard line. These guard lines terminate in pulse to dc converter units, which in turn feed the final 2-out-of-3 circuits. It was considered prudent to retain at least one physical break in the control rod trip circuits, and contactors are retained to switch the low frequency power supplies to the control rods. To provide the power supplies necessary to operate the contactors, the final 2-out-of-3 circuits feed into four inverters which are rated at 2 kW dc. The system is so arranged that no single fault produces a reactor trip, for example the control rods remain held if one inverter fails. The over-all safety system is shown in Fig. 5.

Development and testing

Numerous laddic modules have been made and tested, employing a variety of ferrite materials and various combinations of windings and drive circuits, in an attempt to optimize the design and to make the laddic "fail safe" to all conceivable faults.

The form of laddic finally adopted is proof against all short circuits and open circuit windings. The arrangement is proof also against all cracks in the ferrite core other than a crack across the first control

rung (a). From a study of ferrite material, it is concluded that a significant crack could not develop in the first control rung without a corresponding crack appearing in the side rails which would cause the laddic to "fail safe". However, if it is considered necessary to protect against such a contingency, a later form of laddic has been developed which is proof against all cracks.

The original laddic guard line has been in operation on a test bench for more than 20 000 hours. Further experimental guard lines have been built and a prototype system now on test consists of three guard lines, complete with pulse to dc converters, final 2-out-of-3 circuits and four inverters.

Extensive parameter testing has been completed on the laddic modules to determine the effects of variations in every parameter. The results have shown that the laddic system is remarkably insensitive to parameter variations and also to interference as indicated below:

(a) variations in control currents of $\pm 70\%$ have no effect on the laddic performance;

(b) variations in pulse height and width of $\pm 70\%$ and in frequency from 50 c/s to 2.5 Kc/s have no effect on laddic performance;

(c) variations in transistor supply voltage of $\pm 50\%$ have no effect on laddic performance;

(d) variations in ambient temperature from 0 °C to 55 °C have no effect on laddic performance;

(e) injection of 24 mA ac peak to peak into the control windings in the frequency range 20 c/s to 200 Kc/s in the absence of the normal dc control current, fails to hold the laddic, and the laddic "fails safe".

CONTROL ROD LOW FREQUENCY SUPPLIES

System requirements

As described elsewhere [2], British gas-cooled power reactors employ control rods suspended from actuators driven by very low frequency motors. This arrangement reduces gear trains and clutches in the reactor to an absolute minimum and if the power supplies are interrupted the weight of the control rod is able to rotate the motor thus giving a fast controlled shut down.

There are 9 to 16 groups of regulating rods in each reactor with up to 3 control rods per group and the supply frequency is continuously varied by a control circuit to move the rods to maintain a preset reactor temperature. The coarse and safety rods are usually stationary, but can be moved at low fixed speeds by the operator and are generally split into groups of 20 to 40 control rods.

Rotating generators were provided at the first nuclear stations [2], but to reduce maintenance, particularly of brush gear, static equipment has been developed and found to have the additional advantage of reduced capital cost. Extreme reliability is required to avoid a reactor shutdown and a design criterion

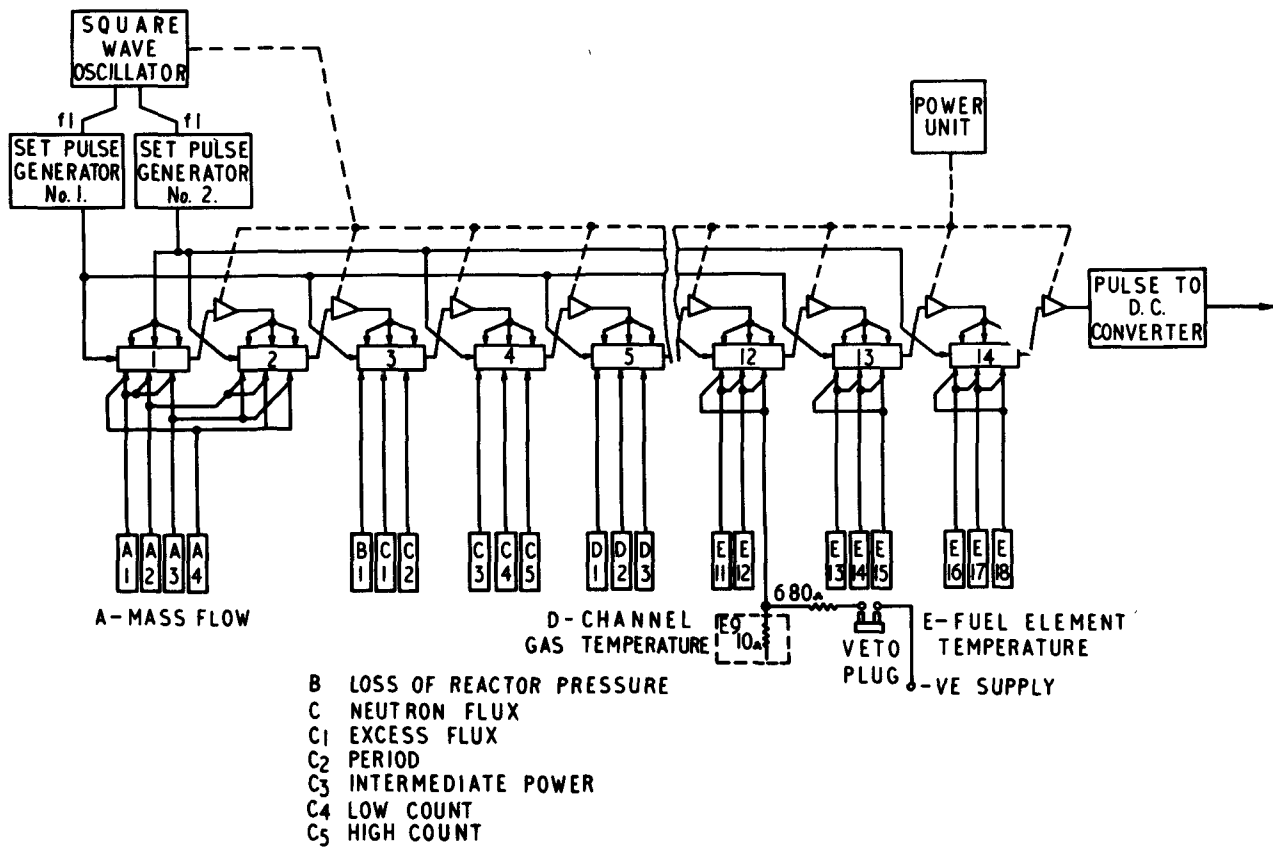


Figure 4. Block diagram of laddic guard line

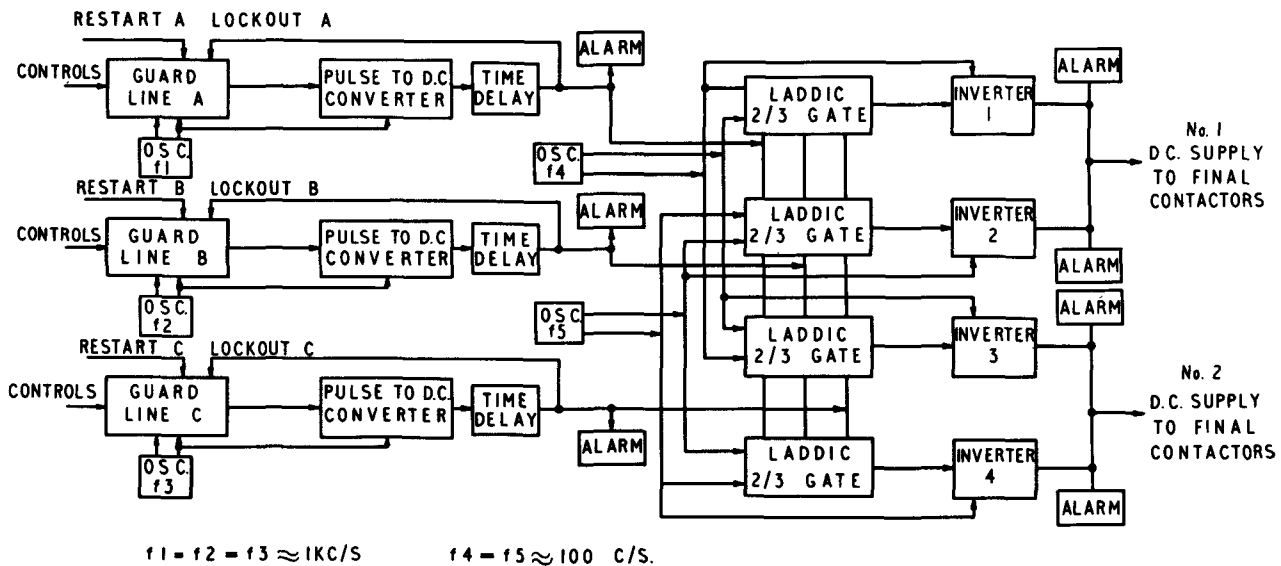


Figure 5. Block diagram of laddic safety system

adopted is that no single fault shall cause a reactor trip. The only exception to this is a main busbar fault on more than one phase. The system must be proof against transient disturbances on the mains supply which could drop the input voltage to low values for periods of time up to 200 ms. Static equipment has the serious disadvantage that it has no inherent inertia but this may be overcome by designing the static

system so as to maintain an adequate output during a transient or using very reliable ac/ac motor generators with high inertia for the supply system.

Static generators

A static generator consists of a 2 or 3 phase modulator unit feeding magnetic amplifiers to raise the power from the milliwatt level to the kilowatt range.

The signal is derived from a synchro-resolver fed at 50 c/s and rotated by a motor which defines frequency and rod speed. Two or three 50 c/s wave forms are produced, modulated in amplitude as the synchro-resolver rotates, which are fed through bridge rectifiers to the control windings of magnetic amplifiers. Further amplifier stages may follow if necessary.

Phase reversal every half cycle is required in amplifier outputs, and in the case of coarse rod generators where the operation is infrequent, contactors or cam-switches driven from the synchro-resolver drive can carry out this function. In one design shadow cams on the synchro-resolver drive interrupt a beam of light falling on photo-transistors and control the contactors without mechanically loading the shaft. It will be noted that the phases should be reversed when the phase current is zero. This will vary slightly relative to the synchro-resolver position with the load on the generator and its power factor, and an optimum position must be found.

For the continuously moving temperature regulator rods, the phase reversal duty is higher and the contactors may be dispensed with at the expense of employing two magnetic amplifiers and connecting the motors and an equivalent resistor in a bridge circuit with the amplifiers.

With the recent development of thyristors of suitable power, phase reversal may be easily obtained without moving parts. Each phase is connected to the load through thyristors which are fired at the appropriate time to give a low frequency output of the correct polarity.

Another approach is employed in a new design [4]. The basic output is derived from a power selsyn as three 50 c/s waves modulated by the required low frequency which is proportional to the selsyn speed of rotation. The output from the selsyn for each of the three phases is passed through a pair of bridge demodulators each of which is switched at 50 c/s by a circuit using two thyristors. The usual low efficiency and heavy current requirements of the bridge demodulator are avoided in this way and a compact supply produced.

Although in some respects the principle of static equipment is lost, the generator moves only when the

control rods are moved and then at a very slow speed so no mechanical wear is expected, and there is no commutator. The main problem is heat dissipation, as there is no windage at the low speed of operation.

With a static system, the output wave form is a true multiphase low frequency supply but has superimposed on it a 50 or 100 c/s harmonic. Tests have confirmed that this is insufficient to cause wear of the control rod actuators. The control rod motors are often of the permanent magnet rotor type and speeds attained during a "scram" are far higher than those reached in normal operation. The correspondingly high voltages generated must not be permitted to reach rectifiers or thyristors.

CONCLUSION

The paper has described the considerable advances being made in the control of British power reactors and the instrumentation provided, compared with that installed in the first stations. Further advances appear to lie in the direction of computer control of the reactor, developments in analogue displays, and the extended use of static control systems.

ACKNOWLEDGEMENTS

The authors wish to acknowledge the use of information from The Nuclear Power Group, United Power Company, and English Electric Company Limited in the preparation of this paper.

REFERENCES

1. Weaving, A. H., and Sherlock, J., *Magnetic logic applied to reactor safety circuits*, J. Brit. Nucl. Energy Soc., 74 (January 1963).
2. Vaughan, R. D., and Southwood, J. R. M., *Symposium on Berkeley and Bradwell nuclear power stations*. Papers 1 and 2 (June 27th 1963). Published by the Institution of Mechanical Engineers (January 1964).
3. Jervis, M. W., *Nuclear Reactor Safety Systems*, AEI (Assoc. Elec. Ind.) Eng., 222 (September/October 1962).
4. Pearce, N., and Price, D. A. C., *A new control rod motor-supply for Sizewell nuclear power station*, Control, 288 (December 1963).

ABSTRACT—RÉSUMÉ—АННОТАЦИЯ—RESUMEN

A/126 Royaume Uni

Tendances récentes dans l'instrumentation et le pilotage des grands réacteurs à réfrigérant gazeux

par D. S. Hiorns *et al.*

Depuis la conception du premier réacteur de puissance britannique à réfrigérant gazeux il y a cinq à sept ans, on s'est attaché à simplifier et rendre plus sûr le pilotage des réacteurs. Le mémoire discute trois

aspects du problème: l'amélioration de l'affichage des principales données, l'application des techniques de l'état solide aux circuits de sécurité et aussi à la commande des barres de contrôle.

L'application de grandes unités de traitement des données, maintenant disponibles sous une forme qui a fait ses preuves, a facilité la centralisation des fonctions de commande. Les informations provenant de l'installation et représentant quelque 7 000 lectures dans une centrale à deux réacteurs sont analysées, et seules les indications nécessaires au personnel de

conduite sont affichées. L'utilisation de tubes à rayons cathodiques, permettant de reproduire des données alpha-numériques, assure la souplesse nécessaire pour cette application. Les améliorations correspondantes sont également décrites pour les panneaux abritant les commandes.

Jusque récemment, tous les réacteurs de puissance civils britanniques utilisaient des relais électromagnétiques dans les systèmes de protection. Pour améliorer la sécurité inhérente d'un système de protection et réduire les essais d'entretien au minimum, on a étudié l'application de dispositifs utilisant l'état solide et on a trouvé que le système Laddic répondait aux exigences de sécurité. Le Laddic est un noyau ferritique à ouvertures multiples sur lequel peuvent être effectués des calculs logiques: sa mise au point dans ce but est décrite, ainsi que son application à un système de protection des réacteurs.

Des courants basse fréquence sont prévus pour actionner le dispositif de commande de barres de pilotage. Cela évite la nécessité d'embrayages et de trains d'engrenages à rapport élevé à l'intérieur du réacteur. Le courant basse fréquence, qui dans les premiers réacteurs était fourni par des machines tournantes, provient maintenant de générateurs statiques à amplificateurs magnétiques, appelés aussi thyristors, qui modulent le courant de sortie pour donner la basse fréquence requise. Pour obvier au manque d'inertie dans un système de génération statique, on incorpore des caractéristiques destinées à maintenir le courant basse fréquence durant les perturbations transitoires de la fourniture principale de courant, ce qui augmente le temps de fonctionnement utile du réacteur.

A/126 Соединенное Королевство

Приборы и регулирование больших реакторов с газовым охлаждением

Д. С. Хиорнс *et al.*

Пять — семь лет назад, в период проектирования первых в Великобритании энергетических реакторов с газовым охлаждением, проводились работы по упрощению эксплуатации системы регулирования и повышению ее надежности. В докладе излагаются три аспекта этих работ: усовершенствование основной системы регулирования, применение твердых переключателей к схемам аварийной защиты и питание регулирующих стержней.

Применение крупных установок по обработке данных, имеющихся в настоящее время и обеспечивающих достаточную надежность, облегчает рост централизации функций контроля. Информация от двух работающих реакторов атомной станции доходит до 7000 показаний, но воспроизводится только информация, требуе-

мая для операторов. Использование электронно-лучевых трубок, на которых может воспроизводиться численная информация, обеспечивает необходимую гибкость для данного применения. Описываются также соответствующие усовершенствования панелей системы контроля.

До последнего времени во всех гражданских ядерных энергетических реакторах Великобритании в системах защиты использовались электромагнитные реле. С целью усовершенствования надежности срабатывания системы защиты и сведения до минимума испытаний системы в процессе эксплуатации изучалось применение твердых переключателей, и было найдено, что переключатель «Laddic» вполне удовлетворяет требованиям безопасности. «Laddic» — это многоканальный ферритовый сердечник, при помощи которого можно выполнять различные логические операции. В докладе описывается разработка прибора для указанных целей и использование его в системе защиты реактора.

Низкочастотное питание обеспечивает работу привода регулирующих стержней энергетических реакторов. Это устройство избавляет от необходимости использования внутри реактора муфт сцепления и высококоэффициентных зубчатых передач. Низкочастотное питание, получаемое для первых реакторов от ротационной установки, в настоящее время поступает от статического генератора с магнитными усилителями или тиристорами, которые модулируют выходное напряжение генератора, чтобы получить необходимую низкую частоту. С целью снижения инерции статической системы генерации все ее элементы объединены, что позволяет обеспечить низкочастотное питание в случае выхода из строя основной системы питания; таким образом повышается надежность работы реактора.

A/126 Reino Unido

Progresos recientes en instrumentación y control de grandes reactores refrigerados por gas

por D. S. Hiorns *et al.*

Desde que se diseñaron los primeros reactores de potencia británicos refrigerados por gas (hace de ello entre 5 y 7 años), se ha trabajado continuamente en la simplificación del control de operación y en el aumento de la seguridad de funcionamiento. En este documento se tratan tres aspectos de esta cuestión relativos a mejoras en la presentación de los datos principales de control y empleo de técnicas de estado sólido en los circuitos de seguridad, así como en las fuentes de alimentación de las barras de control.

El empleo de grandes unidades de tratamiento de datos, disponibles actualmente en modelos bien probados y de funcionamiento seguro, ha permitido

una mayor centralización de la función de control. Se trata adecuadamente la información procedente de la central, que puede elevarse a 7 000 lecturas en una central de dos reactores, y sólo se muestrana los operadores los datos requeridos. El empleo de tubos de rayos catódicos en los que se puede representar la información en forma de números y de letras, da la flexibilidad necesaria para esta aplicación. También se describen las mejoras correspondientes a los paneles que alojan los elementos de control.

Hasta hace poco tiempo se empleaban relés electromagnéticos en los sistemas de protección de todos los reactores de potencia británicos para usos civiles. Para mejorar la seguridad inherente a un sistema de protección y para reducir a un mínimo las pruebas de mantenimiento, se has estudiado el empleo de dispositivos de conmutación de estado sólido y se ha encontrado que el sistema *Laddic* satisface los requerimientos de seguridad. El *Laddic* es un núcleo de ferrita de aperturas múltiples en el cual pueden

hacerse operaciones lógicas; se describe el desarrollo de este dispositivo para el fin mencionado, así como su aplicación a un sistema de protección de reactores.

En la instrumentación se incluyen fuentes de alimentación de baja frecuencia que hacen funcionar el actuador de las barras de control de los reactores de potencia. Con esto se elimina la necesidad de embragues y de trenes de engranajes de alta relación de reducción dentro del reactor. Las tensiones de baja frecuencia, que se obtenían en los primitivos reactores mediante convertidores rotatorios, se obtienen actualmente mediante generadores estáticos que emplean amplificadores magnéticos o thyristores, los cuales modulan la salida del generador para dar la baja frecuencia requerida. Para evitar los efectos de la falta de inercia en un generador estático se han incluido elementos que conservan los valores de las tensiones de baja frecuencia durante transitorios de la red, mejorando así el comportamiento de la instalación.

Improvements in instrumentation for high-performance power reactors

By S. H. Hanauer*

The design and operation of nuclear power plants with enhanced performance require development of improved instrumentation for the control and safety of these plants. Both safety and economic considerations lie behind the need for better instrument systems. High performance in reactor cores must generally be obtained at least partly at the expense of decreasing the margin between operating conditions and undesirable overloads. The safety factor which is thus given up for the sake of low power cost has to be regained by the action of instruments. Also, if high-performance reactors lack self-regulating features, the required safety and control must be provided by instrumentation. Finally, optimization of operating conditions in a power station requires knowledge, often detailed, of plant variables whose measurement might otherwise be unnecessary. It is the object of this paper to describe some recently developed instrumentation techniques aimed at fulfilling the needs of present and future power reactors.

Advances in instrumentation fall generally into two classes: creation of new functions not previously realized, and improving the components and configurations used in execution of instrument functions. A major advance of the latter type has resulted from the development of series of instrument modules, each of which is intended to be a functional unit in one or more reactor instruments. To the compactness of transistor circuits are thus added the flexibility of modular design and the accessibility of plug-in construction, the latter made possible by the development of reliable connectors. The serviceability provided by the plug-in feature makes practical the application to power reactors of complex systems, such as those described later.

INSTRUMENT SYSTEMS

Coincidence and testing in safety systems

Coincidence techniques are widely applied to safety systems employing redundant channels of information, generally in the belief that serviceability (freedom from false scrams) can thereby be improved without payment of an exorbitant price in loss of safety (freedom from failure to scram when required).

However, much experience appears to demonstrate the incorrectness of this belief, at least with regard to serviceability. For example, in a recent study [1], safety-system failure rates experienced in the field were found not to be correlated with the presence or absence of coincidence. The very low failure rates predicted by theories [2, 3] of the statistical behavior of such systems are not usually realized in practice [4,5]. Although the study cited was for test reactors, the conclusion may be generally applicable. A disturbing aspect of this discrepancy between theory and experience is the suspicion that the low failure-to-danger (unsafe failure) rates predicted by the same theory may also not be achieved in operating plants.

The non-applicability of the theoretical treatments is caused, in the main, by their neglect of coupling between systems, channels, or components that are supposed to be independent of each other [6]. The probability of non-random simultaneous failure of such coupled devices is of course much higher than the product of the individual failure probabilities. Coupled failures may be caused directly by the same event, or one failure may induce another. Coupling may also be introduced via such auxiliary functions as supply power, equipment ventilation, and test instrumentation. Coupling is impossible to eliminate completely; the devices in question are related to a single reactor system, and must usually be located in a single control room, detector array, or group of actuators.

It is therefore suggested [7, 8] that the principal value of coincidence in reactor safety systems is not improvement of serviceability but the ability to test safety instrumentation while the reactor is operating, without disabling any safety action and without disturbing the operation.

Testing in a coincidence safety system can be limited by the coincidence element or elements. This problem is fundamental, because the purpose of the coincidence element is to initiate a scram only if more than one input demands it, and because the tests while the reactor is in operation must not actually produce a scram. Such tests can therefore confirm the correct functioning of the system only up to the coincidence elements.

To circumvent this problem, special testers have been devised which simultaneously pulse two or more

* Oak Ridge National Laboratory, Oak Ridge, Tennessee.

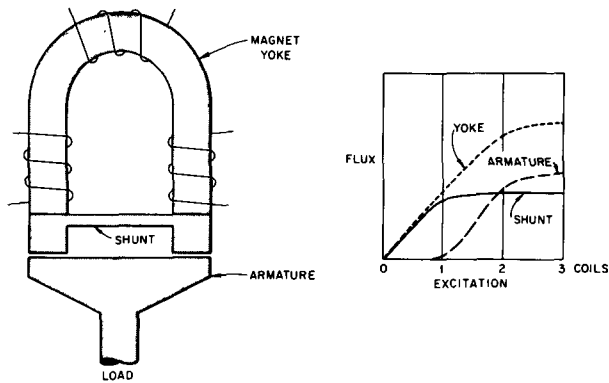


Figure 1. Coincidence magnet with saturating shunt

inputs too fast to affect the safety actuators, but the necessary auxiliary equipment compromises the independence of channels, and to date proposed systems of this type perform tests of limited extent.

Coincidence magnet. A coincidence magnet has been developed for scram mechanisms by Brown *et al.* [9], in which the magnet itself is the coincidence element. Each of the three electrically independent coils on each magnet is controlled by one channel of safety instrumentation; the magnet releases when any two (or three) coils are de-energized. The use of coincidence magnets makes it possible to keep redundant safety channels electrically independent of each other, because the required mixing takes place only in the common magnetic circuit. Testing can be performed during operation by locally perturbing process variables to make each sensor in turn detect an abnormal condition. Observation that the corresponding coil in each coincidence magnet is de-energized by the test confirms the operability of the entire safety channel, except only for the ability of the mechanism to release.

A saturating shunt in the magnetic circuit (Fig. 1) provides the coincidence characteristic. The dimensions and the coil currents are chosen so that when any one coil is energized, the flux will be bypassed through the shunt, with negligible flux in the armature, and hence negligible force on the load. As the excitation is increased by turning on the second coil, the shunt becomes saturated, and force is developed on the load. Energizing the third coil saturates the yoke or the armature, or both, with little increase in force. Thus the magnet has two-out-of-three logic, producing nearly full force when any two, or all three, coils are energized and nearly zero force when one or no coil is energized.

Magnets of this type have been built with forces in the range 20–700 kg. The largest magnet built so far is 20 cm long and 20 cm in diameter. It has forces of 45, 625, and 735 kg for 1, 2, and 3 coils energized, respectively. The release time, for a 400 kg load, is 4.5 ms when all three coils are de-energized simultaneously, and 6.5 ms when two coils are de-energized, and the remaining coil remains energized.

Multiple reactor controllers

Application of redundancy to reactor controllers has been proposed [10] to minimize the reactor down time which would otherwise result from controller failure. When redundancy is applied to regulating rod servos, it is necessary to combine all the outputs to drive a single rod or group of rods, since separate servos driving individual rods would be unstable. Mann and Weaver have demonstrated [11, 12] the feasibility of this approach analytically. The mixing, or coincidence, is accomplished in a mechanical (or hydraulic) multiple-input differential so arranged that the rod velocity is the algebraic sum of the output velocities of the individual servos. The system is equivalent to a single servo with n times the gain of one of the n redundant servos. In a three-servo system, paralysis of one servo will reduce the over-all gain by one-third, provided only that the failed servo cannot be turned by the remaining two. The reactor will remain under control. Runaway of one servo will be combatted by the other two, each turning at half-speed in the opposite direction. For this case, the controlled variable will be offset by the error necessary to run the operating servos at half speed; higher servo gain will thus give smaller error. For on-off servos, this error will in any case be less than the dead band. For continuous servos, the error depends on the gain allowed by stability considerations; in the examples studied the error was small.

Since the differential mechanism and the rod are common to the three regulating channels, their failure will cause the system to fail. The potential improvement in serviceability of the coincidence system can therefore be realized only if these components are trouble-free.

Studies using the analog computer, both with simulated controllers and with electromechanical controller models, have confirmed the theoretical predictions.

Wide range counting channel

A new instrument system has been developed and tested [13,14] in which the entire dynamic range of reactor power can be measured from source level to full power without any range change or other hiatus in the measurement. The principle of operation, illustrated in Fig. 2, uses motion of a detector in an attenuating medium to extend the range of the instrument. A signal proportional to the logarithm of the attenuation (as a predetermined function of detector position) is added to a signal proportional to the logarithm of the detector output; the resultant is proportional to the logarithm of the reactor power. A derivative network gives a measurement of reactor period.

In the instruments constructed to date, a fission chamber is used as the detector to achieve the maximum discrimination against high gamma-ray backgrounds during reactor start-up. The pulses from the chamber are fed to an amplifier, a discriminator, and a logarithmic counting-rate meter. The flexible

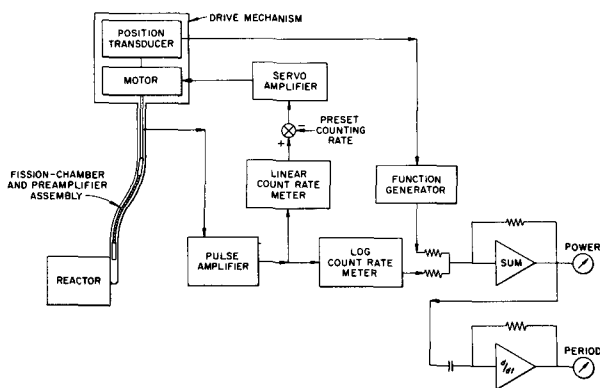


Figure 2. Wide-range counting channel. Block diagram

chamber and preamplifier assembly described later is particularly suitable for this application.

If the chamber can be moved through a shielding medium, the neutron attenuation will approximate to an exponential function of position over several decades. Where required, a nonlinear analog function generator is used to correct the signal proportional to chamber position so it will conform more accurately to the logarithm of the neutron attenuation. Lack of adequate shielding may limit the useful attenuation range, and therefore the range of the entire instrumentation system. Under favorable conditions, a total range of ten decades has been achieved.

Variation of the neutron profile in the shield as reactor operating conditions change may limit the accuracy of the system.

The chamber is positioned by a servomechanism whose input signal is the difference between the actual counting rate and a preset value, typically 10^4 counts/s. The servo system need only be fast enough to follow a stable period; any transient which the servo cannot follow causes the counting rate to increase momentarily above the preset value until the servo can catch up. The reactor power and period are measured correctly during the transient, however, limited only by the time response of the logarithmic counting-rate meter.

When the reactor is to be started after having been shut down for some time, the multiplied source usually produces less than 10^4 counts/s in the detector, so the servo inserts the chamber fully. During start-up, reactor power increases cause counting-rate increases, until the counting rate reaches the preset value. Further power increases cause the servo to withdraw the chamber at a speed commensurate with the reactor period.

Since the counting rate will be $\sim 10^4$ counts/s over most of the operating range of the reactor, the output signals have the fast response and low statistical fluctuation characteristic of this counting rate.

NEUTRON DETECTORS

Neutron flux is universally used as a process variable for reactor control and safety. The first two instru-

ments discussed in this section, and to some extent the third, have been developed to avoid the effects of gamma radiation on what is intended to be a neutron measurement. This is done in order to obtain the desired range of measurement, since the gamma flux decreases much more slowly than the neutron flux when the reactor power is reduced rapidly. A signal proportional to gamma flux can therefore interfere with measuring low values of neutron flux to monitor the neutron chain reaction.

Neutron flux measurements using ion chamber current fluctuations

To decrease interference due to gamma-ray and leakage currents, DuBridge has investigated [15] a new measuring technique utilizing the fluctuation, rather than the average, of the current from an ionization chamber. The mean-squared fluctuation signal is given by $\langle V^2 \rangle = \langle V \rangle^2 + N \int_0^t V(t)^2 dt$, where $V(t)$ is the signal from an ionizing event in the chamber, and N is the average rate of occurrence. Only the last term is measured, the other being eliminated by a low-frequency cutoff,

The discrimination against signals caused by gamma radiation has been analyzed by Snyder [16] who considered the signal given by

$$V(t) = \sum_k V_k \exp [-(t - t_k)/T],$$

where the times of occurrence of the events t_k are randomly distributed and the signal heights V_k have an arbitrary probability distribution. The clipping time constant is T . The mean square of this signal is

$$\langle V^2 \rangle = \langle V \rangle^2 + \frac{1}{2} NT \langle V_k^2 \rangle,$$

with N the average rate of occurrence of events. According to this theory, the gamma radiation contributes a fraction of the fluctuation signal which is proportional to the square of the ratio of gamma to neutron sensitivity, which can give a large improvement in gamma discrimination over direct current measurements.

Experiments have been conducted with fission chambers coated with 2 mg/cm^2 of enriched U_3O_8 . An amplifier with a passband from 0.5 to 13.6 kHz was used with an rms voltmeter. The rms signal was proportional to the square root of the neutron flux, as expected.

The neutron and gamma sensitivities of such an arrangement depend on the gas species and pressure and the gain and bandwidth of the electronics. Typical values, for the gain and bandwidth used, are given in Table 1, together with direct-current sensitivities of the same chamber.

Experiments using He, N_2 , and Ar at pressures from 0.8 to 2.3 atm, in neutron fluxes as high as $6 \times 10^{11} \text{ nv}$, show that the form of the saturation curves is the same for the fluctuation signal as for the more conventional direct-current measurements, which leads to the expectation that operation in higher

Table I. Comparison of chamber sensitivities^a

Fluctuation	Ar, 1.34 atm	N ₂ , 1.34 atm
Volts rms per $\sqrt{(nv)}$	4.5×10^{-6}	3.7×10^{-6}
Volts rms per $\sqrt{(R/h)}$	$<10^{-5}$	$<10^{-5}$
Ratio neutron/gamma	>0.45	>0.37
<i>Direct current</i>		
Amperes per nv	8.2×10^{-17}	6.2×10^{-17}
Amperes per R/h	3.6×10^{-14}	2.6×10^{-14}
Ratio neutron/gamma	0.0023	0.0024

^a See Ref. [15].

fluxes will be possible. The saturation characteristics are also independent of amplifier bandwidth, if the low-frequency cutoff is less than $1/(2\pi T)$ where T is the positive-ion collection time in the ion chamber.

It is evident from the sensitivities given in Table I that the fluctuation method has an advantage of a factor of more than 100 over the direct-current measurement with this chamber insofar as gamma-ray discrimination is concerned. For reasonable sizes and presently available insulators, the fluctuation signal due to electrical leakage in the chamber and cable is not significant at temperatures at least up to 500 °C. The ultimate limitation is amplifier noise, but usually the gamma-ray signal will be large enough that amplifiers of commercial quality will be adequate. Of course, electrical pick-up interference must be held to a tolerably low level.

Snyder has pointed out [16] that the neutron-to-gamma sensitivity ratio of a proton-recoil fast-neutron detector would be enhanced by using the fluctuation signal. By contrast to conventional pulse-counting methods, the fluctuation method would presumably have no pile-up problem.

The applicability of fluctuation measurements to in-core neutron detectors is clearly indicated, and experiments are now forseen to establish the feasibility and limitations of this technique.

Electrically adjustable gamma compensation

Another way to reduce the effect of gamma radiation is compensation: a signal proportional to the gamma flux is subtracted from the chamber current containing components proportional to the neutron and gamma

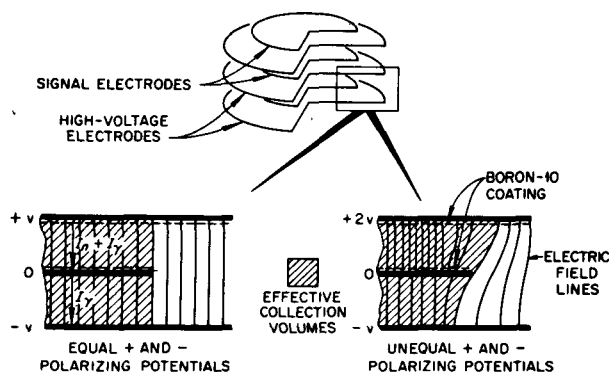


Figure 3. Diagram of adjustable electrical gamma compensation

fluxes. The signal to subtract is obtained from an auxiliary gamma-sensitive chamber section (Fig. 3). Although compensation is simple in principle, it is difficult to achieve and maintain a high degree of compensation in practice. Therefore, either an error must be tolerated or a means of adjustment of compensation must be provided. Roux *et al.* [17] have developed a parallel-plate configuration for which the adjustment of compensation can be accomplished electrically to avoid the disadvantages of fixed compensation.

Figure 3 shows the principle of the adjustable compensated chamber. The signal electrodes are made smaller in diameter than the high voltage electrodes. For equal positive and negative polarizing potentials (as shown on the left side of Fig. 3), the zero-potential surface is an extension of the signal electrode plane, and as a consequence the electric field lines are straight. For unequal polarizing potentials (as in the right side of Fig. 3), the field lines are distorted and the effective collection volumes are changed accordingly. This technique has the advantage over methods previously used that both the neutron and gamma sections are well saturated at all polarizing voltages ordinarily used, so that electrical compensation is not obtained at the expense of saturation. In the present configuration, the compensation does not vary with flux intensity up to 100 μ A gamma current, if the polarizing voltages are at least as large as 100 V.

The chamber electrodes are made of Ni plates, 0.012 cm thick, spaced 0.1 cm apart. The chamber is filled with N₂ at 800 torrs. It contains 16 signal plates (3.9 cm in diameter), 9 positive high-voltage plates (4.6 cm), and 8 negative high-voltage plates (4.6 cm). Without gamma compensation, the chamber sensitivities are 5.4×10^{-15} A/nv and 1.3×10^{-12} Ah/r.

Manufacturing tolerances are such that initially the gamma currents cancel within 3%, allowing the final adjustment of compensation to be made as precisely as desired by varying the voltage ratio. The compensation changes by 2% per 100 V change in the negative polarizing voltage, with the positive voltage equal to 300 V.

The experimental results of Table 2 show the insensitivity of the gamma compensation to wide variations in intensity, energy, and geometry of the gamma source. This results from the close spacing and high symmetry of the electrodes.

Miniature fission chamber and preamplifier assembly

To meet the space and environment requirements of high-performance reactors, Roux *et al.* [18] have developed an articulated assembly consisting of a fission chamber, a preamplifier, and flexible cables. High-flux reactor cores are often inaccessible, and it is desirable to use a detector that is small and movable in a tube which can be bent as required by the access problems of each reactor. The relatively low sensitivity of the small chamber is compatible with the high neutron source level encountered in these reactors.

Table 2. Typical gamma compensation obtained in a single chamber for various gamma sources with fixed electrode voltages (+300 V, -200 V)^a

Gamma source facility	Source condition	Shield and Geometry	Deviation from total compensation ^b
Hot cell, ⁶⁰ Co	2 000 curies	10 cm air, source at front of chamber	+0.8%
Hot cell, ⁶⁰ Co	2 000 curies	10 cm air, source at side of chamber	+1.3%
BSR, ^c fission products	10 min after reactor scram	20 cm of water	+0.9%
BSR, fission products	90 min after reactor scram	20 cm of water	+0.9%
BSR, fission products	1 week after reactor scram	20 cm of water	+0.6%
BSR, fission products	1 week after reactor scram	40 cm of water	+0.5%

^a From Ref. [17].

^b The sign + means undercompensation.

^c Bulk Shielding Reactor.

Placing the preamplifier close to the chamber reduces drastically the susceptibility of the system to pulse noise pick-up, so that the counting channels can be depended on to count neutrons and assure the reactor operator of the presence of an adequate source. The assembly is particularly suited for use as part of the wide-range counting channel described previously, but can also be used with conventional counting instrumentation.

The entire assembly is waterproof. The maximum outside diameter is 1.9 cm and the maximum rigid length is 30 cm. The chamber and the cable connecting it to the preamplifier can withstand at least 10^{10} r; the preamplifier, at least 10^8 r. The preamplifier is potted in epoxy resin for heat transfer and can operate in air or water at 100 °C ambient.

The chamber has a sensitive length of 7.6 cm, is coated with 1 mg/cm² of ²³⁵U, and is filled with Ar + 3% CO₂ at a pressure of 1.7 atm. Its sensitivity is 0.025 count/nvt.

The preamplifier circuit consists of two cascaded feedback amplifier stages using subminiature vacuum tubes. The gain of the charge-sensitive input stage does not vary with changes in its input capacitance: variation of 0 to 200 pF produces a gain change of only 10%. The second stage is a voltage amplifier with the output fed to a balanced shielded signal cable, terminated at its receiving end by a pulse transformer. The preamplifier output signal pulse height is 150 mV into 160 m of cable, for a nominal 50 MeV fission fragment.

During a reactor re-start, the neutron-to-gamma flux ratio is a minimum, and attention must be paid to pulse pile-up and radiation damage problems under these conditions. For Be- or D₂O-moderated reactors, the photoneutron flux will be high, giving a more favorable neutron-to-gamma flux ratio. For reactors moderated or shielded with ordinary water, the natural abundance of D₂O creates a photoneutron flux of 0.2 nv per r/h; at a photoneutron counting rate of 10⁴ counts/s, the gamma flux is 2×10^6 r.h.

Gamma-ray pulse pile-up is minimized by using double RC clipping, with time constants of 150 ns, and by using a low gas density in the chamber. The experimental results shown in Fig. 4 demonstrate the satisfactory signal-to-pile-up ratio at 2×10^6 r/h.

The useful service life is greater than one year [14].

Extensive experimentation has been required to achieve in practice the freedom from electrical noise pick-up which is believed necessary. The principal source of pulse noise is electromagnetic radiation from ac power lines which are shock-excited when some piece of equipment is turned on or off. The sensitivity to noise has been minimized by the large output signal from the preamplifier, the balanced configuration with common-mode rejection, and multiple electrical shielding. Contrary to popular belief, the lowest noise is achieved when the inner and outer shields are connected together in several places, for example, at the preamplifier, at the pulse transformer 100 metres away, and at one other place in between. Apparently, the capacitive coupling between shields

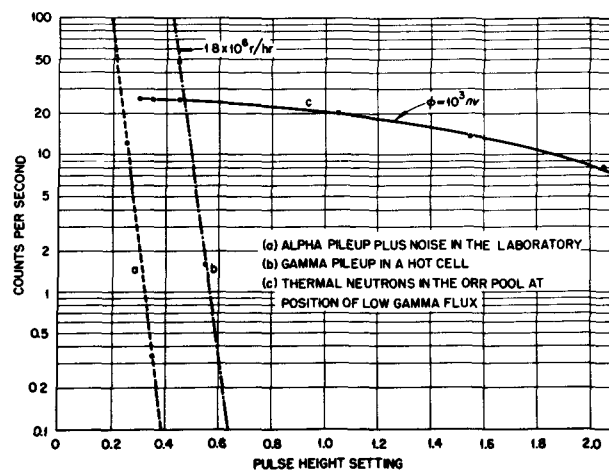


Figure 4. Performance of 22 cm flexible fission chamber and preamplifier assembly

defeats any attempt at isolation. With the correct connections, the instrument operates in the noisiest locations available with no noise pulses as large as alpha-particle pulses from the fission chamber, even when cranes, welders, or rod-drive motors are operated.

Subminiature in-core ion chamber

It is generally recognized that in-core measurements are important for safety, control, and economic optimization of many power reactors. A variety of in-core neutron and gamma-ray detectors have been developed to operate in the adverse environment required for making such measurements.

An ionization chamber developed by Boyd [19] is 0.23 cm in diameter and 1.25 cm long. It is constructed of Ti and special ceramics* that have equal coefficients of expansion, permitting fabrication and thermal cycling without excessive stress. The chamber is hermetically sealed; the final closure weld is made in a bell jar in an atmosphere of the Ar filling gas at a pressure of approximately 1 atm. The chamber is capable of monitoring neutron flux up to 10^{15} at temperatures up to 535 °C.

Because of the small size of the chamber, special techniques are needed to incorporate the neutron-sensitive material. A boron coating is obtained by vapor deposition of elemental boron on the inside surface of the shell. For a fission chamber, a small slug of Zr-U alloy is pressed into the shell and machined in place to a thin-walled cylinder. This alloy can withstand the temperature the chamber experiences in the brazing cycle.

The small size of such a chamber permits a number of interesting applications. In one configuration, the chamber was sealed in a 0.3 cm diameter tube at the end of an alumina-insulated stainless steel sheath cable of the same diameter. The tube-to-cable transition did not exceed the diameter of the cable and the tube; therefore, the probe could be inserted into the interstices of core structures with a minimum of perturbation.

In another application, two of these chambers were enclosed in a 0.6 cm diameter capsule to measure local moderator void fraction in a boiling-water reactor. One chamber was cadmium shielded to measure the cadmium ratio, which is related to the void fraction.

Finally, this chamber can be attached to a flexible cable to form a probe, which is used to traverse a dry thimble through the pressure vessel wall and through the reactor core.

Studies are under way [20, 21] on the use of mixtures of fissionable and fertile isotopes for in-core detectors to prolong their burn-up life. The optimum mixture may be a sensitive function of the neutron spectrum because of variation with energy of the fission and absorption cross sections. Preliminary calculations suggest [21] that a mixture of isotopes can be devised

whose total fission cross section will vary less than 20% during a lifetime of 5×10^{21} nvt.

SENSORS FOR NON-NUCLEAR VARIABLES

In order that they can function in the reactor environment, sensors for non-nuclear variables must be specially designed for this service. In the instruments discussed in this section, this problem is circumvented to a degree by transmitting the information to a secondary transducer in a more favorable environment, and there converting the signal to an electrical signal in a form more easily utilized by other instrumentation.

Acoustic thermometer

A method of measuring temperature developed by Apfel [22] uses the variation of sound velocity with temperature. To first order, the velocity depends only on the molecular weight, the ratio of specific heats, and the absolute temperature, and is independent of pressure. A burst of acoustic energy is transmitted through a small-diameter tube to a cavity containing the gas whose temperature is to be measured. When the frequency of the signal is equal to the cavity resonant frequency, the reflected echo returning from the cavity will be a minimum.

In the experiments, He gas was used in a cavity 1.3 cm in diameter and 25 cm long. The connecting tube was 0.3 cm in diameter and was made 6 m long to simulate a reactor installation, with the transducer safely away from the core. The acoustic temperature measurement agreed within 1% with a thermocouple over the range 20–925 °C. The transducer need not withstand the reactor core environment, but must provide adequate containment.

Ultrasonic liquid-foam-vapor height gauge

A height gauge described by DePrisco *et al.* [23] utilizes the acoustic impedance mismatch between a small vibrating plate and the fluid under test. The vibrating plate is moved vertically by a calibrated drive mechanism. The marked difference in impedance between liquid, foam and vapor, permits easy identification, during a vertical traverse of the plate, of the three components. Further, a calibrated probe can be used to measure the liquid content of a foam.

Experiments using water foams, both stabilized and unstabilized, demonstrated unambiguous detection of liquid-foam and foam-vapor interfaces over the range 20–250 °C. Foam water content of 1 to 8% was measured.

By use of force-insensitive mounts, the ultrasonic transducer can be located outside the reactor, with the energy transmitted through a bar which may have the shape of a tortuous wire.

Ultrasonic detection of incipient boiling and cavitation

An instrument similar to the one described in the preceding section was used by DePrisco *et al.* [24] to detect incipient boiling. The power to a vibrating

* Fosterite, GE-F202.

surface was increased until cavitation was induced. The cavitation was detected by its characteristic acoustic noise, which was transmitted back through the coupler to the transducer. The power required to induce cavitation is a measure of the pressure and temperature margin below the boiling point.

Measurements were made on water over the range 24–155 °C and 1–5.7 atm. In this region, the sensitivity was not pressure dependent.

The advantage of such a measurement would be the ability to monitor continuously the margin to incipient boiling and, hence, to possible burn-out in a non boiling system.

SUMMARY

Although some of the developments described are one-for-one improvements of existing devices, the general trend in reactor instrumentation is clearly toward greater complexity. This is inevitable because of the increasing complexity of reactor systems and because of the wider scope of instrumentation in these systems. Improvement of the safety, serviceability and economy of the nuclear power plant must be the justification of improving plant instrumentation, with safe and economical power always the ultimate goal.

It is a pleasure for the author to acknowledge his indebtedness to the many persons in the field whose private communications of work not yet published were invaluable in the preparation of this paper. The author is also grateful for helpful comments by Dr. S. H. Bush and his colleagues, and by Dr. D. P. Roux.

REFERENCES

1. Garrick, B. J., Costley, W. J., and Gekler, W. C., USAEC report HN-172 (1963).

2. Jacobs, I. M., Trans. Am. Inst. Elec. Eng., Paper 57-906 (1957).
3. Underkoffler, V. S., Cockrell, J. L., and Magee, J. H., IRE (Inst. Radio Engrs.) Trans. Nucl. Sci., NS-8 130 (1961).
4. Lennox, C. G., and Pearson, A., IRE (Inst. Radio Engrs.) Trans. Nucl. Sci., NS-8 155 (1961).
5. Schultz, M. A., Nuclear Safety 4, No. 2, 1 (1962).
6. Ditto, S. J., Nuclear Safety 2, No. 4, 16 (1961).
7. Siddall, E., USAEC report ORNL-2695, 179 (1960).
8. Hanauer, S. H. *et al.*, USAEC report ORNL-3191, 66 (1962).
9. Brown, W. D., Hanauer, S. H., and Wintenberg, R. E., Trans. Am. Nucl. Soc., 7 (1964) (in press).
10. Lennox, C. G., and Pearson, A., IRE (Inst. Radio Engrs.) Trans. Nucl. Sci., NS-5, No. 2, 64/72 (1958).
11. Mann, E. R., private communication to the author.
12. Weaver, C. H., USAEC report ORNL-CF-61-1-82 (1961).
13. Wintenberg, R. E., and Anderson, J. L., Trans. Am. Nucl. Soc., 3, 454 (1960).
14. USAEC report ORNL-3614, 8 (1964).
15. Du Bridge, R. A., Trans. Am. Nucl. Soc., 6, 306 (1963) USAEC reports GEAP-3914 (1962), GEAP-4304 (1963), GEAP-4386 (1963); also private communication to the author.
16. Snyder, T. M., General Electric Company report APED-4475 (1964).
17. Roux, D. P., Gundlach, J. C., and Hanauer, S. H., Trans. Am. Nucl. Soc. 7 (1964) (in press).
18. Roux, D. P. *et al.*, Trans. Am. Nucl. Soc., 5, 185 (1962); see also USAEC report ORNL-3191, 72 (1962).
19. Boyd, Leo R., private communication to the author.
20. Hegberg, D. E., USAEC report HW-73335 (1962).
21. Bunch, W. L., private communication to the author.
22. Apfel, Joseph H., Rev. Sci. Instr., 33, 428 (1962).
23. De Prisco, Carmine F. *et al.*, USAEC report NYO-10011 (1962).
24. De Prisco, Carmine F. *et al.*, USAEC report NYO-10010 (1962).

ABSTRACT—RÉSUMÉ—АННОТАЦИЯ—RESUMEN

A/229 Etats-Unis d'Amérique

Améliorations dans l'instrumentation des réacteurs de puissance à haute performance

par S. H. Hanauer

La mise au point de centrales nucléaires capables de fournir de l'énergie à bas prix a exigé l'amélioration des performances du cœur. Pour que le fonctionnement du réacteur ne soit pas limité par les possibilités de l'instrumentation, de nouveaux appareils ont été réalisés, à la fois pour répondre à de nouvelles fonctions et pour mieux satisfaire aux fonctions déjà utilisées. Pour que l'énergie soit à bas prix, il faut également que la centrale soit disponible à tout instant, et des efforts importants ont été consacrés à améliorer à cet effet la fiabilité des instruments. On décrit quelques nouvelles techniques instrumentales.

La réalisation d'instruments modulaires à fonctions spécialisées utilisant des composants actifs à l'état

solide, a constitué une amélioration essentielle de l'équipement électronique des réacteurs. En plus des avantages que sont des performances meilleures, la fiabilité, le faible volume et la faible consommation d'énergie, ces nouveaux modules peuvent être combinés pour constituer des systèmes d'instruments de caractéristiques très améliorées. On décrit un élément de comptage, à gamme très large, qui utilise un mouvement contrôlé continu du détecteur pour mesurer la puissance du réacteur et sa période, dans tout le domaine de fonctionnement, sans changement de gamme ni autres discontinuités. On a réalisé des ensembles multiples de contrôle de réacteurs, pour lesquels la panne d'un canal de mesure ou d'un servo-mécanisme ne compromet pas la régulation automatique du processus. On a construit des systèmes de sécurité recevant à l'entrée des fonctions complexes qui, par des essais en cours d'utilisation, garantissent une sûreté convenable sans sacrifier la disponibilité de la centrale.

Les détecteurs nucléaires améliorés décrits comprennent des chambres d'ionisation compensées, des chambres comprenant plusieurs sections, des chambres à haute température, et un ensemble chambre de fission – préamplificateur insensible aux parasites électriques. Des modules d'instrumentation non nucléaire utilisant des composants à l'état solide ont été réalisés et donnent de meilleures performances et une meilleure fiabilité.

Des détecteurs spéciaux pour la mesure de variables non nucléaires au voisinage du réacteur sont décrits. Les techniques ultrasoniques servent à la mesure des niveaux liquides, des interfaces liquide – mousse – vapeur, et de la densité des mousses. Des détecteurs expérimentaux comprennent des détecteurs soniques, ultrasoniques, la détection par réactivité du début d'ébullition, la mesure pneumatique des températures et la mesure des hautes températures par variation de la constante diélectrique de certains matériaux céramiques. La mesure en pile de variables nucléaires et non nucléaires facilite l'optimisation du fonctionnement du réacteur et de son contrôle.

L'utilisation de ces nouveaux instruments et de ces nouvelles techniques a pour but d'augmenter la sûreté, les performances et la disponibilité de la centrale. L'augmentation certaine de la complexité et du prix de l'instrumentation doit donc être compensée par ces gains, pour aboutir à un prix de revient global plus bas dans des conditions satisfaisantes de sécurité.

A/229 США

Усовершенствование контрольно-измерительных приборов для энергетических реакторов высокой производительности

С. Г. Ханauer

Разработка ядерных энергетических установок, вырабатывающих дешевую электроэнергию, связана непосредственно с улучшением параметров активной зоны реакторов. Для того чтобы высокие эксплуатационные качества реактора не ограничивались возможностями существующих контрольно-измерительных приборов, были разработаны новые приборы как для выполнения новых, до сих пор не применявшихся функций, так и для улучшения контроля и измерения уже известных параметров. Дешевое производство энергии требует, чтобы установки обладали высокими качествами. Поэтому много усилий было потрачено на повышение надежности приборов. В докладе описаны некоторые новые приборы.

Большие достижения в ядерной электронике позволили оснастить реакторы приборами специального назначения. По сравнению с прежними новые приборы обладают более высокой

точностью и надежностью работы, имеют небольшие размеры и характеризуются малым потреблением энергии. В докладе описывается широкодиапазонный счетчик с непрерывным регулируемым движением датчика. Он предназначен для определения мощности реактора и периода его работы в ходе эксплуатации. Счетчик не требует никаких переключений диапазонов или каких-либо других перерывов в работе. Созданы многоканальные контрольные приборы, в которых авария одного измерительного канала или одного сервомеханизма не приводит к прекращению автоматической регулировки всего процесса. Также созданы системы контроля безопасности со сложными входными функциями, которые определяют состояние системы в процессе работы и тем обеспечивают требуемую безопасность без лишнего простоя.

К описанным усовершенствованным системам относятся компенсационные ионизационные, многосекционные и высокотемпературные камеры и аппараты с предварительным усилением импульсов камеры деления, что обеспечивает нечувствительность к электрическим помехам датчика. Разработаны также модели ядерных приборов, основанных на принципах физики твердого тела, в результате чего повысилась их надежность и точность в работе.

Описываются специальные датчики для измерения ядерных переменных в реакторе. Так, ультразвуковая техника применяется для измерения уровня жидкости или поверхностей раздела между водой, пеной и паром, а также плотности пены. Экспериментальные датчики включают указатели начала кипения, работающие по звуковому и ультразвуковому принципу или же с детектором реактивности, пневматические измерители температуры и измерители высокой температуры, основанные на изменении диэлектрической константы некоторых керамических материалов. Датчики внутри активной зоны, контролирующей ядерные и неядерные переменные, применяются для оптимизации работы реактора и облегчения его управления.

Применение этих новых приборов и методов имеет целью повысить безопасность и улучшить работу и обслуживание установки. Несомненное усложнение и удорожание реакторов, применяющих такую аппаратуру, окупается указанными преимуществами и более низкой стоимостью энергии при соответствующем уровне безопасности.

A/229 Estados Unidos de América

Mejoras en la instrumentación para reactores de potencia de alto rendimiento

por S. H. Hanauer

El desarrollo de centrales nucleares capaces de suministrar energía a bajo precio ha exigido un mayor

rendimiento del núcleo del reactor. Para que el rendimiento del reactor no esté limitado por las posibilidades de la instrumentación, se han desarrollado nuevos instrumentos tanto para funciones no utilizadas hasta ahora, como para mejorar funciones ya en uso. Un bajo coste de la energía requiere también un alto aprovechamiento de la central y para este fin se ha puesto un gran empeño en aumentar la seguridad de funcionamiento de la instrumentación. Se describen algunas de las técnicas sobre instrumentación recientemente desarrolladas.

Se ha obtenido una importante mejora en la electrónica de la instrumentación de reactores mediante el desarrollo de instrumentos moduladores para fines especiales, empleando componentes activos de estado sólido. Además de las ventajas de presentar mejor rendimiento y un mayor grado de confiabilidad, como también menores requerimientos en cuanto a tamaño y suministro de energía, estos módulos pueden ser combinados para formar equipos con características grandemente mejoradas. Se describe un canal de recuento de amplio margen que emplea el movimiento continuo controlado del elemento detector para medir la potencia y período del reactor en todo el margen de operación sin cambio de escala u otras discontinuidades. Se han desarrollado sistemas de control múltiple para reactores en los cuales la avería de un canal de medida o de un servo no produce pérdida de regulación automática del proceso. Se han construido sistemas de seguridad con funciones complejas de entrada en las que realizan verificaciones durante el funcionamiento normal para asegurar unas caracterís-

ticas de seguridad adecuadas sin sacrificio en el uso de la central.

En los detectores nucleares mejorados que se describen se incluyen cámaras de ionización compensadas, cámaras de secciones múltiples, cámaras para altas temperaturas y un sistema preamplificador de impulsos para cámaras de fisión insensible al ruido eléctrico captado. Se han desarrollado módulos para instrumentación no nuclear empleando componentes de estado sólido que proporcionan mayor rendimiento y seguridad de funcionamiento.

Se describen elementos sensibles especiales para la medida de variables no nucleares en las proximidades del reactor. Se emplean técnicas de ultrasonidos para medir niveles de líquidos, o de interfases líquido-espuma de vapor, así como densidades de espuma. Se incluyen elementos sensibles experimentales para la detección de ebulliciones nacientes por sonidos, por ultrasonidos y por reactividad, así como para la medida neumática de temperatura y para la medida de altas temperaturas por variación de la constante dieléctrica de ciertas cerámicas. Para hacer óptimo más fácilmente el rendimiento y el control de reactores se analizan variables nucleares y no nucleares del interior del núcleo.

El empleo de estos nuevos instrumentos y técnicas tiene por objeto aumentar la seguridad, el rendimiento y el grado de utilización de la central. El aumento indudable en la complejidad y costes de la instrumentación tiene que compensarse con las ventajas anteriormente mencionadas conduciendo a unos costes totales inferiores con una seguridad aceptable.

Система управления реакторами

И. Я. Емельянов, А. Г. Филиппов, С. Л. Уманская, А. И. Хлудов

Разрабатываемые в настоящее время атомные реакторы отличаются большим разнообразием по назначению, мощности, конструктивному исполнению. Это разнообразие требует в каждом отдельном случае индивидуального подхода к решению системы управления. В то же время для всех типов реакторов остается безусловным требование безопасной работы. Безопасная работа установки может быть обеспечена только при надежной системе управления. В связи с этим уделяется большое внимание разработке систем управления. Усилия конструкторов системы направляются на обеспечение безопасности работы при минимальных материальных затратах.

ДВЕ ОБЛАСТИ УПРАВЛЕНИЯ

Одним из определяющих факторов при разработке системы управления является допустимая скорость изменения мощности установки. Из эксплуатационных соображений желательна максимально возможная скорость изменения мощности. Однако, учитывая специфику атомных установок, на скорость изменения мощности всегда накладываются ограничения, гарантирующие безопасную работу. Эти ограничения увеличивают время выхода на мощность или изменения уровня мощности. На исследовательских реакторах с плотностями потоков нейтронов до $10^{15} \div 10^{16}$ нейтр/см²·сек в связи с интенсивным процессом отравления остановленного реактора пуск и выход установки на рабочий уровень должны осуществляться за время порядка 30 мин. На автономных энергетических установках в связи с отсутствием резервных источников питания пуск и выход на рабочий уровень должны осуществляться за время порядка 15 мин, в течение которого образующийся за счет аккумулированной энергии пар может удовлетворять собственные нужды станции. В этих случаях должно быть найдено компромиссное решение, позволяющее обеспечить работоспособность и безопасность установки.

Минимальное время выхода на мощность можно было бы получить при разгоне по экспоненциальному закону с безопасным периодом. Однако не на всех реакторах допустим такой разгон во всем диапазоне изменения мощ-

ности до номинальных значений. Энергетические и мощные исследовательские реакторы допускают разгон по экспоненциальному закону только до уровня, составляющего несколько процентов от номинального, то есть в диапазоне изменения мощности, где гарантирован отвод тепла, образующегося в реакторе, и не может появиться опасных для реактора перепадов температуры.

На более высоких уровнях мощность реактора должна находиться в соответствии с расходом теплоносителя; чтобы избежать тепловых ударов, на скорость изменения мощности накладываются ограничения. В этом диапазоне мощности наиболее целесообразен, на наш взгляд, разгон по линейному закону изменения мощности.

Требования сочетания минимального времени выхода на мощность с безопасностью установки и удобством ее эксплуатации могут быть удовлетворены осуществлением разгона по экспоненциальному закону при пусках и на малых уровнях и разгона по линейному закону в рабочем диапазоне мощности. В соответствии с этим весь контролируемый диапазон мощности разбивается на две области: пусковую и рабочую. Пусковая система должна обеспечивать управление в диапазоне от полностью остановленного реактора до $1 \div 10\%$ от номинальной мощности, рабочая система — в диапазоне от $1 \div 10\%$ до номинальной мощности. Граница перехода от пусковой системы к рабочей определяется в каждом конкретном случае.

ОСНОВНЫЕ ФУНКЦИИ СИСТЕМЫ

Пусковая система должна обеспечивать изменение мощности в логарифмическом масштабе, измерение периода разгона, высвобождение реактивности для компенсации подкритичности и создания надкритичности, обеспечивающей заданный период разгона, поддержание заданного периода до выхода на необходимый уровень и далее стабилизацию мощности на этом уровне, поступление сигналов в системы предупредительной защиты и автоматической аварийной остановки реактора при превышениях допустимой скорости разгона или заданного уровня мощности. Для пусковой

системы можно считать приемлемой точность поддержания периода и уровня мощности $20 \div \pm 25\%$ от заданного значения.

Система, действующая в рабочем диапазоне, должна обеспечивать измерение мощности, поддержание и изменение уровня мощности, компенсацию всех возмущений реактивности, поступление сигналов в системы предупредительной защиты и автоматической аварийной остановки реактора при превышениях мощности. Точность поддержания уровня мощности обычно порядка 1% от заданного значения.

Формирование сигналов превышения мощности в рабочем диапазоне обеспечивается системой контроля превышения мощности. Эта система может реагировать на относительные или абсолютные превышения мощности во всем диапазоне ее работы. Предпочтение, на наш взгляд, следует отдавать системам, реагирующим на абсолютные превышения мощности. На номинальном уровне мощности эти системы равноценны, на уровнях ниже номинального чувствительность системы, реагирующей на абсолютные превышения, ниже, чем чувствительность системы, реагирующей на относительные превышения. Такое снижение чувствительности уменьшает вероятность появления аварийных сигналов из-за небольших, не опасных для реактора, превышений мощности, то есть делает систему более надежной. Кроме того, появляется возможность упрощения прибора в связи с тем, что не требуется регулировать коэффициент передачи в зависимости от уровня мощности и поэтому порог чувствительности прибора может быть сделан выше примерно в 100 раз (если диапазон рабочего прибора составляет 2 декады). Такое упрощение также способствует повышению надежности системы.

Сигналы превышения скорости нарастания мощности или превышения уровня мощности из пусковой системы и сигналы превышения мощности из системы, действующей на рабочих уровнях, поступают в системы предупредительной защиты и автоматической аварийной остановки реактора. Система предупредительной защиты предупреждает оператора об отклонении контролируемых параметров и блокирует перемещение стержней вверх, то есть не позволяет увеличивать избыточную реактивность. Система автоматической аварийной остановки реактора обеспечивает гашение реакции введением того или иного количества стержней в зависимости от характера аварийной ситуации.

Так как рабочие уровни лежат в пределах двух декад, а система автоматической остановки достаточно быстродействующая, то есть уверенность, что сигнал о превышении мощности обеспечит остановку реактора прежде, чем период разгона достигнет опасных значений, а потому защита по скорости разгона

в рабочем диапазоне, как правило, не предусматривается.

Система, действующая в рабочем диапазоне мощностей, должна удовлетворять повышенным требованиям надежности, так как она контролирует реактор в наиболее энергетически напряженных режимах и рассчитана на длительную работу (в отличие от пусковой системы). Требуемая надежность обеспечивается наличием минимум двух автоматических регуляторов мощности и трех независимых каналов контроля превышения мощности. Наличие нескольких независимых дублирующих каналов требует согласования их работы. Должны предусматриваться средства автоматизации, обеспечивающие удобства обслуживания такой системы и предотвращающие нарушения работоспособности системы из-за неправильных действий оператора.

ТРЕБОВАНИЯ К ЗАДАТЧИКУ МОЩНОСТИ

Каждый канал автоматического регулирования и контроля превышения мощности должен получать сигнал, соответствующий заданному уровню мощности. Этот сигнал сравнивается с сигналом, поступающим от ионизационной камеры, являющейся датчиком фактической мощности реактора. Если в каждом канале имеются свои независимые органы задания сигнала уставки, при переходе на новый уровень мощности оператор должен выполнить операции, заключающиеся в поочередном изменении уставок в каждом канале до устранения разбалансов на соответствующих приборах. При этом во избежание ложных остановок реактора важно соблюдать определенную очередность в задании новых уставок: при увеличении уровня мощности реактора сначала нужно изменять уставки каналов контроля превышения мощности, затем каналов автоматического регулирования, рабочего и резервного; при снижении уровня мощности реактора сначала нужно изменять уставки регуляторов, рабочего и резервного, а затем каналов контроля превышения мощности. При такой системе задания уставок нежелательны изменения мощности сразу в большом диапазоне, так как при этом будет иметь место существенное снижение чувствительности системы контроля превышения мощности и, следовательно, снижение безопасности установки.

Необходимость выполнения большого количества операций вручную отвлекает оператора от других обязанностей. От опыта оператора также зависят надежность системы и безопасность установки: ошибки оператора могут приводить к ложным остановкам реактора.

В наиболее распространенных схемах задатчиков мощности в качестве задающих элементов используются наборы сопротивлений с переключателем (ступенчатые задатчики) и потенциометры или вращающиеся трансформа-

торы с ручным управлением (плавные задатчики). Изменение уставки в ступенчатых задатчиках приводит к отключению автоматического регулятора из-за появления большого разбаланса.

Использование плавного задатчика мощности позволяет осуществлять изменение мощности реактора вслед за изменением уставки в задатчике, но допустимый диапазон изменения уставки ограничен из-за возможности отключения автоматического регулятора при больших разбалансах (обычно 20% от заданного уровня).

Если система автоматического регулирования не обеспечивает слежения мощности за уставкой задатчика мощности, то изменение уровня мощности оператор должен осуществлять при выключенном автоматическом регуляторе с помощью стержней ручного управления. Это также снижает безопасность установки: ошибки оператора могут привести к разгонам с недопустимой скоростью.

Из изложенного можно сделать вывод, что система, действующая в рабочем диапазоне, должна иметь общий задатчик мощности, обеспечивающий плавное изменение уставки с определенной, не зависящей от оператора скоростью, гарантирующей отсутствие разбалансов которые могут привести к отключению каналов автоматических регуляторов. Определяющими при выборе скорости изменения мощности, как уже отмечалось, должны быть условия съема тепла, выделяемого в реакторе.

Такой задатчик в сочетании с автоматическим регулятором обеспечит слежение мощности реактора за уставкой задатчика и следование уставки каналов контроля превышения мощности за уставкой автоматического регулятора.

ПРИНЦИПЫ ПОСТРОЕНИЯ СИСТЕМЫ ЗАДАНИЯ МОЩНОСТИ

Учитывая важность функций, выполняемых задатчиком мощности, и то, что один задатчик обслуживает всю систему, чрезвычайно важно гарантировать надежную работу системы задания мощности. Надежность этой системы обеспечивается максимальным повышением надежности самого задатчика за счет упрощения его схемы и использования надежных элементов, а также резервированием задатчиков: устанавливаются 2 задатчика, выходы которых запараллелены через логическую схему или на диодах. При исчезновении напряжения на выходе одного задатчика напряжение на общем выходе системы остается без изменения. Развернутая блок-схема системы задания мощности приведена на рис. 1.

Основным элементом задатчика мощности является бесконтактный сельсин $1'$, управляемый двигателем 6 (блок IV). Напряжение между фазами обмотки сельсина является функцией положения ротора. Это напряжение через переключатель диапазонов 9 , трансформаторы

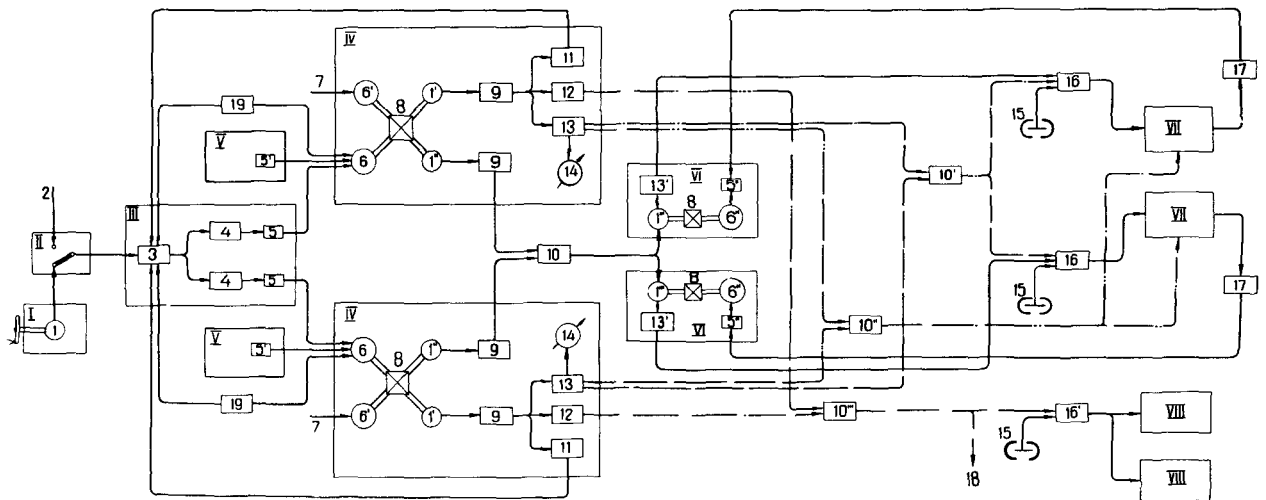


Рис. 1. Развернутая блок-схема системы задания мощности:

— — — — сигнал задания мощности, поступающий в каналы автоматических регуляторов; — · — · — сигнал регулировки коэффициентов передачи автоматических регуляторов; — · — · — сигнал задания мощности, поступающий в каналы превышения мощности; I — блок установок; II — переключатель режимов; III — блок следящей системы; IV — задатчик мощности; V — корректор мощности; VI — автоматический корректор уставки; VII — усилитель регулятора; VIII — усилитель контроля превышения мощности; 1 — сельсин; 2 — сигнал из системы задания расхода теплоносителя; 3 — схема коммутации и сравнения; 4 — усилитель следящей системы; 5 — реле; 6 — двигатель; 7 — сигнал на быстрое снижение уставки задатчика мощности; 8 — редуктор; 9 — переключатель диапазонов; 10 — схема «или»; 11 — трансформатор; 12 — выпрямитель; 13 — трансформатор с выпрямителями; 14 — указатель заданной мощности; 15 — ионизационная камера; 16 — схема сравнения; 17 — схема переключения задатчиком мощности; 18 — сигнал на другие каналы контроля превышения мощности; 19 — ключ ручного управления

и выпрямители 11, 12, 13 поступает на выходы задатчика.

Сигнал постоянного тока с выходов трансформатора с выпрямителями 13 поступает на указатель заданной мощности 14, через логическую схему или 10' на схемы сравнения 16 токов уставок с токами ионизационных камер 15 и через схему, или 10'' в цепи регулирования коэффициентов усиления усилителей регуляторов VII для обеспечения одинаковой чувствительности автоматических регуляторов во всем диапазоне работы задатчика. Сигнал постоянного тока с выпрямителя 12 через схему, или 10''' поступает в каналы контроля превышения мощности. С трансформатора 11 сигнал переменного тока поступает в схему коммутации и сравнения 3 блока следящей системы III.

Диапазон изменения выходных токов задатчика равен 300 и соответствует токам ионизационных камер от 2 до 600 мкА для автоматических регуляторов и от 1 до 300 мкА для каналов контроля превышения мощности. Указанные токи приняты соответствующими мощности реактора 0,5÷150% от $N_{ном}$. Если при столь большом диапазоне изменения уставок обеспечить одинаковую скорость во всем диапазоне, то оказывается практически невозможно удовлетворить два противоречивых требования: минимальное время перехода на новый уровень мощности и безопасность разгона. Если обеспечить безопасность разгона, то есть не допускать коротких периодов разгона на малых уровнях, то общее время изменения уставки окажется очень большим, что неприемлемо в условиях эксплуатации.

Представляется целесообразным разделить весь диапазон работы задатчика на два диапазона: первый, соответствующий уровням 0,5÷15%, и второй, соответствующий уровням 15÷150% от номинальной мощности.

В задатчике используется синусоидальная зависимость среднего значения напряжения между фазами трехфазной обмотки сельсина от угла поворота ротора относительно статора. Разделение на диапазоны осуществляется за счет подключения к выходным цепям различных фаз сельсина. Угол поворота в пределах каждого диапазона ограничен 60°, что обеспечивает практически линейный характер зависимости выходного напряжения от угла поворота ротора сельсина.

На рис. 2 изображены расчетные зависимости токов в выходных цепях задатчика мощности от угла поворота ротора сельсина и заданной мощности, а также зависимости токов камер от мощности реактора на I и II диапазонах работы задатчика для каналов автоматических регуляторов и контроля превышения мощности.

На рис. 3 приведены кривые изменения токов задатчиков и входных токов усилителей при переключении диапазонов.

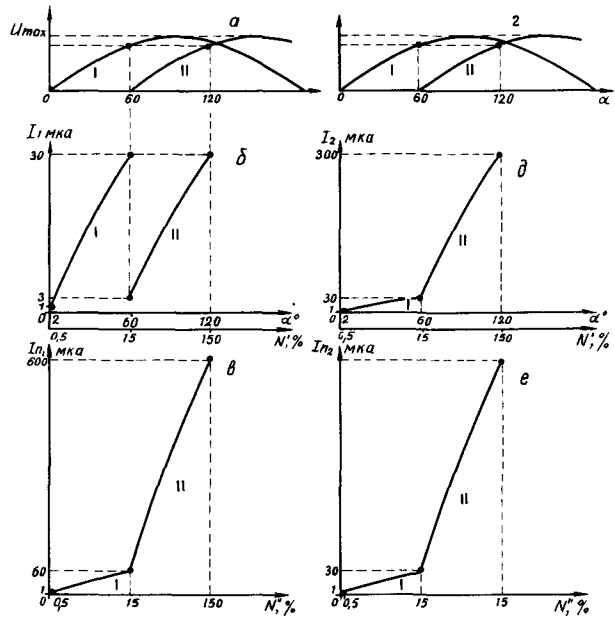


Рис. 2. а и г—зависимость средних напряжений между фазами сельсина U от угла поворота ротора α ; б и д—зависимость токов задатчиков I_1 и I_2 от угла α и заданного уровня мощности реактора N' для каналов автоматических регуляторов и контроля превышения мощности соответственно; в и е—зависимость токов камеры I_{n1} и I_{n2} от мощности реактора N'' для каналов автоматических регуляторов мощности и контроля превышения мощности соответственно

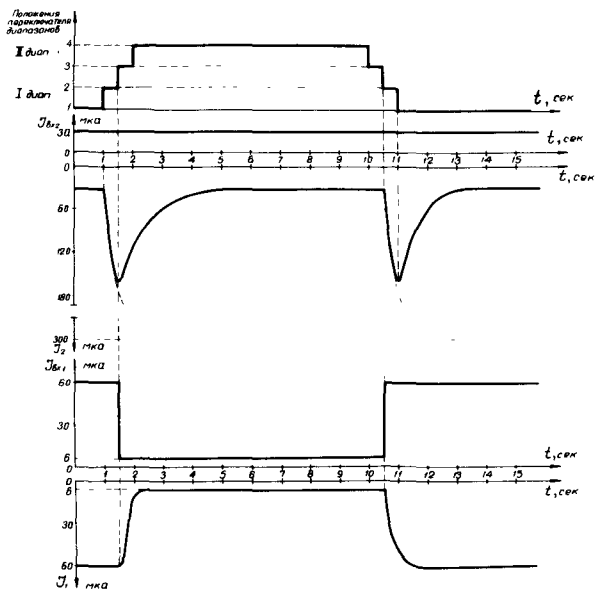


Рис. 3. Кривые изменения токов задатчика (I_1 и I_2) и входных токов усилителей ($I_{вх1}$ и $I_{вх2}$) при переключении диапазонов:

1 и 4—основные; 2 и 3—промежуточные положения переключателя диапазонов; I_1 и $I_{вх1}$ —для каналов автоматического регулирования; I_2 и $I_{вх2}$ —для каналов контроля превышения мощности. Длительность нахождения переключателя в промежуточных положениях принята равной 0,5 сек

Так как при переключении с I на II диапазон ток, поступающий в каналы автоматических регуляторов, уменьшается в 10 раз, то ток, поступающий от ионизационной камеры, тоже должен быть уменьшен в 10 раз. Это достигается подключением шунтирующего сопротивления ко входу усилителя регулятора.

Характеристика зависимости токов задатчика от угла поворота ротора для каналов контроля превышения мощности (рис. 2, б) выполнена непрерывной во всем диапазоне работы задатчика.

Сохранение величины выходного сигнала при переключении фаз и получение требуемой зависимости выходного сигнала от угла поворота ротора сельсина обеспечиваются наличием в выходной цепи I диапазона гасящего сопротивления.

Промежуточные положения 2 и 3 переключателя диапазонов обеспечивают изменение выходных токов задатчика, поступающих в каналы контроля превышения мощности, только в сторону увеличения, что исключает появление ложных аварийных сигналов при переключении диапазонов.

Задатчик может выполняться с разными скоростями изменения уставок. Одна из модификаций задатчика обеспечивает скорость 0,02% от номинальной мощности в секунду на I диапазоне и 0,2% от номинальной мощности в секунду на II диапазоне (при одинаковой скорости поворота сельсина). Разделение на два диапазона позволило значительно повысить точность задаваемого уровня мощности при работе на низких уровнях.

Наряду с нормальной скоростью изменения уставки предусмотрена и повышенная примерно в 10 раз скорость. Повышенная скорость используется для быстрого снижения мощности работающего реактора или перевода уставки задатчика мощности в требуемое положение при отключенной системе регулирования. Управление сельсинами I и I' в этом случае осуществляется от отдельного двигателя 6' со своим редуктором.

Для сохранения величины выходных сигналов системы задания уровня мощности при отключении или неисправности одного из двух параллельно работающих задатчиков применена схема компенсации, в которой используется изменение величины запирающего напряжения в случае отключения одного задатчика.

В качестве указателя заданной мощности используется вольтметр со шкалой 270°. Вольтметр измеряет выходное напряжение задатчика. Указатель заданной мощности имеет два диапазона измерений соответственно двум диапазонам работы задатчика. Большой угол шкалы и два диапазона измерений обеспечивают удовлетворительную точность отсчета.

Для удобства работы в системе имеется блок уставок I, с помощью которого задается уро-

вень мощности, на который требуется вывести реактор. Блок уставок содержит бесконтактный сельсин I, ротор которого соединен с внешней рукояткой. При повороте рукоятки до требуемого положения (по имеющейся на блоке шкале) на выходе блока появляется напряжение, пропорциональное уставке. Оно поступает в схему коммутации и сравнения 3 блока следящей системы III, где сравнивается с напряжениями, поступающими с выходов задатчиков мощности. Следящая система, включая двигатели задатчиков, обеспечивает приведение уставок каждого задатчика в соответствие с заданным положением рукоятки блока уставок.

Имеются также ключи 19 независимого управления каждым из задатчиков. При таком способе управления тот задатчик, ключом которого ведется управление, принимает на себя функции ведущего. Следящая система вырабатывает сигнал рассогласования задатчиков и, включая двигатель второго (ведомого) задатчика, обеспечивает приведение его уставки в соответствие с уставкой ведущего. При этом способе управления оператор должен держать нажатым ключ управления на протяжении всего времени изменения уровня мощности; при управлении от блока уставок вмешательство оператора требуется только для изменения положения рукоятки.

Сигнал в следящую систему III может поступать и из системы 2 регулирования расхода теплоносителя (вместо сигнала с блока уставок). В этом случае осуществляется синхронное изменение расхода теплоносителя и мощности реактора. Предусмотрена также возможность коррекции уставки мощности по сигналам из схем регулирования температуры или давления теплоносителя. Срабатывающие при отклонениях регулируемого параметра реле 5 в корректоре V обеспечивает включение двигателей задатчиков и, таким образом, приведение мощности реактора к требуемому уровню.

Учитывая возможность наличия расхождений в настройке усилителей и в величинах токов ионизационных камер, а также возможность появления расхождений в величинах токов камер в процессе работы реактора, предусматриваются индивидуальные для каждого канала ручные корректоры токов камер и автоматические корректоры заданной уставки мощности. Ручные корректоры токов камер представляют собою шунты ко входу усилителей и позволяют изменять коэффициент передачи цепи от камеры к усилителю до трех раз с точностью до 1%. Автоматические корректоры уставки VI имеются только в каналах регуляторов и представляют собою следящую систему, обеспечивающую отсутствие разбаланса на выходе усилителя регулятора, находящегося в резерве. Корректор гарантирует отсутствие разбаланса и, следовательно, возможность включения резервного автомата при отказе рабочего.

Основным элементом корректора является сельсин I''' , выполняющий функции бесконтактного индукционного потенциометра. Угол поворота ротора сельсина ограничен так же, как и в задатчике 60° . Напряжение с сельсина через трансформатор с выпрямителем $13'$ задает ток коррекции в схему сравнения 16 . Ток коррекции является составной частью тока компенсации, с которым сравнивается ток камеры. На статор сельсина I''' напряжение подается с отдельного сельсина задатчика мощности I'' , этим обеспечивается зависимость тока коррекции от уставки задатчика и одинаковая эффективность корректора во всем диапазоне работы задатчика.

Ротор сельсина I''' связан через редуктор 8 с двигателем $6''$. Двигатель включается с помощью двух реле $5''$, обмотки которых подключаются к выходу усилителя регулятора VII, если он находится в резерве. При появлении на выходе усилителя разбаланса срабатывает одно из реле (в зависимости от полярности разбаланса), включается двигатель, который вращает ротор сельсина в направлении устранения разбаланса. Автоматический корректор уставки имеет зону нечувствительности, превышающую зону нечувствительности автоматического регулятора. Имеющие место включения корректора при отклонениях мощности, превышающих его зону нечувствительности, окупаются постоянной готовностью резервного автомата к работе.

ОПИСАНИЕ СИСТЕМЫ УПРАВЛЕНИЯ

На рис. 4 приведена блок-схема системы управления, содержащей описанную систему задания мощности, два канала автоматического регулирования мощности и три канала контроля превышения мощности. Каждый канал работает от своих независимых камер.

В каждом канале контроля превышения мощности имеется два одинаковых усилителя 18 . Входы усилителей включены последовательно и получают с общей схемы сравнения 16 сигналы, равные разности токов камеры и задатчика. Выходы усилителей соединены по схеме совпадения «два из двух». Неисправность прибора дает на выходе сигнал, аналогичный сигналу превышения мощности реактора. Однако на выходе схемы совпадения сигнала при этом нет. Но достаточно появиться выходному сигналу от второго усилителя из пары (из-за его неисправности или вследствие фактического превышения мощности реактора), как сформируется сигнал, который поступит в логическую схему управления приводами и удерживающими электромагнитами. Логическая схема управления может обеспечивать отпусkanie электромагнитов и включение двигателей приводов стержней по схеме «один из нескольких» или «два из нескольких», например из трех.

Выбор схемы производится в зависимости от конкретных особенностей установки.

Для увеличения степени автоматизации установки автоматическое регулирование мощности и периода разгона осуществляется как стержнями самого автоматического регулятора, так и компенсирующими стержнями. Если в процессе регулирования стержни автоматического регулятора выходят в крайнее положение, то происходит автоматическое подключение к системе регулирования компенсирующих стержней и перемещение их в том же направлении, в котором двигался стержень регулятора. Количество одновременно перемещаемых компенсирующих стержней и последовательность их работы определяются заданной программой. Компенсирующие стержни перемещаются до тех пор, пока стержни автоматического регулятора не вернуться в среднее положение. Такая схема связи между стержнями эквивалентна увеличению эффективности органов регулирования самого автомата и позволяет осуществлять автоматически, без вмешательства оператора, пуск реактора, изменение уровня мощности, компенсацию эффектов выгорания, отравления, изменения температуры, изменения реактивности при догрузке тепловыделяющих элементов на работающем реакторе, то есть осуществлять автоматическое регулирование реактора при возмущениях, значительно превышающих компенсирующую способность стержней самого автоматического регулятора.

Однако при наличии описанной связи между стержнями, когда автоматический регулятор фактически управляет целой группой стержней, способных создать избыточную реактивность, значительно превышающую β , особенно остро встает вопрос о безопасности установки. Должны быть наложены ограничения на величину положительной реактивности, которая может быть введена при перемещении группы стержней, и на скорость введения положительной реактивности.

Если стержни по эффективности примерно одинаковы, то используется схема, блокирующая перемещение стержней, когда подготовленное к извлечению число стержней превышает допустимое.

Если стержни по эффективности разные, то используется схема, в которой учитывается эффективность каждого стержня и подсчитывается суммарная эффективность стержней, подготовленных к извлечению. Если суммарная эффективность стержней превысит порог настройки схемы (чаще всего $0,5 \pm 0,8 \beta$), то блокируется всякое извлечение стержней.

Безопасность установки обеспечивается и наличием в каналах автоматических регуляторов реле, срабатывающих при появлении больших разбалансов, являющихся явно следствием неисправности канала. Эти реле блокируют выход усилителя и, таким образом,

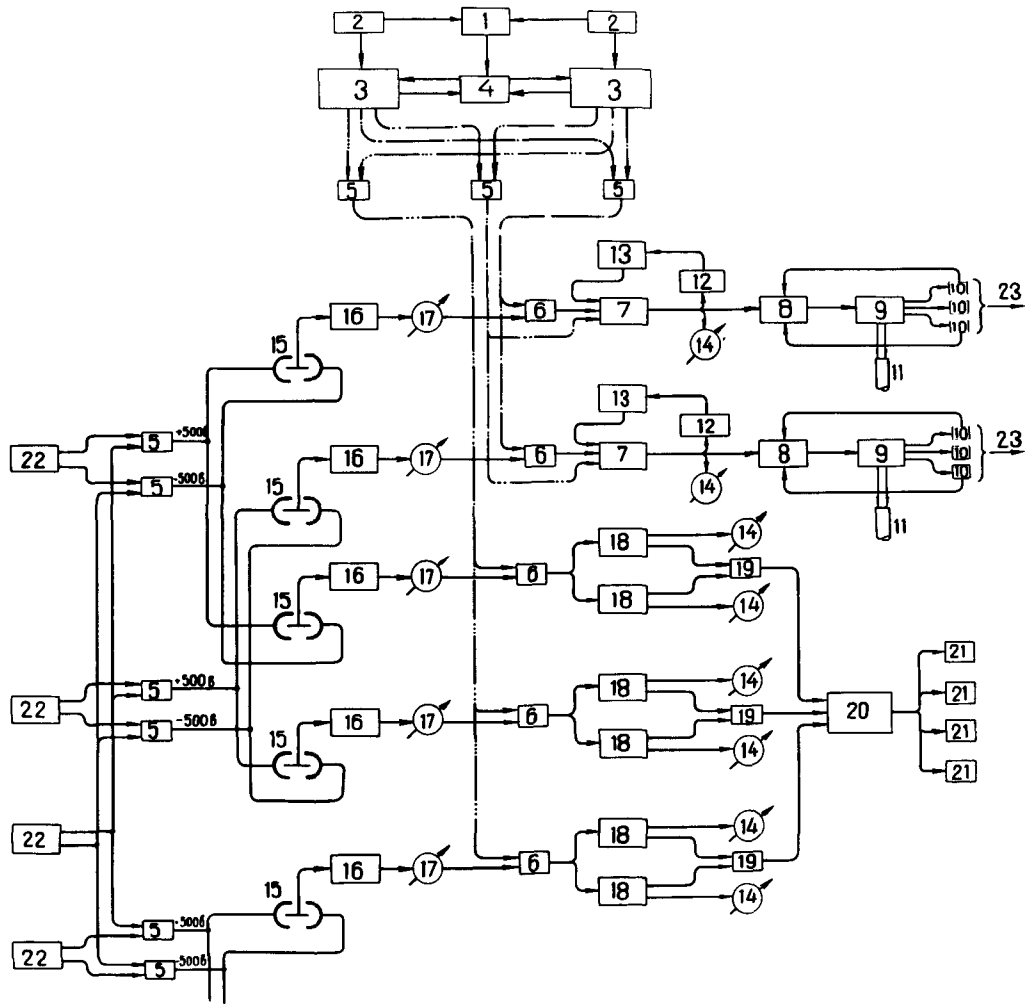


Рис. 4. Блок-схема системы управления:

1—блок уставок; 2—ключ ручного управления задатчиком мощности; 3—здатчик мощности; 4—блок следящей системы; 5—схема «или»; 6—схема сравнения; 7—усилитель регулятора предварительный; 8—усилитель регулятора выходной; 9—сервопривод автоматического регулятора; 10—датчики конечных и промежуточных положений стержня; 11—поглощающий стержень автоматического регулятора; 12—схема переключения «работа—резерв»; 13—автоматический корректор уставки; 14—индикатор разбаланса; 15—ионизационная камера; 16—корректор тока камеры; 17—указатель тока камеры; 18—усилитель контроля превышения мощности; 19—схема совпадения «два из двух»; 20—логическая схема управления приводами и удерживающими электромагнитами; 21—удерживающие электромагниты аварийных стержней; 22—источник питания ионизационных камер; 23—связь с системой управления компенсирующими стержнями

предотвращают воздействие на реактор ложных сигналов. Все эти меры направлены на исключение возможности появления опасной избыточной реактивности.

НАДЕЖНОСТЬ СИСТЕМЫ УПРАВЛЕНИЯ

Надежность системы управления достигается поканальным дублированием, резервированием отдельных приборов, обеспечением непрерывного и периодического контроля отдельных приборов, максимальным повышением надежности отдельных приборов за счет максимально возможного упрощения их и применения надежных элементов.

Измерение любого параметра осуществляется не менее чем двумя независимыми приборами с независимыми датчиками сигнала. Контроль превышения мощности осуществляется не менее чем по трем независимым каналам. Контроль скорости разгона — не менее чем по двум независимым каналам. В рабочем диапазоне аварийный сигнал по скорости разгона блокируется во избежание ложных срабатываний. Ложные срабатывания предотвращаются и введением схем совпадений. Так, например, в системе АЗ по превышению мощности в каждом из трех независимых каналов используются два усилителя, выходы которых соединены по схеме совпадения «два из двух». Такая схема позволяет снимать для ремонта приборы,

посылать контрольный сигнал для проверки прибора без снижения надежности системы.

О резервировании задатчиков мощности уже упоминалось. Аналогично резервируются источники питания ионизационных камер. При исчезновении на выходе одного из параллельно включенных источников напряжение на камерах сохраняется. Один источник может выполнять функции резервного для нескольких цепей питания камер.

Описанная система надежна и в то же время проста. Система имеет такое резервирование, что нет необходимости организовывать сквозную проверку цепей. Создание сквозных контрольных цепей усложняет систему и может привести к снижению надежности. Можно обойтись простыми средствами периодической или непрерывной проверки отдельных наиболее ответственных приборов. Другие элементы, трудно поддающиеся контролю, в случае выхода их из строя приводят к остановке реактора. Однако это относится к очень ограниченному числу элементов, например удерживающим электромагнитам стержней.

Тщательное изготовление, правильная организация испытания перед установкой и соблюдение условий эксплуатации этих элементов делают чрезвычайно редкими выходы их из строя. При таком положении было бы неоправданным усложнение системы введением сквозного контроля цепей.

Значительное повышение надежности получено за счет перехода на транзисторные и магнитные схемы приборов вместо ламповых. Сейчас существует целая серия приборов систем управления реакторами, выполненных на транзисторах и магнитных усилителях. Магнитные усилители используются преимущественно в силовых цепях, для управления двигателями и электромагнитными муфтами. Для этой же цели разработаны и схемы на управляемых вентилях, отличающиеся от схем на магнитных усилителях простотой и меньшими габаритами приборов.

Надежность системы повышается и благодаря способности приборов работать при значительных колебаниях напряжения сети; допускается снижение питающего напряжения на 30÷40%.

Все более широкое применение в приборах и схемах управления находят бесконтактные элементы. Разработаны схемы управления приводами и приборами на транзисторных логических элементах (вместо реле и контакторов). Используемые в схеме логические элементы выполнены в виде модулей, которые легко komponуются на стандартных панелях. Схема управления получается значительно более компактной, чем при использовании реле и контакторов.

Вообще, переход на системы, выполненные полностью на бесконтактных элементах, привел бы к громоздкой, сложной в обслуживании

(из-за трудностей в нахождении повреждений) и, в конечном итоге, недостаточно надежной системе. В каждом отдельном случае приходится конкретно решать вопрос о разумном объеме использования бесконтактных элементов. Значительное число контактных элементов еще представляется целесообразным сохранить в схемах управления приводами, в задатчиках мощности, корректорах (командоаппараты: кнопки, ключи, а также реле и контакторы).

РЕЗУЛЬТАТЫ ИСПЫТАНИЯ СИСТЕМЫ

Описанная система была испытана с моделью реактора. Испытания подтвердили работоспособность системы.

Отклонение мощности модели реактора при отключении одного задатчика не превышает 2% от установленного уровня, погрешность в каналах контроля превышения мощности не более 1% от номинального уровня. При переходе с одного уровня мощности на другой в пределах одного диапазона расхождения в отдельных каналах не превышают 1% от номинальной величины. При переходе с одного диапазона на другой отклонения мощности не превышают 1÷2% от установленного уровня, погрешность в каналах контроля превышения мощности не более 0,5% от номинальной мощности. При колебаниях напряжения сети +10 и -15% отклонения не более ±1%, при снижении напряжения сети на 40% не более +3%.

В настоящее время описанная система используется на ряде установок, в том числе на материаловедческом реакторе МИР.

ВЫВОДЫ

Разработанная система отличается универсальностью, так как может содержать разное количество каналов автоматического регулирования (до 3) и контроля превышения мощности (до 6) и может принимать извне сигналы, обеспечивающие разные способы регулирования параметров установки.

В системе довольно широко применена автоматизация, что освобождает оператора от ряда функций и резко снижает зависимость надежности системы от опыта оператора.

Применение транзисторов, магнитных усилителей, управляемых вентилях, транзисторных логических элементов в сочетании с реле и контакторами (в менее ответственных цепях) позволило получить надежную и сравнительно простую систему.

Дублирование каналов и резервирование отдельных наиболее ответственных приборов с применением простых средств периодической или непрерывной проверки отдельных приборов позволило получить надежную систему без введения сквозной проверки каналов.

Разработанная система обеспечивает безопасность работы установки.

ABSTRACT—RÉSUMÉ—АННОТАЦИЯ—RESUMEN

A/330 USSR

Control system of nuclear reactorsBy I. Y. Emelyanov *et al.*

The paper briefly discusses the main design principles of nuclear reactor control systems.

The requirements to the system design: maximum simplicity, channel duplicating, use of reliable elements (transistors, magnetic amplifiers, non-contact elements). The paper describes reactor monitoring, beginning from the subcritical condition, by means of instruments operating from the current ionisation chambers and gives the characteristics of the instruments which provide the means for the measurement of the period and power on a logarithmic and linear scale.

Two systems of automatic power level control are described, one exponential with a preset period, and the other linear. An emphasis is made on the advantages of one power controller, common for the entire system, with automatic and manual level correctors. The paper describes rod interrelation which enables automation of the processes requiring introduction of reactivity and compensation for the reactivity deviations which exceed the effectiveness of one rod.

The paper goes on to discuss the safety provisions, alarm system and emergency shut-down systems, the relation between the circumstances which require reactor shut-down and the means for quenching the reaction; specific features of the system for the power level overshoot control are noted.

The paper shows the advantages of the actuator control schemes using transistorised elements as compared with the control schemes using relays and contactors.

A/330 URSS

Système de contrôle des réacteurspar I. Y. Emelyanov *et al.*

Les auteurs exposent brièvement les principes essentiels de la structure des systèmes de contrôle et de sécurité des réacteurs nucléaires.

Les conditions que ces systèmes doivent remplir sont mises en évidence: simplicité maximale, chaînes doubles, fiabilité des éléments (transistors, amplificateurs magnétiques, éléments sans contact). Ils décrivent le contrôle des réacteurs—en commençant par l'état sous-critique—au moyen d'appareils alimentés par des chambres d'ionisation à courant et donnent les caractéristiques des appareils d'enregistrement linéaire et logarithmique du temps de doublement et la puissance.

Ils décrivent deux systèmes de contrôle automatique du niveau de puissance, l'un exponentiel avec temps de doublement préétabli, l'autre linéaire. Ils font valoir

les avantages d'un appareil de contrôle de la puissance commun à l'ensemble du système et muni de correcteurs de niveau automatiques et manuels. Ils décrivent la relation entre les barres qui permet d'automatiser les opérations qui nécessitent l'addition de réactivité et la compensation des écarts de réactivité, supérieurs à l'efficacité d'une seule barre.

Les auteurs étudient ensuite les mesures de sûreté, les divers systèmes d'avertissement et d'arrêt brusque du réacteur, l'interdépendance des causes qui imposent un tel arrêt et les moyens d'arrêter la réaction; ils signalent les particularités du système de contrôle des excursions de puissance.

Enfin, ils font ressortir les avantages que les systèmes de contrôle par transmission à l'aide d'éléments "logiques" transistorisés et de soupapes commandées présentent par rapport aux systèmes à relais et à contacteurs.

A/330 URSS

Sistema de control de los reactorespor I. Y. Emelyanov *et al.*

En la memoria se exponen brevemente los principios básicos de la estructura de los sistemas de control y protección de los reactores nucleares.

Se enfocan las condiciones a que han de satisfacer esos sistemas: máxima sencillez, duplicación de la indicación, empleo de elementos fide dignos (transistores, amplificadores magnéticos, elementos sin contacto). Se describe el control de los reactores, partiendo del estado subcrítico, mediante aparatos alimentados por cámaras de ionización de corriente. Se presentan las características de los instrumentos que permiten las medidas y el registro del período y de la potencia en las escalas lineal y logarítmica.

Se describen dos sistemas de control automático del nivel de potencia: uno exponencial, con un período dado y otro lineal. Se señalan las ventajas de un marcador de potencia, común para todo el sistema, con correctores automáticos y manuales del nivel prefijado. Se describe la relación entre las barras, que permite automatizar los procesos que exigen la introducción de reactividad, y la compensación de su desviación por encima del valor correspondiente a una barra sola.

A continuación se discuten las medidas adoptadas para la seguridad de la instalación, los sistemas de protección preventiva y de parada brusca del reactor, la interdependencia de las causas que exigen la parada y los medios de parar la reacción; se señalan las particularidades del sistema de control del exceso de potencia.

Se indican las ventajas del sistema de control mediante circuitos lógicos transistorizados y válvulas controladas, con respecto a los esquemas a base de relés y contactores.

Résultats pratiques et perspectives de l'utilisation de poison en solution dans les réacteurs à eau sous pression

par M. Plumier*, P. Stacquez*, P. Dozinel**, R. Muylle**, M. Preat**, G. Beuken***, M. Gueben*** et L. Maesen***

Le contrôle chimique est appelé à jouer un rôle de plus en plus important dans l'exploitation des centrales nucléaires de puissance du type à eau sous pression.

En vue de réduire le coût du kWh, on a cherché à augmenter les durées d'irradiation du combustible ainsi que la puissance spécifique du cœur. Or les barres de contrôle n'ont qu'une efficacité limitée et, d'autre part, elles provoquent des pointes de flux de chaleur impliquant une réduction de la densité moyenne de puissance dans le cœur. L'emploi de poison en solution pour contrôler la réactivité pendant toute la durée de vie du cœur pallie ces inconvénients. En effet, un empoisonnement homogène de l'eau du circuit primaire permet une répartition plus uniforme du flux neutronique en éliminant les barres de compensation; il rend possible un plus grand excès initial de réactivité et conduit ainsi à une augmentation de la durée de vie du cœur en se rapprochant de l'optimum économique.

Un contrôle chimique est prévu dans les centrales du type à eau sous pression (PWR) actuellement en construction ou en projet; il permettra de compenser l'épuisement du combustible et de suivre les transitoires lents, tels que ceux dus à l'effet xénon. La combinaison des propriétés neutroniques et chimiques de l'acide borique l'a fait choisir comme poison.

D'autres poisons chimiques sont cependant également utilisés; par exemple, le sulfate de cadmium est utilisé dans l'eau lourde du réacteur canadien de Douglas Point.

Le contrôle chimique entraîne un certain nombre de problèmes relatifs à la chimie des eaux de refroidissement du réacteur, à la corrosion des circuits, à la dynamique du réacteur, à la souplesse de la compensation de réactivité, ainsi que certaines modifications dans la conception et l'exploitation des centrales, notamment en ce qui concerne le traitement des effluents radioactifs.

La présente communication examine, dans une première partie, les problèmes qui se sont posés lors de

l'essai de marche en puissance de la centrale nucléaire BR3 en présence de bore, puis, dans la seconde partie, les particularités introduites, par ce procédé de contrôle, dans la conception des centrales à eau sous pression, ainsi que dans le traitement des effluents radioactifs.

MARCHE EN PUISSANCE DE LA CENTRALE NUCLÉAIRE BR3 EN PRÉSENCE DE BORE DANS LE CIRCUIT PRIMAIRE^a

La centrale nucléaire BR3 possède un réacteur du type PWR d'une puissance thermique nominale de 40,9 MW. La puissance électrique brute correspondante est de 11,7 MW.

Mise en service industriel en fin 1962, la centrale a, pendant les 12 premiers mois de marche en puissance, produit 70 000 000 kWh électriques, soit l'équivalent de 6 000 heures à pleine charge. Il en résulte une utilisation moyenne proche de 70%. Les principaux résultats d'exploitation de la première année de fonctionnement de la centrale sont décrits dans le document BLG 261 [1].

Le réacteur n'ayant pas été conçu pour être contrôlé par voie chimique, avant de procéder aux essais pratiques, la sécurité des expériences envisagées a été étudiée sur simulateur analogique.^b

Simulateur analogique

Les principaux phénomènes examinés sont:

a) L'influence de la réduction, en valeur absolue, du coefficient négatif de température de l'eau (modérateur) lors de transitoires importants de charge. On en conclut que l'introduction de bore, particulièrement à des concentrations supérieures à 100 ppm, conduit à une réponse transitoire du système moins favorable que lors du fonctionnement sans bore, mais néanmoins parfaitement acceptable.

b) Les conséquences de la disparition rapide du bore contenu dans l'eau du circuit primaire. Malgré des

* Ateliers de constructions électriques de Charleroi.

** Bureau d'études nucléaires, Bruxelles.

*** Groupe industriel pour l'exploitation du BR3, du centre d'étude de l'énergie nucléaire, Mol.

^a Les expériences menées sur le BR3 ont été réalisées sous les auspices de la Fondation nucléaire.

^b La simulation analogique a été réalisée sur les installations du CEN à Mol par J. P. Contzen et F. de Greef.

- Puissance électrique : $P_e = 10 \text{ MW (e)}$
- Température moyenne : $T_{ave} = 262^\circ \text{C}$
- Pression : $p = 140 \text{ kg/cm}^2$
- Hauteur de référence pour les barres de contrôle : $H = 93 \text{ cm}$

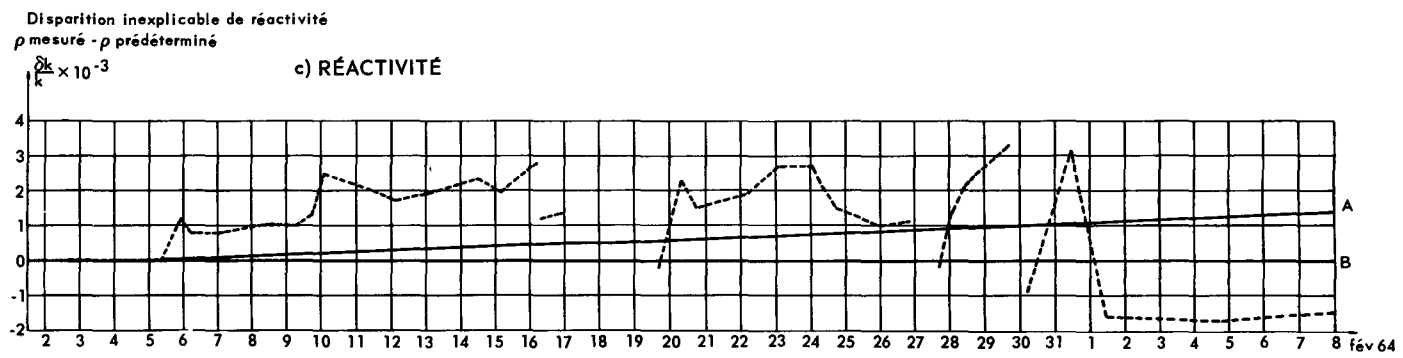
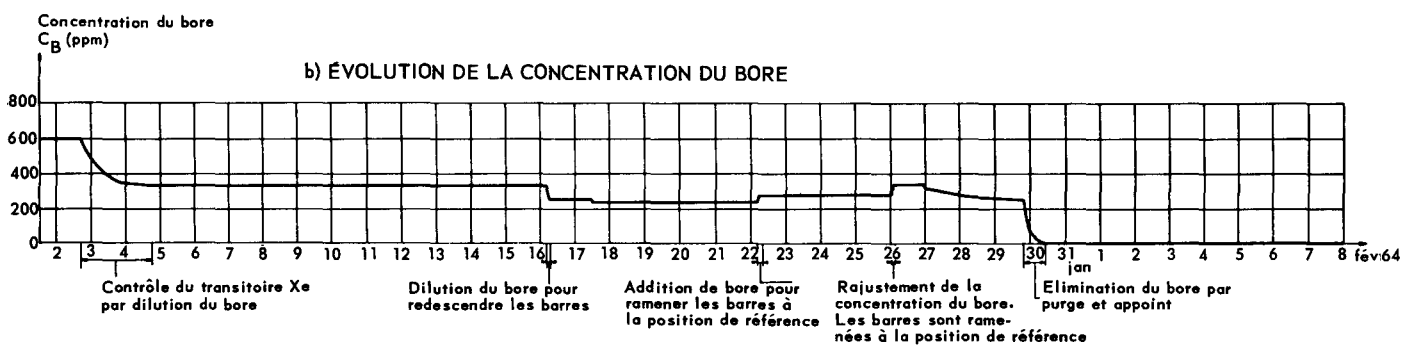
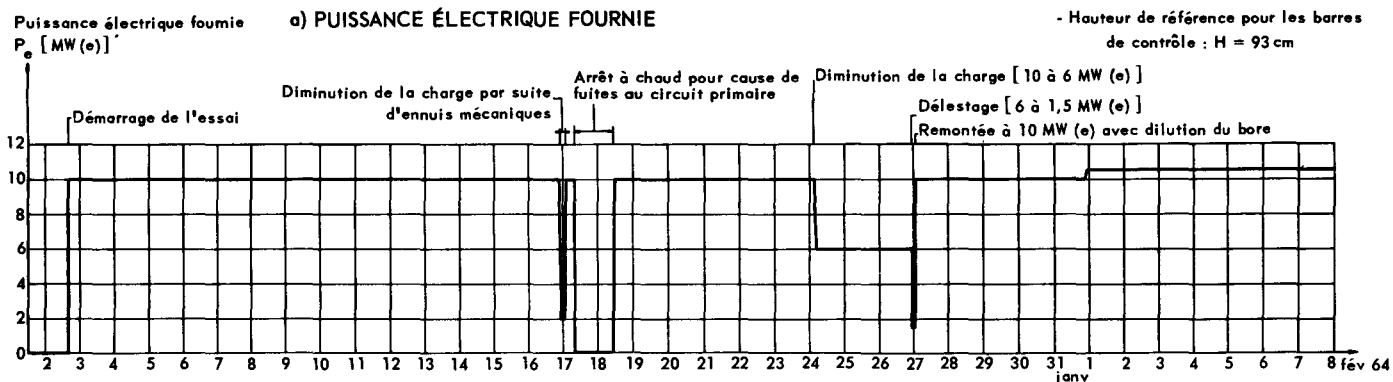


Figure 1. Marche du réacteur BR3 en présence de 400 ppm de bore.
 Partie c) Réactivité—Courbe A: burn-up: 110 EFPH = 0,123% $\delta k/k$ (100 ppm = 1% $\delta k/k$), Sm: 1 000 EFPH = 0,2% $\delta k/k$; courbe B, Burn-up: 110 EFPH = 0,1% $\delta k/k$ (100 ppm = 1% $\delta k/k$), Sm: 1 000 EFPH = 0,2% $\delta k/k$

hypothèses extrêmement pessimistes, aucune température limite du combustible et de l'eau n'est atteinte. Cependant, afin de se prémunir contre des variations « inexplicables » de la réactivité, l'exploitant fixe une limite (0,65 % $\delta k/k$ en 24 heures) à de telles variations. Cette limite n'est jamais atteinte au cours des essais, ainsi qu'en témoigne la fig. 1, extraite des documents BLG 205 et 262 [2].

Essais réalisés

Ces essais ont été réalisés par étapes successives afin de connaître la répercussion de chacune des modifications introduites dans le fonctionnement des systèmes.

1. Marche préalable à puissance normale, sans purification par le déminéraliseur à lit mélangé, les résines échangeuses d'ions n'étant pas saturées en ions BO_3^{3-} et, de ce fait, ne pouvant pas être utilisées pendant le fonctionnement avec bore.

2. Marche préalable à la puissance normale sans utilisation du déminéraliseur, avec réduction du pH de 9,5 à 7 environ.

Pendant ces deux étapes préalables, l'augmentation de l'activité de l'eau primaire, d'ailleurs prévisible, est loin de conduire aux limites admissibles. L'activité de l'air, elle aussi, reste partout en dessous des concentrations maximales admissibles.

3. Marche en puissance, l'eau du circuit primaire contenant 125 ppm de bore. Ce premier pas dans l'étude du contrôle chimique permet de déterminer l'effet global du « by-passage » du déminéraliseur, de la réduction du pH et de la présence de bore dans l'eau du circuit primaire. Il donne des renseignements sur l'évolution des caractéristiques chimiques des eaux, de la concentration en bore, de la réactivité du noyau (cœur) et sur la possibilité de compenser l'empoisonnement Xe.

4. Marche en puissance avec une concentration en bore plus élevée (350 ppm) dans l'eau du circuit primaire.

Cette dernière étape, réalisée après un changement de configuration du noyau permet de pousser l'étude plus loin :

- Démarrage et montée en puissance des installations en présence de bore ;
- Compensation totale de l'effet Xe par réduction de la concentration en bore ;
- Fonctionnement en puissance, toutes les barres de contrôle étant hors du noyau à l'exclusion de deux barres de pilotage ;
- Compensation de l'empoisonnement Sm et de l'usure du combustible par élimination de bore. En outre, différents délestages et montées rapides en puissance permettent de tester le comportement dynamique du réacteur.

Ici encore, la réactivité du noyau, la concentration du bore, les produits en solution ou en suspension dans l'eau primaire, ainsi que les caractéristiques physico-chimiques et la radioactivité de cette eau sont systématiquement suivis pendant et après les essais.

Examen des résultats obtenus

Caractéristiques physico-chimiques et radiochimiques de l'eau primaire (tableau 1).

Evolution du pH

Le pH suit régulièrement les variations de la concentration en bore. Il est assez sensible à la présence de quelques traces de lithium et d'ammoniac.

Evolution des constituants chimiques en solution

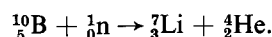
a) *Bore*.—L'acide borique ne paraît pas se décomposer : en effet, des analyses faites par des méthodes différentes, l'une déterminant la concentration du bore sous forme d'acide borique uniquement, l'autre déterminant la concentration du bore sous ses différentes formes, donnent des résultats identiques.

b) *Chlorure*.—La concentration en chlorure fluctue sans jamais atteindre la valeur maximale admissible de 0,1 mg Cl^- par litre.

c) *Silice*.—La silice—sous forme colloïdale—serait introduite dans le circuit avec l'eau déminéralisée d'appoint. En marche normale, avec déminéraliseur et à pH élevé, la silice passerait en solution avec une vitesse de réaction suffisamment faible pour être retenue sur l'échangeur d'ions au fur et à mesure de sa dissolution. Ces conditions n'étant pas réalisées lors des présents essais, la teneur en silice s'accroît et se maintient à un niveau relativement élevé.

d) *Oxygène*.—La teneur en oxygène est toujours restée nulle au cours des différents essais. Rappelons, à ce sujet, que la quantité d'hydrogène contenue dans l'eau du circuit primaire s'élève à 25 à 35 cm^3/kg .

e) *Lithium*.—La concentration du lithium, qui est utilisé en fonctionnement normal comme régulateur de pH, avait été abaissée à une valeur non détectable afin de contrôler sa production éventuelle par la réaction nucléaire



Aussitôt après l'addition d'acide borique et avant la criticité de réacteur, la concentration du lithium remonte à 100 $\mu\text{g}/\text{l}$ par remise en solution des dépôts fixés aux parois. Cet accroissement subit de la teneur en lithium a empêché toute possibilité de bilan de la production de lithium à partir du bore 10.

f) *Sodium*.—Le sodium présent dans l'eau primaire provient d'impuretés contenues dans l'acide borique.

g) *Ammoniac*.—De l'ammoniac se forme à partir de l'azote présent dans l'eau d'appoint sous l'action du flux neutronique ; cette formation est, en régime, prépondérante par rapport à la décomposition radiolytique sous l'action du flux gamma. Des transitoires de charge provoquent en conséquence des variations de concentration, par suite de la modification du rapport de ces flux.

h) *Nitrates et nitrites*.—Si les teneurs en nitrites sont restées nulles, les nitrates n'ont pas pu être dosés en présence d'acide borique par la méthode d'analyse habituellement utilisée.

i) *Fer et autres constituants de l'acier inoxydable*.—La quantité de fer soluble à bas pH est assez importante ; elle diminue lorsque le pH augmente, à cause de

Tableau I. Analyses chimiques et radiochimiques de l'eau primaire

	Marche avec déminéraliseur sans bore (mesure faite avant déminéraliseur) préalable à l'addition de 350 ppm de bore	Marche avec déminéraliseur sans bore (mesure faite après déminéraliseur) préalable à l'addition de 350 ppm de bore	Marche sans déminéraliseur sans bore préalable à l'addition de 350 ppm de bore	Marche sans déminéraliseur avec 125 ppm de bore	Marche sans déminéraliseur avec 350 ppm de bore	Marche sans déminéraliseur sans bore après retrait des 350 ppm de bore	Marche avec déminéraliseur sans bore après retrait des 350 ppm de bore (mesure faite avant déminéraliseur) ^a	Marche avec déminéraliseur sans bore après retrait des 350 ppm de bore (mesure faite après déminéraliseur) ^a
pH	9,72	9,72	9,70	6,75	6,0	8,12	8,86	8,85
<i>MATIÈRES EN SOLUTION DANS L'EAU PRIMAIRE</i>								
<i>Analyse chimique</i>								
B (mg/l)	0	0	0	113,1	334	2,2	0	0
Cl ⁻ (μg/l)	24	12	80	10	40	0	68	28
SiO ₂ (μg/l)	29	11	300	196	158	254	44	21
O ₂ (μg/l)	0	—	3	0	0	0	0	—
Li ⁺ (μg/l)	780	780	430	100	135	0	180	175
Na ⁺ (μg/l)	8	6	6	120	270	6	0	0
NH ₃ (μg/l)	171	160	220	180	125	208	0	0
NO ₂ ⁻ (μg/l)	0	0	0	0	0	—	—	—
NO ₃ ⁻ (μg/l)	0	0	30	—	—	—	—	—
Fe _{tot} (μg/l)	25	12	12	—	—	38,5	35,5	44
<i>Analyse radiochimique</i>								
Activité sol. (μCi/ml)	7,1 × 10 ⁻²	2,0 × 10 ⁻³	12 × 10 ⁻²	17 × 10 ⁻²	22 × 10 ⁻²	10,9 × 10 ⁻²	6,6 × 10 ⁻²	1,45 × 10 ⁻²
Activité gaz (μCi/ml)	1,4 × 10 ⁻²	1,4 × 10 ⁻²	1,8 × 10 ⁻²	2,1 × 10 ⁻²	2,2 × 10 ⁻²	1,4 × 10 ⁻²	1,4 × 10 ⁻²	1 × 10 ⁻²
¹³¹ I (μCi/ml)	4,4 × 10 ⁻⁴	—	—	1 × 10 ⁻³	6,1 × 10 ⁻⁴	—	—	—
¹³³ I (μCi/ml)	0,8 × 10 ⁻³	0,6 × 10 ⁻³	—	0,86 × 10 ⁻²	1 × 10 ⁻²	—	—	—
⁵⁴ Mn (μCi/ml)	—	—	—	8,4 × 10 ⁻⁴	3,8 × 10 ⁻⁴	—	—	—
²⁴ Na (μCi/ml)	1,3 × 10 ⁻³	—	—	0,8 × 10 ⁻¹	1,5 × 10 ⁻¹	—	—	—
¹³³ Xe (μCi/ml)	1,1 × 10 ⁻³	2,0 × 10 ⁻³	—	—	1,6 × 10 ⁻³	—	—	—
¹³⁵ Xe (μCi/ml)	2,0 × 10 ⁻³	1,1 × 10 ⁻³	—	—	1 × 10 ⁻²	—	—	—
¹⁴⁰ La (μCi/ml)	—	—	—	—	3,3 × 10 ⁻⁴	—	—	—
¹⁸ F (μCi/ml)	5,5 × 10 ⁻²	2,6 × 10 ⁻⁴	—	—	—	—	—	—
⁴¹ A (μCi/ml)	1,6 × 10 ⁻³	4,4 × 10 ⁻³	—	—	—	—	—	—
<i>MATIÈRES EN SUSPENSION DANS L'EAU PRIMAIRE</i>								
<i>Analyse chimique</i>								
Mat. en susp. (ppb)	—	2,1	4,2	0,42	2,25	—	—	—
Fe (%)	—	46,5	65	71	59	—	—	—
Ni (%)	—	2,6	0	0,9	1,7	—	—	—
Cr (%)	—	1,84	2,5	1,2	1,6	—	—	—
Mn (%)	—	1,82	—	0	0	—	—	—
B (%)	—	0	—	—	6,65	—	—	—
<i>Analyse radiochimique</i>								
⁵⁹ Fe (μCi/mg Fe)	—	1,28 × 10 ⁻¹	—	1,23	0,07	0,67	1,02	—
⁵⁸ Co (μCi/mg Fe)	—	1,42 × 10 ⁻¹	—	1,33	2,6	2,60	3,60	—
⁶⁰ Co (μCi/mg Fe)	—	2,85 × 10 ⁻¹	—	0,65	0,69	0,93	1,76	—
⁵¹ Cr (μCi/mg Fe)	—	2,3 × 10 ⁻¹	—	5,7	45	3,40	8,65	—
⁵⁴ Mn (μCi/mg Fe)	—	0,75 × 10 ⁻¹	—	2,55	0,65	0,8	1,27	—
^{110m} Ag (μCi/mg Fe)	—	1,50 × 10 ⁻¹	—	0,27	6,8	0,014	0,098	—

^a Ces colonnes donnent les valeurs relevées après purge du bore, mais avant addition de LiOH pour la correction du pH.

^b Ces chiffres ne sont pas directement comparables à ceux résultant de l'essai avec 350 ppm de bore. En effet, contrairement aux autres éléments de ce tableau, les données relatives aux analyses radiochimiques des matières en suspension, préalables à l'essai à 350 ppm de bore, diffèrent sensiblement des mêmes données à la veille de l'essai à 125 ppm de bore, qui sont données ci-dessous:

	Avec démin. sans bore	Sans démin. sans bore
⁵⁹ Fe	0,67	1,02
⁵⁸ Co	2,60	3,60
⁶⁰ Co	0,93	1,76
⁵¹ Cr	3,40	8,65
⁵⁴ Mn	0,8	1,27
^{110m} Ag	0,014	0,098

la formation d'hydroxydes peu solubles. On constate également la présence de manganèse en solution pour des pH voisins de 6; celui-ci passe sous forme d'hydroxydes lorsque le pH croît. Le chrome et le nickel ne sont généralement pas détectables.

Evolution des matières en suspension

Ainsi que le laissent prévoir les courbes de solubilité des hydroxydes, on constate le passage en solution de fer et de manganèse tandis que les autres métaux constitutifs de l'acier inoxydable continuent à se retrouver sous forme filtrable.

Evolution des éléments radioactifs solubles

Cette activité augmente rapidement au début de

l'essai et se stabilise à une nouvelle valeur correspondant à 0,24 μCi/ml environ, approximativement triple de l'équilibre atteint lorsque les résines sont en service. Cette variation est due à: a) la mise hors service de l'échangeur d'ions; les produits de fission ne sont plus éliminés (¹³¹I, ¹³³I, etc.) et atteignent un nouvel équilibre, de valeur plus élevée; b) la formation de ²⁴Na provenant de l'activation du Na présent comme impureté de l'acide borique; c) la présence de ⁵⁸Co, ⁵⁴Mn, ⁵⁶Mn provenant de la dissolution des matières en suspension.

Evolution des matières en suspension

Le fonctionnement à bas pH provoque, comme il

fallait s'y attendre, la libération des produits de corrosion déposés sur les parois en acier inoxydable et leur passage progressif en solution. On y retrouve les composants de l'acier inoxydable (par exemple ^{51}Cr) ainsi que l'isotope $^{110}\text{Ag}^m$, résultant de l'attaque des barres de contrôle Ag-In-Cd à travers les défauts du recouvrement en nickel. De nombreuses mesures ont permis de vérifier que la concentration en bore des matières en suspension reste extrêmement faible.

Variation de réactivité

Pendant la marche en régime ou lors de transitoires, la réactivité varie de façon limitée dans les deux sens, mais toujours très lentement (un facteur 2 ou 3 est toujours conservé vis-à-vis de la limite fixée).

Le graphique donné à la figure 1 montre l'évolution, en fonction du temps, de la disparition « inexplicable » de réactivité lors de l'essai à 350 ppm de bore. Ce terme désigne la différence entre, d'une part, la valeur déduite expérimentalement de la position des barres et de la concentration du bore et, d'autre part, la valeur prédéterminée à partir d'une position de référence, en tenant compte d'un taux dépuisement constant du combustible tout au long de l'essai, du coefficient de puissance et des empoisonnements Xe et Sm. Aucune explication certaine n'a pu être donnée pour ces variations; on peut tout au plus émettre l'hypothèse d'une adaptation progressive du noyau du réacteur à son nouvel environnement tant au point de vue empoisonnement (Xe et Sm) qu'au point de vue thermique et métallographique.

D'autre part, ces variations sont en partie imputables aux approximations faites et au manque de précision inhérent aux méthodes de mesure employées. Citons entre autres:

a) L'étalonnage des barres a été fait dans un noyau boré, mais à puissance nulle et sans xénon, c'est-à-dire dans un environnement bore seul, qui, du fait de sa répartition uniforme, donne une forme de flux plus pointue au centre du noyau que l'environnement borexénon et donc une importance spécifique trop grande aux barres de pilotage.

b) La position des barres n'est définie qu'avec une précision de ± 1 cm (ce qui correspond, en équivalent bore, à 5 ppm), tandis que la mesure de la concentration du bore se fait avec une précision de l'ordre de 1 ppm.

c) La distribution de flux et la répartition du xénon changent avec la position des barres, c'est-à-dire avec le niveau de puissance et la concentration du bore. On conçoit dès lors que la valeur de la disparition inexplicable de réactivité soit plus forte dans les 48 heures qui suivent un transitoire que lorsque le réacteur est stabilisé depuis plus de deux jours.

Influence sur les coefficients de température et de puissance

La diminution du coefficient de température du modérateur (de l'ordre de 15%) due à la forte concentration du bore n'a pas d'incidence fâcheuse sur le comportement dynamique du réacteur. Un délestage,

réalisé sans déplacement des barres de contrôle, a permis de s'en rendre compte. Le coefficient de puissance est inchangé.

Variation de la concentration du bore

La concentration du bore est modifiée à différentes reprises, au cours des essais, pour compenser l'épuisement du combustible, les transitoires Xe et Sm et les modifications lentes de charge. La dilution s'opère aisément et ne pose aucun problème particulier. Il semble cependant que le bore ait tendance à se concentrer progressivement dans le pressuriseur. Ceci ne constitue en aucun cas un inconvénient majeur.

Les analyses chimiques de l'eau et le bilan de réactivité après élimination du bore montrent qu'il n'y a pas rétention dans le noyau ou le circuit primaire.

Conclusions des essais de marche en puissance avec contrôle chimique

Ces essais permettent notamment de se rendre compte de la sécurité de ce procédé comme système de compensation de la réactivité:

1. Les variations « inexplicables » de réactivité sont toujours restées d'amplitude limitée. Elles se développent lentement, beaucoup plus lentement qu'un transitoire dit « lent » comme l'empoisonnement Xe. Il a toujours existé un rapport minimal de 2 à 3 entre leur vitesse de changement et la valeur de $0,65 \delta k/k$ par jour admise comme étant la limite au-delà de laquelle l'essai devait être interrompu. Un système de contrôle normal pourra donc les compenser facilement.

D'autre part, ces variations de réactivité ne dépendent pas proportionnellement de la concentration du bore. On pourrait donc envisager de fonctionner avec des concentrations bien supérieures, si toutefois la diminution du coefficient de température ne l'empêche pas.

Des variations inexplicables de réactivité se produisent d'ailleurs en fonctionnement sans bore.

Enfin, ces pertes de réactivité sont temporaires; on les récupère intégralement après l'élimination du bore. Un bilan de perte de réactivité en fonction du temps a permis de vérifier ce fait.

2. Aucune variation brusque et importante de la concentration du bore ne se produit. La concentration dans le pressuriseur est cependant toujours plus forte que dans le reste du circuit primaire.

3. Le bore ne s'incruste pas de façon appréciable à l'intérieur du cœur ou sur les parois des tuyauteries.

4. L'évolution du pH ne pose pas de problème particulier pendant le fonctionnement. L'acide borique étant un acide très faible, les hydroxydes LiOH et NH_4OH , même en faible concentration, ont une influence non négligeable sur le pH.

5. La corrosion de l'acier inoxydable ne pose pas de problème. Seules les barres de contrôle Ag-In-Cd gainées au nickel sont attaquées de façon plus importante lors d'une marche avec bore.

6. L'activité de l'eau primaire reste inférieure aux limites admises, bien que le déminéraliseur soit resté

hors service pendant plus de six semaines. L'activité ambiante reste normale également.

CONCEPTION DES CIRCUITS HYDRAULIQUES DES RÉACTEURS PWR CONTRÔLÉS PAR POISON SOLUBLE

Exposé du problème

Il serait judicieux de chercher à simplifier les circuits auxiliaires, tout en les adaptant aux sujétions du contrôle chimique, ce qui nécessite de repenser chaque fonction à la lumière des résultats d'expérimentation et d'exploitation.

Nous n'examinerons que le cas où le poison soluble est un composé de bore, sans perdre de vue que d'autres éléments pourraient être envisagés (Cd, terres rares, etc.).

La concentration des effluents et leur élimination est relativement onéreuse si l'on désire dimensionner les installations en fonction des hypothèses généralement admises pour le calcul d'un réacteur à eau sous pression, à savoir 1% de gaines défectueuses d'éléments de combustible. D'autre part, le contrôle chimique d'une centrale d'une puissance de l'ordre de 250 MW(e) conduit à éliminer annuellement 2 à 10 t d'acide borique, selon le programme d'exploitation (variations de charges, arrêts).

Le nombre nécessaire de fûts blindés pour évacuer ces résidus solides dépend soit de la quantité de produits de fission libérés dans l'eau primaire si celle-ci est importante, soit de la quantité de BO_3H_3 si la contamination est faible. Etant donné la haute qualité technologique des combustibles actuellement fabriqués et en service, les fissures de gaine sont extrêmement rares et l'eau primaire est peu radioactive. Dans ce cas, afin de réduire le nombre de fûts actifs, il faut tenter de séparer BO_3H_3 des produits de fission et des produits de corrosion.

Procédés de concentration

La concentration des impuretés contenues dans les effluents, telles que acide borique, produits de fission et de corrosion, peut être obtenue par plusieurs procédés:

Distillation

Le choix du type d'appareil sera guidé par des considérations techniques et économiques, dépendant principalement des volumes à traiter. Si les variations de charge sont contrôlées à l'aide d'acide borique, les volumes à traiter sont relativement élevés, et il est recommandé d'utiliser un type de distillateur d'exploitation peu coûteuse. Parmi ceux-ci, le type à recompression de la vapeur est utilisé notamment à Shippingport aux Etats-Unis, et prévu pour la centrale SELNI en Italie. La distillation à simple effet, d'un coût d'investissement plus réduit, présente certains avantages de simplicité de conception et d'exploitation, et il peut se justifier si les volumes à traiter ne sont pas trop importants et si le coût de la calorie-vapeur disponible est relativement faible (soutirage à la turbine par exemple).

On pourrait envisager également de greffer le distillateur sur le circuit primaire en mettant à profit les différences de pression et de température y existant, les consommations de calories étant ainsi réduites au minimum.

Electrodialyse

Ce procédé consiste essentiellement à faire migrer les ions dans un champ électrique et à les isoler ensuite à l'aide de parois de perméabilité sélective. Quoique connu de longue date, il n'a été développé que récemment. Les progrès de sa technologie ont permis ces dernières années de réaliser des installations industrielles.

Si l'électrodialyse s'avère pratiquement applicable à la séparation d'acide borique, on en retirerait les avantages suivants: a) un coût très faible pour le traitement des effluents, la consommation d'énergie électrique étant minime; b) la possibilité de traiter directement toute du purge circuit primaire en réduisant sensiblement le volume des réservoirs d'effluents et d'eau d'appoint ainsi que la station de traitement des effluents; c) la possibilité de récupérer l'acide borique ainsi concentré et de réduire la quantité des résidus radioactifs solides.

Echange d'ions

Ce procédé n'est économiquement acceptable pour l'enlèvement de l'acide borique que si sa concentration est faible. Etant donné que, pour traiter des effluents à haute concentration, un autre procédé est nécessaire, plus celui-ci sera économique, moins la présence d'un déminéraliseur sera justifiée.

Purification de l'eau primaire

La purification, telle qu'elle est généralement conçue pour les réacteurs à eau sous pression, suffit à diminuer la concentration des substances radioactives à un niveau acceptable, même si 1% des éléments de combustible est endommagé [3]. Cette hypothèse paraît pessimiste à la lumière de l'expérience acquise dans de nombreux réacteurs. Si la proportion d'éléments défectueux est inférieure à 1‰, la purification n'est plus indispensable, et l'échange ionique tel qu'utilisé actuellement peut être abandonné. Cependant outre leur fonction d'échange, les déminéraliseurs jouent vis-à-vis des produits de corrosion le rôle de filtres, par ailleurs difficilement colmatables. Ces produits se présentent, en général, sous forme d'oxydes et d'hydroxydes en grande partie insolubles, se déposant sur les parois des équipements dont ils restreignent l'accessibilité. Leur extraction est donc indispensable et peut être effectuée simplement sur des filtres adéquats, placés par exemple en dérivation sur une des pompes de circulation du circuit primaire.

De plus, l'enlèvement du bore par purge du fluide primaire constitue un moyen de déconcentration supplémentaire qui peut être suffisant du point de vue des produits de fission, lorsque le nombre d'éléments défectueux est relativement faible.

Déchets solides

Le contrôle de la réactivité par poison dissous

entraîne la manipulation de quantités importantes de boues après concentration des effluents. Si la radioactivité de l'eau primaire est élevée, la totalité des boues doit être traitée comme résidu radioactif, nécessitant un nombre élevé de fûts. L'insolubilisation et la prise en masse de ces boues posent certains problèmes. Leur incorporation à du bitume plutôt qu'à du ciment pourrait y apporter une solution intéressante, tout en réduisant le nombre de fûts. Si au contraire, ainsi que le montre l'expérience acquise, on pouvait réduire les valeurs maximales supposées pour le pourcentage de défauts d'éléments de combustible on pourrait: soit réutiliser tel quel l'acide borique reconcentré; soit le séparer des produits radioactifs par précipitation. Le nombre de fûts de déchets radioactifs s'en trouverait fortement réduit. Des essais ont montré qu'une telle précipitation pouvait être effectuée sans entraînement de produits radioactifs.

CONCLUSIONS

Les expériences effectuées sur le réacteur BR3 ainsi que sur d'autres réacteurs à eau sous pression ont montré la facilité et la souplesse de fonctionnement du contrôle de la réactivité par acide borique dissous

même avec des installations qui n'avaient pas été spécialement prévues à cet effet. Aucun inconvénient marquant n'a été rencontré des points de vue: du contrôle de la réactivité; de la stabilité et de la sécurité du fonctionnement du réacteur; de la corrosion de l'acier inoxydable.

Néanmoins, le contrôle chimique du réacteur peut conduire à la production de quantités d'effluents liquides et résidus solides assez élevées; il serait souhaitable d'avoir recours à des méthodes de traitement et de séparation susceptibles de réduire les coûts d'investissements et d'exploitation correspondants. Ces simplifications d'équipements semblent d'autant plus facilement réalisables que l'hypothèse de calcul choisie comme fraction d'éléments de combustible défectueux est faible.

BIBLIOGRAPHIE

1. Rapport BLG 261: *Résultats de la 1^{re} année de fonctionnement de la centrale BR3.*
2. Rapports BLG 205 et 262: *Essai de marche en puissance de la centrale nucléaire BR3 en présence de bore dans le circuit primaire (1^{re} et 2^e parties).*
3. Proksch E. *Purification of reactor moderator—coolants*, Revue d'Energie Atomique, Vol. 1, n° 1, p. 5.

ABSTRACT—RÉSUMÉ—АННОТАЦИЯ—RESUMEN

A/518 Belgium

Practical results and prospects for the use of a soluble poison in the pressurised-water reactors

By M. Plumier *et al.*

The control by chemical shim is going to play an important role in the economics of pressurised-water reactor operation. The homogeneous poisoning of the primary circuit water, avoiding the perturbing action of control rods, allows a more uniform distribution of the neutron flux; it opens the way towards a large initial investment of reactivity, and leads to an increase of the core life-time.

Chemical shim is provided in the pressurised-water plants now being erected or planned; it will compensate for the fuel burn-up and follow the slow transients, such as those resulting from the xenon effect. The combination of the nuclear and chemical properties of the boric acid designates it as poison.

This paper covers, in the first part, the problems encountered with boron during the power operation of the BR3 plant and, in the second part, the influence of this type of control on the design and the operation of the pressurised-water type plants, as well as in the treatment of radioactive wastes.

Power operation of the BR3 plant with boron in the primary loop

After analogue computer studies and preliminary

tests proved that power operation using boron was safe, two series of tests were run successively; the first one with 125 ppm, the second one with 350 ppm of boron (in boric acid form) dissolved in the water. Most practical cases have been covered: power operation at fixed load; operation at reduced load; slow and fast load transients; slow reactivity transients; especially the xenon effect without rod displacement.

The paper describes some of the problems encountered and gives, with comments, the results of the tests showing the evolution of the primary loop parameters (reactivity, water chemistry, activities).

Influence of the circuits

The introduction of the chemical shim did not radically modify the auxiliary circuits of the reactors now being designed. However, it seems desirable to review the whole of the hydraulic circuits, especially the purification and the waste treatment system.

Some solutions of the purification system problem are discussed in connection with the various methods of boric acid removal.

Furthermore, feed and bleed needed for boric acid dilution increase the quantities of liquid wastes. The paper discusses the problem of the boric acid removal, either by concentration and separation (different methods are suitable: single pass distillation or vapour recompression, demineralization, electro-dialysis, or by controlled disposal, after storage and dilution.

A/518 Бельгия

Практические результаты и перспективы применения поглотителя в растворе в ядерных реакторах с водой под давлением

M. Плюмье *et al.*

Химический контроль призван играть все более важную роль в экономике эксплуатации атомных электростанций с реакторами, охлаждаемыми водой под давлением. Гомогенный поглотитель в воде первичного контура позволяет получить более однородный поток нейтронов, устраняя нарушающее действие регулирующих стержней; он дает возможность увеличивать начальный вклад реактивности и таким образом приводит к увеличению срока службы активной зоны.

Химическое регулирование предусматривается для атомных электростанций типа с водой под давлением, строящихся или проектируемых в настоящее время; оно позволит компенсировать истощение топлива и будет следить за медленными переходными режимами мощности, возникающими в результате эффекта ксенона. В качестве поглотителя была выбрана борная кислота благодаря сочетанию ее ядерных и химических свойств.

В первой части доклада рассматриваются проблемы, возникшие во время испытаний на мощности атомной электростанции BR-3 при наличии бора; во второй части — особенности, которые вводит этот метод регулирования в конструкцию и эксплуатацию атомных электростанций такого типа, а также в методы переработки жидких радиоактивных отходов.

А. Эксплуатация на мощности атомной электростанции BR-3 в присутствии бора в первичном контуре

После того как исследования на счетно-решающих машинах и предварительные испытания эксплуатации показали, что работа реактора на мощности в присутствии бора совершенно безопасна, последовательно были проведены две серии испытаний: одна — при наличии 125 частей бора на миллион и вторая — при наличии 350 частей бора на миллион (в виде борной кислоты), растворенного в воде первичного контура. Исследовались случаи, наиболее возможные на практике:

- работа на мощности при постоянной нагрузке;
- работа при сокращенной нагрузке;
- медленные или быстрые изменения нагрузки;
- медленные изменения реактивности; в частности, можно было проследить эффект ксенона без перемещения стержней.

В докладе описываются некоторые возникшие проблемы, приводятся результаты испытаний с комментариями и описываются изменения параметров первичного контура (реактивность, химия воды, радиоактивность).

В. Влияние на контуры

Введение химического регулирования не привело к большим изменениям во вспомогательных контурах проектируемых реакторов. Однако представляет интерес рассмотреть в совокупности гидравлические контуры и особенно системы очистки и переработки радиоактивных отходов.

Приводятся некоторые решения проблемы очистки в зависимости от различных методов выделения борной кислоты.

Кроме того, значительно увеличиваются количества отходов в результате последовательных разбавлений, необходимых для удаления бора. В докладе рассматривается проблема удаления борной кислоты методом концентрации и разделения (можно применять различные методы: простое выпаривание или со сжатием, деминерализация, электродиализ, осаждение) или контролируемый сброс после хранения и разбавления.

В конце рассматривается экономика этого метода.

A/518 Bélgica

Resultados prácticos y perspectivas del empleo de veneno en solución en los reactores de agua a presión

por M. Plumier *et al.*

El control químico habrá de desempeñar un papel de creciente importancia en la explotación económica de las centrales nucleoelectricas del tipo de agua a presión. El envenenamiento homogéneo del agua del circuito primario permite repartir con mayor uniformidad el flujo neutrónico al eliminar la acción perturbadora de las barras de control: hace posible una inversión inicial más elevada de reactividad y conduce así a un aumento de la vida útil del núcleo del reactor.

En las centrales del tipo de agua a presión que actualmente se construyen o proyectan, está previsto un control químico que permitirá compensar el agotamiento del combustible y seguir variaciones lentas como las debidas al efecto del xenón. Como veneno se ha escogido el ácido bórico debido a la combinación de sus propiedades neutrónicas y químicas.

En la primera parte, la memoria examina los problemas que se han planteado durante los ensayos de funcionamiento en carga de la central nuclear BR3 en presencia de boro y, en la segunda parte, las

particularidades que este procedimiento: de control introduce en la concepción y la explotación de las centrales de este tipo y en el tratamiento de los efluentes radiactivos.

Funcionamiento en carga de la central nuclear BR3 en presencia de boro en el circuito primario

Los estudios analógicos y los ensayos preliminares de explotación mostraron que el funcionamiento en carga en presencia de boro era posible en condiciones de perfecta seguridad; por consiguiente, se han realizado dos series sucesivas de ensayos, uno con 125 y otro con 350 partes por millar de boro disuelto en el circuito primario (en forma de ácido bórico). Se ha examinado la mayor parte de los casos que podrían presentarse en la práctica: funcionamiento a carga constante; funcionamiento a carga reducida; variaciones lentas o rápidas de la carga; variaciones lentas de la reactividad; se ha podido seguir el efecto del xenón sin desplazar las barras de control.

La memoria señala algunos de los problemas que se han encontrado, indica y comenta los resultados de los ensayos, y describe la evolución de los parámetros

del circuito primario (reactividad, química del agua, actividades).

Influencia sobre los circuitos

La introducción del control químico no entrañó modificaciones fundamentales en los circuitos auxiliares de los reactores en proyecto. Sin embargo, parece interesante revisar el conjunto de los circuitos hidráulicos y, en particular, los sistemas de purificación y tratamiento de los desechos radioactivos.

La memoria presenta algunas soluciones del problema de la purificación en función de los diversos métodos de separación del ácido bórico.

Por otra parte, las diluciones sucesivas que exige la eliminación del boro han hecho aumentar notablemente las cantidades de desechos. La memoria examina el problema de la eliminación del ácido bórico, sea por concentración y separación (lo que puede efectuarse por diversos métodos: evaporación simple o con recompresión, desmineralización, electrodiálisis, precipitación), sea por eliminación controlada después de un almacenamiento y dilución.

Por último se examinan los aspectos económicos del procedimiento.

Les caissons en béton précontraint des réacteurs français de la filière uranium naturel – graphite – gaz carbonique

par G. Lamiral *, L. Laurent *, R. Bonnelle *, N. Beaujoint * et P. Faurot **

Lors des études d'avant-projet des premières centrales nucléaires françaises de la filière uranium naturel – graphite – gaz carbonique, le manque d'expérience en matière de construction de très grandes enceintes sous pression et les avantages techniques et économiques respectifs des diverses solutions en présence justifiaient la mise en concurrence de ces solutions.

Cette mise en concurrence fut favorable à la solution « béton précontraint » pour les caissons des réacteurs des centrales G2, G3 de Marcoule; par contre, elle fut favorable à la solution « acier » pour les caissons des centrales EDF1 et EDF2 de Chinon.

Pour la centrale EDF3 de Chinon la conjoncture avait évolué; les centrales de Marcoule étaient en service, et les constructeurs de caissons en béton précontraint avaient pu tirer les enseignements de la construction de ces centrales; par ailleurs, les constructeurs de caissons en acier avaient une connaissance exacte des difficultés liées à la construction de grandes capacités sous pression en acier: la mise en concurrence fut favorable au béton précontraint et une solution sensiblement différente de celle de Marcoule fut adoptée.

Pour la centrale EDF4 de Saint-Laurent-des-Eaux et les centrales suivantes, la mise en concurrence des deux solutions « béton » et « acier » aurait certainement été envisageable si la décision n'avait été prise pour ces centrales d'intégrer les échangeurs dans le caisson du réacteur.

L'augmentation des dimensions des caissons liée à cette intégration proscrit l'adoption de solutions « acier »: les solutions « béton précontraint » sont les seules envisageables, et dès lors l'évolution de la filière uranium naturel – graphite – gaz carbonique se trouve étroitement liée à l'évolution de la technique de construction des caissons en béton précontraint.

CAISSON DE LA CENTRALE EDF3 DE CHINON (fig. 1)

Les caissons en béton précontraint des réacteurs des centrales G2, G3 de Marcoule, construits entre 1956 et 1960 par le Commissariat à l'énergie atomique

* Electricité de France.

** Commissariat à l'énergie atomique.

Tableau 1. Caissons en béton précontraint des centrales G2, G3 de Marcoule ^a

Puissance thermique du réacteur: 250 MW (thermique).
Pression nominale: 15 bars.
Température entrée CO ₂ : 140 °C.
Température sortie CO ₂ : 350 °C.
Forme du caisson: cylindrique à axe horizontal.
Dimensions extérieures: diamètre, 20 m; largeur hors tout, 33,7 m.
Forme de la cavité intérieure: cylindrique à axe horizontal.
Dimensions de la cavité intérieure: diamètre, 14 m; longueur, 15,7 m.
Nombre et dimensions des ouvertures: face de chargement, 1 200, Ø 107 mm; face opposée, 14, Ø 1,2 m.
Câbles de précontrainte:
Cerces: 57 (797, Ø 5, par câble).
Nombre: tirants longitudinaux: 46 (715, Ø 5, par câble). tirants transversaux: 58 (715, Ø 5, par câble).
Type: monotoron.
Tension à la précontrainte: 1 200 t.
Charge de rupture minimale garantie: 2 200 t.
Type d'ancrage: épanouissement dans culot de béton fretté.
Disposition des câbles: cerces à l'extérieur; autres câbles dans le béton sous gaine métallique.
Protection contre la corrosion: circulation air sec.
Épaisseur de la peau d'étanchéité: 30 mm.
Température maximale admise dans le béton: 50 °C.
Mode de réfrigération: circuit auxiliaire de CO ₂ .
Calorifuge employé: ALFOL entre circuit principal de CO ₂ et circuit auxiliaire.

^a Bureau d'études: Société Coyne et Bellier.

et dont les caractéristiques sont rappelées dans le tableau 1, comportent des câbles de précontrainte de grande puissance (1 200 t) répartis en câbles rectilignes et en cerces, la précontrainte des cerces étant transmise aux caissons par des patins de glissement.

L'expérience de la réalisation de ces caissons a conduit les constructeurs à proposer pour la centrale EDF3 des solutions mettant en œuvre des câbles de puissance sensiblement plus faible et ne nécessitant pas de patins de glissement (tableau 2).

La solution retenue a sensiblement la forme d'un parallépipède de 32,06 m de hauteur: les faces latérales vues en plan forment un carré de 27,45 m dont les angles sont abattus sur 1,59 m; les milieux des faces sont engraisés suivant des arcs de cercle donnant une flèche de 0,8 m pour une corde de 15,54 m.

La cavité intérieure a la forme d'un cylindre de révolution à fonds légèrement coniques et à axe

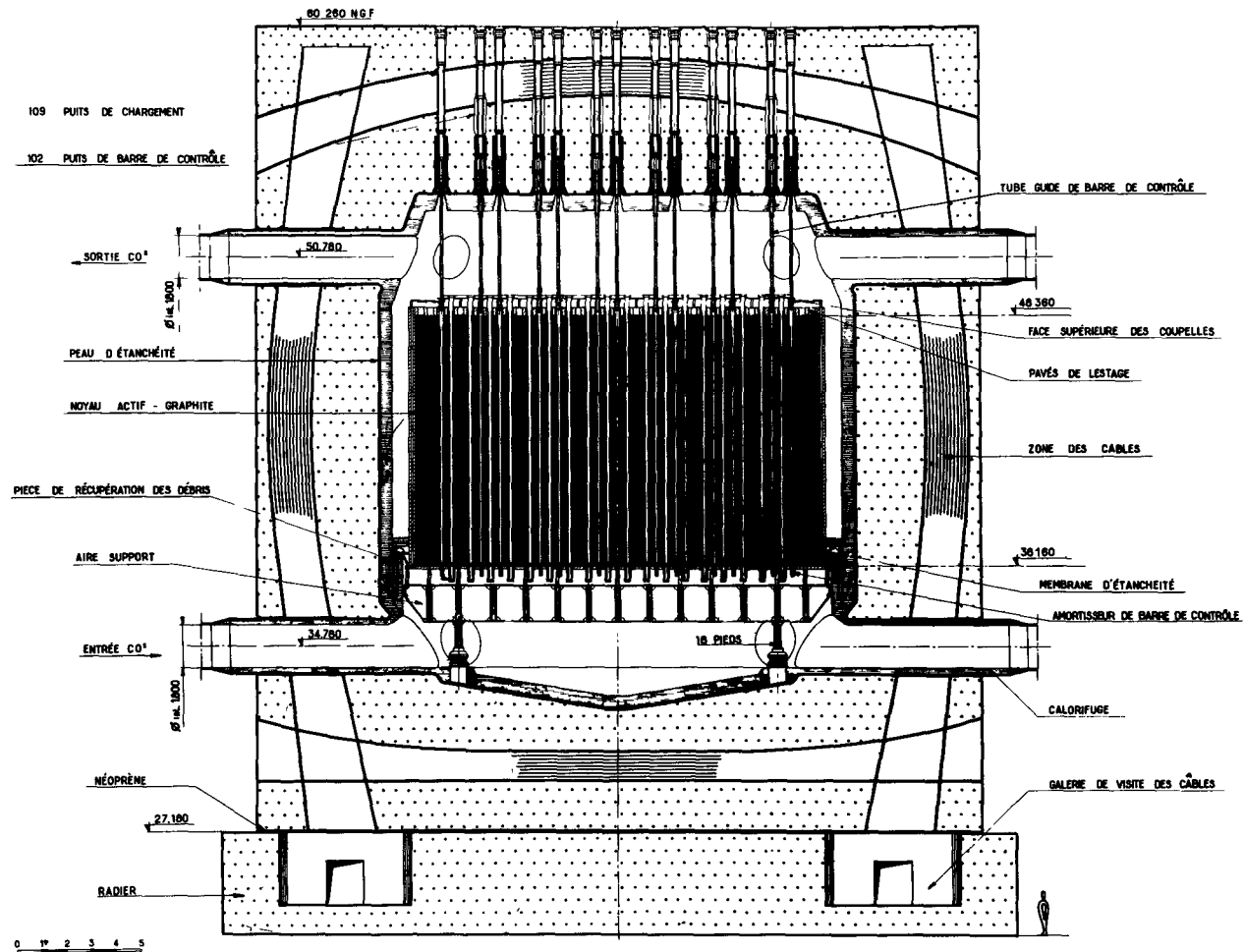


Figure I. Caisson EDF3

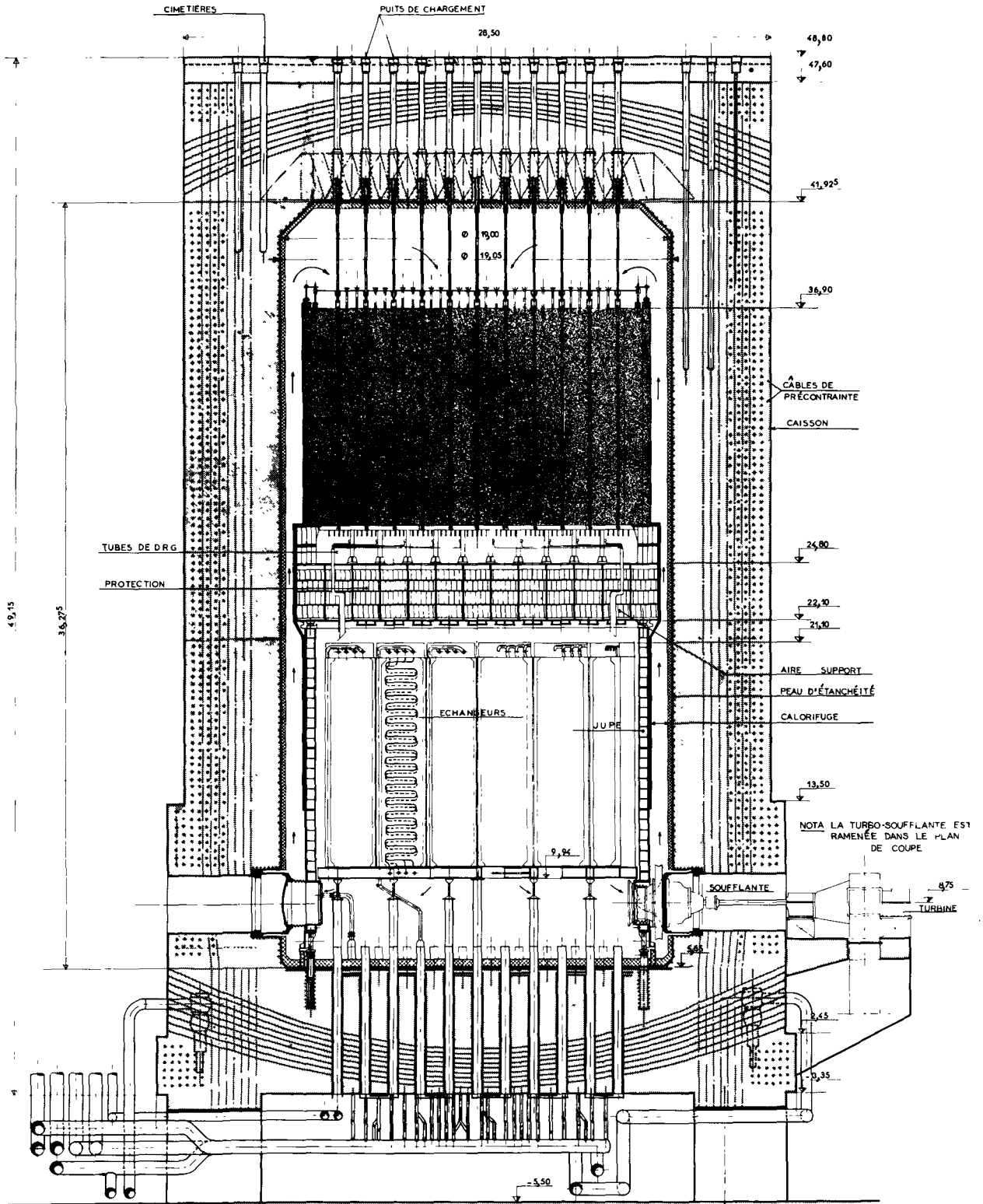


Figure 2. Caisson EDF4

Tableau 2. Caisson en béton précontraint de la centrale EDF3 de Chinon ^a

Puissance thermique du réacteur: 1 560 MW (thermique).
 Pression nominale: 30 bars.
 Température entrée CO₂: 240 °C.
 Température sortie CO₂: 410 °C.
 Forme du caisson: parallélépipédique.
 Dimensions extérieures: 27,45 m × 27,45 m; hauteur, 32,06 m.
 Forme de la cavité intérieure: cylindrique à axe vertical avec parties tronconiques en haut et en bas.
 Dimensions de la cavité intérieure: diamètre intérieur, 19 m; hauteur, 21,09 m.
 Nombre et dimensions des ouvertures: 16 tubulures, Ø 2,2 m; 5 tubulures, Ø 1 m; 211 tubulures, Ø 0,47 m.
 Câbles de précontrainte:
 Nombre: câbles verticaux, 2 360; câbles horizontaux dalles, 2 360; câbles horizontaux fût, 4 000.
 Type: monotoron de 810 mm² de section (61 fils en acier 180 de 4,1 mm de diamètre).
 Tension à la précontrainte: 115 t.
 Tension utile: 95 t.
 Charge de rupture minimale garantie: ≥ 130 t.
 Type d'ancrage: SEEE à manchon filé.
 Disposition des câbles: dans le béton, sous gaine métallique.
 Protection contre la corrosion: injection de coulis de ciment.
 Épaisseur de la peau d'étanchéité: 25 mm.
 Température maximale admise dans le béton: 75 °C.
 Mode de réfrigération: circulation de liquide organique dans des tubes en demi-lune soudés sur la peau d'étanchéité.
 Calorifuge employé: béton de ponce avec casing dilatable étanche en acier inoxydable.

^a Bureau d'études: Société d'études et d'équipement d'entreprises.

vertical, dont les angles supérieurs et inférieurs sont abattus par des goussets tronconiques. Le diamètre intérieur est de 19 m et la hauteur de 21,09 m; la cavité est tapissée par une enveloppe en tôle soudée* de 25 mm d'épaisseur, destinée à assurer une étanchéité parfaite.

L'enveloppe est traversée par 16 tubulures de 2,2 m de diamètre pour la circulation du gaz carbonique, par 5 tubulures de 1 m de diamètre pour le passage des tubes de détection de rupture de gaines et des câbles de thermocouples, et la dalle supérieure est traversée par 211 tubulures de 0,47 m de diamètre pour le chargement du combustible et la commande des barres de contrôle.

L'enveloppe est précontrainte par 8 720 câbles en acier du type monotoron antigiratoire à torsions alternatives, formés, chacun, par 61 fils de 4,1 mm de diamètre donnant une section de 810 mm², en acier clair de 170/190 kg/mm² de charge de rupture. La tension unitaire des câbles est de 115 t, donnant, après déduction des pertes par frottement, retrait, fluage, relaxation, une tension résiduelle supérieure à 95 t.

Les ancrages sont réalisés par filage à froid sur les câbles de manchons métalliques cylindriques, à travers la matrice d'un vérin de filage; l'accrochage manchon-câble est assuré par un ressort à spires jointives qui s'imprime dans le manchon et dans le câble au moment du filage. Les manchons des culots

actifs sont filetés après filage; le blocage après mise en tension des câbles est réalisé par des écrous vissés sur les manchons et s'appuyant sur des plaques métalliques circulaires appuyées elles-mêmes sur le béton. Les manchons des culots morts s'appuient directement sur les plaques métalliques.

Ces câbles sont répartis suivant les six faces du parallélépipède; quatre nappes de câbles horizontaux compriment les parois latérales; des câbles verticaux entourent la cavité interne et chaque dalle horizontale contient un réseau de câbles suivant trois directions à 120°. Le tracé de tous ces câbles est légèrement courbe; ils sont tous disposés dans des gaines métalliques à l'intérieur du béton, et une distance minimale a été respectée entre les armatures et les parois internes du caisson de façon que le rayonnement nucléaire reçu par les câbles soit relativement faible et leur température en fonctionnement peu différente de la température ambiante.

CAISSON DE LA CENTRALE EDF4 DE SAINT-LAURENT-DES-EAUX

(fig. 2, tableau 3)

Pour la centrale EDF4 de Saint-Laurent-des-Eaux, l'intégration des échangeurs dans le caisson en béton précontraint pouvait se concevoir suivant différents schémas: schémas à cavités réacteurs et échangeurs

Tableau 3. Caisson en béton précontraint de la centrale EDF4 de Saint-Laurent-des-Eaux ^a

Puissance thermique du réacteur: 1 560 MW (thermique).
 Pression nominale: 30 bars.
 Température entrée CO₂: 225 °C.
 Température sortie CO₂: 400 °C.
 Forme du caisson: prisme droit à section hexagonale.
 Dimensions extérieures: largeur sur plats: 28,5 m en partie haute, 31 m en partie basse; hauteur: 49,15 m.
 Forme de la cavité intérieure: cylindrique à axe vertical avec partie tronconique en haut.
 Dimensions de la cavité intérieure: diamètre 19 m, hauteur: 36,275 m.
 Nombre et dimensions des ouvertures: 6 orifices Ø 3,20 m à l'intérieur, Ø 2,70 m à l'extérieur; 211 trous Ø 0,4 m, et 2 trous d'homme Ø 0,5 m en partie haute; 211 trous Ø 0,4 m en partie basse.
 Câbles de précontrainte:
 Nombre: câbles verticaux, 1 080; câbles horizontaux dalles, 1 566; câbles horizontaux fût, 2 500.
 Type: F 16: 19 torons de 7 fils de diamètre 3,6 mm en acier 190, 6 fils intercalaires de 4,1 mm et 12 fils intercalaires de 2,4 mm.
 Tension de précontrainte: 225 t.
 Tension utile: 185 t.
 Charge de rupture garantie: ≥ 280 t.
 Type d'ancrage: SEEE à manchon filé.
 Disposition: dans le béton, sous gaine métallique.
 Protection contre la corrosion: injection de coulis de ciment.
 Épaisseur de la peau d'étanchéité: 25 mm.
 Température maximale admise dans le béton: 75 °C.
 Mode de réfrigération: circulation d'eau dans des tubes cylindriques soudés sur la peau d'étanchéité.
 Calorifuge employé: béton de ponce.

^a Bureau d'études: Société d'études et d'équipement d'entreprises.

* Acier doux Martin A48C3SR (norme AFNOR NF A 36-205).

séparées; schémas à une seule cavité avec échangeurs disposés autour du réacteur; schémas à une seule cavité avec échangeurs et réacteur superposés.

Les solutions du premier type conduisaient à accoler plusieurs caissons et ne permettaient pas un dessin simple du circuit de CO₂; elles furent éliminées au profit des solutions à «cavité unique» et parmi ces dernières solutions l'étude a finalement fait préférer les solutions du type «superposé» aux solutions du type «concentrique»:

A volume utile égal, les solutions superposées conduisaient à des caissons de 10 à 15% moins coûteux que les solutions concentriques; les problèmes de précontrainte des dalles étaient plus faciles à résoudre; enfin, les caractéristiques de la centrale EDF4 étant identiques à celles de la centrale EDF3, la disposition superposée permettait la reconduction d'un certain nombre de dispositions élémentaires.

Finalement, le caisson du réacteur de la centrale EDF4 de Saint-Laurent-des-Eaux se présente sous la forme d'un prisme droit de section hexagonale de 28,5 à 31 m sur plats et de 49,15 m de hauteur.

La cavité intérieure a la forme d'un cylindre de révolution à fond plat et à axe vertical dont les angles supérieurs sont abattus par des goussets tronconiques; le diamètre intérieur est de 19 m et la hauteur de 36,275 m; la cavité est tapissée par une enveloppe en tôle soudée de 25 ou 35 mm d'épaisseur.

L'enveloppe est traversée par une ouverture provisoire de 2,5 m de diamètre environ destinée à l'introduction des éléments de calorifuge et de l'empilement du réacteur, et par 6 ouvertures de 2,7 m à 3,2 m pour le logement des soufflantes, l'accès et la ventilation à l'arrêt.

La dalle supérieure, identique à celle du caisson de la centrale EDF3, est traversée par 211 tubulures pour le chargement du combustible et la commande des barres de contrôle, 3 tubulures pour les appareils de mesure de puissance (faible flux) et par deux trous d'homme.

La dalle inférieure est traversée également par 211 tubulures pour les entrées d'eau, sorties de vapeur des échangeurs, détection de rupture de gaine et câbles de thermocouples du réacteur. Elle porte la jupe support de l'empilement de graphite par l'intermédiaire de 54 pieds d'appui encastrés de 2,5 m environ.

Les études ont conduit à l'adoption de câbles plus puissants que ceux de la centrale EDF3, et la précontrainte est obtenue par 5 200 câbles ancrés par manchons filetés; leur tension unitaire initiale est de 225 t, donnant une tension résiduelle supérieure à 185 t.

Ces câbles sont répartis suivant les huit faces du prisme; le fût est précontraint horizontalement par familles couvrant chacune deux côtés de l'hexagone du caisson et verticalement par une famille de 1 100 câbles répartis en 7 nappes concentriques. Chaque dalle horizontale contient un réseau de câbles suivant 3 directions à 120°. Le tracé des câbles verticaux est quasi rectiligne; celui des câbles horizontaux du fût et des câbles des dalles est courbe.

BASE DES CALCULS DES CAISSONS EN BÉTON PRÉCONTRAIT

Réglementation en vigueur

Lors des études des centrales de Marcoule et de Chinon, la construction des caissons en béton précontraint n'était pas réglementée en France; la réglementation des appareils à pression de gaz, et notamment le décret du 18 janvier 1943 *, n'intéressait que les «appareils métalliques de production, d'emmagasinage et de mise en œuvre de gaz comprimés», et les constructions en béton précontraint n'étaient soumises qu'aux «instructions provisoires relatives à l'emploi du béton précontraint» de la circulaire n° 141 du 26 octobre 1953 du Ministère des travaux publics **. Cette circulaire, conçue en vue de la construction d'ouvrages d'art, ne s'appliquait que très imparfaitement aux caissons en béton précontraint, et il devenait dès lors indispensable de définir pour ces ouvrages particuliers des conditions de calcul et des conditions de vérification de ces calculs.

Conditions imposées au caisson de la centrale EDF3

Les premières conditions imposées ont concerné le mode de travail du béton du corps du caisson en béton précontraint pur (le coefficient d'homothétie définissant le domaine de sécurité à partir de la courbe intrinsèque étant celui des instructions provisoires de 1953, soit 1/0,28) sous les sollicitations résultant du fonctionnement normal de l'installation, c'est-à-dire sollicitations dues à la pression nominale (30 bars), sollicitations dues à la température en absence de pression et à la pression en absence de température.

Le calcul en phase élastique a été conduit en admettant que l'enveloppe extérieure était constituée d'un anneau cylindrique et de deux disques reliés par deux ceintures annulaires. On a appliqué à ce solide les théories des voiles et plaques minces en tenant compte des corrections dues à l'épaisseur. On a pris pour inconnues intermédiaires du calcul les paramètres définissant les déformations des deux ceintures annulaires, soit la variation du rayon de la fibre moyenne et la rotation de la ceinture autour de la fibre moyenne.

Dans un premier stade de calcul on a déterminé les efforts dans le système en supposant les ceintures indéformables; dans un deuxième stade on a déterminé les efforts sous une déformation quelconque donnée aux ceintures; on a ensuite écrit que les ceintures étaient en équilibre sous l'effet simultané des deux stades ci-dessus. Les équations ont donné la valeur des déformations d'équilibre, donc les efforts dans le système.

* Depuis ce décret, un autre décret en date du 21 septembre 1961 a supprimé le mot «métallique» du décret précité; toutefois, à l'exception des articles 8 et 10, relatifs à la sécurité et aux déclarations à faire en cas d'accident, le décret du 21 septembre 1961 n'entrera en vigueur pour les appareils à pression non métalliques qu'à des dates ultérieures qui seront fixées par arrêté ministériel.

** Circulaire actuellement en cours de révision.

Les contraintes d'origine thermique ont été prises en compte et calculées suivant l'hypothèse élastique avec un coefficient d'élasticité de béton de $100\,000\text{ kg/cm}^2$ acceptable pour le béton mis au point*.

Ces conditions n'étaient toutefois pas suffisantes, et il était nécessaire de définir des coefficients de sécurité globaux et des tests ou épreuves de vérification des appareils.

Le comportement du béton précontraint sous charge est très différent de celui de l'acier; les contraintes dans le béton sont maximales en absence de charge; elles diminuent avec la charge alors que parallèlement les contraintes dans les câbles augmentent, ces dernières restant inférieures aux valeurs correspondant à la mise en précontrainte pour autant que l'on ne dépasse pas sensiblement la charge de service. La mise en précontrainte constitue de ce fait une première épreuve des éléments de la structure. Par ailleurs, la fissuration du béton commence à se manifester alors que les câbles sont encore dans le domaine élastique et que la structure n'a pratiquement pas perdu sa résistance.

Dès lors, les méthodes utilisées pour les appareils métalliques sous pression ne sont pas transposables aux caissons en béton précontraint.

Les caissons des centrales de Marcoule furent calculés avec des coefficients de sécurité très larges, et l'un d'eux subit une épreuve à deux fois la pression de service; le coût relatif du surdimensionnement étant important, il s'avéra nécessaire pour les centrales suivantes, plus puissantes, de chercher à réduire ces coefficients.

Les études faites pour le caisson de la centrale EDF3 conduisirent à l'adoption, en plus de la condition de comportement élastique sous les sollicitations nominales, d'une condition de rupture, celle-ci ne devant intervenir que pour des pressions supérieures à trois fois la pression nominale, soit 90 bars; et d'une condition intermédiaire qui fut une condition de fissuration permanente, cette dernière ne devant être atteinte que pour des pressions supérieures à 1,6 fois la pression nominale, soit 48 bars.

L'épreuve hydraulique d'un caisson métallique constitue une adaptation des points singuliers par déformation plastique; elle constitue aussi une vérification globale des calculs et une vérification globale de la construction si elle s'accompagne de la surveillance d'un nombre important de jauges de contrainte.

Une épreuve à 1,5 fois la pression de service d'un caisson en béton précontraint calculé suivant les critères ci-dessus provoquerait des phénomènes irréversibles (fissurations) sans toutefois altérer la résistance de la structure. Par ailleurs, l'hétérogénéité de celle-ci et son épaisseur ne permettraient pas, même avec un grand nombre de dispositifs de mesures (témoins, sondes, pendules), de conserver à l'épreuve ce caractère

de test de vérification des calculs qu'elle a dans le cas des récipients métalliques.

Aussi a-t-il été jugé préférable de ne prévoir, sur l'ouvrage lui-même, qu'une épreuve pneumatique à une pression inférieure à la pression de fissuration du béton (1,25 fois la pression de service pour le caisson de la centrale EDF3) en donnant à des essais hydrauliques, conduits jusqu'à la rupture sur maquettes à échelle réduite, le caractère d'essais de vérification globale des calculs.

Ces dispositions purent être adoptées compte tenu de la grande expérience du Centre de recherches et d'essais de Chatou, acquise dans le domaine de l'expérimentation des maquettes de barrages hydro-électriques.

Deux maquettes furent réalisées à l'échelle de 1/6; elles furent construites avec le même béton et les mêmes armatures que l'ouvrage définitif. Ces dernières sont, évidemment, en nombre 36 fois plus faible. Le poids propre de l'ouvrage n'était représenté que pour 1/6; les efforts dus à la pression interne étant prépondérants, la correction en résultant avait été évaluée par un calcul qui avait montré que la résistance du caisson réel serait supérieure d'environ 5% à celle des maquettes. Les dalles supérieures comportaient la même proportion de vide et de plein que les dalles du caisson définitif; la courbure et la tension des câbles avaient été ajustées pour tenir compte d'une correction de frottement.

Par ailleurs, des dispositions avaient été prises permettant de noter l'apparition des premières tensions dans le béton et dans la tôle, ainsi que l'apparition des premières fissures; de suivre l'évolution de la tension des câbles de précontrainte au cours de la montée en pression; de vérifier si les points singuliers de l'ouvrage inaccessibles au calcul ne subissaient pas des contraintes inquiétantes; cela au moyen de mesures de déformation au sein du béton, de mesures de déformations superficielles, de mesures des déplacements extérieurs et intérieurs en certains points, et de mesures de la tension de certains câbles.

La première maquette avait été revêtue intérieurement d'une peau en caoutchouc armé ne jouant aucun rôle de résistance mais assurant l'étanchéité du béton jusqu'à une ouverture des fissures de 10 cm. La seconde maquette avait été revêtue intérieurement d'une tôle de 5 mm d'épaisseur représentant la peau d'étanchéité de l'ouvrage définitif. La comparaison des résultats obtenus avec les deux maquettes devait situer le rôle de la peau d'étanchéité dans la résistance d'ensemble.

Les deux maquettes présentèrent un comportement élastique pas toujours linéaire jusqu'à une pression située entre 27 et 35 bars pour la première et entre 35 et 40,5 bars pour la seconde. La pression n'entraîna aucun accident généralisé jusqu'à 48 bars pour la première maquette et 60 bars pour la seconde.

La première fuite considérée comme test de rupture n'apparut qu'à 93 bars pour la première maquette et 110 bars pour la seconde, sans qu'aucun câble ne se soit rompu.

* Béton de porphyre ($\leq 35\text{ mm}$) dosé à 375 kg/m^3 de ciment CPAL de la classe 215/315 ayant une résistance à la rupture par compression de 450 kg/cm^2 à 90 jours.

Conditions imposées au caisson de la centrale EDF4

Les principes directeurs du calcul du caisson de la centrale EDF4 de Saint-Laurent-des-Eaux sont très semblables à ceux utilisés pour le caisson de la centrale EDF3.

Les cas de charge envisagés sont:

a) Les conditions nominales: pression 30 bars, et écart thermique entre les faces interne et externe 50 °C; les contraintes du béton doivent être inférieures aux contraintes limites admissibles en béton précontraint, la paroi interne étant toujours en compression;

b) Les conditions de service exceptionnelles: pression nominale augmentée de 20% et écart thermique augmenté de 50%; la contrainte limite admissible de compression du béton est augmentée de 50% et celle de traction de 150%;

c) Les conditions de rupture: les conditions ci-dessus étant remplies, on doit vérifier que la rupture n'intervient que pour une pression supérieure à 2,5 fois la pression nominale.

La grande importance relative des efforts d'origine thermique, dans les conditions de service exceptionnelles en particulier, a poussé à chercher à les diminuer le plus possible. Cela est obtenu par l'utilisation d'un béton ayant à la fois un module d'élasticité et un coefficient de dilatation faibles et de hautes performances mécaniques (résistance à la compression de l'ordre de 500 kg/cm²) permettant de réduire l'épaisseur des parois.

L'augmentation de précontrainte correspondante est possible dans de bonnes conditions d'emploi grâce à la mise au point de câbles plus puissants unitairement (tension initiale 225 t — tension résiduelle supérieure à 185 t).

Le calcul est confirmé et précisé par expérimentation sur une maquette au 1/5 construite avec le béton et les câbles de l'ouvrage et essayée dans les meilleures conditions possibles de représentativité des contraintes d'origine thermique, de brève et même de longue durée.

PROBLÈMES ANNEXES POSÉS PAR LA RÉALISATION DE CAISSONS EN PRÉCONTRAIT

La construction de caissons de réacteurs en béton précontraint n'a pu être envisagée qu'en fonction de la grande expérience des constructeurs français dans l'utilisation de cette technique pour la réalisation d'ouvrages d'art.

Protection des câbles contre la corrosion

Pour les caissons des centrales G2, G3, le nombre relativement peu important des câbles sous gaine a permis de réaliser une protection des câbles contre la corrosion par simple ventilation d'air sec; par contre, le grand nombre et la longueur des câbles employés dans les caissons des centrales EDF3 et EDF4 ont fait préférer la technique utilisée à peu près systématiquement pour les autres utilisations du béton précontraint et qui consiste à dégraisser les câbles au moyen d'une

solution détergente et à les injecter ensuite avec un coulis de ciment.

Protection thermique du béton précontraint

L'expérience acquise dans le domaine du béton précontraint ne couvrait que des utilisations de béton à des températures relativement modérées. La sécurité demandée aux caissons en béton précontraint imposait de ne pas sortir du domaine d'utilisation expérimenté et par suite de prévoir, compte tenu des températures de fonctionnement du réacteur, une protection thermique de celui-ci.

Pour les caissons des centrales G2, G3 de Marcoule, dont la température maximale de béton avait été fixée à 50 °C, cette protection fut réalisée par circulation du gaz carbonique d'un circuit auxiliaire, solution simple dans son principe mais conduisant à une complication des circuits de gaz carbonique.

Pour le caisson de la centrale EDF3, il fut préféré à cette solution celle comportant un circuit de réfrigération parcouru par un liquide entraînant l'utilisation d'un calorifuge dans la cavité intérieure du caisson (fig. 3). Le circuit de réfrigération, constitué par des tubes en demi-lune de 50/60 soudés sur la peau d'étanchéité, est parcouru par un liquide organique dérivant de ceux utilisés dans les réacteurs à modérateur organique; il comporte deux séries de circuits fonctionnant normalement en parallèle, l'un d'eux étant suffisant pour maintenir le béton à une température inférieure à la température de 75 °C, considérée comme étant la température à ne pas dépasser pour rester dans les limites du comportement connu des structures.

Contrairement à ce que l'on pouvait supposer, les principales difficultés vinrent de la conception du calorifuge. A l'époque des études de la centrale EDF3, le comportement sous pression de gaz des matériaux habituellement utilisés sans pression était mal connu, et, les premiers essais réalisés ayant montré que le coefficient de conductibilité de ces matériaux augmentait très fortement avec la pression par suite de l'accélération des phénomènes de convection, l'Electricité de France s'est rapidement trouvée dans la nécessité d'entreprendre un programme d'études et d'essais très important allant des études fondamentales en strioscopie interférentielle des phénomènes de convection dans des cellules contenant du gaz carbonique sous pression aux essais de conductibilité en température et en pression dans un réservoir de grandes dimensions (3 m de diamètre, 8 m de haut).

Ces études et essais conduisirent à l'élimination de toutes les solutions primitivement envisagées: multicouches en feuilles d'aluminium (Alfol) ou en feuilles d'acier inoxydable, pavés en feuilles d'acier inoxydable et laine de verre; finalement, des considérations techniques et économiques conduisirent à l'utilisation d'un béton de pierre ponce spécialement composé, coulé, traité thermiquement et chimiquement, ayant une parfaite stabilité physique, chimique et dimensionnelle dans le gaz carbonique et sous rayonnement dans les conditions d'emploi.

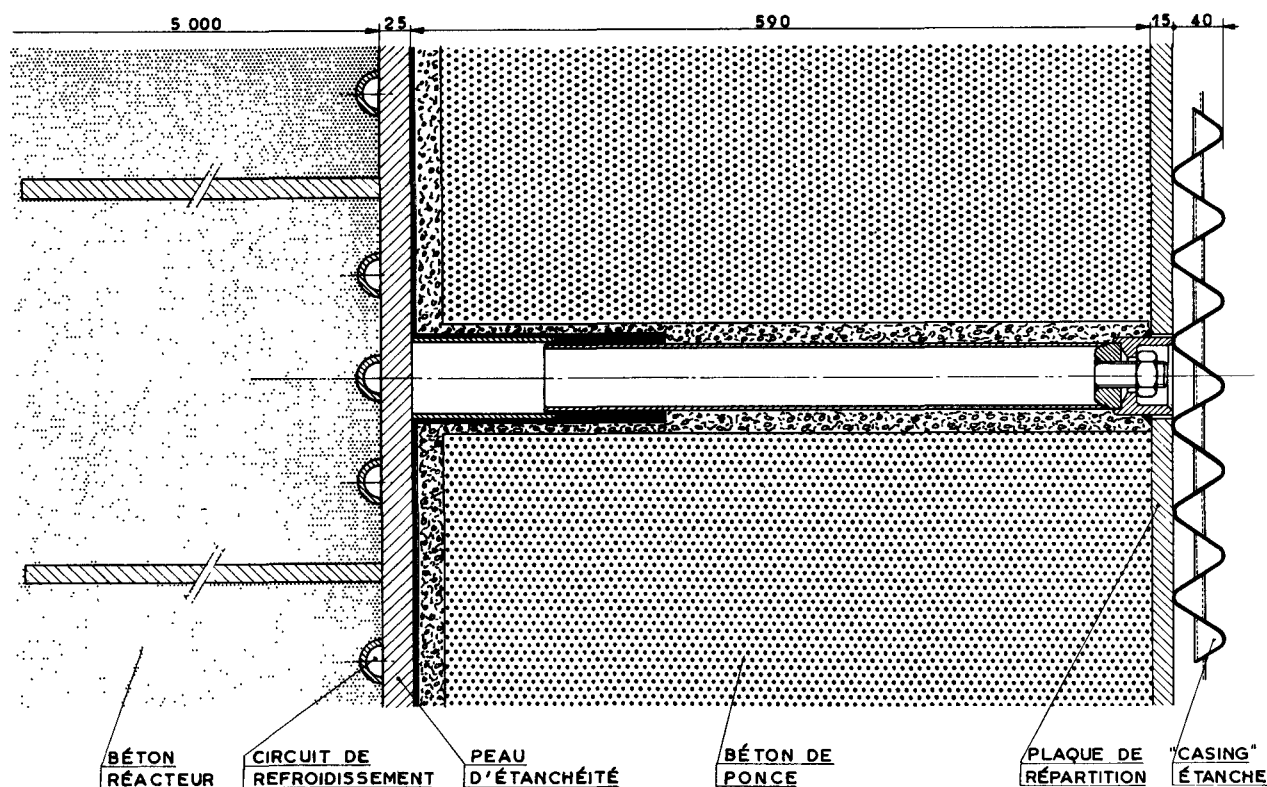


Figure 3. Constitution interne de la paroi du caisson EDF3

La densité du béton de pierre ponce est voisine de 1 ; sa porosité est de l'ordre de 1 000 fois celle du béton ordinaire ; sa conductibilité pour les épaisseurs envisagées est de l'ordre de $0,45 \text{ kcal/hm}^2 \text{ } ^\circ\text{C}$, avec un coefficient de dilatation de $7 \text{ à } 7,5 \times 10^{-6}$, une résistance à la compression de l'ordre de 100 kg/cm^2 et un module d'élasticité de l'ordre de $40\,000 \text{ kg/cm}^2$.

Le calorifuge est réalisé sous la forme de pavés de $1,5 \text{ m} \times 1,2 \text{ m}$ et $0,5 \text{ m}$ d'épaisseur contrôlés au moyen d'un équipement sonore après traitement thermique. Les pavés sont montés sur des potelets soudés sur la peau d'étanchéité et maçonnés au mortier de ponce. La face intérieure du calorifuge est protégée par des tôles de répartition non jointives en acier doux, de 1 cm d'épaisseur, qui supportent un casing étanche et dilatable en tôle d'acier inoxydable, de $1,2 \text{ mm}$ d'épaisseur. Le rôle principal de ce casing est de faire étanchéité aux poussières ; il peut néanmoins supporter la pression interne du réacteur et permettre une utilisation du caisson du réacteur, le calorifuge étant à la pression atmosphérique.

Pour la centrale EDF4, les problèmes de réfrigération du béton et d'isolation thermique sont résolus d'une façon semblable ; le circuit de réfrigération est constitué par des tubes cylindriques soudés sur la peau d'étanchéité ; quant au calorifuge, les épaisseurs de béton de ponce sont plus faibles, car, compte tenu des dispositions adoptées, intégration des échangeurs et disposition réacteur - échangeurs superposés, les parois de la cavité interne du caisson ne sont soumises qu'à la température la plus basse du gaz carbonique ($225 \text{ } ^\circ\text{C}$).

PROBLÈMES DE SÉCURITÉ

La sécurité d'emploi du béton précontraint a donné lieu à un certain nombre d'études, et il est reconnu que la construction et la mise en précontrainte constituent déjà à elles seules une épreuve des matériaux : a) pour les armatures de précontrainte, puisque leur tension à la mise en précontrainte est supérieure à leur tension de service ; b) pour le béton, puisqu'en général les contraintes du béton à vide sont supérieures aux contraintes en service.

Dans les caissons en béton précontraint actuellement en cours de réalisation, les câbles de précontrainte sont en grand nombre et indépendants les uns des autres ; ils travaillent en parallèle et la rupture de l'un d'entre eux n'affecte pas les autres. Néanmoins les problèmes de corrosion sous tension des câbles ne sont pas encore connus de façon parfaite.

Dans le but d'étudier les effets éventuels d'une corrosion étendue des câbles ou d'une détente généralisée des câbles, la troisième maquette du caisson de la centrale EDF3 a donné lieu à un certain nombre d'essais de détente de câbles.

Après un premier essai à 25 et 30 bars, des cycles $0 - 25$ bars ont été faits successivement après détente de : 6 câbles verticaux ; 3 câbles de la dalle supérieure ; 8 câbles horizontaux du fût ; 10 câbles verticaux ; 3 câbles de la dalle supérieure et 8 câbles horizontaux du fût ; 3 câbles de la dalle supérieure et 12 câbles horizontaux du fût ; 6 câbles verticaux et 3 câbles de la dalle inférieure. Pour ce dernier essai, correspondant à

la détente d'environ 10% des câbles de la maquette, la pression a été limitée à 20 bars.

La première remarque faite à la suite de ces essais est que l'effet de la détente d'un câble du modèle qui représente 36 câbles de l'ouvrage n'a qu'une influence très localisée; la tension des câbles voisins n'est pratiquement pas modifiée et les contraintes dans le béton ne sont perturbées que de quelques kg/cm² dans la zone intéressée par le câble; la représentativité de la maquette peut toutefois être mise en doute car les contraintes ne sont analysées qu'en des points espacés et il n'est pas certain que le maximum de l'effort supplémentaire ait été repéré; néanmoins, le dernier essai, correspondant à la détente d'environ 10% des câbles symétriquement répartis, montre que la répartition des contraintes est tout à fait acceptable pour la pression de 20 bars et que les points les plus perturbés se comportent comme s'ils étaient sollicités par une pression de l'ordre de 25 bars sur le modèle, aucun câble n'étant détendu.

L'essai n'a pas été poursuivi jusqu'à la rupture; de même, les essais de rupture sous pression de gaz n'ont pas encore été effectués. Néanmoins, les études, compte tenu des règles adoptées pour la conception des ouvrages, tendent à démontrer que, dans les cas très improbables où la résistance des câbles viendrait à diminuer très notablement, des fissures décelables à l'œil apparaîtraient sur les faces extérieures du caisson bien avant qu'il y ait des risques de rupture totale ou même de fuite. Ce contrôle visuel, joint à la surveillance périodique des indications des témoins sonores et pendules disposés dans la structure, doit garantir une sécurité totale d'exploitation des ouvrages.

ÉTUDES EN COURS

L'avenir des réacteurs de la filière uranium naturel – graphite – gaz carbonique paraît actuellement orienté vers l'utilisation d'éléments combustibles du type annulaire refroidis intérieurement et extérieurement, conduisant à l'adoption de pressions de gaz carbonique plus élevées: 40 à 60 bars.

La puissance spécifique des éléments combustibles envisagés est sensiblement plus importante que celle des éléments combustibles des centrales EDF3 et EDF4; néanmoins, comme les puissances unitaires des réacteurs risquent d'augmenter, les caissons en béton précontraint des réacteurs futurs semblent devoir se présenter comme ayant des dimensions utiles du même ordre que celles de la centrale EDF4, avec des épaisseurs de parois plus fortes et un plus grand nombre de câbles de précontrainte.

L'emploi d'éléments combustibles annulaires diminue le nombre de canaux du réacteur; néanmoins, la recherche de la simplicité de l'appareillage de chargement et de déchargement du combustible ne diminue pas le nombre de puits traversant la dalle supérieure du caisson; elle peut même dans certains cas sensiblement l'augmenter. Par ailleurs, l'intégration des échangeurs dans le caisson conduit à un grand nombre d'ouvertures dans la dalle inférieure.

Dans ces conditions, les problèmes les plus difficiles à résoudre deviennent ceux de la conception des dalles qui ne peuvent plus être traversées par des réseaux de câbles de précontrainte.

L'augmentation des pressions rend le problème de l'isolation thermique plus difficile à résoudre; les solutions du type EDF3 ou EDF4 paraissent toutefois extrapolables, et il n'est pas impossible d'envisager, pour un avenir plus ou moins lointain, un relèvement des températures maximales admises dans le béton précontraint.

Les développements envisagés pour les caissons de réacteurs en béton précontraint ont conduit le CEA et l'EDF à lancer un vaste programme d'étude et d'expérimentation sur la composition optimale de bétons devant travailler en béton précontraint à différentes températures et sous différents gradients thermiques, sur la corrosion des câbles de précontrainte, sur la conception de nouveaux câbles avec des aciers autres que ceux utilisés jusqu'à présent, enfin sur le comportement des structures.

Des essais en température ont été exécutés jusqu'à 140 °C sur une troisième maquette du caisson de la centrale EDF3; parallèlement, le CEA a essayé une maquette de 2,62 mm de diamètre et 5 m de haut avec des gradients thermiques allant jusqu'à 160 °C pendant des durées variant de deux à six mois.

BIBLIOGRAPHIE

1. Bulletin d'informations scientifiques et techniques du Commissariat à l'énergie atomique (août 1958).
2. Bellier, J., et Fabreguette, J., *Les caissons en béton précontraint des réacteurs atomiques G2, G3*, Association scientifique de la précontrainte (février 1959).
3. Bellier et Tourasse, Conférence à la Société des ingénieurs civils de France, Annales de l'Institut technique du bâtiment et des travaux publics (juillet – août 1959).
4. Direction des études et recherches d'Electricité de France, *Etudes sur modèles de structure*, Annales de l'Institut technique du bâtiment et des travaux publics (novembre 1961).
5. Ségot, C., *Intérêt de l'emploi du béton précontraint dans les caissons des réacteurs de Marcoule*, Conférence au centre de perfectionnement technique (mars 1962).
6. Tourasse, *Quelques particularités de la technique française des réacteurs de puissance*, Conférence de Melbourne (octobre 1962).
7. Conversy, *Etude des caissons sous pressions, en béton, pour réacteurs nucléaires*, Congrès franco-japonais, Tokyo (novembre 1962).
8. Bellier, J., Fabreguette J., et Laroche, L., *Description et construction des caissons en béton des réacteurs G2, G3*, Congrès franco-japonais, Tokyo (novembre 1962).
9. Lamiral, G., et Leclerc, R., *Les réalisations à Chinon des caissons des réacteurs EDF1 et EDF2*, Annales de l'Institut technique du bâtiment et des travaux publics (mars – avril 1963).
10. Conte, F., *Quatre années d'exploitation des réacteurs G2, G3*, Conférence de Vienne (juin 1963).
11. Dambrine, C., Conte, F., et Gaussot, D., *Les caissons en béton précontraint dans le programme français des réacteurs de puissance*, Conférence de Vienne (juin 1963).

ABSTRACT—RÉSUMÉ—АННОТАЦИЯ—RESUMEN

A/52 France

The prestressed concrete pressure-vessels of the French natural uranium-graphite-carbon dioxide gas sequence reactors

By G. Lamiral et al.

The first prestressed concrete pressure-vessels for nuclear reactors were built at Marcoule between 1956 and 1960 by the French Atomic Energy Authority (CEA).

After recalling the features of these pressure-vessels, the report defines the basic components and describes the pressure-vessels of the reactors of EDF3 and EDF4, built respectively at Chinon and at Saint-Laurent-des-Eaux by Electricité de France.

The pressure-vessel of the EDF3 reactor, designed for an operating pressure of 30 bars, has approximately the shape of a square prism with a base having sides 25 m long, and its height is 32 m; its effective capacity is bounded by a cylinder 19 m in diameter and 21 m high.

The pressure-vessel of the EDF4 reactor, which houses the reactor core and the heat exchangers, is designed for an operating pressure of 30 bars; its effective capacity is bounded by a cylinder 19 m in diameter and about 37 m high.

The design of these structures sets many problems, which can only be overcome after trials on scale models.

Since the high temperatures reached by the carbon dioxide gas are today considered incompatible with prestressed concrete, the concrete has to be insulated from the gas and cooled; many tests have been carried out and new solutions found for these problems.

The inclusion of the primary circuit within the reactor pressure-vessel meant such huge dimensions that prestressed concrete was the only feasible solution; any development of natural uranium-graphite-carbon dioxide gas type reactors are therefore tied to the development of this technique; problems concerning the use of prestressed concrete for reactor pressure-vessels are at present being subjected to various studies in France.

A/52 Франция

Корпуса давления из предварительно напряженного бетона на французских уран-графитовых реакторах, охлаждаемых углекислым газом

Ж. Ламираль et al.

Первые корпуса давления из предварительно напряженного бетона для ядерных реакто-

ров были созданы Комиссариатом по атомной энергии в Маркуле в период 1956—1960 годов.

После краткого описания характеристик корпусов, работающих под давлением, рассматриваются основные элементы корпусов реакторов фирмы «Электрисите де Франс»: EDF-3 в Шиноне и EDF-4 в Сен-Лоран-дез-О. Корпус давления реактора EDF-3, рассчитанный на рабочее давление 30 бар, имеет форму параллелепипеда с квадратным основанием со стороной 25 м и высотой 32 м; ее полезный объем определяется цилиндром, имеющим диаметр 19 м и высоту 21 м.

Корпус давления EDF-4, в котором размещаются активная зона и теплообменники, рассчитана на рабочее давление 30 бар; ее полезный объем определяется цилиндром диаметром 19 м и высотой около 37 м.

При проектировании этих сооружений возникают многочисленные проблемы, которые можно решить только с помощью испытаний на макетах уменьшенной величины.

Углекислый газ достигает высокой температуры, которая в настоящее время считается несовместимой с предварительно напряженным бетоном; необходимо предусмотреть устройства для изоляции и охлаждения бетона; были проведены многочисленные исследования, и эти проблемы получили оригинальное решение.

Установка первичного контура внутри корпуса реактора доводит его до таких размеров, которые можно осуществить только с помощью предварительно напряженного бетона; поэтому разработка уран-графитовых реакторов, охлаждаемых углекислым газом, связана с разработкой этой техники; проблемы использования предварительно напряженного бетона для корпусов давления реактора, являются в настоящее время объектом обширных исследований во Франции.

A/52 Francia

Las vasijas de hormigón pretensado de los reactores franceses del tipo uranio natural - grafito - gas carbónico

por G. Lamiral et al.

Las primeras vasijas de hormigón pretensado para reactores nucleares han sido construidas por el Commissariat à l'énergie atomique, en Marcoule, entre 1956 y 1960.

Después de recordar las características de estas vasijas, la memoria trata de los elementos que los definen y hace una descripción de las vasijas de los reactores de las centrales EDF3 y EDF4, construidas por Electricité de France en Chinon y Saint-Laurent-des-Eaux, respectivamente.

La vasija del reactor EDF3, proyectada para una presión de trabajo de 30 bares, tiene, aproximadamente, la forma de un paralelepípedo de base cuadrada de 25 m de lado y 32 m de altura; su volumen útil está limitado por un cilindro de 19 m de diámetro y 21 m de altura.

La vasija del reactor EDF4, que contiene el núcleo del reactor y los cambiadores de calor, está proyectada para una presión de trabajo de 30 bares; su volumen útil está limitado por un cilindro de 19 m de diámetro y unos 37 m de altura.

La concepción de estas obras plantea numerosos problemas que no pueden resolverse más que haciendo ensayos en maquetas a escala reducida.

El gas carbónico alcanza temperaturas elevadas que, según se estima actualmente, son incompatibles con el hormigón pretensado, por lo que se deben proveer medios para aislar y refrigerar el hormigón. Se han efectuado muchos ensayos y se han obtenido soluciones originales para estos problemas.

La integración del circuito primario en la vasija del reactor obliga a dar a ésta dimensiones tales que sólo parecen realizables soluciones en las que se utilice hormigón pretensado; por lo tanto el desarrollo del tipo de reactores de uranio natural - grafito - gas carbónico, depende de los adelantos de esta técnica; los problemas relativos al empleo del hormigón pretensado en vasijas de reactores, actualmente son objeto de muchos estudios en Francia.

The design and construction of prestressed concrete pressure vessels with particular reference to Oldbury nuclear power station

By **A. Houghton Brown,* J. D. Hay,** R. B. Hyde* and T. W. Spruce***

The nine commercial size nuclear power stations constructed or under construction in the UK are based on gas-cooled, graphite-moderated reactors.

The first seven in the series have reactors contained in steel pressure vessels connected by external ducts to heat exchangers. The increase in pressure vessel size with the progression in station capacity, coupled with an upward trend in coolant gas pressure, made the design of steel vessels reach towards practical limits for their construction. This inspired the consideration of prestressed concrete vessels.

It was soon established that, if the whole pressure circuit, embracing reactor and heat exchangers, was placed within one concrete vessel which also provided the radiation shielding, then a practical and economical design could be developed. This concept gave many advantages in cost, compactness and additional safety and a considerable potential for further increases in size.

Sir. R. McAlpine & Sons Ltd., originated and developed this type of design for inclusion in The Nuclear Power Group's tender to the CEGB for the station at Oldbury. This tender was accepted and construction on site started in April, 1962.

BASIC REQUIREMENTS OF THE DESIGN

The safety of a nuclear power station is the first consideration in every design. It follows that the modes of failure of a pressure vessel must be predictable and it is highly desirable that warning should be given by failure being slowly progressive.

These requirements can be attained with a prestressed concrete vessel.

However, the use of concrete for this type and scale of structure is a new departure in civil engineering and the basic requirements are deemed to be:

(a) The gas pressure shall be contained under working conditions throughout the anticipated life of the station;

(b) Under maximum credible fault condition the gas pressure shall be contained without nearing ultimate failure;

(c) The mode of ultimate failure shall be progressive without sudden rupture. The practical requirements are that:

(d) The vessel can be constructed in a way that satisfies the design requirements;

(e) The plant requirements can be met with respect to support, penetrations of the vessel and access for installation and maintenance.

To meet the requirements the structural behaviour of the vessel should be substantially elastic up to proof test pressure (say $1.15 \times$ design pressure). Analysis of the behaviour of the vessel in this range is necessary but difficult to carry out fully and accurately even with the extensive use of computers, photo-elastic analysis and other techniques. This is due to the massive nature of the structure, the pattern of penetrations and the lack of precise knowledge of the short and long term behaviour of concrete under operating conditions due to shrinkage, creep, thermal stresses and moisture movement, particularly as the strains due to these phenomena are of the same order as the strains due to design loadings. It is therefore, at present, necessary to supplement mathematical analysis with model testing in confirmation of results.

For requirements (b) and (c) an ultimate load analysis is carried out in which various modes of failure are examined and the necessary forces provided to maintain equilibrium at the load factor decided upon. In the ultimate, the design should be such that the prestressing cables determine the failure. The ultimate tensile strength of a cable is easily determined by testing; in the Oldbury design, every cable can be withdrawn and tested at any time during the life of the vessel. It is suggested that the load factor could safely be 2.0 to 2.5. The ultimate load factor was taken as 3.0 for the Oldbury design as this was the first vessel to be designed and a conservative approach was made as methods were not fully developed.

There is no great problem in producing concretes of adequate workability with compressive strengths of up to 7 000 psi (490 kg/cm²) at 28 days, and such concretes are more than adequate for a satisfactory vessel design. The physical properties of these high strength concretes for normal structures are well known, but there is little information with regard to

* The Nuclear Power Group, Knutsford, Cheshire.

** Sir Robert McAlpine & Sons Ltd., London.

their performance in large masses at elevated temperatures. Consequently an insulating and cooling system to reduce temperatures to an acceptable level, and an impermeable lining to avoid the effects of hot CO₂ upon the inner concrete surface and to ensure gas-tightness, are required. A steel membrane insulated on its inner face and with cooling water pipes attached to its outer face satisfies these requirements. Further advantages of a steel lining are gained by its use as concrete shuttering, and its convenience for the fixing of attachments, such as cooling pipes, insulation studs, brackets and penetration liners.

The basis for the design of a liner is the calculated strain distribution to which it is subject, due to straining of the inner surface of the concrete vessel, and due to restrained differential thermal expansion between the liner and the concrete. It is anchored to the concrete at points such as penetrations, and it is considered necessary to further key it to the concrete at intervals over its surface in order to cause its strain distribution to approximate to that of the vessel inner surface, and so limit any accumulation of strain, and excessive shear load on any particular attachment. In addition to the keys, ties are necessary to keep buckling within acceptable limits.

The liner thickness is chosen taking account of the desirability of it being thin to minimize the loads on the keys, the need for it to withstand evacuation of the vessel without collapse, and its use as concrete shuttering.

PRESTRESSING MATERIALS AND METHODS

The ideal prestressing system for a PCPV should have cables which are sufficiently flexible for each handling, the cable and anchorage should be as compact as possible, and the cable should have small relaxation under load and temperature; such a system would have a GUTS (Guaranteed ultimate tensile strength) in the range of 300–500 tons per cable. Irradiation tests carried out to date have not indicated any significant effects on concrete or high tensile wire at the flux level to which they are likely to be subjected.

The prestressing force may be applied to the pressure vessel either externally or within the thickness of the concrete. Cables applied externally would be very large cables on special saddles or many layers of smaller cables wrapped on to the concrete or arranged so that they may be jacked off the concrete at frequent intervals. Cables may be accommodated within the thickness of the concrete in ducts, thus giving a very compact arrangement albeit with an associated problem of placing the concrete around the ducts.

THE INTERRELATION OF VESSEL SHAPES, PRESTRESSING METHODS AND PLANT ARRANGEMENT

There are two basic shapes for the pressure vessel, the cylinder and the sphere.

The reactor core, in this type of reactor, is a right vertical cylinder requiring access from the top for fuel handling, control, etc. In the integral design the boilers are best placed surrounding the core as great complication is introduced to the plant if placed above or below. The cylinder is the obvious choice to contain, with economy of space, plant arranged in this way. If the ends are closed by flat slabs, there is the further advantage of a flat floor which can accept plant supports in any location and a flat soffit parallel to the top of the core which simplifies the design of the fuel handling plant and reduces the length of charge tubes, hence the height of the charging machine and of the building generally.

The authors have carefully investigated the relative costs of spherical and cylindrical vessels to contain equivalent plant in the range from 200 to 800 psig (14 to 56 kg/cm²) design pressure and for sizes from 50 to 100 ft (15.3 to 30.5 m) diam and in all cases find the cylinder to be the less costly. These costs took into account the effect on station layout and probable construction methods.

For pressure containment a simple sphere is the mathematical optimum. It would at first appear to be amenable to detailed stress analysis but this advantage fades when a prestressing system is imposed. Whatever arrangement of prestressing cables is adopted, it is necessary to provide for anchors and the only solution appears to be the addition of ribs to the outside of the sphere, and the uncomplicated stress pattern immediately disappears.

With increase in size and pressure the problem of disposing the anchorages becomes more acute and it would seem that the external shape of the vessel would become increasingly cubical or at best a series of right vertical cylinders.

It is generally considered that the major problems in cylindrical vessels are associated with the ends and the conditions of fixity at the junction of wall and ends. Various schemes have been proposed to avoid this problem by introducing a hinge at this junction, but no satisfactory solution has been found. However, detailed analysis and model testing have shown that the stresses in areas of fixity are not excessive when a suitable prestressing arrangement is used.

The two basic structural forms available for closing the ends of the cylinder are the flat slab and the dome. Various forms of hemispherical dome have been suggested, such as the Marcoule hemisphere and the tension dome. These systems result in a considerable increase in the over-all height of the vessel with extra length of prestressing cables. They also result in increases in the length of the standpipes and the distance from the top of the core to the charge floor. This, in turn, has an adverse effect on rates of charging and discharging, increases the height of the charge machine and charge hall, and of course gives considerable cost penalties.

A thick flat slab can be designed with greater ease of construction and a smaller over-all height. The slab can be prestressed with cables in two or more directions

across the slab, or circumferentially outside the standpipe zone.

The basic way of stressing a cylinder is to dispose the cables vertically and circumferentially, the circumferential cables being anchored on a series of vertical ribs on the external surface of the walls.

A more elegant solution is to combine vertical and circumferential prestress by using cables in a helical pattern with layers of cables alternately clockwise and anti-clockwise, thus giving anchorages at the ends of the vessels only. This results in a very compact arrangement in which access to the anchorages may be obtained from permanent galleries which are used for the insertion and stressing of cables during construction and are a permanent feature for inspection, testing and replacement at any time if required. This is the system which has been adopted for the vessels at Oldbury. To achieve a comparable facility with the circumferential and vertical stressing system for the cylinder or any system for the spherical vessel would require a complicated arrangement of galleries with the consequent expenditure of valuable space.

A reactor pressure vessel is of necessity penetrated at several places, the design of small openings is simply effected by replacing the concrete displaced by the opening with a steel tube the wall thickness of which is about 1/10 of its radius—the ratio being that of Young's moduli for concrete and steel. For larger penetrations the plate thickness so assessed would be beyond practical limits and in such cases secondary reinforcing steel could be introduced to reduce concrete stresses to acceptable levels.

DESIGN OF OLDBURY PRESSURE VESSELS

General description

A typical cross section of the vessel is shown in Fig. 1. The vessel is a vertical cylinder of 77 ft (23.5 m) id and 60 ft (18.3 m) internal height. The cylinder wall is 15 ft (4.6 m) thick and the end slabs 22 ft (6.7 m) thick. The vessel is constructed of high strength concrete, using limestone aggregate and sulphate resisting cement to give a minimum cube strength of 6 000 psi (420 kg/cm²) at 28 days.

Each prestressing cable is composed of twelve 0.6 in nominal diameter high-tensile steel strands; each strand is of 7 wires and has a minimum GUTS of 51 000 lb (23 200 kg) giving a guaranteed minimum ultimate load for the cable of 273 tons. The cables are contained within seam welded mild steel tubes of 3½ in (8.9 cm) od which are jointed by means of reinforced rubber sleeves, which locate the ends and form a seal against ingress of grout during concreting.

The multistrand anchorage shown in Fig. 2 is composed of two forged steel components between which the twelve strands of the cable are gripped and spaced circumferentially by grooves in the male and female components. The grooves of the male cone are roughened to improve the grip on the strands.

The grip is obtained by jacking the inner cone into the outer with the stressed strands of the cable lying

between them. A steel bearing plate is supplied under the anchorage. The entire anchorage remains outside the concrete and is arranged so that the specially designed stressing jack can be used at any time to lift the anchorage off the bearing plate without upsetting the grip on the cable between the male and female cones. With a calibrated jack and pressure meter the force to do this can be ascertained to give a measure of the load in the cable. Means are available (by shims between the anchorage and the bearing plate) to adjust the cable load in event of relaxation.

Arrangement of prestressing cables

The prestressing cables are arranged in two principal systems, one approximately helical within the wall thickness and continuing to the outer surface of the slabs and the other horizontally within the end slabs as shown in Fig. 2. In the helical system, the layers are arranged alternately clockwise and anti-clockwise, with 160 cables in each of 22 layers on a 45° helix. In the slabs, the cables are arranged horizontally in layers, the direction of the cables in the centre part of the layers alternating at right angles.

The arrangement of the prestressing cables was adopted as being the most satisfactory after the study of several alternatives. It fully satisfies the structural requirements in an economical manner, and gives a reasonably uniform distribution around penetrations.

Structural analysis for ultimate load

The vessel is designed to withstand an ultimate pressure up to 1 155 psig (81 kg/cm²) at ambient temperature, which is three times the maximum operating pressure.

The ultimate analysis is based on a consideration of the forces required to maintain equilibrium of the structure at failure. The mode of failure has been indicated in model tests, but other modes of failure have also been examined.

The forces acting on the concrete were simplified to the reactions of a single anchorage at the centre of the helical system, a reaction between the helical cables and the concrete of the cylinder wall and the forces from the equivalent number of vertical rows of anchorages of the horizontal cable system on the edges of the slabs. At failure, the wall was assumed to be cracked into vertical strips with horizontal cracks providing hinges at the first line of slab cable anchorages and at the mid-height of the vessel. By equating moments about hinge points the number of helical cables required was derived.

Similarly, for the slabs, sufficient cables are provided to maintain equilibrium. The slabs were also checked to ensure they will not fail in shear due to the domed configuration of the maximum principal stresses.

Elastic analysis

A preliminary analysis was made in which the vessel was split into three structural elements, a thin cylindrical shell and two circular plates. All sections were considered as thin with regard to rotations and

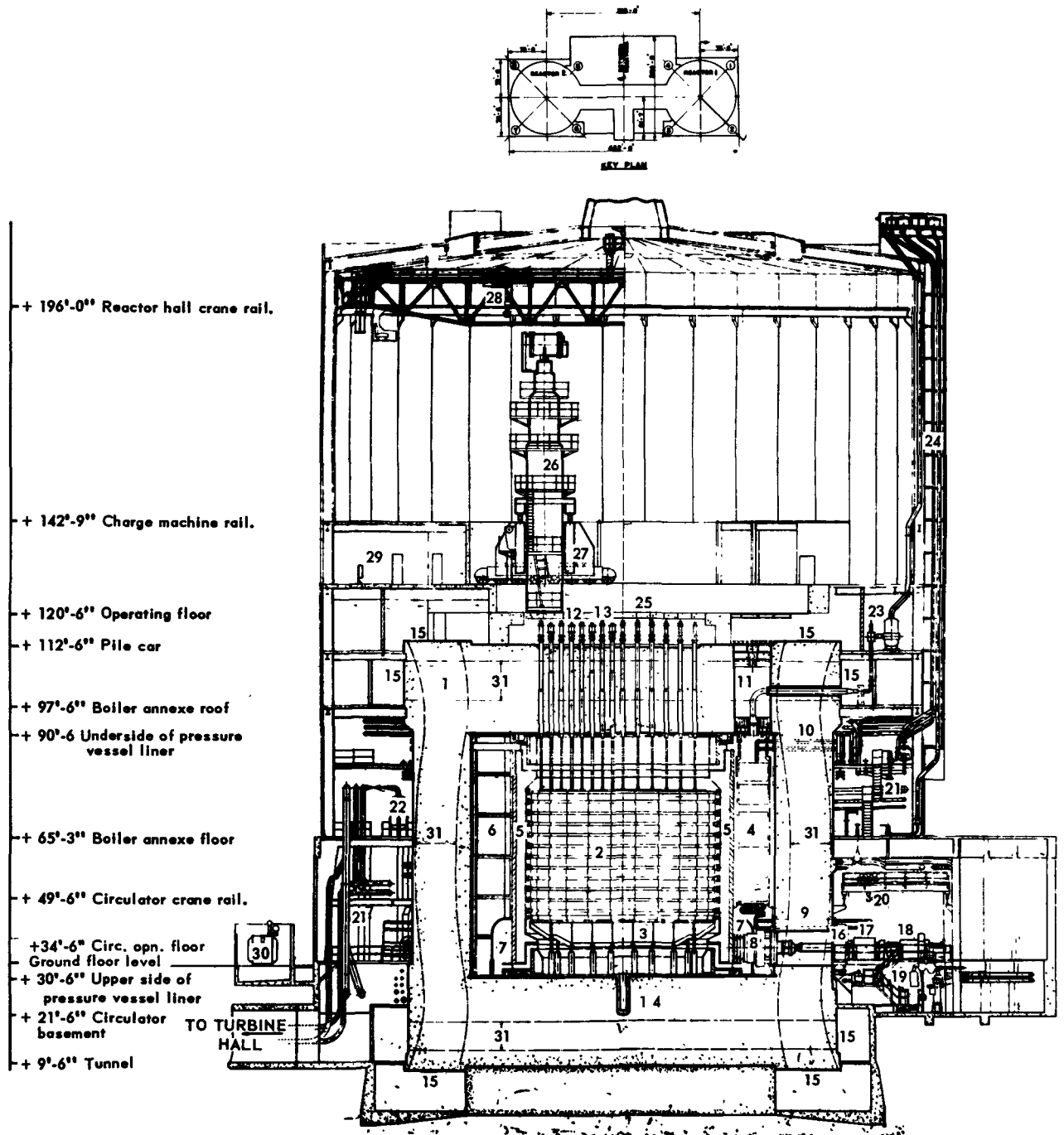
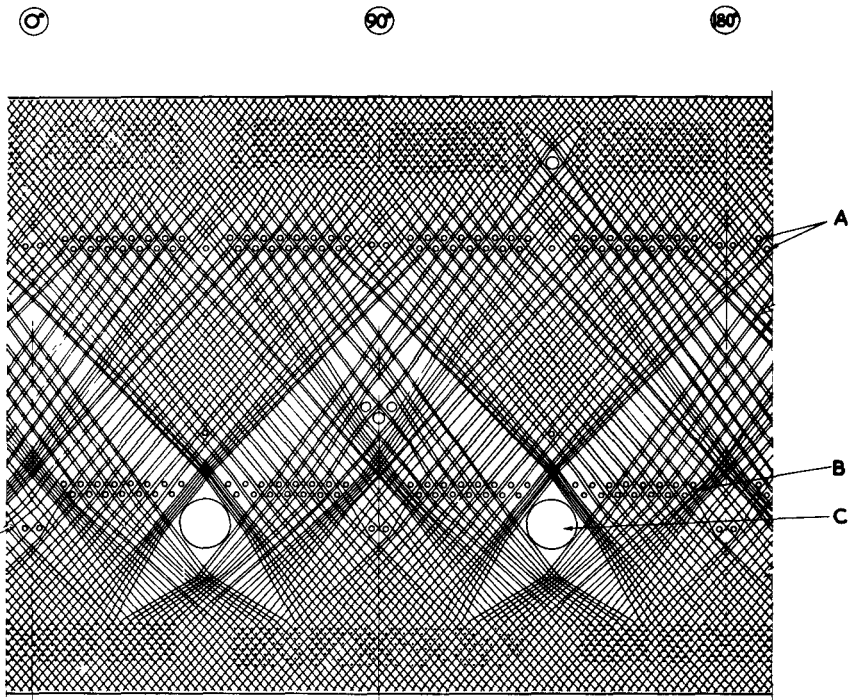


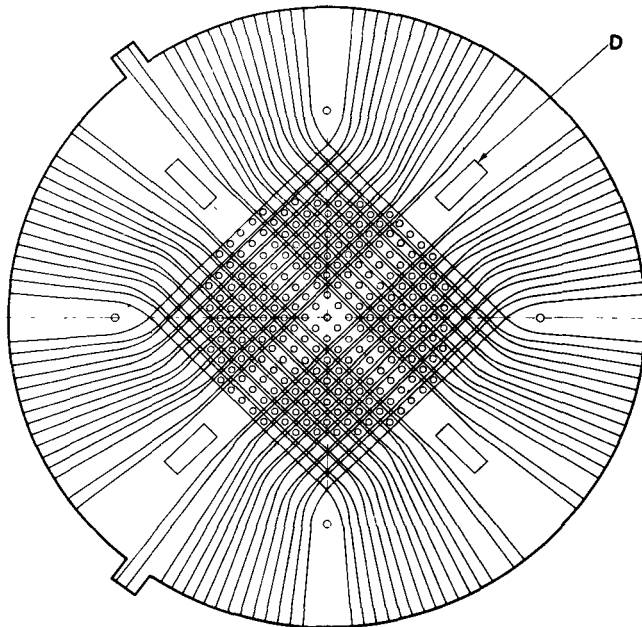
Figure 1. Oldbury power station. Prestressed concrete vessel transverse elevation

1: Prestressed concrete pressure vessel; 2: Graphite core; 3: Core support grid; 4: Boiler; 5: Boiler shield wall; 6: Boiler end piece; 7: Gas circulator outlet duct; 8: Gas circulator; 9: Boiler feed penetrations; 10: HP and LP steam penetrations; 11: Boiler loading slot; 12: Charge standpipe; 13: Control standpipe; 14: Debris mortuary tube; 15: Pressure vessel stressing galleries; 16: Gas circulator shield doors; 17: Gas

circulator pony motor; 18: Gas circulator turbine; 19: Gas circulator auxiliaries; 20: Gas circulator crane 25 T; 21: Steam and feed pipework; 22: Boiler start-up vessels; 23: Reactor safety valves and filters; 24: Relief valve pipes to atmosphere; 25: Charge floor; 26: Charge/discharge machine; 27: Charge/discharge machine gantry; 28: Charge hall crane 25 T; 29: B.C.D. room; 30: Transformers; 31: Stressing cables

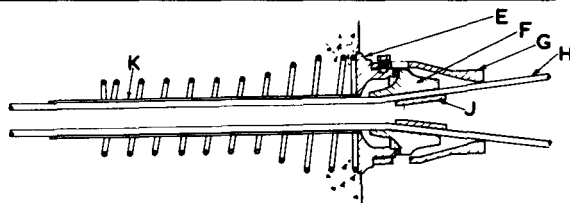


HALF DEVELOPED ELEVATION OF PRESTRESSING CABLE NET.



REF	DESCRIPTION
A	STEAMPIPE PENETRATIONS
B	FEED & REHEAT PENETRATIONS
C	BLOWER PENETRATIONS
D	BOILER ACCESS OPENING
E	BEARING RING
F	FEMALE ANCHORAGE CONE
G	BRIDGING STOOL
H	12 x 0.6" STRANDS
J	MALE CONE
K	3 1/2" O.D. DUCT

ARRANGEMENT OF CABLES IN VESSEL TOP SLAB.



DETAIL OF CABLE ANCHORAGE.

Figure 2. Oldbury power station. Prestressed concrete vessel. Details of cables and anchorages

deformations but for direct stresses in the cylinder, thick cylinder theory was adopted. The rotations and displacements at points of connexion of the three systems were equated. This method gave a pessimistic indication of the stresses at the junction of wall and slabs.

A more sophisticated analysis has been carried out with the aid of the computer. The results of both methods compare satisfactorily with observations from model tests.

Liner

The liner strains vary considerably over its surface, the greatest value which has been considered is one of 1710 microstrain (compressive) in the vertical direction near the bottom of the cylindrical wall. In operation, large parts of the liner will be beyond compressive yield strain.

The liner top and side wall is keyed and tied to the concrete by flat fins and hooked bars, whilst the bottom is keyed and tied by its attachment to a framework set into the concrete. At the stiffened junctions of the side wall with the top and bottom liners, large keys have been incorporated on to which the concrete bears in order to strain the liner.

The liner materials, $\frac{1}{2}$ in (12.7 mm) mild steel for the top and side wall and a 7/16 in (11.1 mm) Fortiweld for the bottom, were chosen for ductility and weldability; the use of Fortiweld, a high yield steel, permitting a 1 ft (30.5 cm) pitch of bottom framework members.

Penetrations

Penetrations of the vessel fall into two categories, the first consisting of the eight large openings for boiler access and the gas circulators; these, being closed at their inner ends, are not subject to gas pressure and temperature along their lengths; and the second consisting of the numerous relatively small openings for steam and water feed pipes, charge and control rod tubes, instrumentation pipes, etc., which are closed at their outer ends.

The closures for the circulator openings are the circulator casings themselves, whilst the closures for the rectangular boiler access slots are made by plating against a rigid grillage which is supported across the inner end of each penetration.

Cooling system and insulation

Both the vessel and smaller penetration liners are insulated from the hot gas and have completely duplicated cooling water pipes welded to their external surfaces. The cooling system and insulation were primarily designed to ensure that the temperature distribution in the concrete is acceptable, but they also determine the liner temperatures and hence the thermal component of the liner strains. The design conditions were that the bulk concrete temperature in the top and side walls should not exceed 55 °C and the temperature difference across the walls should not exceed 30 °C. The bulk concrete temperature in the

floor is limited to 60 °C. It was possible to achieve these conditions without exceeding a liner mean temperature of 65 °C.

The primary cooling medium is demineralized de-aerated water of boiler feed quality, dosed to give a high pH for corrosion inhibition. Tests have shown that for the water quality used, radiolysis has little effect on tube corrosion. The secondary cooling medium is river water, with a maximum temperature of 24 °C, the heat being transferred from primary to secondary coolant in shell and tube type heat exchangers.

The insulation on the liner inner surface is made up of layers of thin stainless steel sheet with suitable spacers incorporated between each layer.

RESEARCH AND TESTING

As the vessel design evolved each step was consolidated by a series of tests mounted either to obtain realistic parameters or to prove and develop the components.

Cables and ducts

With the adoption of the helical cable pattern it was decided in 1959 to construct a full scale test bed consisting of a 3 ft 9 in (1.14 m) square helical section of the vessel wall containing five pairs of different types of cable duct. This test bed was used to determine the relative suitability of various types of cable, ducts and jack and to establish the friction and anchorage losses developed and the effect of various lubricants.

Other full-scale models of parts of the vessel structure were made to examine the feasibility of duct erection and concreting in areas of apparent congestion.

Anchorage

The final design of anchorage and bearing ring adopted is shown in Fig. 2. Various anchorage designs were tested in order to arrive at one which might be readily manufactured and yet be capable of withstanding at least 95% of the guaranteed minimum ultimate strength of the cable and this standard has been obtained with the first production anchorages.

Concrete

Research into the properties of concrete has concentrated on those using limestone aggregates obtained from quarries located near Oldbury. Mixes having adequate site workability and compressive strength have been tested to determine their properties of creep, moduli of elasticity, Poissons ratio, shrinkage, thermal expansion, thermal conductance and their relative variation with moisture content, temperature and age.

Liner

To allow a margin above the calculated concrete strain values and the predicted temperature distribution, it was decided that the liner design should be demonstrated to be adequate for strains of 1.5 times the calculated strains. As the buckling behaviour of

panels at biaxial strains well beyond compressive yield strain is not amenable to simple calculation, it was necessary to undertake an extensive test programme in order to determine this. Plates, both flat, and with various forms of initial bowing and dimpling, including under-thick and over-thick specimens of nominally $\frac{1}{2}$ in (12.7 mm) mild steel and 7/16 in (11.1 mm) Fortiweld were tested. Simulated vacuum conditions were included in some of the tests.

This programme, together with tests to determine the load deflection characteristics of the keys into the concrete, enabled simple calculations to be made demonstrating the adequacy of the liner design.

Vessel models

A concrete model vessel to $\frac{1}{8}$ scale of an early design was built in 1959 at Hayes in Middlesex. This model preceded the settlement of detail of the Oldbury design but is a near simulation in general.

The prestressing cable arrangement and levels of prestress simulated as nearly as possible those employed in the full-scale design using a $\frac{1}{2}$ in diam, 7 wire strand (having a 36 000 lb (16 300 kg) guaranteed minimum ultimate strength) in 6 helical layers in the walls. It was necessary, from practical considerations, to use an out-of-scale model steel liner thickness of $\frac{1}{8}$ in.

The model vessel was subjected to a protracted series of onerous tests for pressure, temperature and a combination of the two. The pressure was hydraulically applied and temperature effects were simulated by heating the water. However, to investigate reactor fault conditions, pneumatic testing was employed and high temperatures induced by internal heaters.

The Hayes model vessel was designed for an ultimate pressure of 675 psig (47 kg/cm²). Cracking of the vessel concrete was first observed at a pressure of 470 psig (33 kg/cm²). This pressure was equivalent to a concrete tensile stress of about 700 psi (49 kg/cm²), a figure which previously had been obtained in tensile tests of concrete specimens.

At an average temperature in the concrete of 100 °C there was no measurable increase in the forces in the cables. No damage was detected in the model structure as a result of application of heat, with peak temperatures of about 180 °C and local recorded gradients of 18 °C/in (7 °C/cm). Extensive cycling of pressure at ambient temperature and with the water at 90 °C indicated only small changes in the deflection characteristics in the cylinder wall.

A similar model vessel to $\frac{1}{8}$ scale but constructed to simulate closely the Oldbury design was built at Leatherhead, Surrey, for the CEGB. In this case, the ultimate pressure was 1 155 psig (81 kg/cm²). Testing continues but the behaviour pattern of the Hayes model is expected to be repeated.

To avoid the cost of constructing complete model pressure vessels, several small-scale end slabs, each about 2 ft (61 cm) diam were tested. The tests of these prestressed concrete discs have confirmed the methods of end slab failure and the influence of the varying boundary conditions. It is considered that the general

pattern of cracking can be forecast, together with the corresponding pressures and the deflected forms, at any stage up to failure.

CONSTRUCTION

Oldbury power station (Fig. 3) is located in flat farming country on the south bank of the Severn estuary just north of Bristol.

The construction craneage for the reactor buildings is a system of fixed monotower cranes, of which two of 15 tons capacity with 130 ft (40 m) high towers serve each of the two pressure vessels (Fig. 4).

All the concrete at Oldbury is mixed in a central weighbatcher plant having two 2 yd³ (1 $\frac{1}{2}$ m³) tilting drum mixers, transported to the various parts of the site in Dumpcrete lorries, tipped into laydown hopper-bottomed concrete skips and hoisted into position by the cranes.

Foundations

The pressure vessels are supported by $\frac{1}{2}$ in (12.7 mm) thick Neoprene mats which cover the top surface of 80 ft (24.5 m) diam mass concrete bases and which reduce the resistance to radial movement on both prestressing and pressurization.

Ground exploration revealed that at Oldbury about 13 ft (4 m) thickness of recent alluvium overlay Keuper Marl which, in turn, at a great depth rests upon sandstone. A series of layers of siltstone and sandstone were found in the marl containing solution cavities which by their interconnexion formed horizontal aquifers at some levels.

The mass concrete bases were founded directly upon the hard surface of one of these sandstone layers at an average bearing pressure of 12 tons/ft² (13 kg/cm²).

Vessel

The part of the vessel base slab which extends radially outwards beyond the mass concrete foundation contains, on the underside, the bottom anchorages for the helical stressing cables (Figs. 5, 6). There are 22 circumferential rows of anchorages; each row facing in the opposite direction at right angles to the adjacent row and at slightly different angles in plan and elevation. The accuracy called for in placing and fixing these anchorages was achieved by forming radial precast concrete beams which each contained two radial rows of 11 anchorages. The beams were temporarily supported at their outer ends on timber props, which were removed when the vessel walls reached mid-height. As prestressing cannot start until the vessel structure is complete, high tensile reinforcement was built into the lower part of the walls to make the vessel self-supporting (Figs. 7, 8).

The base slabs were poured in 5 lifts, each lift being broken into pours with a maximum size of 290 yd³ (225 m³). The stressing ducts which were fixed in position either on precast concrete stools, or temporarily held by scaffolding, were cut into lengths

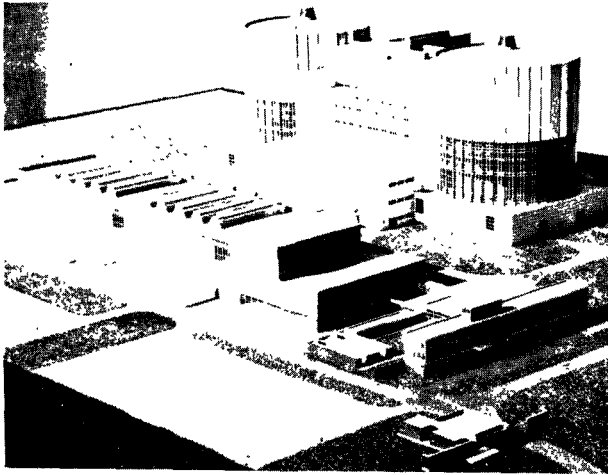


Figure 3. A model showing the Oldbury station completed. The blower houses form square plinths for the two reactor buildings, the upper parts of these being halls for the charging machines. A block for fuel handling and charge machine maintenance stands between the two circular buildings, forming a complex 480 ft long, 157 ft wide and 193 ft above ground level. The control room block stands in front of this, facing the turbine house which is 380 ft long, 155 ft wide and 67 ft 6 in above ground. Workshops, stores, welfare and administration buildings run to the right of the turbine house

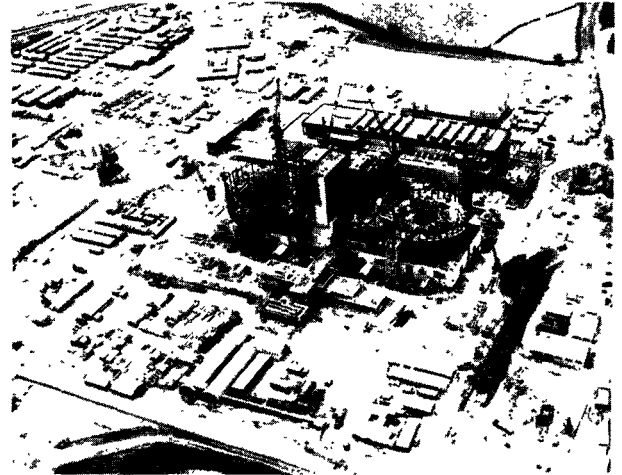


Figure 4. An aerial view of the Oldbury site, taken from the opposite direction to Fig. 5. The main buildings are seen in the centre, with working sites around them to a total area of about 60 acres. The camp and offices are in the top left corner and the River Sever is seen on the right-hand side

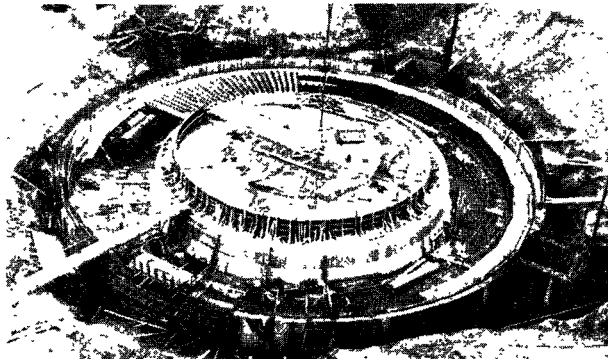


Figure 5. Construction of the foundation for the first vessel, in a battered excavation 25 ft deep. The central mass foundation is encircled by the wall of the lower stressing gallery. On the further side can be seen the first of the precast beams from which the helical stressing system starts

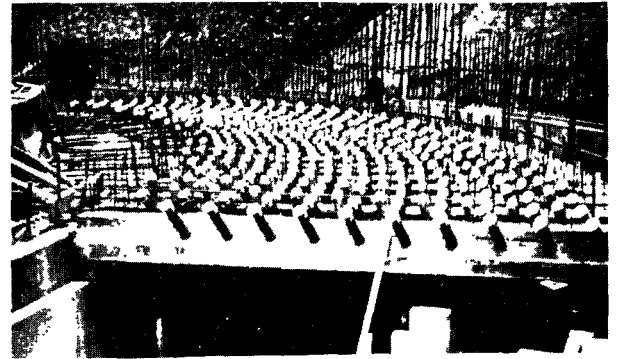


Figure 6. A closer view, showing the precast beams in more detail. Short lengths of the ducts for the cables, with temporary caps on them, can be seen cast into the beams

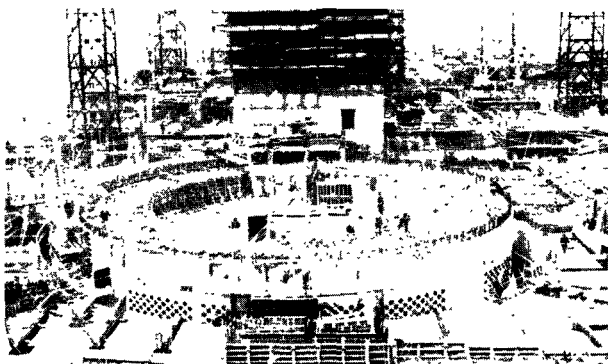


Figure 7. Concrete in the form of a ring is here placed to contain the ducts of the helical stressing system, in advance of the central lifts of the bottom disc. The bearing plate for the horizontal stressing system of the bottom disc can be seen at the bottom of the photo

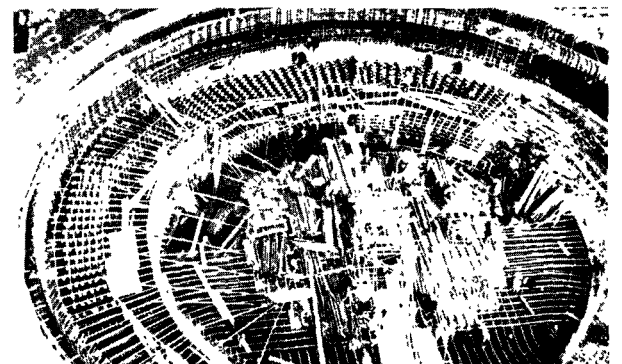


Figure 8. Prestressed concrete vessel construction; the stage following that shown in Fig. 7

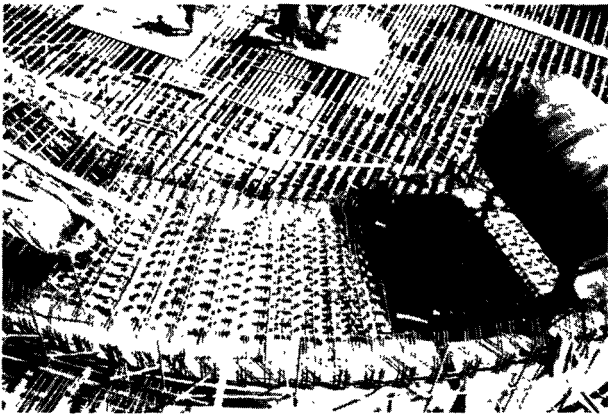


Figure 9. The position immediately before placing the top lifts of the bottom disc. In the upper half, steel framing is in position for concreting-in, and this receives the plating of the bottom of the liner

corresponding to the size of each pour and bent to shape on site with a hydraulically operated pipe bending machine.

Before casting the top lift of the base a steel framework of T-section joists was constructed at the upper surface. The concrete which anchored the framework was accurately trowelled to be flush with the top surface of the Ts, which were later used as backing strips for the butt welding of the steel floorplates of the liner (Fig. 9).

Whenever possible timber stop end shutters were used. However, throughout the vessel at positions within the helical cable zone expanded metal shuttering was used which was left permanently in position.

The liner side wall, and top centre disc without penetrations, together with other internal structures such as the graphite support grid, were concurrently fabricated on temporary works areas near the reactor locations.

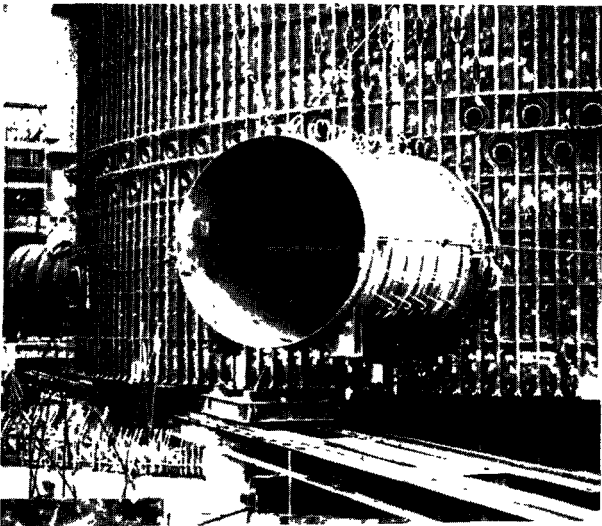


Figure 11. A closer view than in Fig. 10, at Reactor 2 where liners for blower penetrations were attached to the main liner before roll-in

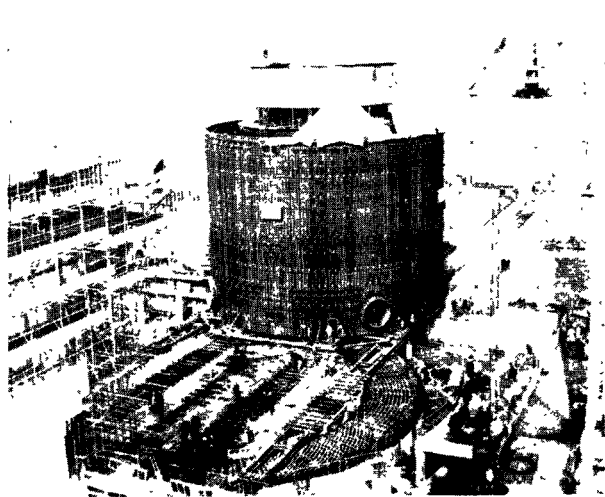


Figure 10. Rolling-in the vessel liner on Reactor 1

This completed 77 ft (23.5 m) diam fabrication weighing about 1 000 tons, suitably braced, was rolled on to the reactor floor using winches and bogies on rails (Figs. 10, 11). When in position it was jacked down, and the liner bottom corner angle was butt welded to the floor plating using the annular plate forming the framework ring member as a backing strip. The walls were then concreted in lifts 6 ft (1.8 m) high, each broken into four parts of about 230 yd³ (180 m³). Work proceeded in a spiral sequence climbing between the base and top slabs of the vessel (Figs. 12, 13, 14).

Shortly in advance of the concreting, the roof plating was completed and the penetration liners for the side walls and top slab were welded in (Figs. 15, 16).

At the time of writing the roof slab is temporarily supported by the vessel liner which is propped internally to act as a soffit shutter. These props are to be removed after some 12 ft (3.7 m) depth of top slab

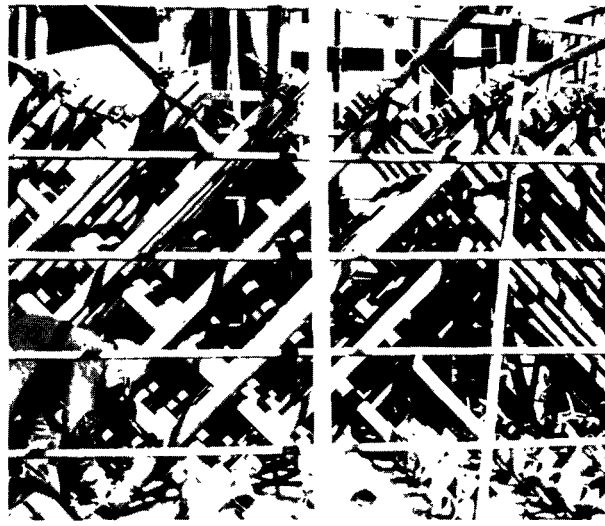


Figure 12. A close-up of ducts for the wall helices. The method of temporary attachment to radially fixed scaffold poles can be seen

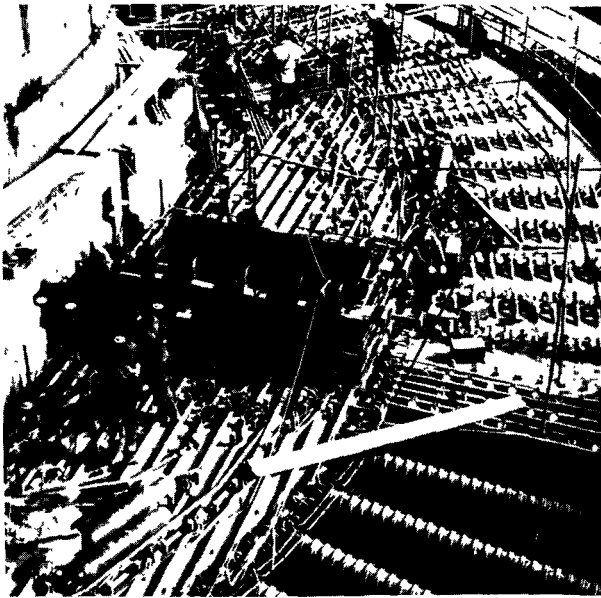


Figure 13. The concreting of the walls approaching the level of the top of the liner. The upper surface of the liner can be seen in the right foreground, with two men standing on it in front of a boiler-loading slot. Upper steam pipe penetrations are in the left foreground

has been poured, the liner itself temporarily acting as constructional reinforcement before prestressing.

The liner inspection was aimed at the detection of any possible leakage paths. All butt welds in the liner wall and top, and in penetrations, were radiographically examined. All butt welds in the liner floor made against a framework set in the concrete, were ultrasonically crack detected. The pressure-retaining fillet welds were subjected to magnetic crack detection. Weld quality control was maintained by the usual tensile and bend tests and macro-section examinations.

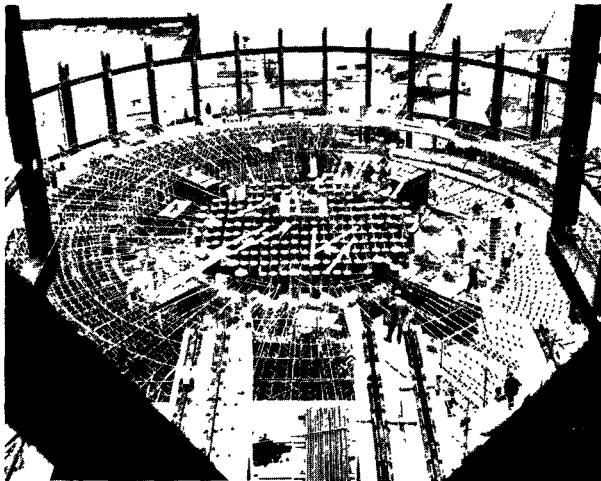


Figure 15. The top of the vessel, preparing for the last lifts of concrete. Standpipes occupy the central zone; linings for the four boiler slots can be seen. The structural steelwork for the charge hall forms the periphery

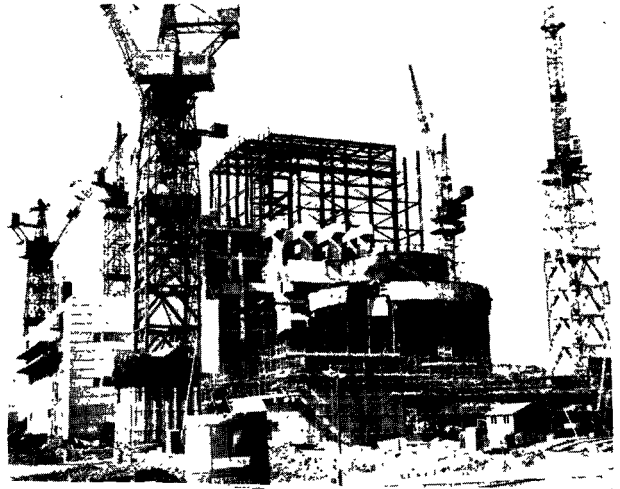


Figure 14. A general view of the station with Reactor 2 in the foreground. The liner has been rolled in and a temporary housing erected on top of it to proceed with standpipe erection and welding. Beyond, and above, four beams are prominent, and these are to carry the rails for traversing the charge machines to the fuelling positions in the central block or to the other charge hall. Structural steelwork is erected over the central block

Threading and stressing

The strand for the stressing cables is delivered to site on drums in 5 000 ft (1 500 m) lengths. The cables are made up by drawing off twelve drums simultaneously on to a table where the strands are bundled and the cable cut to length. The cables are transported in to the works on a reel and pulled into the ducts by winch-operated ropes.

The stressing sequence is arranged so that disparity between zones does not exceed 10%. Jacks for stressing are carried on gantries or bogies with hydraulic lifting arms where required. A jack is attached to both ends of a cable by temporary anchors

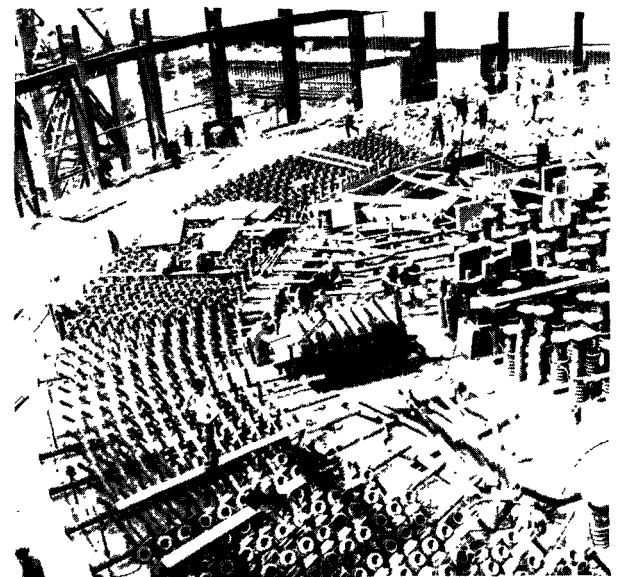


Figure 16. A closer view than Fig. 15 at a slightly later stage. The last lift of concrete has been placed in the outside annulus, at the right in the photograph

and the two jacks are operated together to stress the cable to 210 tons (i.e., 77% GUTS). This loading is maintained for two minutes, when the male cone of the permanent anchorage is driven by hydraulic jack into the female cone to form the grip on the cable, and the cable loading is then relaxed into the permanent anchorage. The anchorage is then retracted as a unit until a force of 191 tons (i.e., 70% GUTS) is in the cable and shims of suitable thickness are inserted between the anchorage and the bearing plate to maintain this extension in the cable. This last operation can be repeated at any time to test the load in a cable with readjustment if necessary by variation in the shims.

A system of sonic strain gauges, thermocouples and moisture cells are built into the concrete of the vessel and resistance and mechanical strain gauges fixed to the surface of the liner. These are read at intervals, at the same time as vessel surface deflections are measured, to compare the actual performance of the vessel and liner with calculated predictions and results from model testing.

Pressure testing

Following the completion of prestressing, the vessel will be subjected to a proof pressure test. As clean conditions have been established within the vessel and as a graphite core will be installed, a pneumatic pressure test will be carried out. The pressure is expected to be raised in successive stages from zero to 130, 260 and 385 to 443 psig (zero to 9, 18 and 27 to 31 kg/cm²) which is 1.15 times the design pressure (385 psig 27 kg/cm²). At each of these stages the vessel and liner strain measurements will again be compared with those obtained by calculation and from the model testing.

Progress

At the time of reading this paper, pressure vessel No. 1 concrete work will be complete, threading and stressing of cables will be proceeding, the enclosing building will be completed up to pile cap level and preparations will be in hand for the erection of the

charge hall. The construction of pressure vessel No. 2 will be following No. 1 closely, with half the top slab completed.

CONCLUSION

The adoption of prestressed concrete pressure vessels enclosing the complete reactor, coolant gas circuits and boilers is a major advance in the design of nuclear power stations.

The principal advantages are:

(a) A high standard of safety arising from the containment of the coolant gas circuit in a single vessel capable of withstanding the pressure under the maximum credible fault conditions.

(b) The vessel may be designed so that ultimate failure is progressive and gives ample warning.

(c) The massive nature of the structure gives assurance against accidental damage from large external forces such as earthquakes.

(d) The thick concrete vessel required structurally gives a standard of radiation shielding several orders of magnitude in excess of international requirements.

(e) Large vessels for high pressures outside the range of practical steel designs are possible.

(f) The integral design with a concrete vessel gives a significant reduction in the over-all station costs, compared with designs using steel or concrete pressure vessels with external gas ducts and boiler shells.

(g) The facilities for testing, retensioning or replacing the stressing cables ensure that the life of the vessel may be extended without limit.

(h) Prestressed concrete vessels may be economically constructed with semi-skilled labour and using local concreting materials in any part of the world.

(i) There is no foreseeable gas-cooled reactor design advance in either pressure or size which cannot be contained within a prestressed concrete pressure vessel.

The Oldbury pressure vessel described in the paper has proved that the design and construction of prestressed concrete vessels can be carried out successfully in practice.

ABSTRACT—RÉSUMÉ—АННОТАЦИЯ—RESUMEN

A/140 Royaume-Uni

Etude et construction de cuves sous pression en béton précontraint, notamment pour la centrale nucléaire d'Oldbury

par A. Houghton Brown *et al.*

Le mémoire commence par un aperçu historique du développement des centrales nucléaires commerciales en Grande-Bretagne, qui a abouti à l'adoption de cuves sous pression en béton précontraint contenant la totalité du circuit sous pression des gaz réfrigérants.

Un examen des principales exigences auxquelles doit répondre la construction est suivi d'un rappel des

principes du comportement de la structure de la cuve en deçà de la charge limite et au point de rupture. On décrit la conception générale de la gaine d'étanchéité et du système de refroidissement. On énumère les exigences auxquelles doivent satisfaire les matériaux et les systèmes de précontrainte.

La corrélation entre la forme de la cuve, les méthodes de précontrainte et l'implantation des installations est examinée pour les cuves sphériques et cylindriques, et on compare leurs prix de revient. On discute du choix des fermetures d'extrémité et des systèmes de précontrainte pour cylindres et on donne les raisons de la préférence des auteurs pour les solutions adoptées à Oldbury.

La thèse générale est alors illustrée par l'exemple de l'étude et de la construction de la centrale d'Oldbury.

Une brève description de la cuve indique les principales dimensions et l'agencement du système de précontrainte. On décrit les méthodes utilisées pour l'analyse à la charge limite et à la charge de rupture, ainsi que la conception de la gaine d'étanchéité, des orifices de pénétration, du système de refroidissement et de l'isolement.

On décrit les recherches sur le béton et les essais de possibilité de construction. D'autres essais ont porté sur les éléments du système de précontrainte et de la gaine d'étanchéité, ainsi que sur des maquettes des dalles d'extrémités et des cuves complètes.

Un aperçu de la construction de la centrale d'Oldbury, qui a commencé en 1962, décrit le plan de construction, la disposition des fondations et la préparation du radier de la cuve, la mise en place de la partie préfabriquée de la gaine d'étanchéité, l'achèvement de celle-ci et la coulée du béton. On décrit ensuite la technique de précontrainte et les essais de pression proposés.

Le mémoire se termine par une description des avantages des cuves sous pression en béton précontraint pour contenir les circuits d'un réacteur nucléaire, et par une estimation des possibilités qu'offre ce mode de construction.

A/140 Соединенное Королевство

Проектирование и строительство корпусов под давлением из предварительно напряженного бетона; сооружение корпуса атомной электростанции в Олдбери

A. Хоутон Браун *et al.*

Доклад начинается кратким историческим обзором разработки промышленных атомных электростанций в Соединенном Королевстве, которая привела к введению реакторных корпусов под давлением из предварительно напряженного бетона, вмещающих весь контур газового теплоносителя, находящегося под давлением.

Основные конструктивные требования рассматриваются в докладе одновременно с кратким обзором принципов статической работы корпуса в упругой зоне, а также в случае максимальной аварии. Описывается конструкция лейнера корпуса и системы охлаждения и перечисляются требования, предъявляемые к материалам и предварительно напряженным системам.

Взаимосвязь формы корпуса, методов предварительного напряжения и компоновки установки анализируется применительно к сферическим и цилиндрическим корпусам и с учетом расходов. В докладе обсуждается выбор кон-

цевых крышек и систем предварительного напряжения для цилиндрических корпусов и причины предпочтения, отдаваемого авторами конструкции корпуса в Олдбери.

Основная тема доклада иллюстрируется ссылками на конструкцию и строительство атомной электростанции в Олдбери.

Краткое описание корпуса включает основные параметры и устройство системы предварительного напряжения. Описываются методы анализа статической работы корпуса в упругой зоне, а также при максимальной аварии, конструкции лейнера, фиттингов, системы охлаждения и изоляции.

В докладе описываются работы по исследованию бетона и испытания, касающиеся демонстрации возможности строительства корпуса такого типа. Дополнительные исследования включали испытания узлов системы предварительного напряжения корпуса, частей лейнера, а также моделей концевых плит и целых корпусов.

Дается общее описание строительства атомной электростанции в Олдбери, которое началось в 1962 году. Это описание включает строительное оборудование, устройство фундамента и подготовку концевых плит корпуса, а также соединение вальцовкой предварительно изготовленных частей лейнера, установку лейнера корпуса и бетонирование. Затем обсуждается методика предварительного напряжения корпуса. В докладе даются предложения, касающиеся пробных испытаний под давлением.

В заключение коротко говорится о преимуществах корпусов под давлением из предварительно напряженного бетона при размещении внутри них контуров реактора и дается оценка потенциальных возможностей корпусов такого типа.

A/140 Reino Unido

Proyecto y construcción de vasijas de presión de hormigón pretensado referidos particularmente a la central nuclear de Oldbury

por A. Houghton Brown *et al.*

La memoria comienza con un breve resumen histórico del desarrollo de las centrales nucleares comerciales en el Reino Unido, que condujo a la adopción de vasijas de presión de hormigón pretensado conteniendo todo el circuito de presión de los gases refrigerantes.

Se establecen y explican los requisitos básicos de proyecto, junto con un breve resumen de los fundamentos del comportamiento estructural de la vasija en la zona elástica y a la rotura. Se describe el proyecto general del revestimiento y del sistema de refrigeración. Se mencionan las condiciones a cumplir por los materiales y los sistemas de pretensado.

Se examina la relación entre la forma de la vasija, métodos de pretensado y disposición del equipo para vasijas esféricas y cilíndricas y se comparan los costes. Se discute la elección de los cierres terminales y los sistemas de pretensado de los cilindros y se dan las razones de la preferencia de los autores por la solución adoptada en Oldbury.

Se aclaran después los principios generales expuestos haciendo referencia al proyecto y construcción de la central de Oldbury.

Se da una descripción breve de la vasija incluyendo las dimensiones principales y la disposición del sistema de pretensado. Se señalan los métodos empleados para los análisis elásticos y a la rotura y también el proyecto de revestimiento, penetraciones, sistema de refrigeración y aislamiento.

Se describen los trabajos de investigación de hormigones y ensayos sobre posibilidad de construc-

ción. Se emprendieron otros ensayos tales como los de componentes del sistema de pretensado, detalles del revestimiento y modelos de las losas extremas y vasijas completas.

Se da una descripción esquemática de la construcción de Oldbury, iniciada en 1962. Esta descripción comprende las instalaciones de construcción, la disposición de la cimentación y la preparación de la losa base de a vasija. Continúa con la conformación de la parte prefabricada del revestimiento, la terminación del revestimiento de la vasija y el hormigonado. Se describe después la técnica de pretensado y se establecen las propuestas para los ensayos de prueba de presión.

La memoria termina con un resumen de las ventajas de las vasijas de presión de hormigón pretensado para la contención de los circuitos de un reactor nuclear y con una estimación de sus posibilidades.

The design of prestressed concrete pressure vessels, with particular reference to Wylfa

By R. S. Taylor* and A. J. Williams**

The first generation of power producing gas-cooled reactors follow closely the design of Calder Hall, the principal developments having been increased output, improved layout and higher component performance.

Parallel development has proceeded towards combining the biological shield and the pressure vessel in a prestressed concrete vessel, a system pioneered at Marcoule.

In Britain, the flexibility of design conferred by prestressed concrete has been exploited to integrate reactor components in a single vessel. Two such reactors are under construction for the 600 MW(e) Oldbury station. A second British station, designed to produce 1 180 MW(e) from two reactors, is being built for the Central Electricity Generating Board at Wylfa Head by the English Electric/Babcock & Wilcox/Taylor Woodrow Construction Consortium. This paper describes the development of prestressed concrete vessels for the Wylfa design.

Advantages of prestressed concrete pressure vessels

Common features of early stations are steel pressure vessels containing the reactor core, connected to external boiler and circulator vessels by heavy ducting, the whole complex being surrounded with massive concrete shielding.

For the range of gas pressures currently considered, it is possible for concrete vessels to be made large enough to accommodate not only the reactor core, but also the boilers and circulators. This layout eliminates all external gas circuits, which in itself, is an important contribution to the safety of the system.

A concrete pressure vessel is inherently safe. The progressive deformations with pressure, as shown in Fig. 1, are characteristic and give clear warning of overstrain or impending failure. The failure of a single prestressing tendon or component would have an insignificant effect on the strength of the structure, and would not lead to sequential failure of other tendons.

The shielding provided by the vessel concrete permits inspection of surface concrete and prestressing components during reactor operation. If

required, tendons may be retensioned or even replaced in service. Further, internal shielding permits the greater part of the vessel internal surface to be inspected during reactor shut down.

The construction of a concrete vessel employs well-proved civil and mechanical engineering materials and techniques, enabling simple and established inspection procedures to be used during construction.

Functional requirements for prestressed concrete vessels

Balanced specifications for vessel and reactor are achieved by including the vessel parameters in over-all optimisation studies. With fixed output and fuel element conditions, the internal dimensions of the vessel are governed mainly by plant arrangement.

The vessel design is influenced considerably by penetrations. The stand-pipe array is affected by

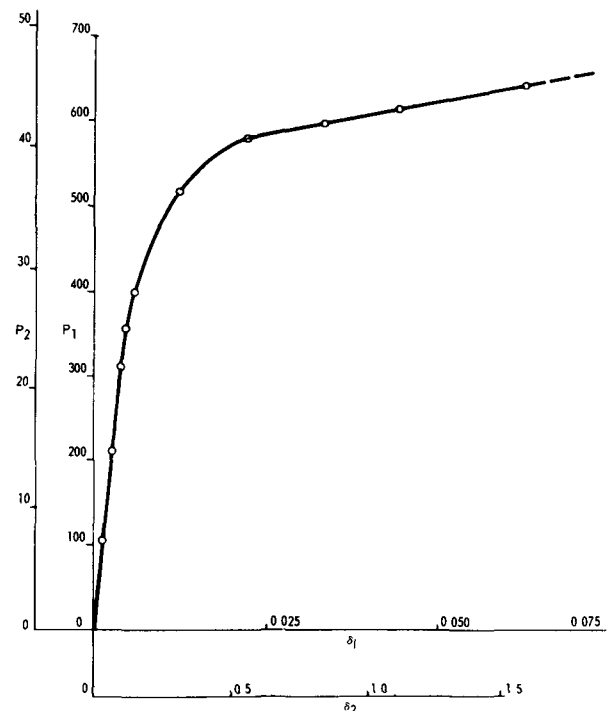
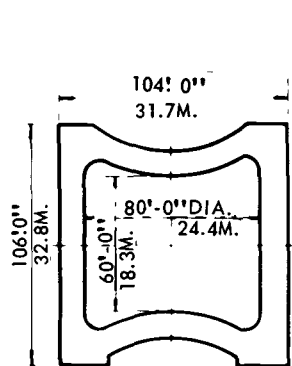


Figure 1. 1/40th scale model deflection at top cap. p_1 = internal pressure lb/in²; p_2 = internal pressure kg/cm²; δ_1 = deflection in.; δ_2 = deflection mm

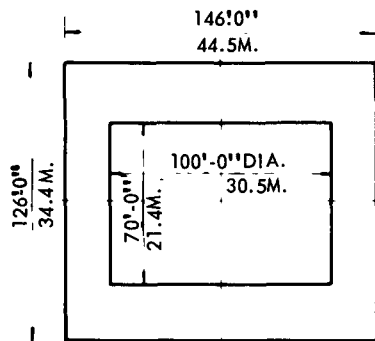
* Taylor Woodrow Construction Limited, Southall.

** The English Electric Company Limited, Whetstone, Leicester.

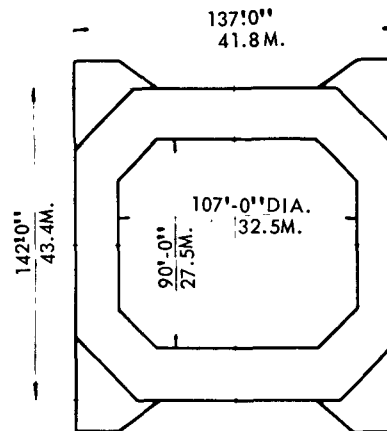
A. CYLINDRICAL VESSELS



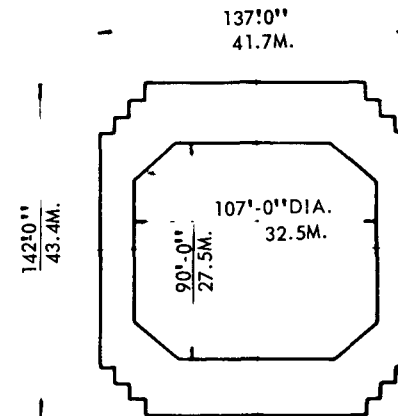
A.1.



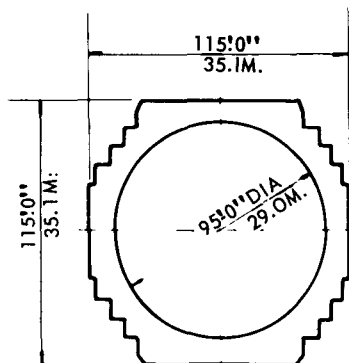
A.2.



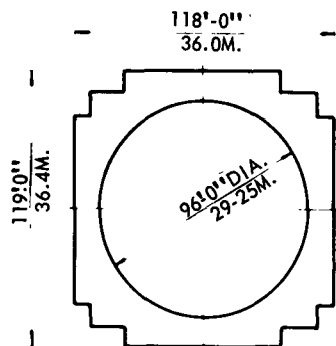
A.3.



A.4.



B.1.



B.2.

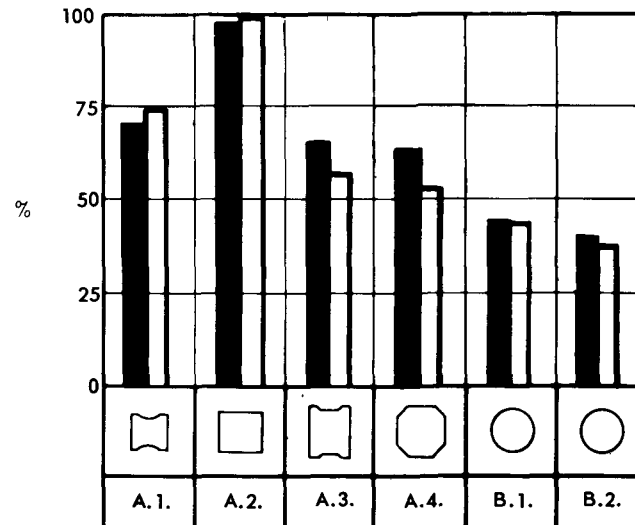


Figure 2. A: Cylindrical vessels; B: Spherical vessels; C: Specific quantities

reactor optimisation, the design of fuelling plant, the structural behaviour of the top cap of the vessel and the feasibility of construction.

Current safety considerations require at least four main gas circulators, whilst economy requires the minimum number consistent with reasonable development costs. The size of circulator openings is such as to influence profoundly the arrangement of prestressing tendons. Both spherical and cylindrical vessels with square standpipe lattices are well suited to accommodate four circulators.

Boiler penetrations are significant on account of their number rather than their size, and thus the once-through boiler is preferable to the forced-circulation type.

Boiler quality steel provides a satisfactory vessel liner which is impervious to carbon dioxide. Vessel and liner designs must be such that the latter experiences acceptable deformations. Similarly, the movement imposed on plant accommodated by penetrations must be acceptably small.

Optimisation of system pressure, vessel diameter and temperature crossfall has favoured high pressures. In Wylfa the working pressure has been limited to 400 psia (28.3 kg/cm² (a)) by consideration of graphite-carbon dioxide reaction.

Gas temperatures reach 400 °C in a uranium-magnox reactor. The concrete temperature must be limited to about 70 °C to avoid deterioration of its properties and to lower values in most areas to control thermal stresses. This requires internal insulation and an elaborate cooling system, the cost of which are significant. The temperature crossfall through the concrete is usually controlled to between 15 °C to 25 °C.

In the Wylfa design an internal shield controls the radiation levels over most of the vessel, and thermal shielding elsewhere ensures that no part of the liner or concrete receives a radiation dose exceeding 3×10^{19} nvt, at which value their properties do not appear to be significantly affected. The prestressing tendons are sufficiently shielded by vessel concrete to ensure that radiation effects are negligible.

The vessel design is influenced in detail by construction considerations, and the construction programme must be carefully phased to take account of the concentration of men and materials implicit in an integrated scheme.

Development of the Wylfa vessel design

The final design of the Wylfa vessels was selected after an extensive programme of development in which various possible vessel types were examined. This work was carried out concurrently with the development of the reactor layout and the structures described were conditioned by the requirements of the latter. A design pressure of 300 psi (21.1 kg/cm²) was generally used, with internal plan diameters of between 100 ft (30.5 m) and 110 ft (33.5 m).

This development is illustrated in Fig. 2 together

with comparative specific quantities for each type of vessel. The first four vessels have cylindrical walls and various forms of end closure were investigated, (Figs. A1-4, Fig. 2). These vessels were characterised by the high specific quantities and large concrete thicknesses required. It should be noted that the specific quantities of the cylindrical design A2 appears to decrease at a rate somewhat greater than a proportional reduction in vessel diameter. Prestress efficiencies were found to be relatively low and bending moments and shear forces large. The strains imposed on the vessel liners were subject to heavy peaks at the junctions of walls and end closures, and the structural behaviour of the vessels when approaching ultimate pressure was difficult to predict.

Development of the reactor layout enabled a spherical vessel to be considered and further work was concentrated in this direction.

It was clear that the specific quantities and concrete thicknesses of a spherical vessel were notably less than in the cylindrical designs previously considered. Furthermore, the mode of behaviour at operating and ultimate load conditions was essentially similar and capable of confident prediction. In the designs illustrated (Figs. B1 and 2, Fig. 2), the internal surface is truly spherical, whilst the external surface approximates to a series of concentric right cylinders.

Design criteria

There are no existing codes of practice which deal adequately with the design and construction of prestressed concrete pressure vessels, and in designing the Wylfa vessels it has been necessary to consider all design criteria objectively and in detail.

A prestressed concrete pressure vessel should satisfy three basic design criteria:

- (a) It should behave in a substantially elastic manner under test conditions, and under all operating conditions throughout its working life.
- (b) No sudden increase in strain or deformation should occur under conditions of over load.
- (c) Final failure of the vessel should be associated with a satisfactory level of vessel strain, and an acceptable load factor.

Compliance with these criteria must be demonstrated for any particular vessel design by theoretical analysis, supported, if necessary, by model tests. The range of elastic behaviour is primarily determined by the level of prestress available. This must be chosen, and applied, so as to control the direct and bending stresses induced by gas pressure, temperature distribution and temperature crossfall, to levels which do not induce irrecoverable deformations. In the case of a spherical vessel, membrane stresses predominate, and the application of efficient prestress is accordingly made easier.

Sudden increase of strain or deformation under overload conditions is avoided by ensuring that cracking or rupture of the concrete is well distributed

and controlled, by the provision of adequate bonded steel reinforcement. A typical load-deformation curve for a spherical vessel is shown in Fig. 1. Subject to any requirement that prestressing tendons should be capable of retensioning or replacement, most of the required bonded reinforcement can be obtained by grouting the prestressing tendons. If grouting is not permitted, it will be necessary to provide bar reinforcement in quantities sufficient to ensure compatibility of strain with the prestressing steel up to ultimate load conditions. Whilst shear stresses are generally minimal in a spherical vessel, they can be heavy in cylindrical designs, and security must be obtained by the provision of adequate prestress, or additional bonded bar reinforcement.

The gas pressure necessary to cause failure of a spherical vessel can be closely determined by reference to the membrane forces carried by prestressing steel, bonded reinforcement and the vessel liner, and it has been found that theory and experiment show good agreement. Re-distribution of moments and shear forces in a cylindrical vessel make it more difficult to determine the mode of failure and the failure pressure by purely theoretical means. It is, therefore, most desirable to demonstrate the behaviour of the vessel at ultimate load by adequate model testing.

In the Wylfa design, compressive stresses in concrete have been limited to 1/3 of the cube strength at 28 days, an increase of 10% being permitted under transient conditions. For local stress concentration at penetrations, double these values are permitted. Tensile stresses of up to 200 psi are allowed on the outer surface of the concrete but no tensile stresses are permitted adjacent to the vessel liner. Reinforcement is provided where local tensile stress concentrations exceed 1/10 of the concrete cube strength.

Since prestressing cables are subject to temperatures above ambient, allowance is made for the additional relaxation losses which occur. The use of stabilised prestressing strand, which has a maximum relaxation loss at 60 °C of 5% after 1 000 hours under load, has been found to be advantageous.

The proof test pressure should be selected sufficiently above the design pressure to allow the vessel performance to be checked against design predictions. If the proof test pressure is selected at too high a value, this may impose uneconomic consequences on the design. In the Wylfa vessels the proof test pressure has been selected at 1.15 times the design pressure.

The Authors consider that the ruling criterion for the selection of the ultimate load factor should be that the load factor at the time of proof testing should be at least 2. The ultimate load factor of the Wylfa vessel is 2.65 times the design pressure.

Design and Research

An extensive research programme was undertaken to obtain the necessary information upon which competent design could be based. This programme was not directed at any single type of vessel, but was designed to cover as wide a field as possible.

Epoxy resin model vessels

A series of model vessels was made in epoxy resin with the object of determining stress patterns in vessels of complex shape. This work has enabled analytical tools to be developed which closely reproduce the behaviour of these model vessels. Three models, corresponding to Fig. 2 (A2, A3 and B1), have been examined, using frozen stress photo-elastic techniques. Stresses have also been measured in a series of models whose internal surfaces were spherical, and whose external shapes varied from true cylinders to the generator form of the Wylfa vessels.

Pile cap behaviour

The presence of the standpipe penetrations in the top cap of the vessel produce stress concentrations and a change of rigidity which must be fully considered in the design.

The problem was studied by subjecting zircon-filled epoxy resin discs to edge moments and radial forces. Each disc was tested before and after an array of holes was drilled through it. The holes were then lined with steel tubes and the test repeated. Comparison of the measured strain patterns indicated that for the Wylfa vessel the rigidity of the pile cap was reduced to 65% of the unperforated cap. Reduction of the effective modulus of the concrete due to creep increases the degree of compensation afforded by the liners to the standpipe. The initial loading condition is thus the most critical.

Stress concentrations

The Wylfa design is characterised by the large number of penetrations in the vessel walls. The most important of these are the standpipe penetrations in pile cap and the four 10 ft (3.05 m) id circulator penetrations. These penetrations produce stress concentrations in the concrete, the magnitude and distribution of which must be kept to specified limits. It has been found desirable and economic only partially to compensate these penetrations, and to accept relatively high levels of stress which are limited to localised zones. Photo-elastic techniques have been used to study the stress concentrations occurring in plates under uniaxial tension containing various patterns of holes. Varying degrees of compensation were provided by lining the holes with a magnesium alloy which gave a modular ratio lying in range expected to occur in the Wylfa vessel. A further study has been made of the stress concentration around single circular openings in concrete blocks subjected to biaxial compression. This showed agreement with results obtained using elastic materials.

Concrete models

Experiments with relatively small models of elastic material provided results to check and modify the analytical studies, but it was also essential to carry out tests on models made of concrete. These models allow the effects of concrete creep, prestress and thermal loadings to be studied, and so demonstrate

vessel behaviour under working and ultimate load conditions.

Five such models have been tested. These comprise two spherical vessels generally similar to the Wylfa design, and three cylindrical vessels corresponding to Fig. A1, Fig. 2. One vessel of each type was tested at operating and moderate overload conditions. The remainder have been tested to destruction. In this paper it is only possible to give brief descriptions of the spherical vessel models.

(a) *1/12th scale concrete model*: This model resembled the Wylfa vessel in structural shape and general arrangement of prestressing cables. A simulated standpipe pattern was constructed on the top cap of the vessel and the four major circulator penetrations were reproduced in simplified form. The vessel was pressurised with water and the inner spherical surface lined with a rubber membrane. A temperature crossfall through the concrete wall was produced by heating the water with immersion heaters. The vessel was generally stressed by 0.6 in (15.3 mm) diameter strand and was reinforced with a total of 0.5% ribbed high tensile bar. All instrumentation was situated on two meridians approximately normal to each other.

The behaviour of the vessel under the application of prestress was studied and a comprehensive series of pressure tests with and without a temperature crossfall have been carried out.

Accepting the limits of stress used in the Wylfa design, the theoretical working conditions in the model were 300 lb/in² (21.1 kg/cm²) internal pressure plus 15 °C crossfall. The maximum loadings applied were 550 lb/in² (38.8 kg/cm²) at ambient conditions and 400 lb/in² (29.2 kg/cm²) with a 25 °C crossfall.

The theoretical stresses have been translated into strain for comparison with the experimental strains and are indicated in Fig. 3 for internal pressure loading and prestress. These results, from 18 individual pressure tests, have been normalised to a pressure of 100 lb/in² (7.03 kg/cm²). The normalised curve is given as well as the maximum and minimum values recorded during all the tests.

The whole series of tests indicated a close correlation between theory and experiment.

(b) *1/40th scale concrete model*: A 1/40th scale model similar in shape to the 1/12th scale model has been built and tested to destruction. This model had an inner diameter of 28½ in (72 cm), wall thickness of 3 in (7.6 cm), and was reinforced with a total of 0.2% mesh reinforcement. Meridional prestress was by means of 5/16 in (8 mm) diameter high tensile strand and 8 swg wire. Hoop prestress was applied by winding on 20 swg wire under tension. A preformed copper liner was used and structural failure occurred before rupture of the liner.

The equivalent working pressure of the vessel was 270 lb/in² (19.0 kg/cm²) and failure occurred at 820 lb/in² (57.8 kg/cm²). During the test, cracking developed gradually and without any sudden release of energy. Figure 1 shows the deflection of the top cap of the vessel with increasing pressure and indicates

that the behaviour of the vessel followed a progressive deformation pattern giving adequate warning of impending failure.

Bonded reinforcement

A minimum of 0.3% of bonded reinforcement has been provided in the Wylfa vessel in order to control cracking in the working range and to ensure that the integrity of the liner is maintained until structural failure occurs.

Uniaxial tensile tests on a series of large reinforced concrete beams have suggested that compatibility of strain between bonded reinforcement and prestressing steel will be achieved at the failing pressure.

Properties of concrete

The concrete materials and mix for the vessel were designed to meet structural and site requirements, and the physical properties of this material were fully studied. An important factor in the vessel design was the effect of temperature on the creep behaviour of concrete. Knowledge of this particular aspect was necessary in order to predict:

- (a) The deformation pattern of the vessel and liner with time, particularly as the expected life of the structure is 30 years.
- (b) Losses in prestress.
- (c) The re-distribution of stress in the vessel caused by the change in temperature through the shell of the structure producing different rates of creep strain.

Concrete specimens were made using the concrete specified for Wylfa. These specimens were sealed to simulate the condition in mass concrete and were subjected to a sustained compressive stress whilst maintained at various temperatures within the range 20–95 °C. Stress was applied at various ages after casting, and deformations have been recorded over a period of two years. This work showed that:

(a) Creep deformation, but not initial elastic deformation, was significantly increased for concrete maintained at elevated temperatures. For example, concrete one year old, loaded for 100 days at 93 °C, deformed 50% more than the same concrete at 20 °C.

(b) At 20 °C, the greater the specimen age at load application, the lower was the creep rate. This reduction with age occurred less at the higher temperatures. For example, at 20 °C, the 100 day deformation for concrete aged 180 days prior to loading was 50% less than concrete aged 7 days. At 93 °C the corresponding figure was only 16%.

(c) The application of heat to concrete already under sustained load caused an increase in the creep rate.

Prestressing system

Since, in the Wylfa design, the prestressing tendons are ungrouted, it was necessary to demonstrate rigorously the ultimate strength and strain capacity of the prestressing system. The 12/0.6 in (15.3 mm) strand Freyssinet system was adapted by using three such cables to form each tendon; this tendon has an

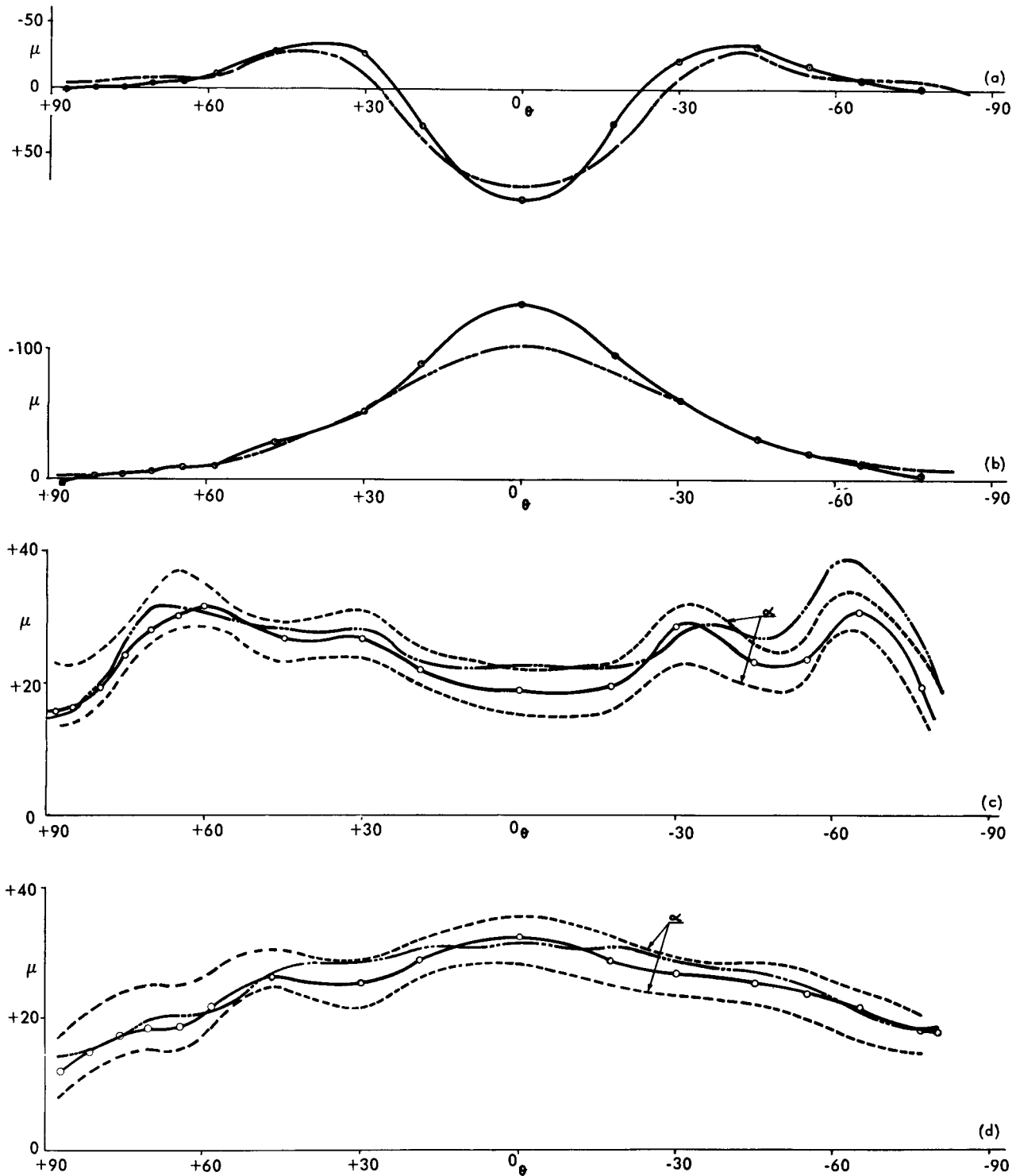


Figure 3. Experimental results 1/12th scale model

[Key]

(a): Internal meridional strains due to application of equatorial band of hoop prestress; (b): Internal hoop strains due to application of equatorial band of hoop prestress; (c): Internal meridional strains due to pressure. Experimental results are the average of 14 sets of results between 250 lb/in² and 350 lb/in² each normalised to 100 lb/in²; (d): Internal hoop strains due to pressure. Experimental results are the average of 18 sets of results between 250 lb/in² and 350 lb/in² each normalised to 100 lb/in²; Theoretical strain; —○—: Average experimental strain (limits of strain shown on c and d by α) $\mu = \text{strain} = 10^{-4}$; $\theta = \text{angle from equator of vessel}$

initial force of 615 tons (630 tonnes) and is contained in a 5½ in (14.0 cm) diameter duct.

The tests were designed to establish the efficiencies and ultimate strain capacities of the 36 strand tendons in straight and curved ducts, the strength of the specially developed concrete bearing plate, friction coefficients and the long term security of the system.

Analysis of vessel

A method of calculation based on the standard methods of analysis of indeterminate structures was developed, and a computer programme written to obtain a solution. The accuracy of the assumptions or approximations used in the calculations was checked against the behaviour of the various models and the experiments previously described.

Liner and closures

The vessel liner carries various construction loads but the main strains are imposed by the deformation of the concrete. A typical strain history indicates a maximum value of $2\,000 \times 10^{-6}$. This exceeds the compressive yield strain but the cyclic component is well within the limit of fatigue failure.

A more important consideration is the buckling of the liner, which must be prevented by tying the liner back into the concrete. The design should, however, be such that:

- (a) The strain at any point lies within the limit of high strain fatigue.
- (b) The ties will not fracture if buckling does occur.

As the onset of buckling cannot be theoretically predicted, compression tests have been carried out on a series of specimens formed by placing concrete between two 6 ft (1.83 m) diameter portions of the full size liner. These specimens have been subjected to strains of $2\,800 \times 10^{-6}$ before buckling.

In the detailed design of penetrations it is generally necessary to compensate for the opening in the liner, provide support for equipment in the opening, anchor the penetration liner in the concrete, isolate the closure from concrete deformations and provide radiation shielding.

Cooling system

Control of concrete temperature and hence thermal stresses is most positively achieved by insulating the liner and the providing of cooling pipes buried in the concrete. Demineralised, de-oxygenated water treated to a pH value of about 10.5 appears to give the best performance.

Optimisation of the Wylfa system has led to an array of square pipes of 1.7 in² (11 cm²) section area, welded to the liner and penetrating at a pitch not exceeding 12 in (30.5 cm), giving a local mean concrete temperature of 35 °C. The standpipes, which present a special problem, have annular water jackets.

To ensure that the liner and concrete are never overheated, alternate pipes are connected to separate systems, and pumps, coolers, power supplies, control and instrumentation equipment are duplicated. Potential hazards lie in the aggravation of corrosion of pipes

by radiolysis. The provision of internal shielding and an overpressure of hydrogen in the coolant, however, reduces the corrosion rate to a predicted 0.001 in (0.025 mm)/year. A treatment loop is fitted with centrifuges and ion exchange units to remove both insoluble and soluble impurities.

Insulation

Insulation must be compatible with fuel element materials and of a non dusting nature. Stainless steel foil is the only currently acceptable insulating material inside reactor vessels. The low conductance required, combined with material costs, make accurate prediction of performance essential. This is made difficult, however, by the results of convection, particularly leakage convection, aggravated by high system pressure and large vertical heights involved.

Tests have been carried out specifically to evaluate leakage convection, and advantage has been taken of the results of pressurised tests of large representative panels.

Wylfa vessels

The two reactors at Wylfa are each housed in a reactor hall, and served by a common reactor equipment building. The reactors are illustrated in Fig. 4.

Each reactor vessel has a spherical internal surface of 96 ft (29.2 m) diameter and a minimum concrete wall thickness of 11 ft (3.35 m). The external shape of the vessel has been evolved to facilitate construction and in order to accommodate plant, penetrations and prestressing components. The external surface of the vessel thus approximates closely to five concentric right cylinders with 16 vertical ribs. All external surfaces are plane, and either vertical or horizontal. The internal surface of the vessel is formed by a ¾ in (19 mm) thick steel liner, which maintains gas tightness and also serves as formwork against which the concrete is cast. The liner is tied to the concrete by angle-bars welded at a maximum pitch of 2 ft (61 cm).

The vessel is prestressed by three systems of tendons. One system consists of external hoop tendons, anchored on the vertical ribs. The other two systems are located within the concrete structure, and generally lie on vertical planes. In the first of these, tendons are arranged on vertical great circles in the barrel region of the vessel and the second provides an orthogonal grid of tendons in the upper and lower caps of the vessel. The latter grid conforms to the arrangement of 18 in (45.6 cm) od standpipes on a square lattice of 31 in (78.5 cm) pitch. The 36/0.6 in (15.3 mm) strand tendon was developed in order to achieve the necessary concentration of prestress, without undue congestion of ducts and anchorages.

The core and associated shielding are carried on a radial grid supported on rollers from the vessel at sixteen points. Access to the core from the standpipes is provided by guide tube assemblies carrying thermal shield plates.

The once-through boiler tubes are accommodated in the space between the shield tank and a cylindrical outer casing. This presents a single gas passage, but

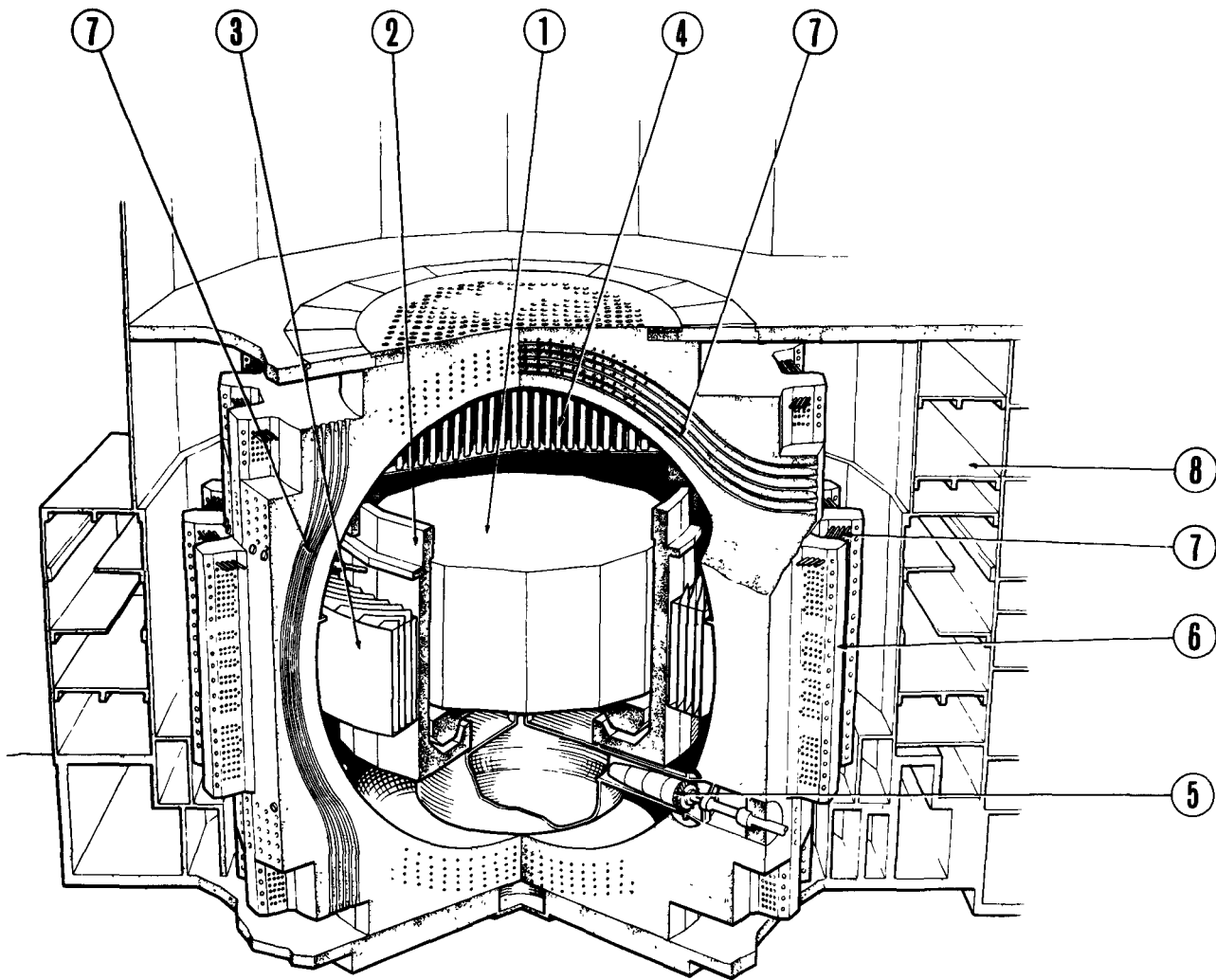


Figure 4. Wylfa nuclear power station reactor
1: Core; 2: Shield; 3: Boilers; 4: Standpipes; 5: Blowers; 6: Ribs; 7: Cables; 8: Equipment building

the boiler feed and steam pipes are arranged to give effectively four separate pipes but interwoven boilers. Bypassing of the boilers is prevented by a gas seal between the casing and the vessel.

The circulators are supported from their closure in the cylindrical part of these penetrations. They draw from the common boiler outlet into hemispherical volutes and discharge into a common plenum sealed to the radial grid.

Two construction access penetrations are fitted in positions corresponding to the circulators above the vessel equator. One of these accommodates the duct to the safety valves.

The interior of the vessel is accessible except above the core. Isolation of boiler tubes and routine maintenance, however, can be achieved without such access.

FUTURE DEVELOPMENT

The development of the Wylfa vessels shows that, for uranium-magnox applications, the present design

has not reached limiting conditions of dimensions and pressure, and hence reactor output.

Prestressed concrete pressure vessels can be readily designed to meet the requirements of the advanced gas-cooled reactor (AGR). Although reactor gas outlet temperatures will be higher—about 600°C —it appears to be economically preferable to provide a "hot-box" over the core, thus exposing the vessel to gas at inlet temperature only. Hence the duty on insulation and cooling system is decreased. The improved thermal performance of AGR leads to a reduction of vessel dimensions for a given output.

The most critical design problem arises in the pile cap region, where the high ratio of fuel element diameter to lattice pitch and the desirability of single channel access for fuelling, lead to very small concrete ligaments. This results in a notable loss of rigidity of the top cap and considerable construction problems.

Water cooled reactors are likely to require vessels with diameters and pressures variously in the ranges 12 to 25 ft (3.6 to 7.6 m) and 1 000 and 2 000 psi

(70 to 140 kg/cm²) respectively, whilst fast reactors may require larger vessels carrying much lower pressures. Preliminary studies indicate the prestressed concrete vessels would be generally feasible for these duties, although insulation would doubtless be a problem.

Until detailed designs are prepared, it is not possible to say whether they might offer an attractive alternative to steel. Over-riding considerations of reactor safety may well be an important influence in favour of prestressed concrete.

ABSTRACT—RÉSUMÉ—АННОТАЦИЯ—RESUMEN

A/141 Royaume-Uni

Étude de cuves sous pression en béton précontraint, notamment pour la centrale de Wylfa

par R. S. Taylor et A. J. Williams

Le mémoire décrit brièvement l'évolution des cuves sous pression en béton précontraint pour les réacteurs nucléaires modérés au graphite à réfrigérant gazeux, en se référant tout particulièrement aux cuves des réacteurs jumeaux en construction à la centrale nucléaire de Wylfa.

Un aperçu des caractéristiques et des limitations des cuves en acier est suivi d'une récapitulation des principaux avantages des cuves en béton précontraint. On examine l'intérêt de ces cuves pour les systèmes de réacteurs intégrés ainsi que leurs avantages du point de vue de la sûreté de ces réacteurs et de la souplesse dans la conception de ceux-ci.

On décrit comment la conception de la cuve est influencée par celle du réacteur. On examine l'optimisation d'une centrale nucléaire comprenant des cuves sous pression en béton précontraint, ainsi que les problèmes que posent les orifices de pénétration, les effets de l'irradiation, l'enveloppe de sécurité du système et le contrôle de la température de la cuve.

On passe en revue les différents systèmes de cuves sous pression en béton précontraint étudiés avant l'adoption du type de Wylfa. On donne les avantages et les limitations de chaque type, et on compare les diverses valeurs.

On examine les principaux facteurs influençant le choix des critères de construction des cuves sous pression en béton précontraint, et on récapitule les efforts admissibles pour le béton, l'acier de précontrainte et l'armature de renforcement. On étudie le comportement de la cuve au cours de sa durée utile en service et les déformations imposées à la garniture de la cuve et des orifices de pénétration, ainsi que la manière de déterminer le facteur de charge limite.

On décrit les principaux problèmes posés par l'étude et la construction de cuves sous pression en béton précontraint, ainsi que les recherches qui ont été entreprises pour arriver aux solutions adoptées. On examine les problèmes particuliers que posent les efforts et déformations de la cuve, les propriétés du béton, les concentrations de contraintes et le renforcement des orifices de pénétration, l'armature de renforcement, les organes de précontrainte, le comportement et l'étude de la gaine d'étanchéité et des

fermetures, le système de refroidissement et l'isolement. On décrit ensuite le comportement des maquettes de cuves dans les conditions de service et de charge limite.

On explique comment les résultats de ces recherches et perfectionnements ont été appliqués dans la conception des cuves pour les réacteurs de Wylfa.

On décrit les cuves jumelles de 96 pieds (29 mètres) de diamètre en construction à Wylfa, ainsi que l'agencement de l'installation principale des réacteurs.

Le mémoire se termine par une analyse sommaire des possibilités d'évolution des cuves sous pression en béton précontraint pour les centrales nucléaires.

A/141 Соединенное Королевство

Проектирование баков высокого давления из предварительно напряженного бетона. Конструкция баков в Уилфе

Р. С. Тэйлор *et al.*

В докладе кратко представлено развитие техники баков высокого давления из предварительно напряженного бетона для ядерных реакторов с газовым охлаждением и графитовым замедлителем. Особое внимание уделено двум реакторным бакам, строящимся на атомной электростанции в Уилфе.

Приводится краткий обзор характеристик и ограничений для стальных систем, сопровождаемый указанием основных преимуществ баков из предварительно напряженного бетона. Обсуждается пригодность таких баков для интегрированных реакторных установок и получающиеся в результате повышения безопасности и гибкости конструкции реактора.

Описывается влияние, которое конструкция реактора оказывает на конструкцию бака. Наряду с проблемами, связанными с проницаемостью, радиационными эффектами, поддержанием давления и контроля за температурой бака, обсуждается оптимизация атомной электростанции с баками высокого давления из предварительно напряженного бетона.

Приводится обзор различных конструктивных решений баков высокого давления из предварительно напряженного бетона, имевших место

до принятия конструкции в Уилфе. Описываются преимущества и ограничения каждого из них, и сравниваются отдельные величины.

Обсуждаются основные факторы, влияющие на выбор конструктивных критериев, и рассматриваются допустимые напряжения в бетоне со стальной арматурой. Обсуждается поведение бака за время его жизни при рабочих условиях, возникновение деформаций в самом баке и в фиттингах и определяются величины предельных нагрузок.

Рассматриваются основные проблемы, встречающиеся при конструировании и строительстве систем из предварительно напряженного бетона, и приводятся исследования, предпринятые в поисках конструктивных решений. Разбираются отдельные вопросы, такие как напряжения и деформации в баке, свойства бетона, концентрация напряжений, проницаемость, арматура, предварительно напряженные узлы, работа и устройство лейнеров и крышек, система охлаждения и изоляция. Рассматривается поведение моделей баков в рабочих условиях и при предельной нагрузке.

Приводится описание того, как исследования и разработки были объединены в конструкции баков реактора в Уилфе.

В докладе дается описание баков диаметром 29 м, строящихся в Уилфе, и способа размещения главной реакторной установки.

В конце доклада кратко обсуждаются возможности разработок баков высокого давления из предварительно напряженного бетона для атомных электростанций в будущем.

A/141 Reino Unido

El proyecto de vasijas de presión de hormigón pretensado, referido particularmente a Wylfa

por R. S. Taylor y A. J. Williams

Esta memoria describe brevemente la evolución de las vasijas de presión de hormigón pretensado para los reactores nucleares moderados por grafito y refrigerados por gas y se refiere, en particular, a las vasijas de los reactores gemelos, en construcción, en la central nuclear de Wylfa.

Después de pasar una breve revista a las características y limitaciones de los sistemas en acero, expone las

ventajas principales de las vasijas de hormigón pretensado. Se discute la adecuación de dichas vasijas para sistemas de reactor integrados y las características de la mejora de la seguridad que resultan, así como la flexibilidad de proyecto del reactor.

Se describe en qué forma influye el proyecto del reactor sobre el de la vasija. Se considera la «optimización» de una central nuclear que emplee vasijas de presión de hormigón pretensado, junto con los problemas relacionados con penetraciones, efectos de la radiación, contención de la presión del sistema y control de la temperatura de la vasija.

Se pasa revista a los diversos conceptos sobre proyecto de vasijas de presión de hormigón pretensado, estudiados antes de la adopción del proyecto Wylfa. Se exponen las ventajas y limitaciones de cada concepto y se comparan cantidades específicas.

Se discuten los factores principales que influyen en la elección de los criterios de proyecto de las vasijas de presión de hormigón pretensado y se consideran las tensiones admisibles en el hormigón, en el acero de pretensado y en la armadura de adherencia. Se discute el comportamiento de la vasija durante su vida en las condiciones de servicio y las deformaciones impuestas a la vasija y a los revestimientos de penetración, junto con la determinación del factor de rotura.

Se describen los problemas principales planteados en el proyecto y construcción de un sistema de vasija de presión de hormigón pretensado y la investigación emprendida para obtener solución al proyecto. Se examinan problemas individuales incluidos las deformaciones y tensiones de la vasija, propiedades del hormigón, concentración de tensiones y armadura de las penetraciones, armadura de adherencia, componentes del pretensado, comportamiento y proyecto del revestimiento y cierres, sistema de refrigeración y aislamiento. Después se describe el comportamiento de modelos de vasijas en condiciones de servicio y de carga de rotura.

Se expone la forma en que se ha incorporado esta investigación y desarrollo al proyecto de las vasijas del reactor Wylfa.

Se describen las vasijas gemelas de 28,8 m (96 pies) de diámetro que se construyen en Wylfa y la forma en que se ha dispuesto el equipo principal del reactor.

La memoria termina con una estimación sucinta del posible desarrollo futuro de las vasijas de presión de hormigón pretensado para centrales nucleares.

Investigations to predict the performance of steel reactor pressure circuit components in service

By C. H. A. Townley and E. Procter*

As owner and operator of a large number of nuclear power stations, the Central Electricity Generating Board has a responsibility to ensure the safety and integrity of its plant throughout its whole working life. The purpose of this paper is to outline the structures research work which the Board is undertaking, with this object in view, in the field of pressure circuit equipment.

The reactor pressure vessels and the pressure circuits generally are designed according to BS 1500 fusion welded pressure vessels for use in the chemical, petroleum and allied industries supplemented where appropriate, and where this is possible, with a detailed elastic stress analysis of certain features. Each vessel and each separate portion of the pressure circuit is subjected to an overpressure proof test before being put into service, and, in most cases, there is little doubt that initially the equipment is satisfactory for the duties imposed on it. However, neither a code of practice based largely on experience, nor a proof test of this nature, is adequate guarantee that the pressure parts will remain satisfactory throughout their working life. In the case of conventional plant, the annual statutory inspection provides a means of checking deterioration of the structure. For reactor pressure vessels and certain other parts of the pressure circuits, no inspection is possible once the plant has been in operation, and continued confidence in the integrity of the equipment must be sought indirectly.

A large part of the Board's pressure circuit research programme is, therefore, directed towards obtaining as detailed a knowledge as is possible, of the behaviour of the plant in service, taking into account, where necessary, changes in operating conditions and changes in material properties. In this context the main areas of interest are creep distortion, creep rupture and high strain fatigue. In some cases, it has also been necessary to investigate the margins between operating conditions and those which create distortion by short-term yielding. All of these effects are critically dependent on the geometry of the component and on the loading system, and must be given as much consideration as the purely metallurgical considerations of the material properties.

As well as leading to an improved understanding of pressure vessel performance in service, an important by-product of the work is the contribution it makes to the improvement of future designs. This is likely to be of importance in the conventional as well as the nuclear fields.

THE IMPORTANCE OF INELASTIC EFFECTS

As far as elastic stress analysis is concerned, the design of reactor pressure vessels has provided a stimulus for developing new mathematical techniques, particularly in the field of thin shells. Examples of this are the investigations by Hicks [1] on the discontinuity stresses at the intersections between the support skirt and the reactor vessel shell, by Rose [2] and by Penny [3, 4] on the stresses at nozzle penetrations, and the more recent work on the same subject by O'Connell and Chubb [5, 6]. On the experimental side, elastic stress analyses have been carried out on features such as support systems [7] and standpipe nozzles [8], and a more extended treatment of the latter feature is in progress at the Board's Leatherhead Laboratory. In addition, much information on the initial elastic stresses in the vessels is also now available from measurements taken during proof testing. Here, in addition to the strain gauges necessary for control purposes, it has been the Board's policy to provide comprehensive strain gauging round one particular feature in each vessel, such as a standpipe nozzle or a support skirt intersection, in order to obtain basic data.

Nevertheless, these elastic analyses are, in themselves, insufficient to provide a full understanding of the performance of the plant in service. Because of the high stresses which exist in certain parts of the vessels, a knowledge of inelastic behaviour is essential. For example, although creep rates at nominal design stress and design temperature are generally low, high discontinuity stresses of unknown magnitude, probably greater than yield, will tend to relax, and in so doing will cause distortion of such areas as the standpipe nozzles. Since any marked distortion of the standpipe nozzles will interfere with the correct operation of the refuelling machinery, no estimate of the useful life of a reactor vessel can be made without considering creep. In a similar way, when estimating the probability of high strain fatigue cracking at

* Central Electricity Generating Board, Research and Development Department, Berkeley Nuclear Laboratories.

discontinuities such as the vessel support, a further knowledge of inelastic behaviour is required.

Unfortunately, it is only recently that some attention has been directed to creep and plasticity effects in pressure retaining structures, and very little information is yet available which is of direct application to the problems under consideration. The Board's present research programme embraces two lines of approach: the theoretical and experimental.

The theoretical work is aimed at providing means of calculating strains and distortions in a complex shape using the data obtained from simple uniaxial materials tests. Once this has been done, it will be relatively simple to allow for changes in material properties brought about by irradiation. Progress is being made in this direction for simple shell structures with discontinuities such as nozzles operating in both inelastic regimes, but owing to the nature of the work, it will be several years before results are available.

In the immediate future, therefore, predictions about the performance of pressure circuit plant in service must be obtained from the experimental work. This involves testing models, or actual components, under a variety of loadings so as to induce creep and plasticity effects.

The experimental work has so far been concentrated on those component parts of the pressure circuit which are likely to be of critical importance in service. Because this represents a considerable departure from previous experimental stress analysis, the remainder of this paper deals, in some detail, with tests which have so far been completed. While the quantitative results apply only to the shapes tested, it is considered that some of the deductions made can be applied, in general terms, to other shell structures.

In some of the experiments, additional work has been undertaken to provide data which will be of use in future designs of pressure vessels. This is particularly the case in the tests concerned with short-term yielding. As well as demonstrating that the shapes tested had adequate ductility near to design conditions, and defining the limiting pressure range for high strain fatigue to occur, pressurization has been continued to pressures well above those which could credibly be applied in service. The object of this has been to observe the redistribution of stresses and strains which occur due to inelastic material properties. This is of considerable fundamental importance, since creep and plasticity are beginning to feature prominently in advanced thinking of shell structures.

YIELD TEST ON DUCT ELBOW

The corner unit in the coolant ducts are portions of the pressure circuit for which a detailed elastic stress analysis cannot be carried out. A unit of each design is, therefore, subjected to a proof test before type approval is given by the insurance authority.

In the case of one-design, localized yielding occurred at $1\frac{1}{4}$ times design pressure. This cast doubts on the fitness of the unit for the duty imposed on it, and

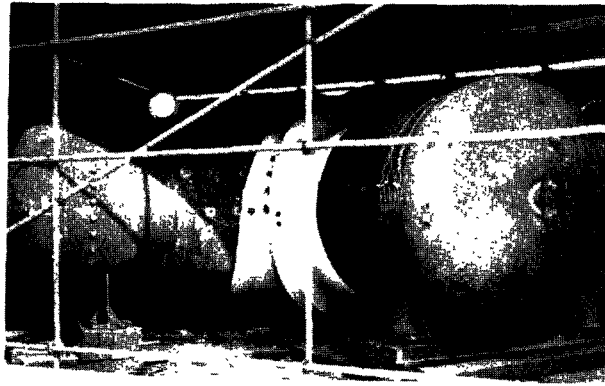


Figure 1. Duct elbow prepared for test

further tests were carried out at the Board's Berkeley Nuclear Laboratories. Since the unit concerned was intended for operation at temperatures not exceeding 250 °C., creep was not involved. The work at Berkeley was purely concerned with short-term plasticity and consisted of pressurizing beyond yield and ultimately to complete failure, at ambient temperature, using water as the working fluid [9]. Strains at critical points in the structure were monitored by electric resistance strain gauges and by replica gauges, at each stage of the pressurization.

The unit prepared for test is shown in Fig. 1. Figure 2 gives the dimensions of the vessel and the positions of the strain gauges. The unit has been manufactured from BS 1501/161C. steel and had been stress relieved prior to the test work at Berkeley.

The unit behaved in a perfectly elastic manner up to a pressure of 350 psig (24.6 kg/cm²) when the strain gauges at the intrados started to show deviations from linear behaviour. As pressures were increased further, the strains in this region increased very quickly and, at the same time, the zone of yielded material spread to other parts of the structure. A typical plot of strains in the duct leg adjacent to the discontinuity is shown in Fig. 3 while Fig. 4 shows how the stresses on the same section are redistributed as yielding proceeds.

Significant distortion first began to appear at a pressure of 700 psig (49.2 kg/cm²), and at 800 psig (56.2 kg/cm²) the curve of pressure versus volume of water pumped (Fig. 5) shows that general yielding of the whole vessel took place. The vessel finally failed at a pressure of 1 390 psig (97.7 kg/cm²) when a fast running crack propagated from a point at the intrados where two welds joined. Adjacent to the point of failure, the reduction in plate thickness was approximately 20% in the duct leg, and approximately 10% in the reinforcing band. Measurements at positions remote from the failure point showed reductions of thickness of between 6% and 7%, which can be compared with an 8% reduction of thickness on a simple tensile test piece of the vessel material. The results illustrate the capacity with which a structure in a ductile material, such as mild steel, can accommodate large overloads through redistribution of stress by yielding. The initial elastic stress concentration

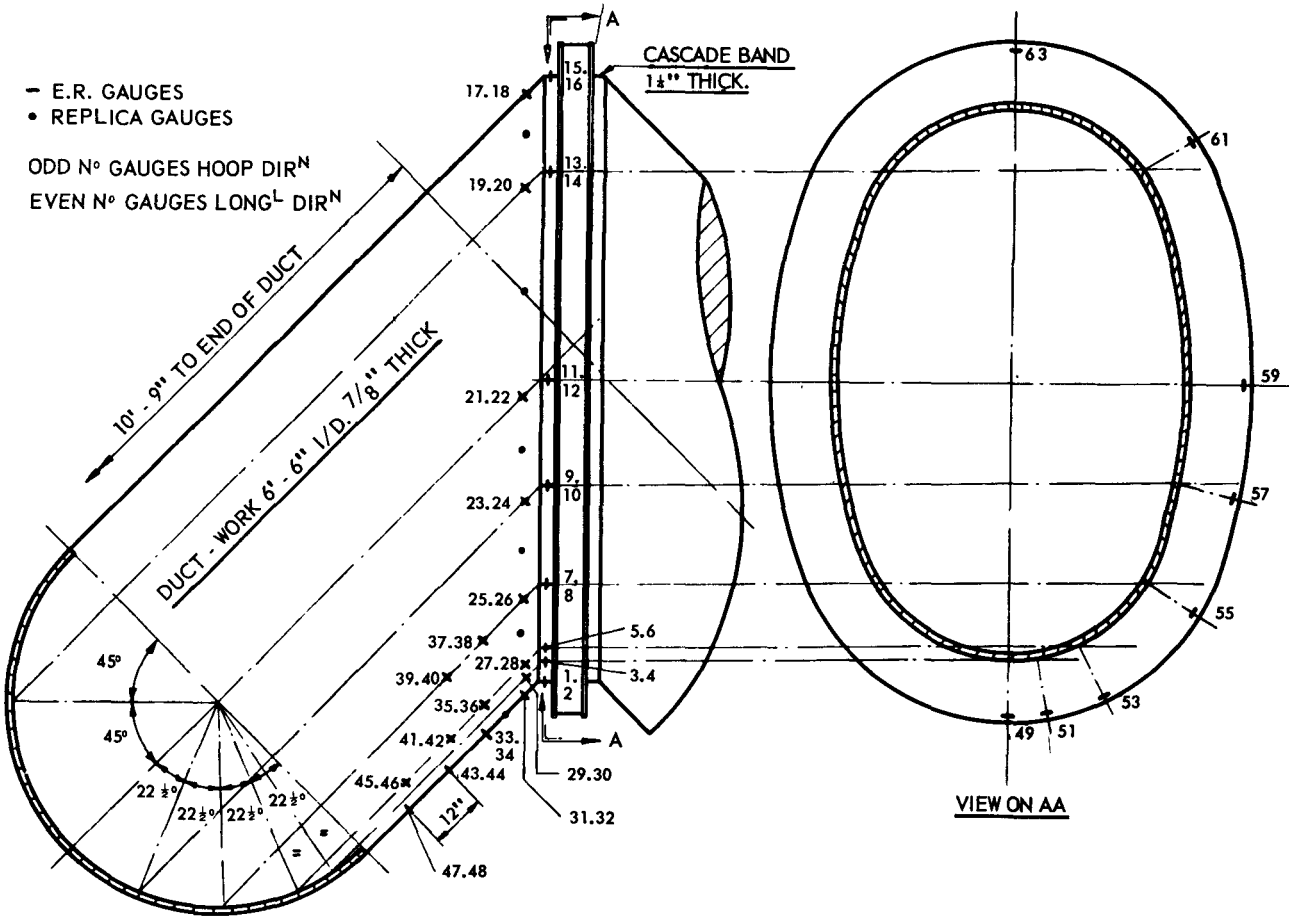


Figure 2. Duct elbow. Dimensions and strain gauge positions

was 2.1, and at failure this had been reduced to approximately 1.1.

The design pressure for the duct corner is 295 psig (20.71 kg/cm²). In addition to the internal pressure, the corner unit is subjected to external bending moments, under certain service conditions. However, from work previously carried out, the effect of this

bending moment, when added to the pressure stress, is inconsequential. Thus for the unit tested, after making allowance for corrosion, there is a factor of 2.2 between the pressure at which distortion occurs and design pressure. The factor between failure pressure and design pressure is 4.4.

The experiment clearly demonstrates that the unit

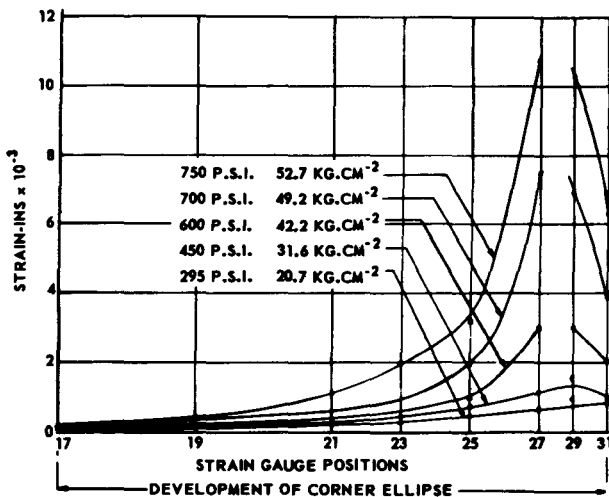


Figure 3. Hoop strains on duct leg

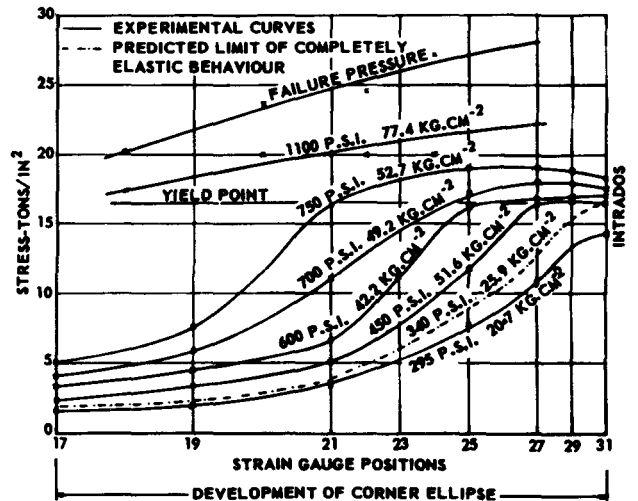


Figure 4. Hoop stresses on duct leg

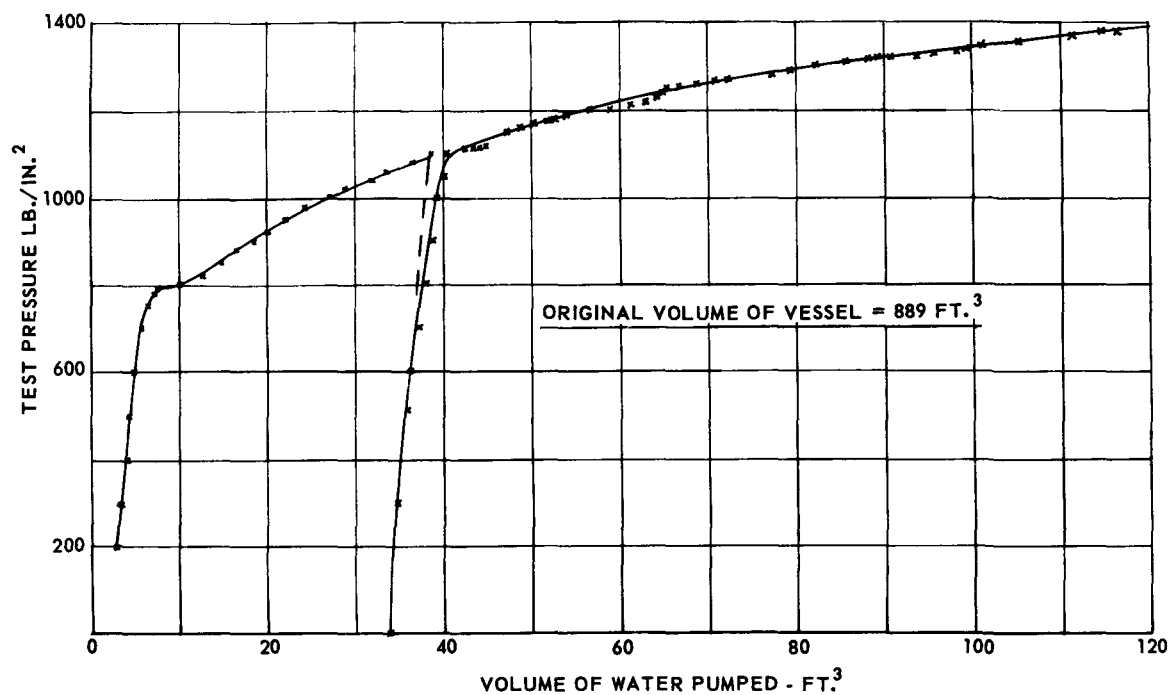


Figure 5. Volume change during pressurization

is satisfactory for operation at the design pressure of 295 psig (20.71 kg/cm²) in that it has adequate ductility to sustain accidental overpressure. Detailed considerations of the strain gauge readings, dealt with more fully in reference [9], also show that at this pressure, there is no problem from high strain fatigue.

TESTS ON STANDPIPE NOZZLES

Yield test on standpipe nozzle cluster

Because it was known that high stresses exist in the regions of reactor vessels, which include the standpipe penetrations, it was decided to carry out a series of preliminary tests at a relatively small scale. These were intended to show in which direction, if any, further large-scale work would be required. It was recognized that to make predictions about high strain fatigue and creep rupture, a certain amount of work on fully strain-gauged, large-scale vessels would be necessary at a later date.

Due to the availability of press dies, and also because of the size of vessel which could be safely shielded during subsequent tests, using gas as the pressurizing medium, the vessels, for the preliminary tests, were designed to 1/13th scale size. A carbon/manganese steel similar to that used in the full size reactor vessel was chosen for the models. Special attention was given to procedure to ensure that the areas to be tested were, as far as possible, geometrically identical to the full sized vessel. Figure 6 shows a section through a typical nozzle area prior to test. While the scale was too small to permit comprehensive strain gauging of the highly stressed areas, a number of gauges were attached to give an over-all indication of vessel behaviour.

In the first test, the vessel was pressurized beyond yield, and eventually to failure at ambient temperature [10, 11]. The object was to find the margin between operating pressure and failure pressure and to observe the way in which the standpipe nozzle area behaved as yielding proceeded. The latter object, as well as being of fundamental value, had a more immediate interest. Since creep and plasticity are both examples of general inelastic behaviour, the test permitted a qualitative prediction of creep distortion, which was required in advance of the long-term creep experiments.

In general, the vessel behaved in a similar way to the duct corner unit described previously. Failure occurred at a pressure of 1 670 psig (117.4 kg/cm²), which is 5.58 times the design pressure. The membrane stress in the shell remote from the nozzle at failure was 36.6 tons/in² (5 765 kg/cm²), and when this is compared with the ultimate tensile strength of the material of between 36 tons/in² (5 670 kg/cm²) and 37 tons/in² (5 828 kg/cm²), it is quite clear that yielding has reduced the stress concentration factor to a little over unity. The initial elastic stress concentration factor was approximately 2 and the result is somewhat surprising. The geometry is such that from an initial consideration it might be concluded that yielding would not redistribute the forces as readily as in the case of the duct corner.

The experiment shows that the nozzle region has adequate ductility to sustain occasional overpressure, and dispels any doubts about the presence of triaxial stress effects, which would cause sudden failure without significant yielding. The tests were carried out above the transition temperature of the material used for the construction of the model vessels. This is



Figure 6. Section through a typical nozzle area prior to test

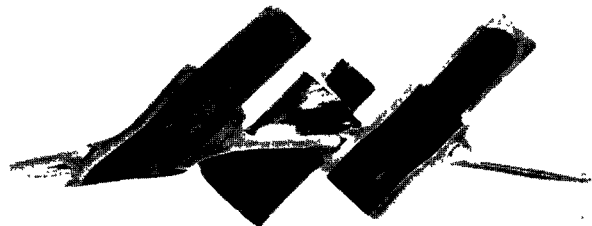


Figure 7. Section through nozzles showing failure

consistent with the Board's practice for operation of the reactors. At all times when the vessels are pressurized, they are maintained above their transition temperature.

The failure was caused by a fracture in the hoop plane of the outer nozzle welds. This is shown in Fig. 7, which also gives an indication of the distortion which took place prior to failure. The position and direction of the fracture are what would be expected from elastic considerations. This means, that although the relative magnitude of the maximum stresses are reduced as yielding takes place, their position and direction are unchanged.

Creep test on standpipe nozzle cluster

A second spherical vessel, identical to that previously described, was subjected to a long-term test under creep conditions [12]. The purpose of this was to form an estimate of the amount of creep distortion likely to take place in the vicinity of the standpipe nozzles during the working life of the reactor, assuming that the top of the vessel was operated continuously at its design temperature.

On the full-size vessels, material properties are such that the creep strain in the unpierced membrane portion of the vessel will not exceed 0.05%, or in some designs 0.1%, in 200 000 hours. The test conditions were chosen so that, in the model, about 0.07% creep strain was obtained in the unpierced portion of the vessel in 3 000 hours. Most of this acceleration was achieved by increasing the temperature of the test vessel, but because of limitation of the equipment, a further acceleration was obtained by increasing the pressure 20% above the operating pressure of the full-sized vessel.

Because of the nature of the test, gas pressurization was the only feasible method and for safety reasons the test was carried out in an underground pit, to prevent damage in the case of failure. The heating was by means of electric blanket heaters, and apart from one shut-down during running, for readjustment, the temperature was maintained to within $\pm 2^\circ\text{C}$ of the desired value.

In addition to the pressure loading, an external load was applied to one nozzle to simulate the restraint of

the top of the standpipe in the pile cap. This load was progressively increased as the test proceeded, since the restraining force varies as the vessel creeps.

The area of the vessel containing the nozzle cluster was surveyed before and after the test. The data obtained show that the circumferential growth of the vessel in the standpipe region is approximately three times that of the unpierced portion of the vessel. This is thought to be pessimistic because the amount of flattening of the shell profile which occurred during the manufacture of the model vessel was greater than on a full-sized reactor vessel. However, using this factor of 3, and assuming that the unpierced portion of the reactor vessel creeps by 0.1% in 200 000 hours, then it can be predicted that the maximum outward displacement of an outermost standpipe nozzle will not exceed 1 in (2.54 cm) in twenty years.

The rotation of the nozzles in the test vessel was less than 1° . There was difficulty in obtaining accurate measurements with such small deflections, but the indications were that the more oblique standpipes rotated to a greater extent than the less oblique ones. The direction of rotation was in the sense of decreasing the angle of obliquity and this adds to the effect of outward displacement as far as restraining forces at the pile cap are concerned. Calculations show that even relatively small angular rotations can produce high stresses in the standpipes, and that the rotations are more important in this respect than the outward deflections [13].

The experimental results serve to disprove pessimistic speculation about large distortions in the region of oblique nozzles. Nevertheless, because even small rotations could give rise to embarrassment in operation, provision is to be made on the reactor vessels to check the deflection of representative standpipes.

Cyclic load test on standpipe nozzle cluster

A third spherical vessel has been tested under conditions identical to those in the steady creep test already described. The main difference is that the pressure is reduced to atmospheric forty times during the period of the experiment to simulate the effect of reactor shut-downs.

The results so far obtained show that distortions are

generally similar to those which took place during the steady-state creep test. It seems that such elastic-plastic shakedown as has occurred has been small compared with creep relaxation.

SKIRT TO SHELL INTERSECTION

Yield test

Elastic calculations show that, under operating conditions, on several reactors, the stresses in the vicinity of the intersection between the main pressure shell and the support skirt approach yield [14]. This particular situation is unusual, in that the overpressure acceptance test is, in itself, no conclusive proof that the vessel is satisfactory from the start. Although the proof test is carried out at 1½ times design pressure, the maximum stress at the intersection, under these conditions, differs insignificantly from that when the

vessel is operating. This is because additional items, such as standpipes, added to the vessel after the proof test, increase the self-weight and because severe temperature gradients occur near the intersection when the vessel is hot.

Calculations of the behaviour of the intersection after yielding has occurred was not possible, and it was, therefore, decided to carry out experimental work to establish the margin between operating pressure and the pressure at which distortion of the vessel first becomes significant [15]. Considerations of cost and convenience led to the choice of a small vessel which would provide information of a general nature and show whether operational problems were of sufficient magnitude to justify more detailed research. The scale was finally decided to suit availability of components and machining facilities. The portion of the vessel containing the intersection and the support skirts was

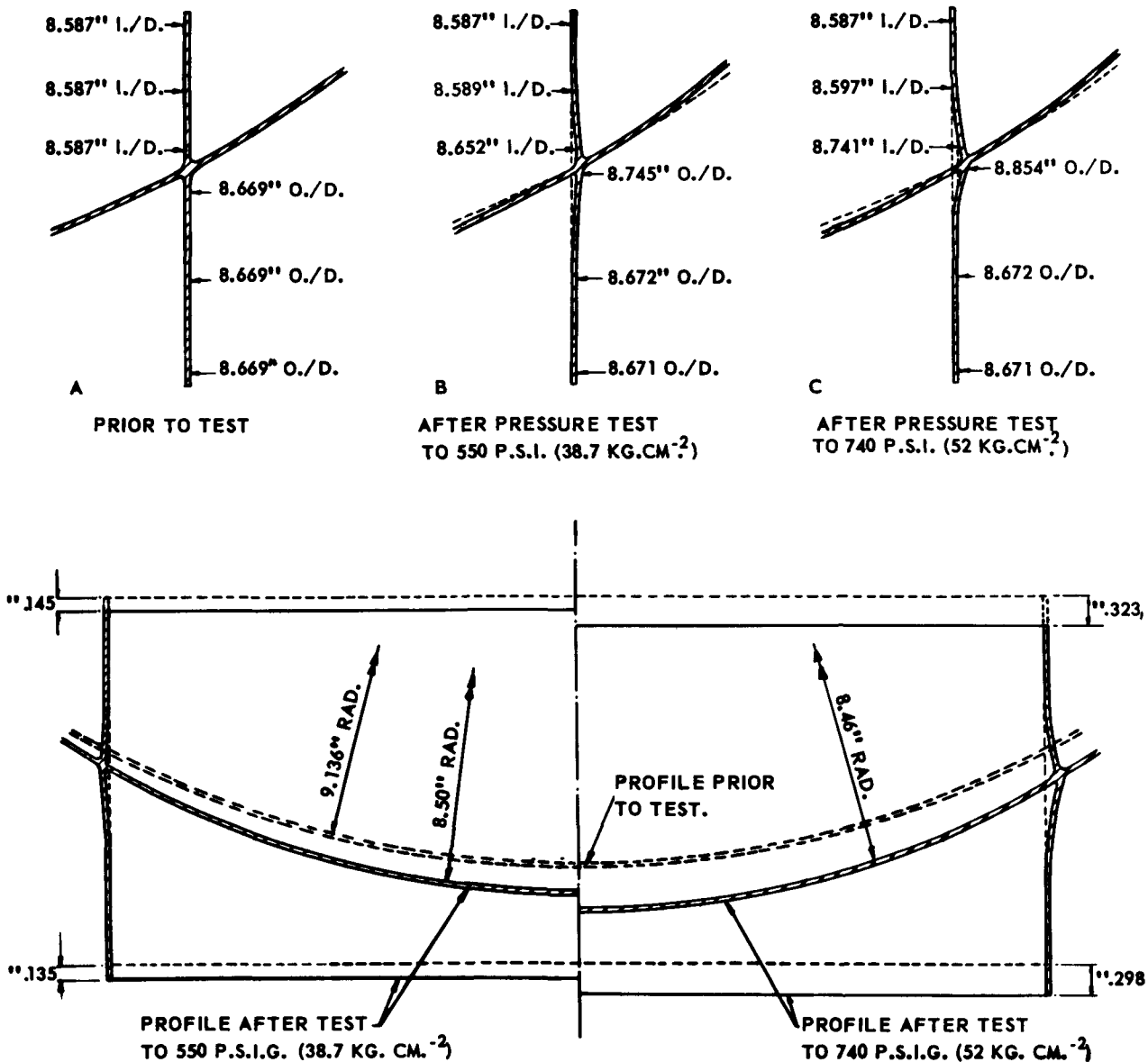


Figure 8. Distortion of intersection and lower portion of vessel at various test pressures

reproduced accurately at 1/44th full size. The steel used for this part of the model was a carbon/manganese steel typical of that used in the full sized vessels.

The vessel was hydraulically pressurized at ambient temperature. In order to obtain correct stresses at the intersection due to the self weight of the vessel and attachments, an external load of 0.81 tons (823 kg) was applied at the top of the model. Shape changes were measured by means of dial gauges, and by taking plaster casts of the intersection at various stages of the pressurization. Figure 8 gives a general indication of how the distortion of the intersection proceeded with increasing pressure. Significant distortion did not occur until $1\frac{1}{2}$ times design pressure was reached, and at 4 times design pressure, there was no sign of failure in the vicinity of the intersection.

It is concluded that the vessel design is satisfactory in this respect despite the high surface stresses. The explanation appears to lie in the relatively large ratio between the pressure to cause first yield and the pressure to form a plastic hinge circle.

Cyclic load test

As well as short-term plastic deformation, cyclic loading is important in structures which contain zones of material initially above the yield point. Even if such a structure eventually shakes down into a pseudo-elastic state, this may be accompanied by significant distortion.

A second test was, therefore, set up with an identical model, which was subjected to forty pressure cycles from atmospheric pressure up to design pressure and back to atmospheric pressure. The test was carried out at a temperature of 225 °C and a temperature gradient was introduced in the outer skirt to simulate that occurring in practice.

The measurements so far made of the model after the test suggest that the distortion due to this shake-down is so small as to be of no practical importance. There is no evidence of continued plastic cycling of a sufficiently large magnitude to cause high strain fatigue.

CONCLUSIONS

The work reported here has mainly been concerned with plastic effects and creep distortion, and, to a lesser extent, high strain fatigue. The results so far obtained are encouraging, in that in most of the

components tested, high local stresses do not lead to a deterioration in integrity under the service conditions investigated.

Further experimental work is required to predict fully the behaviour in service of the whole of the reactor plant. Large-scale tests are now in progress to examine strain concentrations around the standpipe nozzles in detail, from the point of view of high strain fatigue and creep rupture. It is likely that the range of components tested will need to be extended to include, for example, parts of the vessels where operational data shows that there are high thermal stresses. Also, because there is a strong economic incentive for moderate increases in operating pressures and temperatures, further work will be required in this direction.

REFERENCES

1. Hicks, R., *Proc. I. Mech. E.*, 172, 707 (1958).
2. Rose, R. T., and Thompson, J. M. T., in *Proceedings of Symposium on Nuclear Reactor Containment Buildings and Pressure Vessels*, Royal College of Science and Technology, Glasgow (1960).
3. Penny, R. K., *J. Mech. Eng. Sci.*, 3, 369 (1961).
4. Penny, R. K., in *Proceedings of Symposium on Nuclear Reactor Containment Buildings and Pressure Vessels*, Royal College of Science and Technology, Glasgow (1960).
5. O'Connell, J. M., and Chubb, E. J., C.E.G.B. Report RD/B/N.137 (1963).
6. O'Connell, J. M., and Chubb, E. J., to be published in *Proceedings of Applied Mechanics Group Convention*, I. Mech. E., London (1964).
7. Noone, M. J., and Bishop, R. F., *Proc. I. Mech. E.*, 175, 471 (1961).
8. Rose, R. T., Mantle, K. G., Procter, E., Horseman, R. W., Mackenzie, A. C., and Spence, J., in *Proceedings of the Symposium on Pressure Vessel Research Towards Better Design*, I. Mech. E., London (1962).
9. Townley, C. H. A., and Procter, E., *The Engineer*, 216, 1057 (1963).
10. Townley, C. H. A., Procter, E., Grindrod, A., and Gadd, B. W., C.E.G.B. Report RD/B/N. 165 (1963).
11. Townley, C. H. A., Procter, E., Grindrod, A., and Gadd, B. W., to be published in *Proceedings of Applied Mechanics Group Convention*, I. Mech. E., London (1964).
12. Townley, C. H. A., Procter, E., and Gadd, B. W., C.E.G.B. Report RD/B/N.240, (1964).
13. Chubb, E. J., C.E.G.B. Report RD/B/N.162 (1964).
14. O'Connell, J. M., and Townley, C. H. A., C.E.G.B. Report RD/B/N.45 (1962).
15. Procter, E., and Strong, J. T., C.E.G.B. Report RD/B/N.212 (1964).

ABSTRACT—RÉSUMÉ—АБСТРАКТ—RESUMEN

A/144 Royaume-Uni

Recherches tendant à prévoir le comportement en service de composants en acier des circuits sous pression des réacteurs

par C. H. A. Townley et E. Procter

Le mémoire traite des recherches dans le domaine mécanique concernant les cuves sous pression et les

composants du circuit primaire de refroidissement. Il indique les problèmes qui sont d'un intérêt primordial pour le Central Electricity Generating Board, c'est-à-dire ceux concernant la sûreté et l'intégrité de l'installation pendant sa durée utile. Il décrit le travail effectué jusqu'ici dans cette direction et passe en revue ce qui reste à faire.

A l'heure actuelle, il n'est généralement pas possible de calculer à l'avance le comportement en service de

composants du circuit sous pression, spécialement s'il faut tenir compte du fluage et d'autres formes de comportement inélastique. C'est pourquoi dans l'avenir immédiat les données requises doivent provenir d'essais, sur les pièces elles-mêmes et sur des maquettes, effectués le cas échéant dans des conditions d'environnement simulées.

Les études de ce genre dont traite le mémoire comprennent:

a) Trois essais au-delà de la limite de résistance de pièces soumises à des efforts élevés: un coude de conduite, un groupe de tubulures des canaux de chargement et une jonction entre une bordure de support et une coque sphérique.

b) Un essai de fluage sur un groupe de tubulures des canaux de chargement.

c) Deux essais de charge cyclique sur un groupe de tubulures des canaux de chargement et sur une intersection entre une bordure de support et une coque sphérique.

A/144 Соединенное Королевство

Исследования, связанные с предсказанием характеристик действующих узлов стальных реакторных баков давления

С. Х. А. Таунли, Э. Проктер

В докладе представлены исследования инженерных проблем, связанных с баками высокого давления и узлами первичных контуров теплоносителей в ядерных реакторах. Кратко рассматриваются проблемы, представляющие большой интерес для Центрального энергетического управления, а именно проблемы безопасности и исправности установок в течение всего периода эксплуатации. Приводятся работы, выполненные в этом направлении, и рассматриваются задачи, требующие своего решения.

В настоящее время обычно не удается с помощью расчета предсказывать эксплуатационные характеристики действующих узлов контура давления, особенно если наблюдаются ползучесть металла и другие виды неупругих деформаций. Поэтому необходимые данные в ближайшем будущем должны быть получены из испытаний действительных узлов и моделей, которые в случае необходимости будут проводиться в имитированных условиях окружающей среды.

Рассматриваемые в докладе исследования этого типа включают:

a) три испытания за пределом текучести таких узлов контура высокого давления, как колленчатый трубопровод, пучок вертикальных наконечников труб и соединение опорного цилиндра со сферической оболочкой;

b) испытание на ползучесть с пучком вертикальных наконечников труб;

c) два испытания на циклическую нагрузку с пучком вертикальных наконечников труб и с соединением между опорным цилиндром и сферической оболочкой.

A/144 Reino Unido

Investigaciones para predecir el comportamiento en servicio de las componentes del circuito de presión de acero de los reactores

por C. H. A. Townley y E. Procter

Esta memoria trata de la investigación, desde un punto de vista técnico, de las vasijas de presión de los reactores nucleares y de las componentes del circuito primario de refrigeración. Se perfilan los problemas que son de mayor interés para la Central Electricity Generating Board, problemas que conciernen a la seguridad e integridad de la central durante su vida de funcionamiento. Se describe el trabajo que en este sentido se ha terminado ya, y se revisa lo que todavía debe hacerse.

Actualmente, por medio del cálculo, no es posible predecir de un modo general el comportamiento en servicio de las componentes del circuito de presión, especialmente si aparece la fluencia lenta u otras formas de comportamiento inelástico. Por tanto, en un futuro inmediato, la información necesaria debe obtenerse a partir de las pruebas en las componentes reales y en los modelos, efectuadas, si fuese necesario, en condiciones de ambiente simuladas.

Las investigaciones de este tipo, tratadas en la memoria, comprenden:

a) Tres ensayos por encima del punto de fluencia en componentes sometidas a tensiones elevadas — una zona angular en un tubo, un conjunto de toberas adyacentes, y una intersección entre un soporte circular y una vasija esférica.

b) Una prueba de fluencia lenta en un conjunto de toberas adyacentes.

c) Dos pruebas de carga cíclica en un conjunto de toberas adyacentes y en una intersección entre un soporte circular y una vasija esférica.

Problems in the design and construction of large reactor vessels

By A. L. Gaines* and L. Porse**

The Atomic Energy Commission of the United States has encouraged and assisted in the development of nuclear plants for the production of electrical power. In the past two years, however, many utility companies have signed contracts for nuclear-fueled power stations for a purely economic reason, without Government funding being a factor in their decision. Although prototype plants using liquid metal and gaseous coolants have been built, commercial application of atomic energy in the United States has concentrated on water systems for economical production of electrical power from nuclear fuel. The commercial plants being constructed use either pressurized water or boiling water reactor systems, therefore the vessels for other systems will not be discussed.

Increasing the size of the reactor system greatly reduces the cost of nuclear power generation. The most recent nuclear stations in the 500 to 600 MW(e) capacity range are advertised as capable of producing electricity at a cost that will be competitive with fossil-fueled power plants even in the coal mining regions of the United States. Vessel designs now permit construction of water system plants in capacities of 1 000 to 1 500 MW(e). Fossil-fueled plants will have difficulty in competing with nuclear-fueled plants in sizes of 600 to 700 MW(e) capacity.

The relation between reactor vessel size and the power rating of the two water cycle systems is illustrated in Fig. 1. Only the large power producing systems that are built or are being built are plotted on this figure. The band width covers plant sizes being investigated for current and future offerings to the utility industry.

DESIGN CONSIDERATIONS

Until very recently, the design and fabrication of reactor vessels in the United States have conformed to the basic requirements of Sections I or VIII of the ASME Power Boiler and Unfired Pressure Vessel Codes. Additional precautions, considered advisable in consultation between responsible system designers and governmental agencies, have been taken due to

concern for the public interest and have resulted in components of exceptionally high integrity. This need for higher standards led, in 1956, to the initial formulation of ASME Code Cases, which gave supplementary requirements for nuclear vessels, and later, to the preparation of Section III, Rules for Construction of Nuclear Vessels. Section III was approved by the ASME late in 1963 and issued in March of 1964.

The rules of Section III differ from those of the older sections of the Code in the following respects:

(a) Section III requires the detailed calculation and classification of all stresses and the application of different stress limits to different classes of stress. On the other hand, the older sections, I and VIII, gave formulas for minimum allowable wall thicknesses. The higher, more localized stresses were controlled by a safety factor and a set of design rules for determining the shape of details such as heads and nozzles. The major stress categories used in Section III are primary, secondary, and peak. Their chief characteristics may be described briefly as follows:

(i) Primary stress is that developed by the imposed loading necessary to satisfy the laws of equilibrium between external and internal forces and moments. The basic characteristic of a primary stress is that it is not self-limiting. If a primary stress exceeds the yield strength of the material through the entire thickness, the prevention of fracture depends entirely on the strain-hardening properties of the material.

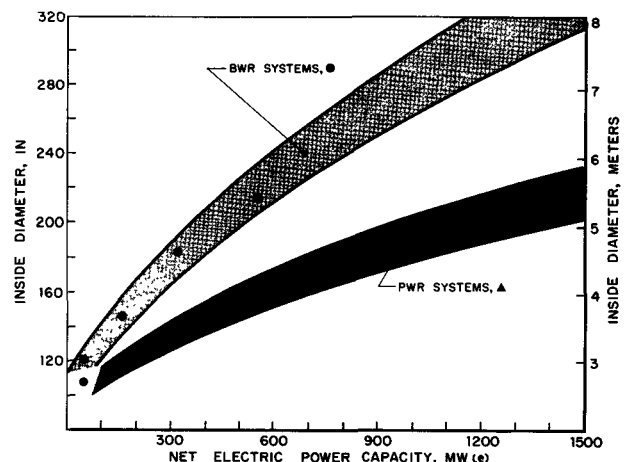


Figure 1. Reactor vessel diameter vs. plant power rating

* Combustion Engineering, Inc., Chattanooga, Tennessee.
 ** Westinghouse Electric Corporation, Pittsburgh, Pennsylvania.

(ii) Secondary stress is a stress developed by the self-constraint of a structure. It must satisfy an imposed strain pattern rather than being in equilibrium with an external load. The basic characteristic of a secondary stress is that it is self-limiting since minor distortions can satisfy the discontinuity conditions or thermal expansions which cause the stress to occur.

(iii) Peak stress is the highest stress in the region under consideration. The basic characteristic of a peak stress is that it causes no significant distortion and is objectionable mostly as a possible source of fatigue failure.

Secondary stresses are assigned higher allowable values than primary stresses. Peak stresses are limited only by fatigue considerations. The allowable value of primary-plus-secondary stress is three times as high as the allowable value of primary stress.

(b) Because of its more detailed stress analysis, the rules of Section III necessitate the use of the maximum shear stress (Tresca) theory of failure instead of the maximum stress (Rankine) theory.

For the simple analyses on which the thickness formulas of Sections I and VIII are based, it makes little difference whether the maximum stress theory or the maximum shear stress theory is used. When a more detailed stress analysis is made, however, the difference between the two theories becomes important. A good example is the knuckle region of a dished head, where the largest stress is meridional tension on the inside surface. This stress is accompanied by a circumferential compression, so that the stress intensity is larger than the highest stress component. For one particular case, a 2:1 ellipsoidal head on a 48 in (1 219 mm) diameter vessel designed for 133 psi (0.0934 kg/mm²), calculations indicated that the maximum stress was 23 480 psi (16.5 kg/mm²) and that the highest stress intensity was 33 360 psi (23.4 kg/mm²). The basic design stress in the cylinder was 20 000 psi (14.05 kg/mm²); thus the maximum stress theory would indicate that the stresses exceeded the basic design stress by only 17%, but the maximum shear stress theory shows that the basic design stress was exceeded by 67%.

(c) Section III requires the calculation of thermal stresses and gives allowable values for them. Thermal stresses fall into either the secondary or peak stress categories depending on how much general distortion they might produce.

(d) Section III considers the possibility of fatigue failure and gives rules for its prevention. Design fatigue curves based on strain-controlled fatigue tests are provided, but the strain values are multiplied by the elastic modulus of the material to give values which have the dimensions of stress. Direct comparison can therefore be made to stress values calculated by the usual methods of the theory of elasticity.

(e) Basic stress limits of Sections I and VIII for ferritic materials below the creep temperature range are the lower of $\frac{1}{4}$ of the specified minimum tensile strength or $\frac{2}{3}$ of the specified minimum yield strength at the temperature. In Section III these factors have

been increased to $\frac{1}{3}$ and $\frac{2}{3}$, respectively. Therefore, vessels designed to the rules of Section III will usually have thinner walls than those designed to the older sections. Higher integrity is obtained by replacing a large safety factor to cover unknown localized stresses with a detailed stress analysis.

(f) Requirements for materials, fabrication and inspection are more restrictive in Section III than in Sections I and VIII, and reflect the practices which have been developed and used in the United States during the past several years in the construction of reactor vessels.

For each of the Code Sections, the designer must select pressure vessel details to meet all Code requirements, while striving for optimum utilization of available materials and fabrication facilities. Figure 2 illustrates reactor vessel cross sections for 1 000 MW(e) capacity, water reactor systems. The left side of these cross sections shows the design made to Section VIII requirements, while the right side shows the redesign to Section III requirements. These designs are typical of present United States practices. Although the weights are great and the materials are of unusual thickness and dimension, careful investigations have verified the present capability to produce either vessel. Under Sections I or VIII, all nozzle opening reinforcement was permitted to be in the nozzle—now, under Section III, the reinforcement must be nearer the vessel wall. Therefore, the nozzles are much shorter and thicker for Section III designs. For example, the upper nozzle on the illustrated BWR vessel extended 42 $\frac{1}{4}$ in (1 073 mm) from the inside diameter and was 35 $\frac{3}{8}$ in (911 mm) maximum diameter for the Section VIII design. This nozzle extended only 28 $\frac{1}{4}$ in (819 mm) out from the inside diameter but had to be 42 $\frac{3}{8}$ in (1 076 mm) maximum diameter for the Section III design. Fabrication costs are greater for the shorter, larger-diameter nozzles. Savings in total material weight obtained by using Section III requirements result from the thinner vessel walls. The PWR vessel weight was reduced by 16% (from 1 407 000 lb or 637 000 kg to 1 189 000 lb or 540 000 kg). The BWR vessel weight was reduced 25% (from 2 088 000 lb or 948 000 kg to 1 558 000 lb or 706 000 kg).

MATERIAL CONSIDERATIONS

Large vessels require wall thicknesses in excess of the thicknesses referenced in the ASME Material Specifications for each grade of material used. The availability of acceptable materials, therefore, must be determined. Three types of problems are associated with materials:

(a) designing the vessel to utilize materials that can be manufactured with the needed dimensions, and that will satisfy the exacting requirements of chemical and mechanical properties;

(b) inspecting the vessel to assure that the specified quality is obtained in materials, and maintained through all phases of fabrication; and,

(c) planning each operation to permit handling and

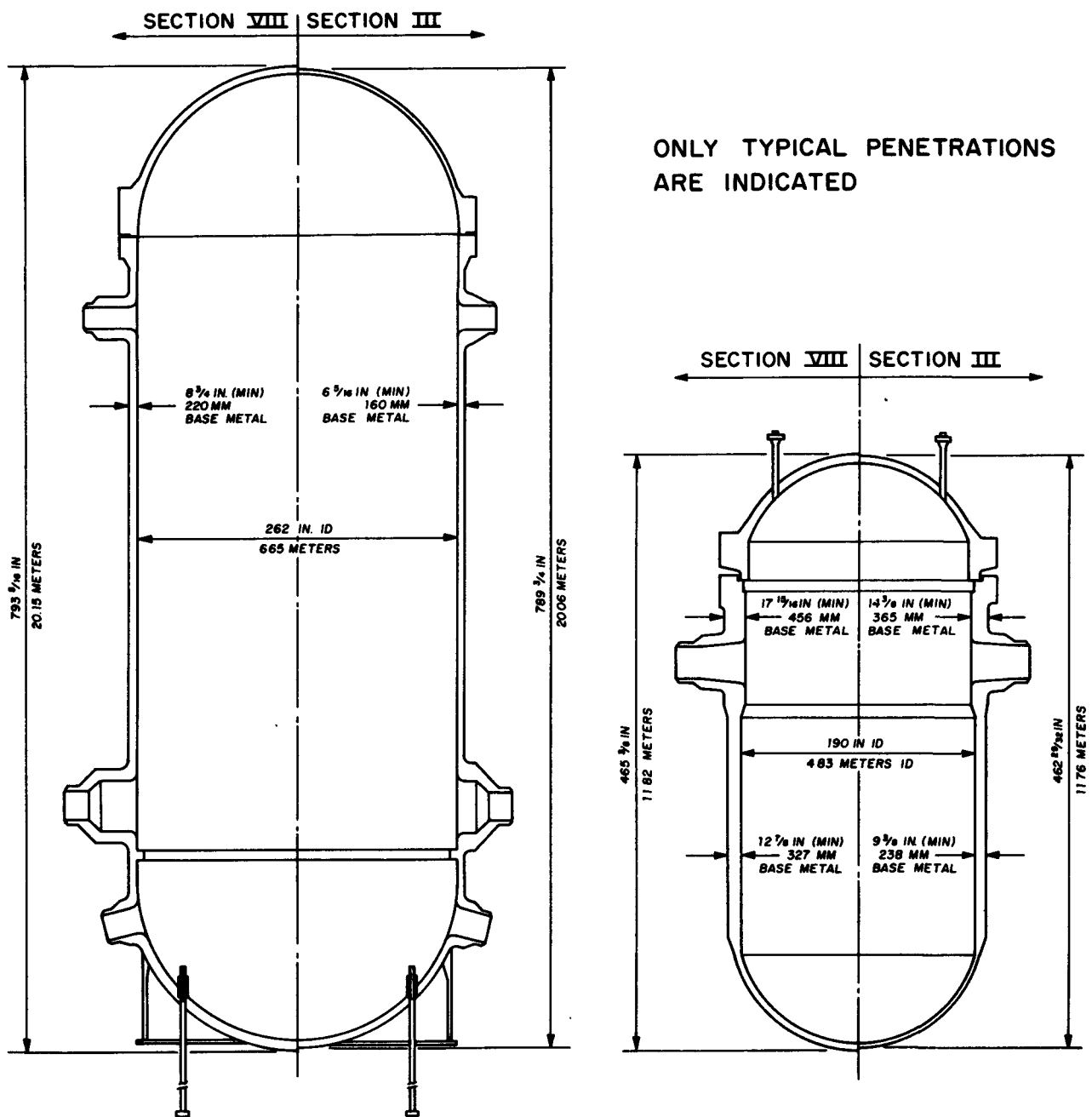


Figure 2. Typical reactor vessel designs for 1 000 MW(e) capacity plants, comparing ASME Code Sections VIII and III

transporting materials and assemblies of such large sizes and weights.

Large reactor vessels for nuclear service are fabricated from ASME SA-302, Grade B, carbon-manganese-molybdenum low alloy plate material, and/or ASME SA-336 carbon-manganese-molybdenum and nickel-chromium low alloy forged materials to ASME Code Case 1236. These materials have a minimum specified ultimate strength of 80 000 psi (56.3 kg/mm²) and a minimum specified yield strength of 50 000 psi (35.2 kg/mm²). A design stress value of 20 000 psi (14.05 kg/mm²) is permitted by Sections I or VIII of

the ASME Codes, and 26 700 psi (18.78 kg/mm²) is permitted by Section III. The mechanical properties, in the extreme material thicknesses delivered for large vessels, are obtained by restricting the limits on certain chemical elements within the range permitted by ASME Material Specifications.

Of the materials accepted by the ASME Codes, only SA-302 Grade B is suitable for fabrication of large reactor vessels. Carbon steels, having ultimate strengths of 70 000 psi (49.2 kg/mm²) and yield strengths of 38 000 psi (27.7 kg/mm²), would require wall thicknesses too great for quality procurement and

fabrication. The high strength properties of low alloy steels, obtainable by quenching and tempering heat treatments, are not recognized by the Codes in the thicknesses required for reactor vessels. Thus, the alloy compositions producing minimum ultimate strength of 80 000 psi (56.2 kg/mm²) and minimum yield strength of 50 000 psi (35.2 kg/mm²) are the only practical, economic choices under present regulations.

Plate manufacturers can produce plates, in the maximum finished sizes obtainable, weighing only 100 000 lb (45 300 kg). Furthermore, considerable research has shown that materials of the normal chemical composition specified by the ASME Material Specifications will develop the required mechanical properties only in thicknesses up to approximately 12 in (305 mm).

Forging manufacturers can produce parts weighing up to approximately 140 000 lb (63 500 kg). If mandrel forged, the largest outside diameter that can be secured is 205 in (5 200 mm). Rolled-ring type forgings can be secured to approximately 325 in (8 225 mm) outside diameter. For diameters exceeding 325 in (8 255 mm), one-piece forged flanges cannot now be obtained. Therefore, these flanges must be fabricated from multi-piece formed forged bars. The United States' present material suppliers do not all have the capability for machining these forged flange segments in the necessary diameters. Therefore, the responsibility for acceptable flange segment material may be divided, and final material processing and qualification may be performed in the vessel manufacturer's plant.

DESTRUCTIVE MATERIAL TESTING

Qualification testing of materials is based on both destructive and non-destructive testing. Quality control begins with the raw materials at the steel mill. Normal ASME Code requirements include chemical composition analyses and verification of minimum mechanical properties, which include values for ultimate and yield strength and percentages for elongation and area reduction. For the low alloy steels used in reactor vessels, toughness properties also must be ascertained as acceptable. Both mechanical and toughness properties must be obtained from samples that are representative of the material in the vessels. The location from which sample materials are taken and the simulation in the sample of the heat treatments anticipated for the material are both of great concern.

Sampling practices in the forging industry permit removal of sample material for mechanical and impact testing (for toughness) at a distance below the heat treated surface equal to the distance below this heat-treated surface at which the most highly stressed area in the completed vessel exists. Forging practices require $\frac{1}{2}$ in of excess material during quenching and tempering heat treatments to provide for dimensional changes during quenching. (The quenching and

tempering are performed to obtain the desired toughness properties, but no advantage is taken in the design of the higher strength simultaneously obtained.) These practices result in the samples being removed approximately $\frac{3}{4}$ to $1\frac{1}{2}$ in (19 to 38 mm) below the surface of the material.

Sampling practices in the plate industry, on the other hand, require samples for material qualification to be taken from the region midway between the center of thickness and the surface. These samples must be taken from material integral with the production part during quenching and tempering operations and no closer to the plate edges than one plate thickness (T), or from a separate plate from the same heat treated in identical manner and $3T \times 3T \times T$ in dimensions. For materials under 6 in (154 mm) thick, the sampling practices for plate material are comparable to those for forgings. At the thicknesses required for large reactor vessels, the sample location is much less demanding in forgings than in plate. At $1\frac{1}{2}$ in (38 mm) below the surface, excellent values for strength and toughness are obtained from both material types. At one-quarter thickness locations in material greater than 10 in (254 mm) thick, the temperature at which acceptable toughness values are obtained is often higher than the desired 10 °F (−12.2 °C).

Toughness properties are usually determined by Charpy V-notch impact tests and furnish a measurement of the brittle fracture characteristics. Through correlations with NDTT (Nil-Ductility Transition Temperature) for each grade of steel, the required Charpy V-notch impact requirements are obtained. For 35 000 psi (24.6 kg/mm²) yield strength steels, the generally accepted equivalent Charpy V-notch test value at a given temperature is 15 ft lb (26 kg/cm²). For 50 000 psi (35.1 kg/mm²) yield strength steels, the value is 30 ft lb (5.18 kg/cm²). Recent plant operation limitations concerning stress loadings at a given temperature have been based on these notch toughness properties. This transition temperature approach, illustrated in Fig. 3, gives a stress/temperature relationship for safe reactor vessel operation. The transition

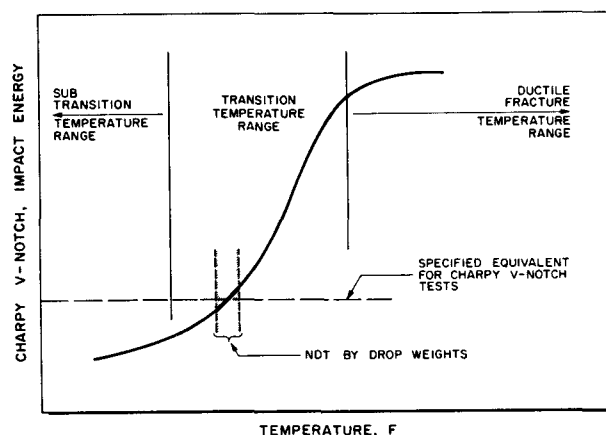


Figure 3. Transition temperature approach to notch toughness property of materials

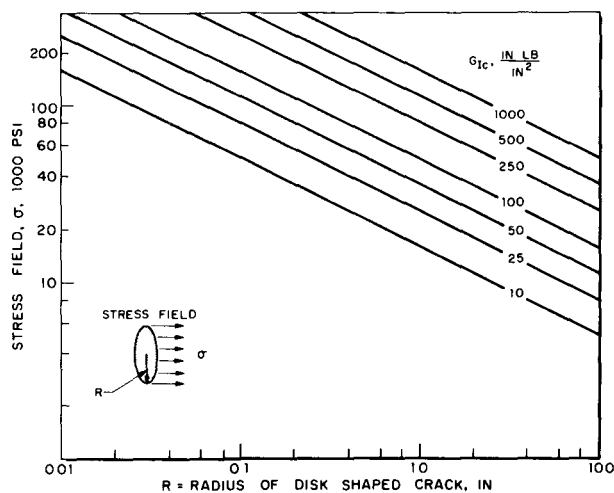


Figure 4. Fracture strength vs. defect size for various fracture toughness values

temperature approach established three temperature ranges corresponding to three types of fracture behaviour: (a) the subtransition temperature range, in which the material will fracture in a brittle manner at relative low stresses; (b) the transition temperature range, in which the material shows a rapidly increasing rise in fracture strength; and (c) the ductile temperature range in which the material will fracture only by ductile tearing. Plant operating limitations based on transition temperature approach maintain low stresses in the reactor vessel wall throughout the subtransition and transition temperature ranges.

In the future, destructive testing of materials probably shall include determination of fracture toughness properties. Fracture toughness is considered a basic property for strain rate sensitive materials, very much like the yield strength and quite different from the notch toughness criterion determined by Charpy impact testing. The fracture toughness value, generally referred to as G_c , has the potential of being very useful to the designer and plant operator. Through application of fracture mechanics (Griffith-Irwin theory) a critical fracture stress can be equated to a specific flaw size and geometry. When further developed, fracture mechanics may be used to establish plant operational limitations. These limitations may permit higher stress levels while the vessel is operating in the transition temperature range. The permissible stress level is a function of flaw size and the fracture toughness value, G_c , as shown in Fig. 4. The fracture toughness value, G_c , is established for each material at temperatures covering the anticipated operational temperature range. The development of this theory will require establishing the changes in G_c occurring because of exposure to various levels of nuclear radiation throughout the operating temperature range. The application will require determination, in each area being considered, of: (a) the initial G_c value for all materials used; (b) the maximum size of flaws originally existing as well as growth of flaw size, if any; and, (c) knowledge of the total nuclear radiation

accumulating during service. Initial determination of flaw size and location is accomplished by nondestructive testing techniques.

NONDESTRUCTIVE TESTING

Nondestructive testing is intended to assure that quality materials are obtained and that the quality is maintained throughout fabrication. Therefore, these tests are performed after several stages of manufacturing.

Ultrasonic testing techniques are used in many investigations of vessel quality. A complete ultrasonic survey is made upon receipt of all materials to predetermine quality prior to fabrication. This survey discloses the location, depth, size, and orientation of defects, if any, in the materials. If other inspection methods, such as radiography of welds, disclose defects, ultrasonic examination is used to furnish additional information regarding the defect. Corrosion-resistant surfaces on the inside of reactor vessels are inspected using special ultrasonic equipment. Weld-deposited stainless steel cladding is examined for continuity of bonding in the as-deposited surface condition using a wheel-type device containing the transducer. Double crystal devices have been developed to disclose defects, if any, in the cladding. (These devices require a machined clad surface, however.)

The surfaces of weld joint preparations are examined by magnetic particle inspection. Surface discontinuities and sub-surface flaws can be detected by magnetic particle inspection and removed prior to welding. Critical areas of welds, such as the root section, can be examined as an in-process inspection. Thus welding operations will not cause extension of imperfections in the material adjacent to the joint. After the hydrostatic test, magnetic particle inspection may also be performed on all magnetic material of pressure boundaries, and on discontinuities, such as supports.

Surfaces of nonmagnetic materials and welds are examined for cracks and imperfections by liquid penetrant inspection. The final surfaces of vessel cladding and nozzle extensions are examined for surface defects, repaired, and re-examined until acceptable. Liquid penetrant inspection serves the same purpose on nonmagnetic materials for surface indications as magnetic particle inspections serve on magnetic materials.

Radiographic examination is performed on all pressure-containing welds in the vessel. The designer must exercise great care during detailing to obtain a weld geometry suitable for radiographic examination. The more stringent requirements for nuclear reactor vessels are exemplified by the mandatory radiography of all nozzle attachment welds, while, for non-nuclear vessels, Sections I or VIII of the ASME Code require mandatory radiography only of attachment welds for nozzles larger than 10 in (254 mm) in diameter. One exception, however, is permitted by a Nuclear Code Case; nozzles, such as control rod penetrations and

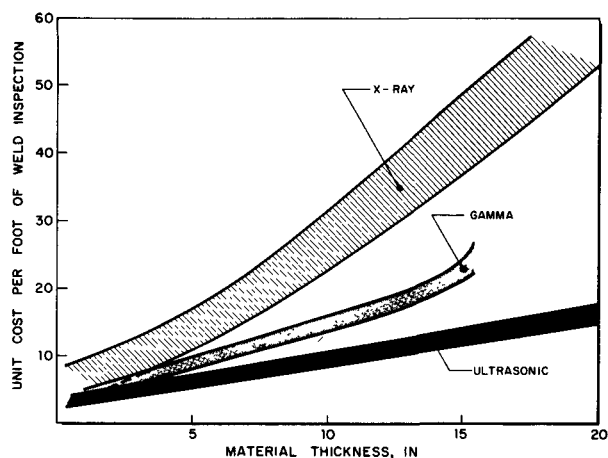


Figure 5. Relative cost for various weld inspection methods

instrumentation wells, on which there are substantially no applied moments or forces, are not required to be attached by full penetration welds. Since interpretation of radiographs of such welds would be questionable, progressive inspection of the attachment weld is required by liquid penetrant or magnetic particle means. One per cent radiographic sensitivity is required for weld thicknesses in excess of 6 in (152 mm). This sensitivity is often difficult to obtain and requires the use of high energy precision built equipment. The relative costs of various weld inspection methods is shown in Fig. 5.

Upon completion of each assembly machining operation, dimensional verification must occur. Complex dimensional inspection techniques are required to assure matching of large-diameter, close-tolerance component assemblies. Optical tooling is a necessity in obtaining component alignment.

One of the last nondestructive tests for integrity given to the vessel is a hydrostatic test at either one and one-half times the rated pressure for Sections I or VIII, or one and one-quarter times the rated pressure for Section III, each pressure corrected for the temperatures involved. Hydrostatic testing will flex the vessel and result in local yielding of material at points of large local discontinuities. It will result in a vessel of quite stable dimensions; one not likely to be further affected by operational service. After this test, the surfaces may be inspected for material flaws which might not have been detectable before this flexing of the vessel.

Radiographic inspection considerations

Since the reactor vessel has the longest fabrication time of any nuclear plant component, all time-consuming inspection techniques must be critically examined. With the wall thickness necessary for the typical 1 000 MW(e) PWR system reactor vessel designed to Section VIII, the exposure time needed for radiography may amount to 2 500 hours or more when using a 15 MeV betatron. For inspection of segmented flange welds and nozzle attachment welds on large

vessels, other equipment for radiography or other inspection techniques should be considered.

Equipment for radiographic examination has been undergoing rapid development. Betatron devices themselves were a major advance of ten years ago. At present, most promising equipment utilizes the principles of linear acceleration of particles. A limited number of these very powerful linear accelerators are in use in the United States. These machines may reduce exposure time for the large vessel from 2 500 h to 250 h.

Other inspection techniques (to substitute for time consuming radiographic examinations) are not generally approved in the United States. Considerable work is, however, being done by the ASTM and ASME in preparing specifications for techniques and acceptance/rejection criteria for ultrasonic testing. Individual companies are investigating comparative capabilities of ultrasonic and radiographic examinations (see Fig. 5). Ultrasonic examination can be used to examine areas that cannot be radiographed. It can detect defects that are not properly oriented for radiography, and can examine thicknesses beyond the capability of radiographic equipment. It is at a disadvantage in obtaining a consistently reliable and well-defined permanent record. Such records, however, are possible to obtain, and will permit comparison of initially existing flaw indications with indications determined after various service periods by remote, if necessary, ultrasonic inspection. This record will permit re-establishment of operational limitations during the service life, by application of fracture mechanics.

MATERIAL DEVELOPMENTS

Another development area for future application is the use of high-strength steels. In the thicknesses required for reactor vessels, the Code does not now accept the mechanical properties obtained in alloy steels by quenching and tempering heat treatments. Certain steels having nickel, chromium and molybdenum constituents have yield strengths of 85 000 psi (59.8 kg/mm²) and ultimate strengths of 105 000 psi (73.8 kg/mm²) and higher in the quenched and tempered condition. The high strengths are maintained throughout simulated fabrication heat treatments and are obtainable in the welds and heat affected zones in the desired thicknesses. Reactor vessel designs using these steels will reduce the material weight by approximately one-fourth. Reduction in material thickness also reduces the amount of welding and the radiography time. These reductions are offset in part by a threefold increase in cost per pound for the material and increase in welding costs.

Before such materials will be accepted by Code authorities, extensive test results must be available on high-temperature strength values, on fatigue properties, and on the effect of probable fabrication and heat treatment errors. Data on the effects of radiation on this material are now being obtained; some information has already been acquired on steels

of comparable analysis. In particular, changes in mechanical and toughness properties because of radiation effects must be established. These higher alloy steels have exhibited lower transition temperatures than the lower alloy steels such as SA-302 Grade B in the extreme plate thicknesses since hardenability due to alloying is considerably improved. However, it appears that, although the transition temperature is lower, the upper shelf of the impact energy versus temperature curve is also lowered. Additional investigation of this lower upper shelf energy is required before full advantage can be taken of the higher strength steels. Low cycle fatigue tests of pressure vessel steels performed at the Southwest Research Institute, under Atomic Energy Commission Contract No. AT(11-1)-1228, Task A, have shown premature failure in a vessel fabricated from one of the high strength quenched and tempered steels. It has been postulated that the observed low upper shelf energy may have contributed to this failure; therefore, care must be exercised in the design and operation of vessels made from these potential steels.

MANUFACTURING AND HANDLING CONSIDERATIONS

Fabrication techniques for the large vessels have evolved from the techniques used on large boiler drums. Base metal welding and joint designs were proved in the lighter walled drums and gradually enlarged for the thick walled reactor vessels. Cladding techniques have been developed in each supplier's shop especially for this service. The first vessels were built from roll-bonded mill clad plate. Economics and quality required that weld deposited cladding techniques be developed for thick-walled vessels. Machine tools are large versions of horizontal and vertical boring mills but have much more stringent precision capabilities than similar tools used in boiler manufacture. The greatest change has come in floor space requirements and crane capacities. A reactor vessel may have from five to eight full diameter sub-assemblies proceeding in parallel toward final assembly. One such sub-assembly may weigh over 200 000 lb (90 700 kg). The completed vessel may weigh over 1 600 000 lb (725 metric tons). These problems are being solved in the new facilities being built by the manufacturers of large reactor vessels.

Flanges can be transported from the forge shop to the fabricator by rail, only if the diameter does not exceed 205 in (5 210 mm). Larger diameter ring forged flanges are shipped by inland waterways. Completed vessels exceeding 11 ft 3 in (3 429 mm) in inside diameter usually have nozzle clearance dimensions that prohibit rail movement. Therefore, for a shop fabricated and inspected vessel to be used in a power plant, the plant must be close to navigable water. Movement of the very large and heavy vessels by trailer from a barge unloading facility to the site is technically feasible. In the United States, the authority to issue permits for such moves is not centralized, a situation that would probably result in prohibitive cost for the transportation. Field fabrication of large reactor vessels is also technically feasible. However, field assembly of the large vessels to the quality required will result in great expense and delay of plant start-up.

SUMMARY

Large reactor vessels present complex problems and require more lead time than other components for nuclear systems. Therefore, the fabrication span for the vessel makes it the first component purchased. Because the combination of vessel diameter and design pressure requirements offset each other, vessels for either boiling water or pressurized water systems require roughly the same fabrication spans for a given power capacity. These spans are as follows:

Plant capacity	Section VIII	Section III
250 MW(e) net	100 weeks	95 weeks
500 MW(e) net	125 weeks	120 weeks
750 MW(e) net	155 weeks	145 weeks
1 000 MW(e) net	175 weeks	165 weeks
1 500 MW(e) net	220 weeks	205 weeks

Due to paralleled operations on most welding operations, Section III schedules are not reduced by the same factor as the weight is reduced. To the above time must be added approximately 20 weeks for initial engineering and material procurement.

In conclusion, the authors wish to thank the many engineers who have generously contributed to this paper. Particular recognition is given to the contributions of Messrs. B. F. Langer, of Westinghouse Electric Corporation, and T. F. Robinson, of General Electric Company.

ABSTRACT—RÉSUMÉ—АННОТАЦИЯ—RESUMEN

A/227 Etats-Unis d'Amérique

Problèmes de conception et de construction de cuves de réacteur de grandes dimensions

par A. L. Gaines et L. Porse

Des cuves de réacteur pour des centrales nucléaires à eau sous pression ou à eau bouillante de 500 à

600 MW(e) sont en construction aux Etats-Unis. On achève les plans de cuves de réacteur pour des centrales de 1 000 MW(e) et l'on étudie des cuves pour des centrales allant jusqu'à 1 500 MW(e). On indique le rapport entre la taille de la centrale et la taille de la cuve sous pression du réacteur pour les réacteurs à eau pressurisée (conçus pour 175 kg/cm², 2 500 psi) et à eau bouillante (conçus pour 88 kg/cm², 1 250 psi).

La conception des cuves sous pression est en train de changer. Les sections I et VIII du code ASME exigent que les cuves soient dimensionnées selon la « théorie de la contrainte maximale ». Le nouveau principe de la section III du code est basé sur la « théorie de la contrainte de cisaillement maximale ». On discute les raisons de ce changement de principe, et l'effet de ce changement sur la conception des cuves de réacteur de grandes dimensions.

Une cuve de réacteur pour une centrale à eau sous pression de 1 000 MW(e) conçue en fonction des sections I ou VIII du code ASME utiliserait des plaques épaisses d'environ 35 cm (14 pouces). La virole de la cuve aurait un diamètre extérieur de 585 cm (230 pouces) et une épaisseur d'environ 46 cm (18 pouces). Une cuve de réacteur pour une centrale à eau bouillante suivant les mêmes exigences du code aurait des plaques dont l'épaisseur serait d'environ 23 cm (4 pouces). La virole de la cuve aurait un diamètre extérieur de 750 cm (292 pouces) et une épaisseur de 38 cm (15 pouces). On examine le problème de l'étude détaillée des cuves de grandes dimensions en vue de l'achat de matériaux de qualité pour leur construction. Les différentes nuances d'acier acceptable selon le code et utilisables pour les cuves de réacteurs sont comparées du point de vue économique et du point de vue industriel.

On décrit les problèmes que pose l'inspection de ces matériaux en vue de s'assurer que leur qualité correspond aux exigences particulières d'utilisation. Le mémoire n'analyse pas l'effet des radiations sur les matériaux des cuves de réacteur. L'influence de l'utilisation d'aciers à haute résistance, obtenus par trempe et par traitement thermiques, sur la conception des cuves est examinée ainsi que les problèmes de charge pour cycles lents.

On passe en revue l'évolution des méthodes de construction de cuves lourdes de grandes dimensions. Les problèmes d'encombrement et de manutention que pose l'emploi de plus en plus fréquent de cuves de 4,5 à 7 mètres de diamètre (15 à 22 pieds) pesant jusqu'à 800 tonnes sont discutés. On précise les conditions auxquelles doit répondre l'implantation des centrales pour permettre la fabrication complète en usine, les essais et le transport de ces cuves. On donne une estimation des délais entre la commande et la livraison pour les cuves des réacteurs qu'exigent des centrales nucléaires allant jusqu'à 1 500 MW(e).

A/227 США

Вопросы расчета и строительства больших реакторных корпусов

А. Л. Гейнс, Л. Порс

В настоящее время в США строятся корпуса ядерных реакторов, охлаждаемых водой под давлением, и водяных кипящих реакторов электрической мощностью 500—600 Мвт. В стадии окончательного проектирования находятся кор-

пуса реакторов электрической мощностью 1000 Мвт, изучаются также конструкции корпусов для реакторов электрической мощностью 1500 Мвт. В докладе указывается соотношение между мощностью электростанции и размерами корпусов высокого давления, предназначенных как для реакторов, охлаждаемых водой под давлением (расчетное давление 175,8 кг/см²), так и для кипящих реакторов (расчетное давление 87,9 кг/см²).

В подходе к расчету корпусов высокого давления для ядерных установок происходят перемены. Так, согласно разделам I и VIII кодекса Американского общества инженеров-механиков, выбор размера корпусов высокого давления должен быть основан на теории предельного напряжения. Однако новые требования в разделе III этого кодекса основаны на теории предельного напряжения при сдвиге. В докладе рассматриваются причины, вызвавшие эти перемены, и их влияние на конструкцию больших реакторных корпусов.

Корпус реактора, охлаждаемого водой под давлением, электрической мощностью 1000 Мвт, рассчитанный согласно разделам I и VIII упомянутого кодекса, потребовал бы листового материала толщиной около 36 см. Внешний диаметр такого корпуса оказался бы равным 584,2 см, а толщина фланцев — 45,7 см. Корпус водяного кипящего реактора той же мощности, рассчитанного согласно тем же разделам кодекса, потребовал бы применения листового материала толщиной 2 см. Внешний диаметр и толщина фланца в этом случае были бы 741,7 см и 38 см соответственно. Рассматривается вопрос о деталях конструкции больших корпусов, чтобы обеспечить поставку качественных конструкционных материалов. Экономические показатели и конструкционные качества различных марок стали, рекомендуемые кодексом, сравниваются применительно к реакторным корпусам высокого давления.

Описаны вопросы, связанные с контролем качества этих материалов для данного применения. Исследования радиационных повреждений материалов для реакторных корпусов в докладе не рассматриваются. Исследуется влияние на конструкцию высокопрочных сталей, полученной закалкой и термической обработкой, а также определяются вопросы, связанные с низкими усталостными циклическими нагрузками.

Дается обзор развития методов производства больших и тяжелых корпусов. Рассматриваются вопросы размещения и установки реакторных корпусов диаметром 4,57—6,70 м и весом 725,7 т. Рекомендуются также условия выбора места для полного заводского производства и испытания реакторных корпусов, а также правила их перевозки. Определяется время с момента поступления заказа до доставки для нескольких вариантов реакторных корпусов, применяемых в атомных энергетических установках электрической мощностью до 1500 Мвт.

A/227 Estados Unidos de América

Problemas en el proyecto y la construcción de grandes vasijas de presión para reactores por A. L. Gaines y L. Porse

En la actualidad se están construyendo en los Estados Unidos vasijas para reactores de centrales nucleares de agua a presión y de agua en ebullición con potencias del orden de 500 a 600 MW(e). Están prácticamente terminados algunos proyectos de vasijas para reactores de centrales de 1 000 MW(e) y se están realizando estudios sobre vasijas para centrales con potencias de hasta 1 500 MW(e). La memoria da la relación entre la potencia de la central y el tamaño de la vasija de presión para los reactores de agua a presión, con presiones de proyecto de 170 atm (2 500 lb/in²) y de agua en ebullición, con presiones de proyecto de 85 atm (1 250 lb/in²).

Está cambiando el criterio en el proyecto de vasijas de presión para aplicaciones nucleares. Las secciones I y VIII del Código ASME exigían que las vasijas de presión tuviesen dimensiones con arreglo a la teoría del esfuerzo máximo. El nuevo criterio de la sección III del Código utiliza la teoría del esfuerzo cortante máximo. Se discuten en la memoria las razones para este cambio de criterio y el efecto de dicho cambio sobre los proyectos de vasijas para reactores de gran tamaño.

Una vasija para un reactor de una central de agua a presión de 1 000 MW(e), proyectada de acuerdo con la sección I o la VIII del Código ASME, requeriría chapas de unos 350 mm (14 in) de espesor. Las bridas de la vasija serían de unos 6 m (230 in) de diámetro y de unos 460 mm (18 in) de espesor. Una vasija para un reactor de una central de agua en

ebullición de 1 000 MW(e), proyectada de acuerdo con las exigencias de dicho Código, requeriría chapas de 230 mm (9 in) de espesor, y bridas de 7,5 m (292 in) de diámetro exterior y de unos 380 mm (15 in) de espesor. Se discuten los problemas de redacción de proyectos de vasijas de gran tamaño de manera que se puedan acopiar materiales de buena calidad. Se comparan, desde los puntos de vista económico y de proyecto, los diversos tipos de aceros admisibles en el Código para su empleo en vasijas de presión de reactores.

Se describen los problemas de inspección de dichos materiales para lograr que la calidad cumpla con los requisitos específicos de esta aplicación. No se incluye en esta memoria la investigación del deterioro por irradiación de los materiales que forman la vasija de presión. Se da cuenta del efecto que tiene sobre los proyectos la elección de aceros de alta resistencia producidos por tratamientos térmicos de temple y revenido, y al mismo tiempo se presenta un bosquejo de los problemas asociados con los ciclos de fatiga provocados con esfuerzos pequeños.

En la memoria se hace una revisión de cómo han evolucionado las técnicas de fabricación de las grandes vasijas. Se discuten los problemas de espacio y de manejo que se presentan con el creciente uso de vasijas para reactores de 4,5 a 6,7 m (15 a 22 ft) de diámetro y de más de 800 t de peso. Los requerimientos de emplazamiento de la central están condicionados, pues han de permitir la fabricación completa en taller, ensayos y transporte de las vasijas de presión. Se predice el tiempo que se requiere desde la fecha en que se ordena la construcción de la vasija hasta su entrega dentro del intervalo de dimensiones requeridas en centrales nucleares con potencias hasta de 1 500 MW(e).

Корпуса водо-водяных энергетических реакторов высокого давления

**В. В. Стекольников, А. А. Хохлачев, В. П. Денисов,
Ю. В. Вихорев, Н. И. Пригоровский, Н. А. Лугов,
Б. И. Коваленко, В. Б. Добронравов***

ВВЕДЕНИЕ

Корпуса мощных водо-водяных энергетических реакторов высокого давления проектировались в СССР для Нововоронежской АЭС, АЭС в ГДР и опытно-промышленной Ульяновской АЭС. При проектировании предусматривались законченный цикл заводского изготовления, чтобы на монтажных площадках осуществлялись лишь установочные, сборочные работы и подсоединение коммуникаций, а также транспортабельность по железнодорожным путям до места монтажа на большегрузных транспортерах.

Срок службы корпусов в соответствии с техническим заданием должен составлять 20 лет, чем и определялся весь комплекс проектно-исследовательских работ.

ОСНОВНЫЕ ОСОБЕННОСТИ КОРПУСОВ ВЫСОКОГО ДАВЛЕНИЯ

Сложность проектирования и изготовления корпусов крупных водо-водяных реакторов, работающих под высоким давлением, определялась следующими особенностями:

высоким рабочим давлением теплоносителя, что при большом диаметре обуславливает значительную толщину стенок корпуса; это обстоятельство усложняло решение технологических и сварочных проблем, так как связано с увеличением напряжений от температурных перепадов, особенно при переменных режимах;

высокой температурой теплоносителя, значительным объемом первичного контура и как следствие большим значением аккумулированной энергии, представляющей серьезную опасность в случае нарушения плотности корпуса; наличием радиоактивного излучения, вызывающего дополнительный температурный перепад на стенке корпуса в районе активной зоны и изменение физико-механических свойств ме-

талла в процессе эксплуатации, и необходимостью в связи с этим осуществлять периодический контроль за изменением свойств металла; условиями нагружения корпуса, связанными с периодическим изменением нагрузок от давления и температуры.

Количество циклов нагружения для расчетной и экспериментальной проверки работоспособности материала корпуса в пределах заданного срока службы оценивалось:

1) с колебанием давления $\pm 5 \text{ кг/см}^2$ при установившемся режиме работы вследствие неидеальности системы авторегулирования при поддержании мощности на заданном уровне — величиной 10^4 ;

2) то же с колебанием давления $\pm 7 \text{ кг/см}^2$ при переходных режимах — величиной 10^3 ;

3) с понижением давления до атмосферного и температуры до $60\text{--}70^\circ \text{C}$, при плановых и аварийных остановках аппарата с расхолаживанием — величиной 200 циклов.

Немаловажной особенностью является также недоступность для ремонта и осмотра большинства элементов и соединений корпуса после начала эксплуатации.

Эти особенности корпусов вынудили предъявить к их проектированию, выбору стали и технологии изготовления дополнительные требования, более жесткие, чем предписания Госгортехнадзора, по которым обычно ведется проектирование паровых котлов и сосудов, работающих под давлением.

В качестве металла для корпусов реакторов больших габаритов могли быть использованы как обычные котельные стали, так и специальные стали, имеющие более высокие механические свойства. Поскольку было принято решение об изготовлении корпуса в заводских условиях, что обеспечивает более высокое качество, то для снижения веса из условий транспортабельности корпусов была выбрана легированная сталь, предложенная проф. П. Г. Пашковым и инж. Е. Я. Тепловой, сварочные материалы инженерами А. Г. Молчановой и

* Государственный комитет по использованию атомной энергии СССР.

Т. И. Ивановой. Это дает весовой выигрыш примерно в 2 раза.

Выбранная хромо-молибдено-ванадиевая сталь обладает высокими прочностными и пластическими свойствами.

Так, например, предел текучести при рабочей температуре составляет величину ≥ 50 кг/мм², а предел прочности 70—80 кг/мм² при относительном удлинении $\geq 20\%$ и ударной вязкости не менее 10 кг/см². Причем химический состав определил получение однородных механических свойств по всему сечению детали.

Помимо высоких механических и пластических свойств сталь обладает теплоустойчивостью при рабочей температуре и допускает перегревы до 450° С. Сталь эта обладает всеми требуемыми технологическими свойствами, а именно: свариваемостью, возможностью качественного нанесения на нее плакирующего слоя и получения поковок весом 100 т и более при толщине до 600 мм.

При разработке конструкции корпусов реакторов был выдержан ряд специфических требований. Так, обечайки корпусов выполнены все коваными без продольных швов.

Учитывая недостаточные возможности контроля корпуса в процессе эксплуатации, патрубки подвода и отвода воды для охлаждения активной зоны были вынесены в среднюю относительно доступную часть корпуса, что увеличивает также надежность с точки зрения обслуживания активной зоны.

Электросварные швы предусмотрены со сплошным проваром на всю глубину и равнопрочны основному металлу. В тех же местах, где сварку можно было выполнить только односторонней, предусматривалось удаление корня шва механическим способом.

Патрубки выполнялись с двойными сварными швами. При такой конструкции в случае нарушения плотности одного из швов его функции переходят к другому и только после нарушения плотности второго шва возможна протечка среды в атмосферу.

Для узлов, выполненных из сталей с разными коэффициентами линейного расширения, предусмотрены мероприятия, снимающие дополнительные напряжения в рабочем режиме введением термического натяга.

Учитывая необходимость поддержания достаточной чистоты теплоносителя, было решено внутреннюю поверхность корпусов плакировать нержавеющей сталью аустенитного класса. В то же время, имея в виду незначительную долю поверхности корпуса ($\sim 1\%$) в общей поверхности первичного контура, которая в основном определяется поверхностью трубок парогенераторов, пришлось предусмотреть всесторонние исследования коррозионной стойкости корпусной стали и подбор оптимального водного режима, обеспечивающие минимальное загрязнение контура продуктами коррозии.

В результате этих исследований выяснилось, что коррозионная стойкость выбранной марки стали достаточна, чтобы в дальнейшем отказаться от применения плакировки.

Конструктивные размеры корпуса определялись¹ в основном принципиальной схемой реактора:

внутренний диаметр — размерами активной зоны аппарата, вытекающими из физических и тепловых расчетов и толщиной экрана для защиты металла корпуса от радиационных повреждений;

высота — принятым способом регулирования мощности реактора, способом перегрузки, а также высотой слоя над активной зоной для обеспечения необходимой биологической защиты верха реактора;

толщины элементов — расчетами на прочность по нормам Госгортехнадзора на заданные рабочие условия, а в необходимых случаях и для элементов, к которым рекомендации Госгортехнадзора не могли быть применены, — по специальным методикам, разработанным на базе теории упругости².

ОПИСАНИЕ КОРПУСА РЕАКТОРА НОВОВОРОНЕЖСКОЙ АЭС

Корпуса для трех водо-водяных энергетических реакторов разработаны и изготовлены на основе одинаковых принципиальных решений, что позволило сократить количество экспериментальных и опытных технологических работ и уделить большое внимание их глубине и качеству.

Корпус реактора, установленный на Нововоронежской АЭС, представлен на рис. 1.

Корпус представляет собой вертикальный цилиндрический сосуд с эллиптическим днищем и плоской крышкой. По высоте корпус разбит на три зоны. Нижняя зона высотой 6000 мм, к которой приварено эллиптическое днище толщиной 120 мм, имеет наружный диаметр 3800, толщину стенок 100 мм и состоит из трех цельнокованных обечайек. Патрубки и отверстия в нижней зоне отсутствуют.

Средняя зона высотой 2900 мм состоит из двух цельнокованных обечайек наружным диаметром 3880 и толщиной стенки 180 мм. На нижней обечайке снаружи имеется кольцевой выступ, служащий опорой корпуса. В нижней и верхней обечайках средней зоны расположено по 6 патрубков Ду 500 для входа и выхода воды.

Верхняя зона представляет собой цельнокованный фланец высотой 1100 мм с наружным диаметром 3900 мм. На верхней обечайке (фланце) насажен с натягом бандаж, уменьшающий деформации фланца от распорной силы клиновой прокладки и тем самым изгибающие напряжения в шпильках корпуса и сварном шве приварки фланца, и произведена проточка под уплотнение крышки. Необходимость установки банджа на фланце диктовалась техно-

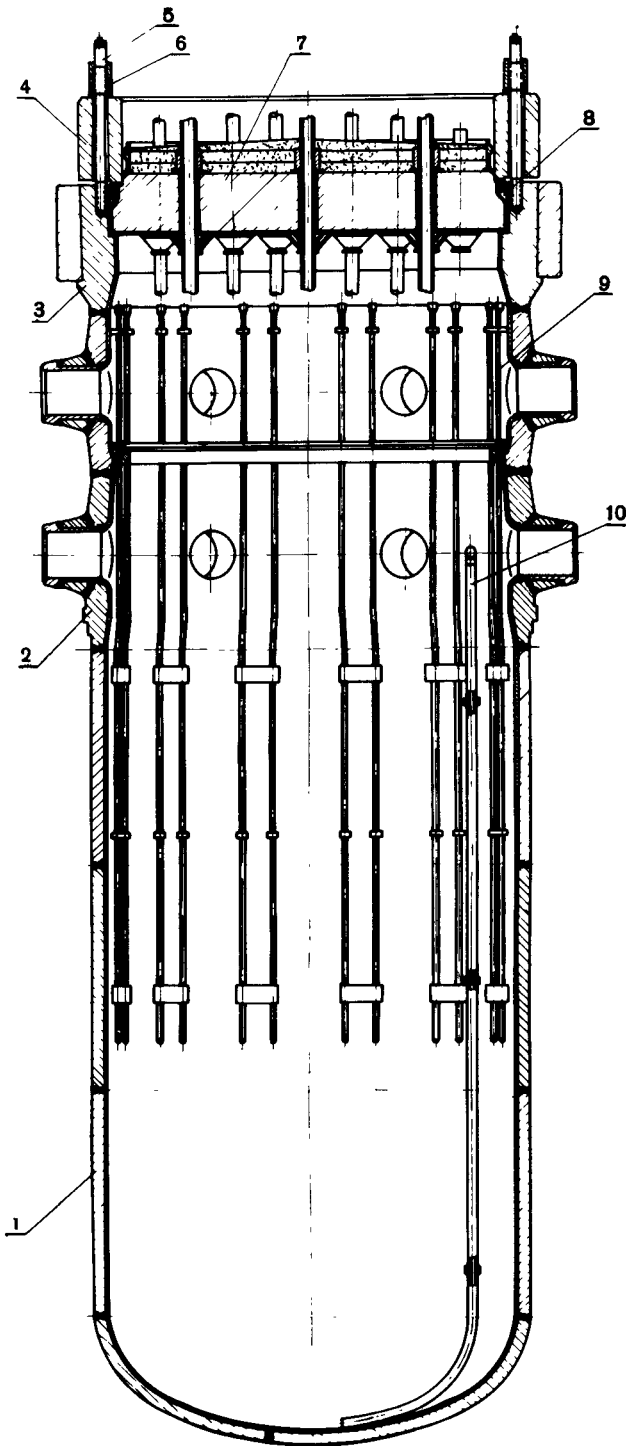


Рис. 1. Корпус реактора Нововоронежской АЭС: 1 — нижняя зона; 2 — средняя зона; 3 — верхняя зона; 4 — нажимное кольцо; 5 — шпилька; 6 — гайка; 7 — крышка; 8 — клиновидная прокладка; 9 — каналы под загрузку образцов корпусной стали; 10 — труба продувки и опорожнения

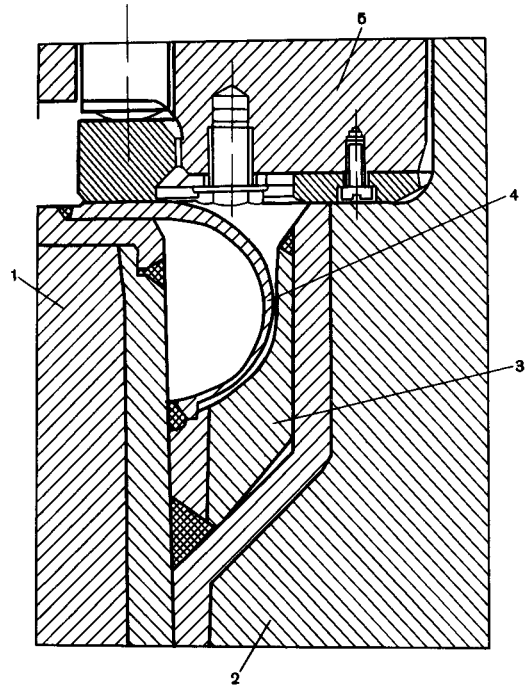


Рис. 2. Резервный вариант уплотнения:

1 — фланец; 2 — крышка; 3 — вкладыш; 4 — полуторовый компенсатор; 5 — нажимное кольцо

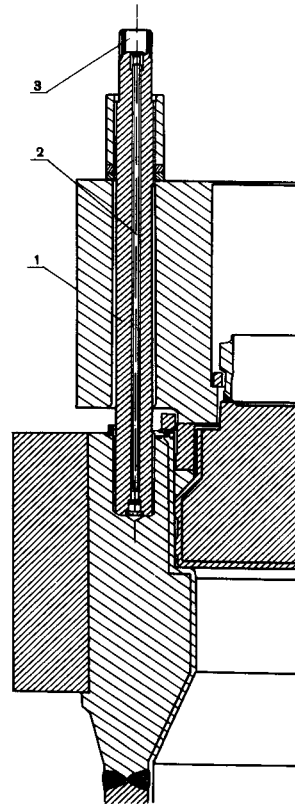


Рис. 3. Устройство для контроля удлинения шпильки:

1 — шпилька; 2 — измерительный стержень; 3 — гнездо под установку индикатора

логическими трудностями изготовления фланца толщиной 500 мм.

Уплотнение места разъема крышки и фланца выполнено в виде самоуплотняющегося затвора с клиновидной никелевой прокладкой⁴. Прижим прокладки к крышке и фланцу осуществляется шпильками через нажимное кольцо. Суммарное усилие затяжки шпилек принято 1,25—1,5 от силы давления на крышку. Для компенсации неточностей, получающихся при изготовлении шпилек, гаек и нажимного кольца, под гайки устанавливается по две сферические шайбы, проскальзывание которых при сборке гарантирует шпильки от изгиба.

Отсутствие опыта длительной эксплуатации клинового уплотнения таких больших размеров, несмотря на положительные результаты испытаний, вынудило создать резервный вариант, основной частью которого является полоторовый компенсатор, привариваемый с одной стороны к фланцу корпуса, а с другой к наплавке крышки (рис. 2). Резервный вариант уплотнения полностью взаимозаменяем с клиновым уплотнением, причем применение гибкого элемента в полоторе позволяет компенсировать силовые и термические деформации фланца корпуса и крышки.

Для контроля величины затяга шпилек предусмотрены измерительные устройства, принцип действия которых основан на контроле удлинения шпильки. Такие устройства позволяют определить величину затяга с точностью до $5 \div 10\%$ (рис. 3).

Крышка корпуса выполнена в виде плоской кованой плиты толщиной 500 и диаметром 3350 мм. Крышка имеет 55 сквозных отверстий диаметром от 90 до 200 мм, на которых установлены патрубки органов управления и контрольно-измерительных приборов. Патрубки выполнены в виде двойных «колокольчиков», находящихся один внутри другого, а швы приварки их к крышке вынесены из зоны наибольшей концентрации, то есть удалены от контура отверстий.

Вся внутренняя поверхность корпуса покрыта антикоррозионной наплавкой, выполненной аустенитными электродами вручную или автоматически лентой. Наплавка выполнена толщиной ~ 20 мм. Изготовление, контрольная сборка и гидроиспытание корпуса полностью выполнены на заводе-изготовителе.

При разработке проекта корпуса обращалось внимание на обеспечение его надежной работы, в связи с чем был предусмотрен ряд мер по контролю за состоянием корпуса в процессе эксплуатации. К ним следует отнести установку в корпусе 24 каналов для загрузки образцов-свидетелей, выполненных из припусков деталей корпуса. Предусмотрена возможность периодического выема образцов для контроля за изменением механических и пластических свойств металла корпуса и сдвига критической температуры хрупкости.

Для контроля за напряженным состоянием корпуса в первый период эксплуатации на нем установлено несколько тензометров в точках, наиболее чувствительных к изменению температурного режима. Такими точками являются стебли шпилек и швы приварки фланца к обечайке средней зоны.

Установленные на шпильках тензометры подключены к приборам, имеющим запись и звуковую сигнализацию. Для уменьшения напряжений в шпильках при переменных режимах (пуск и остановка реактора) предусмотрена специальная следящая система разогрева — охлаждения нажимного кольца, которая ликвидирует разницу температур между фланцем и нажимным кольцом, тем самым уменьшая дополнительные напряжения в шпильках.

Применение этой системы позволяет при необходимости производить разогрев и расколдование реактора с большей скоростью, чем это предусмотрено эксплуатационными инструкциями.

Показанные в описании реактора Нововоронежской АЭС способы решения проблем, связанных с постройкой крупных корпусов, являются общими лишь в принципиальной части.

Вследствие специфики реакторов отдельные элементы корпусов отличаются как по своему конструктивному исполнению, так и по спосо-

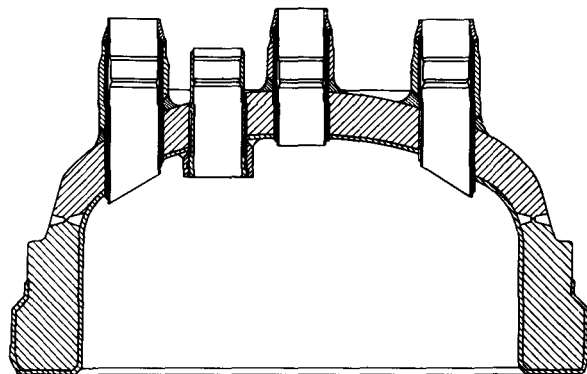


Рис. 4. Крышка реактора, поставленного в ГДР

бу решения некоторых узлов. Например, если из-за сравнительно низкого напряженного состояния на реакторах Нововоронежской и Ульяновской атомных станций применена плоская крышка, отличающаяся простотой изготовления, то на реакторе, поставленном в ГДР, — сферическая (рис. 4). Это вызвано тем, что на последнем запроектирована перегрузка без съема крышки, что потребовало увеличить диаметр отверстий. Сферическая крышка позволяет это выполнить, сохраняя невысокий уровень напряжений.

На Ульяновской АЭС установлен реактор кипящего типа, а поэтому при конструктивном

оформлении патрубков корпуса приняты дополнительные меры по их тепловой защите.

ИССЛЕДОВАТЕЛЬСКИЕ РАБОТЫ

Наряду с большим объемом проектных и расчетных работ была выполнена намеченная программа исследований по изучению напряженного состояния корпуса при работе в стационарных и нестационарных режимах, по изучению прочности выбранных для изготовления основных и сварочных материалов, а также проверке уплотняющей способности места разъема между крышкой и фланцем корпуса. Вся программа была разбита на следующие этапы.

1. Проверка напряженного состояния корпусов на моделях из пластмасс с помощью тензометров и на смоляных моделях оптическим методом.

2. Проверка напряженного состояния корпусов на стальных моделях в рабочих условиях, включая моделирование нестационарных режимов работы корпуса.

3. Исследование прочности выбранных материалов в рабочих условиях.

4. Исследование работоспособности уплотнения крышки на стенде натурной величины, имитирующей верхнюю часть корпуса; отработка вспомогательных устройств для обслуживания узла уплотнения и следящей системы.

5. Контрольная проверка напряженного состояния и перемещений элементов корпусов в период гидравлических испытаний на заводе-изготовителе.

Ниже кратко изложены задачи, решаемые на каждом этапе опытных работ и основные результаты их.

Проверка напряженного состояния корпусов на моделях из пластмасс

На данном этапе определялись напряжения в районе патрубков входа и выхода теплоносителя, зависимость напряжений в верхней части корпуса от величины распорной силы при затяжке клиновидной прокладки, а также напряжения от насадки банджа на фланец корпуса. Тщательно изучались прогибы и напряжения в крышке в месте расположения клиновой прокладки и около отверстий. Исследования проводились на модели из органического стекла, выполненной в масштабе 1 : 20, и на моделях из эпоксидной смолы.

В результате экспериментов было установлено, что все детали корпуса работают в упругой области и имеют достаточный запас упругих свойств для обеспечения работы в нестационарном режиме, когда возникают дополнительные термические напряжения. В нижнем днище корпуса были обнаружены существенные изгибные напряжения в центре, составляющие до 25% от мембранных, которые не учитывались примененной методикой расчета днища. На

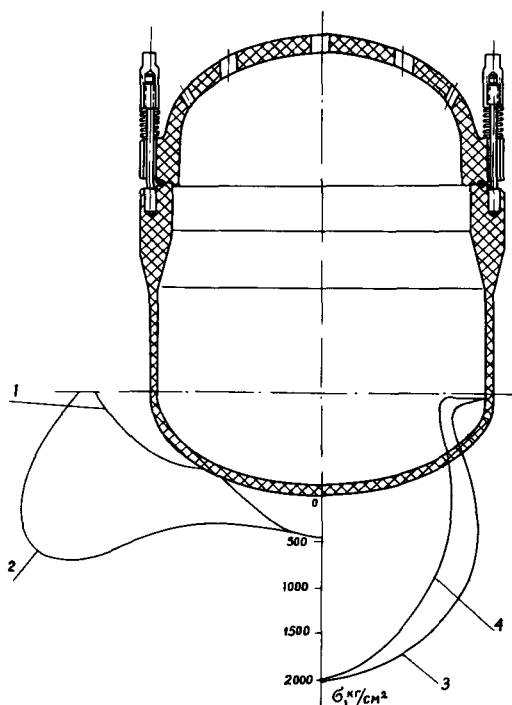


Рис. 5. Модель корпуса из смолы и эпюра напряжений в днище:

1 — кольцевые напряжения по внутреннему контуру; 2 — меридианальные напряжения по внутреннему контуру; 3 — меридианальные напряжения по наружному контуру; 4 — кольцевые напряжения по наружному контуру

рис. 5 показан эскиз модели и приведена эпюра напряжений. Данные расчета, проведенного с учетом изгиба от давления, удовлетворительно совпали с результатами, полученными при тензометрировании натурального корпуса.

Проверка напряженного состояния корпусов на стальных моделях

Предварительные расчеты на прочность показали, что ввиду сложной формы корпусов, наличия деталей большой толщины и переменных сечений, сопрягаемых между собой, могут появиться значительные напряжения при пуске реактора или остановке его с последующим расхолаживанием. Для проверки напряженного состояния была изготовлена стальная модель корпуса в масштабе 1 : 4,5 (рис. 6), которая была подвергнута всесторонним испытаниям. Модель находилась под давлением 100 кг/см² и разогревалась электронагревателем. При достижении температуры 275° С производился сброс горячей воды с одновременной подачей в модель холодной воды из буферного бака, которая на выходе в модель перемешивалась с находящейся в ней горячей водой. Скорости охлаждения воды в модели выбирались пропорционально квадрату масштаба, то есть $b_m = b_n \cdot m^2$, где b_m , b_n — скорость охлаждения воды в модели и натурном корпусе соответственно; m — масштаб модели.

рительно, несмотря на заметные взаимные перемещения уплотнительных поверхностей.

Исследование прочности выбранных материалов в рабочих условиях

На базе заданного срока службы корпуса определялось возможное число как плановых, так и аварийных режимов, при которых корпус наряду с внутренним давлением испытывают наибольшие влияния нагрузки и термические воздействия. Задача исследования прочности материалов решалась по следующим направлениям:

испытания стандартных образцов основного металла, наплавки и сварных соединений на прочность;

испытания образцов материалов после облучения в каналах опытного реактора;

повторностатические испытания малогабаритных образцов;

повторностатические испытания образцов с размерами, соответствующими натурным деталям вплоть до толщины 500 мм (рис. 7);

испытания образцов для определения критической температуры хрупкости и сдвига этой температуры в зависимости от размера детали и степени облучения;

испытание образцов с наплавкой на тепловой удар с перепадом температур 300° С.

В результате проведения этой программы было установлено, что принятые для проекта материалы обладают достаточной теплоустойчивостью, мало изменяют свои свойства при облучении интегральным потоком нейтронов, соответствующем 20-летнему сроку службы корпуса. Повторностатические испытания образцов показали, что имеющийся в корпусах уровень напряжений с учетом концентрации является допустимым для заданного срока службы с 10-кратным запасом по числу циклов-остановок реактора.

При исследовании значения критической температуры хрупкости установлено, что наиболее толстые детали — крышка и фланец — накладывают ограничения на эксплуатацию корпуса, так как их критическая температура хрупкости

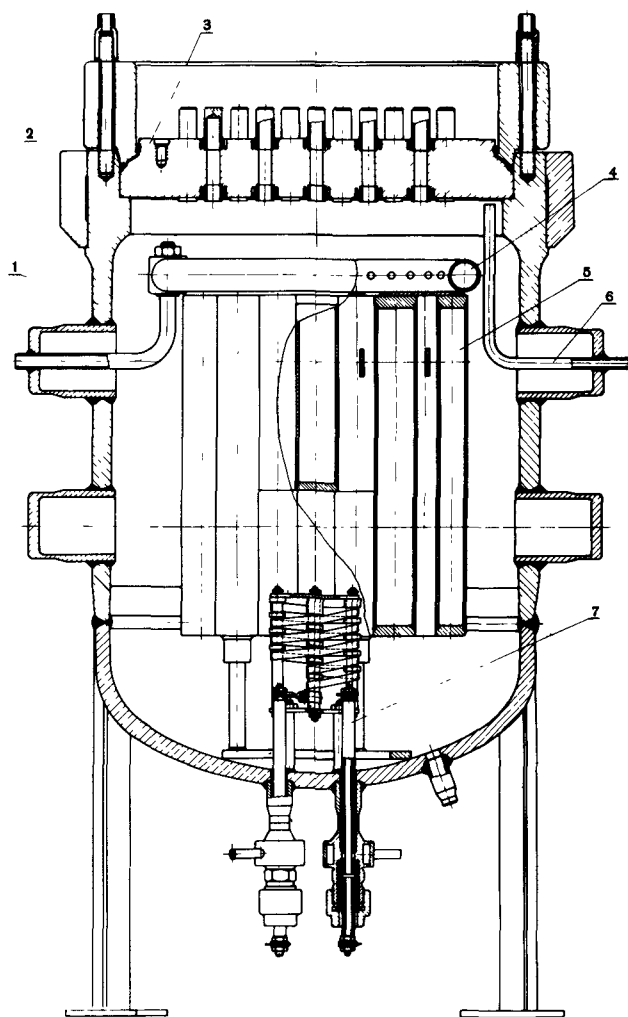


Рис. 6. Стальная модель корпуса Нововоронежской АЭС:

1 — корпус; 2 — нажимное кольцо; 3 — крышка; 4 — охладитель; 5 — вытеснитель; 6 — воздушник; 7 — электронагреватель

Для регистрации напряжений применялись термостойкие тензометры с базой 10 мм, которые устанавливались как внутри модели, так и снаружи в специальных защитных колпачках. Запись показаний производилась потенциометрами через каждые 2 сек.

Результаты обработки измерений показали, что напряжения в районе патрубков корпуса снижаются при охлаждении корпуса модели, что выбранная расчетом скорость охлаждения 30° С/ч является допустимой для данной конструкции корпуса, так как не вызывает напряжений, выводящих основной металл за предел текучести, а прогибы крышки за установленные нормы по условиям работы механизмов управления, монтируемых на ней. Было показано также, что уплотнение модели работает удовлетво-

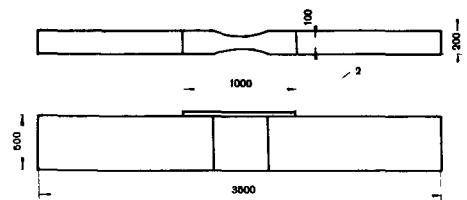


Рис. 7. Крупногабаритный образец: 1 — основной металл; 2 — наплавка

лежит в пределах 50 ÷ 80° С в исходном состоянии. Эти же материалы исследовались под облучением; для них с ростом интегральной

дозы облучения значение критической температуры хрупкости возрастает до 100—120° С.

Поскольку, как показали исследования, несущая способность корпусов не уменьшалась, то на заводах-изготовителях корпуса подвергались гидроиспытанию холодной водой, а на месте монтажа водой, подогретой до 80—90° С. Подъем давления в дальнейшем намечено также производить при наличии подогретой воды в контуре.

Как указывалось выше, конструкция патрубков корпусов выполнена с переходной втулкой из аустенитной стали, имеющей коэффициент линейного расширения $17 \cdot 10^{-6} 1/^\circ\text{C}$, а сам патрубок выполнен из стали с коэффициентом $12 \cdot 10^{-6} 1/^\circ\text{C}$. Прочность такого типа патрубков проверялась на специальном стенде, где патрубок в натуральную величину подвергался периодическим теплосменам, одновременно испытывая напряжения от внутреннего давления.

Исследование работоспособности уплотнения крышки

Проверка уплотнения, устройств системы затяжки шпилек и устройств следящей системы

производилась на стенде, схема которого приведена на рис. 8. Стенд изготовлен из деталей в натуральную величину и снабжен необходимой тензометрической аппаратурой, позволяющей следить за напряженным состоянием и температурами в различных точках конструкции при испытаниях.

Испытания проводились в два этапа: сначала на холодной воде произведено 50 циклов подъемов и сбросов давления от 0 до 100 кг/см^2 , а затем проводились разогревы стенда до 275° С с последующим охлаждением при увеличении скорости охлаждения от цикла к циклу.

В результате испытаний было установлено: сборка узла уплотнения должна производиться весьма тщательно, несоосность крышки и фланца должна быть в пределах 0,1—0,2 мм;

прокладка может быть установлена повторно несколько раз;

следящая система охлаждения — разогрева нажимного кольца снижает напряжения изгиба в шпильках и при необходимости может поддерживать напряжения на уровне стационарного режима;

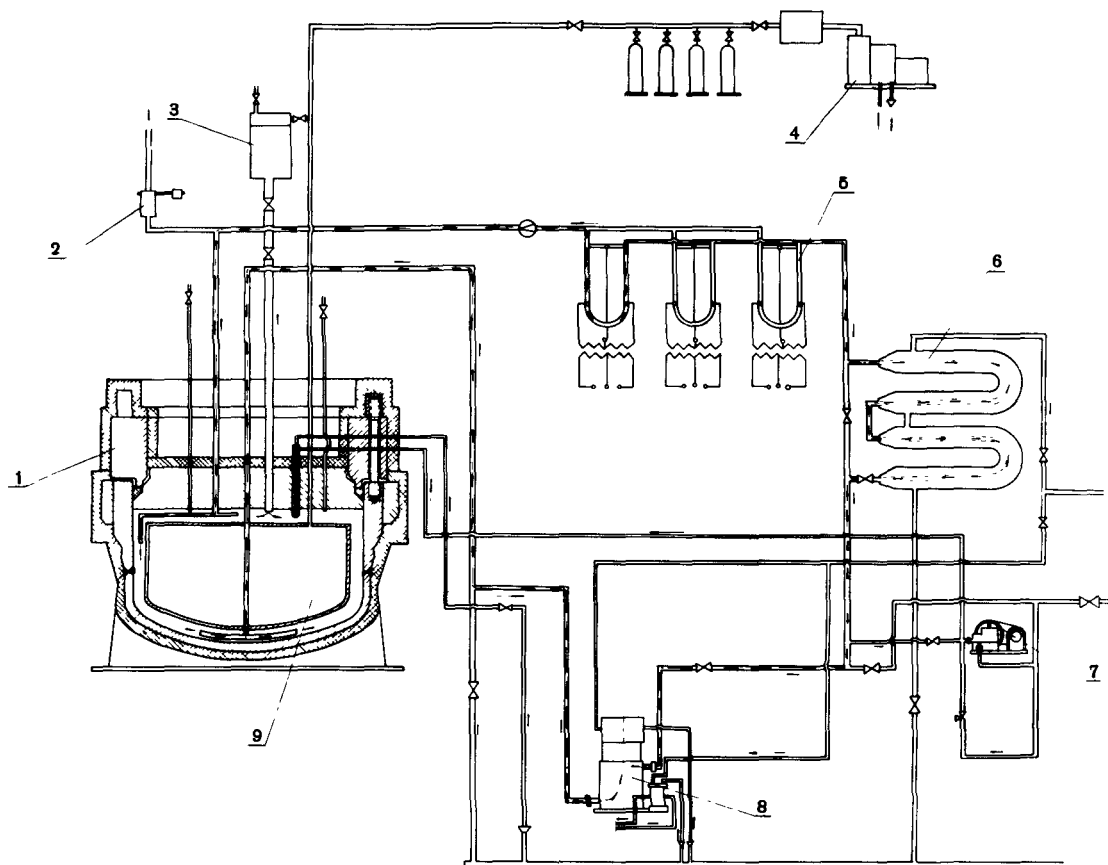


Рис. 8. Натурный стенд:

- 1 — натурная модель корпуса; 2 — предохранительный клапан; 3 — бак холодной воды; 4 — компрессор; 5 — электронагреватели; 6 — теплообменники; 7 — подпиточный насос; 8 — циркуляционный насос; 9 — вытеснитель

плотность разъема не нарушается на всех проведенных режимах вплоть до охлаждения со скоростью 120°C/ч ;

определено напряженное состояние узлов и деталей верхней части корпуса в различных режимах охлаждения; показано, что намеченная расчетом скорость охлаждения с точки зрения прочности, является допустимой;

определена величина затяжки шпилек, обеспечивающая плотность соединения, которая оказалась равной $0,7-0,9 \text{ мм}$ при замере по индикатору или в пересчете на суммарное усилие $P_{\text{зат}} = 1,5P_{\text{гидр}}$, где $P_{\text{зат}}$ — суммарное усилие затяжки всех 60 шпилек; $P_{\text{гидр}}$ — усилие, действующее на крышку от внутреннего давления.

Контрольная проверка напряженного состояния корпусов на заводе-изготовителе

Для головных корпусов реакторов в качестве обязательного испытания проводятся тензометрические измерения при их гидроиспытаниях, а результаты измерений являются отчетными при приемке службами Госгортехнадзора. С точки зрения использования результатов измерений для целей дальнейшей эксплуатации они являются весьма полезными для окончательного решения вопроса о месте установки контрольных тензометров, по которым эксплуатационный персонал следит за правильностью проведения режима пуска и остановки реактора.

При гидроиспытаниях корпусов были проведены измерения напряжений в тех точках, в которых по техническим причинам не могли быть измерены напряжения на моделях или стендах. Общее число тензометров, устанавливаемых на корпусе, не превышает 100 штук.

ПОРЯДОК ИЗГОТОВЛЕНИЯ И КОНТРОЛЯ КАЧЕСТВА

Организация исследовательских работ по технологии

При начале организации исследовательских работ по проверке технологии выбранного металла было принято решение, что обработка технологии получения слитков, поковок, листов, обработка технологии сварки и сварочных материалов, а также и обработка методов контроля качества должна производиться на заводе-изготовителе на деталях и узлах штатных размеров при самом тесном участии научно-исследовательских институтов и конструкторских организаций.

Предстояло решить вопросы получения поковок и плит толщиной до 600 мм с незначительным разбросом механических свойств по толщине, а также выбрать надежные методы контроля качества поковок и плит. В области сварки необходимо было разработать методы ручной и автоматической сварки обечайки толщиной

до 180 мм из легированной стали и наплавки лакирующего слоя, а также методы ремонта дефектных швов. В области термообработки необходимо было добиться таких режимов, которые обеспечили бы получение заданных механических свойств основного металла и сварных соединений при одновременном гарантированном незначительном уровне остаточных напряжений в конструкции. В области контроля необходимо было показать вклад разного рода дефектов в прочность конструкции, накопить статистические данные и на базе указанных материалов создать нормы для оценки качества конструкции. Программа этих исследовательских работ была наиболее дорогой и обширной.

Изготовление полуфабрикатов

Для получения необходимых механических свойств поковки и листы подвергались закалке и последующему отпуску. При сварке корпусной стали выяснилось, что для получения качественного сварного соединения с необходимыми механическими свойствами сварного шва, а также для отпуска подкаленной зоны и снятия напряжений требуются повторные отпуска. Поэтому в исходном состоянии основной металл (поковки, листы) имел повышенные значения предела текучести и предела прочности с тем, чтобы после отпусков при сварке получались необходимые свойства.

Изготовление деталей корпусов

Все основные детали и узлы корпусов — фланец, бандаж, обечайки зоны патрубков и средней части корпуса, нажимное кольцо, крышка, крепеж, патрубки — изготавливались из поковок. Днище корпуса изготавливалось из двух листов толщиной 120 мм , сваренных между собой электрошлаковым способом, с последующей штамповкой под прессом. Для заготовки днища использовались листы нетермообработанные. Перед сваркой листы тщательно контролировались на отсутствие флокенов.

После электрошлаковой сварки заготовка подвергалась термообработке (закалка и отпуск) для получения одинаковых механических свойств основного металла и сварного шва, затем производился тщательный ультразвуковой контроль по всей поверхности заготовки. На отштампованном днище механической обработке подвергались только кромки под сварку с цилиндрической частью корпуса.

Цилиндрические обечайки средней части корпуса, обечайки зоны патрубков, фланец, а также бандаж, нажимное кольцо изготавливались каждая из одной кованой заготовки путем механической обработки. После механической обработки каждая заготовка подвергалась контролю на отсутствие флокенов и других дефектов ультразвуком.

Сварочные работы

При изготовлении корпус был разделен на три технологических узла: днище с обечайкой; две обечайки средней части корпуса; две обечайки зоны патрубков с фланцем. Сварка деталей между собой в каждом из этих узлов, а также сварка узлов производилась с сопутствующим подогревом деталей в местах сварки на специальных кантователях, со сварочными и нагревательными приспособлениями. Сварка в основном была автоматическая. После сварки кольцевых швов узел направлялся в печь на термообработку (отпуск) для обеспечения необходимых механических свойств сварного соединения.

Кольцевые сварные швы и околошовная зона сваренных деталей после сварки и термообработки подвергались тщательному контролю рентгенопросвечиванием и ультразвуком.

Перед сваркой узел корпуса между собой на внутренней поверхности каждого из узлов наносилась защитная нержавеющая наплавка. Для обеспечения высокого качества наплавленного слоя перед проведением работ по наплавке производился селективный по механическим свойствам отбор электродов и сварочных материалов, предварительная отработка режимов сварки и проверка качества на образцах. Наплавка производилась по всей внутренней поверхности узла, кроме участка, расположенного около кромок под дальнейшую сварку. Этот участок заплавлялся после сварки узлов между собой. Проверка механических свойств стыковых сварных швов производилась путем испытания образцов, вырезанных из контрольных пластин, сваренных одновременно с изготовлением контролируемых швов, с применением тех же исходных материалов, методов сварки, сварочных режимов и термообработки.

Для обеспечения необходимой точности геометрических размеров корпуса окончательная механическая обработка деталей и узлов производилась в основном после сварки и термообработки. Большое внимание обращалось на точность выполнения определяющих размеров

в каждой детали и каждом узле. В результате общая кривизна корпуса по вертикальной оси при длине 11 м составила не более 8 мм.

Посадка банджа; прочие виды контроля

На окончательно сваренный и проверенный корпус была произведена насадка банджа на фланец с натягом 1,5 мм на сторону. Бандж перед насадкой нагревался в печи. Благодаря большой точности обработки посадочных мест банджа и фланца после посадки горловина корпуса по диаметру установки крышки имела незначительную эллиптичность — 0,2 мм.

При изготовлении крышки корпуса, нажимного кольца, крепежных деталей, патрубков и т. д. также производился тщательный пооперационный контроль, особенно на отсутствие флокенов и других внутренних дефектов.

Изготовленный корпус после контрольной сборки подвергался на заводе-изготовителе гидравлическому испытанию с одновременной проверкой напряженного состояния основных элементов корпуса с помощью тензомерирования.

ЗАКЛЮЧЕНИЕ

Опыт изготовления показал, что корпуса реакторов высокого давления, изготовленные в заводских условиях, обеспечивают достаточную надежность, подтвержденную технологическими испытаниями и расчетно-исследовательскими работами на образцах, моделях, натурном стенде и выполненных изделиях.

ЛИТЕРАТУРА

1. С. А. Скворцов. Водо-водяные энергетические реакторы (ВВЭР) в СССР. Труды Второй международной конференции по мирному использованию атомной энергии, Женева, 1958, P/2518.
2. Э. Б. Канторович. Основы расчета химических машин и аппаратов. М., Машгиз, 1960.
3. Котлонадзор. «Справочник по котлонадзору». М., Госэнергоиздат, 1951.
4. Б. А. Корндорф. Техника высоких давлений в химии. М., Госхимиздат.

ABSTRACT—RÉSUMÉ—АННОТАЦИЯ—RESUMEN

A/331 USSR

Vessels for power reactors cooled and moderated by water at high pressures

By V. V. Stekolnikov *et al.*

The high-pressure vessels for water-water reactors built in the USSR have been designed to ensure their full manufacture at the works with the possibility of shipment over the USSR railways.

The designers had to solve many problems (including metallurgical, engineering, welding, structural strength, etc.) and had to carry out research to determine the structural features which would enhance the vessel reliability.

The paper discusses the requirements for the materials of a vessel for a large water-cooled, water-moderated reactor; i.e. the problems involved in the choice of the materials, their corrosion resistance, etc.

A great deal of attention is devoted to investigations of the vessel in a stressed condition, investigation of the material strength at repeated static loading under conditions which approximate to the actual working conditions, evaluation of the residual strength, and strength tests on full-size and scale models. Choice of the seals and seal performance tests on full-size and scale models are also discussed.

The paper touches upon the vessel performance under alternating conditions, since large thicknesses and non-uniform heating of the vessel by the coolant result in considerable stresses caused by the differential temperatures at various parts of the vessel. A description is given of the method of solution of these problems, including the reliability of electrically-welded butt joints from steels with different coefficients of linear expansion.

The correct solution of the engineering problems determines, to a large degree, the performance, life and reliability of the vessel. Therefore, the paper deals with some of the key engineering problems and with the problems of quality control.

A/331 URSS

Cuves pour réacteurs de puissance refroidis et ralentis à l'eau sous pression élevée

par V. V. Stekolnikov *et al.*

Les cuves sous pression élevée que l'on fabrique en Union soviétique pour les réacteurs ralentis et refroidis à l'eau ont été étudiées de manière que l'on puisse les monter entièrement à l'atelier et les transporter par chemin de fer.

Les ingénieurs d'études ont dû résoudre un grand nombre de problèmes (de métallurgie, de mécanique, de soudage, de résistance, etc.); il leur a fallu, en outre, faire des recherches pour déterminer les

caractéristiques de construction spéciales qui permettraient d'accroître la fiabilité de l'ouvrage.

Les auteurs examinent les conditions auxquelles doivent satisfaire les matériaux dont se composent les cuves destinées aux grands réacteurs ralentis et refroidis à l'eau, les problèmes que pose le choix des matériaux, leur résistance à la corrosion, etc.

On a consacré beaucoup de temps et d'efforts à étudier le comportement de la cuve sous contrainte et la résistance des matériaux utilisés sous l'action répétée d'une charge statique dans des conditions voisines des conditions réelles de fonctionnement et à évaluer la résistance résiduelle et les essais de résistance sur des maquettes de différentes grandeurs. Les auteurs discutent le choix du système d'étanchéité et les essais de ce système sur un banc en vraie grandeur.

Les études ont également porté sur le comportement de la cuve sous l'effet d'efforts alternés, car, étant donné la grande épaisseur des parois et le fait que le fluide de refroidissement ne chauffe pas la cuve uniformément, il en résulte des tensions considérables dues aux différences de température des divers éléments de la cuve. Les auteurs décrivent la manière de résoudre ces problèmes, ainsi que ceux de la viabilité des soudures électrique d'aciers ayant des coefficients de dilatation linéaire différents.

La solution des problèmes technologiques détermine dans une large mesure les performances, la durée et la sûreté de la cuve. Aussi les auteurs traitent-ils également certains des problèmes essentiels de technologie et de contrôle de la fabrication.

A/331 URSS

Vasijas para reactores de potencia de alta presión, refrigerados y moderados por agua

por V. V. Stekolnikov *et al.*

Las vasijas de los reactores de alta presión, refrigerados y moderados por agua, que se fabrican en la URSS, cumplen la condición básica de su total acabado en fábrica y de la posibilidad de transportarlas por ferrocarril.

Se ha exigido de los proyectistas la solución de muchos problemas (metalúrgicos, mecánicos, de soldadura, de resistencia, etc.); como también la realización de estudios de los métodos de construcción, capaces de aumentar la seguridad de funcionamiento de las vasijas.

Los autores estudian las condiciones que deben satisfacer los materiales de las vasijas de los grandes reactores, moderados y refrigerados por agua, los problemas que plantea la elección de los materiales, su resistencia a la corrosión, etc.

Se ha prestado gran atención al estudio del comportamiento de la vasija sometida a tensión, a la investigación de la resistencia de los materiales

empleados bajo la acción de cargas estáticas repetidas, en condiciones próximas a las de trabajo, a la evaluación de la resistencia residual y a la comprobación de ésta sobre modelos de diferentes tamaños. Se estudia la elección del tipo de cierre y la comprobación de su buen funcionamiento sobre modelos a escala natural.

En la memoria se ha prestado atención al comportamiento de la vasija en regímenes variables, puesto que los grandes espesores y la irregularidad de su calentamiento por el refrigerante conducen, como se sabe, a la aparición de tensiones considerables provocadas

por la diferencia de temperaturas en los diferentes elementos de la vasija. Se describen métodos para resolver estos problemas, incluyendo entre ellos la seguridad en el trabajo de las soldaduras eléctricas de aceros que poseen diferentes coeficientes de dilatación lineal.

De la buena solución de los problemas tecnológicos depende, en gran parte, la capacidad de trabajo, duración y seguridad de funcionamiento de la vasija. Por consiguiente, los autores también estudian algunos aspectos esenciales de la tecnología y del control de fabricación.

Pressure vessel for the first Czechoslovak nuclear power station

By J. Hauer, St. Havel, J. Němec and St. Štěpánek*

NOMENCLATURE

- x, y, z : orthogonal co-ordinates
 x, r, θ : polar co-ordinates
 a : radius of opening
 a_N : radius of vessel
 a_c : central radius of cylindrical shell (branch)
 b : pitch of openings
 t_N : thickness of vessel wall
 t_c : thickness of cylindrical shell (branch)
 l : length of cylindrical shell (branch)
 t : temperature
 k : stress concentration factor
 P : internal pressure
 r_A, r_B : fillet radius
 ρ : radius of notch sharpness
 σ : normal stress
 σ_K : yield point
 σ_P : breaking strength
 ϵ : elongation per unit length
 δ : ductility
 ψ : contraction
 v : coefficient respected state of stress
 $\beta_N^A = 3(1 - \nu^2)a_N^2 t_N^2$
 ν : Poisson's ratio
 E : Young's modulus
 K : central value of energy, consumed on 1 cm² crack's surface
 V : volume
 F : surface of crack
 L : length of test piece
 M : bending moment
 R_M : notch toughness
 Y_M : deflection
 L : energy of the state of stress
 $X = t_c/a_c$
 $Y = t_c/t_N$
 $Z = 1/(2a_c t_c)^{1/2}$

*
* * *

The design of a pressure vessel for a heavy water moderated and carbon dioxide cooled reactor is unique because of the size and technical complexity.

For an output of 150 MW(e), the reactor requires a pressure vessel of outer diameter 5 m and an over-all height of approximately 20 m, and for a working pressure of 65 atm(a), the thickness of the cylindrical shell would be 150 mm (Fig. 1).

The pressure vessel is cylindrical with hemispherical top and bottom domes, the top dome being removable. The connection between the top dome and the vessel is provided by two loose flanges and by bolted joints.

The leak tightness of the connection is provided by a welded annular ring.

The head is very difficult to manufacture. Internally and externally, there are more than 190 nozzles for the connection of charge tubes and the control system of the reactor. Inlet and outlet tubes for D₂O, burst can detection tubes, bottom tubes for inlet cooling gas, cable outlets and the drain are attached to the bottom nozzles by the same method. The bottom inside surface is the main support face, having internal lugs. The support system of the vessel is located on the bottom outer surface and is provided with a conical skirt well insulated to reduce thermal stresses. The cylindrical part of the vessel has in the upper region twelve inlet coolant nozzles and in the lower region twelve outlet coolant nozzles which are made by thickening the wall; and in addition the nozzles penetrate slightly into the vessel.

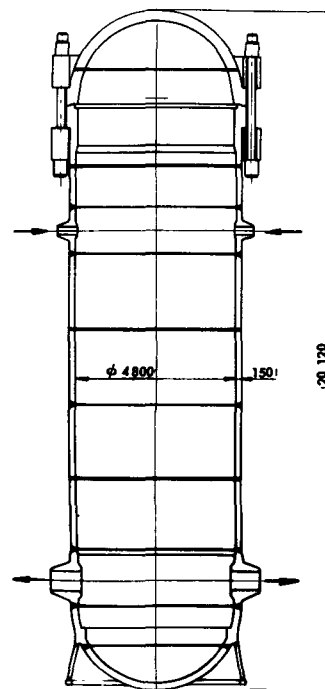


Figure 1. Section of the reactor pressure vessel

* V. I. Lenin Works, Pilsen.

The cooling system keeps the temperature of the vessel within the range 120 to 150 °C. The vessel is designed so that at all openings there is a reduction in stress-concentration and the wall centre line is continued through to the hemispherical top and bottom domes.

To ensure the reliability of operation and to enable checks on the manufacturing technology of the pressure vessel to be carried out, a broad research programme was completed which was taken beyond that usual for design, calculation and research work; the aims were:

(a) research on and proof testing of suitable shapes of the highly stressed parts of the pressure vessel;

(b) development and consolidation of steel properties;

(c) research into and development of suitable welding techniques;

(d) the manufacture of a shortened model of the pressure vessel to a scale 1:1.

Some of the results of this work are given below.

Analysis of stresses in nozzle rings

In the theoretical selection of the shape of nozzle rings from the point of view of their strength, the following factors were taken into consideration.

The effect of a number of openings on the periphery of the vessel

As a first approximation this problem was solved by considering a flat plate with a number of circular holes loaded at suitable points to stress levels equalling the membrane stresses of a plain cylindrical vessel.

A calculated [1] maximum stress concentration factor in relation to a membrane periphery stress in the vessel is solved by:

$$k = 2.5 - 2\left(\frac{\pi}{2}\right)^2\left(\frac{a}{b}\right)^2 + \frac{583}{180}\left(\frac{\pi}{2}\right)^4\left(\frac{a}{b}\right)^4$$

The calculation was made on the assumption that the ratio a/b is small; for greater values of a/b the calculation was replaced by photoelastic measurements. The results of the calculations and experiments are given in Fig. 2.

The effect of the curvature and thickness of the vessel wall

The theoretical results of Lurje can be expressed as a factor of stress concentration

$$k = \frac{\sigma_{\theta}}{p_{a_N}} \cdot t_N = \frac{1}{4} \left[3 \left(1 + \frac{a^2}{r^2} \right) + \left(1 + 3 \frac{a^4}{r^4} \right) \cos 2\theta \right] + \frac{\pi}{4} a^2 \beta_N^2 \left[1 + \frac{a^2}{r^2} \frac{5}{8} \left(1 + 3 \frac{a^4}{r^4} \right) \cos 2\theta \right]$$

For large circular openings in a given cylindrical vessel relatively high stresses are obtained.

An experimental confirmation of this calculation was made, with the help of space photoelasticity, on a model of a cylindrical pressure vessel with five circular openings of various diameters and by taking

the same boundary conditions as there were in the calculation. The model has been manufactured from transparent material, E 12-MF, which is a suitably hardened epoxy resin. Figure 3 is a photograph of "iced" isochromatic lines around a hole in a cylindrical shell.

Figure 4 shows experimental results with a stress factor concentration round about the hole for a longitudinal plane $\theta = 0^\circ$, this is the plane containing the axis of the vessel and of the opening; and for the transversal plane $\theta = 90^\circ$, this is the plane perpendicular to the axis of the vessel and containing the axis of the opening; also plotted are the calculated values by Lurje and, for example, the value of an opening in a plane plate by Kirsch. The experimental values lie between the calculated values. A segment containing the opening was cut along the thickness of the wall of the cylindrical shell and in this segment the size of the added stresses were checked. In the longitudinal plane, there were no bending stresses, but in the transversal plane the bending stresses were as high as 40% of the membrane stress.

The previous considerations lead to the conclusion that from a strength point of view in order to be certain of the value of a/b it is preferable to have a large number of small holes in the periphery of a cylindrical pressure vessel, rather than a smaller number of large diameter holes.

The effect of reinforcing and the local arrangement of nozzles passing into the vessel

At the places where the nozzles are connected to the vessel the possibility of deformation due to internal pressure is reduced, but at these joints there are additional shell stresses.

Direct and accurate calculation of this problem is very difficult. For consideration of the reciprocal effects an approximate calculation was used for one nozzle by Waters [2], the vessel has been replaced by the plane containing the holes and the nozzle by the cylindrical shell (Fig. 5).

If we suggest that $l_A \geq l_B$ the maximum periphery stress in the plate is on the contour of the opening where the nozzle B is connected.

For reasonably large nozzles, the change of stress-concentration factor $k = \frac{\sigma_{\max}}{s}$, where s is a force in

the system in all directions, shown in Fig. 6, with variables $Z_B = l_B/(2act_c)^{1/2}$, $Y = t_c/t_N$, $X = t_c/a_c$.

The nature of the dependence of the stress-concentration factor on variable parameters remains the same for the stresses in the cylindrical shell of the pressure vessel.

From the diagram it is evident that the pipe or the nozzle attached at one side to the pressure vessel causes a bending moment and in the thinner shell of the nozzles an increase of the stress-concentration factor. The most effective way of minimizing the stress-concentration factor is achieved by placing the nozzles symmetrically on both sides of the vessel shell.

At every change of shape of the stressed vessel, the magnitude of the stress is dependent on the degree of

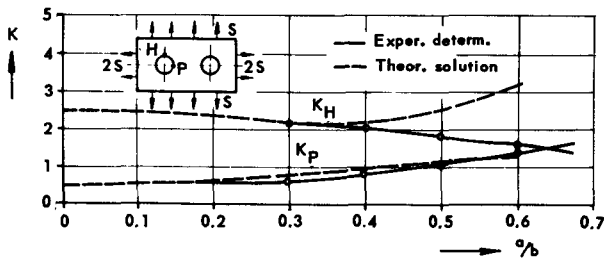


Figure 2. S.c.f. (stress concentration factor) for the row of holes in the plate

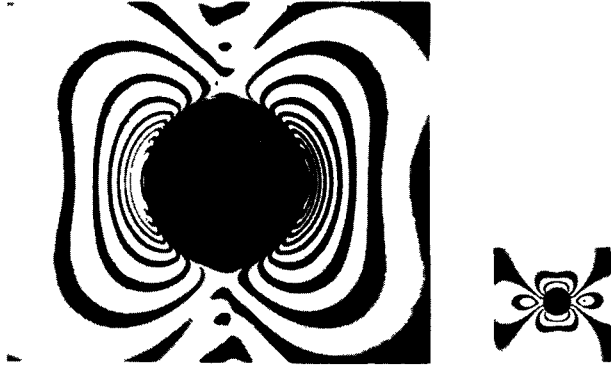


Figure 3. Isochromatic lines around holes in cylindrical shell

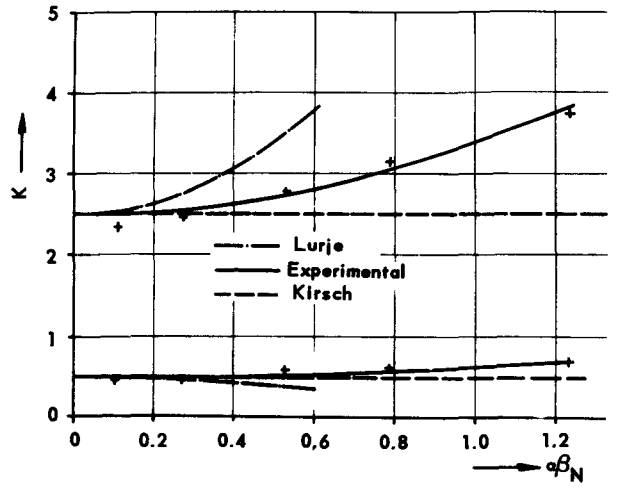


Figure 4. Effect of curvature and thickness of the vessel wall

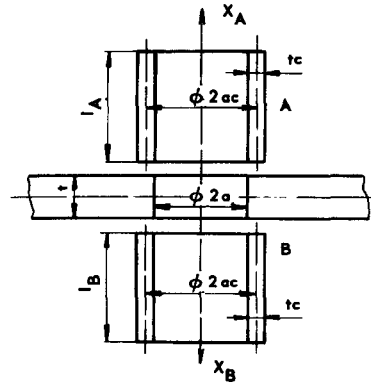


Figure 5. Plate with hole, reinforced by cylindrical shell

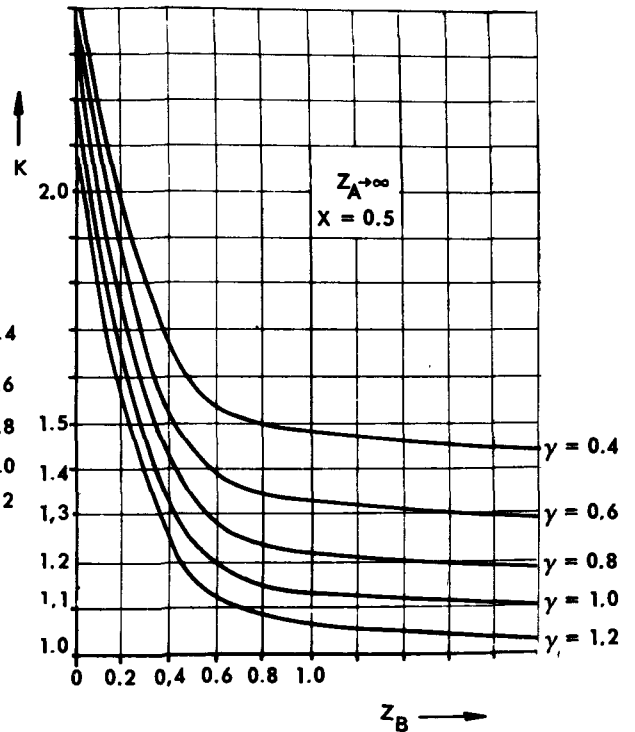
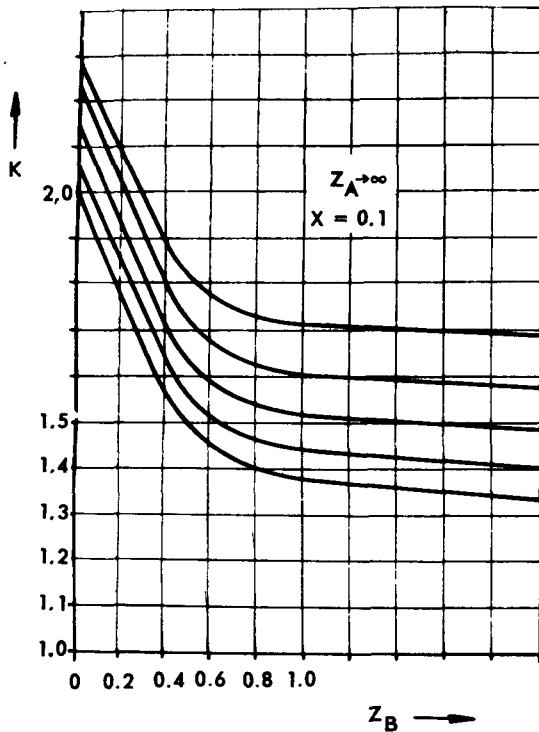


Figure 6. S.c.f. in the plate, reinforced by cylindrical shell

transition. This occurs where the nozzle is connected to the cylindrical vessel; at this joint, the degree of transition is given mainly by two radii r_A and r_B in Fig. 7.

In general, it is considered that the bigger the radius of transition from one shape to the other, the more satisfactory is the change of stress. In the case considered, this principle is valuable only for the radius r_A . By increasing this radius, the stress is minimized in the "notch" on the outside surface and on the inside surface of pressure vessel, because the increased radius r_A acts partially as a reinforcement.

The effect of the size of radius r_B and the general effect of the form of transition on the inside surface of the vessel on the stress concentration factor were measured on five different forms of transition of the inside surface of one nozzle type R 25 in the cylindrical vessel and on two different forms of another nozzle type R 58. For both types, all 12 nozzles were placed in one line on the periphery of the vessel, so that the lines of nozzles did not influence one another and they were not influenced by the flange joint and the bottom of the cylindrical vessel. In Figs. 8 and 9, the dimensions of the nozzles, their arrangement and type are given. The nozzle R 25-3 was developed from R 25-2.

The stress was measured by means of electrical resistance tensometers always on the middle nozzle from the total number of three or six in order to eliminate the effect of the adjacent shape on measured values [3]. The results of the measurements indicate that the effect of the number of orifices, curvature and wall thickness is greatly reduced by the reinforcement effect of the nozzle.

The results gained by measurements on the nozzles R 25-1, R 25-2 and R 25-3 indicate that a fixed optimum radius r_B exists for any given type of nozzle (Fig. 10).

The other nozzles R 25-4, R 25-5, R 58-1 and R 58-2 were already made with a constant ratio $r_B/t_N = 0.5$ as well as the nozzle R 25-2, but on the inside surface of the vessel the shape of the opposite nozzle was marked. It is evident from the diagram in Fig. 11, based on the results of measurements, that the effect of the opposite nozzle on the reduction of the concentration stress factor is large and more effective for higher values t_c/a_c . This factor is also evident from later calculations (Fig. 6).

On the basis of these experiments and considering the other circumstances of manufacture, assembly and function, types R 25-4, R 58-2 were chosen (12 nozzles in one line) for inlet and outlet cooling gas nozzles. The rings, including nozzles, are made so that their rigidity measured by increasing the radius depending upon the inside overpressure is equal to that for rings without nozzles. In a similar way, the remaining highly stressed parts of the pressure vessel were dealt with. Complex states of stress verification in the pressure vessel were made on a metallic model (scale 1:5) by tensometric measurement and on plastic models (scale 1:20) by spacephotoelasticity.

The development of the steel and evaluation of its mechanical properties

The modified boiler steel ČSN 13030 containing up to 0.20% C, 1.10–1.40% Mn and with a maximum of 0.01% Co plus aluminium and titanium to increase structural stability and give a fine grain structure was used. The steel, of "nonageing" quality, was made in open-hearth furnaces and the following steel casting of 45 ton ingots was achieved without using vacuum melting.

The development of the steel and research into its properties was achieved in the laboratory, special care being given to development and technology under manufacturing conditions. Careful manufacturing operations and the appraisal of the effect of technological deviations on resultant quality and properties became a very significant part of the steel development process.

The development was unusual in that the amount of research carried out exceeded that performed in the development of any other mark of steel in the CSSR. On the basis of this programme, which ran from 1957 to 1961, production casts of more than 5 500 tons of steel were made in 43 to 180 t ingot sizes. Studies were made of various alternatives of: (a) charge composition, (b) complex deoxydation, (c) the effect of furnace units and technological parameters on the melting and casting processes, (d) the possibility of using the vacuum casting process, (e) the shape of ingot moulds and (f) various forming processes. In the application of combined forming methods (pressing and rolling processes) to forging ingots it is necessary to obtain isotropy of mechanical properties in all directions (Fig. 12). It is evident from Fig. 13 that accepted technology ensures homogeneity of the mechanical properties for large differences of thickness.

The cobalt content was examined systematically in all the melts and raw materials to determine the best way of maintaining it within permissible levels. Studies were made on problems of heat treatment and the effect of temperature cycles on the resultant structure and properties of the steel. These experiments included studies dealing with the significance of segregation of important elements from the point of view of mechanical properties and welding and internal defects and their size and characteristics. The requirements of nondestructive examination became continually more important and eventually 100% ultrasonic control by calibrated instruments was required for all products. The types of defect and their actual size were determined and questions of their permissible form and size were studied. Mechanical properties were investigated with conventional test specimens, attention being paid to transition curves of notch toughness for steels in various conditions of heat treatment and after artificial ageing, and tensile strength properties of various orientations of the ingots. The effects of sulphide segregates, the effects of grain size and line structure on the main mechanical properties were also determined. The values of notch toughness in a

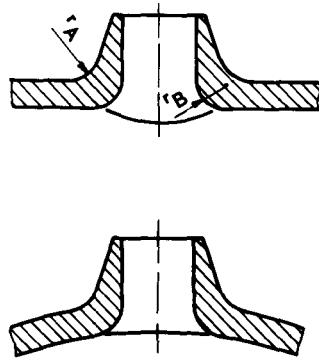


Figure 7. Designation of transition radius

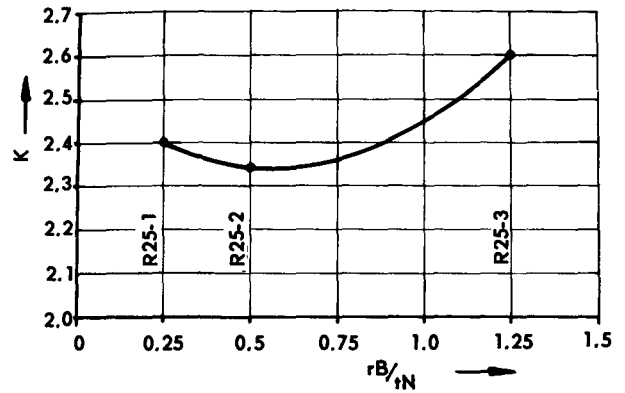


Figure 10. Effect of radius r_B on s.c.f.

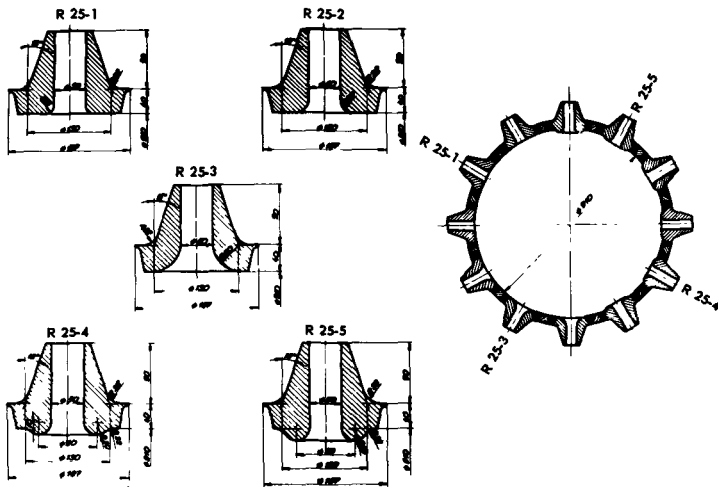


Figure 8. Dimensions of measured nozzles R 25

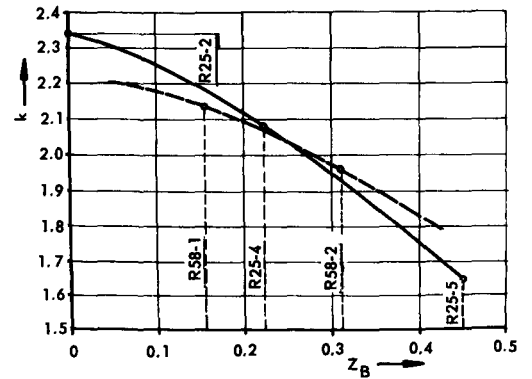


Figure 11. Effect of Z_B on s.c.f.

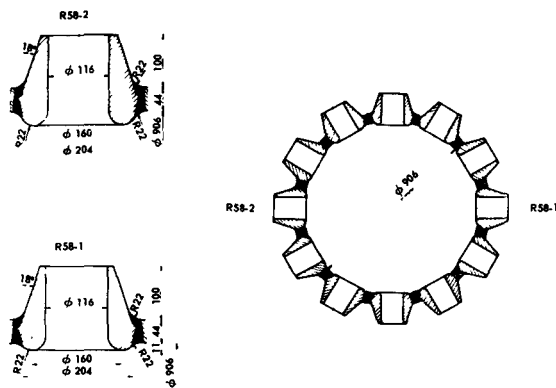


Figure 9. Dimensions of measured nozzles R 58

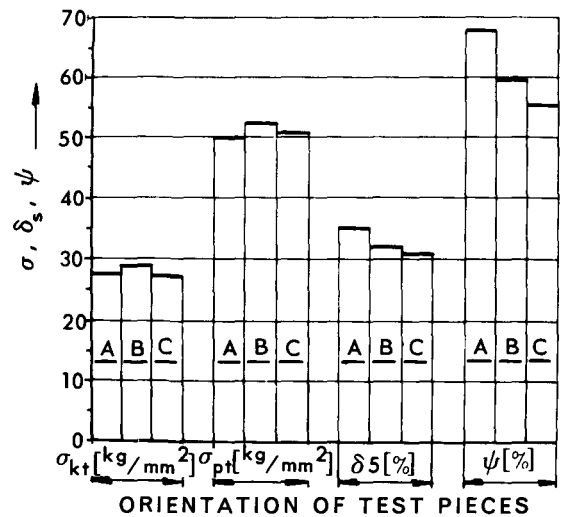


Figure 12. Isotropy of mechanical properties

A: In direction of ingot axis, i.e., in direction of forming
 B: In direction perpendicular to ingot axis
 C: In direction of thickness of semi-finished product

semi-finished product are shown in Fig. 14. It follows that it is necessary to give advance consideration to the values of notch toughness as an acceptance condition for the material.

Figure 15 shows the accuracy of notch toughness values obtained from 108 ingots. The diagram confirms the previously mentioned hypothesis about classification of notch toughness tests.

The irradiation stability of the steel was studied extensively under pressure vessel operating conditions. Base material, weld metal and the weld-affected zone of samples welded by different methods were irradiated. Research was carried out on the radiation stability of different types of test samples, which had undergone dimensional changes or changes in properties and stress state. The purpose of this work was in evaluating the permissible neutron flux and the permissible integral neutron dose. The number of these tests and studies have increased during the development of the steel.

The pressure vessel steel requirements and technical conditions have changed in extent and in content during the project, design work, and during the development of the steel. The most important factor has been the statistical information, which was gained during manufacture and testing of many large dimensioned semi-finished products. The technical requirements cover the complete cycle of technological operations and maintain semi-finished product standards in different phases of manufacture; it is thus possible to eliminate a defective semi-finished product at an early stage [5]. The requirement of high quality steel means that up to 50% of the semi-finished products are rejected.

The study of steel brittleness

A study of the steel properties has enabled the special problem of steel and pressure vessel brittle strength to be solved.

The resistance against brittle fracture is a basic requirement of strength [6]. A programme has been planned, therefore, which has comprised research on large bodies with notches under steady stresses. This programme has taken into account both the effect of local stress concentration and notches induced in welded joints.

Although the tensile testing of large components (cross sections greater than 103 cm²) is difficult and costly, it is the best way to take account of the size factor, because there is no reliable theoretical information available to ascertain the strength of a metallic structure made from complicated components.

Thus from the beginning of the studies in the CSSR the design and manufacture of a special test machine for a maximum tensile loading of 6 000 tons on flat steel test specimens was commenced (Fig. 16).

First information about the strength of large components made from the modified boiler steel ČSN 13030 containing notches was obtained from static bending tests. If the steel passed this test it was

a good choice of steel for pressure vessel manufacture. The steel with a higher yield point ČSN 11523 was also tested but with fewer bending tests.

Information on the strength and toughness of components subjected to bending stresses and the analysis of results

Rods of triangular cross section of various sizes and flat plates with cross sections of 2 500 cm² having notches of different sharpness and depth in tensile stressed parts of the cross section have been tested. The strength and the deformation properties have been determined in relation to size at normal temperature and on smaller rods at temperatures within the range -40 to +100 °C [7]. In Fig. 17 the logarithm of relative strength (expressed as the ratio of the strength of a large test specimen to the strength of a basic test specimen with a cross section of 10 × 10 mm²) is plotted against the logarithm of cross-sectional area for both tested steels. The diagram of changes of bending strength is for notches of constant depth and sharpness $\rho = 2$, and is for a practically constant relative stress gradient. If the size of the cross section is about 0.1 cm², the logarithm of the relative strength decreases linearly as the logarithm of the exposed area increases. By this means, the ultimate strength is calculated by the principles of elastomechanics. Up to a certain critical size, the elastic limit is lower than the limit of plastic macro-deformation and cracking occurs at the phenomenological elastic stress of the body. This is brittle fracture, though also in this case residual plastic deformation can be determined on the surface of the fracture area. If the size is larger than the critical size, the plastic deformation is restrained only on a microscopic volume of metal around the tip of the propagating crack. The stronger and more brittle the material (a smaller ratio σ_P/σ_K), the greater the strength decrease with increasing size of the specimen. A greater slope is shown for steel ČSN 11523 (Fig. 17). Although the material is stronger, the critical size of the body is evidently smaller. Therefore the choice of mild steel for pressure vessels has been made. There are three important sections. In section 1-2 there are ductile fractures and they are marked as slow fractures. In this manner the standard test rods are fractured. Between points 2 and 3 ductile fractures occur also on larger bodies but they are marked as fast fractures. At first the component undergoes plastic deformation and then fast fracture occurs ($\sigma_P/\sigma_K > 1$). After point 3, plastic deformation is concentrated in the narrowest part of the propagating crack and the fracture is brittle and very fast. The consequent deformation characteristics are shown schematically in Fig. 17. The phenomena of ductile-fast fractures are basically defined. By increasing the test specimen size, the occurrence of fast fracture is increased and the amount of plastic deformation decreases as an enhanced effect of notches appears. Fast fracture can occur as well in the elastic-plastic region above the limit of purely elastic deformation

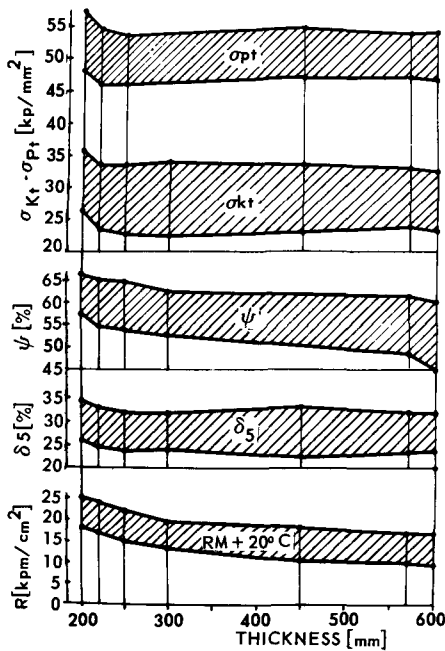


Figure 13. Effect of semi-finished product thickness on mechanical tests of the steel. In the diagram, minimum and maximum values only plotted

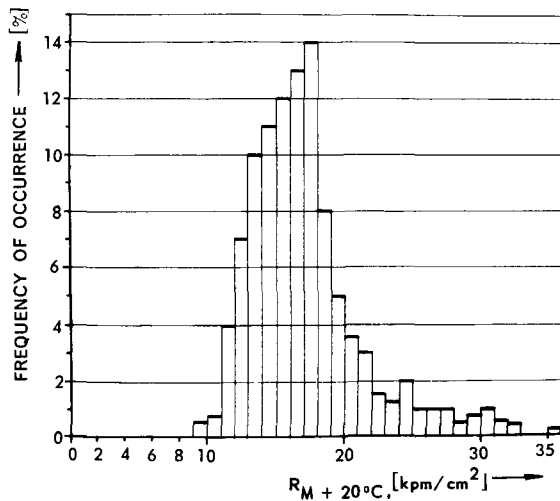


Figure 14. Histogram of notch toughness values at 20°C for one semi-finished product

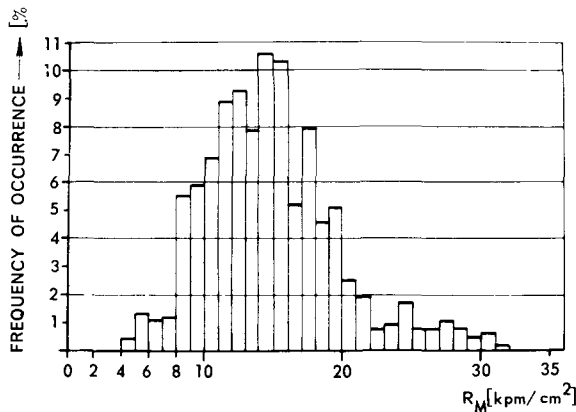


Figure 15. Histogram of notch toughness values from 108 ingots

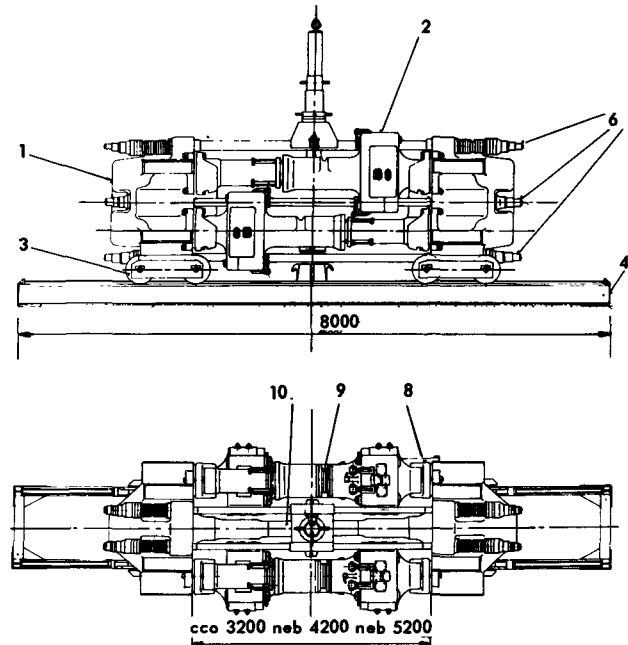


Figure 16. 6 000-ton loading machine

8 000-ton maximum working capacity; 1 500 kg maximum energy of impact; weight, 64 000 kg; -40 °C to +300 °C cooling and heating storage capacity. At top: Front elevation; Centre: Plan view; Below: End elevation 1: Two heads; 2: Four hydraulic members with internal pressure of 4 × 6 200 or 7 400 or 8 700 kg; 3: Chassis; 4: Foundation frame; 5: Support; 6: Bars with shock absorbers; 7: 460-kg pneumatic hammer; 8: Seating of hydraulic members; 9: Distance pieces; 10: Specimen

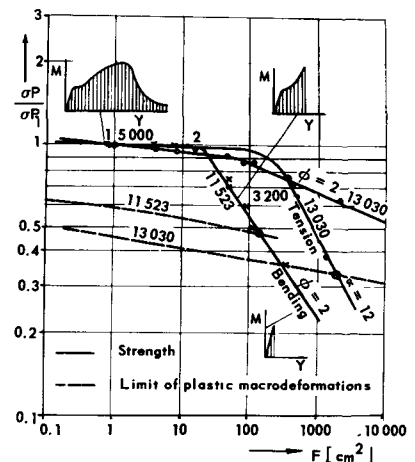


Figure 17. Strength dependence on size of specimens

as in the region under this limit. For this fracture phenomenon to occur in samples from construction steels it is necessary to have sufficient stored energy from elastic stressing in the system and an adequate initial notch-effect. The linear dependence of the logarithm of limiting stress on the logarithm of cross-section size shows the importance of storage of elastic energy in the sample and this has also been proved by calculation. Therefore, it can be expected with tensile tests, where stressing of the sample is more uniform, that a decrease in strength compared with that from bending tests will occur. When the initiation conditions of fracture are fulfilled the formation of a crack is dependent on the energy of elastic stressing $\vartheta \frac{2}{2E}$ in the specimen, and can be expressed by the basic equation [8]:

$$LeI = \vartheta \frac{\sigma^2}{2E} \cdot v = K \cdot 2F$$

For bending

$$\vartheta \text{ bending} < \vartheta \text{ tensile}$$

and

$$K \text{ bending} > K \text{ tensile}$$

Without the notch effect, which stops local plastic deformation due to the stress concentration and without the effect of multiaxial stress, fast fracture cannot occur. Under these circumstances the strength will not decrease with increasing size of specimen. Figure 18 shows this schematically. This principle is important if we want to apply the results of tests on large components with notches to the pressure vessel. The basic conditions of an adequate strength of component are that the level of stress concentration arising from forming the vessel shape and the number of large defects in the material which are perpendicular to the stress direction must be decreased. The lower the temperature the more important is the complex effect of size of stressed area and the notch effect and the critical dimension for possibility of brittle fracture is smaller. In Fig. 19, this is shown for the condition when the sharpness of the notch is constant. These and other important information have been gained by tests of large components subjected to bending stresses. The bending tests are not entirely suitable because the pressure vessel has to withstand the basic tensile stress. The energy consumed on propagation of fast cracks during fracture is unevenly distributed in bend specimens. For this and other reasons, tensile tests have been decided on and large tensile test specimens and a large tensile test machine with a loading of 6 000 tons have been prepared.

Tests on large samples and the evaluation of the results

Test specimens for the large tensile machine were made from the pressure vessel steel and were 50, 100 and 150 mm thick, 1 200 mm in width and had a test length of about 1 200 mm. Prior to the tests,

results on tensile tests with specimens 380 mm wide and 150 mm thick made from the basic material and also from weld joints made by hand-welding and electro-slag-welding. The properties of the basic material have been studied at different temperatures within the range -40 to 60 °C on rods with a central notch made in the axis of the specimen in the form of a circular hole at one side with a sharp cut perpendicular to the stress direction. The greatest theoretical stress concentration checked on the photoelasticity model has been $k = 12$. In parallel, tests have been carried out on geometrically similar specimens with an approximate scale 1:6. The material has been tested in several different states, normalized, annealed, long-term annealed and with artificial ageing. Tests have been made on the tensile machine at 6 000 t in the normalized, annealed and long-term annealed states with and without notches and the first series of Robertson type tests have been carried out with a temperature gradient and at a constant temperature to determine the so-called "temperature of crack arrest."

The deformation characteristics of the test piece as a whole are very important (tensile diagram). If we express the dependence of conventional stress which is calculated on the smallest cross section of deformation, $(\epsilon_c/\epsilon_{el})\sigma/\epsilon_c$ is all the strain and ϵ_{el} is the elastic strain which depends on the level of stress, information like that shown in Fig. 20 is obtained. Evidently the deformation characteristics are different for specimens without notches and they are not greatly different for specimens of various sizes. It can be said that the effect of specimen size in the absence of a notch is unimportant at normal temperatures. However, with specimens containing notches the effect of size is important. The curves c and d should be compared. The gradient of strain hardening is practically identical, only the strength of the larger specimen is decreased by the stored elastic stress in the system which enables easier and faster crack propagation. The curve e has a higher level of strain hardening (this is affected by lowering the specimen temperature to -40 °C) and accordingly (Fig. 18) the size factor plays a more important role. In spite of the relatively high stress concentration factor ($k = 12$), large amounts of local plastic deformation have been shown in the proximity of the tip of the notch in all test specimens ($\epsilon_{c, \text{notch}} \gg \epsilon_c$). Also at temperatures of -40 °C local plastic deformation was observed at the tip of the notch in amounts greater than 10% of that on the surface of the specimen. From this it is evident that relaxation of the peak stress always occurs.

The dependence of the strength of large test specimens containing notches on the temperature is shown in Fig. 21. The smaller the stress concentration, the smaller the dependence of impact strength on temperature. With increasing specimen size, the whole system of curves move to higher temperatures.

If the slope of the curve $\left(\frac{d\sigma_P}{dt}\right)_{\text{max}}$ is small, the risk of undesirable fast fracture will also be small.

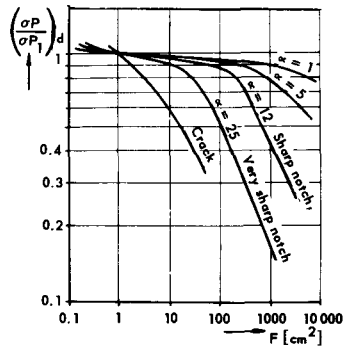


Figure 18. Foressen diagram of strength dependence on s.c.f. and size of component

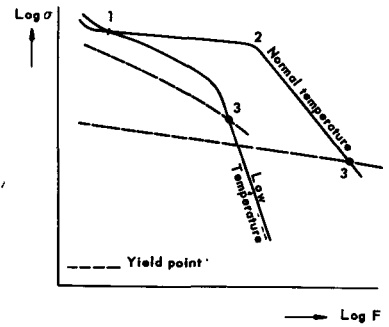


Figure 19. Diagram of dependence of limit conditions on temperature and size for $k = \text{const.}$

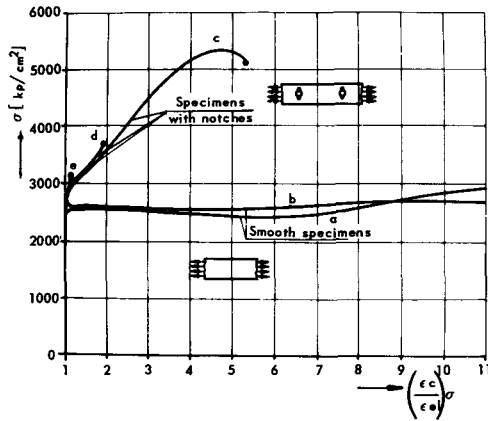


Figure 20. Tension characteristics of pressure vessel steel
 Curve a: Large specimen ($F = 1\,200\text{ cm}^2$) at normal temperature;
 Curve b: Small bar ($F = 1\text{ cm}^2$) at normal temperature;
 Curve c: Small bar ($F_{\text{min}} = 1\text{ cm}^2$) at normal temperature;
 Curve d: Large bar ($F_{\text{min}} = 480\text{ cm}^2$) at normal temperature;
 Curve e: Large bar ($F_{\text{min}} = 480\text{ cm}^2$) at temperature $-40\text{ }^\circ\text{C}$

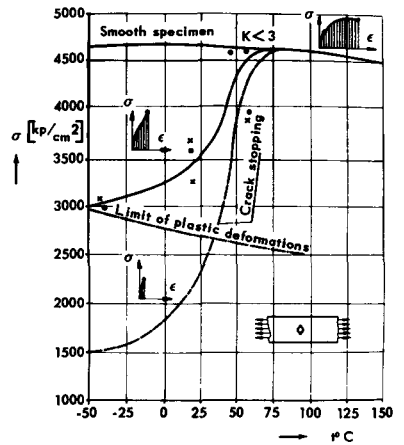


Figure 21. Strength dependence on temperature of large test specimens with notch

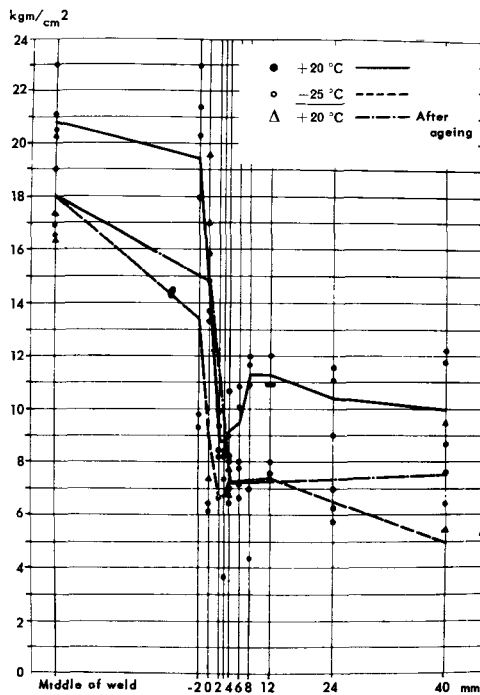


Figure 22. Notch toughness diagram of the manual circumferential weld

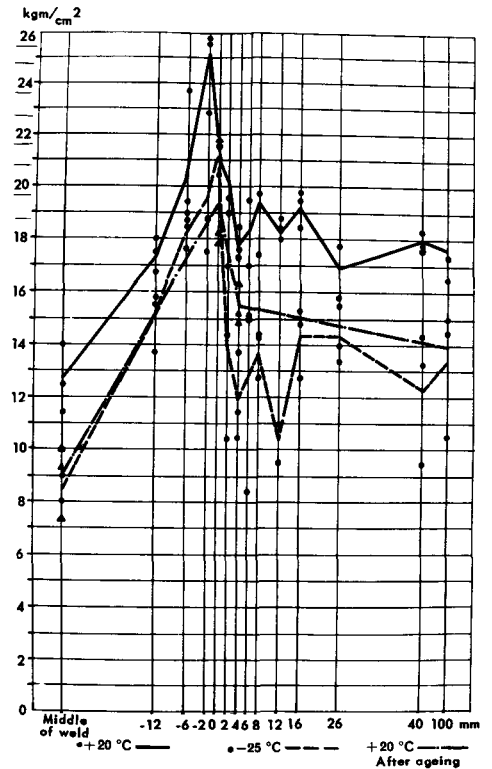


Figure 23. Notch toughness diagram of automatic electro-slag welding

The smaller k (the stress concentration) the smaller is the value $\left(\frac{d\sigma_P}{dt}\right)_{\max}$.

Tensile tests of large specimens with welded joints has shown that the temperature dependence of the stress-strain curve is not very different from the behaviour of the basic material, if it has been stress relieved.

Tests for crack arrest have also been carried out on the large tensile machine and these indicate the lowest above-mentioned value for maximum notch effect.

It is shown that the determination of the nil-ductility temperature is not reliable enough and depends on geometry of the test specimen and on the relative distribution of the temperature in the specimen. The criterion of nil-ductility temperature according the appearance of fracture is not satisfactory. Crystal appearance of fracture face does not indicate that the body is in the field of brittle fracture.

An experiment which has followed the effect of residual stress on impact strength of large cross sections has been interesting. Test specimens were welded to the heads of the tensile machine using an automatic welding machine and were not annealed.

The first tests on the tensile machine with specimens of the basic material without notches have shown that fast fractures have occurred in welded joints although their cross section was larger than in the test part of the specimens. This could be due to stress concentration, a bad weld structure or to the action of residual stresses. If a welded test specimen was warmed to 100 °C and stressed to 2 200 kg/cm², residual stresses were decreased by means of the plastic deformation that occurred. Subsequently, fracture did not occur even at normal temperatures when reloaded. This indicates the importance of residual stress since neither defects nor weld structures would be altered.

From these results it is clear that the large pressure vessel must be stress relieved. The selected material has a sufficient amount of plasticity, even in large cross sections. Evaluation of nil-ductility temperature from test results is a problem. It depends mainly on the fact that the impact strength is safely above the limit for plastic deformation. This condition is fulfilled in fine-grained mild steel, with increased resistance against ageing.

The decrease in strength of large steel samples due to the presence of notches, arises from storing elastic energy from the stress in the system. The greater this store the faster the crack propagates and the value of energy consumed for fracture to occur is therefore lower with an area of 1 cm². The initiation of a fast crack is affected by stress in the tip of the notch and by local properties of the material. If we eliminate the propagation of fast cracks, the pressure vessel can work well in principle in the size field above the critical size but if it is possible vessels below the critical size should be used. This decides the mean value of consumed energy for fracture occurrence (K), which must be tested. Under this condition a complex basis of

design rigidity can be defined for $\sigma = \sigma_K$

$$\frac{EK}{\sigma_K^2 \frac{V}{F}} = \frac{EK}{\sigma_K^2 L} = \text{const.}$$

As this value increases, the resistance against fast fracture also increases.

Development of the pressure vessel welding process

The welding technology of the plates and forgings between 150–600 mm in thickness for the pressure vessel was influenced by the following requirements:

(a) The chosen welding technique and filler metal must meet the isotropy of mechanical properties and homogeneity of the welded joints requirements (Figs. 22 and 23).

(b) The large number of very thick welds in the design of the vessel and the weight limitations of 43 tons for the ingots used necessitates the use of automatic welding.

All rings and spherical parts of the vessel are welded from plates by circumferential joints. The pressure vessel is assembled from rings joined by site welding.

Using this technique the selection of the welding process is very important. Many test plates were automatically welded together in the laboratory using hand-operated arc-welding, semi-automatic welding in carbon dioxide, submerged arc-welding and automatic electro-slag processes. For the rings and top and bottom domes whose axes are parallel to the pressure vessel axis, the automatic electro-slag process was used (Fig. 24).

The selection of circumferential joint welding on the rings met the requirements of dimensional rigidity and the manufacturer's conditions during construction at the site. This was decided by comparing all the above described techniques by welding test rings of the 1:1 scale model of the pressure vessel (Fig. 25).

The shortened pressure vessel model, scale 1:1

The shortened pressure vessel scale 1:1 was produced to gain statistical data for forming tentative technical specifications for steel production requirements on the pressure vessel and for complex verification of the strength and frictional reliability of the pressure vessel. During the production of the model, the production technology was developed and verified in individual operations (forming, heat treatment, welding, machining, ultrasonic inspection, measuring of residual stress, measuring of shape changes, etc.).

New production techniques for forming the ring with ducts in twelve separate segments were developed (Fig. 26). Individual segments with ducts were forged in the die from ingots of 30 tons weight. The forging of ingots was carried out with the object of placing the ingot parts with unfavourable properties in such joints of the vessel which are less strained in service. At the same time new technology for automatic welding of

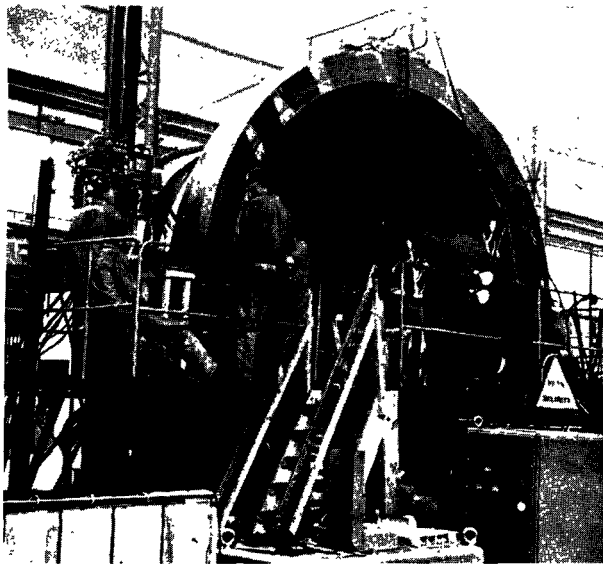


Figure 24. Location of welding parts before automatic electroslag welding

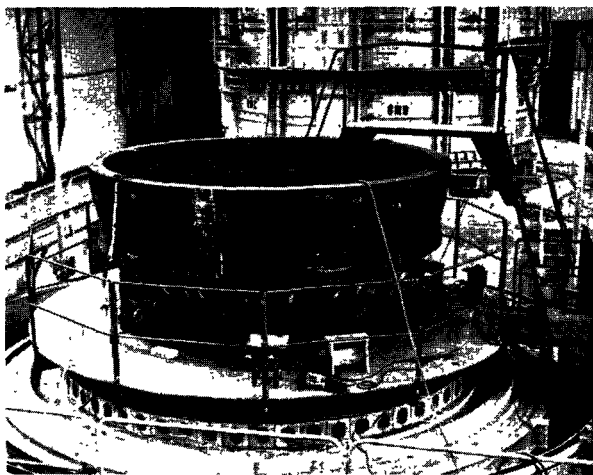


Figure 25. Location of welding parts on the bottom of electric resistance furnace

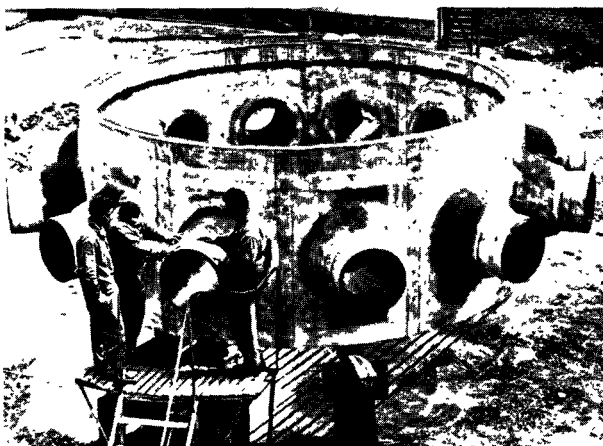


Figure 26. Nozzle rings

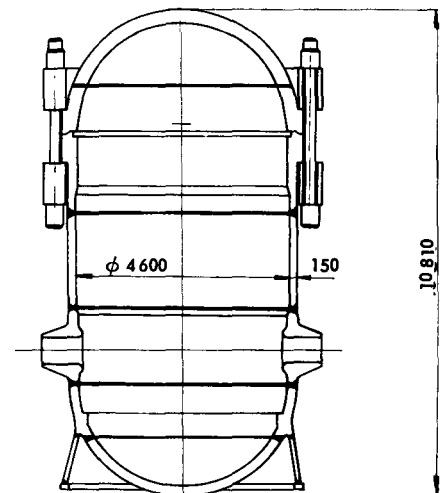


Figure 27. Section of the shortened model of the pressure vessel

thick plates was acquired. The development and production of unique equipment for heat treatment of separate pressure vessel sections and a whole vessel were enforced using the production method mentioned. Dimensions of the vessel and requirements of machining accuracy occasioned the design and production of a new self-turnable cutting machine for machining inner surfaces of the vessel over all its height.

The shortened model of the pressure vessel, scale 1:1, has an average diameter of 5 m and is 12 m high including the domed cover. Height shortening of the vessel was performed by excluding identical parts of the vessel column rings and one ring with ducts. The volume of the model is 150 m³, about half the volume of the real pressure vessel (Fig. 27).

The results of the research and development programme and experience gained during the production of the model are useful not only for verifying the accuracy of the project for the design of the reactor pressure vessel for the first Czechoslovakia nuclear power station. In addition, they have given a large amount of useful technical data for design and production of large dimensioned pressure vessels. These results also have wide importance and extensive use in many technical and production fields related to the national economy of Czechoslovakia.

REFERENCES

1. Ae 559/Dok, Research information, Škoda Works, Pilsen.
2. Waters, E. O., Transactions, Series A, Journal of Engineering for Power (April 1959).
3. Ae 0203/Dok, Research information, Škoda Works, Pilsen.
4. Ae 1006/Dok, Research information, Škoda Works, Pilsen.
5. Ae 0291/Dok, Research information, Škoda Works, Pilsen.
6. Němec, J., *Analysis of Brittle Strength of a Reactor Vessel*, Nuclear Reactor Containment Buildings and Pressure Vessel, Glasgow (1960).
7. Ae 343/Dok, Research information, Škoda Works, Pilsen.
8. Němec, J., *Kovové materiály, č. 1, SAV (Metal materials)* (1963).

ABSTRACT—RÉSUMÉ—АННОТАЦИЯ—RESUMEN

A/522 Tchécoslovaquie

Cuve sous pression pour la première centrale nucléaire tchécoslovaque

par J. Hauer et al.

Un des types fondamentaux de réacteur de puissance qui ont été mis à l'essai dans le cadre d'un vaste programme de recherches sur prototypes, exécuté en Union soviétique et dans les démocraties populaires, est le réacteur à cuve sous pression et à aiguilles d'uranium naturel, ralenti à l'eau lourde et refroidi par un gaz.

Les dimensions générales de la cuve sont fonction à la fois de la conception du réacteur et de la puissance nominale, qui est de 150 MW(e). Etant donné les spécifications relatives aux espaces minimaux entre les canaux pour combustible, les dimensions de la cuve et l'épaisseur des parois sont telles que la fabrication, le soudage et les essais de contrôle sont très difficiles à réaliser. Pour cette raison, il faut, au stade des études, déterminer les formes et dimensions optimales pour les parties les plus délicates de la cuve, telles que le couvercle, le joint à collier, le support conique, et surtout les branchements à l'entrée et à la sortie des conduites du fluide de refroidissement. On a pu trouver les solutions théorique et expérimentale de ces problèmes en appliquant à des modèles des méthodes de tensométrie et de photoélasticité. On a étudié la concentration des contraintes dans les parties de la cuve cylindrique qui sont affaiblies par la présence des branchements, ainsi que les effets, sur cette concentration, des variations de certains paramètres: dimensions et forme du trou, nombre de trous sur la circonférence, renforcement du trou au moyen du branchement et traitement local du branchement au passage à travers la paroi de la cuve.

Lorsque la cuve est soudée, il y a un risque de cassure nette soudaine.

En conséquence, on a fait des essais de flexion sur grandes éprouvettes entaillées. Les résultats montrent que la résistance varie selon la dimension de l'éprouvette et l'effet d'entaille. Les auteurs traitent de l'analyse des caractéristiques des déformations et précisent les notions de cassure rapide nette et de cassure rapide plastique.

En outre, on a mis au point l'essai systématique de grandes éprouvettes dont l'épaisseur correspondait à l'épaisseur réelle de la paroi de la cuve. Ces éprouvettes ont été essayées sur un grand appareil d'une force de 6 000 t. On a étudié les résultats de certains des essais faits jusqu'à présent sur de grandes éprouvettes et on les a évalués au point de vue des conditions extrêmes auxquelles sera soumise la cuve du réacteur.

On a fait un examen critique de l'importance que présentent des essais portant sur de petites éprouvettes et leurs résultats, selon la température de transition et la température d'arrêt des fissures.

La cuve du réacteur sera en acier ordinaire au carbone et au manganèse, à grain fin; cet acier, qui ne subira pas de vieillissement, sera produit au four Martin-Siemens et coulé à la pression atmosphérique en lingots de 43 tonnes.

Les pièces forgées (demi-produits avec branchements) et les brames dont on fait les demi-produits plats sont obtenus par forgeage des lingots avec une presse de 12 000 t. Aux demi-produits, on fait subir un matriçage à la presse de 12 000 t pour obtenir des pièces ébauchées. Avec les pièces finies, on construit les diverses parties de la cuve par soudure électrique. Les parties de la cuve sont assemblées, par soudure électrique, soudure semi-automatique dans une atmosphère de CO₂, et soudure manuelle pour former le couvercle et le corps de la cuve. Pour éliminer les tensions, la cuve est traitée dans un four électrique spécial.

Avant le soudage, il a fallu procéder à diverses expériences pour contrôler la soudabilité de l'acier, mettre au point les meilleurs matériaux complémentaires pour les différentes méthodes de soudure, approfondir la technologie du soudage et du préchauffage, vérifier la grandeur des contraintes et des tensions, déterminer un traitement thermique approprié après soudure, etc. Ces essais ont été faits non seulement sur des tôles, mais également sur des pièces fabriquées à l'échelle grandeur.

Tout le processus technologique de la construction de la cuve — depuis la fabrication de l'acier jusqu'aux essais de la cuve soudée et ayant subi un traitement thermique — comporte une série d'opérations qui influent sur la qualité du métal de base et des joints soudés. Pour cette raison, on a intercalé entre les diverses phases de la construction un certain nombre d'essais de réception en vue de dépister en temps utile les pièces défectueuses.

Pour éprouver la technologie de la construction de modèles et en tirer des conclusions en ce qui concerne la sûreté de la cuve, on a presque achevé la fabrication à l'échelle grandeur d'un modèle de cuve plus court que la normale. Ce modèle ne comporte ni la partie cylindrique simple ni le collier avec branchement pour l'arrivée du fluide de refroidissement. Il sera soumis à des essais de résistance et de bon fonctionnement.

A/522 Чехословакия

Корпус реактора первой чехословацкой атомной электростанции

Й. Хауер et al.

Одним из основных типов энергетических реакторов, разрабатываемых в СССР и странах народной демократии, является реактор корпус-

ного типа на природном уране с тяжеловодным замедлителем, охлаждаемый газом, с тепловыделяющими элементами пруткового типа.

Такая конструкция и мощность реактора 150 Мвт (эл.) определяют основные размеры его корпуса. При соблюдении заданного минимального шага между тепловыделяющими элементами габариты корпуса и толщина его стенок достигают значительных размеров, которые усложняют изготовление, особенно сварку и контроль. Поэтому конструкция должна обеспечивать оптимальные размеры и формы узлов корпуса, испытывающих наибольшую нагрузку, таких, как крышка, фланцевые соединения, конусное основание, а главное, входные и выходные патрубки для охлаждающего газа. Эти проблемы были решены теоретически и экспериментально на моделях при помощи тензометрического и оптического методов исследования напряжений. При этом изучалось влияние различных факторов на концентрацию напряжений в местах цилиндрического корпуса реактора, ослабленных патрубками, таких, как размеры и формы отверстий, количество отверстий по диаметру, жесткое крепление отверстия патрубка и местная модификация перехода патрубка в корпус.

У сварных корпусов опасно появление внезапных хрупких изломов.

Поэтому проводились предварительные испытания на изгиб крупногабаритных образцов с надрезами. Результаты показали зависимость прочности от размеров образцов и надреза. Был проведен анализ характеристик деформации и уточнены понятия быстрого пластического и быстрого хрупкого изломов.

Далее был разработан проект систематических испытаний крупных узлов и образцов небольших размеров в натуральную толщину стенки корпуса. Испытания этих образцов проводятся на тяжелой грузочной машине с усилием 6000 т. Изучались результаты некоторых проведенных к настоящему времени испытаний на изгиб крупногабаритных образцов с точки зрения оценки предельного состояния корпуса реактора.

Был проведен критический анализ и оценка испытаний образцов небольших размеров по величине переходной температуры и температуры, необходимой для прекращения растрескивания.

Корпус реактора будет изготовлен на малоуглеродистой марганцевой конструкционной мелкозернистой стали. Нестареющая сталь производилась в СМ-печах и отливалась в слитки весом 43 т без применения вакуума.

Из слитков свободной ковкой на 12 000 т прессе изготавливались фасонные поковки заготовок с горловинами и слябы, из которых прокатывались листовые заготовки. Из заготовок на 12 000 т прессе штамповались сегменты, которые электрошлаковой сваркой сваривались в отдельные узлы корпуса. Из узлов после их

обработки электрошлаковой полуавтоматической в атмосфере CO_2 и ручной сваркой были сварены кольцевыми швами крышка и корпус реактора. Отжиг корпуса для устранения напряжений проводился в специальной электропечи.

До непосредственного проведения сварки корпуса в широком объеме проводились экспериментальные работы по проверке стали на свариваемость, по разработке наиболее пригодных присадочных материалов для всех видов сварки и овладению технологией сварки и предварительного нагрева при сварке, а также исследования по определению величины внутренних напряжений и деформаций и по разработке режимов термообработки после сварки и т. д.; испытания проводились не только на плитах, но и на узлах натуральных размеров и толщин.

Весь технологический процесс изготовления корпуса от варки стали до проведения испытаний сваренного и термически обработанного корпуса включает ряд операций, которые влияют на качество основного металла и сварных соединений. Поэтому в различные фазы производства включены пооперационные приемочные испытания с целью своевременного обнаружения деталей с наличием дефектов.

В настоящее время для проверки разработанной технологии производства и комплексной оценки безопасности эксплуатации корпуса реактора закончено изготовление сокращенной модели корпуса в масштабе 1 : 1. Модель сокращена по длине за счет гладкой цилиндрической части и кольца с патрубками для подвода охлаждающего газа. Модель будет подвергнута прочностным и функциональным испытаниям.

A/522 Checoslovaquia

Vasija de presión para la primera central nuclear de Checoslovaquia

por J. Hauer et al.

Uno de los tipos fundamentales de reactores de potencia ensayados dentro del marco de una amplia investigación de diferentes prototipos en la URSS y los Estados democráticos populares, es el reactor con vasija de presión, alimentado con elementos combustibles, de uranio natural, en forma de varilla, moderado con agua pesada y refrigerado por gas.

De acuerdo con el concepto de reactor y con la potencia establecida, de 150 MW(e), se fijaron las dimensiones fundamentales de la vasija de presión del reactor. Se obtuvieron así, para el espaciado mínimo previsto de los canales del combustible, grandes dimensiones de la vasija y grandes espesadores de pared lo que lleva consigo dificultades para efectuar las soldaduras y para inspeccionarlas. Por esta razón, el proyecto debe resolver el problema de las dimensiones óptimas y el diseño particular de las partes más difíciles de la vasija, tales como la tapa

superior, las juntas de las bridas, el soporte cónico, y especialmente, las conexiones interior y exterior para las conducciones del gas refrigerante. Estos problemas fueron resueltos teóricamente y experimentalmente sobre modelos siguiendo técnicas tensiométricas y fotoelasticimétricas. Se estudiaron diversos efectos sobre el grado de concentración de tensiones en lugares débiles de la vasija de presión cilíndrica, debidos a las conexiones de las tubuladuras: magnitud y forma del agujero, número de agujeros situados sobre una misma circunferencia, refuerzo del agujero con las tubuladuras de unión y modificación local transitoria de la tubuladura en la pared de la vasija de presión.

En las vasijas de presión soldadas existe el peligro de la aparición repentina de fracturas frágiles.

Por esta razón se realizaron ensayos previos de plegado en grandes componentes con entalla. El resultado demuestra la dependencia de la resistencia con la magnitud y el efecto de la entalla. Se indica el análisis de las características de la deformación y la especificación de las fracturas compacta plástica y compacta frágil.

Además, se llevó a cabo un proyecto para el ensayo sistemático de componentes normales y probetas de gran tamaño con espesores análogos a los de la pared de la vasija de presión real. Estos ensayos, con tales probetas, se realizaron con grandes máquinas de ensayo de 6 000 t de carga. Se han estudiado los resultados de algunos ensayos realizados hasta la fecha con componentes de gran tamaño, así como lo que su valor representa con respecto a la condición de contorno de la vasija del reactor.

Se llevó a cabo un análisis crítico de la importancia de los ensayos sobre probetas pequeñas y de los resultados de los mismos, de acuerdo con la temperatura de transición y con la temperatura a la que las grietas no prosiguen.

La vasija de presión será fabricada con acero de construcción al manganeso, de bajo contenido en carbono, de grano fino, producido, en calidad estabilizada, en hornos Martin-Siemens y colado a la presión atmosférica, en lingotes de 43 t de peso.

A partir del lingote, se conforman, con forja libre, en prensas de 12 000 t, tanto los productos semiacabados incluyendo las tubuladuras, como los

desbastes planos (palanquillas) de los cuales se sacan por prensado, las chapas semiacabadas. A partir de éstos, se conforman los segmentos por estampación, en prensas de 12 000 t, soldándose las diferentes partes de la vasija de presión según la técnica de soldadura con electroescoria. Las unidades completas, es decir, la parte central y superior de la vasija de presión, se forman, a partir de los componentes terminados, soldando circunferencialmente, según la técnica de electroescoria, semiautomática, bajo atmósfera protectora de CO₂ y por soldadura manual. Las tensiones introducidas por estas operaciones, en la vasija de presión, se eliminan, introduciendo ésta en un horno de resistencia eléctrica especialmente diseñado para este objeto.

Antes de la soldadura, fue necesario llevar a cabo un amplio trabajo experimental para garantizar la soldabilidad del acero, desarrollar los restantes materiales más adecuados para todos los métodos de soldadura, conocer a fondo la tecnología de la soldadura y del precalentamiento, comprobar la magnitud de las tensiones y las deformaciones, encontrar un tratamiento térmico adecuado para después de la soldadura, etc. Estos ensayos fueron realizados no solamente en las chapas sino también en partes de la vasija, a escala natural.

El ciclo tecnológico completo que cubre la fabricación de la vasija de presión, desde la producción del acero hasta el ensayo de la vasija soldada y tratada térmicamente, incluye una secuencia de operaciones que afectan a la calidad del material de base y de las juntas soldadas. Por este motivo es necesario realizar ensayos especiales entre las distintas operaciones de las diversas fases de fabricación, que tienen por objeto detectar a tiempo una pieza defectuosa.

Está finalizando la construcción de un modelo simplificado de esta vasija, a escala 1:1, con objeto de comprobar el desarrollo de la tecnología de fabricación y poder dar conclusiones en lo que se refiere a la seguridad de la vasija de presión. El modelo carece de la porción cilíndrica y del anillo con las tubuladuras para la entrada del gas refrigerante. El modelo se destinará a ensayos de resistencia mecánica y de funcionamiento.

Design and manufacture of the reactor pressure vessels for the Ågesta and Marviken Power Stations and some future developments

By O. Hellström*

Reactor development work in Sweden has been concentrated, since 1958, on heavy water reactors of the pressure vessel type. The first example of this type in Sweden, the Ågesta PHWR reactor, went critical in July 1963 and after a research programme of core physics and thermal behaviour the reactor was increased to full power, 65 MW, at the beginning of March 1964. From a general point of view the Ågesta reactor—in itself too small to be an economical power production unit—might be regarded as the starting point for two attractive outlines of pressure vessel unit development for competitive nuclear power, namely:

(a) The uniform lattice reactor (*homogenized*), PHWR, and

(b) The natural circulation direct cycle boiling heavy water reactor equipped with facilities for internal superheating, BHWR.

The Marviken Power Station is of the second type and is designed for an electrical output of 140 MW with saturated steam operation and 200 MW with nuclearly superheated steam. The pressure vessel for this plant has been designed and the manufacture has started.

The general aim of the power plant operators is to increase power rating and to use more advanced thermal behaviour and fuel handling facilities within the reactor vessels. This is accompanied by an increase in both pressure vessel dimensions and the various difficulties of obtaining practical solutions to design, materials and fabrication problems. The increase in geometrical size can be taken care of by using more advanced designs, better materials and adjusted fabrication methods.

Design basis

The basis for the design of nuclear pressure vessels in Sweden has been the Swedish Pressure Vessel Code. In addition to Code requirements, several special rules have to be complied with.

The Swedish Pressure Vessel Code is based on yield strength with regard to thickness calculations. For each material, a certain yield strength at room temperature is specified. For different temperatures,

a calculation value is given, corresponding to a stress value slightly below the yield strength at this temperature.

To obtain the allowable stress, the *calculation value* is modified by a safety factor and a weld joint factor. The latter has a value of 0.9 for qualified vessels. The factor of safety for membrane stresses is 1.5 and for bending plus membrane stresses 1.1–0.73.

When starting work on the Ågesta vessel, comparatively little was known about radiation damage of the material used. It was therefore considered safest to assume the whole vessel to be brittle and allow for no plastic flow. In other words, all the calculated stresses were below the yield point of the material.

During the work on Ågesta it became apparent that with more knowledge about material properties it was unnecessary to have this requirement of stresses below yield.

For the Marviken vessel slightly different rules are used. They are given briefly below:

(a) Swedish Pressure Vessel Code shall be complied with, and

(b) The stress calculation shall take into account all stresses (membrane, bending, stress concentrations and thermal stresses). Where multi-axial stresses exist, a combined stress shall be calculated.

The calculated stresses shall be in accordance with the allowable level for all normal conditions of the reactor (even fast shut-downs, scrams, etc.). For certain types of more serious accidents it shall be determined that plastic deformation of the components is not great enough to preclude the use of components afterwards.

All stresses shall be calculated assuming complete unlimited elastic behaviour of the material.

The maximum allowable stress in a point shall be less than twice the calculation value divided by D_F . Mean stress in a section shall always be below two thirds the calculation value. Values of D_F are given in Table 1.

For internal components which do not carry any pressure, and are mainly subjected to thermal and bending stresses, the allowable stress is

$$\sigma_{all} = (\sigma_y \text{ at } 20^\circ\text{C} + \sigma_y \text{ at desired temperature})/S_F$$

* Uddeholms Aktiebolag, Degerfors, Järnverk

Table 1. The factor D_F

Part	D_F
Flange, head and cylindrical shell subject to bending	1.8
Unsymmetrical nozzle	1.6
Symmetrical nozzle	2.2-1.6
Thermal stress in transition between two materials of different coefficient of expansion	1.8

This means a safety factor of S_F against repeated plastic flow. For non-local stresses $S_F = 1.5$ and for local stresses $S_F = 1.2$.

Ågesta PHWR vessel

The reactor pressure vessel is shown in Fig. 1 and the principal data are given in Table 2.

The pressure vessel consists of a bottom dome and a cylindrical shell with an upper flange. The shell is made of sandwich rolled stainless clad pressure vessel steel. The flange is made of forged parts welded together. Its inside and sealing joint surfaces are clad with stainless steel by overlay welding.

The bottom dome is of an ellipsoidal shape with eight main nozzles for the coolant inlet and outlet. Originally this dome was designed torispherical. Strain measuring on a scale model, however, gave stress concentrations of too high a magnitude. Consequently the shape was changed to ellipsoidal which was assumed to decrease the stress concentrations around the nozzles. The theoretical results were confirmed by strain measurements on the full scale vessel in connection with the final pressure test.

The top cover has the form of a flat lid, comprising two main plates, separated by a grid of 50 mm thick and 1 200 mm high plates and surrounded by a cylindrical shell. The lid is equipped with light water circulation for balanced heating and cooling guided by and controlled against the reactor coolant temperature. The height of the top cover is dictated not only by the need for a rigid lid to avoid too high stresses in the nozzles passing through it, but also by the need to keep a low radiation level at the upper

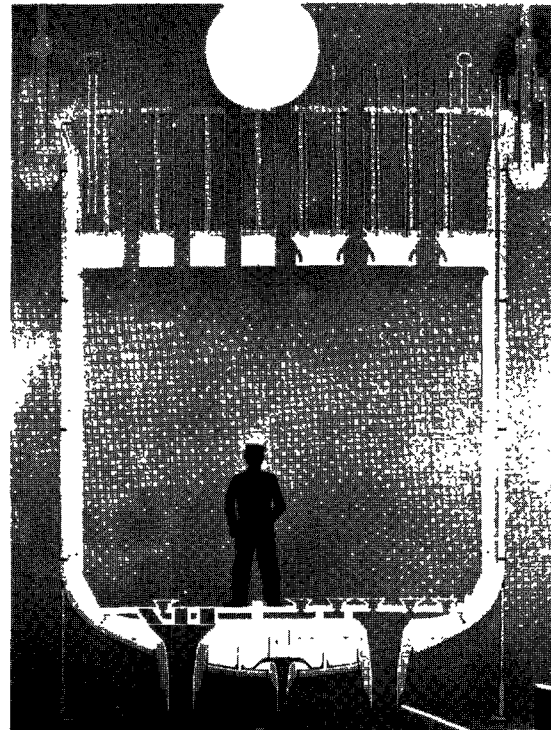


Figure 1. Ågesta PHWR vessel

closing plate and the tightening flange so that the top plate can be assessable whenever the reactor is shut down.

The flange design permits reactor start-up or shut-down in ten hours without producing over-stresses in either the vessel or the top cover. The flange itself is sealed by a primary lens-formed silver gasket and a secondary seal-welded torus.

All heavy water surfaces are smoothed to a micro-depth of profile of the order of 0.016 mm to prevent contamination.

To investigate the embrittlement of the vessel steel, special channels for boxes containing test pieces are arranged in the outer portion of the radial stainless steel shielding.

Table 2. Survey of reactor vessel data

	Ågesta PHWR	Marviken BHW	BASHFUL-660
Design pressure . . .bar	40	57.5	80
Design temperature .°C	251	272	293
Vessel inner diameter . .m	4.555	5.22	6.6
Cylindrical wall thickness mm	65	76	120
Bottom dome wall thickness mm	65	70	175
Vessel steel type .	carbon-manganese	carbon-manganese-molybdenum	9% ni-steel
Vessel height. .m	9.5	23.96	26.75

Marviken BHW vessel

The reactor vessel is shown in Fig. 2 and the principal data are listed in Table 2.

Contrary to the Ågesta vessel the internal shell surface is clad with stainless steel by overlay welding. The welding is to be carried out by the submerged arc process with a 60 mm broad and 0.6 mm thick band as additional material instead of wire rods. The requirement for the micro-depth of profile is a maximum of 0.035 mm and investigations have shown that the weld deposit has a surface finish which satisfies this requirement without any machining or grinding.

The bottom dome is hemispherical with the central cap of thicker plates than the rest of the dome. The penetrations are:

- 32 superheater nozzles;

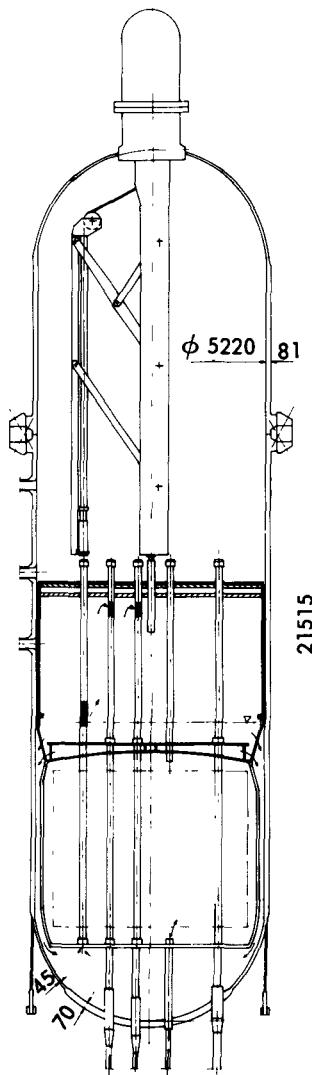


Figure 2. Marviken BWR vessel

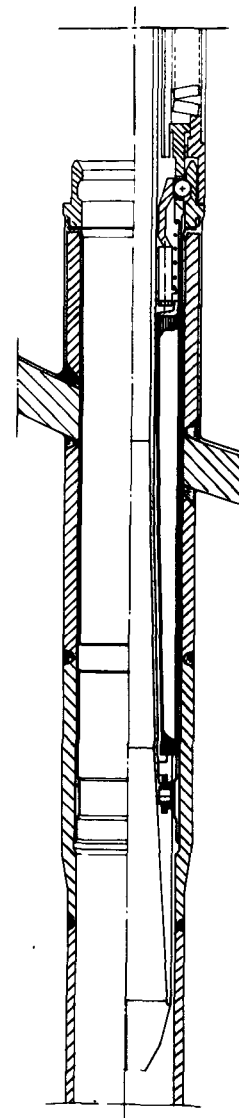


Figure 3. Superheater nozzle

34 nozzles for indicating position of the control rods by ultrasonics;

12 nozzles for neutron detectors;

8 nozzles for start-up heating and coolant inlet;

1 nozzle for transport channel for control rods and fuel elements.

The bottom dome design and manufacture requires high quality work and careful studies of all technical details have been made. The nozzles are of the set-on type and for welding of these to the dome bent electrodes will be used to some extent.

Special attention has been paid to the superheater nozzle itself, illustrated in Fig. 3. The temperature distribution and the corresponding thermal stresses have been carefully studied, and suitable insulation between the steam and the nozzle walls has been developed.

The design also involves some rather intricate problems of joining different structural materials.

As the hydraulic driving devices for the control rods are arranged internally, penetrations for these

driving units are eliminated from the vessel itself. The cylindrical shell is penetrated by nozzles for: feed water, control rods (drives), pressure relief valves, emergency cooling of boiler fuel elements, canning leak detection and for emergency cooling of superheater fuel elements.

For a vessel of this size and pressure, the main flange gives rise to difficult problems. A conventional solution would give very heavy sections. This is a manufacturing problem and also a thermal stress problem, due to gradients through the sections.

A solution similar to the Ågesta flange was found to be unsatisfactory for various reasons.

In conventional flanges, the flange dimensions are chosen such that the flange has a sufficient torsional stiffness to withstand the twisting moment, without giving too high stresses in the shell. In the new flange concept (patented) the twisting moment is eliminated. The flange design is shown in Fig. 4, and the forces acting are shown schematically in Fig. 5. The bolt (1)

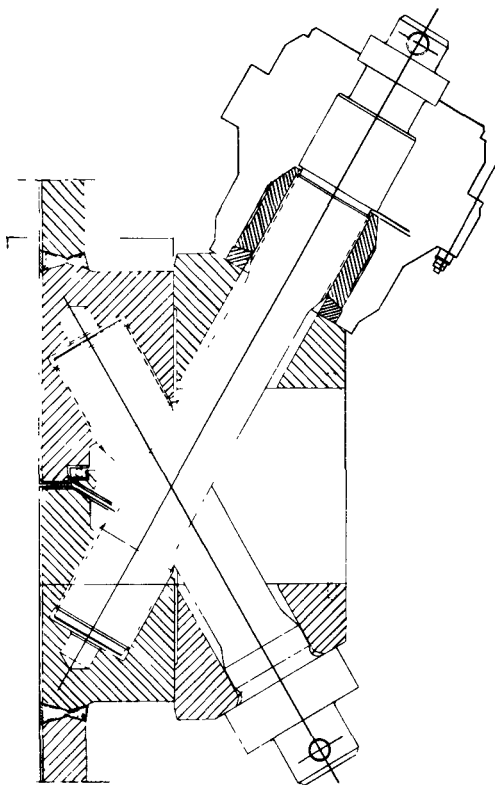


Figure 4. Marviken flange

passes through a piece (2) the length of which is approximately the bolt pitch. (1) engages in the fixed flange ring (4). To keep the pieces (2) apart, supporting legs (3) are spaced between the bolts.

As will be seen from Fig. 5 all the forces acting in the fixed flange rings are passing through one point, giving no moment on the ring. Some bending will be introduced in the bolts during tightening, due to parallel movement of centre-lines in piece (1) and bolt holes, but its magnitude is small. Only the bolts on one side require tightening. The whole arrangement except the upper set of bolts may be mounted on the upper flange before placing the cover in position. There are 112 details of each sort in the flange.

The material in the flange rings can be made of a lower quality steel than the rest of the shell due to the fact that practically no bending occurs. The loose details are made of high quality tough-hardened chromium-molybdenum quenched steel.

A model of the flange about 1 metre in diameter has been built (Fig. 6). Practical tests have verified the theoretical results.

Because of its relatively small dimensions and the symmetry of the bolt arrangement the flange is very advantageous from the thermal stress point of view.

The bolts are to be tightened by specially designed hydraulic tools. These are designed to operate under water if necessary and be remotely controlled. This may be necessary should certain types of accidents occur.

The closing cover consists of a cylindrical part with a flange and a hemispherical head. In the hemisphere

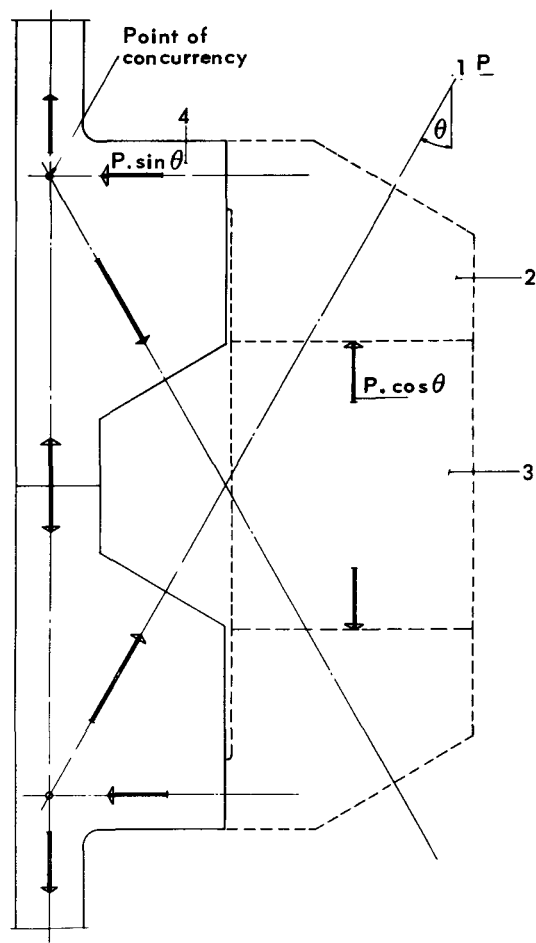


Figure 5. Force diagram of Marviken flange

there are three nozzles for television cameras for inspection of the internal surface and internal parts. The charging machine is supported in the large central nozzle. This machine can be lifted out of the reactor through this nozzle for service and the main flange need not be opened.

One of the more difficult stages in the manufacture is to keep the very narrow tolerances between the support of the charging machine, and the nozzles for superheaters in the bottom flange.

Project study BASHFUL—660 vessel

A drawing of this pressure vessel is shown in Fig. 7 and the principal data are given in Table 2.

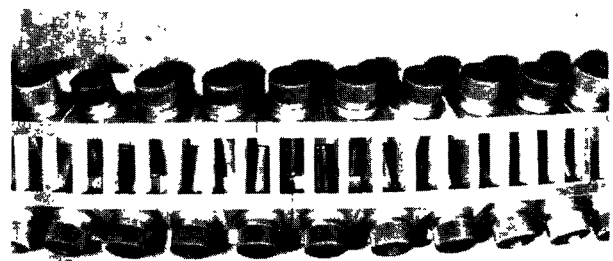


Figure 6. Model of Marviken flange

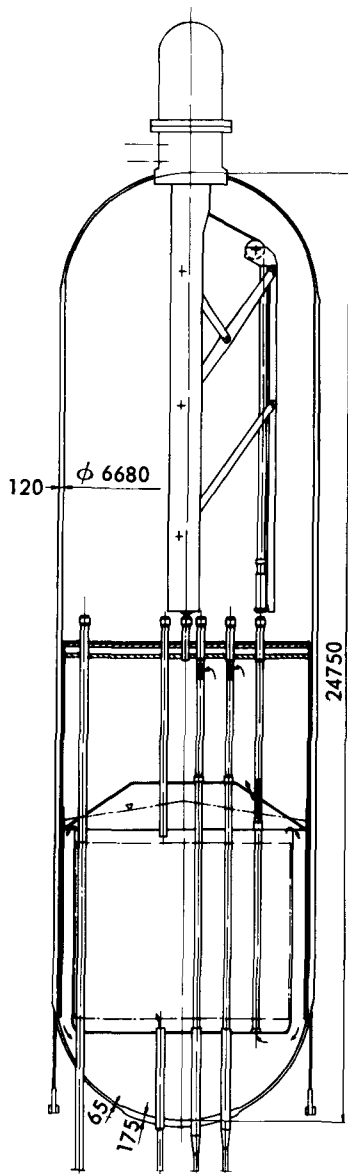


Figure 7. BASHFUL-660 vessel

This design is different from Marviken in the following respects:

- (a) Dimensions and plate thickness are increased,
- (b) The vessel has no main flange,
- (c) The superheater element has been concentrated in the centre of the core. This decreases the pitch between the nozzles in the bottom to about half the pitch in the Marviken vessel. This gives a very difficult welding problem, as the space between the nozzles will be very limited,
- (d) The thermal shields have been replaced by a thin Zircaloy tank, surrounding the core.

As the vessel is designed without a main flange it is necessary to assemble the internals before welding the shell completely together. It is not practical to insert the internals prior to transport, and the vessel will therefore have to be shop manufactured in at least two pieces which will be welded together on site.

This method also makes it possible to choose a suitable transport weight.

The Marviken vessel will give valuable experience for manufacturing a vessel in this way.

Due to the limited size which can be taken into the machines the vessel will be made in two or three finished parts which are welded together and locally heat treated. A mock-up assembly of the internals will be carried out before the vessel leaves the workshop.

Steels for reactor vessels

For the Ågesta vessel a carbon-manganese steel containing 0.16% C and 1.6% Mn was used. This steel is a slight modification of the standard Swedish pressure vessel steel SIS-14-2103. Yield strength is 30 kp/mm² at 20 °C and 24 kp/mm² at the design temperature of 250 °C. Impact strength is a minimum of 2.8 kpm at -20 °C in the Charpy V test.

For the Marviken vessel it was considered necessary to use a steel of higher strength in order to restrict the thicknesses and thereby obtain easier welding and better quality control. As radiation embrittlement data was necessary to have before definitely choosing material, it was considered advantageous to choose a material which had been tested by others and used previously for reactors.

After a study of suitable materials to fit the above mentioned requirements it was decided to use the American pressure vessel steel ASTM-A-302 B with some light modification in order to get better welding and impact properties. Our own steel DE-631 A has the following specification for mechanical properties: yield strength at room temperature minimum 42 kp/mm², yield strength at 275 °C minimum 33 kp/mm² and Charpy V-notch impact strength minimum 2.8 kpm at -20 °C.

For BASHFUL-660 studies a steel is required which, without being too expensive, has the following properties:

- (a) High tensile strength;
- (b) Good impact strength;
- (c) Good welding properties.

By a survey of existing materials in practical use, it was found that for instance a 9% nickel steel satisfactorily combines the above properties. This type of steel was developed for cryogenic service. The steel is fine grain treated, has a low carbon content (0.08%) and is alloyed with nickel and a small amount of manganese. The structure is composed of austenite, bainite and low carbon annealed nickel-martensite.

The strength properties are very good; the ultimate tensile strength is 71 kp/mm² and the yield strength at 20 °C is 59 kp/mm² and at 300 °C 53 kp/mm². Impact tests show that the energy absorption exceeds 2.8 kpm at -180 °C.

It should be mentioned that the above figures refer to thinner plate than will be used in BASHFUL-660. It is not to be expected that the increase in thickness will influence the properties appreciably, but the

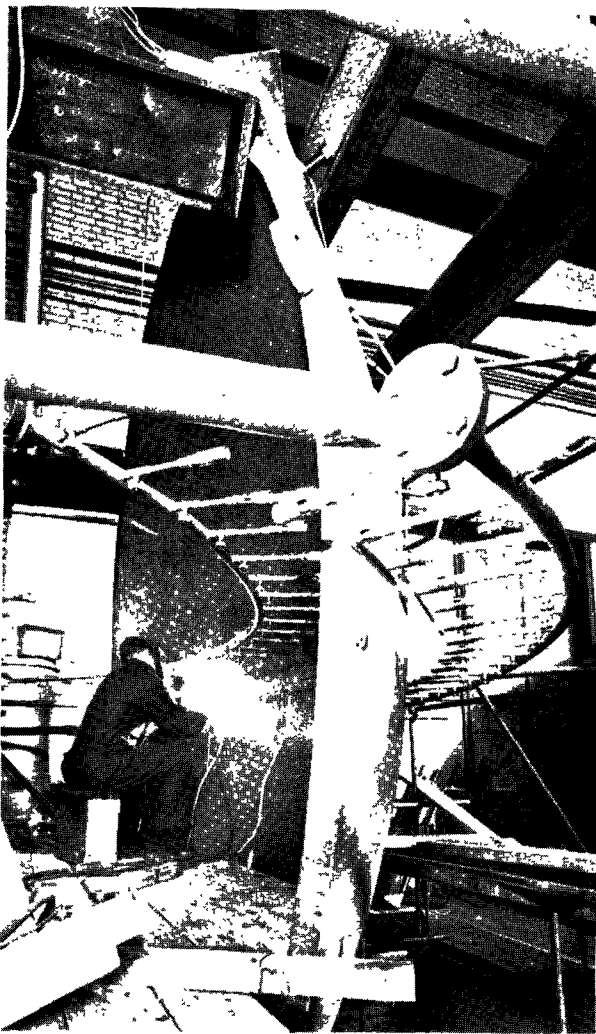


Figure 8. Welding of bottom dome cap for Marviken

thickness 120 mm is calculated using a yield strength of 42 kp/mm². It is probable that the allowable value will be higher, when more tests have been carried out.

For the time being no welding material exists which has the same properties as the plate. For vessels built in this material an electrode has been used which gives the required properties, but has lower tensile strength. It is to be expected, however, that with the large amount of research going on, suitable electrodes will be developed in the near future.

Shop fabrication

To manufacture large nuclear pressure vessels it is necessary to have heavy shop facilities, especially large lathes, boring machines and welding positioners. Lifting facilities of the order of 250 tons are necessary for current vessels. Future developments may require still heavier equipment. The development of suitable manufacturing methods requires a number of experts in various fields and close co-operation between them. It necessitates a large amount of experimental work on development of materials, welding techniques, pre-heating temperatures, etc., in order to get a perfect result in the shop or on site. Figure 8 shows the welding of the bottom dome cap, which will illustrate the special arrangements for preheating and temperature measurements all through the welding operation. It is to be expected that future vessels will be too large to be shop fabricated completely. A smaller or larger amount of site fabrication will be necessary. Development work on suitable welding techniques, electrode testing and heat treatment will be necessary.

It may be assumed safely that with suitable materials and techniques, the size limits for steel vessels will be large enough for the need of the reactor designer for a considerable time to come.

ABSTRACT—RÉSUMÉ—АННОТАЦИЯ—RESUMEN

A/810 Suède

Conception et réalisation des cuves sous pression pour les réacteurs d'Ågesta et de Marviken et quelques perspectives d'avenir par O. Hellström

Le programme suédois de production d'électricité nucléaire a été, dès le début, concentré sur des réacteurs à eau lourde et à uranium naturel. Après étude, il a été décidé de construire le réacteur d'Ågesta selon le type à cuve sous pression. Du point de vue général, le réacteur d'Ågesta peut être considéré comme un prototype pour deux filières intéressantes à cuve sous pression en vue de la production d'électricité nucléaire compétitive, à savoir:

- a) Le réacteur à réseau uniforme (homogénéisé), PHWR,
- b) Le réacteur à eau lourde bouillante à cycle

direct et à circulation naturelle, équipé de dispositifs de surchauffe interne, BHWB.

La centrale nucléaire de Marviken est du deuxième type et est prévue pour 140 MW(e) en fonctionnant avec de la vapeur saturée et 200 MW(e) en fonctionnant avec surchauffe nucléaire. L'étude de la cuve sous pression pour cette installation est maintenant achevée et sa construction est commencée.

Le mémoire décrit l'étude et la construction des cuves sous pression pour les réacteurs d'Ågesta et de Marviken. Les impératifs du code, les types et les propriétés des matériaux et les calculs d'étude spéciaux sont examinés. De plus, on expose les problèmes spéciaux de construction résultant des exigences de poids, des dimensions géométriques et des tolérances strictes fixées pour ces cuves sous pression. La capacité de l'atelier doit être suffisante pour que ces caractéristiques spéciales soient respectées. Quant à l'accroissement des dimensions

géométriques, on peut prévoir que l'emploi de matériaux meilleurs et la revision des méthodes de construction faciliteront la solution des problèmes de dimensions durant les 5 à 10 années à venir.

Pour des installations dépassant de beaucoup 500 à 600 MW(e), il est probable que les cuves sous pression devront être préfabriquées à l'usine pour ensuite être assemblées sur place selon des techniques spéciales.

A/810 Швеция

Проектирование и изготовление реакторных корпусов под давлением для атомных электростанций в Агесте и Марвикене и некоторые будущие разработки

О. Хеллстрём

В шведской программе развития атомной энергетики с самого начала основное внимание уделялось тяжеловодным реакторам на природном уране. После проведения ряда исследований было решено построить в Агесте реактор с корпусом под давлением. С общей точки зрения реактор в Агесте можно рассматривать как прототип двух замкнутых типов реакторов с корпусом под давлением, предназначенных для производства конкурентоспособной атомной энергии, а именно:

a) реактора с однородной решеткой (гомогенный) PHWR;

b) кипящего реактора BHWK с прямым циклом и естественной циркуляцией, снабженного оборудованием для ядерного перегрева пара.

Реактор Марвикенской атомной электростанции относится ко второму типу и рассчитан на электрическую мощность 140 Мвт при работе с насыщенным паром и 200 Мвт при работе с ядерным перегревом. Корпус под давлением для этого реактора уже спроектирован, и началось его изготовление.

В докладе дается описание конструкции и изготовления корпусов под давлением для реакторов в Агесте и Марвикене. Обсуждаются требования программы — код, типы и свойства материалов, а также специальные конструктивные расчеты важных узлов. Кроме того, рассматриваются специальные проблемы изготовления корпусов, связанные с весом, геометрическими размерами и жесткими допусками. Мастерские по изготовлению таких корпусов должны быть готовы к выполнению работ с учетом этих специальных условий. Что касается увеличения геометрических размеров,

то следует предположить, что с использованием лучших материалов и методов изготовления этим проблемам может быть уделено особое внимание в течение следующих 5—10 лет. Для установок электрической мощностью значительно выше 500—600 Мвт корпуса под давлением, по-видимому, следует изготавливать в мастерских и монтировать на месте строительства с использованием специальных методов.

A/810 Suecia

Proyecto y construcción de vasijas de presión para los reactores de las centrales de Ägesta y Marviken y desarrollos futuros

par O. Hellström

El programa sueco de producción de energía se ha limitado desde sus comienzos a los reactores de uranio natural y agua pesada. Después de algunos estudios se decidió construir el reactor de Ägesta, del tipo de reactores con vasija de presión. Desde un punto de vista general, el reactor Ägesta podría considerarse como un prototipo para desarrollar dos aspectos interesantes de reactores con vasijas de presión, capaces de hacer la energía nuclear competitiva, es decir: a) reactor con espaciado uniforme (homogeneizado) PHWR, y b) reactor de agua pesada en ebullición, de ciclo directo, con circulación natural, equipado con instalaciones adecuadas para el recalentamiento interno, BHWK.

La central de Marviken es del segundo tipo y está proyectada para 140 MW(e) con vapor saturado y 200 MW(e) con recalentamiento. Se ha proyectado y ha comenzado ya la construcción de la vasija de presión para este reactor.

La memoria describe el proyecto y la construcción de las vasijas de presión para los reactores de Ägesta y Marviken y se discuten los códigos necesarios, las clases de materiales, las propiedades y los cálculos especiales de las partes interesantes del proyecto. Además, se presta especial atención a problemas especiales de fabricación debidos al peso, a las dimensiones geométricas y a la necesidad de tolerancias muy estrechas, de estas vasijas de presión. Los talleres deben ser adecuados para atender a estas características especiales. En lo que respecta al aumento en las dimensiones geométricas, puede postularse que, usando mejores materiales y métodos de fabricación más adaptados, los problemas del tamaño podrán resolverse adecuadamente, durante los próximos 5 a 10 años.

Para centrales con potencias muy superiores a 500—600 MW(e) es probable que las vasijas de presión tengan que ser prefabricadas en el taller y montadas « in situ » utilizando técnicas especiales.

Design, development and manufacture of control rod drives for heavy-water power reactors

By S. Ericsson and B. Ahlnäs*

GENERAL REQUIREMENTS

Irrespective of the type of reactor there are a number of fundamental requirements which the design of a control rod drive must fulfil in order to be considered suitable as one of the most important parts of a nuclear power plant. There is in particular the severe requirement for absolute reliability and safe function during all reactor operating conditions, normal as well as abnormal. The control rod drives must be regarded as auxiliary equipment and consequently their design must be adapted to the design of the complete core as optimized from an economic, heat transmission and reactor physics point of view. This leads to certain requirements with regard to location, allowable space, etc., which it is the task of the designer to meet.

Among the more apparent special requirements associated with control rod drives for heavy-water reactors is the requirement for complete drainability. This is important in order to keep the unavoidable loss of heavy water as small as possible when the drives are removed from the reactor, for cost as well as for health physics reasons. The high cost of heavy water also makes it necessary to minimize the amount of water in the control rod drive and in the manoeuvring and coolant system. The techniques for removing and replacing the drives in heavy water reactors must also be carefully worked out in order to avoid the hazards connected with possible leakage of heavy water containing tritium.

CONTROL RODS AND DRIVE MECHANISMS FOR THE ÅGESTA REACTOR

Principal design

The reactor for the Ågesta nuclear power plant has a pressure vessel with a flat lid penetrated by standpipes through which the fuel is charged [1]. The control rod drives are located in the standpipes. Pipes for the manoeuvring, cooling, etc., of the drives are welded to the top of the standpipes.

The drive mechanisms are of two kinds. Sixteen coarse control rods and eleven safety rods are driven by hydraulically operated step mechanisms (Fig. 1).

The two fine control rods have drives comprising a piston in a hydraulic cylinder. Only the former will be dealt with in this paper.

The tubular control rod is driven by a hydraulically operated jack mechanism. The hydraulic medium is D_2O which is taken from the reactor coolant circuit and fed to the drive mechanisms through an outer manoeuvring system. Scram action is obtained by releasing the hydraulic pressure from the mechanism. The control rod then drops into the core by gravity.

Control rod design and manufacture

The control rods are tubular with an outer diameter of 104 mm, an inner diameter of 87 mm and a total length of 4 400 mm. The neutron absorbing material is silver with 15% indium and 5% cadmium and has a thickness of 3.5 mm and a length of 3 000 mm. With regard to the demands for mechanical strength and corrosion resistance the silver alloy is clad with stainless steel equivalent to AISI type 304 L, the outer cladding being 2 mm thick and the inner cladding 3 mm. The cladding is metallurgically bonded to the silver alloy.

The first step in the production of the 80/15/5 Ag-In-Cd tubes was the preparation of a master alloy of silver plus 30% cadmium. This master alloy together with silver and indium was subsequently melted to obtain the desired 80/15/5 composition. The alloy thus produced was, after analysis control, remelted and cast into billets suitable for extrusion. These billets were given a homogenizing heat-treatment prior to piercing and extrusion. The extruded tubes were cold-drawn to the required dimension in five draws without intermediate annealing.

From a thermal conductivity point of view it is necessary to avoid a gap between the silver alloy and the cladding. Therefore a special technique was developed to obtain a metallurgical bond between the silver alloy and the cladding.

This technique involved pre-treating the surfaces of the cladding that come in contact with the silver alloy by electroplating first with nickel and then with copper. After assembly and end-seal welding, the cladding tubes and the silver-indium-cadmium tube were co-drawn to the final dimensions. The co-drawing, which resulted in a reduction in wall thickness of about 10% in each of the three tubes, was made mainly to obtain good contact between the silver

* ASEA, Västerås, Sweden.

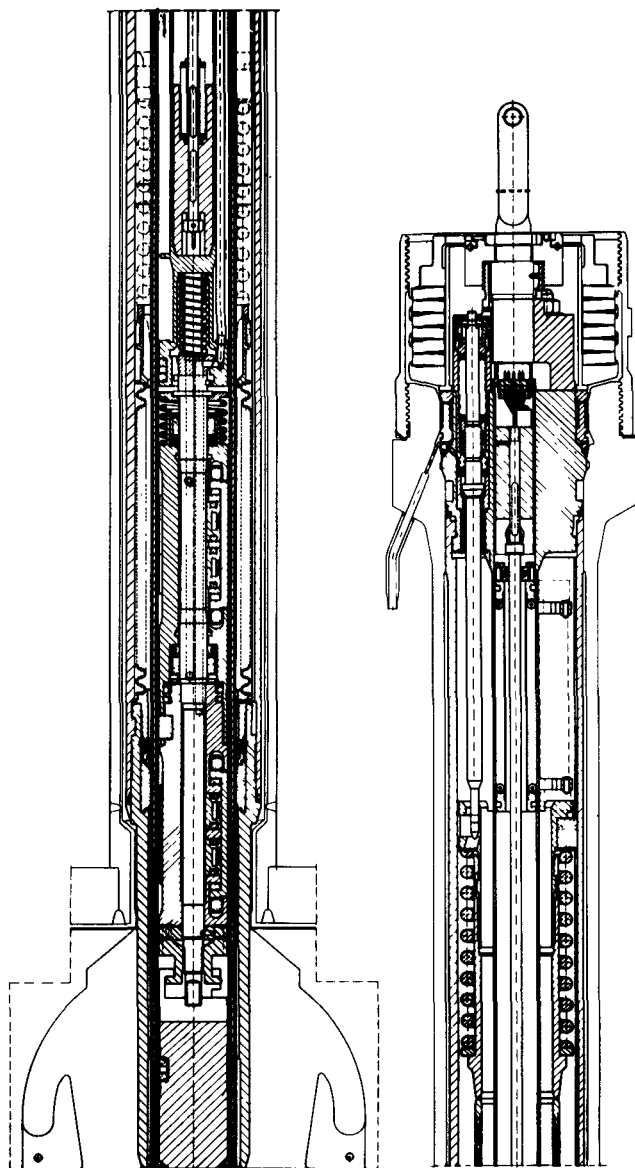


Figure 1. Control rod drive for the Ågesta reactor

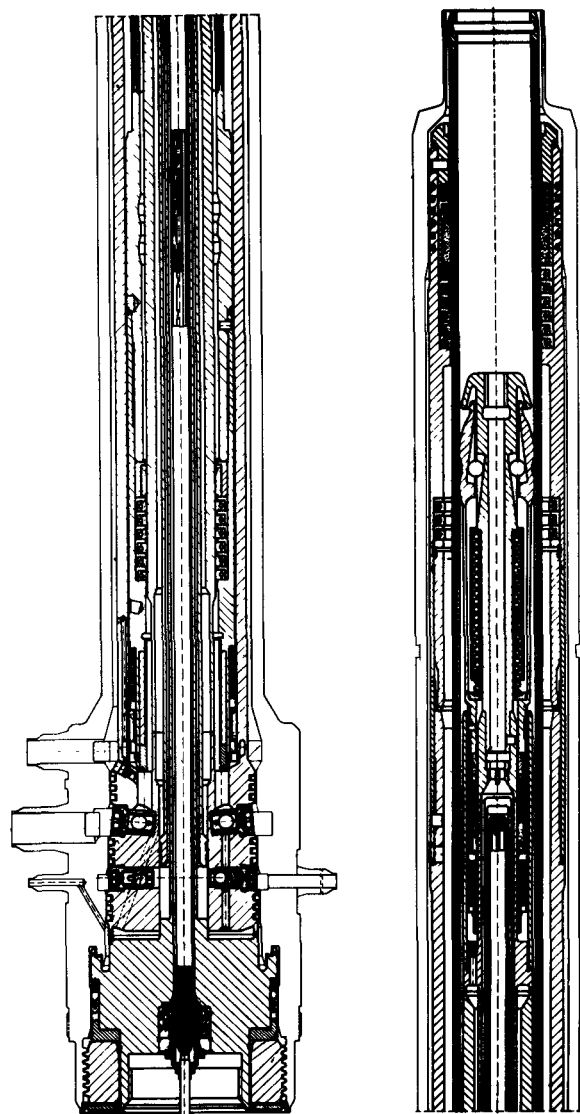


Figure 2. Bottom-mounted control rod drive for a pressurized-water reactor proposal

alloy and the cladding so that metallurgical bonding between the silver alloy and the cladding could be achieved by vacuum annealing. This anneal results in an intermetallic compound between copper and silver-indium-cadmium being formed.

During the development work on this bonding technique extensive tests were carried out to determine suitable bonding temperatures, times and nickel and copper plating thicknesses. The shear and tensile strengths of the metallurgical bond were determined and the tendency for carbide precipitation in the stainless steel cladding was examined.

The quality of the metallurgical bond was tested by ultrasonic inspection. Satisfactory strength properties of the metallurgical bond were shown by mechanical testing.

The next step after bonding was to remove the ends of the co-drawn tubes. The silver alloy was then machined out at each end of the tube to a depth of 10–15 mm. End rings were welded into each end using an automatic TIG-method.

With regard to the function of the control rod drives a good surface finish on the control rods was required and therefore the rods were electro-polished to a surface finish of 3 μm .

Drive mechanism

The hydraulic step mechanism inside the control rod has press plates which can be pressed against the inside of the rod to hold it in position by friction. The step mechanism has two chucks of which the lower one is fixed while the upper can be moved

axially a distance of 10 mm when pressurized D₂O is fed into the space between the chucks. The return action is accomplished by a spring and by the weight of the chuck.

The step action is obtained by means of pressurized water, and the three manoeuvring functions, "Keep" (lower chuck), "Grip" (upper chuck) and "Lift", are used for stepping the rod upwards according to the following programme:

Pressurize	"Keep"
Pressurize	"Grip"
Evacuate	"Keep"
Pressurize	"Lift"
Pressurize	"Keep"
Evacuate	"Grip"
Evacuate	"Lift"

Stepping downwards is done in principally the same way. Scram is obtained by evacuating the manoeuvring pressure for all three functions. The grip of the press plates against the control rod is then released irrespective of the position of the rod, which then drops by gravity into the core. The rod velocity is limited by the hydraulic resistance from the water passing from the moderator, past the rod, into the space above. Close to the bottom position an hydraulic dash pot is arranged to decrease the velocity of the rod before it hits the spring buffer.

The safety and coarse control rod drives have the following working data:

Working pressure	34 atm
Working temperature	220 °C
Step length	10 mm
Manoeuvring speed	15 steps/minute
Drop speed	1.6 m/s max
Time taken for rod to reach max drop speed after breaking current to solenoid valve	0.5 s
Rod travel	3 000 mm
Total length of control rod drive with rod in top position	5 100 mm
Max diameter of drive	182 mm
Total weight of drive	~ 400 kg
Weight of control rod with position indicator magnets	~100 kg

The drive can be regarded as consisting of three concentric tubes. The innermost of these is the position indicator tube which contains the transducer for the position indicating system, the step mechanism being fixed at the lowest part of this tube. The indicator tube is surrounded by the control rod and the outermost parts are the guide tubes which form a container for the inner parts of the drive.

The plug in the top of the drive seals the standpipe by means of a primary seal, which consists of a silver ring, and a secondary seal in the shape of a pressed sheet metal ring with Teflonized sealing lips. Through holes in the conical seat pressurized water for the step action is fed to the step mechanism.

The control rod consists of the absorber tube and a guide head. Connected to the guide head there is a spring buffer for deceleration of the rod in the bottom position on scram occasions.

The step mechanism forms the real working device of the drive. It gives the rod its step action and consists of two chuck systems on a vertical shaft. One of the chucks is fixed and the other can be moved axially a distance of 10 mm. Each chuck has three press plates, 120 degrees apart, which can be expanded radially against the inner surface of the control rod. The press action is obtained hydraulically by pistons behind the press plates. For the axial movement of the upper chuck there is a working cylinder formed between the fixed and movable chucks.

In the lower part of the guide tube, there is a bellows-shaped buffer. The object of this is to absorb by plastic deformation the energy from a rod accidentally dropped when there is no water in the drive for braking.

The transducer for the position indicating system is located in the central tube. It consists of an axial bifilar-wound potentiometer coil. A contact device is driven along the potentiometer coil by permanent magnets standing on the control rod head thus causing a short-circuit between two adjacent turns. For indicating the end limits of the rod travel there are three glass switches.

The control rod drives are exchanged in the reactor by the fuel charge machine when the reactor is shut down.

The material in the control rod drive is almost entirely austenitic stainless steel. In some special cases where there is a need both for good corrosion resistance and for reasonably high hardness, for example in the press plates of the step mechanisms, a precipitation hardening steel has been chosen. All springs in contact with the reactor water are made from Inconel-X. For bushings and seal rings graphite has been used.

Testing

During the design and development stage for the Ågesta control rod drives extensive testing has been carried out both as component tests with the most important parts and as full-scale prototype tests.

Among the component tests especially worth mentioning are those aimed to develop graphite seal rings with a leak tightness good enough to keep the amount of manoeuvring water at an acceptable value. Extensive tests have also been made with the position indicator coil in order to reach a solution which satisfies the requirements both for acceptable life and for easy manufacturing.

The greatest effort, however, has been concentrated on the testing of a full-scale prototype of the coarse control rod drive. For this reason a test rig has been built, in which the conditions to which the control rod drive will be subjected in the reactor at normal as well as at conceivable abnormal conditions can be simulated. Thus the pressure, temperature, flow pattern and water chemistry was the same in the test rig as in the reactor.

The prototype of the coarse control rod drive has been run through an extensive test programme for

more than 1½ years. The programme has covered prolonged wear tests with stepping and scrambling at reactor operating conditions to check important factors for the life of the drive, such as the variation with time of wear and seal ring leakage. Furthermore, the function of the drive has been tested at certain abnormal conditions such as with water flow inclined to the rod, boiling in the moderator, pressure excursions in the moderator, a substantially bent absorber rod, etc. Very good results have been obtained from the tests and therefore it has been necessary to introduce only minor alterations and modifications to the design. An example of components which have been changed are the graphite seal rings for the step mechanism, where the leakage in the beginning was too large, but where design modifications have brought the leakage down to acceptable values. At an initial stage of the testing it was found that the primary seal silver ring had inadequate creep strength. This has been solved by modifying the analysis of the silver alloy.

During the tests the coarse control rod drive prototype has performed more than 1 million steps and 1 400 scrams with very good results.

Manufacturing problems

The manufacture of the kind of components represented by control rod drives for nuclear reactors no doubt offers many new problems to the workshop. As the requirements for safe function of the product at all instants are so severe, the best machine tools and the best personnel must be selected to carry out the work. It is also essential to have properly applied inspection of the most important parts.

Many of the manufacturing difficulties can be assigned to the relatively bad machining properties of low-carbon, austenitic stainless steel, and the very severe surface finish requirements on surfaces which work against graphite components, such as seal rings. However, methods have been developed which satisfy both the functional requirements and the manufacturer's desire for high production capacity.

For the welding of the more important parts with high requirements on shape accuracy after welding, an automatic tube welding machine, specially developed for site welding of piping systems in Ågesta, has been used. The welding is done as argon-arc welding without filler metal. The design of the automatic welder is such that unavoidable warping can be kept well under control and can also be effected in a desired direction during the welding procedure.

The manufacture of the very long coil with a small diameter for the position indicating system has presented considerable problems. Through successive tests it has been possible, however, to develop a winding method and an insulating material with qualities suitable for working at 220 °C.

Operational experience

At the time of writing the control rod drives have been working in the reactor for more than one year,

first during the light water test period and after that during the low and high power tests with D₂O.

The control rod drives as well as their manoeuvring system have performed very well with only minor exceptions. Some problems have arisen with the position indicator coils where dust, probably from the binding material in the insulating material, has stuck to the winding and caused increased contact resistance. A modification has been made and will soon be tested in the reactor.

CONTROL ROD DRIVES FOR THE MARVIKEN REACTOR

Principal design

The Marviken nuclear power plant will have a direct cycle boiling heavy-water reactor [2]. In order to leave space enough for individual outlets in the bottom of the reactor vessel from each superheating channel, it has been necessary to locate the control rods with their drive mechanisms wholly inside the pressure vessel above the core.

The same design principle is used as in Ågesta, e.g., the drive consists of a hydraulic step mechanism working against the inner surface of the tubular control rod.

In principle the difference in design between the Marviken and Ågesta drives is due to differences in location in the pressure vessel, in environmental conditions and in the weight of the control rod.

Control rod

In the Marviken reactor it is intended to use the same type of control rods as in the Ågesta reactor the dimensions being slightly changed. Thus the outer diameter will be 122 mm, the inner diameter 100 mm and the total length approximately 5 100 mm.

Compared with the control rods in the Ågesta reactor some modifications to the bonding technique are to be made. Tests have shown that a metallurgical bond between the stainless cladding and the silver alloy can be obtained using only nickel plating.

In order to further reduce the risk of carbide precipitation in the grain boundaries of the austenitic stainless cladding material during the bonding treatment a stainless steel equivalent to AISI type 316 L is to be used.

Drive mechanism

The drive is placed in a guide tube in the core top by the internal fuel handling machine. Seal rings in the top of the drive mechanism must be designed to give adequate sealing action only by the weight of the drive itself against the different tube connections in the core top through which the manoeuvring and cooling water is to be fed. The water is fed from the manoeuvring system in the reactor building outside the reactor biological shield to the control rod drives through pipes welded to the core top and passing

through the pressure vessel wall. Because of a heavier control rod the step mechanism has to work with higher pressures in the manœuvring functions than in Ågesta.

Different types of suitable seals in the top of the drive have been theoretically and experimentally investigated. The best solution seems to be a special design of metallic piston ring. There are not many conceivable types of seal which can perform the sealing action in the very limited space and with the small sealing force available.

In Marviken the drive works in steam and therefore it is necessary to keep the drive filled with water from a supply outside the reactor in order to obtain the hydraulic limitation of drop speed which is necessary on scram occasions. Care must also be taken to avoid boiling in the manœuvring or braking volumes of the drive at any working condition as this would cause malfunction of the drive. To prevent damage to the drive or core top if the control rod should drop when there is not water enough in the hydraulic braking volume, the drive is equipped with a bellows-shaped buffer of the same kind as in Ågesta.

The position indication system consists of a transducer located in a tube welded to the bottom of the reactor vessel and a reflector plate which forms the lowest part of the control rod. The transducer emits ultrasonic pulses against the reflector plate from whence they are reflected back against the transducer. By measuring the time taken for the sound to go to the rod and back again and comparing it with the corresponding time in a calibration channel, which is also located in the reactor core, the position of the control rod can be determined.

Experiments and prototype tests

A number of experiments with the most important elements of the control rod drive have already been made and will continue. A great deal of work has been devoted to experimental investigations on suitable types of piston ring seals in the top head of the drive.

A full-scale prototype of the drive will be thoroughly tested in a test rig where the working conditions in the reactor can be simulated. Although the design of the drive is similar to that of Ågesta the different ambient conditions and other special requirements make it necessary to perform these very laborious and costly prototype tests. After completion of the prototype tests the test rig will be dismantled from the ASEA laboratories and reassembled in the reactor station, where it will be used to test control rod drives before they are put back into the reactor after service.

OTHER CONCEIVABLE TYPES OF CONTROL ROD DRIVES

As the development costs for a new type of control rod drive are very high, one must try to use types already developed as far as possible. The Ågesta

design principle, described in the preceding chapters, has demonstrated its suitability during operation in the reactor and it will now be further developed for use in the Marviken reactor with its different conditions. However, for a boiling heavy-water reactor for a direct cycle with saturated steam the mechanically best solution might be to locate the control rod drives below the reactor in standpipes welded to the pressure vessel bottom. Much design and development work has already been done on a bottom-mounted control rod drive for Marviken in an alternative form as a pressurized-water reactor.

This drive is designed as a hydraulic cylinder with an annular piston (Fig. 2). The piston has seal rings at its outer and inner diameter against the manœuvring space below the piston. Furthermore, the drive has seal rings acting against the absorber rod at the top of the drive. To move the rod upwards a defined quantity of water per unit time is fed by a plunger pump into the space below the piston. In the same way a defined quantity of water is pumped out of the drive to move the rod downwards. When the control rod does not move it is kept in the desired position by a locking chuck working by friction against the inside of the absorber rod. The chuck is self-locking and is opened hydraulically before manœuvring the rod. Scram action is obtained by connecting the space below the piston to pressure water accumulators. At the same time, the space between the outer piston seal and the seal against the rod is connected to a dump tank with a pressure lower than that of the reactor.

During the design stage of this drive component, tests have been performed with the most important parts such as the piston rings. A simplified and shortened prototype drive was tested in order to check the design, and it worked very well both in cold and hot conditions.

How control rod drives for future reactors will look cannot be regarded as an isolated question. The drives and the other components of the reactor must be designed together to obtain the best solution for the reactor as a whole. As the control rod drives with their manœuvring systems represent quite a considerable cost for a large heavy-water reactor, there will always be a striving to minimize the number of control rods by using simpler and cheaper methods for reactivity control. Boron systems and burnable poisons might be used in as large an extent as the growing experience from reactors in operation shows is desirable with respect to the operation and safety of the reactor. To the extent that it will be necessary to use control rod drives, however, designers have to seek simple and cheap solutions which interfere as little as possible with the layout of the reactor core for best economy.

Regardless of drive location it will certainly be possible in the future to reduce today's severe requirements on design and manufacture, as more and more experience from the operation of power reactors is gained. Lower requirements on materials, tolerances and surface finish will result in cost reductions, when

it has been shown during reactor operation that wear and length of service intervals are acceptable even with not quite so high requirements.

In cases, however, where the safe function depends on very high design and manufacturing quality, there can never be consideration of reducing the requirements.

ABSTRACT—RÉSUMÉ—АННОТАЦИЯ—RESUMEN

A/809 Suède

Construction, développement et fabrication des mécanismes des barres de commande pour réacteurs de puissance à eau lourde

par S. Ericsson et B. Ahlnäs

Les mécanismes des barres de commande d'un réacteur nucléaire doivent être considérés comme équipements auxiliaires, et, par conséquent, leur construction doit être adaptée à l'architecture du cœur complet et constituer une solution optimale du point de vue de l'économie de la transmission thermique et de la physique du réacteur. Cela entraîne certaines exigences quant à l'emplacement, l'espace disponible, etc., la solution de ces problèmes incombant à l'ingénieur constructeur. Il peut, par contre, être impossible d'obtenir les propriétés qui sont théoriquement souhaitables. Il est donc important que l'étude du cœur et du mécanisme des barres de commande se poursuive simultanément et en collaboration étroite.

En outre, les exigences relatives à la sûreté de fonctionnement sont extrêmement élevées dans le cas du mécanisme des barres de commande. Pour les réacteurs à eau lourde on rencontre en outre les problèmes spéciaux résultant des dangers sanitaires résultant de la présence de tritium dans l'eau lourde. Il convient de tenir compte de ces problèmes lors de l'étude du remplacement des mécanismes dans le réacteur, des travaux d'entretien, etc.

Le mémoire présente l'expérience acquise lors des travaux suédois concernant des réacteurs à caisson sous pression, modérés et refroidis à l'eau lourde, l'un actuellement en service à Ågesta et l'autre devant être installé à Marviken, dont les travaux de construction sont déjà très avancés et dont la divergence est prévue pour 1968.

Dans ces deux réacteurs, les barres absorbantes sont tubulaires et l'alliage absorbant (argent, indium et cadmium) est chemisé intérieurement et extérieurement avec de l'acier inoxydable. Dans les zones limites, l'alliage absorbant et le métal de chemisage sont métallurgiquement unis l'un à l'autre. Le mémoire traite des travaux de mise au point et de la fabrication des barres de commande.

Les mécanismes de commande d'Ågesta et de Marviken sont construits selon le même principe.

REFERENCES

1. Hellström, O., *Design and manufacture of the reactor pressure vessels for the Ågesta and Marviken power stations and some future developments*, P/810, this volume.
2. Margen, P. H., Leine, L., and Nilson, R., *The design of the Marviken heavy water reactor with nuclear super-heat*, P/603, Vol. 6, these Proceedings.

Cependant, en raison de l'emplacement et des conditions environnantes, un certain nombre de modifications ont été nécessaires pour Marviken. Le mémoire contient une description de la construction des mécanismes de commande, des résultats des travaux de développement poussés faits à Ågesta et des essais sur prototype projetés pour Marviken.

Un certain nombre de problèmes spéciaux ont dû être résolus lors de la fabrication des mécanismes des barres de commande pour Ågesta. Le mémoire présente les plus importants de ces problèmes ainsi que les premiers résultats de fonctionnement en service.

Finalement, on mentionne plusieurs types éventuels de mécanismes de commande pour réacteurs de puissance à eau lourde. L'une des solutions, à laquelle une grande somme d'études et de travaux expérimentaux a été consacrée, est un mécanisme destiné à être placé au fond du caisson sous pression, sous le cœur du réacteur. On présente une brève description des travaux consacrés à ce système.

A/809 Швеция

Конструкция, разработка и изготовление приводов регулирующих стержней для тяжеловодных энергетических реакторов

С. Эрикссон, Б. Альнес

Приводы регулирующих стержней ядерного реактора должны рассматриваться как вспомогательное оборудование. Поэтому их конструкция должна выбираться в зависимости от конструкции полной активной зоны с точки зрения экономики, теплопередачи и физики реактора. В связи с этим решение задач, касающихся размещения приводов, допусков и т. д., входит в задачу конструктора. С другой стороны, было бы невозможно удовлетворить требования, касающиеся теоретически желаемых свойств. Поэтому важно поддерживать одновременное и тесное сотрудничество конструкторов во время проектирования активной зоны и приводов регулирующих стержней.

Кроме того, к безопасной работе приводов

регулирующих стержней предъявляются очень высокие требования. При эксплуатации тяжеловодных реакторов имеет место также особая проблема — проблема опасности для здоровья обслуживающего персонала в связи с содержанием в тяжелой воде трития. Это обстоятельство необходимо учитывать при замене приводов в реакторе или при обслуживании механизмов и т. д.

В настоящем докладе приводится описание опыта эксплуатации шведских реакторов с корпусом давления, использующих в качестве замедлителя и теплоносителя тяжелую воду. Один из этих реакторов в Агесте находится в настоящее время в эксплуатации, а другой реактор в Марвикене совершенствуется и должен достичь критичности в 1968 году.

В обоих этих реакторах поглощающие стержни являются трубчатыми, причем поглощающей нейтроны сплав серебра, индия и кадмия покрывается снаружи и внутри оболочкой из нержавеющей стали. Поглощающий нейтроны сплав и материал в месте их соприкосновения соединяются металлургическим способом. В настоящем докладе рассматриваются разработка и изготовление регулирующих стержней.

Механизмы приводов имеют одну и ту же принципиальную конструкцию на реакторах в Агесте и Марвикене. Отличия в размещении приводов и окружающих условиях для реактора в Марвикене привели к необходимости внести ряд модификаций. В докладе приводится описание конструкции приводных механизмов, результатов обширных разработок, которые были выполнены для реактора в Агесте, и планируемых испытаний прототипа реактора в Марвикене.

Предстоит еще решить ряд специальных проблем, касающихся изготовления приводов регулирующих стержней для реактора в Агесте. Наиболее важные из них, а также первый опыт эксплуатации рассматриваются в данном докладе.

Упомянуты некоторые возможные типы приводов регулирующих стержней для разрабатываемых тяжеловодных энергетических реакторов. Один привод, которому была посвящена большая конструкторская и экспериментальная работа, был размещен ниже активной зоны реактора на дне корпуса давления. Приводится краткое описание работы над этой конструкцией привода регулирующих стержней.

A/809 Suecia

Дизайн, разработка и fabrication de mecanismos de operación de barras de control para reactores de potencia de agua pesada

por S. Ericsson y B. Ahlnäs

Los mecanismos de operación de las barras de control en un reactor nuclear deben considerarse como

equipo auxiliar y, por tanto, su proyecto debe adaptarse al diseño completo del núcleo que sea óptimo desde los puntos de vista económico, de transmisión de calor y de la física del reactor. Esto conduce a ciertos requisitos con respecto a situación, espacio permisible, etc., que constituyen la tarea del proyectista. Por otro lado, pudiera resultar imposible el satisfacer las propiedades teóricas deseadas. Por ello es importante mantener una estrecha colaboración simultánea durante el diseño del núcleo y el de los mecanismos de operación de las barras de control.

Por otra parte, el requisito de seguridad funcional de estos mecanismos es de extrema importancia. Además para reactores de agua pesada existe el problema particular debido a los peligros derivados del contenido en tritio del agua pesada. Esto tiene que ser tomado en cuenta al planear el intercambio de los mecanismos dentro del reactor, así como los trabajos de mantenimiento, etc.

En la memoria se da una descripción de la experiencia adquirida en el trabajo sueco sobre reactores de recinto a presión moderados y refrigerados por D_2O , uno de ellos el Ågesta que se encuentra ahora en operación y el otro el Marviken que está en una fase avanzada de diseño y que deberá alcanzar la criticidad en 1968.

En ambos reactores las barras absorbentes son tubulares y la aleación absorbente, plata, indio y cadmio, está recubierta en el interior y exterior por acero inoxidable. En la zona de contacto, la aleación absorbente y el material de recubrimiento están adheridos metalúrgicamente. En la memoria se describe el trabajo de desarrollo y de fabricación de las barras de control.

Los mecanismos de operación de las barras de control son esencialmente del mismo tipo de diseño en Ågesta y Marviken. Sin embargo, las diferencias en posición y en el medio que las rodea hacen necesario para Marviken un cierto número de modificaciones.

En la memoria se describe el diseño de tales mecanismos, los resultados de un amplio trabajo de desarrollo llevado a cabo en Ågesta y las pruebas con prototipo planeadas para Marviken.

Durante la fabricación de los mecanismos de operación de las barras de control para Ågesta, se tuvieron que resolver una serie de problemas especiales. Los más importantes así como la primera experiencia operacional se mencionan en la memoria.

Finalmente se mencionan también algunos tipos posibles de mecanismos para barras de control en reactores de potencia avanzados de agua pesada. Una solución a la que se ha dedicado mucho trabajo experimental y de diseño, se refiere a un mecanismo de barras de control para ser colocado debajo del núcleo del reactor en la parte inferior del recinto de presión. Se da una breve descripción del trabajo sobre este diseño.

Les appareils de chargement et déchargement du combustible dans les réacteurs uranium naturel-graphite-gaz

par B. Saitcevsky* et D. Gaussois*

La manutention du combustible est certainement la plus délicate des opérations normales d'exploitation d'une centrale nucléaire.

Dans le cas d'une centrale à réacteur du type uranium naturel-graphite-gaz, le dispositif principal de manutention (ensemble des appareils permettant d'effectuer la manutention du combustible) est un des éléments les plus importants de la centrale, tant au point de vue prix qu'au point de vue fonctionnement.

En nous appuyant sur les exemples concrets d'EDF2 et d'EDF3, nous allons examiner les options fondamentales qui doivent être prises et les impératifs généraux qui doivent être respectés pour arriver à un ensemble de fonctionnement aussi sûr que possible.

FONCTIONNEMENT ET SÉCURITÉ

Rôle du dispositif principal de manutention

Le dispositif principal de manutention doit essentiellement effectuer les opérations suivantes: extraction des éléments combustibles irradiés hors du réacteur; évacuation de ces éléments à la piscine; introduction dans le réacteur des éléments neufs.

Ils doit en outre, en général, assurer la manutention de tous les objets actifs situés à l'intérieur du réacteur ou sur la dalle supérieure tels que: éléments absorbants, barres de contrôle et sécurité, bouchons, échantillons pour irradiation, etc.

Nombre des opérations à effectuer

Le nombre des opérations à effectuer est très grand.

Par exemple, pour les éléments combustibles, il faut évacuer environ 6 000 éléments irradiés par an à EDF2, 11 000 à EDF3, et les remplacer par autant d'éléments neufs.

Parmi les fonctions auxiliaires, la plus fréquente est la manutention des absorbants. La fréquence de cette opération est cependant inférieure d'un ordre de grandeur à celle de l'opération principale.

La répartition dans le temps des diverses opérations peut être très différente suivant la stratégie de chargement et de déchargement, la puissance spécifique, la fréquence des ruptures de gaines.

Conditions de fonctionnement

Le fonctionnement est rendu délicat à la fois par les caractéristiques des éléments combustibles eux-mêmes et par les conditions d'ambiance.

Les éléments combustibles sont relativement fragiles (l'élément proprement dit est supporté à l'intérieur d'une chemise en graphite); ils sont très radioactifs; ils chauffent; l'enceinte dans laquelle on opère est chaude, 200 à 400 °C, sous pression élevée de CO₂, et radioactive; quand le réacteur est en marche, un rapide courant ascendant de CO₂ provoque la lévitation des derniers éléments d'un canal en cours de déchargement.

Il en résulte essentiellement les nécessités suivantes: exécution des opérations à distance derrière protection et en télécommande; étanchéité parfaite des ouvertures; refroidissement permanent des éléments en cours de manutention; fonctionnement de certaines parties mécaniques, avec le maximum de sécurité, à température élevée et sous radiations, donc sans graissage.

Incidents possibles et conséquences

Les incidents les plus graves sont ceux qui peuvent entraîner la détérioration d'un élément combustible irradié par chute ou cisaillement. Dans le tableau 1 quelques-uns des incidents possibles et leurs conséquences prévisibles ont été résumés.

Enfin, il faut souligner que le risque de chute d'élément combustible dans un canal est plus grand, et ses conséquences plus graves, en marche qu'à l'arrêt, à cause du violent courant de CO₂ sous pression et des conditions beaucoup plus sévères de température et de dégagement de chaleur.

OPTION FONDAMENTALE : DÉCHARGEMENT EN MARCHÉ OU À L'ARRÊT

Suivant les cas, on peut envisager que le dispositif principal de manutention opère: réacteur en marche à pleine puissance; réacteur arrêté sous pression; réacteur arrêté hors pression

A première vue, le dispositif opérant en marche est le plus avantageux au point de vue exploitation. Cependant, il est évidemment le plus cher et les risques d'incident en cours de fonctionnement sont plus

* Electricité de France.

Tableau I. Incidents possibles en cours d'exploitation d'un appareil de chargement

Incident	Cause possible	Conséquences possibles	Conséquences pour la centrale
Chute hors réacteur (dans la machine ou le bâtiment de combustible irradié).	Erreur de commande. Défaillance de la signalisation. Défaillance du grappin. Rupture de la chemise par suite d'un choc.	Contamination. Blocage de l'appareil intéressé.	Si deux appareils, pas d'arrêt.
Chute dans le réacteur.	Comme ci-dessus.	Blocage d'un canal. Incendie de cartouche. Contamination du réacteur.	Arrêt pour dépannage. Détérioration permanente de certaines parties du réacteur.
Cisaillement hors réacteur.	Erreur de commande d'un aiguillage (bras, barillet, etc). Défaillance de la signalisation.	Comme dans le premier cas.	Comme dans le premier cas.
Cisaillement dans le réacteur.	Comme ci-dessus.	Comme dans le deuxième cas.	Comme dans le deuxième cas.
Rupture d'étanchéité.	Mauvais accouplement. Défaillance d'un joint ou d'un organe d'obturation.	Fuite du CO ₂ et vidange plus ou moins rapide suivant l'importance de l'ouverture. Contamination à l'extérieur du réacteur.	Arrêt pour réparation.

élevés, à cause des conditions plus difficiles dans lesquelles il doit travailler. Le gain apparent de disponibilité peut ainsi être en partie diminué.

Le dispositif opérant à l'arrêt en pression n'est pas beaucoup moins cher que le précédent, les étanchéités à assurer, en particulier au droit des accouplements, étant très coûteuses.

Le dispositif opérant à l'arrêt hors pression est beaucoup plus léger et plus simple que les deux précédents. Les appareils, étant plus légers, peuvent être plus nombreux. On peut certainement atteindre, en toute sécurité, des cadences de l'ordre de 600 éléments par jour. L'indisponibilité correspondante serait de l'ordre de 7% pour EDF3.

En fin de compte, un choix rationnel ne pourra être effectué que lorsque l'expérience d'exploitation des centrales du même type aura permis de déterminer: a) la fréquence et la gravité des ruptures de gaine; b) la fréquence et le nombre des opérations normales d'exploitation, telles que: chargement et déchargement des éléments combustibles, redistribution des absorbants; c) la disponibilité des dispositifs opérant réacteur en marche.

Dans l'ignorance de ces éléments, la solution déchargement en marche a été choisie pour EDF2 et EDF3, car elle donne la plus grande souplesse du point de vue exploitation.

DESCRIPTION RAPIDE DES DISPOSITIFS PRINCIPAUX DE MANUTENTION EDF2 et EDF3

Caractéristiques communes

Il est impossible de donner une description complète des ensembles très complexes que sont les dispositifs principaux de manutention EDF2 et EDF3.

Ils remplissent les mêmes fonctions dans des conditions identiques, et présentent des similitudes nombreuses, notamment: a) ils opèrent par la partie supérieure du réacteur; b) chaque puits à travers la paroi du caisson dessert 34 canaux disposés suivant un réseau triangulaire; c) la continuité entre puits et canal est assurée par un bras descendu par la machine à travers le puits; d) la machine, après extraction des éléments combustibles hors du réacteur, les évacue par l'intermédiaire d'un ensemble dénommé bâtiment du combustible irradié, que nous ne décrivons pas ici pour abrégé l'exposé; e) le fonctionnement est complètement automatique.

Ensemble EDF2

Généralités

Le dispositif principal de manutention EDF2 comporte plusieurs machines spécialisées par fonction: a) chargement et déchargement du combustible (2 machines identiques); b) mise en place du bras de chargement, manutentions autres que celles du combustible (barres de contrôle, bouchons, etc.) (1 machine); c) liaison machine - puits et commande du bras (5 fourreaux amovibles); d) dépannage (1 machine).

Déplacement

Les machines sont placées sur des chariots automoteurs. Le transport des machines est assuré par un pont tournant sans pivot à quatre boggies de deux galets, dont les caractéristiques sont les suivantes: longueur totale, 19,2 m; largeur, 11,2 m; diamètre du chemin de roulement, 17,5 m; poids total à vide, 146 t; poids en charge, 1 136 t; vitesse moyenne de rotation, 1°/s.

La rotation est assurée par deux roues dentées motorisées prenant appui sur une crémaillère fixe. Un groupe Ward Leonard assure une grande précision de positionnement.

Protection

La protection neutron et gamma est constituée par du béton à la baryte de densité 3,4 complété par des écrans en fer de 3 cm d'épaisseur sur les machines principales. Ce type de protection a été jugé économiquement que les écrans composites en couches successives de matériaux légers hydrogénés et de matériaux lourds.

Le problème difficile de la protection à la jonction de la machine et du puits de chargement est facilité par la présence d'une deuxième dalle de protection au-dessus du réacteur. Les treuils de barres de contrôle et les têtes des puits de chargement débouchent dans le grenier intermédiaire. De cette manière, la dalle supérieure, dans laquelle une seule ouverture à la fois est nécessaire, assure une excellente continuité de la protection.

Principe général de fonctionnement

La machine principale est chargée en éléments neufs sur un des postes fixes du bâtiment de combustible irradié.

Pendant ce temps, la machine auxiliaire vient sur le puits choisi, sur lequel le fourreau amovible a été préalablement mis en place à l'aide du pont auxiliaire, verrouillé et connecté automatiquement.

Après connexion de la machine et ouverture des deux clapets, la machine auxiliaire extrait les bouchons et descend le bras de chargement. Elle est ensuite évacuée et remplacée par la machine principale. Celle-ci extrait les éléments irradiés à l'aide d'un grappin mécanique accroché à un câble enroulé sur un tambour entraîné électriquement, et les stocke dans les alvéoles d'un tambour fixe. Les éléments neufs sont introduits dans le réacteur par le même processus. Après remplissage, la machine est déconnectée de la pièce intermédiaire et mise en place sur le poste d'évacuation du combustible.

Description des machines (fig. 1)

La *machine principale* comprend : a) un chariot porteur automoteur; b) une carcasse principale cylindrique remplie de béton lourd à la baryte de densité 3,4 constituant la protection secondaire; c) un corps de machine disposé à l'intérieur de la protection secondaire, comportant : une carcasse avec protection primaire en béton lourd à la baryte, $d = 3,4$; un réservoir de machine comprenant 30 alvéoles de stockage de trois éléments combustibles et, dans le nez inférieur de machine, un clapet de fermeture; un ensemble treuil - potence avec grappin mécanique de prise des éléments combustibles. Le poids total et la hauteur sont de 440 t et 9,2 m.

La *machine auxiliaire* comprend : a) un chariot automoteur; b) une carcasse principale cylindrique remplie de béton lourd assurant la protection secon-

daire; c) un corps de machine disposé à l'intérieur de la protection secondaire, comprenant : une carcasse avec protection primaire en béton lourd; un réservoir et un nez de machine; un barillet de stockage des éléments avec ses mécanismes de commande; deux treuils de manœuvre et leurs mécanismes de commande; les accessoires. Le poids total et la hauteur sont de 370 t et 14,6 m.

La *machine de dépannage* ressemble à la machine principale. On peut lui adapter des matériels d'intervention. Son poids est de 185 t.

Le *bras de chargement* est télescopable et comporte un poteau de centrage. Ses caractéristiques principales sont les suivantes : diamètre intérieur minimal, 0,14 m; longueur totale, déplié, 12,2 m; longueur bras télescopé, 8,12 m; poids, 1 t.

Le *fourreau amovible* comprend essentiellement : a) un dispositif de raccordement sur les têtes de puits de chargement (accrochage à baïonnette); b) un dispositif de raccordement aux machines (vérin pneumatique d'accostage et tête d'accrochage à billes); c) un clapet d'obturation avec bouchon biologique; d) un dispositif de commande du bras de chargement (levage, inclinaison, orientation). Son poids est 2,8 t et sa hauteur totale de 4 m.

Ensemble EDF3

Généralités

L'ensemble EDF3 est d'une conception très différente de celle de l'ensemble EDF2. Toutes les fonctions sont remplies par une seule machine qui est de ce fait beaucoup plus grande et plus lourde. Pour les fonctions exceptionnelles, en particulier les dépannages, des appareillages spéciaux peuvent être ajoutés ou substitués. Deux machines identiques sont montées sur EDF3.

Déplacement

Le caisson du réacteur étant en béton précontraint, la dalle supérieure est capable de supporter des charges très élevées et les têtes de puits sont fixes, à la différence d'EDF2. Ces conditions ont conduit à adopter pour EDF3 le déplacement de la machine sur un réseau de rails fixés sur la dalle supérieure du caisson. À une des extrémités de la dalle réacteur, un transbordeur permet le transfert de la machine d'une paire de rails à une autre, ou sur les postes fixes d'évacuation et d'essai.

Protection

La protection est assurée par des caissons métalliques remplis de béton au fer de densité 5,4. La protection à la liaison puits - machine est assurée par une large jupe qui s'abaisse quand la machine arrive sur le puits, et qui couvre les puits adjacents. Cela nécessite qu'aucun des appareils à poste fixe sur la dalle du réacteur ne dépasse de celle-ci.

Principe de fonctionnement (fig. 2)

Il est évidemment analogue à celui d'EDF2, mais plus simple, la machine unique intégrant toutes les

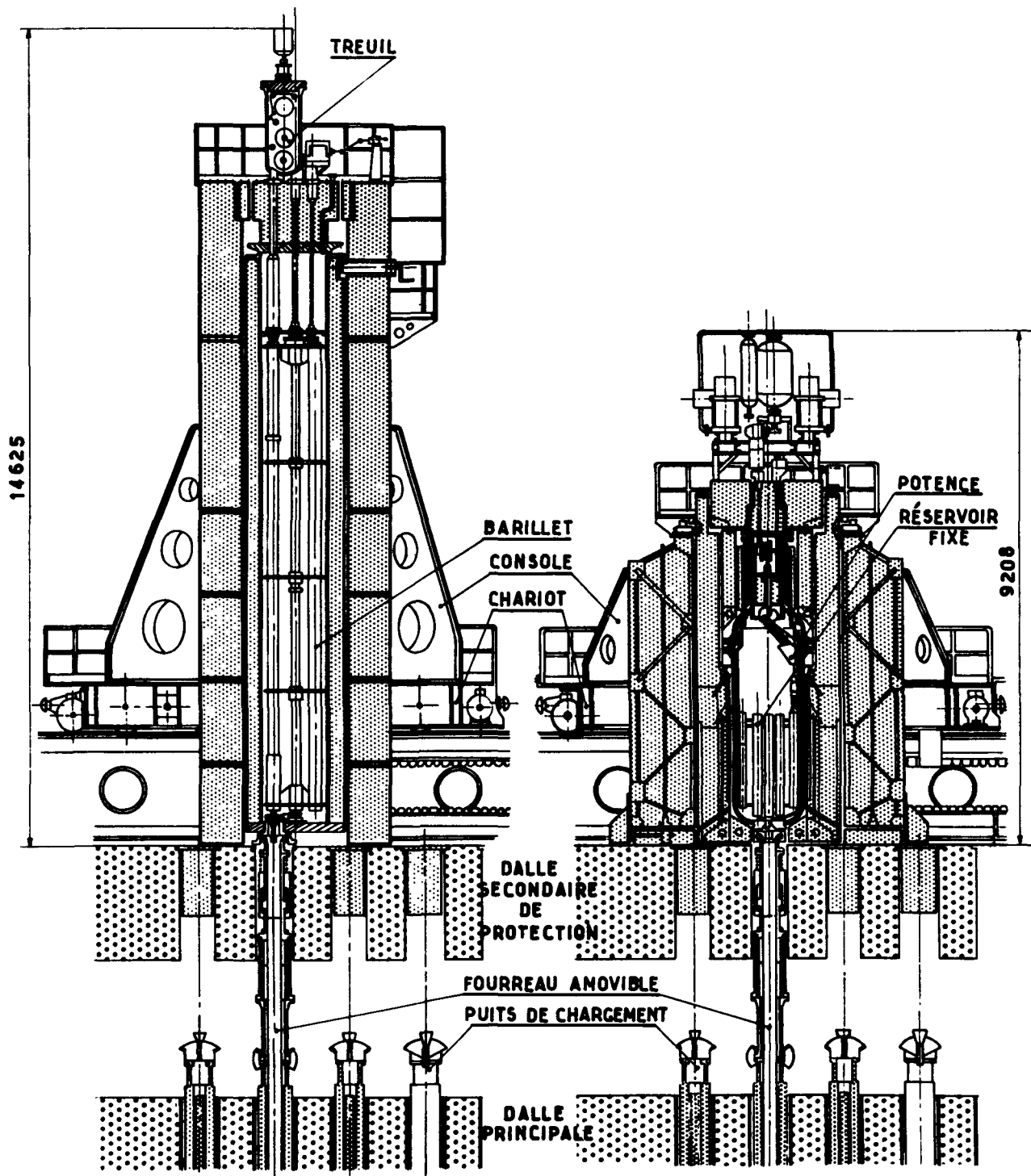
MACHINE AUXILIAIREMACHINE PRINCIPALE

Figure 1. Dispositif principal de manutention EDF2

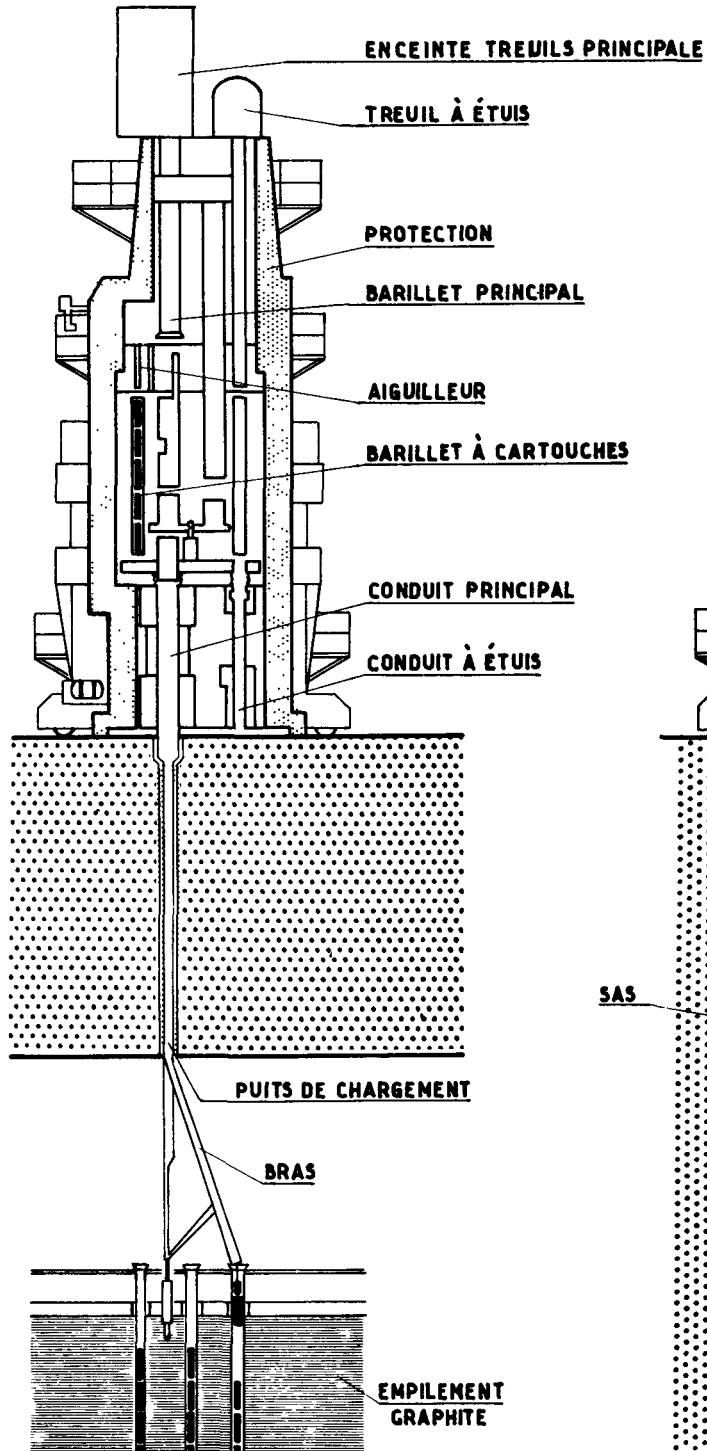
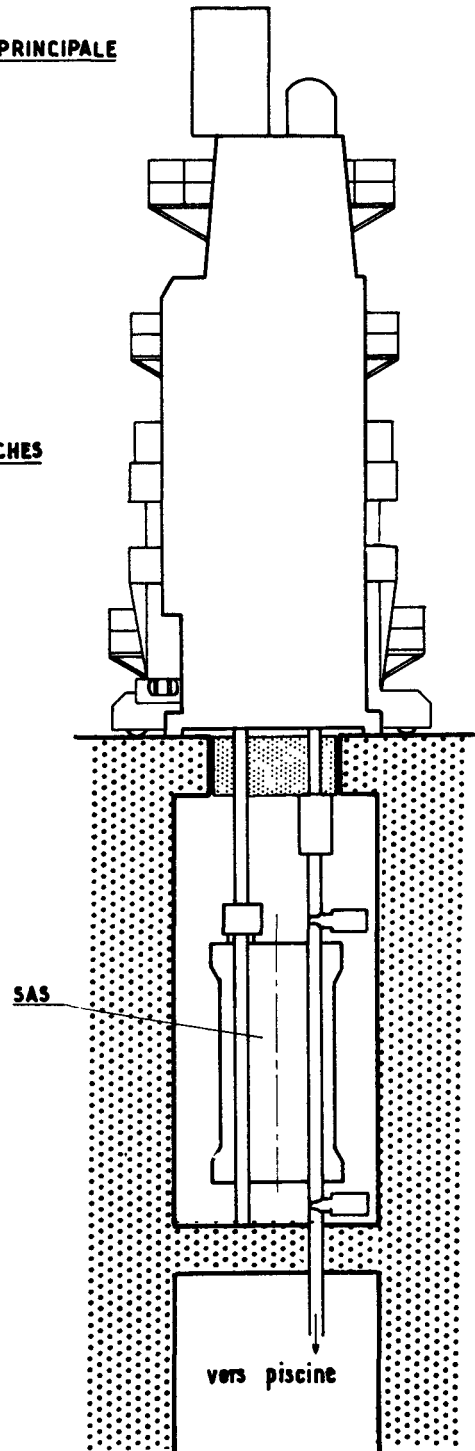
EXTRACTION HORS
DU RÉACTEURÉVACUATION A
LA PISCINE

Figure 2. Machine EDF3, schéma de fonctionnement

fonctions. La machine vient sur le puits, se branche dessus, le déverrouille, extrait les bouchons, descend le bras, le dirige sur le canal choisi, extrait les cartouches irradiées par un grappin fixé à un câble et entraîné par un treuil. Dans les alvéoles du barillet, les éléments sont stockés par 5 dans des étuis en acier qui sont évacués ensuite à la piscine, ce qui permet d'accélérer les opérations d'évacuation hors de la machine et le rechargement en éléments neufs.

Description (fig. 3)

Machine intégrée

La machine comporte quatre éléments juxtaposés, facilement séparables les uns des autres: la partie inférieure amovible; la partie principale; l'enceinte treuils principale; l'enceinte treuil à étuis. Le poids total est de 550 t, la hauteur de 16,5 m et la section hors tout de 6,2 × 6,2 m.

Partie inférieure amovible

Cet ensemble, fixé par boulons sous la partie principale, rétablit la continuité entre les organes de stockage logés dans cette partie principale et les divers postes de travail de la machine intégrée.

Il possède lui-même les organes et mécanismes nécessaires à l'obturation inférieure de la partie principale, ainsi qu'à la commande du bras de chargement.

La partie inférieure comporte essentiellement: a) un conduit principal constitué par: à sa partie supérieure, une vanne à opercule tournant et double étanchéité; à sa partie médiane, une enceinte étanche contenant les différents mécanismes de commande du bras de chargement; à sa partie inférieure, un joint à soufflets métalliques qui absorbe les écarts radiaux et axiaux et dont la bride inférieure, munie de joints, assure la liaison étanche avec les puits; b) un conduit à étuis, de constitution analogue au conduit principal à l'exclusion des mécanismes de commande du bras.

Partie principale

La partie principale est constituée essentiellement d'une enceinte métallique étanche timbrée à 36 bars, d'axe vertical, contenant deux barillet, et entourée d'une protection biologique.

L'enceinte étanche est composée de deux cylindres concentriques reliés par une partie tori-conique, les différentes parties étant assemblées par brides boulonnées. Sa partie inférieure comporte deux orifices venant se raccorder, l'un au dispositif d'accouplement sur les orifices d'évacuation, l'autre au dispositif d'accouplement sur puits réacteur de la partie inférieure amovible. Sa partie supérieure comporte également deux orifices, l'un permettant le raccordement soit sur l'enceinte treuils principale, soit sur l'enceinte de dépannage, l'autre le raccordement soit sur l'enceinte du treuil à étuis, soit sur le château de secours. Un conduit assure la continuité de passage entre l'orifice supérieur correspondant à l'enceinte du treuil à étuis et l'alvéole du barillet à cartouches situé dans l'axe de cet orifice.

L'enceinte étanche contient:

a) Un barillet principal, qui comporte six alvéoles

de diamètre différent, d'environ 10 m de hauteur, servant de magasin de stockage aux pièces suivantes: bras de chargement, bouchons, tubes guides, barre de contrôle, etc;

b) Un barillet extérieur, concentrique au précédent, qui comporte 24 alvéoles identiques d'environ 3 m de haut pour le stockage des éléments combustibles;

c) Un aiguilleur pour le transfert des cartouches entre barillet et canal; il peut recevoir un grappin à cartouches et lui faire occuper deux positions: dans l'axe du conduit de déchargement et dans l'axe de l'un des alvéoles du barillet à cartouches. L'une des poulies de renvoi du câble à cartouches est munie d'un dispositif de peson permettant la détection de sous-tension et de surtension du câble.

d) Un treuil à cartouches disposé dans une enceinte annexe reliée à l'enceinte principale par un conduit muni de soufflets et comportant une protection de plomb pour se protéger de l'activité du câble. Le tambour d'enroulement se translate horizontalement, afin de permettre le déroulement du câble suivant un axe fixe. Les vitesses de manœuvre du grappin sont de 1 m/s et 0,33 m/s.

Enceinte treuils principale

L'enceinte treuils principale est constituée essentiellement d'une enceinte métallique étanche, entourée d'une protection biologique, qui contient: à la partie supérieure, le treuil principal, capable de 2 t; à la partie inférieure, le treuil auxiliaire, capable de 200 kg.

Enceinte treuil à étuis

L'enceinte treuil à étuis est constituée essentiellement d'une enceinte métallique étanche contenant le treuil qui sert à la manutention des étuis par l'intermédiaire d'un grappin lors de l'évacuation des éléments combustibles à la piscine ou du chargement en éléments neufs.

SOLUTIONS ADOPTÉES

POUR LES PROBLÈMES CLÉS

Généralités

Après les descriptions succinctes précédentes, ce chapitre est consacré aux solutions qui ont été adoptées sur des points particulièrement importants du point de vue fonctionnement ou sécurité.

Le grappin

Le grappin à élément combustible est une des pièces maîtresses du dispositif principal de manutention. Il doit être d'un fonctionnement extrêmement sûr, la chute d'un élément en cours de manutention pouvant être extrêmement grave de conséquences. Il doit être très endurant; en une année un grappin effectuera environ 24 000 manœuvres. Les conditions de travail sont particulièrement dures: radiations, CO₂ à 25 bars et 20 m/s, température jusqu'à 410 °C. Enfin, la place laissée pour loger la mécanique est faible, car le grappin doit laisser passer tout le débit de gaz de refroidissement avec une perte de charge très faible.

A EDF2, le grappin est à commande mécanique. Le mouvement des trois griffes qui s'engagent dans la

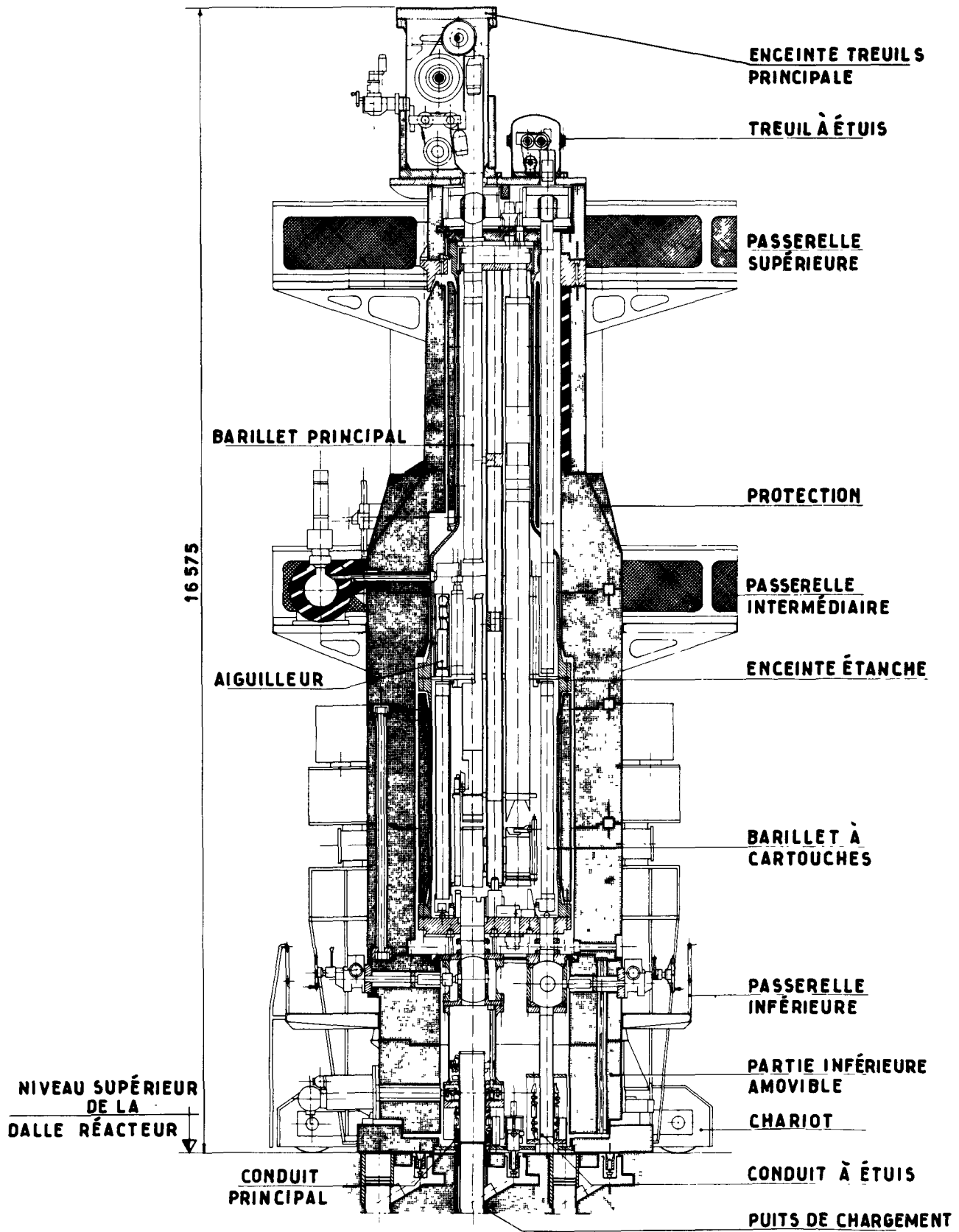


Figure 3. Dispositif principal de manutention EDF3

gorge d'accrochage de la chemise en graphite est commandé par le poids de la masselotte supérieure quant cette dernière est libérée par le contact avec l'élément. Une rampe hélicoïdale transmet un mouvement d'ouverture une fois sur trois, et de fermeture deux fois sur trois. Ainsi, on peut accepter un choc avec fonctionnement intempestif sans provoquer de chute de cartouche. L'ensemble est très ajouré et caréné de façon à laisser passer le gaz avec un minimum de perte de charge.

A EDF3, les développements effectués depuis EDF2 ont permis la mise au point d'un câble électrique porteur résistant à la température.

Le grappin est électrique et comprend essentiellement deux pinces fixées sur un corps par l'intermédiaire d'une lame élastique. Les pinces constituent les armatures mobiles du circuit magnétique d'un électro-aimant et sont constamment ramenées en position d'accrochage sur l'élément à manipuler par la lame élastique. Le manipulateur n'est en position de décrochage que quand l'électro-aimant est sous tension. Pour éviter tout décrochement intempestif, un deuxième électro-aimant, dit électro-aimant de verrouillage, interdit tout fonctionnement des pinces en dehors des lieux de pose ou de prise de l'élément manipulé.

Dans les deux cas, un dispositif sensible permet de déceler immédiatement un excès de tension de façon à arrêter immédiatement le mouvement de montée et à éviter la rupture du câble.

Le dispositif contre-envol

La forte perte de charge régnant entre le bas et le haut du réacteur provoque la lévitation des derniers éléments restant dans un canal au cours d'un déchargement en marche. Pour éviter leur envol, le trajet défini par le bras est relativement étanche.

A EDF2, un débit important de gaz est injecté dans le bras à partir de la machine. Ce débit de contre-envol, qui s'échappe par des événements ménagés dans le bas du bras, est réglé suivant le nombre de cartouches présentes dans le canal.

A EDF3, le bras est muni d'un clapet automatique qui maintient un débit constant en maintenant une perte de charge constante entre l'intérieur du bras et l'extérieur. Comme à EDF2, la mise en place du bras se traduit par une légère diminution du débit de gaz dans le canal et par une légère augmentation de la température de gaine.

Étanchéité

Le problème de l'étanchéité à la pression élevée du CO₂ est particulièrement important sur les grandes ouvertures que constituent les puits de chargement et à la liaison puits - machine.

A EDF2, tous les obturateurs de grand diamètre sont des clapets auto-claves à joint en élastomère. Leur manœuvre n'est physiquement possible que quand la pression est égalisée sur les deux faces. L'étanchéité entre machine et puits est assurée par des joints toriques.

A EDF3, la fermeture permanente du puits est assurée par un bouchon à double joint torique et verrouillage à billes. Un dispositif de sécurité basé sur la pression empêche l'ouverture intempestive du verrouillage. La liaison puits - machine est assurée par une bride raccordée à la machine par l'intermédiaire d'un soufflet de dilatation.

Refroidissement

Sur les postes de travail, le refroidissement des éléments combustibles est assuré par une circulation de CO₂. Quand la machine n'est pas raccordée, le refroidissement est assuré à l'intérieur de la machine par convection naturelle du CO₂.

A EDF2, des échangeurs CO₂ - eau et eau - air assurent l'évacuation de la chaleur.

A EDF3, les calories sont évacuées directement par une circulation forcée d'air dans l'espace compris entre l'enceinte étanche et la protection biologique.

Possibilité de dépannage

L'une des pannes les plus probables est un blocage du bras dans le réacteur. Il est toujours possible d'extraire le bras en cisailant par traction des goupilles de sécurité qui le ramènent à la position fermée. D'autre part, il est toujours possible de laisser le bras dans le réacteur et d'emmener la machine, le réacteur étant en pression.

A EDF2, la manœuvre est normale.

A EDF3, la partie inférieure, qui comporte une vanne sphérique, peut être laissée sur place.

Le maximum de possibilités a été ménagé tant à EDF2 qu'à EDF3 pour extraire des débris éventuels dans les canaux du réacteur ou la machine.

Commande et sécurité

Le dispositif de commande très automatisé a été étudié, tant à EDF2 qu'à EDF3, dans un esprit de très grande sécurité. D'une manière générale, tous les incidents du genre cisaillement ou arrachement sont interdits par des limiteurs d'effort. Au point de vue réalisation, les dispositifs sont assez différents.

A EDF2, l'automatisme se distingue à deux niveaux:

Ensemble fonctionnel

Chaque organe mécanique fait partie d'un ensemble fonctionnel comprenant tout le matériel électromécanique nécessaire au fonctionnement de l'ensemble considéré isolément. Il y a environ 80 ensembles fonctionnels dans l'ensemble EDF2, par exemple: positionnement du bras de chargement, treuil de machine de chargement, etc.

S'agissant en grande partie d'asservir en position un organe mécanique, il a été fait usage de servomécanismes analogiques comprenant: a) un dispositif de comparaison entre la position affichée provenant du programme de travail et la position réelle de l'organe mécanique; b) un amplificateur tournant commandé par un groupe Ward Leonard alimentant un moteur à courant continu d'entraînement de l'organe mécanique; c) des dispositifs annexes nécessaires à la stabilité et à la sécurité de fonctionnement du système

(génératrice tachymétrique, variomètre de détection de mou de câble, relayage d'asservissement entre ensembles fonctionnels, etc.).

Programme de travail

Les programmes de travail sont inscrits sur des bandes de papier perforées selon un système codé. Des programmeurs lisent les bandes perforées et distribuent successivement les ordres de manœuvres aux ensembles fonctionnels concernés avec indication de position.

A EDF3, nous avons:

Un ensemble électro-mécanique

Chaque organe mécanique est entraîné soit par un moteur asynchrone, soit par un vérin commandé par électro-aimant. Toutes les positions discrètes occupées par chaque organe sont matérialisées par des contacts électriques « fins de course ». Pour manœuvrer un organe mécanique, il suffit de fermer le contacteur électrique de commande de l'organe (moteur ou électro-aimant). La bobine du contacteur est montée en série avec le contact « fin de course », qui s'ouvre lorsque l'organe mécanique a atteint la position désirée.

Une télécommande centralisée

Un ensemble électronique semi-universel, s'apparentant aux calculateurs numériques industriels, assure la commande et le contrôle de l'ensemble des installations du dispositif principal de manutention.

Il comprend:

a) Une mémoire constituée par un tambour tournant sur lequel sont inscrits en permanence des cycles d'opérations. Chaque opération inscrite comprend: le code de l'opération à effectuer + 6 conditions de sécurité à vérifier pendant l'exécution de l'opération;

b) Les programmes de travail sont inscrits sous forme codée sur des bandes de papier perforées et comprennent la succession des cycles d'opérations à utiliser. A chaque cycle, le lecteur de bande fait avancer la bande perforée;

c) Une matrice de commande permet de manœuvrer les organes mécaniques comme indiqué ci-dessus (contacteur ou électro-aimant);

d) Une matrice d'analyse permet d'analyser en permanence les conditions de sécurité nécessaires à chaque opération et matérialisées par des contacts électriques;

e) Une machine à écrire permet de communiquer avec l'ensemble de l'automatisme (défauts, informations, etc.).

CONCLUSION

Seule, une longue expérience montrera la validité des solutions adoptées pour les nombreux problèmes que pose un dispositif de manutention de combustible dans le cas d'un réacteur uranium naturel - graphite - gaz. Une évolution vers la simplification de fonctionnement peut être observée entre EDF2 et EDF3.

Ces appareils nécessitent pour leur étude et leur réalisation des moyens très puissants, en particulier:

a) tous les composants sont soumis à des essais d'endurance très poussés;

b) l'ensemble est essayé dans les conditions réelles de température, d'écoulement gazeux et de pression avant d'être envoyé sur le site;

c) les études et les essais représentent environ 35% du coût.

En conclusion, on peut dire que les résultats des essais déjà effectués sur les diverses parties des deux ensembles semblent favorables, ce qui donne à penser que les dispositifs principaux de manutention EDF2 et EDF3 devraient donner satisfaction après la mise en service des centrales correspondantes.

REMERCIEMENTS

Nous tenons à remercier tout particulièrement les constructeurs français qui étudient et réalisent les dispositifs principaux de manutention pour le compte de l'Electricité de France, et qui sont:

Pour EDF2, la Société INDATOM;

Pour EDF3, la Société des forge set ateliers du Creusot (groupe Schneider) et le Groupement Atomique Alsacienne-Atlantique (GAAA).

ABSTRACT—RÉSUMÉ—АННОТАЦИЯ—RESUMEN

A/54 France

Fuel loading and unloading devices for the natural uranium-graphite-gas sequence reactors

By B. Saitcevsy and D. Gaussot

The refuelling system is one of the vital parts of a natural uranium-graphite-gas sequence nuclear power plant.

From the costs standpoint, it involves 8 to 10% of total capital expenditure, at the moment. From the technical standpoint, the question is complex, both as

regards the tasks the equipment must fulfil and the high safety requirements.

In the first section of the paper, the various fundamental aspects of operation and safety are reviewed, enabling principles universally applicable to be brought out.

The authors then go on to analyse factors governing the basic choice and conclude by emphasising the replacement of fuel on load and the value of actual operation so as to accumulate long operational experience.

They then give a brief description of the equipment for EDF2 and EDF3 and show how the above

principles have been applied to two solutions differing very widely technically:

At EDF2, several machines, each specialising in a given task; preparing the standpipes, auxiliary operations, charging and discharging of the fuel elements into and from the reactor, and maintenance;

At EDF3, a single machine carrying out all these tasks.

In both cases, the equipment is very heavy, owing to the very stringent safety standards adopted.

The results of initial pressure and temperature tests justify consideration that the equipment will give every satisfaction.

A/54 Франция

Машины для загрузки и разгрузки топлива уран-графитовых реакторов с газовым охлаждением

Б. Зайчевский, Д. Госсю

Установка для перегрузки топлива является одним из основных элементов атомной электростанции, использующей уран-графитовый реактор с газовым охлаждением.

С экономической точки зрения ее стоимость составляет 8—10% от общих капитальных затрат; с технической точки зрения она является сложной как по выполняемым функциям, так и по высокой степени безопасности, которая требуется при ее работе.

В первой части доклада рассматриваются основные аспекты работы и безопасности, которые позволяют установить принципы, применимые ко всем системам.

Затем авторы анализируют выбор основных принципов и описывают, какой интерес представляет работа установки для накопления опыта эксплуатации.

Авторы вкратце описывают оборудование реакторов EDF-2 и EDF-3 и показывают, как вышеприведенные принципы были применены к двум технически очень разным решениям:

— на реакторе EDF-2 несколько машин выполняют различные функции—подготовка труб и вспомогательные операции, извлечение тепловыделяющих элементов из реактора и загрузка их в реактор, ремонт;

— на реакторе EDF-3 одна машина выполняет все функции.

В обоих случаях машины очень тяжелы вследствие очень строгих мер защиты, которые были приняты.

Результаты первых испытаний под давлением и при температуре позволяют думать, что установки окажутся весьма удовлетворительными.

A/54 Francia

Máquinas de carga y descarga del combustible de los reactores de uranio natural – grafito – gas

por B. Saitcevsy y D. Gausso

El dispositivo principal de manejo del combustible constituye uno de los elementos esenciales de una central de los reactores de uranio natural – grafito – gas.

Desde el punto de vista económico, su coste representa, actualmente, de 8 al 10% de la inversión total. Desde el punto de vista técnico, el dispositivo es complejo, tanto por las funciones a realizar como por el alto grado de seguridad exigido.

En la primera parte se examinan los diversos aspectos fundamentales de funcionamiento y de seguridad que permiten deducir los principios aplicables a todos los sistemas.

Los autores analizan después los criterios de selección de las bases de partida y llegan a la conclusión de que presenta interés repostar el combustible cuando el reactor está en marcha en espera de disponer de una mayor experiencia de explotación.

Los autores describen brevemente, a continuación, los dispositivos de las centrales EDF2 y EDF3, y ponen de manifiesto cómo se han aplicado los principios precedentes a dos soluciones técnicamente muy diferentes:

a) En la central EDF2, varias máquinas especializadas por su función: preparación de los pozos y operaciones auxiliares, extracción e introducción de los elementos en el reactor, reparación de averías.

b) En la central EDF3 una sola máquina realiza todas las funciones.

En los dos casos las máquinas son muy pesadas, a causa de las muy severas normas de protección que se han adoptado.

Los resultados de los primeros ensayos efectuados a presión y temperatura permiten suponer que las máquinas funcionarán satisfactoriamente.

Experience with Bradwell and Latina on-load fuel handling equipment and its influence on future designs

By J. O. Joss,* W. H. Shipley,** G. H. Branch* and J. E. Taylor*

THE BRADWELL MACHINERY

Description

The original specification called for two universal refuelling machines per reactor, one operational and one standby, each capable of handling fuel elements, absorbers, neutron sources, support/gags, chutes and charge standpipe assemblies on load; graphite samples and control standpipe assemblies off-load. Storage capacity for 64 elements, one chute, two charge assemblies and one control assembly was specified together with a normal handling rate of 112 elements per week. The reactor condition in which on-load operations were to be conducted was CO₂ at 400 °C and 132 psig.

Each refuelling machine (Fig. 1) consists of a shielded vertical pressure vessel containing a rotatable turret, a service hoist and two element hoists at the upper end, a shield plug positioned between the turret and the hoists, and a shielding/sealing valve at the lower end. All three hoists are aligned with a bottom outlet in the vessel which can be closed with the valve. The service hoist handles standpipe components, while the element hoists are used for all in-pile components. Each turret storage tube can be aligned over the machine outlet [1-5].

Each charge standpipe has a flap-valve at its top end and normally contains a shield-pipe assembly. The top element in the channel below the standpipe is used for temperature measurement and can be retracted into the assembly tube. A telescopic chute headbox forms the pressure connection between the machine and a standpipe and contains the drives to rotate and radius a charge chute (Fig 2) which sits on the top of the core and guides an element grab to reach 37 channels from one standpipe [4].

Development of the design for Bradwell

Prior to and during manufacture a number of changes were made to the design, the more important of which are given below:

(a) Redesign of turret facilities to put all storage tubes into a simple circular section turret, with fixed instead of swivelling hoist units. Later, three of the

fuel storage tubes were modified for preheating new fuel elements. The introduction of sleeved fuel channels caused the capacity to be modified to four channels of fuel and four channels of sleeves. Elimination of channel sleeving resulted in a total element storage capacity of 66, 18 of which were stored in a magazine latched into the control assembly storage tube (Fig. 1) [4].

(b) Addition of the auxiliary element hoist, originally intended for sleeve handling but retained when sleeves were discarded (Fig. 1).

(c) Due to uncertainty regarding the reliability of an electric cable for element hoist duty, the original electrically operated grab was redesigned for automatic gravity operation. An electric solenoid lock was retained which unlocked on the application of current, manually initiated within certain defined zones. Continued uncertainty over the cable led to the addition of a form of mechanical lock which required the grab to be landed twice to release the component from its jaws, and at the same time the electric lock was changed to unlock when de-energised. Mineral insulated and glass fibre insulated single-core cables were tested but had an inadequate life before failure. Finally, a ceramic-bead insulated plough steel conductor in a hollow stranded steel-wire cable was developed which gave a satisfactory life on test.

(d) Extension of the versatility of the charge machine to deal with a great many additional components due to changes in reactor design requirements, such as steel specimens, axial string and other special support struts and special handling tools and chutes.

(e) The addition of stabilising arms to the lifting head of the fuel elements required guide fins or petals to be added to the fuel element grabs (Fig. 3) to orient these so that the hooks would not foul the stabilising arms and prevent pick-up [4]. It was also necessary to modify the grab mechanism so as to prevent hook closure except when the grab was correctly landed on the element lifting head.

(f) The charge machines were each erected on rails and functionally tested at ambient and hot conditions before dismantling and despatch to site. No standpipe components could be handled at this stage because of height and space limitations. Chutes and grabs were first of all tested cold, and then at

* The Nuclear Power Group, Knutsford, Cheshire.

** Messrs. Strachan & Henshaw Ltd, Bristol.

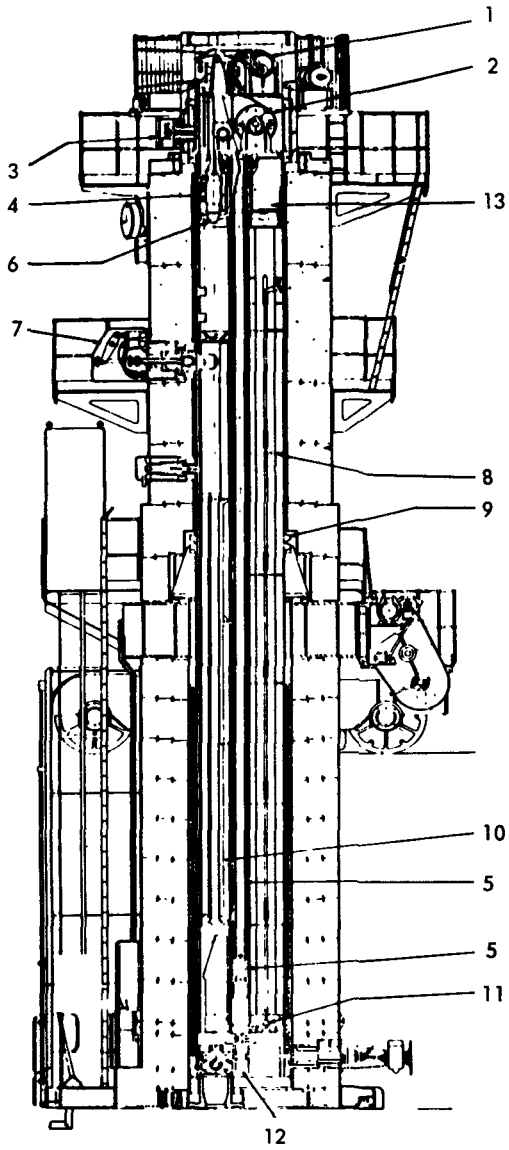


Figure 1. Bradwell charge machine

1: Auxiliary hoist; 2: Element hoist; 3: Weighting device; 4: Element grab; 5: Service hoist chain, etc.; 6: Service grab; 7: Element deflector; 8: Turret; 9: Pressure vessel; 10: Turret magazine; 11: Latches; 12: Machine valve; 13: Shield plug

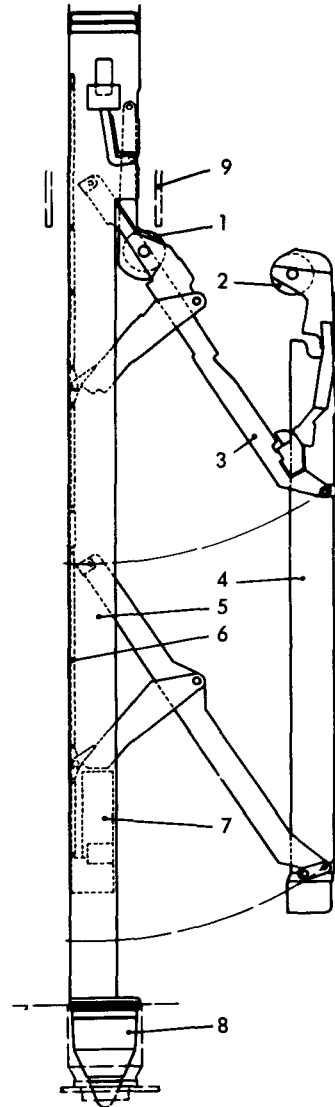


Figure 2. Bradwell charge chute

1: Upper pulley; 2: Lower pulley; 3: Radiusing link; 4: Radiusing tube; 5: Main support tube; 6: Radius drive rod; 7: Counterweight; 8: Nose cone; 9: Standpipe nozzle



Figure 3. Bradwell fuel grab

full reactor temperature (400 °C). In the case of chutes the hot testing was for convenience carried out by loading the chute into a test rig and then heating up to temperature.

Commissioning at Bradwell

The early tests over the test well and the reactor produced only minor troubles, mainly in optimising and maintaining the settings on limit switches and interlocks. Six channels of fuel were loaded and unloaded from the reactor, as well as absorbers and specimen containers at 20% mass flow and about 70 °C gas temperature.

The second phase of testing was carried out before fuel loading, at 100% mass flow and 230 °C. The main difficulty was due to apparent obstructions in the bore of the charge chute, preventing free passage of the fuel grab. This was due either to the retractable pulleys not opening out correctly or to the radiusing tube not closing completely (Fig. 2). The pulley mechanism was modified, improved grab guidance provided, the radiusing link geometry and material changed to eliminate thermal effects, and a dead weight added to make closure more positive. After these modifications 22 channels of fuel were handled without trouble.

Following the physics phase, a 7-day test was carried out at 230 °C and full blower speed with the fully loaded core. A great many minor interruptions occurred during this test, broadly classifiable as electrical component faults, spurious loss of grab tension, erratic grab behaviour and intermittent grab cable short circuits. One serious fault was that the 3.8 in diameter grab fins gave insufficient protection to the stabilising arms on the fuel element heads, and these on occasion jammed in turret tube construction joints. The grab fins were increased to 4.1 in diameter and the turrets stripped and rectified, and no further difficulty arose. The other major fault was damage to a fuel element during closing of the chute due to inaccurate positioning in the open state. The level for chute closure was re-assessed and fine limit switches added to cure this defect.

Although the programmed tests were complete, further plant testing at 230 °C allowed further charge machinery work to take place. Before these extra tests the charge machine hoist gears were lubricated, the grab cables replaced by a non-spin type with improved central conductor, and the split and spring-loaded hoist barrels made solid. The split construction was to allow for cable contraction during cooling, but was found to lead to errors in depth measurement. During these tests more trouble was experienced in passing the grab through the chute pulley region, and it was decided to completely modify the chutes to overcome this. On one occasion also the grab cable became trapped in the chute and fairings were added to contain the cable and eliminate narrow gaps.

While reactor commissioning was being completed and during start-up the chutes were modified to overcome the pulley operation defect. An inner tube was

added, forming the bore in the upper end, linking the lifting head to the pulley mechanism. A more rigorous test was applied, similar to the entry and use cycle in the reactor. The revised pulley mechanism worked perfectly but it was discovered that the chute bowed due to differential heating rates where the metal section was circumferentially non-uniform. A heavy counter-weight used to balance the cut-outs at the lower end was mainly responsible and was removed. There was also transient differential expansion between the longitudinal radius operating rods, which caused the radius tube to open sufficiently to obstruct the grab passage. In its original form the time to open and reclose fully was 60 min at 400 °C. Removal of operating rod protection tubes and improved gas circulation to the chute internals halved the amount of self-radiusing and reduced the time to full reclosure to just under 30 min. A 30 min soak period was introduced into the operational sequence of the refuelling machinery and no further cases of grab fouling have been reported.

Early Bradwell operational experience

Since no chutes were available in a form suitable for on-load use, both reactors were started with fuel and absorber handling restricted to a maximum temperature of 150 °C with the reactor off-load. Following the pressure steps to detect faulty fuel elements a total of 20 channels of fuel was discharged and reloaded in the two reactors. In addition to this, 8 channels of fuel were discharged and prepared for loading absorbers, and 5 channels of absorbers changed.

When the first fully modified chute became available it was initially tested over the reactor by handling absorbers at shutdown. Following this, two channels of absorbers were removed and replaced at maximum power and temperature (about 400 MW(th) and 350 °C gas temperature). While handling the second of these channels the electric lock became defective and the work was completed relying on the mechanical lock alone. Shortly after this trial, a full programme of absorber changing at power was begun to keep pace with the core reactivity build-up. Throughout this programme, the electric grab lock gave continuous trouble, which was finally rectified by the production of a cable inner conductor with improved insulation and by improving the mechanical details and insulation of the grab solenoid and end connections.

When a second chute of the final version became available, absorber handling began on the second reactor. By the end of February 1963, a total of 55 absorber channels has been changed on load on the two reactors.

Full operational use of the Bradwell machinery

The Generating Board, as owners and operators of the power station, felt justified, taking account of the off- and on-load performance of the machinery, in proceeding with on-load handling of fuel. A programme was laid out specifying stages of increasing severity

in the approach to full permissible reactor conditions. The stages corresponded to blower speeds of 20%, 60% and maximum; progression within each stage from lower rated to higher rated channels, and from restricted fuel element temperature to the maximum allowable by the station operating rules during fuel handling at the relevant power level. A handling run of 43 fuel channels was specified with an additional requirement that failure of the electric lock on the fuel grab must result in suspension of operations. This programme involved handling either 3 or 4 channels of fuel at each standpipe. By the end of the 60% load stage the fuel grab in use was showing signs of erratic behaviour by a growing failure to pick up elements at the first attempt. This grab was therefore replaced by another for stage 3 (full load).

Because of the success of this full load trial, routine refuelling continued for a further 25 channels, when a failure of the replacement grab occurred, resulting in the spurious release of a new fuel element into the loading magazine. Operations were at once suspended, since it was evident that onset of mechanical failure of a grab could not be deduced from the information available to the operator. The locking solenoid could be energised at any time but could only be effective when the hooks were closed. Proof of current flow was therefore not adequate indication of closed hooks. While the grab was being developed to improve its safety, absorber continued on both reactors and by the time refuelling recommenced, a total of 75 further channels of absorbers had been changed on the two reactors.

This early experience gave a great deal of encouragement as, apart from the grab failures, the remainder of the plant worked well. The time taken to change 3 channels of fuel from a standpipe was however considerably longer than indicated by earlier design

calculations, as shown in Table 1. Several modifications have adversely affected the original time cycles, such as reduction of grab speed by 40%, introduction of the grab "double bounce" mechanism and the chute soaking period. In the design cycle it was also assumed that, in Table 1, operation 1 could be carried out concurrently with operation 7, and operation 5 with operation 10. In practice, it is considered that the time of $20\frac{1}{4}$ hours may be reduced by about 5 hours.

The element grab load indicator was closely examined throughout the fuel handling trials, to try to detect inter-element adhesion. No cases of this were in fact found. The load indication is by measurement of cable tension just below the winding drum at the top of the charge machine, compensated for the weight of cable paid out. Despite the effects of chute pulley friction, channel wall friction and upthrust due to gas flow, it was obvious that the weight indicated at point of pick up in the channel was predictable within small limits and varied as expected according to which element was being picked up and the gas flow in the channel.

Further study of the grab and the requirement for better indication showed that direct indication of hook position was not feasible. Since the electric lock could only function with the hooks fully closed, it was decided to use positive indication that the grab was locked as the required indication. The single-core cable was a limitation, as any signals indicating position had to share this core with the operating current. This problem was solved by fitting a high-temperature micro-switch to the locking plunger, arranged to switch a resistor in series with the solenoid coil when the lock operated correctly, and detecting the reduction in current. The availability of modified grabs incorporating this feature enabled on-load refuelling to be resumed. It was appreciated that this modification had only improved indication and safety, not reliability.

Refuelling was resumed on both reactors and continued subject only to the availability of grabs. By the end of 1963, an additional 100 channels had been changed using 6 grabs, 4 of which had failed mechanically. In each case the symptoms of failure were clearly obvious and operations safely suspended. The problem of grab reliability is still under investigation by testing in gas similar to that in the reactor, and by testing the effects of detailed changes introduced singly into the mechanism. The advantages to be gained by changes in protective surface treatments are also being studied and it is expected that application of the results of one or more of these lines of attack will produce a grab of adequate life.

In the meantime, refuelling continues on-load with no significant impediment, other than periodic grab replacement. It is worth recording that the chutes now in use on each reactor are the same ones used since the very beginning of on-load operation and that no difficulties whatever have occurred with them during this period.

Table 1. Bradwell: charge machine operating cycle times

Operation	Actual time	Design time
	Hours	
1. Inspect 3 channels of fuel and load magazine	$1\frac{1}{2}$	—
2. Load 3 channels of fuel into machine	2	1
3. Travel machine to gas supply and connect	$\frac{1}{2}$	$\frac{1}{4}$
4. Pressurise machine	$\frac{3}{4}$	
5. Re-instate previous standpipe and prepare new one	3	—
6. Connect machine to standpipe	$\frac{1}{2}$	$\frac{1}{2}$
7. Discharge and reload 3 channels	8	$3\frac{3}{4}$
8. Disconnect machine and travel to vent point	$\frac{1}{2}$	$\frac{1}{4}$
9. Depressurise machine	$\frac{1}{2}$	2
10. Connect to discharge hole and unload 3 channels	2)	
11. Travel to vent point and purge machine	$\frac{1}{2}$	—
12. Travel to loading point and connect	$\frac{1}{2}$	$\frac{1}{4}$
Total times	$20\frac{1}{4}$	8

THE LATINA MACHINERY AS A DEVELOPMENT OF BRADWELL

While basically similar to the Bradwell machinery, that at Latina naturally contains many improvements and simplifications. The significant changes are: (a) only one element type hoist which serves both fuel channels and absorbers; (b) the turret is much simpler and more rugged; (c) replacement of Bradwell flap valves by self-locking couplings operated by headbox pressure differential. In addition, more comprehensive testing at works was instituted.

The combined result of improved and more rugged design, of the use of proved designs of chute and grab cable (for example) and past commissioning experience made it possible to curtail site testing and commissioning without introducing uncertainty in finding potential faults. The programme included the same unit tests, cold and hot reactor tests as for Bradwell, but interchangeability of tests between cold and hot phases, reduction of number of handling cycles and other artifices were practised as necessary to maintain the decreed time scale.

In fact, little trouble was experienced, except for one case of failure of the insulation of a grab solenoid coil. A few modifications were included during or after commissioning either as a result of commissioning or later Bradwell experience. These included adding the mechanical double setting down lock to the grab, and re-design of the locking solenoid as a replaceable encapsulated unit, as measures to increase grab safety and reliability.

On-load working at Latina

Soon after the reactor was raised to power, a short demonstration programme was initiated. This consisted of handling two channels of absorber and one of fuel at 20% power and also at 50% power followed by one channel of each type at 70% power. These were all completed without incident.

Following the trial programme absorber cycling was begun at loads corresponding to blower speeds in the range 1 500–2 000 rpm (full design load was ultimately attained at 2 150 rpm). Up to the end of 1963 about 35 channels of absorbers had been handled with only a few minor stoppages. Four fast bursts were also discharged at reduced load and gas temperature, with, in one case, an initial delay owing to the automatic mechanical mechanism of the grab getting out of step and having to be reset, a condition which had been observed on occasion at Bradwell.

The Latina performance, while based on less extensive operations than Bradwell, has been generally extremely satisfactory.

THE DUNGNESS AND OLDBURY MACHINERY

In the same way that Latina developed from Bradwell, so Dungeness followed logically from Latina. There has been a continuous tendency towards simple

and rugged construction, towards reliability rather than elegance in control systems, and use of the maximum number of proved features from earlier designs.

The element grab cable, turret drive, service grab and bottom isolating valve are among the features thus carried forward.

The Dungeness machine turrets are further improved by eliminating as many construction joints as possible. The fuel element hoist is in a separate pressure vessel which may be removed from the main section of the machine while the latter is pressurised, and all shielding is integral with the machine, whereas both Bradwell and Latina use separate shielding rings below the machine. The chute is completely new, eliminating the features found to cause trouble at Bradwell and Latina. Mainly, the retractable pulley on the radiusing tube has been replaced by a fixed pulley, and the radiusing drive from the top of the chute is by rotating tube rather than by pull rods. The chutes have also been made from mild steel in place of the stainless steel of the earlier chutes.

The fuel element grab is a new design both mechanically and electrically, and in particular provides indication both of "hooks open" and "hooks closed". Since automatic control forms part of the element hoist system, petals have been eliminated and a more sophisticated hook system introduced to reduce the probability of failure to pick up. Such failures, due to a grab petal landing directly on a fuel spider arm, have been observed at Bradwell.

Works testing and the quality of rig simulation has been much improved in an effort to eliminate a higher proportion of faults. For example the series of tests on the standpipe shield plug assemblies included simulated lowering into the reactor as well as long time/temperature tests. These showed the need for modifications to reduce thermally-induced bending as well as to overcome mechanical defects.

The Oldbury equipment is almost identical to that for Dungeness and will closely follow it into production. The only differences are, increased height of the charge machine to cater for the longer chutes and other assemblies, and better mechanical arrangement of the charge-chute allowed by the greater headroom in the flat-roofed cylindrical concrete pressure vessel. Otherwise replication is kept absolute.

LESSONS FOR THE FUTURE

The experience gained in the use of the machinery at Bradwell and Latina has made obvious certain requirements which must be met by successful on-load refuelling machines and associated plant.

Refuelling machine. The main objects must be simplicity, ruggedness and reliability. Separation of main components into detachable or removable units as an aid to availability and ease of maintenance should only be done without reducing the three main objects. Space saved at the expense of simple mechanical design or accessibility is expensively bought.

Of the stoppages at Bradwell and Latina, a fair proportion have been due to faults occurring on electrical components—limit switches, relays, contactors and so on. Massive rather than elegant devices give by far the best service. Limit switches and position indicating devices should avoid the use of long gear trains with resulting back-lash and errors in setting. Settings of such devices should be easily made and include locking devices which make spurious changes impossible. Where extremely fine limits are unavoidable, these are best obtained by a combination of coarse and fine switches.

Chute. The chute must be designed to minimise bending and spurious operation due to transient differential temperatures on entry into the reactor. The former demands circumferentially uniform metal section which is difficult to obtain over the entire length. The bearings used in high temperature sections should be simple, the best solutions found so far being nitrided bushes with generous radial clearances. Robustness is essential, and for this reason thick mild steel sections are to be preferred to thinner ones of stainless or other alloy steel. Rigorous testing under closely simulated reactor conditions is essential to guarantee performance in operation.

Element grabs. In this case the requirements are equally obvious, but less easily attainable. Simplicity is the transcendent objective, with as robust a construction as the space will allow. A positive operating force is necessary, as little affected as possible by friction, shock and aerodynamic effects. The mechanism must not be susceptible to spurious operation due to gas loads when being lowered into a fuel channel. The grab cannot be lubricated, so that the number of relatively moving parts can vitally affect performance. Surface treatment of these parts is still a problem, and whether or not a working life of, say, two or three hundred channels can ever be attained before deterioration of surfaces, and high friction, scuffing or adhesion occurs, is debatable. It may be that a simple but inexpensive grab with a predictable though short minimum life may be the answer, as this would put grab changing on a routine basis, before trouble arises, at a known cost per channel.

Clearances must be generous, as the fuel grab undergoes massive changes in working ambient temperature, and the resulting differential temperatures can be very large. Allowance must be made for temperature gradients in both senses from outer case to internal components. Allowance should be included for gamma heating in the internals while the grab is in the core. This may result in temperatures of up to 50 °C in excess of external gas temperatures.

Indication of the safety of the grab state can now be regarded as essential. As a minimum requirement, proof that the hooks are fully closed when lifting an element is acceptable, proof of correct locking of the mechanism an added safeguard. The indication system should never presuppose the successful development of a new type of cable.

Grab cable. This should be of minimum diameter to minimise winding drum radius, and allow the use of small radius bends in the chute. This requirement conflicts with the necessity for good insulation, both mechanically and electrically, and where required, the incorporation of a gas hose. The resulting compromise affects the entire fuel handling system, and must be carefully chosen. For reliability and good performance the cable should resist forces tending to make it spin or twist. The authors' experience so far has indicated that ceramic insulation is preferable to the mineral or glass type, and that multi-core cables are inferior to the single-core type. Tests on less than full length cables may give misleading results, though such tests can be useful preliminaries. Correct geometry of cable path is essential in the test rig, as is the use of the actual terminal arrangements.

Testing. There is no substitute for comprehensive proof testing of prototypes and in some cases first production units. Inadequate simulation of reactor conditions in testing new devices can give entirely misleading results. Generally test rigs should use the correct coolant medium, moisture content, gas pressure, temperature, flow, geometry and time cycles. Omission of any one or more of these should only be allowed after a careful assessment of the effects on the test. Cross-flow is the most difficult effect of all to simulate in a test rig, and experience so far is that its omission does not lead to later difficulty.

CONTROL BY COMPUTER

The fuel handling equipment for Bradwell and Latina is manually controlled. Experience has shown that, under operational conditions, the effort required by an operator to control the equipment at optimum efficiency is considerably increased as the shift progresses. This is particularly true when on-load fuel handling is taking place over the reactor, and is reflected in the increase in time taken to carry out any operation. Since absolute security of control is necessary, the possibility of an error due to operator fatigue has led to the consideration of other forms of control. It was considered that a digital computer would fulfil the control requirements of the fuel handling system at Bradwell, and a design study was carried out to assess its feasibility.

The study showed that a computer could be used to meet the requirements of a Bradwell or similar system particularly as the control is additive to the existing plant, and that modifications to plant can be carried out in a very short period.

Prior to exercising its control function, the computer generates the handling procedure from a very limited amount of information fed in by the operator. This requires an instruction stating the type and number of components to be moved, their location and destination. During the compilation of the handling procedure, which involves the identification of any additional unspecified components to be handled, as

well as the organisation of the operations involved, a large range of compatibility checks will ensure that only permissible operations can be performed and only then, if the required components are held in their correct positions, the machine is positioned at its correct location, and a range of associated checks are satisfied.

Having determined the handling procedure which may cater for the changing of up to three channels of fuel at a reactor standpipe, it may be performed in the required sequence without operator intervention. This ability of the computer to generate its own handling procedures and detect any error that it may make, using parity checks and self checking routines, replaces the limited concentration of the human operator and removes from him the responsibility of deciding on optimum procedures, storage positions in the charge machine and similar problems. It follows from this that the charge machine can be operated very closely to its maximum design speed for a period dependent only on mechanical and electrical reliability which is normally far from possible using manual control. During the operation of the charge machine, the position of all its actuators is monitored many times a second, and any unscheduled movement causes the operation to be arrested and the operator informed. The performance of the charge machine can also be followed, as the present indication is supplemented by a descriptive print-out and a numerical display.

In addition to carrying all the information necessary to organise the fuel handling procedures, the storage facilities of the computer are used to hold the contents of all the storage tubes both round the reactor and in the charge machine. Reactor contents storage is

limited to that required to decide on the correct handling procedures, as all other information is held in the existing fuel accountancy system. The scope of the scheme embraces all charge machine movements for all types of component involved, with the exception of machine travel, although its "grid" position is monitored for checking purposes.

The use of a computer in a control system of this type, as opposed to simple logic or relay sequence control, ensures that there is almost unlimited flexibility in its application.

ACKNOWLEDGEMENTS

The authors are indebted to the Directors of Strachan & Henshaw Ltd and of The Nuclear Power Group for permission to present this paper. They also wish to thank the Central Electricity Generating Board and SIMEA for the use of information pertaining to operations at Bradwell and Latina respectively.

REFERENCES

1. Bradwell Nuclear Power Station, *Electrical Review, Refuelling Equipment*, 171, p. 7, London (1962).
2. *Fuel Handling at Bradwell*, Nuclear Engineering, Vol. 5, No. 55, 563 (1960).
3. Vaughan, R. D., and Anderson, E., *The Bradwell Power Station*, Proceedings of the Second International Conference of the Peaceful Uses of Atomic Energy, P/263, Vol. 8, p. 450, United Nations (1958).
4. Vaughan, R. D., *Bradwell Nuclear Power Station*, I. Mech. E. Symposium on Berkeley and Bradwell Nuclear Power Stations, Paper No. 1, London (1963).
5. Wordsworth, A. D., *Nuclear Fuel Handling*, Butterworths, 20, 163, London (1963).

ABSTRACT—RÉSUMÉ—АННОТАЦИЯ—RESUMEN

A/139 Royaume-Uni

Expérience acquise avec l'appareillage de chargement de combustible pendant le fonctionnement du réacteur à Bradwell et à Latina, et son influence sur les conceptions ultérieures

par J. O. Joss *et al.*

On donne une description générale des principales caractéristiques de l'appareillage de chargement de Bradwell et de l'installation auxiliaire, surtout des caractéristiques qui ont demandé une mise au point poussée ou des modifications au cours des périodes d'étude, de construction et de mise en service avant de devenir d'un fonctionnement sûr.

La conception originale de la machine de Bradwell

présentait des caractéristiques qui, on le savait, devaient faire l'objet d'essais et de mises au point sur prototype. En outre, il a fallu apporter des modifications par suite de changements faits dans d'autres organes du réacteur. Ces deux séries de facteurs ont profondément influencé la forme définitive de certains composants.

Le programme d'essai de l'installation de manutention de combustible faisait partie intégrante de l'ensemble des essais des mise en service du réacteur avec phases d'essais à froid et à chaud, et d'essais d'endurance, chaque phase étant conçue pour mettre à l'épreuve différents aspects de la construction en général et en détail. Les défauts relevés ont été, pour la plupart, corrigés sur place, mais certains ont exigé des mises au point supplémentaires. En raison de certaines limitations constatées à la mise en service, la machine de Bradwell a été au début utilisée avec le réacteur à l'arrêt, ou à puissance et à température

réduites. Dans ces conditions, la manutention des absorbeurs et des canaux de combustible s'est effectuée sans difficulté et on a acquis une expérience considérable dans l'utilisation de la machine.

Lorsqu'on a pu disposer de canaux de chargement améliorés, on a commencé la manutention des absorbeurs à pleine puissance.

Après une certaine période de manutention des absorbeurs, il a été décidé d'effectuer un essai contrôlé de manutention du combustible à pleine puissance du réacteur. Le Central Electricity Generating Board a établi un programme pour le renouvellement du combustible à 20% de la puissance, puis à 60%, enfin à pleine puissance, programme qui a été exécuté sans incident. Des difficultés relatives aux accrocheurs des éléments combustibles ont fait suspendre le renouvellement du combustible jusqu'à la mise au point ultérieure des accrocheurs. Entre-temps, on a continué la manutention des absorbeurs; un incident s'est produit lorsqu'une partie d'un bouchon écran s'est brisée; à la suite de cet incident, tous les bouchons ont été modifiés.

Lorsque des accrocheurs améliorés devinrent disponibles, on a pu reprendre le rechargement à pleine puissance. Des difficultés mécaniques ont persisté, mais un système d'alerte amélioré a empêché qu'elles ne provoquent des incidents graves. On a poursuivi le renouvellement continu du combustible ainsi que le perfectionnement des accrocheurs.

Bien qu'étant les mêmes quant au principe, les machines de chargement de Latina ont bénéficié pleinement de l'expérience acquise pour Bradwell aux stades de l'étude, de la mise au point, des essais et de la mise en service. De ce fait, il a fallu beaucoup moins de temps pour la mise en service de l'équipement sur les lieux.

Jusqu'ici, il n'y a guère eu de manutention des éléments de combustible pendant le fonctionnement du réacteur, mais un nombre considérable de canaux d'absorbants ont été remplacés sans incident.

Suivant une évolution continue, les installations à peu près identiques de Dungeness et d'Oldbury sont basées sur celle de Latina, mais avec des caractéristiques visant à éliminer les inconvénients qui sont devenus apparents au cours du fonctionnement des machines antérieures. On a fait une utilisation bien plus grande des appareils d'essai donnant une simulation améliorée des conditions dans le réacteur, pour les essais des composants et des machines complètes, à la fois sur prototype et dans leur forme définitive.

Le mémoire expose les exigences principales auxquelles doit répondre une bonne conception des machines de manutention du combustible. Ces exigences n'étaient pas toutes évidentes lors de l'étude des réacteurs de Bradwell et de Latina. Une grande partie de ces connaissances s'applique aux réacteurs avancés à réfrigérant gazeux (AGR) ainsi qu'aux réacteurs à Magnox.

Outre les caractéristiques mécaniques, les améliorations apportées aux systèmes de commande peuvent

beaucoup accroître la sécurité, la rapidité et la commodité de l'exploitation. L'application d'un calculateur numérique au système de renouvellement de combustible du type Bradwell est décrite et discutée.

A/139 Соединенное Королевство

Опыт эксплуатации оборудования по загрузке ядерного топлива при работе реактора на полной мощности в Брадуэлле и Латине и его влияние на разработку загрузочного оборудования для последующих реакторов

Дж. О. Джосс *et al.*

Дается общее описание главных конструктивных особенностей загрузочной машины и вспомогательного оборудования, особенно тех деталей, которые потребовали интенсивной разработки или модификации в период проектирования, строительства и пуско-наладочных работ до того, как они стали надежными.

Первоначальная конструкция загрузочной машины в Брадуэлле имела такие конструктивные особенности, которые, как было решено, необходимо проверить путем разработки и испытания прототипа. Кроме того, требовалось внести некоторые изменения в машину в связи с изменениями других узлов реакторной установки. Эти два обстоятельства сильно повлияли на окончательную разработку некоторых узлов загрузочной машины.

Программа испытаний машины для загрузки ядерного топлива являлась неотъемлемой частью общих пуско-наладочных работ реактора в холодный и горячий периоды и в период испытания на выносливость, причем каждый из этих периодов предусматривает опробование как отдельных узлов, так и конструкции в целом. Обнаруженные при этом дефекты устраняются в основном на месте, однако некоторые из них требовали дальнейшего исследования.

Из-за некоторых ограничений, обнаруженных во время пуско-наладочных работ, загрузочное оборудование использовалось вначале при работе реактора на неполной мощности и при заниженных рабочих температурах. В этих условиях перегрузка поглотителей и топливных каналов осуществлялась без помех и был накоплен значительный опыт использования загрузочного оборудования.

После разработки усовершенствованных желобов началась перегрузка поглотителей при работе реактора на полной мощности.

После периода испытаний по перегрузке поглотителей было решено провести контролирующую подготовку к перегрузке топлива при работе реактора на полной мощности. Энергетическим управлением была разработана программа перегрузки топлива при работе реактора на

20%-ной, 60%-ной и затем на полной мощности, которая была выполнена без каких-либо осложнений. Из-за механического повреждения устройств, захватывающих тепло выделяющие элементы, пришлось приостановить последующие операции по перегрузке топлива до разработки захватывающих устройств. Тем временем перегрузка поглотителей продолжалась, однако произошел инцидент — отошла часть сборки защитной пробки, в результате чего потребовалась модификация всех таких пробок.

После усовершенствования захватывающих устройств были возобновлены операции по перегрузке топлива при работе реактора на полной мощности. Механические повреждения все же имели место, однако модифицированная система обнаружения исключала перерастание этих повреждений в серьезные аварии. Параллельно с продолжающимися операциями по перегрузке топлива ведутся работы над усовершенствованием конструкции захватывающих устройств.

Будучи в основном такой же по конструкции, загрузочная машина в Латине вобрала, однако, в себя все лучшее, что дал опыт проектирования, разработки, испытаний и пуско-наладочных работ загрузочной машины в Бродуэлле. Благодаря этому гораздо меньше времени потребовалось для ее подготовки к работе на месте.

Фактически никакой перегрузки тепло выделяющих элементов при работе реактора на мощности пока еще не проводилось, однако было заменено без каких-либо осложнений значительное число поглотителей.

После продолжительной оценки решено было строить более или менее идентичные загрузочные машины в Дандженессе и Олдбери на базе конструкции загрузочной машины в Латине с использованием характеристик, исключая те неполадки, которые выявились во время работы загрузочных машин ранних конструкций. Значительно шире стали использоваться испытательные стенды, на которых более эффективно моделировались условия реактора, при испытании прототипных и промышленных узлов и целых загрузочных машин.

В докладе показываются основные требования, предъявляемые к конструкции надежных загрузочных машин; не все из этих требований были известны при проектировании загрузочных машин для реакторов в Бродуэлле и Латине. Многие из полученных данных применимы к реактору AGR и магноксовым реакторам.

Кроме механических требований, обеспечению безопасной, быстрой и удобной эксплуатации загрузочной машины в значительной степени способствовало бы усовершенствование системы регулирования. В докладе обсуждается и считается желательным использование в системе перегрузки топлива в Бродуэлле цифрового счетно-решающего устройства.

Experiencia con el equipo de manejo de combustible durante el funcionamiento de Bradwell y Latina, y su influencia en futuros proyectos

por J. O. Joss et al.

Descripción esquemática de las características principales de la máquina de carga Bradwell y su instalación auxiliar, especialmente de aquellas características que necesitaron desarrollo extenso o modificación durante el período de proyecto, construcción y puesta en servicio, antes de llegar a ser aparatos dignos de confianza.

El proyecto original para Bradwell contenía características que se comprendió tendrían que ser comprobadas mediante ensayo de un prototipo y desarrollo ulterior. Además, fueron necesarios cambios debido a alteraciones en otros puntos de la instalación del reactor. Estos dos factores repercutieron profundamente en la forma final de ciertos componentes.

El programa de prueba de la instalación de manejo de combustible constituyó una parte integrante de la puesta en servicio del reactor, con etapas fría, caliente y de duración, cada una proyectada para comprobar diversos aspectos del proyecto en detalle y en general. Los defectos que surgieron fueron corregidos principalmente *in situ*, pero algunos necesitaron más amplio desarrollo.

A causa de ciertas limitaciones encontradas durante la puesta en servicio, se empleó al principio la maquinaria de Bradwell a reactor parado o a potencia y temperatura reducidas. En estas condiciones se manejaron los canales combustibles y los elementos absorbentes sin incidentes, y se obtuvo una considerable experiencia en el empleo de la maquinaria.

Cuando se llegó a disponer de mejores tolvas de descarga comenzó el manejo de los elementos absorbentes a plena potencia del reactor.

Después de un período de manejo de los elementos absorbentes de neutrones se decidió proceder, de manera controlada, al manejo de elementos combustibles a plena carga. El Generating Board presentó un programa para recargar a 20%, 60% y posteriormente a plena potencia; dicho programa se llevó a cabo sin incidentes. Unas averías mecánicas en la garra de manipulación del combustible dieron origen a que se suspendieran las cargas mientras se seguían desarrollando las garras. Entretanto continuó el manejo de los elementos absorbentes, y surgió un incidente cuando parte del conjunto de un tapón de blindaje se desprendió. Como resultado, todos estos tapones necesitaron modificación.

Se llegó a disponer de garras mejoradas y se reanudó la recarga a plena potencia. Persistieron las averías mecánicas, pero un sistema de indicación mejorado evitó que éstas degeneraran en incidentes importantes. Sigue llevándose a cabo la recarga

continua paralelamente al desarrollo del proyecto de las garras.

Aun cuando básicamente coinciden, las máquinas de carga de Latina se han beneficiado enteramente de las experiencias del proyecto, desarrollo, prueba y puesta en servicio de las de Bradwell. Como resultado de esto se empleó mucho menos tiempo en ajustar el equipo para trabajar en el emplazamiento.

Virtualmente no se ha llevado aún a cabo el manejo en carga de los elementos combustibles, pero un número considerable de canales de absorbente de neutrones se han cambiado sin incidentes.

Siguiendo la pauta de evolución continua, la maquinaria, más o menos idéntica, de Dungeness y Oldbury se basa en el proyecto de Latina, incorporando características para eliminar los inconvenientes que se manifestaron durante el funcionamiento de los

primeros proyectos. Se ha hecho un uso mucho mayor de los equipos de prueba, que simulan mejor las condiciones del reactor, en los ensayos de las máquinas y sus componentes, ya sea en forma de prototipo o de serie.

La memoria describe los requisitos principales para un buen proyecto de la maquinaria de manejo de combustible, no todos los cuales eran evidentes cuando se proyectaron Bradwell y Latina. La mayor parte de esta experiencia es aplicable a reactores AGR y a los reactores de Magnox.

Además de las necesidades mecánicas, las mejoras en los sistemas de control pueden aumentar mucho la seguridad, velocidad y comodidad de funcionamiento. Se describe y discute la aplicación de una calculadora digital a un sistema de recarga del tipo de Bradwell.

Fuel handling equipment for the Ågesta D₂O moderated pressure vessel reactor

By G. Granelli,* G. Fagerlund,** S. O. Brunzell*** and G. Fröman*

The object of the report is to describe the design of the fuel handling equipment in the main, and to give some information about unconventional details which have required special attention.

For the design work the following criteria were fixed:

(a) Fuel charging will occur during the off-load condition;

(b) Storage and fuel charging will occur under gas-tight and radiation shielded conditions. The radiation level on the exposed surfaces to the reactor hall should not exceed 0.75 mr/h;

(c) The handling will also concern control rods and plugs.

(d) Storage area will be found in the reactor hall for about 300 fuel assemblies and about 60 control rods and plugs together with the requisite test and service equipment;

(e) The fuel assemblies will be cooled effectively in all operation and storage situations;

(f) D₂O will be taken care of and prevented from mixing with H₂O;

(g) The refuelling machine's operating system will be fool-proof;

(h) The refuelling machine will be ventilated and decontaminated;

(i) The risk of contaminating the refuelling machine must be kept down through the use of suitable materials and well-thought-out design without pockets. Lubrication ought to be used as little as possible and if absolutely necessary one should use molybdenum disulphide.

(j) The refuelling equipment should be provided with suitable emergency and auxiliary equipment for electrical and water supply. The more important components should be duplicated. The refuelling machine's hoist and rotational movements should have a reserve hand operation;

(k) A minimum of 2 fuel assemblies should be charged at a time or 4 during plundering;

(l) Can-damaged fuel assemblies must be handled in gas-tight shielded flasks.

Lay-out for the reactor hall

The storage part has been laid out as follows: (see Fig. 1).

* AB Atomenergi, Stockholm.

** Nohab, Trollhättan.

*** Asea, Västerås.

Storage for new or low activated control rods and plugs, 26 positions.

Storage for activated fuel assemblies, 294 positions.

Storage for activated can-damaged fuel assemblies, 20 positions.

Storage for activated control rods and plugs, 42 positions.

Storage for activated new fuel assemblies, 8 positions.

At the far end of the hall, seen from the reactor, a station is situated for changing inlet throttle rings on the activated fuel assemblies, exhaust and decontamination connections, a reactor mock-up, shielded transport casks for fuel assemblies and control rods and service equipment for the refuelling machine.

The travelling bridge with crab

The refuelling machine consists of a travelling bridge with a crab which carries the machinery with its necessary operating system and shielding. The shielding consists of cast iron with a maximum thickness of 630 mm and is dimensioned to give a dose rate of 0.75 mr/h during normal fuel charging. The refuelling machine's central chamber has also been provided with a neutron shield consisting of a water mantle about 70 mm thick, filled with boronated water. The whole fuelling machine weighs about 220 tons of which the shielding weighs about 170 tons (Fig. 2).

The operating equipment for the traverse crab as well as the travelling bridge has been designed as a Ward-Leonard system with transducer regulation for step speed control from maximum down to zero. The refuelling machine's positioning at the different working stations will be controlled manually from the operating platform with the help of selsyn indicators and a periscope. Maximum travelling speed for the travelling bridge as well as the crab is 0.25 m/s and creep speed about 0.005 m/s.

The refuelling machine's hoisting and rotating machinery

The fuel assemblies as well as the control rods and plugs are provided with lifting hooks of similar design into which the refuelling machine's grab lifts during handling. There are equivalent supporting hooks fitted in the reactor as well as in the storages and also in the refuelling machine's chamber. In the reactor

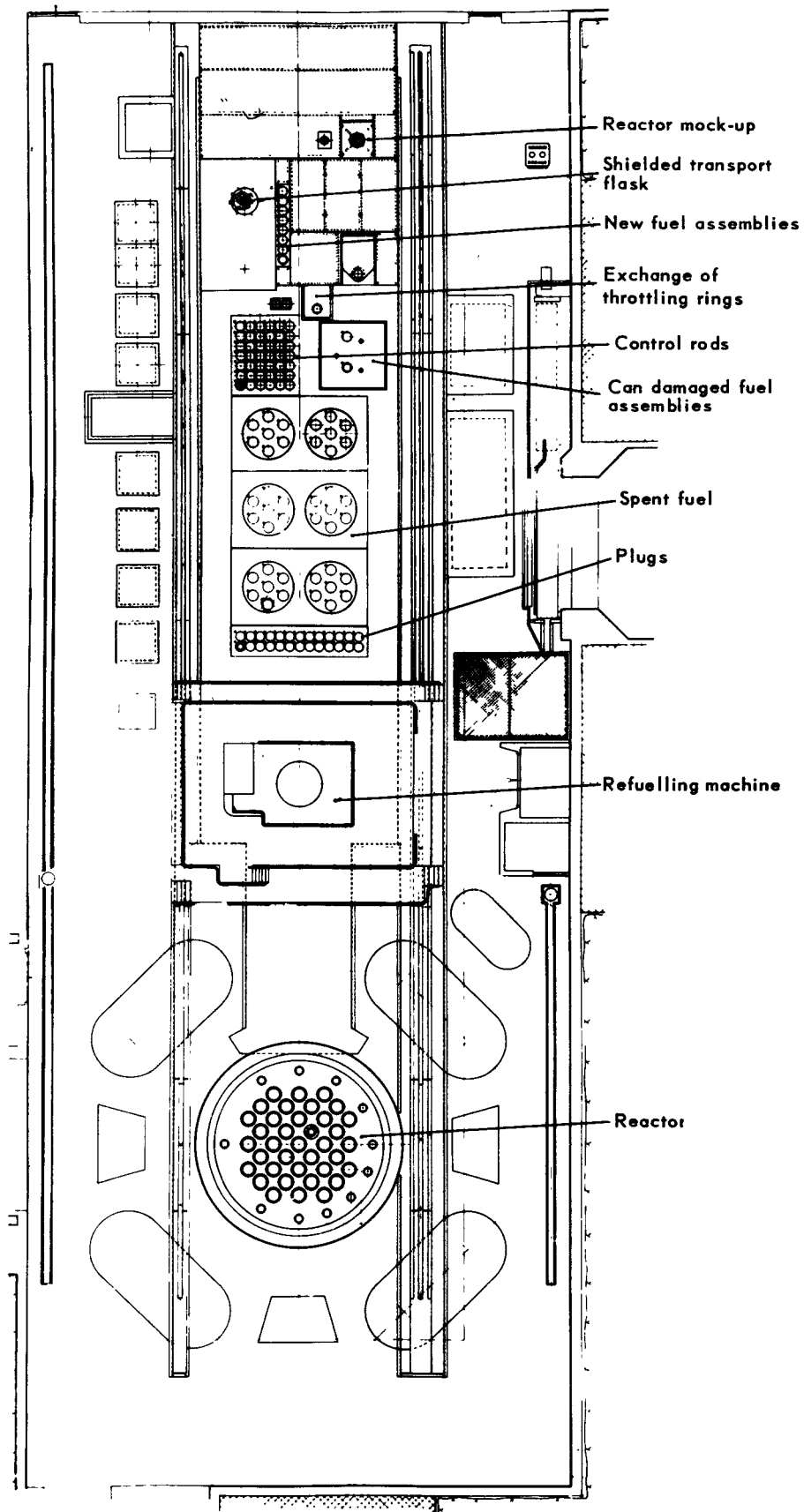


Figure 1. Lay-out for the reactor hall

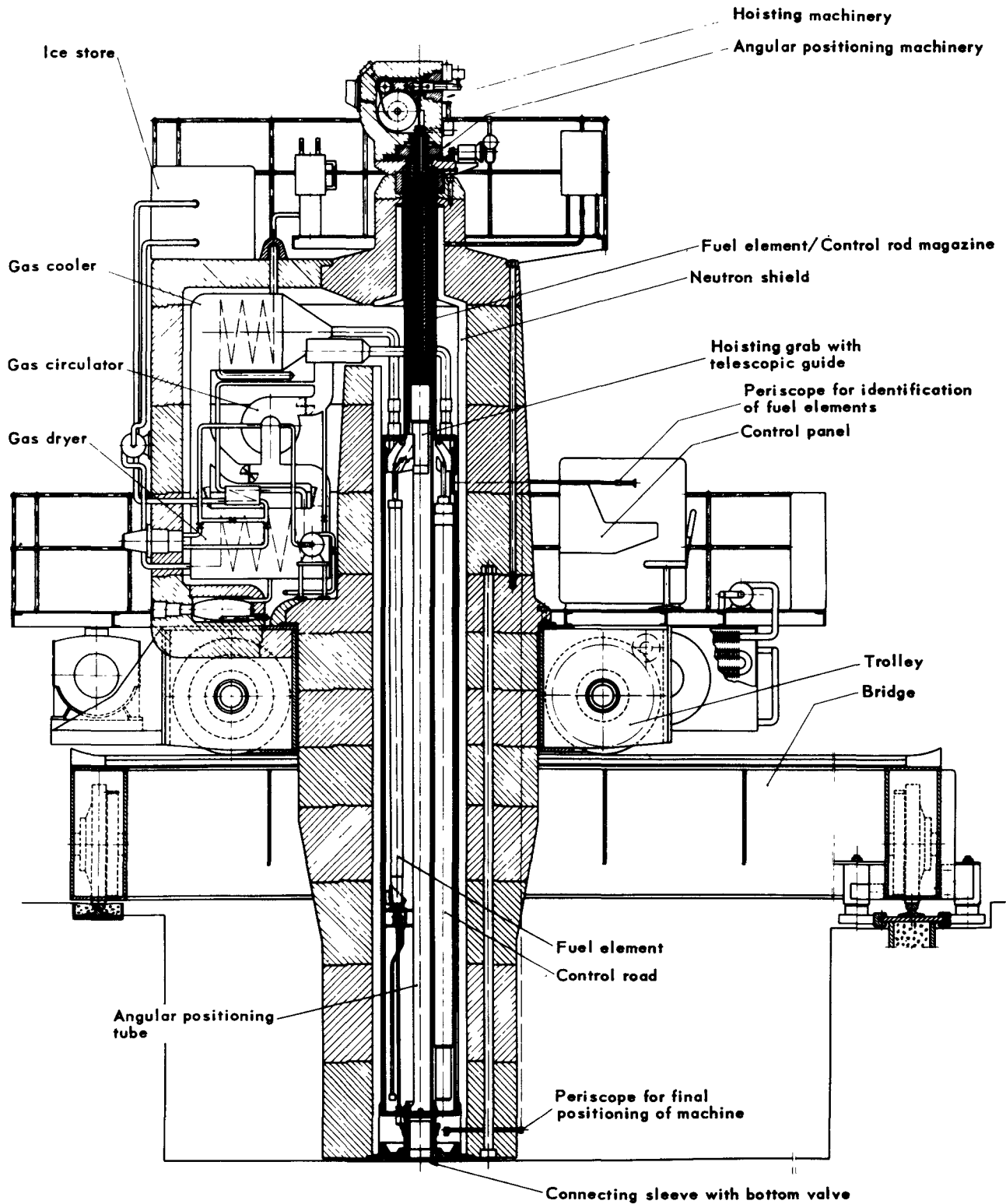


Figure 2. Vertical section through the refuelling machine

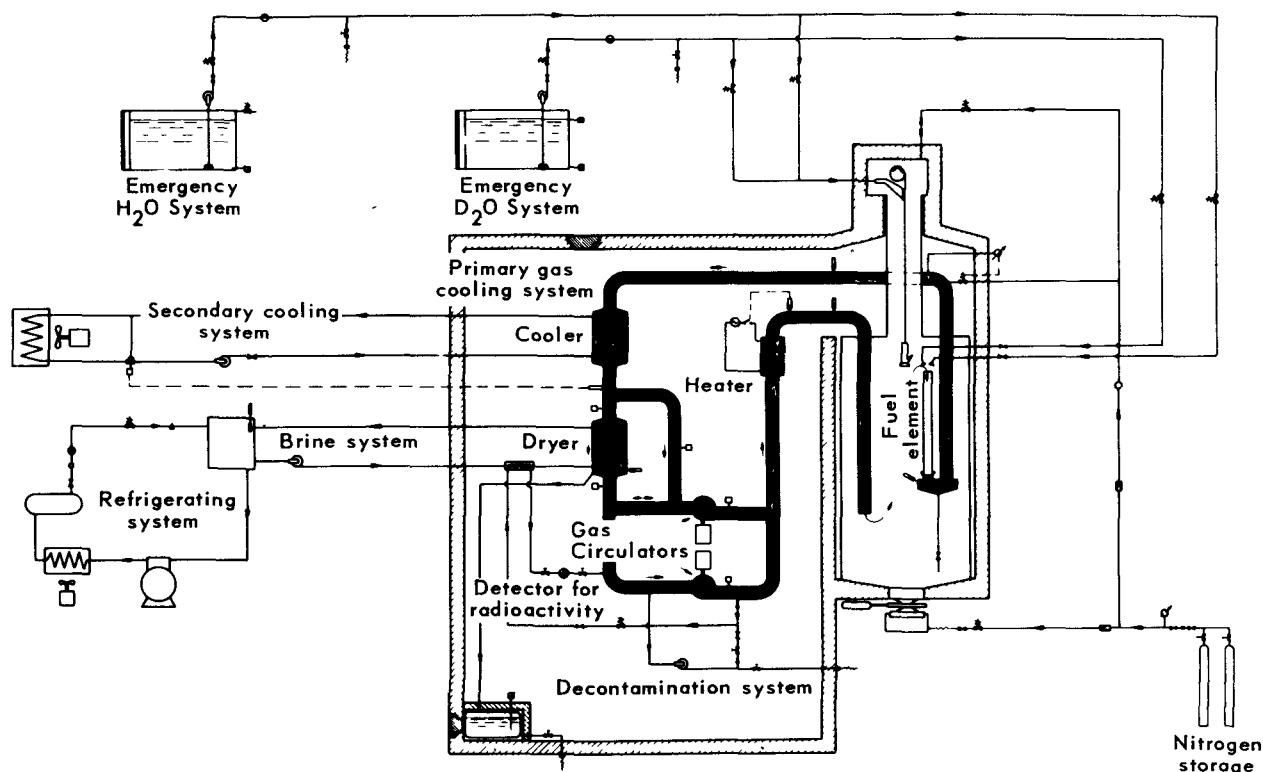


Figure 3. Simplified scheme of cooling and drying circuit

4 fuel assemblies are grouped around each charge pipe which is to be sealed centrally with either a control rod or a plug. During each change of fuel the control rod or the plug must be changed since the primary as well as the secondary sealing must be changed after each visit. There are, in the refuelling machine, supporting hooks for 4 fuel assemblies and 2 control rods or plugs which allow 3 fuel assemblies to be changed at the same time. Four fuel assemblies can be taken at a time during plundering. The charge equipment is largely built up from a cylindrical chamber in whose centre a telescopic guided manipulator runs in a cut-away guide tube. The manipulator with the help of the telescopic arrangement is guided down into the reactor's charge pipe to a level in line with the fuel assembly supporting hooks.

The lifting and lowering operations are done with a woven flat rope which runs from the hoisting machine in the top of the chamber. The hoisting drum is driven through a sliding clutch by a motor. The rope from the hoisting drum is guided up and over 2 smaller rollers of which one is supported in an arm that swings about a horizontal pivot. This pivot arm indicates the rope tension by operating against an electrical pressure switch which is used as protection against overload and also as an impulse unit to operate signal lamps and a continuous graphical recorder.

The bottom of the chamber is provided with a valve and a telescopic sleeve which enables it to be coupled gas tight to the reactor or the storages.

The refuelling machine's cooling system

In the design criteria it is stated that the fuel assemblies will be cooled effectively in all storage and operating situations. When the assembly is removed from the reactor it normally has a surface temperature of about 70° and the fuel continues to give off a decay heat equivalent to 11 kW fairly constantly for several hours. This heat must be removed, otherwise the temperature will rise abnormally causing damage to the assembly. The assembly need not be cooled for about 5 min which occurs when changing from the reactors D_2O to the storages H_2O . The system has, of course, several limitations; for instance the assembly cannot be gas cooled during all moments of handling. For this reason the system has been designed with a spray cooling system for D_2O or H_2O . The spray system is also a reserve for the gas cooling system if for instance a fault occurs in the circulators.

The system (Fig. 3) consists of a cooler, a dryer, an electric heater and a circulator which is duplicated. Clean nitrogen is used as the cooling medium. The gas flow is 0.4 kg/s at a pressure rise of 1 500 mm water gauge. The cooler works between $+210$ to $+80^{\circ}C$ and transmits the heat by a water circuit to an air cooler which in turn transmits the heat to the atmosphere in the reactor hall. The dryer, which is placed in series with the cooler, is dimensioned so that all the D_2O steam in the cooling circuit will be condensed within 5 min after the refuelling machine has left the reactor (Fig. 4). A freon-cooling system combined with an ice box divided into compartments is chosen

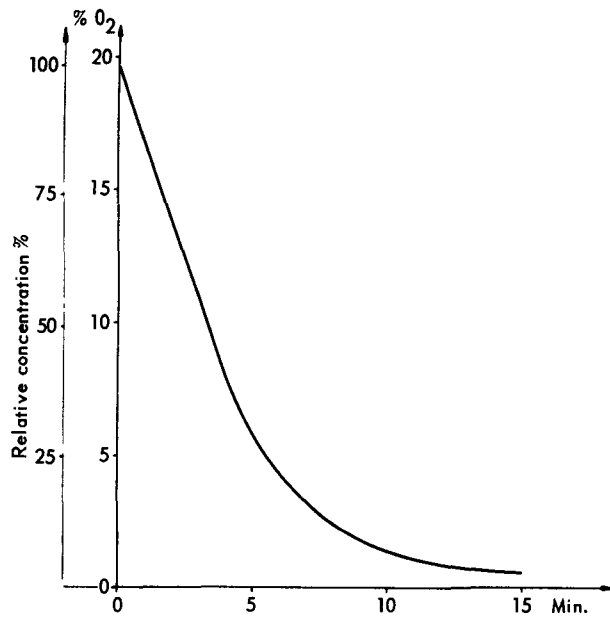


Figure 4. The ventilating efficiency in the refuelling machine

for the dryer. The electric heater has a consumption of 6 kW and works between $+75$ to $+85$ °C. The task of the heater is to warm up the gas and the inner surfaces to at least $+80$ °C before the refuelling machine is connected to the reactor. An escape of D_2O from the reactor up into the refuelling machine is thus prevented.

The gas circulators are one of the machine's most interesting components. They ought to be totally closed with little or no risk of oil leakage into the gas circuit as per the design criteria. Having considered various schemes, an invitation was accepted by a British company to supply a wholly canned circulator using gas lubricated bearings. The manufacturers had not built circulators of this size before, but they presented very positive reports of many years development work. Unfortunately the manufacturer was unsuccessful in spite of extraordinary attempts to produce a circulator with sufficient reliability. Due to the pressing time schedule there was unfortunately no possibility of continuing work with the gas lubricated bearings and the circulator had to be rebuilt using ball-bearings.

The ball-bearings selected for this application were a special, bronze-machined cage type (Fig. 5). Similar bearings had been submitted to many years of observation and thousands of running hours under far more arduous load conditions, greater temperature extremes, and nearly double the speed.

Nevertheless, the essential feature of this redesigned assembly was, of course, oil-free operation under normal and extreme conditions of operating cycles. The source of oil leakage most detrimental to this application was from the front seal next to the impeller, although to a lesser degree, internal leakage into the casing could be troublesome over long periods. Thus, to eliminate this possibility, comprehensive

investigations during manufacturing tests were carried out such that no oil leakage was observed or detected. Labyrinth type, self-cutting, carbon oil seals were specified, based on successful results and negligible leakage on a similar test rig assembly.

In order to supply the bearings with oil, at consistent flows and temperature conditions, an oil tank assembly was also designed in which heating/cooling coils were housed together with oil pump and motor etc, as an independent sealed unit.

During commissioning, however, some oil leakage from the front seal was detected. At first this problem seemed part of the learning process towards normal operating/control techniques. But, subsequent experience showed that the operating circulator unit appeared to effect the other non-operational unit *in situ*. A programme of investigation into relative pressure levels throughout both circulator units under various operating conditions was therefore carried out in the refuelling machine.

Sealing arrangement

Resulting from the findings and analysis of this investigation, adjustments to the lubricant drain systems and the general running procedure of the circulators successfully enabled oil-free operation.

In order to meet the requirement to keep the gas leakage down to a minimum, double sealing by means of synthetic rubber is used and positioned so that back-up gas is pressurized between them. The use of elastomers is strongly limited where one has ionising

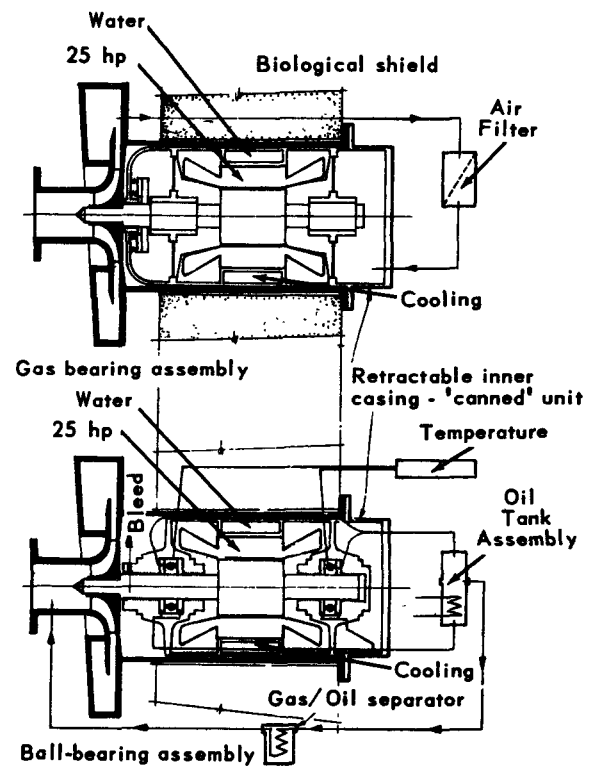


Figure 5. Comparison/conversion of gas bearing to ball-bearing machines

radiation and thus this sealing element must be positioned in a relatively well-shielded part of the machine. Provision of back-up gas is made from the nitrogen supply which is stored on the machine. Also, nitrogen is used for filling and flushing clean the refuelling machine's primary circuit and for other pneumatic operations. It is stated that when one uses dry nitrogen the friction properties of the seal become worse; these are then compensated for by applying molybdenum disulphide to the friction surfaces of the seal.

Radiation detection and decontamination

As already mentioned the shielding is designed to give a dose rate of 0.75 mr/h. If, however, in the fuel assembly large can damage occurs, there is a risk that activity will spread to parts of the refuelling machine, which, due to its space and weight, cannot be given the same shielding. In order to get an immediate alarm by an increased gas activity in the machine a radiation detector is connected to a by-pass in the gas circuit.

In order to make inspection and service easier the primary system has been fitted with a pump so that the decontamination fluid can be circulated round the gas circuit and in this manner reduce the activity level of the inner components.

Control equipment

The design criteria require that safety is met by:

- (a) Electrical interlocks incorporated so that an incorrect operation cannot be carried out;
- (b) Indication of the operating positions on symbol diagrams which gives the operator the information he requires for manipulating the machinery;
- (c) Essential instrumentation for measuring temperatures, mass flows, pressures, loading in the hoisting rope etc.

The travelling and traversing movements are automatically stopped when the refuelling machine approaches the outer positions of its movement. Before the refuelling machine's travelling movement is stopped the speed changes to creep.

The hoisting and lowering speeds are to be changed automatically from maximum to creep at fixed levels. The electrical interlocks are arranged in such a way that only determined operations in an arranged sequence are possible with the following considerations: (a) Which station is to be served; (b) In which turning position the grab rests; (c) At which level the grab rests; (d) Which hooks in the refuelling machine are occupied; (e) Which hooks in the reactor or storage are occupied; (f) If the grab is engaged or free; (g) Plug control rod or fuel assembly operation; (h) The grab out or in.

Information is normally given from switch-governed relay-circuits except for (e) where it is relayed from a memory-relay-circuit and for (f) from switches which are influenced by the hoisting ropes weighing equipment with associated relay functions.

After the refuelling machine is closed and disconnected the memory is erased, that is, the hooks in the reactor and stores are shown to be *occupied*. When the refuelling machine is again connected to the reactor or any of the fuel stores, a *trial run* is carried out in order to trigger the *memory* system so that the correct fuel changing sequence is obtained.

The drive for the bottom nozzle and bottom valve continues to move to a fixed stop position, when the clutch slips, causing the governor to break the current.

A frequency changer supplies the gas circulator squirrel cage motor with 440 V 260 cps which gives the circulator a speed of 16 000 rev/min. The drive of the circulator and its auxiliary system is completed with sufficient interlocks and the starting up of the complete system is actuated in a fixed sequence.

The control system is designed for a change of 2 spent fuel assemblies for 2 new ones. If any other operation is required, this is possible only by overriding the actual interlocks. A special box, normally closed, is placed in the control panel, in which there are several handles that enable the interlocks to be over-ridden.

The reactor mock-up

A fuel handling machine of this type needs to be rather complicated. With regard to the safety aspects it has been considered important that all functions of the refuelling machine be thoroughly checked before any fuel changing is started. A reactor mock-up has, for this reason, been placed in the service area. In this mock-up it is possible to carry out almost a complete check of all functions.

Storage for fuel assemblies, control rods and plugs

The main principle during the design of the storage has been with adherence to the criteria that all handling of activated or decontaminated components has to be done under gas-tight and shielded conditions (Fig. 6).

The storage for new fuel assemblies

This is a transfer station placed inside the refuelling machine's working area. It consists of 8 vertically placed protecting pipes of stainless steel whose top end is designed so that the refuelling machines bottom nozzle seals against them, the fuel assemblies being supported at the lower end in a guide. Every storage pipe is connected to the ventilating system in the station, in order to ventilate the machine's sliding sleeve.

The storage for activated undamaged fuel assemblies

This consists of 6 tanks for 49 assemblies each. The contents of the store is thus a total of 294 assemblies. The spent fuel will be kept 6 months in the store in order to reduce the decay heat to such a value that the assemblies can be transported without special cooling. Every tank pair is connected to a cooling system to dispose of the decay heat. For the ventilating operations the tanks are also connected to

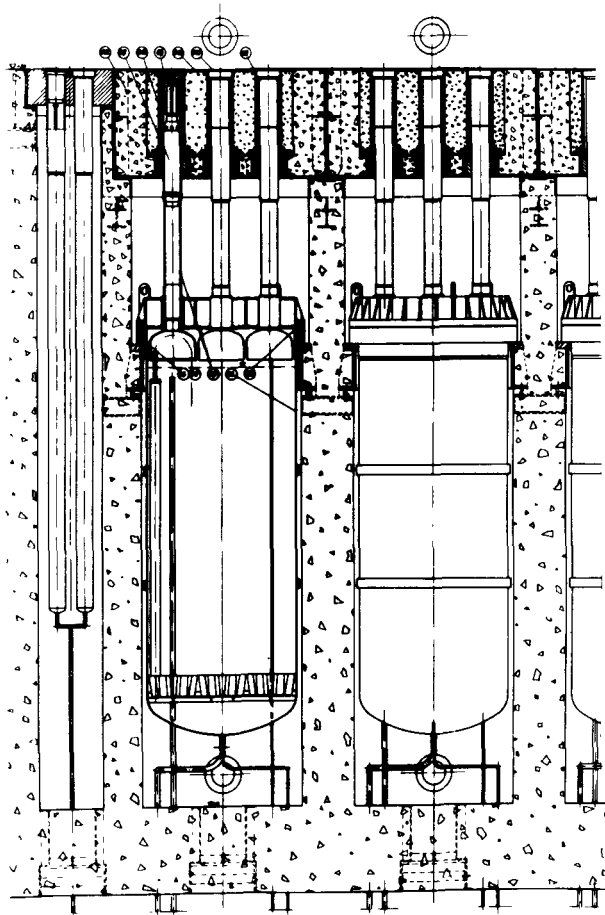


Figure 6. Vertical section of storage

the active gas system. This is normally kept below atmospheric pressure.

The store for active can-damaged fuel assemblies

This is designed, so that the damaged assembly can be placed in a separate flask, which is provided with a seal plug. The plug contains lifting hooks similar to the assembly for handling in the refuelling machine. The operation of the plug-handling equipment and the store's turning machinery is carried out from an operating panel placed in the bottom end of the reactor hall. All functions are started manually with push-buttons. The operations are indicated with signal lamps on a symbol scheme. The turning movement and the lifting and lowering movement can be followed on selsyns. The different operations are interlocked so that the impulses must be given at correct time intervals. The store is electrically connected to the refuelling machine to maintain correct interlocking.

The store for control rods and plugs

The store is from the design point of view similar to that above. The storage pipes are connected to the station's ventilating system.

The station for the exchange of throttling rings on fuel assemblies

Fuel assemblies in different positions in the reactor require different cooling mass flows. The mass flow is regulated with a throttling ring clipped into the bottom end of the assembly. The change of the ring is carried out with a manipulator during gas-tight and shielded conditions.

Experience from manufacture, erection and tests

As a general rule all details with surfaces exposed to heavy water should be made from stainless steel with low carbon content and from the decontamination point of view, made to a certain minimal surface finish. For erection purposes the manufacturers have arranged clean areas of a high standard.

The final erection and test run has clearly shown that it is necessary to use large tolerances when two stainless surfaces have to work together. The risk of seizing is considerable. All changes in dimension must be provided with good guiding faces without sharp edges. This is particularly apparent later when a dull oxide-protection has covered the surfaces.

Summary and conclusions

In order to lower the stress in the flat lid the number of charge pipes has been limited for one of each four fuel assemblies. The traverse movement of the assemblies to respective hooks has thus to be managed inside the reactor vessel and the grab has to be designed to meet this requirement.

The same geometry must, however, be used in the fuel stores and this fact together with the safety requirements has certainly meant an increase of the plant costs. Since the design is a prototype, and the necessity is to keep down the costs, it is not considered justifiable to use automation for the fuel handling as might be considered for a more commercial plant. Experience from the operations which is now available shows also that the auxiliary functions take an unproportionally long time in comparison with the proper fuel handling.

The request for limiting the choice of construction material and the requirement for high cleanliness during manufacture has raised certain complications. The wish to keep down the dimensions has also necessitated designs which have caused certain manufacturing problems.

After necessary corrections during the final erection and tests it was, however, shown that all functions corresponded well with the estimated design performance.

ABSTRACT—RÉSUMÉ—АННОТАЦИЯ—RESUMEN

A/808 Suède

Équipement de manutention du combustible pour le réacteur d'Ågesta à cuve sous pression modéré à l'eau lourdepar G. Granelli *et al.*

L'objet du mémoire est d'indiquer quelques aspects des idées de base et de l'expérience acquise dans l'étude, la construction et les essais.

Certains paramètres fondamentaux de la conception étaient fixés. La manutention du combustible doit s'effectuer avec étanchéité aux gaz et protection contre les rayonnements; le mécanisme de manutention du combustible et le stockage du combustible doivent être dotés d'un système de refroidissement efficace sous toutes conditions de fonctionnement concevables; le système de commande doit être à l'épreuve de toutes les fausses manœuvres; enfin, l'eau lourde condensée dans la machine de chargement doit être récupérée et ne doit en aucun cas être susceptible de se mélanger à l'eau légère.

Afin d'obtenir une construction aussi simple que possible, il a été décidé d'utiliser un tube de chargement commun pour les quatre positions d'éléments les plus rapprochées. Le tube de chargement contient également la barre de contrôle qui est desservie par la machine de chargement. Les éléments de combustible sont suspendus à des crochets sous le capot du réacteur et sont manutentionnés à l'aide d'une pince à griffes logée dans la machine de chargement.

Le réservoir de combustible se présente sous forme de récipients normalement maintenus en dépression par rapport à la pression atmosphérique afin d'éviter les fuites d'activité vers la salle du réacteur. Pendant le chargement du combustible, qui s'effectue lorsque le réacteur n'est pas en fonctionnement, la machine de chargement est reliée, de manière étanche, aux gaz, au tube de chargement du réacteur ainsi qu'aux tubes du réservoir de combustible.

L'eau lourde présente dans le système est recueillie par drainage du gaz de refroidissement. Le condensat du sécheur est acheminé dans un bac de condensation spécial. Tout mélange avec l'eau légère est évité par épuisement rigoureux du tube de chargement et de la machine de chargement avant toute manutention de combustible.

Chaque opération est mise en route et arrêtée manuellement. La sûreté contre les fausses manœuvres résulte de dispositifs de verrouillage et de la possibilité d'intervention manuelle pour toutes les opérations principales.

La demande d'un choix limité de matériaux de construction et les exigences relatives à une propreté rigoureuse en cours de fabrication ont soulevé certaines complications. Le désir de maintenir les dimensions à un minimum a également exigé des modes

de construction qui ont posé certains problèmes de fabrication.

Après les corrections nécessaires au cours du montage final et des essais, il a été démontré que toutes les fonctions correspondaient bien aux performances prévues.

A/808 Швеция

Оборудование для работы с тепло-выделяющими элементами тяжело-водного реактора в Агесте с корпусами давленияГ. Гранелли *et al.*

Цель доклада состоит в том, чтобы рассмотреть некоторые аспекты физики реактора и опыта его проектирования, изготовления и испытания.

Обсуждаются некоторые основные параметры конструкции. Работа с тепловыделяющими элементами должна проводиться в газонепроницаемой системе, снабженной защитой от радиации. Для проведения всех опытов машина для работы с твэлами и хранилище для топлива должны быть снабжены эффективной системой охлаждения. Маневрирующая система должна быть несложной. Конденсат тяжелой воды в загрузочной машине должен собираться так, чтобы не допустить его смешивания с обычной водой.

Чтобы сделать конструкцию возможно более простой, было решено использовать соединительные загрузочные трубы для четырех наиболее плотных положений элементов. Загрузочная труба содержит также регулирующий стержень, который управляется загрузочной машиной. Тепловыделяющие элементы, подвешенные на крюках ниже крышки реактора, берутся захватом, установленным на машине для загрузки топлива.

Хранилище топлива состоит из чанов, в которых обычно поддерживается давление ниже атмосферного, чтобы избежать утечки активности в реакторный зал. Во время загрузки топлива, которая проводится в условиях, когда реактор работает без нагрузки, загрузочная машина присоединяется к загрузочной трубе в реакторе, а также к загрузочным трубам хранилища для топлива. При этом обеспечивается газонепроницаемость системы.

Тяжелая вода в системе собирается путем осушения охлаждающего газа. Конденсат из сушилки направляется в специальный бак-конденсатор. Всякое смешивание тяжелой воды с обычной водой предотвращается путем полного откачивания воздуха из загрузочной

трубы и машины для загрузки топлива, прежде чем проводится какая-либо загрузка.

Каждая операция начинается и прекращается вручную. Чтобы сделать систему несложной в управлении, применена система блокировки. В проведении всех основных операций преобладает ручное управление.

Требование ограничения выбора конструктивных материалов и необходимость в высокой чистоте материалов в процессе их изготовления несколько повысили сложность конструкции. Желание уменьшить рост размеров тепловыделяющих элементов привело к необходимости создать конструкции, изготовление которых вызывало некоторые трудности.

После введения необходимых поправок во время окончательной отработки и испытаний было показано, что параметры конструкции находились в хорошем соответствии с расчетными рабочими характеристиками.

A/808 Suecia

Equipo de manejo de combustible para el reactor de vasija a presión moderado por D_2O de Agesta

por G. Granelli *et al.*

El objeto de la memoria es el de presentar algunos aspectos de las bases teóricas y de la experiencia del proyecto, la fabricación y los ensayos.

Se establecieron para el proyecto ciertos parámetros básicos. El manejo de combustible tiene que ser realizado en condiciones de hermeticidad a los gases y protección contra la radiación, la máquina de manejo de combustible y el almacén del combustible deben estar provistos de un sistema de refrigeración efectivo en todas las condiciones de funcionamiento concebibles, el sistema de maniobra debe ser a prueba de

falsas maniobras y, finalmente, el agua pesada condensada en la máquina de carga tiene que ser recogida y no debe mezclarse con H_2O .

A fin de hacer el diseño lo más sencillo posible, se decidió emplear un tubo de carga común para las cuatro posiciones de elementos más próximas. El tubo de carga contiene también la barra de control, a la que sirve la máquina de carga. Los elementos combustibles cuelgan de ganchos debajo de la tapa del reactor y son manejados por medio de un gancho horquillado situado en la máquina de carga del combustible.

El depósito de combustible consiste en unos tanques que se mantienen normalmente por debajo de la presión atmosférica para evitar fugas de elementos radiactivos a la sala del reactor. Durante la carga de combustible, la cual se realiza con el reactor fuera de funcionamiento, la máquina de carga se empalma con una conexión hermética a los gases, al tubo de carga del reactor y a los del depósito de combustible.

El agua pesada del sistema se recoge desecando el gas de refrigeración. El condensado procedente del desecador se lleva a un condensador especial. Se evita la mezcla con H_2O vaciando a fondo el tubo de carga y la máquina de carga de combustible antes de realizar la operación.

Cada operación se inicia y se detiene manualmente. Para hacer el sistema a prueba de falsas maniobras se emplean enclavamientos y se ha dispuesto un sistema de control manual predominante en todas las operaciones básicas.

Los requisitos para la elección de materiales de construcción y la necesidad de una gran limpieza durante la fabricación han dado lugar a algunas complicaciones. El deseo de limitar las dimensiones ha sido causa también de adoptar diseños que han originado ciertos problemas de fabricación.

Después de las necesarias correcciones durante la instalación final y las pruebas se ha demostrado que todo el funcionamiento correspondía bien al comportamiento previsto.

Etude de structures nouvelles adaptées aux réacteurs graphite-gaz et eau lourde-gaz

par R. Martin et R. Roche*

FILIÈRE GRAPHITE - GAZ

L'expérience acquise par l'exploitation des réacteurs de Marcoule, la construction et le démarrage des réacteurs d'EDF, d'une part, les conclusions des études et essais effectués hors pile, d'autre part, conduisent à un changement considérable de la physionomie des réacteurs de la filière graphite - gaz.

Éléments combustibles annulaires

La recherche de puissances spécifiques de plus en plus élevées a d'abord orienté vers des éléments combustibles creux, puis vers des éléments annulaires refroidis extérieurement et intérieurement. Cette disposition supprime tout risque de flambement sous l'effet de la pression du gaz et accroît la surface d'échange. La résolution du problème de gainage interne est facilitée par l'accroissement de la pression qui va de pair avec l'augmentation de puissance spécifique. Les ailettes externes conservent la configuration en chevrons, qui offre un excellent rendement, tandis que la paroi interne présente des micro-chevrons ou des corrugations de faible amplitude.

Sens de circulation du fluide

L'accroissement de la puissance développée par canal entraîne une augmentation corrélative du débit de fluide; le sens de l'écoulement doit être inversé pour écarter le risque de lévitation des éléments combustibles. Cela implique la conservation des chemises pour soulager les cartouches des efforts dus à la poussée du gaz. L'inversion du sens de soufflage apporte de très nombreux autres avantages (suppression du dispositif de contre-envol des éléments combustibles, fonctionnement du treuil et du grappin en zone relativement froide, meilleur refroidissement des cartouches irradiées pendant leur manutention, diminution d'épaisseur du calorifuge du caisson, possibilité de régler le débit de gaz dans les canaux au moyen d'un organe de laminage accessible, amélioration de la stabilité des éléments combustibles, dégagement du dôme, les tubes de prélèvement — DRG, débits, températures — étant reportés au niveau de la sole). En contrepartie, il convient de citer quelques inconvénients (nécessité de renforcer les supports d'éléments combustibles pour tenir compte en

particulier de la poussée aérodynamique lorsque le débit est momentanément accru, durant les opérations de renouvellement en marche; alourdissement de la sole portée à la température de sortie du gaz et qui doit résister au poids du cœur majoré de la poussée aérodynamique du gaz; incompatibilité du soufflage descendant avec un refroidissement par thermosiphon du réacteur arrêté ou fonctionnant à puissance réduite).

Compte tenu des avantages attendus de l'inversion du sens traditionnel de soufflage, et en dépit des inconvénients mineurs qui viennent d'être cités, il a été décidé d'adopter cette solution sur le réacteur EDF4, en construction à Saint-Laurent-des-Eaux.

L'empilement de graphite

L'accroissement de la masse d'uranium par canal a pour conséquence de réduire très sensiblement le nombre des canaux. Celui-ci peut, à puissance de réacteur égale, être divisé par trois ou quatre. Corrélativement, le pas du réseau est augmenté et l'empilement de graphite doit être adapté à cette nouvelle condition.

Le CEA a pu imaginer et mettre au point un type d'empilement tel que le pas du réseau est rigoureusement insensible à l'expansion Wigner, que celle-ci soit positive ou négative. Il consiste à juxtaposer des blocs de graphite prismatiques, de section généralement hexagonale, et à les relier entre eux par des clavettes également en graphite. Un jeu est ménagé entre chaque bloc afin d'autoriser une certaine expansion. Le choix de ce jeu suppose évidemment la connaissance de la borne supérieure de l'expansion Wigner, ce qui est généralement le cas. Ce procédé, déjà adopté pour les réacteurs EDF2, EDF3, EDF4, ainsi que dans divers réacteurs construits à l'étranger, est évidemment transposable aux réseaux à grande maille moyennant l'augmentation de section des blocs. Une autre disposition, basée sur le même principe mais faisant usage de blocs non forés, a été envisagée; dans ce cas, les canaux sont créés par le retrait de certaines colonnes de graphite réparties selon un réseau régulier. Ce système a reçu le nom d'empilement lacunaire.

Des études ont été lancées concernant, d'une part, la possibilité de production de barres en graphite nucléaire de gros module, d'autre part, le comportement d'empilements lacunaires, notamment au moyen d'un montage expérimental de grandeur quasi réelle

* Commissariat à l'énergie atomique.

installé à Chinon, en coopération avec Electricité de France.

Les gradients de flux neutroniques et de température au travers d'un bloc de graphite sont susceptibles d'engendrer des contraintes (blocs de gros module) ou de provoquer des arcures (blocs d'empilement lacunaire), dont l'importance est en cours d'évaluation.

Le caisson

L'emploi de béton fretté, à Marcoule, dès 1956, a ouvert des perspectives nouvelles dans le domaine des caissons de réacteurs. Cette technique autorise des pressions notablement plus fortes qu'avec l'acier et, par conséquent, des puissances unitaires plus grandes, toutes choses restant égales par ailleurs.

Indépendamment des facilités de construction qu'il apporte incontestablement, le béton précontraint est aujourd'hui considéré comme offrant une sécurité supérieure à celle de l'acier. Tandis que le caractère monolithique d'un caisson métallique exige impérativement l'absence de tout défaut local, la résistance d'un caisson en béton précontraint est fournie par une multitude de câbles, généralement indépendants les uns des autres, de sorte que la rupture éventuelle de l'un d'eux n'aboutit qu'à une surcharge légère et très acceptable des câbles voisins. Sous réserve d'une étude sérieuse et d'une surveillance régulière en service, un caisson en béton précontraint peut être considéré comme inexplosible. Cet avantage a été jugé d'une telle importance qu'il a conduit à étudier l'intégration des échangeurs, des canalisations de CO₂ et des soufflantes dans le caisson contenant le cœur. Des études ont été entreprises en vue de comparer les différentes possibilités quant à la disposition relative du cœur et des échangeurs; compte tenu des commodités de construction du caisson, d'une part, des servitudes imposées par la manutention du combustible, d'autre part, il est apparu judicieux de placer les échangeurs sous le cœur; cette disposition, qui se concilie facilement avec l'inversion du sens de soufflage, a été adoptée sur le réacteur EDF4.

La manutention du combustible

La manutention du combustible reste un des problèmes majeurs des piles à graphite-gaz. Cette partie de l'installation est l'une des plus coûteuses et des plus délicates par l'ampleur des moyens mis en œuvre. C'est aussi celle qui a le plus de répercussions sur les conditions d'exploitation de la centrale.

Certes, avec la disposition proposée pour le réacteur, le problème est simplifié: le nombre des canaux à desservir est fortement réduit; l'inversion du sens de soufflage supprime tout système de contre-envol et permet aux mécanismes d'évoluer dans une ambiance relativement froide.

Par contre, la grande section des éléments combustibles annulaires, encore accrue par la présence de leurs chemises en graphite, conduit à des appareils dont les dimensions, le poids et la complexité s'accroissent

d'inquiétante façon, principalement lorsqu'on désire opérer pile en marche. Or, on sait que la France s'est résolument orientée dans la voie du renouvellement du combustible « pile en marche », qui procure un certain nombre d'avantages importants.

Par ailleurs, la trajectoire curviligne ou brisée imposée aux éléments combustibles dans les solutions classiques est peu satisfaisante à plusieurs égards (chocs, risques de fonctionnement intempestif du grappin, difficultés de ramonage d'un canal avarié. . .).

Cette situation nous a conduits à reconsidérer le problème sur des bases nouvelles et à proposer, dès 1957, un dispositif de manutention incorporé, caractérisé par l'emploi de mécanismes qui évoluent à l'intérieur même du caisson, dans un compartiment relativement froid (70 °C environ) situé au-dessus du cœur et appelé « grenier » [1]. Ainsi, la fonction de blindage est demandée au caisson lui-même. Une dalle de protection, percée d'un orifice en regard de chaque canal, constitue le plancher de ce grenier. Les orifices de cette dalle sont normalement obturés par des bouchons semi-étanches qui ont pour but de limiter les échanges d'atmosphère entre le cœur et le grenier et d'atténuer l'intensité des rayonnements susceptibles d'induire une certaine radioactivité dans les parois de ce dernier. Grâce aux dispositions prévues, l'accès au grenier devrait être possible 48 heures après l'arrêt de la pile.

Trois circonstances ont favorisé le développement de cette solution. Ce sont: l'adoption du béton précontraint pour la construction des caissons; l'augmentation de pas du réseau; l'inversion du sens traditionnel de soufflage.

Parmi les points originaux que comporte cette solution, citons le repérage des canaux au moyen d'un dispositif optico-électronique. Des mires portant un repère (nombre binaire) sont disposées auprès de chaque canal. Leur image est transmise au tableau de contrôle au moyen d'une caméra de télévision. Un dispositif électronique compare ces repères à un code préalablement inscrit en mémoire et la machine s'arrête lorsque la concordance est obtenue, la coïncidence des images autorisant du même coup le déclenchement des séquences suivantes. Des caméras d'ambiance, équipées d'objectifs grand angulaire, permettent de suivre le déroulement des opérations.

Les paniers contenant les éléments combustibles usagés séjournent quelque temps dans l'enceinte avant d'être évacués par l'un des deux sas prévus. Ceux-ci sont constitués chacun par un tube de diamètre inférieur à deux mètres et fermé à chacune de ses extrémités par des portes autoclaves qui ne peuvent en aucun cas être manœuvrées si les pressions ne sont équilibrées de part et d'autre; elles présentent donc une très grande sécurité intrinsèque. Du point de vue de leur étanchéité les conditions de température en cet endroit permettent l'emploi d'élastomères.

Un « robot », sorte de machine de dépannage, de conception simple, peut être introduit dans le grenier, sans arrêter le réacteur, pour intervenir en cas de besoin.

Les avantages procurés par le dispositif de manutention intégré sont nombreux :

a) Les machines, dépourvues de tout blindage, sont simples et rustiques. Leur mise en position ne nécessite aucun raccordement étanche amovible avec le réacteur. L'accessibilité aux organes mécaniques est plus grande que dans les machines conventionnelles en dépit des apparences. La modicité de leur prix permet d'envisager l'échange standard d'une machine défaillante contre une autre en bon état;

b) Les éléments combustibles suivent une trajectoire rectiligne au cours de leur manutention, ce que l'on doit considérer comme un avantage fondamental. Leur course est réduite au minimum;

c) L'évacuation par convection naturelle de la puissance résiduelle des éléments combustibles stockés dans l'enceinte ne pose aucun problème compte tenu des conditions ambiantes (pression élevée, température modérée);

d) Chaque manœuvre de sas intéresse un tonnage de combustible important (représentant la charge de cinq canaux);

e) Le réarrangement du combustible à l'intérieur d'un canal demeure une opération simple; la permutation entre canaux devient même possible avec une remarquable facilité;

f) Les bouchons de la dalle-plancher reposent sur leurs sièges par gravité; ils ne comportent aucun dispositif de verrouillage ni d'étanchéité;

g) Le recours à la télévision pour les repérages et verrouillages simplifie considérablement l'équipement des machines en supprimant tout contact électrique interne et en réduisant le nombre des conducteurs qui, autrement, seraient nécessaires pour acheminer les informations. Par ailleurs, l'exactitude des informations recueillies est indiscutable;

h) La télévision d'ambiance permet de travailler à vue, ce qui constitue un facteur psychologiquement très appréciable;

i) Le dépannage est possible commodément et en toutes circonstances.

Compte tenu de l'importance du sujet, le CEA a entrepris avec la participation d'EURATOM la construction d'une maquette en vraie grandeur qui fonctionne à Saclay depuis plusieurs mois. Les essais, menés à la pression atmosphérique et à la température ambiante, sont complétés par d'autres, d'envergure plus limitée, dans le CO₂ comprimé et chaud.

En dépit de son apparence révolutionnaire, le dispositif de manutention intégré ne fait appel, en réalité, qu'à des procédés industriellement éprouvés.

Au moment où les commodités offertes par le béton précontraint permettent d'envisager l'intégration des échangeurs dans le caisson, l'incorporation des machines de manutention du combustible ne fait que marquer un pas de plus dans la voie de l'intégration totale.

Les barres de contrôle

Le développement du dispositif de manutention intégré était subordonné à la possibilité de loger les

barres de contrôle et leurs treuils au-dessus du cœur sans entraver le mouvement des machines de chargement - déchargement. La solution a été trouvée dans l'emploi de chaînes en acier boré. Certains bouchons de la dalle-plancher du grenier sont conçus de manière à contenir le treuil de commande et la réserve de chaîne stockée en vrac.

Un treuil défaillant peut être remplacé à tout moment d'une manière très simple et sans nécessiter le dégonflage du caisson.

Conclusion

En résumé, le réacteur de demain de la filière graphite-gaz se présente, à l'heure actuelle, sous la forme d'un cœur à canaux verticaux de forte section, en nombre réduit, chargés d'éléments combustibles annulaires de forte puissance spécifique supportés par des chemises en graphite, refroidis par l'intérieur et par l'extérieur au moyen d'un courant de gaz inversé.

Le caisson, en béton précontraint, calculé pour résister à une pression de l'ordre de 50 bars, apparaît sous la forme d'une tour relativement haute, abritant le cœur, les échangeurs, les soufflantes et, dans un grenier, la machine de manutention du combustible, tandis que les barres de contrôle, constituées de chaînes absorbantes, sont actionnées par des treuils disposés dans le plancher du grenier.

FILIÈRE EAU LOURDE - GAZ

Les réacteurs de puissance, modérés à l'eau lourde et refroidis au gaz, constituent une filière si récente (la construction du prototype n'étant pas encore achevée) que l'on pourrait considérer toutes les structures possibles comme nouvelles.

Une brève revue des problèmes fondamentaux de la filière et des grandes options qu'elle présente permet cependant de concevoir les deux évolutions possibles des structures utilisées: l'une vers un réacteur voisin de EL4 mais à faible nombre de canaux et à concentration des circuits, l'autre vers des réacteurs apparentés à ceux de la filière graphite-gaz et qui en hériteraient les caractères essentiels: verticalité, caisson, intégration.

Caractères propres à la filière eau lourde - gaz

La conception des structures mécaniques des réacteurs de la filière eau lourde - gaz est dominée par des impératifs résultant directement de la définition de la filière.

a) Il convient de séparer le caloporteur gazeux du modérateur liquide; la séparation matérielle généralement appelée « tube de force » doit être complétée par une séparation thermique limitant les fuites de chaleur entre le gaz caloporteur chaud et le modérateur froid ou tiède. La température du gaz caloporteur à la sortie du canal étant incompatible avec la tenue du tube de force, l'isolant thermique doit être placé côté gaz de façon que la température du tube de force demeure voisine de celle du modérateur. Les cartouches doivent donc cheminer sur le calorifuge lors de leur renouvellement. L'ensemble constitué par le tube

de force et l'isolant thermique doit être aussi peu absorbant que possible; le perfectionnement des solutions actuelles est tributaire des progrès de la métallurgie. Néanmoins ces structures resteront relativement fragiles (faible épaisseur, médiocrité des qualités mécaniques des matériaux utilisés); il est donc nécessaire de pouvoir les entretenir, les réparer ou les remplacer sans travaux longs et coûteux. Cette dernière nécessité, jointe aux impératifs de montage et de mise en place, exerce une influence décisive sur la configuration du réacteur et contribue à la différencier de ceux de la filière graphite-gaz.

b) Hors le circuit principal de réfrigération, de nombreux petits circuits sont nécessaires pour l'épuration de l'eau lourde, son dégazage, la recombinaison des gaz radiolytiques, etc. A la puissance qui naît directement dans l'eau lourde (ralentissement des neutrons par exemple) vient s'ajouter celle qui, provenant du gaz, parvient à traverser l'isolation thermique; finalement le circuit de refroidissement du modérateur doit véhiculer 5 à 8% de la puissance de fission. Quoique thermodynamiquement dégradée, il paraît encore rentable de chercher à récupérer cette puissance pour la production d'énergie (réchauffage de l'eau d'alimentation par exemple).

c) L'eau lourde est un liquide coûteux qu'il convient d'employer avec une stricte économie. La relative indifférence des possibilités d'irradiation du combustible vis-à-vis de l'arrangement géométrique du réseau porte à choisir des pas de réseau assez faibles, de façon à réduire l'immobilisation d'eau lourde. La réalisation de ces faibles pas est l'un des impératifs essentiels auxquels doit satisfaire le réacteur; en cette voie et pour certaines solutions, nous verrons l'intérêt de l'utilisation éventuelle de réseaux rectangulaires.

Ces faibles pas exigent des structures peu encombrantes, difficiles à réaliser. Le problème est facilité par l'emploi de gros canaux à grandes contenances en combustible; on dispose ainsi d'un pas relativement plus grand favorisant l'assemblage et le choix de jeux convenables. Le prix des structures qui les composent (en grande partie proportionnel à leur nombre) est fortement diminué. Cette voie est bornée par l'accroissement du creusement de flux dans l'assemblage combustible et les difficultés de refroidissement qui en résultent.

d) Le renouvellement du combustible est un point crucial de cette filière qui vise les irradiations très élevées; il est nécessaire de disposer d'un ensemble de manutention permettant de déplacer, de retirer, de remplacer les éléments combustibles avec le minimum d'influence sur la marche du réacteur. Cela constitue une lourde sujétion. L'un des problèmes essentiels est celui du franchissement de l'enceinte sous pression; en cette matière on se dirige vers une grande simplification des dispositifs d'étanchéité, de fermeture et d'accrochage, à la limite vers leur disparition en utilisant un procédé de manutention du type grenier.

e) En limitant l'investissement d'eau lourde, on s'impose des puissances spécifiques élevées et, par suite, l'usage d'un caloporteur de chaleur volumique

satisfaisante. Pour le gaz, cela signifie l'emploi d'une pression assez forte croissant avec la tenue des matériaux. D'autres solutions à faible pression peuvent se révéler intéressantes (suspension de solides pulvérulents dans un gaz).

Options principales de la filière

Les principales directions possibles résultent de la combinaison des principales options, c'est-à-dire des choix faits pour résoudre chacun des problèmes essentiels exposés précédemment.

Chacune des directions envisagées est, bien entendu, susceptible de poser des problèmes particuliers en sus de ceux que nous venons de voir.

a) L'option la plus décisive est, sans aucun doute, celle qui concerne le choix de la forme du réservoir contenant le gaz caloporteur sous pression. Deux grandes classes se présentent: la solution « caisson » et la solution « tubes de force ».

La seconde est caractérisée par la limitation au strict minimum de l'enceinte contenant le gaz, les tubes de force étant dimensionnés de façon à résister mécaniquement à la totalité de la pression du gaz; c'est la solution retenue pour EL4. La première est au contraire caractérisée par le logement du réacteur et d'une partie plus ou moins étendue de ses annexes dans un réservoir dont les parois sont dimensionnées pour résister à la pression du gaz.

b) On peut penser que le défaut majeur de la solution caisson résulte de la dépendance étroite de la pression vis-à-vis du diamètre du caisson, et l'on n'a pas manqué d'affirmer que cette solution, parfaitement valable pour les petites unités, ne serait pas transposable aux réacteurs de grandes dimensions imposés par la philosophie de la filière (réduction des fuites neutroniques). Or, les études dérivées de celles menées pour la filière graphite-gaz montrent que cette crainte est vaine et que les grosses unités ne sont nullement incompatibles avec des caissons en béton résistant à des pressions élevées. Disons, pour préciser, qu'un réacteur destiné à procurer une puissance électrique de 1 000 MW se loge aisément dans un caisson résistant à une pression supérieure à celle employée pour EL4. Cette conclusion est valable pour un dispositif de manutention du combustible n'exigeant qu'un faible nombre d'ouvertures dans le caisson, mais il n'est pas exclu qu'on puisse l'étendre au cas limite où le caisson présenterait un orifice de déchargement en regard de chaque canal.

c) Ce préjugé étant dissipé, il convient de jauger les avantages immédiats procurés par l'emploi du caisson et de préciser les problèmes qu'il pose.

La diminution d'épaisseur du tube de force qui n'est plus soumis à la totalité de la pression du gaz procure un gain de réactivité appréciable, mais moins important qu'il ne paraît de prime abord. Il doit, en effet, résister encore aux variations de pression des circuits de gaz et d'eau lourde (pression hydrostatique, perte de charge); finalement, on peut escompter une réduction de moitié.

La disposition à tubes de force résistants entraîne une complication particulière visant à autoriser sans contraintes excessives les dilatations différentielles, qui ont leur origine dans l'écart de température entre le gaz et l'eau lourde: la cuve contenant l'eau lourde définit le pas du réseau tandis que les canaux sont liés à un circuit de gaz carbonique chaud. Un tel système, qu'il fasse usage d'isolations internes ou d'organes élastiques (dont les plus communs sont les tubulures de faible diamètre), est toujours coûteux, délicat et long à mettre en place. La solution caisson procure de ce point de vue un gain important encore majoré par les simplifications permises pour la cuve d'eau lourde, libérée des efforts exercés par les canalisations de gaz.

d) Un autre groupe d'avantages se rattache au précédent: il concerne les conséquences de la défaillance du circuit de gaz.

Dans le cas où les tubes de force contiennent la totalité de la pression du gaz, la rupture de l'un d'eux entraîne l'irruption soudaine du gaz dans la cuve où apparaît une surpression momentanée; la cuve doit donc être dimensionnée de façon à résister à cette pression, et des organes de séparation de l'émulsion eau - gaz doivent être prévus. Toute cette complication disparaît lorsqu'on emploie un caisson [2].

Il convient également de considérer les conséquences de la rupture éventuelle d'un gros collecteur de gaz: ce sont elles qui conduisent à loger l'installation dans une enceinte étanche. L'intégration du circuit caloporteur dans le caisson, contenant le cœur, permet de s'aligner sur la filière graphite - gaz, et de faire l'économie de l'enceinte étanche.

e) A ces avantages, s'ajoute, bien entendu, la possibilité de coordonner les études de développement des deux filières à gaz, qu'elles soient modérées au graphite ou à l'eau lourde. Cependant, l'utilisation de l'eau lourde dans une disposition intégrée pose, comme nous l'avons vu, certains problèmes qu'il est bon d'examiner à nouveau. La pression et les températures visées pour la filière eau lourde sont de nature à compliquer la réalisation des accessoires internes du caisson: la pression aggrave le problème de l'isolation thermique du béton et la température entraîne l'usage, dans les zones chaudes, d'aciers résistant au fluage et à la corrosion par le gaz carbonique qui sont plus coûteux et d'une mise en œuvre plus délicate.

L'installation dans le caisson d'une structure compliquée, encombrante et fragile destinée à contenir l'eau lourde et à l'isoler matériellement et thermiquement du gaz pose également un problème. Le montage, le contrôle et la vérification d'une telle structure sont incontestablement longs et délicats; mais l'essentiel du problème est dans la nécessité d'en pouvoir assurer l'entretien, la réparation et le remplacement éventuel après le fonctionnement du réacteur. En l'état de la technologie des structures, on ne peut considérer que les dispositions présentant les dégagements indispensables à ces opérations, ce qui ne va pas sans majorer le coût de l'installation. Le choix concomitant de la manutention du combustible par une seule extrémité accentue grandement cette nécessité

par suite du risque de destruction que courent les structures en cas de lâcher intempestif de l'élément combustible par le grappin de manutention.

Pour bénéficier des avantages du caisson, il faut que l'eau lourde et le gaz carbonique soient à des pressions voisines; il apparaît en conséquence un problème d'équilibrage de ces deux pressions. Cet équilibrage ne paraît pas pouvoir être réalisé par simple contact des deux fluides avec niveau libre; il serait difficile, dans ces conditions, de contrôler efficacement la teneur en humidité du gaz caloporteur, d'où des risques accrus de corrosion: il paraît non moins difficile d'assurer un faible taux de radiolyse et une épuration bon marché avec de l'eau lourde saturée par du gaz carbonique en solution à pression élevée. L'équilibre étant maintenu, tout le circuit d'eau lourde se trouve à haute pression; aussi pour éviter d'accroître sensiblement son prix, d'une part, et de risquer qu'une fuite soit catastrophique, d'autre part, on est conduit à placer la plus grande partie de ce circuit dans le caisson.

f) Une autre option importante a trait à l'orientation des canaux, qui peuvent être horizontaux ou verticaux. L'horizontalité permet d'accéder à un canal par ses deux extrémités et autorise une circulation équicourant du combustible, ce qui entraîne de nombreux avantages (absence de canaux vides à certains moments, homogénéité des irradiations, absence de cyclages thermiques, disposition du combustible le plus irradié dans les zones les plus froides).

En revanche, cette disposition implique des contraintes supplémentaires sur les structures (écrasement de l'isolant thermique par le poids des éléments combustibles, flexion du tube de force à la fois sous l'influence du refroidissement non homogène par l'eau et du poids des éléments). Les contraintes provoquées de ce chef sont particulièrement importantes pour les tubes minces de la solution intégrée dans un caisson, ce qui nous conduit à ne retenir, dans ce cas, que la disposition verticale, nous rapprochant ainsi de la filière graphite - gaz, malgré les inconvénients que cela présente pour le combustible.

Deux directions pour les structures nouvelles

Cette analyse des problèmes fondamentaux et des types de solutions qu'ils peuvent recevoir montre le vaste champ de possibilités offert à la filière. Néanmoins, deux types principaux se dégagent, qui correspondent d'ailleurs à des cheminements historiques très caractérisés. L'un, à tubes de force horizontaux alimentés par des tubulures souples et qui découle simplement du perfectionnement, du développement des éléments utilisés pour EL4. L'autre, à caisson résistant, équipé de canaux verticaux, avec un circuit de gaz et un système de manutention du combustible totalement intégrés et qui naît de la transposition des techniques évoluées décrites à propos de la filière graphite - gaz.

Examinons rapidement, pour terminer, les principaux traits caractéristiques de ces deux évolutions possibles.

a) La technique des tubes de force horizontaux évoluera, bien entendu, avec les fortes puissances; on doit, à ce sujet, noter que l'augmentation de la puissance ne s'accompagne pas d'un grossissement notable de l'installation. L'évolution de la technique sera surtout sensible sur les points suivants:

i) Le relèvement des contraintes admissibles dans les tubes de force (par perfectionnement du matériau et du mode d'élaboration du tube) conduira à majorer la pression utilisée; on évoluera donc vers un circuit présentant des conduits de diamètre relativement petit, compacts et peu encombrants;

ii) Les tubulures d'alimentation individuelles seront plus compactes et plus simples [4]; elles seront quasi planes et leur montage sera réalisé rapidement grâce à une certaine préfabrication. Leurs caractéristiques aérodynamiques seront améliorées, l'accroissement de leur diamètre rendu possible par l'adoption d'un pas rectangulaire sans augmenter la quantité d'eau lourde immobilisée;

iii) Les canaux immobilisés seront proportionnellement moins nombreux et contiendront une masse plus importante de combustible. Les tubes de force seront ainsi beaucoup plus résistants en flexion; l'absorption parasite de l'isolation thermique sera diminuée ainsi que celle correspondant aux tolérances de fabrication. On diminuera, surtout, le nombre des canaux et, par là, les investissements correspondants;

iv) Le modérateur sera à une température plus élevée grâce à la mise en pression hydrostatique de l'eau lourde (cela implique que la cuve autorise la dilatation différentielle entre la virole et les tubes de force); on pourra alléger le circuit, diminuer la quantité d'eau lourde qu'il immobilise et récupérer l'énergie contenue dans l'eau lourde.

b) Le type « intégré » présente pour l'essentiel de son architecture les principes constructifs exposés dans la première partie de ce texte à propos de la filière graphite-gaz (caisson en béton précontraint, verticalité des canaux, intégration des échangeurs et des machines de déchargement). Nous pouvons donc nous limiter à examiner rapidement comment cette adaptation peut être effectuée [3].

L'équilibrage de pression se fera par des pots

spéciaux où un piston flottant séparera les deux fluides, ces pots d'équilibrage seront placés sur les circuits d'épuration en amont des dispositifs d'épuration proprement dits; on pourra sans danger les placer extérieurement au caisson ainsi que tous les petits circuits.

Le circuit principal d'eau lourde sera intégré, les échangeurs et les pompes étant placés dans le grenier de grande hauteur contenant la machine de maintenance, et d'où l'on pourra remplacer les tubes de force et les isolants thermiques.

Le bouclier intermédiaire ne supportera pas la cuve qui sera suspendue au bloc tubulaire supérieur par les goulottes de guidage prolongeant les canaux. Ce bouclier pourra donc être exécuté assez grossièrement à partir d'aciers au chrome, probablement non soudables, la mise en œuvre s'effectuant par assemblages mécaniques; la protection proprement dite exigera acier et graphite nucléaire du fait des risques de corrosion. Par contre, les amortisseurs-crêpines des pieds de canaux seront supportés par ce bouclier (le fond mince de la cuve ne pouvant résister à la chute éventuelle d'un élément combustible).

Les dimensions et les poids des différents éléments: échangeurs, bouclier, cuve, bloc tubulaire, permettent leur mise en place à l'état fini dans le caisson à l'aide de moyens de levage comparables à ceux mis en œuvre pour la filière graphite-gaz.

On voit ainsi comment les deux filières considérées ici sont susceptibles d'évoluer et comment cette double évolution laisse entrevoir la possibilité d'une unification de techniques, au départ très différentes.

BIBLIOGRAPHIE

1. Bazin, L., et Martin, R., *Problèmes mécaniques rencontrés dans les réacteurs de centrales appartenant à la filière graphite-gaz*, tiré à part BIST n° 79.
2. Roche, R., Vrillon, B., et Hareux, F., *Etude expérimentale des conséquences de la rupture d'un tube de force dans la cuve d'un réacteur modéré à l'eau lourde et refroidi au gaz*, rapport CEA à paraître.
3. Gaudet, J. C., et Roche, R., *Conception générale et principaux problèmes d'un réacteur de puissance « eau lourde-gaz » contenu dans un caisson résistant*, rapport CEA à paraître.
4. Aubert, G., Hassig, J. M., Laurent, N., Peuchmaur, A., et Thomas, B., *Perfectionnements au système d'alimentation en gaz des canaux d'un réacteur modéré à l'eau lourde*, rapport CEA à paraître.

ABSTRACT—RÉSUMÉ—АННОТАЦИЯ—RESUMEN

A/51 France

Study of new structures adapted to gas-graphite and gas-heavy-water reactors

By R. Martin and R. Roche

The experience acquired as a result of the operation of the Marcoule reactors and of the construction and start-up of the EDF reactors on the one hand, and the conclusions of research and tests carried out out-of-pile on the other hand, lead to a considerable change

in the general design of reactors of the gas-graphite type.

The main modifications envisaged are analysed in the paper. The adoption of an annular fuel element and of a down-current cooling will make it possible to increase considerably the specific power and the power output of each channel; as a result there will be a considerable reduction in the number of the channels and a corresponding increase in the size of the unit cell. The graphite stack will have to be adapted to

these new conditions. For security reasons, the use of prestressed concrete for the construction of the reactor vessel is becoming more widespread; they could lead to the exchangers and the fuel-handling apparatus becoming integrated inside the vessel (the so-called "loft" device). A full-size model of this loft has been built at Saclay with the participation of EURATOM; the operational results obtained are presented as well as a new original design for the control rods.

As far as the gas-heavy-water system is concerned, the research is carried out on two points of design; the first, which retains the use of horizontal pressure tubes, takes into account the experience acquired during the construction of the EL4 reactor of which it will constitute an extrapolation; the second, arising from the research carried out on the gas-graphite system, will use a prestressed concrete vessel for holding the pressure, the moderator being almost at the same pressure as the cooling fluid and the fuel being placed in vertical channels.

The relative merits of these two variants are analysed in the present paper.

A/51 Франция

Изучение новых конструкций, принятых для реакторов с графитовым замедлителем и газовым охлаждением и тяжеловодных реакторов с газовым охлаждением

Р. Мартен, Р. Рош

Опыт, накопленный при эксплуатации реакторов в Маркуле, строительство и пуск реакторов фирмы Электрисите де Франс, с одной стороны, и результаты исследований и испытаний, проводившихся вне реактора, с другой стороны, ведут к значительному изменению конструкции графитовых реакторов с газовым охлаждением.

В докладе дается анализ основных намеченных модификаций. Применение кольцевого тепловыделяющего элемента и нисходящей воздушной струи позволят значительно увеличить удельную мощность и мощность на канал; это приведет к значительному сокращению числа каналов и соответствующему увеличению отверстий решетки. Для этих новых условий необходимо принять использование графита. Соображения безопасности ведут к использованию предварительно напряженного бетона для строительства оболочек, что может позволить устанавливать внутри оболочек теплообменники и машины для перегрузки топлива (устройство, называемое «чердачным»). В Сакле при участии Евратома был построен макет такого «чердака» в натуральную величину. Приводятся результаты эксплуатации, а также новые оригинальные конструкции регулирующих стержней.

нальные конструкции регулирующих стержней.

Для тяжеловодного реактора с газовым охлаждением исследования проводятся по двум главным направлениям: 1) сохранение использования горизонтальных трубок, работающих под давлением, с учетом опыта строительства реактора EL-4; 2) на основе исследований, выполненных для графитовых реакторов с газовым охлаждением, следует прибегнуть к использованию корпусов из предварительно напряженного бетона для сохранения давления, причем замедлитель будет находиться почти под таким же давлением, что и теплоноситель, а топливо будет размещаться в вертикальных каналах.

В докладе анализируются относительные преимущества этих двух вариантов.

A/51 Francia

Estudio de nuevas estructuras adaptadas a los reactores grafito-gas y agua pesada-gas por R. Martin y R. Roche

La experiencia adquirida con la explotación de los reactores de Marcoule, la construcción y la primera etapa de funcionamiento de los reactores EDF por una parte, y las conclusiones de los estudios y ensayos efectuados fuera de los reactores por otra, originan grandes cambios en los reactores del tipo grafito-gas.

En la memoria se analizan las principales modificaciones consideradas. La adopción de un elemento combustible anular y el soplado descendente permitirán aumentar considerablemente la potencia específica y la potencia desarrollada por canal, con lo que resultará una reducción sensible del número de canales y un aumento correlativo del paso de la red; y habrá que adaptar la estructura de grafito a estas nuevas condiciones. Razones de seguridad obligan a generalizar el empleo del hormigón pretensado para la construcción de las vasijas de presión. Por las mismas razones se podrá llegar a introducir en el interior de éstas los cambiadores de calor y la máquina de carga y descarga del combustible (disposición que en Francia llaman « en desván »). En Saclay se ha construido, con la participación de EURATOM, una maqueta a tamaño natural de este « desván ». Se presentan los resultados de su explotación así como unos esquemas de barras de control de nueva concepción.

En lo que se refiere al tipo de reactores de agua pesada-gas, se continúan los estudios en dos direcciones principales. La primera, en la que se seguirán empleando tubos de presión horizontales, se basa en la experiencia adquirida durante la construcción del reactor EL4, y constituye una extrapolación del mismo. En la segunda, inspirada en los estudios que se han continuado realizando sobre el tipo grafito-gas, se recurre a una vasija de presión de hormigón pretensado para soportar la presión, estando el moderador sensiblemente a la presión del refrigerante y el combustible dispuesto en canales verticales.

En la memoria se analizan las ventajas respectivas de estas dos variantes.

Les circuits de gaz carbonique dans les centrales nucléaires

par E. Robert, J. Hustache et P. Sevin*

Il n'est pas dans notre intention d'aborder ici, dans sa généralité, l'étude des problèmes de conception et de réalisation des matériels constituant les circuits primaires de CO₂ des centrales nucléaires d'Electricité de France. Nous essaierons seulement de dégager les impératifs auxquels doivent satisfaire les matériels les plus caractéristiques. De ce fait, nous n'aborderons que les matériels les plus importants, c'est-à-dire les échangeurs et les groupes de soufflage et pour une moindre part les organes de dilatation et d'isolement.

D'autre part, nous sacrifierons volontairement la description des installations afin de mettre en évidence les évolutions subies par ce genre de matériel ainsi que les avantages et les inconvénients des différentes solutions adoptées. Les caractéristiques essentielles des échangeurs de chaleur et des groupes de soufflage sont données dans le tableau 1.

Dans la filière uranium naturel-gaz-graphite, Electricité de France a en exploitation, en cours de démarrage ou en construction les centrales dénommées EDF1, EDF2, EDF3 et EDF4.

Une évolution importante dans les dispositions générales des circuits primaires de CO₂ permet d'adopter une classification naturelle, suivant que ces circuits sont incorporés ou non dans une seule et même enceinte. Ainsi les centrales EDF1, EDF2 et EDF3 appartiennent à la conception avec circuit primaire non incorporé, alors que EDF4 est conçue avec un circuit primaire incorporé.

Cette évolution très remarquable et qui tend à se généraliser a pour objectif principal la recherche d'une sécurité accrue principalement vis-à-vis des conséquences de l'accident maximal. Cette disposition présente en outre l'avantage de rendre les installations plus compactes et devrait logiquement conduire à un abaissement notable du coût d'investissement.

L'incorporation du circuit primaire de CO₂ a conduit à apporter de très larges modifications à la conception, à la fabrication et au montage des différents matériels constitutifs de celui-ci; c'est le cas des réchangeurs de chaleur et des groupes de soufflage. Elle permet en outre la suppression de certains matériels tels que les organes de dilatation et d'isolement.

LES ÉCHANGEURS DE CHALEUR

Ils ont pour rôle le transfert des calories du fluide primaire au fluide secondaire. Ils doivent assurer cette fonction en réalisant une étanchéité totale entre les circuits primaire et secondaire, tout en constituant naturellement un volant thermique important nécessaire à une bonne protection du réacteur contre les chocs thermiques.

Il y a lieu tout d'abord de remarquer que les quantités de chaleur à transmettre sont importantes étant donné la taille adoptée pour les réacteurs, et que, d'autre part, pour la filière qui nous intéresse, il est demandé aux échangeurs de réaliser le transfert de calories avec des écarts de température réduits et à l'aide d'un fluide primaire de densité relativement faible conduisant à des débits importants. Cet ensemble de considérations conduit, lors de la réalisation, à la mise en œuvre de surfaces d'échanges très importantes, ce qui fait que le prix d'un échangeur représente une part non négligeable du coût total de l'investissement.

Le problème de la recherche d'un optimum se pose donc d'une manière impérative au maître de l'œuvre et au constructeur. Cet optimum concourt :

a) A la recherche du meilleur rendement de transfert de chaleur: cycle thermodynamique le mieux adapté (choix du nombre d'étages de pression et détermination des écarts optimaux d'échanges), coefficient de transfert calorifique le meilleur;

b) A la détermination de la perte de charge à admettre, sans omettre pour autant les impératifs de construction de montage et de transport.

La prise en considération de cet ensemble de réflexions explique à elle seule l'évolution imprimée à la conception des échangeurs utilisés en France. C'est ainsi que, pour ce qui est des centrales à *circuit primaire non incorporé* (EDF1, EDF2, EDF3), l'évolution de la conception des échangeurs peut être examinée essentiellement sous trois aspects :

1. Il a été recherché, d'une manière générale, un compromis entre l'utilisation d'un cycle thermodynamique ayant le meilleur rendement et une réalisation simple. Différents processus ont été considérés et il a été estimé qu'un des plus simples de mise en œuvre était la multiplication du nombre d'étages de pression de vapeur. Pour EDF1 et EDF2,

* Electricité de France.

Tableau I. Caractéristiques des échangeurs et des soufflantes des centrales EDF1, EDF2, EDF3 et EDF4

	Unités	EDF1	EDF2	EDF3	EDF4
I. Echangeurs					
Nombre de tours en parallèle	—	120	96	192	Intégré (30)
Poids d'une tour élémentaire	t	18	40	16,3	80
Puissance thermique	MW	300	781	1 620	1 650
Caractéristiques du CO ₂ :					
Pression	bars	25	25	25	25
Température d'entrée	°C	355	365	410	400
Température de sortie	°C	140	192,5	233,7	220
Débit	t/s	1,590	4,300	8,500	8,200
Pertes de charge	bars	0,325	0,260	0,360	0,450
Caractéristiques de la vapeur HP:					
Pression ballon	bars	21,3	32,6	52,5	36,6
Température	°C	342	340	400	390
Débit	kg/s	79,75	191	574	576
Caractéristiques de la vapeur BP:					
Pression	bars	4,3	8,73	—	—
Température	°C	215	340	—	—
Débit	kg/s	29,6	104,4	—	—
Caractéristiques de la vapeur resurchauffée:					
Pression	bars	—	—	32	—
Température	°C	—	—	400	—
Débit	kg/s	—	—	287	—
Température de l'eau d'alimentation	°C	77	90,5	118,3	88
Surface totale d'échange	m ²	39 000	43 000	87 000	174 000
Constructeurs	—	a	b	c	d
II. Soufflantes					
Nombre de soufflantes	—	1	4	4	4
Débit de CO ₂	t/s	1,59	1,075	2,125	2,05
Pression d'aspiration	bars	25	25	25	25
Pression de refoulement	bars	26,6	26,3	26,6	26,7
Température d'aspiration	°C	140	192,5	233,7	220
Température de refoulement	°C	145,4	198,1	240	226
Rendement global	%	86	85	85	82
Vitesse de rotation	tr/mn	2 980	2 910	3 300	2 850
Puissance à l'accouplement	kW	9 180	5 760	14 300	16 000
Mode d'entraînement	—	Moteur élect.	Moteur élect.	Turbine vapeur	Turbine vapeur
Mode de réglage de vitesse	—	Directrices orientables	Coupleur hydraul.	Turbine vapeur	Turbine vapeur
Constructeurs	—	Sulzer	CEM	Rateau	Sulzer

^a Compagnie des surchauffeurs.

^b Babcock et Wilcox, Chantiers de l'Atlantique, Fives Lille; Compagnie des Surchauffeurs.

^c Fives Penhoët, Chantiers de l'Atlantique, Fives Lille; Babcock et Wilcox.

^d Sulzer, Stein et Roubaix, Alsthom.

il a été adopté un cycle à deux étages de pression avec utilisation de motosoufflantes. Pour EDF3, de puissance très supérieure, cette position a dû être reconsidérée par suite de l'accroissement de la puissance unitaire de soufflage nécessitant l'entraînement des soufflantes par turbines à vapeur. En définitive, il a été choisi un cycle avec resurchauffe du débit total de vapeur qui s'accommode bien de cette disposition. Tous ces échangeurs fonctionnent suivant le principe de la circulation naturelle. Cette disposition permet de faire appel à des techniques classiques pour la régulation de l'alimentation en eau.

2. Les échangeurs de chaleur des centrales EDF1, EDF2 et EDF3 ont été divisés en un grand nombre d'unités complètes (fig. 1). Une telle disposition permet: a) la fabrication en usine d'unités complètes, le montage sur place étant ainsi grandement facilité; b) des manutentions faciles à tous les stades de la

fabrication, du transport et du montage; c) un contrôle de fabrication plus aisé de ces unités; d) la possibilité d'une fabrication en série; e) un traitement plus aisé des surfaces.

Cette subdivision poussée a aussi permis d'obtenir d'autres avantages qui sont la possibilité: en exploitation, d'isolement partiel en cas d'avarie; d'effectuer des essais dans les conditions réelles de fonctionnement sur élément prototype, ces essais étant effectués avant la mise en fabrication de série.

Il apparaît qu'ainsi une solution simple a été trouvée aux problèmes de construction, transport et montage ainsi que de sécurité d'exploitation.

3. Il a été recherché d'une manière constante, par les différents constructeurs, des améliorations dans les domaines suivants:

a) Rendement d'échange par l'adoption de profils de surface toujours mieux adaptés. C'est ainsi que les

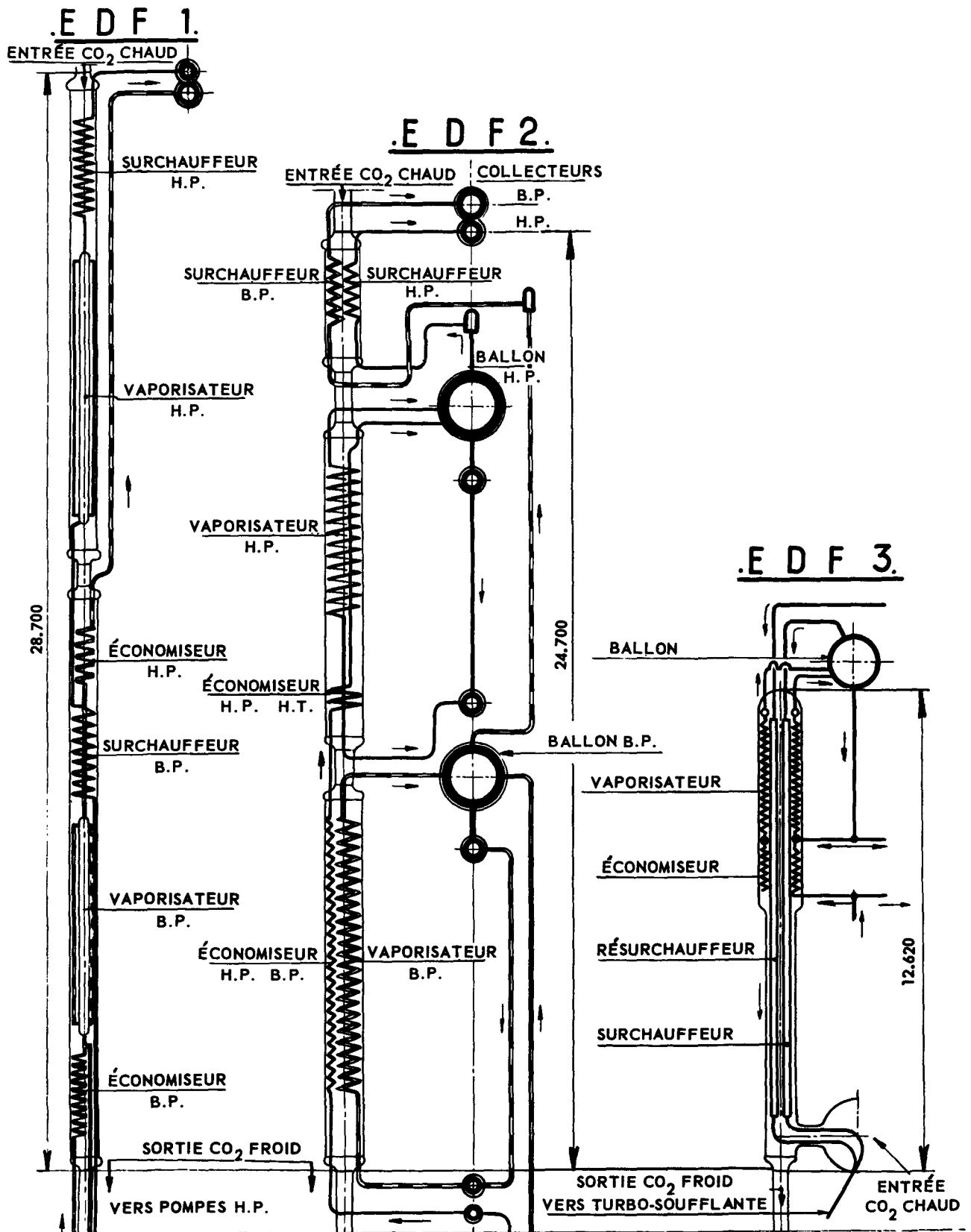


Figure 1. Echangeurs; coupe schématique d'un élément

tubes lisses constituant principalement au départ les surfaces d'échanges ont été remplacés progressivement par des tubes à ailettes de différents profils;

b) Utilisation meilleure des volumes disponibles;

c) Traitement de surface mieux adapté et plus efficace.

Les échangeurs du type à *circuit primaire incorporé* voient leur première réalisation en France pour la centrale EDF4.

Pour une centrale nucléaire avec générateur de vapeur intégré, le constructeur est amené à résoudre des problèmes nouveaux et particuliers qui ne se posent pas dans les installations nucléaires où le générateur de vapeur est placé à l'extérieur de l'enceinte. En effet, dans le cas où réacteur et générateur sont montés séparément, les dimensions de ce dernier peuvent être fixées avec une certaine latitude. Par contre, pour un système intégré, les dimensions du générateur sont tributaires de celles du réacteur. Lorsque les deux unités sont superposées (cas d'EDF4), on doit chercher à adapter le diamètre du générateur à celui du réacteur, ce qui restreint les possibilités de conception. En outre, pour un générateur de vapeur intégré, tout particulièrement dans un caisson en béton précontraint, il est impératif de réduire le nombre de pénétrations nécessaires pour les conduites d'eau d'alimentation et de vapeur. C'est pourquoi, compte tenu de cet ensemble de considérations, il a été adopté un générateur de vapeur monotubulaire qui présente la meilleure solution appropriée, étant donné l'absence de ballons de vapeur et de collecteurs de dimensions importantes dont la présence à l'intérieur du caisson est nuisible à la sécurité de l'installation.

D'autre part, toujours pour les mêmes raisons, le cycle de vapeur a été choisi le plus simple possible, c'est-à-dire un cycle thermodynamique à un seul étage de pression de vapeur, sans resurchauffe.

Enfin, l'adoption d'un générateur de vapeur de conception monotubulaire pose, lors des études de fonctionnement, des problèmes de régulation qui ont pu être correctement résolus.

Description succincte des échangeurs de chaleur

Les générateurs de vapeur des centrales EDF1, EDF2 et EDF3 ne présentent pas de particularités marquantes; c'est pourquoi il n'en est pas entrepris de description; par contre, nous décrivons succinctement ci-après les échangeurs d'EDF4, qui sont d'une conception nouvelle.

Les générateurs de vapeur d'EDF4 occupent un volume cylindrique ayant 15,5 m de diamètre et 10 m de hauteur. Ils sont constitués de 26 tours standards et de 4 demi-tours (fig. 2). Chaque tour comprend un certain nombre de panneaux tubulaires formés d'un seul tube aileté continu entre les distributeurs d'eau d'alimentation et les collecteurs de vapeur; chaque faisceau composant une tour est formé par l'imbrication de 4 circuits indépendants. En alternant ainsi 4 circuits vapeur indépendants les uns des autres à l'intérieur du caisson, il est possible d'effectuer, en cas d'incident sur l'un d'entre eux, son isolement, afin que,

de toute manière, le fonctionnement de la centrale à charge réduite soit assuré et qu'en toute circonstance le refroidissement du réacteur soit suffisant. Pour ce faire, chaque circuit peut être isolé de l'extérieur du caisson, les autres restant en service normal. Pour ce qui est du montage, il est à noter que l'ensemble (y compris les charpentes) a été conçu de façon à pouvoir être mis en place en six semaines.

L'ampleur du problème que pose la réalisation d'échangeurs de chaleur et l'importance de celui-ci expliquent l'effort exceptionnel effectué par Electricité de France afin de parvenir, dans tous les cas, à la solution la plus valable. C'est pourquoi, en particulier, il est réservé une grande part aux essais intervenant, soit au stade du projet, soit à celui de la réception: car c'est finalement l'intérêt commun du maître d'œuvre et du constructeur que d'installer des échangeurs dont les caractéristiques de fonctionnement soient les plus proches de celles recherchées.

Dans cet esprit, EDF a construit une « station d'essais ». Grâce à celle-ci, vraisemblablement unique en son genre, il a pu être essayés les prototypes d'EDF1, d'EDF2, d'EDF3 et d'EL4 (et sera sous peu essayée EDF4) avant que ne débute la fabrication de série. Il y a lieu de remarquer que, indépendamment de leur intérêt sur le plan contractuel, ces essais permettent aux constructeurs de réaliser des progrès appréciables en ce domaine.

Cette politique trouve sa pleine justification lorsque l'on considère l'évolution du coût des échangeurs. La réduction constatée résulte de l'action sur plusieurs facteurs qui sont: principalement, la conception d'ensemble de la centrale; également la conception particulière des échangeurs; ainsi que la fabrication proprement dite de ceux-ci.

LES SOUFFLANTES

Le débit-poids de gaz nécessaire au refroidissement des réacteurs de puissance de la filière gaz-graphite est très important. Il s'ensuit que les puissances absorbées par les soufflantes sont considérables (de l'ordre de 10% de la puissance nette de l'installation). De plus, le fonctionnement de ces machines est étroitement lié à celui du réacteur et conditionne même celui-ci.

Dans ces conditions, les soufflantes (non susceptibles de la duplication classique normale-secours) ne doivent pas être considérées comme de simples organes auxiliaires, mais au contraire comme des organes tournants vitaux devant présenter une grande sûreté de fonctionnement. Cette condition est difficile à atteindre, d'autant plus que la température de fonctionnement de ces machines est déjà assez élevée — de l'ordre de 200 à 250 °C — et que celles-ci véhiculent du gaz radioactif sous pression. De ce fait, leur étanchéité vers l'extérieur devra être absolue, notamment au droit des traversées d'arbre de transmission.

Ces machines peuvent être de différents types: axial à un seul étage centrifuge, hélico-centrifuge, chacun de ces types présentant des avantages particuliers. Le type axial a été retenu pour les centrales de

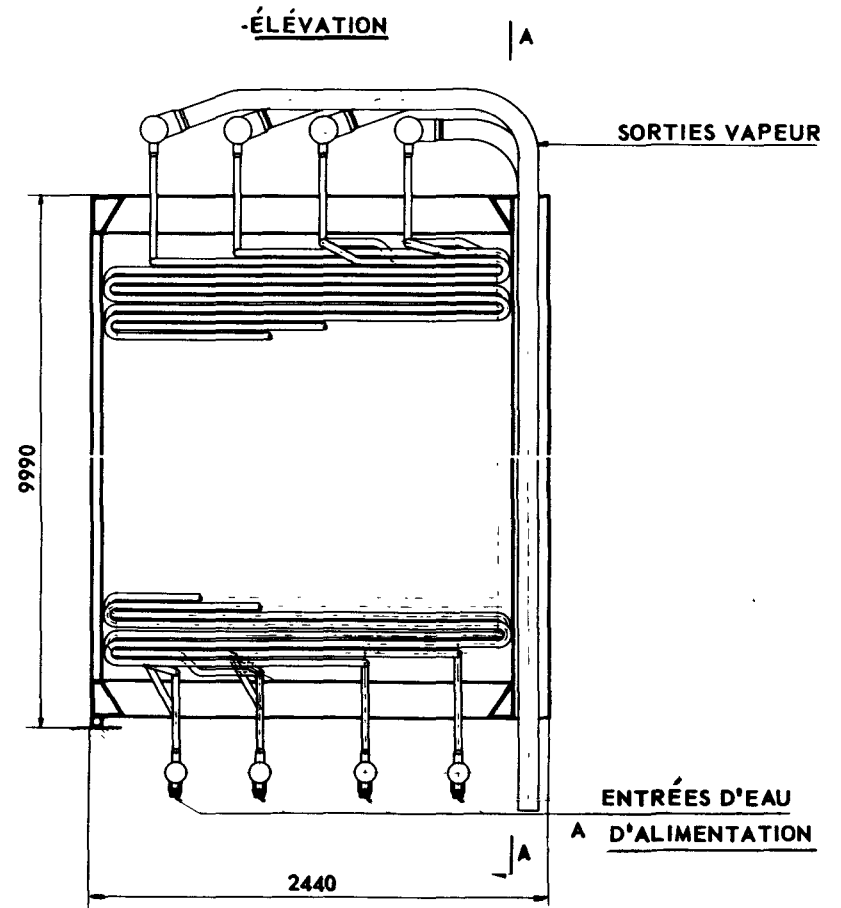
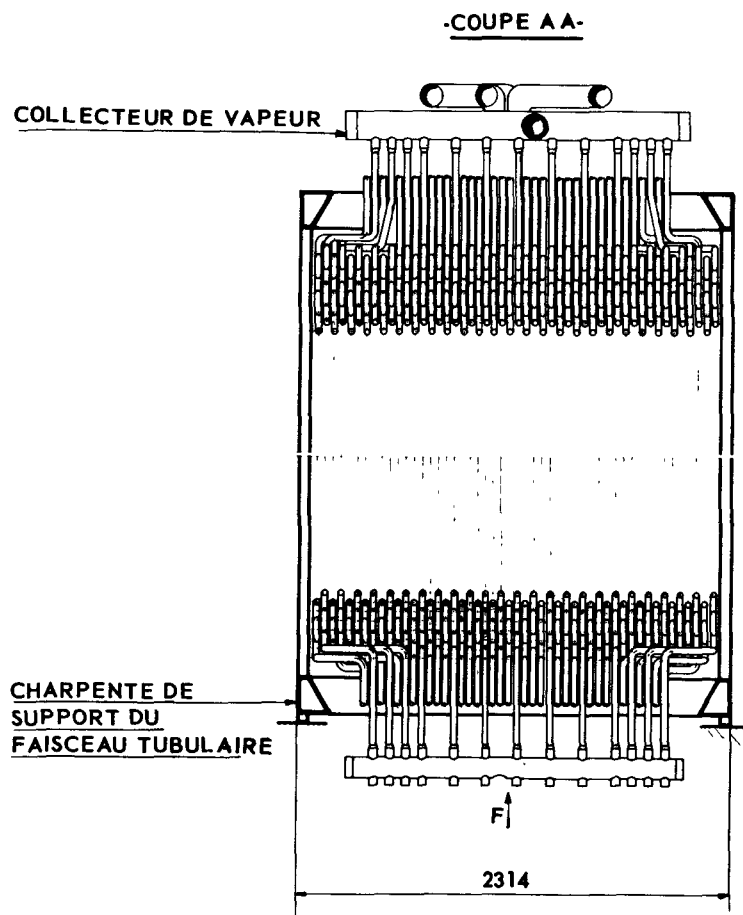


Figure 2. Echangeurs EDF4

Chinon, EDF1, EDF2, EDF3, et de Saint-Laurent-des-Eaux (EDF4) pour les raisons suivantes:

a) Possibilité d'adaptation aux caractéristiques réelles du circuit primaire, car, d'une part, les caractéristiques de celui-ci sont évaluées avec une certaine marge d'imprécision lors de l'établissement du projet, et d'autre part, le réacteur est chargé d'éléments combustibles dont les caractéristiques sont susceptibles d'évolution au cours de la vie de la centrale. Les soufflantes axiales permettent facilement cette adaptation par modification du calage des pales mobiles, la machine étant à l'arrêt;

b) Facilité d'installation. Ces machines se prêtent bien à une implantation à axe horizontal avec répartition des tubulures d'entrée et de sortie symétrique. Leur encombrement est réduit du fait que leur vitesse optimale se situe à une valeur déjà assez élevée.

L'étude et l'amélioration des conditions aérodynamiques d'écoulement du gaz dans les machines du type axial ont permis d'atteindre des valeurs de rendements élevées, de l'ordre de 0,85.

L'entraînement des machines est effectué pour EDF1 et EDF2 par des moteurs électriques asynchrones, et la simplification du schéma de l'installation et la facilité de conduite qui en résultait ont justifié ce choix. L'augmentation des puissances de soufflage, le désir de réaliser des groupes de puissance unitaire élevée, la difficulté de réalisation de moteurs électriques très puissants et les problèmes posés par leur démarrage ont conduit par la suite à s'orienter vers un entraînement des soufflantes par turbines à vapeur, pour lesquelles aucune limitation de puissance n'intervient. Cette solution a été adoptée pour EDF3 et EDF4.

De plus, l'entraînement par turbine à vapeur permet de réaliser le réglage du débit de CO_2 du circuit par variation de vitesse du groupe turbo-soufflante. Dans les solutions à moteurs électriques, cette variation de débit peut être obtenue de différentes façons:

a) Utilisation d'un ensemble d'aubes prédirectrices orientables équipant la soufflante: solution adoptée pour EDF1;

b) Utilisation d'un coupleur hydraulique intercalé entre moteur et soufflante: solution adoptée pour EDF2;

c) Utilisation de pales mobiles orientables en marche. Ce mode de réglage (qui permet de surcroît une adaptation immédiate de la machine aux caractéristiques du circuit) a été essayé en endurance durant 4 000 heures sur une machine prototype représentative d'une puissance de 6 MW. Les résultats obtenus furent très satisfaisants, mais l'accroissement très rapide de la puissance unitaire de soufflage n'a pas encore permis l'adoption de ce principe.

Sur le plan constructif, les soufflantes décrites comportent toutes les dispositions suivantes:

a) Une roue porteuse de pales en porte à faux par rapport aux paliers afin de n'avoir qu'une seule étanchéité à assurer à la traversée par l'arbre de l'enceinte sous pression;

b) Un dispositif d'étanchéité en marche normale assuré par un ensemble comprenant généralement une chambre de barrage alimentée en CO_2 «neuf» à pression plus élevée que celle du circuit primaire, associée à un dispositif d'étanchéité sur l'arbre tournant alimenté en huile sous pression;

c) Un dispositif d'étanchéité utilisable lors d'arrêts prolongés de la machine, ce dispositif permettant, tout en maintenant le circuit primaire sous pression, le démontage et l'entretien des paliers et du dispositif d'étanchéité tournant;

d) Un arbre intermédiaire facilitant les opérations de montage et de démontage du rotor;

e) Un système général de distribution d'huile (de graissage, de barrage et de fonctions annexes éventuelles).

La difficulté des problèmes posés conduit à effectuer un certain nombre d'essais préliminaires lors de la construction de ces machines: essai de résistance des pales; essais aérodynamiques sur maquette à échelle réduite de l'ensemble de la soufflante, permettant la détermination des sections d'entrée et de sortie et la mesure des pertes de charge; essais aérodynamiques d'une maquette tournante à échelle réduite, permettant de s'assurer que la machine projetée répondra bien aux caractéristiques demandées; épreuve de maquette de résistance des corps ou des fonds; essai en endurance d'une maquette échelle grandeur reproduisant le dispositif d'étanchéité et son appareillage annexe.

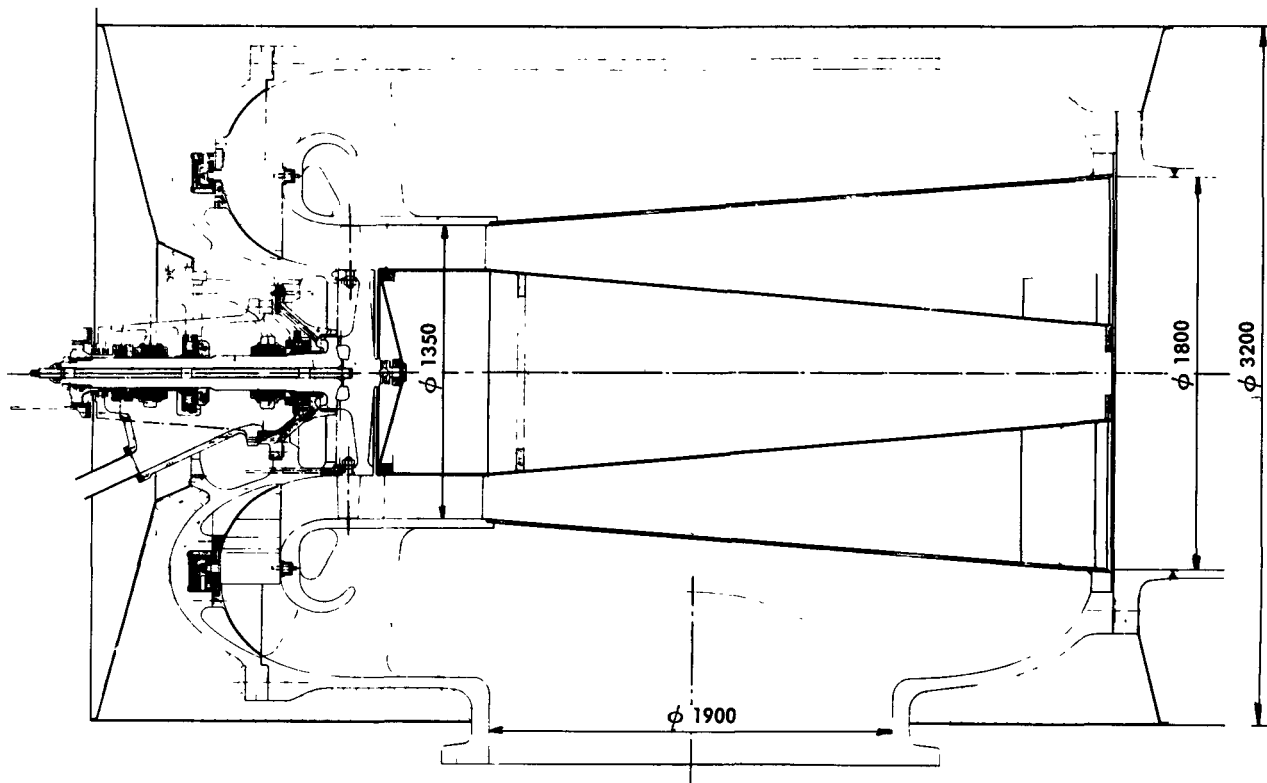
Cet ensemble d'essais préliminaires est complété, lorsque la machine est réalisée, par un essai de fonctionnement à la pression atmosphérique permettant le contrôle des caractéristiques, et par un essai d'endurance dans les conditions normales de fonctionnement.

Description succincte des soufflantes EDF1, EDF2 et EDF3

Soufflante EDF1. — Le corps en tôle d'acier spécial est soudé directement aux tuyauteries. Le couvercle en acier coulé et soudé renferme les aubes prédirectrices avec leur cercle de vannage et porte les servo-moteurs hydrauliques de commande. Bâche et couvercle sont fixés entre eux par une bride de 3,35 m de diamètre (fig. 3a). Un support conique est fixé au couvercle; il renferme le carter des paliers, comprenant successivement un palier radial, une butée double, le palier radial côté machine. Ce dernier palier est combiné avec des anneaux flottants assurant l'étanchéité entre l'huile de barrage et l'atmosphère. La roue comporte 15 ailettes en acier au chrome; elle est suivie d'aubes redresseuses fixes. Le réglage du débit est obtenu par l'action du cercle de vannage en liaison aux aubes directrices orientables par l'intermédiaire de biellettes. L'adaptation de la soufflante à des conditions de marche différentes se fait par modification du calage à l'arrêt des aubes mobiles; la plage d'adaptation permet tous les débits compris entre 1 365 et 1 800 kg/s.

L'étanchéité à l'arrêt est obtenue par déplacement de l'ensemble carter des paliers et rotor, grâce à un certain nombre de pistons hydrauliques fixés sur le support conique.

EDF 1



EDF 2

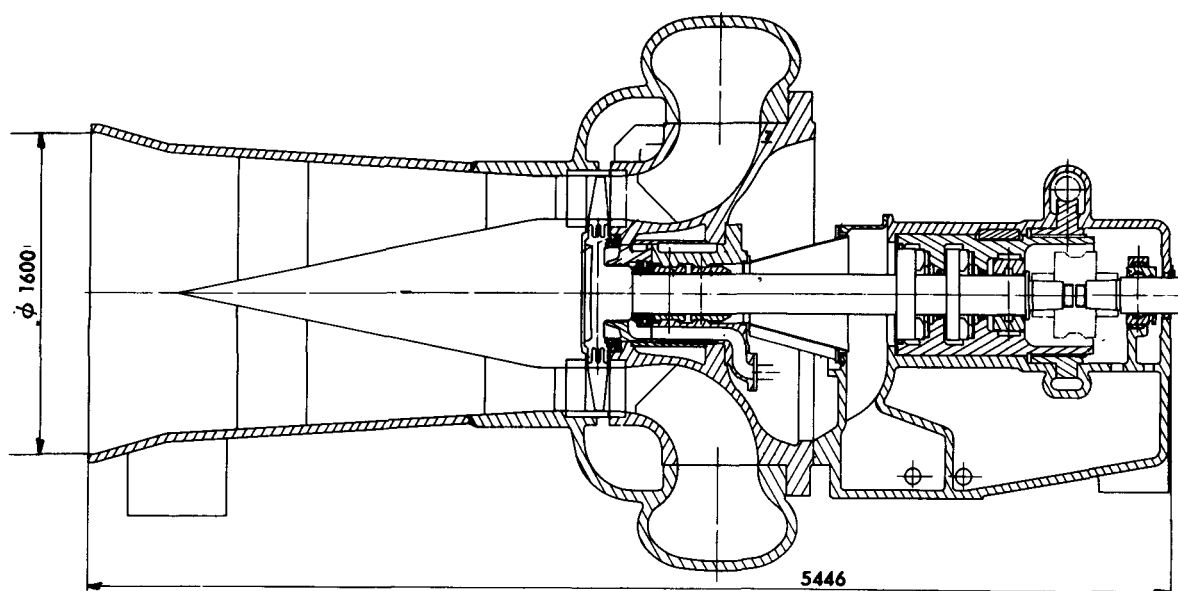


Figure 3. Soufflantes EDF1 et EDF2

Soufflante EDF2. — La soufflante (fig. 3b) est constituée d'un corps en acier moulé, formé par l'assemblage de la volute comportant ses deux entrées, du diffuseur constitué par un corps central et une enveloppe externe, et du convergent; d'un rotor en acier forgé de construction monobloc, comprenant la roue destinée à recevoir les dix aubes mobiles; d'un palier porteur disposé à proximité de la roue; d'un ensemble palier – butée comprenant le deuxième palier et la double butée ainsi que le mécanisme de déplacement du mobile; des dispositifs d'étanchéité.

Le rotor de la soufflante est entraîné par le coupleur hydraulique au moyen d'un arbre intermédiaire supporté par deux paliers sur lequel est disposé un frein anti-dévireur.

L'étanchéité à la sortie d'arbre est réalisée à l'aide de CO₂ de barrage provenant d'un circuit de CO₂ à pression plus élevée. Le CO₂ s'échappe d'une part vers le circuit principal à travers des labyrinthes, d'autre part vers une chambre où il se mélange avec l'huile en provenance de la bague d'étanchéité. Ce dispositif d'étanchéité est disposé entre la roue et le premier palier porteur; il est normalement utilisé lors du fonctionnement ou en cas d'arrêts brefs. Lors d'arrêts prolongés, le mobile de la soufflante est déplacé et deux portées viennent s'appliquer sur des parties correspondantes du stator. Du CO₂ de barrage est introduit entre les deux portées.

Soufflante EDF3. — Ces machines, bien que plus puissantes, sont d'une conception assez analogue à celles qui ont été précédemment décrites. Signalons cependant que le débit de CO₂ est séparé en deux après le diffuseur dans une culotte de bifurcation solidaire du corps de la machine (fig. 4).

Soufflantes EDF4. — Les soufflantes EDF4 sont situées à la base du caisson, sous les échangeurs, le plus près possible de la cavité interne, de manière à supprimer toute conduite de refoulement et d'aspiration (fig. 5).

Cette situation a conduit à prévoir des machines du type semi-axial; l'aspiration s'effectue axialement et les gaz sont refoulés radialement dans un espace annulaire formé par la paroi interne du caisson et la jupe support du réacteur.

Chaque soufflante est fixée à une pièce d'ancrage très rigide scellée directement sur le béton du caisson. Cette fixation pose des problèmes de refroidissement et de liaisons avec la peau d'étanchéité.

Une vanne cylindrique, à l'intérieur du carter, permet, en cas d'arrêt de l'une d'entre elles, d'éviter un flux de retour des gaz; cependant, pour éviter l'inversion du sens de rotation, il est prévu un dispositif de blocage du rotor.

La faible place disponible et la conception générale du circuit de CO₂ ne permettent pas d'installer un circuit anti-pompage pour le démarrage. La mise en service d'une soufflante supplémentaire lorsque les autres sont en service, et plus spécialement si trois soufflantes sont déjà à leur régime nominal, pose certains problèmes d'instabilité aérodynamique que l'absence du circuit anti-pompage rend plus difficiles à

résoudre. Les études préliminaires ont montré que la mise en service de la quatrième soufflante devant débiter sur le circuit commun pouvait être effectuée en diminuant la vitesse des trois autres machines et en ouvrant la vanne cylindrique dans certaines conditions.

L'entraînement est prévu avec des turbines à vapeur à condensation situées à l'extérieur du caisson, les deux machines étant reliées par l'intermédiaire d'un long arbre de transmission et d'un accouplement à dents.

Les orifices tunnels aménagés dans la paroi du caisson pour l'installation des turbo-soufflantes ont pu être ainsi réduits au minimum, diamètre 2,20 m, mais les opérations de démontage de la soufflante sont rendues délicates et doivent être étudiées très en détail dès le début de la conception de la machine.

Les quatre soufflantes fonctionnant toujours en parallèle à la même vitesse sur un circuit unique; le réglage du débit s'effectuera en changeant simultanément la vitesse des quatre soufflantes, l'arrêt d'une d'entre elles n'intervenant seulement qu'à la suite d'une panne.

TUYAUTERIES ET ORGANES ANNEXES

Le texte ci-après ne concerne que les centrales à *circuits primaires non incorporés* puisque cet ensemble de matériels est totalement supprimé dans la conception incorporée.

Les liaisons entre les différents organes constituant le circuit principal sont réalisées à l'aide de tuyauteries de grand diamètre. D'autre part, sur ces tuyauteries sont disposés des obturateurs destinés à l'isolement de certaines parties du circuit ainsi que des joints de dilatation.

Tuyauteries

Les différents diamètres des tuyauteries ont été déterminés à la suite d'une étude économique faisant intervenir la puissance de soufflage. De ce fait, les vitesses de circulation du gaz dans les tuyauteries sont de l'ordre de 20 m/s. Toujours dans le but de réduire les pertes de charge, des grilles à ailes profilées sont prévues de façon systématique aux changements de direction des tuyauteries.

Ces tuyauteries sont réalisées à partir de tôles d'acier. Elles sont formées de tronçons raccordés par soudure entre eux avec les appareils intercalés dans le circuit.

Organes de dilatation

Les dilatations des tuyauteries aux différents régimes de fonctionnement sont encaissées par un système d'organes de dilatation qui peuvent être de différents types: universels compensés (fig. 6); charnière ou cardans (simple ou double).

La détermination et l'implantation de ces joints de dilatation est effectuée de manière à réduire au strict minimum le nombre de points fixes situés sur le caisson, les échangeurs et les soufflantes, et à créer sur ces points fixes des réactions aussi réduites que possible.

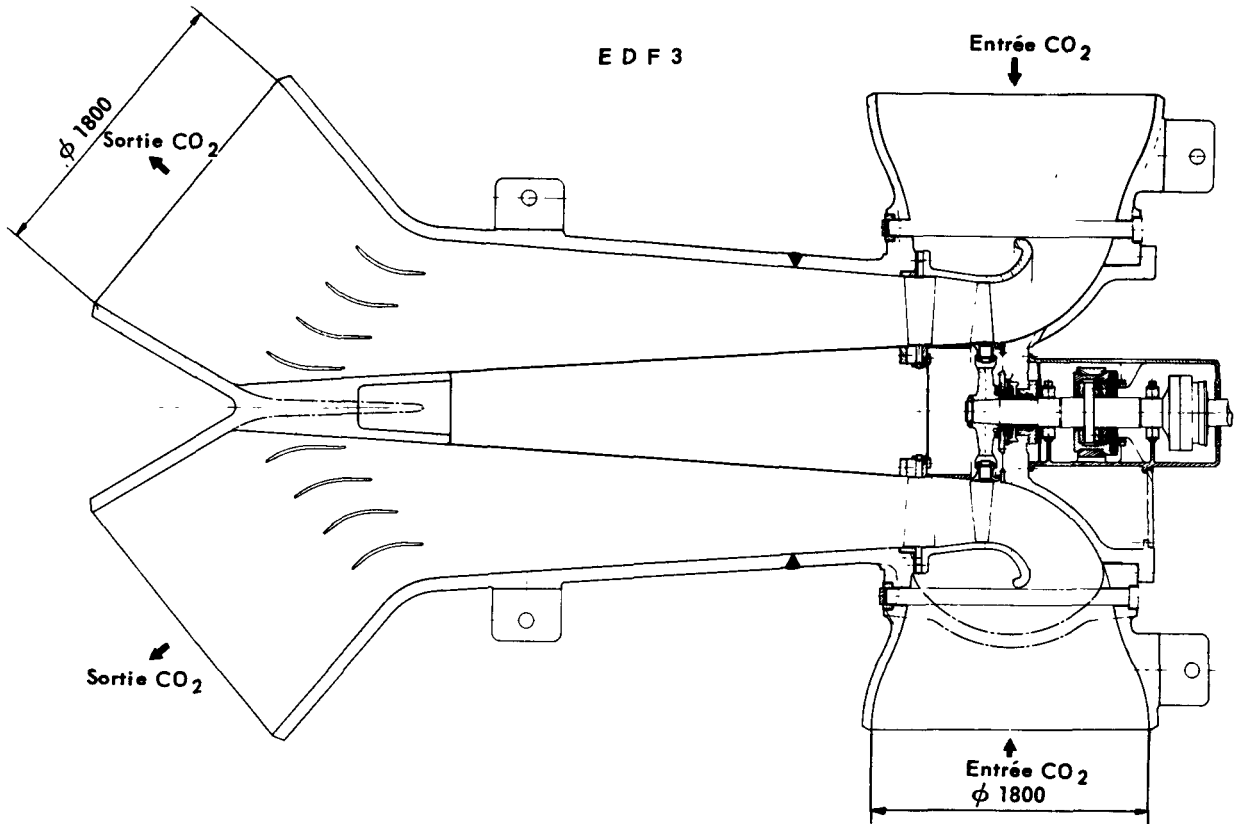


Figure 4. Soufflante EDF3

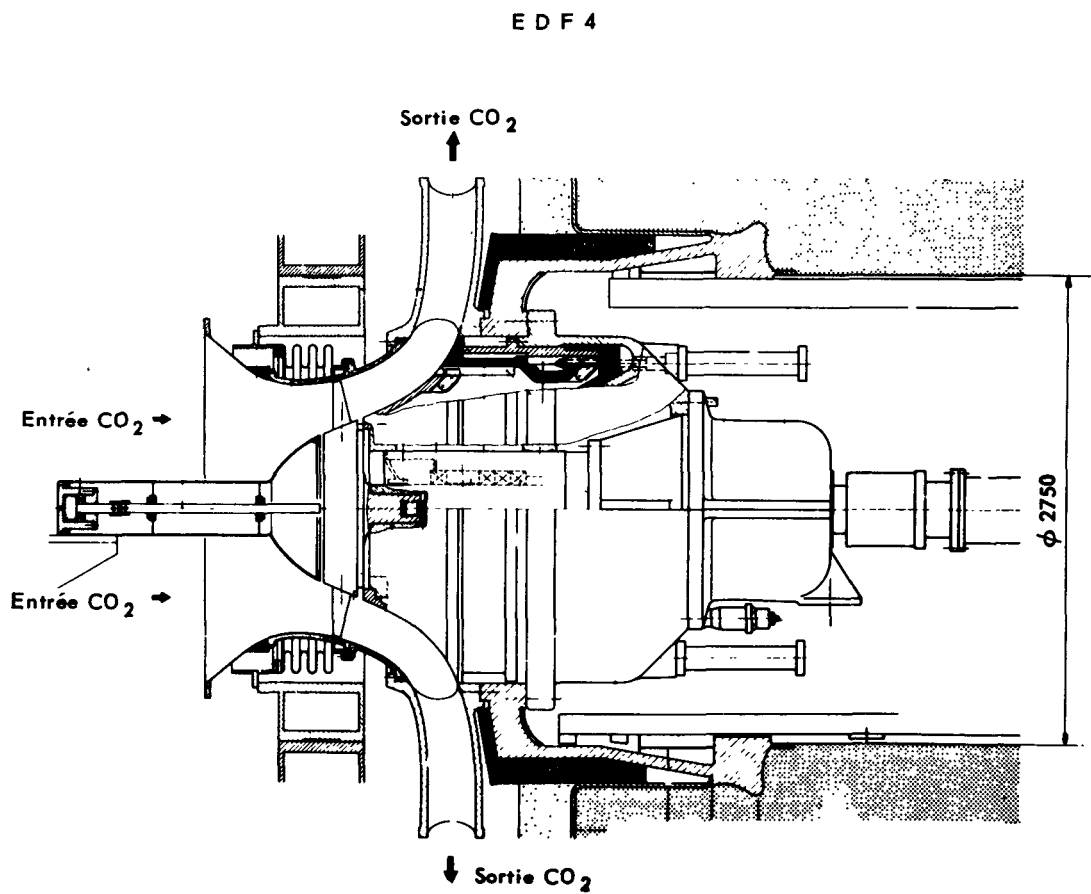


Figure 5. Soufflante EDF4

- COMPENSATEUR -

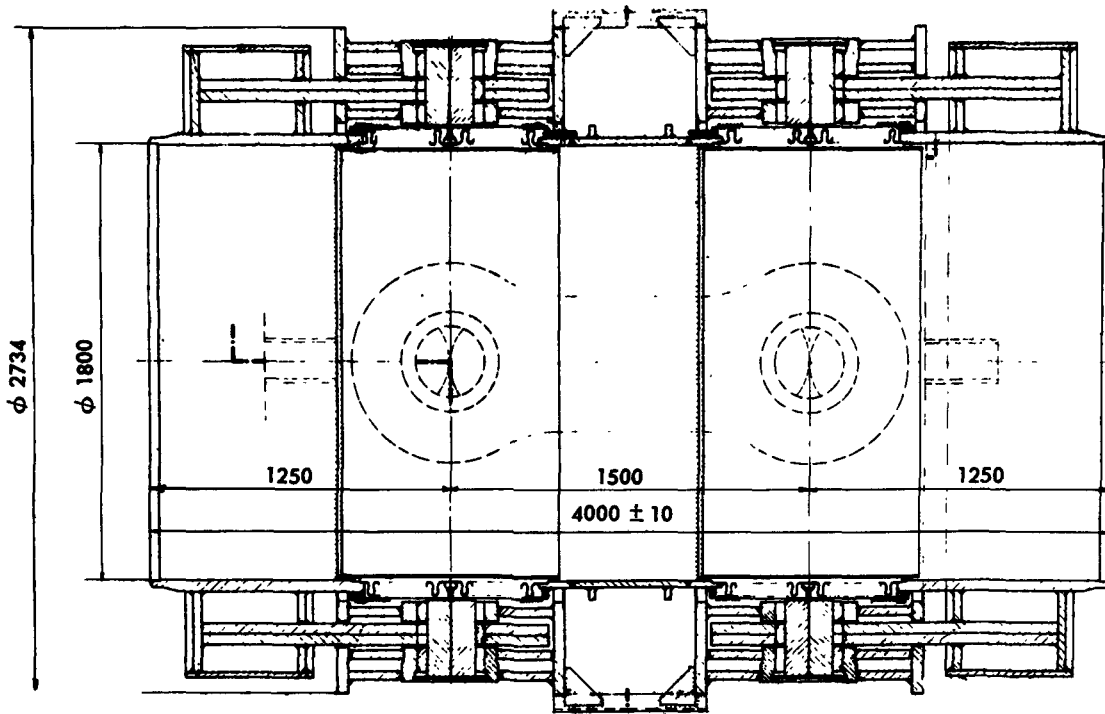


Figure 6. Compensateur

- OBTURATEUR -

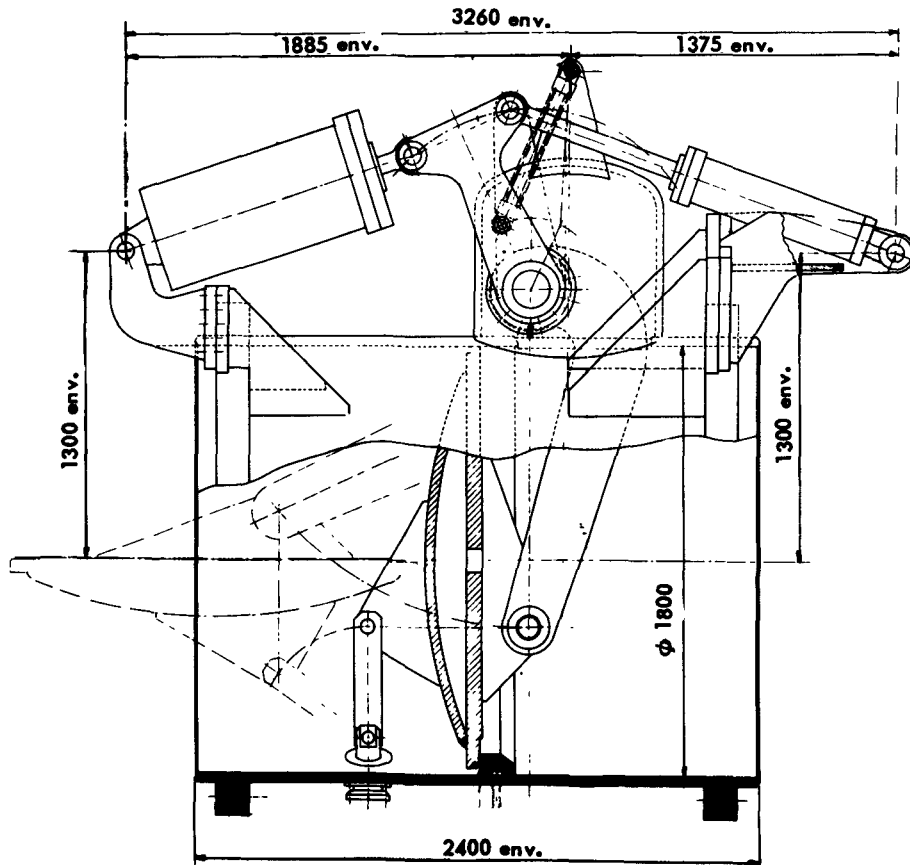


Figure 7. Obturateur

Ces organes de dilatation sont constitués par des soufflets réalisés en tôles de faible épaisseur (une ou plusieurs) roulées, soudées sur une seule génératrice et plissées. Ces soufflets sont ensuite raccordés par soudure circulaire sur leurs manchettes de raccordement. Les effets de fonds sont repris par un ensemble de tirants articulés disposés entre les manchettes.

Obturbateurs

Les obturbateurs disposés sur chaque boucle sont destinés à isoler du réacteur l'ensemble échangeur-soufflante (fig. 7).

Chaque obturbateur est constitué par un corps cylindrique disposé dans l'alignement de la conduite.

L'obturation est réalisée à l'aide d'un battant pivotant grâce à un système de leviers qui vient s'appliquer sur les deux sièges concentriques entre lesquels a été ménagée une gorge de récupération des fuites. Lorsque l'obturbateur est en position fermée, le circuit de récupération des fuites est mis à la pression atmosphérique. L'étanchéité amont-aval est garantie d'une manière absolue sous l'effet d'autoclave.

La manœuvre de l'obturbateur est réalisée à l'aide de dispositifs de commande par vérins à double effet, alimentés soit en CO₂ à une pression supérieure de 10 bars à celle régnant dans le circuit principal (solution EDF1 et EDF2: servo-moteur incorporé à l'obturbateur); soit par air comprimé (solution EDF3: servo-moteur non incorporé à l'obturbateur).

ABSTRACT—RÉSUMÉ—АННОТАЦИЯ—RESUMEN

A/94 France

CO₂ circuits in nuclear power stations

By E. Roberts et al.

This report deals with the typical equipment employed in the primary CO₂ circuits of French nuclear power stations using carbon dioxide gas as coolant. This equipment consists essentially of: heat exchangers; fans; units peculiar to the circuit (valves, compensating devices).

The heat exchangers associated to the reactor of a nuclear power station of the natural uranium-graphite-CO₂ sequence consist in all plants now built or now being completed (Chinon, EDF1, EDF2 and EDF3) of a certain number of identical units working in parallel.

A brief description of the different types is given, together with a list of advantages of this type of solution.

In new power stations of the integrated type (EDF4) the heat exchanger is housed within the pressure-vessel and thus forms a monobloc unit. Because of this, it has different structural and operational characteristics, which are also mentioned.

As regards the blowers, first and foremost, the vital part played by these in a nuclear power station is explained. Indeed, these machines must operate both reliably and efficiently.

The way in which the best-suited type of machine is chosen, how it is to be driven, the possibilities of adapting it to suit the characteristics of the circuit and the principal problems arising in installing the machines are then examined.

The various solutions adopted by Electricité de France for the different power stations are reviewed, and a list is given of all the difficulties encountered during development and starting up.

Lastly, special mention is given of the various characteristics of the blowers employed in integrated solutions.

Bellows and valves are also mentioned. These primary circuit devices are difficult to design and implement.

A/94 Франция

Контуры углекислого газа на атомных электростанциях

Э. Робер et al.

В настоящем докладе рассматривается характерное оборудование первичных контуров CO₂ на французских атомных электростанциях, использующих в качестве теплоносителя углекислый газ. В основном оборудовании включается:

- теплообменники;
- газодувки;
- механизмы, свойственные этому контуру (клапаны, компенсирующие механизмы).

Теплообменники атомных электростанций с натрий-графитовым реактором, охлаждаемые углекислым газом почти на всех установках, строительство которых закончено или находится в стадии завершения (EDF-1, EDF-2, EDF-3 в Шиноне), состоят из ряда идентичных элементов, работающих параллельно.

Приводится краткое описание различных типов; подводятся итоги преимуществ этого типа.

На новых атомных электростанциях компактного типа (EDF-4) теплообменник устанавливается внутри оболочки, в результате чего создается моноблочная конструкция. Этот факт обуславливает различие в характеристиках и эксплуатации, которое также рассматривается в докладе.

В докладе рассматриваются группы газодувки с точки зрения первостепенной роли, которую они играют на атомной электростанции. Не-

обходимо, чтобы они имели хорошую производительность.

Затем излагаются: метод выбора наиболее пригодного типа установки, способ питания, возможности приспособления к характеристикам установки и основные проблемы, возникшие при ее создании.

Приводятся различные решения, принятые фирмой «Электрисите де Франс» для разных атомных электростанций, и подводятся итоги трудностям, встретившимся при их наладке и вводе в эксплуатацию.

Отмечается различие в характеристиках газодувок, используемых на компактной атомной электростанции.

Описаны также расширительные устройства и клапаны первичного контура, которые являются важной частью конструкции и сложны в исполнении.

A/94 Francia

Los circuitos de CO₂ en las centrales nucleares

por E. Robert et al.

La presente memoria trata de los elementos característicos de los circuitos primarios de CO₂ de las centrales nucleares francesas que utilizan el gas carbónico como refrigerante. Esencialmente estos elementos son: los cambiadores de calor, las soplantes y los órganos específicos de este circuito (obturadores, órganos de compensación).

Los cambiadores de calor acoplados al reactor de

una central nuclear del tipo de uranio natural-grafto - CO₂, constan, en todas las centrales actualmente acabadas o próximas a su terminación (Chinon, EDF1, EDF2, EDF3), de un cierto número de elementos idénticos que trabajan en paralelo.

Se presenta una breve descripción de los diferentes tipos y al mismo tiempo se hace un balance de las ventajas de esta clase de solución.

En las nuevas centrales del tipo integrado (EDF4) el cambiador está colocado en el interior de la vasija del reactor y constituye un conjunto monobloque. Por lo tanto su constitución y explotación presentan características diferentes que también se reseñan.

Por lo que respecta a los *grupos de soplado*, se expone primero el papel primordial que se les reserva en una central nuclear. En efecto, se exige que estas máquinas tengan un funcionamiento seguro y un buen rendimiento.

A continuación se examina la manera de decidir la elección del tipo de máquina más apropiado, el procedimiento de puesta en marcha, sus posibilidades de adaptación y las características del circuito y los principales problemas que plantea su construcción.

Se describen las diferentes soluciones adoptadas por Electricité de France para las diferentes centrales y se hace un balance del conjunto de dificultades que se han encontrado durante su desarrollo y su puesta en servicio.

Por último se hace una mención particular de las diferentes características que presentan las soplantes utilizadas en las soluciones del tipo integrado.

Se reseñan también *las juntas de dilatación y los obturadores*, órganos importantes de concepción y de construcción delicada, situados en el circuito primario.

Graphite core structures for large gas-cooled power reactors

By P. C. Warner and M. A. Bayer*

The core of a gas-cooled graphite-moderated reactor consists of a stack of graphite pierced by vertical channels for control and fuel. For first generation reactors having a net electrical output of about 250 MW and contained in a steel pressure vessel the graphite stack is about 45 ft (15 m) in diameter and about 30 ft (10 m) high. Gas enters the pressure vessel through ducts at its lower end, flows vertically upwards through fuel channels in the core and is led out to boilers through ducts at the top of the pressure vessel. Since neutron absorbing material in large quantities has to be avoided the graphite of the moderator and reflector must itself be the medium in which the fuel and other channels are formed.

The essence of the design is to maintain integrity of these channels under all working conditions and following any credible faults, so that control holes remain operational, fuel elements can be put in or taken out, and coolant gas is directed over the fuel. There are therefore two main objectives: (a) to provide a structure which keeps channels reasonably straight, and (b) to prevent gas by-pass of the fuel channels.

The present paper discusses how these objectives are attained, especially as illustrated by the design and construction of three of the first generation reactors at Hunterston, Trawsfynydd, and Tokai Mura, and by an outline design for a unit of 500 MW net electrical output which is evolved from this experience.

Main structural design

Graphite is available in blocks of regular cross section up to about 3 ft (1 m) long, formed by extruding a coke and pitch mix which is then baked, impregnated and graphitised. The face dimensions of these extrusions are conveniently of the same order as a fuel lattice pitch, and it is therefore reasonable to design on one block per pitch with a hole up the centre of the block to form the fuel channel. The blocks have to be stacked on one another, and the core as a whole stands on a steel platform supported on the base of the pressure vessel. The requirement is for a core structure able to accept differential thermal movements and irradiation distortions, but stable under gas pressure differences, fuel handling loads and in some cases earthquakes.

Thermal expansion of graphite is approximately one quarter that of steel. Since there is a temperature gradient of nearly 200 °C through the core, the lower part being close to inlet gas temperature and the top close to outlet, differences in thermal expansion between the graphite and the various parts of any steel structure surrounding it must be catered for. An early solution was to butt the block vertical faces and to hold the stack solid with garters at the periphery; the expansion characteristic of graphite then dictated the behaviour of the whole system, but provided the garters had enough elasticity and were temperature compensated their stabilising load was effective at all temperatures; thermal movement between the base of the stack and the mild steel platform was accommodated by a ball race under each graphite column. This broadly was the solution adopted on the Calder reactors.

Under irradiation graphite undergoes long term strains which vary with temperature and total dose. In the solid type of structure just described, lateral growth would accumulate along a diameter and push out the peripheral blocks, while lateral shrinkage would create internal slackness. These effects can be tolerated only in the small diameter cores of prototype reactors. For the three large power reactors discussed in this paper, the potential misalignment of channels would be unacceptable: for example the permissible fuel channel misalignment over an element length would be between 1/4 in (6 mm) and 1/2 in (12 mm) depending whether they were stacked or sleeved. All are built from graphites which exhibit growth at temperatures close to the inlet, and shrinkage in the hotter regions. On Trawsfynydd, for instance, a column of blocks in the flattened zone may have a growth strain of about 2% and a shrinkage strain of about 1%, and the misalignment of peripheral channels could reach several inches if the core were built solid. Consequently, these large cores must have a structural skeleton which holds each column of blocks nearly vertical and which is contrived to be unaffected by their lateral strain. This has the added advantage that the design is much less sensitive to uncertainties in the irradiation data for these graphites.

A framework of some material like zirconium which is free from irradiation strain could have been used, but was considered too expensive and poisonous. The solution adopted on the designs covered by this paper

* United Power Company Limited, London.

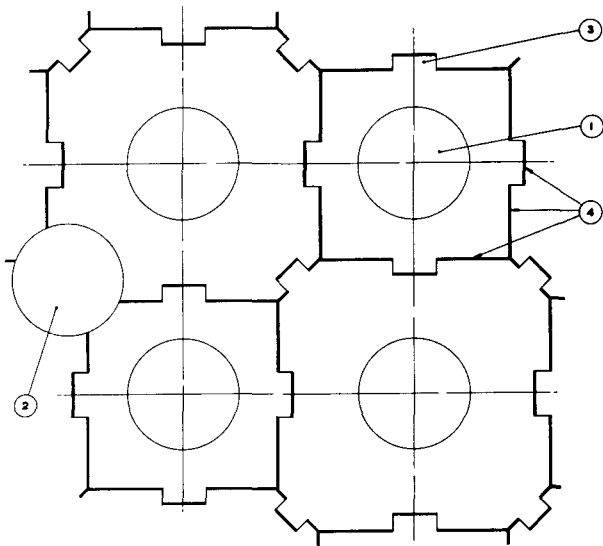


Figure 1. Plan view of keyed layer in graphite core structure (square pitch and integral keys)

1: Fuel channel; 2: Interstitial hole; 3: Integral key; 4: Expansion gap for thermal or irradiation strain

is to locate the individual columns by means of keys radial to the column centre line, as shown for instance in Figs. 1 and 2. A layer must be keyed in at least three directions and its outer blocks must be tied together circumferentially for it to form a structure. Slackness between columns is confined to backlash in keys; this can be kept small, and because irradiation damage at a key and keyway is nominally the same it hardly changes with reactor life. If, however, the boundary is expanded or contracted as a whole, the layer becomes a mechanism which changes its pitch in a consistent pattern. Thermal expansion of the layer is dictated by that of the boundary which may expand as graphite or as steel. For instance, on Trawsfynydd the boundary of every layer consists of a ring of graphite reflector blocks, which are virtually free from irradiation strains, held together by garters. The stack as a whole expands as graphite and is similar in this respect to the Calder design. On the other hand, the Tokai Mura boundary consists of a steel structure fixed to the outer ring of blocks. It therefore expands as steel; there is no need for ball races underneath the stack and the bottom blocks spigot directly to the steel platform. This solution gives the greatest resistance to lateral loads, and indeed seems to be the only form of structure strong enough for large earthquake design loads.

Whatever the core design, flux varies and therefore so does irradiation strain. Where this happens within a block, incompatible strains lead to internal stresses. One example is the hoop strain in a block around a fuel channel, and this is why it is advantageous to have a block no greater at any rate than the lattice dimension. Generally speaking, for the reactors reviewed here the problem is not serious and is relieved by irradiation creep.

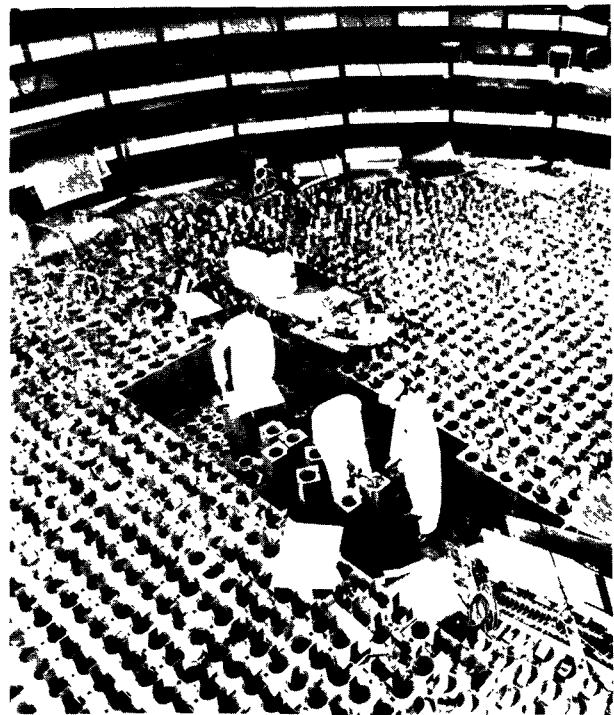


Figure 2. Erection of Hunterston core. Note the cruciform keys in the tile layer and the shims between block faces (Courtesy of General Electric Co. Ltd.)

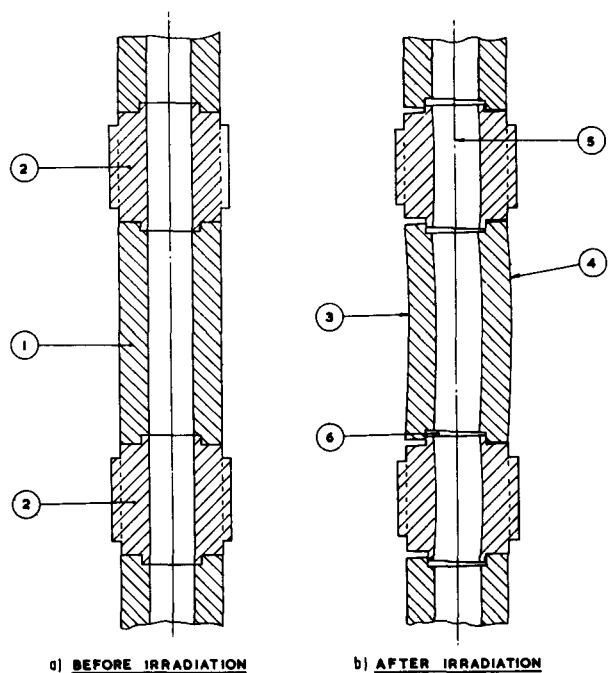


Figure 3. Block bowing caused by a flux gradient
1: Plain block; 2: Keyed tile; 3: Face with high flux causing fast shrinkage; 4: Face with low flux causing slow shrinkage; 5: column centre line is held fixed by tile keyed into tile layer; 6: Separation of block end faces

Flux gradients across a block, for instance near absorber or in the unflattened zone, cause one of its faces to shrink faster than the other so that the block becomes bowed as shown in Fig. 3 and slightly obstructs the channels. This causes block end faces to tilt relative to each other, and has an effect on gas leakage, which is dealt with in the next section: the magnitude of the separation for a typical block may reach 0.030 in (nearly 1 mm). It also makes columns of blocks unstable so that they buckle laterally against the key or other structural framework which must apply small restraining forces. Differential bowing of adjacent blocks or differential shrinkage of the material forming a key and mating keyway could lead to jamming and prevent free thermal or irradiation movements. Clearances for machining tolerances and ease of erection are generally large enough to avoid this, especially as the degree of bowing depends on the length of the block. Moreover, a small local jam, either from these causes or from trapped fragments, can be accommodated in the backlash of the surrounding keys.

This review of the structural features shows that the essential factor determining the choice of core design has been the nature of the thermal and irradiation strains. Once that was catered for, and remembering that the core is made up of small blocks, the forces within them are of a secondary order. Gravity loads are of consequence only on Trawsfynydd, which has an overhung steel platform whose deflection tends to make the blocks run outwards on their ball races; this puts a little extra load on the bottom garters of the same order as the frictional load resulting from thermal movement of the bottom blocks relative to the steel platform. Gas bursting forces may be important, especially under burst duct fault conditions, as explained in more detail in the next section. The Tokai Mura reactor also has the particular requirements to cater for large earthquake forces under lateral accelerations of 0.7 gravity.

Flow control

Coolant gas must flow from the header under the stack to the header above it via the channels containing fuel, as shown in Fig. 4. This gives three sealing problems; the spaces between bricks, the annulus around the stack, and the channels themselves.

The spaces between bricks must be vented to the outlet header, because a generally high pressure within these spaces could be obtained only by putting a sealing plate of some sort across the top of the core which would be extremely difficult to anchor down. It follows that the bottom of the core must prevent gas leaking between the brick spaces and by-passing the fuel channels; if the core is arranged to expand as graphite as on Trawsfynydd the bottom layer of reflector bricks is clamped up solid; on Tokai Mura and on Hunterston, the plate into which the bottom blocks are spigoted is gas tight.

The seal in the annulus between the stack and the pressure vessel must accommodate differential thermal movements in all directions. These are greatest if it is

located at the top of the core. Moreover, with the seal in that position there is a radial inward pressure on the outer ring of blocks which must both resist this load and be gas tight; gas is also liable to seep under the top peripheral blocks and lift them. For these reasons the gas seal was put at the bottom on all three projects, giving a small outward pressure differential between inter-brick spaces (fed by out-of-channel leakage) and the annulus (at outlet pressure); in the event of a top duct failure, venting of the inter-brick spaces lags behind the outlet header and large bursting forces may be experienced, so that an adequate restraint system is needed around the core.

Leakage out of fuel channels may be through the permeable graphite or through the joints between blocks. The driving pressure varies from approximately the core pressure difference near the bottom to nearly nothing at the top. In the two reactors with sleeved fuel elements, the sleeves form an intermediate seal which helps to inhibit out of channel leakage. When the core is new, some 75% of the leakage is through the graphite. As it ages, oxidation increases the permeability of the graphite by a small factor, but the joint leakage may rise considerably where bowing causes the block faces to separate as shown in Fig. 3 unless special sealing features are used. On Tokai Mura these take the form of conical graphite spigots on which the blocks can rock without separation, and on Trawsfynydd of magnox rings in annular grooves in the end faces. Coolant flow must be controlled by a gag in each channel adjusted according to its radial position. It must be removable for resetting, but during normal refuelling it must not become buoyant in the increased gas flow up the empty channel.

Requirements for fuel handling

Handling fuel and other components into and out of their channels sets requirements other than alignment. In each design, there are steel components to engage the charge tubes, guide them into place against any over-all movements of the core relative to the stand-pipes, take their weight and seal onto them if necessary. The interior surface of all the channels is free from steps and recesses which might catch components being withdrawn. Except on Hunterston, there is provision against dropping of components by accident, enough to protect the permanent structure and enable fragments to be withdrawn without too much difficulty.

General comparison of the Hunterston, Trawsfynydd and Tokai Mura designs

Design features of three first generation reactor projects [1, 2, 3] are given in Table 1, together with those for a current 500 MW(e) design to be discussed later.

In their basic structural design to cater for thermal and irradiation strains, Trawsfynydd follows the conventional lines of a structure that expands as graphite, and Tokai Mura one that expands as steel. Hunterston is a mixed design, with the bottom blocks spigoted into the steel platform to suit fuel

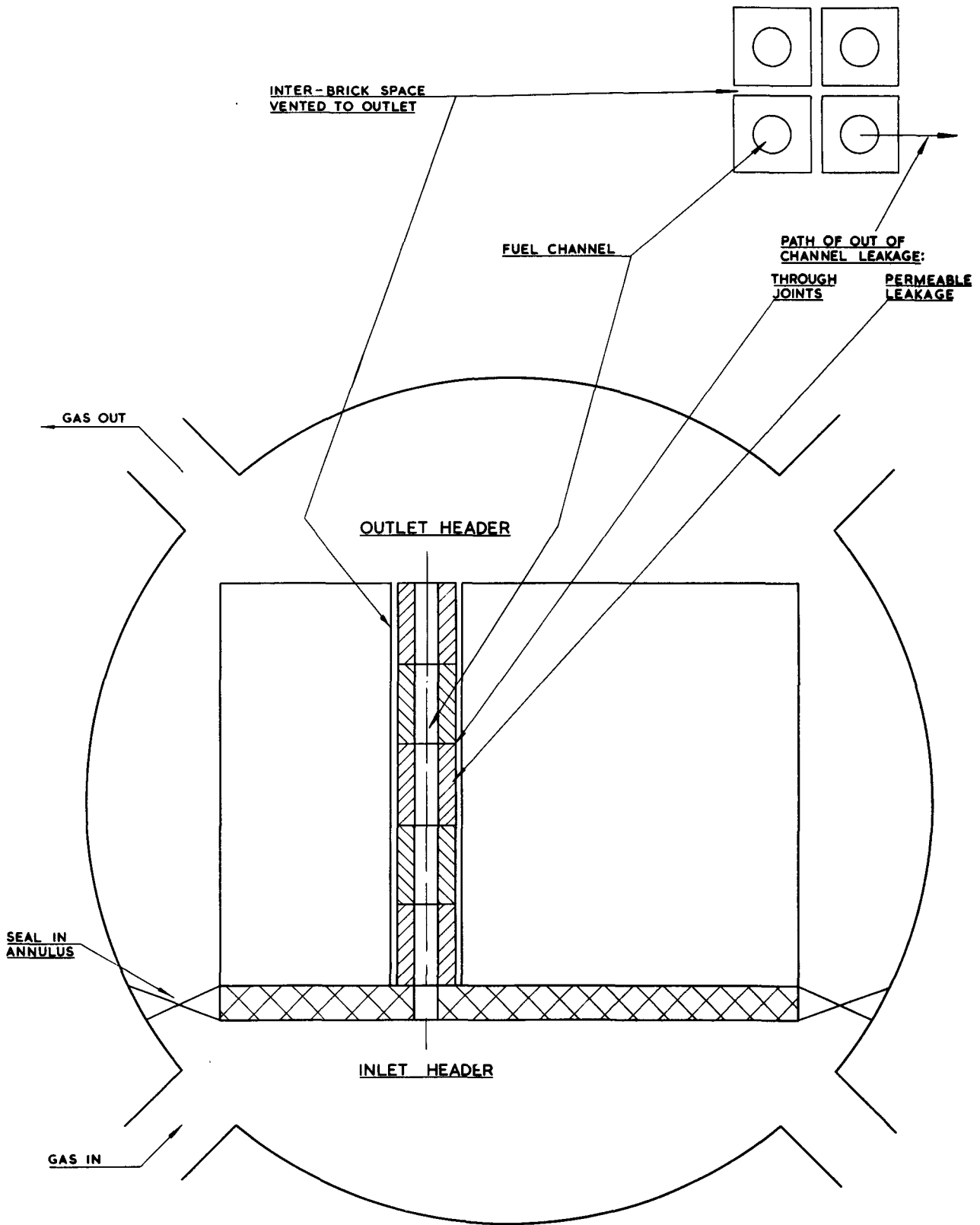


Figure 4. Arrangement of seals and leak paths

Table I. Four core designs compared

	Hunterston	Trawsfynydd	Tokai Mura	500 MW Unit
Net electrical output	160 + MW	250 MW	149 MW	500 MW
Fuel element type	Sleeved	Stacked	Sleeved	Stacked
Weight of graphite	2 180 tons	1 900 tons	1 000 tons	3 600 tons
Number of fuel channels	3 288	3 740	2 052	—
Position of control holes	Interstitial	Interstitial	On fuel lattice	Interstitial
Structural system	Plain blocks keyed tiles	Plain blocks keyed tiles	Keyed blocks	Plain blocks keyed tiles
Tile thickness	3 in (7.6 cm)	4 in (10.2 cm)	Block depth	15 in (38 cm)
Type of key	Loose cruciform, loose face	Loose cruciform, integral face	Integral	Integral
Thermal expansion	Mixed	As graphite	As steel	As steel
Lattice geometry	Square	Square	Triangular	Square
Lattice pitch	8.25 in (21 cm)	7.75 in (19.7 cm)	9.3 in (23.6 cm)	7.625 in (19.4 cm)
Fuel channel diam	5.28 in (13.4 cm)	3.75 in (9.5 cm)	5.28 in (13.4 cm)	3.75 in (9.5 cm)
Restraint system	Top garters with hinged vertical beam	Garters	Fixed to steelwork	Fixed to steelwork
Core pressure drop	3.5 lb/in ² (0.25 kg/cm ²)	7.2 lb/in ² (0.51 kg/cm ²)	10.2 lb/in ² (0.72 kg/cm ²)	4.2 lb/in ² (0.29 kg/cm ²)
Inter block seals	None	Magnox rings	Graphite cones	Magnox rings
Channel gags	Orifice, locked mechanically	Venturi, self-seating	Orifice, locked mechanically	Sleeve self-seating
Shock absorber for dropped fuel	—	Swage on fuel element strut	Graphite sleeve	Swage on fuel element strut
Shock absorber for control rods	Collapsing coil	Swage	Collapsing coil	Swage
Gas seal in annulus	Toroidal steel shell	Steel flaps	Toroidal steel shell	—

loading from underneath, but the top blocks held together at their periphery by garters; the intermediate layers are free standing between beams hinged to the platform and connected to the garters at the top. All of them employ a keyed system. For Trawsfynydd and Hunterston the keying is confined to thin layers spigoted between thick layers of blocks with plain faces, but on Tokai Mura the much greater strength required to restrain earthquake forces dictates that keys should extend over the whole depth of all core blocks, which are staggered axially to maintain alignment. Lateral strength is also the reason for using hexagonal blocks rather than square.

Gas bursting forces are not high on Hunterston because of the low core pressure drop and the use of sleeved elements, and this is why garters are not needed on every layer. On Trawsfynydd the core pressure drop is much higher and elements are stacked; taken with a very conservative assessment of out-of-channel leakage, this gives high radial gas forces under a top duct failure requiring garters at all layers; as an ultimate safeguard a steel structure around the garters acts as a stop to limit deflection. On Tokai Mura, earthquake loads are paramount so that gas forces lose significance.

A feature of the Hunterston design is that the decision to adopt a keyed system was made fairly late, after new irradiation information had developed. By choosing loose cruciform keys at tile corners, and loose side keys between tile faces, it was possible to use the raw material sizes already ordered. This restriction did not apply on Trawsfynydd where side keys were made integral, giving lower handling costs

and a reduction in the backlash between adjacent columns. The complex shape of the tiles is readily machinable on the type of broach shown in Fig. 5. The outer rings of the Hunterston tile layers are not tied so that any layer can displace laterally within the thermal expansion gap between it and the hinged beams but not enough to obstruct fuel elements. The Trawsfynydd layers have to be tied by steel dowels between tiles and side reflector because the stacked elements have less clearance and require a straighter channel.

The main erection difficulty turned out to be setting up the Trawsfynydd side reflector rings to their correct radius. When garters were tightened as each

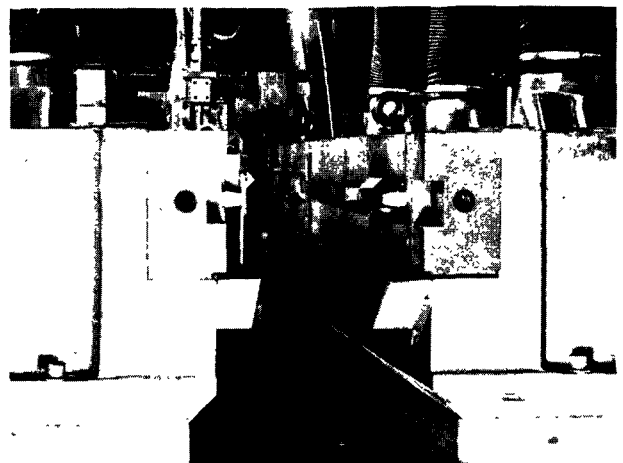


Figure 5. Tile broaching machine (Courtesy of Fairey Engineering Limited)

layer was placed, the ring went out of circular because blocks bedded in where their machined faces were not exactly parallel. Steel shims had been provided to take up machining tolerances on block face widths, and there was an adjustable screw in the dowels linking tiles to reflector. But bigger shims had to be put in to preset the arch outwards by twice the amount necessary for purely elastic shortening, and it took five layers to develop a satisfactory technique for selecting shim sizes, packing the bricks and finding a sequence for tightening the two garters on each layer. There were no technical difficulties of the same order during erection of the Hunterston core (see Fig. 2). Garters could not be tightened until the stack was completed, and so it was most important to prevent the side reflector from going out of circular since corrective action would have demanded major dismantling. This was achieved by using the experience of steel shimming from Trawsfynydd.

It was found as erection proceeded at Hunterston that progressive deflection of the platform caused the columns to tilt inwards and reduce the lattice pitch. This could have caused difficulties in fitting the top reflector layer which is clamped up tight by the garters to the pitch dimensions, and steel shims had to be placed between every block and removed as the tiles were laid; the frictional resistance of the tiles was enough to maintain true pitch at least until the next layer had been placed. On Trawsfynydd, the platform is much stiffer and this did not happen. Shims were not used within the block layers.

The Tokai Mura core has not been erected at the time of writing, but trial erections have shown that there should be no problem in assembling the long keyed blocks and in holding them upright on their conical seals until the outer blocks are fastened to the restraining structure.

Development and test experience

Extensive testing was needed to develop the above core designs. Models of the tile layers were built to investigate general kinematic properties, to show how backlash builds up across a group of tiles and whether there are any modes of distortion which the designer has not visualised; for instance the tendency for the tiles to fan out when the boundary is disturbed in an unsymmetrical manner, and the way in which local displacement or rotation of one tile is disseminated through the layer. The model tiles can be of graphite, but this is not essential and a convenient tool for investigation is a layer of thin metal tiles to a reduced scale held in a flat box. By using loose keys it is also possible to investigate the degree of redundancy so as to see how many of the corner keys can be omitted from the layer (for instance at an interstitial hole) without impairing its structural properties. It is not easy to calculate the strength of a graphite component because of the scatter of properties and the microscopic cracks which act as internal stress raisers. Moreover, most components whose strength is of interest in the design have a complex geometry.

For these reasons a large sample of tiles has to be subjected to ultimate strength tests. They are loaded through yokes representing the keys of adjacent tiles. The work on the Tokai Mura hexagonal blocks has already been reported [4]. Similar work was done for the Trawsfynydd tiles, but was not judged essential on the conservative Hunterston design. The object of the tile tests is to demonstrate that the margin of strength over loads in service is enough for scatter of properties and for such effects as loss of strength through oxidation.

Measurements of gas leakage through various components are needed. For most purposes, a test with nitrogen from a bottle exhausting to atmosphere is adequate provided the pressure ratio is kept well below the critical value: results are readily converted to carbon dioxide at reactor conditions. The magnox sealing rings on the block end faces operate by creeping on to the walls of the grooves under the pressure difference, and a special technique using lead rings was employed to demonstrate this.

The permeability of graphite is one of the properties subject to the largest scatter, and reactor performance calculations were based on test results from a number of blocks and sleeves. The mean permeability depends on the raw material type and the number of pitch impregnations during manufacture, but to impregnate repeatedly would give fast diminishing returns and is seldom justified as an economic means of improving performance.

A wide variety of reactor components was functionally tested. Thus the ball bearings in the Trawsfynydd design were subjected to friction and life tests; the devices for absorbing the energy of dropped fuel elements or control rods in all the designs were proved; the elastic garters for Trawsfynydd were calibrated and proof loaded; and the behaviour of seal flaps, mechanical locks, and other components was demonstrated in reactor atmospheres and temperatures.

The supporting programme of graphite irradiation tests by the UKAEA and others is outside the scope of this paper. For the graphites used in each project, information was provided about such properties under irradiation as Wigner strain, creep, thermal conductivity, and weight and strength loss due to oxidation. A result of special importance was that Wigner energy measurements had shown that no special measures were necessary to keep the temperature high and minimise the amount stored.

The graphite for each of the three reactors discussed here was machined by three different contractors, and the development work on machining techniques tended to vary according to local circumstances. Mention may be made of the broaching process which was used on the side faces of all Trawsfynydd blocks and tiles (Fig. 5) and of the trepanning of the channel bore for Hunterston and Trawsfynydd. On Hunterston, blocks and sleeves were trepanned simultaneously. Other developments in the machine shops included the usual work on jigs and inspection method in association with the final stages of drawings.

A general conclusion from the experience on these reactor projects is that the development and test programme needs to be carefully investigated at the conceptual design stage and related to the programme of detail design.

Core design for a unit of 500 MW(e)

A current design for a unit of 500 MW(e) is illustrated in the last column of Table 1. This has a keyed system attached to a steel structure so continuing the sequence which was traced previously from Calder via Trawsfynydd to Tokai Mura, while retaining and developing preferred subsidiary features from all three designs. In the keyed system itself (Fig. 1), the number of key to keyway transitions has been halved and backlash much reduced by increasing the size of the cruciform component on the Trawsfynydd system and putting a fuel channel through it. It is assumed here that there are no earthquake problems, so that a square lattice gives adequate strength: it makes the design of vessel penetrations easier, especially with a concrete pressure vessel. Layers of plain blocks alternate with keyed layers increased to half the block depth compared with the shallow layers on Trawsfynydd and Hunterston. This gives reasonable raw material utilisation. The layers are deep enough to give a reserve of strength against increased oxidation caused by a higher circuit gas pressure, but not so deep as to cause relative interference due to bowing. It also reduces the number of brick joints and hence the leakage, and the number of components to be handled.

CONCLUSIONS

Design practice for the cores of large gas-cooled power reactors is now thoroughly established. The fundamental problem is to maintain adequate channel alignment as the graphite undergoes thermal and irradiation strain, and in all cases this is done by building the stack from keyed layers which hold the columns in position. There should be no serious trouble from jamming or irradiation cracking because

the constituent blocks are kept small, namely one per lattice pitch and reasonably short. They are made strong enough for the fault loads, but under normal running they are virtually unstressed.

The comparison between Hunterston, Trawsfynydd and Tokai Mura is especially interesting because they were designed by different organizations which have since merged. Yet they all exhibit the same basic principles, and the similarity, for instance, in the development programme of Trawsfynydd and Tokai Mura is remarkable. Points of difference are largely due to differences in requirements. Thus Hunterston being the earliest has a very low core pressure drop and hence is lightly loaded even under a fault. In the other two the design is more stringent, and Tokai Mura must also resist earthquakes. Trawsfynydd is the only one with stacked elements, so that some channel problems are special to it.

The development potential of graphite cores does not stop at the design in the last column of Table 1, and the same principles can be extended to larger units. They can also be applied to a core design for an advanced gas-cooled reactor, which has a smaller diameter and a higher flux but where the structural problem is basically the same. The ultimate size limitation is likely to be the keys since their strength has to increase with core diameter, but this is not yet in sight for conventional conditions. However, if the core has to withstand earthquakes, it would be reached sooner even allowing for graphites of increased strength.

REFERENCES

1. Nuclear engineering, Articles and data on Hunterston (April 1964).
2. Nuclear engineering, Articles and data on Trawsfynydd (January 1961).
3. Nuclear power: Articles and data on Tokai Mura (March 1960).
4. Kiyoshi Muto, Bailey, R. W., and Mitchell, *Special requirements for the design of nuclear power stations to withstand earthquakes*, I. Mech. E. Proc., Vol. 177, No. 7 (1963).

ABSTRACT—RÉSUMÉ—АБНОТАЦІЯ—RESUMEN

A/137 Royaume-Uni

Structure des cœurs en graphite pour les grands réacteurs de puissance à réfrigérant gazeux

par P. C. Warner et M. A. Bayer

Le cœur d'un réacteur modéré au graphite et à réfrigérant gazeux se compose de colonnes de graphite percées de canaux verticaux pour les barres de contrôle et pour les éléments de combustible. La structure doit être capable de supporter les déformations provoquées par l'irradiation et les mouvements thermiques différentiels en même temps que les

contraintes dues aux différences de pression du gaz, à la manutention du combustible et, dans certains cas, aux forces séismiques. Pour les cœurs de grande taille, il est indiqué de prévoir la structure de telle façon que chaque colonne conserve sa place, indépendamment des contraintes latérales, et soit maintenue verticale par une armature appropriée. De cette manière les colonnes sont insensibles aux contraintes variables dues à l'irradiation, et en outre le défaut d'alignement des colonnes est réduit à un minimum.

La solution habituelle consiste à utiliser des assemblages à clés radiales sur les pièces de graphite de façon à former une couche qui change de pas d'une manière régulière lorsque le contour est dilaté ou

contracté dans son ensemble. La périphérie peut être fixée à une structure en acier ou à une arche en graphite maintenue en place par des brides élastiques compensées pour tenir compte des différences de température. Des problèmes de structure résultent aussi du cintrage des blocs provoqué par le rétrécissement différentiel et des forces de dilatation du gaz, notamment en cas de défaut dans les conduites. L'autre problème important est d'assurer que le gaz circule dans les canaux de combustible. Les espaces entre les briques nécessitent une aération par la partie supérieure du cœur en raison des exigences du contrôle, et la couche inférieure doit par conséquent former un joint étanche sur la base, soit sous forme d'une plaque en acier, soit par un assemblage étanche des blocs réflecteurs. Le gaz s'échappe des canaux de combustible à travers le graphite perméable et à travers les joints entre les blocs et un système sans chemise doit comprendre des éléments d'étanchéité spéciaux entre les blocs pour éviter les fuites excessives après déformation à long terme.

Les cœurs utilisés à Hunterston, à Trawsfynydd et à Tokai Mura comprennent tous des couches assemblées par clés radiales en vue de compenser les contraintes thermiques et d'irradiation; mais pour Trawsfynydd on a adopté la dilatation du graphite, pour Tokai Mura celle de l'acier et pour Hunterston une solution mixte. Une étude des ces types de cœur montre que les problèmes se sont présentés d'une façon légèrement différente dans chaque cas et ont reçu des solutions différentes. Il est intéressant d'examiner les mêmes problèmes pour un gros réacteur du type Magnox actuel destiné à produire 500 MW(e) et de définir un modèle de cœur pour ce réacteur basé sur l'expérience des trois réacteurs précédents. On est amené à proposer un cœur avec des couches à assemblages par clés radiales profondes, alternant avec des couches sans assemblage, encastrées dans de l'acier à la partie inférieure et à la périphérie. Des principes analogues peuvent être adoptés pour le cœur d'un réacteur d'avant-garde à réfrigérant gazeux.

A/137 Соединенное Королевство

Структура активных зон из графита для больших энергетических реакторов с газовым охлаждением

П. К. Уорнер, М. А. Байер

Активная зона реактора с замедлителем из графита и с газовым охлаждением состоит из графитовых колонн с вертикальными каналами для управления и для топлива. Структура активной зоны должна воспринимать радиационные искажения и дифференциальные тепловые сдвиги и в то же время должна оставаться стабильной в отношении нагрузок, обусловленных изменениями давления газа, манипуляциями

с топливом и в некоторых случаях сейсмическими силами. Для больших активных зон рекомендуется конструкция, обеспечивающая независимую от поперечных деформаций установку каждой колонны. При этом в вертикальном положении колонны могут поддерживаться с помощью любого подходящего устройства. Таким образом исключается необходимость в точном знании величин деформаций под действием облучения и обеспечивается минимальная разрегулированность колонн. Обычным конструктивным решением является использование радиальных пазов на графитовых блоках, с тем чтобы образовать слой, который способен согласованным образом изменять свой шаг, когда граница в целом расширяется или сжимается. Фиксация по периферии может быть обеспечена с помощью стальной конструкции или графитовой арки, закрепленной на упругих подвесках с температурной компенсацией. Другие проблемы включают деформацию блоков, обусловленную дифференциальным сжатием и ударными силами в газе, особенно в случае разрыва трубопровода. Еще одна важная задача при конструировании активной зоны состоит в том, чтобы предотвратить газовое байпасирование топливных каналов. Промежутки между блоками должны продуваться в направлении верхней части активной зоны, что обусловлено требованиями регулирования. Поэтому нижний слой по основанию должен иметь уплотнение или в виде стальной пластины или путем плотной пригонки блоков отражателя один к другому. Утечка газа из топливных каналов может происходить через проницаемый графит и через соединения между блоками. Чтобы предотвратить чрезмерные утечки после длительных искажений, в системе без соединительных рукавов должны быть предусмотрены специальные уплотнения между блоками.

В конструкциях активных зон энергетических реакторов в Хантерстоне, Траусфиниде и Токай-Муре, чтобы противостоять тепловым и радиационным напряжениям, используются пазовые слои. Однако в конструкции реактора в Траусфиниде применен графит, для реактора в Токай-Муре — сталь, а для реактора в Хантерстоне принято смешанное решение. Изучение активных зон этих реакторов показывает, как одни и те же проблемы несколько по-разному проявились в каждой из них и привели к различным решениям и конструктивным требованиям. Интересно рассмотреть те же проблемы для современного большого магноксового реактора мощностью 500 Мвт (эл.) и на основании накопленного с тремя предыдущими реакторами опыта описать конструкцию активной зоны. Это приводит к активной зоне с глубокими пазовыми слоями, перемежающимися с плоскими слоями, и с втулочными соединениями со сталью у основания и по периферии. Аналогичные принципы могут распространяться на активные зоны других газовых реакторов.

A/137 Reino Unido

Estructuras de núcleos de grafito para grandes reactores de potencia refrigerados por gas

por P. C. Warner y M. A. Bayer

El núcleo de un reactor moderado por grafito y refrigerado por gas está constituido por columnas de grafito atravesadas por canales verticales para el combustible y los elementos de control. La estructura debe ser capaz de admitir deformación por irradiación y movimientos térmicos diferenciales y, al mismo tiempo, ser estable frente a cargas debidas a diferencias de presión del gas, manejo del combustible y, en algunos casos, fuerzas sísmicas. Para núcleos grandes, es aconsejable proyectar la estructura de modo que cada columna tenga determinada su posición independientemente de sus deformaciones laterales y quede soportada verticalmente por una armadura adecuada. De este modo, no sólo es insensible la posición al valor exacto de las deformaciones por irradiación, sino que el defecto de alineación de las columnas es mínimo. La solución más corriente consiste en emplear chavetas radiales en los componentes de grafito, a fin de formar una capa que cambia su parámetro reticular de manera regular cuando el contorno se dilata o contrae globalmente. La periferia puede sujetarse a una estructura de acero, o a un anillo de grafito fijado por ligaduras elásticas compensadas a efectos de temperatura. Otros problemas estructurales consisten en el arqueamiento de los bloques causado por contracciones diferenciales y fuerzas de expansión del gas, especialmente bajo condiciones de accidente por rotura de un conducto.

El otro problema principal en el proyecto del núcleo consiste en evitar derivaciones del flujo de gas fuera de los canales de combustible. Los espacios entre los ladrillos tienen que estar ventilados a la parte superior del núcleo por necesidades de control; por tanto, la capa del fondo tiene que cerrar herméticamente en el plano de la base, bien por medio de una placa de acero o poniendo a tope de forma compacta los bloques del reflector. El gas se fuga fuera de los canales de combustible a través del grafito permeable y a través de las uniones entre bloques, y a un sistema sin manguitos debe dotársele de características de hermeticidad especiales entre los bloques para evitar pérdidas excesivas después de un largo período de deformación.

Los núcleos proyectados para Hunterston, Trawsfynydd y Tokay Mura emplean todas las capas enchavetadas para acomodar las deformaciones térmicas y de irradiación. No obstante, Trawsfynydd dilata como grafito, Tokay Mura como acero y Hunterston emplea una solución mixta. Un estudio de estos proyectos muestra cómo los problemas se han presentado de modo ligeramente diferente en cada uno, y han dado origen a diferentes soluciones y necesidades de desarrollo. Es interesante considerar cómo los mismos problemas se manifiestan también en una unidad de magnox grande actual para 500 MW eléctricos netos de salida, y describir un proyecto de núcleo para esta unidad basado en la experiencia de los tres primeros reactores. El proyecto conduce a un núcleo con capas enchavetadas profundas alternando con capas planas, machihembradas a elementos de acero en el fondo y en la periferia. Para un reactor de gas avanzado pueden adoptarse principios similares.

Gas circulators and their drives for large gas-cooled power reactors

By H. Bateman, G. L. Duffett and W. Johnson*

The circulation of large quantities of high pressure carbon dioxide used as the heat transport medium in large gas-cooled power reactors demands a high power and the circulators with their drives feature as principal plant. The output and design features of the reactor together with the technical and economic factors relating to the circulator and drive affect the choice of equipment for a particular reactor.

Two basic types of circulator have been used and of the large number of types of drive available several very different schemes have been engineered. Most of these are briefly discussed or mentioned in the present paper which takes the systems used at Hunterston, Trawsfynydd and Tokai as examples of solutions adopted for steel pressure vessel stations. The development of concrete pressure vessels containing reactor boilers and circulators has introduced different problems which are discussed in this paper.

TYPES OF CIRCULATOR

In a large power reactor the circulator power is about 7% to 12% of the station output. The pressure ratio is in the range of 1.05 to 1.1 and the pressure head can be generated easily in a single stage. All circulators so far built or under construction have a single stage on an overhung rotor and are of axial flow or centrifugal design.

An axial flow circulator normally runs at a higher speed than a centrifugal one and is more easily matched to the speed of a two-pole motor or a multistage turbine. A centrifugal design is likely to require a speed of about 1 000 to 1 500 rpm and is suitable for dc or multipole ac motor drive but requires a gearbox if driven by a high speed steam turbine.

The choice of an ac motor direct drive dictates the circulator speed and may necessitate some compromise in the design, although the resulting difference in performance is small or even negligible. Adjustment of the full load operating point of an axial circulator can be obtained by providing variable inlet guide vanes, the adjustment being performed either as an initial presetting or on load.

Although axial circulators must be designed to operate stalled due to maloperation, it is considered preferable to avoid fluctuating loads on the blading by opening a bypass to avoid stall. At Trawsfynydd

a cooling circuit is provided in a bypass to enable the circulator to be run continuously in an isolated circuit.

Centrifugal circulators are robust machines and there is no risk of damage from running stalled provided there is not an excessive temperature rise. Both Hunterston and Tokai have centrifugal circulators where an isolated unit is brought into service by running up to speed against a closed valve which is opened when the differential pressure is zero.

Both axial and centrifugal circulators operate stably in the stalled region, i.e., there is no surging. The design point, which is close to the maximum efficiency contour may not be further removed from stall in the centrifugal than in the axial design. The axial characteristic is steeper and with a constant speed drive the gas flow is less sensitive to variations in the system resistance from the calculated figure.

CIRCULATOR DRIVES

There was an extensive choice of drive available for the early reactors from steam turbines to dc motors and ac motors with many possible variations. However, the choice of drive becomes more limited as circular ratings increase.

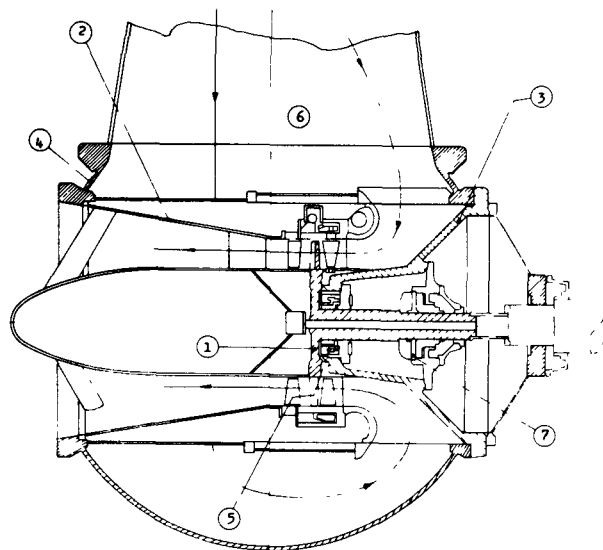


Figure 1. Trawsfynydd axial flow circulator
1: Rotor; 2: Diffuser; 3: Removable circulator unit; 4: Pressure casing; 5: Gas seal; 6: Inlet ducting; 7: Thrust bearing

* United Power Company Limited, London.

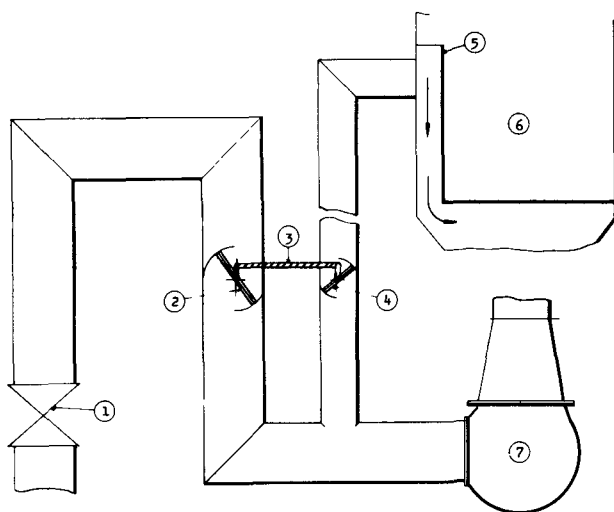


Figure 2. Trawsfynydd gas flow control system
1: Isolating valve; 2: Throttle valve; 3: Linkage; 4: Bypass valve; 5: Baffle; 6: Economizer; 7: Circulator

The selection of a circulator drive is influenced by the following factors: reliability; capital cost; efficiency at full load; low maintenance; method of gas flow control; operating and commissioning requirements; and ease of incorporating an auxiliary drive for emergency purposes.

Electric drive

The various types of electric drive are:

(a) *DC motors with variable speed control*

This drive is very suitable for speed control but there are limiting factors on maximum speed and on circulator rating. DC systems suffer from conversion losses whether incurred in rectifiers or in rotating machinery.

(b) *AC constant speed motor with hydraulic coupling*

The ac motor is an efficient electric drive but the hydraulic coupling reduces the efficiency at full load, and further still at part load.

(c) *AC constant speed motor with bypass control of gas flow*

This form of drive has a high efficiency at full load particularly when variable guide vanes are incorporated. However, gas bypassing leads to a poor part load efficiency.

(d) *AC motor supplied from variable frequency alternators*

Turbo-electric drive is the most costly but it has a good speed variation facility with a relatively high efficiency over the whole range. Individual motor speed control is not available and a gas bypass system is required to enable a boiler/circulator unit to be brought into service whilst the remaining circulators are operating.

(e) *AC slip ring induction motors*

This form of variable speed drive has a good part load efficiency if used with a slip recovery system but the associated electrical plant produces a complex and expensive system.

Steam drive

Optimization of a dual pressure plant leads to a HP steam generation of about 65% of the total. If all the HP steam is expanded through auxiliary back pressure turbines to the LP system it is found that the power generation is about equal to the circulator power demand although some adjustment of steam conditions may be necessary to achieve exactly the circulator power required.

A good full load efficiency depends on matching the design points of the turbo-circulator to the full load operating conditions of the plant and upon a high internal efficiency from the auxiliary turbine. If a high speed turbine design is selected, gearbox losses are introduced.

The circulator power varies approximately as the cube of speed and of reactor gas flow while the steam generation is approximately proportional to the gas flow. Consequently, if the circulator turbine is designed to accept all the HP steam at full load, then as load and speed are reduced there is an excess of HP steam. This excess may be pressure reduced and bypassed around the circulator turbine or the part load efficiency can be improved by utilizing the excess in the HP stages of the main turbines. With larger sizes of main turbine the design problems and costs associated with providing an HP section increase greatly so that there is an incentive to use a single pressure machine.

Emergency drives

Emergency drives are required to ensure adequate gas flow in the unlikely event of rapid depressurization coinciding with the loss of electrical supplies. In these circumstances natural circulation is negligible and auxiliary power is essential to run the circulators. On the earlier reactors pony motors are provided which take their power from batteries, except at Hunterston where the main dc motors fulfil this function. At Trawsfynydd, flywheels extend the rundown time and ac motors with double windings supplied from diesel alternators produce about 50% speed at atmospheric pressure and 20% at full pressure.

A system with steam driven circulators can be designed so that sudden and simultaneous loss of drive to all circulators is not a credible fault. Reduction in water pressure or low drum level causes a reactor trip and there is a delay before the steam available to drive the circulators becomes inadequate. The rundown time of the turbo-circulators following rapid depressurization can be extended by providing sufficient water and thermal capacity in the boiler and by opening an atmospheric exhaust valve to utilize these capacities to the maximum extent. When the reactor is shut down, fission product heat must be removed and pony motors may be used to run two or more circulators at slow speed.

With turbine driven circulators, auxiliary power may be provided by auxiliary boilers. However, such boilers take some time to generate steam to provide

power for cooling following rapid depressurization and pony motors may be installed. At Tokai, for instance, dc pony motors are provided which can drive the circulators under atmospheric conditions. Reliance is placed on auxiliary boilers when the system is pressurized as natural circulation occurs under this condition and time is available to raise steam.

Gas seals

Running seals are necessary around the circulator drive shafts. There are basically three types of seal, pneumatic, hydrodynamic and carbon ring. In the pneumatic seal the running clearance between a rotating and a stationary face is provided by a layer of air which acts as a lubricant. The air pressure distribution across the seal face is so arranged that ingress of air into the gas circuit and loss of CO₂ is prevented. A small but controlled loss of CO₂ is permitted which is piped to the station stack.

The hydrodynamic seal is a development of those used on hydrogen cooled alternators in which an oil film is produced and maintained between a white metal face and hydrodynamic pads under the influence of shaft rotation. A small quantity of oil is permitted to flow across the contact faces and it is collected with gas leaking through a labyrinth at a controlled rate and passed to a separating tank. Oil diffusion to the circuit is prevented by the labyrinth controlling the outward flow of gas.

In a carbon ring seal, oil is delivered to an adjacent journal bearing and flows past a spring loaded carbon ring. The oil pressure is controlled so that it is just lower than the circuit gas pressure but oil migration occurs across the seal face due to centrifugal action of the ring and the oil lubricates the interface and produces pressure balance.

CONTROL

The general requirements of the control system are:

- (a) Variation of reactor gas mass flow;
- (b) A reasonable balance of flow between circuits, i.e., ganged operation;
- (c) Satisfactory operation with one or more circuits isolated;
- (d) Control of an individual circulator and associated gas circuit to allow a shut-down circuit to be reinstated while the reactor is at power;
- (e) Design features to limit transient conditions during normal operation and under fault conditions.

The range of mass flow varies with the plant design and at Calder Hall and the earlier civil stations a very wide range of flow control was specified. Later the requirements were not so restrictive and at Trawsfynydd, for instance, the minimum reactor flow on main motors with all circuits operative is about 30% of the full load value.

The ease with which ganged operation is achieved depends upon the drive system. With turbo-electric drive, ganged response is inevitable, but with other systems it is necessary for individual circuits to respond

to a single demand signal. Slight unbalance between circuits at partial load due to slightly different characteristics of individual circuits is acceptable, but to utilize the plant capacity to a maximum, a facility for trimming individual circuits at full load is usually provided. Such a facility may take the form of variable guide vanes in equal speed systems, or small differences in speed settings in systems where speed is variable between circuits.

Circulator isolation due to a fault makes it necessary to operate at power with at least one circuit isolated. There is no problem in removing a circulator from service, but for operational flexibility it is preferable to reinstate the circuit without reducing the reactor power.

To achieve reinstatement, it is necessary to achieve a circulator condition such that the gas isolating valves can be opened without producing a significant transient condition in the reactor. The method whereby this condition is achieved varies with the type of circulator and type of drive. With a variable speed centrifugal system as at Hunterston and Tokai, the isolated circulator speed is increased against a closed valve until there is no pressure difference across the isolating valve. The valve can then be opened and the circulator speed raised until it corresponds to that of the other running circulators. In the case of the constant speed axial design at Trawsfynydd, a stalled condition is avoided by closing the gas throttle valve and opening the interconnected bypass valve. When the incoming circulator is up to speed, the gas isolating valve is opened. With the throttle valve closed the flow transient is small and is reduced further by opening the isolating valve in steps and a suitable valve control is provided. The throttle valve is then opened until it matches the opening on the other circuits, when the actuator can be brought into ganged control. The gas flow control system is normally operated with the circuits ganged, whether the control is by circulator speed variation or by gas valve movement. However, the rate of change of flow is restricted by the design, so that a dangerous reactor gas flow transient condition cannot occur despite a fault in the station over-all control system or through operator maloperation.

COMMISSIONING

The major commissioning tests which influence the design of the circulators and their drives are:

(a) *Filtration and vibration run*

This operation and test is performed with air in the vessel at atmospheric pressure and with all circulators operating at full speed. Although the power input is relatively small, minor problems may arise because of the static pressure at the circulator being sub-atmospheric.

(b) *Hot dynamic run*

This test is performed with air at pressure and in the latter stages of the run at or even above the normal full load temperature. A major object of the test

is to dry out the graphite core, but it is not essential to run the circulators at full speed to produce a dry core as the length of the operation can be extended.

(c) Mechanical proving run

This run is performed with CO₂ at pressure in the circuit and has the object of demonstrating that the circulator and drive is mechanically sound and that all items in the gas circuit behave satisfactorily under flow conditions. The operation is performed before first raising the reactor to power.

There is little variation in the gas density around the circuits during commissioning tests as there is no heat output from the reactor core and flow conditions only approximate to those which occur during operation.

Electrically driven circulators present no fundamental problems of commissioning, provided that in the case of variable frequency drive from steam the design full load frequency is 50 c/s, so that imported electrical supplies can be used. In the latter case, the behaviour over the controlled speed range cannot be found.

With steam driven circulators, the total full load steam flow cannot be produced economically from auxiliary boilers. Full load velocities may be obtained in the cold gas circuit by running the circulators at full speed but at reduced reactor pressure. This test should show up any circuit vibrations although the amplitudes will be less than at full pressure. An alternative scheme is to block off flow from part of the gas circuit, including the core itself, and so obtain local velocities which are representative of the full load operating conditions.

DESIGN

Development has fallen into broad chronological stages which are found to contain common factors. These stages represent the philosophy prevailing at the time and contain reactors of similar fundamental design representing the stage of development attained.

The United Power Company's stations are selected as examples of the stages of development and the

other stations designed in the UK are also briefly mentioned. Table 1 lists the stations together with the ratings of the associated circulators and drives.

Stage 1 (1956–1958)

Stations in this first stage of development, of which Hunterston is an example, have circulator powers up to 5 000 hp. It was considered essential for the circulators to have a wide range of speed control and desirable to utilize proved equipment wherever possible for plant directly associated with the reactor. The choice for these early stations was largely influenced by the type of equipment directly available to the firms responsible for the design. These factors led to the use of centrifugal circulators driven by dc motors with double armatures. Eight boiler/circulator units were selected with the large radial diffuser of the circulator mounted within the boiler pressure casing in a vertical position which simplified the ducting and foundations. The motors are rated at 2 200 hp at 1 000 rpm with an overload capacity of 2 920 hp at 1 100 rpm. A double armature was chosen to limit the length of commutator bars, to limit the current density in brushes and the surface velocities at the commutator.

A wide range of speed control is obtained by using grid controlled mercury arc rectifiers. Individual speed regulation is available and ganged control can be obtained by manual operation from the control room desk or by the automatic station control system. The speed control system is designed so that the maximum rate of change of speed is limited to 3% per minute to avoid a large transient under certain possible fault and operational conditions.

The dc motors eliminate the requirement of pony motors for emergency conditions as two circulators are preselected and are automatically connected to the station battery system at the appropriate run-down speed.

The supply to each circulator from the station 6.6 kV system is so arranged that under all fault conditions other than total loss of supplies only one of the circulators is lost. This is achieved by quick

Table 1. Circulators and drives for power reactors of UK design

Station name	Output MW(e)	Gas circuits per reactor	Horse power	Circulator	
				Type	Drive
Berkeley	2 × 140	8	3 800	Axial	Constant speed electric motor with variable slip fluid coupling
Bradwell	2 × 150	6	4 400	Axial	Variable frequency electric motor
Hunterston	2 × 150	8	2 354	Centrifugal	Variable speed dc motor
Latina	1 × 200	6	4 750	Axial	Variable frequency electric motor
Hinkley	2 × 250	6	7 800	Axial	Variable frequency electric motor
Trawsfynydd	2 × 250	6	7 000	Axial	Constant speed ac motor
Tokai	1 × 150	4	8 700	Centrifugal	Variable speed steam turbine
Dungeness	2 × 275	4	8 916	Axial	Variable speed steam turbine
Sizewell	2 × 290	4	9 850	Axial	Constant speed ac motor
Oldbury	2 × 290	4	6 600	Axial	Variable speed steam turbine
Wylfa	2 × 590	4	18 500	Axial	Constant speed ac motor
AGR	2 × 500	4	15 000		

switching between the busbar systems. Reacceleration of the circulators subsequent to a quick switch is delayed until the starting load of induction motors fed from the same source has decreased to the full load value. A flywheel is incorporated in each drive to extend the run-down time of the circulators.

Hunterston is now operating at power, the maximum output from both reactors being well in excess of the design figure. The behaviour of the circulators and drives both during commissioning and operation has been very satisfactory. There have been no major troubles. The long vertical shafting has not created any operational problems and the gas seals have run well. The design efficiency seems to have been achieved but the design gas mass flow is obtained at lower than design speed, that is, the impeller is a few per cent oversize. This is not an undesirable feature in a variable speed system.

The firms responsible for the other reactors in the first stage of development based their designs on axial flow circulators which were located in the duct system between the boilers and the reactors. Steam turbine drive appeared non-competitive for the smaller ratings. As a result, all these stations are designed for a wide range of speed control based on an ac motor. At Berkeley this is achieved by driving through a scoop-controlled fluid coupling, whereas at Bradwell, Latina and Hinkley Point variable speed auxiliary turbo-alternators are installed.

Stage 2 (1959–1961)

The second stage of development began in a highly competitive atmosphere and in most cases there was an increase in net electrical output per reactor to 250–290 MW with associated circulator powers up to 10 000 hp. This led to the use of constant speed electric motors or variable speed steam turbines.

At Trawsfynydd, the choice of an axial circulator with a diffuser contained within the cold gas duct (Fig. 1) and the preference for electric drive by the customer narrowed the choice of drive to a 3 000 rpm electric motor. This speed was about the optimum for an axial circulator of the required rating and therefore suitable for direct drive from a two-pole motor. A new factor was the acceptance of the reasoning that a variable speed drive was not a necessity but that a more limited form of gas flow control was acceptable for bringing boilers on and off load and also to obtain a flow variation from the design point.

As about 80 000 hp of circulator power was to be installed for base load operation on a competitive tender, maximum consideration was paid to the economics at rated power. Any drive, therefore, which tended to produce a lowering of efficiency at rated power was eliminated. The following alternative drives were reviewed based on a rating of 6 000 to 7 000 hp:

(a) variable frequency alternators proved attractive as they allowed easy operation and provided good gas flow control. They were rejected because of the high

first cost and because the reactor would trip on loss of the variable frequency set;

(b) dc drives and ac commutator motors required brush gear of high capacity due to the power required being high, and gearboxes would have to be incorporated to produce the speed required for an axial circulator;

(c) two-pole slip ring motors of the size required were not considered a reliable proposition at the time and therefore gearing would have to be introduced to match the speed of an axial circulator to a four-pole motor;

(d) slip ring motors using slip recovery techniques appeared to be very attractive when considering part load operation. In this system, the losses of a slip ring motor are fed back into the main electrical system after rectification, inversion and transformation or are used to supply a dc motor on the same shaft as the main ac slip ring motor. This system was discarded due to the low speed available which required a gearbox and due to the cost of the auxiliary equipment;

(e) hydraulic couplings had not been designed at the time for the ratings required and proved designs of high power were not available;

(f) squirrel cage motors with gas flow control by a system of gas throttle and bypass valves were finally adopted for high full load efficiency and low capital cost. With nuclear stations, the financial penalty for loss of efficiency at part load is less than for conventional plant and is not of prime importance, but to obtain the best performance the circulator inlet guide vanes at Trawsfynydd are remotely adjustable on load. These guide vanes can be used to compensate for any prolonged reduction in system frequency as well as allowing the system to be set to its optimum condition at full load.

Experience of the circulators and drives during commissioning has been very satisfactory. The hydrodynamic gas seals in particular have behaved well. Site tests have not indicated any problems due to pressure oscillations in the gas circuit.

The throttle valves are butterfly valves with a large annular gap between the disc and duct and with a central hole in the disc. Hence ganged movement of the throttle valves cannot completely shut off the reactor flow. The bypass valves are mechanically linked with the throttle valves so that they move in antiphase which not only prevents circulator stall but ensures adequate natural circulation under fault conditions with the circulators stationary (Fig. 2).

There is an ac emergency pony motor on the main shaft. The pony motor has two speeds: 20% speed for full pressure operation and 50% for operation at atmospheric pressure. The use of the ac pony motors led to an ac emergency system which is very simple, the pony motors being started from the control room when emergency conditions arise.

Constant speed circulators driven by squirrel cage motors are also used at Sizewell but in this design the circulators, although of the axial flow type, are

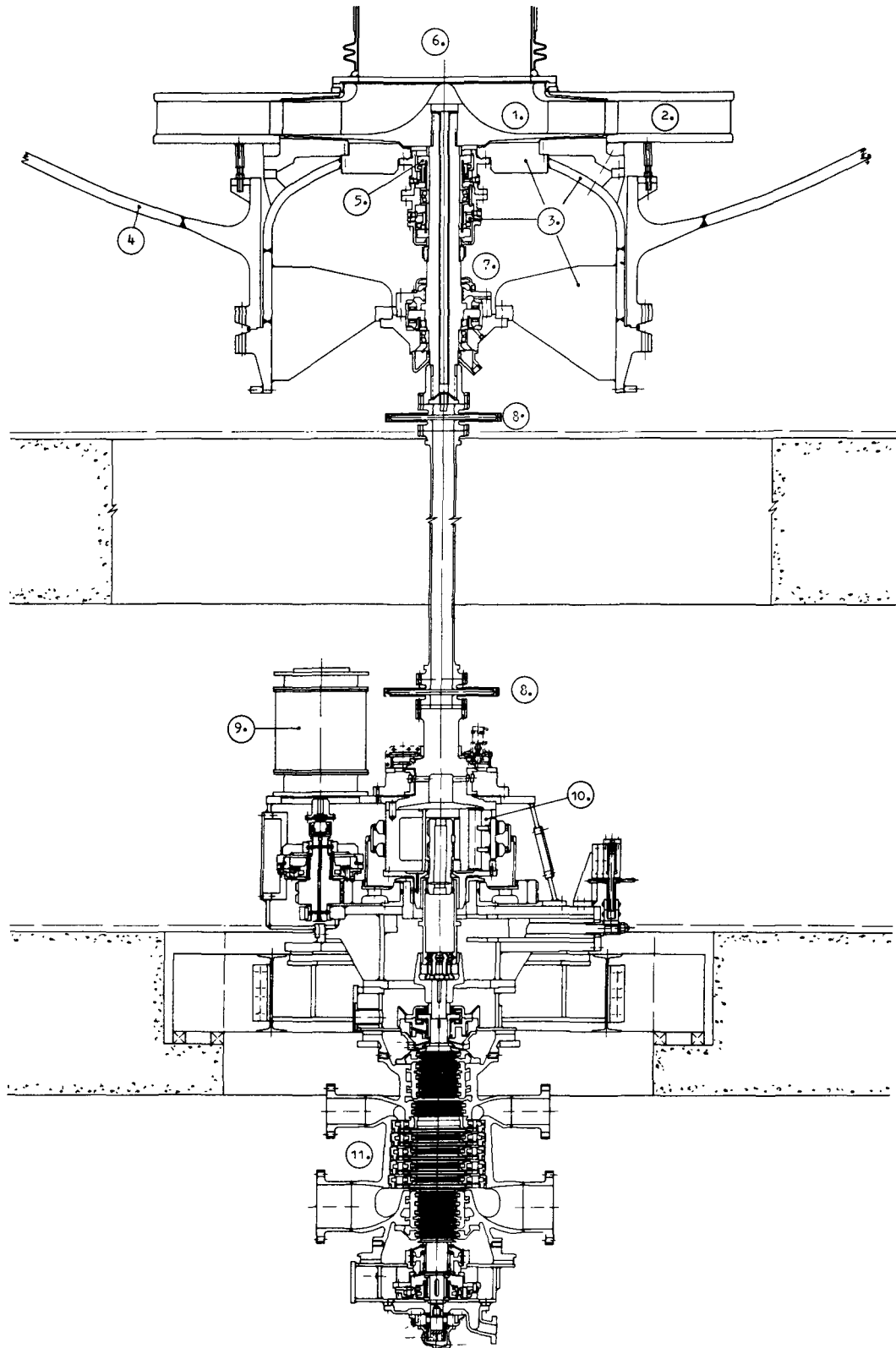


Figure 3. Tokai nuclear power station gas circulator and drive turbine
 1: Impeller; 2: Diffuser; 3: Removable circulator unit; 4: Pressure casing; 5: Gas seal; 6: Inlet ducting; 7: Thrust bearing;
 8: Flexible disc coupling; 9: Pony motor; 10: Epicyclic gearbox; 11: Steam turbine

arranged with vertical shafts with upward gas flow. Gas flow control is obtained by means of gas bypass valves and inlet guide vane movement.

At Tokai, steam turbine drive was selected because of the high power demand associated with highly rated hollow fuel and the economic and safety advantages. The optimum HP steam generation for the dual pressure cycle is compatible with the circulator power requirement at full load and a wide range of speed control is available. Furthermore, an adequate dryness in the main turbine exhaust is obtained by passing the partly expanded HP steam into the LP system before superheating all the steam in the LP superheater.

The excess HP steam available at part load conditions is utilized in HP stages of the main turbines with a resulting improvement in part load efficiency. Although the circulators run at a rather higher speed (1 200 rpm), the design for Tokai (Fig. 3) follows closely that for Hunterston, a high speed turbine and epicyclic gearbox replacing the dc motor. The spindles are vertical and the main boiler shell forms the pressure casing. There is no flywheel, as the boiler thermal capacity limits the rate of reduction in the steam supply.

The circulator turbine exhaust steam may take any of three paths depending upon the operating conditions. Under normal operation, it passes through a non-return valve to the LP superheater inlet, where it is reheated before passing into the LP steam range and to the main turbines. Under these conditions, the back pressure on the circulator turbine cannot be less than the LP steam pressure. Under certain fault conditions, an exhaust valve to atmosphere is opened to make maximum use of the capacity of the HP boiler to provide power for cooling. The third path is used during start-up and when the steam from auxiliary boilers is providing power for gas flow under shut-down conditions on the reactor. In this case, the exhaust steam is passed through a pressure regulating valve to a dump condenser. The pressure setting is variable but usually set to a low value. Construction of the Tokai station is well advanced and the circulators have run at full speed at atmospheric pressure, driven by the turbines using steam from the auxiliary boilers.

Back pressure turbines are also used for the circulator drive at Dungeness, but for this station direct coupled 13 stage units were adopted. The steam cycle is slightly different from the Tokai system, for the partially expanded HP steam is separately reheated before it combines with the LP steam for passage to the main turbines. The latter are single pressure units, so that the design and control problems are simplified and the costs associated with providing a high pressure cylinder on the main turbine are eliminated.

Stage 3 (1962-1964)

The third stage of development is characterized by concrete pressure vessels containing the reactor

core, boilers and gas circulators with circulator powers up to 20 000 hp. This basic change in reactor design has permitted the development of larger reactors with increased gas pressures and has improved economics.

The duty required from gas circulators and their drives has therefore increased, but at the same time limitations on the physical dimensions have been imposed for two reasons. Firstly, the allowable number and size of penetrations in the wall of the concrete pressure vessel must be minimal since they prevent stressing cables being located in these areas. Secondly, although the maximum rate of rapid depressurization under postulated fault conditions is much less than with a steel vessel, the pressure casing which seals the circulator penetration is the limiting component.

The concrete pressure vessel introduces further restrictions on the choice of drive because the circulators are less accessible and maintenance becomes more difficult both physically and radiologically. A variable speed circulator is preferred for it results in the elimination of flow regulating devices within the vessel.

The circulator power required for Magnox stations and for advanced gas-cooled reactors under development in the UK are so large for reactors of over 500 MW(e) (Table 1) that variable speed ac electric motors have speed limitations and are uneconomic. The types of drives suitable for this duty are restricted to steam turbines or constant speed ac motors. As scoop-controlled fluid couplings are now being developed for the powers required, these allow constant speed motors to drive variable speed circulators.

The high pressure, high temperature, steam conditions of the AGR makes steam turbine drive relatively expensive when account is taken of pipework and control equipment. Special commissioning facilities must also be provided. An over-all assessment of station cost and performance indicates that electric drive is the more economic solution for a net output of about 500 MW. However, if the reactor design output is increased a stage is reached when steam drive is more economic because, by reducing the generator output required, it avoids changing to two main turbines and so prevents a major step change being necessary.

The relatively large pressure losses of an AGR core and the smaller volume flow due to the higher pressure and smaller mass flow than comparable Magnox stations make the centrifugal circulator an attractive proposition.

CONCLUSIONS

Circulator and drive development and application over the past eight years has shown that the progressive increases in reactor output and reduction in circulator numbers have impelled designers to constantly review the circulator designs and drives available and to make a selection most appropriate to the station rating and its economics.

Hunterston and Tokai both show that the incorporation of a simple centrifugal circulator at the base of each boiler shell has produced an attractive design for the lower reactor ratings whilst the increase in gas flow for the subsequent reactors has concentrated development upon axial flow machines. The steam turbine drive first incorporated at Tokai is relatively efficient over a wide range of speed and flow control whilst the constant speed ac motor drive pioneered at Trawsfynydd is a low cost, simple system that has a high efficiency at full load, is very suitable for base load operation, and can be operated over the complete power range for commissioning tests.

The large advanced gas-cooled reactors in concrete pressure vessels now under development require circulators with speed control. For reactors producing about 500 MW(e), the most satisfactory drives are constant speed ac motors in conjunction with scoop-controlled fluid couplings, but steam turbines

become competitive at higher outputs when they avoid a step change in the number of main sets.

The paper illustrates that the very different choice of gas circulators and their drives all have justification for their respective reactors. The factors which influence the choice are not constant, and the designer must be prepared to change the design as reactor development proceeds.

ACKNOWLEDGEMENTS

The authors wish to thank Richardsons, Westgarth & Co., Ltd., and the General Electric Company Limited for permission to use the illustrations and to the United Power Co., Ltd. for permission to publish the paper.

The authors wish to thank their colleagues, and particularly Mr. L. M. Dartnell, for help in the preparation of the paper.

ABSTRACT—RÉSUMÉ—АННОТАЦИЯ—RESUMEN

A/138 Royaume-Uni

Circulateurs de gaz et leur commande pour de grands réacteurs de puissance à réfrigérant gazeux

par H. Bateman *et al.*

On examine les deux principaux types de circulateurs et les nombreuses formes de commande disponibles, ainsi que des exemples de leur application et les raisons pour leur choix.

On décrit les principales caractéristiques des circulateurs centrifuges et axiaux et on discute en détail des mérites relatifs de la commande par turbine à vapeur; de la commande par moteur électrique à courant alternatif à vitesse fixe, par moteur électrique à courant alternatif à vitesse variable et par moteur électrique à courant continu à vitesse variable.

La commande par moteur électrique a l'avantage de la simplicité, mais les moteurs à courant alternatif à vitesse constante demandent soit une boîte de vitesses, soit que la vitesse du circulateur soit adaptée à celle du moteur bipolaire ou quadripolaire, ce qui peut compromettre la conception du circulateur. Les moteurs à courant alternatif à vitesse variable demandent soit une alimentation à fréquence variable, ce qui entraîne des coûts d'installation initiale élevés, soit des porte-balais à haute capacité de transport de courant qui nécessitent beaucoup d'entretien, tandis que les moteurs à courant continu ont une capacité limitée et exigent un équipement coûteux de redressement ou de transformation.

La commande par turbine à vapeur semble attrayante si le niveau optimal de génération de vapeur à haute pression s'harmonise avec la puissance de la soufflerie lorsque la pression d'échappement coïncide avec la pression du système à basse pression dans un

cycle à double pression. Le réchauffage de la vapeur à haute pression partiellement détendue et le mélange avec de la vapeur à basse pression fournit une méthode simple et économique de régler l'humidité de la vapeur dans les cylindres à basse pression de la turbine principale.

On insiste sur la nécessité de joints exempts d'ennuis pour éviter des fuites de gaz toxiques venant du circuit sous pression du réacteur.

Une partie du mémoire est consacrée aux aspects les plus importants de la commande du circulateur et à l'influence des considérations de sécurité sur la conception des commandes. On examine l'incorporation et l'utilisation de moteurs démarreurs.

Les essais de mise en service effectués avant la divergence afin de vérifier la solidité mécanique du circulateur et l'absence de vibrations dans les circuits sous pression ont une influence sur le type de commande, et on décrit le but des différents essais effectués sur les lieux.

Le mémoire donne une récapitulation des caractéristiques des circulateurs et des commandes des réacteurs de puissance civils construits au Royaume-Uni, qui permet de discerner trois stades dans le développement et la conception des réacteurs.

Ceux du premier stade utilisaient des commandes par moteurs électriques et le principe du réglage du débit du gaz réfrigérant au moyen de la variation de la vitesse, tandis que ceux du second stade avaient des turbines à vapeur à vitesse variable ou des moteurs électriques à vitesse fixe avec réglage du débit du gaz par vannes.

Les caissons en béton d'une seule pièce contenant le cœur du réacteur, les chaudières et les circulateurs que l'on construit actuellement constituent le troisième stade et posent de nouveaux problèmes. Le nombre d'orifices de pénétration dans la cuve et leur diamètre

doivent être réduits au minimum. Le réglage du débit du gaz par vannes est difficile à réaliser, car les dispositifs de réglage devraient se trouver à l'intérieur de la cuve avec les circulateurs; le réglage du débit par variation de vitesse semble donc de nouveau intéressant. Le mémoire se termine par un bref coup d'œil sur les tendances futures.

A/138 Соединенное Королевство

Газовые циркуляционные насосы и их приводы для больших энергетических реакторов с газовым охлаждением

Х. Бэйтмен et al.

В докладе исследуются и обсуждаются два основных типа циркуляционных насосов и различные виды приводов, а также даются примеры их использования и основания для выбора. Описываются основные свойства центробежных и аксиальных циркуляционных насосов и широко обсуждаются относительные достоинства паротурбинного привода и электрических приводов с двигателем переменного тока с фиксированной скоростью, двигателем переменного тока с переменной скоростью и двигателем постоянного тока с переменной скоростью.

Электромоторные приводы благодаря своей простоте обладают определенными преимуществами, однако двигатели переменного тока с постоянной скоростью требуют либо использования коробки передач, либо подгонки скорости насоса к скорости двух- или четырехполюсного мотора, что может усложнить конструкцию насоса. Двигатели переменного тока с переменной скоростью требуют либо подачи переменной частоты, что связано с повышенной первоначальной стоимостью установки, либо передачи на щетки больших токов, что связано с необходимостью в текущем обслуживании. Двигатели постоянного тока имеют ограниченную мощность и требуют дорогостоящего оборудования для выпрямления или преобразования.

Паротурбинный привод кажется заманчивым, если оптимальный уровень генерации пара высокого давления соответствует мощности продува, когда давление на выходе совпадает с давлением в системе низкого давления в двойном цикле давления. Подогрев частично расширенного пара высокого давления и смешивание с паром низкого давления дает точный и экономичный метод регулирования влагосодержания пара в цилиндрах низкого давления основной турбины.

Особенно подчеркивается необходимость в мерах предосторожности, с тем чтобы предотвратить утечку токсичных газов из реакторного контура высокого давления.

Один раздел доклада посвящен важным проблемам управления циркуляционными насосами и влиянию на системы управления соображений безопасности; обсуждается применение пусковых моторов.

Тип привода определится в результате испытаний докритических условий, которые должны доказать механическую надежность машинного оборудования насосов и отсутствие вибраций в контуре высокого давления. Описываются цели проведения отдельных испытаний.

В докладе приводится обзор характеристик циркуляционных насосов и приводов, используемых в энергетических реакторах Великобритании. Обзор показывает, что разработки делятся на три стадии.

К первой стадии относятся электрический привод и управление потоком охлаждающего газа изменением скорости. Ко второй стадии относится паротурбинный привод с переменной скоростью или электрический привод с двигателями постоянной скорости и клапанным управлением потока газа.

Строящиеся в настоящее время баки высокого давления из монолитного бетона с активной зоной внутри, бойлеры и циркуляционные насосы относятся к третьей стадии и представляют новые проблемы. Диаметр и число трубопроводов, входящих в такие баки, должны быть минимальными. Использование для регулирования газового потока клапанной системы также вызывает трудности, так как регулирующие приборы в этом случае должны помещаться внутри бака с насосами. Регулирование потока изменением скорости опять становится заманчивым. В конце доклада кратко обсуждаются возможные направления в будущем.

A/138 Reino Unido

Las soplantes y sus sistemas de accionamiento para grandes reactores de potencia refrigerados por gas

por H. Bateman et al.

Se investigan y discuten los dos tipos básicos de soplantes y las muchas formas de accionamiento disponibles, junto con ejemplos de su aplicación y las razones para su elección.

Se describen las principales características de las soplantes centrífugas y axiales, incluyendo una extensa discusión de las ventajas relativas de los accionamientos por turbina de vapor, motor eléctrico de c.a. y velocidad fija o velocidad variable, y de c.c. de velocidad variable.

El accionamiento por motor eléctrico tiene la ventaja de la simplicidad, pero los de c.a. de velocidad constante necesitan una caja de cambios o que la velocidad de la soplante coincida con la de un motor de 2 ó 4 polos, lo cual puede comprometer el diseño de la soplante. Los motores de c.a. de velocidad variable

requieren una fuente de alimentación de frecuencia variable que supone una fuerte inversión inicial o un sistema de conmutación para corriente elevada de mantenimiento delicado. Los motores de c.c. tienen una capacidad limitada y requieren un equipo costoso de rectificación y conversión.

El accionamiento por turbina de vapor es interesante si el nivel óptimo de generación de vapor de alta presión se corresponde con la potencia de la soplante cuando la presión de escape se hace coincidir con la del sistema de baja presión en un ciclo de dos presiones. El recalentamiento del vapor de alta presión parcialmente expandido y su mezcla con vapor de baja proporcionan un método elegante y económico de controlar el contenido de humedad del vapor en los escalonamientos de baja presión de la turbina principal.

Se subraya la necesidad de cierres herméticos a prueba de fallos para impedir el escape de gases tóxicos del circuito de presión del reactor.

Se dedica una sección de la memoria a los aspectos más importantes del control de la soplante y a la influencia de las consideraciones de seguridad sobre los criterios de control, y se discute la incorporación y uso de motores auxiliares de arranque.

Se describe el conjunto de pruebas de puesta en servicio previas a la criticidad para comprobar la resistencia mecánica de la maquinaria de la soplante y la ausencia de vibraciones del circuito de presión.

Estas pruebas tienen influencia sobre el tipo de accionamiento. También se describe la finalidad de varias pruebas efectuadas «in situ.»

Se incluye una visión de conjunto de las características de la soplante y su accionamiento para los reactores comerciales de potencia proyectados en el Reino Unido. Se infiere que el desarrollo y los criterios de proyecto han pasado naturalmente por tres grandes etapas.

La primera etapa poseía accionamiento por motor eléctrico y control del caudal de gas refrigerante mediante variación de la velocidad, mientras que en la segunda etapa se empleaban turbinas de vapor de velocidad variable o motores eléctricos de velocidad fija con control del caudal de gas por medio de válvulas.

Las vasijas de presión de hormigón de un solo bloque que se construyen actualmente conteniendo el núcleo del reactor, los cambiadores de calor y las soplantes, constituyen la tercera etapa y presentan nuevos problemas. El diámetro y número de orificios de penetración en la vasija deben ser mínimos. El control del caudal de gas mediante válvulas es difícil de conseguir ya que los mecanismos reguladores tendrían que estar dentro de la vasija junto con las soplantes. El control del caudal por variación de la velocidad ha vuelto a ser interesante. La memoria concluye con una breve discusión sobre las tendencias futuras.

Some engineering problems of the SGHW 100 MW(e) prototype reactor

By N. Bradley,* P. J. Cameron** and N. G. Worley***

The direct steam cycle Steam Generating Heavy Water (SGHW) prototype reactor [1] is of the vertical pressure tube type, and principal components of engineering interest are shown in Fig. 1. Dual moderation results from the high pressure boiling-light-water coolant in the pressure tubes and the low pressure heavy water in the calandria.

The core consists of 112 zirconium alloy pressure tubes connected to the external stainless steel coolant system by mechanical joints. Two coolant circuits are each provided with a steam separation drum and two glandless recirculating pumps. Saturated steam, produced by boiling in 104 of the channels, passes from the steam drum to the 100 MW(e) saturated steam turbine at 900 psig. A portion of the steam from the drums flows to 8 superheat channels which are designed for 1 000 °F (538 °C) maximum outlet temperature, this steam being subsequently mixed with the main saturated steam flow to the turbine.

Experimental loop facilities are provided for tests under boiling and superheat conditions. One of the boiling channels can be connected to a self-contained circulating and heat rejection equipment and two small pressure tubes are located in inter-lattice positions and provided with their own boiling loop circuit for fuel development work. The output of one superheat pressure tube can be diverted direct to the turbine condenser.

The reactor will be refuelled whilst operating at power for both superheat and boiling channels. In the presence of a two-phase mixture or a condensable gas (steam) it is impracticable to cool the joint seals to less than the saturation temperature (280 °C). This temperature eliminates the use of organic seals and so a metal to metal joint between the refuelling machine and pressure tube is under development. Since the fuel and its associated components are handled as a rigid assembly some 32 ft (10 m) long during refuelling, the refuelling machine is tall and protrudes through the main biological shielding surrounding the core and reactor coolant system. As this shielding also serves as a low pressure containment, the rotating shield associated with the refuelling machine must be provided with a gas tight seal to the main concrete shielding.

* U.K. Atomic Energy Authority, Reactor Group, Risley.

** The Nuclear Power Group, Knutsford.

*** Babcock and Wilcox Ltd., London.

CALANDRIA OR MODERATOR VESSEL

The use of dual moderation leads to a lower heavy water investment and closer pressure tube lattice pitch, compared with a D₂O moderated and cooled reactor, thus accommodation of Zircaloy/steel joints and coolant circuit connecting pipes is a major problem. This is further aggravated in the prototype reactor by the experimental requirements to vary the quantity of heavy water in the lattice to less than that required for an economic reactor design.

A solution has been developed in which tubes at inter-lattice positions are built into the calandria. These tubes are open to the helium gas blanket at the upper end and connected to a drainage system at the lower end. With empty inter-lattice tubes, the pressure-tube lattice pitch becomes sufficient to accommodate the Zircaloy/steel joints and coolant pipes and achieve the low heavy water/fuel ratios that are required. Flooding selected numbers of inter-lattice tubes permits the heavy water/fuel ratio to be increased.

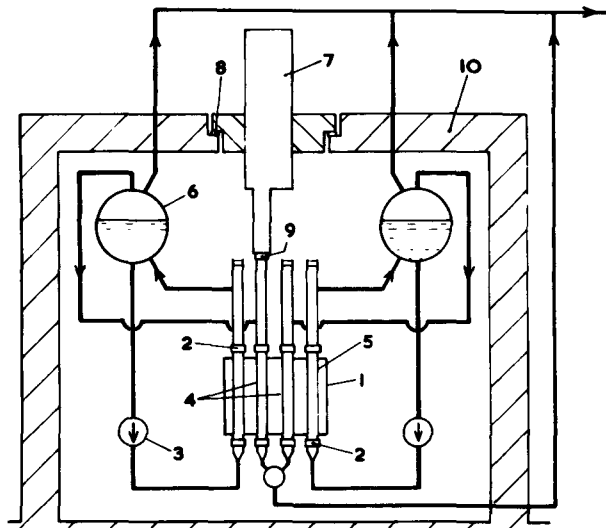


Figure 1. Diagram of SGHW prototype reactor
 1: Calandria (moderator vessel); 2: Mechanical joints; 3: Glandless recirculating pumps (4 off); 4: Superheat channels (8 off); 5: Boiling channels (104 off); 6: Steam separation drums (2 off); 7: Refuelling machine; 8: Rotating shield seal; 9: Refuelling machine to pressure tube joint; 10: Biological shielding

Moderator level variation, which is used for limited reactivity control, leads to a problem in extracting water from the top end of the core to feed the moderator cooling system. Moderator must also be pumped to the top of the calandria to cool the portions not submerged in the bulk moderator. The simplest arrangement has all the re-cooled moderator returned through the top of the core tank and extracted from the bottom.

To investigate the circulation system in the calandria a quarter-scale model was made at The Nuclear Power Group, Knutsford. The heat generated in the calandria tubes, inter-lattice tubes and the moderator bulk was simulated. Extensive thermocouple readings at three different levels showed that radial variations did not exceed 8 °C and that vertical axial variations were less than 2 °C although the water inlet temperature was 40 °C below the bulk moderator temperature. Temperature traverses local to the top cold water inlets indicated efficient mixing. The tests showed that natural circulation of the water in the calandria predominates and that the coolant return flow can all be pumped to the top of the core.

MECHANICAL JOINTS

A low neutron cross-section material is necessary for the pressure tubes and this must be of sufficient strength at the operating temperature to allow a high coolant pressure to be employed without excessive thickness. The only suitable materials are zirconium alloys and of these, cold-worked Zircaloy-2 has been selected. This material is costly and therefore steel has to be used for the external coolant circuit where there is no need for neutron economy. In view of the uncertainty on the long-term corrosion of mild steel or low alloy steels in oxygenated water, austenitic stainless steel was selected.

A strong leak tight joint has therefore to be made between the zirconium alloy pressure tube and the steel piping of the rest of the circuit, both above and below the reactor core. This joint must accept the forces and temperature changes associated with the layout of the plant and the coolant. It also has to remain leak tight despite the dimensional changes due to the differences in the coefficients of expansion between the materials of the joint. The close pitch of the pressure tubes restricts the size of the joints to 8in (203 mm) od.

For the SGHWR, simultaneous development work on a bolted joint for which a design theory is available and on a simpler but empirically designed expanded joint was carried out. Development on a flanged and gasketed bolted joint started at the U.K. Atomic Energy Authority's Reactor Engineering Laboratories in 1958. This work was later transferred to the Babcock & Wilcox Research Station, Renfrew, where tests of an expanded joint were also carried out. In fact, tests on developed designs based on both of these concepts have produced joints which are satisfactory for SGHWR service.

Testing

For proving the bolted and expanded designs, tests must, as far as possible, reproduce in 1 year the whole life of the joint, i.e., 20 to 30 years. Clearly, a realistic number of load and thermal cycles have to be applied and also some attempt made to reproduce the creep and relaxation that will occur in service. In the reactor system, the torques and bending moments exerted on the joint are limited by physical restrictions, but to ensure that the joints are sufficiently robust, tests were carried out with bending moments of 1 000 lb ft (139 kg m) and torques of 500 lb ft (69 kg m) simultaneously with 1 000 full thermal and pressure cycles. These test parameters are 4 times the predicted reactor condition. The pull-out strength of the expanded joints was specified as 94 000 lb (43 000 kg), 4 times the sum of the axial pressure and pipework loads.

All joints of the final designs, when subjected to these tests, had a leak rate less than the 0.1 clusecs (0.1 cm³/d at atmospheric pressure) limit associated with the sensitive helium mass spectrometer measuring equipment employed.

Bolted joint

The initial development work covered the experimental and theoretical assessment of a number of principles for sealing faces of ferritic steel and Zircaloy, including a survey of gasket materials and joint geometry. The assessment of hard and soft gasket materials demonstrated the superiority of the soft materials, in particular their ability to accommodate the relative movements of the faces and acceptance of small defects in the surface without leakage.

This work led to the recommendation of a design with a soft silver gasket, held between gramophone finish flanges compensated for axial expansion. An interlocking flange arrangement is used which reduces the bolt load when the system is under pressure by loading the gasket directly from the pressure forces and fits in the limited space available. After 800 stress and temperature cycles, leaks of several hundred clusecs developed in two of the joints under test. Calculations, confirmed by bolt relaxation tests, demonstrated that the design had insufficient resilience to allow for the effects of creep of the component parts. Tests also suggested that the corrosion resistance of silver in oxygenated water was inadequate whilst gold would be satisfactory. The design was therefore modified (Fig. 2) to increase resilience by lengthening the bolts, reduce some high local stress and incorporate a gold gasket. This design has now successfully passed its trials.

Expanded joint

Smaller expanded joints have been applied successfully to NPD, the Canadian pressure tube reactor and a joint arrangement similar to that proposed by the NPD team for the SGHWR conditions, was used (Fig. 3). Cold-worked Zircaloy-2 has a high strength at room temperature and must be deformed plastically

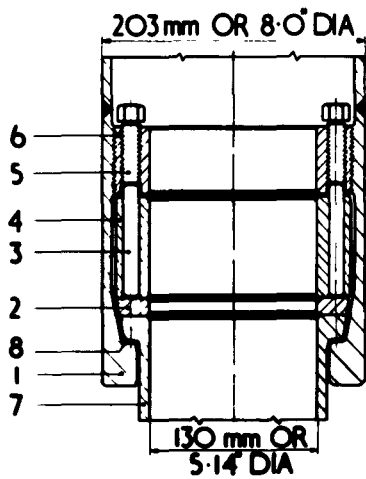


Figure 2. Final top pressure tube bolted joint

1: 12% chromium steel hub; 2: 12% chromium steel compensator ring; 3: Precipitate hardened stainless steel studs; 4: Stainless steel support ring; 5: Precipitate hardened stainless steel bolts; 6: Precipitate hardened bolt flange; 7: Zircaloy pressure tube; 8: Gold gasket

during rolling. The hub material against which it has to be compressed must combine high elastic modulus and strength. Heat treated 12% chromium martensitic steel which also has an expansion coefficient intermediate between Zircaloy and austenitic steel was chosen. Subsequent pull-out, creep, load temperature cycling and thermal shock tests on 12 rigs, each with 2 joints, demonstrated that the design is suitable for SGHWR application. Two failures have occurred in tests, one in which joints were subjected to a high temperature of 320 °C and the other as a result of an accidentally large shock bending moment. These joints only leaked at a rate of about 60 clusecs after initial failure and in one case, during subsequent tests, the leak resealed. In the other case, the low leak rate was not increased appreciably during further

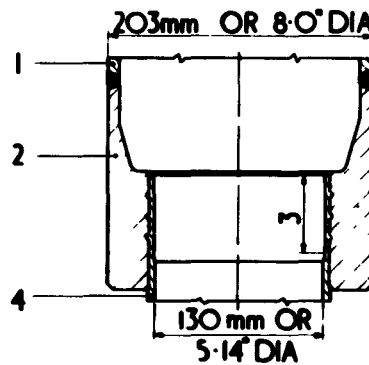


Figure 3. Rolled joint between Zircaloy-2 and 12% chromium steel

1: Stainless steel (18/8/1 Ti); 2: Heat treated 12% chromium steel; 3: Expansion length; 4: Zircaloy-2 (cold-worked)

When pumping power fails, the margin between the cooling required and that available immediately reduces, Fig. 4. The inertia that has to be built into the pump system to ensure curve (1) never decays to a value below curve (2) has been investigated taking into account the delay in tripping the reactor, the normal running margin and the hydraulic characteristics of the circuit.

The effect of pump inertia, normal running margin and the time to trip upon burn-out margin or fuel can overheating is shown in Fig. 5. Glandless pump design studies showed that an inertia of 1 000 lb ft² (42.2 kg m²) was possible without going beyond current design knowledge, although efficiency must be sacrificed. Optimum pump unit efficiency would occur with about 200 lb ft² (8.4 kg m²) inertia and represents normal practice if no rundown limitations applied.

An inertia of about 1 000 lb ft² was required and three alternatives were studied and compared with units designed for optimum efficiency.

	Cost	Efficiency to pump shaft %
(a) Glandless, wet stator, 1 000 lb ft ²	1.0	72
(b) Glandless, wet stator, 200 lb ft ² plus 800 lb ft ² electrically coupled	1.3	72
(c) Glanded, external flywheel, 1 000 lb ft ²	1.3	82
(d) Glandless, wet stator, 200 lb ft ² approximately	0.9	82
(e) Glandless, dry stator, 200 lb ft ² approximately	1.3/1.8	80/82

cycling tests. Expanded joints will be used in the SGHWR because they are simpler in design and cost less than a bolted joint.

PRIMARY CIRCULATING PUMPS

The primary circulating pumps must be leak free and simple in design, since failures require reactor shutdown for maintenance. Whilst in North America the trend has been towards limited-leakage glanded units on grounds of inertia requirements, capital cost and efficiency, study of these factors has led to the choice of a glandless unit for SGHWR.

The unit with an electrically coupled motor-alternator-flywheel is more expensive than the 1 000 lb ft² glandless unit, it depends upon questionable electrical coupling integrity, and has no better over-all efficiency. For case (c) the most reliable pump gland with adequate potential for the duty appears to be the floating ring design development for Central Electricity Generating Board feed pumps. For the 4 pumps each of 450 kW shaft power, the gland sealing requirement represents an appreciable fraction of the pump energy and the capital cost of the seal water plant is also significant at this pump size. An important factor in the capital cost comparison is that the wet

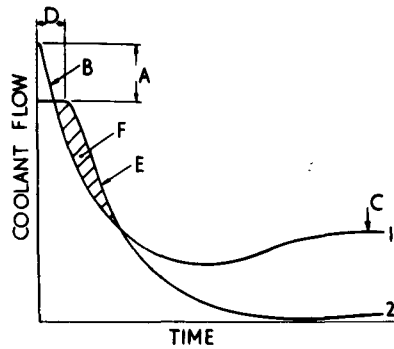


Figure 4. Pump rundown characteristics

1: Coolant flow curve; 2: Coolant flow requirement curve; A: Normal running margin; B: Rapid decay due to pump rundown; C: Stable natural circulation; D: Reactor trip time; E: Decay of nuclear and stored heat input; F: Deficit of cooling capability

stator glandless units, case (d), are considerably lower in price than dry stator units, case (e), as extensively used in North America.

Wet stator units have already been built for commercial power stations, are operating at the size required for the prototype reactor and are suitable for 1-2 years continuous operation. Operational experience of the activity problems in a reactor circuit, available from the use of smaller units in our materials testing reactors and loops, indicate no difficulties.

SUPERHEAT CHANNEL DESIGN

The primary object of the prototype reactor is to demonstrate the reliability, economy and safety of the system when producing saturated steam. Superheat has proved economically attractive in power station practice and in order to demonstrate the development potential of the SGHW system, 8 superheat channels are incorporated into the prototype to raise the steam temperature from 280 °C saturation to 538 °C maximum.

The pressure tubes and standpipes are very similar to those in the boiling channel and consist of a Zircaloy in-core section rolled into heat treated ferritic stainless steel hubs at either end. Materials other than Zircaloy are unsuitable for the in-core section either because they are too weak at the operating conditions proposed or, alternatively, their neutron absorption is too high in the thicknesses required.

Zircaloy is not an ideal material as both corrosion and hydrogen embrittlement increase with increasing temperature. For design purposes a zirconium temperature limitation of 320 °C has been adopted. It follows therefore, that the Zircaloy in the pressure tube (and in any other Zircaloy superheat channel component) must be insulated from the superheated steam and cooled to remove both the heat transmitted through the insulation and that generated within the Zircaloy due to nuclear heating. The integrity of the

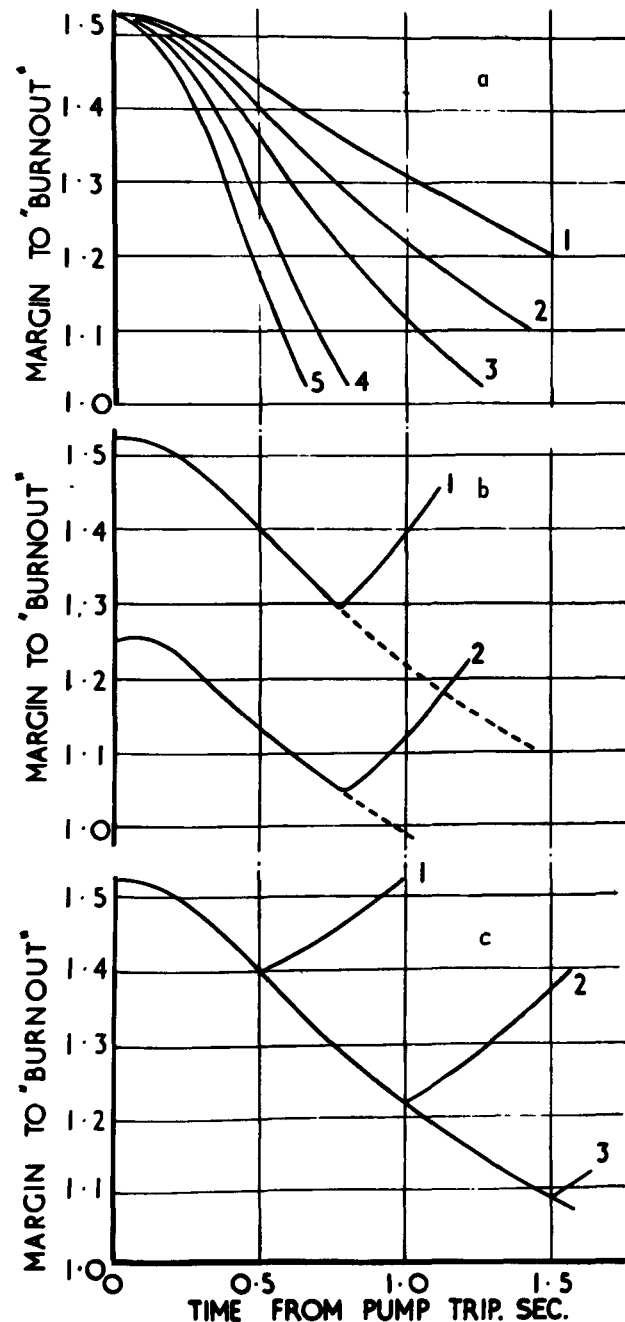


Figure 5. Coolant circuit performance characteristics
(a) Effect of pump inertia (assuming no reactor trip):

Curve	lb ft ²	kg m ²
1	1 500	62.3
2	1 000	42.2
3	700	29.6
4	350	14.8
5	200	8.4

(b) Effect of normal running margin (assuming 1 000 lb ft² inertia 0.8 s trip): Curve 1: 110% rating; Curve 2: 125% rating; and (c) Effect of reactor trip delay (assuming 1 000 lb ft²): Curve 1: 0.5 s trip; Curve 2: 1.0 s trip; Curve 3: 1.5 s trip

pressure tube is essential and the cooling must be both positive and have ample margin to cover differences in calculated and actual performance.

Several designs of superheat channel have been investigated and that shown in Fig. 6 appears to be the most satisfactory. In this design, a fixed internal liner is welded to the standpipe and tailpipe so as to form an annulus between it and the pressure tube extending over a length of channel equivalent to about twice the core height. The in-core section of the liner is in Zircaloy and the out-of-core section predominantly ferritic stainless steel. Rolled joints connect the Zircaloy and stainless steel sections together. The annulus formed between the pressure tube and Zircaloy/steel liner is cooled by circulating drum water through it. This water is tapped from the discharge side of the reactor circulating pumps, flows upwards through the annulus and returns to the drum. The steam quality at exit from the cooling annulus is approximately 15% by weight, thus allowing a considerable margin for uncertainty in heat loss calculation and a very positive method of heat removal. The latter, coupled with the similarity of materials at each point on the two walls of the annulus results in a low differential expansion under all steady operating conditions. Nevertheless, a bellows expansion piece is included in the upper end of the liner wall to allow for transient conditions. A further point to be noted is that the inner wall of the annulus must be designed to withstand the maximum differential pressure occurring between the drum and the channel steam outlet. This differential pressure acts inwards tending to collapse the liner.

In order to insulate the Zircaloy components from the superheated steam, a further removable liner of 0.020 in thick stainless steel is inserted inside the Zircaloy and steel annulus. This liner which is at steam temperature is located at the upper end on a conical seat and is spaced from the Zircaloy and steel liner by stainless steel spring spacers of the type shown in Fig. 6. A sufficiently thin liner can be designed to avoid a serious penalty from neutron absorption. The spring spacer design allows partial closing of the gap between the two liners to occur without overheating the Zircaloy liner where it touches the spring of the spacer even when the latter is fully compressed.

The insulating properties of the annulus between the stainless steel liner and the Zircaloy-steel liner depends on the steam in the annulus being substantially stagnant. For this reason, the conical seat on which the stainless steel liner sits is backed up by a labyrinth seal and all heat transfer calculations are based on the assumption that the leakage flow in the stagnant annulus is equal to that across the labyrinth with the sealing effect of the conical seat ignored.

The Zircaloy and stainless steel liner tubes are manufactured by a helical welding technique which provides a tube straightness better than 1 in 3000.

Test rigs are being set up to investigate the problems of vibration on the liner and fuel element system, fuel element insertion into the channel and past the steam

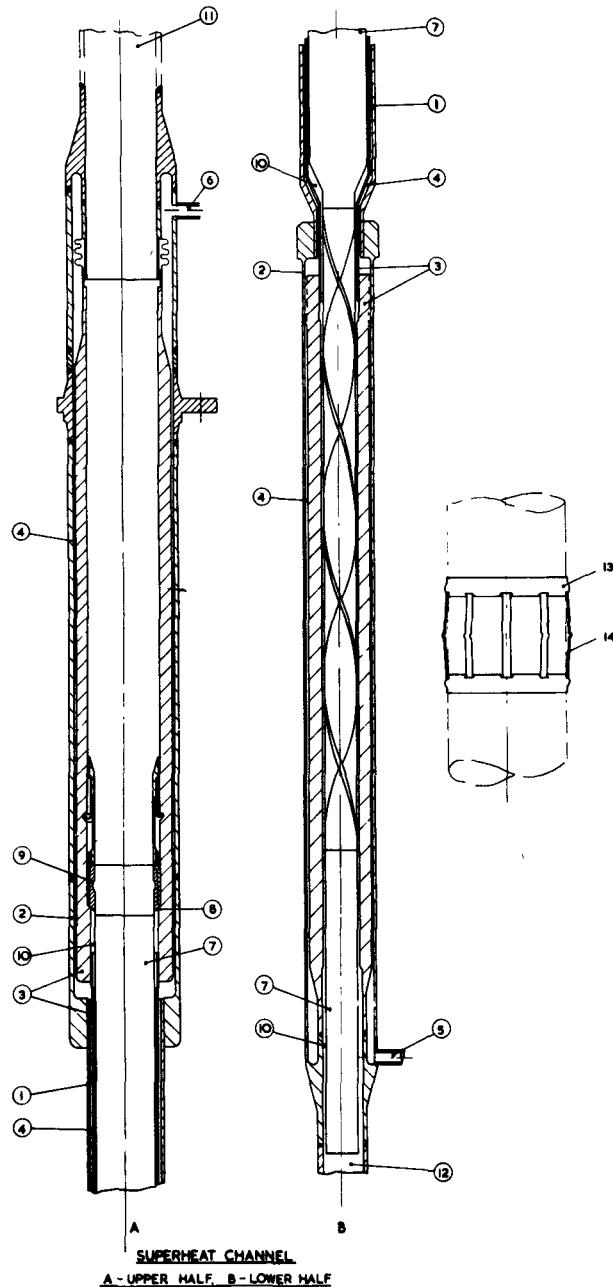


Figure 6. SGHW 100 MW(e) prototype reactor

1: Pressure tube, zirconium in-core section; 2: Pressure tube, steel out-of-core section; 3: Zirconium steel liner; 4: Cooling annulus; 5: Coolant inlet from drum; 6: Coolant outlet to drum; 7: Inner stainless steel liner; 8: Conical seat for inner liner; 9: Inner liner labyrinth seal; 10: Stagnant steam insulation; 11: Saturated steam inlet; 12: Superheated steam outlet; 13: support ring; 14: Free leaf springs

inlet port and fretting between the stainless steel spacers and the Zircaloy liner. A test is also being carried out on the labyrinth seal to confirm the leakage calculation.

EXPERIMENTAL LOOPS

Loops are provided on the prototype SGHW reactor to demonstrate and exploit its potential

particularly with respect to the use of less expensive primary circuit materials and the development of more advanced fuel element designs. Two loops are installed; one large boiling loop constructed from ferritic steel connected to a standard reactor channel providing a self-contained heat rejection system for the output from that channel and one boiling pencil loop constructed from austenitic stainless steel connected to two stainless steel small pressure tubes connected in parallel and located at inter-lattice positions in the reactor core.

The coolant circuit material of the prototype reactor is stainless steel but economics studies have shown it would be desirable to use mild steel and the suitability of this both at power and during shutdown will be investigated with the large loop. The technique of hydrogen overpressure used in PWR systems to suppress oxygen levels may not be applicable to the SGHW direct boiling cycle as hydrogen will be continuously stripped out in the power plant condenser off-gas system. Recycling the hydrogen introduces further problems. Experiments carried out in a small loop are not conclusive since the ratio of the coolant volume to the loop surface area is not representative for a power reactor. Hence, operation of a full-size prototype loop having facilities for adding and recirculating any excess hydrogen is a prudent requirement before an SGHW reactor using a mild steel coolant circuit is constructed. Provision for adding ammonia and hydrazine and for the accommodation of test coupons is also provided.

Tests of fuel pins in the small loop covers the early development stages for advanced fuel designs, whilst the large loop enables the cluster design to be endorsed under irradiation conditions without risk to the main circuit and power plant. The large loop is designed for a maximum working pressure of 1 500 psig (105 kg/cm²) to have a heat rejection capacity of 200% of the normal boiling channel heat output and to handle up to 150% of the normal boiling channel flow. Prediction of the safe operating margin to burn-out has so far been based upon using out-of-reactor tests in conjunction with calculation and very restricted in-reactor measurements. The 200% heat rejection capacity will enable an adequate margin to burn-out to be demonstrated for a given cluster design.

Information is available from the advanced gas cooled reactor system relating to stainless steel clad UO₂ fuel, supplemented by steam-cooled single-fuel-pin tests in the Canadian NRX reactor (carried out under a joint AECL/UKAEA development programme). A major feasibility problem not encountered in the CO₂ cooled reactor system is stress corrosion at the inlet end of the fuel. Since this depends upon the moisture carried over from the steam drum, its chloride content and the oxygen level, the correct conditions would not be obtained in a recirculating loop. Therefore, to avoid risk of contaminating the reactor and turbine when testing advanced fuel designs, one superheat channel is arranged so that

coolant of the correct composition can be used and passed directly to the turbine condenser and clean-up plant after leaving the superheat channel.

REFUELLING EQUIPMENT

The principal design problems for an on-load SGHWR machine are the same as those of the gas-cooled stations, for which there is extensive design and operating experience, with the additional problem that no organic seal is adequate for operation at the saturation temperature of 537 °F (280 °C). The shielded machine must be accurately positioned over and sealed to the pressure tube (whose location will depend on the reactor temperature) and then remove the fuel element assembly into the machine and replace it by a fuel assembly already stored in the machine. The irradiated fuel will be releasing a significant proportion of its full power heat and this heat must be removed all the time the fuel is in transit to the machine as well as in the machine itself. The machine has also to operate successfully with the reactor off-load, unpressurized, and cold.

The fuelling machine is mounted eccentrically in rotating shields which permit it to be positioned over any reactor pressure tube as well as the discharge facility and other positions (Fig. 1). These rotating shields form part of the primary containment structure and seals are provided so that the primary containment boundary is maintained at all times.

Seals for the rotating shields

The seal, which is 36 ft (11 metres) long, must have a high standard of leak tightness under any possible condition, including accidents, during the life of the plant. The use of hydrostatic bearings in supporting the shield has also led to an acceptable solution of the sealing problem.

The performance of the hydrostatic bearing depends on the introduction of a pressurized oil film between the rotating and the stationary member. The latter comprises a large number of seal pads. Oil at about 150 psig is fed to the seal pads and flows radially across the pads into weirs from which it returns to the pump suction by gravity. Assembly of these pads as a continuous ring around the shield periphery provides a hydrostatic oil seal.

Under both normal and accident conditions the oil pressure resists the difference in pressure between the primary and secondary containment. Frictional resistance to shield rotation is negligible during normal operation and even should the oil supply fail, there is adequate time to stop shield rotation before there is a significant increase in bearing friction.

To take account of inaccuracies in the large concrete shield structures, the bearing pads are mounted on rubber blocks. The relative stiffnesses chosen for the oil film and the rubber have been shown to be tolerant to radial tilting of the pads to 0.2 in (5 mm) and individual pad levelling of 0.08 in (2 mm).

A small-scale bearing rig 5 ft (1.6 m) diam, with pads 4 in × 12 in (100 × 300 mm) was constructed at Fairey Engineering Ltd., Stockport. This showed that because the oil was held up in the weirs, leakage would only occur many minutes after the oil supply to the bearing failed. There was no measurable leakage in normal operation.

Nose unit to standpipe seal

During refuelling operations, the nose unit of the machine forms a pressure boundary with the top of the reactor pressure tube, but as this is located within the primary containment boundary, some leakage at the junction is permissible. The nose unit must cater for positional inaccuracies between the rotating shield and the pressure tube axes and must not exert undue vertical forces on the standpipe. The seal must be capable of withstanding a temperature of about 300 °C at a pressure of 1 000 psig and a leakage of about 1 lb of water per day is considered acceptable.

The nose unit face should be able to operate without replacement for a large number of operations over a period of about 1 year. A spherical component mating with a conical seat has been chosen as the most suitable arrangement for the seal since it can accommodate misalignment between the pressure tube and machine nose unit while still maintaining an adequate seal, Fig. 7. It is necessary, in order to achieve a low leak rate, to counter the steam pressure forces and to maintain a heavy load across the seal and therefore a number of equally spaced clamps are used to load the components. The angle of the surface on the pressure tube is greater than the angle of repose so that large dirt particles falling on the surface are unlikely to remain.

Initial tests at English Electric, Whetstone, with several make and break operations, in some cases with components at angles up to 20 minutes, gave leakage rates of less than 0.15 lb/day. Tests are being carried out with the following hard components: (a) two faces of tungsten carbide, (b) Stellite 6 (66% Co, 26% Cr) and Stellite 12 (59% Co, 29% Cr, 9% W, 1.8% C), (c) two faces of Fontargen 716 (a cast iron with 35% Cr), (d) die steel (16½% Cr, 0.5% Mo) and spheroidal graphite Ni-resist (a cast iron with 3% C, 3% Si, 0.8% Mn, up to 22% Ni, 1% Cr), (e) two faces of die steel (16½% Cr, 0.5% Mo).

Tests with the components at several misalignment angles up to ½° and at various attitudes will be included. Information will also be obtained from the tests upon the effect of ovality of the faces and erosion

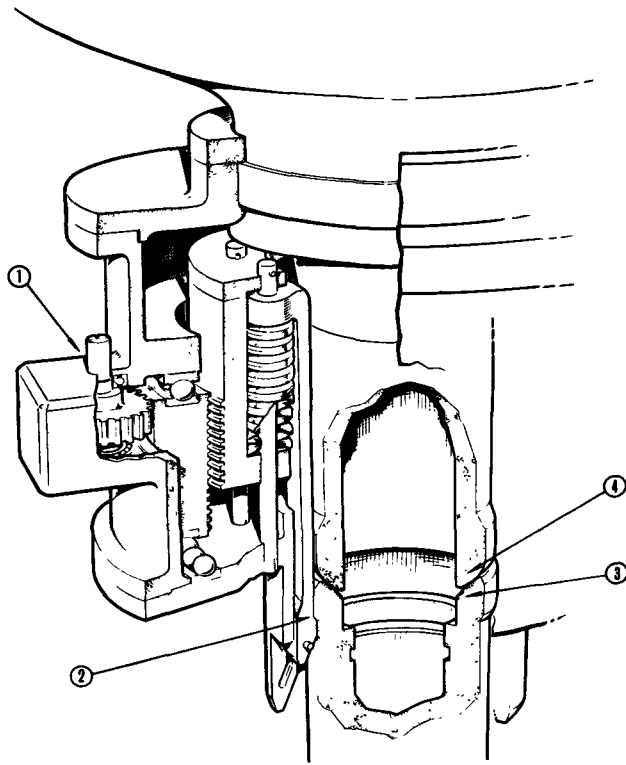


Figure 7. Metallic seal, nose unit to standpipe
1: Drive and compensating mechanism; 2: loading finger;
3: Conical face on standpipe; 4: Spherical face on nose unit

of the surfaces from wet steam flowing across the faces. Other tests will be carried out to prove the suitability of the materials for superheat channel refuelling.

SUMMARY

The paper has described some of the more novel engineering features of the SGHWR system and the associated development work currently being carried out in the laboratories of the three UK nuclear consortia, their member firms and the UKAEA.

Based upon interest shown during collaborative international discussions, the authors have elaborated on those topics which are likely to have widest appeal. Even so, the space available has only permitted restricted presentation of the work carried out.

REFERENCE

1. Fawcett, S., Firth, A., and Holmes, J. E. R., *General Design of the SGHWR*, P/129, Vol. 5, these Proceedings.

ABSTRACT—RÉSUMÉ—АННОТАЦИЯ—RESUMEN

A/143 Royaume-Uni

A/143 Соединенное Королевство

Quelques problèmes de construction
relatifs au réacteur prototype à eau lourde
et générateur de vapeur de 100 MW(e)

par N. Bradley *et al.*

Le mémoire étudie certaines solutions mécaniques nouvelles adoptées pour le réacteur à eau lourde et générateur de vapeur décrit par Fawcett, Firth et Holmes dans le mémoire P/129 (voir les présents Actes, vol. 5).

Le problème de la fixation des tubes de force en zirconium sur le circuit primaire en acier a été étudié et deux types de joints mécaniques, à savoir laminés et boulonnés, ont été mis au point et essayés avec succès.

La double modération entraîne un pas très serré du réseau de tubes de force et on décrit la solution mécanique adoptée. On donne les résultats des essais concernant la distribution de la température dans le modérateur.

Des canaux surchauffés sont prévus pour démontrer que les futurs réacteurs à eau lourde générateurs de vapeur pourront exploiter les avantages du surchauffage sans sacrifier la sécurité ou la disponibilité du prototype. Dans ces canaux, la chaleur gamma engendrée dans le tube de force en zirconium est évacuée par la circulation d'eau bouillante à travers un anneau interne fonctionnant en parallèle avec les canaux principaux à eau bouillante. Une mince garniture en acier inoxydable empêche le transfert convectif de la chaleur de la vapeur surchauffée à l'anneau interne.

On décrit les boucles expérimentales, prévues pour une grappe d'éléments de combustible en régime d'eau bouillante avec un circuit en acier au carbone, et deux canaux pour élément combustible en «crayons» avec un circuit en acier inoxydable. On a prévu la possibilité de vider le réfrigérant d'un canal surchauffé dans le condenseur lors d'essais de combustibles d'un type avancé.

Le rechargement en combustible du réacteur en fonctionnement pose nombre de problèmes techniques qui exigent des solutions originales. On décrit les essais entrepris en vue de résoudre les problèmes principaux.

On indique les paramètres qui influencent le temps d'évacuation de la pompe de circulation primaire et les moyens de donner au système l'inertie requise. On donne également les raisons du choix d'une pompe de circulation sans garniture, à moteur immergé.

Некоторые инженерные проблемы,
связанные с прототипным реактором
SGHW электрической мощностью
100 Мвт

Н. Брэдли *et al.*

В докладе рассматриваются некоторые из более новых инженерных особенностей реактора SGHW, описанного Фосеттом, Фертом и Холмсом (в докладе P/129, т. 5 настоящего издания).

Исследовалась проблема соединения циркониевых труб под давлением со стальными трубами первичного контура, и были успешно разработаны и испытаны два типа механических соединений (болтовое соединение и вальцовка).

Двойное замедление (тяжелая и обычная вода) ведет к использованию тесной решетки труб под давлением, и в докладе описано принятое инженерное решение этой проблемы. Приводятся также результаты испытаний по распределению температуры в массе замедлителя.

В прототипном реакторе предусмотрены (без ущерба для безопасности и эксплуатации прототипа) каналы для перегрева пара, предназначенные для того, чтобы продемонстрировать возможность использования в будущих энергетических реакторах SGHW преимуществ перегрева. В этих каналах тепло, генерируемое в циркониевой трубе под давлением, переносится циркулирующей кипящей водой через внутренние кольцевые каналы, работающие параллельно с главными каналами кипения. Тонкая оболочка из нержавеющей стали предотвращает конвективную теплопередачу от перегретого пара к кольцевым каналам.

В докладе дается описание испытательных петель, предназначенных для исследования сборки тепловыделяющих элементов в условиях кипящей воды для контура из углеродистой стали и тепловыделяющего элемента из двух узких стержней для контура из нержавеющей стали. Предусматриваются меры для отвода теплоносителя из одного канала перегрева в конденсатор при испытании усовершенствованных конструкций топливной сборки.

Перегрузка топлива во время работы реактора представляет ряд конструктивных проблем, требующих новых решений. Сообщается об испытаниях, ведущих к решению основных проблем.

В докладе обсуждаются параметры, влия-

ющие на время реверса циркуляционного насоса первичного контура, и средства, с помощью которых можно обеспечить системе необходимую инерцию. Сообщаются причины выбора бессальникового циркуляционного насоса.

A/143 Reino Unido

Algunos problemas de ingeniería del reactor prototipo SGHW de 100 MW(e)

por N. Bradley et al.

La memoria comenta algunas de las características menos usuales del reactor SGHW descrito por Fawcett, Firth y Holmes en el documento P/129 (véase el Vol. 5 de las presentes Actas).

Se ha investigado el problema de unión de los tubos de presión de zirconio al circuito primario de acero y han sido desarrollados y probados con éxito dos tubos de juntas mecánicas, mandriladas y atorilladas.

La moderación dual conduce a un reticulado de tubos de presión muy compacto. Se describe la solución adoptada para la construcción. Se dan los resultados de las pruebas de distribución de temperatura en todo el volumen del moderador.

Se disponen canales de sobrecalentamiento para demostrar que los futuros reactores de potencia

SGHW pueden aprovechar las ventajas del sobrecalentamiento sin sacrificar la seguridad y factor de utilización del prototipo. En estos canales, el calor gamma generado en el tubo de presión de zirconio es extraído por circulación del agua hirviendo a través de un anillo interno que trabaja en paralelo con los canales de ebullición principales. Una delgada capa de acero inoxidable impide la transmisión de calor por convección desde el vapor sobrecalentado al anillo.

Se describen los circuitos experimentales, preparados para un elemento combustible de haz de barras con agua en ebullición y circuito de acero al carbono, y dos canales con elemento combustible del tipo lápiz y circuito de acero inoxidable. Se ha previsto descargar refrigerante de un canal de sobrecalentamiento al condensador cuando se prueben diseños de combustible avanzado.

La carga de combustible en el reactor durante el funcionamiento presenta un número de problemas de proyecto que requieren soluciones no usuales. Se indican los ensayos conducentes a hallar soluciones para los problemas principales.

Se destacan también los parámetros que afectan al tiempo de parada de la bomba de circulación principal y los medios por los cuales se puede conseguir la inercia requerida en el sistema. Se dan las razones para la elección de una bomba de circulación de rotor sumergido y sin prensaestopas.

Components for sodium reactors

By H. O. Monson,* F. A. Smith,* W. J. Hallett** and J. J. Morabito***

Components for sodium cooled power reactors have evolved through many years of development and application [1]. Significant progress has been made. However, further improvements are needed to satisfy operational requirements of future central station power plants in respect to increased size, higher temperature of operation, and improved reliability. This paper discusses the major components: steam generators, heat exchangers, reactor vessels and pumps for sodium reactor systems. Recent operating experience, difficulties encountered and necessary corrective modifications are described. Procedures for installation, removal and cleaning of components are treated in another paper [2] presented at this Conference.

Since the Second Geneva Conference, the United States has gained experience with diverse designs of major components in sodium reactor systems. The Hallam Nuclear Power Facility [3, 4], a 256 MW(th) graphite-moderated reactor, has been thoroughly tested and operated for several months as a load-following plant. The Experimental Breeder Reactor II [5, 6], a 62.5 MW(th) fast breeder, has completed pre-operational testing and is presently starting low power operation. The Enrico Fermi plant [7, 8], a 300 MW(th) fast breeder,**** has conducted pre-operational testing and is undergoing low power operation. Smaller and older installations continue to provide information, e.g., Los Alamos Molten Plutonium Reactor Experiment (LAMPRE) [9], Sodium Reactor Experiment (SRE) [10], and Experimental Breeder Reactor I (EBR-I) [11]. The experience being gained from these systems is expected to be augmented strongly in the future by specific component tests and test programs, some currently in progress, fostered by the Sodium Components Development Program of the U.S. Atomic Energy Commission.

STEAM GENERATORS

Steam generator development since the 1958 Geneva Conference has been principally concerned with larger units of higher temperature capability. Most of

this effort has been associated with reactor plant project developments. The successful operation of the Hallam steam generators and the demonstrated ability of the Fermi units to accommodate a large sodium-water reaction are important contributions to the field of steam generator development.

Design

Figure 1 and Table 1 illustrate the principal features of the Hallam, EBR-II, and Fermi steam generators [12]. The Hallam and EBR-II units are natural circulation boilers employing double wall tubes, whereas Fermi is a once-through type with single wall tubes.

In the Hallam units, re-entrant tubes are utilized to permit free differential expansion between tubes and shell and minimize thermal gradients in the high pressure tube sheets. In the EBR-II units, a compensatory initial differential expansion between tubes and shell was provided during fabrication by cold springing, i.e., the shell was heated and elongated approximately 1/8 in while the tubes were being welded to the tubesheets. In the Fermi units, flexibility of the return bend involute tubes accommodates differential expansion.

For direct detection of possible leakage, helium gas is used to monitor the spaces between the two walls of the duplex tubes and between the water and sodium tubesheets in the Hallam units. In the EBR-II steam generator, the duplex tubes function only as a double barrier between sodium and water, and the spaces between water and sodium tube sheets are completely open to the atmosphere.

In EBR-II, two modified evaporators have been substituted for the four superheaters originally contemplated. This became necessary because of difficulty encountered in making consistently reliable tube-to-tubesheet welds on the thin wall duplex tubes employed in the design of the original superheaters. The modification of evaporators to render them useful as superheaters consisted of installing inserts in the evaporator tubes so as to restrict the flow channel to a 1/8 in annulus and effect the requisite steam velocity. With these two substitute units the generator is capable of producing 800 °F steam at full load. Provisions have been made for installation of another two such units to enable generation of steam at 840 °F in the future.

* Argonne National Laboratory, Argonne, Illinois.

** Atomics International, Canoga Park, California.

*** Atomic Power Development Associates, Detroit, Michigan.

**** Nominal rating: the plant is designed for maximum of 430 MW. Operation with first core loading will be limited to 200 MW.

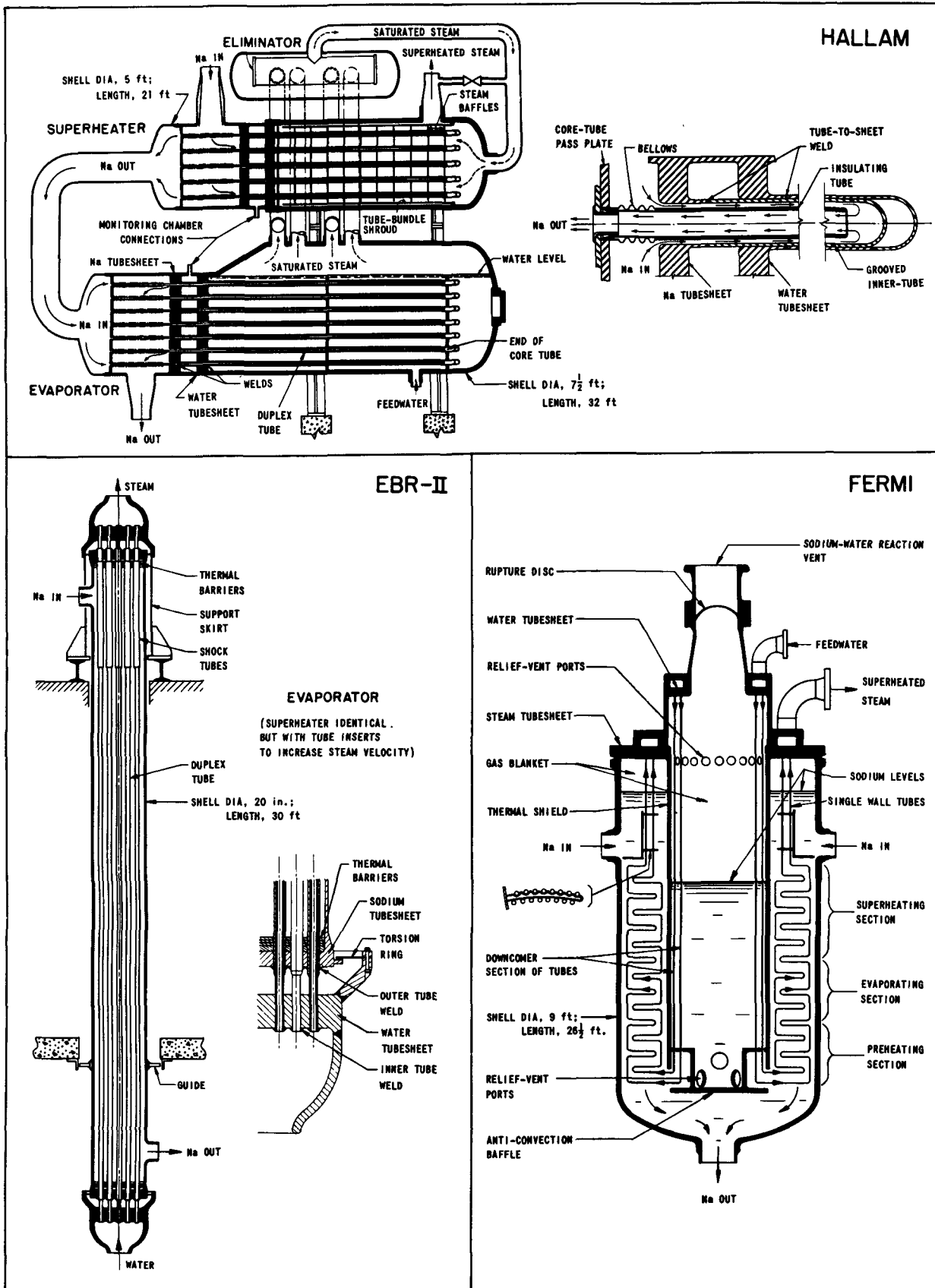


Figure 1. Sodium-to-water steam generators

Table 1. Sodium-to-water steam generator characteristics

	HALLAM		EBR-II		FERMI
	Evaporator	Superheater	Evaporator	Superheater	Once-through
Full load heat transfer per unit, MW	69	16	5.7	4.2	143
Number of units	3	3	8	4	3
Steam pressure, psig	900	895	1 310	1 300	900
Shell side fluid	Water	Steam	Sodium	Sodium	Sodium
Flow rate, lb/hr.	2.51×10^5	2.51×10^5	3.12×10^5	6.24×10^5	5.30×10^6
Temp "in", °F	304	530	794	866	820
Temp "out", °F	530	875	588	794	520
Tube side fluid	Sodium	Sodium	Water	Steam	Water and Steam
Flow rate, lb/hr.	2.82×10^6	2.82×10^6	0.31×10^5	0.62×10^6	4.76×10^6
Temp "in", °F	830	895	550	580	380
Temp "out", °F	555	830	580	840	780
Heat transfer area, ft ²	3 680	2 150	620	620	10 800
Number of tubes	680	560	73	73	1 200
Outer tube size, in	1.52 od	1.52 od	1.438 od	1.438 od	0.625 od
Inner tube size, in	0.072 wt	0.072 wt	0.094 wt	0.094 wt	0.042 wt
Material: water side.	A212 Gr B	2½ Cr-1 Mo	2½ Cr-1 Mo	2½ Cr-1 Mo	2½ Cr-1 Mo
Na side.	2½ Cr-1 Mo	5 Cr-½ Mo-½ Ti	2½ Cr-1 Mo	2½ Cr-1 Mo	2½ Cr-1 Mo
core tube	304 SS	304 SS	—	—	—
Manufacturer	Griscom-Russell		ANL		Griscom-Russell

Operating experience

The Hallam steam generators have operated for a period of months at various power levels up to full power. More than 5 000 MWd had been accrued at the end of March 1964. The only difficulty experienced with these generators has been carryover of water due to variation of water level in the evaporator with change in load [13]. A program of water level regulator setting versus load was established to maintain carryover within the 25% design limit. This program required controlling the water level within ± 1 in to keep the level low enough to prevent carryover and yet high enough to cover the upper tubes of the evaporator. With the exception of this one problem, operation of the units has been completely satisfactory.

The EBR-II steam generator has not experienced power operation to date; however, it has been filled with sodium and water as part of the pre-operational test program and has operated for several days isothermally at 580 °F with full flow on the sodium side and 1 250 psig steam on the water side. No troubles have developed.

The Fermi steam generators have not yet been placed into power operation, but have undergone significant testing and modification. In 1961, after installation, it was discovered that many of the tubes in the No. 2 unit were leaking. Examination established that the leakage was due to stress corrosion cracking at the tube bends which was attributed to residual cleaning solution containing sodium hydroxide and sodium nitrate. Examination of the No. 1 and No. 3 units indicated that their tubing was sound. The No. 2 unit was completely retubed [14].

In late 1962, the No. 1 unit was filled with sodium and water and operated isothermally at a maximum sodium flow for approximately two weeks, when

failure of several tubes caused a sodium-water reaction to occur. On noting a rise in pressure, the operator triggered the safety system which dumped the water from the generators. The reaction, however, generated enough hydrogen to raise the cover gas pressure above the 60 psi setting of the rupture disc. All systems designed to accommodate such a reaction functioned satisfactorily, and the separator collected all the sodium expelled from the unit. Subsequent examination indicated that the failures were due to flow-induced vibration of tubes opposite the sodium inlets, with the damage occurring four feet below the steam manifold where the tubes make the first horizontal pass through the inner support bar. In addition to the primary failures, wall thinning and pressure ruptures occurred on four of the tubes in the area of the sodium-water reaction. The units have since been modified to incorporate a baffle and tube clips in the vertical section of tubing (Fig. 1), and subsequent testing indicates that the vibration has been eliminated. Since modification, the No. 3 unit has been placed in service without water, but with sodium on the shell side, and has operated satisfactorily up to a maximum temperature of 600 °F and full flow for a period of about one month.

At Los Alamos Scientific Laboratory, a smaller, once-through, single wall tube steam generator has been successfully tested for 9 500 hours [12]. This unit consisted of an evaporator section and a superheater section with a tempering heat exchanger installed between the superheater and evaporator to reduce the temperature of the sodium entering the evaporator. The 2 MW unit operated with temperatures of 1 000 °F sodium entering, 750 °F sodium leaving, producing steam at a temperature of 925 °F and 900 psia.

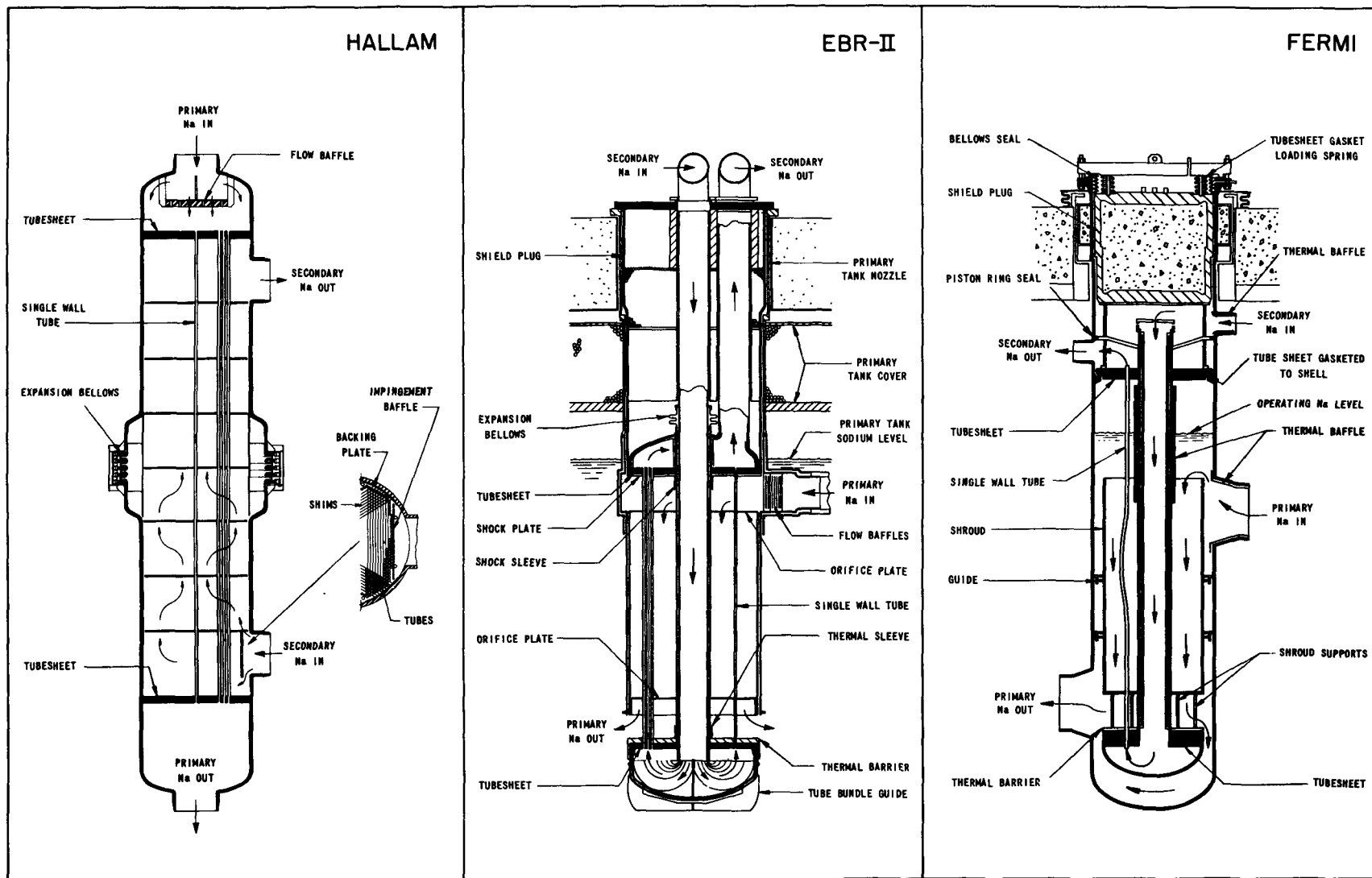


Figure 2. Sodium-to-sodium heat exchangers

Table 2. Sodium-to-sodium heat exchanger characteristics

	HALLAM	EBR-II	FERMI
Full load heat transfer per unit, MW	42.6	62.5	143
Number of units	6	1	3
Shell side fluid	Secondary Na	Primary Na	Primary Na
Flow rate, lb/hr.	1.3×10^6	3.7×10^6	5.3×10^6
Temp "in", °F	555	883	900
Temp "out", °F	895	695	600
Tube side fluid	Primary Na	Secondary Na	Secondary Na
Flow rate, lb/hr.	1.4×10^6	2.5×10^6	5.3×10^6
Temp "in", °F	945	588	520
Temp "out", °F	610	866	820
Heat transfer area, ft ²	2 870	4 539	5 840
Number of tubes	1 395	3 026	1 860
Tube size, in	0.625 od	0.625 od	0.875 od
	0.031 wt	0.052 wt	0.049 wt
Material, tube and shell	304 SS	304 SS	304 SS
Manufacturer	M. W. Kellogg	Struthers-Wells	Alco

In addition to steam generator development related to specific reactor projects, the Atomic Energy Commission, under its Sodium Components Development Program, has undertaken the construction of a 35 MW facility capable of testing steam generators (and heat exchangers) with maximum sodium temperature of 1 200 °F [15]. A 30 MW model of a once-through type generator utilizing duplex tubes of 316 stainless steel and Inconel is presently under construction and scheduled for testing in this facility in 1964 [16]. The Commission is also sponsoring the design of a 1 000 MW steam generator and the fabrication and testing of a 30 MW model of this unit [17].

HEAT EXCHANGERS

The chief interest in sodium-to-sodium heat exchanger design continues to be directed toward development of larger units for service at higher temperatures. Operating experience acquired since 1958, although not extensive, has been encouraging. Perhaps the most significant development is the demonstration of repairability of a failed heat exchanger without removal of the unit from the system (as described later).

Design

The general arrangement and characteristics of the Hallam, EBR-II and Fermi intermediate heat exchangers are depicted in Fig. 2 and Table 2. All are of shell-and-tube design and are installed with the tubes vertical to preclude the problem of thermal stratification which occurred with the Sodium Reactor Experiment heat exchanger [18]. A special feature of the EBR-II and Fermi exchangers is the provision for removal of the tube bundle from the shell without disconnecting the shell from the system. In the Hallam unit, a distinctive feature is the use of a bellows expansion joint in the shell to accommodate differential expansion of the shell and tubes.

Not described in the figure or table is a 30 MW heat exchanger [16] under construction for testing in the

Sodium Component Test Installation [15]. This unit is designed for 1 200 °F operation.

Operating experience

The most significant operating experience under design conditions has been obtained with the Hallam heat exchangers. Heat transfer coefficients for the three units have been determined from measurements of sodium temperatures and flow rates on both primary and secondary sides at several power levels. These measurements have established that the heat transfer coefficients are within 10 per cent of the predicted values and that the exchangers are performing satisfactorily. Only one malfunction has occurred in several months of operation. A leak developed between the secondary and primary systems as a result of tube failure in one of the units. This unit was removed from the system and the defective tube identified. This tube and sixteen others were removed to determine the cause of the initial failure and to permit an estimate of the condition of the remainder of the tubes. Extensive metallurgical and mechanical property tests were conducted, together with analyses, which showed the failure to have been caused by flow-induced vibration. Vibration dampening shims were then installed in the exchanger near the shell side inlet as illustrated in Fig. 2. The same modification was made on the remaining five units without removing them from the system by cutting entry holes through their sides and later welding in appropriate closures. Subsequent performance has been completely satisfactory.

The three Fermi heat exchangers have been subjected to rated flow of sodium at a maximum temperature of 1 000 °F isothermally on the shell (primary) side, with no evidence of malfunction. The tube sides of two units have been operated at 600 °F at rated flow (again isothermally) without difficulty, but no significant transfer of heat has been effected.

The EBR-II intermediate heat exchanger has been subjected to rated flow on the primary, or shell, side

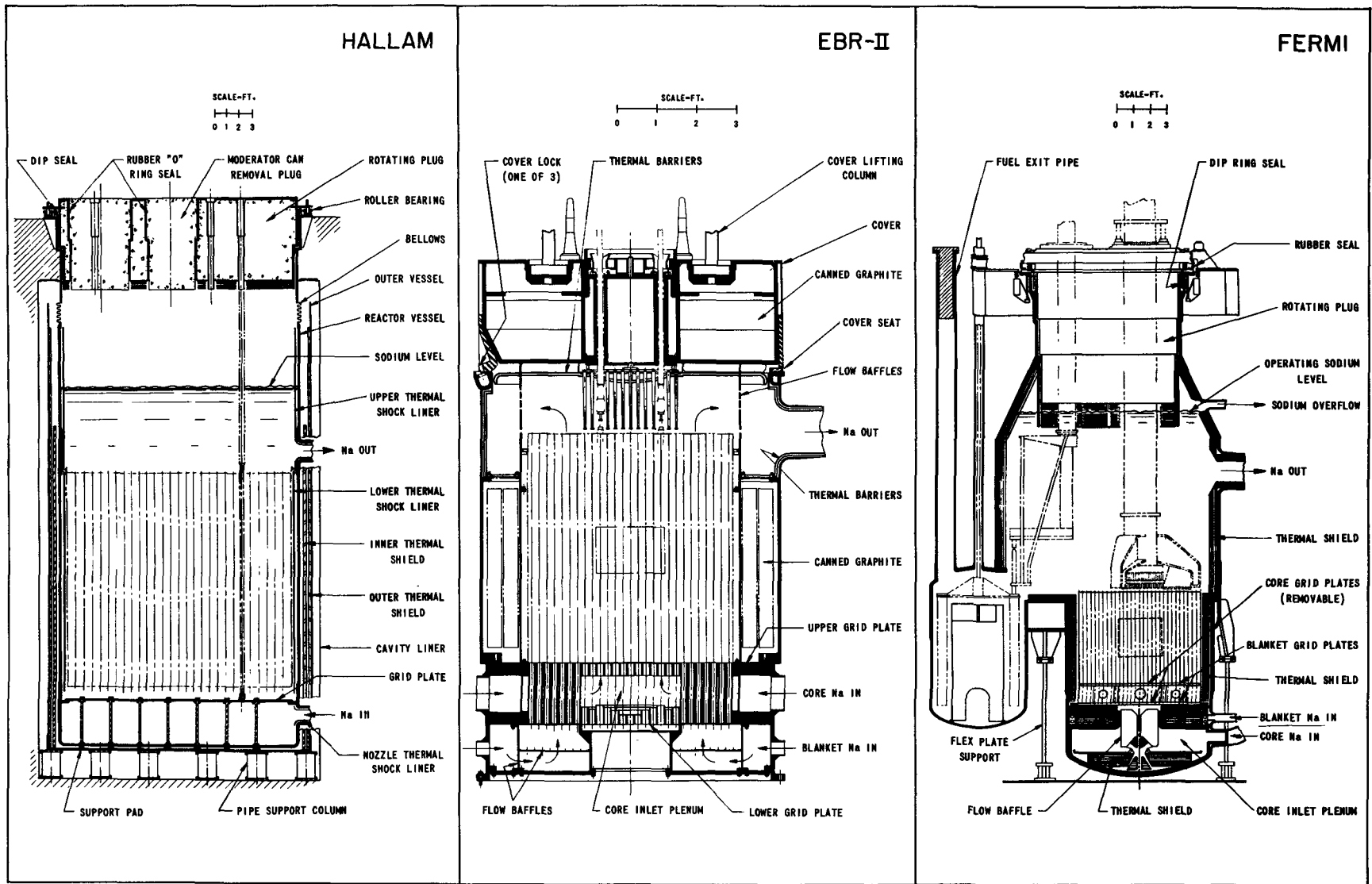


Figure 3. Sodium reactor vessels

Table 3. Sodium reactor vessel characteristics

	HALLAM	EBR-II	FERMI
Reactor type	Thermal	Fast	Fast
Reactor power, MW	256	62.5	430
Operating temperature:			
Coolant "in", °F	610	700	600
Coolant "out", °F	945	833	900
Operating pressure:			
Coolant "in", psig	30	60	100
Coolant "out", psig	negligible	10	negligible
Size of vessel:			
Height, ft	33	13	36
Diameter, ft	19	8	14
Material	304 SS	304 SS	304 SS
Manufacturer	Baldwin-Lima-Hamilton	Blaw-Knox	Combustion Engineering

at 650 °F (isothermal) with no evidence of difficulty. The tube side of the exchanger recently has been filled with sodium; however, the approach to power is only starting and no performance data are yet available.

REACTOR VESSELS

Reactor vessels employed for sodium-cooled reactors have encountered only insignificant operational problems. Perhaps of most interest at this time are the large differences in vessel configurations, their relative design complexities, provisions for thermal shock protection, and fabrication problems.

Design

The Hallam, EBR-II and Fermi reactor vessels are briefly described in Fig. 3 and Table 3. Major variations in configuration are evident. These variations are related to differences in the primary system concepts, particularly in respect to fuel handling, shielding and containment provisions.

The Hallam vessel is of relatively simple design [19]. It incorporates an expansion bellows (19 feet diam) for accommodating thermal expansion of the vessel wall (Fig. 3). A fabrication problem arose in making the weld at the reactor site between the lower angle on the bellows assembly and the reactor vessel wall. Shrinkage of this weld rotated the lower angle excessively and caused significant distortion in the two lowest convolutions of the bellows. Extensive investigation substantiated the conclusion that the bellows in this distorted condition could perform properly in operation. The same vessel earlier had suffered minor damage during transport to the construction site. Again, intensive analysis was required which indicated that re-work was not necessary and that vessel integrity was not jeopardized.

The EBR-II reactor concept is unique in that the entire vessel is submerged in the primary system bulk sodium within a large "primary tank," thus obviating any need for leak tightness of the vessel or its connecting piping. The chief fabrication problem was the difficulty of keeping the relatively complicated grid structure (Fig. 3) clean throughout the assembly process. After installation of the reactor vessel in the

primary tank, a thorough final cleanup of the grid to remove chips, turnings and other foreign matter had to be performed. This required extensive use of specially designed retrieval tools, borescopes and mirrors, and proved costly and time consuming.

The Fermi vessel is the most complicated of the three. Thermal shielding is particularly extensive, and removable core grid plates are incorporated. Fabrication of the vessel and its transport to the site required substantial effort and represented a significant achievement.

Operating experience

The Hallam reactor vessel experienced approximately five months of nuclear power operation (more than 5 000 Mwd) by the end of March 1964, at temperatures from 350 °F to 945 °F. Although presently undergoing only low power operation, the Fermi vessel has experienced about three years of pre-operational testing with isothermal sodium temperatures from 400 °F to 900 °F, and one week at 1 000 °F. The EBR-II vessel has undergone more than a year of pre-operational testing in isothermal sodium at 270 °F to 650 °F. No problem has been encountered with any of these units to date other than a cavitation erosion effect in a Fermi vessel grid plate attributable to abnormal circumstances [2].

SODIUM PUMPS

A distinct trend toward use of mechanical centrifugal pumps—as opposed to ac or dc electromagnetic pumps—for high capacity service has become evident. Very significant operating experience with this type of pump has been accumulated. Although several instances of operational difficulty have occurred, no basic or inherent deficiency has been identified. Extrapolation to the very large pump sizes required for the advanced plants under study [20–23] is considered clearly feasible.

Design

Arrangement and principal features of the Hallam, EBR-II and Fermi plant primary system pumps are indicated in Fig. 4. In all of these plants the primary

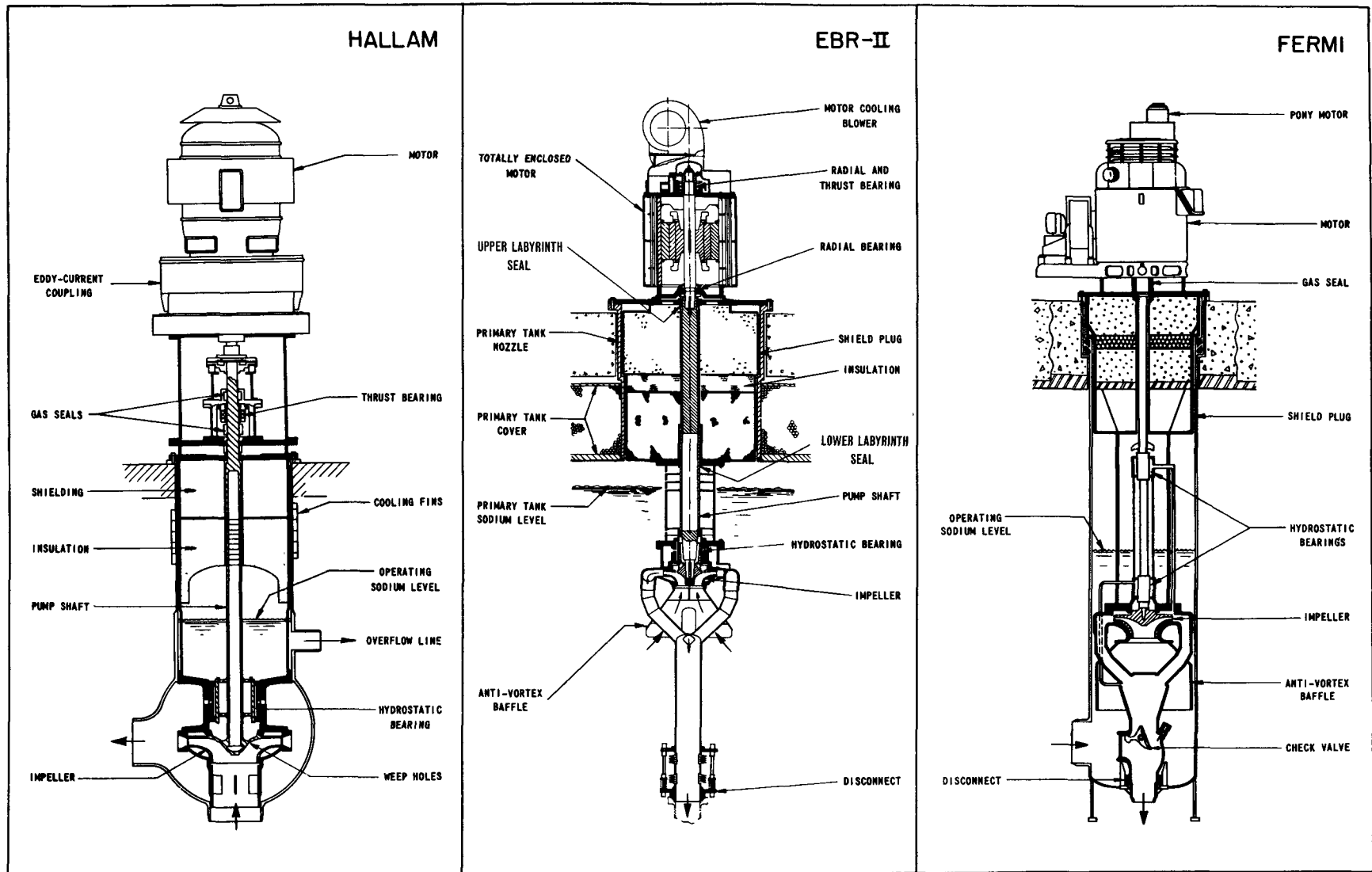


Figure 4. Primary system sodium pumps

Table 4. Sodium pump (design) characteristics

	HALLAM	EBR-II	FERMI
Primary system pumps:			
Type	Mechanical free surface	Mechanical free surface	Mechanical free surface
Number of units	3	2	3
Capacity, gpm	7 200	5 500	11 800
Dynamic head, ft	160	200	310
Design temperature, °F	1 000	800	1 000
Motor speed, rpm	900	1 075	900
Motor power, hp	350	350	1 060
Sealing arrangement	Mechanical shaft seal	Totally enclosed drive motor	Mechanical shaft seal
Material	304 SS	304 SS	304 SS
Type of speed control	Eddy current coupling	Variable frequency and voltage	Wound rotor motor with liquid rheostat
Manufacturer	Byron-Jackson	Byron-Jackson	Byron-Jackson
Secondary system pumps:			
Type	Mechanical free surface	AC linear induction	Mechanical free surface
Number of units	3	1	3
Capacity, gpm	7 200	6 500	13 000
Dynamic head, ft	170	142	100
Design temperature, °F	1 000	700	1 000
Motor speed, rpm	900	1 180 (M.G. Set)	900
Motor power, hp	350	500 (M.G. Set)	350
Sealing arrangement	Mechanical shaft seal	Total metal enclosure	Mechanical shaft seal
Material	304 SS	304 SS	2½ Cr-1 Mo
Type of speed control	Eddy current coupling	Variable voltage (M.G. Set)	Eddy current coupling
Manufacturer	Byron-Jackson	General Electric	Byron-Jackson

system pumps differ in some degree from the secondary system pumps. The general design characteristics for both primary and secondary pumps are indicated in Table 4.

Operating experience

The Hallam pumps have operated for several thousand hours at temperatures ranging from 300 °F to 950 °F, including 1 000 hours or more at about 950 °F. Operation has been generally satisfactory, although all six have had to be removed for maintenance and minor modification at least once.

The three primary pumps exhibited too low a sodium level within the pump casing under high speed conditions. This was found to result from excessive flow through the impeller weep holes, and necessitated removal of the pumps and plugging of four of the eight weep holes in each. Since this correction, level control has been satisfactory.

After a number of months of uneventful operation, binding of one of the secondary pumps occurred, causing a system scram and stopping all three pumps. It then was found that, in addition to the one pump being tightly bound, the other two were difficult to turn and could not be restarted. The pumps were dismantled and inspection revealed accumulations of small amounts of foreign material in the 0.010 in clearance of the hydrostatic bearings and in the larger clearances of the impeller wear rings. It was concluded that these accumulations constituted the primary cause of the pump seizures, but that a contributing

cause was misalignment of pump internals caused by uneven temperature distribution in the pump casings. Cleanup of the bearings, enlargement of the wear ring clearances, correction of pump casing cooling systems, and filtration of the secondary system sodium were all undertaken as remedial measures. Subsequent operation has been satisfactory.

In EBR-II binding of both primary pumps occurred after less than 200 hours of operation at 550 °F to 650 °F. Inspection after dismantling showed that in both pumps rubbing had occurred between the pump shaft and the lower labyrinth seal (Fig. 4) which eventually resulted in binding. The initial cause of the rubbing has not been definitely established. Possible causes include insufficient initial clearance and warpage of the shafts (of three-piece welded construction) prior to operation. The pumps were fitted with new shafts of modified design to minimize possibility of warpage, and clearances at both lower and upper labyrinth seals were increased. The re-installed pumps have been put into operation satisfactorily, but insufficient operating time has been accumulated to support additional conclusions.

The three Fermi primary pumps have performed exceptionally well. Operating time exceeds 7 000 hours, including about two weeks at 1 000 °F. No difficulties have arisen with the pumps themselves. The associated check valves, however, were found to close with too high a velocity resulting in excessive piping strains. To eliminate this, a dash-pot snubber (illustrated in Fig. 4) is being added to each unit.

Modification of two pumps has been completed and one of these returned to service.

Only two of the three Fermi secondary pumps have yet been put into operation. These have performed without difficulty of any kind, operating approximately two months at temperatures of 500 °F to 600 °F.

CONCLUSIONS

Operating experience with major components since the Second Geneva Conference has been generally encouraging. Difficulties have arisen in a number of instances which required corrective modifications; however, no basic or inherent deficiencies have become apparent. Experience with such components should increase at an accelerated pace in the future, particularly as present sodium reactor plants become more fully operational and the U.S. Atomic Energy Commission Sodium Components Development Program matures. It is expected that this experience will assure timely development of components eminently suitable for very large, high-efficiency, central station power plants.

REFERENCES

1. Smith, F. A., *Sodium Technology for Nuclear Power Plants*, Proceedings of the Second International Conference on the Peaceful Uses of Atomic Energy, P/2291, Vol. 7 p. 57, United Nations (1958).
2. Koch, L. J., et al., *Sodium Cooled Fast Breeder Reactors*, P/207, Vol. 6, these Proceedings.
3. Atomics International, NAA-SR-5700 (1961).
4. Dickinson, R. W., and Starr, C., *Sodium Graphite Reactors*, Addison-Wesley Publishing Co., Reading, Mass. (1958).
5. Koch, L. J., et al., USAEC report ANL-5719 (1957), and ANL-5719 Addendum (1962).

6. Koch, L. J., et al., *Construction design of EBR-II: An Integrated Unmoderated Nuclear Power Plant*, Proceedings of the Second International Conference on the Peaceful Uses of Atomic Energy, P/1782, Vol. 9, p. 323, United Nations (1958).
7. Power Reactor Development Co., *Enrico Fermi Atomic Power Plant, Technical Information and Hazards Summary Report*, Vols. 1-6 (1961).
8. Amorosi, A., and Yevick, J. G., *An Appraisal of the Enrico Fermi Reactor*, Proceedings of the Second International Conference on the Peaceful Uses of Atomic Energy, P/2427 Vol. 9, p. 358, United Nations (1958).
9. Los Alamos Scientific Laboratory, LA-2833 (1963).
10. Parkins, W. E., *The Sodium Reactor Experiment*, Proceedings of the Second International Conference on the Peaceful Uses of Atomic Energy, P/499, Vol. 3, p. 295, United Nations (1958).
11. Lichtenberger, H. V., et al., *Operating Experience and Experimental Results obtained from a NaK-cooled Fast Reactor*, Proceedings of the First International Conference on the Peaceful Uses of Atomic Energy, P/813, Vol. 3, p. 345, United Nations (1956).
12. USAEC Report, TID-18072 (1962).
13. Foust, O. J., *Hallam Nuclear Power Facility Reactor Operation Analysis Program Monthly Report*, No. 15, 56 (1963).
14. Heidel, C. M., *Modification of Enrico Fermi Reactor Steam Generators*, Power Reactor Development Co., 15th Quarterly Report (Sept. 10, 1962).
15. Atomics International, NAA-SR-Memo 4754 (1960).
16. Alco Products Co., APAE-112, Vols. I-IV (1962).
17. Babcock and Wilcox Co., BW-67-1 (1964).
18. Foster, K. W., NAA-SR-3775 (1960).
19. Mahlmeister, J. E., et al., NAA-SR-7366 (1960).
20. Combustion Engineering, Inc., CEND-200, Vols. I and II (1964).
21. Allis-Chalmers Mfg. Co., ACNP-64503 (1964).
22. Westinghouse Electric Corp., WCAP-3251-1 (1964).
23. General Electric Corp., GEAP-4418, Vols. I and II (1964).

ABSTRACT—RÉSUMÉ—АННОТАЦИЯ—RESUMEN

A/228 Etats-Unis d'Amérique

Composants pour réacteurs à sodium

par H. O. Monson et al.

Malgré les nombreux succès et les améliorations apportées pendant les dernières années à la technologie des systèmes à sodium, presque tous les aspects de ces systèmes font encore appel à la technique et à l'esprit d'invention et sont susceptibles d'améliorations importantes. Le mémoire décrit les composants essentiels d'un réacteur à sodium — caissons, générateurs de vapeur, échangeurs de chaleur et pompes — et indique les problèmes en cours d'étude.

Les Etats-Unis ont la chance d'avoir pu acquérir, depuis la deuxième Conférence de Genève en 1958, une expérience notable concernant divers modèles de composants essentiels de réacteur à sodium. Le réacteur prototype de Hallam, réacteur à sodium modéré au graphite de 256 MW(th), a été essayé, mis en service, et a fonctionné pendant des mois à pleine puissance. Le réacteur surgénérateur expérimental

n° II (EBR-II), surgénérateur à neutrons rapides de 62,5 MW(th), a commencé son fonctionnement à pleine puissance après de multiples essais. L'installation Enrico Fermi, comprenant un surgénérateur à neutrons rapides de 300 MW(th), a subi également ses essais et fonctionne à puissance réduite. Des installations plus petites et plus anciennes continuent à fournir des renseignements; par exemple, le réacteur expérimental à plutonium fondu de Los Alamos (LAMPRE), le réacteur expérimental à sodium (SRE), et le réacteur EBR-I. De plus, l'expérience que ces systèmes permettront d'acquérir doit être considérablement accrue par des essais de composants particuliers et des programmes d'essais, dont certains sont en cours, sous l'égide du Programme de développement des composants pour sodium de l'U.S. Atomic Energy Commission.

Pour les générateurs de vapeur et les échangeurs de chaleur, on s'attache surtout à éviter tout contact entre le sodium et l'eau, et à limiter la corrosion sous contrainte, les chocs thermiques et les vibrations. On a

observé des incidents sur un échangeur de chaleur intermédiaire de Hallam et un générateur de vapeur de Fermi. Un tube s'est rompu dans l'un des six échangeurs de chaleur de Hallam. On a attribué cette défaillance à une vibration du tube, produite par la grande vitesse du sodium à proximité d'un point d'entrée. Des vibrations analogues ont provoqué la rupture de plusieurs tubes dans l'un des trois générateurs de vapeur de Fermi, conduisant à une notable réaction eau-sodium. Ce problème a été supprimé par modification des supports de tubes et/ou des chicanes d'écoulement. Pour EBR-II, ces composants n'ont encore donné aucune difficulté, mais le réacteur vient d'entrer en fonctionnement.

Aucun des caissons n'a encore subi d'accident ou de difficultés sérieuses. Cependant, seul le réacteur d'Hallam a été soumis aux principales conditions de fonctionnement pour lesquelles il a été conçu. On s'intéresse tout spécialement à la complexité relative de ces caissons, qui vise en particulier à éviter les contraintes thermiques excessives, et à l'effort de fabrication qui en résulte.

Les pompes du réacteur d'Hallam, du type mécanique centrifuge, ont subi des incidents et des difficultés de fonctionnement dus à différentes causes, telles que l'accumulation de corps étrangers dans les bagues de rattrapage de jeu des pompes et le mauvais alignement du corps de la pompe par suite d'une mauvaise distribution de températures. Il a fallu démonter les six pompes pour corriger ces défauts. Les deux pompes primaires d'EBR-II sont tombées en panne durant les essais préliminaires. Dans les deux cas, la panne était due au frottement entre le rotor de la pompe et un labyrinthe d'étanchéité destiné à empêcher la vapeur de sodium de passer le long du rotor. On pense avoir résolu ce problème en utilisant des rotors moins sensibles aux déformations et des labyrinthes d'étanchéité moins ajustés. Les pompes centrifuges du réacteur Fermi ont fonctionné de façon entièrement satisfaisante plusieurs milliers d'heures. Dans tous ces réacteurs, les paliers (hydrodynamiques), lubrifiés au sodium, des pompes n'ont causé aucun ennui.

A/228 США

Основные узлы натриевых реакторов

Г. О. Монсон *et al.*

Несмотря на многочисленные успехи и прогресс, достигнутые за последние годы, технология натриевых реакторов все еще требует совершенствования. В настоящем докладе рассматриваются основные узлы натриевых реакторов: реакторные баки, парогенераторы, теплообменники, насосы и описываются некоторые проблемы, которые в настоящее время исследуются.

После Второй международной конференции по мирному использованию атомной энергии

в 1958 году в США накоплен значительный опыт в конструировании основных узлов натриевых реакторов. Натриевый реактор с графитовым замедлителем Холлэмской атомной электростанции тепловой мощностью 256 Мвт был испытан, пущен в эксплуатацию и работает уже несколько месяцев на полную мощность. Закончились предварительные испытания экспериментального реактора-размножителя EBR-II на быстрых нейтронах тепловой мощностью 62,5 Мвт, реактор сдан в эксплуатацию. Закончились предварительные испытания реактора-размножителя на быстрых нейтронах атомной электростанции имени Энрико Ферми тепловой мощностью 300 Мвт, реактор уже работает на пониженном энергетическом режиме. Менее мощные и более старые установки продолжают работать и обеспечивать информацию. К ним относятся Лос-Аламосский экспериментальный реактор на расплавленном плутонии (LAMPRE), экспериментальный натриевый реактор (SRE) и экспериментальный реактор-размножитель на быстрых нейтронах (EBR-I). Кроме того, опыт, приобретаемый на этих установках, со временем сильно увеличится благодаря экспериментальному применению в них специальных узлов и проведению испытательных программ. Некоторые из них уже осуществляются в соответствии с программой разработки узлов натриевых реакторов при Комиссии по атомной энергии США.

Главное внимание в разработке парогенераторов и теплообменников сосредоточено на способах предотвращения контакта между натрием и водой и на сведении к минимуму коррозии под напряжением тепловых ударов и вибраций.

В промежуточном теплообменнике Холлэмской атомной электростанции и в парогенераторе атомной электростанции имени Энрико Ферми произошли аварии. В одном из шести теплообменников Холлэмской атомной электростанции лопнула труба. Установлено, что это произошло из-за вибрации трубы, вызванной большой скоростью потока натрия около входного отверстия. Аналогичная вибрация вывела из строя несколько труб в одном из трех парогенераторов атомной электростанции имени Энрико Ферми и вызвала значительную реакцию между натрием и водой. Изменением способа закрепления труб и (или) применением перфорированных перегородок удалось успешно решить эту задачу. В реакторе-размножителе EBR-II никаких трудностей с этими узлами пока не отмечалось, правда, его эксплуатация лишь только началась.

Ни один из реакторных корпусов еще не вышел из строя и не наблюдалось серьезных трудностей в эксплуатации. Однако пока лишь одна Холлэмская атомная электростанция работает в расчетных эксплуатационных условиях. В настоящее время основное внимание уделяется совершенствованию конструкции этих кор-

пусов, в особенности устройству теплоизоляционных перегородок для устранения чрезмерных термических напряжений и вызываемых ими производственных затруднений.

Центробежные насосы Холлэмской атомной электростанции испытывали несколько аварий и эксплуатационных трудностей по разным причинам, в том числе вследствие накопления инородных веществ в зазорах кольцевых прокладок и искривлений кожухов из-за неправильного распределения температуры. Для устранения этих дефектов пришлось заменить все шесть насосов. На реакторе EBR-II оба главных насоса первого контура выбыли из строя во время предварительных испытаний. В каждом из этих случаев авария произошла из-за трения между валом насоса и «лабиринтной прокладкой», предназначенной для предотвращения утечки паров натрия вдоль вала. Установлены новые валы с более высокой прочностью к искривлению и новые «лабиринты» с большим зазором. Этим как будто была решена и эта задача. Центробежные насосы атомной электростанции имени Энрико Ферми работают вполне удовлетворительно уже много тысяч часов. Во всех этих насосах подшипники с натриевой смазкой работают безаварийно.

A/228 Estados Unidos de América

Componentes para reactores de sodio

por H. O. Monson et al.

A pesar de los muchos éxitos y avances conseguidos durante los últimos años en la tecnología de los sistemas de sodio, prácticamente cada uno de sus aspectos es un reto a la pericia y al ingenio, y cabe efectuar mejoras sustanciales. En esta memoria se describen las principales componentes de los reactores de sodio — vasijas del reactor, generadores de vapor, cambiadores de calor y bombas — y se señalan algunos problemas en los que se está trabajando actualmente.

Desde la Segunda Conferencia de Ginebra, que tuvo lugar en el año 1958, los Estados Unidos han podido adquirir un considerable acervo de experiencias gracias a diversos proyectos de componentes principales de reactores de sodio. Los reactores de los que más experiencia se ha obtenido son la instalación de potencia de Hallam, reactor de sodio-grafito de 256 MW térmicos, en la que se realizaron muchos ensayos, y que durante varios meses ha operado a plena potencia. El EBR-II (Reactor reproductor experimental II), de 62,5 MW térmicos, ha comenzado ya la operación a potencia después de un gran número de ensayos previos. La central Enrico Fermi, reactor reproductor rápido de 300 MW térmicos, ha sido también objeto de ensayos previos a la entrada en operación, y actualmente se halla operando a baja potencia. Además de estas tres instalaciones, hay otras más pequeñas y más antiguas que aún continúan suministrando información, como, por ejemplo, el

LAMPRE (Experimento de reactor de plutonio fundido de Los Alamos), el SRE (Experimento de reactor de sodio) y el EBR-I (Reactor reproductor experimental I). Además, se espera que en el futuro aumente notablemente la experiencia obtenida con estos reactores, gracias a los ensayos de componentes específicas y a los planes de experimentación, algunos en fase de realización, fomentados por el Programa para el Desarrollo de las Componentes de Reactores de Sodio, de la Comisión de Energía Atómica de los Estados Unidos.

En los diseños de generadores de vapor e intercambiadores de calor se dedica especial interés al proyecto de los dispositivos utilizados para prevenir posibles contactos entre el sodio y el agua, y para minimizar las tensiones por corrosión, el choque térmico y la vibración. Se han presentado fallos en un intercambiador intermedio de calor de la central de Hallam y en un generador de vapor de la planta Fermi. Uno de los seis intercambiadores de calor de Hallam sufrió la rotura de un tubo debida a la vibración producida por la alta velocidad del sodio cerca de la entrada. Análoga vibración hizo fallar varios tubos en uno de los tres generadores de vapor de la central Enrico Fermi, produciéndose una importante reacción del sodio con el agua. Se resolvió el problema de modo efectivo modificando los soportes de los tubos, o mediante distribuidores de flujo o aplicando ambas soluciones a la vez. En el EBR-II no se ha presentado hasta la fecha ninguna dificultad con estas componentes, aunque la operación apenas ha comenzado.

Tampoco las vasijas han fallado ni han planteado dificultades de importancia hasta ahora. Sin embargo, únicamente la unidad de Hallam ha operado ya en las condiciones principales para las cuales fué diseñada. Del mayor interés son la relativa complejidad de estas vasijas, particularmente en cuanto se refiere a los distribuidores para prevenir excesivas tensiones térmicas, y los efectos resultantes en el esfuerzo que represente su fabricación.

Las bombas de la instalación de Hallam, bombas mecánicas del tipo centrífugo, han sufrido fallos o dificultades de operación debido a varias causas, tales como acumulación de material extraño en los espacios libres de los segmentos y desalineación de la caja de la bomba, debido a una distribución inadecuada de temperaturas, y ha sido necesario sacarlas para su corrección. Las dos bombas primarias principales del EBR-II fallaron durante las pruebas previas a la entrada en operación. En ambos casos los fallos se atribuyeron a la fricción entre el árbol de la bomba y un «cierre en laberinto» destinado a reducir el flujo de vapor de sodio a lo largo del árbol. Se piensa que el problema podrá resolverse con el empleo de ejes menos susceptibles al alabeo y de cierres en laberinto con mayores espacios libres. Las bombas centrífugas de la central Enrico Fermi han funcionado a entera satisfacción durante varios miles de horas. En todas estas instalaciones, los cojinetes hidrodinámicos lubricados por sodio no tuvieron averías.

Mild steel in primary circuits of water-cooled power reactors

By K. Videm*

Despite the extensive use of carbon and low-alloy steels in conventional steam generating plants, it has been questioned whether such steels have a sufficiently good corrosion resistance for nuclear reactor applications.

The possibility for using normal boiler steels in pressurized water reactors has been investigated in the US [1, 2] and results have been so promising that carbon steel is used in primary system components of a pressurized water reactor at the US National Reactor Test Station in Idaho [3] and in out-of-core sections in the NPD reactor at Hanford [4]. However, nothing has been published so far regarding experience with these steels. Carbon steel has also been used in the primary steam circuit in the Halden Boiling Water Reactor (HBWR) and, as described later, with good results.

There are two factors specific for reactors which make the application of carbon and low-alloy steels difficult: the water in a reactor cannot easily be treated as is done in conventional plants in order to minimize corrosion, and corrosion products in the water must be maintained at a low level in order to prevent fouling of the heat transfer surfaces and to minimize radioactive contamination of the outer parts of the primary system.

A direct-cycle boiling reactor is used as a reference for the present discussion of the application of mild steel. For the assessment, information is required about the water quality wherever mild steel is to be applied (pressure vessel, steam pipeline, condensate and feed water system), and about the corrosion properties of the steel under these conditions. Associated problems are purification of the water and induced activities. The present paper will discuss all these problems with the main emphasis on corrosion.

WATER QUALITY IN BOILING-WATER REACTORS

It is difficult to keep the oxygen concentration in a boiling reactor at the same level as in a conventional power plant because of radiolytic decomposition of the water. With a normal recombination unit in a bypass system, the water phase will contain about 0.02–0.1 ppm oxygen, and the steam phase 5–20 ppm [5]. Experiments in the Halden Boiling Water Reactor

have shown that the decomposition rate increases linearly with power, which means that the oxygen content in the steam is about constant. Increased pressures tend to decrease the amount of oxygen in the steam. In comparison with light-water reactors, it appears that the oxygen production is reduced to about 1/3 if heavy water is used as coolant [6].

The normal maximum oxygen content in the water for a once-through-boiler is 0.02–0.04 ppm, i.e., as in the water phase of a boiling reactor. The oxygen content in the reactor steam is, however, two orders of magnitudes higher than that in the conventional boiler. The steam pipelines and the turbine in a direct cycle reactor will be exposed to this oxygenated steam. Accumulation of gases in the condenser is not permitted. The gases must be evacuated as is done with infiltrated air in conventional plants. The oxygen content in the condensate will, therefore, be much lower than in the steam, and as low as in a conventional plant.

The amount of oxygen in the moderator and steam can be reduced by the injection of hydrogen into the feed water or directly into the reactor. However, a high dosage rate is required to reduce the oxygen to low values.

In conventional power plants alkalies are usually added to the water to maintain pH at 10–11 (measured cold). The use of fixed alkalies (NaOH, KOH, LiOH) is not recommended in a boiling reactor because the large heat flux on the fuel elements can locally concentrate the hydroxides with serious corrosion problems as a consequence. A volatile base like ammonia would be ideal in this respect.

The behaviour of ammonia in a boiling reactor has been investigated in HBWR [6]. The ammonia would oxidize to nitric and nitrous acids, unless the moderator contained more than 0.03 ppm dissolved deuterium. With smaller amounts of ammonia, addition of deuterium gas was required to reach 0.03 ppm. With larger quantities of ammonia, its own decomposition supplied enough deuterium to inhibit the oxidation. The nitrogen and hydrogen (or deuterium) will have to be removed from the condenser in a direct cycle reactor, and some ammonia must be added to compensate for decomposition losses. In the reactor tank, only a low concentration of ammonia can be maintained under boiling. Ammonia addition will therefore mainly affect the corrosion of the condensate and feed water system.

* Institutt for Atomenergi, Kjeller Research Establishment, Kjeller.

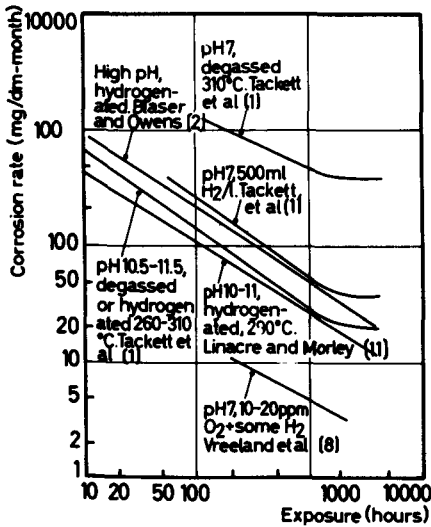


Figure 1. Corrosion rate of mild steel vs. exposure. Literature data

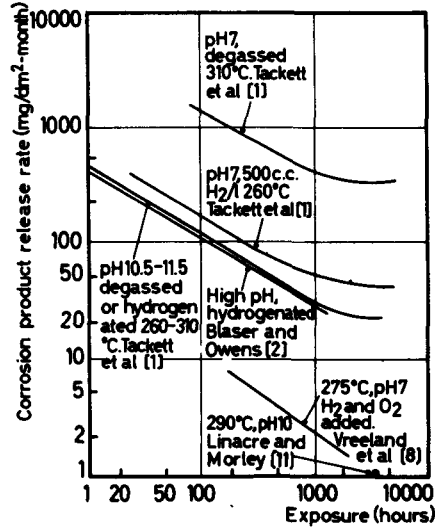


Figure 2. Rate of corrosion product release vs. exposure. Literature data

CORROSION OF MILD STEEL

High temperature corrosion

Corrosion experiments with mild steel in water at elevated temperatures have been performed by many workers. Some of their results are shown in Figs. 1 and 2. It appears that each worker gets his own set of data and this makes it difficult to isolate the effect of the many variables.

In an effort to clarify the situation, we are carrying out a study of some of the more crucial points. For this work we have available two loops made of stainless steel operated with a small over-pressure and a boiling natural circulation loop of carbon steel. In order to simulate the water conditions in a carbon steel system in the stainless steel loops, rust generators consisting of carbon steel sheets are exposed in addition to the actual corrosion specimens. In this way we can vary the area of steel surface to the water volume ratio. The experimental technique is as follows: the specimens, some of them with a pre-formed oxide film, are mounted in the loop and the system evacuated. If NH₃ is to be added, this is done immediately while oxygen is admitted when the system has reached 80 °C. The water is continuously purified in mixed-bed ion exchangers. The steel used in the experiments has the following composition: 0.1 % C, 0.6 % Mn, 0.02 % P, and 0.03 % S.

The corrosion rate of steel decreases with time for a long period until a constant corrosion rate is reached. The metal loss in the first period can be expressed as a function of time *t* by an equation of the following type:

$$\text{Metal loss} = kt^p \quad (1)$$

where *k* and *p* are constants.

In Fig. 3 is shown the effect of oxygen in neutral water on the instantaneous corrosion rate after a month. Vreeland *et al.* [7, 8, 9] were the first to report that small amounts of oxygen could act as an inhibitor.

It is seen that this occurs in the range 0–10 ppm oxygen, larger amounts accelerating the corrosion. Very high oxygen contents lead again to inhibition as described by Gerasimov [10] and Ruther and Hart [12]. The type of oxide films formed under the various oxygen levels are indicated at the top of Fig. 3. Bloom [13] suggests that the inhibition by small amounts of oxygen in the water is due to the development of γ -Fe₂O₃. Stereo electron micrographs showed many oxide whiskers on steel exposed to deoxygenated conditions while a much smoother and tighter oxide occurred when small amounts of oxygen was added.

The reaction order, *p*, is indicated on the figure

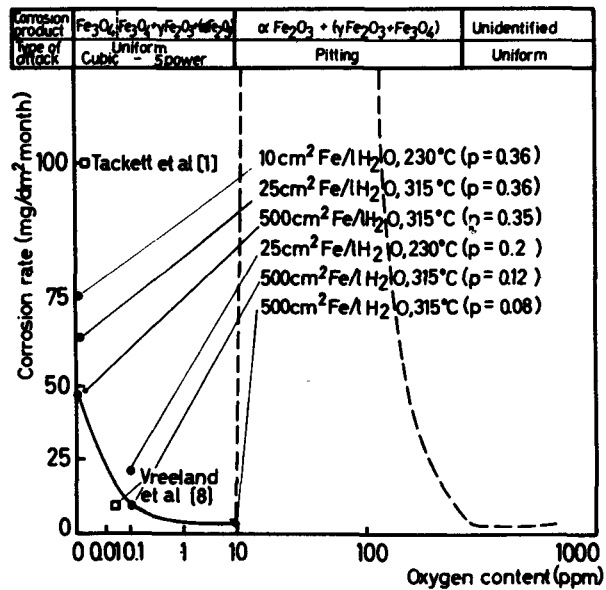


Figure 3. Effect of oxygen on the corrosion rate in high temperature water. Corrosion rate measured after one month's exposure

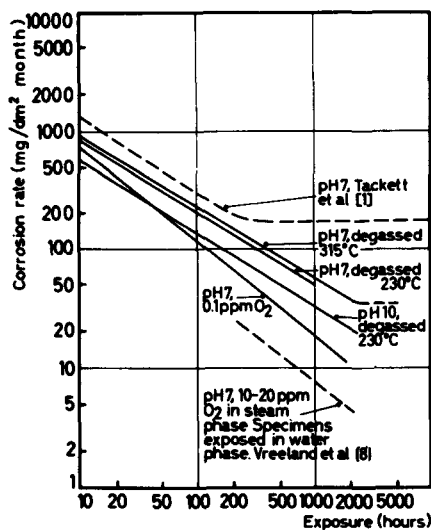


Figure 4. Corrosion rate of mild steel vs. exposure. Present results

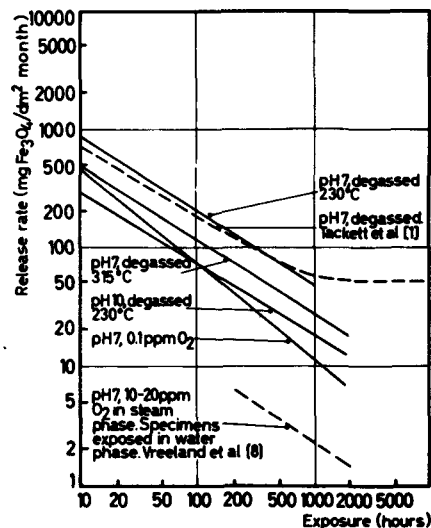


Figure 5. Rate of corrosion product release vs. exposure. Present results

and it is seen that p is reduced from 0.36 under degassed conditions to 0.08 at 10 ppm. A low p means a rapid decrease of the corrosion rate with time. Oxygen is thus a more effective inhibitor the longer the exposure.

Figure 3 indicates significantly different corrosion rate points for the same oxygen content. We believe this is mainly due to variation in the mild steel surface area to water volume ratio, a high ratio giving lower corrosion rates. With a high surface area to water volume ratio, specimens added after the test had started corroded with the higher rates typical for experiments with low ratios. In an experiment at 315 °C with 0.1 ppm O_2 and with 500 cm^2/l , specimens which had been exposed from the start (320 hours) had a metal loss of 70 mg/dm^2 , specimens which joined the test 20 hours after the first ones, lost 90 mg/dm^2 , and still newer specimens (150 hours) lost 180 mg/dm^2 .

Vreeland *et al.* [7, 8, 9] observed that the corrosion rate, and especially the corrosion product release rate, could be much reduced by increasing the heating-up rate. They also emphasized the special importance of having a good oxygen control at the start of the experiment. In addition to varying the mild steel surface area to water volume ratio, the variation in the results by various workers can possibly be explained by insufficient control of the heating-up rate and the oxygen content.

Results from some prolonged experiments are shown in Figs. 4 and 5. It is seen that the corrosion rates had not reached a constant value when the tests were interrupted. At this point the rates were:

40 $mg/dm^2/month$ for neutral, degassed water at 315 °C

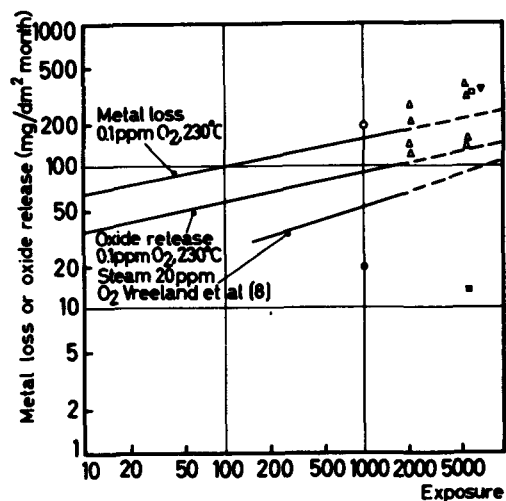
30 $mg/dm^2/month$ for degassed water with ammonia to pH 10, at 230 °C

12 $mg/dm^2/month$ for neutral water with 0.1 ppm O_2 at 230 °C.

The last figure was found in an experiment with a fairly low steel to water ratio; still lower corrosion rates can be achieved as indicated in Fig. 3.

The effect of oxygen in water with ammonia has less interest since the two constituents are not compatible under irradiation. Some results are, however, given in Table 1.

The effect of a static pre-filming operation varied with the environment used in the subsequent dynamic exposure in a complex way. The following conclusions are tentatively drawn.



- Metal loss, HBWR 150° C steam
- Release of oxide - - - - -
- ▲ Metal loss - - - - - 230° C - - - - -
- Release of oxide - - - - -
- ▼ Metal loss - - - - - 1000 hours 150° C, 5800 hours 230° C
- ▲ - - - - - EBWR (Breedon (5))

Figure 6. Result of in-pile exposure of steel specimens compared with out-of-pile tests

Table 1. Behaviour of mild steel in dynamic tests with water containing ammonia additions at 230 °C

pH	Steel area to water volume ratio (cm ² /l)	Oxygen content (ppm)	Corrosion rate after 1 month's exposure (mg/dm ² /month)	Order of corrosion rate reaction constant k^a		Release rate constant k_r^a (mg/dm ² /month ^{-p})
				p^a	(mg/dm ² /month ^{-p})	
10	10	less than 0.22	40	0.36	105	95
10	20	less than 0.02	35	0.36	95	50
10	500	less than 0.02	11	0.36	60	30
10	20	10	2	0.1	20	—

^a p , k , and k_r in the following equations:
 metal loss = $k \times t^p$
 oxide released = $k_r t^p$

Pre-filming in static degassed water reduced the corrosion rate under degassed dynamic conditions. The rate was increased in neutral oxygenated water. Pre-exposure in neutral water, with sufficiently high oxygen content to cause passivation, decreased the corrosion rate significantly under dynamic conditions in neutral oxygenated water and in high pH water, but had very little effect in neutral degassed water. A somewhat reduced rate was always found for specimens pre-exposed in static water of the same type as used in the subsequent dynamic test. It is possible that the reduced corrosion rates found in the natural circulation loop compared to the forced circulation systems can be explained by this, because the flow was very small during the heating-up period. This could then act as a static pre-filming exposure. A similar effect will probably operate during the heating-up of a reactor.

We have seen from the previous section that the oxygen content in the steam is much higher than in a conventional plant, and one may conclude that this will cause excessive corrosion. Vreeland, Gaul and Pearl [7, 8, 9] have, however, shown that the corrosion rate in saturated steam is in fact somewhat lower than in the corresponding water phase, and the release rates are much lower in steam since the corrosion products are not so easily washed away. In the experiments described, the steam lines and steam test sections were not heated so that water condensed both on piping and on specimens, and the samples in the so-called steam corrosion tests had presumably a water film. If this is correct and the oxygen distribution not too far from equilibrium, the close correlation between corrosion rates in steam and water is not surprising.

Reactor experience

ASTM-A-212 A steel has been used for the main steam pipe line in HBWR. After the first fuel charge operation at 150 °C, the surface had a good appearance and was covered with a black magnetite film. Machined areas had been attacked uniformly, while very shallow pits occurred on the as-rolled surface. The pits were less than 2 microns deep. The exposure period was: 1½ years of which 1 000 hours were on temperature. The metal loss was determined to be 200 mg/dm² and the release as low as 20 mg/dm². These values are plotted in Fig. 6 and are in the normal range for steel in neutral water and steam.

Before operation with the second fuel charge at 230 °C, extra steam pipes were installed. The appearance of the old and new pipelines was identical after operation. The metal loss was 306 mg/dm² and 330 mg/dm² for steel exposed 5 800 hours at 230 °C only and 1 000 hours at 150 °C + 5 800 hours at 230 °C respectively. The release value for specimens exposed at 230 °C was only 16 mg/dm².

The corrosion behaviour of carbon steel installed in EBWR was good for the first 6 569 hours [5]. Accelerated attack occurred in the last month prior to shutdown for rebuilding to 100 MW operation. Values for metal loss for different steels exposed for 2 249 and 5 771 hours in EBWR are included in Fig. 6 [5]. As seen from Fig. 6, the in-pile values correspond well with the present out-of-pile corrosion tests in neutral water with 0.1 ppm oxygen.

Corrosion in water up to 100 °C

Data regarding rates of release of corrosion products under dynamic conditions in low temperature water are lacking. In order to accumulate such data, we have erected two forced circulation loops operating at atmospheric pressure. A deoxygenated resin is used for oxygen removal. By electrolytic decomposition of water in a separate cell, without liquid contact with test environment, oxygen can be maintained at 0.005–10 ppm. Some results are given in Table 2. We see that steel dissolves in water with a low oxygen content at room temperature. If the water is maintained reasonably pure, the corrosion product will also be dissolved. The corrosion rate was found to be constant with time in experiments lasting 1–250 hours. The rate was higher than anticipated (10 mg/dm²/month at 25 °C and 50 mg/dm²/month at 50 °C), as many publications state that steel reacts very slowly with oxygen-free water.

If the temperature is above 60–70 °C, magnetite forms in the absence of oxygen, and the corrosion rate is somewhat decreased. Larger amounts of oxygen lead to nonadherent rust (α - or γ -FeOOH or α -Fe₂O₃ depending on temperature and oxygen level) and the corrosion rate is high.

The change from a slow attack to rapid rusting was rather irreproducible and could not be correlated with oxygen content, pH and temperature only as it was extremely sensitive to the purity of the water and to flow conditions. We have observed that mild steel

Table 2. Results of corrosion tests of steel in water below 100 °C

Type of test	Oxygen ppm	Temp. °C	pH	Type of attack	Rate law	Corrosion rate (mg/dm ² /month)	Oxide film	Appearance
Boiling under reduced <i>A</i> pressure Loop, continuously purified water	0	25	7	uniform	linear	10 ^a	none	bright
Loop, continuously purified water	0.02	25	7	uniform	linear	15 ^a	none	bright
Loop, continuously purified water	0.4	25	7	uniform	cubic	10 ^a	none	bright
Loop, continuously purified water	8	25	7	uniform	not known	less than 3	unidentified, very thin	bright
Agitated, no purification	8	25	7	rusting	linear	2 000	γ-Fe ₂ O ₃	rusty
Stirred, no purification	8	25	10	uniform	not known	less than 3	unidentified, very thin	bright
Stirred, no purification	8	25	10	uniform	not known	less than 3	unidentified, very thin	bright
Boiling under reduced <i>A</i> pressure Loop, continuously purified water	0	50	7	uniform	linear	50 ^a	none	bright
Loop, continuously purified water	0.2	50	7	uniform	linear	400 ^a	unidentified, thin	grey
Loop, continuously purified water	6	60	7	rusting	linear	2 000	γ-Fe ₂ O ₃	rusty
Agitated, no purification	6	60	7	rusting	linear	1 500	γ-Fe ₂ O ₃	rusty
Agitated, no purification	6	60	10	uniform	not known	less than 5	unidentified	bright
Boiling in <i>A</i> atmosphere	0	100	7	uniform	cubic	10	Fe ₃ O ₄	grey
Boiling with reflux condensers	?	100	7	uniform	cubic	15	Fe ₃ O ₄	grey
Boiling with reflux condensers	?	100	10	uniform	not known	less than 5	unidentified	bright

^a All corrosion products formed were released to the water in these tests: rate of release of oxide (calculated as Fe₃O₄) = 1.38 corrosion rate.

could be exposed in our loops to 30 °C water with 8 ppm oxygen with practically no attack (<3 mg/dm²/month) provided that the water was kept flowing and maintained at a high purity with ion exchange clean-up. Concentration gradients of oxygen in the environment is assumed to be important in the rusting process, and it is assumed that the effect of flow is to reduce such gradients.

The corrosion rate in water with 8 ppm oxygen was, as seen from Table 2, lower than in water with 0.025 ppm oxygen. This is difficult to explain without

assuming formation of an oxide film on the metal. Ellipsometric investigations have, however, not revealed much difference between polished and corroded steel specimens and the films must consequently be very thin. The low rate in oxygenated water is in sharp contrast with the normal rusting of steel and it is hoped that further work will clarify the details.

Increase in pH makes iron more stable thermodynamically and makes the oxides less soluble. The result is a decrease in corrosion rate for all oxygen levels (see Tables 2 and 3).

Table 3. Exposure at low temperature of steel earlier exposed at higher temperature

Type of test	Oxygen ppm	Temp. °C	pH (NH ₃)	Behaviour of pre-filmed specimens ^a	Behaviour of specimens without pre-formed film
Loop, continuously purified water	0.02	25	7	Practically no change after 200 hours	Reacted slowly to dissolved Fe(OH) ₂
Loop, continuously purified water	0.4	25	7	Practically no change after 200 hours	Remained bright
Loop, continuously purified water	4	25	7	Little affected, lost 0.01 mg/dm ² after 200 hours	Remained bright
Loop, continuously purified water	8	25	7	Little affected, lost 0.01 mg/dm ² after 200 hours	Remained bright
Agitated, no purification	8	25	7	Pits 0.2 mm deep	Severe rusting
Agitated, no purification 0.1 M NaCl	8	25	7	Oxide coating completely destroyed after 48 hours	Severe rusting
Loop, continuously purified water	0.2-0.4	60	7	Little affected, lost 0.1 mg/dm ² after 200 hours	Metal loss 13 mg/dm ² after 200 hours
Loop, continuously purified water	4	60	7	Little affected, lost 0.6 mg/dm ² after 75 hours	Rusted, metal loss 26 mg/dm ² after 75 hours
Agitated, no purification	6	60	7	Oxide coating completely destroyed after 700 hours	Severely rusted
Loop, continuously purified water	0.02	70	7	Little affected after 120 hours	Metal loss 14 mg/dm ² after 120 hours
Boiling with reflux condensers	low	100	7	Little affected after 700 hours	Developed uniform magnetite film
Agitated, no purification	8	25	10	Little affected after 700 hours	Little affected
Agitated, no purification	6	60	10	Little affected after 700 hours	Little affected
Boiling with reflux condensers	low	100	10	Little affected after 700 hours	Little affected

^a The pre-treatments were 2 days exposure in (1) superheated steam 400 °C, 100 kg/cm² (2) degassed water at 315 °C (3) water with 1 ppm O₂ at 315 °C (4) water with 2 000 ppm O₂ at 315 °C (5) degassed water at 230 °C (6) water with 1 ppm O₂ at 230 °C (7) water with 1 000 ppm O₂ at 230 °C (8) water with NaOH to pH 10 at 315 °C

The table is based on treatment (3). Treatments (1, 2, 3, 5, 6 and 8) gave very similar results, while (4) and (7) gave much less resistant films.

Problems associated with the application of mild steel for the condensate and feed water system in a nuclear plant should not be appreciably different from those in the conventional plants. Systems operating with neutral water have usually an oxygen content 50 ppb or lower. Kiekenberg [14] reports that the oxygen content in the turbine condensate in power stations in Hamburg, Germany, was 15–45 ppb. This content was further reduced with thermal degassers to 15–20 ppb. In this water, $\text{Fe}(\text{OH})_2$ released from steel pipes increased the iron content from 5 ppb in the turbine condensate to 50 ppb at the boiler entry.

Corrosion in alternating high and low temperature water

The corrosion of components normally exposed to high temperature water during shut-down periods might be an important problem. The behaviour of mild steel under such conditions has therefore been examined. We see from Table 3 that as long as the oxygen content in the cold water is low, no harmful corrosion will occur on specimens with a corrosion film formed at high temperature. Oxygen monitoring of the water and facilities for reducing the oxygen content during shut down is therefore recommended. The purity of the water is also important and the clean-up system should be allowed to operate in shut-down periods.

If the system is kept at lower temperatures for longer periods and when a low oxygen content is difficult to maintain, addition of alkalies should be considered and preferably even an oxygen scavenger such as hydrazine hydrate.

In agreement with results published by Vreeland, Pearl and Gaul [7, 8, 9] pits formed at low temperature were not found to grow under subsequent high temperature exposure.

We have also carried out experiments with thermal cycling. The cycling as such did not appear to have much influence. In no case did spalling of the oxide occur.

From the preceding sections, we conclude that the oxygen content in the primary water in a reactor is so low that no severe corrosion of mild steel will occur at any temperature. Not even condensed steam with originally 10–20 ppm oxygen is expected to give difficulties.

DISCUSSION

In a boiling-water direct-cycle reactor we can have either neutral water with fair amounts of radiolytically produced oxygen in the steam or ammoniated water with a low content of oxygen. We conclude that normal boiler steels will have a satisfactory corrosion resistance in high temperature water under both conditions. This view is supported by the experience with mild steel steam pipelines in HBWR. After longer exposure periods a corrosion product release rate of 10–15 $\text{mg}/\text{dm}^2/\text{month}$ can be expected (3–5 $\text{mg}/\text{dm}^2/\text{month}$ for stainless steel) [5, 15, 16]. The initial corrosion product release rate is much higher. However, this can

largely be avoided if a conditioning treatment is applied prior to actual reactor operation. If the reactor is to be operated with neutral water with radiolytic gases present, it is essential to use oxygenated water for the pre-treatment.

The rather high corrosion rates in neutral water at low temperature present difficulties. The ferrous hydroxide will be pumped into the reactor tank (if condensate clean-up is not applied), and little is known regarding its behaviour there. Precipitation of corrosion products on the fuel elements is a main objection against the application of mild steels in water cooled power reactors. An increased flow rate in the purification circuit cannot eliminate this problem. It appears that colloidal corrosion products have a pronounced tendency to precipitate shortly after their release, while products which have been in the water for a longer period are more inert in this respect. If the period required to transform corrosion products from the active to the inert form is short compared with the bulk water clean-up time, purification will hardly affect the tendency to precipitation on fuel elements. Precipitation on the fuel elements is irradiation-induced [17], and cannot be simulated by out-of-pile experiments. We therefore plan to install rust generators in HBWR to study this problem.

Relatively large amounts of corrosion products will originate from attack on components exposed in neutral low temperature water. No specific recommendation can be forwarded in this field. However, condensate clean-up will be an advantage. Reactor experiments are badly needed, and more out-of-pile corrosion tests with good water control would certainly be useful. Experiments aimed at finding cheap pre-treatments which can reduce the release rate should be worth while.

Alkalisiation of the water is attractive because the release rates in low temperature water are significantly reduced. Addition of ammonia does not reduce the corrosion rate at high temperatures. However, ammonia changes the nature of the released substance in such a way that a relatively large fraction of the corrosion products will be present as solid particles. Experiments with in-pile loops demonstrate that precipitation and transportation of corrosion products are much easier to handle at higher pH. It should be noted that it is reported that ammonia is much less effective than the hydroxides of the alkalimetals in this respect [16, 18].

The solid particles present in high pH water can be removed by filtering while the ionic and colloidal constituents make filtering less effective in neutral water. We believe that hot filtering can be developed into a technically and economically attractive process fairly easily. Interesting results have been obtained with a bed of magnetite [19, 20]. Beds of more insoluble matter are under investigation. High temperature filtering is suggested, used in combination with cold ion-exchange clean-up, and it is hoped that the ion exchange purification rate can be reduced by the introduction of hot filtering.

The radioactive corrosion products from the core will be transported with the water to out-of-core positions. The absence of nickel, chromium and cobalt in the mild steel system reduces the total activity in spite of the larger amounts of corrosion products. Decontamination of mild and low alloy steels can be carried out. This necessitates removal of the corrosion film and a conditioning treatment of decontaminated surfaces must be considered.

CONCLUSIONS

Oxygen in the range 0–10 ppm is acting as an inhibitor for the corrosion of mild steel in neutral high temperature water. Without additions to the water, apart from oxygen, steel exposed to the steam phase corroded at about the same rate as those in the water phase when oxygen was in equilibrium with the two phases. Small amounts of oxygen act as an inhibitor also in ammoniated high temperature water.

The steel surface area to water volume ratio has a major influence on the corrosion behaviour of steel under dynamic exposure at high temperature.

Only a part of the oxide coating on steel forms a continuous film, the rest of the oxide being whiskers. No correlation between corrosion rate, bulk thickness and type of oxide could, therefore, be found.

The effect of oxygen on the corrosion of steel at 20–100 °C is complex; small amounts of oxygen appeared to accelerate corrosion, but under some conditions larger amounts could cause passivation.

The water and steam in a boiling-water reactor will contain about 0.02–0.05 ppm and 5–20 ppm oxygen respectively without any treatment, this will inhibit corrosion of carbon and low-alloy steels in water and steam at high temperature. The rates of corrosion and corrosion product release will decrease with time to about 10 mg/dm²/month after 2–3 000 hours. Vreeland *et al.* [7, 8, 9] suggest a release rate as low as 2 mg/dm²/month. The steady state corrosion and release rates for low alloy steel at high temperature are nearly as low as those for stainless steel, and on this basis the consequences of using mild steel instead of stainless steel are small.

The initial corrosion product release rate is much higher for mild steel, and the purification system must be designed with this in mind. A significant reduction of the initial release can be achieved with an adequate pre-conditioning treatment.

The corrosion films formed at high temperature offer good protection at low temperature as long as the oxygen content in the water is low, but are destroyed by prolonged exposure in air-saturated water below 100 °C.

The gases borne with the steam will be extracted in the turbine condenser in a direct cycle reactor,

whereby the oxygen content in the condensate will be of the same order as in conventional power plants and the corrosion problems for the two types of plants similar in many respects. The corrosion rate of steel exposed in neutral water at low temperature is much higher than that of stainless steel. If low temperature components are made of mild steel, fairly large amounts of ferrous hydroxide will be present in the feed water if condensate clean-up is not used, with unknown consequences.

Alkalisiation of the primary water is attractive as the release rate from steel at low temperature is significantly reduced. The use of ammonia will facilitate water purification by hot-filtering. It is, however, not clear whether ammonia has sufficiently good stability under reactor conditions for general applications in light- and heavy-water reactors.

ACKNOWLEDGEMENT

This paper is partly based on work carried out as a joint project by Reactor Centrum Nederland and Institutt for Atomenergi, Norway. The author is grateful to these organizations for their interest and support.

REFERENCES

1. Tackett, D. E., Brown, P. E., and Esper, R. T., USAEC report WAPD-LSR(C)-134 (1955).
2. Blaser, R. U., and Owens, J. J., Symposium on High-Purity Water Corrosion, ASTM Special Publication 179, 137 (1956).
3. Kenton, D. E., *Nucleonics* 17, No. 9, 80 (1959).
4. Cosmata, H. R., *Nucleonics* 19, No. 3, 106 (1961).
5. Breeden, C. R., USAEC report ANL-6562.
6. Rose, R., Allison, G. M., and Hammar, L., *Water Chemistry Research at HBWR*, P/595, Vol. 9, these Proceedings.
7. Vreeland, D. C., Gaul, G. G., and Pearl, W. L., *Corrosion* 18, No. 10, 368 (1962).
8. Vreeland, D. C., Gaul, G. G., and Pearl, W. L., *Corrosion* 17, No. 6, 269 (1961).
9. Vreeland, D. C., Kjeller Report KR-53 (1963).
10. Gerasimov, V. V., AEC-tr-5219 (1962).
11. Linacre, J. K., and Morley, H., UKAEA report AERE-C/R 2853 (1959).
12. Ruther, W. E., and Hart, R. K., *Corrosion* 19, 127 (1963).
13. Bloom, G. M., Prov. 21st Annual Water Conference. Engineers Soc., West Pennsylvania (1960).
14. Kiekenberg, H., *Ingeniøren* (Danish) 21, 626 (1960).
15. Videm, K., Unpublished data.
16. Breeden, C. R., AEC-EURATOM Conference on Aqueous Corrosion of Reactor Materials, TID 7587, 48 (1959).
17. Ayers, J. A., HW-SA-2420 (1962).
18. Allison, G. M., AECL-1158 (1960).
19. Larson, R. E., and Williams, S. L., *Corrosion* 14, 424 (1958).
20. Paulson, C. F., *Chem. Engineering Progress* 56, 64 (1960).

ABSTRACT—RÉSUMÉ—АННОТАЦИЯ—RESUMEN

A/592 Norvège

L'acier doux dans les circuits primaires
de réacteurs de puissance refroidi à l'eau

par K. Videm

Pour étudier la possibilité de remplacer des aciers inoxydables par des aciers de chaudière ordinaires dans la construction de réacteurs de puissance refroidis à l'eau, il faut connaître la qualité de l'eau et de la vapeur dans tout le système et le comportement de l'acier dans ce milieu. Le mémoire porte essentiellement sur les problèmes de la corrosion et de la purification dans un ensemble en acier doux et concerne en particulier les réacteurs à eau bouillante à cycle direct.

La vapeur d'un réacteur à eau bouillante contient généralement 5 à 20 ppm d'oxygène. Il est possible de diminuer la quantité d'oxygène en introduisant de l'hydrogène dans le réacteur. Il est aussi possible d'augmenter le pH jusqu'aux valeurs utilisées dans les centrales classiques en introduisant de l'ammoniaque. Cependant des essais effectués au HBWR (sujet traité dans un autre mémoire présenté à la Conférence) ont montré que de très grandes quantités d'hydrogène sont nécessaires dans les deux cas. Il serait préférable d'utiliser des aciers doux avec de l'eau neutre contenant de l'oxygène et de l'hydrogène radiolytiques.

Une série d'essais de corrosion, effectuée hors de pile à des températures élevées aussi bien que basses, a été effectuée dans ce but, et les résultats sont comparés aux données de la littérature et aux résultats d'expériences de corrosion réalisées dans un réacteur à eau bouillante (HBWR). Un effort tout particulier a été fait pour étudier l'effet de l'oxygène et du pH et les moyens de traiter les aciers afin de réduire la corrosion et l'apparition de produits de corrosion.

On arrive à la conclusion que la résistance à la corrosion des aciers de chaudière ordinaires dans les réacteurs à eau bouillante est acceptable à haute température; par contre, les problèmes posés par les éléments se trouvant à basse température, ou dont la température baisse lors des arrêts du réacteur, sont les plus difficiles à traiter.

Dans tous les cas, l'utilisation d'aciers au carbone ou d'aciers faiblement alliés augmente la quantité de produits de corrosion introduits dans l'eau et exige ainsi un système de purification plus efficace.

A/592 Норвегия

Использование низкоуглеродистой
стали в первичных контурах энергетических реакторов с водяным теплоносителем

К. Видем

Оценка возможностей замены нержавеющей стали обычной котельной сталью в энергетическом реакторе с водяным теплоносителем требует знания качества воды и пара на любом участке системы и поведения стали в этих окружающих условиях. Данный обзор связан главным образом с проблемами коррозии и очистки в системе из низкоуглеродистой стали; обсуждение проблем дается на примере кипящего реактора с прямым циклом.

Пар, производимый кипящим реактором, содержит обычно от 0,0005 до 0,002 % кислорода. Содержание кислорода можно снизить путем инжектирования водорода в реактор. Добавлением аммиака можно увеличить также pH до величин, используемых в обычных установках. Однако результаты экспериментов, выполненных на кипящем энергетическом реакторе HBWR (эксперименты описываются в специальном докладе, представляемом на данную конференцию), показывают, что в обоих случаях требуются очень высокие дозы водорода. Более заманчивым решением была бы возможность использовать низкоуглеродистую сталь в нейтральной воде, в которой присутствуют радиолитический кислород и водород.

С этой целью была осуществлена серия коррозионных исследований во вне реакторных испытательных петлях как при высоких, так и при низких температурах; полученные результаты сравниваются с опубликованными в литературе данными и с результатами коррозионных экспериментов, выполненных на кипящем энергетическом реакторе HBWR. Специальные усилия были посвящены изучению эффекта содержания кислорода, величины pH и методов предварительной подготовки сталей в целях уменьшения коррозии и выделения продуктов коррозии.

Пришли к выводу, что коррозионная стойкость обычной котельной стали при высоких температурах в условиях кипящего реактора вполне приемлема и что коррозия отдельных узлов при низкой температуре и корродирование участков, обычно находящихся при высоких температурах, во время остановки реактора являются самыми трудноразрешимыми проблемами.

При всех обстоятельствах использование углеродистой стали или низколегированной стали приведет к увеличению выделения продуктов коррозии в воду и к необходимости применения более эффективной системы очистки.

A/592 Noruega

El acero suave en circuitos primarios de reactores de potencia refrigerados por agua por K. Videm

Para valorar las posibilidades de sustitución de aceros inoxidable por aceros normales de caldera en un reactor de potencia refrigerado por agua, es preciso conocer las características del agua y del vapor a lo largo de todo el sistema, y el comportamiento del acero en este medio. El presente estudio trata fundamentalmente de los problemas de corrosión y de purificación en un sistema de acero suave en un reactor de agua hirviendo de ciclo directo.

El vapor de un reactor de agua hirviendo normalmente contiene de 5 a 20 ppm de oxígeno. Es posible reducir el contenido en oxígeno por inyección de hidrógeno en el reactor. También es posible aumentar el pH, hasta los valores con que operan las instalaciones clásicas por adición de amoníaco. Sin embargo, los resultados de las experiencias realizadas en el HBWR

(descritos en otra memoria de esta Conferencia) demuestran que en ambos casos se requiere un suministro de hidrógeno muy elevado. Sería una solución más interesante el poder emplear acero suave en un agua neutra que contuviera oxígeno e hidrógeno radiolíticos.

Con este fin se han efectuado una serie de experiencias de corrosión sin irradiación, en circuitos a elevadas y bajas temperaturas, y se han comparado los resultados con los datos de la bibliografía y con experiencias de corrosión efectuadas en un reactor de potencia de agua hirviendo (HBWR). Se dedicó un esfuerzo especial a estudiar el efecto del contenido en oxígeno y del pH, y de los métodos de preacondicionamiento de los aceros, con el fin de disminuir la corrosión y la liberación de los productos de corrosión.

Se llega a la conclusión de que el acero de calderas presenta a elevadas temperaturas una resistencia a la corrosión aceptable en reactores de agua hirviendo, y que los problemas más difíciles de tratar son la corrosión de los componentes que operan a baja temperatura y el ataque durante los períodos de parada de las zonas que normalmente trabajan a elevadas temperaturas.

En todos los casos el empleo de acero al carbono o de aceros de baja aleación da lugar a una cantidad de productos de corrosión mayor, que pasan al agua por lo cual se precisará un sistema más eficaz de purificación.

Special problems relating to monotube boilers in nuclear power stations

By J. Kägi and P. Doroszlai*

The merits of the monotube steam generator emphasize its ever-increasing importance in reactor plants with steam production outside of the core. In gas-cooled reactor plants the monotube principle provides appreciable advantages in regard to the integrated steam generator which is located in the same pressure vessel as the reactor core. Owing to the advantages resulting from the reduction of the number of tube passages through the pressure vessel, in conjunction with various possible simplifications, as compared with the conventional monotube boiler, preference is given to the monotube principle already at low steam pressure, for which, in conventional plant, other boiler types would be employed. The following chapters deal with the dynamic properties of nuclear steam generators.

Problems posed

We can distinguish between the dynamic behaviour for small disturbances, which is characteristic of control processes during normal operation, and the behaviour of the boiler as a result of large disturbances, which may occur under special operating conditions such as start-up, shut-down, feedwater cutout, reactor scram, etc., just to mention some examples. Generally in this group of operating conditions the thermodynamic values are subject to changes within wide limits. The classification of the dynamic problems was made in view of the differing methods employed for handling each case, which is essential to ensure a reasonable amount of calculation work, as is shown further below. In both cases the problem is to find the variation in time of characteristic values such as temperatures and pressures after a disturbance. A first solution to the problem consists of course in the application of a non-linear mathematical model for the boiler, according to the practice employed for dynamic investigations of reactor cores. Experience has however shown that the treatment of boiler control problems in this way requires a very great amount of computer capacity. Frequently two heat exchange systems in the gas flow must be partially connected in parallel, partially in series, and represent together with the other plant components, and the control circuits, a very extensive and complicated system. Here it is advisable to use a linearized com-

puting method, starting from the assumption of small disturbances. On the other hand, the linearized model (theory) can of course not be readily employed for large disturbances. Here a non-linear simulation is necessary, whereby it is possible to keep the extent of the work within reasonable limits, since these investigations may often be confined to the boiler itself and the control systems can be disregarded.

From our experience, proper control problems are best solved with the aid of the analogue computer, while for the non-linear simulation the digital computer may also be used.

In all cases it is advisable to supplement the dynamic investigations by stationary analysis, i.e., to calculate the steady state distribution of temperatures and steam conditions in the heat exchange system for various operating conditions. Here again the analogue computer has proved to be a very useful instrument. Manual calculations in the case of systems connected both in series and in parallel immediately become very complicated and time consuming, while with the computer many problems can be solved within a short time. Significant information on energy and mass content of the system such as, for example, steam temperatures as a function of the load may be obtained in this way.

Demonstration with a few examples

The following investigations have been made for the steam generator of the EDF4 nuclear power plant, with the exception of curves (a) and (b) in Fig. 1.

Stationary investigations

Figure 2 illustrates the distribution of CO₂ temperature and water/steam temperatures over the heating surface for 100% load and 25% load. It was assumed that the CO₂ outlet temperature from the boiler does not vary with load. The corresponding heating surface excess at partial load is offset by properly shifting the evaporator end point. In the same illustration the energy content of the tube system as well as the mass content as a function of the load are also depicted. The major amount of mass is stored in the preheater. As the load decreases so also does the water and steam content. Conversely, the stored thermal energy increases quite considerably as the load drops, which is attributed to the corresponding increased size of the superheater, storing a great amount of energy in its

* Sulzer Brothers Ltd., Winterthur.

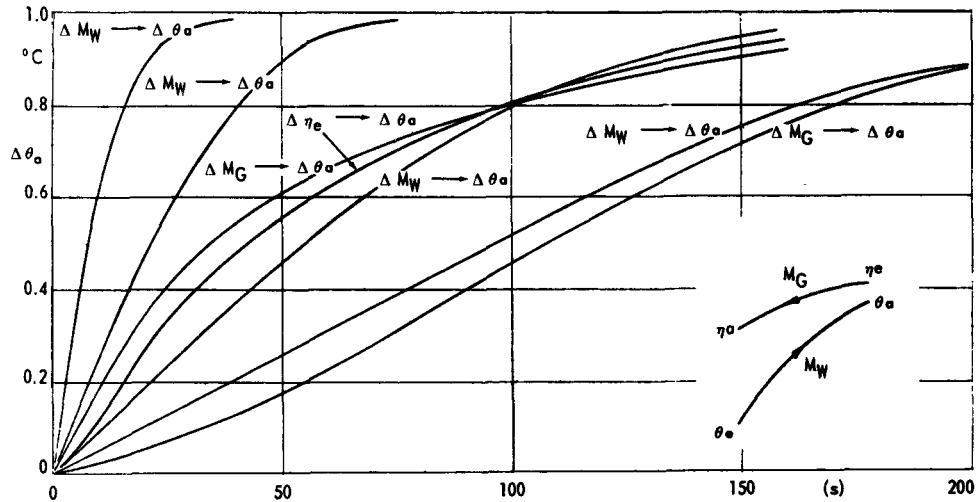


Figure 1. Transfer functions for different preheaters (For details see Figure 3)

hot tubes. As the load drops, the evaporator and preheater sections show a decrease in the energy content. Already from these curves important conclusions can be drawn for the control of the steam generator, which can be verified later on by the results of the control dynamic investigations:

(a) With an increase in load the amount of feed-water that must be temporarily supplied to the boiler is greater than the amount corresponding to the new steady state. The excess water is stored in the preheater which changes its length accordingly;

(b) The steam generator has a considerable load-dependent thermal capacity, which benefits the control system. If the load increases, an appreciable amount of energy is released merely through shifting of the evaporation end point downstream with increased feed flow. If we form the time constant $T = \frac{\Delta E}{H}$ with ΔE = released energy for a load change

of H = thermal rating of the boiler, we obtain a value of approx. 22 seconds. This means that the increased energy requirements after a positive load change during that time can be met by the tube system itself. This value is approximately 20 times greater than the pressure-dependent accumulator time constant. On the basis of these conditions it may be predicted that the quality of the over-all control system will depend to a great extent on feed flow control and in particular on the proper choice of the corresponding anticipation signals. This will be confirmed in a later section.

Dynamic control investigations with linearized model

The dynamic behaviour of the preheater-evaporator-superheater system, subject to constant heat inputs and steam pressure as a function of time, is described in detail in [1]. By applying this theory it is possible to deal with many problems, at least qualitatively.

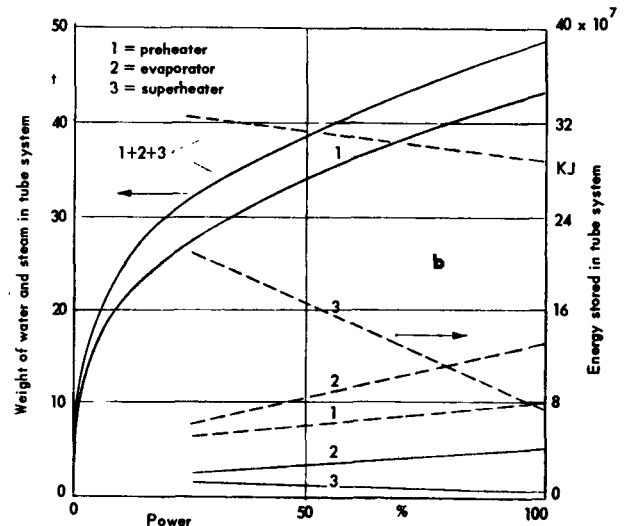
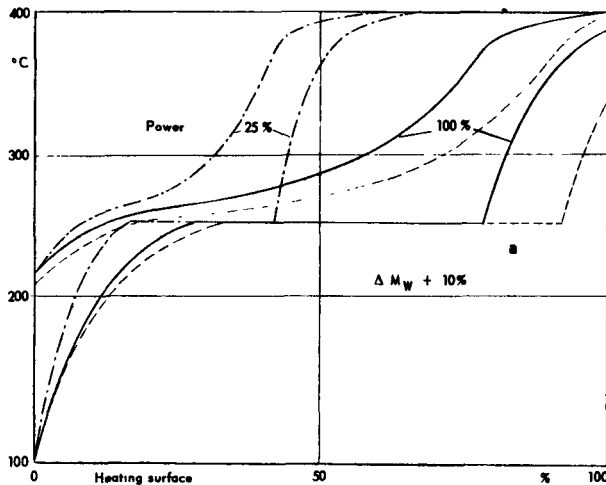


Figure 2a and b. Stationary analysis of once-through boiler at different loads. Thermal power 1 600 MW

More accurate investigations however call for adaptation to the conditions imposed by the counter-flow heat exchange in boilers of nuclear power plants, viz:

(a) To every change in the evaporation pressure there is a corresponding change in heat transfer by reason of a change in the average temperature difference between heat transport medium and working medium;

(b) Changes in the heating surfaces in the individual sections, as shown in Fig. 2, correspond to changes in the temperature field, and in turn in the heating (see heating distribution at full load and after 10% feed flow disturbance in Fig. 2). The assumption of constant heat input in a particular section during partial disturbances on the working-medium side must, therefore, be abandoned.

By dividing the preheater, evaporator and superheater into a number of sections, whereby the energy balance between gas flow and working-medium flow is established for each section, taking into account the variable pressure in the system, a linearized simulation method has been developed that permits of dynamic investigations of the boiler, without requiring excessive computer capacity. A reactor plant having parallel and independent water/steam systems in the common CO₂ flow can still be simulated, under the assumption of an ideal reactor, i.e., constant gas outlet temperature during all load conditions, on a Beckman-Ease computer equipped with 8 dead-time elements of special design.

Preheater

The transfer behaviour of the preheater is of decisive importance, not only as far as the control of the boiler is concerned but also as regards the control of the entire plant and it gives a good example of what has been mentioned earlier. Figure 1 illustrates a number of transient responses for various preheater types of gas-cooled reactors calculated under different assumptions. In general the designation Δ signifies in the following the deviation of a factor from the steady state. The designation $\Delta M_G \rightarrow \Delta \eta_a$ infers that, for the curve in question, $\Delta \eta_a$ is the response of the temperature η_a to a disturbance ΔM_G of the gas flow M_G . The symbols employed are defined in Figs. 8 and 9.

Let us first of all look at curves (c), (d), (e), (f) and (g), which all belong to the same preheater of a steam generator of 1 600 MW thermal for a CO₂ cooled, graphite moderated natural uranium reactor.

Following a change in heat input or changes of the feed water flow, the preheater changes its outlet temperature ϑ_a and its length in the same proportion [1]. This variation in length, in turn affects the process in the evaporator and superheater. Curve (e) shows the outlet temperature for a feed flow change, calculated for constant heat input in space and time. Figure 3 illustrates the relevant tube dimensions and tube lengths. This is a finned tube which, for these calculations, is replaced by a smooth tube having the same mass per unit length and the same inside diameter with a fictitious wall thickness.

Curves (f) and (g) show the temperature responses at preheater outlet for heating or feed flow disturbances at inlet as they actually occur with time-dependent counterflow heating (variable in time). Curves (e) and (f) show an appreciable difference which cannot be neglected. The reason for the much slower temperature response lies in the continuous shift of the heat input as a result of the increase in length of the preheater section, which, in turn, must become apparent over the feed water flow. Only gas flow and temperature disturbances on the gas side at economiser inlet lead to rapid responses of η_a and ϑ_a (see curves (c) and (d)). Curve (b) illustrates a transfer function equivalent to function e , for a steam generator of the same power but having an economiser with a large number of parallel unfinned tubes. It will be seen that, from a control point of view, the widening and shortening of the economiser surfaces is considered desirable. But the very numerous parallel tubes have an adverse effect on design, such as the disadvantage of having many header weldings and tolerance problems. An interesting feature is the transfer behaviour as depicted by curve (a) which is shown for a boiler for a high-temperature reactor of the same output as the examples described above. The intensive heating, with a practically constant temperature difference over the tube length, allows for short heating surfaces with a brief dead time so that a very good control behaviour may be expected.

Transfer behaviour of the entire steam generator

The transfer behaviour of the steam generator may be illustrated by a set of transfer functions, whereby one has to distinguish between the following two cases:

(a) the steam pressure remains constant,

(b) the steam demand M_T of the turbine is an independent variable, forced upon the steam generator and determining the load of the plant.

Figures 4 and 5 refer to case (a), while Figs. 6 and 7 apply to case (b). In the case shown we are again concerned with a steam generator system of 1 600 MW(th) power having the same constants as the ones used for the plotting of curve 3 in Fig. 1. The boiler consists of two absolutely identical tube systems running in parallel and arranged in one and the same gas flow; within certain limits the two systems may operate independently of each other. Consequently, in all illustrations the symmetric cases for simultaneous disturbances in both systems and the asymmetric cases with disturbances on only one system are plotted. Of particular interest here is the mutual interference of the systems resulting from the coupling on the gas side. Generally speaking it may be said that in the present instance the coupling on the gas side is relatively small.

Of special interest is the variation of the boiler gas outlet temperature as the result of a feed water disturbance (Fig. 7). An increase of feed flow primarily leads to a drop in the temperature, as a result of the increased preheater length and of the increased heat transfer coefficient k , in conjunction with the

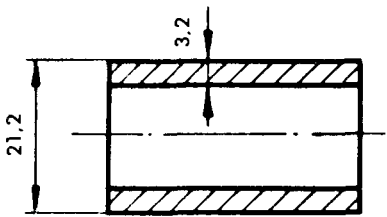
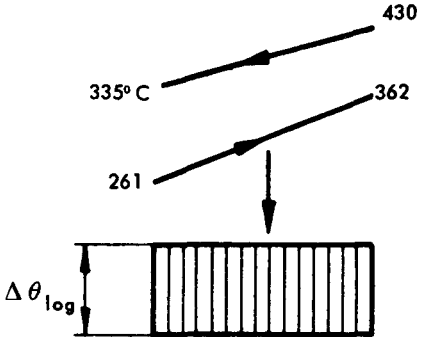
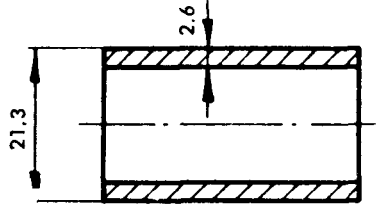
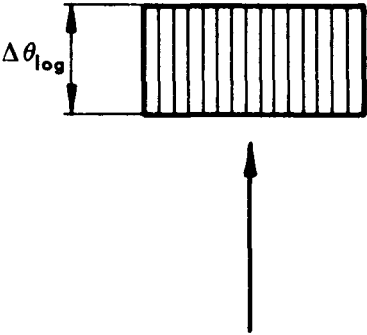
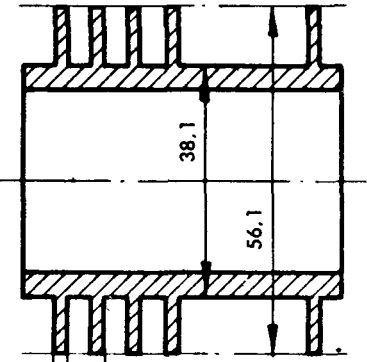
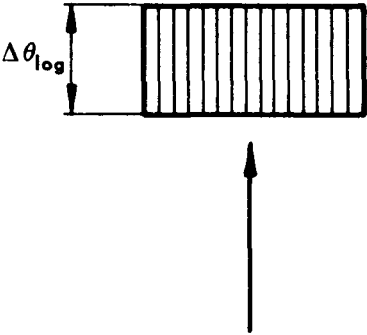
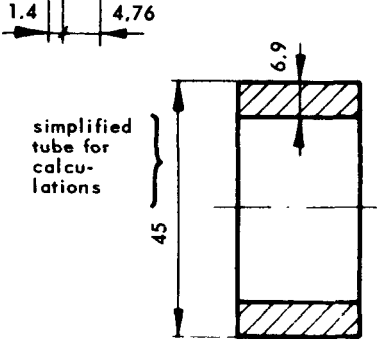
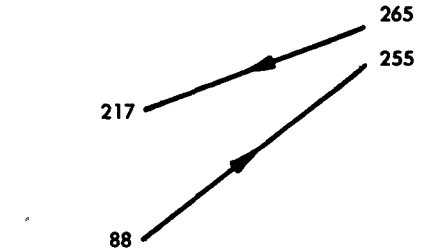
Case	Dimensions of tubes	Number of parallel tubes	Type of heat input
a		<p>3090</p> <p>$L = 20.4$</p>	
b		<p>10 000</p> <p>$L = 12.4$</p>	<p>constant in space and time</p> 
e		<p>1404</p> <p>$L = 58$ m</p>	
c d f g	 <p>simplified tube for calculations</p> <p>45</p> <p>6.9</p> <p>1.4 4.76</p>	<p>$L = \text{length of preheater section}$</p>	<p>variable in space and time (counterflow heating)</p> 

Figure 3. Geometrical and thermal characteristics of the preheaters compared in Figure 2

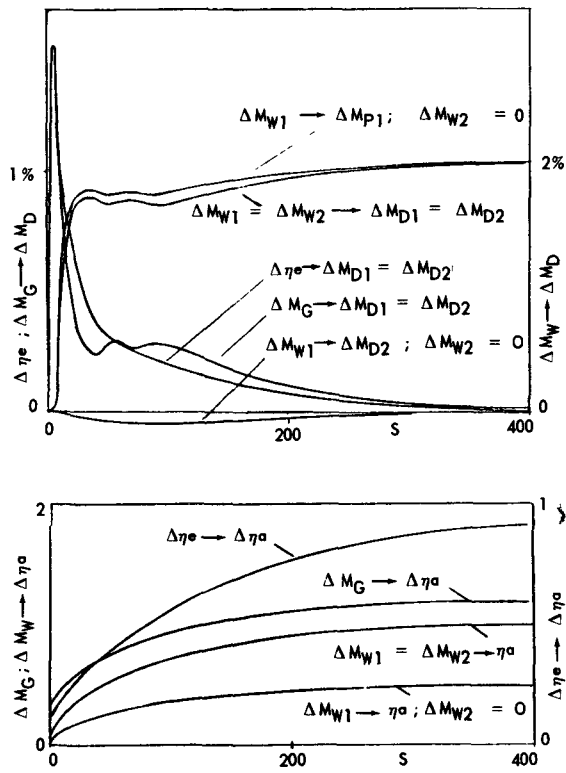


Figure 4. Transfer function of a 1600 MW(th) boiler. Steam pressure constant
Disturbances: 1% for ΔM and 5°C for $\Delta \eta_e$

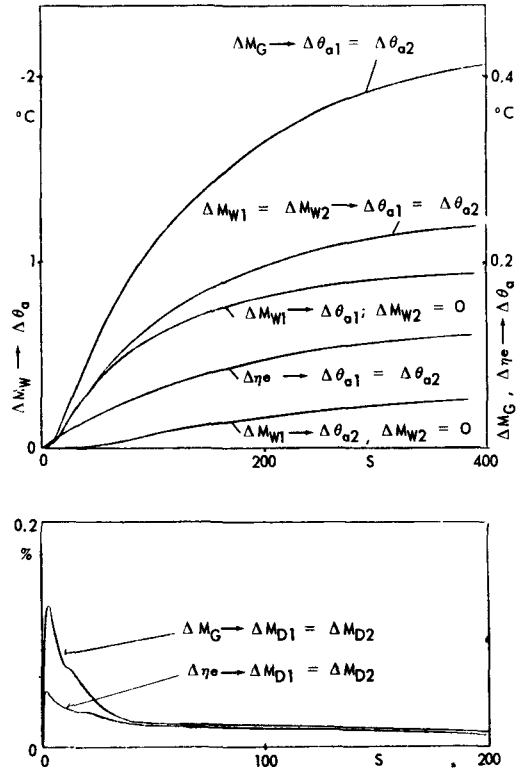


Figure 5. Transfer functions of a 1600 MW(th) boiler. Steam pressure constant
Disturbances: 1% for ΔM and 5°C for $\Delta \eta_e$

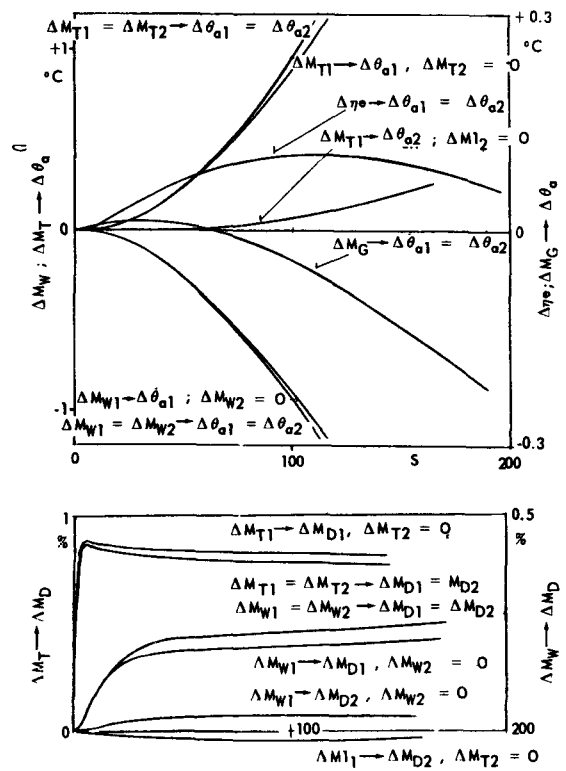


Figure 6. Transfer functions of a 1600 MW(th) boiler. Steam flow M_T is an independent variable
Disturbances: 1% for ΔM and 5°C for $\Delta \eta$

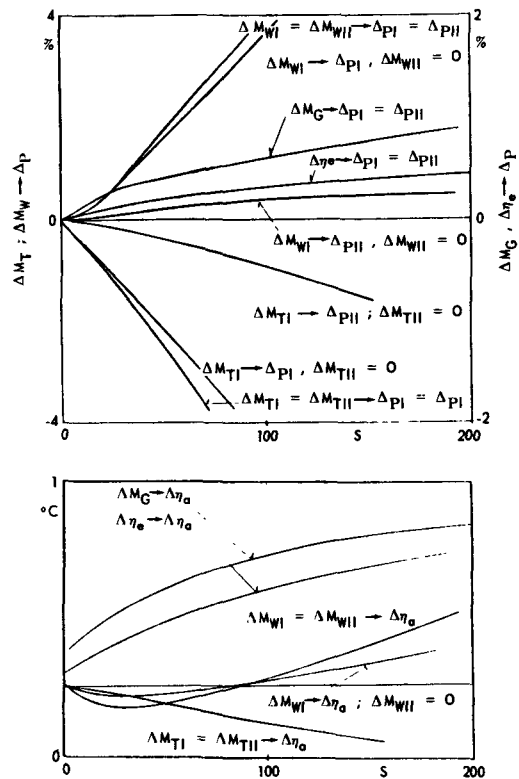


Figure 7. Transfer functions of a 1600 MW(th) boiler. Steam flow M_T is an independent variable
Disturbances: 1% for ΔM and 5°C for $\Delta \eta$

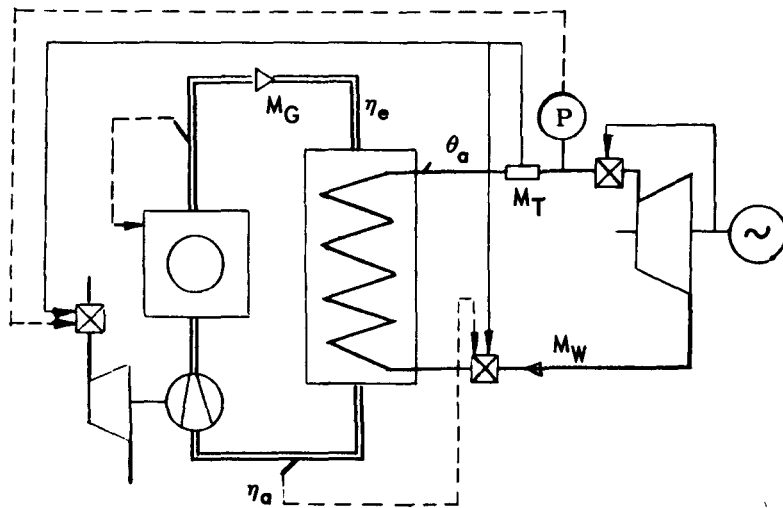
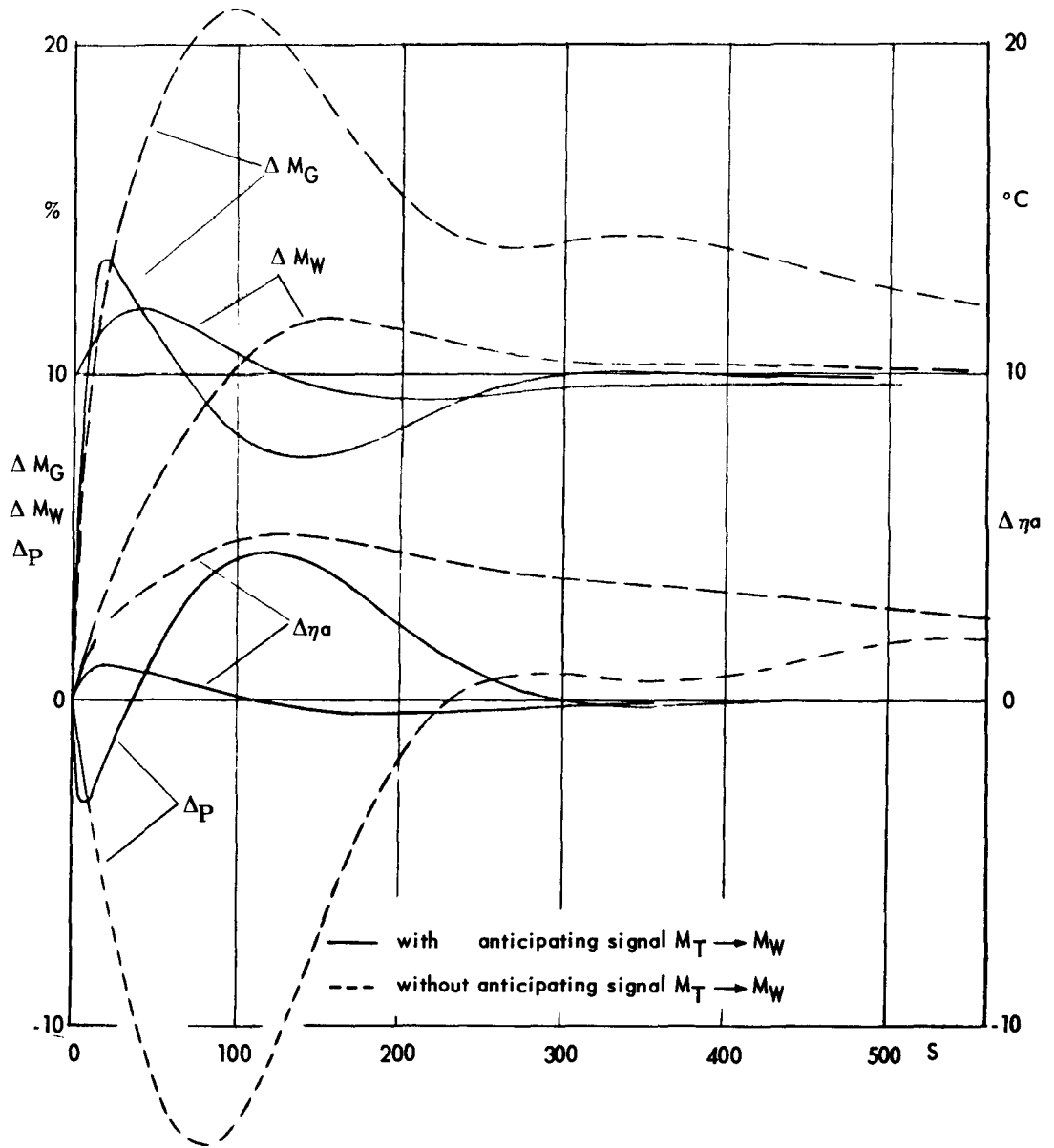


Figure 8. Dynamic behaviour of a 1600 MW(th) power station
Disturbance: $\Delta M_T = 10\%$

corresponding displacement of the temperature field, and rises again after approximately 100 seconds under the influence of the continuously increasing evaporation pressure. On the basis of this curve alone it would appear as if control of feed flow from the gas outlet temperature were not possible, but the following deliberations show that in practice η_a may still be used as the controlling variable.

Entire plant

Figure 8 illustrates the dynamic behaviour of the entire plant following step-disturbance of the turbine steam flow M_T . The control system is shown in the accompanying sketch, the broken line illustrating the control impulses of proportional-integral character, while the full lines illustrate the proportional anticipation signals. In this case the reactor was idealised by putting $\Delta\eta_e = 0$, which is quite permissible for the present purpose. The response of the gas outlet temperature η_a shows that, after an output disturbance the immediately increased gas flow will guarantee the proper functioning of the feed control, by overriding the influence of pressure on η_a , which was described in the previous chapter. An interesting point is the brief drop in the steam pressure within the first 50 seconds, with subsequent pressure peak caused by the anticipating signal from M_T on the feed water flow.

It is clearly seen here that the anticipating signals, as postulated previously, exert a very favourable influence on the control process. If it is omitted, considerably greater control deviations occur for η_a and p , which can be only slowly adjusted by the integral part of the control impulse coming from the adjusting time of the PI controllers. The reset time of the PI controller for η_a must be relatively long on account of the stability (sluggish behaviour of the preheater). Figure 9 shows a slightly different control layout where the feed water flow is controlled by the pressure, while η_a acts on the gas flow. The transfer behaviour essentially corresponds to that of the first control layout, except for the slightly greater deviations of the steam pressure. A close examination of the curves shown and a comparison of the individual transient responses of the steam generator will provide interesting aspects, but a detailed discussion would lead beyond the scope of the present paper. Although the gas outlet temperature η_a depends on the steam pressure as well as on the steam/water content of the steam generator, feed flow control depending on it, is possible.

REFERENCE

1. Dr. Paul Profos, *Die Regelung von Dampfanlagen*, Springer-Verlag (1962).

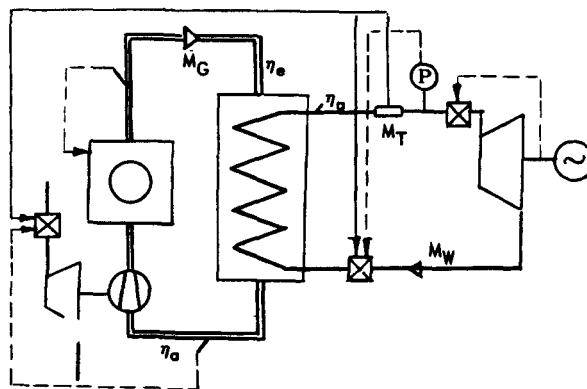
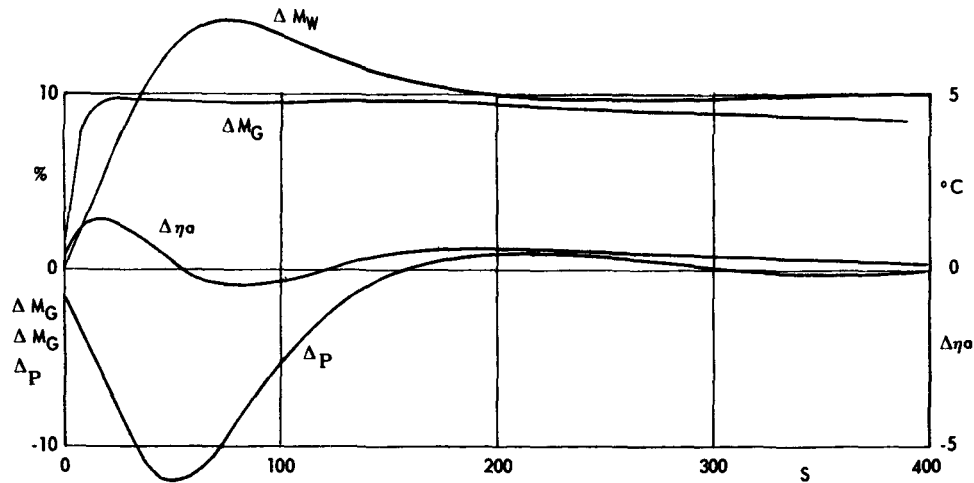


Figure 9. Dynamic behaviour of a 1600 MW(th) power station
Disturbance of steam flow at turbine $\Delta M_T = 10\%$

ABSTRACT—RÉSUMÉ—АННОТАЦИЯ—RESUMEN

A/696 Suisse

Problèmes spéciaux du générateur de vapeur monotubulaire dans la centrale nucléaire

par J. Kägi et P. Doroszlai

Le mémoire traite différents problèmes résultant de l'utilisation du générateur de vapeur monotubulaire dans la centrale nucléaire.

La première partie de l'étude concerne les problèmes relevant du calcul, de la construction, de la fabrication et du montage, ainsi que des conditions de fonctionnement et de questions de sécurité spéciales. A l'aide de différents exemples pris dans le domaine des réacteurs refroidis au gaz [réacteurs à l'uranium naturel refroidis au CO₂, *Advanced gas-cooled reactors* (AGR), réacteurs à haute température (HTGR)], certains problèmes spécifiques sélectionnés sont analysés à la lumière de l'expérience acquise lors de la construction des générateurs de vapeur classiques, compte tenu des essais et études faits récemment. Est considéré tout spécialement le générateur de vapeur dit « intégré », implanté dans le même caisson que le réacteur. Quelques résultats d'études de projets détaillés sont traités spécialement.

Dans la seconde partie, il est question des problèmes dynamiques du générateur de vapeur monotubulaire. Ceux-ci peuvent en principe être divisés en deux groupes, celui des fortes perturbations, comme celles qui se présentent dans des conditions de fonctionnement spéciales, et celui des faibles perturbations, telles qu'elles se manifestent dans le réglage en marche normale. Par fortes perturbations, on entend des états de marche entraînant une variation des valeurs thermodynamiques dans un vaste domaine, comme le démarrage, l'arrêt, la chute des barres du réacteur, les perturbations provoquées par une panne du système de réglage, etc. Un modèle simplifié pour la simulation non linéaire du générateur de vapeur avec une calculatrice analogique est présenté. Les problèmes sont traités d'une manière concrète à l'aide de quelques exemples de calcul pour les types de réacteur susmentionnés.

Les opérations de réglage sont traitées moyennant une théorie linéarisée. Dans un premier paragraphe, on indique à l'aide d'exemples les systèmes de réglage possibles pour les différents champs d'application ainsi que les relations statiques des grandeurs thermiques pour différents états de charge. Les calculs éventuellement très complexes et longs concernant la répartition de la température et de la pression sont résolus au moyen d'une calculatrice analogique.

Dans le deuxième paragraphe, il est question des fonctions de transfert du générateur de vapeur pour différentes perturbations possibles. De plus, le comportement de l'installation dans son ensemble est illustré à l'aide de résultats de calcul. Le but est de nouveau la comparaison entre les trois domaines

d'application principaux indiqués plus haut. A l'aide d'un exemple, la concordance entre le calcul et les résultats d'essais effectués dans une boucle d'essais est mise en évidence.

A/696 Швейцария

Особые проблемы прямоточных парогенераторов на атомных электростанциях

Ж. Кэги, Л. Дорозлаи

В настоящем докладе рассматриваются различные проблемы, возникающие при использовании прямоточного парогенератора на атомной электростанции.

В докладе обсуждаются проблемы, возникающие при расчете, строительстве, изготовлении и монтаже, а также условия эксплуатации и специальные вопросы безопасности. С помощью различных примеров, взятых из области реакторов с газовым охлаждением (реакторов на природном уране с охлаждением CO₂, усовершенствованных реакторов AGR с газовым охлаждением, высокотемпературных реакторов HTGR), анализируются некоторые специфические проблемы в свете опыта, накопленного при строительстве обычных парогенераторов, и с учетом недавно проведенных испытаний и исследований. Особо рассматривается так называемый «включенный» парогенератор, который устанавливается в одной оболочке с реактором. Детально рассматриваются некоторые результаты проектных исследований.

Обсуждаются также проблемы динамики прямоточного парогенератора. В принципе их можно разделить на две группы: проблемы сильных возмущений, возникающих в особых условиях эксплуатации, и проблемы слабых возмущений, проявляющихся в регулировании при нормальной работе. Под сильными возмущениями подразумеваются режимы работы, влекущие за собой изменение термодинамических величин в широком диапазоне, например пуск, остановка, падение стержней реактора, возмущения, вызываемые поломкой в системе регулирования, и т. д. Представлена упрощенная модель для нелинейного моделирования парогенератора с помощью счетно-решающей машины. Проблемы решаются на конкретных примерах расчетов для упомянутых типов реакторов.

Операции регулирования рассматриваются путем усреднения линеаризованной теории. В первом разделе с помощью примеров показаны возможные системы регулирования для различных областей применения, а также статические

отношения тепловых величин для различных состояний нагрузки. Вычисления, касающиеся распределения температуры, в некоторых случаях очень сложные и длинные, решаются с помощью счетно-решающей машины.

Во втором разделе рассматриваются функции переноса парогенератора для различных возможных возмущений. Кроме того, поведение установки в целом иллюстрируется с помощью результатов расчета. Целью является сравнение трех основных областей применения, о которых говорилось выше. С помощью примера выявляется связь между расчетом и результатами испытаний, проведенных в экспериментальной петле.

A/696 Suiza

Problemas especiales del generador de vapor monotubular en una central nuclear

por J. Kägi y P. Doroszlai

En la memoria se examinan diferentes problemas que plantea la utilización de un generador de vapor monotubular en una central nuclear.

La primera parte trata de los problemas relativos al cálculo, construcción, fabricación y montaje, así como de las condiciones de funcionamiento y de las cuestiones especiales de seguridad. Con ayuda de diferentes ejemplos, tomados de los reactores refrigerados por gas [reactores de uranio natural refrigerados por CO₂, *Advanced gas-cooled reactors* (ADR), y reactores de elevada temperatura (HTGR)], se analizan determinados problemas específicos de acuerdo con los experimentos realizados en la construcción de generadores de vapor clásicos, teniendo en cuenta los ensayos y estudios que se han llevado a cabo recientemente. Se considera muy en particular el generador de

vapor denominado « integrado », que va montado en el mismo recipiente que el reactor. Se examinan especialmente algunos resultados de estudios de proyectos detallados.

La segunda parte trata de los problemas dinámicos del generador, que en principio pueden dividirse en dos grupos: el de las grandes perturbaciones, como las que se presentan en condiciones especiales de funcionamiento, y el de las perturbaciones ligeras, tales como las que se manifiestan en el control de marcha normal. Por grandes perturbaciones se entiende estados de funcionamiento que originan una variación en gran escala de los valores termodinámicos como, por ejemplo, la puesta en marcha, la parada, la caída de las barras de control, las perturbaciones provocadas por una avería del sistema de regulación, etc. Se expone un modelo simplificado para la simulación no lineal del generador de vapor con una calculadora analógica y se estudian problemas concretos mediante algunos ejemplos de cálculo relativos a los tipos de reactor mencionados.

Las operaciones de regulación se estudian según una teoría expresada en términos lineales. En el primer apartado se indican, con ejemplos, los sistemas de control posibles para los diferentes campos de aplicación y las relaciones estáticas entre las magnitudes térmicas para varios estados de carga. Los cálculos de distribución de temperaturas y presiones, que serían muy largos y laboriosos, se resuelven con ayuda de una calculadora analógica.

El segundo apartado trata de las funciones de transferencia del generador de vapor para diferentes perturbaciones posibles. Además, se describe con ayuda de los resultados del cálculo el funcionamiento de la instalación en su conjunto, con objeto de comparar nuevamente los tres campos principales de aplicación. Se demuestra con un ejemplo que los resultados del cálculo concuerdan con los de las pruebas realizadas en un circuito de ensayo.

Experience in the design, calculation and manufacture of power reactor components

By K. J. de Jong, C. de Pater and M. C. van Veen*

The Neratoom Group has dealt, or is dealing, with four main components for power reactors, viz.:

Two secondary steam generators for SENN (Società Elettro-nucleare Nazionale, a BWR at Garigliano, Italy);

A core structure for SENN:

A core structure for KRB (Kernkraftwerk RWE-Bayernwerk, a BWR at Gundremmingen, Germany);

A reactor pressure vessel for SEP (Samenwerkende Elektriciteits Productie-bedrijven, a BWR at Dodewaard, Holland).

The components for SENN have been delivered and are operating satisfactorily. The KRB core structure is in the manufacturing stage, whilst the reactor pressure vessel for SEP is in the design stage. In general we want to emphasize one point which is in our opinion very important in order to meet the high standards of reliability and performance required for nuclear components. In a paper by Rickover [1] it has been stated that the (American) industry finds it difficult to reach the manufacturing standards required. Moreover Rickover states that the problems are not only of a technological nature but that organizational problems also play an important role. It is said that industry pays insufficient attention to these problems. Manufacturing procedures would seem to be not sufficiently understood, and specified requirements should be seen more as desirable, rather than as stringent, requirements. In the light of these remarks it is our opinion that in this era where industry is trying to meet the high requirements, the role of the client in the selection of industries that will be the suppliers for nuclear components is very important and delicate. Besides the normal commercial factors, such as price and time of delivery, the technological and organizational possibilities of manufacturers must play a role in the selection. In general clients do not sufficiently take into account these factors in the project stage. Should this be the case then it is our opinion that the results will be better than reported by Rickover. Besides the very important contact between supplier and client in the project stage we think that intimate contact, between all departments and specialists who have to take action at one stage or another at the suppliers works, is inevitable. The design departments which usually have contact with

clients should also discuss manufacturing procedures with qualified work specialists. In our opinion this is the only way to arrive at an integrated design. By having these contacts, the manufacturing problems and also the cost saving possibilities can play a role in the choice between two alternatives. Also when these manufacturing specialists are playing a role in the design stage they gain a better understanding of the meaning of the unusual tolerances and the exacting manufacturing instructions. As an example, for the contract for the secondary steam generators a special group was formed by the supplier, consisting of design office, tooling department, boiler shop and machine shop specialists, and welding and material specialists. In the early stages of design, weekly meetings were held at which the design office outlined their ideas which were in many cases adjusted by the mentioned specialists. During these meetings a manufacturing analysis was born, growing more detailed as the design progressed. Plans for development work of manufacturing methods originated from these meetings in an early stage. The result was that all departments concerned had a clear picture of what was being asked of them when the definitive construction drawings left the design office, and that the design office was well aware of the technical possibilities and could discuss with the client the details of the manufacturing instructions. We are quite certain that due to this special organization time was gained and less mistakes were made than would have been the case if the normal works organization had been used.

SECONDARY STEAM GENERATORS FOR SENN POWER STATION

Description

The two secondary steam generators for SENN are of the vertical type. Design data per generator are as follows:

Design pressure: 90 atm (g),
 Design temperature: 302 °C,
 Operating pressure (primary side): 74 atm (g),
 Primary water inlet temperature: 277 °C,
 Primary water flow: 4 200 t/hr,
 Secondary steam pressure**: 34 atm (g),

* Neratoom Group, The Hague.

** At max continuous load.

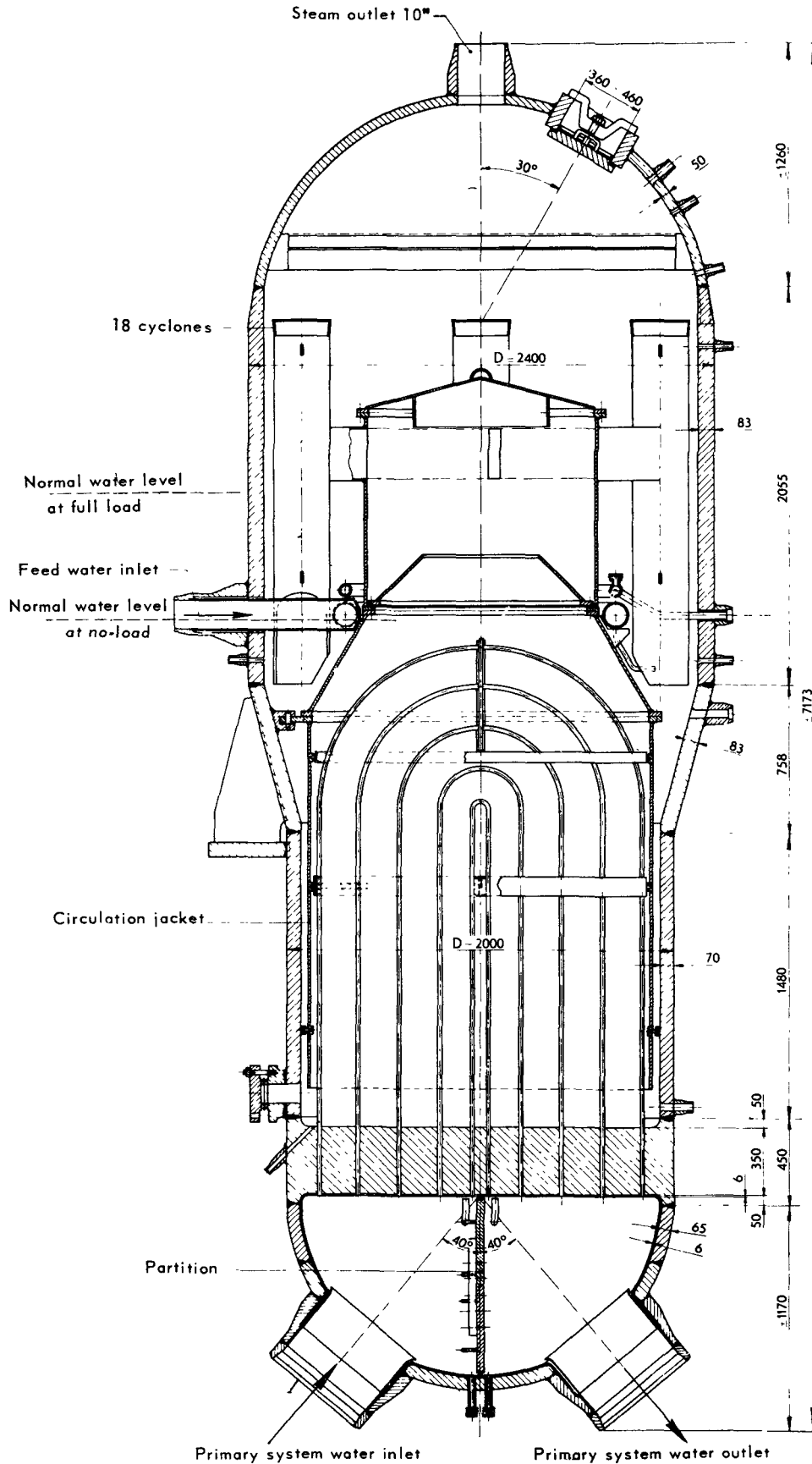


Figure 1. General arrangement of secondary steam generator for SENN

Secondary steam temperature*: 242 °C,
Secondary steam flow*: 109 t/hr,
Feed water temperature: 190 °C.

Figure 1 shows a general arrangement of the steam generator.

Materials used. Vessel: steel plates ASTM-A-302 grade B (max C content 0.20%). Tube plates and nozzles over 6" dia forged from ASTM-A-336-58T grade F1. Tubes: Monel to ASTM-B-163 stress-relieved. Surfaces in contact with primary water were clad by hand welding with Inco 140 Monel electrodes in three layers with a 200 °C preheat. Water partition plate and transition rings: stainless steel ASTM-A-182-59T grade F304. Test requirements for materials were to ASTM standards supplemented by special requirements such as 100% ultrasonic tests for all plates, forgings and tubes. For the tube plate forgings more extensive impact tests were required in order to establish the transition temperature.

Calculations

The calculations which had to be carried out were concerned with heat transfer and strength of the construction.

Heat transfer

In calculating the required heat-transfer surface use was made of the well-known Colburn formula for the heat transfer of water to tubes and of a number of boiling correlations, including those of Rohsenow and Forster and Zuber. In these calculations a fouling factor of 0.0035 h ft² °F/Btu was used. In addition calculations were carried out to ascertain the circulation ratio in the steam generator. From this circulation ratio and the slip ratio, i.e., the ratio of steam velocity to water velocity in the steam/water mixture in the boiling section, follows the water content of the steam generator during operation. This water content is of importance in connection with the dynamic behaviour of the steam generators. Moreover, these data can be used as a basis to calculate the fluctuation of the water level with sudden load fluctuations. The steam generators will in the first instance have to absorb the load fluctuations of the turbine. As carry-over of water by the steam to the turbine must in any case be avoided (guaranteed moisture content in steam 0.1% max), the cyclones have a great length so that they are capable of handling fairly strong level fluctuations. The steam generators were simulated on an analogue computer to study their dynamic behaviour under transient conditions.

Strength calculations [2]

As the applicable codes do not contain any formulae for the calculation of thick perforated plates, we have based our calculations in this respect on a formula proposed by Miller but in a somewhat modified form. The object of the static stress calculation carried out is to prevent relatively considerable quantities of the material exhibiting plastic deformation under working

conditions. This could very well be the case if the designs were to be based exclusively on the code rules, e.g., in the case of structural discontinuities (connection between tube plate and shell, of nozzles on the shell, etc.). In this stress analysis, allowance had to be made for external forces and moments, such as can occur with nozzles. It was made a condition that the stresses thus calculated, exclusive of the stress concentrations, should not be higher than 90% of the yield point of the material at the working temperature. In addition to this stress analysis under static conditions a dynamic stress analysis was made for this component. It is known that materials are susceptible to fatigue and that with a certain number of oscillations, dependent on the amplitude of the load fluctuations, the material collapses. These stress variations occur with load fluctuations, changes in temperatures and pressures and when starting up or shutting down the installation. The stress can be calculated as a function of time at critical points during a transient, for which calculation the results of the above-mentioned analogue computer study are essential. In the case of these stresses the thermal stresses, as well as the stress concentrations, play a very important part. When the stresses are determined it is possible to ascertain with the aid of fatigue diagrams whether the installation can safely withstand the specified number of load fluctuations during the life of the installation. These calculations are very time-consuming. It was shown that the generators can withstand the specified transient conditions.

Manufacturing and quality control

General

Design and manufacture comply with ASME standards Section VIII, 1959, and the qualification of welders and the making and testing of test welds have taken place in accordance with the specification of ASME Section IX, Welding Qualifications. As these codes do not provide the relevant directions, test standards have been drawn up by the principal and the manufacturer in mutual consultation and are largely based on American practice. The general supervision and inspection of welding operations was in the hands of Lloyd's Register of Shipping. Also design and manufacture had to meet the specifications of the ANCC (Associazione Nazionale per il Controllo della Combustione). The generators were divided in several parts so that they could be manufactured in the boiler shop. Further assembly including the making of the first layers of the closing welds, which are the upper and lower circumferential welds, took place in a clean shop. These were finished by an automatic welding machine and stress-relieved by means of induction heating. Interesting features of manufacture are described in the following paragraphs.

Cladding with Monel

When overlaying Monel alloy on carbon steel it is essential that the iron content of the overlay be kept as low as possible to avoid cracking and decrease in

* At max continuous load.

the corrosion resistance of the cladding. In an investigation conducted in our own laboratories, into the welding process best suited for the job we began by manual arc welding without a barrier layer, which is sometimes recommended. When it was found to yield satisfactory results it was adopted. The welding technique used was particularly aimed at reducing penetration to a minimum and this was achieved by using thick electrodes, 5 mm diameter; by welding with the smallest possible current, 140 A; by welding with a relatively low rate of travel, the arc being chiefly directed towards the pool and the bead already deposited; and by adopting a minimum preheat temperature, 200 °C, of the steel to be overlaid. Inspection tests adopted from US Navy standards for austenitic stainless steel overlays were applied. Upon approval of the Procedure Qualification Test, the tube sheets were overlaid and stress-relieved. The top layer was then machined bright and the surface inspected for cracks or other flaws by the liquid absorption method. Apart from a few gas inclusions, no flaws were found. The adhesion of the Monel on the steel substratum was ultrasonically tested and found to be satisfactory.

Tube to tube-plate connection

The two steam generators each contain 1785 hairpin-type Monel tubes of 3/4", each of which had to be welded to the Monel clad tube plate. The tubes were rolled into the tube plate after welding. In this case, too, the ASME code gives no information on quality standards. It was attempted to make a joint free from cracks, gas inclusions or lack of fusion and with sufficient strength and a smooth transition from the weld to the tube and tube sheet, so as to reduce the resistance of the incoming primary system water to a minimum. A smooth transition without narrowed passage is also required in order to allow the tube expander to be easily introduced into the tube after welding. Furthermore, a minimum leak path of 75% of the thickness of the tube wall was required. The welding machine used consists of a water-cooled argon-arc torch that can rotate around a central pivot. With this apparatus the time cycle of the torch is adjustable from 3 seconds upwards. A great number of variables can influence the results of this welding process and many experiments were carried out to study the influence of the following factors:

- Protective gas: argon + 15% hydrogen,
- Electrode: 0.095 in. (2.4 mm) diam thorium oxide tungsten electrode,
- Arc length: 0.03 in. (0.8 mm) between tip of electrode and tube plate,
- Protruding tube length: 0.098 in. (2.5 mm) above tube plate surface,
- Tracking diameter of electrode: 0.8 in. (20.4 mm),
- Starting point: lowest point,
- Rolling tube before welding: no rolling, not even over a short length for fixing only, was allowed.

The main test procedure for checking the quality of experimental welds consisted of the systematic

preparation of cross sections for macroscopic and microscopic examination. To get an idea of the strength of the welded joint before expansion, the tubes were pushed out of the tube sheet under thrust. The forces recorded were of the order of 6 tons. Some non-expanded tube joints were pressure tested with water to 1 000 atm and in these tests no leakage was found. Calculated pressure required for tearing off the tubes was over 2 000 atm. A repair procedure was established for joints that would fail, for whatever reason, during the actual welding to the tube sheet. Defective joints were removed by a special milling machine and rewelded by hand by the argon-arc process using a filler metal.

Inspection. Initially, test specimens were welded by each shift immediately before making the actual welds on the tube sheet and these were tested as described. When, after some ten shifts, the results proved to be good without exception, this check was abandoned. The joints were visually inspected at the end of each working day, where necessary, with a $\times 7$ magnifying glass and, for detail, with a $\times 25$ glass.

The tube rolling process. After welding, the tubes were rolled into the tube plate over the total thickness 350 mm of the plate. Although the weld had sufficient strength to carry the load, rolling was necessary to obtain a good heat transfer between tube and tube plate and to prevent the formation of a crevice between tube and plate that would give rise to crevice corrosion of the tube sheet material. It was postulated that the rolling fit should be such as to require a force 150% that of design pressure to push the tube out of the tube hole without a welded joint. Elliot Company protractive expanding equipment was selected. One reason for the selection of protractive expanding was that the tube extrusion occurring in the direction of the U-bend was well defined. This is important because the clearance between tubes at the top of the tube bundle is of the same magnitude as the extrusion of the tube.

Testing

The secondary shell was pressure tested to 5 atm with air and the tube to tube-plate connections checked for tightness by a soap bubble test. Several leaky connections were found, all of which occurred in hand-welded joints. These were repaired and rechecked. A further test was applied by filling the secondary shell with freon-12 at 2 atm and scanning the tube plate with a halogen detector. Ten more faulty connections were found this way. Out of 7 140 joints, 42 faulty ones, or 0.6% were repaired. A final hydraulic pressure test at 138 atm was carried out.

Welding the transition pieces

The transition pieces between the steel nozzles and the austenitic stainless steel pipes of the primary water system were welded with Inconel welding electrode 182, whereupon the ferritic material and the weld were overlaid on the inside with Monel. Inconel alloy was

preferred to stainless steel because it is less susceptible to iron absorption, less subject to hot cracking and has no tendency to carbon migration and sigma phase formation. A preheat temperature of 200 °C was used. The weld was stress-relieved for 2 hours at 625 °C. Although the stress-relieving effect of annealing is doubtful with such a combination of materials, this treatment was carried out to reduce the hardness of the ferritic nozzles in the transition zone. As a quality test, the joints were X-rayed, tested by ultrasonics and the inner and outer surfaces were checked by the liquid absorption test.

CORE STRUCTURES FOR SENN AND KRB-POWER STATIONS

Material and heat treatment

Figure 2 gives an idea of the dimensions and the intricate construction of the SENN core structure. With structures that support reactor cores and especially structures that have to maintain a very accurate position of the fuel elements in the reactor core, very high dimensional accuracy is required. Usually these structures are made out of stainless steel, at the moment preferably of the ASTM type 304. In cases where machining with high precision must be carried out (for instance ± 0.1 mm on 1 500 mm pitch) it is necessary to aim at a condition of minimum internal stresses (for instance welding stresses) of the

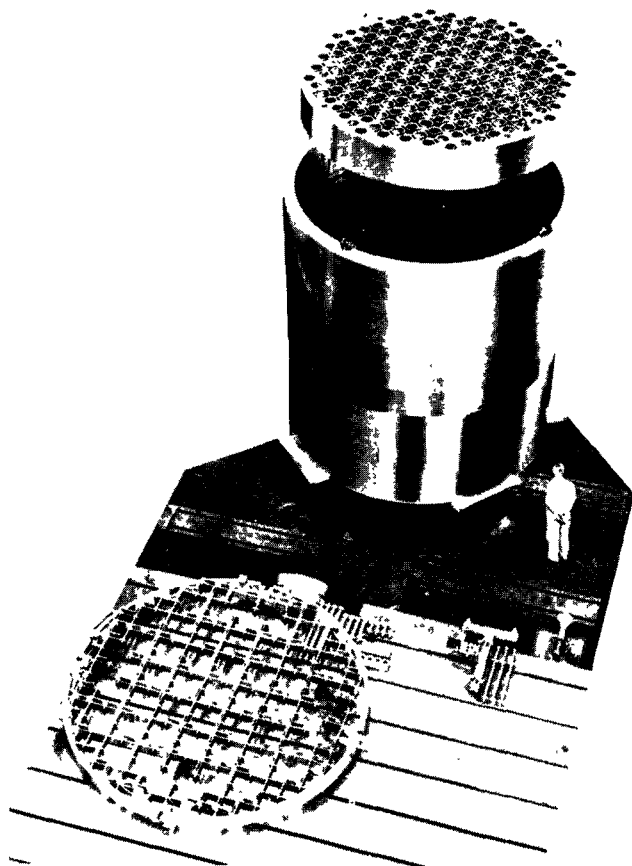


Figure 2. Core structure for SENN

structure. Using normal working practice this condition is difficult to accomplish with stainless steel type 304. The best heat treatment, from the point of view of corrosion, consists of quenching in water from 1 100 °C. In this case however it is almost inevitable that stresses remain in the structure due to non-uniform cooling. With a stress relief at 500–550 °C, which is acceptable from the point of view of inter-crystalline corrosion, only limited stress relaxation occurs even by prolonged annealing. This is the reason why we apply a heat treatment that will sound strange for people accustomed to manufacture in stainless steel. We anneal at 725 °C with maximum heating and cooling speeds of 50 °C/h, the reason being that with annealing at 725–750 °C it is possible to remove about 90% of all internal stresses, while the structure has still sufficient strength to maintain its form. Chromium carbides will indeed be formed along the grain boundaries but, if this is limited by a modest carbon content, it is not these carbides which will cause the corrosion but the dechroming on the grain boundaries. However at 725 °C chromium diffusion takes place over the whole grain, for which reason the effect is limited. This heat treatment has been successfully applied.

Optical measurements

In the case of a core plate of say 3 000 mm diam, where a tolerance of ± 0.1 mm on the co-ordinates of the position of the holes for the fuel elements has to be measured, we are faced with a dimensional control problem of the first order. The problem is in fact the measurement of deviations to a reference system of two perpendicular lines with an accuracy that is a fraction of the allowed tolerance, in this case about ± 0.01 mm. It is our opinion that this kind of dimensional quality control cannot be performed by purely mechanical means. We used an optical method, Fig. 3. The measuring procedure is carried out in this case with an adjustable telescope that could be moved by means of an autocollimator aimed at a mirror connected to it in such a way that the telescope axis remains parallel to it. The telescope is adjusted along a linear measuring machine over the fixed nominal pitch distances by means of measuring block gauges that must make electrical contact. By placing an optical target on the points to be measured the deviation of each measuring point could be read by adjusting the telescope. By means of optical prisms and two optical targets the telescope can be re-located with the linear measuring machine in such a way that measurements can also be made in the second co-ordinate direction. In this way it proved possible to measure in a plane of 6×6 m with very high accuracy. It is also possible to measure deflection in the direction of the third co-ordinate by means of test loading.

Cost saving effects

Both the chosen dimensional tolerances and the choice of the material have a great influence on the cost price of the core structure. During the past years it has been possible to compare costs of two reactor

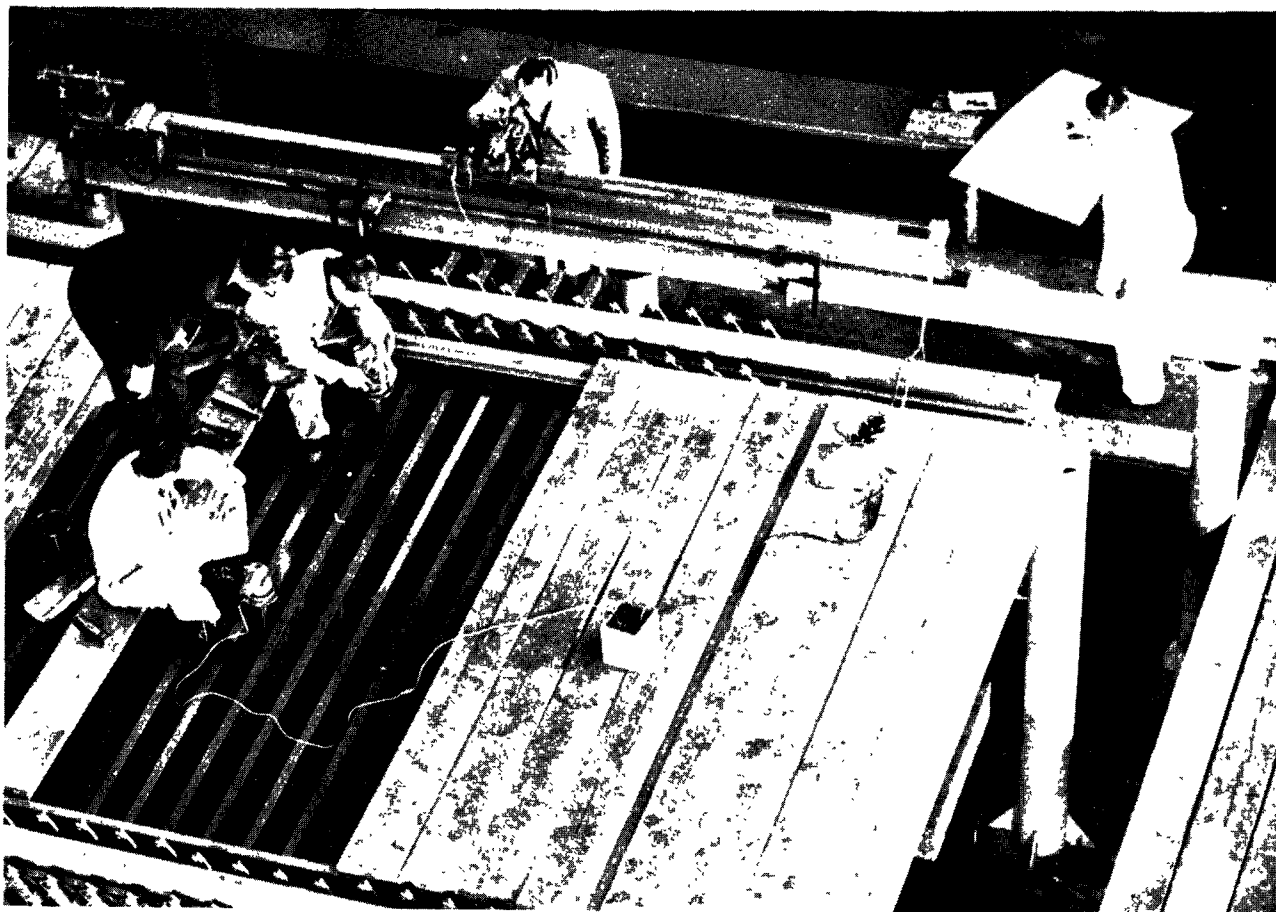


Figure 3. Optical measuring set-up

core structures for the same reactor type and about the same power. For both structures the same material was required, that is to say stainless steel, type 304. By changing the design of the second core structure in view of the manufacturing experiences on the first core structure and also by allowing greater tolerances in many places it proved possible to decrease the manufacturing cost per kilogram of the finished article by about 25%. A further reduction in manufacturing price can be achieved by using the so-called ferritic stainless steels, for instance ASTM type 405 with $11\frac{1}{2}$ – $14\frac{1}{2}$ % chromium. This material is 20% lower in price than type 304, and also machining can be done faster and to a better standard. A further advantage compared to 304 apparent not only in the design but also during manufacture is that ferritic stainless steel has about the same coefficient of thermal expansion as carbon steel. The greater precautions necessary during welding (preheating is required) are in our opinion less important than the mentioned advantages.

REACTOR PRESSURE VESSEL FOR SEP POWER STATION

Description

The SEP power station will use a direct-cycle boiling-water reactor of General Electric design. The

pressure vessel is still in the design stage. The following data are provisional:

- Design pressure: 90 atm (g).
- Design temperature: 350°C ,
- Inner diameter: 2 800 mm.
- Total height: 11 000 mm.
- Wall thickness to ASME code III: 80 mm.
- Total weight: about 100 tons.

Materials

The material that is applied in most cases at the moment for pressure vessels for water reactors, with a wall thickness of over 75 mm, is ASTM-A-302, grade B. In our opinion the 302 B material shows two manufacturing problems. In the first place the weldability is limited due to crack sensitivity which is caused by the high allowed carbon content ($<0.25\%$). In the second place there is a rather high sensitivity for temper-embrittlement which shows itself during the stress-relief annealing operation required after welding. For reactor pressure vessels with very thick walls the total duration of stress-relief annealing can be rather long, especially as the heating and cooling speeds must be limited. In order to avoid these problems a material is proposed known as I.2 MD07, developed by Société des Forges et Ateliers du Creusot. By decreasing the carbon content to 0.18% maximum and 0.16% nominal this is a steel with a

low transition temperature and an improved weldability. By decreasing the carbon content however the strength properties of the steel are influenced; to improve this 0.5% nickel is added, resulting in a yield stress that is the same as for the 302B material. The tensile stress is 6% lower. This however is of less importance when the modern American or European codes are used for calculating the wall thickness of the reactor vessel. The carbon equivalent, an often-used measure for the weldability of steel, calculated according to Cottrell and Bradstreet [3], is 0.311 for 1.2 MD07 steel as against 0.33 for A302-B, and 0.393 for modified A336. The sensitivity for temper-embrittlement of the 1.2 MD07 steel is limited mainly by limiting the molybdenum and manganese content to the lower regions of the 302B specification and by decreasing the phosphor content [4]. Forging tests have shown that for rings with a wall thickness of 300 mm and a total duration of stress-relief of 20 hours at 625 °C, transition temperatures for the Charpy-V test specimen with 5 kgm/cm² at -30 °C can be obtained for tangential test specimens at a quarter of the wall thickness. See Table 1 for the

Table 1. Reactor pressure vessel materials

Quality	ASTM A 302B	ASTM A 336MoD	1.2 MD07
C	<0.25	<0.27	<0.18
Mn	1.15-1.50	0.50-0.80	1.0-1.5
Cr.	-	0.25-0.45	<0.2
Ni.	-	0.50-0.90	0.3-0.7
Mo	0.45-0.60	0.55-0.70	0.35-0.55
Tensile strength	56.3	56.3	52.5 kg/mm ²
Yield stress 20 °C	35	35	35 kg/mm ²
Yield stress 350 °C	28	28	28 kg/mm ²
Allowable stress ASME III	18.7	18.7	17.5 kg/mm ²

comparison of the mentioned reactor pressure vessel steels. Radiation tests with the 1.2 MD07 steel have given results comparable with those found for A302-B steel [6]. The 1.2 MD07 steel that can be worked up as forgings and as plates has also been used for the reactor vessel, the pressurizer and the primary pipelines for the Ardennes power station at Chooz.

The application of forged rings

It is notable that in Europe, and in contrast to the US, a tendency exists to not only forged flanges but also forged rings to form the vessel body for the pressure vessels of water reactors. Often the bottoms and heads are also constructed of one or more forged pieces. Examples are the vessels for the SENN station, the Ardennes station and the KRB station. At the present time, the same procedure is being considered for the pressure vessel of the SEP power station. We consider this method of construction to be the best one technologically for items which are so costly as reactor pressure vessels. We think we can

claim a more perfect working method. We want to show this by the following points:

(a) In the first place during forging the inner part of the forging block is removed. This part of the bloom solidifies last during casting, and thus contains most of the flaws. The result is that, especially when vacuum cast ingots are used, forged rings give a very homogeneous material.

(b) In the second place because only circumferential welds are used the total length of welds is decreased appreciably. A figure of at least 40% is mentioned [5]. As the welding process does not need to be interrupted, circumferential welds are automatically welded more easily than longitudinal welds. Moreover the deformation due to welding stresses is decreased by the higher rigidity of cylindrical rings. If it is specified, as is usually done, that welds may not be segmental, one has a greater degree of freedom in the design, viz., in the positioning of nozzles. As the behaviour of the weld and the heat-affected zone under radiation is to a great extent an unknown factor, the possibility of positioning the welds in such a way so that they are outside the highest radiation intensity is an advantage.

(c) As forgings have to be completely machined after heat treatment a high dimensional accuracy of the vessel can be obtained. The out-of-roundness will be practically nil and the matching of weld preparations is very good.

(d) It may be considered that one disadvantage is that the use of stainless steel cladding on rolled plate is not possible. We do not think this is a disadvantage with steels of the manganese molybdenum type, as described above, that have to be heat treated. It is very difficult, not to say impossible, to carry out a heat treatment that gives good results both in the base material and the stainless steel cladding. We think better results are obtainable by the method of welding on clads, which can of course also be done on vessels made out of plate material.

Pressure vessel codes

We are now in a position where pressure vessels are being offered for power stations in different countries. Usually calculations are required not only according to the codes ruling in the country of the reactor designer, but also to codes ruling in the country where the reactor will be operated. In the case of a marine reactor the requirements of the insurance classification offices also play an important role. In the first place, not all countries have rules for nuclear pressure vessels, thus lengthy discussions with the authorities concerned are required to establish a set of rules. In the second place, where one has to design a vessel to more than one code, conflicting requirements have to be discussed between the authorities concerned. The conventional codes ruling in most cases do not give sufficient information on the design requirements of nuclear vessels, so additional, provisional rules are given or calculation methods have to be agreed upon and much detailed analysis is asked for. All this is very time-consuming and delays the preparing of

construction drawings. This is a disadvantage as the times of delivery for nuclear components are usually rather short. In the view of this philosophy we think it is advantageous to aim at a unified code for reactor vessels. This code should not only contain the calculation methods but also the allowable stresses in different materials and the requirements of quality control on materials and fabrication. If a code should exist which is internationally valid and used by all authorities, we are of the opinion that a growing understanding will show what manufacture and design of nuclear components really means. Much confusion in the earlier design stages would be prevented. We consider the new ASME code, Section III for Nuclear Vessels, a very good basis for such an international code. Another money-saving method of working would be that test and inspection documents issued by an authorized inspection body would be accepted by other authorities concerned. It has happened that authorities of one country would not accept the documents of the authorities of a qualified and neutral inspection body, so that even such simple tests as the tensile tests had to be repeated. Much travelling would be eliminated when an agreement

could be made such that the official bodies charged with the inspection in a country could accept inspection documents reciprocally from inspection bodies having the same authority in other countries. The two mentioned factors have price-decreasing influence and will result in shorter delivery times.

REFERENCES

1. Rickover, H. G., *Quality the Never-ending Challenge*, 44th Annual National Metal Congress (29 October 1962), Nucl. Eng., 8, No. 81 (1963).
2. *Tentative Structural Design Basis for Reactor Pressure Vessels and Directly Associated Components for Pressurized Water Cooled Systems*, Bureau of Ships (December 1958).
3. Cottrell, C. L. M., and Bradstreet, B. J., *British Welding Journal*, 34, 305 (June 1955).
4. Martin P. F. *et al.*, *Etude de la fragilisation d'aciers soudables au manganèse-molybdène au cours des revenus de détente après soudage*, Revue de métallurgie (octobre 1962).
5. Bartocci, A., and Marianeschi, E., *Forged components for the nuclear reactor pressure vessel at the SENN power station, Italy*, Proc. of a symposium on steels for reactor pressure circuits, The Iron and Steel Institute (1961).
6. Skreppe, H. *et al.*, *The Norwegian-Dutch Steel Irradiation Programme*, R.C.N. report 26 (1964).

ABSTRACT—RÉSUMÉ—АННОТАЦИЯ—RESUMEN

A/728 Pays-Bas

Expérience acquise dans l'étude, le calcul et la fabrication de composants pour réacteurs nucléaires

par K. J. de Jong *et al.*

Le groupe Neratoom s'est occupé, ou s'occupe, de quatre composants principaux pour réacteurs de puissance.

Le mémoire décrit des composants étudiés par la General Electric des Etats-Unis pour les centrales nucléaires SENN, KRB et SEP, qui sont du type à eau bouillante.

Sur la base des spécifications de fonctionnement, on a fait l'analyse des contraintes et les calculs de transmission de chaleur pour mettre au point les générateurs de vapeur secondaires destinés à la centrale SENN.

Un travail analogue sera fait pour la cuve du réacteur de la centrale nucléaire SEP de 50 MW(e).

Les supports des éléments combustibles pour la centrale nucléaire SENN ont été construits, et ceux pour la centrale KRB le seront d'après les plans de construction fournis par le client.

Le mémoire signale les calculs détaillés décrivant le comportement dynamique des générateurs de vapeur SENN.

On décrit les exigences rigoureuses en matière de construction et de contrôle et la façon dont elles ont été respectées. Elles concernent les procédés de soudage, les essais et le contrôle des soudures, la détection de criques et les contrôles d'étanchéité.

Les méthodes appliquées en vue de réaliser la précision dimensionnelle élevée exigée dans les spécifications des supports des éléments combustibles sont aussi décrites.

En ce qui concerne les cuves de réacteur, on discute l'influence des règlements en vigueur dans divers pays concernant les cuves sous pression. Etant donné que les exigences pour le calcul et le contrôle ne sont parfois pas suffisamment définies, des désaccords peuvent en résulter. Les auteurs sont d'avis qu'il faut s'efforcer d'élaborer un code internationalement accepté pour le calcul des contraintes et les exigences en matière de contrôle.

En outre, les deux méthodes de construction des cuves de réacteur, à savoir l'utilisation de pièces cylindriques forgées et celle de plaques laminées et cintrées à chaud, sont discutées.

A/728 Нидерланды

Опыт проектирования, расчета и изготовления энергетических узлов реакторов

К. Я. Де Ионг *et al.*

Фирма «Нератом групп» занимается четырьмя основными узлами энергетических реакторов.

В данном докладе описываются узлы для атомных электростанций SENN, KRB и SEP с

книжками реакторами, спроектированными американской фирмой «Дженерал электрик».

На основе рабочих спецификаций были проведены анализ напряжений и расчеты теплопередачи и разработана конструкция парогенераторов вторичного контура для реактора SENN.

Аналогичные работы будут выполнены для реакторного корпуса под давлением для электростанции SEP электрической мощностью 50 Мвт.

Активные зоны для реакторов SENN и KRB будут изготовлены в соответствии с чертежами, представленными заказчиком.

В докладе приводятся подробные расчеты, касающиеся динамического поведения парогенераторов реактора SENN.

Описываются также жесткие требования, предъявляемые к изготовлению и контролю, и пути их выполнения; освещаются следующие вопросы: сварка, испытание и контроль сварных швов, испытание на наличие трещин и на утечку.

Дается описание методов, используемых для достижения высокой точности соблюдения размеров, требуемой в соответствии со спецификацией для конструкции активной зоны.

Что касается реакторных корпусов под давлением, то в докладе описано значение кодовых программ для расчета корпусов под давлением, применяемых в различных странах. Поскольку требования к расчетам и контролю иногда недостаточно определены, это может служить источником расхождений. По мнению авторов, разумно было бы принять международную кодовую программу для расчета напряжения и определить требования к контролю.

Кроме того, рассматриваются два метода изготовления реакторных корпусов под давлением, а именно использование кованных колец и прокатанных и изогнутых плит.

Experiencia adquirida en el diseño, el cálculo y la fabricación de elementos para reactores de potencia

por K. J. de Jong et al.

El Grupo Neratoom se dedica a la fabricación de cuatro tipos principales de elementos para reactores de potencia.

En la memoria se describen los elementos destinados a las centrales nucleo-eléctricas SENN, KRB y SEP, del tipo agua hirviendo, proyectadas por la General Electric de los Estados Unidos. Sobre la base de las especificaciones pertinentes, se han efectuado los análisis de esfuerzos y los cálculos de transmisión de calor y se ha realizado el diseño de los generadores de vapor del circuito secundario de la central SENN.

Un trabajo análogo se efectuará para el recipiente de presión del reactor de la central SEP, cuya potencia es de 50 MW(e). Se ha construido la estructura del núcleo de la central SENN y se construirá la de la central KRB, en ambos casos con arreglo a los respectivos planos facilitados por el cliente.

En la memoria se da cuenta de los extensos cálculos que describen el comportamiento dinámico de los generadores de vapor de la central SENN. Se indican las estrictas normas de fabricación y control aplicadas y la manera en que se han satisfecho. Se examinan las siguientes cuestiones: métodos de soldadura, ensayo y control de soldadura, ensayos para la detección de grietas y escapes. Se describen los métodos utilizados para alcanzar la elevada precisión dimensional requerida en las especificaciones de las estructuras del núcleo.

En lo que respecta a los recipientes de presión, se examina la influencia de las reglamentaciones sobre dichos recipientes vigentes en diferentes países. Como las prescripciones relativas al cálculo y control carecen a veces de precisión, suelen surgir discrepancias.

Los autores estiman conveniente que se procure preparar una reglamentación internacionalmente aceptada en materia de cálculo de esfuerzos y exigencias del control. Se examinan asimismo los dos métodos posibles de fabricación de recipientes de presión para reactores, a saber, el empleo de anillos forjados y el de planchas laminadas y curvadas.

Apport de la réalisation d'une grande centrale nucléaire dans la conception et la construction des équipements pour réacteurs

par P. Klees et C. Gérard *

La réalisation d'une centrale nucléaire impose actuellement à l'industrie manufacturière de franchir une étape significative dans le raffinement des procédés de fabrication. Elle permet aux constructeurs d'accroître leur expérience tant sur le plan de la conception des systèmes et des équipements que sur celui de leur exécution.

Le présent mémoire a pour objet d'illustrer ce gain d'expérience par quelques exemples rencontrés au cours de la construction de la centrale nucléaire des Ardennes.

ELÉMENTS CARACTÉRISTIQUES DE LA CONCEPTION DES SYSTÈMES ET ÉQUIPEMENTS

Caractéristiques fonctionnelles de la centrale considérée

Ces caractéristiques se classent en deux catégories selon qu'elles résultent du fait qu'il s'agit d'une installation nucléaire ou des conditions propres à la centrale des Ardennes. Elles ont toutes une influence directe sur la conception des systèmes et la spécification des équipements.

Dans la première catégorie nous rangeons notamment:

a) La disponibilité importante de l'usine (garantie de 6 000 h/an pendant la première année) nécessaire à réaliser compte tenu du rapport élevé entre les frais fixes et les frais proportionnels;

b) Le confinement des équipements nucléaires dans le but d'empêcher la dispersion non contrôlée de substances radioactives aussi bien en exploitation normale que lors d'un incident.

Dans la seconde catégorie, il faut retenir:

a) L'implantation « mixte » de l'usine, dont la salle des machines est construite sur une plateforme en rive droite de la Meuse et dont les installations nucléaires sont aménagées dans deux cavernes creusées à 100 m à l'intérieur de la colline et distantes de 25 m entre elles;

b) La possibilité d'accroître la puissance thermique fournie par le réacteur, au fur et à mesure de l'instal-

lation des cœurs successifs. Bien que la puissance électrique nette garantie soit de 242 MW(e), les équipements de la partie classique ainsi que les échangeurs de chaleur et les pompes primaires de circulation ont été conçus et réalisés sur la base d'une puissance de 10% supérieure à la puissance nominale garantie, soit 266 MW(e);

c) L'emploi d'un poison chimique (H_3BO_3) dilué dans le modérateur comme agent contrôleur du flux neutronique, en vue de réduire les facteurs de pointe et d'augmenter la densité moyenne de puissance du cœur.

Aspects particuliers de la conception des systèmes

Systèmes auxiliaires

Nous décrivons dans ce paragraphe quelques solutions adoptées dans le cas de la centrale des Ardennes pour la conception des systèmes en vue de respecter les caractéristiques fonctionnelles énoncées ci-dessus:

Maîtrise de la corrosion

La corrosion est maîtrisée dans les systèmes primaire et auxiliaires par: a) l'emploi généralisé pour le circuit primaire et ses auxiliaires d'aciers inoxydables austénitiques du type 18/8 sans stabilisant; b) un traitement chimique de l'eau primaire réduisant le taux des différentes formes de corrosion, assurant la filtrabilité maximale aux produits de la corrosion résiduelle et limitant leur dépôt sur les parois des circuits et sur les surfaces d'échange de chaleur.

Il est nécessaire de tenir compte des réactions nucléaires (n, γ), (n, p) ainsi que de la libération des produits de fission, des réactions radiochimiques entre les constituants du fluide primaire et de l'effet des radiations sur l'incrustation des produits de corrosion. En conclusion, il est apparu que les prescriptions ci-après devaient être suivies pour l'eau de refroidissement du circuit primaire:

Résistivité	déterminés par les quantités de poison chimique et d'inhibiteur de corrosion présentes
pH à 25 °C	
Concentration d'oxygène	< 0,1 ppm

* Ateliers de constructions électriques de Charleroi, Division nucléaire.

Concentration de chlorures	< 0,1 ppm
Concentration de fluorures	< 0,1 ppm
Concentration d'hydrogène	25 – 35 cm ³ (TPN)/kg H ₂ O
Salinité totale	< 0,5 ppm (additions exclues)
Inhibiteur de corrosion	3 ppm de LiOH (2 ppm en Li)

Ces prescriptions sont réalisées par :

a) Un rinçage des circuits à l'eau déminéralisée avant le premier démarrage;

b) L'emploi d'eau déminéralisée de grande pureté pour le remplissage initial et pour l'appoint :

Résistivité (Ω cm)	> 1 000 000
pH à 25 °C	voisin de 7
Concentration d'oxygène	< 0,1 ppm
Concentration de chlorures	< 0,1 ppm
Concentration de fluorures	< 0,1 ppm
Salinité totale	< 0,5 ppm
Concentration d'anhydride carbonique	< 0,2 ppm

c) L'élimination de l'oxygène dissous dans l'eau par réduction à l'aide d'hydrazine (10–20 ppm) pendant les démarrages et par recombinaison avec de l'hydrogène maintenu en léger excès (2–3 ppm) pendant la marche en puissance. De plus l'hydrogène réagit avec l'azote présent dans l'eau de remplissage ou d'appoint pour former de l'ammoniac et empêcher la formation d'acide nitrique;

d) La marche à un pH supérieur au pH neutre, ce qui réduit le salissement des surfaces des éléments de combustible et augmente la filtrabilité des produits de corrosion en suspension dans l'eau;

e) Le contrôle du pH se fait au cours de la purification de l'eau primaire par dérivation d'une fraction de son débit à travers un échangeur d'ions à lit basique de résines cationiques et anioniques de la forme Li⁺ OH⁻. L'addition de LiOH n'est nécessaire qu'après une importante dilution du fluide de refroidissement primaire;

f) L'acide borique, utilisé comme poison chimique, est soumis à des prescriptions analogues à tout autre élément d'addition, en particulier ses teneurs maximales admissibles en chlorures et en fluorures ont été fixées à 4 ppm. Il présente en outre les qualités d'être parfaitement soluble et de ne pas provoquer de corrosion des aciers utilisés.

Le contrôle de la variation de concentration du poison soluble dans l'eau primaire en relation avec l'exploitation du cœur

Ce contrôle est réalisé par :

a) L'injection de H₃BO₃ concentré, à 12% en poids de bore, dans le système primaire au moyen d'une pompe doseuse et d'une pompe d'appoint. La concentration maximale prévue actuellement est de 3 190 ppm de bore, lors d'un arrêt à froid avec le premier cœur;

b) Le retrait du bore par dilution jusqu'à un seuil de concentration fixé à 260 ppm de bore et au moyen

d'un échangeur d'ions à résines anioniques fortement basiques et du type régénérable, dimensionné pour le retrait de 9 kg de bore avant que la régénération ne soit nécessaire, en-dessous du seuil fixé. Le réchauffage des tuyauteries et équipements véhiculant ou contenant des solutions concentrées d'acide borique est assuré par des câbles électriques installés sous l'isolation thermique. Il évite la précipitation du bore. Dans le cas présent, on a préféré un système électrique à un réchauffage par de la vapeur, après examen comparatif de la souplesse, de la sécurité et de l'économie des deux solutions.

La manipulation de charges et de fluides radioactifs

Les assemblages de combustible sont transférés de la piscine du réacteur à la piscine de désactivation et vice versa par un dispositif maintenant l'étanchéité entre les deux piscines et constitué d'un tube dans lequel circule un piston libre.

Le tube de transfert, d'un diamètre intérieur de 406 mm, repose horizontalement à l'intérieur d'une galerie de 25 m de long, creusée dans le roc entre les deux cavernes. Son isolement est réalisé par deux vannes à guillotine du type méplat, commandées par moteur électrique. Le piston libre est réalisé sous la forme d'un chariot contenant un panier qui en fin de course dans l'une ou l'autre des piscines peut basculer en position verticale et recevoir les assemblages de combustible ainsi que les différentes charges à transférer. Le circuit hydraulique qui actionne le piston libre comprend une pompe de circulation commandée par un moteur électrique et se ferme par les piscines et le tube de transfert.

Les circuits véhiculant un fluide radioactif sont conçus de manière à respecter le taux de fuite admis pour le fluide transporté. Les fuites admises pour les circuits primaire et auxiliaires vers l'atmosphère de la caverne du réacteur correspondent à la vaporisation de 1 200 g d'eau primaire par heure et celles des circuits auxiliaires vers l'atmosphère de la caverne des auxiliaires à la vaporisation de 300 g/h. Ces fuites se produisent essentiellement aux bourrages des tiges de commande des vannes. Les vannes à service radioactif dont le diamètre est supérieur ou égal à 2,5 pouces (63,5 mm) sont équipées d'une connexion de reprise des fuites évacuant celles-ci vers un réservoir de drainage. La répartition judicieuse des anneaux de bourrage avant et après l'anneau lanterne de reprise des fuites permet d'assurer le serrage adéquat des bourrages et limite les fuites à la fois vers le réservoir de drainage et vers l'atmosphère.

La conception des joints à bourrages des tiges de commande des pistons des pompes d'appoint permet d'espérer qu'après 2 000 heures de fonctionnement la fuite sera limitée à environ 50 l/j par pompe en régime.

La complète sécurité de fonctionnement et la haute disponibilité des systèmes

Celles-ci sont assurées par une combinaison judicieuse entre la duplication des équipements

vitaux les plus sollicités et l'interconnexion des systèmes en vue de leur interchangeabilité pour remplir une même fonction. Nous citerons : le doublement des pompes d'appoint et des pompes d'injection de sécurité ainsi que l'installation de trois pompes de réfrigération auxiliaire, chacune de ces dernières étant calculée pour la moitié du débit nominal du système.

Contrôle et instrumentation

Notre objectif est de montrer dans ce paragraphe comment sont résolus des problèmes importants d'alimentation et de contrôle spécifiquement liés à la sécurité de fonctionnement de la centrale.

Conception d'une source sûre d'alimentation en énergie électrique

Deux réseaux distincts aboutissent au site de Chooz; leurs tensions respectives sont de 220 kV et 63 kV. Il a été demandé au constructeur de la centrale de tenir compte de la disparition simultanée des deux réseaux. Cette exigence a entraîné la scission du réseau 5,5 kV en deux parties distinctes MA et MB (fig. 1). En marche normale, le jeu de barres MA est alimenté par TS, et MB est alimenté par TD1; TD2 est en réserve et peut être substitué soit à TS, soit à TD1 en cas de défaillance de ceux-ci.

Une raison propre au fonctionnement du réacteur a nécessité l'introduction du troisième jeu de barres MC à 5,5 kV. En cas de défaillance générale de l'alimentation électrique, il est obligatoire d'assurer pendant au moins une minute le fonctionnement de deux des pompes primaires. Cela est réalisé en connectant ces pompes au jeu de barres MC, normalement alimenté par l'alternateur auxiliaire AA. Ce dernier, lors d'un incident sur le réseau, continue à tourner pendant plusieurs minutes par suite de l'inertie importante du groupe turbo-alternateur.

Pour le démarrage, les deux pompes PP1 et PP2 sont branchées sur MB. Chaque transformateur de démarrage alimente les jeux de barres MA ou MB, jusqu'à ce que l'alternateur soit excité et en mesure de fournir au transformateur de soutirage TS la puissance requise par MA. Dès que l'alternateur auxiliaire est prêt, les deux pompes PP1 et PP2 sont successivement branchées sur MC.

En cas de défaut sur l'un des jeux de barres MA ou MB, les jeux 380 V normaux extérieurs (MF et MG) et normaux cavernes (MK, ML) peuvent être connectés automatiquement sur le réseau 5,5 kV restant en fonctionnement.

En cas de défaillance simultanée ou indépendante de MA et de MB, il est nécessaire d'alimenter les jeux de barres secours, tant à l'extérieur qu'en cavité. Cela est réalisé à l'aide de trois groupes diesels de secours. On admet qu'un groupe est en révision et qu'un groupe refuse de démarrer. Le troisième groupe est à lui seul capable d'alimenter les auxiliaires vitaux nécessaires pour assurer l'arrêt de la centrale en toute sécurité.

Il est à remarquer que les pompes d'injection de sécurité (IS1, 2 et 3), dont il est question au para-

graphe suivant, sont raccordées aux jeux de barres secours.

Analyse et prévention des accidents d'origine nucléaire

Le rôle du système d'injection de sécurité est de refroidir le cœur du réacteur avec de l'eau boriquée, en vue d'éviter la fusion des gainages à la suite d'une rupture importante dans le circuit primaire. La conception de ce système repose sur un ensemble de conditions de base dont les principales sont détaillées ci-dessous:

a) La brèche la plus importante à considérer avec une probabilité non négligeable est celle correspondant à la rupture complète d'une tuyauterie de 8 pouces (20,3 mm);

b) Dans ce cas, la température maximale admise pour le gainage des éléments combustibles est égale à 1 100 °C. Une faible fraction des gainages, évaluée à 5 - 10%, peut éventuellement être trouée, ce qui est à considérer comme un accident tolérable;

c) Pour des ruptures de dimensions plus réduites, le calcul montre que la possibilité de dommages aux gaines diminue fortement;

d) La rupture franche d'une tuyauterie de 24 pouces (610 mm) du circuit primaire se présentant avec une probabilité extrêmement faible, on peut lui associer une limite de température moins stricte (fusion des gainages) se situant à 1 400 °C;

e) Dans l'hypothèse d'une vidange complète de la cuve du réacteur, l'élévation de température des gainages cesse dès que l'eau de remplissage atteint la partie inférieure du cœur.

Il a été tenu compte en outre de certaines conditions propres à la centrale des Ardennes: a) le réservoir d'eau boriquée étant situé sur la colline englobant la caverne du réacteur, on dispose d'une hauteur géométrique de 213 m; b) on dispose du débit de 3,8 l/s en provenance des pompes d'appoint du réacteur; c) du fait de la présence des quatre connexions d'injection d'eau boriquée (une par boucle primaire), le débit net déversé dans la cuve du réacteur vaut les 3/4 du débit total des pompes d'injection; et d) l'effet de gravité et la puissance de pompage sont utilisables avec des délais respectifs de 10 et 20 secondes après l'accident.

L'analyse effectuée avec le code SOCO a montré que l'injection forcée de 95 l/s, face à une contre-pression de 105 kg/cm² dans le système primaire, protège efficacement le cœur. L'entrée en action du système est automatique, et déclenchée par la baisse coïncidente du niveau d'eau dans le pressuriseur et de la pression dans le réacteur. Le pilote peut aussi démarrer le système manuellement ou opérer le transfert sur contrôle manuel après un démarrage automatique.

Respect des marges de sécurité imposées par l'étude du cœur

Certaines valeurs maximales des paramètres du cœur sont basées sur les propriétés physiques des

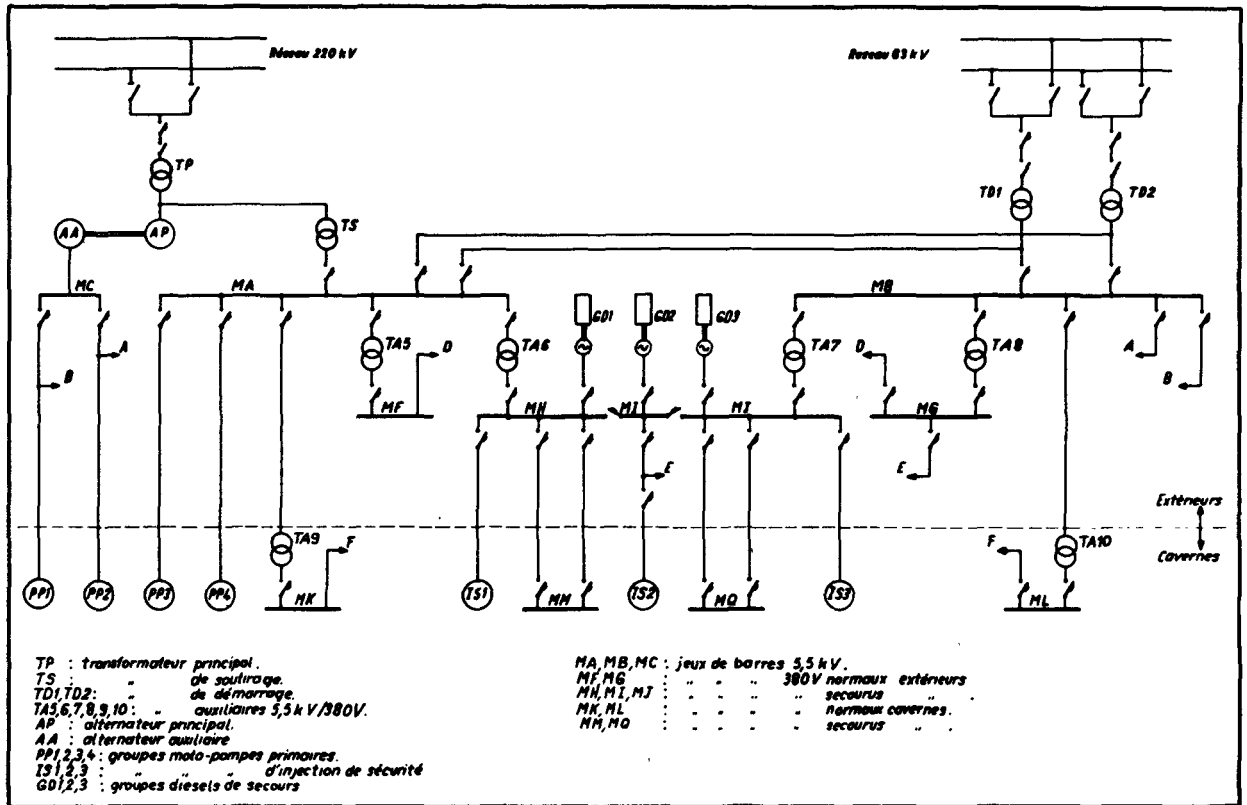


Figure 1. Centrale des Ardennes. Schéma unifilaire de principe

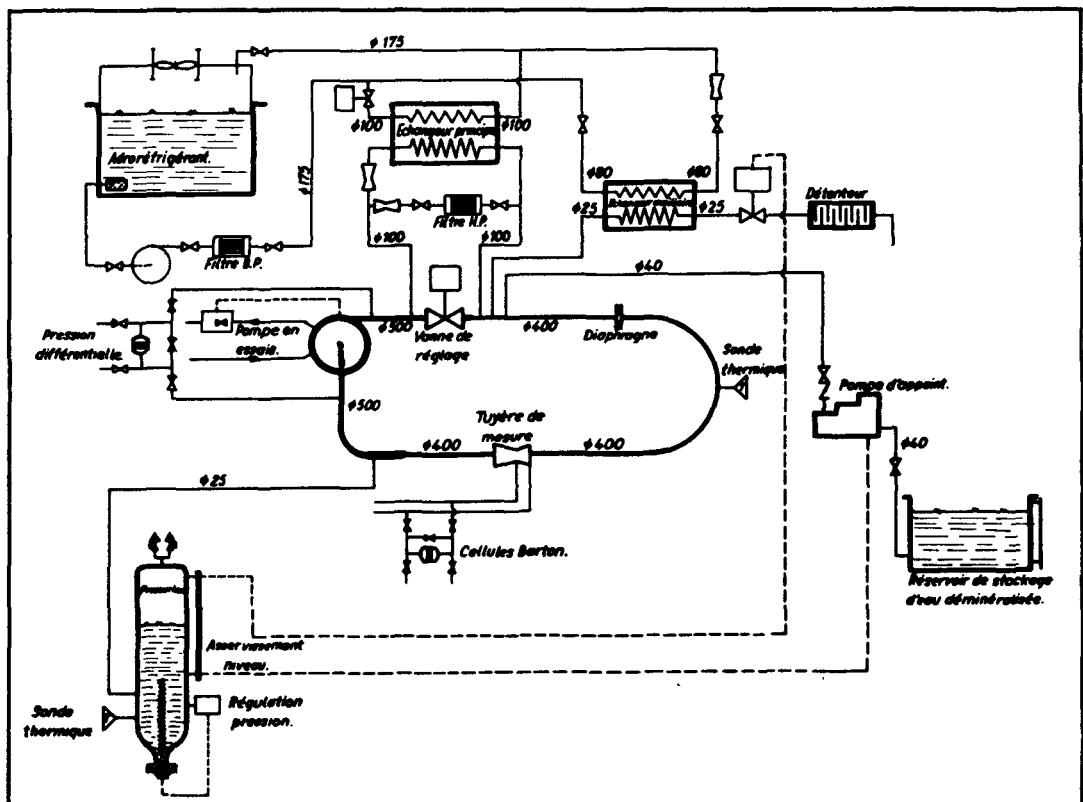


Figure 2. Centrale des Ardennes. Schéma de principe de la boucle d'essais des pompes à HP et HT

matériaux utilisés. Le point de fusion du combustible et le dépassement de l'ébullition nucléée (DEN ou DNB en langue anglaise) constituent deux de ces limites.

Les techniques de calcul disponibles actuellement permettent de déterminer la distribution de puissance et d'analyser les conditions de fonctionnement dans les canaux où le débit calorifique est maximal. Néanmoins, des *mesures* périodiques de la répartition spatiale du flux neutronique et du flux calorifique permettraient de recalculer à tout moment de la vie du cœur les facteurs de pointe et le rapport DEN, ainsi que le facteur global de redistribution du débit entre les différents canaux. Il en résulterait une vérification, beaucoup plus sûre que par calcul seul, des marges de sécurité imposées au départ.

Le système de mesures dans le cœur consiste en 45 thermocouples et 33 tubes à billes. Chacun de ces tubes est situé en lieu et place d'un barreau combustible et est relié à un système d'air comprimé situé en dehors de la cuve du réacteur. Il est ainsi possible d'envoyer et de retirer en différents points du réacteur une colonne de billes d'acier dont l'activation est ensuite mesurée pour dresser la carte du flux.

Philosophie d'isolement de l'enveloppe étanche

Le constructeur a proposé d'adopter la philosophie définie par le projet de norme ASA [1] en notant que: a) le cas d'une rupture simultanée à l'intérieur et à l'extérieur de l'enveloppe d'une tuyauterie pénétrant dans celle-ci n'est pas à envisager puisqu'il est équivalent à la rupture de l'enveloppe elle-même; b) les circuits, à l'exception de ceux de ventilation, pénétrant dans la cavité du réacteur sont éprouvés à une pression d'essai supérieure à celle qui existerait dans la cavité en cas d'accident majeur (3,75 kg/cm² eff.) et font donc partie intégrante de l'enveloppe de sécurité lorsqu'ils forment une boucle fermée à l'extérieur; c) les parois constituant cette enveloppe peuvent, en cas d'accident, être contaminées sur leur face intérieure, et des procédures opératoires évitant tout danger en tout temps sont prévues pour le fonctionnement d'équipements pouvant être ainsi contaminés; d) les circuits pénétrant dans l'enveloppe comportent les catégories suivantes:

- a) Tuyauteries véhiculant des fluides radioactifs;
- b) Tuyauteries transportant des fluides non radioactifs à l'abri d'une rupture, lors d'un accident dans la cavité, par leur disposition ou leur épaisseur de paroi (circuits de vapeur et d'eau alimentaire);
- c) Tuyauteries véhiculant des fluides non radioactifs, susceptibles de subir une rupture provoquée par un accident dans l'enveloppe;
- d) Gaines de ventilation.

Les solutions ci-dessous répondant au projet ASA ont été proposées suivant la catégorie de tuyauteries envisagées:

- a) Addition d'une vanne d'isolement ou d'un clapet dans la tuyauterie, à l'intérieur de la cavité du réacteur, lorsqu'une rupture à l'extérieur de l'enveloppe

risque de provoquer une libération de substances contaminées;

- b) Pas de vannes supplémentaires d'isolement;
- c) Addition d'une vanne d'isolement à l'extérieur de la cavité;
- d) Installation à l'extérieur de l'enveloppe d'une vanne à fermeture rapide, de l'ordre de 3 à 5 secondes.

Il a été demandé au constructeur de prévoir des vannes d'isolement supplémentaires pour éviter la contamination de portions de circuits situés dans la cavité des auxiliaires. Il en résulte l'installation de plusieurs vannes surabondantes.

Codes et normes

Le choix judicieux des codes de calcul peut conduire à des simplifications appréciables. Nous citerons le cas de la cuve du réacteur dont les épaisseurs ont été calculées d'après le principe du document [2] dit *Navy code*.

Il importe de veiller à ce que les normes dimensionnelles spécifiées soient en usage dans la pratique commerciale courante.

Dans le cas de la centrale des Ardennes, on a spécifié pour les circuits véhiculant des fluides radioactifs ou pouvant en véhiculer accidentellement les normes dimensionnelles ASA, et dans les autres cas les normes AFNOR.

Matériaux

En ce qui concerne les matériaux employés dans les centrales à eau, nous renvoyons à la référence [3].

Pour la centrale des Ardennes, on a utilisé les matériaux suivants:

Gainage du combustible	AISI 304
Cuve	
Corps, couvercle et tubulures	ACIER SFAC 1,2 MO7
Revêtement interne	acier équivalent à l'AISI 304
Échangeur de chaleur	
Corps	Soudotenax 52
Plaque tubulaire	Soudotenax 52
Tubes	AISI 316

ASPECTS CARACTÉRISTIQUES DE LA CONSTRUCTION DES ÉQUIPEMENTS

Les constructeurs de la centrale des Ardennes ont acquis une expérience technologique particulière en matière de : soudage et placage par la construction des équipements primaires; chromage par la réalisation de certaines pièces des mécanismes de commande des barres; forgeage dans l'exécution de la cuve du réacteur; réalisation de faible tolérance de fabrication dans les pièces internes de la cuve; traitements thermiques dans l'élaboration des principales pièces des équipements primaires.

Nous insisterons sur la fabrication spécialement délicate de deux de ces équipements:

Les pièces internes du réacteur qui ont comme fonction de localiser et supporter les assemblages combustibles, de guider les barres de contrôle et, enfin, de

répartir le débit dans la cuve du réacteur. Les plus importants problèmes de réalisation portent sur les plaques supérieure et inférieure de support et de maintien du cœur ainsi que sur l'enveloppe du cœur. Les tolérances sur les entre-axes des trous de logement des assemblages dans les plaques par rapport aux axes de celles-ci sont extrêmement serrées: de l'ordre de quelques centièmes de mm. Il en va de même pour la tolérance sur la perpendicularité des axes des plaques, qui est de l'ordre de quelques centièmes de mm/m.

Il est essentiel de se rendre pratiquement indépendant des facteurs énumérés ci-dessous, qui sont d'autant plus importants que les plaques sont grandes et très découpées (200 trous):

i) Erreur de positionnement de la broche de l'aléuseuse;

ii) Différence de coefficient de dilatation entre l'acier au carbone de la machine et l'acier inoxydable de la pièce; soit environ $6 \mu / ^\circ \text{C m}$ (l'importance de ce coefficient est telle qu'une variation simultanée de 1°C de la température de la pièce et de la machine provoque un effet appréciable);

iii) Ecart de température entre la pièce et la machine.

Dans ce but, il fut décidé de fabriquer sur une machine à pointer de grande précision (de l'ordre du micron) un gabarit de forage reproduisant les trous d'axes des plaques ainsi que les axes des trous à y aléser.

En outre, il fut jugé plus précis et plus commode d'utiliser ce gabarit comme étalon et comme moyen de contrôle plutôt que des broches micrométriques placées entre des tampons logés dans les alésages.

Les mécanismes de commande des barres de contrôle, qui sont du type à encliquetage magnétique à trois bobines. Les plus importants problèmes de réalisation ont porté sur :

a) L'usinage de la tige de commande, longue de 5,50 m et présentant des cannelures dans lesquelles s'engagent les cliquets assurant le mouvement de la barre. Il a fallu, pour réaliser ces pièces aux tolérances sévères imposées, transformer provisoirement un tour d'atelier de grande précision et de 3 m d'entrepointes;

b) La soudure des enveloppes sous pression à visser sur le couvercle de la cuve du réacteur. Ces enveloppes, réalisées en acier inoxydable AISI 405, comportent trois cordons de soudure en acier AISI 307 constituant les entrefers pour les trois bobines de commande. L'épaisseur de paroi étant de l'ordre de 35 mm, le volume du métal d'apport est conséquent et des précautions particulières doivent être prises pour éviter les inclusions dans la soudure. La difficulté a été résolue en grande partie grâce à un entraînement intensif des soudeurs.

Par ailleurs, des spécifications extrêmement sévères ont été rédigées pour tous les équipements, primaires et auxiliaires. Nous estimons qu'à l'instar de ce qui s'applique pour la construction des centrales classiques, il y a lieu d'établir une « jurisprudence » en matière

d'application de ces spécifications. Cela est indispensable pour permettre la compétitivité de l'énergie nucléaire. Il est possible selon nous d'apporter, sans toucher au fond de ces spécifications, les simplifications principales ci-après:

a) L'inspection en usine pour toutes les pièces effectuée par les organismes de contrôle étrangers aux constructeurs devrait être limitée à un contrôle par sondage, étant admis que les certificats et rapports d'essais seraient établis par le constructeur dans tous les cas où ils sont nécessaires;

b) Les essais de réception des différentes catégories de matériel doivent pouvoir être exécutés dans les installations permanentes des constructeurs et dans les mêmes conditions que dans le cas de matériel classique;

c) La propreté nucléaire devrait être considérée comme obtenue lorsque seront respectées les procédures de nettoyage spécifiées plutôt que des critères d'inspection du type « gant blanc » dont la définition est entièrement subjective.

INSTALLATIONS D'ESSAIS SPÉCIFIQUES AUX ÉQUIPEMENTS DE CENTRALE NUCLÉAIRE

En vue d'assurer la fourniture des principaux équipements avec une garantie totale, il est nécessaire de disposer d'installations d'essais spécifiques, dont les principales sont citées ci-dessous.

Stand d'essais des pompes primaires (voir fig. 2)

Les caractéristiques hydrauliques et thermiques des groupes essayés peuvent atteindre les valeurs suivantes:

Débit maximal:	7 000 m ³ /h
Pression maximale à l'aspiration:	170 kg/cm ²
Pression différentielle maximale:	10 kg/cm ²
Température maximale:	300 °C
Puissance électrique disponible, à tension et fréquence variables:	2 500 kVA

Installation d'essais pour la robinetterie à haute pression

Pression maximale:	170 kg/cm ²
Température maximale:	320 °C
Pression différentielle:	de 0 à 170 kg/cm ²

Station d'essais pour mécanismes des barres de contrôle, barres de contrôle et éléments combustibles

Un autoclave de 12 m de hauteur et 325 mm de diamètre intérieur est prévu pour l'essai de ces équipements à des température et pression de 260 °C et 154 kg/cm². Un débit réglable de 0 à 250 m³/h simule la circulation du réfrigérant dans le cœur.

Les références [4-6] donnent une description complète de ces installations, qu'il n'est pas possible d'insérer dans le cadre de ce mémoire.

ÉVOLUTION FUTURE DE LA CONCEPTION DES SYSTÈMES ET DES ÉQUIPEMENTS À LA SUITE DE L'AMÉLIORATION DES PARAMÈTRES DES CENTRALES À EAU

Dès à présent, l'état d'avancement des études et de la construction permet de formuler une série d'améliorations pour les centrales futures, sans vouloir prétendre fournir une liste exhaustive.

Amélioration des facteurs de pointe

Habituellement, les facteurs de pointe sont décomposés en une série de sous-facteurs nucléaires et techniques. La méthode de combinaison de ces sous-facteurs par simple produit est très conservative, car elle revient en fait à considérer que toutes les conditions les plus défavorables se produisent en un même point. Une méthode plus réaliste consiste à combiner ces sous-facteurs par une méthode statistique. Si ce procédé est applicable sans trop de difficultés aux sous-facteurs issus des tolérances de fabrication, qui se caractérisent par une distribution connue, il est par contre beaucoup plus difficile de l'appliquer aux sous-facteurs nucléaires.

Augmentation du débit de réfrigération

Cette augmentation permet d'accroître la température moyenne du réfrigérant, pour des conditions données à la sortie du canal critique. Elle accroît également le coefficient de sécurité relatif à l'élévation d'enthalpie et au flux de chaleur provoquant le DEN.

C'est ainsi que le débit total passerait de 5 900 m³/h pour une centrale de 266 MW(e) net à 14 500 m³/h pour 500 MW(e) net.

Ebullition

Le troisième moyen permettant d'accroître la température moyenne du réacteur consiste à admettre une certaine ébullition dans le cœur. Un premier pas en ce sens a été franchi en admettant l'ébullition locale dans le cœur, puis l'ébullition massive à la sortie du canal critique, mais en régime transitoire uniquement. La tendance future sera d'admettre un faible pourcentage d'ébullition à la sortie du canal critique en régime permanent.

Cyclage du combustible

L'introduction dans la centrale des Ardennes d'un noyau à trois régions a permis un gain appréciable vers l'uniformité de la distribution de puissance. Toutefois ce gain se détériore au fur et à mesure de l'accroissement des dimensions physiques du noyau, les trois régions ayant tendance à vivre indépendamment l'une de l'autre. Pour les grands cœurs, un potentiel d'amélioration important réside en une méthode combinant les éléments frais et usés selon une loi déterminée. Tout le problème consiste à définir l'optimum parmi toutes les combinaisons possibles.

Exploitation industrielle des résultats obtenus par l'instrumentation interne du cœur

Jusqu'à présent, le programme moyen d'action des barres de réglage est déterminé à l'avance par calcul pour un cycle d'irradiation.

A partir des renseignements fournis par l'instrumentation interne du cœur, il est possible de connaître à intervalles rapprochés la carte du flux et d'arriver à la modéliser en vue d'une utilisation optimale du combustible. Cette méthode nécessite l'emploi d'un système de traitement des informations et d'un calculateur digital chargé de réviser périodiquement le programme de contrôle.

Simplification des systèmes auxiliaires

Cette simplification doit se concevoir dans l'optique suivante:

a) Suppression des vannes primaires dont la présence est ignorée dans le calcul du système de protection;

b) Remplacement du système de purification par des filtres en dérivation sur le système primaire;

c) Remplacement du système de transfert du combustible décrit ci-avant par l'utilisation d'une seule machine de chargement pour la manutention du combustible dans le réacteur et dans la piscine de désactivation;

d) Application d'une philosophie d'isolement de l'enceinte étanche basée sur le projet de l'ASA [1];

e) Conception des systèmes auxiliaires, et en particulier la ventilation, le traitement des déchets et la protection biologique, sur la base d'un taux de libération de produits de fission conforme à la réalité, compte tenu d'un facteur de sécurité raisonnable (10 au lieu de 500).

Normalisation des équipements primaires

Les boucles primaires sont actuellement standardisées et conçues pour le transfert de 425 MW(th).

CONCLUSIONS

L'exposé ci-dessus a montré jusqu'à quel point a été poussé dans la centrale des Ardennes le souci de la protection des installations, aussi bien en fonctionnement normal qu'en cas d'accident. Ce souci, couplé dans beaucoup de cas à la nouveauté des fabrications, a entraîné comme conséquence: le choix dans les calculs de marges de sécurité très conservatives; l'installation d'équipements surabondants dans certains systèmes; l'utilisation de critères de réception exceptionnellement sévères.

Cette situation, qui pouvait se justifier dans le cas de la construction d'une première centrale, doit faire place progressivement à des règles se rapprochant davantage de la bonne pratique industrielle, spécialement en ce qui concerne la fixation des marges de sécurité, laquelle doit tenir compte de la qualité des équipements. Cette condition, jointe à l'expérience technologique acquise par le constructeur, aux améliorations et simplifications envisagées, doit

normalement conduire les centrales nucléaires à une situation économique favorable pour autant qu'une expansion suffisante du volume des fabrications permette aux constructeurs l'utilisation poussée des moyens mis en place.

BIBLIOGRAPHIE

1. *Proposed safety standard for design, fabrication and maintenance of steel containment structures for stationary nuclear power reactors*, document approuvé par le sous-comité ASA N6-2 et soumis à l'approbation du comité ASA N6.
2. PB 151 987 — *Tentative structural design basis for reactor pressure vessels and directly associated components*,

Superintendent of documents, U.S. Dept. of Commerce, Washington D.C.

3. Kramer, L. B., Westinghouse E. C., *Materials selection for Yankee and subsequent PWRs*, présenté au Congrès mondial de métallurgie (octobre 1962).
4. *Installation d'essais pour pompes centrifuges à haute pression*, document ACEC-FACEJ, disponible aux Ateliers de constructions électriques de Charleroi, division NR, Marcinelle, Belgique.
5. *Installation d'essais pour robinetterie à haute pression*, document ACEC, disponible comme [4].
6. *Station d'essais pour mécanismes de barres de contrôle, barres de contrôle et éléments combustibles*, document ACEC-MMN, disponible comme [4].

ABSTRACT—RÉSUMÉ—АННОТАЦИЯ—RESUMEN

A/770 Belgium

The effect of the construction of a large nuclear power plant on the design and manufacture of reactor equipment

By P. Klees and C. Gérard

The paper shows, on the basis of the experience accumulated during the construction of the Ardennes plant at Givet, the progress made by the manufacturing industry in the refinement of the fabrication procedures, and also outlines future trends.

The paper sums up the functional requirements of the plant considered, which have a direct bearing on the system design and on equipment specifications. These requirements have led to special solutions concerning:

- (a) Corrosion control;
- (b) Regulation of soluble poison concentration and of water quality in relation to core operation;
- (c) Handling and treatment of radioactive charges and fluids;
- (d) Complete operational safety and high system availability.

It shows how several control problems, related to plant operating safety, have been resolved:

- (a) Design of a reliable power supply for vital auxiliaries;
- (b) Analysis and prevention of accidents of nuclear origin;
- (c) Effect of the safety margins imposed by the core design.

The isolation and containment philosophy adopted for the Ardennes nuclear plant is commented upon and conclusions are drawn which are applicable to other plants.

On the basis of practical experience obtained by the constructors of the Ardennes plant, the paper defines new methods and procedures developed for welding and cladding, chroming, application of small fabrication tolerances, and heat treatments.

Attempts are made to define what should be the criteria and the means adopted for the control of

material and fabrication in shops, acceptance tests of the different equipment categories, and nuclear cleanliness.

Also described are the installations especially designed for the development and testing, under operating conditions, of the primary pumps and valves, the core elements, and the control rod drive mechanisms.

Part of the paper is devoted to future trends in system and equipment design, following improvements in the reactor parameters.

A/770 Бельгия

Вклад создания атомной электростанции большой мощности в проектирование и строительство оборудования для ядерных реакторов

П. Клеес, Ш. Жерар

В предлагаемом докладе на базе опыта, накопленного строителями атомной электростанции в Арденнах, в Живе, рассматриваются успехи, достигнутые промышленностью в области отработки методов изготовления, и в общих чертах излагаются дальнейшие пути развития.

В докладе кратко излагаются рабочие характеристики рассматриваемой атомной электростанции, оказывающие непосредственное влияние на проектирование систем и спецификацию оборудования. Вышеуказанные требования привели к специальным решениям, касающимся:

- а) преодоления коррозии;
- б) контроля за изменением растворимого поглопителя и за качеством воды в связи с эксплуатацией активной зоны;
- в) обращения с жидкими и твердыми радиоактивными веществами и их обработки;
- д) полной безопасности работы и высокой доступности систем.

Показано, каким образом решаются некото-

рые проблемы контроля, особенно связанные с безопасностью работы установки:

a) проектирование надежного источника электропитания;

b) анализ и предупреждение ядерных аварий;

c) соблюдение безопасных пределов, налагаемых изучением активной зоны.

Обсуждается изоляционный материал, принятый для атомной электростанции в Арденнах; приводятся положения, применимые к другим установкам.

Приводятся точные примеры, показывающие основное значение выбора кодов и норм. Это тем более является предметом обсуждения, если, как в данном случае, речь идет об объединенном предприятии разных стран.

Описан выбор материалов для основных узлов первичной установки, и объясняются причины выбора.

На основе опыта, накопленного на практике строителями атомной электростанции в Арденнах, определяются новые методы и способы, вновь разработанные или примененные в промышленном масштабе для сварки и плакировки, хромирования,ковки, осуществления небольших допусков изготовления, тепловой обработки.

Делается попытка определить критерии и средства, принимаемые для контроля за материалами и изготовлением на заводе, приемочных испытаний различных категорий материала и ядерной чистоты.

Описаны опытные установки, спроектированные специально для разработки и проверки в действительных рабочих условиях насосов и клапанов первичного контура, элементов активной зоны и приводных механизмов регулирующих стержней.

Часть доклада посвящена будущему развитию систем и оборудованию, связанному с усовершенствованием параметров атомных электростанций с водяным реактором.

В заключение рассматриваются пределы безопасности и методы изготовления, предусматриваемые вначале, и на их основе определяются приемлемые критерии для будущего промышленного строительства.

A/770 Bélgica

Aportación de la realización de una gran central de potencia a la concepción y construcción de equipo para reactores

por P. Klees y C. Gérard

La memoria muestra, tomando como base la experiencia adquirida por los constructores de la Central de las Ardenas en Givet, los progresos realiza-

dos por la industria constructora de equipo para conseguir un perfeccionamiento de los procedimientos de fabricación y da un esquema de la evolución futura.

Se resumen las características funcionales de la central considerada que tienen una influencia directa sobre la concepción de los sistemas y la especificación de los equipos. Los requisitos mencionados han conducido a soluciones especiales que se refieren:

a) Al domino de los problemas de corrosión;

b) Al control de la variación de veneno soluble y de la calidad del agua en relación con la explotación del núcleo;

c) Al manejo y tratamiento de fluidos y cargas radiactivas;

d) A la seguridad completa de funcionamiento y a la elevada disponibilidad que deben tener los sistemas.

Se muestra la forma en que se han resuelto algunos problemas de control, ligados, específicamente, a la seguridad de funcionamiento de la instalación:

a) Concepción de una fuente segura de suministro de energía eléctrica;

b) Análisis y prevención de los accidentes de origen nuclear;

c) Respeto de los márgenes de seguridad impuestos por el estudio del núcleo.

Se analizan las bases del sistema de aislamiento adoptado para la Central de las Ardenas y se obtienen conclusiones aplicables a otras instalaciones.

Se citan ejemplos concretos que demuestran la importancia fundamental que tiene la elección de códigos y normas. Esta elección está más sujeta a discusión si se trata, como en el caso presente, de una empresa común a diferentes países.

La memoria describe, para las piezas importantes del sistema primario, la elección de materiales y explica las razones que se han tenido en cuenta.

Se definen, tomando como base la experiencia práctica que han adquirido los constructores de la Central de las Ardenas, los métodos y los procedimientos nuevos que se han puesto a punto o industrializado para: la soldadura y el chapeado, el cromado, la forja, la realización de tolerancias estrechas de fabricación, y los tratamientos térmicos.

Se intenta definir lo que deberían ser los criterios y medios a adoptar para: el control de los materiales y de las fabricaciones en taller, las pruebas de recepción de las diferentes categorías de material, y la limpieza nuclear.

Se hace una descripción de las instalaciones concebidas especialmente para la puesta a punto y la comprobación, en las condiciones reales de funcionamiento, de: las bombas y válvulas primarias, los elementos del núcleo, y de los mecanismos de mando de las barras de control.

Una parte de la memoria está consagrada a la evolución futura en la concepción de los sistemas y equipos, como consecuencia de la mejora de los diferentes parámetros de las centrales de agua.

Strength problems of the flanged joint

By J. Kuchta*

NOTATION

- p : internal pressure
 σ_1 : total stress
 σ_2 : membrane stress
 $()_z$: dimensions of basic shape
 n : number of bolts
 1: stress on the external surface of wall
 2: stress on the internal surface of wall
 a: figure has value for point 1
 b: figure has value for point 3
 c: figure has value for point 4
 Other dimensions are noted on Fig. 1.

One of the main problems connected with pressure vessels of some nuclear power reactors is the successful design of the joint between the removable top dome and vessel, which is needed for exchange of internals or fuel, or some other reason. The importance of this arises especially in the case of gas-cooled power reactors, of cylindrical shape, moderated by heavy water.

The demand for maximum economy in unit cost leads the designer to increasing the output of reactors, but there are certain limits of heat, physics, strength and technological parameters in the active zone of this reactor type, which require that the achievement of higher unit output can only be done by increasing the diameter of the active zone.

Diameters of 6 000 mm for the active core are quite usual but as the diameter of the vessel increases, and taking into account the fact that the coolant is gas at a pressure of 100 kgf/cm², the requirements for reliability of the joint becomes more important. The design of flange joint must assure with sufficient safety not only the retaining of great axial forces, but also a satisfactory uniform seal against pressure during all operations. The effects of stress-concentration, of size factor, of accumulated energy, neutron flux and other factors connected with choice of material and manufacturing technology must not be neglected. The problem arises of applying some of the classical types of flanged joint or their modification to a highly stressed vessel of unusually large dimensions.

However, not all classical types of flanged joint have the same range of application for increased diameters of vessels. Every joint has some limiting parameter and its effect with increase of dimension grows steadily more expressive, till at a certain value it cannot

comply strictly with strength or technological requirements. At transition sections, where two different thicknesses of components join, i.e., at a spherical top dome and a flange, there are uniform membrane stresses and also bending stresses, which can reach especially in the median section values of considerable magnitude. For design reasons it is not possible to make this joint so smoothly to ensure that notch effect does not occur.

The possibility of decreasing the stress concentration in a local area of transition is, practically speaking, limited. However, there is still the possibility with suitable design, even with the existence of unavoidable notches of eliminating at these points the bending stress and leaving only the uniform membrane stress. In this way the value of stress concentration is usually decreased and the distribution of stress becomes sufficiently uniform.

Therefore it is necessary first to choose a type of flanged joint suitable for the vessel diameter and to accepted materials—the optimising of type, and second to make a choice in detailing the actual dimensions to eliminate bending stresses—the optimising of shape.

But shape optimisation gives no finite form of flanged joint. Its design during development suffers a series of changes, large and small, for design or technological reasons, which arise during the course of the work. Every such design change means a new optimisation.

For successful development the designer needs to gain concrete knowledge about the strength behaviour of the joint in the most important operating conditions, not only about the joint but also about its components. He needs to know, at every stage of the project, how some of the necessary changes affect the state of stress in important cross-sections, especially where unavoidable design notches exist.

The proving of the above-mentioned optimisations and some arising design changes on models would require a great deal of time and money. The whole process is done more effectively on the digital computer. In this way the designer gains a satisfactory basis for the optimum design of a joint and for evaluation of the effect of design changes during a few hours, without losing time by doing many variants of a design which are often ineffective.

It is necessary to note that the calculating methods have some inaccuracies and that they cannot include

* Skoda Works, Pilsen.

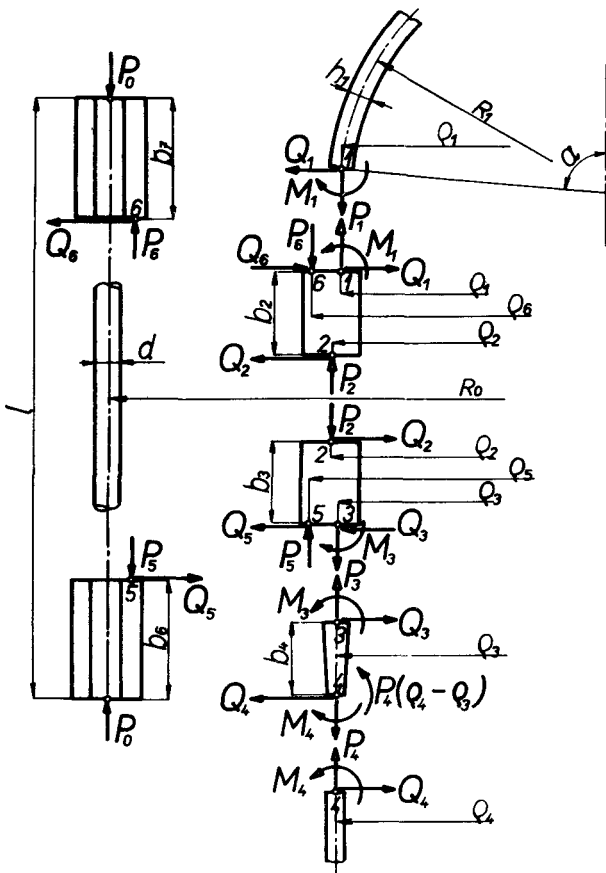


Figure 1

applied to three types of flanged joint, as shown in Fig. 2:

- (a) Loose type flanges;
- (b) Integral type flanges with bolts;
- (c) Integral type flanges with studs.

These have been analysed for a vessel with a mean diameter of approximately 6 000 mm, with an internal pressure of about 70 kgf/cm² and with a temperature difference in the joint reaching 50° C. Usually in these calculations the so-called method of forces is used. Its principle is that the whole joint is sectioned into separate axially symmetric sections for which in the theory of strength of materials more or less accurate expressions for radial deformation, cross-sectional torque and distribution of stress exist.

A simple calculation scheme for a joint with loose flanges indicating the required forces and dimensions is shown in Fig. 1. At the sections shown, the unknown shear forces and bending moments are included and the deformations are determined partly from these and partly from other external forces; pressure, gasket force, temperature differences, weight, etc.

From the condition of continuity of deformations in the sections a system of linear algebraical equations is obtained. Its left hand side expresses the elasticity dependence of the joint, its right side the action of all the external effects. The calculated values of unknown forces, moments and other effects are substituted into the equations for stress, eventually for deformations of separate parts. The more perfect the determination of external effects and the more exact the formulae used, the less the calculated values will differ from reality.

The material of the vessel was chosen in order to allow the membrane circumferential stress in the smooth part, $\sigma_t = 1\,500$ kgf/cm², and membrane stress in the unweakened part of the spherical top dome $\sigma_m = \sigma_t = 500$ kgf/cm² on condition that the largest used thickness of sheet cannot exceed 500 mm. It was also necessary to assume that the sealing force equals 50 per cent of the total force acting on the top dome in the operation.

The first type optimisation for the given parameters of vessel and material has indicated that no applied type of joint with integral flanges fulfilled the strength and technological requirements, and that it was impossible to use them in the design of the vessel.

Only the loose flange joint has fulfilled all conditions and has indicated that it is ready for subsequent shape optimisation. Let us look closer at both optimisation processes. Their preparation consists in the rationalization of general strength calculations for the type of joint which can be considered for application.

The final results are equations for longitudinal and circumferential stresses on the internal and external surfaces of the wall at flanges, bolts—and at all points where a high state of stress can be expected. The equations for the most important deformations of separate parts of the joint have all been determined.

This task as well as the programming of the general calculation on the digital computer, does not take much

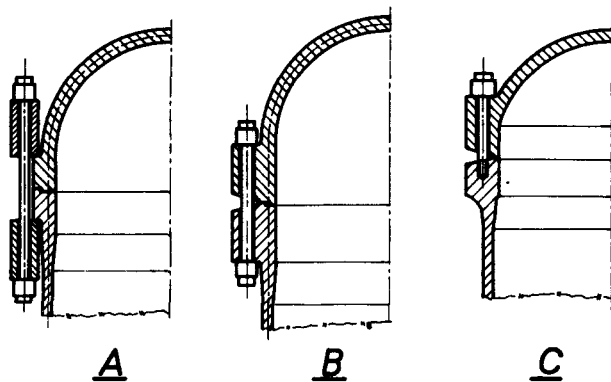


Figure 2. Types of flanged joints

some details and small changes. For comparison of various shapes their accuracy is adequate. The chosen shape is verified on the model and according to the results of measurements the relevant modifications and additions to calculated data are introduced. Such a method for the preparation of the design means a saving of time and expense. In this case it has been

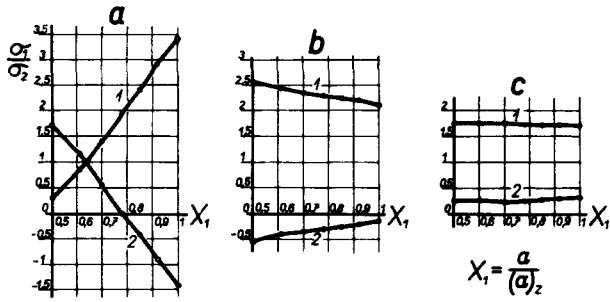


Figure 3. Variation of R_1, h_1, α simultaneously valid are:

$$\frac{R_1}{h_1} = \frac{2\sigma_{\text{membrane}}}{p} = \text{const}; R_1 \sin \alpha = \rho_1 = \text{const}.$$

$$X_1 = \frac{a}{(a)_z}$$

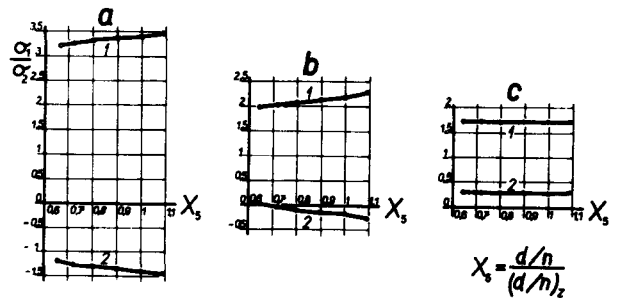


Figure 7. Variation of d, n

$$X_5 = \frac{d/n}{(d/n)_z}$$

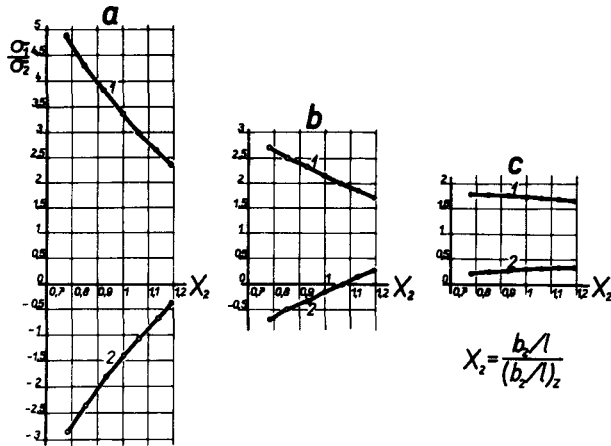


Figure 4. Variation of b_3, l

$$X_2 = \frac{b_3/l}{(b_3/l)_z}$$

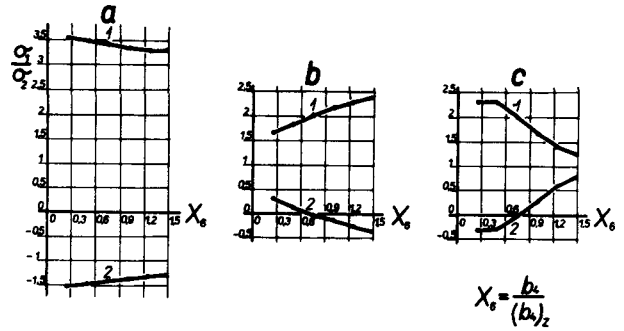


Figure 8. Variation of b_4

$$X_6 = \frac{b_4}{(b_4)_z}$$

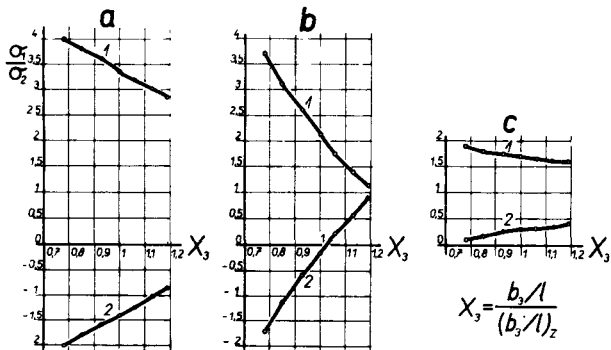


Figure 5. Variation of b_3, l

$$X_3 = \frac{b_3/l}{(b_3/l)_z}$$

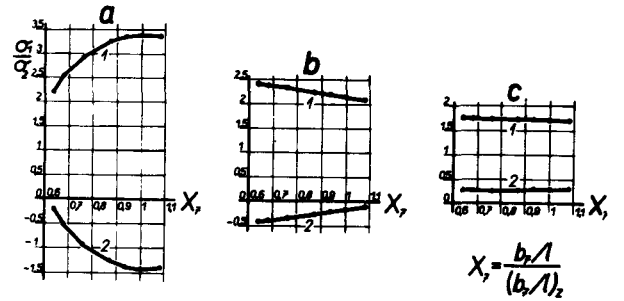


Figure 9. Variation of b_7, l

$$X_7 = \frac{b_7/l}{(b_7/l)_z}$$

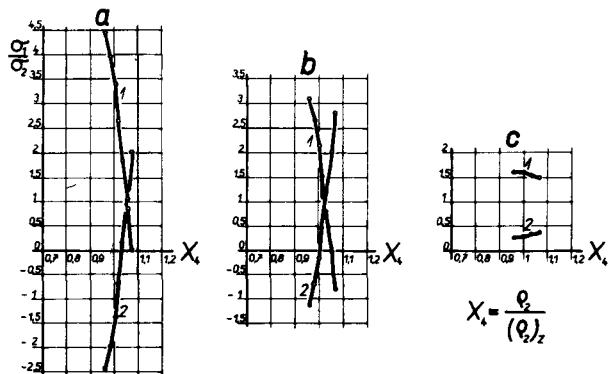


Figure 6. Variation of ρ_2

$$X_4 = \frac{\rho_2}{(\rho_2)_z}$$

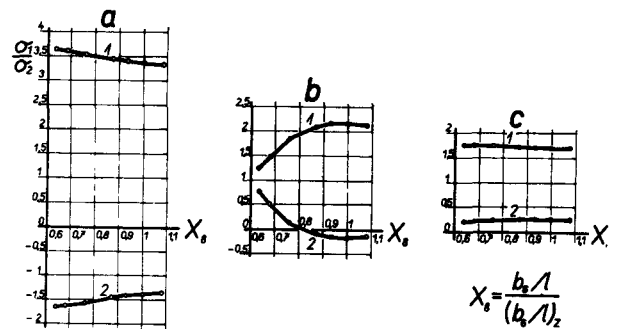


Figure 10. Variation of b_6, l

$$X_8 = \frac{b_6/l}{(b_6/l)_z}$$

time for the experienced worker when he uses various means. In the later process the designer, on the basis of design experience and technological possibilities, determines the so-called "basic shapes", one for each type of joint used in the range of parameters and dimensions of the vessel.

For the determined "basic shapes" a system of dimensional variation is made by means of the above-mentioned general calculations. This process consists in changing one dimension in such a way that its chosen difference in value in the "basic shapes" on both sides does not change the values of other dimensions.

The calculated stresses, and/or the deformations in the above-mentioned sections with a high state of stress which decide the strength reality of the design, are drawn in diagrams. The curves of changes in stress dependence on change of dimension in the most highly stressed points for every applied type of joint are obtained.

In accordance with the values of stress and on the basis of gradients of the curves, it is possible to reach a satisfactory conclusion, if some parts of the "basic shape" are oversized or if it is capable of further dimension correction without affecting the stress in another point, or if the limits of the given range of

technological possibilities and available deformations are not exceeded. In this way the unsatisfactory types of joint can be eliminated without losing time by further work on them.

The type of joint which complies with type optimisation is subjected to the shape optimisation. This task is more simple, because we know the dependence of stress on the changes of dimensions on the basis of the diagrams obtained. It has been shown that there is a sufficient number of other variants in practice to eliminate the bend and to give an adequately strong joint. It is necessary to say that for a simultaneous combination of some changes of various dimensions, the character of the curves is the same, though the gradients are slightly affected. The character of the obtained curves stays the same within a broad dimensional range about the "basic shape."

As examples, in Figs. 3 to 10 are shown some curves of the dependence of stress on changes of dimensions of a "basic shape" joint with loose flanges. For clarity the longitudinal stresses on external and internal surfaces of the wall are shown, from which the effect of dimensions on the existence of the bending stresses can be seen. This is only for points 1, 3, 4 in Fig. 1. At other tested points the same dependences have been obtained and therefore they are not shown.

ABSTRACT—RÉSUMÉ—АННОТАЦИЯ—RESUMEN

A/834 Tchécoslovaquie

Problèmes de résistance des joints à brides

par J. Kuchta

La réalisation d'un joint démontable entre le couvercle et la cuve est l'un des principaux problèmes posés par de nombreux réacteurs de puissance. L'importance d'un joint de conception sûre croît avec le diamètre de la cuve.

On est ainsi amené à adapter certains types de joints à brides classiques ou modifiées à des cuves très grandes et compliquées. Les divers types de joints classiques ne peuvent pas tous convenir à des cuves très grandes.

Il faut donc d'abord choisir le type de joint convenable (optimisation du type), puis en choisir les diverses dimensions (optimisation de la forme). De cette façon on peut choisir des formes réalisables pour les régimes de fonctionnement les plus durs, éliminer les contraintes de flexion indésirables et ne laisser que les tensions de membrane.

La réalisation d'un modèle de ces deux optimisations ne serait économique ni en temps ni en coût. Il faut donc optimiser de façon analytique en utilisant une machine à calculer. Le fabricant obtient en quelques heures les données nécessaires à la conception du joint. Pour vérifier le plan obtenu il suffit de contrôler une variable choisie.

On a analysé trois types de joints à brides pour une cuve de 6 000 mm de diamètre, sous une pression de

70 kgf/cm² environ, avec une différence de température dans le joint atteignant 50°C, avec une pression assurant l'étanchéité de l'ordre de 50% de la pression totale agissant sur le couvercle, et en postulant quelques autres conditions concernant la technologie et les matériaux.

Le joint à bords libres s'est révélé le meilleur et l'on indique pour ce type la procédure d'optimisation de la forme. Pour l'obtenir rapidement il faut disposer de courbes donnant la variation des contraintes dans les sections importantes en fonction des changements de dimensions.

On utilise l'analyse de la résistance générale du joint à bords libres en fonction des effets, que l'on étudie à l'aide d'une machine à calculer. Après avoir défini les variables de dimensions essentielles approximativement dans le domaine des paramètres de la cuve pour laquelle le joint est optimisé, on fait varier les dimensions. L'influence de ces changements de dimensions sur les contraintes dans les sections importantes est traduite en graphiques. A partir de ces courbes on peut tirer des conclusions non seulement sur les possibilités des variables dimensionnelles mais aussi sur le comportement global de la jonction.

Les renseignements obtenus permettent de réaliser les meilleures formes dans un grand domaine de paramètres de la cuve avec un petit nombre d'autres variables.

Le mémoire comprend des graphiques de courbes caractéristiques pour un joint à bords libres.

A/834 Чехословакия

Вопросы прочности фланцевого соединения

Й. Кухта

Хорошая конструкция съемного соединения крышки с корпусом реактора является одной из основных проблем для многих ядерных энергетических реакторов. Значение надежности конструкции этого соединения возрастает с увеличением диаметра корпуса.

Возникает задача применить один из классических типов фланцевых соединений или его разновидность на корпусе чрезвычайно крупного и ответственного аппарата. Различные классические типы фланцевых соединений, по-видимому, не одинаково перспективны в данном случае ввиду увеличенных размеров корпуса.

В связи с этим необходимо в первую очередь отобрать удобный тип соединения (типовая оптимизация) и затем произвести выбор размера деталей (оптимизация формы). Таким путем можно найти технологически приемлемые формы для наиболее тяжелого режима эксплуатации, исключив нежелательные напряжения изгиба и оставив лишь мембранные напряжения.

Ввиду того что с точки зрения денежных расходов и затраты времени моделирование обеих оптимизаций неэкономично, оптимальные решения находят аналитическим путем с помощью счетно-решающей машины. В результате конструктор получает необходимые данные для проектирования фланцевого соединения в течение нескольких часов. Для проверки сделанного проекта достаточно провести измерения одного избранного варианта.

Были рассмотрены три типа фланцевых соединений корпуса диаметром 6000 мм с перепадом давления 70 ат, разностью температур в соединении порядка 50°С и прижимной уплотняющей силой 50% общей нагрузки, действующей на крышку при заданных технологических условиях и конструкционных материалах.

Оптимальным оказалось соединение со свободными фланцами, для которого приводится метод оптимизации формы. Для успешного и быстрого выполнения этой задачи достаточно иметь кривые зависимости напряжения в решающих сечениях от изменений отдельных размеров.

Основой служит расчет на прочность соединения со свободными фланцами, выполненный по методу нагрузок и спроектированный для счетно-вычислительной машины. После разработки основного варианта размеров в пределах параметров корпуса, для которого оптимизируется соединение, приводится система раз-

мерных вариаций. Влияние этих размерных изменений на напряженность в решающих сечениях соединения отображено на графиках. По характеру кривых можно судить не только о возможностях основного варианта размеров, но также и о поведении узла в целом.

При помощи полученных данных можно с минимальным числом следующих вариантов добиться оптимальной формы соединения в достаточно широких границах параметров корпуса.

К докладу приложены графики с характеристическими кривыми соединения со свободными фланцами.

A/834 Checoslovaquia

Problemas de resistencia de las uniones por bridas

por J. Kuchta

La solución del problema de las uniones desmontables entre la cubierta y el recipiente del reactor es de primordial importancia en la construcción de los reactores nucleares de potencia. La importancia de la seguridad de esas uniones crece a medida que el diámetro del recipiente aumenta.

Surge el problema de la aplicación de uno de los tipos clásicos de las uniones por bridas o de sus variantes a los recipientes de dimensiones y cargas extremadamente grandes. Sin embargo, no todos los tipos clásicos de las uniones por bridas son aplicables al aumentar las dimensiones del recipiente.

En primer lugar, se debe escoger un tipo apropiado de unión (optimización del tipo) y a continuación elegir las dimensiones de los componentes (optimización de la forma): de este modo pueden encontrarse para los regímenes de trabajo más severos formas tecnológicamente adecuadas y, al mismo tiempo, evitar las indeseables tensiones en la dobladura, manteniendo sólo las tensiones de membrana.

Debido a que el estudio de las dos optimizaciones sobre modelos es antieconómico desde el punto de vista de su costo y del gasto de tiempo, se recurre a cálculos que se realizan con ayuda de máquinas calculadoras. En consecuencia, el constructor obtiene datos para el diseño de la unión por bridas al cabo de algunas horas. En caso de necesidad basta realizar medidas sobre una de las variantes elegidas.

Se han estudiado tres tipos de uniones por bridas para un recipiente de 6 000 mm de diámetro, a unos 70 kgf/cm² de presión, con diferencia de temperatura en la junta del orden de 50 °C y con el aprovechamiento para el cierre del 50 por ciento de la fuerza total que actúa sobre la cubierta en las condiciones térmicas y tecnológicas dadas.

Se ha mostrado óptima la unión por bridas libres, en la cual se procede a la optimización de la forma. Para la rápida y eficaz solución de este problema se necesitan curvas que relacionen las tensiones en las secciones críticas con las variaciones de las diferentes dimensiones.

Como base de partida se adopta el cálculo general de la resistencia de las uniones por bridas libres, realizado por el método de fuerzas y programado para la máquina calculadora. Después de proponer el sistema dimensional básico con parámetros próximos a los del recipiente real, cuya junta se somete a la optimización, se estudia la influencia de la variación de estos últimos. Los resultados de estos estudios se representan en gráficos.

La forma de las curvas encontradas permite sacar conclusiones no sólo acerca de las posibilidades del sistema básico de las dimensiones, sino también acerca del comportamiento de la totalidad de la instalación. Estos datos permiten obtener con un número mínimo de variantes subsiguientes, formas óptimas de juntas en un margen bastante amplio de parámetros del recipiente. Se adjuntan gráficas con curvas características de la unión por bridas libres.

Some engineering studies conducted in introducing a British type reactor for the Tokai atomic power station

By T. Yoshioka, C. Asada*; M. Kawasaki, R. Ueda, K. Taketani, M. Sasagawa, S. Nomura, Y. Okamoto and S. Sato**

In connection with the construction of the Tokai atomic power station, the Japan Atomic Power Company and the Japan Atomic Energy Research Institute have jointly carried out extensive experimental studies on the engineering and safety aspects of the fuel elements.

Uranium fuel oxidation and fission gas release

Defect test on model fuel elements

The first half of this series of experiments is a so-called defect test [1-2]. Reduced model fuel elements were prepared by canning with Magnox natural as-cast uranium rods, 10 mm in diam and 25 mm in length. Each canned specimen was intentionally punctured with a pinhole 0.2 to 1.0 mm diam. The model was heated externally to 450 °C and to 550 °C in atmospheres of either carbon dioxide, air or an equivolume mixture of the two. The creation of a gap between the uranium and the clad caused oxidation to take place over a wide area around the pinhole, irrespective of the pinhole diam.

In the case of carbon dioxide oxidation, only a slight swelling by oxidation was observed after one day. The weight increase was about 100 mg/day at 550 °C and about 7 mg/day at 450 °C, with little variation due to pinhole diam. Weight increased linearly with time. In the case of air oxidation, swelling grew rapidly, and when after several hours at 550 °C the gain in weight approached 300 mg the cladding burst and uranium oxide powder formed by oxidation was released. The weight increase by oxidation measured about 1 000 mg (see Fig. 1) in 10 hours at 550 °C (slightly lower at 450 °C), irrespective of pinhole diam. The log-log plot of weight increase versus time with air oxidation presented two straight lines connected by a break point.

Fission gas release during oxidation by carbon dioxide

Fission product release from uranium heated in air, steam and carbon dioxide are reported by Hilliard [3], Scott [4] and Parker [5], respectively. The purpose of the present experiment was to determine the correlation of fission gas release with uranium oxidation by

carbon dioxide. The experiment was carried out at relatively low temperatures to enable us to simulate the operating conditions of the reactor concerned.

The specimen used in the experiment was a uranium pellet weighing about 1 g and was irradiated to 10^{15} nvt. After cooling, it was heated in purified carbon dioxide and the oxidation rate was measured gravimetrically in a thermo-balance. The thermo-balance was swept periodically with pure helium to collect fission gas in a low temperature charcoal trap. The fraction of fission gas released during oxidation was determined by measuring the activity of the collected gas. The temperatures investigated were 500, 600 and 700 °C.

Experimental results are shown in Fig. 2. The correlation of fission gas release percentage with oxidation percentage was found to be linear at the temperatures investigated. The fractions of fission gas released to completion of oxidation were about 10, 22 and 40% at 500, 600 and 700 °C, respectively. Plots of the fraction against the reciprocal of the temperature were found to agree with the Arrhenius type relation of small activation energy (5.1 kcal/mole). This temperature dependence indicates that diffusion in the oxide powder is not the exclusive factor in the release of fission gas during oxidation.

Diffusion coefficient of fission gas in the oxide

In connection with the study described in the preceding section, the diffusion rates of fission gas in

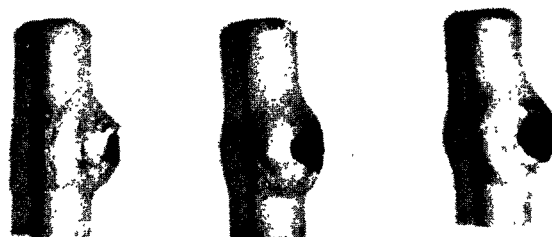


Figure 1. Appearance of specimens after a few hours air oxidation

* Japan Atomic Power Company, Tokyo.

** Japan Atomic Energy Research Institute, Tokai-mura.

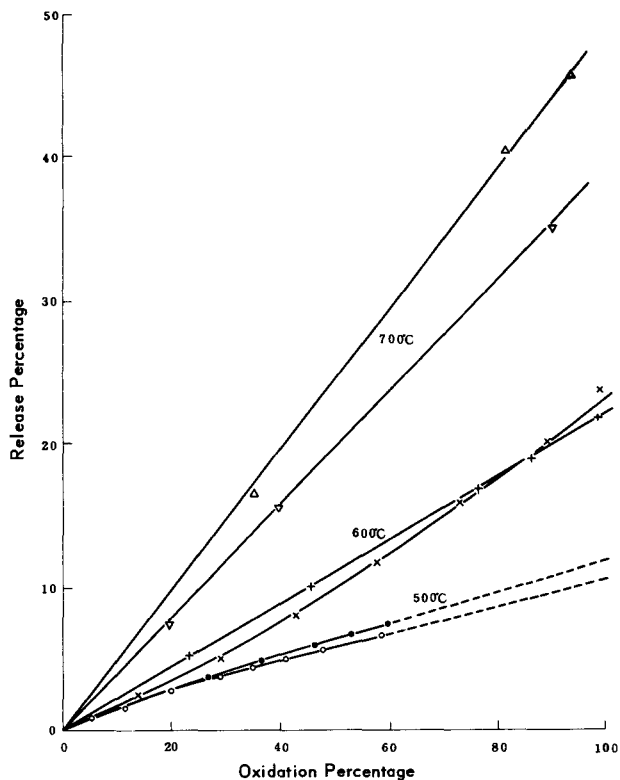


Figure 2. Correlation of fission gas release with oxidation of uranium by carbon dioxide

the uranium dioxide powder produced upon carbon dioxide oxidation of uranium at 600 and 700 °C have been measured at temperatures ranging from 450 to 750 °C.

Two kinds of uranium dioxide powder were used. They were prepared under identical conditions except for the temperatures at which the uranium was oxidized. The powders were irradiated to 10^{15} nvt. They were not subjected to any treatment such as sintering or compacting before or during irradiation. After cooling, fission gas released during isothermal heating was collected in low temperature charcoal traps, and analyzed by gamma ray spectroscopy.

The fraction of fission gas released during heating was apparently proportional to the square root of the heating time as can be explained from the general diffusion mechanism. The apparent diffusion coefficient D' , i.e., diffusion coefficient divided by the square of the radius of the theoretical sphere of the oxide, was 2.0×10^{-12} , 1.8×10^{-11} , 1.5×10^{-10} and $1.4 \times 10^{-9} \text{ s}^{-1}$ at 450, 550, 650 and 750 °C, respectively, for the powder produced at 600 °C, and 5.7×10^{-10} and $2.8 \times 10^{-8} \text{ s}^{-1}$ at 600 and 700 °C, respectively, for the powder produced at 700 °C. For that produced at 600 °C, the logarithms of D' versus the reciprocals of temperature were linear, with activation energy of 16 kcal/mole. By analogy, the Arrhenius plot for the powder produced at 700 °C could also be presumed a straight line though only two points were obtained, and the activation energy was calculated to be 28 kcal/mole. In the present investiga-

tion, all gaseous fission products were collected and measured, and found to be almost exclusively ^{133}Xe .

Oxidation by decomposed carbon dioxide

In the reactor under operation, carbon dioxide is partially decomposed by ionizing radiations and by its contact with graphite. To meet this problem, the oxidation rate of uranium by partially decomposed carbon dioxide was measured gravimetrically and compared with that by non-decomposed carbon dioxide.

Decomposition of carbon dioxide was effected by silent discharge. Precise determination of the decomposition percentage was made by measuring the vapour pressure of the gas remaining uncondensed at liquid nitrogen temperature. But for routine operation, a very simple absorption flask was used, containing 40% KOH aqueous solution to absorb carbon dioxide.

Experimental results are shown in Fig. 3 together with the oxidation rate by non-decomposed carbon dioxide, for comparison. The oxidation rate increases almost proportionally with increase in decomposition percentage. But it is important to note that, in the present case, the decomposition contributes to uranium oxidation purely as source of oxygen supply to the carbon dioxide. This is confirmed by the fact that the rate of oxidation by the decomposed carbon dioxide was the same as that caused by carbon dioxide into which oxygen from water electrolysis was continuously supplied to an equivalent amount.

Creep properties

For the creep tests a vacuum creep testing machine of the author's original design was used, and all the tests were carried out in vacuum to minimize oxidation.

The creep specimens of 8 mm diam and 50 mm gauge length were machined from two groups of cast bars of different composition. Typical compositions determined by analysis and heat treatment data are shown in Table 1.

Table 2 shows the experimental results obtained from the present creep tests. The results are plotted graphically in Fig. 4. The logarithmic relation between the secondary creep rate and the stress for both groups present roughly straight lines.

Figure 5 shows that a straight-line relation exists also between the logarithm of the secondary creep rate and the reciprocal of absolute temperature.

The results presented in Figs. 4 and 5 confirm a well known expression [6-8] of the secondary creep rate:

$$\dot{\epsilon} = \sigma^n \exp(K - Q/RT) \quad (1)$$

where $\dot{\epsilon}$ is the secondary creep rate in bar^{-1} , σ the applied stress in kg/mm^2 , T the absolute temperature in $^{\circ}\text{K}$, Q the activation energy of creep, while n and K are constants.

Using Eq. (1), the values of Q , n and K derived from the present results are summarized in Table 3 for two groups.

In this case, the calculation error was treated by the method of weighted least squares.

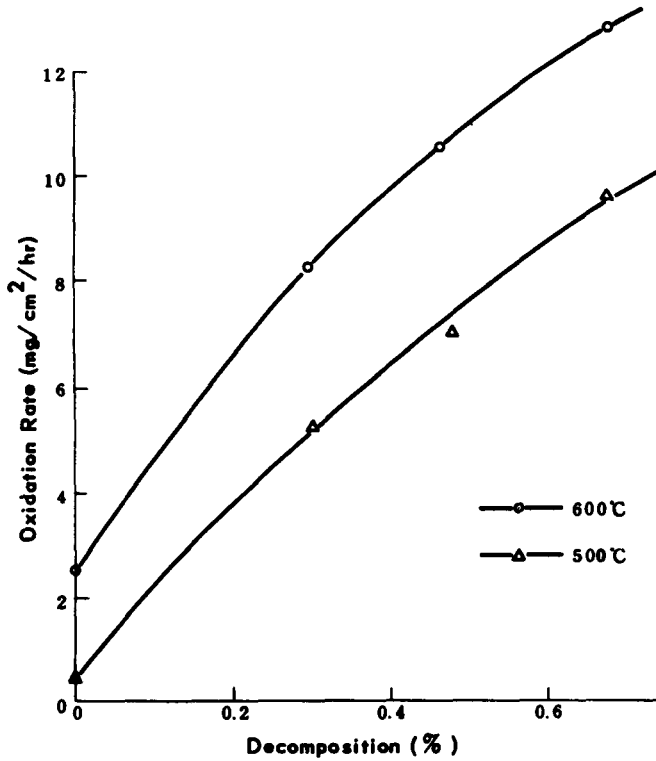


Figure 3. Correlation of oxidation rate with decomposition percentage

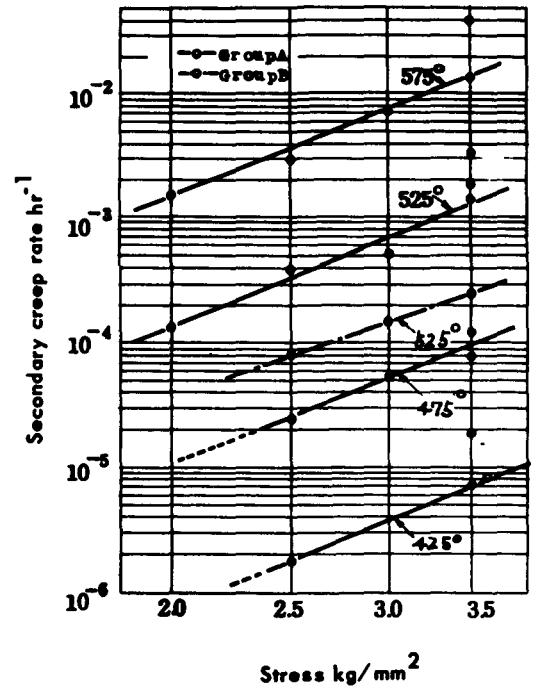


Figure 4. Secondary creep rate versus stress in the temperature range 425-575 °C

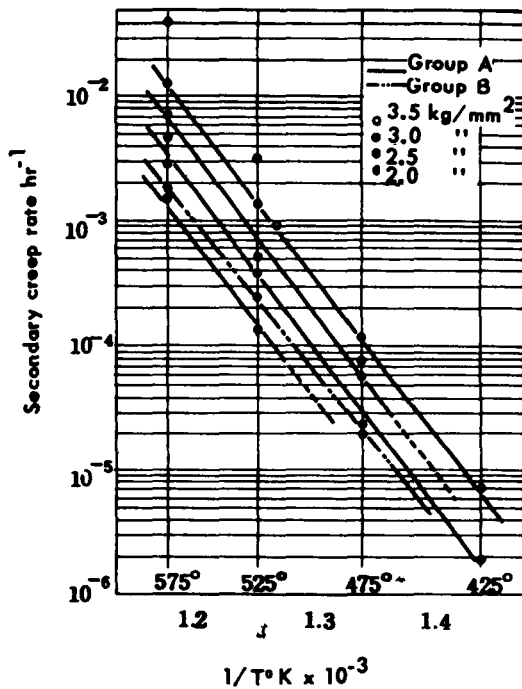


Figure 5. Secondary creep rate versus reciprocal of absolute temperature for various stresses

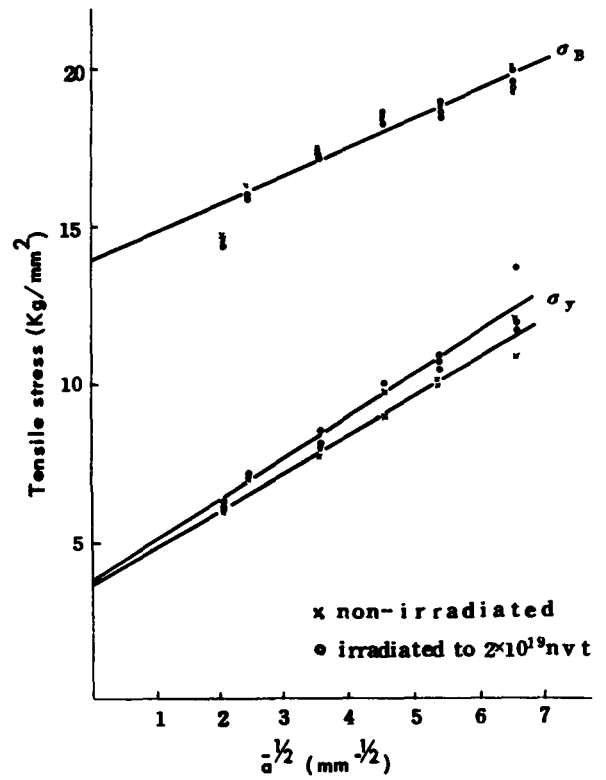


Figure 6. The effect of grain size on yield and fracture stresses of Magnox AL80 specimens at room temperature

Table 1. Typical chemical composition and heat treatment

Group	C ppm	Fe ppm	Al ppm	Heat treatment
A	600	60	39	720 °C × 15 min → W.Q. (twice) 600 °C × 2 hrs
B	350	350	1 100	720 °C × 15 min → W.Q. 600 °C × 1 hr

Table 2. Results of isothermal creep tests

Group	Temp. °C	Stress kg/mm ²	Secondary creep rate hr ⁻¹
A	425	2.5	1.87 × 10 ⁻⁶
	425	3.5	7.20 × 10 ⁻⁶
	425	3.58	9.96 × 10 ⁻⁶
	475	2.5	2.39 × 10 ⁻⁵
	475	3.0	5.52 × 10 ⁻⁵
	475	3.5	7.79 × 10 ⁻⁵
	475	3.5	1.20 × 10 ⁻⁴
	515	3.5	9.12 × 10 ⁻⁴
	525	2.0	1.36 × 10 ⁻⁴
	525	2.5	3.87 × 10 ⁻⁴
	525	3.0	5.20 × 10 ⁻⁴
	525	3.5	3.24 × 10 ⁻³
	525	3.5	1.37 × 10 ⁻³
	575	2.0	1.58 × 10 ⁻³
	575	2.5	4.90 × 10 ⁻³
	575	2.5	2.88 × 10 ⁻³
	575	3.0	7.29 × 10 ⁻³
575	3.5	1.32 × 10 ⁻²	
575	3.5	4.22 × 10 ⁻²	
B	475	3.5	1.94 × 10 ⁻⁵
	525	2.5	8.30 × 10 ⁻⁵
	525	3.0	1.50 × 10 ⁻⁵
	525	3.5	2.44 × 10 ⁻⁴
	575	3.5	1.81 × 10 ⁻³

Grain size ranged between 275 and 650 μ , and the carbon content between 390 and 950 ppm in group A, but these variations did not affect the creep rate in any significant manner. On the other hand a remarkable effect on the creep rate is brought by the presence of even a small amount of cast structure resulting from incomplete heat treatment.

Conclusions

(a) The isothermal creep properties for group A and B may be represented by the following relations:

Group A (temperature range 425 ° to 575 °K)

$$\dot{\epsilon} = \sigma^{3.929} \exp(-1.082 \text{ to } 59.6 \text{ kcal}/RT)$$

Group B (temperature range 475 ° to 575 °K)

$$\dot{\epsilon} = \sigma^{3.202} \exp(1.476 \text{ to } 57.1 \text{ kcal}/RT)$$

(b) The addition of Fe and Al produces high creep resistance and good grain stability.

(c) The presence of texture results in a very marked change of the creep rate.

Irradiation effects on Magnox AL80

To study the effects of neutron irradiation on the mechanical properties of Magnox AL80, room temperature yield and fracture stresses were measured for 2 mm diam polycrystalline wire specimens with grain diameters varying from 0.03 mm to 0.24 mm. After heat treatment to vary grain size, specimens were irradiated in JRR-2 to doses between 10¹⁷ neutrons/cm² and 2 × 10¹⁹ neutrons/cm² at an irradiation temperature of about 50 °C. Tensile tests were performed with an Instron testing machine. The grain size dependence of yield and fracture stresses were measured at a strain rate of 1%/min. And the strain rate dependence of yield and fracture were measured for specimens of 0.07 mm grain diam by changing the strain rate from 1%/min to 100%/min. These results were compared with those of non-irradiated specimens. No definite irradiation effects were obtained in the specimens irradiated to doses up to 10¹⁸ neutrons/cm². After a dose of 2 × 10¹⁹ neutrons/cm², neutron irradiation tends to raise the yield stress of Magnox AL80 specimens as shown in Figs. 6 and 7, although the fracture stress is unchanged. The yield stress, σ_y , can be related to the average grain diam, d , by the equation

$$\sigma_y = \sigma_1 + K_y d^{-1/2}$$

where σ_1 and K_y are constants. The values of σ_1 and K_y , estimated from Fig. 6 are 3.8 kg/mm² and 1.3 kg/mm^{3/2} respectively for irradiated samples and 3.6 kg/mm² and 1.2 kg/mm^{3/2} respectively for non-irradiated samples. Irradiation to 2 × 10¹⁹ neutrons/cm² slightly increases both σ_1 and K_y of Magnox AL80. The changes in yield stress associated with irradiation are independent of the strain rate (Fig. 7).

The present study includes work being conducted by the Japan Atomic Energy Research Institute in co-operation with Furukawa Electric Company Ltd., and Sumitomo Metal Industries Ltd.

Collapse tests

Collapse tests of sub-sized fuel elements have been carried out with high temperature and high pressure CO₂ gas. An autoclave was specially designed for this

Table 3. Values of Q , n and K in the creep equations derived from two groups

Group	M	K	Q (cal/mole)
A	3.929 ± 0.275	-1.082 ± 1.490	59 600 ± 1 200
B	3.202 ± 0.019	1.476 ± 0.617	57 100 ± 1 200

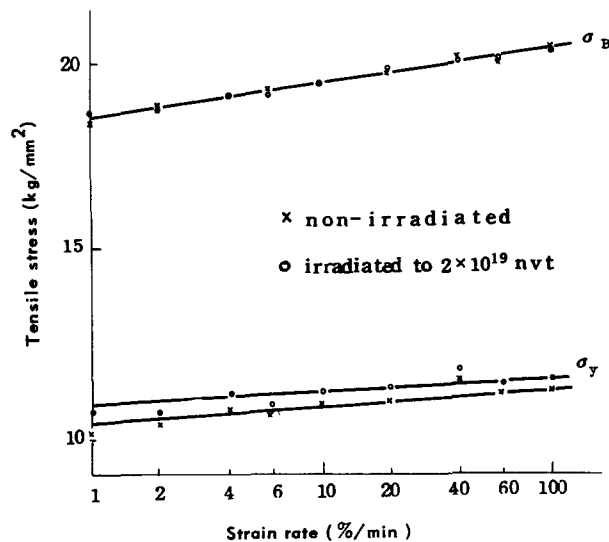


Figure 7. The effect of strain rate on yield and fracture stresses of Magnox AL80 specimens at room temperature

test, and was used to periodically measure with dial gauges change of fuel diam at operation temperature and pressure.

Fuel samples were isotropically compressed with CO_2 gas under the following conditions:

550 °C: 30 kg/cm², 40 kg/cm², 50 kg/cm²
 30 kg/cm²: 550 ± 20 °C, 550 ± 10 °C, 500 ± 20 °C,
 at 6 cycles per day. In order to avoid the effect of primary creep, the samples were exposed to 550 °C at 5 kg/cm² of CO_2 gas for 4 days before starting the thermal cycling tests.

Experimental results are shown in Figs. 8 and 9, and diametric contraction rates are estimated from these curves and summarized in Table 4.

Fluid dynamics and heat transfer

Fluid dynamics and heat transfer tests were undertaken on full-size shells of the power reactor fuel element by means of a high temperature high pressure gas loop. This loop was designed to solve thermal problems of gas cooled reactors. The fuel elements of the Tokai reactor are Magnox clad uranium rods, and the fuel surface carries polyzonal spiral fins. The finned fuel elements 76.3 mm in length, 61 mm diam at fin tip, 45 mm diam at fin root, the fins being 16 in number and helical with a lead of 18.3 mm. Outside the fins are four longitudinal splitters, 20 mm in height, and 2 mm in thickness. Three finned element shells are inserted in the test channel which is 3 m long and 100 mm in diam.

Figure 10 shows the cross section of the test equipment. The test channel is installed in the test section of the gas loop. The three fins in the channel are heated by a 30 kW stainless steel heater. The heater surface is electrically insulated by ceramic coating. Alumel-chromel thermocouples are pinned into the fin roots, and static holes are opened on the channel wall. The space between the fin and the heater is filled with nickel powder. This loop is operated on carbon dioxide at a pressure of 10 kg/cm². A total of 80 kW of electric heating capacity is available for the preheating stage. The gas temperature at the channel inlet is controlled to a constant level of 400 °C. The circulator circulates 70 m³/min of carbon dioxide at a static head of 1 500 mm water column. Measurements of flow rate, gas and fin temperature, pressure drop, and heat input were made.

The heat transfer coefficient is calculated from the temperature distribution, and the friction factor is obtained. The relation to fluid flow of flow resistance and heat transfer is represented in dimensionless units in Fig. 11. The results reproduced on the Bradwell pattern [9–10] are shown for comparison also in the the same figure.

Studies on Tokai graphite

The reactor graphite in Japan was, as explained above, required to be particularly stronger in mechanical strength, due to the requirements of the aseismic design. Accordingly, a decision was made for the Tokai reactor to use the Pechiney graphite of France, which is mechanically stronger, in place of the British AGL previously considered under the original design.

Graphite in the Calder Hall type reactor is one of the materials of utmost importance, in the aspects of both reactor characteristic performance and safety, and therefore, the selection was made only after serious consideration, with various tests performed also in Japan, as are presented hereunder of the AGL, Pechiney (PC-Q₁ and PC-Q₂) and Japan-made (TD-AG) graphite to be of use in coming to the correct decision.

Graphite oxidation

Graphite oxidation in CO_2 gas and in air is one essential point of importance in the fundamental characteristics of graphite, the former, known as mass-transfer, being involved in the problem effecting deterioration in both density and mechanical strength of the graphite, while the latter in the problem affecting performance at the time of an accident.

Table 4. Diametric contraction rates of fuel elements

Conditions	550 °C			30 kgs/cm ²		
	30 kgs/cm ²	40 kgs/cm ²	50 kgs/cm ²	550 ± 20 °C	550 ± 10 °C	500 ± 20 °C
Rates (mm/day)	-0.003	-0.010	-0.011	-0.037	-0.011	-0.014

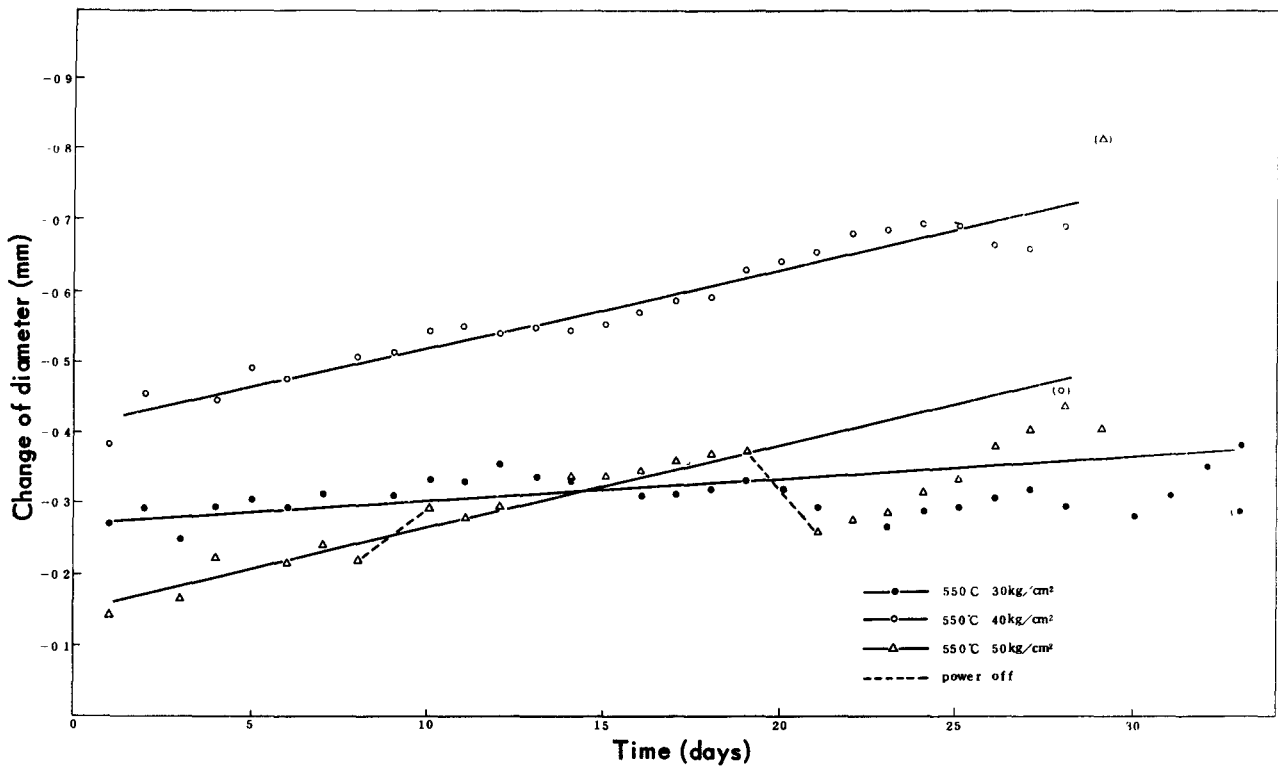


Figure 8. Change of fuel diameter by pressure at 550 °C

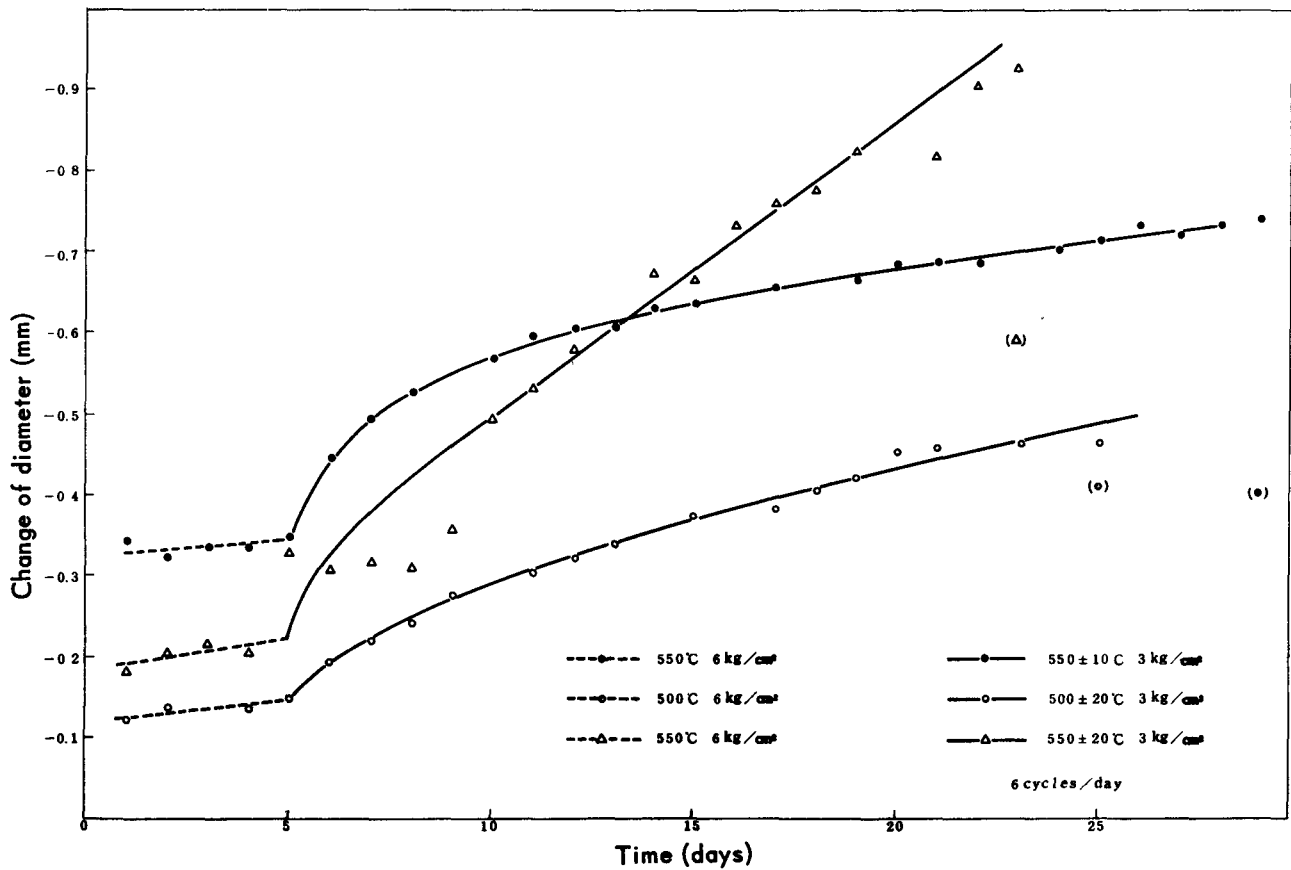


Figure 9. Change of fuel diameter by thermal cycling

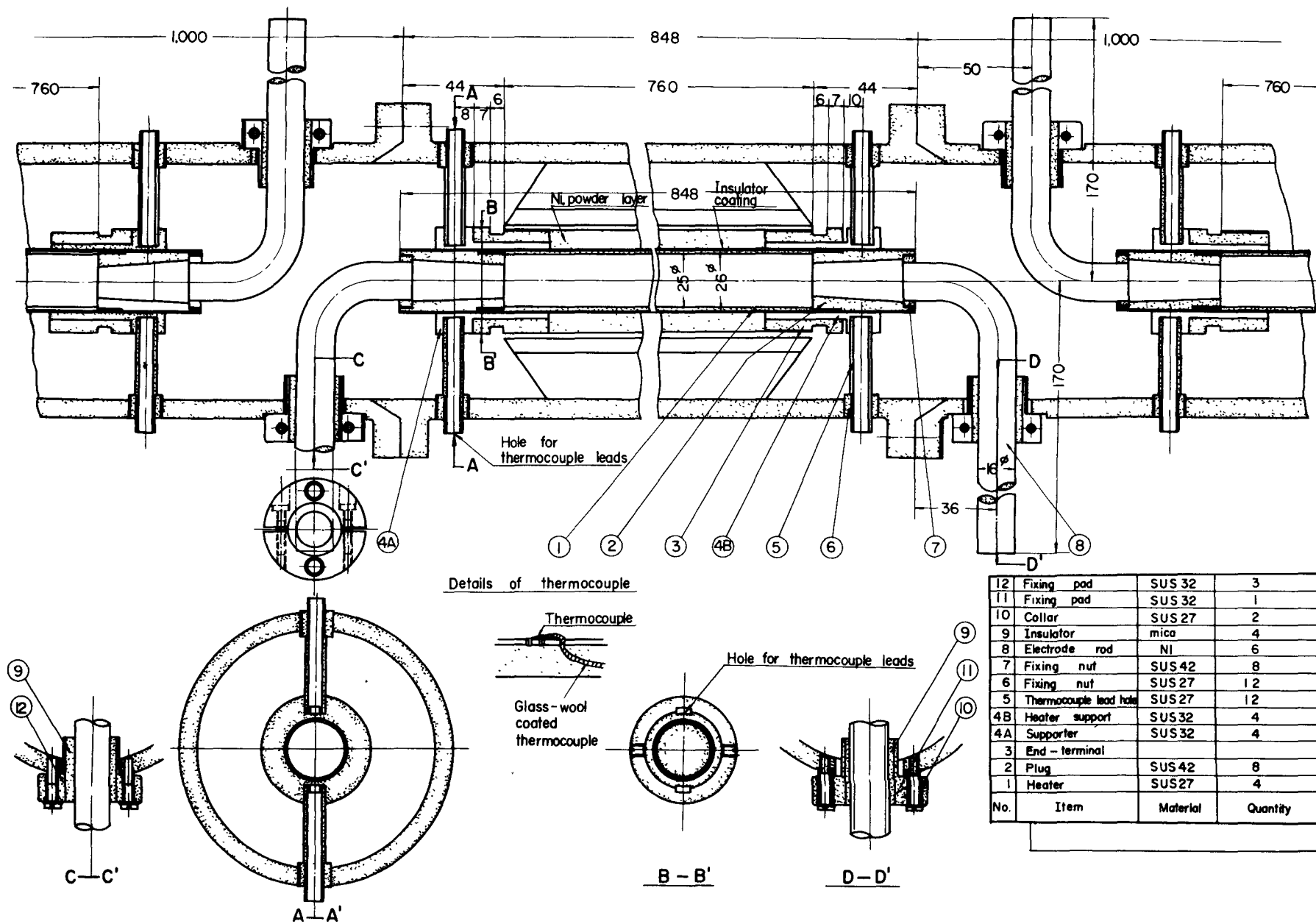


Figure 10. Test equipment for fluid dynamics and heat transfer experiments

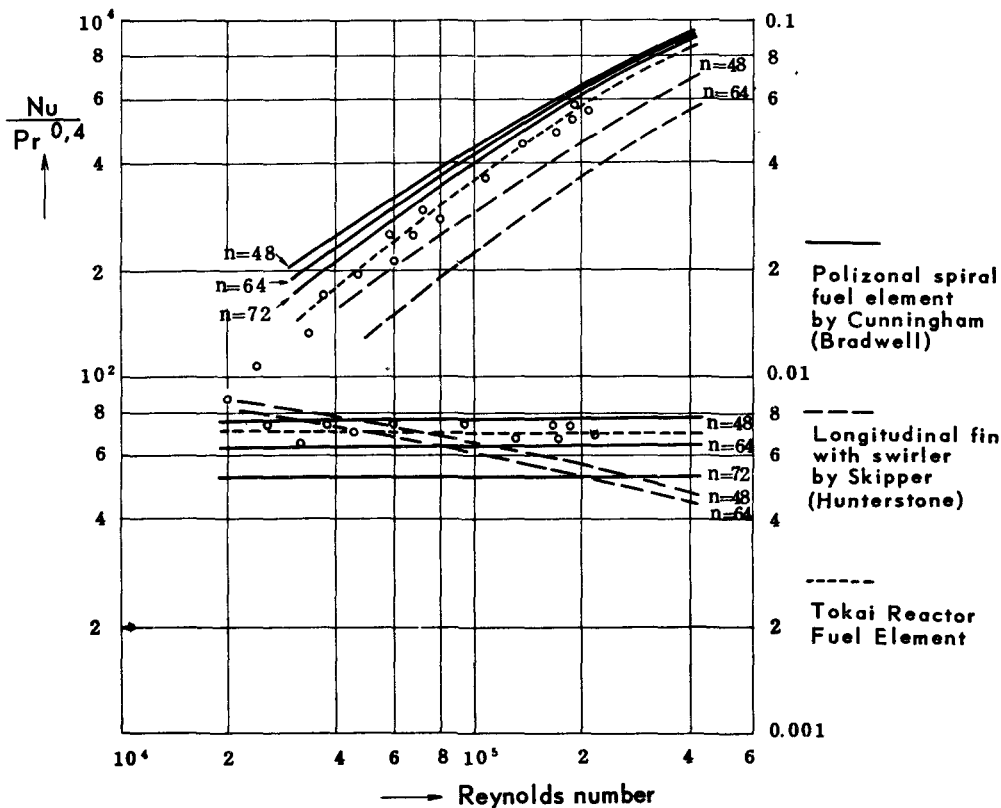


Figure 11. Fluid dynamics and heat-transfer data

The laboratory tests were performed at 800–1 000 °C for the oxidation in CO₂ gas as its rate is slow at low temperature, and those in air at different temperatures of 600 and 700 °C. From the results thus obtained no significant difference was found between the graphites of various manufacturers.

Further in these laboratory tests, investigations were carried out to determine the change arising from oxidation in porosity distribution of the graphite and for the contamination effect relative to oxidation, and certain worthwhile results were obtained.

Mechanical strength of the graphite and the effect of oxidation

The graphite blocks of the Tokai reactor were made in the shape of hexagonal columns, with keys and keyways provided in turn on the faces in the axial direction, so that the blocks are firmly interlocked.

Mechanical strength tests were performed on the complete graphite block. Tests were also performed on the test pieces cut out of the block for the following mechanical properties:

(a) *Ultrasonic measurement of elasticity.* This method is advantageous, as the breaking strength is measurable without breaking the test piece. The elasticity was obtained by measuring the timing of an ultrasonic pulse propagating in the test piece.

(b) *Bending strength tests.* The 3-point bending method was adopted for the tests, with a 12 mm wide, 15 mm high and 76.2 mm long rectangular test piece.

(c) *Compression breaking strength test.* A cylindrical test piece, 15 mm in diam and 15 mm high, was used for the test piece, using Olien compression testing equipment.

(d) *Compression strength test.* The same equipment as that for the compression breaking strength test was used, with a test piece having the same dimensions, but measurements were taken at a loading rate of 0.3 mm/min.

The results obtained may be summarized as follows:

(a) *Mechanical strength of the test piece before oxidation.* Compared with the total average strength of all the types tested, PC-Q₁ was found to be the strongest and PC-Q₃ the lowest, with AGL and TD-AG ranking in between the two. AGL, having the highest specific density and specific gravity, was found to be relatively high in elasticity but not proportionally high in strength.

(b) *Comparison in oxidation rate.* The four types of graphite were placed in a natural convection current reaction tube filled with air, and their oxidation rates were compared.

This made it quite clear that both PC-Q₁ and AGL were more resistant to oxidation. Further, various factors influencing the oxidation rate were investigated. It was shown that apparent density, porosity and porosity distribution as well as thermal expansion influenced the thermal oxidation rate. The true density, graphitisation temperature and magnitude of ash content had a much smaller effect on the oxidation

rate. However, for the AGL certain differences from the above findings were observed for which it was difficult to produce a reasonable explanation in the light of results previously obtained from the measurement of porosity distribution. It was recognized that this was due to other causes, for example differences arising during the course of manufacturing the raw material.

(c) *Size effect in oxidation.* Experiments were performed on test pieces of cylindrical shape in four different sizes ranging from 6.24 mm to 50.0 mm in diam at temperatures ranging from 400 to 700 °C to investigate the effect of the temperature T and the size d on the oxidation rate, and the results approximately indicated that a relationship proportional to the Arrhenius formula and d^{-n} , respectively existed. It also indicated a slight change in the activation energy with the size, becoming smaller as the size got smaller, indicating a certain relationship existed between the oxidation rate and the geometrical surface area.

(d) *Mechanical change arising from oxidation.* Prior to the breaking strength tests, a comparison was made between the change in the modulus of elasticity and the extent of oxidation. It was found that the modulus of elasticity changed faster. The change in mechanical strength relative to the extent of oxidation was found to be similar, which indicates that the modulus of elasticity and mechanical strength, as seen

from the macro-scale interpretation of the micro-structural forces, will be decreased more than the simple decrease in properties due to weight losses arising from oxidation in the internal porosity. It was also shown that changes in the modulus of elasticity and strength were taking place at approximately an equal ratio, thus indicating the effectiveness of the elasticity measurement, by means of an ultrasonic method, for the purpose of non-destructive investigation.

REFERENCES

1. Taketani, K., and Ikawa, K., J. Atomic Energy Soc., Japan 5, 4, 310/315 (1963).
2. Taketani, K., and Ikawa, K., J. Atomic Energy Soc., Japan 5, 6, 481/491 (1963).
3. Hilliard, R. K., USAEC Report HW-60689 (1959).
4. Scott, A. J., USAEC Report HW-62604 (1959).
5. Parker, G. W., USAEC Report ORNL-2983 (1960).
6. Dorn, J. E., J. of the Mechanics and Physics of Solids, 3, 116 (1954).
7. Young, A. G., Gardiner, K. M., and Rotsey, W. B., J. Nuclear Materials, 2, 234 (1960).
8. Gardner, L. R. T., and Miller, W. H., Inst. of Materials, Symposium on Uranium and Graphite No. 4 (1962).
9. Cunningham, C., Proc. Inst. Mech. Eng. Symposium No. 10 57/77 (1960).
10. Skipper, R. G. A., Proc. Inst. Mech. Eng. Symposium No. 10 78/84 (1960).

ABSTRACT—RÉSUMÉ—АБХОТАЦІЯ—RESUMEN

A/857 Japon

Quelques études d'*engineering* faites à l'occasion de l'introduction d'un réacteur de type anglais à la centrale de Tokai

par T. Yoshioka *et al.*

En liaison avec la centrale nucléaire de Tokai, la Japan Power Company et l'Institut de recherches nucléaires du Japon ont effectué ensemble des études expérimentales très poussées sur l'*engineering* et la sûreté des éléments combustibles, ainsi que sur le graphite.

Des recherches ont été effectuées, à diverses températures, sur l'oxydation de modèles perforés d'éléments combustibles, et de blocs de graphite, dans une atmosphère de gaz carbonique ou d'air. Des expériences ont été également effectuées en vue d'étudier la relation entre le dégagement de gaz de fission et le degré d'oxydation, par le gaz carbonique de l'uranium irradié. On a trouvé que la quantité de gaz de fission dégagée durant l'oxydation, est, en gros, proportionnelle à l'étendue de l'oxydation. Le total de gaz de fission dégagé durant la période d'oxydation était, à 500 °C, de 11 % du contenu initial de gaz de fission; à 600 °C, de 25 %; et à 700 °C de 45 %. Les coefficients de diffusion de Xe dans les oxydes d'uranium produits par l'oxydation ont fait l'objet d'expé-

ences supplémentaires. De plus, l'influence de la décomposition du gaz carbonique sur le taux d'oxydation de l'uranium a aussi été étudiée.

Des essais de fluage à température élevée ont été effectués sur l'uranium, en vue d'étudier le phénomène d'écrasement de l'élément combustible. Les vitesses de fluage secondaire se différents uranium ont été mesurés à l'aide d'un essayeur de fluage à vide, sous des charges constantes de 2 à 3, 5 kg/mm², à des températures de 425 à 575 °C. Les graphiques des taux de fluage en fonction du logarithme des charges et de l'inverse de la température, se sont révélés être linéaires, et l'addition de fer ou d'aluminium a causé une augmentation de la résistance de fluage.

Pour étudier l'effet de l'irradiation neutronique sur les propriétés mécaniques du Magnox AL 80, la relation entre la résistance à la traction et la taille du grain et le taux de déformation a été étudiée expérimentalement; les résultats se sont révélés conformes à l'équation de Petch.

Puisque le combustible en question est un cylindre creux, il pourrait s'écraser dans le réacteur. En vue de résoudre ce problème, un modèle réduit d'élément combustible a été soumis à des pressions de gaz carbonique de 30 à 50 kg/cm², à des températures de 450 à 550 °C, et cyclé thermiquement entre des limites de ± 20 °C. Les résultats ont montré que la variation de diamètre était comprise dans les limites

des erreurs expérimentales (0,05 mm/mois de réduction, sous des charges de moins de 30 kg/cm² et de 40 kg/cm², respectivement).

Les caractéristiques du flux de chaleur de l'élément combustible ont été étudiées au moyen d'une boucle d'essai fonctionnant à 10 kg/cm² à 800 °C. Un élément d'uranium gainé de Magnox a été chauffé intérieurement dans la boucle et les caractéristiques de conduction de chaleur, ainsi que le coefficient de point chaud ont été étudiés en mesurant la distribution de température à la surface. L'étendue de la déformation et le comportement durant la réduction de pression ont aussi été observés.

Des essais de résistance mécanique ont été effectués sur des blocs de graphite entiers et des éprouvettes coupés dans ces blocs. Des informations intéressantes ont été obtenues.

A/857 Япония

Некоторые инженерные исследования, связанные с планами использования для атомной электростанции в Токай-Мура реактора типа английских реакторов

Т. Иосиока et al.

В связи со строительством атомной электростанции в Токай-Мура фирма «Джапен атомик пауэр» и Японский научно-исследовательский институт атомной энергии совместно провели обширные экспериментальные исследования инженерных проблем и вопросов безопасности, связанных с тепловыделяющими элементами и графитом.

Исследовалось окисление перфорированных моделей тепловыделяющих элементов и графитовых блоков в атмосфере двуокиси углерода или воздуха при различных температурах. Проводились также эксперименты по изучению взаимосвязи между высвобождением газообразных продуктов деления и степенью окисления облученного урана в атмосфере двуокиси углерода. Было установлено, что количество газообразных продуктов деления, высвобождающихся при окислении, грубо пропорционально степени окисления. Общее количество газообразных продуктов деления, выделившихся за период окисления при температуре 500 °C, составило 11% от первоначального количества газообразных продуктов деления, при температуре 600 °C — 25% и при 700 °C — 45%. При дополнительном эксперименте были измерены коэффициенты диффузии ксенона в окислях урана, образующихся при окислении. Кроме того, изучалось влияние разложения двуокиси углерода на скорость окисления урана.

Были проведены высокотемпературные испытания на крип урана с целью изучения явлений

разрушения тепловыделяющих элементов. Измерения вторичной ползучести урана проводились при помощи вакуумного устройства для испытания на ползучесть при постоянных нагрузках 2—3,5 кг/мм² и температурах 425—575 °C. Графики скорости ползучести как функции логарифма нагрузок и обратной величины температуры оказались линейными, и было установлено, что добавление железа или алюминия повышает сопротивление ползучести.

Проводилось экспериментальное изучение влияния нейтронного облучения на механические свойства магноксового сплава AL-80, зависимости сопротивления разрыву от размера зерен и скорости деформации; полученные результаты согласуются с уравнением Петча.

Поскольку рассматриваемые тепловыделяющие элементы представляют собой полые цилиндры, то в условиях работы реактора могут иметь место разрушения топлива. Для решения этой проблемы проводилось испытание уменьшенной модели тепловыделяющего элемента в атмосфере двуокиси углерода под давлением 30—50 кг/см² при температуре 450—550 °C и тепловом цикле в пределах $\pm 20^\circ$ C. Полученные результаты показали, что при нагрузках менее 30 кг/см² изменение диаметра находилось в пределах экспериментальной ошибки, а при нагрузке 40 кг/см² имело место уменьшение по диаметру, равное 0,05 мм в месяц.

Изучение характеристик теплового потока в тепловыделяющих элементах осуществлялось при помощи испытательной петли, работающей под давлением 10 кг/см² и при температуре 800 °C. Урановый тепловыделяющий элемент в магноксовой оболочке подогревался изнутри в петле, и характеристика теплопроводности и коэффициент местного перегрева исследовались путем измерения распределения температуры на поверхности. Наблюдалась также степень деформации и поведение тепловыделяющего элемента при снижении давления.

Испытания механической прочности графита проводились на графитовых блоках и на опытных кусках, вырезанных из целого блока. Получены разнообразные ценные данные.

A/857 Japon

Estudios de ingeniería realizados al introducir el tipo británico de reactor para la central nuclear de potencia de Tokai

por T. Yoshioka et al.

La Japan Power Company y el Instituto de Investigación sobre Energía Atómica del Japón han realizado conjuntamente un amplio programa experimental, relacionado con la central nuclear de potencia de Tokai, sobre problemas técnicos y de seguridad de elementos combustibles y grafito.

Ha sido investigada la oxidación de modelos de elementos combustibles perforados y de bloques de grafito en atmósfera de aire y dióxido de carbono en

diferentes condiciones de temperatura. Se han realizado también experiencias para estudiar la correlación entre la liberación de productos de fisión gaseosos y la extensión de la oxidación por dióxido de carbono del uranio irradiado. Las cantidades totales de gases de fisión liberados durante el período de oxidación han sido: a 500 °C, el 11 % del contenido inicial de gases de fisión, a 600 °C, el 25 % y a 700 °C, el 45 %. Como experiencia adicional se han medido los coeficientes de difusión de Xe en óxidos de uranio producidos por oxidación. Además, se ha estudiado el efecto de la descomposición del dióxido de carbono en la velocidad de oxidación del uranio.

Se han realizado pruebas de arrastre de uranio para estudiar el fenómeno de deformación de los elementos combustibles. Las velocidades secundarias de agrietamiento de diversos uranios se han medido con un comprobador de arrastre en vacío para diferentes cargas entre 2 y 3,5 kg/mm² y temperaturas comprendidas entre 425 y 575 °C. La velocidad de arrastre es una función lineal del logaritmo de la carga y del inverso de la temperatura, y la resistencia al arrastre aumenta cuando se añaden hierro o aluminio.

Al estudiar el efecto de irradiación neutrónica sobre las propiedades mecánicas del magnox AL 80, se ha investigado experimentalmente la dependencia del límite elástico del tamaño del grano y de la velocidad

de deformación, encontrándose un resultado de acuerdo con la ecuación de Petch.

Como los elementos combustibles son tubos cilíndricos, puede ocurrir una deformación del mismo en las condiciones de operación del reactor. Para resolver este problema, se ha sometido un modelo de elemento combustible a presiones de dióxido de carbono de 30 a 50 kg/cm² y temperaturas de 450 a 550 °C realizando ciclos térmicos entre ± 20 °C. Los resultados demuestran que la variación en diámetro se encontraba dentro del error experimental y una reducción de 0,05 mm/mes para cargas menores de 30 kg/cm² y 40 kg/cm² respectivamente.

Se han estudiado las características de flujo térmico de los elementos combustibles en un circuito experimental que se encuentra sometido a una presión de 10 kg/cm² y 800 °C de temperatura. Se calentó internamente un elemento combustible revestido de magnox situado en este circuito experimental, determinándose los coeficientes de transmisión de calor y de punto de temperatura máxima mediante la medida de la distribución de temperaturas en la superficie. Se observó la extensión de la deformación y el comportamiento durante la reducción de presión.

Se han realizado pruebas mecánicas de bloques de grafito y de diferentes trozos cortados de estos bloques, obteniéndose diversas informaciones útiles.

Reactor plant equipment

Chairman: G. Stiennon (Belgium)

Paper P/330 (presented by A. G. Filippov)

DISCUSSION

D. S. HIORNS (United Kingdom): It is pointed out in the paper just presented that the reliability and safety of a reactor system are prejudiced if the operator has a lot of manipulations to perform. In this connection, I should like to draw attention to paper P/126, which describes a system in which the operator's task is simplified.

J. A. THIE (United States of America): My principal question relates to the blocks numbered 17 in Fig. 1 of the paper. Are both systems operating at the same time, or is just one of the pair operating, with transfer to the other taking place in case of failure? If there is a transfer, what information causes it?

A. G. FILIPPOV (USSR): In view of the possibility that discrepancies may arise in the settings of the amplifiers and ionization chamber currents during reactor operation, automatic correctors (VI in Fig. 1) are provided in the controller channels to prevent unbalance at the output of the reserve controller amplifier. The automatic corrector of the operating controller is at the same time out of circuit. The automatic correctors are switched on and off manually by the operator using blocks 17 in Fig. 1.

J. A. THIE (United States of America): At what percentage of full power does a trip take place when the demand is set at 10% of full power and at 100 or 150% of full power? What exponential period is used before reaching the ramp rate?

A. G. FILIPPOV (USSR): In the power range 10–150% the accident prevention operates for a 20% power increase above the rated value. Before the linear power rise, an exponential rise, normally with a period of 20–30 s, is used.

J. WEILL (France): You say that your reactors have to be started up rapidly. In view of this, what system do you use for the start-up phase?

A. G. FILIPPOV (USSR): In order to reduce the reactor start-up time and for reasons of safety we use automatic systems to go from the subcritical state to 1–10% of the rated power. An exponential law is used.

J. WEILL (France): What type of detectors do you use? If they are ionization chambers, as your paper appears to indicate, are they compensated with regard to gamma rays?

A. G. FILIPPOV (USSR): Ionization chambers with compensation for the gamma background are used in the control systems.

J. WEILL (France): What average speed have you selected for your compensation and control rods (expressed in units of reactivity per second)?

A. G. FILIPPOV (USSR): The average speed of the control rods is about $20 \times 10^{-5} \text{ s}^{-1}$ and of the compensating rods about $10 \times 10^{-6} \text{ s}^{-1}$.

Paper P/52 (presented by G. Lamiral)

DISCUSSION *

P. FORTESCUE (United States of America): Have any of the models been tested to failure or leakage using a gas rather than water to apply the pressure? Would different results be anticipated if a gas were used? Does the existence of a steel liner affect the mode of failure?

G. LAMIRAL (France): For various reasons we have not carried out tests on models under gas pressure, but tests we have made on the third model of the EDF-3 vessel seem to indicate that ruptures caused by gas pressure would not differ essentially from ruptures caused by water pressure. In view of the design of the openings, the cracks would start from the outside of the vessel.

The steel liner could have some effect on the way in which the vessel ruptured; this liner has to withstand considerable strains during prestressing and at the same time it may undergo plastic deformation, so it must be made of good quality soft steel capable of considerable expansion. In tests to failure, especially with threaded prestressed cables, it might be feared that the cables would break before the sealing film and that the break would be very violent, but tests have shown that this fear is not justified. It must also be realized that although tests to failure carried out on models at increased pressure, constitute a check on the calculations, they do not correspond to a possible mode of rupture since the pressure in the reactor during operation could not be more than a few per cent higher than the service pressure.

It is possible, though not likely, that the strength of the cables could decrease (for example, through corrosion) with the reactor at the service pressure. For this contingency, as we have pointed out, it was found necessary to do away with a large number of

* See also later discussion on paper P/140.

cables to ensure that the breaking pressure is achieved and any serious accident preceded, well in advance, by serious cracking clearly visible from the outside of the vessel.

P. FORTESCUE (United States of America): Do you in France see any practical problems in building concrete pressure vessels to contain a working pressure of up to 70 kg/cm² of helium gas?

G. LAMIRAL (France): Studies being carried out on the vessel of the INCA Reactor take into account pressures of 40 and 60 bars. We do not think the design of prestressed concrete vessels raises special problems below pressures of about 100 bars. The only problem connected with the use of helium appears to be in connection with leak-proofing; checks on the metallic skin would have to be very much more stringent than those in the case of a carbon-dioxide-gas-vessel.

P. FORTESCUE (United States of America): At what physical size is it more economical to use a concrete vessel than a steel vessel?

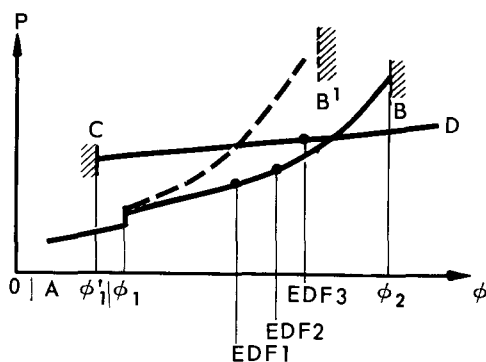


Figure 1

G. LAMIRAL (France): The graph in Fig. 1 compares the economics of steel vessels and prestressed concrete vessels. However, the graph is more in the nature of an aid to explanation than an accurate representation. The vessel price is given as a function of some dimensional parameters, for example the diameter of the reactor core at a given height.

The graph is for a given pressure, say 28 bars. For metal vessels (curve AB) there are no minimum dimensions, and the vessels can be as small as desired. It will be noted that there is a discontinuity in price at ϕ_1 corresponding to the dimensions above which the vessels can no longer be built in the factory and must be built on site. The curve then rises very rapidly and difficulties increase very quickly with the dimensions until, at a certain size ϕ_2 , construction is no longer possible.

In the case of prestressed concrete vessels there is an (intuitive) lower limit, for any given system of pre-

stressing, below which construction is not possible; the price curve is then continuous (using the same materials) and no upper limit to the size can be seen.

For the EDF 1 station, the economic comparison was in favour of steel vessels, and steel was also chosen for EDF 2.

Difficulties encountered in designing vessels of manganese-molybdenum steel led to the development of new manufacturing processes and the curve for steel vessels now becomes AB'. At the same time, experience gained at Marcoule made it possible to reduce the cost of prestressed concrete vessels. For EDF 3, therefore, the comparison was in favour of prestressed concrete. At the present time, if the EDF 3 vessel had to be rebuilt, a saving of 15–20% could be realized and it is probable that if comparisons between steel and concrete were now to be made for EDF 1 and EDF 2, the result would be in favour of concrete for EDF 2 and perhaps even for EDF 1. I would point out that the EDF 2 vessel is in the shape of a sphere, 18.3 m in internal diameter, while the EDF 1 vessel is cylindrical in shape, with a diameter of 10 m and a height of 23 m.

The above comparison has been made for a given pressure of the order of about 28 bars, and it should be noted that for higher pressures the upper limits of the dimensions of metal vessels would be lower, whilst the lower limits of reinforced concrete vessels do not seem to change very much.

Paper P/140 (presented by A. Houghton Brown)

DISCUSSION

P. FORTESCUE (United States of America): Could you specify the time scale implied by item (c) in the second section of your paper, namely that "The mode of ultimate failure shall be progressive without sudden rupture". In other words, in what period of time would the loss of half the initial gas pressure be considered sudden?

A. HOUGHTON BROWN (United Kingdom): The progressive mode of failure mentioned in the paper is not related to time. The progression is with increasing deflections under increasing pressures; the time during which the pressure is applied is not significant.

M. TROOST (United States of America): What is the thickness of the liner insulation and how many layers are used? Secondly, what heat flux is the insulation designed for?

A. HOUGHTON BROWN (United Kingdom): I should like to ask my colleague Mr. Spruce to answer these questions.

T. W. SPRUCE (United Kingdom): The thickness of the stainless steel insulation is of the order of 2 inches, and it is made up of about 30 layers of foil suitably spaced apart.

The heat flux on the insulation varies considerably over the surface, but I am not able to quote the actual values offhand.

R. S. TAYLOR (United Kingdom): I should like to make a few comments relating to the papers on prestressed concrete pressure vessels, especially papers P/52 and P/140. A number of quite different solutions have been proposed to the basic problem of building vessels of large dimensions, operating at high pressures. Each of the designs described clearly results in safe, workable structures. This diversity of approach indicates the inherent flexibility of concrete vessels in meeting the requirements of the reactor designer.

The pressure vessel design adopted must result from close liaison between the vessel and reactor designers, and the optimum solution will depend on the particular criteria applied.

In the case of the Wylfa power station (described in paper P/141) each reactor provides a net electrical output of 590 MW. The internal diameter of each of the two vessels is 96 ft and the design pressures 440 psi. An economic solution was found by adopting a spherical internal surface, with an external surface formed to enable the heavy prestressing gear to be accommodated, and practical and expeditious construction to be achieved. This form of design also yields very low specific quantities in comparison with other vessel shapes and this point is illustrated in Fig. 2 of paper P/141.

Doubt has sometimes been expressed as to whether the spherical vessel, in its practical form, is amenable to close stress analysis. The Wylfa type of vessel has in fact been based upon a wide research and development programme, and as will be seen from Fig. 3 of paper P/141, the correspondence between experimental and predicted strain is very good. The effect of departures from a true sphere are in fact minor in comparison with the discontinuities inherent in the cylindrical form.

The behaviour of the spherical type of vessel is essentially the same both in the working range and at ultimate load and shear forces are very low. The necessity for building in considerable margins to cover the uncertainties of the transition of the cylindrical vessel from working to ultimate load is obviated.

Paper P/810

DISCUSSION

L. CAVE (United Kingdom): In describing the Marviken BHWV vessel, your paper states that the nozzles on the bottom head of the vessel are of the "set-on" type; Fig. 3 shows that the nozzle is rather long, so that any rotation during welding or stress relief will be magnified considerably.

The problem of nozzle rotation received considerable attention in the UK during the development of the earlier civil stations, and we found that it is preferable to use "set-through" nozzles on these large steel vessels. For example, in the case of the Tokai reactor the use of "set-through" nozzles, together with pre-setting to correct for the estimated effects of welding and stress-relief, avoided the need for any major machining of the nozzles after fabrication to correct for misalignment.

In addition, the method of welding for "set-through" nozzles is easier and more reliable than for the "set-on" type. I should be interested to know, therefore, why "set-on" nozzles have been chosen for the Marviken vessel.

O. HELLSTRÖM (Sweden): We have studied this part of the vessel extremely carefully with regard to rotation. The expression "set-on" is generally valid, but some of the nozzles could be more aptly classified as "set-in" nozzles.

A. L. GAINES (United States of America): What method of inspection is performed for the difficult operation of welding the nozzles into the head?

O. HELLSTRÖM (Sweden): Careful inspection of every bead is carried out visually and using magnetic particles and dye penetrants. This assures a weld free from cracks and other defects.

A. L. GAINES (United States of America): During heat-up and cool-down temperature transients, does the unique construction of the vessel closure result in axial position changes of the sealing surfaces? What rate of transient can be withstood during the expected life of the vessel?

O. HELLSTRÖM (Sweden): The closure is acceptable with regard to the technical specifications relating to temperature changes during start-up and shut-down of the reactor. The time is between 8 and 16 hours, depending on the kind of operation.

M. C. VAN VEEN (Netherlands): What is your opinion as to the use of a weld-factor of 0.9, compared with the factor of 1.0 recognized by the ASME codes for the highest class of weld?

O. HELLSTRÖM (Sweden): I think a weld-factor of 0.9 is not necessary for a reactor pressure vessel in view of the high requirements and strict control of the product. However, I am sure that we shall change this factor from 0.9 to 1.0 in our Swedish code.

M. C. VAN VEEN (Netherlands): Have you carried out any welding tests on 9% Ni-steel plates of 5-7" thickness?

O. HELLSTRÖM (Sweden): Not as far as I know.

Paper P/227 (presented by A. L. Gaines)

DISCUSSION

B. SAITCEVSKY (France): It is not always possible to transport very large vessels by water from the factory to the site. Could you say anything about the types of construction and the times and costs involved in the case of site-built vessels?

A. L. GAINES (United States of America): To date, there has been no firm demand for field-fabricated vessels. Existing industrial facilities permit the building of vessels up to 35 feet in diameter and 1 000 tons in weight. Moreover, the large power plants need condenser cooling water in such quantities that they are usually located on navigable rivers. For these reasons, I do not have ready information on times and costs involved in site-assembly of reactor vessels.

C. DE PATER (Netherlands): Section III of the ASME code gives "Rules for the Construction of Nuclear Vessels". Can non-nuclear vessels also be based upon this section in the United States?

A. L. GAINES (United States of America): Section III requirements may be used for vessels other than nuclear with the permission of the local regulatory authorities. These rules are also being applied to petroleum and chemical vessels.

Paper P/522 (presented by A. Komárec)

DISCUSSION

A. L. GAINES (United States of America): The separate forged flange rings, while easing a difficult material procurement and fabrication problem, seem to limit the ability of the design to withstand fast heat-up rates. For what rate of temperature rise over what temperature range (starting to operating) has the vessel been designed and analysed?

A. KOMÁREC (Czechoslovakia): A special feature of our reactor vessel is that the working temperature is low (not more than 150 °C) and the temperature fluctuations, especially in the region of the flange joint, are not sharp. An analysis of starting and operating conditions showed that the flange joint is satisfactory.

A. L. GAINES (United States of America): Did the testing of the 1 to 1 model include temperature and pressure cycling?

A. KOMÁREC (Czechoslovakia): The scale model of the vessel is practically ready, but testing has not yet begun. However, it has been decided to include pressure cycling in the test programme. Not much consideration is given to the effects of temperature cycling as this type of stressing is not characteristic of the vessel.

A. L. GAINES (United States of America): The coincidence of the support ledge for intervals and the vessel support cone attachment would seem to accentuate thermal problems. For what rate of temperature change and what range of temperature, and for how many cycles, has the design analysis shown the vessel to be within design stress limits?

A. KOMÁREC (Czechoslovakia): The lower part of the vessel is cooled by gas, and a careful analysis has shown that the gas temperature (110 °C) varies only slightly for different reactor operating conditions. The starting conditions will be worked out experimentally using the scale model of the vessel.

C. DE PATER (Netherlands): Can you give data regarding impact strengths and transition temperatures of the base metal, the weld metal and the metal of the affected zone, in particular with regard to the electroslag welded joints?

A. KOMÁREC (Czechoslovakia): A special characteristic of vessels of large size is that they represent an integral whole. Although the transition temperatures of the base metal, the weld metal and the metal of the zone affected by the weld can be determined on

standard samples, these data are not representative for the structure of the vessel as a whole. The only true picture of the properties of the structural metals for reactor vessels is given by tests on large samples on which welded joints have been made. Such tests have been carried out in Czechoslovakia and they show that in all the required conditions of manufacture and operation the reactor vessel can support temperatures higher than the critical temperature of the structure as a whole.

Paper P/138 (presented by H. Bateman)

DISCUSSION

P. FORTESCUE (United States of America): Has experience shown that special problems are involved in the parallel operation of blowers with variable speed drive? Do stability considerations impose any especially desirable form of flow characteristic?

H. BATEMAN (United Kingdom): Our experience at Hunterston has not shown that any special problems are involved in the parallel operation of variable-speed blowers. The forms of characteristic obtained from either centrifugal or axial blowers of conventional design are satisfactory.

Paper P/139 (presented by J. O. Joss)

DISCUSSION

P. J. DUNTON (United Kingdom): Experience on Hunterston, Tokai Mura and Trawsfynydd confirms the conclusions given in the section of the paper headed "Lessons for the Future". The comments on testing of prototype and production units are particularly relevant, especially if the site is a long way from the place of manufacture. Both the Hunterston reactors have been brought up to design output, and only minor troubles remain in connection with the fuel-handling plant; there were extensive works and site tests before the reactor was raised to power.

It may be of interest to indicate a few differences between the fuel-handling equipment on Hunterston, Tokai Mura and Trawsfynydd and that on Bradwell. Hunterston is the most radically different arrangement, in that it employs bottom charging of fuel with top charging of control assemblies. One fuelling machine is provided beneath each reactor, and one servicing machine above. Despite some complications and extra cost, this layout has a number of advantages in operation and reliability. First, all fuelling is done at reactor inlet temperatures so that fuel-chute problems are eased, and the machine can be tested under working conditions before the reactor power is raised. Secondly, the channel is removed from the core in only two units. This is done by a compression chain of proved reliability which is also very fast in operation.

Like Bradwell, Tokai Mura and Trawsfynydd both employ universal machines. Each has facilities for removal of a fully-shielded hoist unit from the fuelling machine, when it is pressurized and connected to the reactor. This gives an emergency "back-door"

method for removal of fuel from the fuelling machine if it cannot be removed. One of the main differences from Bradwell arises as a result of the reactor design. The core pressure drop is higher (on Tokai it is much higher because of the need for a small, highly-rated core imposed by earthquake considerations) so that it is uneconomic to prevent fuel element levitation during refuelling by a parasitic pressure drop in every channel. Flow control confined to the channel being fuelled has to be adopted. On Trawsfynydd this is achieved by the use of a temperature-sensitive valve on the fuel chute, which throttles channel flow as successive elements are removed and prevents levitation. On Tokai Mura there is a loop circuit which keeps the channel flow roughly constant during fuelling: after removal from the core, elements are stacked vertically in the fuelling machine and the gas from the channel being fuelled is passed over the elements in the machine and back to the reactor. Both machines have been extensively tested. For Tokai, production testing of the fuelling machines was done over a rig which comprised a mock-up

charge chute and a section of the reactor with hot gas flow.

My final comment on the paper just presented is relevant to the paragraph dealing with commissioning at Bradwell, which mentions the damage that occurs to fuel during fuel handling. Trawsfynydd has a stacked element similar to that of Bradwell, and to minimize damage during fuel handling the grab is fitted with a tubular shroud, or canister, which surrounds grab and fuel at all times except when fuel is actually within the core channel. As a result of this no damage has occurred to the elements either in works or site tests.

B. SAITCEVSKY (France): I should like to mention that the Marcoule industrial reactors G2 and G3 have been running since 1959 with refuelling machines operated when the reactor is at full power. The EDF2 and EDF3 reactors also have refuelling machines operating with the reactor at full power, and a description of them is given in paper P/54. Another machine which the CEA has developed for future use is described in paper P/51.

Compte rendu de la séance 3.7

Equipement des réacteurs

Président: G. Stiennon (Belgique)

Mémoire P/330 (présenté par A. G. Filippov)

DISCUSSION

D. S. HIORNS (Royaume-Uni): On montre, dans le mémoire qui vient d'être présenté, que la sécurité et la sûreté d'un appareillage de réacteur sont diminuées lorsque le conducteur doit accomplir un grand nombre de manœuvres. A ce propos, je voudrais attirer l'attention sur le mémoire P/126, qui décrit un appareillage où la tâche du conducteur se trouve simplifiée.

J. A. THIE (Etats-Unis d'Amérique): Ma principale question vise les blocs numérotés 17 sur la figure 1 du mémoire. Ces deux systèmes fonctionnent-ils en même temps, ou n'y en a-t-il qu'un des deux en marche, avec reprise par l'autre en cas de panne? S'il y a reprise, par quelle information est-elle provoquée?

A. G. FILIPPOV (URSS): Comme des différences peuvent se produire dans les réglages des amplificateurs et des courants des chambres d'ionisation pendant la marche du réacteur, des correcteurs automatiques (VI sur la figure 1) sont prévus dans les circuits de contrôle pour éviter un déséquilibre à la

sortie de l'amplificateur du contrôleur en secours. Le correcteur automatique du contrôleur en service est en même temps hors circuit. Les correcteurs automatiques sont enclenchés et déclenchés manuellement par le conducteur au moyen des blocs 17 de la figure 1.

J. A. THIE (Etats-Unis d'Amérique): A quel pourcentage de la puissance nominale y a-t-il déclenchement quand la demande est fixée à 10% de la puissance nominale, et à 100 ou 150% de la puissance nominale? Quelle période d'exponentielle prend-on avant d'atteindre la croissance linéaire?

A. G. FILIPPOV (URSS): Dans la gamme de puissance de 10 à 150%, la prévention d'accidents fonctionne pour un dépassement de puissance de 20% au-dessus de la valeur nominale. Avant la croissance linéaire de puissance on fait une montée exponentielle normalement d'une période de 20 à 30 s.

J. WEILL (France): Vous dites que le démarrage de vos réacteurs doit être rapide. Dans ces conditions, pour la phase de démarrage, quel système employez-vous?

A. G. FILIPPOV (URSS): Afin de réduire la durée du démarrage du réacteur et pour des raisons de sécurité, nous employons des systèmes automatiques

pour passer de l'état sous-critique à 1 à 10% de la puissance fixée. On suit une loi exponentielle.

J. WEILL (France): Quel type de détecteurs utilisez-vous, et, s'il s'agit de chambres d'ionisation comme semble l'indiquer votre mémoire, ces chambres sont-elles compensées à l'égard du rayonnement gamma?

A. G. FILIPPOV (URSS): Ce sont des chambres d'ionisation avec compensation pour le fond gamma qui sont utilisées dans les dispositifs de contrôle.

J. WEILL (France): Quelles vitesses moyennes avez-vous choisies pour vos barres de compensation et de contrôle (en unités de réactivité par seconde)?

A. G. FILIPPOV (URSS): La vitesse moyenne des barres de contrôle est environ $20 \times 10^{-5} \text{ s}^{-1}$ et celle des barres de compensation de $10 \times 10^{-6} \text{ s}^{-1}$.

Mémoire P/52 (présenté par G. Lamiral)

DISCUSSION *

P. FORTESCUE (Etats-Unis d'Amérique): L'une des maquettes a-t-elle été testée jusqu'à rupture ou fissuration en utilisant un gaz au lieu d'eau pour agent de pression? Les résultats prévus seraient-ils différents si l'on utilisait un gaz? La présence d'une peau d'étanchéité en acier a-t-elle un effet sur le mode de rupture?

G. LAMIRAL (France): Pour des raisons diverses, nous n'avons pas fait d'essais sur maquettes sous pression de gaz, mais des essais effectués sur la troisième maquette du caisson d'EDF3 semblent indiquer que la rupture sous pression de gaz ne serait pas nettement différente de la rupture sous pression d'eau. Vu la conception des ouvertures, les fissures commenceraient de l'extérieur du caisson.

La peau d'étanchéité en acier pourrait avoir quelque influence sur le mode de rupture du caisson; cette peau doit résister à des contraintes considérables au cours de la précontrainte; en même temps elle peut subir des déformations plastiques; elle doit donc être d'acier doux de bonne qualité susceptible d'un grand allongement. Dans des essais jusqu'à la rupture, surtout avec des câbles de précontrainte injectés, on pourrait craindre que les câbles ne cèdent avant la peau d'étanchéité et que la rupture soit très brutale, mais des essais ont montré que cette crainte n'était pas fondée. Il faut aussi réaliser que les essais jusqu'à la rupture faits sur des maquettes à pression croissante constituent une vérification des calculs mais ne représentent pas un mode possible de rupture, car la pression dans le réacteur en fonctionnement ne pourrait dépasser que de quelques unités pour cent la pression de service.

Il est possible, bien qu'improbable, que la résistance des câbles diminue (par exemple par corrosion) le réacteur étant à sa pression de service. Vu cette éventualité — comme nous l'avons montré — nous avons jugé nécessaire de supprimer un grand nombre

de câbles pour nous assurer que la pression de rupture soit atteinte et que tout accident grave soit précédé de loin par l'apparition de grosses fissures bien visibles sur l'extérieur du caisson.

P. FORTESCUE (Etats-Unis d'Amérique): Voyez-vous, en France, des difficultés pratiques à construire des caissons de béton servant d'enceinte à de l'hélium sous une pression de service atteignant 70 kg/cm^2 ?

G. LAMIRAL (France): Des études sont en cours sur le caisson du réacteur INCA avec des pressions de 40 et 60 bars. Nous pensons que la conception des caissons de béton précontraint ne pose pas de problèmes particuliers pour des pressions inférieures à une centaine de bars. Le seul problème lié à l'emploi d'hélium semble être celui de l'étanchéité; les contrôles de la peau d'étanchéité devraient être beaucoup plus stricts que ceux effectués dans le cas d'un caisson à gaz carbonique.

P. FORTESCUE (Etats-Unis d'Amérique): A quelles dimensions devient-il plus économique d'employer un caisson en béton plutôt qu'un caisson d'acier?

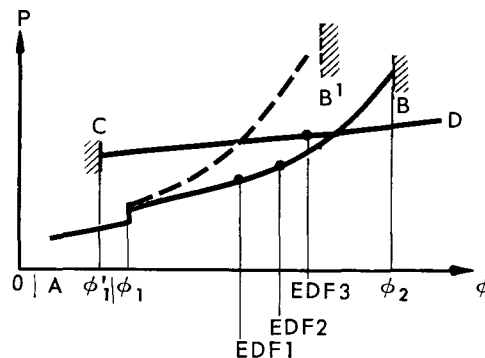


Figure 1.

G. LAMIRAL (France): Le graphique de la figure 1 représente la comparaison économique de caissons d'acier et de caissons de béton précontraint. Cependant, le graphique est plus un outil d'exposé qu'une représentation rigoureuse. Le prix du caisson est donné en fonction d'un paramètre dimensionnel, qui peut être le diamètre du cœur à hauteur constante, par exemple.

Le graphique est établi pour une pression donnée, 28 bars par exemple. Pour des caissons métalliques (courbe AB) il n'y a pas de dimensions minimales, et les caissons peuvent être aussi petits qu'on le veut. On observera une discontinuité de prix à ϕ_1 , correspondant aux dimensions pour lesquelles le caisson ne peut plus être fait en usine et doit être fait sur le chantier. La courbe s'élève très rapidement et les difficultés augmentent très vite avec les dimensions jusqu'au moment où, à une taille ϕ_2 , la construction devient impossible.

* Voir aussi, plus loin, la discussion du mémoire P/140.

Pour les caissons en béton précontraint, il y a des dimensions minimales (intuitives) pour un type de précontrainte donné, au-dessous desquelles on ne peut pas descendre. La courbe de prix est ensuite continue (on emploie les mêmes matériaux) et on ne voit pas de limite supérieure de taille.

Pour la centrale EDF1, la comparaison économique donnait la faveur aux caissons d'acier, et l'acier fut aussi choisi pour EDF2.

Des difficultés rencontrées dans la construction de ces caissons d'acier au manganèse-molybdène nous ont conduits à modifier complètement nos techniques de construction, et la courbe pour les caissons d'acier est alors devenue AB'. En même temps, l'expérience acquise à Marcoule permettait de réduire le coût des caissons de béton précontraint. Ainsi pour EDF3 la comparaison a été en faveur du béton précontraint. S'il fallait à l'heure actuelle refaire le caisson d'EDF3, nous estimons que nous pourrions faire des économies de 15 à 20%, et il est probable que, s'il fallait refaire des comparaisons entre acier et béton pour EDF1 et EDF2, la conclusion serait favorable au béton pour EDF2 sûrement et pour EDF1 peut-être. Je précise que le caisson d'EDF2 est une sphère de 18,30 m de diamètre intérieur, et que le caisson d'EDF1 est un cylindre de 10 m de diamètre intérieur et de 23 m de haut.

La comparaison ci-dessus a été faite pour une pression donnée, d'environ 28 bars, et on observera qu'à des pressions plus élevées la limite supérieure des dimensions des caissons d'acier serait plus basse, alors que la limite inférieure des caissons de béton précontraint ne semble pas varier beaucoup.

Mémoire P/140 (présenté par A. Houghton Brown)

DISCUSSION

P. FORTESCUE (Etats-Unis d'Amérique): Pourriez-vous préciser l'échelle de temps impliquée au point c) de la deuxième section de votre mémoire, à savoir que le mode de rupture définitive sera progressif, sans rupture soudaine. En d'autres termes, en combien de temps doit se produire une chute de pression du gaz à la moitié de sa valeur initiale pour être considérée comme soudaine?

A. HOUGHTON BROWN (Royaume-Uni): Le mode progressif de rupture dont il est question dans le mémoire ne se rapporte pas au temps. La progressivité porte sur des déformations croissantes sous des pressions croissantes; le temps d'application de la pression n'est pas significatif.

M. TROOST (Etats-Unis d'Amérique): Quelle est l'épaisseur de l'isolement de la peau d'étanchéité, et combien de couches utilisez-vous? Deuxièmement, pour quel flux thermique cet isolement est-il prévu?

A. HOUGHTON BROWN (Royaume-Uni): Je voudrais demander à mon collègue M. Spruce de répondre à ces questions.

T. W. SPRUCE (Royaume-Uni): L'épaisseur de

l'isolement en acier inoxydable est d'environ 2 pouces (5 cm), et cet isolement consiste en une trentaine de couches de feuilles espacées convenablement.

Le flux thermique sur l'isolement est très variable sur l'ensemble de la surface, mais je ne puis citer immédiatement les chiffres exacts.

R. S. TAYLOR (Royaume-Uni): Je voudrais faire quelques remarques à propos des mémoires sur les caissons sous pression en béton précontraint, spécialement en ce qui concerne les mémoires P/52 et P/140. Bien des solutions de toutes sortes ont été proposées au problème fondamental de la construction de caissons de grandes dimensions à pressions nominales élevées. Chacune des conceptions présentées aboutit manifestement à des constructions sûres et viables. La diversité de ces solutions indique la souplesse intrinsèque des caissons de béton pour satisfaire aux besoins des projets de réacteurs.

Les plans adoptés pour les caissons sous pression doivent être le fruit d'une étroite collaboration entre les ingénieurs qui établissent le projet du caisson et ceux qui établissent le projet du réacteur, et la solution optimale dépendra des critères particuliers choisis.

Dans le cas de la centrale de Wylfa (décrite dans le mémoire P/141), chaque réacteur fournit 590 MW électriques net. Le diamètre intérieur de chacun des deux caissons est de 96 ft (29 m) et la pression nominale est de 440 psi (31 kg/cm²). Une solution économique a été trouvée par l'adoption d'une surface intérieure sphérique et d'une surface extérieure adaptée au logement du lourd matériel de précontrainte et à la réalisation d'une construction rapide. La forme adoptée dans ce projet donne aussi des valeurs spécifiques très faibles en comparaison d'autres formes de caissons, et cela est illustré par la figure 2 du mémoire P/141.

On a parfois exprimé des doutes sur la possibilité d'analyser de façon précise les contraintes d'un caisson sphérique dans sa forme pratique. Le modèle du caisson de Wylfa s'appuie en fait sur un vaste programme de recherche et de mise au point, et l'on verra d'après la figure 3 du mémoire P/141 que l'accord est très bon entre les mesures et les calculs de contrainte. L'influence des écarts par rapport à une sphère parfaite est en fait peu de chose en comparaison des discontinuités inhérentes à la forme cylindrique.

Le comportement d'un caisson de modèle sphérique est fondamentalement identique dans le domaine d'utilisation et sous la charge de rupture, et les efforts de cisaillement sont très faibles. La nécessité de prévoir dans la construction des marges importantes pour couvrir les incertitudes du passage, dans un caisson cylindrique, de la charge nominale à la charge de rupture, se trouve éliminée.

Mémoire P/810

DISCUSSION

L. CAVE (Royaume-Uni): Dans la description du caisson du BHWR de Marviken, votre mémoire dit que les ajutages sur le fond de la cuve sont du type

« rapporté ». La figure 3 montre que l'ajutage est plutôt long, si bien que toute rotation pendant la soudure ou toute contrainte rémanente sera amplifiée considérablement.

Le problème de la rotation des ajutages a été l'objet d'attentions particulières au Royaume-Uni pendant le développement des premières centrales civiles, et nous avons trouvé préférable d'employer des ajutages « pénétrants » sur ces grands caissons d'acier. Par exemple, dans le cas du réacteur de Tokai, l'emploi d'ajutages « pénétrants », avec mise en place préalable tenant compte des corrections pour les effets estimés de soudure et de contraintes rémanentes, ont rendu inutile tout usinage important sur les ajutages une fois construits pour corriger des défauts d'alignement.

En outre le procédé de soudure pour des ajutages « pénétrants » est plus simple et plus sûr que pour le type « rapporté ». Je voudrais donc savoir pourquoi l'on a choisi des ajutages « rapportés » pour le caisson de Marviken.

O. HELLSTRÖM (Suède): Nous avons étudié de très près cette partie du caisson pour ce qui concerne la rotation. Le terme « rapporté » s'applique en général, mais certains des ajutages mériteraient mieux la classification en ajutages « pénétrants ».

A. L. GAINES (Etats-Unis d'Amérique): Par quelle méthode faites-vous le contrôle de la difficile opération de la soudure des ajutages sur le couvercle?

O. HELLSTRÖM (Suède): On effectue avec soin une inspection de chaque cordon, visuellement et au moyen de limaille aimantée et de teintures pénétrantes. Cela donne la certitude d'une soudure sans fissures ni autres défauts.

A. L. GAINES (Etats-Unis d'Amérique): Pendant les évolutions de température au chauffage et au refroidissement, la structure unique de fermeture du caisson conduit-elle à des écarts d'alignement des surfaces scellées? A quelle vitesse d'évolution le caisson peut-il résister pendant la durée prévue de son existence?

O. HELLSTRÖM (Suède): La fermeture est adaptée aux spécifications techniques concernant les changements de température au démarrage et en cours d'arrêt. La durée est comprise entre 8 et 16 heures, selon le type d'opération.

M. C. VAN VEEN (Pays-Bas): Quel est votre avis sur l'emploi d'un facteur de tenue de soudures de 0,9, comparé au facteur de 1,0 reconnu par les codes ASME pour la meilleure classe de soudures?

O. HELLSTRÖM (Suède): Je pense qu'un facteur de tenue de soudures de 0,9 n'est pas nécessaire pour un caisson de réacteur sous pression, vu les exigences des spécifications et la sévérité du contrôle de la fabrication. Cependant je suis sûr que nous changerons ce facteur de 0,9 en 1,0 dans notre code suédois.

M. C. VAN VEEN (Pays-Bas): Avez-vous effectué

des essais de soudure sur des plaques d'acier à 9% de Ni de 5 à 7 pouces (13 à 18 cm) d'épaisseur?

O. HELLSTRÖM (Suède): A ma connaissance, non.

Mémoire P/227 (présenté par A. L. Gaines)

DISCUSSION

B. SAITCEVSKY (France): Il n'est pas toujours possible de transporter de très grands caissons par voie fluviale de l'usine jusque sur le site. Pourriez-vous nous parler des méthodes de fabrication et des délais et coûts mis en œuvre dans le cas de caissons construits sur place?

A. L. GAINES (Etats-Unis d'Amérique): A ce jour, il n'y a pas eu de demande ferme de caissons fabriqués sur place. Des établissements industriels existants peuvent construire des caissons ayant jusqu'à 35 ft (10,5 m) de diamètre et pesant jusqu'à 1 000 tonnes. En outre, les grandes centrales ont besoin d'eau de refroidissement pour les condenseurs en quantités telles qu'elles sont placées en général sur des rivières navigables. Pour ces raisons, je n'ai aucun renseignement immédiat sur les délais et coûts mis en œuvre dans le montage sur place de caissons de réacteurs.

C. DE PATER (Pays-Bas): La section III du code ASME donne des règles de construction de caissons nucléaires. Des caissons non nucléaires peuvent-ils aussi aux Etats-Unis suivre les principes de cette section?

A. L. GAINES (Etats-Unis d'Amérique): Les dispositions de la section III peuvent être appliquées aux caissons autres que les caissons nucléaires avec l'autorisation des autorités locales responsables. Ces règles s'appliquent aussi aux caissons des industries pétrolières et chimiques.

Mémoire P/522 (présenté par A. Komárec)

DISCUSSION

A. L. GAINES (Etats-Unis d'Amérique): Le forgeage séparé des anneaux de brides, tout en simplifiant un problème difficile d'approvisionnement de matériau et de fabrication, semble limiter les possibilités, pour l'ensemble, de résister à de grandes vitesses d'échauffement. Pour quelle vitesse d'élévation de température et entre quelles limites (démarrage à fonctionnement) le caisson a-t-il été prévu et étudié?

A. KOMÁREC (Tchécoslovaquie): Une caractéristique du caisson de notre réacteur est que la température en fonctionnement est basse (pas plus de 150 °C) et que les fluctuations de température, surtout dans la région de la jonction par la bride, sont peu accusées. L'analyse des conditions de démarrage et de fonctionnement a montré que la jonction par la bride donnait satisfaction.

A. L. GAINES (Etats-Unis d'Amérique): L'essai de la maquette à l'échelle 1 comprenait-il un cyclage en température et en pression?

A. KOMÁREC (Tchécoslovaquie): La maquette du caisson est pratiquement prête, mais les essais n'ont pas encore commencé. Cependant, on a décidé de prévoir un cyclage en pression dans le programme d'essais. On n'a pas prêté une attention excessive aux effets du cyclage en température, car ce genre de contraintes n'est pas caractéristique du caisson.

A. L. GAINES (Etats-Unis d'Amérique): La coïncidence de l'épaulement de support des intervalles avec l'embase conique de support du caisson semblerait devoir accentuer les problèmes thermiques. Pour quelle vitesse d'évolution de la température, dans quelle gamme de températures et pour combien de cycles, l'étude du projet a-t-elle montré que le caisson restait dans les limites de contraintes du projet?

A. KOMÁREC (Tchécoslovaquie): La partie inférieure du caisson est refroidie par gaz, et une analyse poussée a montré que la température du gaz (110 °C) variait peu pour diverses conditions de fonctionnement du réacteur. Les conditions de démarrage seront établies expérimentalement au moyen de la maquette du caisson.

C. DE PATER (Pays-Bas): Pourriez-vous donner des chiffres concernant les résiliences et les températures de transition du métal de base, du métal de soudure et du métal de la région affectée, principalement en ce qui concerne les joints de soudure électrique?

A. KOMÁREC (Tchécoslovaquie): Une caractéristique des caissons de grandes dimensions est qu'ils forment un tout dans leur ensemble. Bien que les températures de transition du métal de base, du métal d'apport de la soudure et du métal de la zone affectée par le soudage puissent se déterminer sur des échantillons types, ces chiffres ne sont pas représentatifs pour la structure du caisson dans son ensemble. La seule image vraie des propriétés des métaux de structure pour les caissons de réacteurs est donnée par des essais sur de grands échantillons sur lesquels on a réalisé des joints soudés. De tels essais ont été faits en Tchécoslovaquie et ils montrent que, dans toutes les conditions voulues de fabrication et de fonctionnement, le caisson du réacteur peut supporter des températures plus élevées que la température critique de la structure dans son ensemble.

Mémoire P/138 (présenté par H. Bateman)

DISCUSSION

P. FORTESCUE (Etats-Unis d'Amérique): L'expérience a-t-elle révélé des problèmes particuliers dans le fonctionnement en parallèle de soufflantes à vitesse d'entraînement variable? Les conditions de stabilité imposent-elles une forme spécialement souhaitable des caractéristiques d'écoulement?

H. BATEMAN (Royaume-Uni): L'expérience que nous avons acquise à Hunterston n'a révélé aucun problème particulier dans le fonctionnement en parallèle de soufflantes à vitesse variable. Les formes de caractéristiques obtenues pour des soufflantes soit centrifuges

soit axiales de conception classique sont satisfaisantes.

Mémoire P/139 (présenté par J. O. Joss)

DISCUSSION

P. J. DUNTON (Royaume-Uni): L'expérience acquise à Hunterston, Tokai Mura et Trawsfynydd confirme les conclusions de la section du mémoire intitulée « Leçons pour l'avenir ». Les remarques sur les essais de prototypes et d'unités de production s'appliquent tout particulièrement, surtout si le site est éloigné du lieu de fabrication. Les deux réacteurs de Hunterston ont été portés à leur puissance nominale, et seuls quelques ennuis peu importants subsistent à l'installation de manutention de combustible; on a fait de nombreux essais en usine et sur le site avant la montée en puissance du réacteur.

Il peut être intéressant de signaler quelques différences entre les appareils de manutention de combustible de Hunterston, Tokai Mura et Trawsfynydd, et celui de Bradwell. La disposition à Hunterston est particulièrement originale, en ceci que le chargement du combustible se fait par la partie inférieure et celui des éléments de contrôle par la partie supérieure. Une machine de chargement se trouve au-dessous de chaque réacteur et une machine de manutention au-dessus. Malgré quelques complications et dépenses supplémentaires, cette disposition présente de nombreux avantages pour l'exploitation et la sécurité. Tout d'abord, tous les chargements se font aux températures d'entrée du réacteur, ce qui simplifie les problèmes des glissières du combustible, et la machine peut subir des essais dans les conditions de service avant la montée en puissance du réacteur. En second lieu, un canal est retiré du cœur en deux éléments seulement. Cela se fait par une chaîne de compression éprouvée, qui est aussi d'un fonctionnement très rapide.

Comme Bradwell, Tokai Mura et Trawsfynydd utilisent toutes deux des machines universelles. Chacune est munie de dispositifs d'enlèvement de treuil sous blindage complet hors de l'appareil de chargement sous pression et couplé au réacteur. Cela offre une « sortie de secours » pour enlever le combustible de l'appareil de chargement s'il ne peut plus bouger. L'une des principales différences par rapport à Bradwell résulte de la conception du réacteur. La perte de charge dans le cœur est plus élevée (à Tokai elle est beaucoup plus élevée, à cause de la nécessité d'avoir un cœur de petites dimensions et à hautes performances, imposée en prévision des tremblements de terre), de sorte qu'il n'est pas économique d'empêcher l'envol des éléments combustibles en cours de chargement par une perte de pression parasite dans chaque canal. Il faut un contrôle de l'écoulement limité au canal où s'effectue le chargement. A Trawsfynydd, cela se trouve réalisé au moyen d'une vanne commandée en température sur la glissière du combustible; cette vanne règle l'écoulement dans le canal

à mesure que les éléments sont retirés et empêche l'envol. A Tokai Mura, il y a une boucle qui maintient l'écoulement dans le canal à peu près constant pendant le chargement: une fois sortis du cœur, les éléments combustibles sont empilés verticalement dans l'appareil de chargement, et le gaz sortant du canal que l'on charge passe sur les éléments dans l'appareil et retourne au réacteur. Les deux appareils ont fait l'objet d'essais très complets. Pour Tokai, les essais de fabrication des appareils de chargement ont été effectués sur un banc qui comprenait une maquette de glissière de chargement et une section du réacteur avec écoulement de gaz chaud.

Ma remarque finale sur le mémoire qui vient d'être présenté concerne le paragraphe où il est question des détériorations subies par le combustible pendant les manutentions. A Trawsfynydd, l'élément

est empilé comme celui de Bradwell, et, pour réduire les détériorations au cours des manutentions, le grappin est équipé d'une enveloppe cylindrique, ou chemise, qui coiffe le grappin et le combustible à tout moment, sauf lorsque le combustible se trouve effectivement dans le canal du cœur. Le résultat est qu'il n'y a eu aucune détérioration d'élément aux essais, ni en usine ni sur le site.

B. SAITCEVSKY (France): Je voudrais rappeler que les réacteurs industriels G2 et G3 de Marcoule fonctionnent depuis 1959 avec des machines de chargement exploitées avec le réacteur à pleine puissance. Les réacteurs EDF2 et EDF3 ont également des dispositifs de chargement fonctionnant lorsque le réacteur est à pleine puissance, qui sont décrits dans le mémoire P/54. Une autre machine développée par le CEA pour l'avenir est décrite dans le mémoire P/51.

Протокол заседания 3.7

Оборудование реакторных установок

Председатель Г. Стеннон (Бельгия)

Доклад P/330 (представил А. Г. Филиппов)

ДИСКУССИЯ

Д. С. БИОРНС (Соединенное Королевство): В представленном докладе указывается, что надежность и безопасность реакторной системы ставится под сомнение, когда оператор должен выполнять значительное число манипуляций. В связи с этим я должен обратить внимание на доклад P/126, в котором описывается система со значительно упрощенными обязанностями оператора.

Дж. А. ТАЙ (Соединенное Королевство): Мой основной вопрос относится к блокам, обозначенным номером 17 на рис. 1 доклада. Работают обе системы одновременно или работает только одна из двух систем с включением второй системы в случае аварии? Если существует такая передача, то в каких случаях она включается?

А. Г. ФИЛИППОВ (СССР): На случай возможного рассогласования в настройке усилителей и токов ионизационных камер во время работы реактора в контролируемые каналы устанавливаются автоматические корректоры предотвращающие рассогласование выходного сигнала резервного контрольного усилителя. Автоматический корректор действующего регулирующего устройства одновременно в цепь не

включается. Автоматические корректоры включаются и выключаются вручную оператором с использованием блоков 17 на рис. 1 доклада.

Дж. А. ТАЙ (Соединенное Королевство): При каком проценте от полной мощности срабатывает выключающее устройство, когда задается ряд уровней мощности: 10, 100 и 150% от полной мощности? Чему равен период экспоненциального роста, который предшествует линейному росту мощности?

А. Г. ФИЛИППОВ (СССР): В диапазоне от 10 и 150% полной мощности аварийная защита срабатывает при 20%-ном превышении номинального значения. Обычно используется период экспоненциального роста мощности до линейного участка порядка 20—30 сек.

Ж. ВЕЙЛ (Франция): Вы сказали, что Ваши реакторы должны быстро выходить на мощность. В связи с этим возникает вопрос: какую систему Вы используете в период пуска реактора?

А. Г. ФИЛИППОВ (СССР): Для сокращения времени пуска реактора и обеспечения безопасности нами используются автоматические системы при подъеме мощности от подкритического состояния до 1—10% номинальной мощности. Подъем мощности следует экспоненциальному закону.

Ж. ВЕЙЛ (Франция): Какой тип детекторов Вы используете? Если это ионизационные

камеры, как указано в Вашем докладе, то используется ли в них компенсация γ -фона?

А. Г. ФИЛИПОВ (СССР): В регулирующих системах используются ионизационные камеры с компенсацией γ -фона.

Ж. ВЕЙЛ (Франция): Какая средняя скорость выбрана Вами для компенсирующих и регулирующих стержней (выраженная в единицах реактивности в секунду)?

А. Г. ФИЛИПОВ (СССР): Средняя скорость регулирующих стержней составляет порядка $20 \cdot 10^{-5} \text{ сек}^{-1}$, а компенсирующих стержней около $10 \cdot 10^{-6} \text{ сек}^{-1}$.

Доклад Р/52 (представил Ж. Ламираль)

ДИСКУССИЯ*

П. ФОРТЕСКЬЕ (США): При испытании каких-либо моделей на аварийное повреждение или утечку используется газ, а не вода для обеспечения необходимого давления? Должны ли получаться совпадающие результаты в случае использования газа? Влияет ли стальная оболочка на форму аварийного повреждения?

Ж. ЛАМИРАЛЬ (Франция): Мы не проводили испытания моделей с газом под давлением для всех случаев. Но, кажется, были испытаны три модели корпуса реактора EDF-3 с целью показать, что разрушения, вызванные газом под давлением, существенно не отличаются от разрушений в случае использования воды под давлением. Принимая во внимание характер трещин, можно заключить, что растрескивание начинается с внешней поверхности корпуса.

Стальная оболочка может оказывать определенное влияние на механизм разрушения корпуса. Эта оболочка должна выдерживать значительные напряжения во время предварительной опрессовки, в то же время она может подвергаться пластическому растяжению. В связи с этим оболочка должна быть изготовлена из высококачественной стали, способной к значительным растяжениям. При испытаниях на повреждение особенно с введенными через уплотнения кабелями может случиться, что кабели разорвутся раньше уплотнений, однако испытания не подтвердили этого факта даже при значительном разрушении. Необходимо также понять, что хотя испытания на повреждение проводятся на моделях при более высоком давлении с целью проверки расчетных данных, они не соответствуют возможной форме натуральных повреждений, поскольку давление в процессе эксплуатации реактора не может превышать рабочее давление более чем на несколько процентов.

Возможно, хотя и маловероятно, что прочность кабелей в реакторе может снизиться (на-

пример, из-за коррозии) при рабочем давлении. Как мы указывали, в этом случае пришлось вынуть значительное количество кабелей, чтобы убедиться, что разрушающее давление достигнуто и любому серьезному инциденту предшествует значительное растрескивание, ясно видимое с внешней стороны корпуса.

П. ФОРТЕСКЬЕ (США): Какие практические проблемы сооружения бетонных корпусов давления, выдерживающих рабочее давление гелия до 70 кг/см^2 , возникают во Франции?

Ж. ЛАМИРАЛЬ (Франция): Проводятся исследования корпуса реактора INEA на давления 40 и 60 бар, принятые в расчетах. Мы не думаем, что в конструкции корпуса из предварительно напряженного бетона возникнут какие-либо проблемы в диапазоне давлений ниже 100 бар. По-видимому, единственной проблемой будет обеспечение герметичности при использовании гелия. Металлическая оболочка должна проверяться более тщательно, чем в случае корпуса для углекислого газа.

П. ФОРТЕСКЬЕ (США): Для каких физических размеров бетонный корпус является более экономичным, чем стальной корпус?

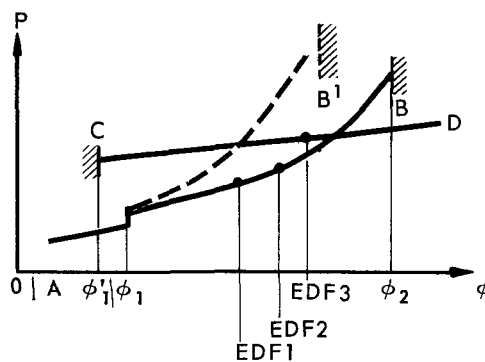


Рисунок 1

Ж. ЛАМИРАЛЬ (Франция): На рис. 1 сравнивается стоимость стальных корпусов с корпусами из предварительно напряженного бетона. Однако график дает скорее качественное объяснение, а не точное представление. Стоимость корпуса дается как функция некоторых геометрических параметров, например, диаметра активной зоны реактора при заданной высоте.

График построен для определенного давления скажем 28 бар. Для металлических корпусов (кривая AB) минимальные размеры отсутствуют, то есть корпус может быть так мал, как это необходимо. Дальше наступает разрыв функции стоимости и соответствующим таким размерам, выше которых корпуса не могут изготавливаться на заводе и должны монтироваться непосредственно на строительной площадке. Затем кривая стоимости и соответствующие трудности быстро возрастают с ростом размеров до тех пор, когда при определенном значении

* См. также ниже дискуссию по докладу Р/140.

φ 2 сооружение становится практически невозможным.

В случае корпусов из предварительно напряженного бетона для любой данной предварительно напряженной системы (интуитивно) есть предел, ниже которого сооружение невозможно. От нижнего предела кривая стоимости непрерывно растет (используются те же материалы) и, как видно на графике, не имеет верхнего предела по размерам.

Для атомной электростанции EDF-1 был выбран стальной корпус, поскольку он оказался экономичнее. Стальной корпус был также выбран для реактора EDF-2.

Трудности, встретившиеся при создании корпусов из марганце-молибденовой стали привели к разработке новых технологических процессов. На графике это показано кривой *AB'* для стальных корпусов. В то же время проведенные в Маркуле эксперименты подтвердили возможность снижения стоимости корпусов из предварительно напряженного бетона. Поэтому для EDF-3 сравнение было в пользу корпуса из предварительно напряженного бетона. Если в настоящее время корпус EDF-3 пришлось бы построить заново, то экономия составила 15—20%. При сравнении стального и бетонного корпуса для реакторов EDF-1 и EDF-2 с учетом современных данных возможно, что преимущество было бы на стороне бетонного корпуса для реактора EDF-2 и даже для реактора EDF-1. Я должен указать, что корпус реактора EDF-2 имеет сферическую форму внутренним диаметром 18,3 м, а корпус реактора EDF-1 цилиндрической формы диаметром 10 м и высотой 23 м.

Приведенное выше сравнение сделано для давления порядка 28 бар. Можно показать, что для более высокого давления верхний предел геометрических размеров металлических корпусов будет ниже, чем бетонных. Оказывается, нижний предел армированных бетонных корпусов изменяется очень незначительно.

Доклад Р/140 (представил А. Хоутон Браун)

ДИСКУССИЯ

П. ФОРТЕСКЬЕ (США): Можете ли Вы уточнить, что Вы понимаете под пунктом с временной шкалой, приведенной во второй части Вашего доклада, а именно под выражением «максимальная авария должна развиваться постепенно без мгновенного разрушения». Другими словами, какой период времени должен рассматриваться как внезапный при снижении давления газа на 50% от первоначального значения?

А. ХОУТОН БРАУН (Соединенное Королевство): Указанная в докладе последовательная форма развития аварии не связана со временем.

Эта последовательность определяется ростом отклонений под действием увеличивающегося давления. Время действия приложенного давления не существенно.

М. ТРУСТ (США): Какова толщина изолирующей оболочки и сколько слоев используется? Какой предполагаемый тепловой поток будет проходить через оболочку?

А. ХОУТОН БРАУН (Соединенное Королевство): Я попрошу моего коллегу д-ра Спрюса ответить на эти вопросы.

Т. У. СПРЮС (Соединенное Королевство): Толщина изоляции из нержавеющей стали порядка 5 см, она изготовлена из 30 слоев фольги с соответствующими зазорами. Тепловой поток на поверхности изоляции существенно меняется, однако я не в состоянии сейчас назвать точную величину.

Р. С. ТЭЙЛОР (Соединенное Королевство): Я хочу сделать несколько замечаний по докладам, в которых описываются корпуса из предварительно напряженного бетона, и, в частности, по докладам Р/52 и Р/140. Предложено несколько различных решений основной проблемы сооружения корпусов больших размеров, работающих при высоких давлениях. Для каждого проекта четко описаны вопросы безопасности, воплощенные в конструкции. Такое разнообразие решений указывает на присущую бетонным корпусам гибкость с точки зрения удовлетворения требованиям конструкторов реакторов.

Разработка проекта корпуса давления должна производиться в тесной связи между конструкторами реактора и корпуса. Оптимальное решение будет зависеть от использования практических критериев.

В случае атомной электростанции в Уилфе (описанной в докладе Р/141) каждый реактор вырабатывает электрическую мощность 590 Мвт. Внутренний диаметр каждого из двух корпусов составляет 29,2 м и рабочее давление 30 ат. Было найдено экономичное решение с использованием сферической внутренней поверхности. Форма внешней поверхности была выбрана в соответствии с тяжелым приспособлением для предварительного напряжения бетона, что оказалось практичным и сократило сроки сооружения. Эта форма имеет очень низкую удельную нагрузку по сравнению с другими формами корпуса, что отмечено на рис. 2 доклада Р/141.

Иногда выражают сомнение в том, что корпуса сферической формы трудно поддаются анализу на сжимающие усилия. Корпус реактора в Уилфе был разработан на основе данных программы научно-исследовательских и опытно-конструкторских работ, и, как показано на рис. 3 доклада Р/141, экспериментальные и расчетные данные хорошо согласуются между собой. Отклонения от сферической формы в действительности играют меньшую роль по

сравнению с отклонениями, присущими цилиндрической форме.

Поведение корпусов сферической формы по существу одинаковое как при рабочей нагрузке, так и при предельной нагрузке, скальвающие усилия очень малы. При сооружении цилиндрического корпуса требуются значительные запасы прочности, чтобы перекрыть неопределенности, связанные с переходом от рабочей к предельной нагрузке. В случае сферического корпуса эта необходимость отпадает.

Доклад P/810

ДИСКУССИЯ

Л. КЕЙВ (Соединенное Королевство): В Вашем докладе описан корпус Марвикенского реактора BNWR, при этом указывается, что патрубок днища корпуса приварен уголкового соединением. На рис. 3 показано, что патрубок довольно длинный, поэтому при сварке или снятии напряжений любое вращение будет заметно возрастать.

Проблеме вращения патрубка уделялось значительное внимание при разработке ранних английских атомных электростанций, и причем было установлено, что для больших стальных корпусов более предпочтительным является тавровое соединение со сквозным патрубком. Например, в реакторе в Токаи-Мура использование сквозного патрубка в сочетании с предварительной проверкой влияния сварки и операциями по снятию напряжений исключает необходимость выполнения трудоемкой механической обработки патрубков для восстановления соосности и ликвидации других дефектов после их изготовления.

Кроме того, сварка сквозных патрубков тавровым соединением проще и более надежна, чем уголкового соединения патрубков. В связи с этим хотелось бы узнать, по каким соображениям для Марвикенского реактора был выбран тип патрубков с уголкового соединением?

О. ХЕЛЛСТРЕМ (Швеция): Мы очень тщательно изучали этот узел корпуса с точки зрения вращения. Название «уголковое соединение», вообще говоря, обосновано, однако для некоторых патрубков наиболее подходящим названием будет термин «уголковое соединение с вставленным патрубком».

А. Л. ГЕЙНС (США): Какой метод использовался для проверки трудных операций по приварке патрубков к днищу?

О. ХЕЛЛСТРЕМ (Швеция): Все дно было тщательно осмотрено визуально, кроме того, для проверки использовались магнитные частицы и окрашенные смачивающие вещества. Это обеспечило сварку без трещин и других дефектов.

А. Л. ГЕЙНС (США): Во время изменения

температуры при нагреве и охлаждении влияет ли аксиальное расположение уникальной конструкции перегородки корпуса на герметичность поверхностей? Какая скорость переходных процессов будет допустимой во время эксплуатации корпуса?

О. ХЕЛЛСТРЕМ (Швеция): Перегородка является технически приемлемой с точки зрения изменения температур во время запуска и остановки реактора. Это время составит от 8 до 16 ч в зависимости от характера эксплуатации реактора.

М. К. ВАН ВИН (Нидерланды): Каково Ваше мнение об использовании показателя качества сварки 0,9 по сравнению с показателем 1,0, установленным нормами ASME для высшего класса сварки?

О. ХЕЛЛСТРЕМ (Швеция): Я думаю, что сварка с показателем качества 0,9 необходима для реакторного корпуса давления с точки зрения высоких требований и строгого контроля их выполнения. Однако я уверен, что в наших шведских нормах этот показатель мы изменим с 0,9 до 1,0.

М. К. ВАН ВИН (Нидерланды): Проводили ли Вы какие-либо опыты по сварке стальных пластин (с содержанием никеля 9%) толщиной 13—18 см?

О. ХЕЛЛСТРЕМ (Швеция): Насколько мне известно, такие опыты не проводились.

Доклад P/227 (представил А. Л. Гейнс)

ДИСКУССИЯ

Б. ЗАЙЧЕВСКИЙ (Франция): Как известно, не всегда возможна транспортировка очень больших корпусов по воде от завода-изготовителя к строительной площадке. Можете ли Вы что-либо сказать о типах конструкции, времени и стоимости сооружения таких корпусов на строительной площадке?

А. Л. ГЕЙНС (США): В настоящее время нет спроса со стороны фирм на изготовление корпусов в полевых условиях. Существующая промышленная техника позволяет строить корпус диаметром до 10 м и весом 1000 т. Кроме того, на крупных атомных электростанциях для охлаждения конденсаторов вода необходима в таком количестве, что обычно приходится строить станции на судоходных реках. По этим причинам я не располагаю данными о времени и стоимости сборки реакторных корпусов на строительной площадке.

К. ДЕ ПАТЕР (Нидерланды): III часть норм ASME содержит «Правила для сооружения корпусов ядерных реакторов». Применяются ли в США эти правила для сооружения неядерных корпусов?

А. Л. ГЕЙНС (США): Требования III части могут быть использованы для корпусов не только ядерных установок с учетом требований местных контролирующих органов. Эти правила применимы также при сооружении корпусов, используемых в нефтяной и химической промышленности.

Доклад P/522 (представил А. Комарек)

ДИСКУССИЯ

А. Л. ГЕЙНС (США): Изготовление различных фланцевых колец, хотя и облегчает трудности, связанные с заготовкой материала, и процессы изготовления, но, по-видимому, ограничивает способность конструкции выдерживать большие скорости нагрева. На какие скорости повышения температуры в диапазоне рабочих температур рассчитан и испытан корпус?

А. КОМАРЕК (Чехословакия): Особенностью нашего корпуса является то, что он работает при низких температурах (не выше 150°С). Температурные флуктуации, особенно в местах фланцевых соединений, не будут резкими. Анализ пусковых и эксплуатационных условий показал, что фланцевые соединения работают удовлетворительно.

А. Л. ГЕЙНС (США): Проводились ли испытания модели в масштабе 1:1, включая циклические режимы температуры и давления?

А. КОМАРЕК (Чехословакия): Масштабная модель корпуса практически готова, но испытания еще не начаты, однако принято решение включить циклический режим давления в программу испытаний. Предварительное рассмотрение показывает, что напряжения, возникающие при температурных качках, не характерны для такого корпуса.

А. Л. ГЕЙНС (США): Согласование интервалов для опорных консолей и конического опорного приспособления корпуса должно, по-видимому, вызвать тепловые проблемы. При какой скорости изменения температуры, в каком температурном диапазоне и с каким количеством циклов испытывалась конструкция, показавшая, что напряжения корпуса не превышают проектных пределов.

А. КОМАРЕК (Чехословакия): Нижняя часть корпуса охлаждается газом; тщательный анализ показал, что температура газа (110°С) незначительно меняется при различных условиях работы реактора. Условия пуска будут проверяться экспериментально с использованием масштабной модели корпуса.

К. ДЕ ПАТЕР (Нидерланды): Можете ли Вы сообщить данные, относящиеся к импульсным нагрузкам и температурам переходных режимов для основного металла, сварного металла и металла в зоне действия сварки и в особенности для электросварных соединений?

А. КОМАРЕК (Чехословакия): Отличительной особенностью крупных реакторных корпусов является то, что они представляют собой единое целое. Хотя переходные температуры для основного металла, сварного металла и металла в зоне действия сварки могут определяться на стандартных образцах, эти данные не являются представительными для конструкции корпуса в целом. Единственно правильная картина свойств конструкционных металлов для реакторных корпусов получается при испытании крупных образцов, на которых выполнены сварные соединения. Такие испытания были проведены в Чехословакии, результаты которых показали, что при всех требуемых условиях изготовления и эксплуатации реакторного корпуса температуру можно поддерживать выше критической температуры конструкции в целом.

Доклад P/138 (представил Х. Бейтмен)

ДИСКУССИЯ

П. ФОРТЕСКЬЕ (США): Указывают ли эксперименты на существование специальных проблем, обусловленных параллельной работой газодувок с переменными скоростями? Налагаются ли условия стабильности на любую желаемую форму характеристики потока?

Х. БЕЙТМЕН (Соединенное Королевство): Опыт работы в Хантерстоне не свидетельствует о наличии каких-либо специальных проблем, связанных с параллельной работой газодувок с переменными скоростями. Формы характеристик, полученных как для центробежных, так и для аксиальных газодувок современной конструкции, являются удовлетворительными.

Доклад P/139 (представили Дж. О. Джосс)

ДИСКУССИЯ

П. Дж. ДАНКТОН (Соединенное Королевство): Опыт эксплуатации реакторов в Хантерстоне, Токаи-Мура и Траусфиниде подтверждает выводы, приведенные в разделе доклада «Уроки на будущее». Замечания по испытанию прототипа и промышленной установки уместны, особенно если строительная площадка расположена далеко от места изготовления. Оба хантерстонских реактора достигли проектной мощности, осталось только решить некоторые вопросы, связанные с машиной для перегрузки топлива. Перед выводом реактора на мощность проведен большой объем работ и различные испытания на строительной площадке. Интересно было бы указать на некоторые различия между оборудованием по перегрузке топлива на реакторах в Хантерстоне, Токаи-Мура и Траусфиниде и соответствующим оборудованием на реакторе в Брадзулле. Наиболее радикальные отличия име-

ет разгрузочное оборудование реакторов в Хантерстоне, где топливо разгружается через низ реактора, а сборки регулирующих стержней — через крышку. Одна перегрузочная машина обслуживает низ реактора, а другая — верх. Несмотря на некоторое усложнение и увеличение стоимости, это оборудование обладает рядом эксплуатационных преимуществ. Во-первых, вся загрузка топлива в реактор производится при входной температуре теплоносителя, что существенно облегчает проблему разгрузочного желоба и машина может быть испытана в рабочих условиях до подъема мощности реактора. Во-вторых, канал удаляется из активной зоны только двумя машинами. Это осуществляется путем уплотнения цепи, обеспечивающей надежность и быстроту выполнения операции по разгрузке на ходу.

На реакторах в Токаи-Мура и Траусфиниде, так же как и на реакторах в Бладуэлле, используются универсальные машины. Каждая станция имеет установки для удаления из разгрузочной машины полностью защищенного подъемного устройства, когда машина опрессована и подсоединена к реактору. Это позволяет использовать аварийный способ «обратная дверь» для удаления топлива из разгрузочной машины, если она потеряла способность к перемещению. Основное отличие этой машины от машины на реакторах в Бладуэлле определяется конструкцией реактора. Перепад давления в активной зоне выше (в реакторах Токаи-Мура перепад значительно выше из-за сейсмических условий, налагаемых на небольшую высоконапряженную активную зону), поэтому экономически нецелесообразно препятствовать подъему тепловыделяющих элементов при разгрузке за счет перепада давления в каждом канале. Во время разгрузки должен быть установлен контроль за расходом теплоносителя в разгружаемом канале. На реакторах в Траусфиниде это достигается путем использования чувствительного к температуре клапана, установленного на разгрузочном желобе, который дросселирует поток в канале при последова-

тельном извлечении элементов и предотвращает их подъем. В реакторах Токаи-Мура имеется петлевой контур, который во время разгрузки топлива поддерживает расход в канале почти постоянным. После выгрузки из активной зоны элементы устанавливаются вертикально в разгрузочной машине, и газ из разгруженных каналов пропускается через элементы, находящиеся в разгрузочной машине, и возвращается обратно в реактор. Обе разгрузочные машины прошли длительные испытания. Производственные испытания разгрузочных машин для реакторов Токаи-Мура проводились с использованием модели разгрузочного желоба и секции реактора с потоком горячего газа.

Последнее мое замечание по обсуждаемому докладу касается параграфа, в котором описаны пуско-наладочные работы по Бладуэллской станции и приведены случаи повреждения тепловыделяющих элементов во время разгрузки топлива. В разгрузочной машине реакторов в Траусфиниде тепловыделяющие элементы устанавливаются так же, как и в Бладуэллской разгрузочной машине. Для уменьшения возможных повреждений во время перегрузки топлива захват снабжен трубчатым кожухом или оболочкой, который окружает захват и тепловыделяющий элемент во время разгрузки за исключением того момента, когда элемент еще находится в канале активной зоны. В результате этого тепловыделяющие элементы не повреждаются ни во время работы, ни при испытаниях.

Б. ЗАЙЧЕВСКИЙ (Франция): Я должен заметить, что промышленные реакторы G-2 и G-3 в Маркуле эксплуатируются с 1959 года с разгрузочными машинами, действующими при работе реактора на полной мощности. Реакторы EDF-2 и EDF-3 также имеют перегрузочные машины, действующие при работе реактора на полной мощности. Эти машины описаны в докладе P/54. Другая машина, разрабатываемая Комиссариатом по атомной энергии Франции для будущего использования, описана в докладе P/51.

Acta de la Sesión 3.7

Accesorios de las centrales dotadas de reactores

Presidente: G. Stiennon (Bélgica)

Documento P/330 (presentado por A. G. Filippov)

DISCUSIÓN

D. S. HIORNS (Reino Unido): En la memoria se señala que la confianza y seguridad del sistema a que pertenece un reactor resultan perjudicadas si el

operador tiene que hacer muchas manipulaciones. En relación con esto, me gustaría llamar su atención sobre la memoria P/126 que describe un sistema con el que se simplifica la tarea del operador.

J. A. THIE (Estados Unidos de América): Mi pregunta se refiere a los bloques número 17 de la

figura 1 de la memoria. ¿Funcionan ambos sistemas al mismo tiempo, o funciona sólo uno de los dos y la transferencia al otro se produce en caso de avería? Si hay transferencia, ¿qué información la produce?

A. G. FILIPPOV (URSS): En vista de la posibilidad de que surjan discrepancias en la fijación de nivel de los amplificadores y de las corrientes de las cámaras de ionización durante el funcionamiento del reactor, se han dispuesto correctores automáticos (VI en la figura 1) en los canales de control para impedir desequilibrios a la salida del amplificador de control de reserva. Al mismo tiempo el corrector automático del regulador en servicio está fuera de circuito. Los correctores automáticos los conecta y desconecta manualmente el operador, empleando los bloques 17 de la figura 1.

J. A. THIE (Estados Unidos de América): ¿A qué porcentaje de la potencia máxima se produce el disparo cuando la demanda es 10 por 100 de la de la potencia total y 100 o 150 por 100 de la misma? ¿Qué período exponencial se emplea antes de alcanzar el régimen lineal?

A. G. FILIPPOV (URSS): En la gama de potencias de 10-150% el sistema de prevención de accidentes entra en funcionamiento para un aumento de potencia del 20% sobre el valor fijado. Antes de la elevación de potencia lineal se emplea un aumento exponencial, normalmente con un período de 20-30 segundos.

J. WEILL (Francia): Dice Vd. que sus reactores tienen que ponerse en marcha rápidamente. ¿Que sistema emplean Vds. en la fase puesta en marcha?

A. G. FILIPPOV (URSS): Para reducir el tiempo de puesta en marcha y por razones de seguridad, empleamos sistemas automáticos para pasar del estado subcrítico al 1-10% de la potencia nominal. Se emplea una ley exponencial.

J. WEILL (Francia): ¿Qué tipo de detectores emplean? Si son cámaras de ionización, como su memoria parece indicar, ¿están compensadas para radiaciones gamma?

A. G. FILIPPOV (URSS): En los sistemas de control se emplean cámaras de ionización con compensación del fondo gamma.

J. WEILL (Francia): ¿Qué velocidad media han elegido para sus barras de control y compensación (expresado en unidades de reactividad por segundo)?

A. G. FILIPPOV (URSS): La velocidad media de las barras de control es aproximadamente $20 \times 10^{-5} \text{ s}^{-1}$ y la de las barras de compensación aproximadamente $10 \times 10^{-6} \text{ s}^{-1}$.

Documento P/52 (presentado por G. Lamiral)

DISCUSIÓN *

P. FORTESCUE (Estados Unidos de América): ¿Se ha probado alguno de los modelos hasta rotura o fuga

empleando gas en vez de agua para aplicar la presión? ¿Se esperarían resultados diferentes si se empleara un gas? ¿Afecta a la forma de la rotura la existencia de un revestimiento de acero?

G. LAMIRAL (Francia): Por diversas razones no hemos llevado a cabo ensayos de modelos sometidos a presión de gas, pero los ensayos que hemos efectuado en el tercer modelo de la vasija del EDF3 parecen indicar que las roturas causadas por presión de gas no diferirán esencialmente de las roturas causadas por presión de agua. A la vista del proyecto de las aberturas, las grietas se iniciarían en el exterior de la vasija.

El revestimiento de acero podría tener algún efecto en la forma de romperse la vasija; este revestimiento tiene que resistir deformaciones considerables durante el pretensado y al mismo tiempo puede sufrir deformaciones plásticas; por ello tiene que ser de acero suave de buena calidad, capaz de un alargamiento considerable. En ensayos de rotura, especialmente con cables de pretensado inyectados, se podría temer que los cables se rompieran antes que la capa de sellado y que la rotura fuese muy violenta, pero los ensayos han demostrado que este temor no es justificado. También hay que tener en cuenta que, aunque los ensayos de rotura llevados a cabo en modelos a presión superior constituyen una comprobación de los cálculos, no corresponden a un modo posible de rotura, puesto que la presión del reactor en funcionamiento no será superior a la presión de servicio más que en un pequeño tanto por ciento.

Es posible, aunque no probable, que la resistencia de los cables disminuya (por ejemplo por corrosión) con el reactor a la presión de servicio. Como hemos señalado, para esta contingencia se estimó necesario suprimir un gran número de cables con objeto de asegurar que se alcanza la presión de rotura y que, mucho antes de cualquier accidente serio, se presenta un agrietamiento importante, claramente visible desde fuera de la vasija.

P. FORTESCUE (Estados Unidos de América): ¿Ven Vds. en Francia algún problema práctico en la construcción de vasijas de presión de hormigón para presiones de trabajo hasta de 70 kg/cm² de gas helio?

G. LAMIRAL (Francia): Los estudios que se realizan sobre la vasija del reactor INCA tienen en cuenta presiones de 40 y 60 bares. No creemos que el proyecto de vasijas de hormigón pretensado plantee problemas especiales para presiones por debajo de los 100 bares. El único problema que plantea el empleo de helio parece estar relacionado con la hermeticidad; la comprobación del revestimiento metálico debe ser mucho más rigurosa que en el caso de vasijas para dióxido de carbono.

P. FORTESCUE (Estados Unidos de América): ¿Para qué tamaño es más económico emplear una vasija de hormigón en vez de una vasija de acero?

G. LAMIRAL (Francia): El gráfico de la figura 1 compara desde un punto de vista económico las

* Ver también, más adelante, la discusión del documento P/140.

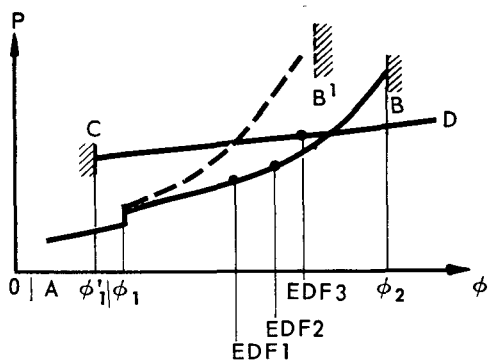


Figura 1

vasijas de acero con las vasijas de hormigón preten-sado. Sin embargo, se ha trazado el gráfico más para facilidad de explicación que como una representación exacta. El coste de la vasija viene dado en función de algunos parámetros dimensionales, por ejemplo el diámetro del núcleo del reactor para una altura dada.

El gráfico es para una presión fija, por ejemplo de 28 bares. Para vasijas metálicas (curve AB) no hay dimensiones mínimas y las vasijas pueden ser tan pequeñas como se desee. Se puede apreciar que hay una discontinuidad del precio en ϕ_1 , correspondiente a las dimensiones máximas de las vasijas que pueden ser construidas en fábrica; por encima de esas dimensiones la vasija debe ser construida en obra. La curva crece después muy aprisa y las dificultades crecen también muy rápidamente con las dimensiones, hasta que para un cierto tamaño ϕ_2 ya no es posible la construcción.

En el caso de vasijas de hormigón pretensado hay un límite inferior (intuitivo), para cualquier sistema de pretensado dado, por debajo del cual no es posible la construcción; la curva de coste es continua a partir de ahí (empleando los mismos materiales) y no puede verse un límite superior de tamaño.

Para la Central EDF1 la comparación económica fué favorable a las vasijas de acero y también se eligió este material para el EDF2.

Las dificultades encontradas en el proyecto de vasijas de acero al manganeso - molibdeno condujeron al desarrollo de nuevos procesos de fabricación y la curva para vasijas de acero pasa ahora a ser la AB'. Al mismo tiempo, la experiencia obtenida en Marcoule hizo posible la reducción del coste de las vasijas de hormigón pretensado. Por consiguiente, para el EDF3 la comparación fue favorable al hormigón pretensado. Si hubiera que volver a construir la vasija del EDF3 en la actualidad, se podría conseguir una economía del 15-20% y es probable que si se hicieran ahora comparaciones entre acero y hormigón para EDF1 y EDF2, el resultado sería favorable al hormigón para EDF2 y quizá incluso para EDF1. Quiero señalar que la vasija del EDF2 tiene forma de esfera con un diámetro interior de 18,3 m mientras la vasija del EDF1 es cilíndrica, con un diámetro de 10 m y una altura de 23 m.

La comparación anterior se ha hecho para presión dada, del orden de 28 bares aproximadamente, y debe señalarse que para presiones más elevadas los límites superiores de las dimensiones de las vasijas metálicas serían más bajos, mientras los límites inferiores de las vasijas de hormigón armado no parece cambien mucho.

Documento P/140 (presentado por A. Houghton Brown)

DISCUSIÓN

P. FORTESCUE (Estados Unidos de América): ¿Puede Vd. especificar la escala de tiempo que se aplicaría al apartado c) de la segunda sección de su memoria, cuando dice, «La forma de rotura será progresiva sin producirse rotura repentina»? En otras palabras, ¿en qué período de tiempo sería considerada repentina la pérdida de la mitad de la presión inicial de gas?

A. HOUGHTON BROWN (Reino Unido): La forma de rotura progresiva mencionada en la memoria no está relacionada con el tiempo. Las deformaciones crecen, de forma progresiva, bajo presiones crecientes; el tiempo durante el cual se aplica la presión no influye sobre ello.

M. TROOST (Estados Unidos de América): ¿Cuál es el espesor del aislamiento del revestimiento y cuántas capas se emplean? ¿Para qué flujo térmico se ha proyectado el aislamiento?

A. HOUGHTON BROWN (Reino Unido): Me gustaría pedir a mi colega Sr. Spruce que conteste a estas preguntas.

T. W. SPRUCE (Reino Unido): El espesor del aislamiento de acero inoxidable es del orden de 50,8 mm (2 pulgadas) y está constituido por unas 30 capas de láminas, convenientemente espaciadas.

El flujo calorífico en el aislamiento varía considerablemente sobre la superficie, pero no puedo en este momento citar los valores reales.

R. S. TAYLOR (Reino Unido): Desearía hacer unos cuantos comentarios en relación con las memorias que tratan de vasijas de presión de hormigón pretensado, especialmente sobre las memorias P/52 y P/140. Se ha propuesto un gran número de soluciones muy diferentes al problema básico de construir vasijas de grandes dimensiones que funcionan a altas presiones. Es evidente que cada uno de los proyectos da como resultado estructuras seguras y realizables. Esta diversidad de soluciones demuestra la flexibilidad inherente a las vasijas de hormigón para cumplir los requisitos del proyectista del reactor.

El proyecto de vasija de presión adoptado debe ser el resultado de una íntima colaboración entre los proyectistas de la vasija y del reactor y la solución óptima dependerá de los criterios particulares que se apliquen.

En el caso de la central nuclear de Wylfa (descrita en la memoria P/141) cada reactor tiene una potencia eléctrica neta de 590 MW. El diámetro interior de cada una de las dos vasijas es de 29,28 m (96 pies) y la presión de proyecto es 30 kg/cm² (440 psi). Se halló

una solución económica mediante el empleo de una superficie interna esférica y una superficie externa de forma adecuada que permitiera acomodar los pesados mecanismos de pretensado y lograr una construcción práctica y expedita. Este tipo de proyecto consigue también dimensiones específicas muy bajas en comparación con otras formas de vasijas y este punto se pone de manifiesto en la figura 2 de la memoria P/141.

Algunas veces se ha expresado la duda de si la vasija esférica, en su forma práctica, se presta a un análisis de tensiones riguroso. La vasija del tipo Wylfa está basada en realidad en un amplio programa de investigación y desarrollo y, como se aprecia en la figura 3 de la memoria P/141, la correspondencia entre las deformaciones experimentales y las pronosticadas es muy buena. El efecto de las diferencias con una esfera geométrica es en realidad mínimo en comparación con las discontinuidades propias de la forma cilíndrica.

El comportamiento de la vasija de tipo esférico es el mismo en esencia para las cargas de trabajo y la de rotura, y los esfuerzos cortantes son muy pequeños. La inclusión de márgenes considerables para tener en cuenta las incertidumbres al pasar en la vasija cilíndrica desde las cargas de trabajo a la de rotura no es aquí necesaria.

Documento P/810

DISCUSIÓN

L. CAVE (Reino Unido): En su memoria, al describir la vasija del BHWR de Marviken, se dice que las boquillas en el fondo de la vasija son del tipo «a tope»; la figura 3 muestra que la boquilla es bastante larga, de forma que cualquier giro que ocurra durante la soldadura o tratamiento térmico posterior, será amplificado considerablemente.

El problema del giro de las boquillas interesó mucho en el Reino Unido durante el desarrollo de las primeras centrales comerciales y encontramos que es preferible el empleo de boquillas «pasantes» en estas grandes vasijas de acero. Por ejemplo, en el caso del reactor Tokai el empleo de boquillas «pasantes» junto con el ajuste previo para corregir los efectos estimados de la soldadura y el tratamiento térmico posterior, evitó la necesidad de una mecanización importante de las boquillas después de la fabricación, para corrección de faltas de alineación.

Además, el método para soldar boquillas «pasantes» es más sencillo y más seguro que el de boquillas «a tope». Por ello estoy interesado en conocer el motivo de la elección de boquillas «a tope» para la vasija de Marviken.

O. HELLSTRÖM (Suecia): Hemos estudiado esta parte de la vasija con gran cuidado en cuanto a los giros. La expresión «a tope» es generalmente válida, pero algunas de las boquillas podrían ser clasificadas más adecuadamente como «penetrantes».

A. L. GAINES (Estados Unidos de América): ¿Qué método de inspección se emplea para la difícil operación de soldar las boquillas a la tapa?

G. HELLSTRÖM (Suecia): Se lleva a cabo una inspección cuidadosa de cada cordón visualmente, con partículas magnéticas y con colorantes penetrantes. Esto asegura una soldadura sin fisuras ni otros defectos.

A. L. GAINES (Estados Unidos de América): Durante los regímenes transitorios de temperatura que tiene lugar durante el calentamiento y el enfriamiento ¿se producen cambios en la posición axial de las superficies de sellado a causa de la construcción singular del cierre de la vasija? ¿Que velocidad de cambio puede ser resistida durante la vida prevista de la vasija?

G. HELLSTRÖM (Suecia): El cierre es aceptable respecto a las especificaciones técnicas que regulan los cambios de temperatura durante la puesta en marcha y parada del reactor. El tiempo está comprendido entre 8 y 16 horas, según la clase de operación.

M. C. VAN VEEN (Países Bajos): ¿Cuál es su opinión respecto al uso de un factor de soldadura de 0,9, en comparación con el factor 1,0 admitido por las normas ASME para las soldaduras de máxima calidad?

G. HELLSTRÖM (Suecia): Creo que un factor de soldadura de 0,9 no es necesario en la vasija de presión de un reactor, si se tienen en cuenta los requisitos elevados y el control riguroso del producto. Sin embargo, estoy seguro que cambiaremos este factor de 0,9 a 1,0 en nuestra norma sueca.

M. C. VAN VEEN (Países Bajos): ¿Han realizado Vds. ensayos de soldadura con chapas de acero al 9% Ni, de 127 a 177,8 mm (5-7 pulgadas) de espesor?

G. HELLSTRÖM (Suecia): No, que yo sepa.

Documento P/227 (presentado por A. L. Gaines)

DISCUSIÓN

B. SAITCEVSKY (Francia): No siempre es posible transportar vasijas muy grandes por vía marítima o fluvial desde la fábrica a la obra. ¿Podría Vd. decir algo sobre los tipos de construcción de vasijas construidas en obra y los tiempos y costes asociados a ellas?

A. L. GAINES (Estados Unidos de América): Hasta la fecha no ha habido una demanda firme de vasijas fabricadas en obra. Las instalaciones industriales existentes permiten la construcción de vasijas hasta 10,65 m (35 pies) de diámetro y 1 000 toneladas de peso. Además las grandes centrales térmicas necesitan tan gran cantidad de agua para los condensadores, que en general se ubican junto a ríos navegables. Por estas razones no dispongo de información sobre tiempos y costes de construcción en obra de vasijas de reactores.

C. DE PATER (Países Bajos): La Sección III de las normas ASME da «Reglas para la construcción de vasijas nucleares». En los Estados Unidos, ¿pueden basarse las vasijas no nucleares también en esta Sección?

A. L. GAINES (Estados Unidos de América): Los requisitos de la Sección III pueden emplearse para otras vasijas, distintas de las nucleares, con el permiso de las autoridades locales correspondientes. Estas normas también se están aplicando a las vasijas de las industrias petrolíferas y químicas.

Documento P/522 (presentado por A. Komárec)

DISCUSIÓN

A. L. GAINES (Estados Unidos de América): Los platillos de brida forjados separados, aunque ayudan a resolver un problema difícil de suministro de material y fabricación, parecen limitar la facultad de este diseño para resistir calentamientos rápidos. ¿Para qué velocidad de elevación de temperatura y para qué intervalo de temperaturas (arranque a funcionamiento normal) ha sido proyectada y analizada la vasija?

A. KOMÁREC (Checoslovaquia): Una característica especial de nuestra vasija es que la temperatura de trabajo es baja (no más de 150 °C) y las fluctuaciones de temperatura, especialmente en la zona de la junta embridada, no son bruscas. Un análisis de las condiciones en el arranque y el funcionamiento normal demostró que la junta embridada es satisfactoria.

A. L. GAINES (Estados Unidos de América): Los ensayos del modelo a escala 1:1 ¿incluyen ciclos de presión y temperatura?

A. KOMÁREC (Checoslovaquia): El modelo a escala de la vasija está prácticamente terminado, pero los ensayos todavía no han empezado. Sin embargo se ha decidido incluir los ciclos de presión en el programa de ensayos. No se da mucha importancia a los efectos de los ciclos de temperatura, pues este tipo de esfuerzos no tiene lugar en la vasija.

A. L. GAINES (Estados Unidos de América): La coincidencia parcial del retallo de soporte con la inserción del cono de soporte de la vasija parece que debe acentuar los problemas térmicos. ¿Para qué velocidad de cambio de temperatura, qué intervalo de temperaturas, y para cuántos ciclos ha demostrado el análisis que la vasija estará dentro de los límites de tensiones fijados en el proyecto?

A. KOMÁREC (Checoslovaquia): La parte inferior de la vasija está refrigerada por gas y un análisis cuidadoso ha demostrado que la temperatura del gas (110 °C) varía sólo ligeramente con los distintos regímenes de funcionamiento del reactor. Las condiciones de puesta en marcha serán investigadas experimentalmente empleando el modelo a escala de la vasija.

C. DE PATER (Países Bajos): ¿Puede Vd. dar datos respecto a resistencia al choque y temperaturas de transición del metal base, metal de aporte y metal de la zona afectada, en particular respecto a las juntas soldadas por electroescoria?

A. KOMÁREC (Checoslovaquia): Una característica especial de las vasijas de gran tamaño es que repre-

sentan un conjunto íntegro. Aunque las temperaturas de transición del metal base, el metal de aporte y el metal de la zona afectada por la soldadura pueden determinarse en probetas normalizadas, estos datos no son representativos de la estructura de la vasija considerada como un conjunto. La única información verdadera de las propiedades de los metales estructurales para vasijas de reactores, es la proporcionada por ensayos con probetas grandes en las que se han hecho juntas soldadas. Estos ensayos se han realizado en Checoslovaquia y han demostrado que, para todas las condiciones que se presentan durante la fabricación y funcionamiento, la vasija del reactor puede soportar temperaturas más elevadas que la temperatura crítica de la estructura considerada globalmente.

Documento P/138 (presentado por R. Bateman)

DISCUSIÓN

P. FORTESCUE (Estados Unidos de América): ¿Ha demostrado la experiencia la existencia de problemas en el funcionamiento en paralelo de soplantes con accionamiento de velocidad variable? ¿Imponen las condiciones de estabilidad alguna forma especialmente conveniente de las curvas características?

R. BATEMAN (Reino Unido): Nuestra experiencia en Hunterston no ha señalado que existan problemas especiales en relación con el funcionamiento en paralelo de soplantes de velocidad variable. Las formas características que se obtienen con soplantes centrífugas o axiales de diseño normal son satisfactorias.

Documento P/139 (presentado por J. O. Joss)

DISCUSIÓN

P. J. DUNCTON (Reino Unido): La experiencia de Hunterston, Tokai Mura y Trawsfynydd confirma las conclusiones expuestas en la sección de la memoria titulada « Lecciones para el futuro ». Los comentarios sobre las pruebas del prototipo y unidades de producción son particularmente apropiados, especialmente si la obra está lejos del lugar de fabricación. Los dos reactores de Hunterston han llegado a su potencia nominal y sólo quedan por resolver pequeños problemas en relación con la instalación de manejo de combustible; se hicieron ensayos amplios en taller y en obra antes de elevar la potencia del reactor.

Puede ser interesante indicar unas pocas diferencias entre el equipo de manejo de combustible de Hunterston, Tokai Mura y Trawsfynydd y el de Bradwell. La instalación de Hunterston es la más diferente esencialmente, en cuanto que emplea carga del combustible por el fondo, con acceso por la parte superior para los conjuntos de control. Bajo cada reactor hay una máquina de carga de combustible y en la parte superior hay una máquina de servicio. A pesar de algunas complicaciones y de un coste más elevado, esta disposición tiene diversas ventajas en cuanto a su funcionamiento y seguridad. Primero: toda la carga y descarga del combustible se hace a las temperaturas

de entrada al reactor, de forma que se simplifican los problemas de la tolva del combustible y la máquina puede ser probada en condiciones de trabajo antes de elevar la potencia del reactor. Segundo: el canal se retira del núcleo en sólo dos unidades. Esto se consigue por una cadena de compresión de seguridad comprobada y que es también de funcionamiento muy rápido.

Igual que Bradwell, Tokai Mura y Trawsfynydd emplean máquinas universales. Cada una tiene dispositivos para sacar de la máquina de carga de combustible una unidad elevadora totalmente blindada, cuando la máquina está a presión y conectada al reactor. Esto proporciona un método de emergencia de «puerta trasera» para retirar el combustible de la máquina de carga si ésta no puede moverse. Una de las principales diferencias respecto a Bradwell es consecuencia del proyecto del reactor. La caída de presión en el núcleo es más grande (en Tokai es mucho mayor por la necesidad de un núcleo pequeño y más compacto impuesta por consideraciones sísmicas), por lo cual es antieconómico impedir el aligeramiento del elemento combustible durante las operaciones de carga por medio de una caída de presión parásita en todos los canales. Se debe adoptar un control de caudal que se limite al canal cuyo combustible se está cargando. En Trawsfynydd esto se consigue mediante el empleo de una válvula gobernada por la temperatura de la tolva de combustible, que estrangula el caudal en el canal a medida que se extraen los elementos evitando así el aligeramiento. En Tokai Mura hay un circuito cerrado que mantiene el caudal en el canal aproximadamente

constante durante la carga de combustible: los elementos combustibles, después de retirados del núcleo, se apilan verticalmente en la máquina de carga y el gas del canal que está siendo cargado pasa por los elementos de la máquina y vuelve al reactor. Ambas máquinas han sido ensayadas concienzudamente. Para Tokai, los ensayos de producción de las máquinas de carga de combustible se hicieron en un circuito que comprendía un modelo de tolva de carga y una sección del reactor con caudal de gas caliente.

Mi comentario final a esta memoria versa sobre el párrafo 12, sobre los daños que sufre el combustible durante su manejo. Trawsfynydd tiene un elemento apilado semejante al de Bradwell, y para reducir a un mínimo el daño durante el manejo de combustible, la garra tiene un aro tubular de refuerzo, o manguito, que rodea garra y combustible en todo momento, excepto cuando el combustible está exactamente dentro del canal del núcleo. Como resultado de esto los elementos no han sufrido daño en los ensayos en el taller ni en la obra.

B. SAITCEVSKY (Francia): Me gustaría mencionar que los reactores industriales G2 y G3 de Marcoule han estado funcionando desde 1959 con máquina de carga de combustible que trabajan con el reactor a plena potencia. Los reactores EDF2 y EDF3 también tienen máquinas de carga de combustible que funcionan con el reactor a plena potencia y que se describen en la memoria P/54. Otra máquina que el CEA ha desarrollado para empleo futuro se describe en la memoria P/51.

List of Volumes

PEACEFUL USES OF ATOMIC ENERGY

Proceedings of the Third International Conference held at Geneva, 31 August-9 September 1964

The full list of the sixteen volumes comprising the multilingual edition of the Proceedings is given below. The sessional titles are included to show the main subjects dealt with in each individual volume.

Volume 1

Progress in Atomic Energy

Programme of the Conference

A Opening of the Conference

B New Economic Data. Energy Needs in Coming Years and the Role of Nuclear Power in Meeting these Needs

1.6 Technical and Economic Aspects of the Use of Nuclear Power

C International Collaboration in Nuclear Reactor Projects, including Developments of Major Co-operative Installations

H Closing of the Conference

Evening Lecture

Scientific Exhibition

Volume 2

Reactor Physics

3.1 New Developments in Reactor Physics

Volume 3

Reactor Studies and Performance

3.2 Lattice Studies and Critical Experiments

3.3 Reactor Performance

Volume 4

Reactor Control

3.4 Reactor Kinetics

3.5 Reactor Control and Shielding

Volume 5

Nuclear Reactors — I. Gas-cooled and Water-cooled Reactors

1.1 Gas-cooled and Graphite-moderated Reactors

1.2 Light-water Reactors

1.3 Heavy-water and Organic Reactors

Volume 6

Nuclear Reactors — II. Fast Reactors and Advanced Concepts

1.4 Fast Reactor Physics and Breeders

1.5 Superheating and Advanced Concepts

1.7 Reactors of Special Applications. Future Developments

Volume 7

Research and Testing Reactors

D Research Reactors

1.9 High Flux Reactors for Material Testing

1.8 Very High Flux Reactors, Construction and Uses

Volume 8

Reactor Engineering and Equipment

- 1.10 Heat Transfer
- 1.11 Hydraulic Problems of Reactor Engineering
- 3.7 Reactor Plant Equipment

Volume 9

Reactor Materials

- 2.8 Structural Materials
- 2.9 Structural and Control Materials and Moderators
- 2.4 Corrosion Studies. Non-destructive Testing

Volume 10

Nuclear Fuels — I. Fabrication and Reprocessing

- 2.3 Fuel Element Fabrication and Experience
- 2.6 Fuel Reprocessing, Part I
- 2.7 Fuel Reprocessing, Part II

Volume 11

Nuclear Fuels — II. Types and Economics

- 2.5 Economics of the Fuel Cycle
- 2.1 Metallic and Various Fuels
- 2.2 Ceramic Fuels

Volume 12

Nuclear Fuels — III. Raw Materials

- 2.11¹ Resources and Requirements
- 2.12 Prospecting Techniques and Recovery from Ores
- 2.10 Isotope Separation

Volume 13

Nuclear Safety

- 3.9 Nuclear Safety Research
- 3.8 Chemical Processing Plant Safety; Fuel Transport
- 3.6 Reactor Safety; Location and Containment; Reactor Tests

Volume 14

Environmental Aspects of Atomic Energy and Waste Management

- 3.10 Safety Aspects of Large-scale Use of Atomic Energy. Measurement and Limitation of Exposure in Radiation Emergencies
- 3.11 Radioactive Waste Management

Volume 15

Special Aspects of Nuclear Energy and Isotope Applications

- E Controlled Nuclear Fusion
- 4.1 Direct Conversion of Heat to Electricity
- F Applications of Isotopes and Radiation Sources in the Physical Sciences
- G Applications of Isotopes and Radiation Sources in the Life Sciences
- 4.2 Miscellaneous Applications of Atomic Energy

Volume 16

List of Papers and Indexes

- List of Papers
- Author Index
- Country Index
- Sessional Index